G.N. Tiwari
Arvind Tiwari
Shyam

Handbook of Solar Energy

Theory, Analysis and Applications

Springer

Energy Systems in Electrical Engineering

Series editor

Muhammad H. Rashid, Pensacola, USA

More information about this series at http://www.springer.com/series/13509

G.N. Tiwari · Arvind Tiwari
Shyam

Handbook of Solar Energy

Theory, Analysis and Applications

Springer

G.N. Tiwari
Centre for Energy Studies
Indian Institute of Technology Delhi
New Delhi
India

Shyam
Centre for Energy Studies
Indian Institute of Technology Delhi
New Delhi
India

Arvind Tiwari
Qassim University
College of Engineering
Buraydah
Saudi Arabia

Printed on acid-free paper

Our respected teacher and guruji, Padmashri Prof. M.S. Sodha, FNA, on his 84th birthday (February 08, 2016)

Preface

Solar energy is clean, environmentally friendly and freely available over the planet earth. Life on earth also owes its existence to solar energy. Solar energy is used to produce thermal as well as electrical power. If fossil fuels continue to be depleted at the present rate, they will be exhausted soon. The use of fossil fuels is also largely responsible for increasing pollution and resulting climate change. Solar energy and other renewable sources, enable us to meet the demand for energy, while offering a cleaner and greener footprint.

In the recent past, there has been rapid development in solar thermal technologies and photovoltaic (PV) materials. This development brought cost effectiveness to solar devices. Based on the developments in the field of solar technology, we decided to compose a handbook of solar energy, which goes beyond the usual and brings together a myriad of current topics such as Day-lighting, Solar cell materials, Photovoltaic thermal (PVT) systems, Energy conservation, Solar power generation, Thermodynamics, Solar cooling of houses, Energy and exergy analysis, CO_2 credit, Energy Matrices, Life Cycle analysis with and without CO_2 credit.

The main objective of writing this book is to create a comprehensive and easy-to-understand source of information on the advances in this rapidly growing research area. This book includes enough information on the basics to be used as a textbook undergraduate coursework in for engineering and the sciences. The inclusion of advanced concepts and research trends will also make it useful as a reference for scientists and professionals. An attempt has also been made to give solved examples and exercise problems with hint and objective questions at appropriate place in each chapter for better understanding of solar energy applications.

This book consists of twenty chapters. The basics of hourly, daily, monthly solar radiation on horizontal and inclined surfaces and sun-earth angles have been discussed briefly in Chap. 1. The various natural day lighting system with examples have been discussed in Chap. 2. Chapter 3 deals with the basic elements of heat transfer mechanisms, laws of thermodynamics and exergy which have been used

throughout text. Effects of nano-particles with water as a base fluid have also been discussed briefly. Chapter 4 discusses different solar cell materials, PV modules, PV arrays and its applications in various sectors. Solar fluid collectors namely conventional flat plate collectors (FPC's), solar concentrators and evacuated tubular collectors (ETC's) are dealt with in Chaps. 5−7. Chapter 8 discusses industrial solar water heating systems for different modes of operation. The modeling of PVT solar air heaters and their applications are reported in Chap. 9. The various passive concepts of heating/cooling of a house with approximate methods and solar cooling houses have been briefly discussed in Chaps. 10 and 11, respectively. Chapters 12 and 13 cover other solar thermal applications namely solar crop drying and solar distillation systems with basic heat transfer, thermal modeling and examples. Energy analyses of solar thermal and PV systems have been covered in Chap. 14. Solar energy storage in different modes is discussed in Chap. 15. Solar power generation by means of photovoltaic (grid and off-grid) and solar concentrating have been considered in Chap. 16. Chapters 17 and 18 report applications of solar thermal energy, which has not been covered in preceding chapters and cover energy conservation in different sectors. Study of exergy, CO_2 mitigation, carbon credit, and life cycle cost analysis of some solar thermal and PV system, which is the backbone of its success, is included in Chaps. 19 and 20, respectively.

SI units are used throughout the book. Some conversion units, various physical and chemical properties of water, air, metals and non-metals are also given as appendices.

Acknowledgements

G.N. Tiwari
Arvind Tiwari
Shyam

Contents

About the Authors

Prof. G.N. Tiwari received postgraduate and doctoral degrees in 1972 and 1976, respectively, from the Banaras Hindu University, India. Since 1977, he has been involved in the teaching program at the Centre for Energy Studies, IIT Delhi. His research interests in the field of solar-energy applications are solar distillation, water/air heating systems, greenhouse technology for agriculture and aquaculture, earth-to-air heat exchangers, passive building design, hybrid photovoltaic thermal (HPVT) systems, climate change, energy security, etc. He has guided approximately 80 Ph.D. students and published more than 550 research papers in journals of repute. He has authored 20 books associated with reputed publishers. He was a corecipient of the Hariom Ashram Prerit S.S. Bhatnagar Award in 1982. He taught at the University of Papua, New Guinea, from 1987 to 1989 as an expert in energy and the environment. He was also named European Fellow in 1997 and has been nominated for the IDEA award. He is responsible for the development of the Solar Energy Park at IIT Delhi and the Energy Laboratory at the University of Papua, New Guinea, Port Moresby. Dr. Tiwari has successfully coordinated various research projects funded by the Government of India. Dr. Tiwari was editor of the *International Journal of Agricultural Engineering* for 3 years (2006–2008). He is associate editor for the *Solar Energy Journal* (SEJ) in the area of solar distillation and has been editor of the *International Journal of Energy Research* since 2007. He is also the editor-in-chief of *Fundamentals of Renewable Energy Applications* and servers as a reviewer for many international journals. He was conferred the title of Vigyan Ratna by the State of Uttar Pradesh, India, on March 26, 2008. He is also founder president of the Bag Energy Research Society, which is responsible for energy education in rural India.

Dr. Arvind Tiwari holds a bachelor's degree in physics and a mater's of science degree majoring in material science from Jamia Millia Islamia as well as a master's degree in technology in microelectronics from Punjab University (2002). He completed his doctorate in hybrid photovoltaic thermal systems in 2006 from IIT Delhi. He is a postdoctoral fellow from the University of Twente, Netherlands. Besides holding several other teaching engagements throughout his career,

Dr. Tiwari has worked as an Indian expert in the capacity of senior lecturer at Manmohan Memorial Polytechnic, Morang, Nepal, on deputation by the Government of India from January 2010 to January 2012. At present, he is working as a professor at Qassim University, Kingdom of Saudi Arabia.

To his credit, he has written more than 20 research papers published in international journals of repute. He cosupervised three Ph.D. students at IIT Delhi and is currently supervising an additional four Ph.D. students. He is also reviewer of many international journals including *Solar Energy*, *Energy Research*, and *Journal of Open Access*.

Mr. Shyam holds a bachelor's of science degree (B.Sc.) majoring in mathematics, physics, and chemistry and a master's of science degree (M.Sc.) in physics from the University of Allahabad. He also holds a master's of technology degree (M.Tech.) in cryogenic engineering from the Indian Institute of Technology, Kharagpur, India. During his M.Tech. programme he studied the giant magnetoimpedance (GMI) effect in manganites and developed a magnetic-position sensor based on the GMI effect. He worked as an assistant professor at the Marathwada Institute of Technology, Bulandshahr, from August 2008 to October 2012 and taught engineering physics at the undergraduate level.

Presently, he is pursuing a doctoral degree under the supervision of Professor G.N. Tiwari at the Centre for Energy Studies, Indian Institute of Technology Delhi. His areas of research interest include solar thermal collectors (modelling and experiments), photovoltaics, heat and mass transfer, exergy, CO_2 mitigation, climate change and carbon trading, and exergoeconomic and enviroeconomic analyses.

Approximate Values of Various Constants in Solar Energy

S.No	Constants	Actual value	Approximate value
1	Diameter of the Sun	$1.39 \times 10^9\,m$	$1.50 \times 10^9\,m$
2	Distance of the Sun from the Earth	$1.5 \times 10^{11}\,m$	$150 \times 10^9\,m$
3	Black-body temperature of the Sun	$5777\,K$	$6000\,K$
4	Centre core temperature of the Sun	$8{-}40 \times 10^6\,K$	$9{-}30 \times 10^6\,K$
5	Energy generated in the Sun's centre core	$90\,\%$	$90\,\%$
6	Diameter of the Earth	$1300\,km$	$1.5 \times 10^6\,m$
7	Solar constant	$1367W/m^2$	$1500W/m^2$
8	Short-wavelength radiation	0.23–2.6 μm	0.3–3.0 μm
9	Average temperature of the Earth	$298\,K$	$300\,K$
10	Stefan–Boltzmann constant	$5.67 \times 10^{-8}\,W/m^2\,K^4$	$60 \times 10^{-9}\,W/m^2\,K^4$
11	Wein's displacement law (λT)	$2897.6\,\mu m K$	$3000\,\mu m K$
12	Long-wavelength radiation from the Earth	$10\,\mu m$	$9\,\mu m$
13	Wavelength radiation from the Earth	$0-30\,\mu m$	$0-30\,\mu m$
14	Sunshine hour at the equator	$12\,h$	$12\,h$
15	Sunshine hour at the North Pole	$24\,h$	$24\,h$
16	Optimum tilt angle for maximum solar radiation	$\phi \pm 15$	$\phi \pm 15$
17	Convective heat-transfer coefficient for air	$2.8 + 3\,V$	$3(1 + V)$
18	Sky temperature (T_{sky})		$(T_a{-}12)$
19	Long-wavelength radiation exchange between the ambient air and the sky	$60\,W/m^2$	$60\,W/m^2$
20	Order of the radiative heat-transfer coefficient	$6\,W/m^2\,K$	$6\,W/m^2\,K$

(continued)

S.No	Constants	Actual value	Approximate value
21	Convective and radiative heat-transfer coefficient for air	$5.7 + 3.8\, VW/m^2\, K$	$3(2 + v)\, W/m^2\, K$
22	Order of the convective heat-transfer coefficient between a hot plate and water		$90 - 300\, W/m^2\, K$
23	Overall heat-transfer coefficient for a single glazed FPC		$6\, W/m^2\, K$
24	FPC-efficiency factor(F')		0.9
25	Insulation thickness	$0.10\, m$	$0.09\, m$
26	Fin efficiency (F)		0.9
27	Flow-rate factor		<0.9
28	Transmittivity of window glass		0.9
29	Threshold intensity		$> 300\, W/m^2$
30	FPC connected in series		≤ 3
31	Thermal conductivity of an insulating material	$0.03 - 0.04\, W/mK$	$0.03\, W/mK$
32	Maximum temperature in a concentrating collector		$3000\, °C$
33	Ideal efficiency of solar efficiency	$60\,\%$	$60\,\%$
34	Optimum depth of a basin of water	$0.02 - 0.03\, m$	$0.03\, m$
35	Effect of the climatic parameter on solar-still yield		$9 - 12\,\%$
36	Emissivity of a surface	0.9	0.9
37	Optimum water depth in a collection-cum-storage water heater	$0.10\, m$	$0.09\, m$
38	Optimum temperature for the fermentation of slurry for biogas production	$25-27\, °C$	$27\, °C$
39	Cooking time by solar cooker	$2 - 3\, h$	$3\, h$
40	Latent heat of vaporization	$2.3 \times 10^6\, J/kg$	$3.0 \times 10^6\, J/kg$
41	Band gap for silicon	$1.16\, eV$	$1.2\, eV$
42	Boltzmann's constant (k)	$1.38 \times 10^{-23}\, J/K$	$12 \times 10^{-24}\, J/K$
43	V-group impurity concentration	$10^{15}\, cm^3$	$10^{15}\, cm^3$
44	Effective density of states in the conduction band	$2.82 \times 10^{19}\, cm^3$	$28 \times 10^{18}\, cm^3$
45	Saturation current in reverse bias	$10^{-8}\, A$	$10^{-8}\, A$
46	Thickness of an n-type semiconductor in a solar cell	$0.2\, \mu m$	$0.3\, \mu m$
47	Thickness of a p-type semiconductor in a solar cell	$0.5\, \mu m$	$0.6\, \mu m$
48	Diffusion path length	$50 - 100\, \mu m$	$60 - 90\, \mu m$

(continued)

(continued)

S.No	Constants	Actual value	Approximate value
49	Junction near an n-type semiconductor in Si	$0.15\,\mu m$	$0.15\,\mu m$
50	Solar intensity in the terrestrial region		$\approx 900\,W/m^2$
51	Efficiency of a solar cell under standard conditions	$15\,\%$	$15\,\%$
52	Efficiency of a PV module with an Si- solar cell	$12\,\%$	$12\,\%$
53	Specific heat of water	$4190\,J/kgK$	$4200\,J/kgK$
54	Specific heat of air	$1000\,J/kgK$	$1000\,J/kgK$
55	Density of air	$1.2\,kg/m^3$	$1.2\,kg/m^3$
56	Absorptivity of a bare surface		≈ 0.3
57	Absorptivity of a blackened surface		> 0.9
58	Heating value of coal	$29000\,kJ/kg$	$30000\,kJ/kg$
59	Heating value of biogas	$20000\,kJ/kg$	$21000\,kJ/kg$
60	Heating value of wood/straw	$15000\,kJ/kg$	$15000\,kJ/kg$
61	Heating value of gasoline/kerosene	$42000\,kJ/kg$	$42000\,kJ/kg$
62	Heating value of methane	$50000\,kJ/kg$	$51000\,kJ/kg$
63	Energy contained in an infrared region	$51.02\,\%$	$51\,\%$
64	Energy contained in a visible region	$36.76\,\%$	$36\,\%$
65	Energy contained in an ultraviolet (UV) region	$12.22\,\%$	$12\,\%$

Chapter 1
Solar Radiation

Abstract Solar energy from the Sun gives life to human beings and all living organism on planet Earth. The existence of an atmosphere with greenhouse gases (GHG) between the Sun and the Earth is responsible for the survival of human beings in the terrestrial region. The Sun is responsible for all renewable energy sources on Earth, which meet the needs of human being. Solar radiation is treated as an electromagnetic wave with wavelength between 0.30 and 3 μm as well as photons in a visible wave length.

Keywords Solar energy · Sun-Earth angles · Solar radiation models · Beam radiation · Global radiation

1.1 General Introduction

1.1.1 Basic Concept of Energy

Today, energy is one of the major needs of society. The total amount of energy in the universe is constant. Energy can neither be created nor destroyed; it can only be transformed from one state to another. For example, two billiard balls colliding may come to rest with the resulting energy becoming sound and perhaps a bit of heat during collision.

Energy, the environment, and economic development of a country are closely related. The proper use of energy requires consideration of social impacts as well as technological ones. Indeed, the sustainable economic growth of a country may be possible only by the well-planned and efficient use of fossil fuel and locally available natural resources such as solar energy, wind, hydro, and biomass. This improves the quality of everyone's lives on planet Earth.

1.1.2 Source of Solar Energy

The source of solar energy is the Sun [1], which is the largest member of the solar system with other members revolving around it. The Sun, having a diameter of 1.39×10^9 m, is at an average distance of 1.5×10^{11} m from the Earth. It is a sphere of intensely hot gaseous matter. The Sun rotates on its axis approximately once every 4 weeks.

It is known that 90 % of the Sun's energy is generated in a spherical region having a radius 0.23 times the Sun's radius. The average density (ρ) and the temperature (T) in this region are 10^5 kg/m^3 and approximately $(8 - 40) \times 10^6$ K, respectively. Energy generated in the region is due to several fusion reactions. In fusion, two hydrogen molecules (i.e., four protons) combine to form one helium nucleus at approximately 10^7 K. The mass of the helium nucleus is less than that of four protons. The mass, having been lost in the reaction, is converted into energy by the relation given by Einstein, i.e., $E = mc^2$. The fusion reaction is given by

$$H_2 + H_2 = He + 25\,MeV \tag{1.1}$$
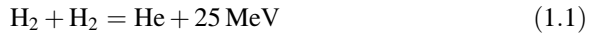
The produced energy ($E = mc^2$) is transferred to the outer surface of the Sun by convection. The temperature and the density drop, respectively, to approximately 1.3×10^5 K and 70 kg/m^3 from the centre to $0.7R$. Therefore, in the region beyond $0.7R$, convection dominates the heat transfer; hence, the region from $0.7R$ to R is termed the "convective zone." The outer layer of the convective zone is known as the "photosphere."

The periphery of the photosphere has low density. Above the photosphere there is a layer of cooler gases called the "reversing layer." Outside the reversing layer, there is a layer referred to as the "chromosphere." The Sun has an effective black-body temperature (T_s) of 5777 K($\sim 6000\,K$).

Solar energy is radiated into space, which is calculated using the following formula:

$$E = \epsilon \sigma T_s^4 \tag{1.2}$$

ε and σ are, respectively, the emissivity of the surface and the **Stefan-Boltzmann constant**.

Solar energy from the Sun can be classified as a heat (electromagnetic waves) and light (photons), respectively. Basically, the Sun is responsible to produce directly most of the renewable energy sources (Fig. 1.1) [2]. It is also responsible for providing indirect sustenance for nonrenewable sources such as fossil fuels. Fossil fuels are actually solar energy stored millions and millions of years ago.

A schematic diagram of the structure of the Sun is depicted in Fig. 1.2a [1].
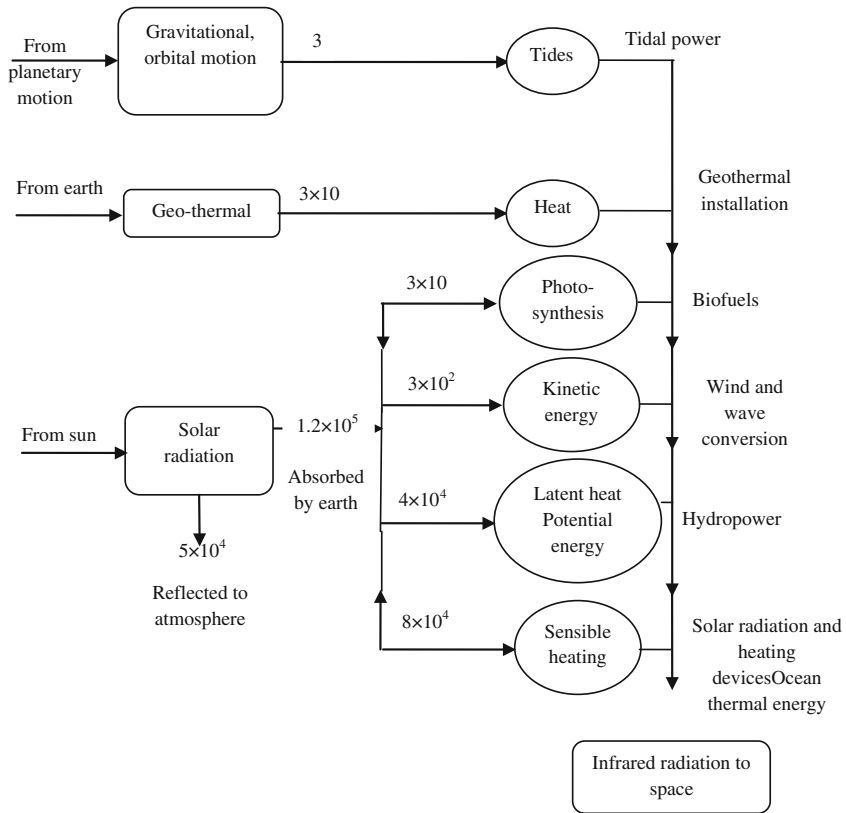
Fig. 1.1 Continuous flow of natural energy as renewable energy on the Earth. Units, terawatts (10^{12}W) [from 12]

1.1.3 Formation of the Atmosphere

The Earth, another member of the solar system, came into existence some 4.6×10^9 years ago. The Earth revolves around the Sun in an elliptical shape once per year as shown in Fig. 1.2b [2]. The Earth is almost round in shape and has a diameter of approximately 13,000 km. The Earth is inclined at $23.5°$ and rotates about its self-axis (Fig. 1.2c [2]). The inner core of the Earth is a solid comprising iron and nickel unlike the Sun. Its outer core constitutes a melted state of iron and nickel. The outer core is the Earth's mantle comprises solid rock. The outermost crust that covers the mantle also constitutes solid rock. The oldest rocks of sedimentary origin appear to be approximately 3.7×10^9 years old. Nearly 70 % of the Earth is covered by water, and the remaining 30 % is land. It is estimated that the black-body temperature of Earth is approximately 288 K ($15 °C$).

(a)

Corona $T \sim 10^6$ K, $\rho \sim$ very low

Chromosphere, $T \sim 5000$ K +

$T = 5000$ K

$\rho = 10^5$ kg/m^3

Convective zone

$T = 1.3 \times 10^5$ K ; $\rho = 10^5$ kg/m^3

40 % of mass
1.2 % of volume

0.7 R

0.23 R

R

90 % of
Energy

$T \sim 8.40 \times 10^6 K$

$\rho = 10^5$ kg/m^3

Reversing layer

Photosphere
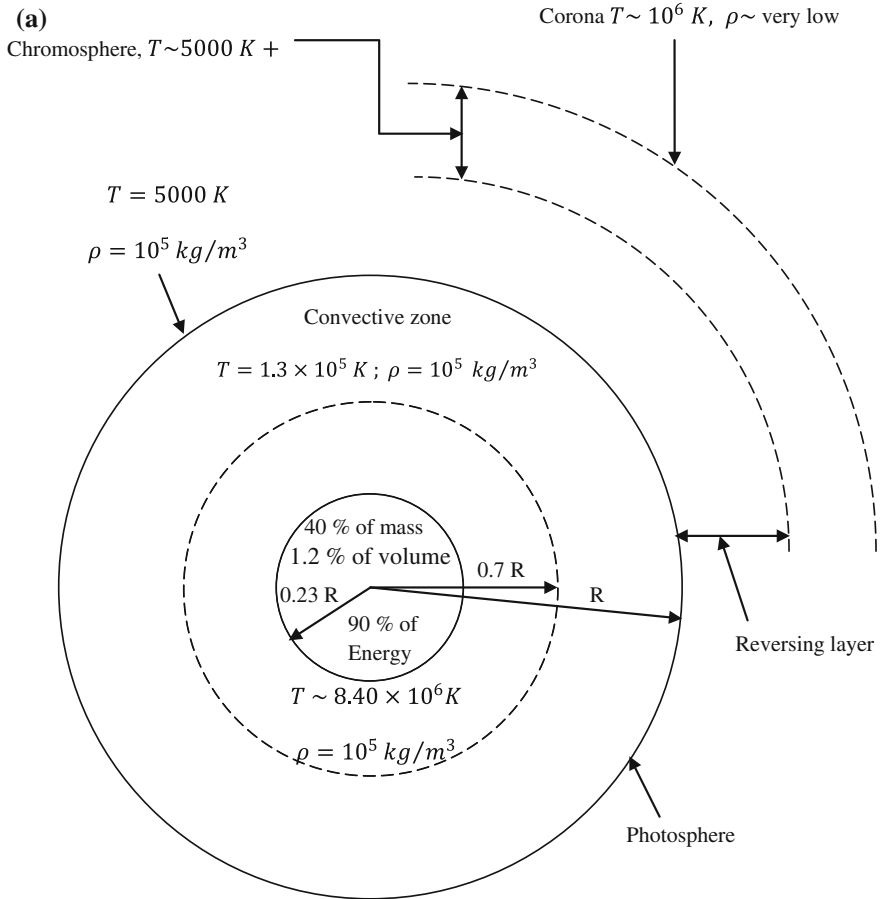
Fig. 1.2 a Structure of the Sun, **b** The Earth orbits around the Sun with different positions [from 12], **c** The Earth is always inclined at 23.5° and rotating around its axis [from 12]

The Earth's crust and uppermost mantle form the lithosphere.

According to plate tectonic theory, the rigid outer shell, or lithosphere, of the Earth is divided into plates, which pull away from each other, slide past each other, or move toward each other. The various gases stored inside the Earth might have escaped 1 million years back into atmosphere in the form of **greenhouse gases (GHG)**. The GHG are ozone (O_3), oxygen (O_2), nitrogen (N_2), carbon dioxide (CO_2), carbon mono-oxide (CO), and water vapour (H_2O). GHG move toward the Sun and becomes stable between the Sun and the Earth. The region of these stable gases between the Sun and the Earth is known as the "atmosphere," (Fig. 1.3), which is porous in nature. It is also referred as the "Earth's atmosphere" due to it being nearer to the Earth.

(b)

(c)
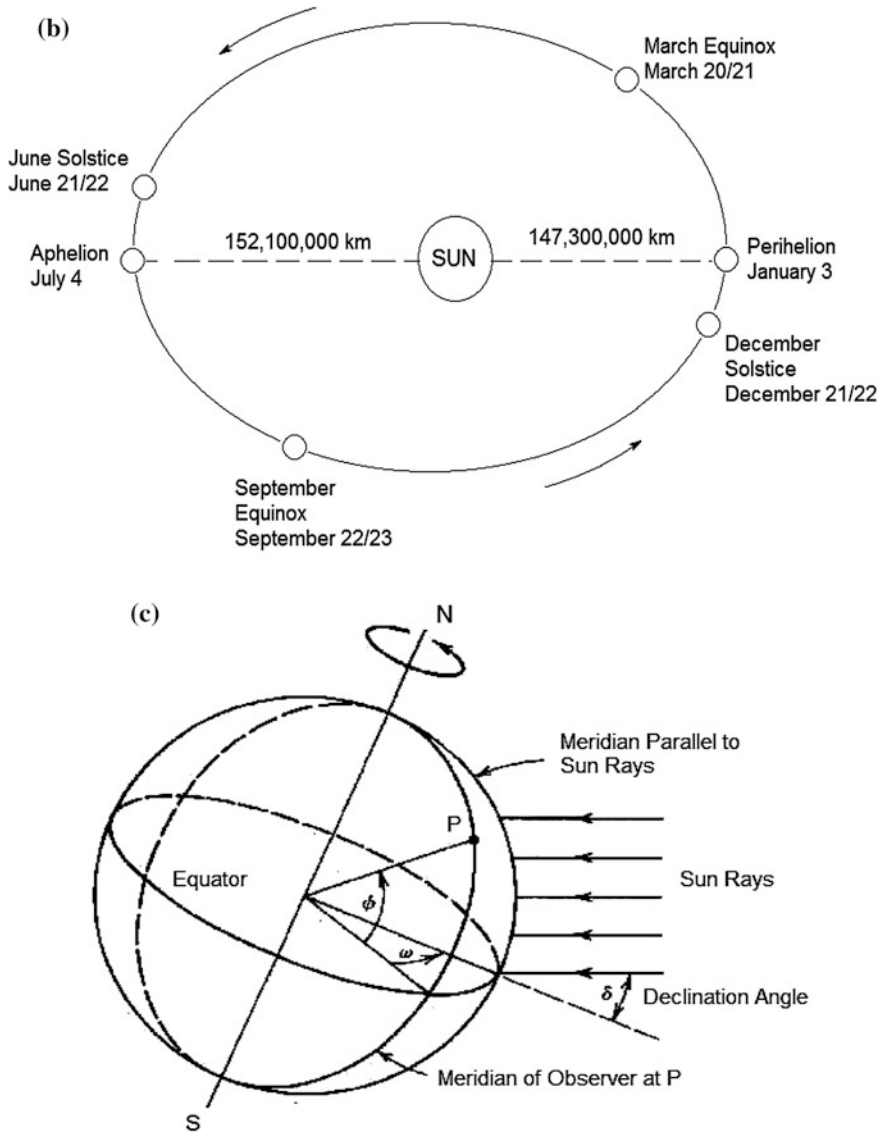
Fig. 1.2 (continued)

The atmosphere has two unique properties:

(i) It transmits short-wavelength radiation (0.23–2.26 μm) coming from the Sun.
(ii) It behaves as opaque for long-wavelength radiation (>2.26 μm).

The region between the Sun and atmosphere is known as the "**extraterrestrial region**." The **terrestrial region** is defined as the area between the atmosphere and the Earth.
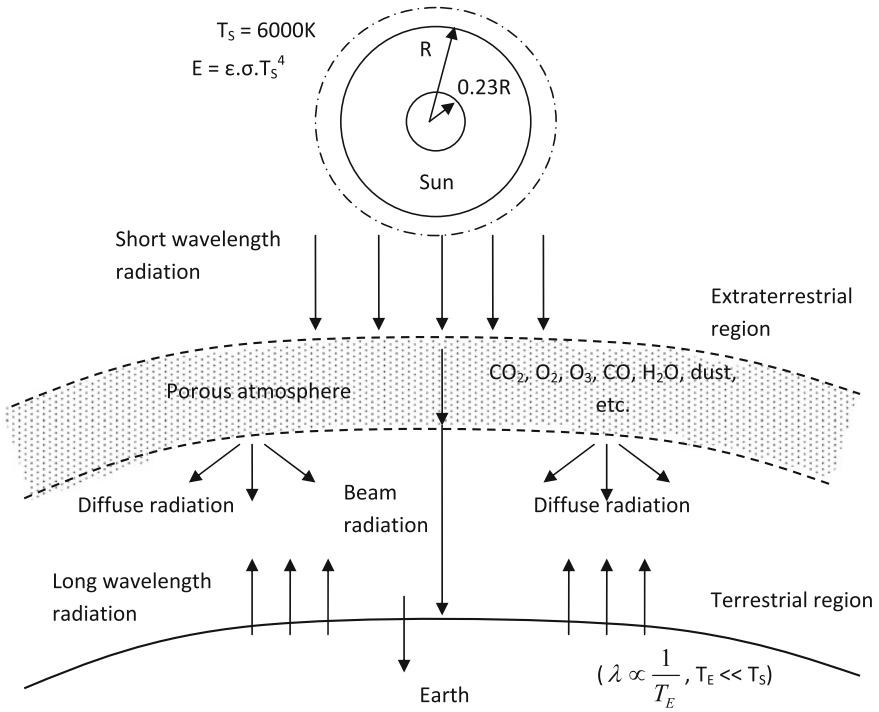
Fig. 1.3 View of the atmosphere between the Sun and the Earth

Half of the Earth is lit by short wavelength sunlight at a time. The Earth constantly spins around its axis. The inclined axis (at approximately 23.5°) of the Earth causes variable lengths of day and night.

Solar radiation coming from the Sun is reflected back to space from the Earth (approximately 4 %) and its atmosphere (26 %). The amount of radiation reflected back to space is known as "albedo." The amount of albedo depends on type of soil, plantation cover over the Earth's surface, and cloud distribution [3].

1.1.4 Solar Spectrum

The emitted solar spectrum (solar radiation having wavelength from zero to infinity) from the Sun is obtained due to the combined effect of solar radiation emitted and absorbed in different layers. Most of the solar spectrum (solar radiation) is emitted from the photosphere. The photosphere is opaque and strongly ionized; hence, it can absorbs and emit the whole spectrum of radiation. The spectral distribution of
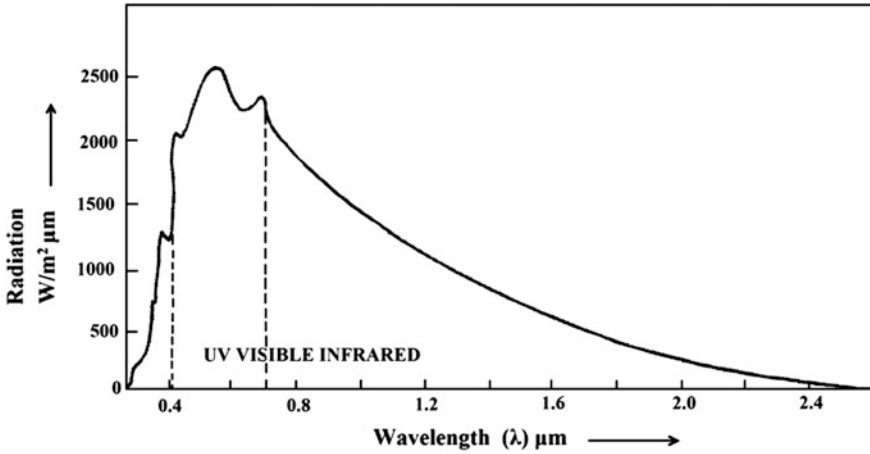
Fig. 1.4 Solar spectral with wavelength in the absence of atmosphere

extraterrestrial radiation with wavelength (λ) in the absence of the atmosphere is shown in Fig. 1.4.

Furthermore, it is clear from Fig. 1.4 that the maximum intensity observed near $0.48\,\mu m$ wavelength falls in the green region of the visible spectrum. The fraction of energy contained in the ultraviolet region $(\lambda < 0.40\,\mu m)$ is minimum $(\sim 8.73\,\%)$, whereas it is maximum $\sim 53.12\,\%$ for the infrared region $(\lambda > 0.70\,\mu m)$. Nearly $38.15\,\%$ of total energy is contained in the visible region $(0.40\,\mu m < \lambda < 0.70\,\mu m)$.

According to **Plank's law radiation** for the black body at temperature T (Kelvin), the magnitude of the solar spectrum with function of wavelength (μm) is given by

$$E_{\lambda b} = \frac{C_1}{\lambda^5 \left[e^{\frac{C_2}{(\lambda T)}} - 1 \right]}$$

where $E_{\lambda b}$ represents the energy emitted per unit area per unit time per unit wavelength (μm) interval at a given wavelength, $C_1 = 3.742 \times 10^8\,W\mu m^4/m^2$ $(3.7405 \times 10^{-16}\,Wm^2)$ and $C_2 = 14387.9\,\mu m K (0.0143879\,mK)$.

In Eq. (1.2), the following cases will be discussed:

(a) For $\lambda T \gg C_2$

$$E_{b\lambda} = \frac{C_1}{(\lambda)^5} \frac{\lambda T}{C_2}$$

The above equation is known as **Rayleigh–Jean's** law.

(b) For $\lambda T \ll C_2$

$$E_{b\lambda} = \frac{C_1}{(\lambda)^5} e^{\frac{-C_2}{\lambda T}}$$

The variation of $E_{\lambda b}$ for temperature of 6000 K (the Sun's temperature) and 288 K (the Earth's temperature) with wavelength in μm is shown in Fig. 1.5a, b, respectively. Furthermore, the comparison between two results is shown in Fig. 1.5c.

It should be noted from Figs. 1.5a that the wavelength of solar radiation emitted from the Sun at approximately 6000 K varies from zero to infinity in the absence of the atmosphere. However, only solar radiation of wavelength between 0.23 and 2.26 μm is allowed to pass through the atmosphere from the extraterrestrial region to the terrestrial region. The remaining solar radiation is either reflected from the top of atmosphere (albedo) or absorbed by the atmosphere. The solar radiation of wavelength between 0.23 and 2.26 μm is known as "short wavelength radiation." The wavelength of radiation emitted by the Earth at $288\,\mathrm{K}(25\,°\mathrm{C})$ lies in the range of more than 3 μm and it is referred to as "long wavelength radiation," which is not allowed to pass through the atmosphere from the terrestrial region to the extraterrestrial region. Some time, the atmosphere is also referred to as device that traps the desired solar radiation in the terrestrial region. The comparison of this radiation from the Sun and the Earth is shown in Fig. 1.5c.

According to **Wein's displacement law**, the wavelength corresponding to the maximum solar irradiance from the Sun can be obtained from

$$\lambda_{\max}.T = 2897.8 \approx (3000)\,\mathrm{\mu m K} \tag{1.3}$$

The derivation of Eq. (1.3) can be seen in the book by Tiwari [1].

The total emitted radiation (**emissive power**) from zero to any wavelength (λ) from the Sun can be obtained from Eq. (1.2) as follows:

$$E_{0-\lambda,b} = \int_0^\lambda E_{\lambda b}\mathrm{d}\lambda \tag{1.4a}$$

If the above equation is integrated between 0 and ∞

$$E_{0-\lambda,b} = \int_0^\lambda E_{\lambda b}\mathrm{d}\lambda = \sigma T^4 \tag{1.4b}$$

Equation (1.4b) is known as the **Stefan–Boltzmann law**.

Fig. 1.5 The effect of
black-body temperature on
emissive power
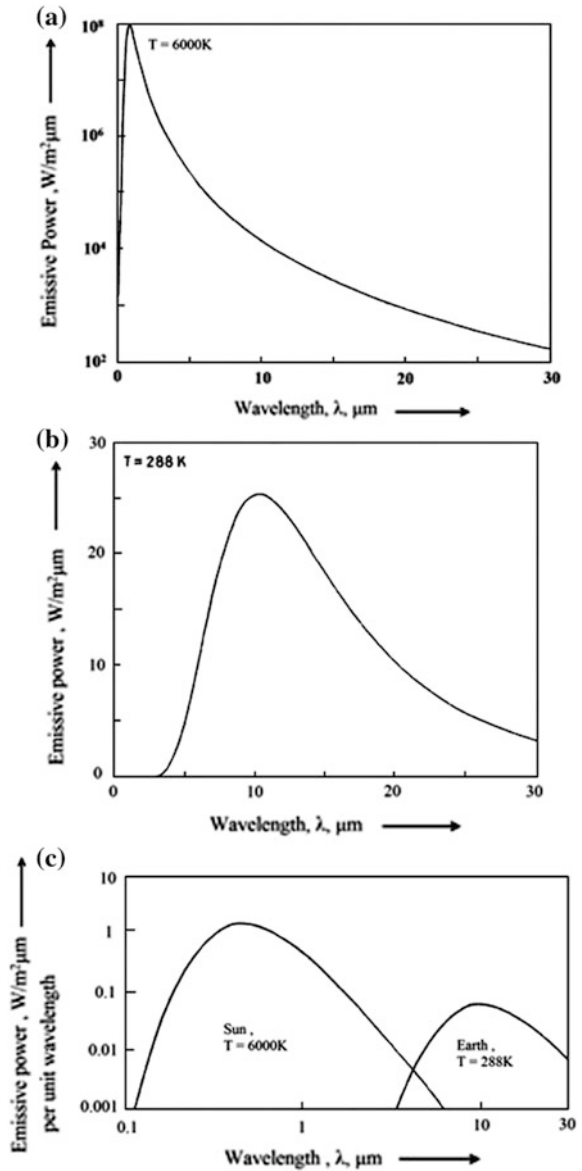
If Eq. (1.4) is divided by σT^4, then the above integral can be rearranged as a
function of λT as follows:

$$
f_{0-\lambda T} = \frac{E_{0-\lambda T}}{\sigma T^4} = \int\limits_{0}^{\lambda T} \frac{C_1 \mathrm{d}(\lambda T)}{\sigma(\lambda T)^5 \left[e^{(C_2/\lambda T)} - 1 \right]}
\tag{1.5}
$$

The values of $f_{0-\lambda T}$ for different λT (in μmK) are given in Appendix II.

Example 1.1 Determine the total energy contained in the visible region $(0.40\,\mu m < \lambda < 0.70\,\mu m)$ using Appendix II.

Solution

By using Appendix II,

 (i) The value of $\lambda T = 2310.8\,\mu mK$ for $T = 5777$ K and $\lambda = 0.40\,\mu m$
 (ii) The value of $\lambda T = 4043.9\,\mu mK$ for $T = 5777$ K and $\lambda = 0.70\,\mu m$

The energy contained in fraction at $2310.8\,\mu mK = 0.1200 + \frac{0.1402 - 0.1200}{100} \times 10.8 = 0.1218$

The energy contained in fraction at $4043.9\,\mu mK = 0.4829 + \frac{0.4987 - 0.4829}{100} \times 43.9 = 0.4898$

The energy contained (**emissive power**) in W/m^2 between $2310.8\,\mu mK$ and $4043.9\,\mu mK$

$$= (0.4898 - 0.1218) \times 1367 = 0.36947 \times 1367 = 503.06\,W/m^2$$

Similarly the energy contained in W/m^2 in the ultraviolet region $(0 < \lambda < 0.40\,\mu m)$ and in the infrared region $(0.70\,\mu m < \lambda < \infty)$ can be determined.

Example 1.2 Determine the maximum monochromatic emissive power at 288 K.

Solution

From Eq. (1.3), one gets $\lambda_{max} = 2897.8/288 = 10.06\,\mu m$.

Now by using Eq. (1.2), the maximum monochromatic power can be obtained as follows:

$$E_{\lambda b} = \frac{3.742 \times 10^8}{(10.06)^5 [e^{(14387/2897.6)} - 1]} = 25.53\,W/m^2\mu m$$

1.1.5 Solar Constant

Due to elliptical orbit of the Earth's motion around the Sun, the Sun–Earth distance is not fixed but rather varies around the year, and the maximum variation is up to 1.7 %. The solar intensity (solar radiation/solar irradiance) in the extraterrestrial region has been measured (by NASA through satellite). For the nth day of the year,

the solar intensity on a plane perpendicular to the direction of solar radiation is given by [4]:

$$I_{ext} = I_{sc}[1.0 + 0.033\cos(360n/365)] \tag{1.6}$$

where I_{sc} is the **solar constant** defined as the radiant solar (energy) flux received in the extraterrestrial region on a plane of unit area kept perpendicular to the solar radiation at the mean Sun–Earth distance. The value of solar constant is 1367 W/m^2.

   For June 22, 2013, $n = 173$, $I_{ext} = 1322.49\,\text{W}/\text{m}^2$ (Eq. 1.6)

   For December 21, 2013, $n = 355$, $I_{ext} = 1411.43\,\text{W}/\text{m}^2$ (Eq. 1.6)

   It should be noted that for leap year, February month has 29 days and, accordingly, the value of n is increased by 1 in Eq. (1.6) after February 28. For a normal year, the variation of extraterrrestrial radiation on the Earth's surface for end of each month using Eq. (1.6) can be determined as follows (Fig. 1.6):

Example 1.3 Determine the temperature of the Sun for the following data: $I_{sc} = 1367\,\text{W}/\text{m}^2$, radius of Sun $(R_s) = 0.619 \times 10^9\,\text{m}$, mean Sun–Earth distance $(L_{se}) = 1.5 \times 10^{11}\,\text{m}$, and $\sigma = 5.67 \times 10^{-8}\,\text{W}/\text{m}^2\text{K}^4$.

Solution

The amount of solar radiation emitted by the surface of the Sun $= \sigma T_s^4 (4\pi R_s^2)$.

   The total emitted radiation from the Sun will be received by a sphere having a radius equal to the mean Sun–Earth distance $= I_{sc} \times (4\pi L_{se}^2)$; hence, $\sigma T_s^4 (4\pi R_s^2) = I_{sc} \times (4\pi L_{se}^2)$ or
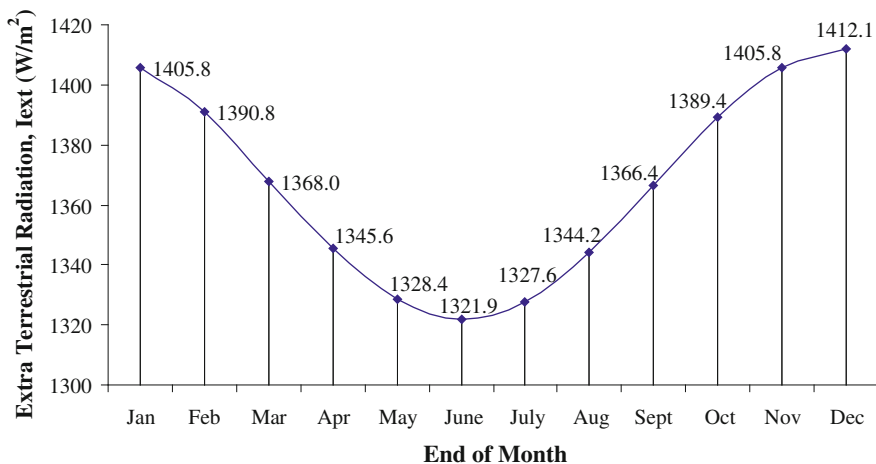
Fig. 1.6 Variation of I_{ext} with month of the year [from 2]

$$T_s = \left[\frac{I_{sc}\left(4\pi L_{se}^2\right)}{\sigma\left(4\pi R_s^2\right)} \right]^{\frac{1}{4}} = 6134\,\text{K}$$

The result is approximately the same as the temperature of the Sun reported earlier.

1.1.6 Air Mass

It is important to mention that the solar radiation in the extraterrestrial region has a certain direction. When the radiation passes through atmosphere consisting of GHG, there is atmospheric attenuation. The amount of attenuation is governed by the air mass. The air mass is a ratio between the paths travelled by the solar radiation through the atmosphere to the mass travelled by the solar radiation if the Sun is at its zenith. For noon time, this ratio is unity. The larger values of air mass implies greater attenuation. An expression for air mass referring to Fig. 1.7 is given by

$$\text{Air mass}(m) = \frac{\text{path length traversed in the atmosphere}}{\text{vertical depth of atmosphere}} = \frac{AB}{AC}$$

$$= \frac{m_o}{H_o} = \sec\theta_z = \frac{1}{\cos\theta_z} \quad \text{for} \ \ \theta_z \leq 0$$

(1.7a)

At noon, $\theta_z = 0, m = 1$; for $\theta_z = 60°, m = 2$ and $m = 0$ for outside the Earth's atmosphere.
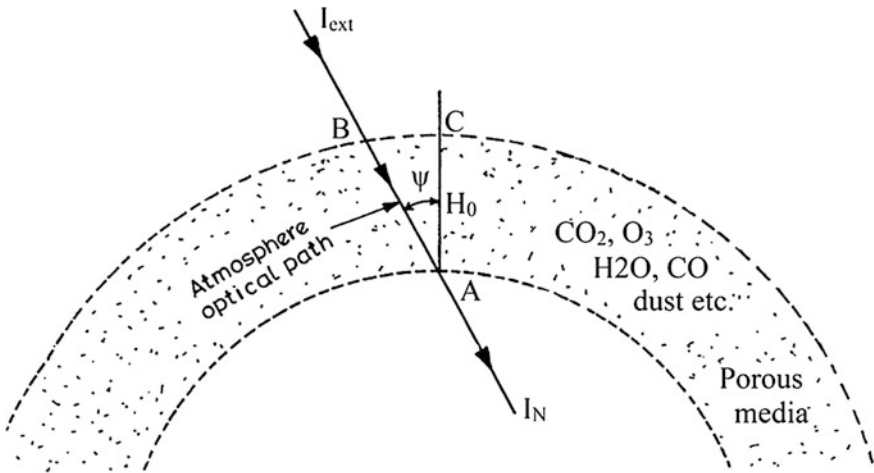
Fig. 1.7 Direction of the Sun's rays passing through the atmosphere

Furthermore, Kasten [5] proposed the modified expression for air mass as follows:

$$m = \left[\cos \theta_z + 0.15 \times (93.885 - \theta_z)^{-1.253}\right]^{-1} \tag{1.7b}$$

Example 1.4 Determine the air mass of normal direct irradiance coming from the Sun at New Delhi at 2.30 pm on February 20, 2013.

Solution
Here, $\cos \theta_z = 0.587$ and $\theta_z = 54.03°$ at 2.30 PM on February 20, 2013, at New Delhi.

Now substituting the previous values in Eq. (1.7b), we have

$$m = \left[0.587 + 0.15((93.885 - 54.03))^{-1.253}\right]^{-1} = 1.699$$

The variation of air mass with the time of the day for the latitude of New Delhi for different number of days of the year is shown in Fig. 1.8. It is observed that the sunshine hours are shorter and the air mass higher for the month of December on the 21st compared with other days as expected.

1.1.7 Solar Time

Solar time is a reckoning of the passage of time with reference to the position of the Sun in the sky, which has the fundamental unit of a day. Solar time is of two types,

Fig. 1.8 Variation in air mass with hour of the day
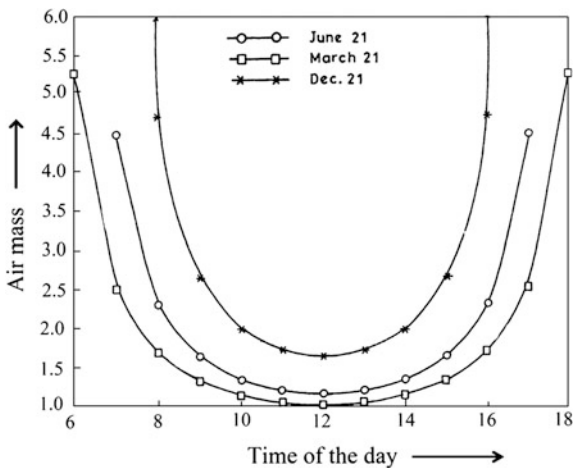
namely, **apparent solar time** and **mean solar time** (clock time or standard time). The difference in minutes between solar time and standard time is

$$\text{Solar time} - \text{standard time} = 4(L_{st} - L_{loc}) + E \qquad (1.8a)$$

where L_{st} is the **standard meridian** for the local time zone. L_{st} for India has the value $81°44'$. L_{loc} is the longitude of the location in question (in degrees west) (Table 1.1), and E is the equation of time (in minutes), which is given by the expression:

$$E = 229.2(0.000075 + 0.001868\cos B - 0.032077\sin B - 0.014615\cos 2B - 0.04089\sin 2B)$$
$$(1.8b)$$

where $B = (n - 1) \times 360/365$, $n = n$th day of the year.

The equation of time (minutes:seconds) for typical days for different months for New Delhi (Longitude $77°\ 12'$E) are given in Table 1.1.

Example 1.5 Determine the solar time (ST) for Indian Standard Time (IST) (longitude $81°\ 54'$E) on May 8, 2014, for New Delhi corresponding to 12:00 noon.

Solution
The equation of time for May 8 is 3 min. 31 s. (Table 1.1). In this case, the longitude correction would be negative because New Delhi is west of the standard meridian. By using Eq. (1.8), one gets

$$ST = 12\,h.0\,min.0\,s. + 3\,min.\ 31\,s. - 4\left(81.9° - 77.2°\right)min$$
$$= 11\,h.44\,min.43\,s.$$

Table 1.1 Latitude, longitude, and elevation for different places in the world

Place	Latitude (ϕ)	Longitude (L_{loc})	Elevation (E_o)
New Delhi	28° 35′N	77° 12′E	216 m above msl
Mumbai	18° 54′N	72° 49′E	11 m above msl
Chennai	13° 00′N	80° 11′E	16 m above msl
Kolkata	22° 32′N	88° 20′E	6 m above msl
London	51° 30′N	00° 07′W	35 m above msl
New York	40° 42′N	74° 00′W	10 m above msl
Paris	48° 51′N	02° 21′E	35 m above msl
Moscow	55° 45′N	37° 37′E	156 m above msl
Singapore	01° 17′N	103° 50′E	6 m above msl
Beijing	39° 54′N	116° 23′E	50 m above msl
Berlin	52° 31′N	13° 23′E	34 m above msl

1.2   Sun–Earth Angles

A better understanding of Sun–Earth angles is essential for estimating solar intensity throughout year for any surface at any place with a desired inclination and orientation. These Sun–Earth angles are defined below.

Latitude (ϕ): The latitude of an observer (location) on the Earth's surface is the angle made between the radial line joining the observer (location) with the centre of the Earth, and its projection on the equatorial plane as shown in Fig. 1.9. For an observer in the northern hemisphere, latitude is positive, whereas for the southern hemisphere it is negative. The latitude for some places in world are given in Table 1.1.

Declination (δ): Declination is defined as the angle between the line joining the centres of the Sun and the Earth, which also determines the direction of the direct rays coming from the Sun and their projection on the equatorial plane as shown in Fig. 1.9. Declination is due to the rotation of the Earth around an axis, which makes an angle of either 66.5° with the plane or 23.5° with normal rotation around the Sun as shown in Fig. 1.9. The declination is calculated by the following relation [4]:

$$\delta = 23.45 \sin\left[\frac{360}{365}(284 + n)\right] \tag{1.9a}$$
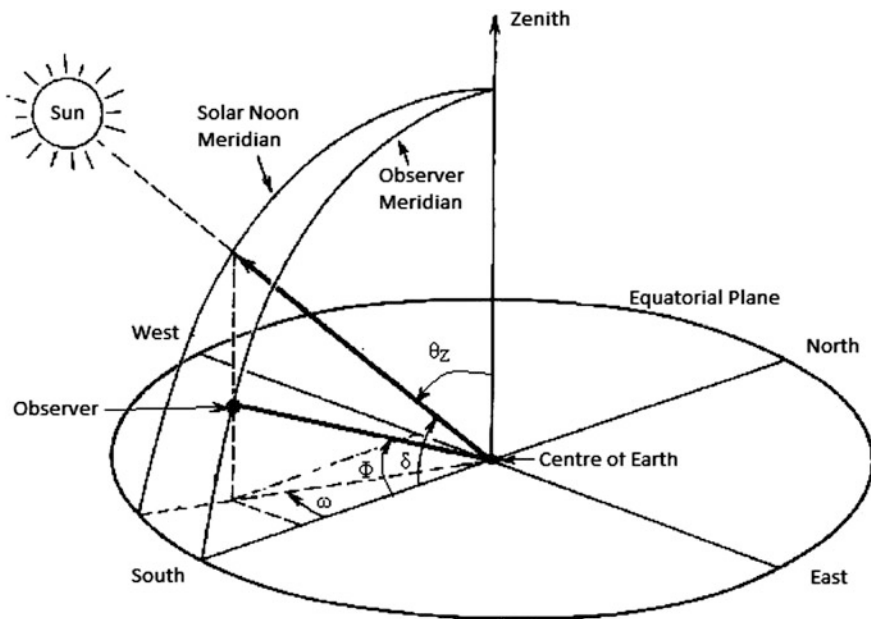
Fig. 1.9 View of different Sun–Earth angles [from 12]
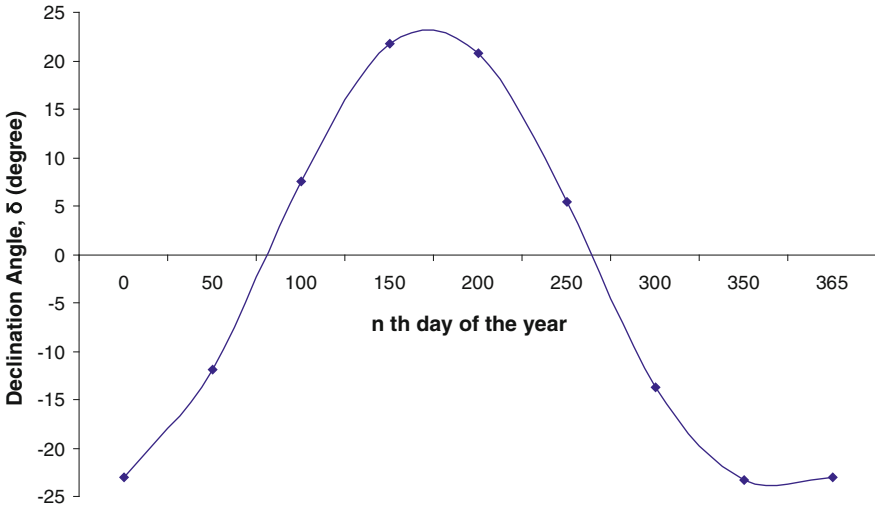
Fig. 1.10 Variation of declination angle with *n*th day of the year [from 12]

The variation of the declination angle with the *n*th day of year is shown in Fig. 1.10. The maximum value of δ is 23.45° (June 21), and minimum value of δ is −23.45° (December 21)

Hour angle (ω): This is the angle between projections of the Sun's rays (solar meridian) and the line running south–north through centre. The south–north line is also referred to as the "line due south." In other words, the hour angle is defined as the angular displacement of the Sun from the local meridian because of the Earth's rotation around its own axis. The hour angle corresponding to 1 h is 15°. The values of the hour angle in the northern hemisphere are listed in Table 1.2. Expression for the hour angle is given by

$$\omega = (\text{ST} - 12) \times 15° \tag{1.9b}$$

where ST is the local solar time. The total hour angle from sunrise to sunset is $(2\omega_s)$. The $\pm\omega_s$ correspond to an hour angle with reference to sunrise and sunset, respectively.

Zenith (θ_z): The angle between Sun's rays; the line perpendicular to a horizontal plane is known as the "zenith angle" (Fig. 1.9).

Table 1.2 The value of hour angle with time of the day for the northern hemisphere

Time of the day (h)	6	7	8	9	10	11	12
Hour angle (°)	−90	−75	−60	−45	−30	−15	0
Time of the day (h)	12	13	14	15	16	17	18
Hour angle (°)	0	+15	+30	+45	+60	+75	+90

Altitude or solar altitude angle (α): The angle made between a horizontal plane and the Sun's rays is known as the "altitude angle." Referring to Fig. 1.9, $\alpha = 90 - \theta_Z$.

Slope (β): This is the angle between the plane surface under consideration and the horizontal surface (tangential plane at observer), Fig. 1.11. Its numerical value is considered positive for slope toward the south and negative for slope toward the north.

Surface azimuth angle (γ): The angle made between the line due south and the projection of normal to the inclined surface on the horizontal plane (tangential plane at observer on the surface of the Earth, Fig. 1.11) is termed the "surface azimuth angle." In the northern hemisphere, conventionally γ is negative (positive for the southern hemisphere) for projections in east of south and positive (negative for southern hemisphere) for projections falling west of south. The values of γ for some orientations are given in Table 1.3.
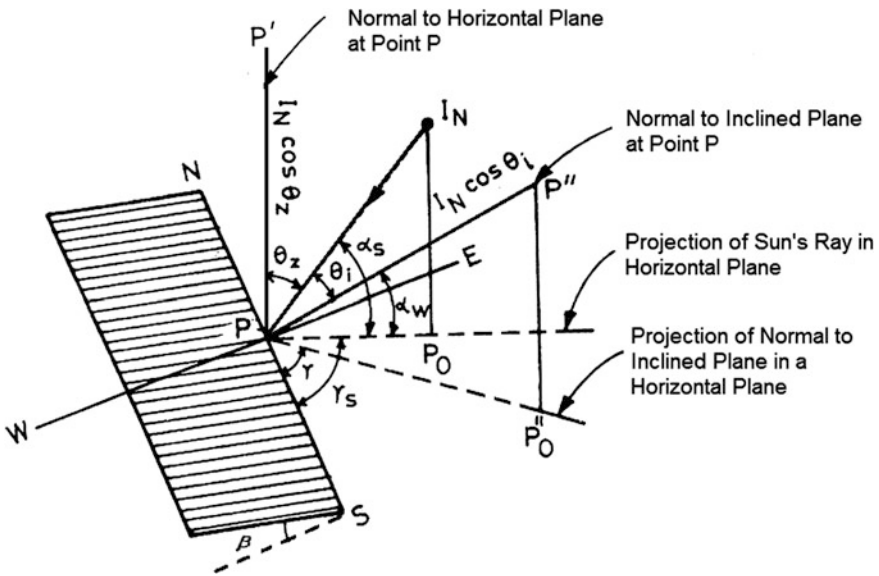
Fig. 1.11 View of various Sun–Earth angles on an inclined surface [from 12]

Table 1.3 Surface azimuth angle (γ) for various orientations in the Northern hemisphere

Surface orientation	γ (°)
Sloped towards the south	0
Sloped towards the north	180
Sloped towards the east	–90
Sloped towards the west	+90
Sloped toward the southeast	–45
Sloped toward the southwest	+45

Solar azimuth angle (γ_s): The angle made between the projection of beam radiation on the horizontal plane and the line due south is known as the "solar azimuth angle" (Fig. 1.11). The sign convention of the solar azimuth angle is the same as the sign convention of the surface azimuth angle.

Sunshine hour (N): The total duration in hours of the Sun's movement from sunrise to sunset. It is defined in terms of the hour angle as

$$N = \frac{2\omega_S}{15}$$

Here 1 h = 15°.

Angle of incidence (θ_i): The angle made between normal to the inclined surface and the solar beam radiation falling on the inclined surface is known as the "angle of incidence" (Fig. 1.11). In general, the angle of incidence (θ_i) can be expressed as [6],

$$\begin{aligned}
\cos\theta_i = {}& (\cos\varphi\cos\beta + \sin\varphi\sin\beta\cos\gamma)\cos\delta\cos\omega + \cos\delta\sin\omega\sin\beta\sin\gamma \\
& + \sin\delta(\sin\varphi\cos\beta - \cos\varphi\sin\beta\cos\gamma)
\end{aligned}$$

$$(1.10)$$

For a horizontal plane facing due south, $\gamma = 0, \beta = 0, \theta_i = \theta_z$ (zenith angle)

$$\cos\theta_z = \cos\varphi\cos\delta\cos\omega + \sin\delta\sin\varphi \tag{1.11}$$

Referring to Fig. 1.9, the zenith angle (θ_Z) will be 90° in the morning as well as in the evening before sunrise and after sunset and $\omega = \omega_s$. Thus, Eq. (1.11) can be written as follows:

$$\begin{aligned}
0 &= \cos\varphi\cos\delta\cos\omega_s + \sin\varphi\sin\delta \\
\omega_s &= \cos^{-1}(-\tan\varphi\tan\delta)
\end{aligned} \tag{1.11a}$$

The total hour angle from sunrise to sunset is given by

$$2\omega_s = 2\cos^{-1}(-\tan\varphi\tan\delta)$$

As mentioned previously, 1 h = 15°; hence, the number of daylight (sunshine) hours (N) is given by

$$N = \frac{2}{15}\cos^{-1}(-\tan\varphi\tan\delta) \tag{1.12}$$

The variation of N with the nth day of the year for different latitudes in the Northern hemisphere is shown in Fig. 1.12.

Fig. 1.12 Variation of sunshine hour (N) with nth day of the year for different latitudes in the Northern hemisphere
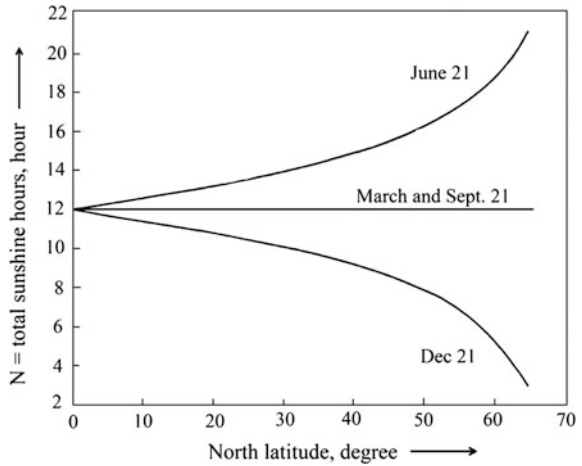
It is important to note here that the values of N cannot be determined at $\varphi = 90°$; hence, N should be calculated for values less than $90°$.

Example 1.6 Determine the angle of incidence of direct irradiance/solar radiation on an inclined surface at $45°$ from the horizontal with orientation of $30°$ west of south and located at New Delhi at 1:30 (solar time) on February 16, 2013.

Solution

For the present case, the value of n is 47, and $\delta = -13.0°$ (Eq. 1.9a); $\omega = +22.5°$ (Eq. 1.9b);

$\gamma = 30°$; $\beta = 45°$; $\varphi = +28.58°$ (New Delhi).

Now, the angle of incidence of direct irradiance/solar radiation on an inclined surface can be calculated using Eq. (1.10) as follows:

$$\begin{aligned}
\cos\theta_i &= \sin(-13°)\sin(28.58°)\cos(45°) - \sin(-13°)\cos(28.58°)\sin(45°)\cos(30°) \\
&\quad + \cos(-13°)\cos(28.58°)\cos(45°)\cos(22.5°) \\
&\quad + \cos(-13°)\sin(28.58°)\sin(45°)\cos(30°)\cos(22.5°) \\
&\quad + \cos(-13°)\sin(45°)\sin(30°)\sin(22.5°) = 0.999
\end{aligned}$$

$$\theta_i = \cos^{-1}(0.999) = 2.56°$$

Example 1.7 Determine the number of sunshine hours for New Delhi on December 22 and June 22, 2013.

Solution

For the present example, we have $\varphi = 28.58°$ (New Delhi); For December 22, 2013, $n = 356$, and $\delta = -23.44°$. From Eq. (1.12), one gets

$$N = \frac{2}{15}\cos^{-1}[-\tan(-23.44°)\tan(28.58°)]$$
$$= \frac{2}{15}\cos^{-1}[(0.434)(0.545)]$$
$$= \frac{2}{15}\cos^{-1}[0.237] = 10.18\,\text{h}$$

Similarly, for June 22, 2013, $n = 173$; $\delta = 23.45°$ (Eq. 1.9a).
From Eq. (1.12), we have

$$N = \frac{2}{15}\cos^{-1}(-\tan 23.45° \tan 28.58°) = 13.82\,\text{h}$$

Example 1.8 Determine the zenith angle of the Sun at New Delhi at 2.30 pm on February 20, 2013.

Solution
For the present case, $n = 51$; $\varphi = 28.58°$ (New Delhi); $\delta = -11.58°$ (Eq. 1.9a); $\omega = 37.5°$ (Eq. 1.9b).
From Eq. (1.11), we have

$$\cos\theta_Z = \cos(28.58°)\cos(-11.58°)\cos(37.5°) + \sin(-11.58°)\sin(28.58°)$$
$$= 0.587$$
$$\theta_z = \cos^{-1}(0.587) = 54.03°$$

1.2.1 Solar Radiation

Solar radiation, while passing from the extraterrestrial region to the terrestrial region through the Earth's atmosphere, suffers scattering losses and atmospheric absorption. After absorption by the atmosphere, the rate of normal solar flux (normal solar radiation/irradiance) reaching the Earth's surface is determined by

$$I_\text{N} = I_\text{ext} \times \exp[-(m.\varepsilon.T_\text{R} + \alpha)] \tag{1.13}$$

where m is the air mass. This is given by Eq. (1.7b), and T_R, the turbidity factor, is defined as the cloudiness/haziness factor for the lumped atmosphere. The values of T_R and α for different weather and flat-land conditions (cases **a, b, c and d** as defined earlier) are given in Appendix IIIA. These values were calculated from the 10-year average data obtained at the airport, which is the only flat condition from the Indian Metrological Department (IMD), Government of India, Pune, India.

These values have been calculated for New Delhi, but they valid for latitude after meeting the weather conditions defined previously.

The expression for ε, known as the integrated optical-thickness of the terrestrial clear and dry atmosphere/Rayleigh atmosphere (dimensionless), is given by

$$\varepsilon = 4.529 \times 10^{-4} \times m^2 - 9.66865 \times 10^{-3} \times m + 0.108014$$

The α in Eq. (1.13) is known as "lumped atmospheric parameters," which accommodate further attenuation of direct normal irradiance in the terrestrial zone because of cloudiness/haziness level, anisotropic behaviour, and unpredictable changes in atmospheric conditions while reaching toward the Earth's surface. The values of α for different weather conditions are given in Appendix IIIA. Case "e" in the appendix is the average value of all weather conditions.

The additional depletion in direct normal irradiance can be attributed to the reasons given below:

 (i)   the variation of particle content and size or both in aerosol;
 (ii) irregular variation of disturbances in the terrestrial region due to different temperatures in different layers.

For $\alpha = 0, T_R = T_L$ and Eq. (1.13) reduces to the classical equation given by Linke [7]. It is important to mention here that the value of T_L is taken by considering the combined effect of aerosol and other particulate matter in the clear sky.

Furthermore, Perez et al. [8]. have proposed another correlation to predict direct **normal irradiance** (solar radiation) in the terrestrial region, which is given by

$$I_N = I_{ext} \times \exp\left[\frac{-T_R}{(0.9 + 9.4 \cos \theta_Z)}\right] \qquad (1.14)$$

The Linke turbidity factor (T_R) for different months and for different conditions, namely, city, flat land, and mountain, are given in Appendix IIIB. It is also important to mention that the value of the Linke turbidity factor (T_R) is for clear-sky conditions only. Furthermore, one can see that the values of T_R (Appendix IIIB) for clear (case **a**) sky and flat condition only are nearly same. Differences in values occur because of α in Eq. (1.13).

The wavelength range of **normal irradiance**/solar radiation (I_N) in the terrestrial region is between 0.23 and 2.26 μm.

Nearly (30 %) of the normal solar irradiance/radiation coming toward the Earth's surface is reflected back into the atmosphere without changing its wavelength range (0.23–2.26 μm) and is further allowed passage from the terrestrial region to the extraterrestrial region. The remainder of normal solar radiation is absorbed by the Earth's surface. The extraterrestrial, atmosphere, and terrestrial regions are depicted in Fig. 1.13a. Nitrogen, oxygen, and other gases present in the ionosphere absorb X-rays and very small ultraviolet radiations. Ultraviolet radiations ($\lambda < 0.40$ μm) are absorbed by the ozone, and infrared radiations ($\lambda < 2.3$ μm)
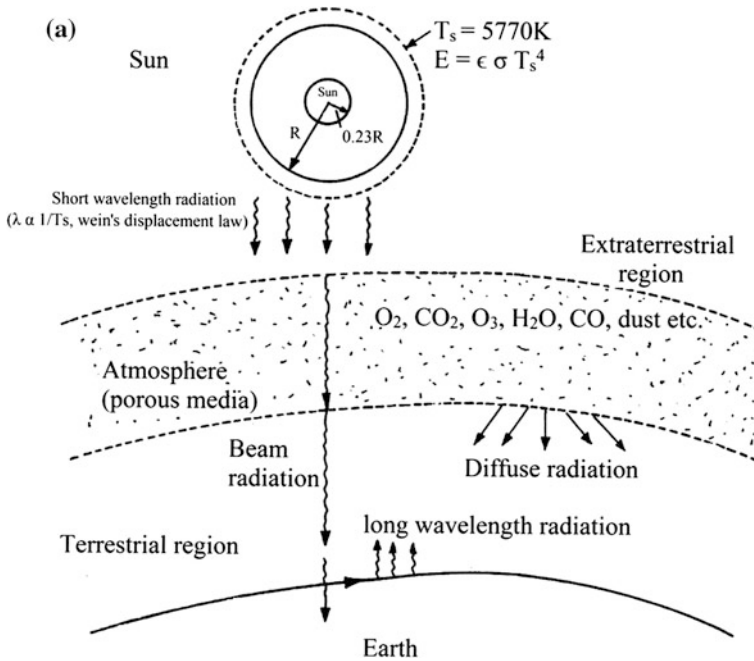
Fig. 1.13 a The terrestrial and extraterrestrial regions, **b** Propagation of solar radiation to the Earth through atmosphere [from 55]

are absorbed by water vapor. Therefore, after passing through the atmosphere, the wavelength below 0.29 μm and above 2.3 μm in solar radiation will be almost completely absorbed. Solar radiations are further attenuated due to scattering by water vapour, air molecules, and other particulates. This scattered solar radiation is known as "diffuse radiation." Figure 1.13b represents the attenuation of solar radiation as it propagates through the atmosphere from the extraterrestrial to the terrestrial region. It also depicts the solar radiation emitted from the Sun and Earth (which is also referred as "**radiosity/radiant existence**" (W/m^2)).

Therefore, the wavelength range of solar radiation available in the terrestrial region for the use of solar energy applications is 0.29–2.3 μm. Due to scattering in the atmosphere, solar radiation has two components (beam and diffuse radiation) in the terrestrial region.

Beam radiation (I_b): This is a normal component of solar radiation (normal irradiance) in W/m^2 propagating along the line joining the receiving surface and the Sun on a horizontal/inclined surface. It has a direction and also termed "direct radiation."

Diffuse radiation (I_d): This is the solar radiation (in W/m^2) scattered by aerosols and other particulates; diffuse radiation does not have any definite direction.

(b)
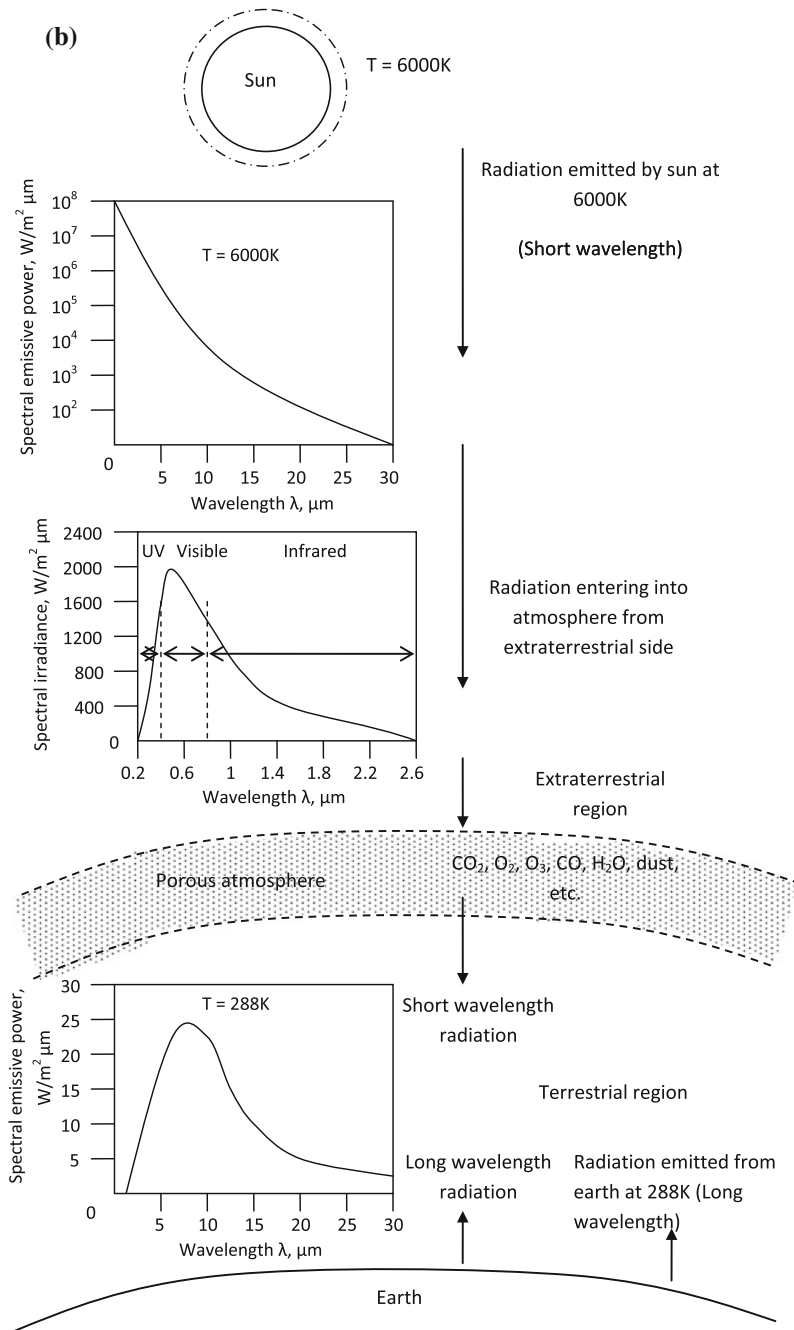
Fig. 1.13   (continued)

The total radiation (I): This is the sum of the beam (direct) and diffuse radiation in W/m^2. It is also known as "global radiation."

Irradiation (radiant exposure): The incident solar radiation/irradiance on a surface in J/m^2 per hour or per day is known as "irradiation." It is obtained by integrating beam/diffuse/total radiation over 1 h or day.

Equation (1.13) gives the magnitude of normal irradiance (solar radiation) in the terrestrial region. This means that the magnitude of diffuse radiation, which has no direction due to scattering from below the atmosphere, will depend on $(I_{ext} - I_N)$. Therefore, the expression for diffuse radiation in W/m^2 has been proposed by Singh and Tiwari [9] as follows:

$$I_d = K_1(I_{ext} - I_N)\cos\theta_Z + K_2 \qquad (1.15)$$

where the numerical values for K_1 and K_2 for different weather are given in Appendix IIIA. Equation (1.15) is applicable to a horizontal surface (tangential surface to the observer at the outer surface of the Earth).

Furthermore, weather classifications for a given climatic condition are defined according to sunshine hours (N) and ratios of daily diffuse to daily global radiation. These are briefly described as follows:

(a) **Clear day (blue sky)**: For clear days, the ratio of daily diffuse radiation in J/m^2 to daily total (global) radiation in J/m^2 is ≤0.25 and for sunshine hours (N) is ≥9 h.
(b) **Hazy day (fully)**: For hazy days, the ratio of daily diffuse radiation in J/m^2 to daily total (global) radiation in J/m^2 is between 0.25 and 0.5 and for sunshine hours (N) is between 7 and 9 h.
(c) **Hazy and cloudy (partially)**: For hazy and cloudy days, the ratio of daily diffuse radiation in J/m^2 to daily total (global) radiation in J/m^2 is between 0.5 and 0.75 and for sunshine hours (N) is between 5 and 7 h.
(d) **Cloudy day (fully)**: For cloudy days, the ratio of daily diffuse radiation in J/m^2 to daily total (global) in J/m^2 radiation is ≥0.75 and for sunshine hours is ≤5 h.

Example 1.9 Determine the average temperature of the Earth in the absence of atmosphere.

Solution
In the absence of atmosphere, there is neither extraterrestrial region nor terrestrial region. The average normal irradiance (beam/direct) will be equal to the solar constant (I_{SC}) i.e., 1367 W/m^2.

The diameter of the Earth (D_e) = 12.75×10^6 m.

The total heat flow in W from the sun to the earth
= the projected area of the earth $\times$ average solar flux (solar constant)

or,

$$\pi(D_e/2)^2 I_{sc} = (\pi/4) \times (12.75 \times 10^6)^2 \times 1367 = 1.75 \times 10^{14}\,\text{kW}$$

In this case, it is assumed that the rate of incoming solar radiation is absorbed by the Earth without any reflection, and the temperature of Earth becomes T_e.

For, T_e, the temperature of the Earth,

$$\text{the rate outward radiation emitted by earth} = \text{the surface area of the earth} \times \in \sigma T_e^4$$
$$= \pi D_e^2 \in \sigma T_e^4$$
$$= \pi(12.75 \times 10^6)^2 \times 5.672 \times 10^{-11}\,(\text{kW/m}^2\text{K}^4).T_e^4$$

If the **incoming average rate of solar radiation on Earth = the rate of outward-emitted radiation from the Earth**,

then

$$\pi(12.75 \times 10^6)^2 \times 5.672 \times 10^{-11} \cdot T_e^4 = 1.75 \times 10^{14}\,\text{kW}$$

or

$$T_e = 278.7\,\text{K} = 5.7\,^\circ\text{C} \varepsilon = 1 \text{ here } \varepsilon = 1$$

If the total thermal energy from the Sun to the Earth is multiplied by 0.7 due to the Earth's albedo, then the Earth's temperature, $T_e = 195\,\text{K} = -78\,^\circ\text{C}$. In this case, it will be a frozen world. This shows that the existing atmosphere between the Sun and the Earth blocks maximum outgoing long-wavelength radiation so that the average temperature of Earth would be raised to approximately $15\,^\circ\text{C}(288\,\text{K})$.

Example 1.10 Calculate the fraction of outgoing radiation from the Earth that is blocked by the atmosphere.

Solution
The albedo from the Earth and atmosphere is nearly 30 %; therefore, only 70 % of incoming solar radiation from the Sun is absorbed by the Earth.

If we assume the average Earth's surface temperature to be approximately 15 °C (288 K), (Example 1.9), then

$$\text{Fraction emitted} = \frac{0.7 \times \text{the rate of incoming solar radiation from the sun}}{\text{the rate of emitted radiation from the earth}}$$
$$= \frac{0.7 \times (1.75 \times 10^{14})}{3.14 \times (12.76 \times 10^6)^2 \times 5.672 \times 10^{-11} \times (288)^4} = 0.614$$

The atmospheric outward transmission of radiant energy = 0.614/ 0.7 = 0.88
Of the inward transmission of solar energy, 88 % is blocked by atmosphere.

1.3 Energy and Environment

During the conversion of nonrenewable energy (fossil fuels) from one form to another (high-grade energy, i.e., electricity), there is an emission of pollutants, which generally affects the environment. The study of energy, particularly **solar energy**, must include the impact of energy production/use on the environment. Currently fossil fuels are an essential necessity for industrial growth and day-to-day activities, but they have undesirable ill effects on environment. The environment has been paying a heavy price for humans using high-grade energy (electricity) to meet their energy-based requirements.

During the combustion of fossil fuels (coal, oil, and natural gases, vehicle engines, furnaces, and even fireplaces) for producing power, the emitted pollutants, namely carbohydrates, are strongly responsible for smog, acid rain, global warming, and climate change. The high level (>400 ppm) of environmental pollution is a serious concern for human health, plant growth, and wildlife. Air pollution caused by the emission of GHG creates problems for human health as well as that of wildlife. Air pollution also damage the ozone layer, which leads to ill effects on the environment and its assets. The impact of air pollution is independent of the source of air pollution, i.e., it may affect places other than the source of the pollution. Pollutants responsible for the air pollution along with their sources are listed below.

Carbon monoxide (CO): This is produced from the combustion of carbon-based fuels as well as some natural and synthetic products. It has very bad effects on human health.

Carbon dioxide (CO_2): This is emitted mainly due to the burning of fossil fuels.

Chlorofluorocarbons (CFC): Prime sources of CFCs are refrigeration and air-conditioning systems. These gases are mainly responsible for deterioration of the ozone layer.

Lead: The major sources of lead are lead batteries, gasoline, petroleum, paints, and dye products, etc.

Ozone (O_3): This is produced from the reaction between volatile organic compounds and oxides of nitrogen emitted from vehicles and industries.

Nitrogen oxide (NO_x): This is produced due to the combustion of fossil fuels such as diesel, coal, and petroleum.

Suspended particulate matter (SPM): These are very fine solid particles suspended in air in the form of vapour, smoke, and dust.

Sulphur dioxide (SO_2): This is a gas produced from burning coal in different process and industries. The major sources of sulphur dioxide production are metal industries, paper industries, and thermal power plants.

The major areas of environmental problems may be classified as follows:

- Water pollution
- Ambient air quality

- Hazardous air pollutants
- Maritime pollution
- Solid waste disposal
- Land-use and land-siting impacts
- Acid rain
- Stratospheric ozone depletion
- Global climate change (greenhouse effect).

1.4   Instruments to Measure Solar Radiation

Instruments used to measure solar radiation are as follows:

1.4.1   Pyrheliometer

Solar radiations are measured by comparing the temperatures of two identical blackened Manganin strips. Each strip is connected with a thermocouple and electric heater (Fig. 1.14). For measuring the radiation, one strip is shaded and heated by an electrical current passing through it, whereas the other is heated by absorbing the solar radiations incident on it. The roles of strips are interchanged for second set of observations to nullify the effect of unavoidable minor differences in the properties of the strips. When the temperatures of both strips are same, the electrical energy used in heating the first strip will be equal to the solar energy absorbed by the second strip. Solar radiation absorbed by second strip is obtained by dividing the electrical energy with the product of the strip area and its absorptivity.

Fig. 1.14 Circuit diagram for thermoelectric-type pyrheliometer
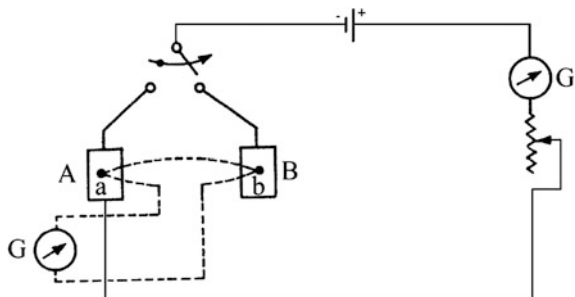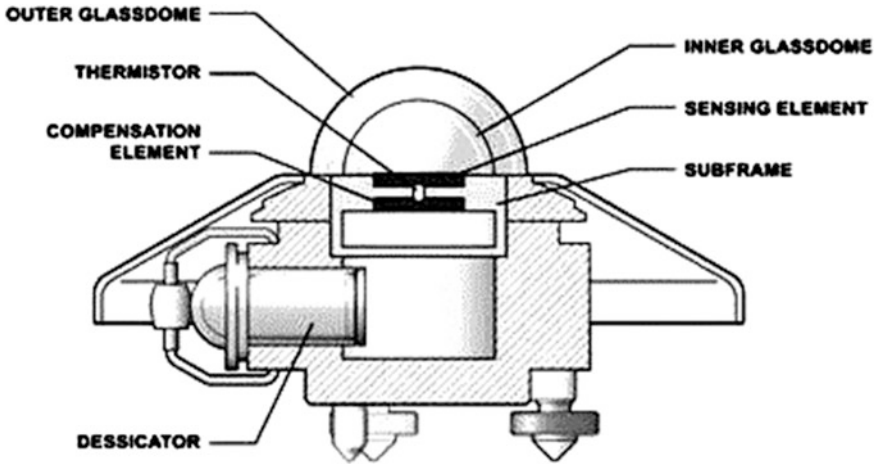
Fig. 1.15 Schematic diagram of pyranometer

1.4.2 Pyranometer

A **pyranometer** is used to measure the global solar radiation received from the entire hemisphere on a horizontal surface as shown in Fig. 1.15. The working principle is the same as that of a pyrheliometer. In this case, the sensitive surface, i.e., hot junction (blackened multijunction circular thermopiles) is exposed to total (beam + diffuse + reflected from Earth and surroundings) radiations. The temperature difference between hot and cold junctions is a function of the solar radiation falling on the surface. The sensitive surface is covered by two concentric hemispherical glass domes. This shields it from wind and rain. and also reduces the convection currents.

A pyranometer measures diffuse radiation with an occulting disc. This disc blocks the beam radiation from the surface. It may be noted that the pyranometers are calibrated to measure the solar radiation on a horizontal surface.

The output voltage corresponding to the incident solar radiation is detected and measured by a potentiometer. Electronic integrators are used to record the solar radiation during a certain time period. Pyranometers based on the silicon solar cell are commonly used for solar-energy measurement because the light current in these solar cells linearly varies with incident solar radiation.

For the measurement of **diffuse solar radiation**, a shading circular ring is used over a sensor of the pyranometer to block all incoming direct/beam solar radiation. The position of the shading circular ring is fixed for a particular day due to fixed path of Sun's motion for a given nth day of the year.

1.4.3   Sunshine Recorder

This is an instrument for measuring the duration of bright sunshine in hours. It consists of a glass sphere mounted in a section of a spherical brass bowl with grooves to hold the recorder cards. The sphere burns a trace on the card after being exposed to the Sun. The length of the trace is a direct measure of the duration of bright sunshine. There are sets of grooves to take three sets of cards, namely, (i) a long curved card for summer, (ii) a short curved card for winter, and (iii) straight cards for equinoxes.

1.5   Solar Radiation on a Horizontal Surface

1.5.1   Extraterrestrial Region

Here, the solar radiation (I_o) incident on a horizontal plane in the extraterrestrial region/outside the atmosphere in W/m^2, which is equivalent to being in the absence of atmosphere, is a component of I_{ext} along the normal to horizontal surface and can be obtained from Eqs. (1.6) and (1.11) as follows:

$$I_o = I_{ext} \times \cos \theta_Z$$

or,

$$I_o = I_{sc} \left[1.0 + 0.033 \cos \left(\frac{360n}{365} \right) \right] \cos \theta_z \qquad (1.16)$$

where I_{SC} is the **solar constant** (1367 W/m^2), and n is nth day of the year (Table 1.4).

Substitution of $\cos \theta_z$ from Eq. (1.11) in the previous equation gives

$$I_o = I_{sc} \left[1.0 + 0.033 \cos \left(\frac{360n}{365} \right) \right] (\cos \varphi \cos \delta \cos \omega + \sin \delta \sin \varphi) \qquad (1.17)$$

The extraterrestrial radiation on a horizontal surface for a given period from hour angles ω_1 to ω_2 (where ω_2 is larger) can be calculated by integrating Eq. (1.17) for a period, and it is given by

$$I_o \left(J/m^2 \right) = \frac{12 \times 3600}{\pi} I_{sc} \left[1.0 + 0.033 \cos \left(\frac{360n}{365} \right) \right] \left(\cos \varphi \cos \delta (\sin \omega_2 - \sin \omega_1) + \frac{2\pi(\omega_2 - \omega_1)}{360} \sin \delta \sin \varphi \right)$$

$$(1.18)$$

Table 1.4 Recommended average days of months for the average radiation of the month

Month	N for ith Day of month	Day of the year (n)
January	17	i
February	16	$31 + i$
March	16	$59 + i$
April	15	$90 + i$
May	15	$120 + i$
June	11	$151 + i$
July	17	$181 + i$
August	16	$212 + i$
September	15	$243 + i$
October	15	$273 + i$
November	14	$304 + i$
December	10	$334 + i$

For calculations of daily solar radiation on a horizontal surface in the extraterrestrial region (H_o) in J/m^2, Eq. (1.17) can be integrated during the period from sunrise $-\omega_s$ to sunset $+\omega_s$, and one gets

$$H_o = \frac{24 \times 3600}{\pi} I_{sc} \left[1.0 + 0.033 \cos\left(\frac{360n}{365}\right) \right] \left(\cos\varphi \cos\delta \sin\omega_s + \frac{2\pi\omega_s}{360} \sin\delta \sin\varphi \right)$$

(1.19)

The monthly average daily extraterrestrial radiation, $\bar{H}_o$, also in J/m^2, can be obtained from Eq. (1.19) by using the day numbers listed in Table 1.4.

Example 1.11 Determine the daily solar radiation in J/m^2 on a horizontal surface (H_o) in the extraterrestrial region at latitude 30°N on May 31, 2014.

Solution
In the given problem, n = 151 and δ (from Eq. 1.9a) = 21.90°, φ = 30°.
    From Eq. (1.15), $\omega_s = \cos^{-1}(-\tan\varphi \tan\delta) = 103.41°$

Now, the daily solar radiation on a horizontal surface in the extraterrestrial region can be obtained from Eq. (1.19) as follows:

$$H_o = \frac{24 \times 3600 \times 1367}{\pi} \left[1.0 + 0.033 \cos\left(\frac{360 \times 151}{365}\right) \right] (\cos 30° \cos 21.90° \sin 103.41°$$

$$+ \frac{\pi 103.41}{180} \sin 30° \sin 21.90°$$

or, $H_o = 40.87 \, \text{MJ/m}^2$

Example 1.12 Calculate the solar radiation in MJ/m^2 on a horizontal surface for Example 1.11 between 10 and 11 am.

Solution
Given $\omega_1 = -30°$ and $\omega_2 = -15°$ (Eq. 1.9b).

First Method:
   From Eq. (1.18), one gets

$$I_o = \frac{12 \times 3600}{\pi} \times 1367 \left[1 + 0.033 \times \cos\left(\frac{360 \times 151}{365}\right)\right] \left[\cos 30° \times \cos 21.9°.\right.$$
$$\times \{\sin(-15°) - \sin(-30°)\} + \left\{\frac{\pi(-15 - (-30))}{180}\right\} \sin 30° \times \left.\sin 21.9°\right]$$
$$= 4.43 \times 10^6 \, \text{J/m}^2 = 4.43 \, \text{MJ/m}^2$$

Second Method:
   The hourly extraterrestrial radiation can also be approximated by using the relation (Eq. 1.17)

$$I_o = 3600 \times I_{sc} \left[1 + 0.033 \cos\left(\frac{360n}{365}\right)\right] [\cos\varphi \times \cos\delta \times \cos\omega + \sin\varphi \sin\delta]$$

where ω is determined at the midpoint of the hour, i.e., $\omega = (\omega_1 + \omega_2)/2 = -22.5°$.
   Now,

$$I_o = 3600 \times 1367 \times 0.972 \times (0.743 + 0.187) = 4.44 \times 10^6 \, \text{J/m}^2$$
$$= 4.44 \, \text{MJ/m}^2$$

   The differences between hourly radiations determined by both methods will be slightly higher at times near sunrise and sunset.

1.5.2   Terrestrial Region

(a) Without knowing any data of solar radiation in the terrestrial region

   Referring to Fig. 1.9 and Eqs. (1.11), (1.13), and (1.4), the component of normal irradiance (solar radiation), I_N, along a normal to horizontal surface in the terrestrial region, is known as beam/direct radiation on a horizontal surface. It is expressed as follows:

$$I_b = I_N \times \cos\theta_Z \tag{1.20}$$

By using Eq. (1.15) for diffuse radiation, the hourly total solar radiation, $I(t)$, the sum of beam/direct and diffuse radiation on a horizontal surface in the terrestrial region, is written as

$$I(t) = I_b + I_d \tag{1.21a}$$

In addition, the hourly total solar radiation in W/m^2 can be calculated from known daily solar radiation data in J/m^2.

Collares Pereira and Rabl [11] proposed the following relation to determine the hourly total solar from known daily solar radiation data in J/m^2:

$$r_t = \frac{I(t)}{\sum I(t)} = \frac{I(t)}{H_o} \tag{1.21b}$$

Or

$$
\begin{aligned}
I(t) &= r_t H_o \,\text{J/m}^2\text{h} = \frac{r_t H_o}{3600}\,\text{W/m}^2 \\
r_t &= \frac{\pi}{24}(a + b \times \cos\omega)\frac{\cos\omega - \cos\omega_s}{\sin\omega_s - (2\pi\omega_s/360)\cos\omega_s}
\end{aligned} \tag{1.21c}
$$

The coefficients 'a' and 'b' are given by

$$
\left.
\begin{aligned}
a &= 0.409 + 0.5016\sin(\omega_s - 60) \\
&\text{and} \\
b &= 0.6609 - 0.4767\sin(\omega_s - 60)
\end{aligned}
\right\} \tag{1.21d}
$$

where ω is the hour angle in degrees for the time in question, and ω_s is the sunset-hour angle.

Example 1.13 Determine the ratio of hourly to daily total radiation, (r_t), on a horizontal surface in New Delhi in the month of May, 2013, at 2 pm. In addition, determine the hourly solar radiation for $H_o = 39.98\,\text{MJ/m}^2$.

Solution
Given $\varphi = 28°35' = 28.58°$ (Table 1.1); $\delta = 18.86°$ (Eq. 1.9a)

$\omega_s = 100.74°$ (Eq. 1.11) and $\omega = 30°$ (Eq. 1.9b)
From Eq. (1.21d), the values of 'a' and 'b' can be obtained as

$$a = 0.409 + 0.5016\sin(100.74 - 60) = 0.736$$
$$b = 0.6609 - 0.4767\sin(100.74 - 60) = 0.350$$

After knowing the numerical values of 'a' and 'b', from Eq. (1.21c) one obtains

$$r_t = \frac{\pi}{24}(0.736 + 0.350 \times \cos 30°)\frac{\cos(30°) - \cos(100.74)}{\sin(100.74) - (2\pi \times 100.74/360)\cos(100.74)}$$
$$= 0.109$$

By using Eq. (1.21b) for a given value of $H_o = 39.98\,\text{MJ/m}^2$ (from Example 1.19), the total radiation in 1 h (1.30–2.30 pm) is calculated as

$$I(t) = r_t \times \bar{H}_o = 0.109 \times 39.98\,\text{MJ/m}^2 = 4.36\,\text{MJ/m}^2$$

The daily total solar radiation (H) in J/m^2 on a horizontal surface in the terrestrial region can be written as

$$H = \sum_{t=1}^{t=N} I(t) \times 3600 \qquad (1.21e)$$

The average monthly solar radiation ($\bar{H}$) in J/m^2 on a horizontal surface in the terrestrial region can be written as

$$\bar{H} = \frac{\sum_i^{n_0} H_i}{n_0} \qquad (1.21f)$$

Evaluation of the monthly average of daily total radiation ($\bar{H}$) in J/m^2 on a horizontal surface.

For many applications, one needs the knowledge of the monthly average of daily solar radiation ($\bar{H}$) in J/m^2 available on a horizontal surface. It can be calculated with 10 % accuracy using following correlation:

$$\frac{\bar{H}}{\bar{H}_o} = a + b\left(\frac{\bar{n}}{\bar{N}}\right) \qquad (1.21g)$$

where $\bar{n}$ and $\bar{N}$ are the observed monthly average of daily bright sunshine hours and the total length of average day of month. $\bar{H}$ and $\bar{H}_o$ Eq. (1.19) are the monthly average of daily total solar radiation on a horizontal surface in the terrestrial and extraterrestrial region, respectively.

The regression coefficients a and b are given by

$$a = -0.309 + 0.539\cos\varphi - 0.0693E_o + 0.290(\bar{n}/\bar{N})$$
and,
$$b = 1.527 - 1.027\cos\varphi + 0.0926E_o - 0.359(\bar{n}/\bar{N}) \qquad (1.21h)$$

where φ is latitude of the place, and E_o is the height of the place (in kilometres) above sea level (Table 1.1). The elevation of the location above sea level is in kilometres.

The regression coefficients can also be determined as follows:

$$a = -0.110 + 0.235 \cos \varphi + 0.323(\bar{n}/\bar{N})$$

and   (1.21i)

$$b = 1.449 - 0.553 \cos \varphi - 0.694(\bar{n}/\bar{N})$$

for different periods of year, the range of $\bar{n}/\bar{N}$ for validity of the previous correlations are as follows:

$0.2 \leq (\bar{n}/\bar{N}) \leq 0.6$ for monsoon period

$0.4 \leq (\bar{n}/\bar{N}) \leq 0.9$ for premonsoon and postmonsoon periods

Example 1.14 Determine the total solar radiation on a horizontal surface for 12.1 h of the monthly average daily hours of bright sunshine (*n*) observed at New Delhi in May 2013.

Solution
Given $\delta = 18.79°$ (Eq. 1.9), $\varphi = 28°35' = 28.58°$ (New Delhi)
and $\omega_s = \cos^{-1}(-\tan 28.58° \tan 18.79°) = 100.68°$ (Eq. 1.15).

The average daily extraterrestrial radiation is obtained as (Eq. 1.19):

$$H_o = \frac{24 \times 3600 \times 1367}{\pi} \left[1.0 + 0.033 \cos\left(\frac{360 \times 135}{365}\right)\right](\cos(28.58)° \cos(18.79)° \sin(100.68)°$$
$$+ \frac{\pi \times 100.68}{180} \sin(28.58)° \sin(18.79)°\right) = 39.96 \text{ MJ/m}^2$$

The number of daylight hours (Eq. 1.12) is obtained as

$$N = \frac{2}{15} \cos^{-1}(-\tan 28.58° \tan 18.79°) = 13.42$$

The values of '*a*' and '*b*' (from Eq. 1.21i) can be obtained as follows:

$$a = -0.309 + 0.539 \cos \varphi - 0.0693 E_o + 0.290(\bar{n}/\bar{N})$$

and,

$$b = 1.527 - 1.027 \cos \varphi + 0.0926 E_o - 0.359(\bar{n}/\bar{N})$$

The previous values of '*a*' and '*b*' is used in Eq. (1.28) to obtain the monthly average daily solar radiation incident on a horizontal surface as follows:

$$\frac{\bar{H}}{\bar{H}_o} = a + b\left(\frac{\bar{n}}{\bar{N}}\right) = 0.388 + 0.338\left(\frac{12.1}{13.42}\right) = 0.693$$

For $H_o = 39.96\,\text{MJ/m}^2$, we obtain $\bar{H} = 27.66\,\text{MJ/m}^2$

(b) **With knowing data of solar radiation $I(t)$ hourly in W/m²; H daily in J/m², and $\bar{H}$ monthly in J/m² in the terrestrial region**

For estimating diffuse radiation from the hourly, daily, and monthly data of solar radiation, one must know the clearness index parameters as follows:

(i) **Hourly clearness index (k_T)**

This is the ratio of hourly data of solar radiation, Eq. (1.21a), in the terrestrial region to hourly data solar radiation, Eq. (1.17), in the extraterrestrial region. $I(t)$ It is given by

$$k_T = \frac{I}{I_o} \tag{1.22a}$$

where I is the measured hourly solar radiation, and I_o is obtained from Eq. (1.18).
Estimation of hourly beam and diffuse solar radiation
For a known k_T, the hourly solar radiation can be obtained from Eq. (1.22a). For the estimation of hourly total solar radiation on any inclined surface, the hourly values of beam and diffuse radiation on a horizontal surface are required.

If $I_d/I(t)$, the ratio of hourly diffuse radiation in W/m² to the hourly total solar radiation on a horizontal surface in W/m² at a given time of hour of a day, then there is correlation developed by Orgill and Hollands [10] given by

$$
\begin{aligned}
I_d/I(t) &= 1.0 - 0.249 k_T & &\text{for } k_T < 0.35 \\
I_d/I(t) &= 1.557 - 1.84 k_T & &0.35 < k_T < 0.75 \\
I_d/I(t) &= 0.177 & &\text{for } k_T > 0.35
\end{aligned}
\tag{1.22b}
$$

(ii) **Daily clearness index (K_T)**

A daily clearness index, K_T, is the ratio of daily solar radiation Eq. (1.21e) on a horizontal surface in the terrestrial region to daily solar radiation on a horizontal surface (Eq. 1.19) in the extraterrestrial radiation for that day.

$$K_T = \frac{H}{H_o} \tag{1.23a}$$

where H is measured daily total solar radiation, and H_o is obtained from Eq. (1.19).

Estimation of beam and diffuse components of daily solar radiation

For a known K_T, the daily solar radiation in J/m^2 on a horizontal surface can be obtained from Eq. (1.23a). The separation of daily solar radiation, H, on a horizontal surface into its beam and diffuse components is important to classify weather conditions (cases a, b, c, and d discussed in Sect. 1.2.1).

If H_d/H is the ratio of daily diffuse radiation to daily total solar radiation, a correlation was proposed in terms of K_T by Collares-Pereira and Rable [11], as follows:

$$
\left.
\begin{array}{ll}
H_d/H = 0.99 & \text{for } K_T \leq 0.17 \\
H_d/H = 1.188 - 2.72K_T + 9.473K_T^2 - 21.865K_T^3 + 14648K_T^4 & \text{for } 0.17 < K_T < 0.75 \\
H_d/H = -0.5K_T + 0.632 & \text{for } 0.75 < K_T < 0.80 \\
H_d/H = 0.2 & \text{for } \geq 0.80
\end{array}
\right\}
$$

(c) **Monthly clearness index** $(\bar{K}_T)$

The monthly average clearness index, $\bar{K}_T$, is the ratio of monthly average solar radiation on a horizontal surface, Eq. (1.21f), in the terrestrial region to the monthly average extraterrestrial solar radiation, i.e.,

$$
\bar{K}_T = \frac{\bar{H}}{\bar{H}_o}
\tag{1.24a}
$$

where $\bar{H}$ is the measured monthly solar radiation, and $\bar{H}_o$ is given by Eq. (1.19) for n given in Table 1.4.

Estimation of the monthly average of daily diffuse solar radiation on a horizontal surface

For a known $\bar{K}_T$ sunshine hour, N, based on the measured data for Chennai, New Delhi, and Pune, Gopinathan [12] has proposed the following correlation

$$
\frac{\bar{H}_d}{\bar{H}} = 1.194 - 0.838\bar{K}_T - 0.0446\frac{\bar{n}}{N}
\tag{1.24b}
$$

The prediction based on the above equation has been compared with that obtained using the following correlations:

$$
\frac{\bar{H}_d}{\bar{H}} = 1.403 - 1.672\bar{K}_T
\tag{1.24c}
$$

and

$$
\frac{\bar{H}_d}{\bar{H}} = 0.931 - 0.814\frac{\bar{n}}{N}
\tag{1.24d}
$$

1.6   Solar Radiation on an Inclined Surface

1.6.1   Conversion Factors

For any inclined surface, there are three type of solar radiation, namely, (i) beam, (ii) diffuse, and (iii) reflected solar radiation from a horizontal surface and the surfaces surrounding it. Hence, there are three conversion factors, namely, for beam (R_b), diffuse (R_d), and reflected (R_r) solar radiations. These conversion factors convert the beam and diffuse solar radiations of a horizontal surface to those of an inclined surface. These conversion factors are as follows:

For beam radiation: The conversion factor for beam radiation (R_b) is defined as the ratio of beam radiation incident on an inclined surface $\left(I_b'\right)$ in W/m^2 to that on a horizontal surface in W/m^2, Eq. (1.20) ($I_b = I_N \times \cos\theta_Z$).

The flux of beam radiation incident on an inclined surface (I_b') is given by

$$I_b' = I_N \cos\theta_i \tag{1.25}$$

where θ_z and θ_i are the angles of incidence on the horizontal and inclined, surfaces respectively (Fig. 1.11), and I_N is the intensity of normal irradiance/solar radiation incidence to the inclined surface (Eq. 1.3). Now, (R_b) for beam radiation can be obtained as,

$$R_b = \frac{I_b'}{I_b} = \frac{\cos\theta_i}{\cos\theta_z} \tag{1.26}$$

Depending on the orientation of inclined surface, the expression for $\cos\theta_i$ and $\cos\theta_z$ can be obtained from Eqs. (1.10) and (1.11), respectively.

The variation of R_b with nth days of the year for is shown in Fig. 1.16.

For diffuse radiation: The conversion factor for diffuse radiation (R_d) is defined as the ratio of diffuse radiation incident on an inclined surface in W/m^2 to that on a horizontal surface in W/m^2. Lack of any established method for finding the distribution of diffuse radiation over the sky makes its estimation very difficult. However, diffuse radiation can be estimated by considering the sky as the isotropic source of diffuse radiation. For a tilted surface at an angle β from the horizontal surface, the conversion factor for diffuse radiation is given as follows:

$$R_d = \frac{1 + \cos\beta}{2} \tag{1.27}$$

For reflected solar radiation: Reflected solar radiations are radiations reflected from the ground and other objects near surface of interest. Assuming that reflected radiations are diffuse and isotropic, the conversion factor for reflected solar radiation (R_r) is given by:

Fig. 1.16 Variation of R_b with nth day of the year for different **a** latitudes, **b** inclination angles, and **c** times of the day

(a)

Conversion factor, R_b

$\omega = 0°$
$\beta = 45°$
$\gamma = 0°$

latitude =
60°
45°
30°
13°

nth day of the year, days from january 1 ⟶

(b)

Conversion factor, R_b

$\omega = 0°$
$\phi = 28.58°$
$\gamma = 0°$

Beta =

15°
30°
45°
60°

nth day of year, days from january 1 ⟶

(c)

Conversion factor, R_b

Omega =

60°

30°

0°

$\beta = 45°$
$\gamma = 0°$
$\phi = 30°$

nth day of the year, days from january 1 ⟶
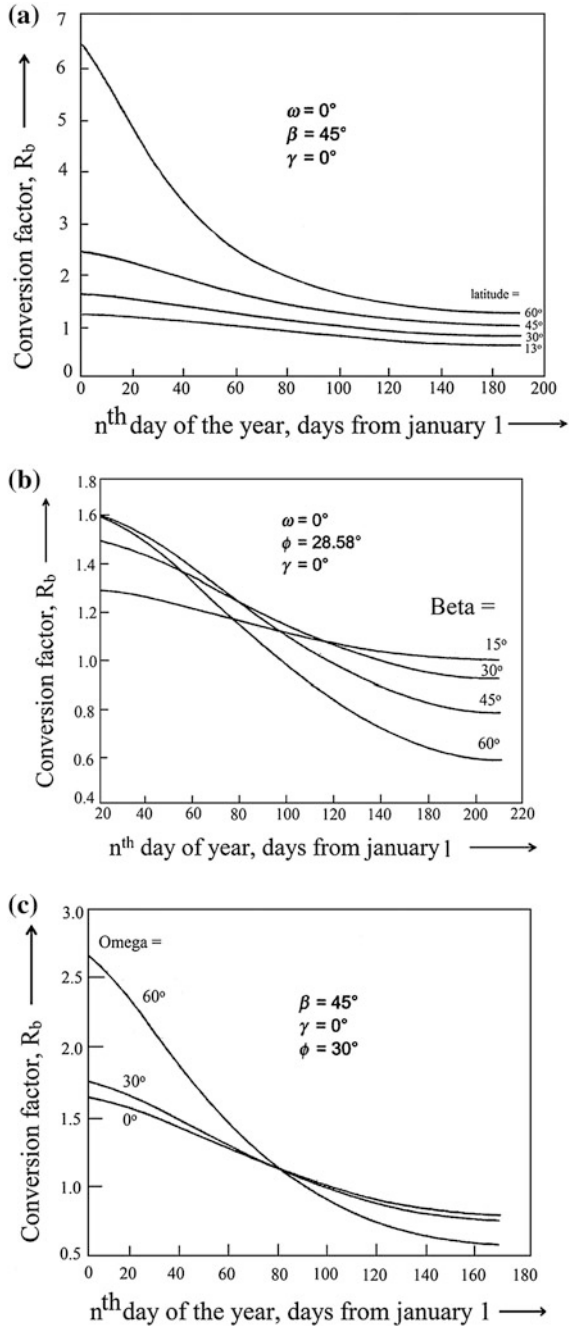
Fig. 1.17 Variation of R_d and R_r with inclination (β)
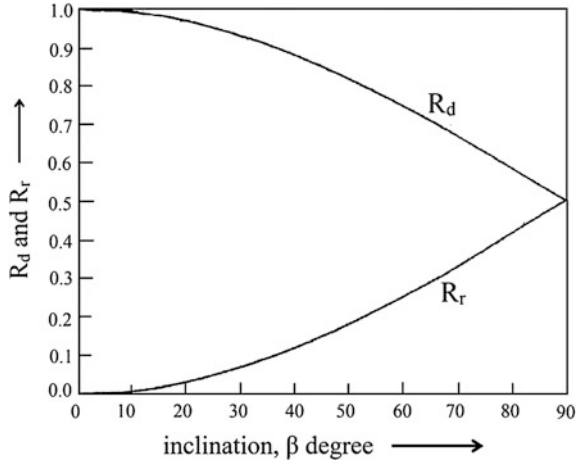
$$R_r = \frac{1 - \cos \beta}{2} \tag{1.28}$$

It may be mentioned here that both the beam and diffuse components of solar radiation undergo reflection from the ground and the surroundings. The variations of (R_d) and R_r with inclination (β) are shown in Fig. 1.17.

For total solar radiation: The ratio of total solar radiation incident on a inclined/tilted (I_T) surface to that on a horizontal surface, $I(t)$, is the conversion factor of total solar radiation on inclined/tilted surface, R', which is calculated as follows:

$$R' = \frac{I_T}{I(t)} = \frac{I_b R_b + I_d R_d}{I_b + I_d} + R_r \tag{1.29}$$

Example 1.15 Determine the conversion factor for beam radiation for the inclined surface for the time specified in Example 1.6.

Solution
For horizontal surface, $\cos \theta_z = \sin \delta \times \sin \varphi + \cos \delta \times \cos \varphi \times \cos \omega$, (Eq. 1.11) is given by

$$\cos \theta_z = \sin(-13°) \times \sin(28.58°) + \cos(-13°) \times \cos(28.58°) \times \cos(22.5°)$$
$$= 0.683$$

From Example 1.6, $\cos \theta_i$ is given by

$$\cos \theta_i = 0.999$$

Furthermore, from Eq. (1.26), R_b is given by

1.6.2   Total Solar Radiation on an Inclined/Tilted Surface

For any inclined surface, Liu and Jordan [13] estimated total solar radiation using the following relation:

$$I_{\mathrm{T}} = I_{\mathrm{b}}R_{\mathrm{b}} + I_{\mathrm{d}}R_{\mathrm{d}} + \rho R_{\mathrm{r}}(I_{\mathrm{b}} + I_{\mathrm{d}}) \qquad (1.30)$$

I_{b} and I_{d} are calculated using Eqs. (1.20) and (1.15) respectively; R_{b}, R_{d}, and R_{r} are estimated using Eqs. (1.26–1.28). The value of the reflection coefficient ρ is 0.2 for ordinary ground, and for snow-covered ground its value is 0.6.

Equation (1.30) can only be used for known measured data of hourly beam and diffuse solar radiation as discussed in Sect. 1.4.2.

If measured data of hourly beam and diffuse solar radiation are not available, then the following expression is used to determine the total radiation on an inclined/tilted surface of arbitrary orientation. It is given by:

$$I_{\mathrm{T}} = I_{\mathrm{N}} \times \cos\theta_{\mathrm{i}} + I_{\mathrm{d}}R_{\mathrm{d}} + \rho R_{\mathrm{r}}(I_{\mathrm{N}} \times \cos\theta_{\mathrm{Z}} + I_{\mathrm{d}}) \qquad (1.31)$$

where an expression for hourly variation of I_{N} and I_{d} can be obtained from Eqs. (1.13) and (1.15), respectively. In addition, the hourly values of $\cos\theta_{\mathrm{i}}$ and $\cos\theta_{\mathrm{Z}}$ can be determined from Eqs. (1.10) and (1.11), respectively. Various radiation models for solar radiation calculation are given in Appendix IIIC [14–43].

Example 1.16 Calculate the beam, diffuse, reflected, and total solar radiation on a south-oriented tilted surface inclined at 45° at a place having latitude 40°N for 2:00 to 3:00 pm on May 31, 2015. Given that: $I = 1.04\,\mathrm{MJ/m^2}$ and $\rho = 0.60$.

Solution
For the present case: $n = 151$; $\delta = -11.6°$ (Eq. 1.9a); $\varPhi = 40°\mathrm{N}$; $\omega_2 = 45°$ and $\omega_1 = 30°$ (Eq. 1.9b).

The hourly extraterrestrial solar radiation in $\mathrm{J/m^2}$ (Eq. 1.18) is given by,

$$\begin{aligned} I_{\mathrm{o}} = {} & \frac{12 \times 3600 \times 1367}{\pi}\left[1 + 0.033\cos\left(\frac{360 \times 151}{365}\right)\right] \times \left[\cos 40° \times \cos(-11.6°)\right. \\ & \left. \times(\sin 45° - \sin 30°) + \frac{\pi \times (45 - 30)}{180}\sin 40° \times \sin(-11.6°)\right] \end{aligned}$$

or,

$$I_{\mathrm{o}} = \frac{12 \times 3600 \times 1367}{\pi} \times 0.972 \times 0.121 = 2.21\,\mathrm{MJ/m^2}$$

The hourly clearness index is obtained by Eq. (1.22a) as,

$$k_{\mathrm{T}} = \frac{I}{I_{\mathrm{o}}} = \frac{1.04}{2.21} = 0.471$$

For the above value of k_{T}, the diffuse component can be determined from Eq. (1.22b) and is given by,

$$\frac{I_{\mathrm{d}}}{I} = 1.557 - 1.84 k_{\mathrm{T}} = 0.690$$

For a given value of $I \left(1.04\,\mathrm{MJ/m^2} \right)$

$$I_{\mathrm{d}} = 0.690 \times 1.04 = 0.718\,\mathrm{MJ/m^2}$$

and

$$I_{\mathrm{b}} = 0.253 \times 1.04 = 0.263\,\mathrm{MJ/m^2}$$

The conversion factor for beam radiation at midpoint of the hour ($\omega = 37.5°$) is given by,

$$R_{\mathrm{b}} = \frac{\cos(40° - 45°)\cos(-11.6°)\cos 37.5° + \sin(-11.6°)\sin(40°)}{\cos 40° \cos(-11.6°)\cos 37.5° + \sin(-11.6°)\sin 40°}$$
$$= 1.38$$

The total radiation is given as,

$$I_{\mathrm{T}} = 0.263 \times 1.38 + 0.718 \times \frac{(1 + \cos 45°)}{2} + 1.04 \times 0.60 \times \frac{(1 - \cos 45°)}{2}$$

Or

$$I_{\mathrm{T}} = 0.363 + 0.613 + 0.091 = 1.067\,\mathrm{MJ/m^2}$$

The contribution of beam, diffuse, and reflected components is 0.363, 0.613 and 0.091 MJ/m², respectively.

Example 1.17 Determine the values of R_{b}, R_{r}, R_{d}, and R' with the data given below:

Latitude $(\varphi) = 28°51' = 28.85°$, day of the year = October 6, 2013
Surface azimuth angle $(\gamma) = 0°$, inclination of the surface $(\beta) = 45°$; reflectivity of the ground $(\rho) = 0.2$

Time (h)	Radiation on a horizontal surface (W/m^2)			Hour angle (ω) ($°$)	Observed radiation on inclined surface (W/m^2)	Calculated radiation on inclined surface (W/m^2)
	Total	Diffuse	Beam			
9:00 am	472.44	174.94	297.5	−45	570.65	535.37
10:00 am	647.41	203.30	444.11	−30	753.7	734.63
11:00 am	752.40	222.22	530.18	−15	839.83	851.607
12:00 pm noon	769.9	231.0	538.70	0	832.9	867.93
1:00 pm	752.40	236.4	516.00	15	872.9	846.60

Solution

In the present example, $n = 279$, $\delta = -6.18°$ (Eq. 1.9a)

Calculation for R_b:

From Eqs. (1.10), (1.11) and (1.26), one can have

$$\cos \theta_i = 0.985; \cos \theta_z = 0.819; R_b = \cos \theta_i / \cos \theta_z = 1.203$$

Calculation for R_d and R_r:

From Eqs. (1.27) and (1.8),

$$R_d = \frac{1 + \cos 45°}{2} = 0.8536 \text{ and } R_r = \rho \left(\frac{1 - \cos 45°}{2} \right) = 0.029$$

Hence, the total solar radiation on an inclined surface can be obtained from Eq. (1.30) by using the data given in problem for 12 noon. This is given by

$$I = I_b R_b + I_d R_d + R_r (I_b + I_d) = 648.19 + 197.18 + 22.56 = 867.93 \text{ W/m}^2$$

The above-calculated value of total solar radiation (867.93) is very close to the observed value (832.9) in the table provided in the current example.

Calculation for R':

From Eq. (1.29), R' is calculated as $R' = \frac{648.19 + 197.18}{769.7} + 0.029 = 1.127$

The calculations for total solar radiation can be repeated for other data given in the table provided in the current example.

1.6.3 Monthly Average Daily Solar Radiation $\bar{H}_T$ on Inclined Surfaces

The monthly average solar radiation on an inclined surface can be estimated according to the similar procedure discussed in previous section for calculating the

hourly total solar radiation on an inclined surface. If $(\bar{H} - \bar{H}_d)$, $\bar{H}_d$, and $\rho\bar{H}$ are the contributions from beam, diffuse, and reflected radiation, then the monthly mean daily solar radiation on an unshaded inclined surface can be expressed by assuming all radiations to be isotropic as Klein [14]:

$$\bar{H}_T = (\bar{H} - \bar{H}_d)\bar{R}_b + \bar{H}_d\left(\frac{1 + \cos\beta}{2}\right) + \rho\bar{H}\left(\frac{1 - \cos\beta}{2}\right)$$

where $\bar{R}_b$ is the conversion factor for average daily beam radiation. In this case, the monthly average values of $\cos\theta_i$ and $\cos\theta_z$ can be obtained from the recommended average days of the month (Table 1.4).

Example 1.18 Determine the monthly average clearness index, $(\bar{K}_T)$, for a surface at latitude 30° for March 16, 2013, and for the monthly average daily terrestrial radiation on a horizontal surface 28.1 MJ/m^2.

Solution
For March 16, 2013 $n = 75$; $\delta = -2.4°$ (Eq. 1.9a), and
   $\omega_s = \cos^{-1}(-\tan 30° \tan(-2.4°)) = 88.61°$ (Eq. 1.11a)

   For the above data, the monthly average daily extraterrestrial radiation is calculated as
   $\bar{H}_o = \frac{24 \times 3600 \times 1367}{\pi}(1.01)(0.832) = 31.57\,\text{MJ/m}^2$ (Eq. 1.19)
   Now, the monthly average clearness index is given by

$$\bar{K}_T = \frac{\bar{H}}{\bar{H}_o} = \frac{28.1}{31.57} = 0.890$$

Example 1.19 Calculate the average diffuse and beam solar radiation on a horizontal surface in Madras (May, 2013). The average solar radiation for May $(\bar{H})$ for Madras is 22.69 MJ/m^2.

Solution
For the present problem, $\delta = 18.86°$ (Eq. (1.9) and Table 1.4), $\varphi = 13°$
   here $\omega_s = \cos^{-1}(-\tan 13° \tan(18.86°)) = 94.5°$ (Eq. 1.11a)

   The monthly average daily extraterrestrial radiation $\bar{H}_o$ (from Eq. (1.19) and Table 1.4) is calculated as

$$\bar{H}_o = 38.18\,\text{MJ/m}^2$$

   The monthly average clearness index $\bar{K}_T$ is calculated as follows:

$$\bar{K}_T = \frac{\bar{H}}{\bar{H}_o} = \frac{22.69}{38.18} = 0.594$$

Using the previous value of K_T in Eq. (1.24c), one gets the diffuse component of monthly average daily radiation ($\bar{H}_d$) as

$$\frac{\bar{H}_d}{H} = 1.403 - 1.672\bar{K}_T = 0.410 \Rightarrow \bar{H}_d = 0.410 \times 22.69\frac{MJ}{m^2} = 9.30\,MJ/m^2$$

Furthermore, the beam component of monthly average daily radiation ($\bar{H}_b$) can be calculated as follows:

$$\bar{H}_b = \bar{H} - \bar{H}_d = 22.69 - 9.30 = 13.39\,MJ/m^2$$

Objective Questions

1.1 Diffuse radiation in the extraterrestrial region is
(a) maximum   (b) minimum   (c) zero   (d) none of these
Answer: (c)

1.2 The solar constant is measured
(a) near the Sun   (b) near the Earth   (c) in the extraterrestrial region   (d) in the terrestrial region
Answer: (c)

1.3 The short-wavelength radiation reaching on the Earth is
(a) 0.03 to 0.30 μm   (b) 3 to 30 μm   (c) 0.3 to 3 μm   (d) none of these
Answer: (c)

1.4 The value of solar radiation in summer is maximum on the surface having an inclination equal to
(a) latitude   (b) zero   (c) 45°   (d) 90°
Answer: (b)

1.5 The Earth emits
(a) long-wavelength   (b) short-wavelength   (c) ultraviolet radiation   (d) infrared radiation
Answer: (a)

1.6 The atmosphere reflects
(a) long-wavelength radiation   (b) short-wavelength radiation   (c) all radiation   (d) none of above
Answer: (a)

1.7 The sunshine hour (N) at the equator
(a) varies with 'n'   (b) is constant   (c) is zero   (d) is 24 h
Answer: (b)

1.8 The relation between the zenith (φ_z) and solar altitude (α) angles is
(a) $\theta_z + \alpha = 60$ (b) $\theta_z + \alpha = 90$ (c) $\theta_z + \alpha = -90$ (d) $\theta_z + \alpha = 0$
Answer: (c)

1.9 The energy generated at the core of the Sun is due to
(a) fission reaction   (b) fusion reaction   (c) conduction   (d) radiation
Answer: (b)

1.10 The wavelength range of infrared region in the solar spectrum is
      (a) 7–∞ μm   (b) 0.7–∞ μm   (c) 70–∞ μm   (d) none of these
      Answer: (b)
1.11 In Wein's displacement law, i.e., $\lambda T = C$, the value of C is
      (a) 300 μm K   (b) 30 μm K   (c) 3000 μm K   (d) none of these
      Answer: (c)
1.12 Air-mass at early morning and late evening is
      (a) zero   (b) minimum   (c) maximum   (d) none
      Answer: (c)
1.13 The sunshine hour in the northern hemisphere on December 21 is
      (a) maximum   (b) minimum   (c) zero   (d) none
      Answer: (a)
1.14 Solar radiation is measured in the
      (a) extraterrestrial region   (b) terrestrial region   (c) on Earth   (d) on
      mountain
      Answer: (a)
1.15 The latitude angle at equator is
      (a) ±90°   (b) ±45°   (c) ±30°   (d) zero
      Answer: (d)

Problems

1.1 Determine the Sun's temperature for different months and compare the
     results for the following data:

$$\text{Solar Constant} = 1367\,\text{W/m}^2, \quad \text{Sun Diameter}(2RS) = 1.39 \times 10^9\text{m}$$
$$\text{Sun}-\text{Earth distance}(L_{se}) = 1.5 \times 10^{11}\text{m}$$

     Hint:
$$I_{ext} = \sigma T_S^4 \left(4\pi R_s^2\right) / \left(4\pi L_{se}^2\right).$$

$$\sigma = \text{Stefan}-\text{Boltzmann constant} = 5.67 \times 10^{-8}\,\text{W/m}^2\text{K}^4.$$

1.2 Determine the declination angle (δ) for March 31, 2014.
     Hint: Use Eq. (1.9a).
1.3 Determine the hour angle (ω) at 2.30 p.m.
     Hint: Use Eq. (1.9b).
1.4 Calculate the daily variation of the extraterrestrial solar intensity (I_{ext}) and
     the declination angle (δ) for the month of June, 2014.
     Hint: Use Eq. (1.6) and Eq. (1.9a). respectively.
1.5 Calculate the air mass for the Sun's position at 10:00 am, 12:00 noon, and
     02:00 pm.

Hint: Airmass $= m/H = \sec\psi$.

1.6 Determine the hourly direct radiation (I_b) on (i) a horizontal surface and
(ii) an inclined surface with an inclination of 45° on January 15, 2014, in the
terrestrial region.
Hint: Use Eq. (1.14), $\alpha = 90 - \theta_z$, for the horizontal surface, $I_b = I_N \cos\theta_z$;
and for inclined surface, $I_b' = I_N \cos\theta_i$.

1.7 Derive an expression for the number of sunshine hours (N).
Hint: Use $\theta_z = 90°$ (sunset/sunrise) in Eq. (1.11) with $\omega = \omega_s$ and
$1\,h = 15°$, $N = 2\omega_s$

1.8 Derive an expression for the extraterrestrial radiation on a horizontal surface
(H_0)
Hint: Use Eq. (1.16) for I_{ext} and integrate the following expression:

$$H_{OT} = \frac{12}{\pi} \times 3600 \int\limits_{-\omega_s}^{\omega_s} I_{ext} \cos\theta \, d\omega$$

1.9 Determine the number of sunshine hours for the places mentioned in
Table 1.1 on June 21 and December 21, 2014.
Hint: Use Eq. (1.12).

1.10 Calculate the diffuse radiation (I_d) on a horizontal surface and an inclined
surface $(\beta = 45°)$ for Problem 1.6.
Hint: Use the following expression:

$$I_d = \frac{1}{3}(I_{SC} - I_N)\sin\alpha$$

1.11 Calculate the conversion factor for beam (R_b) and diffuse radiation (R_d) for
New Delhi (Table 1.1) at 12:00 noon for an 45°-inclined surface facing east–
south on February 16, 2014.
Hint: Use Eqs. (1.26) and (1.27).

1.12 Derive an expression for extraterrestrial radiation on a horizontal surface for
a 1-h period.
Hint: Integrate between ω_1 and ω_2 from Problem 1.8.

1.13 Derive an expression for extraterrestrial radiation on a south-facing $(\gamma = 0)$
tilted surface

$$(H_{OT}).$$

Hint: Use the following expression:

$$H_{OT} = \frac{12}{\pi} \times 3600 \int\limits_{-\omega_s}^{\omega_s} I_{ext} \cos\theta \, d\omega.$$

1.14 Determine the wavelength range of solar radiation received on the Earth.
      Hint: See Fig. 1.4.

1.15 Discuss the basic difference between solar radiation in the extraterrestrial
      region compared with that in the terrestrial region.
      Hint: Refer to Sect. 1.5.

1.16 Prove that $\cos \theta_z = \sin \alpha$
      Hint: Use $\theta_z = 90 - \alpha$.

1.17 Determine the percentage of total radiation that falls in the ultraviolet region
      (0.2–0.38 μm), the visible region (0.38–0.78 μm), and the infrared region
      (0.78–3 μm)
      Hint: Use Fig. 1.4 and Table 1.1 with Example 1.1.

1.18 Calculate the solar altitude angle (α) for Problem 1.2 for different hour
      angles.
      Hint: See Problem 1.16.

1.19 Determine the hourly variation of direct and diffuse radiation on a horizontal
      surface for June 01, 2014, for the locations mentioned in Table 1.1.
      Hint: Use the expressions given in Problems 1.6 and 1.10, respectively

1.20 Calculate (N) for each month for the locations mentioned in Table 1.1.
      Hint: Use Eq. (1.12) and Table 1.4 for δ and n.

1.21 Determine the average temperature of Earth without atmosphere and
      assuming 30 and 45 % reflection losses from the Earth's surface (neglect the
      heat capacity of the Earth).
      Hint: Use the following expression:

$$0.7\pi(D_e/2)^2 I_{SC} = 4\pi D_e^2 \varepsilon \sigma T_e^4$$

1.22 Calculate an average Earth temperature without atmosphere considering the
      heat capacity of the Earth.
      Hint: Use the following expression:

$$\pi(D_e/2)^2 I_{SC} = (4/3)\pi(D_e/2)^3 \rho_e C_e \Delta T.$$

1.23 Determine the variation of monochromatic emissive power with λ in μm for
      different temperatures of black body (6000, 3000, 1000, and 288 K) and
      verify Wien's displacement law.
      Hint: Calculate $E_{b\lambda}$ for different λ and show the variation between $E_{b\lambda}$ and λ
      and determine λ_{max} for each temperature and verify Wien's displacement
      law.

1.24 Calculate the beam and diffuse radiation on a horizontal surface for
      December 21, March 21, and June 21, 2014, for the locations given in
      Table 1.1.
      Hint: See Problem 1.6.

References

1. G.N. Tiwari, *Solar Energy: Fundamental, Design, Modelling and Applications* (Narosa Publishing House, New Delhi and CRC Press, New York, 2004)
2. G.N. Tiwari, R.K. Mishra, *Advance Renewable Energy Sources* (RSC publishing, UK, 2012)
3. D. Budikova, Albedo (2013). Retrieved from http://www.eoEarth.org/view/article/149954
4. J.A. Duffie, W.A. Beckmann, *Solar Engineering of Thermal Processes* (Wiley, New York, 1991)
5. F. Kasten, A.T. Young, Appl. Optics **28**, 4735 (1989)
6. B.Y.H. Liu, R.C. Jordan, Sol. Energy **4**(3), 1 (1960)
7. F. Linke, Beitr. Phys. Fr. Atom **10**, 91 (1922)
8. R. Perez, P. Ineichen, E. Maxwell, R. Seals, A. Zelenka, ASHRAE Trans. **98**, 3578 (1992)
9. H.N. Singh, G.N. Tiwari, Energy **30**, 1589 (2005)
10. J.F. Orgill, K.G.T. Hollands, Sol. Energy **19**, 357 (1977)
11. M. Collares-Perira, A. Rabl, Sol. Energy **22**, 155 (1979)
12. K.K. Gopinathan, Sol. Energy **41**, 379 (1988)
13. B.Y.H. Liu, R.C. Jordan, ASHRAE J. **3**(10), 53 (1961)
14. H.C. Hottel, A. Whiller, in *Transactions of the Conference on Use of Solar Energy*. The Scientific Basis, vol. II(I), Section A (University of Arizona Press, Tucson, 1958), 74
15. F. Kasten, A.T. Young, Appl. Opt. **28**, 4735 (1989)
16. R. Perez, P. Ineichen, E. Maxwell, R. Seals, A. Zelenka, ASHRAE Trans. **98**, 354 (1990)
17. American Society of Heating, *Refrigeration and Air-conditioning Engineers. ASHRAE Applications Handbook (SI)* (ASHRAE, Atlanta, 1999)
18. N. Nijigorodov, WREC **1**, 1270 (1996)
19. M.A. Machler, M. Iqbal, ASHRAE Trans. **91**(1a), 106 (1985)
20. G.V. Parishwad, R.K. Bhardwaj, V.K. Nema, Renew. Energy **12**(3), 303 (1997)
21. H.N. Singh, G.N. Tiwari, Energy **30**, 1589 (2005)
22. M.J. Ahmad, G.N. Tiwari, CIGR E-J **10**, 1 (2008)
23. B.Y.H. Liu, R.C. Jordan, Sol. Energy **4**, 1–19 (1960)
24. J.F. Orgill, K.G.T. Hollands, Sol. Energy **19**, 357 (1977)
25. D.G. Erbs, S.A. Klein, J.A. Duffie, Sol. Energy **28**, 293 (1982)
26. J.W. Spencer, Sol. Energy **29**(1), 19 (1982)
27. T. Muneer, M.M. Hawas, K. Sahili, Energy Convers. Manag. **24**(4), 265 (1984)
28. M.N.A. Hawlader, Int. J. Ambient Energy **5**, 31 (1984)
29. D.T. Reindl, W.A. Beckman, J.A. Duffie, Sol. Energy **45**, 1 (1990)
30. J. Chandrasekaran, S. Kumar, Sol. Energy **53**, 505 (1994)
31. J.C. Lam, D.H.W. Li, Build. Environ. **31**(6), 527 (1996)
32. J. Boland, L. Scott, M. Luther, Environmetrics **12**, 103 (2001)
33. A. Miguel, J. Bilbao, R. Aguiar, H. Kambezidis, E. Negro, Sol. Energy **70**, 143 (2001)
34. A.P. Oliveira, J.F. Escobedo, A.J. Machado, J. Soares, Appl. Energy **71**, 59 (2002)
35. S. Karatasou, M. Santamouris, V. Geros, Int. J. Sustain. Energ. **23**, 1 (2003)
36. J. Soares, A.P. Oliveira, M.Z. Boznar, P. Mlakar, J.F. Escobedo, A. Machado, J. Applied Energy **79**, 201 (2004)
37. A. Whillier, Arch. Meteorol. Geophys. Bioclimatol. **B8**, 197 (1956)
38. M. Collares-Pereira, A. Rabl, Sol. Energy **22**, 155 (1979)
39. T.A. Newell, Sol. Energy **31**, 339 (1983)
40. P.C. Jain, Solar Wind Technol. **1**, 123 (1984)
41. C. Gueymard, J. Sol. Energy Eng. Trans. ASME **108**, 320 (1986)
42. H.P. Garg, S.N. Garg, Sol. Wind Technol. **4**, 113 (1987)
43. A. Baig, P. Akhter, A. Mufti, Renew. Energy **1**, 119 (1991)

Additional References

44. Edward W. Law, Abhnil A. Prasad, Merlinde Kay, Robert A. Taylor, Sol. Energy **108**, 287 (2014)
45. Fariba Besharat, Ali A. Dehghan, Ahmad R. Faghih, Renew. Sustain. Energy Rev. **21**, 798 (2013)
46. Amit Kumar Yadav, S.S. Chandel, Renew. Sustain. Energy Rev. **23**, 503 (2013)
47. Ali N. Celik, T. Muneer, Energy Convers. Manag. **67**, 117 (2013)
48. M. Jamil Ahmad, G.N. Tiwari, Int. J. Energy Environ. **1**(3), 513 (2010)
49. Kadir Bakirci, Renew. Sustain. Energy Rev. **13**(9), 2580 (2009)
50. M. Jamil Ahmad, G.N. Tiwari, *Open Environ. J.* **2**, 6 (2008)
51. M. Jamil Ahmad, G.N. Tiwari, Agric. Eng. Int. CIGR Ej. **10**, 1 (2008)
52. N.K. Bansal, Minke, Gernot, *Climatic Zones and Rural Housing in India, Part 1 of the indo-German Project on Passive Space Conditioning* (1988)
53. S.A. Klein, Sol. Energy **19**(4), 325 (1977)
54. M.P. Thekaekara, Solar irradiance, total and spectral, Chapter III. *In Solar Engineering*, ed. by A.A. M. Sayigh (Academic press, Inc. New York, 1977)
55. G.N. Tiwari, S. Dubey, *Fundamentals of Photovoltaic Modules and Their Applications* (RSC publishing, UK, 2010)

Chapter 2
Daylighting

Abstract Solar energy directly provides illumination (lux) inside a building without any additional heat (thermal energy) source, unlike artificial lighting, and saves the use of conventional (fossil) fuels. This can be treated as one method to conserve available fossil fuels.

2.1 Introduction

Daylighting is the general practice of having vertical windows and openings in a wall exposed to incoming solar radiation to receive natural light inside the room during the day time. The reflective surfaces outside the building can also provide effective internal lighting through an opening in the wall. This process of having natural light inside a room is known as **daylight harvesting**.

Windows in an exposed wall are the most common way to allow daylight into a living space as shown in Fig. 2.1. The amount of solar radiation (daylight in *lux*) available on the vertical window ($\beta = 90°$) and with any orientation for known γ (wall azimuth angle) can be evaluated as discussed in Chap. 1. This means that the window selectively allows for direct and diffuse sunlight for different hours and days of the year. Different manufacturing technologies and process treatments improve the transmissivity of the glass, which in turn increases the amount solar radiation transmitted from the window.

A **clerestory window** is a band of narrow windows placed at the top of a high wall as shown in Fig. 2.2. The solar radiation transmitted from the clerestory windows illuminate the interior walls. Radiations falling on interior walls are further reflected to the living space. Light obtained using this method provides more diffuse radiation, which reduces shadow formation.

Daylight obtained using the concept of a skylight is very simple. These concepts are widely used in residential, community, and commercial buildings. Greater use

Fig. 2.1 Window fitted in the exposed walls of a room for daylighting

Fig. 2.2 View of a clerestory window

of daylighting ensures less use of artificial light, thus saving significant nonrenewable (electrical) energy. Hence, this concept is cost-effective and environment friendly.

2.2 History of Daylighting

Architectural design of building for daylight was an art and science for harnessing the visible portion of the solar spectrum into the built environment. Our historical buildings exhibit good daylight uses. Daylighting has important advantages such as creating psychological visual comfort in a living space [1]. It also reduces electrical energy consumption kWh for artificial lights [2]. This consequently reduces the sensible heat gain associated with artificial lights. Hence, the cooling requirement of the building decreases due to the provision of natural daylight. The **daylight coefficient concept** offers a more effective way of computing indoor daylight

illuminance in lux [3]. Similarly, Joshi et al. [4] gave a brief review on different mathematical models for the estimation of daylight in buildings.

Reddy and Manish [5] modeled the variation of global solar radiation with space and time using an artificial neural network (ANN) model. The validation results and comparison of ANN model with other models showed that the ANN model is more suitable compared with other classical regression models for predicting global solar radiation. Solar radiation for any place and weather condition (Sect. 1.2.6) can be predicted using an ANN model.

In modern architecture, daylighting is an inescapable concept used for meeting the visual needs and thermal comfort of the occupants and ensuring energy-efficient buildings [6]. Daylighting concepts provide maximum possible natural light to the occupant, which is strongly needed for visual as well as mental comfort. The openings provided for daylighting through a window also visually connect occupants to the outside environment, which confers a positive psychological effect.

The high consumption of electricity in buildings for many applications, viz., cooling, heating, illumination, etc., is directly or indirectly related to pollution and global warming due to the electricity produced mainly from conventional fuels [7]. In the US, energy consumption is almost 14 % of total energy required in residential applications as shown in Fig. 2.3. The lighting contribution is approximately 11 % of building energy consumption [8] as shown in Fig. 2.4.

Approximately 20–40 % of the total energy consumption of the building is due to lighting; hence, it is a prime source of carbon emission in buildings [9, 10]. Various researchers and architects have proved that the daylighting is also a good solution for illumination in buildings (through windows, skylights, wind tunnel, etc.) and for saving electrical energy based on fossil fuels during the daytime.

Daylight is the visible part of solar radiation as perceived by the human eye. It is composed of a spectral power distribution (SPD) of electromagnetic radiation in the
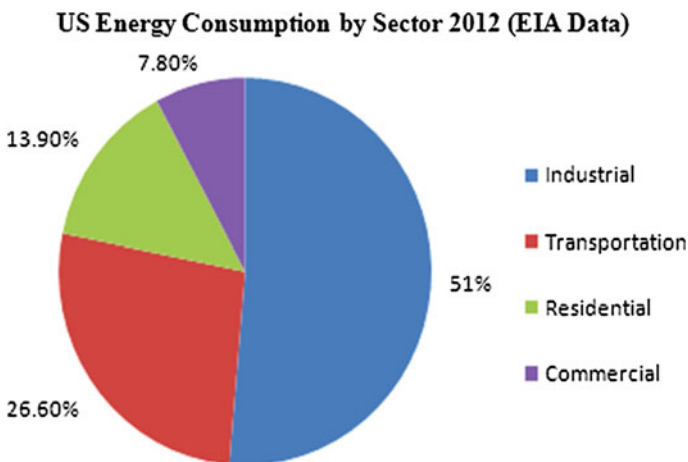
Fig. 2.3 Energy consumption by different sectors

US Building Sector Expenditures, March 2012

6.7%

16.3%

22.7%

2.2%

2.7%

2.8%

3.6%

4.7%

6.0%

9.6%

11.0%

11.6%

■ Space Heating (3)
■ Space Cooling
■ Lighting
■ Water Heating
■ Refrigeration (4)
■ Computers
■ Wet Cleaning (7)
■ Cooking
■ Other (8)
■ Adjust to SEDS (9)
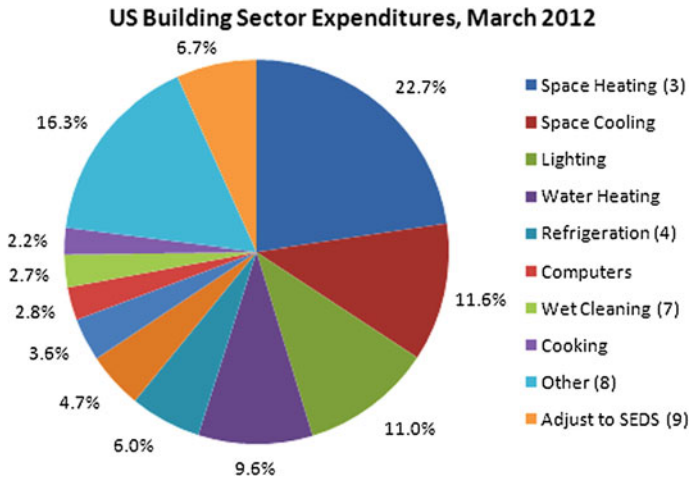
Fig. 2.4 Energy consumption by building equipment

visible wavelength range (0.38–0.78 µm) of solar radiation [11]. Daylight is one of the cheapest and efficient ways of using solar energy in buildings. Architects and building designers are also concerned about energy conservation in buildings due to the use of daylight [12]. It is reported that daylighting improves student performance and health in schools [11] because natural light gives more comfort and is beneficial for human health. With smart control systems, the use of conventional lighting can be considerably reduced and even eliminated inside a community center or office building. Daylight proportion can vary due to the structure of the house or building because the position, direction, and area of the windows play major factor in influencing the amount of natural light inside a room of a house.

Nevertheless, arrangements made for daylighting have direct and indirect impacts on the heating and cooling loads of building [13]. The optimization of daylight has been studied by many researchers [14–16]. The effects of daylighting optimization on thermal loads are also presented in the literature [17]. Some material-based optimization solutions with innovative approaches for lighting energy savings have also been reported [18–20].

The approach adopted for the optimization of daylighting inside a building must be as universal as much as possible so that it can be applicable to most of the building [21]. For the prediction of daylighting, building-simulation software [22] can be used. The annual variation in the availability of daylight at any place is important, particularly for daylight optimization for the annual performance of building [23, 24]. Stokes et al. [25] presented a simple model for the estimation of daylight throughout the year. The existing building can be retrofitted for the inclusion of daylighting concepts; a study regarding the economic analysis of retrofits has been performed by Mahlia et al. [26]. The amount of daylight inside a building strongly depends on the building design and the materials used for the openings for daylighting. Orientation of the living space with respect to light source, geometry of the

living space, optical properties of interior surfaces of the living space, obstructions outside the room, and optical characteristics of glazing play a major role in harnessing daylight [27]. The daylight coefficient for complex fenestration has been examined, and it was concluded that the daylight coefficient does not depend on luminance distribution in the sky [28, 29]. The illuminance level from natural light has been estimated by Rosa et al. [30] for overcast sky conditions.

2.3 Components of Daylighting (Natural Light)

2.3.1 Daylight Factor (DF)

The estimation of illuminance inside a living space can be predicted by an expression for the daylight factor, which is given by

$$DF = SC + ERC + IRC \tag{2.1}$$

where SC, ERC, and IRC are the sky, external, and internal reflection components falling on a building as shown in Fig. 2.5a. The sky component (SC) is the sum of beam and diffuse solar radiation coming from the Sun and the external (ERC) and internal (IRC) reflection components that are only beam/direct solar radiation coming from the Sun due to its direction.

The daylight factor (DF) is a guideline to determine the quantitative suitability (characteristic) of daylight in a particular room (work space) in terms of illuminance (lux). Based on this, there can be some changes in the design of the working space through the size of the windows.

2.3.2 Daylight Factor Due to Sky Components

The daylight factor due to the sky component (SC) is a ratio of inside illuminance, L_i (lux), on the horizontal work plane and outside diffuse illuminance, L_o (lux), on a horizontal surface.

$$SC = \frac{L_i}{L_o} \tag{2.2a}$$

In terms of percentage, it is expressed as follows:

$$SC = \frac{L_i}{L_o} \times 100 \tag{2.2b}$$
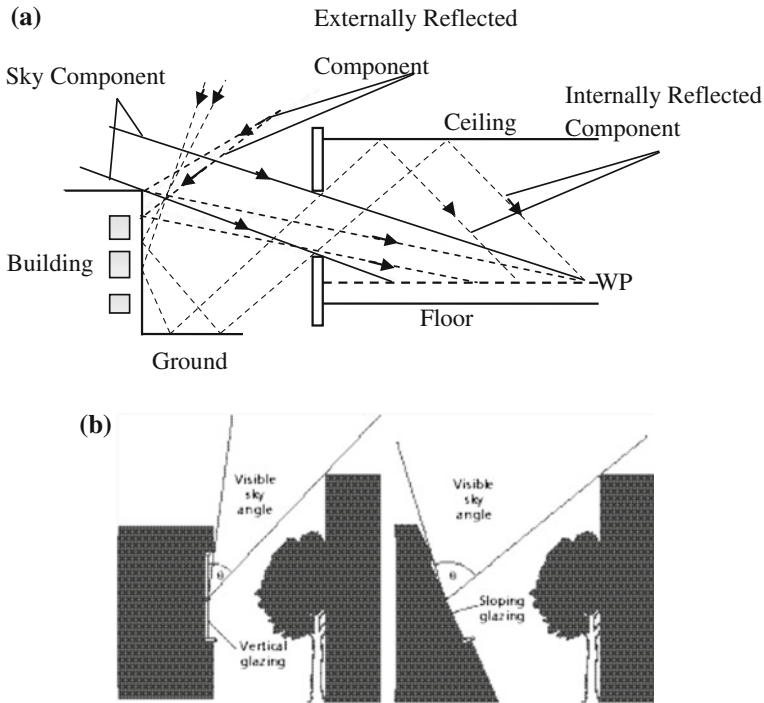
Fig. 2.5 a Different components of the daylight factor. **b** Obstruction and visible sky angle

The daylight factor for a skylight integrated with a vertical window in a building at ground level was developed by Chartered Institute of Building Services Engineers (CIBSE) [10] as follows:

$$\text{SC} = \left[\frac{L_i}{L_o}\right] = \left[\frac{\tau \times A_w \times \theta \times O_F \times M}{A \times (1 - R^2)}\right] \tag{2.3}$$

Equation (2.3) is applicable to CIE overcast conditions (completely cloudless conditions, weather condition '**a**' as described in Chap. 1). Furthermore, the Chartered Institute of Building Services Engineers (CIBSE) is denoted SC by DF because they have not considered external (REC) and internal (IRC) reflection components falling on a building where:

- τ is the transmittance of window materials ($\tau = 0.8$, and 0.7 for single- and double-glazed clear glass, respectively). This also depends on the thickness of the window materials. The numerical value of τ decreases with an increase in the thickness of the window materials.
- A_w is the area a window in m^2, which is inversely proportional to τ.

- θ is the visible-sky angle as shown in Fig. 2.5b, which is approximately written as,

$$\theta = 90 - \text{Obstruction angle} \qquad (2.4)$$

The previous equation is valid for a window without an above-situated overhang. If there is no obstruction, then $\theta = 90°$. The values of θ for different obstruction angle are given below:

Obstruction angle (degree)	0	20	40	60	80	90
θ (degree)	90	70	50	30	20	0

- R is the area-weighted average reflectance ($R = 0.6$ for a white wall, 0.5 for a medium-white wall, and 0.4 for a dark wall). High reflectance confers a double benefit, namely, (i) an increase in daylight factor and (ii) improvement in the distribution of daylight.
- A is the total area of the interior surfaces (including ceiling, floor, walls, and windows).
- M is the maintenance factor, which is generally considered to be <0.88.
- O_F is the orientation factor for glazing ($0.77 \leq O_F \leq 1.20$). For a vertical window facing north–south, the value of O_F is 0.77 and 1.20, respectively; otherwise $O_F = 1$ for a vertical east–west window.

The various parameters in Eq. (2.3) were tabulated with their numerical values for skylight components (SC) in an experimental dome-shaped mud house for a working place at the centre of the floor at IIT Delhi (Fig. 2.6) in Table 2.1. The left-hand side of Fig. 2.6 is a view of the sky component at the top of the mud house in a conical shape, and the right-hand side is the view of the central table as a working place. The conical shape at the top of the dome has been considered equivalent to a vertical window. In this case, an external reflection component (ERC) falling on the building can be neglected.

Equation (2.3) was modified by Chel et al. [31] by considering the effect of height (of a workplace from the floor of mud house) and the time of day ω, Eq. (1.9b). The modified daylight factor for the sky component (SC) is given as follows:

$$\text{SC} = \left[\frac{L_i}{L_o}\right] \times 100 = \left[\frac{\tau \times M \times A_w \times \theta \times O_F}{A_t \times (1 - R_f^2)}\right] \times \left(1 + \frac{h}{H}\right)^m (\cos\theta_z)^n \qquad (2.5a)$$

where h, the vertical height of the table in the workplace above the floor surface inside the skylight-integrated living space (dome structure); H is the central height of the dome and M ($0.5 \leq M \leq 0.9$) is the correction factor for glazing due to dust, etc. In this case too, Chel et al. [31] also did not consider the external (REC) and internal (IRC) reflection components falling on the building because DF is replaced by SC.

Fig. 2.6 Skylight components (SC) in experimental dome-shaped mud house for working place at the centre of floor at IIT Delhi

Table 2.1 Parametric values considered for daylight-factor evaluation

Sr. no.	Parameter	Value	Sr. no.	Parameter	Value
1	Total area of room surfaces in large dome (A_t, m^2)	80	8	Total area of room surfaces in small dome (A_t, m^2)	25
2	Floor area of large dome (A_f, m^2)	26	9	Floor area of small dome (A_f, m^2)	5
3	Transmittance of glazing (τ)	0.8	10	Vertical angle of visible sky from horizon (θ, degrees)	90
4	Correction factor for glazing due to poor maintenance/dust ($0.5 \leq M \leq 0.9$)	0.6	11	Vertical height of work plane above floor surface (h, m) [0, 0.75, 1.5 m]	0, 0.75, 1.5
5	Orientation factor for glazing ($0.97 \leq O_F \leq 1.55$)	1	12	Average reflectance of all room surfaces ($0 \leq R_f \leq 1$)	0.3
6	Total area of glazing (A_g, m^2) for large dome	2.6	13	Total area of glazing (A_g, m^2) for small dome	1.5
7	Ballast factor (B_F)	0.9	14	Artificial light luminous efficacy (ε, lm/W) (CFL lamp)	40

Equation (2.5a) needs further modification for vertical windows with reference to Fig. 2.1 as follows:

$$SC = \left[\frac{L_i}{L_o}\right] = \left[\frac{\tau \times A_w \times \theta \times M \times O_F}{A_t \times \left(1 - R_f^2\right)}\right] \times \left(1 + \frac{h}{d}\right)^m (\cos \theta_i)^n \qquad (2.5b)$$

where h, the mid-height of the window, and d is normal distance from the window and

$$\cos \theta_i = \sin \varphi \cos \gamma \cos \delta \cos \omega + \cos \delta \sin \omega \sin \gamma - \sin \delta \cos \varphi \cos \gamma$$

The above equation, obtained from Eq. (1.10) for $\beta = 90°$ (vertical windows) takes care of orientation (γ), Table 1.3, and the shading effect due to a nearby building/obstruction. The values of γ for east-, south-, west-, and north-facing windows can be considered as $-90°$, $0°$, $90°$, and $\pm 180°$, respectively. For a south-facing vertical window $\beta = 90°$ and $\gamma = 0°$, and then the form of Eq. (2.5) is the same as Eq. (2.4).

Equation (2.5b) is currently modified because Eq. (2.3) developed by CIBSE [10] was expressed as a fraction and not as a percentage.

The constants 'm' and 'n' are determined by regression method using experimental values of inside and outside luminance.

After taking the log of both side of Eq. (2.5), one gets

$$\ln\left[\frac{L_i}{L_o}\right] = [n \times \ln(\cos \theta_i)] + \left[m \times \ln\left(1 + \frac{h}{d}\right) + \ln\left[\frac{\tau \times A_w \times \theta \times M \times O_F}{A_t \times \left(1 - R_f^2\right)}\right]\right]$$

$$(2.6)$$

The previous equation is a linear equation and can be rewritten as:

$$y = m'x + c \qquad (2.7)$$

where $y = \ln\left[\frac{L_i}{L_o}\right]$, $x = \ln(\cos \theta_i)$ and $c = \left[m \times \ln\left(1 + \frac{h}{d}\right) + \ln\left[\frac{\tau \times A_w \times \theta \times M \times O_F}{A_t \times \left(1 - R_f^2\right)}\right]\right]$

Here, $m' = n =$ slope of line and $c =$ intercept of line on y axis

or

$$m = \frac{\left[c - \ln\left[\frac{\tau \times A_w \times \theta \times M \times O_F}{A_t \times \left(1 - R_f^2\right)}\right]\right]}{\ln\left(1 + \frac{h}{d}\right)} \quad \text{and} \quad m' = n \qquad (2.8)$$

After knowing 'm' and 'n', the inside luminance (L_i) in lux can be obtained for the given outside luminance by using Eq. (2.5b).

Sudan et al. [42] further modified the model developed by Chel et al. [31] by considering the effect of tilt, location (latitude), orientation of the window, and position of a point of interest inside the living space:

$$\mathrm{DF} = \left(\frac{L_{\mathrm{i}}}{L_{\mathrm{o}}}\right) \times 100 = \left[\frac{\tau \times A_{\mathrm{g}} \times M \times \theta}{A_{\mathrm{t}} \times (1 - R^2)}\right] \times \left[1 + \frac{L}{2l}(\cos\theta_w)\right]^q \times (1 + \cos\theta_i)$$
$$(2.8a)$$

where θ_{w} is the angle between a line connecting point of interest with the centre of the window and the perpendicular axis from the window directing inside the room. The term $(L/2l)\cos\theta_{\mathrm{w}}$ gives the three-dimensional variation of DF. The value of $\cos\theta_{\mathrm{w}}$ can be given in terms of length, width, and height of the point of interest from the centre of the window. After substitution, Eq. (2.8a) becomes

$$\mathrm{DF} = \left(\frac{L_{\mathrm{i}}}{L_{\mathrm{o}}}\right) \times 100$$
$$= \left[\frac{\tau \times A_{\mathrm{g}} \times M \times \theta}{A_{\mathrm{t}} \times (1 - R^2)}\right] \times \left[1 + \frac{L}{2}\left(\frac{1}{\sqrt{l^2 + h_{\mathrm{cw}}^2 + w^2}}\right)\right]^q \times (1 + \cos\theta_i) \quad (2.8b)$$

where, L, l, and w are the total length of a room, perpendicular length of a given point from the window (m), and perpendicular length of a given point from the perpendicular axis along the width axis of the wall window (m), respectively. The unknown constant q, known as model exponent in Eq. (2.8a), can be found by regression method using the experimental data as follows:

$$q = \frac{\ln\left[\frac{\mathrm{DF} \times A_{\mathrm{t}} \times (1 - R^2)}{(1 + \cos\theta_i) \times \tau \times A_{\mathrm{g}} \times M \times \theta}\right]}{\ln\left[1 + \frac{L}{2}\left(\frac{1}{\sqrt{l^2 + h_{\mathrm{cw}}^2 + w^2}}\right)\right]}$$
$$(2.8c)$$

2.3.3   Daylight Factor Due to External Reflection Components (ERC)

External reflection components (ERC) will be zero if the building is not surrounded by any outside obstruction as shown in Fig. 2.6. In the presence of any outside obstruction, there will be a non-zero ERC value. To obtain this value, one can use the following expression for a window with inclination of β for an overcast sky,

$$\mathrm{ERC} = 0.2 \times \left(\frac{1 + \cos\beta}{2}\right) \times \mathrm{SC}$$
$$(2.9a)$$

For any inclination (β), the factor 0.20 is incorporated, which is generally considered equivalent to the reflection coefficient of the surrounding.

$$\text{For a vertical window, } (\beta = 90°), \quad \text{ERC} = 0.1 \text{ SC} \tag{2.9b}$$

2.3.4 Daylight Factor Due to Internal Reflection Components (IRC)

For vertical window, the average internal reflection (IRC) is determined using the following formula:

$$\text{IRC} = \frac{\tau \times A_{\text{w}}}{A(1-R)}[CR_{\text{fw}} + 5R_{\text{cw}}] \tag{2.10}$$

Here, R_{fw} is the weighted reflectance due to floor and lower height (from the centre of window) of the window; R_{cw} is the weighted reflectance due to the ceiling and upper height (from the centre of window) of the window; and τ, A_{w}, A, and R are the same as defined in Eq. (2.3), for a dome-type mud-house construction, $R_{\text{cw}} > R_{\text{fw}}$. Due to the poor reflectance of the floor, it may be slightly higher.

The coefficient 'C' of Eq. (2.10) can be expressed as follows [10, 33]:

$$C = \left[40 - \frac{\text{angle of obstruction}}{2}\right] \tag{2.10a}$$

$$= \left[40 - \frac{\arctan\left\{\left(\frac{h_1 - h_2}{2}\right)/d\right\}}{2}\right] \tag{2.10b}$$

$$= \frac{\theta}{2} - 5 \tag{2.10c}$$

where θ is given by Eq. (2.4).

Furthermore, the value of C for a different obstruction angle is also given in Table 2.2 [32].

The weighted reflectance can be obtained as

$$R_{\text{w}} = \frac{\sum_{i=1}^{n} A_i R_i}{\sum_{i=1}^{n} A_i} \tag{2.11}$$

Table 2.2 The values of coefficient 'C'

Obstruction angle	0	10	20	30	40	50	60	70	80
Coefficient 'C'	39	35	31	25	20	14	10	7	5

2.4   Different Concept of Daylighting

Generally, most conventional buildings have vertical windows in walls depending on the availability of solar flux on the wall. However, there are many other concepts to have natural daylight in a living space. These are as follows:

2.4.1   Modern Sky Light

Skylights are a light-transmitting fenestration from outside a building into a building living space through the roof as shown in Fig. 2.7a. It can be fixed or

Fig. 2.7   a View of skylight on inclined roof of a building. **b** A pair of skylights installed in a cathedral ceiling
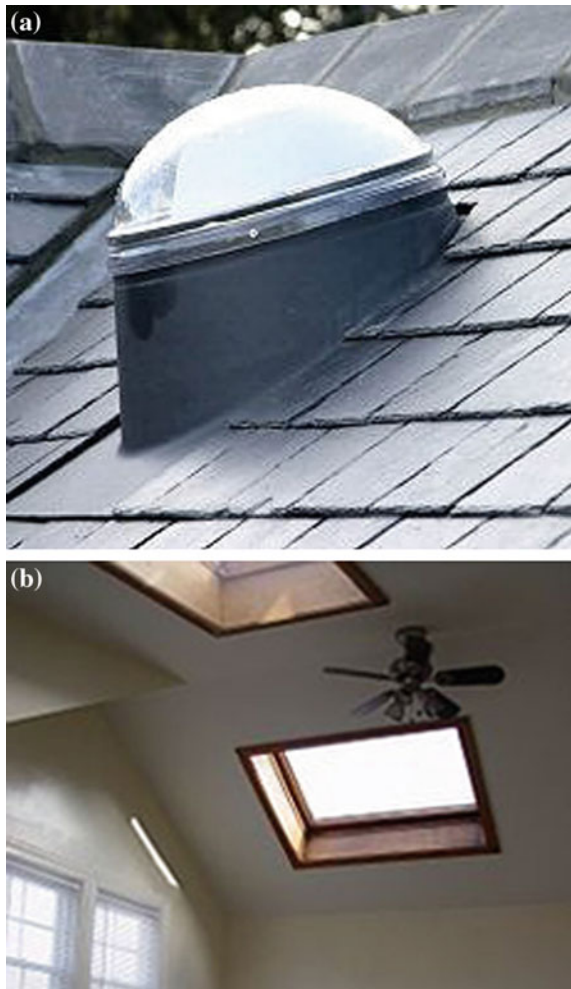
operable (for ventilation) glazing area on the roof of a building. Unit skylights and the sloped glazing in the centre of the roof are used to convey abundant daylight or top lighting into a living space. A skylight, if operable, can also serve for ventilating fresh air inside the building able.

   The structure to be installed (fixed or operable) on a skylight opening is termed "unit skylight." It is made from transparent glass or plastic (fixed with frame) in different shapes and sizes as per the building requirement.

2.4.2   Solar Pipe (SP)/Light Tube

Solar pipes/light tubes have less surface area exposed for heat transfer; therefore, the use of solar pipes reduces heat transfer from the outside environment. In addition, they provide light on a focused area (Fig. 2.8) of interior space of a building.

2.4.3   Semitransparent Solar Photovoltaic Lighting System (SSPLS)

In this case, a semitransparent photovoltaic (PV) (Sect. 4.4.1) module with a reasonable nonpacking factor (NPF) is considered. A set of semitransparent
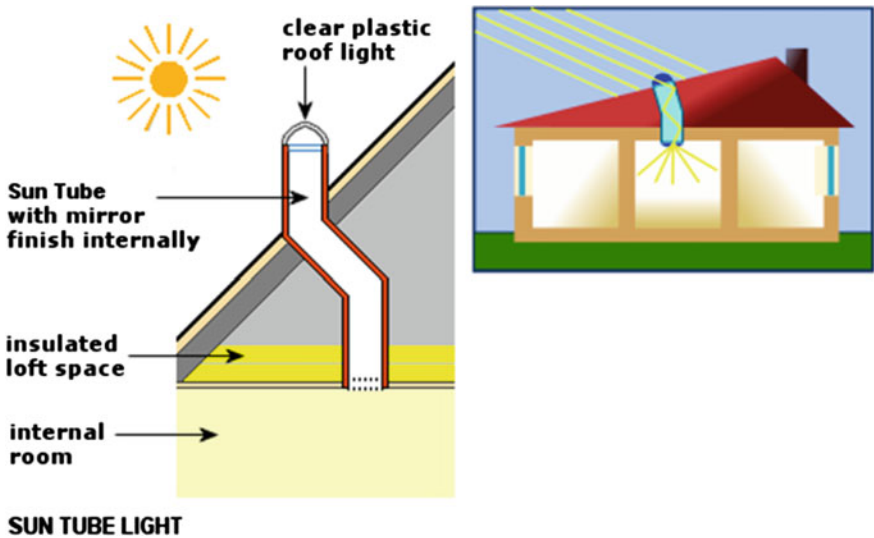
Fig. 2.8 View of solar pipe/light tube/tubular daylighting device (TDD)

Fig. 2.9 View of roof-integrated semitransparent photovoltaic (PV) module

photovoltaic (PV) modules connected in series and parallel combination is integrated with an inclined roof to receive the maximum solar radiation for daylighting and electrical power required by the building as shown in Fig. 2.9. There is a daylighting effect inside the building through the nonpacking area of the PV module. Such roof- integrated semitransparent photovoltaic (PV) modules also provided a greenhouse effect, which can be used for many applications such as

  (i) Daylighting
 (ii) Solar crop-drying
(iii) Sun bath
(iv) Electrical power

2.4.4 Light Shelves

Light shelves are an effective way to enhance the daylighting provided through windows on a wall exposed to incoming solar radiation. A highly reflective metal light shelf is attached to the outside of the window at the top as shown in Fig. 2.10. This arrangement with the window will protect direct solar radiation coming into the living space during summer season due to projection.

This arrangement is also referred as a "light shelf." Solar radiation falling on a light shelf is reflected toward the ceiling of the living space; some radiation will be absorbed (responsible for heating of ceiling an undesirable situation in the summer), and the rest will be reflected back to the living space and illuminate the living area. In case of intense solar radiation, glare-control techniques are needed for proper daylighting.

Fig. 2.10   View of light shelves integrated into a wall of a building

2.4.5   *Light Reflector*

Figure 2.11 shows the manually adjustable **light reflector**, which was mostly used in office buildings in past. Currently it is seldom used. The adjustment of the reflector depends on the season in order to have maximum daylighting into a living space.

Fig. 2.11   View of adjustable light reflector attached to an exposed window
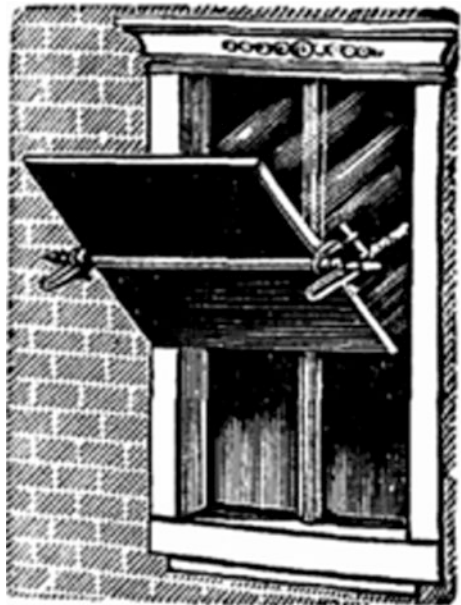
2.4.6 Tubular Daylighting Devices (TDDs)

Tubular daylighting devices (**TDDs**) are devices that provide daylight through tubes integrated with walls or the roof of the building. These tubes collect daylight from a transparent dome structure mounted on them. TDDs can be a simple tube with a high reflective coating or filled with bundles of optical fibers. The daylight carried by TDDs is distributed using a diffuser assembly for the homogeneous distribution of light in a whole living area. These devices are promising techniques to provide daylighting in multistory residential and commercial buildings.

2.4.7 Sawtooth Roof

A sawtooth roof is very old concept used in old factories for using daylight inside the building. It is an arrangement of vertical glass opposite the exposed area of the roof. A sawtooth roof allows diffuse solar radiation. The prime disadvantage of these structures is that the exposed area increases unwanted thermal losses during winter seasons because it allows loss of thermal energy from the exposed glass.

2.4.8 Heliostats

A heliostat, as shown in Fig. 2.12, is a mirror that rotates with the motion of the Sun. The heliostat move in phase with the direction of the Sun and reflects solar radiation in a single direction. These advanced technology devices are used to shine the glazed portion of the building such as the window, a skylight (Fig. 2.7), and tight tubes (Fig. 2.8). The light received from these glazed portions is further used

Fig. 2.12 View of a heliostat mirror

to illuminate the interiors of a room. A heliostat is more energy efficient technique because it uses maximum available solar radiation throughout day.

2.4.9 Smart-Glass Window

The glazing window made of smart-glass materials is known as a smart-glass window. Smart-glass is a material that changes its optical properties significantly on application of a voltage to the material or by applying some mechanical treatment. These materials can behave as a transparent glass sheet or as a reflective surface or retro-reflective surface with a variation of voltage or mechanical treatment. Therefore, these materials can be tuned per the daylighting requirement inside the living space.

2.4.10 Fiber-Optic Concrete Wall (FOCW)

Fiber-optic concrete wall/translucent concrete wall, also known as a **light-transmitting concrete wall**, is made of enhanced light-transmitting building materials having compatibility with concrete. These materials are embedded with optical fiber cables as shown in Fig. 2.13. Solar radiation falls on the outer portion of the fiber-optic concrete wall and is captured by the optical fiber cables and transmitted to the inner space of the wall. The quantity and quality of the daylight in living space depend on the material as well as other structural properties of the optical fiber.

Light-transmitting concretes are mainly used on windows and the interior surface of walls. These materials are made by mixing fine-grain concrete (approximately 95 %) with optical fiber cables (approximately 5 %). After casting processes, these translucent concretes can be cut in the desired shape and sizes per

Fig. 2.13 View of translucent concrete wall at Expo Bau 2011, München/Germany

the building requirement using advanced machines. The mounting of translucent concrete structures on the façade and walls of the building must be performed in such a way that it results in a uniform distribution of day/artificial lighting inside living area.

2.4.11 Hybrid Solar Lighting (HSL)

Hybrid solar lighting was developed by the Oak Ridge National Laboratory (ORNL). This technology can eliminate the requirement for artificial light during day time. Hybrid solar-lighting system comprise a light-collector system mounted on the roof of building, optical fiber cables, and fluorescent lighting fixtures with transparent rods attached to optical fiber cables.

During evening hours, when the intensity of the sunlight decreases, fluorescent fixtures gradually turn on and maintain a nearly constant luminance level in the interior space. At night hours, the fluorescent lighting system is electronically operated. The cost of these systems is a major concern that must be addressed. In near future, hybrid solar lighting may become a promising technology for daylighting.

2.4.12 Solarium

A solarium is a glass house attached to a building having orientation toward either the south in northern hemisphere or the north in southern hemisphere to receive the maximum solar radiation. In this case, the partition opaque wall between the solarium and the building can have a provision of (i) glazed window (Fig. 2.1), (ii) smart glass window, and (iii) Fiber-optic concrete wall (FOCW), (Fig. 2.13) for daylighting. In addition to daylighting, the solarium can be used for many other applications such as (i) daylighting (ii), sun bath, and (iii) heating of the attached room, etc. There can be another application for producing electricity if glass materials are replaced by a semitransparent photovoltaic module as shown in Fig. 2.9.

2.5 Experiments on Skylight for Natural Lighting for a Mud House: A Case Study [34]

2.5.1 Experimental Results

Most of the studies on skylights have been performed for houses with octagonal-pyramid and/or conical dome-shaped roofs. In the present case study, experiments have been performed for a mud house having an octagonal-shaped
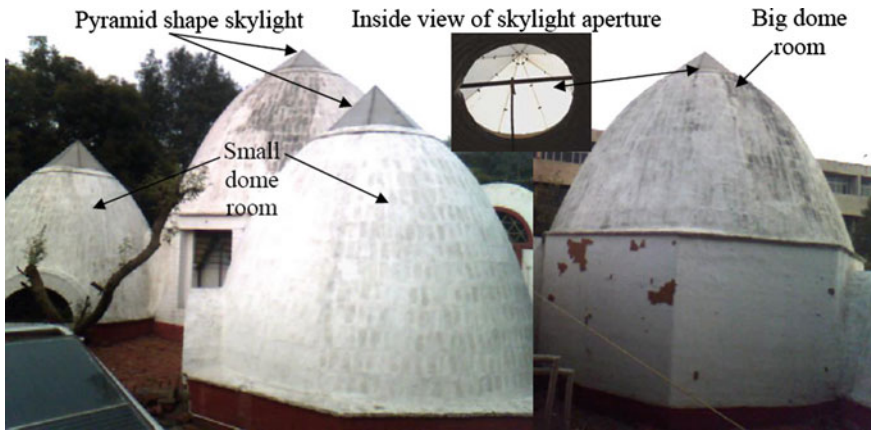
Fig. 2.14 Photograph of octagonal pyramid-shaped skylight for existing dome-shaped buildings: one large and two small-domes rooms

dome-structure roof as shown in Fig. 2.14. Hourly illuminance levels were recorded from 7 a.m. to 5 p.m. inside two rooms having different surface areas of skylight. The view of the large dome and the small dome are also shown in Fig. 2.14. The large dome with the skylight had a conference room with a conference table as shown in Fig. 2.6. Luxmeter (least count = 1 lx; accuracy ±6 % of reading ±1 minimum effective digit; range 0–999,000 lx) was used to record the hourly illuminance inside the rooms at the floor and planes >0.75- and 1.5-m heights from the floor. Hourly variations of global and diffuse radiations were also recorded using same luxmeter. A calibrated glass thermometer was used to measure the ambient air and room air temperature. Experimental observations inferred that the luminance levels inside the rooms were different at different heights from the floor surface. In addition, the luminance level was different for different times (winter or summer) of the year. However, only the results for winter (sun at low altitude) are shown in Fig. 2.15.

Figure 2.15a shows the hourly variation of outside illuminance in lux and solar flux in W/m^2 including the diffuse component for each case for a typical clear day in winter. It can be observed from this figure that 1 W/m$^2 \cong 100$ lx. Furthermore, it should be noted that the ratio of diffuse to total radiation is <0.25, which requires clear-/blue-sky conditions (Sect. 1.2.6) for better daylighting.

The hourly illuminance inside the small and the large dome at a height of (i) 0 cm (floor) (ii) 75 cm from the floor and (iii) 150 cm from the floor is shown in Fig. 2.15b. It is observed that the level of illumination increases with height in the small as well as the large dome due to the decrease in distance between the skylight and the point of observation as expected. It can also be observed that the illumination level in the large dome has a lower value compared with that of the small

(a)

Outside Illuminance on January 19, 2008

(b)   **Illuminance inside big and small dome rooms on January 19, 2008**
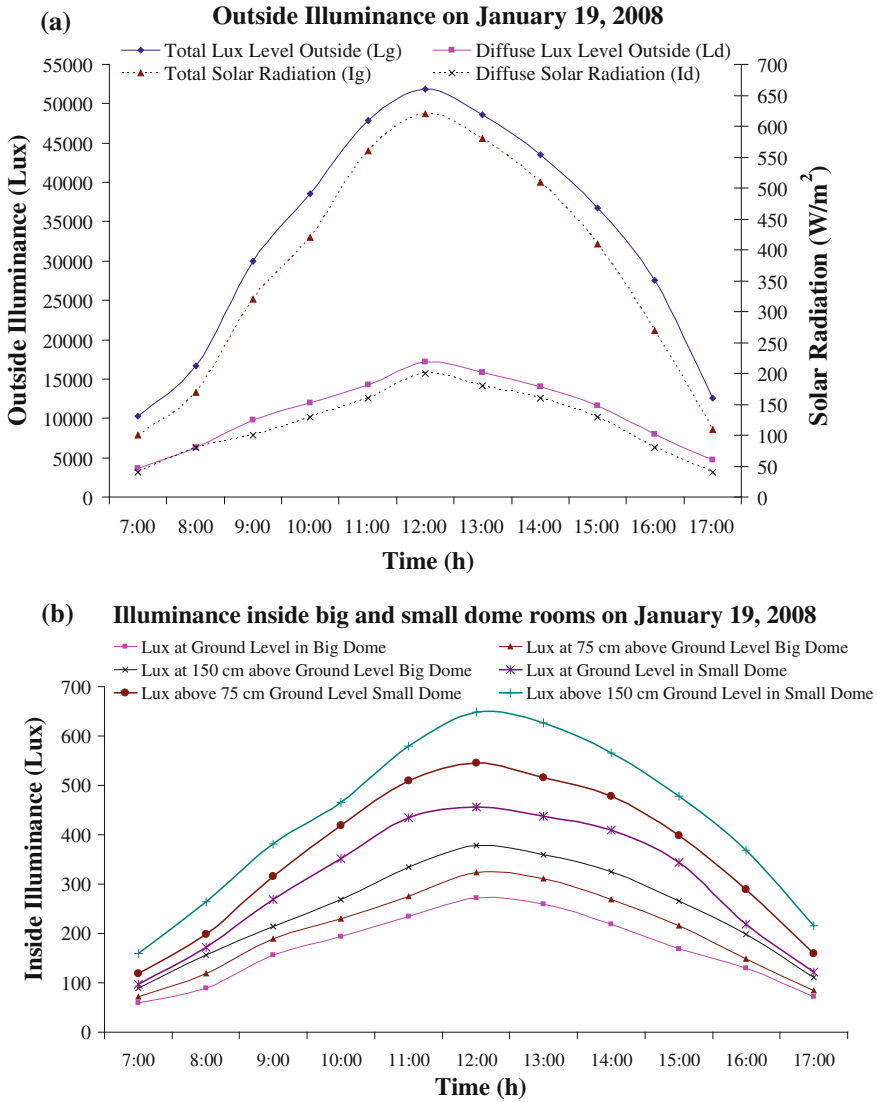
Fig. 2.15 a Outside illuminance at a horizontal surface on January 19, 2008. **b** Inside illuminance at three horizontal work planes on January 19, 2008

dome due to (i) the larger floor area and (ii) the larger distance between the skylight and the point of observation.

The dome-structure rooms in present study have been used for harnessing natural light inside an office building from a skylight. Various training programs,
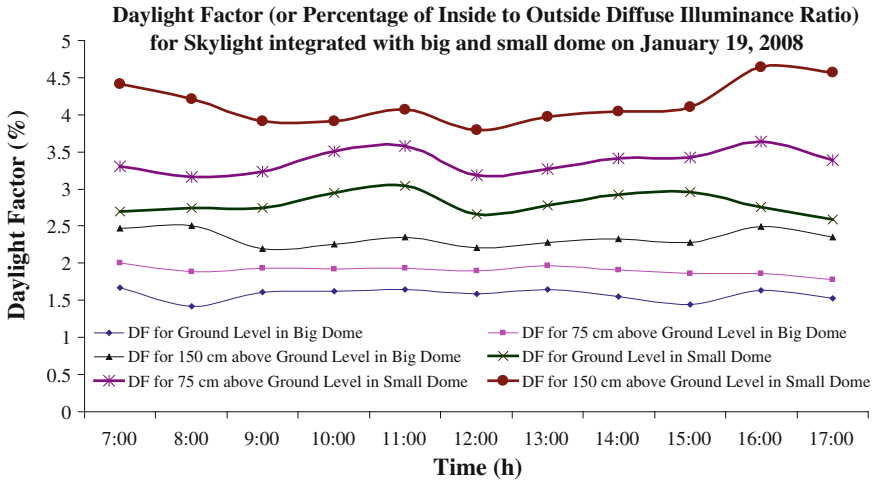
Fig. 2.16 Experimental daylight factor for the same building on January 19, 2008

seminars, and conferences have been performed at this site to show the practical utility of these structures under real operating conditions.

The illuminance level at the floor of the rooms varies from 100 to 250 lx for a large-domed room and 200 to 400 lx for a small-dome room (Fig. 2.15) in month of January. The illuminance levels inside the rooms were suitable for office (working hours) activities.

The experimental hourly values of the daylight factor (DF in %) due to skylight condition can be determined by using Eq. (2.2) in terms of percentage. The results are shown in Fig. 2.16.

From Fig. 2.16, one can conclude the following:

(i) The daylight factor (DF) due to the skylight at top of small dome is maximum as expected.
(ii) The daylight factor (DF) due to the skylight for a large dome has a lower value compared with a small dome.

For daylighting in a large-domed mud house, the size of the skylight system should be increased and optimized.

2.5.2   Modeling of the Skylight for a Dome-Shaped Mud House

Performances of the skylight in both rooms have been evaluated by comparing the luminance level inside the room with the diffuse solar radiation outside the room.

In this case study, the performance of skylight was evaluated from theoretical analysis as well as from experimental observation.

2.5.2.1 Total Luminous Flux, ϕ (Lumen)

According to Jenkins and Newborough [35] the total luminous flux, (ϕ (lumen) needed from an artificial (electrical) lighting system to produce the desired level of illuminance (L_i(Lux or lumen/m^2)) on a horizontal working surface of area ($A_s(m^2)$) is given as follows:

$$\phi = \left[\frac{L_i A_s}{U_F M_F}\right] \tag{2.12}$$

The use factor (U_F) is the fraction of light actually falling on the working area. Its value depends on the dimension of the living area and varies between 0.5 and 0.7 for office buildings; the maintenance factor, M_F, depends on the life and working condition of the light source, and it varies from 0.7 to 0.9. For the horizontal surface of area A_s (m^2) and the measured illuminance level L_i, total luminous flux ϕ can be obtained using following relation:

$$\phi = [L_i \times A_s] \tag{2.13}$$

The electrical energy equivalent corresponding to total luminous flux (ϕ) can be found using Eq. (2.15). This equivalent electrical energy is the conservation of conventional energy due to the incorporation of a skylight in dome-shaped building. The recommended values of the illuminance level for various activities are listed in Table 2.3.

Table 2.3 Recommended illuminance for various activities

Activity	Illumination (lux, lm/m^2)
Public areas with dark surroundings	20–50
Simple orientation for short visits	50–100
Working areas where visual tasks are only occasionally performed	100–150
Warehouses, homes, theaters, archives	150
Easy office work, classes	250
Normal office work, pc work, study library, groceries, show rooms, laboratories	500
Supermarkets, mechanical workshops, office landscapes	750
Normal drawing work, detailed mechanical workshops, operation theatres	1000

2.5.2.2   Total Lighting Power, $P(W)$

Luminous efficacy ε_e (lm/W) is a measure of visible light produced by a light source. It is the ratio of **luminous flux** (ϕ) to **power** (**P**) and is mathematically expressed as

$$\varepsilon_e = (\text{lm/W}) = \phi/P \tag{2.14}$$

where ϕ can be obtained from Eq. (2.13). In the case of daylighting, power (P) is the solar radiation flux on the given area; for artificial light sources, power (P) is the electrical power consumed in a light source. In the case of daylighting, ε_e is also termed the "luminous efficacy" of solar radiation, and it is known as the luminous efficacy of the artificial source.

The luminous efficacy of an artificial source (electrical) reflects the ability of a source to convert electrical energy into visible light. The overall luminous efficacy depends on how efficiently the source generates electromagnetic radiation from electrical energy and to what degree the human eye is susceptible to the radiation emitted from the source. Luminous efficacy of solar radiation is a measure of visible light produced by electromagnetic radiation coming from the Sun.

The total electrical power savings $P(W)$ corresponding to the luminous flux for the measured illuminance level on a given horizontal surface can be obtained using the following equation [35]:

$$P(W) = \left[\frac{\phi}{B_F \times \varepsilon_e}\right] \tag{2.15}$$

where B_F is ballast factor.

Equation (2.15) can be used to evaluate the daily, monthly, and annual power consumed in kWh for a given illuminance.

Monthly and annual daylighting energy savings potential due to a skylight at the floor of large-domed mud house is shown in Fig. 2.17. It can be observed that the potential annual daylighting energy savings varies from 467 to 662 kWh. The average annual potential daylighting energy savings for a large-domed mud house is 564.5 kWh. The monthly energy savings in kWh is greater during the summer months (April–September) due to a high level of insolation. The monthly average energy savings in kWh is 70 during the summer months and 40.7 kWh during winter months. This indicates that the monthly average energy savings in kWh during the summer months 70 % higher than during the winter months (Fig. 2.18).

Similar trends were observed for a small-dome mud house. However, the potential annual daylighting energy savings varies from 169 to 239 kWh. Thus, the average annual potential daylighting energy savings for small-dome mud house is 204 kWh. It is also important to note that the average annual potential daylighting

Monthly Lighting Energy Saving Potential of Skylight for Illuminance on Mudhouse Floor in Big Dome

Annual Lighting Energy Saving Potential = 467 to 662 kWh/year
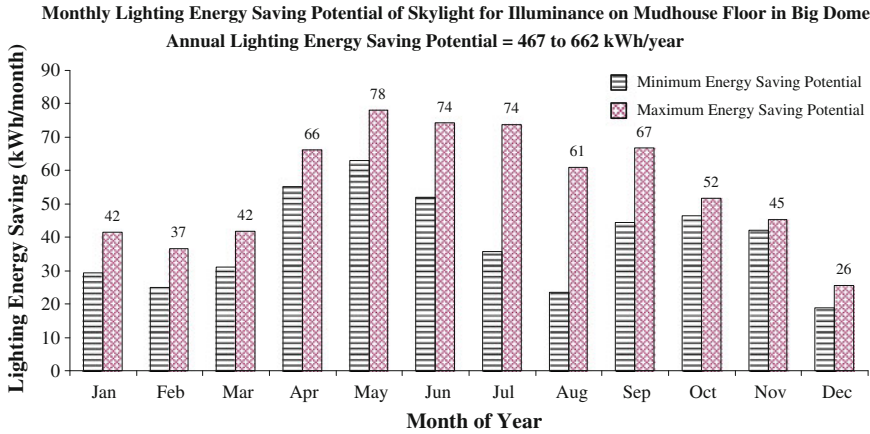
Fig. 2.17 Monthly lighting energy savings corresponding to illuminance at ground level inside room with a large-domed skylight

Monthly Lighting Energy Saving Potential of Skylight for Illuminance on Mudhouse Floor in Small Dome

Annual Lighting Energy Saving Potential = 169 to 239 kWh/year
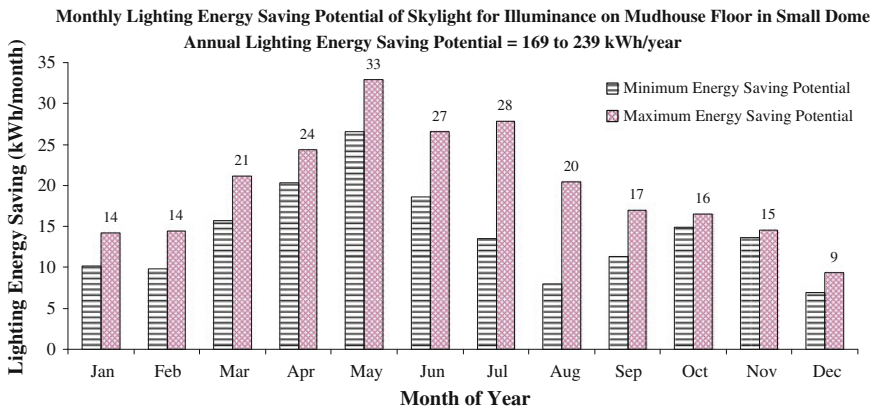
Fig. 2.18 Monthly lighting energy savings corresponding to illuminance at ground level inside a room with a small-domed skylight room

energy savings for a large-domed mud house is 177 % higher than the average annual potential daylighting energy savings for a small-dome mud house, which is in contrast to the illuminance parameter

Furthermore, the total annual potential daylighting energy savings in kWh for small-dome and large-domed mud houses were calculated for all weather conditions (type 'a' to type 'd', Sect. 1.2.6) for five different climatic condition in India, and the results are shown in Fig. 2.19. It is observed that the total annual daylighting energy savings in kWh for small-dome and large-domed mud houses for Srinagar is minimum due to the low level of insolation as well as sunshine hours.
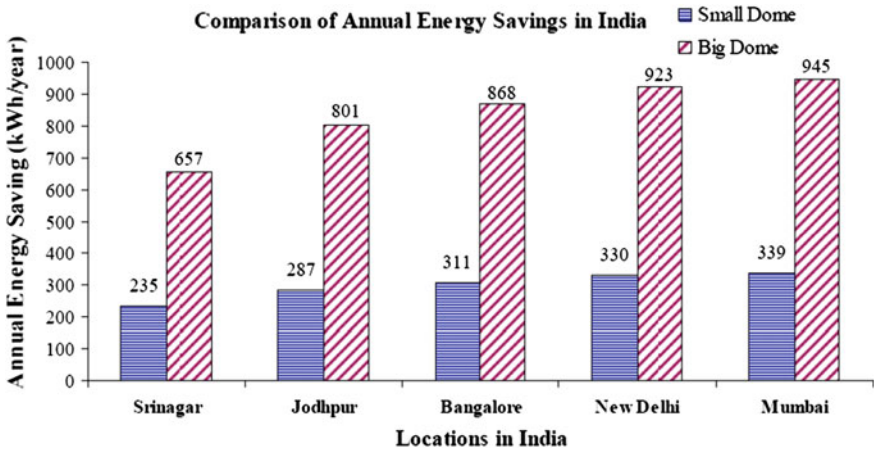
Fig. 2.19 Annual energy saving of skylight for small- and large-domed rooms in India, For $P_i = 5200$, $R = 4615$/year, $M = 2400$/year and $n = 50$ years

2.5.3 Life-Cycle Cost Analysis for Skylight in the Mud House

A similar analysis was used to determine the cost investment for a skylight over the domed roof structures of the mud house. There were annual energy savings for large and small domes of 923 and 339 kWh/year, respectively, which equals the respective annual rate of returns (R) Rs. 4615/year and Rs. 1695/year, respectively, with a unit energy savings cost of Rs. 5/kWh in India. There were total investments in skylight transparent diffuse glass (P_i) for 2.6 m^2 a large dome of Rs. 5200 and Rs. 1200 for a 1.5 m^2 glass area for the skylight, including labor costs, for making a pyramid-shaped skylight. Life-cycle cost analyses were performed for this skylight for different rates of interest. The annual minor maintenance of the mud-house skylight (M) was considered as Rs. 2400 for cleaning the skylight four times per month at rate of Rs. 50 per washing and cleaning. The end-of-life salvage value of the skylight glass was neglected with a 50-year lifetime for a pyramid-shaped skylight. The payback period for different interest rates were determined as shown in Fig. 2.20.

It can be seen that the payback period at lower rate of interest is minimum (2.5 years) as per expectation. Energy matrices of a building by using the day-lighting concept have also been studied by Sudan and Tiwari [36].
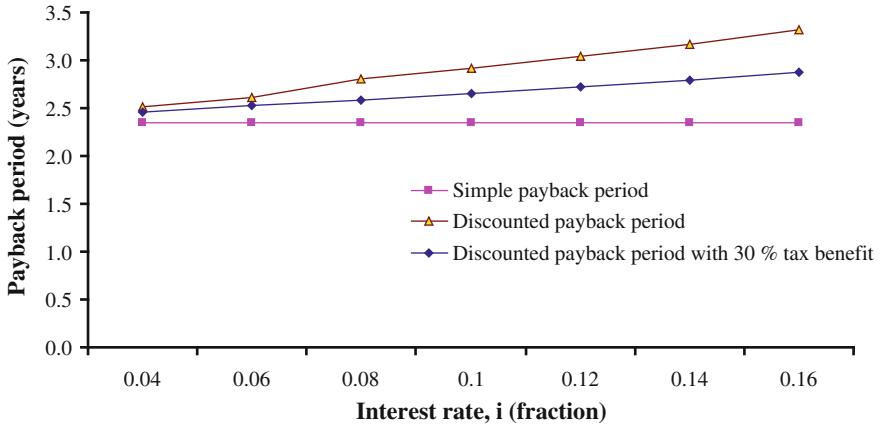
Fig. 2.20 Payback period, with interest rates, for investment in large-domed skylight

Solved Examples

Example 2.1 Calculate the sky components of the configuration given below for the following parameters by using The Building Research Establishment (BRE) Table 2.4:

Table 2.4 The BRE table for vertical glazed rectangular windows

h/d ratio ↓	Obstruction angle (degree)	h = height of window head above working plane; W = width of window to one side of normal; d = distance from window										
		W/d ratio →										
		0	0.2	0.4	0.6	0.8	1.0	1.2	1.4	1.6	2.0	∞
8		0.1	0.02	0.03	0.04	0.05	0.05	0.06	0.06	0.06	0.07	0.08
11		0.2	0.06	0.11	0.14	0.20	0.21	0.22	0.22	0.22	0.23	0.24
17		0.3	0.14	0.26	0.34	0.42	0.47	0.49	0.50	0.50	0.51	0.53
22		0.4	0.25	0.45	0.62	0.75	0.89	0.92	0.95	0.95	0.96	0.98
27		0.5	0.39	0.70	0.97	1.10	1.30	1.40	1.40	1.40	1.50	1.50
31		0.6	0.53	0.98	1.30	1.60	1.80	1.90	1.90	2.00	2.00	2.10
35		0.7	0.68	1.30	1.70	2.10	2.30	2.50	2.50	2.60	2.60	2.80
40		0.8	0.83	1.60	2.20	2.60	2.90	3.10	3.20	3.30	3.30	3.31
42		0.9	0.99	1.90	2.60	3.10	3.40	3.70	3.80	3.90	4.00	4.20
45		1.0	1.10	2.20	3.00	3.60	4.00	4.30	4.50	4.60	4.70	5.00
48		1.1	1.30	2.50	3.40	4.10	4.60	4.90	5.10	5.30	5.40	5.70
50		1.2	1.40	2.70	3.80	4.50	5.00	5.40	5.70	5.90	6.10	6.30
52		1.3	1.50	2.90	4.10	4.90	5.50	5.90	6.20	6.40	6.70	7.00
54		1.4	1.60	3.20	4.40	5.20	5.90	6.40	6.70	7.00	7.30	7.60
56		1.5	1.70	3.30	4.60	5.60	6.20	6.80	7.10	7.40	7.80	8.10
63		2.0	2.0	4.0	5.6	6.7	7.5	8.3	8.7	9.1	9.7	10.3
90		∞	2.5	4.9	6.9	8.4	9.6	10.7	11.6	12.2	13.0	15.0
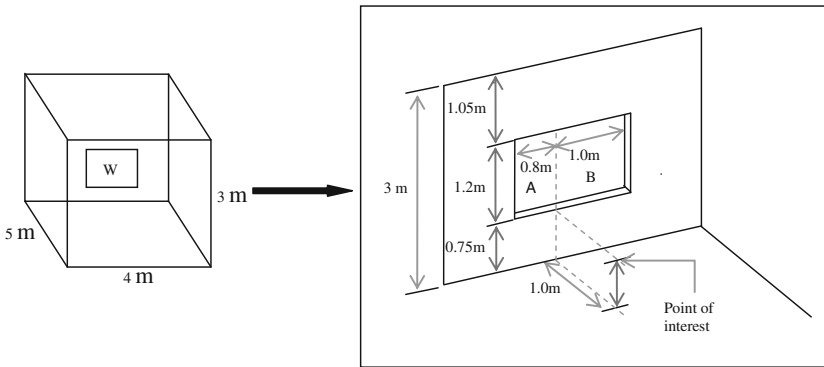
$h_1 = 1.95$ m, $h_2 = 0.75$ m, $W_1 = 0.8$ m, $W_2 = 1$ m and $d = 1$ m.

Solution

Sky component for window A (SC$_1$):

$$\frac{\text{Height of window}}{\text{Distance of point of interest from window}} = \frac{h_2 - h_1}{d} = \frac{1.95 - 0.75}{1} = 1.2$$

and $$\frac{\text{Width of window}}{\text{Distance of point of interest from window}} = \frac{W_1}{d} = \frac{0.8}{1} = 0.8$$

Using Table 2.4, the sky component for window A (SC$_1$) for 1.2 (y-axis) and 0.8 (x-axis) can be written as SC$_1 = 4.5$

Sky component for window B (SC$_2$):

$$\frac{\text{Height of window}}{\text{Distance of point of interest from window}} = \frac{h_2 - h_1}{d} = \frac{1.95 - 0.75}{1} = 1.2$$

and $$\frac{\text{Width of window}}{\text{Distance of point of interest from window}} = \frac{W_2}{d} = \frac{1}{1} = 1$$

Using Table 2.4, the sky component for window B (SC$_2$) for 1.2 (y-axis) and 1 (x-axis) can be written as SC$_2 = 5.0$.

Thus, the total sky component is given as $\text{SC} = \text{SC}_1 + \text{SC}_2 = 4.5 + 5.0 = 9.5\ \%$.

Example 2.2 Evaluate the sky component of Example 2.1 if a half portion of window A and window B is obstructed.

Solution

The sky component for the lower half of window A:

$$\frac{\text{Height of half window}}{\text{Distance of point of interest from window}} = \frac{(h_2 - h_1)/2}{d} = \frac{0.6}{1} = 0.6$$

Using Table 2.4.

The sky component for the half lower portion of window *A* for 0.6 (same *y*-axis) and 1 (same *x*-axis) = 1.6.

Similarly,

The sky component for the half lower portion of window *B* for 0.6 (*y*-axis) and 0.8 (same *x*-axis) = 1.8.

The sky component for the half upper portion of windows *A* and *B* = 9.5 − 1.6 − 1.8 = 6.1 %.

Example 2.3 Calculate the externally reflected component (ERC) of Example 2.2.

Solution

The sky component for the half lower portion of windows *A* and *B* = 1.6 + 1.8 = 3.4.

This sky component for the half lower portion of windows *A* and *B* is reflected from the obstruction back into building and can be evaluated from Eq. (2.9b) as

$$\text{ERC} = 0.1 \times 3.4 = 0.34$$

Example 2.4 Evaluate coefficient '*C*' for obstruction angle of 0°, 40°, and 90° and compare the results of Table 2.3.

Solution

From Eq. (2.10a), we have

$$C = \left[40 - \frac{0}{2}\right] = 40$$

$$C = \left[40 - \frac{40}{2}\right] = 20$$

$$C = \left[40 - \frac{90}{2}\right] = -5$$

From Eq. (2.10c), we have

$$C = \frac{90}{2} - 5 = 40$$

$$C = \frac{50}{2} - 5 = 20$$

$$C = \frac{0}{2} - 5 = -5$$

This suggests that both equations give same results, but its validity is only for obstructions <90°. The values of the calculated coefficient 'C' is nearly the same as reported in Table 2.3.

Example 2.5 Evaluate coefficient 'C' using Eq. (2.10b) for the following configuration.
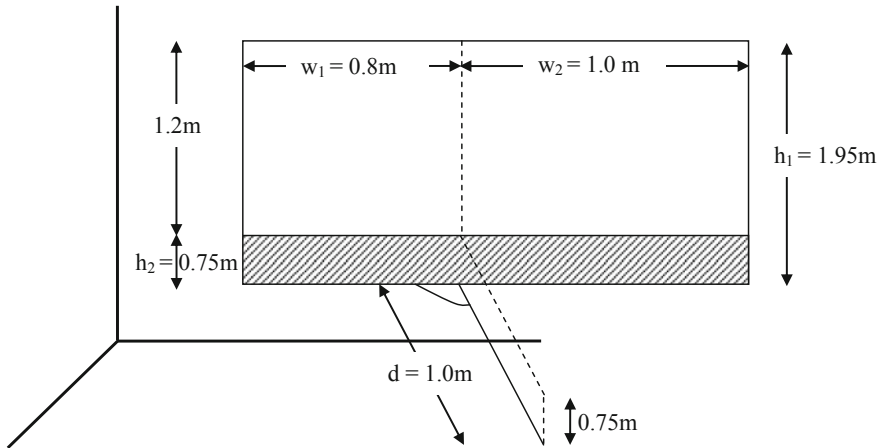
Solution
From Eq. (2.10b), we have

$$= \left[40 - \frac{\arctan\left\{\left(\frac{h_1 - h_2}{2}\right)/d\right\}}{2}\right]$$

Here, $h_1 - h_2 = 1.2$ m and $d = 1$ m.
For the above values, we have

$$C = \left[40 - \frac{\arctan 0.6}{2}\right] = 40 - \frac{30.96}{2} \cong 24.52$$

In this case, the value of coefficient 'C' depends mainly on the size of window and the point of observation unlike in Example 2.4.

Example 2.6 Evaluate the internally reflected component of a house having dimensions of 5 m × 4 m × 3 m with a window configuration of the same as in Example 2.1.

Solution

$$\text{Window area } (W) = \text{width} \times \text{height} = 1.8 \text{ m} \times 1.2 \text{ m} = 2.16 \text{ m}^2;$$
$$\text{Ceiling area} = \text{Floor area} = 4 \times 5 = 20 \text{ m}^2;$$

Height between the floor and the mid-height window

$$= \text{mid-height window} + \text{sill} = 0.6 + 0.75 = 1.35 \text{ m}$$

Height between the ceiling and the mid-height window

$$= \text{mid-height window} + \text{above window} = 0.6 + 1.05 = 1.65 \text{ m}$$

Total area of the side walls = perimeter × height

$$= (4 \times 3) \times 2 + (5 \times 3) \times 2 = 18 \text{ m} \times 3 \text{ m} = 54 \text{ m}^2$$

Total internal area of the roof/floor and walls (A)

$$= (4 \times 5) \times 2 + (4 \times 3) \times 2 + (5 \times 3) \times 2 = 94 \text{ m}^2$$

For various reflectance, namely, the ceiling $(R_C) = 0.70$, floor $(R_F) = 0.20$, window $(R_{W1}) = 0.10$, and the walls $(R_W) = 0.50$, the weighted average reflectance inside the building can be calculated by Eq. (2.11) as

$$R = \frac{20 \times 0.7 + 20 \times 0.2 + 2.16 \times 0.10 + (54 - 2.16) \times 0.5}{94} = 0.469$$

The weighted reflectance of the floor and part of the walls below the mid-height of the window wall (mid-height window + sill = 1.35 m), excluding the window, can also be calculated using Eq. (2.11) as

$$R_{\text{fw}} = \frac{[(5 + 5 + 4) \times 1.35] \times 0.5 + 20 \times 0.2}{[(5 + 5 + 4) \times 1.35] + 20} = 0.589$$

The weighted reflectance of the ceiling and part of the walls above the mid-height of the window wall (mid-height window + above = 1.65 m), excluding the window, can also be calculated by using Eq. (2.11) as

$$R_{\text{cw}} = \frac{[(5 + 5 + 4) \times 1.65] \times 0.5 + 20 \times 0.7}{[(5 + 5 + 4) \times 1.65] + 20} = 0.3$$

From Example 2.5, coefficient $C = 24.55$.

Now the internally reflected component (IRC) can be obtained from Eq. (2.10) by considering $\tau = 0.85$ as

$$IRC = \frac{0.85 \times 2.16[24.55 \times 0.589 + 5 \times 0.3]}{94 \times (1 - 0.469)} = 0.587$$

Objective Questions and Answers

2.1 The daylight factor consists of
     (a) a sky component   (b) an ERC   (c) an IRC   (d) all of these
     Answer: (d)

2.2 The externally reflected component is zero for an obstruction angle of
     (a) 90°   (b) 0°   (c) 45°   (d) none of these
     Answer: (a)

2.3 The externally reflected component is maximum for an obstruction angle of
     (a) 90°   (b) 0°   (c) 45°   (d) none of these
     Answer: (b)

2.4 The sky component is zero for an obstruction angle of
     (a) 90°   (b) 0°   (c) 45°   (d) none of these
     Answer: (a)

2.5 The sky component is maximum for obstruction angle of
     (a) 90°   (b) 0°   (c) 45°   (d) none
     Answer: (b)

2.6 The internally reflected component (IRC) is maximum for a transmissivity of
     (a) 0.6   (b) 0   (c) 0.45   (d) 0.90
     Answer: (d)

2.7 The internally reflected component (IRC) is minimum for a transmittivity of
     (a) 0.6   (b) 0.75   (c) 0.45   (d) 0.90
     Answer: (c)

2.8 The internally reflected component (IRC) is maximum for internal walls of
     (a) yellow paint   (b) green paint   (c) white paint   (d) blue paint
     Answer: (c)

2.9 The daylight factor is maximum for
     (a) a dome-structure building, Fig. 2.6   (b) a vertical window
     (c) an inclined window   (d) none of these
     Answer: (a)

2.10 Daylight provides
     (a) an emission of CO_2 (b) a mitigation of CO_2
     (c) energy conservation   (d) none of these
     Answer: (b) and (c)

2.11 Daylight provides
     (a) thermal heat   (b) no thermal heat
     (c) electrical heat   (d) none of these
     Answer: (b)

Problems

2.1 Calculate the sky components of a window having dimension of 4 m × 3 m equal to the south wall area and a point of interest that is 2 m from the window.
Hint: See Example 2.1.

2.2 Determine the effect of a point of interest from window on the sky components for Problem 2.1.
Hint: Vary the point of interest (d) from 0.5 to 5 m at an interval of 0.5 m,

2.3 Evaluate the sky component of Problem 2.1 if a half portion of the south window is covered by an opaque curtain.
Hint: Follow Example 2.2,

2.4 Calculate the externally reflected component (ERC) of Problem 2.3,
Hint: Follow the procedure given in Example 2.3,

2.5 Calculate coefficient 'C' using Eq. (2.10b) for different points of interest,
Hint: See Example 2.5 and vary "d" from 1 to 5 m.

2.6 Evaluate the internally reflected component of a house having dimensions of 5 m × 4 m × 3 m with a north wall as a window and a point of interest that is 1 m from the window.
Hint: See Example 2.6,

2.7 Determine the effect of a point of interest on the internally reflected component (IRC) of Problem 2.6,
Hint: Vary d from 1 to 5 m.

2.8 Calculate the daylight factor (DF) for Problems 2.1–2.6 for each case.
Hint: Use Eq. (2.1).

References

1. T. Muneer, *Solar radiation and daylight models for the energy efficient design of buildings* (Architectural Press, UK, 1997)
2. U. Choi, R. Johnson, S. Selkowitz, Energy Build. **6**(4), 387 (1984)
3. D.H.W. Li, H.W. Gary, C. Cheung, C.S. Lau, Build. Environ. **41**(5), 578 (2006)
4. M. Joshi, R.L. Sawhney, D. Buddhi, SESI J. **16**(1), 45 (2006)
5. K.S. Reddy, R. Manish, Energy Convers. Manag. **44**(15), 1884 (2003)
6. A.R. Webb, Energy Build. **38**(7), 721 (2006)
7. H.N. Singh, G.N. Tiwari, Energy **30**(9), 1589 (2005)

8. International Energy Agency (IEA), *Daylight in buildings: a source book on daylighting systems and components, Energy Conservation in Buildings and Community Systems Programme*. Task 21, LBNL 47493, http://www.ieashc.org/task21/publications/source/daylighting-c1.pdf. Accessed on 23 May 2011

9. Building Research Establishment (BRE), *Energy consumption guide 19, Energy Use in Offices, Energy Efficiency Best Practice programme*, BRECSU Enquiries Bureau, Garston, Watford 1997

10. Chartered Institute of Building Services Engineers (CIBSE), *Daylighting and window design, Lighting Guide 10* (1999)

11. M. Joshi, R.L. Sawhney, D. Buddhi, Renew. Energy **32**(8), 1363 (2007)

12. M. Krarti, *Energy audit of building systems: an engineering approach*, 2nd edn. (Boca Raton, FL: CRC Press, 2010)

13. A.D. Peacock, M. Newborough, P.F.G. Banfill, *Technology assessment for the existing built-asset base (TARBASE)*, WREC, Aberdeen, 22–27 May 2005

14. P. Greenup, J.M. Bell, I. Moore, Renew. Energy **22**(1), 45 (2001)

15. C.F. Reinhart, Sol. Energy **77**(1), 15 (2004)

16. D.H.W. Li, J.C. Lam, Appl. Energy **76**(4), 363 (2003)

17. C. Franzetti, G. Fraisse, G. Achard, Energy Build. **36**(2), 117 (2004)

18. E.S. Lee, D.L.D. Bartolomeo, S.E. Selkowitz, Energy Build. **38**(1), 30 (2006)

19. T.D.W. Tong, S.L. King, T.M. Cheung, C.S. Leung, Light Res. Technol. **34**(2), 121 (2002)

20. G.B. Smith, Sol. Energy Mater. Sol. Cells **84**, 395 (2004)

21. C.F. Reinhart, A. Fitz, Energy Build. **38**(7), 824 (2006)

22. ASHRAE, *Fundamentals handbook*, Chapter 29 (2001)

23. D.R.G. Hunt, *Availability of daylight, Building Research Establishment (**BRE**) Report* (Department of Environment, London, Watford, Garston, 1979)

24. D.R.G. Hunt, Build. Environ. **14**(1), 21 (1979)

25. M. Stokes, M. Rylatt, K. Lomas, Energy Build. **36**(2), 103 (2004)

26. T. Mahlia, M. Said, H. Masjuki, M. Tamjis, Energy Build. **37**(6), 573 (2005)

27. A. Laouadi, M.R. Atif, Lighting Res. Technol. **32**(4), 175 (2000)

28. A. Laouadi, C.F. Reinhart, D. Bourgeois, J. Build. Perform. Simul. **1**(1), 3 (2008)

29. P.R. Tregenza, I.M. Waters, Lighting Res. Technol. **15**(2), 65 (1983)

30. A.D. Rosa, V. Ferraro, D. Kaliakatsos, V. Marinelli, Appl. Energy **87**(3), 806 (2010)

31. A. Chel, G.N. Tiwari, H.N. Singh, Appl. Energy **87**(10), 3037 (2010)

32. Anon 1, personal.cityu.edu.hk/~bsapplec/methods.htm

33. Anon 2, www.blc.lsbu.ac.uk/webcreatif/BES/lighting-9/T9-5.html

34. A. Chel, *Thermal performance assessment and economic analysis of integrated systems for IIT Delhi mudhouse*, Ph.D. Thesis, IIT Delhi, New Delhi, India, 2010

35. D. Jenkins, M. Newborough, Appl. Energy **84**(6), 608 (2007)

36. M. Sudan, G.N. Tiwari, J. Renew. Sustain. Energy **6**, 122 (2014)

Additional References

37. E.J. Gago, T. Muneer, M. Knez, H. Köster, Renew. Sustain. Energy Rev. **41**, 1 (2014)

38. A.H. Fakra, F. Miranville, H. Boyer, S. Guichard, Energy Convers. Manag. **52**(7), 2724 (2011)

39. J.T. Kim, G. Kim, Build. Environ. **45**(2), 256 (2010)

40. D.H.W. Li, Appl. Energy **87**(7), 2109 (2010)

41. B. Calcagni, M. Paroncini, Sol. Energy **76**(6), 669 (2004)

42. M. Sudan, G.N. Tiwari, I.M. Al-Helal, Sol. Energy **115**, 379 (2015)

Chapter 3
Law of Thermodynamics and Element of Heat Transfer

Abstract Knowledge of thermodynamical law is a basic need to understand the energy and exergy of solar thermal and photovoltaic systems. All heat-transfer phenomena depend on these laws to derive the output/yield from any photovoltaic–thermal (PVT) system in terms of an overall energy and exergy efficiency.

Keywords Exergy · Conduction · Convection · Radiation · Heat and mass transfer

3.1 Introduction

Energy transfer takes place in different forms for different processes, namely, thermal, mechanical, electrical, and chemical. Energy transfer by thermal processes is basically a heat-transfer phenomena. It is a well-established topic. It does not require detailed deliberation due to the small operating-temperature difference (ΔT) in most solar thermal applications. Very few applications of solar energy are at a high operating-temperature difference (ΔT), i.e., solar power generation.

Heat coming from the Sun is in the form of thermal energy. It can be transferred generally from higher to lower temperature as a result of temperature difference (ΔT). No net-heart transfer takes place between two mediums at the same temperature. The rate of heat transfer in a particular direction is directly proportion to the temperature gradient (ΔT) in that direction.

In order to understand heat transfer phenomena's, it is necessary to know basic law of thermodynamics.

3.2 Law of Thermodynamics

A collection of a large number of atoms or molecules of a physical system is known as a "thermodynamic system." The macroscopic properties of a physical system are the temperature (T), pressure (P), mass density (ρ), and heat capacity (MC), etc.

The number of atoms or molecules contained in a physical system must be sufficiently large for higher volume of the system. The macroscopic properties of the system are governed by the condition of the physical system within the system. In principle, a physical system is considered to be infinitely large where the volume of the system is proportional to the number of molecules/atoms in the system. Thermodynamic limit is the condition where the volume of the physical system and number of atoms/molecules increases in a manner that keeps the density of atoms/molecules constant.

In a **thermodynamic process**, macroscopic properties of the system, such as volume, heat (thermal energy), and flow of atoms or molecules of the system, changes with time. In the absence of any thermodynamic process, the macroscopic properties of the systems do not change with time, and the system is said to be in thermal equilibrium.

There are basically four laws of thermodynamics as follows:

3.2.1 The Zeroth Law of Thermodynamics

When two thermodynamic systems (*A* and *B*) independently in thermal equilibrium are brought into thermal contact, either a thermodynamic process will take place or no thermodynamic process will take place between them. In the absence of any thermodynamic process, both systems will said to be in thermal equilibrium with each other.

The Zeroth law of thermodynamics establishes an equivalence relation between the two systems. If two systems, *A* and *B*, are in thermal equilibrium with another system, *C*, then systems *A* and *B* are also in thermal equilibrium with each other. This equivalence is governed by a common property between these systems known as **temperature**.

3.2.2 The First Law of Thermodynamics

Suppose a macroscopic physical system reversibly changes its equilibrium state from P_1 to P_2 on the addition of thermal energy Q, and W is the amount of mechanical work performed on the system. This change can be achieved by following many ways (with different values of Q and W), but first the law of thermodynamics states that the sum $(Q + W)$ is independent of different paths as long as the two equilibrium states are fixed. For an infinitesimally small change, quantity $d'Q + d'W$ will depend on the initial and final states of the system. $d'Q + d'W$ is known as the change in internal energy (dU) of the system as in goes from equilibrium state P_1 to state P_2. Mathematically it can be expressed as:

$$dU = U_{P_2} - U_{P_1} = d'Q + d'W \tag{3.1}$$

Mathematically, $d'Q$ and $d'W$ are path dependent, whereas the sum $d'Q + d'W$ is path independent.

Equation (3.1) is valid for a closed system based on sign convention of International Union of Pure and Applied Chemistry (IUPAC).

According to sign convention of Clausius for cyclic processes, Eq. (3.1) is written as

$$\Delta U = Q - W \tag{3.2}$$

where ΔU is the mechanical equivalent of heat; Q is the heat supplied, and W is the work done by the system.

Furthermore, the **first law of thermodynamics** is also termed as the "energy conservation law for thermodynamic systems."

Thermal analysis of solar energy systems is based on the law of **conservation of energy,** which is also considered as **the reversible process.**

In this case, according to the law of **conservation of energy,**

$$\text{The available solar energy} = \text{the useful energy} + \text{the lost energy} \tag{3.3a}$$

or

$$\text{The rate of available solar energy} = \text{the rate of useful energy} + \text{the rate of lost energy} \tag{3.3b}$$

It is to be noticed that the first law of thermodynamics is applicable to the medium operating temperature (<100 °C) of solar thermal systems.

3.2.3 The Second Law of Thermodynamics

The second law of thermodynamics gives a relation between heat supplied to the system and work extracted on application of the heat. There are several statements of the second law of thermodynamics; the most established statements are given below:

Clausius' principle: It is impossible to transfer heat spontaneously from a colder to a hotter body without causing any other changes in the system.

Caratheodory's principle: Any state infinitesimally close to the thermal equilibrium state cannot reached from it by adiabatic change.

Kelvin's principle: Heat extracted from the hot reservoir cannot be completely used to do work. The amount of heat that must be rejected to a cold reservoir is the difference of heat extracted from a hot reservoir and work obtained from the system, i.e., $Q_C = Q_H - W$. It is impossible to extract an amount of heat (Q_H) from a hot

Fig. 3.1 Heat engine cycle
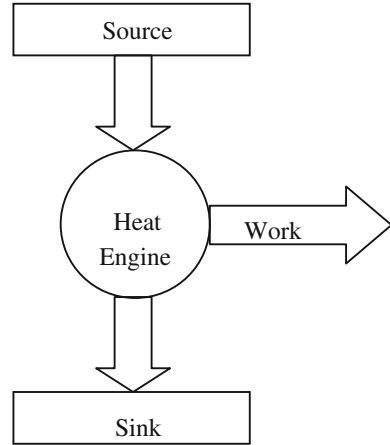
reservoir and use it all to do work (W). The remaining amount of heat ($Q_C = Q_H - W$) must be an exhausted/transfer to a cold reservoir. This is the basis of a perfect **heat engine**. This is a measure of the amount of energy ($Q_C = Q_H - W$) that is unavailable to do work, which is known as "**entropy**," as shown in Fig. 3.1. This is sometimes called the "first form" of the second law of thermodynamics or the **Kelvin–Planck statement of the second law**.

Furthermore, the thermal efficiency of a heat machine/engine working between two energy levels is defined in terms of absolute temperature in Kelvin as:

$$\eta = \left[1 - \frac{T_c}{T_h}\right] \tag{3.4}$$

where η = the thermal efficiency of heat engine; T_h = temperature of the hot reservoir (K); and T_c = temperature the cold reservoir (surrounding) (K).

Here it is also important to mention that the second law of thermodynamics is mostly used for a system with a higher range of operating temperature range ($\gg 400\,°C$).

The second law of thermodynamics also leads to the concept of **exergy**, which is defined as the maximum possible work that can be extracted from the system as it reaches equilibrium with the cold-reservoir/surroundings. For a system in equilibrium with the surroundings, exergy will be zero.

The first law ensures that energy can never be destroyed, which can be achieved only for reversible processes. On the contrary, exergy of the system depends on the irreversibility of the system, which is directly proportional to the increase in entropy of the system in its surroundings. When a process occurs between two different temperatures, energy is destroyed. The destroyed energy is known as "**anergy**."

Exergy analysis
Exergy analysis of any system incorporates irreversibility, which occurs at any part of the process. Irreversibility causes entropy generation and an increase in the entropy of the system and the surroundings. This entropy increase produces unrecoverable loss of exergy. The total exergy destroyed from the system is the sum of exergy destroyed at every point of the system.

For example, consider a water fall: When water falls from a height, the potential energy is converted into kinetic energy and ultimately into thermal energy; in this process energy is converted from one to another form, but it is conserved. At the same time, no work has been extracted in this process, i.e., it is destroyed or lost, and the lost quantity in this case is known as exergy.

The quality of energy directly relates to the exergy available from the system. The exergy analysis of any thermal process (in scope of the present book, the solar thermal process) takes into account the irreversibility at every point of system and the inefficiency of each component of the system. The prime objective of exergy analysis is the improvement of efficiency and a reduction in losses as much as possible. The optimization of solar thermal systems after exergy analysis yields insights into the quality of energy attainable from the system, and exergy-based optimization provides a more efficient system, which in turn yields greater return and capital savings.

"**Exergy is the property of system, which gives the maximum amount of useful work obtained from the system when it comes in equilibrium with a reference to the environment.**"

The above definition infers that out of input thermal energy, some part is converted into useful work and the rest is lost (i.e., cannot be recovered) to the environment. Hence, one can have:

$$\text{Heat supplied (energy)} = \text{Available energy (exergy)} + \text{unavailable energy (anergy)}$$
$$(3.5)$$

Exergy of a process
For the process taking place between two temperatures [source T_1 (in K)] and [sink T_2 (in K)], the maximum work ($W_{\max}$) drawn during this process is given by:

$$W_{\max} = \text{exergy} = \left(1 - \frac{T_0}{T_1}\right) \times Q_1 \qquad (3.6)$$

where Q_1 is the thermal energy available at T_1.

For a given sink temperature T_0, the unavailable energy is proportional to entropy change (Δs) during the process and is given by:

$$\text{The unavailable energy} = T_0 \Delta s \tag{3.7}$$

or

$$\Delta s = \frac{\Delta Q}{T} \tag{3.8}$$

Example 3.1 Calculate the maximum work available W_{max} from the heat source at $T_1 = 40, 60, 80\ °C$ and ambient temperature $= 20\ °C$ when $Q_1 = 150$ kWh.

Solution
Using Eq. (3.6) for 40 °C, we have

$$W_{max} = \left(1 - \frac{20 + 273}{40 + 273}\right) \times 150 = 9.58 \text{ kWh}$$

Similarly, for 60 and 80 °C,

$$W_{max} = 18 \text{ and } 25.5 \text{ kWh, respectively.}$$

It is concluded that the maximum work is available at higher source temperature when the sink temperature is constant.

Exergy efficiency
Exergy efficiency is defined as the ratio of energy output to exergy input. Performance of the system evaluated by incorporating exergy efficiency is based on the second law of thermodynamics unlike energy analysis, which is based on the first law of thermodynamics. Exergy efficiency of the system is obtained by writing the exergy balance of the system, which includes exergy input, exergy output, and exergy destroyed from the system.

The exergy balance for any system can be given as follows:

$$\sum \dot{Ex}_{in} - \sum \dot{Ex}_{out} = \sum \dot{Ex}_{dest} \tag{3.9a}$$

or

$$\left(\sum \dot{Ex}_{heat} + \sum \dot{Ex}_{mass,in}\right) - \left(\sum \dot{Ex}_{work} + \sum \dot{Ex}_{mass,out}\right) = \sum \dot{Ex}_{dest} \tag{3.9b}$$

or

$$\left(\sum \left(1 - \frac{T_0}{T_k}\right) \times \dot{Q}_k + \sum \dot{m}_{in}\psi_{in}\right) - \left(\sum \dot{W} + \sum \dot{m}_{out}\psi_{out}\right) = \sum \dot{Ex}_{dest} \tag{3.9c}$$

where $\dot{Q}_k$ is the rate of thermal energy transfer at the boundary of interest at location k and temperature T_k (K).

The ψ is the exergy flow per unit mass defined as follows:

$$\psi = (h - h_0) - T_0(s - s_0) \tag{3.10}$$

where h and s are the specific enthalpy and entropy, respectively. h_0 and s_0 are the specific enthalpy and entropy at dead-state temperature T_0.

Now, the exergy destruction $(\dot{Ex}_{dest})$ or the irreversibility $(\dot{I})$ may be written as:

$$\dot{Ex}_{dest} = \dot{I} = T_0 \dot{S}_{gen} \tag{3.11}$$

where the rate of entropy generation

$$\dot{S}_{gen} = \sum \dot{m}_{out} s_{out} - \sum \dot{m}_{in} s_{in} \sum \frac{\dot{Q}_k}{T_k}.$$

Exergy efficiency is improved by minimizing the inefficiency and irreversibility, which can be achieved by minimizing the term $\sum \dot{Ex}_{in} - \sum \dot{Ex}_{out}$. The concept of "improved potential (IP)" due to the improvement of exergy efficiency is directly related to the exergy efficiency and term $\sum \dot{Ex}_{in} - \sum \dot{Ex}_{out}$. It is defined as follows:

$$IP = (1 - \varepsilon)\left(\sum \dot{Ex}_{in} - \sum \dot{Ex}_{out}\right) \tag{3.12}$$

where ε is the exergy efficiency of the system defined as [1]:

$$\varepsilon = \frac{\text{rate of useful product energy}}{\text{rate of exergy input}} = \frac{\dot{Ex}_{out}}{\dot{Ex}_{in}} = 1 - \frac{\dot{Ex}_{dest}}{\dot{Ex}_{in}} \tag{3.13}$$

where $\dot{Ex}_{dest}$ is the rate of exergy destruction.

Solar radiation exergy

Exergy of any system is obtained due to the matter (substance) or field (radiation field, magnetic field, gravitational field etc.) involved in the system. Exergy depends on the temperature of the source if the sink temperature is taken to be constant throughout out the process. Therefore, the term "exergy of heat" should "change in exergy of the heat source" [2]. Solar radiation exergy is defined as the input exergy from the Sun that is available to solar thermal systems.

Solar radiations received from the Sun are utilized by human beings, wildlife, plants, and by almost all processes on planet Earth. It can be converted into work, heat, or other necessary process for life on Earth. The energy efficiency and exergy efficiency can be calculated from the work or heat equivalent of thermal radiations using the relations given in Table 3.1.

The unified efficiency expression (U_{ee}) expresses the capacity of the utilization of thermal radiation. Unified efficiency expression (U_{ee}) for different input and output is given in Table 3.2. Solar radiation exergy can be estimated using following relation:

Table 3.1 Conversion efficiency of thermal radiation

S. no.	Efficiency	Radiation to work conversion	Radiation to heat conversion
1.	Energetic, η_e	$\eta_e = W/e$ $\eta_{e\,max} = W_{max}/e$	$\eta_e = 1 - (T_a/T)^4$
2.	Exergetic, η_{ex} [a]	$\eta_{ex} = W/W_{max}$	$\eta_{ex} = W_q/W_{max}$

[a] η_{ex} is exergetic efficiency where W is the work performed due to utilization of the radiation, and W_{max} is the exergy of radiation

$$\dot{Ex}_{sun} = b = e \times U_{ee} \tag{3.14}$$

If $I(t)$ is solar radiation (Eq. 1.31) falling on a unit surface area, the energy contained in solar radiation falling on any surface of area A will be $\{I(t) \times A\}$. The equivalent exergy from the incident solar radiation is then given as [3]:

$$\dot{Ex}_{sun} = \{A \times I(t)\} \times U_{ee} = \{A \times I(t)\} \times \left[1 - \frac{4}{3} \times \left(\frac{T_0}{T_s}\right) + \frac{1}{3} \times \left(\frac{T_0}{T_s}\right)^4\right]$$
$$\tag{3.15}$$

$T_0 = $ Surrounding or ambient temperature $(K) = T_a$;
$T_s = $ Sun surface temperature $= T_{sun} = 6000$ K;

Example 3.2 Calculate the unified efficiency (U_{ee}) using the expression of Petela model and radiation exergy when the surrounding temperature $= 20$ °C, $A = 2$ m^2, $I(t) = 750$ W/m^2.

Solution
Using Table 3.2 and Eq. (3.15), we have

$$\dot{Ex}_{sun} = \{2 \times 750\} \times \left[1 - \frac{4}{3} \times \left(\frac{20+273}{6000}\right) + \frac{1}{3} \times \left(\frac{20+273}{6000}\right)^4\right] = 1.4 \text{ kW}$$

Table 3.2 The input, output, and unified efficiency expression (U_{ee}) of utilization of thermal radiation

S. no.	Researcher	Input	Output	U_{ee}
1.	Petela [2]	Radiation energy	Absolute work	$1 - \frac{4}{3} \times \left(\frac{T_0}{T_s}\right) + \frac{1}{3} \times \left(\frac{T_0}{T_s}\right)^4$
2.	Battisti and Corrado [4]	Radiation energy	Useful work radiation exergy	$1 - \frac{4}{3} \times \left(\frac{T_0}{T_s}\right)$
3.	Lewis and Keoleian [5]	Heat	Net work of a heat engine	$1 - \left(\frac{T_0}{T_s}\right)$

Where T_s and T_0 are surface temperature of sun and environment temperature in Kelvin at Earth, respectively

3.2.4 The Third Law of Thermodynamics

The third law of thermodynamics states that the entropy of any system approaches a minimum constant value as the temperature approaches absolute zero. In statistical thermodynamics, entropy is associated with the degree of disorder in the system. As the temperature of the system decreases, the thermal motion within the system also decreases, which gives it a more ordered state. A highly ordered state gives a minimum value of entropy at low temperature (near absolute zero). Furthermore, absolute entropy cannot be defined due to its constant minimum value of entropy near absolute zero; hence, only the change in entropy can be obtained for different systems at different temperatures.

3.3 Element of Heat Transfer

3.3.1 Introduction

Heat/thermal energy is a very important area. It is freely available from the Sun (Chap. 1). Furthermore, without heat/thermal energy, one cannot even imagine defining the concept of thermodynamic laws. To understand the mechanism for heat/thermal energy transfer from a higher temperature to a lower temperature (see the first and second laws of thermodynamics), it is necessary to first understand heat/thermal energy transfer by different modes, namely, (i) **conduction**, (ii) **convection**, and (iii) **radiation**. It is also important to note the following:

 (i) **Each heat transfer mode acts independently; and**
(ii) **only one heat transfer mode behaves strongly in comparison to the others**.

Usually all three methods are involved in overall heat-transfer problems [6]. All three heat-transfer modes will be discussed in the next sections.

3.3.2 Conduction

Conduction is the transfer of heat/thermal energy from the more energetic particles (means higher temperature) of a substance to the adjacent lower energetic (lower temperature) ones. Conduction can take place in solids, liquids, or gases. Collision between the molecules and the diffusion of molecule is responsible for thermal conduction in liquids and gases. In contrast, thermal vibration and collision between free electrons are responsible for thermal conduction in solids.

Fourier's law of heat conduction

Let us consider steady-state heat transfer through a large vertical plane wall of (a) thickness $\Delta x = L$ and (b) surface area A and $\Delta T = T_2 - T_1$. On the basis of experimentation, it can be shown that the rate of heat transfer $\dot{Q}$ through the vertical wall can be expressed as

$$\text{Rate of heat conduction} \propto \frac{(\text{cross sectional area})(\text{temperature difference/drop})}{\text{change in thickness of slab}}$$

or

$$\dot{Q} = -KA\frac{\Delta T}{\Delta x} \tag{3.16a}$$

where the constant K is the proportionality constant known as "thermal conductivity of the materials" (Appendix V), and thermal conductivity is ability to transport thermal energy from a higher temperature to a lower temperature through conduction. For limiting case, $\Delta x \rightarrow 0$, Eq. (3.16a) reduces to a differential form:

$$\dot{Q} = -KA\frac{\mathrm{d}T}{\mathrm{d}x} \tag{3.16b}$$

Equation (3.16b) is known as Fourier's law of heat conduction. Here $\frac{\mathrm{d}T}{\mathrm{d}x}$ is the slope (temperature gradient) of the temperature curve on a T–x diagram at point x. The negative sign indicates the temperature decreases as one move from a higher temperature point toward the lower temperature. The positive direction of x is taken from the higher temperature to the lower temperature.

Thermal conductivity

Thermal conductivity of a material (K) is defined as the rate of heat transfer per unit of surface area $(A = 1 \text{ m}^2)$ per unit of thickness $(\Delta x = 1 \text{ m})$ between two points having unit temperature difference $(\Delta T = 1 \,°C)$. Higher value of thermal conductivity give higher rate of heat transfer through the material. The thermal conductivity of gases, liquids, and solids depends on temperature. Experimental studies have shown that for many materials, the dependence of thermal conductivity on temperature can be assumed to be linear.

$$K = K_0[1 + \beta(T - T_0)] \tag{3.17}$$

where K_0 is the thermal conductivity at temperature T_0; and β is a constant for the material. The values of K will increase for $T > T_0$ and decrease for $T < T_0$; however, the value of K is unaffected during the medium temperature range of renewable energy technologies in the present book.

Thermal diffusivity

Thermal diffusivity is property of the material that governs the diffusion of heat through the material. The higher the value of thermal diffusivity, the greater the diffusion of heat through the material. It is defined as the ratio of thermal conductivity to the heat capacity per unit volume. Mathematically it is expressed as follows:

$$\alpha = \frac{\text{Heat conducted}}{\text{Heat stored}} = \frac{K}{\rho C_{\text{p}}} \, (\text{m}^2/\text{s}) \qquad (3.18)$$

where ρ and C_{p} are the density and specific heat capacity of the material, respectively. The higher value of thermal conductivity confirms that more heat is conducted through the material and less heat is stored in the material. The thermal diffusivity of some common materials is given in Appendix V.

Similarly, one dimensionless parameter, the Biot number (B_i), is also used in heat-conduction problems, The Biot number is important in cases where a solid body is immersed in hot fluid for heating. In this situation, the outer surface of the solid body is heated through convection, and the heat is transferred to the inner parts of the body by conduction. This is defined as the ratio of convective heat transfer coefficient at the surface of solid body to the conductive heat transfer coefficient through the solid material. Mathematically it is given as follows:

$$B_i = \frac{h_{\text{c}} L}{K} = \frac{h_{\text{c}}}{K/L} \qquad (3.19)$$

or

$$B_i = \frac{\text{heat transfer coefficient at the surface of the solid}}{\text{internal conductance of solid across length } L}$$

In terms of thermal resistance, it is the ratio of thermal resistance faced by conductive heat transfer to the thermal resistance faced by convective heat transfer. A smaller Biot number implies lower thermal caused to the conduction through the solid body.

Equation (3.16b) for the rate of heat transfer in W can be rearranged as follows:

$$\dot{Q}_k = A \frac{K}{L} (T_2 - T_1) \qquad (3.20a)$$

Here −ve sign has been removed because the length has no negative sign. Equation (3.20a) can also be written for the rate of heat transfer per unit area in W/m^2 due to conduction as

$$\dot{q}_k = \frac{\dot{Q}}{A} = h_k(T_2 - T_1) \tag{3.20b}$$

where h_k is the heat transfer coefficient due to conduction. This is defined as the rate of heat transfer due to conduction for unit area and unit temperature difference in $W/m^2\ °C$ and is given by

$$h_k = \frac{K}{L} = \frac{\dot{q}_k}{(T_2 - T_1)} \tag{3.20c}$$

Example 3.3 Evaluate the rate of heat transfer $(\dot{Q}_k)$ through a rectangular-plane wall of 0.1524 m thickness and thermal conductivity (K) of 0.432 W/m K under steady-state uniform surface temperatures of $T_1 = 21.1$ and $T_2 = 71.1\ °C$.

Solution
From Eq. (3.20a), we have the following expression for $\dot{Q}_k$

$$\frac{\dot{Q}_k}{A} = \frac{K(T_2 - T_1)}{L} = \frac{0.432 \times 50}{0.1524} = 141.73\ W/m^2$$

The value of conductive heat transfer coefficient (h_k) is given by

$$h_k = \frac{K}{L} = \frac{0.432}{0.1542} = 2.80\ W/m^2\ °C$$

Here it is important to mention that the unit of heat-transfer coefficient can be expressed either in $W/m^2\ °C$ or in $W/m^2\ K$ due to the cancellation of 273 in the temperature difference.

3.3.3   Convection

By using the definition of heat-transfer coefficient due to conduction (Eq. 3.20c), it becomes simpler to write an expression for the rate of heat transfer between the fluid and the boundary surface in W due to convection as follows:

$$\dot{Q}_c = h_c A \Delta T \tag{3.21a}$$

where h_c is the local convective heat-transfer coefficient in $W/m^2\ °C$.

The rate of heat transfer per unit area in W/m^2 due to convection is given by

$$\dot{q}_c = \frac{\dot{Q}}{A} = h_c(T_2 - T_1) \tag{3.21b}$$

Also, the expression for h_c can be written as

$$h_c = \frac{\dot{q}_c}{(T_2 - T_1)} \tag{3.21c}$$

Dimensionless heat-convection parameters

To evaluate the numerical value of h_c, the following dimensionless numbers, depending on the physical parameters of fluid above the solid surface due to a boundary problem, are used:

Nusselt number (**Nu**): The Nusselt number gives insight about the dominance of convective heat transfer or conductive heat transfer for fluids. It is an important parameter for problems related to convective heat transfer. It is defined as the ratio of the convective heat-transfer coefficient to the conductive heat-transfer coefficient for fluids. Mathematically it is expressed as follows:

$$\text{Nusselt number}, Nu = \frac{h_c X}{K} \tag{3.22a}$$

In the above equation, K is the thermal conductivity of a fluid above solid surface; and h_c is the convective heat-transfer coefficient between solid and fluid.

Reynold's number (**Re**): Reynold's number is defined for the heat-transfer problem in force mode of operation. It is the ratio of fluid dynamic force (ρu_0^2) to viscous drag force $(\mu u_0/X)$ and is given by

$$\text{Reynolds number}, Re = \frac{\rho \mu_0^2}{\mu u_0/X} = \frac{\rho u_0 X}{\mu} = \frac{u_0 X}{v} \tag{3.22b}$$

where ρ is the density; μ is the dynamic viscosity; and $v =$ kinematic viscosity $= \frac{\mu}{\rho}$ and X is the characteristic length for the system of interest. The Reynold's number signifies the flow behavior in forced convection. The value of the Reynold's number indicates the flow type (laminar flow/turbulent flow) of a fluid.

Prandtl number (**Pr**): The Prandtl number relates fluid motion and heat transfer to the fluid. It is defined as the ratio of momentum diffusivity (μ/ρ) to thermal diffusivity $(K/\rho C_p)$ and is given by

$$\text{Prandtl number}, Pr = \frac{\mu/\rho}{K/\rho C_p} = \frac{\mu C_p}{K} \tag{3.22c}$$

where μ is the dynamic viscosity; C_p is the specific heat at a constant pressure; and K is the thermal conductivity of the fluid.

Grashof number (Gr): This is the ratio of buoyancy force to viscous force. It is given by

$$\text{Grashof number}, Gr = \frac{g\beta'\rho^2X^3\Delta T}{\mu^2} = \frac{g\beta'X^3\Delta T}{v^2} \qquad (3.22\text{d})$$

where β is the coefficient of volumetric thermal expansion; g is the acceleration due to gravitation; and ΔT is the operating temperature difference between the surface and the fluid.

Rayleigh number (Ra): This is the ratio of the thermal buoyancy to viscous inertia. It is expressed as

$$\text{Rayleigh number}, Ra = GrPr = \frac{g\beta'\rho^2X^3C_p\Delta T}{\mu K} \qquad (3.22\text{e})$$

All of the numbers defined in this section can be obtained using the properties of air and water listed in Appendix V. The properties are calculated at average temperature T_f given as follows:

$$T_f = \frac{T_1 + T_2}{2} \qquad (3.23\text{a})$$

where T_1 is hot surface temperature; and T_2 is fluid temperature.

The thermal expansion coefficient (β') at hot surface temperature and fluid temperature is calculated using Eqs. (3.23b) and (3.23c), respectively

$$\beta' = \frac{1}{(T_2 + 273)} \qquad (3.23\text{b})$$

$$\beta' = \frac{1}{(T_f + 273)} \qquad (3.23\text{c})$$

The characteristic dimension (X) for different shapes is calculated as follows:

$$X = \frac{A(\text{Area})}{P(\text{Perimeter})} \qquad (3.23\text{d})$$

In some specific cases, the characteristic dimension for a rectangular horizontal surface is determined using relation given below:

$$X = \left(\frac{L_0 + B_0}{2}\right) \qquad (3.23\text{e})$$

Now, the heat transfer by convection is further classified as free and forced convection, which will be discussed as follows:

Free convection
The gravitational force and nonuniform density due to temperature difference between adjacent layers of fluid are the two prime factors responsible for fluid motion. The Nusselt number, as given in Eq. (3.22a), depends on the type of flow (free or forced).

For free convection,

$$Nu = \frac{hL}{K} = C'(GrPr)^n K' \tag{3.24}$$

The above relation is obtained using dimensional analysis at the boundary layer. The values of C' and n are estimated using experimental data for systems with same geometrical shapes and size. For some geometrical shapes used in solar thermal technology, given in Table 3.3, K' governs the entire physical behavior of the problem [7]. Some empirical relations used for free convention are also given in Table 3.4.

Example 3.4 Estimate the convective heat transfer coefficient for a horizontal rectangular surface $(1.0 \text{ m} \times 0.8 \text{ m})$ maintained at $134\,°C$. The hot surface is exposed to (a) water and (b) air at $20\,°C$.

Solution
For the present exercise in both cases, the average temperature, Eq. (3.23a), $T_f = (134 + 20)/2 = 77\,°C$ and the characteristic dimension $(L = X) = (1.0 + 0.8)/2 = 0.90 \text{ m}$, are the same for water or air as a fluid.

(a) For water

From Appendix V, the water thermal properties at $T_f = 77\,°C$ are $\mu = 3.72 \times 10^{-4} \text{ kg/m s}$; $K = 0.668 \text{ W/m K}$, $= 973.7 \text{ kg/m}^3$, $Pr = 2.33$ and $\beta' = 1/(77 + 273) = 2.857 \times 10^{-3}\ K^{-1}$.
From Eq. (3.22d), the Grashof number can be calculated as

$$Gr_L = \frac{g\beta'\rho^2(\Delta T)X^3}{\mu^2} = \frac{9.8 \times 2.857 \times 10^{-3}(973.7)^2 \times 114 \times (0.9)^3}{(3.72 \times 10^{-4})^2}$$
$$= 1.594 \times 10^{13}$$

This is a turbulent flow and for a heated plate facing upward, the values of $C = 0.14$ and $n = 1/3$ (Table 3.3). Now the convective heat-transfer coefficient can be calculated as

Table 3.3 Free convective heat transfer of various systems [8]

System	Schematic	C'	n	k'	Operating conditions
Horizontal cylinder		0.47	0.25	1	Laminar flow condition
		0.1	–	1	Turbulent flow condition
		0.0246	0.4	$[Pr^{1/6}/(1+0.496Pr^{2/3})]^{2/3}$	Turbulent flow condition; to obtain local Nu use $C'=0.0296$, $X=x$
Vertical cylinder with small diameter		0.686	0.25	$[Pr/(1+1.05Pr)]^{1/4}$	Laminar flow condition $\overline{Nu}_{local}=\overline{Nu}+0.52(L/D)$
Heated horizontal plate facing upward		0.54	0.25	1	Laminar flow condition $(10^5<GrPr<2\times10^7)$ $X=(L_0+B_0)/2$; Laminar flow condition $(10^7<GrPr<10^{11})$, $X=A/P$ for circular disc of diameter D, use $X=0.9D$
		0.14	0.33	1	Turbulent flow condition $(2\times10^7<GrPr<3\times10^7)$, $X=(L_0+B_0)/2$
		0.15	0.33	1	Turbulent flow condition $(10^7<GrPr<10^{11})$, $X=A/P$
Heated horizontal plate facing downward		0.27	0.25	1	Laminar flow condition only
Moderately inclined plane		0.8	0.25	$\left[\dfrac{\cos\theta}{1+\left(1+\frac{1}{\sqrt{Pr}}\right)^2}\right]^{1/4}$	Laminar flow condition (multiply Gr by $\cos\theta$ in the formula for vertical plate)
Two vertical parallel plates at the same temperature		0.04	1	$(d/L)^3$	Air layer

(continued)

Table 3.3 (continued)

System	Schematic	C'	n	k'	Operating conditions
Hollow vertical cylinder with open ends		0.01	1	$(d/L)^3$	Air column
Two horizontal parallel plates hot plate uppermost		0.27	0.25	1	Pure conduction $\dot{q} = K(T_h - T_c)/d$ Laminar flow condition (air) $(3 \times 10^5 < GrPr < 3 \times 10^{10})$
Two concentric cylinders		0.317	0.25	$\left[X^3 \left(\dfrac{1}{d_i^{3/5}} + \dfrac{1}{d_o^{3/5}} \right)^5 \right]^{-1/4}$	Laminar flow condition
Two vertical parallel plates of different temperatures (h for both surfaces)		0.18	0.25	$\left(\frac{L}{d}\right)^{-1/9}(Pr)^{-1/4}$	Laminar flow condition (air) $(2 \times 10^4 < Gr < 2 \times 10^5)$
		0.065	–	$\left(\frac{L}{d}\right)^{-1/9}(Pr)^{-1/3}$	Turbulent flow condition (air) $(2 \times 10^5 < Gr < 2 \times 10^7)$
Two inclined parallel plates				$\overline{Nu} = \sqrt{\dfrac{\overline{Nu}_{vert}\cos\theta + \overline{Nu}_{horz}\sin\theta}{2}}$	
Two horizontal parallel plates cold plate uppermost		0.195	0.25	$Pr^{1/4}$	Laminar flow condition (air) $(10^4 < Gr < 4 \times 10^5)$
		0.068	–	$Pr^{1/3}$	Turbulent flow condition (air) $Gr > 4 \times 10^5$

Table 3.4 Simplified equations for free convection from various surfaces to air at atmospheric pressure

Cases	Surface	Laminar $10^4 < Gr_f Pr_f < 10^9$	Turbulent $Gr_f Pr_f > 10^9$
1	Horizontal hot plate facing upward	$h = 1.32(\Delta T/L)^{1/4}$	$h = 1.52(\Delta T)^{1/3}$
2	Hot plate facing downward	$h = 0.59(\Delta T/L)^{1/4}$	
3	Vertical plane and cylinder	$h = 1.42(\Delta T/L)^{1/4}$	$h = 1.31(\Delta T)^{1/3}$
4	Horizontal cylinder	$h = 1.32(\Delta T/d)^{1/4}$	$h = 1.24(\Delta T)^{1/3}$

$$h_c = \frac{K}{L}(0.14)(Gr_L Pr)^{1/3} = \frac{0.668}{0.9}(0.14)\left(1.594 \times 10^{13} \times 2.33\right)^{1/3} = 3467 \text{ W/m}^2\text{K}$$

(b) For surrounding air

By using the physical properties of air at $T_f = 77\ °C$ (Appendix V) and $L = 0.90$ m

$$Gr_L \cdot Pr = \frac{(9.8) \times (134 - 20) \times (0.90)^3 \times (0.697)}{(293) \times (2.08 \times 10^{-5})^2} = 4.51 \times 10^9$$

Using Table 3.3 for a hot surface facing upward and turbulent flow condition, the heat-transfer coefficient can be calculated as

$$h_c = \left(\frac{K}{L}\right) \times 0.14 \times (Gr_L Pr)^{0.333} = \left(\frac{0.03}{0.9}\right) \times (0.14) \times \left(4.91 \times 10^9\right)^{0.333}$$
$$= 2.83 \text{ W/m}^2\ °C$$

It is important to note that the convective heat-transfer coefficient changes from 3467 to 2.83 W/m² °C with a change of fluid from water to air for the given same other parameters because it depends on the physical properties of fluid.

Example 3.5 Estimate the Biot number (B_i) for Example 3.1a for the following conditions:

   (i)   Insulating solid surface $(K = 0.04$ W/m °C)
   (ii) Concrete solid surface $(K = 1.279$ W/m °C)
   (iii) Metallic solid surface $(K = 386$ W/m °C)

Solution

The expression for the Biot number (B_i), Eq. (3.19), is given by

For water as a fluid:

$$
B_i = \begin{cases}
\dfrac{3473 \times 0.9}{0.04} = 78,007.7 & \text{for insulation} \\[3mm]
\dfrac{3473 \times 0.9}{1.279} = 2445.97 & \text{for concrete} \\[3mm]
\dfrac{3473 \times 0.9}{386} = 8.1 & \text{for copper}
\end{cases}
$$

For air as a fluid:

$$
B_i = \begin{cases}
\dfrac{2.83 \times 0.9}{0.04} = 63.67 & \text{for insulation} \\[3mm]
\dfrac{2.83 \times 0.9}{1.279} = 1.99 & \text{for concrete} \\[3mm]
\dfrac{2.83 \times 0.9}{386} = 6.60 \times 10^{-3} & \text{for copper}
\end{cases}
$$

Forced convection [9]

For forced convection, the rate of heat transfer is enhanced by circulating the fluid over the hot surface using an external source of energy such as pump (liquid) or fan (air/gas). Externally supplied energy overcomes the pressure drop due to fluid motion and viscous force (frictional force) due to viscosity of fluid. The heat transfer is dominantly affected by flow behavior (laminar/turbulent) and fluid motion (momentum diffusivity), which in turn is directly related to Reynold's number and Prandtl number, respectively. Therefore, the Nusselt number in forced convection depends on Reynold's number and Prandtl number. It is expresses by the following correlation:

$$
Nu = C(RePr)^n K \tag{3.25}
$$

where C and n are constants for a given type of flow and geometry; and K is a correction factor (shape factor) added to obtain a greater accuracy.
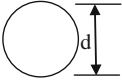
The empirical relation for forced convective heat transfer through cylindrical tubes may be represented as

$$
\overline{Nu} = \frac{hD}{K_{th}} = CRe^m Pr^n K \tag{3.26}
$$

where $D = 4A/P$ is the hydraulic diameter (m); P is the perimeter of the section (m); and K_{th} is the thermal conductivity (W/m K).

The values of C, m, n, and K for various conditions are given in Table 3.5.

Table 3.5 The value of constants for forced convection

Cross-section	D	C	m	n	K	Operating conditions
	d	3.66	0	0	1	Laminar flow case long tube $Re < 2000,\ Gz < 10$
	d	1.86	0.33	0.33	$(d/l)^{1/3}(\mu/\mu_w)^{0.14}$	Laminar flow case short tube for $Re < 2000,\ Gz > 10$
	d	0.027	0.8	0.33	$(\mu/\mu_w)^{0.14}$	Turbulent flow case of highly viscous liquids for $0.6 < Pr < 100$
	d	0.023	0.8	0.4	1	Turbulent flow case of gases $Re > 2000$

For fully developed laminar flow in tubes at constant wall temperature, we have the relation

$$Nu_{\mathrm{d}} = 3.66 + \frac{0.0668(d/L)RePr}{1 + 0.04[(d/L)RePr]^{2/3}} \tag{3.27}$$

The heat-transfer coefficient calculated from this relation is the average value over the entire length of the tube. When the tube is sufficiently long, the Nusselt number approaches a constant value of 3.66.

For the plate heated over its entire length, the average Nusselt number is given by

$$\overline{Nu}_{\mathrm{L}} = 0.664 Re_{\mathrm{L}}^{1/2} Pr^{1/3} \tag{3.28}$$

The thermo-physical properties of water (or any base fluid) can be improved for higher values of heat-transfer coefficient by mixing nano-particles in water (or base fluid). The correlations [10–44] for the thermo-physical properties of nano-fluid are given in Appendix V.

Example 3.6 Calculate an average convective heat-transfer coefficient and the rate of heat transfer per m^2 from a hot plate of 1 m length to flowing water (0.20 m/s) if the hot-plate temperature is 27.8 °C above the flowing-water temperature. The water's physical properties at the fluid film temperature are: $v = 7.66 \times 10^{-7}$ m^2/s, $K = 0.621$ W/m K, $Pr = 5.13$.

Solution
The Reynolds number can be calculated from Eq. (3.22b) as

$$Re_{\mathrm{L}} = \frac{(0.20)(1.0)}{7.66 \times 10^{-7}} = 261{,}096$$

Because the flow is laminar, the average convective heat transfer coefficient can be evaluated from Eq. (3.28) as

$$\bar{h} = \frac{K}{L}(0.664)Re_{L}^{1/2}Pr^{1/3}$$

$$= \frac{0.621}{1.0}(0.664)(261,096)^{1/2}(5.13)^{1/3} = 363.45 \text{ W/m}^2 \text{ K}$$

The average rate of heat transfer, per metre-squared, to the water is given by

$$\frac{\dot{Q}}{A} = \bar{h}\Delta T = (363.45)(27.8) = 10.104 \text{ kW/m}^2$$

Example 3.7 Calculate the convective heat-transfer coefficient from a blackened surface to (a) water (base fluid) and (b) nano-fluid (Al_2O_3 nano-particles) of a passive double-slope solar still for the following parameters;

Water mass (M_w) = 40 kg, solar still area (A_b) = 2 m × 1 m, ambient temperature (T_a) = 35 °C, average glass temperature (T_{gi}) = 50.7 °C, solar intensity ($I(t)$) = 940 W/m^2, wind velocity (v) = 1.5 m/s, C = 0.54, n = 0.25, inclination angle (θ) = 30 °, characteristic length (d) = 1.5 m, absorptivity of glass (α_g) = 0.85, absorptivity of water (α_w) = 0.65, absorptivity of basin (α_g) = 0.8, ε_{eff} = 0.741, and thermal conductivity of glass (K_g) = 0.004(W/m °C)

Properties of Al_2O_3 nano-particles: C_{pp} = 880(J/kg K), β_p = 8.1 × 10^{-6}(K^{-1}), φ_p = 0.004 %, ρ_p = 3.89 × 10^3(Kg/m^3), thermal conductivity of particle k_p = 39.5 (W/m °C), diameter of Nan particle, (d_p) = 15 nm.

Take temperature of water (T_w) = 72.25 °C, Temperature of Nan fluid (T_{nf}) = 74.45 °C.

Solution

(a) From Appendix V (Table V(b)), all of the thermo-physical properties of water can be obtained as follows:

$$\rho_w = 9.7716 \times 10^3 (\text{kg/m}^3), \quad \mu_w = 0.3984 \times 10^{-3}(\text{kg/m s}), \quad k_w = 0.661(\text{W/m °C}),$$
$$C_w = 4.190 \times 10^3 (\text{J/kg K}), \quad \beta_w = 0.0029 \text{ K}^{-1}$$

$$Nu = C(GrPr)^n = 2.289 \times 10^2; \text{ where } Gr = \frac{g\beta d^3 \rho^2 \Delta T}{\mu^2} \text{ and } Pr = \frac{\mu C_p}{k}$$

$$\text{Convective heat transfer coefficient}(h_{cw}) = Nu \times \left(\frac{k_w}{d}\right) = 100.9(\text{W/m}^2 \text{ °C})$$

(b) From Appendix V (Tables V(g–m)):

$$C_{nf} = \frac{[(\varphi_p \rho_p C_p + (1 - \varphi_p)\rho_w C_w)]}{\rho_w} = 4164.2 \text{ (J/kgK)}; \rho_{nf} = \varphi_p \rho_p + (1 - \varphi_p)\rho_w$$

$$= 1.0954 \times 10^3 \text{(kg/m}^3\text{)}; \mu_{nf} = \mu_w \left[1 + 2.5(\varphi_p) + 6.2\varphi_p^2\right]$$

$$= 0.4327 \times 10^{-3} \text{(kg/m s)}$$

$$k_{nf} = k_w \left[1 + (1.0112)\varphi_p + (2.4375)\varphi_p\left(\frac{47}{d_p(\text{nm})}\right) - (0.0248)\varphi_p\left(\frac{k_p}{0.613}\right)\right] = 0.7544 \text{ (W/m }^\circ\text{C)};$$

$$\beta_{nf} = (1 - \varphi_p)\beta_w + \varphi_p \beta_p = 0.0028 \text{ K}^{-1}.$$

$$Nu = C(GrPr)^n = 7.1848 \times 10^2; \text{ where, } Gr = \frac{g\beta d^3 \rho^2 \Delta T}{\mu^2} \text{ and } Pr = \frac{\mu C_p}{k}$$

$$\text{Convective heat transfer coefficient}(h_{cw}) = Nu \times \left(\frac{k_{nf}}{d}\right) = 361.3 \text{(W/m}^2 \text{ }^\circ\text{C)}$$

Convective heat transfer due to wind

The correlation for the heat-transfer coefficient for the flat plates exposed to ambient air/wind has also been studied by many researchers. The correlations for this case depend on the wind speed (V). The typical correlation for this case is given as follows:

$$h_c = 5.7 + 3.8V \quad \text{for} \quad 0 \le V \le 5 \text{ m s}^{-1} \tag{3.29a}$$

For zero wind speed, Eq. (3.29a) will give the heat-transfer coefficient for natural convection. This correlation is an approximate correlation because it is valid for wind blowing parallel to the exposed surface.

The correlation given in Eq. (3.29a) includes the effect of both convection and radiation. The correlation for the heat-transfer coefficient due to convection only is given as follows:

$$h_c = 2.8 + 3.0V \quad \text{for} \quad 0 \le V \le 7 \text{ m s}^{-1} \tag{3.29b}$$

The sensibility of these parameters is also demonstrated through comparison, and another expression for the convective heat-transfer coefficient is given by

$$h_c = 7.2 + 3.8V \tag{3.29c}$$

Several other correlations are also available in the literature, and generally h_c is determined from an expression in the form expressed as

$$h_c = a + bV_a^n \qquad (3.29d)$$

where $a = 2.8, b = 3$ and $n = 1$ for $V_a < 5$ m/s   and $a = 0, b = 6.15$ and $n = 0.8$ for $V_a > 5$ m/s. (The source and reference of Eq. (3.29) can be obtained from Tiwari [6]).

3.3.4   Radiation

Radiation is transmitted/propagated through space/vacuum in the form of electro-magnetic waves. Thermal radiation is the electromagnetic waves of wavelength between 0.1 and 100 μm in the terrestrial region. All of the rules applicable to light are also obeyed by thermal radiation. When thermal radiation strikes a solid surface, it can be absorbed, reflected, or refracted according to the same rule as that for light.

Radiation involving real surfaces
When radiant energy, solar radiation in the present case, falls on a solid surface, a part of it is reflected; another part is absorbed; and the rest is transmitted through it if it is a transparent solid body. The conservation of energy states that the total sum must be equal to the incident radiation; thus,

$$I_r + I_a + I_t = I_T \qquad (3.30a)$$

Dividing the above equation by I_T, one gets

$$\rho + \alpha + \tau = 1 \qquad (3.30b)$$

where $\rho = \frac{I_r}{I_T}$ is the ratio of the solar energy reflected to the incident solar energy ("reflectivity"); $\alpha = \frac{I_a}{I_T}$ is the ratio of the solar energy absorbed to the incident solar energy ("absorptivity"); and $\tau = \frac{I_t}{I_T}$ is the ratio of the solar energy transmitted to the incident solar energy ("transmittance of the intercepting body").

For an opaque surface, $\tau = 0$, therefore $\rho + \alpha = 1$. However, when $\rho = \tau = 0$; $\alpha = 1$, that is, the substance absorbs the whole of the solar energy incident on it. Such a substance is called the "black body." Similarly, for a white body which reflects the whole of the radiation falling on it, $\alpha = \tau = 0, \rho = 1$.

The energy absorbed is converted into heat, and this heated body, by virtue of its temperature, emits radiation according to Stefan–Boltzmann's law. The radiant energy emitted per unit area of a surface in unit time is referred to as the "emissive power" $(E_\lambda b)$ as given by Eq. (1.2).

However, this is defined as the amount of energy emitted per second per unit area perpendicular to the radiating surface in a cone formed by a unit solid angle between the wavelengths lying in the range $d\lambda$; it is called the "spectral emissive power" $(E_{0-\lambda,}b)$ as given in Eq. (1.4a). Furthermore, emissivity, defined as the

ratio of the emissive power of a surface to the emissive power of a black body of the some temperature, is the fundamental property of a surface.

Kirchoff's law

This law states that for a body in thermal equilibrium, the ratio of its emissive power to that of a black body at the same temperature is equal to its absorptivity, i.e.,

$$\frac{E_{b\lambda}}{E_b} = \alpha \quad \text{or} \quad \varepsilon = \alpha \tag{3.31}$$

Thus, a body can absorb as much incident radiation as it can emit at a given temperature. However, this may not be valid if the incident radiation comes from a source at a different temperature. Furthermore, it applies to surfaces bearing grey surface characteristics, viz., radiation intensity is taken to be a constant proportional to that of a black body. The radiative properties α_λ, ε_λ, and ρ_λ are assumed to be uniform over the entire wavelength spectrum.

Laws of thermal radiation

Some other thermal radiation laws were also defined in Chap. 1.

Sky radiation

In order to evaluate radiation exchange from a horizontal body directly exposed to the sky, a certain equivalent black-body sky temperature is determined. This accounts for the fact that the atmosphere is not at a uniform temperature and that it radiates only in certain wavelength regions. Thus, the net radiation exchange between a horizontal surface (T_1) with emittance (ε) and area (A) and the sky temperature, T_{sky}, is given by

$$\dot{Q} = A\varepsilon\sigma\left(T_1^4 - T_{sky}^4\right) \tag{3.32}$$

In order to express the equivalent sky temperature, T_{sky}, in terms of ambient air temperature, various expressions have been given by different people. These relations, although simple to use, are only approximations. The sky temperature in terms of local air temperature can be given by the relation,

$$T_{sky} = 0.0552 T_a^{1.5} \tag{3.33a}$$

where T_{sky} and T_a are both in degrees Kelvin.

Another commonly used relation is given as

$$T_{sky} = T_a - 6 \tag{3.33b}$$

or

$$T_{sky} = T_a - 12 \tag{3.33c}$$

Example 3.8 Determine the rate of long-wavelength radiation exchange (R) between the ambient air $(T_a = 15\ °C)$ and the sky temperature (Eq. 3.33).

Solution

From Eq. (3.32), we have an expression for (R) as follows:

$$\Delta R = \sigma \left[(T_a + 273)^4 - (T_{sky} + 273)^4 \right]$$

From Eq. (3.33), we have

$$T_{sky} = 0.0552(15)^{1.5} = 3.2\ °C$$
$$= 15 - 6 = 9\ °C$$
$$= 15 - 12 = 3\ °C$$

Now, $\Delta R = 5.67 \times 10^{-8} \left[(15 + 273)^4 - (3.2 + 273)^4 \right] = 60.11\ \text{W/m}^2$

$$= 5.67 \times 10^{-8} \left[(15 + 273)^4 - (9.0 + 273)^4 \right] = 31.50\ \text{W/m}^2$$

$$= 5.67 \times 10^{-8} \left[(15 + 273)^4 - (3.0 + 273)^4 \right] = 60.06\ \text{W/m}^2$$

Here, it is important to mention that the value of T_{sky} is nearly same for two cases; hence, the numerical value of ΔR should be considered as 60 W/m^2.

Heat-transfer coefficient due to radiation

The radiant heat exchange between two infinite parallel surfaces per m^2 at temperatures T_1 and T_{sky} may be determined from Eq. (3.32) as

$$\dot{q}_r = \varepsilon\sigma \left[(T_1 + 273)^4 - (T_{sky} + 273)^4 \right] \tag{3.34a}$$

The above equation may be rewritten as

$$\dot{q}_r = \varepsilon\sigma \left(T_1^4 - T_a^4 \right) + \varepsilon\sigma \left(T_a^4 - T_{sky}^4 \right) \tag{3.34b}$$

or

$$\dot{q}_r = \varepsilon\sigma \left(T_1^4 - T_a^4 \right) + \varepsilon\Delta R \tag{3.34c}$$

where $\Delta R = \sigma \left[(T_a + 273)^4 - (T_{sky} + 273)^4 \right]$ is   the   difference   between   the long-wavelength radiation exchange between the horizontal surface at temperature T_a to the sky temperature at T_{sky}. Because T_a and T_{sky} are at low temperature, according to Wein's displacement law, Eq. (1.3), the emitted radiation, will be long- wavelength radiation, which is blocked by the atmosphere.

Using the expression for relation between T_a and T_{sky} given by Eq. (3.33); for $T_a = 25\ °C$, the values of

$$\Delta R = \sigma\left[(T_a + 273)^4 - (T_{sky} + 273)^4\right] = 60\ W/m^2 \tag{3.34d}$$

Furthermore, after linearization of first term of Eq. (3.34c), one can have

$$\dot{q}_r = h_r(T_1 - T_a) + \varepsilon\Delta R \tag{3.34e}$$

where

$$h_r = \varepsilon\sigma\left(T_1^2 + T_2^2\right)(T_1 + T_2) = \varepsilon(4\sigma\bar{T})^3 \quad \text{for} \quad \bar{T}_1 \cong \bar{T}_2 \tag{3.34f}$$

It is necessary to discuss here that the numerical value of ΔR becomes zero for surfaces not directly exposed to sky conditions.

Example 3.9 Determine the radiative heat-transfer coefficient between the surface of a wall at 25 °C and the room air temperature at $T_a = 24\ °C$.

Solution
Because the temperatures are approximately the same, from Eq. (3.34f), we have

$$h_r = 4\varepsilon\sigma T^3 = 4 \times 5.64 \times 10^{-8} \times (25 + 273)^3$$
$$= 6\ W/m^2\ °C$$

3.3.5 Evaporation (Mass Transfer)

In this case, one surface will be a wetted surface for mass transfer to either the surrounding or any cooler surface unlike other cases discussed previously.

For the wetted surface, too, convective heat transfer will always be present. The rate of heat transferred in this case is given as:

$$\dot{Q} = h_{cw}(T_w - T_a) \tag{3.35}$$

where T_w is the fluid temperature; and T_a is the ambient air temperature. The evaporation process involves the transfer of mass from one location of the system to another location of the system. The rate of mass transfer is given as

$$\dot{m} = h_D\left(\rho_w^0 - \rho_a^0\right) \tag{3.36}$$

where $\dot{m}$ is the rate of mass flow per unit area, $(\text{kg/m}^2\text{s})$; h_D is the mass-transfer coefficient $[(\text{kg/s})(\text{m}^2/\text{kg/m}^3)]$; ρ_w^0 is the partial mass density of water vapor, kg/m^3; and ρ_a^0 is the partial mass density of air (kg/m^3).

According to Lewis relation for a mixture of air and water vapor, we know that

$$\frac{h_{cw}}{h_D} = \rho^0 C_{pa} \tag{3.37}$$

By assuming $T_w = T_a = T$ at the water–air interface, using Eq. (3.37), Eq. (3.36) becomes

$$\dot{m} = \frac{h_{cw}}{\rho^0 C_{pa}} \frac{M_w}{RT} (P_w - P_a) \tag{3.38}$$

The rate of heat transfer on account of mass transfer of water vapor is given by

$$\dot{Q}_{ew} = \dot{m}L \tag{3.39}$$

where L is the latent heat of vaporization and P_w and P_a are partial pressure of water vapor and air respectively.

After substituting an expression for $\dot{m}$ from Eq. (3.38) into (3.39), we get

$$\dot{Q}_{ew} = \frac{L h_{cw}}{\rho^0 C_{pa}} \frac{M_w}{RT} (P_w - P_a) \tag{3.40}$$

Let $H_0 = \frac{L h_{cw}}{\rho^0 C_{pa}} \frac{M_w}{RT}$

Then

$$\dot{Q}_{ew} = H_0(P_w - P_a) \tag{3.41}$$

Using the perfect gas equation, $\rho^0 = \frac{P_a M_a}{RT}$, for air (for 1 mol of air) and by substituting in the expression for H_0, one has

$$\frac{H_0}{h_{cw}} = \frac{L}{C_{pa}} \frac{M_w}{M_a} \frac{1}{P_a} \tag{3.42}$$

For small values of P_w, $P_T = P_a$, and the above equation become

$$\frac{H_0}{h_{cw}} = \frac{L}{C_{pa}} \frac{M_w}{M_a} \frac{1}{P_T} \tag{3.43}$$

where P_T is the total pressure of the air–vapor mixture. The values of the different parameters used in Eq. (3.43) are as follows:

L = latent heat of vaporization = 2200 KJ/kg; C_{pa} = Specific heat of air 1.005 KJ/kg °C.

M_w = 18 kg/mol (molar mass of water); P_T = Total pressure of air–vapour mixture = $1atm$.

1 atm = 101,325 N/m^2.

Substituting all of these values in Eq. (3.43) and solving

$$\frac{H_0}{h_{cw}} = 0.013$$

The best representation of the heat- and mass-transfer phenomenon is obtained if the value of $\frac{H_0}{h_{cw}}$ is taken to be 16.276×10^{-3} instead of 0.013. Thus, the rate of heat transfer on account of mass transfer is written as

$$\dot{q}_{ew} = 16.276 \times 10^{-3} \times h_{cw} \times (P_w - P_a) \tag{3.44}$$

If the surface is exposed to the atmosphere, then the above equation reduces to

$$\dot{q}_{ew} = 16.276 \times 10^{-3} \times h_{cw} \times (P_w - \gamma P_a) \tag{3.45}$$

where γ is the relative humidity of air in fraction.

Furthermore, after linearization of Eq. (3.45), one can have

$$\dot{q}_{ew} = h_{ew}(T_w - T_a) \tag{3.46}$$

where the evaporation heat transfer coefficient can be given as

$$h_{ew} = \frac{16.276 \times 10^{-3} \times h_{cw} \times (\bar{P}_w - \gamma \bar{P}_a)}{(T_w - T_a)} \tag{3.47}$$

For a wetted surface exposed to ambient moving air with velocity 'V', then the numerical value of h_{cw} can be considered as given by Eq. (3.29b).

The values of partial vapor pressure at temperature T for the ranges of temperature 10–90 °C can be obtained from the following expression [43]

$$P(T) = \exp\left[25.317 - \frac{5114}{T + 273}\right] \tag{3.48}$$

Example 3.10 Determine the rate of evaporative heat-transfer coefficient in W/m^2 °C from a wetted surface (35 °C) to an ambient air temperature (15 °C) with a relative humidity of 50 %.

Solution

The vapor pressure $P(T)$ in N/m^2 at any temperature T (in °C) can be calculated from Eq. (3.48).

Thus, the vapor pressures at wetted and ambient air temperatures can be calculated as

$$P(T_w) = \exp\left(25.317 - \frac{5144}{273 + 35}\right) = 5517.6 \text{ N/m}^2$$

and

$$P(T_a) = \exp\left(25.317 - \frac{5144}{273 + 15}\right) = 1730 \text{ N/m}^2$$

Using $h_c = 2.8$ W/m^2 °C (Eq. (3.29b) for $V = 0$) and substituting the values in Eq. (3.45), we have the rate of evaporation in W/m^2 as:

$$\dot{q}_{ew} = 16.273 \times 10^{-3} \times 2.8 \times (5517.6 - 0.5 \times 1730) = 211.99 \text{ W/m}^2$$

The evaporative heat-transfer coefficient can be calculated from Eq. (3.47) as

$$h_{ew} = \frac{\dot{q}_{ew}}{(T_w - T_a)} = \frac{211.99}{35 - 15} = 10.60 \text{ W/m}^2 \text{ °C}$$

3.3.6   Total Heat-Transfer Coefficient

The **total heat transfer per m^2** ($\dot{q}_T$) from any solid surface to the surrounding (air) will be the sum of heat transfer by conduction (Eq. 3.20b), convection (Eq. 3.21b), radiation (Eq. 3.34e), and evaporation (Eq. 3.46). As the thermal conductivity of air is very small, conductive heat transfer from any solid surface to the air can be neglected.

$$\dot{q}_T = \dot{q}_c + \dot{q}_r + \dot{q}_{ew} \tag{3.49}$$

The above equation can also be written in terms of respective heat-transfer coefficient as

$$\dot{q}_T = (h_c + h_r + h_{ew})[T_s - T_a] \tag{3.50}$$

where an expression for h_c, h_r, and h_{ew} are given by Eqs. (3.20c), (3.21c), and (3.34f), respectively. It is important to mention here that T_s represents the temperature of the solid dry/wetted surface as required in the analysis.

In Eq. (3.50), the sum of convective, h_c, and radiative, h_r, heat transfer coefficients, i.e., $(h_c + h_r)$, can be considered as given by Eq. (3.23a) as follows:

$$h = h_{\mathrm{c}} + h_{\mathrm{r}} = 5.7 + 3.8V \tag{3.51}$$

Equation (3.51) is also **the total heat-transfer coefficient** without evaporation. Sometimes it is denoted as h_{o}.

With evaporation it becomes

$$h = h_{\mathrm{c}} + h_{\mathrm{r}} + h_{\mathrm{ew}} \tag{3.52}$$

It can be defined as the total heat-transfer coefficient, which includes convective, radiative, and evaporative transfer from the solid surface to the surrounding air.

3.4 Overall Heat-Transfer Coefficient

Heat transfer from a medium (generally fluid [air/water]) at higher temperature to another medium (may be either air or fluid) at a lower temperature may occur between many layers with different thermo-physical properties and different thicknesses. In addition, there may be more than one mode of heat transfer (conduction, convection, radiation, and evaporation) involved in the process. In such cases, the concept of the overall heat-transfer coefficient (U) is adopted for the evaluation of the heat-transfer coefficient from one medium to a second medium by way of a third medium.

(A) **Parallel slabs** [6]

Consider a composite wall with a hot surface at temperature T_A and a cold surface at temperature T_B (Fig. 3.2). Heat is transferred from the hot surface to the cold surface through different conducting slabs. Assuming a steady state, i.e., the heat transfer rate, $\dot{Q}$, through structure is the same through each layer and it can be written as

$$\dot{Q} = Ah_{\mathrm{a}}(T_A - T_0) = \frac{AK_1(T_0 - T_1)}{L_1} = \frac{AK_2(T_1 - T_2)}{L_2} = \frac{AK_3(T_2 - T_3)}{L_3}$$
$$= Ah_{\mathrm{b}}(T_3 - T_B) \tag{3.53}$$

where terms like $h\Delta T$ represent heat transfer by either convection or radiation or both depending on the situation, and terms like $K(\Delta T/L)$ represent heat transfer by conduction through various layers.

In addition, the rate of heat transfer per unit area is

$$\dot{q} = \frac{\dot{Q}}{A} = \frac{T_A - T_0}{R_{\mathrm{a}}} = \frac{T_0 - T_1}{R_1} = \frac{T_1 - T_2}{R_2} = \frac{T_2 - T_3}{R_3} = \frac{T_3 - T_B}{R_{\mathrm{b}}} \tag{3.54}$$

where the R's are the thermal resistances, which is inversely proportional to the respective heat transfer coefficient at various surfaces and layers, and are defined by
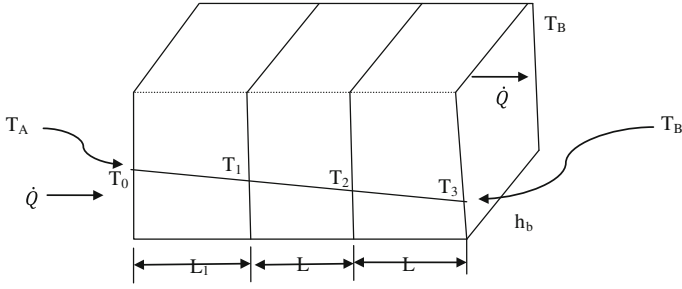
Fig. 3.2 One-dimensional heat flow through parallel perfect contact slabs

$$R_\mathrm{a} = \frac{1}{h_\mathrm{a}}, \quad R_1 = \frac{L_1}{K_1}, \quad R_2 = \frac{L_2}{K_2}, \quad R_3 = \frac{L_3}{K_3}, \quad R_\mathrm{b} = \frac{1}{h_\mathrm{b}}.$$

Equation (3.46) can also be written the following form:

$$T_A - T_0 = \dot{q}R_\mathrm{a};$$
$$T_0 - T_1 = \dot{q}R_\mathrm{a};$$
$$T_1 - T_2 = \dot{q}R_\mathrm{a};$$
$$T_2 - T_3 = \dot{q}R_\mathrm{a};$$
$$T_3 - T_B = \dot{q}R_\mathrm{a}.$$

Addition of the above equations results in:

$$\dot{q} = \frac{T_A - T_B}{R} = U(T_A - T_B) \tag{3.55}$$

where $R = R_\mathrm{a} + R_1 + R_2 + R_3 + R_\mathrm{b}$; and U is the overall heat-transfer coefficient, W/m^2 K.

An overall heat-transfer coefficient, U, is related to the total thermal resistance 'R' of the composite wall by

$$R = \frac{1}{U} = \frac{1}{h_\mathrm{a}} + \frac{L_1}{K_1} + \frac{L_2}{K_2} + \frac{L_3}{K_3} + \frac{1}{h_\mathrm{b}} \tag{3.56}$$

(B) Parallel slabs with air cavity [6]

A roof structure with an air cavity, as shown in Fig. 3.3, includes the effect of air conductance (C) for estimation of the overall heat-transfer coefficient. The value of air conductance (C) varies nonlinearly with the thickness of the air gap, and it becomes constant at larger air gaps as shown in Fig. 3.4.
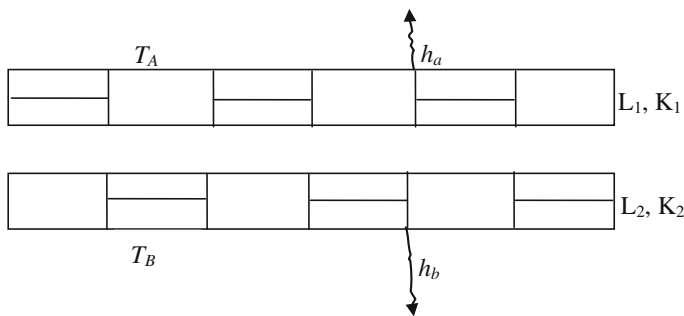
Fig. 3.3 Configuration of parallel slabs with air cavity

Fig. 3.4 Variation of thermal air conductance with air-gap thickness
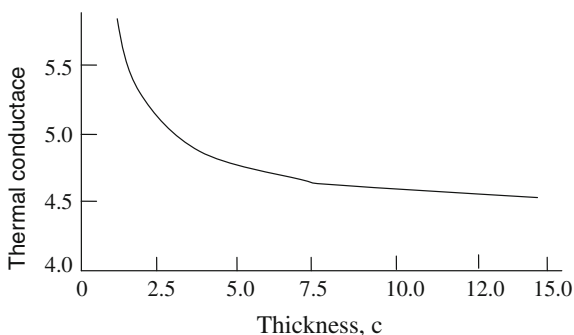
In steady-state condition, the rate of heat transfer at different layers is given as follows:

$$
\dot{Q} = Ah_a(T_A - T_0) = \frac{AK_1(T_0 - T_1)}{L_1} = AC(T_1 - T_2) = \frac{AK_2(T_2 - T_3)}{L_2}
$$
$$
= Ah_b(T_3 - T_B) \tag{3.57}
$$

Following derivation of Eq. (3.50), the equation for U can also be derived for the present case, and its expression is given by through Eq. (3.51) as

$$
\dot{Q} = UA(T_A - T_B) \tag{3.58}
$$

where

$$
U = \left[\frac{1}{h_a} + \frac{L_1}{K_1} + \frac{1}{C} + \frac{L_2}{K_2} + \frac{1}{h_b} \right]^{-1} = \frac{1}{R}.
$$

In general, the overall heat-transfer coefficient (U) for the configuration with air cavities is given as follows:

$$U = \left[\frac{1}{h_a} + \sum_i \frac{L_i}{K_i} + \sum_i \frac{1}{C_i} + \frac{1}{h_b}\right]^{-1} \qquad (3.59)$$

Example 3.11 Calculate the overall heat-transfer coefficient (U) for

(a) Single concrete $(K = 0.72 \text{ W/m } °\text{C})$ slab with thickness (L) of 0.10 m
(b) Two-layered horizontal slab with same material and thickness
(c) Two-layered horizontal slab with air cavity (0.05 m)
(d) Two-layered horizontal slab with two air cavities (each 0.05 m air gap)

for the following parameters:

$h_a = 9.5 \text{ W/m}^2 \text{ °C}, \quad L_1 = L_2 = 0.05, \quad K_1 = K_2 = 0.72 \text{ W/m °C}; \quad C_1 = C_2 = 4.75 \text{ W/m}^2 \text{ °C}$ for 0.05 m air cavity, and $h_b = 5.7 \text{ W/m}^2 \text{ °C}$.

Solution

From Eq. (3.59), one can evaluate an overall heat-transfer coefficient in W/m² °C as follows:

For a single concrete slab,

$$U = \left[\frac{1}{9.5} + \frac{0.10}{0.72} + \frac{1}{5.7}\right]^{-1} = 2.38 \text{ W/m}^2 \text{ °C}$$

For a two-layered horizontal slab,

$$U = \left[\frac{1}{9.5} + \frac{0.05}{0.72} + \frac{0.05}{0.72} + \frac{1}{5.7}\right]^{-1} = 2.38 \text{ W/m}^2 \text{ °C}$$

For a two-layered horizontal slab with a single air cavity,

$$U = \left[\frac{1}{9.5} + \frac{0.05}{0.72} + \frac{1}{4.75} + \frac{0.05}{0.72} + \frac{1}{5.7}\right]^{-1} = 1.59 \text{ W/m}^2 \text{ °C}$$

For a two-layered horizontal slab with a two air–cavity gap separated by metal foil,

$$U = \left[\frac{1}{9.5} + \frac{0.05}{0.72} + \frac{1}{4.75} + \frac{1}{4.75} + \frac{0.05}{0.72} + \frac{1}{5.7}\right]^{-1} = 1.19 \text{ W/m}^2 \text{ °C}$$

It is clear from the above calculations that an increase of the number of air cavities from one to two reduces U from 1.59 to 1.19 W/m² °C, respectively.

Objective Questions

3.1 The first law thermodynamics process is
(a) reversible   (b) irreversible   (c) both   (d) none of these
Answer: (a)

3.2 Energy conservation process depends on
(a) The first law of thermodynamics (b) the second law of thermodynamics
(c) the Zeroth law of thermodynamics   (d) the third law of thermodynamics
Answer: (a)

3.3 The existence of temperature depends on
(a) the first law of thermodynamics   (b) the second law of thermodynamics
(c) the Zeroth law of thermodynamics   (d) the third law of thermodynamics
Answer: (c)

3.4 The second law of thermodynamics states that heat transfer takes place
(a) from a colder body to a hotter body   (b) from a hotter body to a colder body
(c) from equal temperature of both bodies   (d) None of these
Answer: (b)

3.5 The second law of thermodynamics process is
(a) reversible   (b) irreversible   (c) both   (d) none of these
Answer: (b)

3.6 The thermal conductivity of material depends on
(a) temperature   (b) length   (c) thickness   (d) none of these
Answer: (a)

3.7 The heat-transfer coefficient is inversely proportional to
(a) thermal resistance   (b) thermal conductivity   (c) thickness   (d) none of these
Answer: (a)

3.8 The rate of heat transfer from higher to lower temperature is due to
(a) conduction   (b) convection   (c) radiation   (d) all of these
Answer: (d)

3.9 Conductive heat transfer is governed by
(a) Fourier's law   (b) Stefan–Boltzmann law
(c) Wein's displacement law   (d) None of these
Answer: (a)

3.10 Radiation heat transfer is governed by
(a) Stefan–Boltzmann's law   (b) Fourier's law
(c) Wein's displacement law   (d) none of these
Answer: (a)

3.11 Expression for an overall heat-transfer coefficient (U) is derived under
(a) Transient condition   (b) Periodic conduction
(c) Quasi–steady state condition   (d) Steady-state condition
Answer: (d)

3.12 Conduction, convection, and radiation losses are
  (a) dependent on one another   (b) independent on one another
  (c) independent of temperature (d) none of these
  Answer: (b)

3.13 Convective heat transfer depends on
  (a) physical properties of the fluid   (b) physical properties of the solid
  (c) characteristics dimension   (d) all of these
  Answer: (a) & (c)

3.14 Radiation heat transfer between two surfaces is mainly due to
  (a) short wavelength   (b) infra-red
  (c) UV   (d) long-wavelength radiations
  Answer: (d)

3.15 The evaporative heat transfer coefficient (h_{ew}) is
  (a) proportional to h_{cw} (b) inversely proportional to h_{cw}
  (c) independent of h_{cw} (d) none of these
  Answer: (a)

3.16 The evaporative heat-transfer coefficient (hew) depends on convective heat
  transfer coefficient due to
  (a) Lewis relation   (b) Newton's law
  (c) Fourier's law   (d) none of these
  Answer: (a)

3.17 The shape (geometrical) factor for parallel surfaces is
  (a) 1   (b) 10   (c) <1   (d) infinity
  Answer: (a)

3.18 The expression for the radiative heat-transfer coefficient (h_r) for surfaces
  having temperatures almost same but different is
  (a) $4\varepsilon\sigma T^4$ (b) $4\varepsilon\sigma T^3$ (c) $\frac{1}{4}\varepsilon\sigma T^3$ (d) $0.4\varepsilon\sigma T^3$
  Answer: (b)

3.19 For an inclined surface, an expression for the free convective heat-transfer
  coefficient can be obtained from
  (a) $Nu = C(GrPr)^n$ (b) $Nu = C(GrPr\sin\theta)^n$
  (c) $Nu = \frac{1}{C}(GrPr)^{1/n}$ (d) $Nu = C(GrPr\cos\theta)^n$
  Here $C = 0.54$ and $n = 1/4$.
  Answer: (d)

3.20 The partial vapour pressure depends on temperature
  (a) linearly   (b) proportionally   (c) exponentially   (d) none of these
  Answer: (c)

3.21 The value of heat transfer for a hot surface facing upward is maximum for
  (a) a horizontal surface   (b) an inclined surface
  (c) a vertical surface   (d) None of these
  Answer: (a)

Problems

3.1 Determine the convective heat-transfer coefficient and rate of convective heat loss from a horizontal rectangular plate (1.0 m × 0.8 m) at 134 °C to a plate at 20 °C placed at a distance of 0.10 m above the first plate.
Hint: Use Eq. (3.24), Table 3.3, Appendix V, and characteristic length = 0.10 m.

3.2 Determine the convective heat-transfer coefficient and rate of convective heat loss from a horizontal rectangular plate (1.0 m × 0.8 m) at 134 °C to water at 20 °C.
Hint: Use Eq. (3.24), Table 3.3, Appendix V, and characteristic length = 0.90 m.

3.3 Determine the convective heat-transfer coefficient and rate of convective heat loss from a vertical wall (2.40 m × 1.80 m high) exposed to air at 1 atm pressure and 15 °C. The wall temperature is maintained at 49 °C.
Hint: Use Eq. (3.24), Table 3.3, Appendix V, and characteristic length = 1.8 m.

3.4 Determine the convective heat-transfer coefficient and rate of convective heat loss from a vertical wall (2.40 m × 1.80 m high) at 49 °C exposed to a plate placed at a distance of $d = 0.10$ m at 15 °C.
Hint: Use Eq. (3.24), Table 3.3, Appendix V, and characteristic length = 0.10 m

3.5 Calculate the average convective heat-transfer coefficient and rate of convective heat loss from a rectangular (0.91 m × 0.61 m) horizontal plate at 127 °C to air flowing with 4.57 m/s at 27 °C.
Hint: Use Eq. (3.28), Appendix V, and characteristic length = 0.76 m

3.6 Calculate the average convective heat-transfer coefficient and rate of convective heat loss from a 1 m horizontal flat surface to flowing water (20 m/s). The plate temperature is maintained at 27.8 °C above the water temperature.
Hint: Use Eq. (3.28), Appendix V, and characteristic length = 1 m

3.7 Derive an expression for the interface temperature of two material composite walls in a steady-state condition.
Hint: Use the following expression

$$\dot{q} = -K_a A \frac{T_2 - T_1}{L_a} = -K_b A \frac{T_3 - T_2}{L_b}.$$

3.8 Determine the surface temperature of a horizontal plate (0.3 m × 0.3 m) exposed to water at 20 °C. The rate of heat transfer to the horizontal plate ($\dot{q}$) is 900 W.
Hint: Assume that surface temperature $T_s = 30\,°C$ and take $T_f = (30 + 20)/2 = 25\,°C$. Calculate Gr and Pr using physical properties of the water at 25 °C (Appendix V), then calculate $\bar{h} = \frac{K}{L}(0.14)(Gr \cdot Pr)^{1/3}$. And use $T_s^1 - T_0 = \frac{\dot{q}}{hA}$ with $T_a = 20\,°C$.

Repeat the computation with new T_s^1. Repeat the process until the value of T_s^1 becomes constant.

3.9 Calculate the evaporative heat-transfer coefficient for a wetted surface at 60 °C with surrounding temperature of 35 °C and a relative humidity of about 60 %.

   Hint: See Example 3.9.

3.10 Repeat Problem 3.9 to estimate the evaporative heat-transfer coefficient for different levels of relative humidity ($\gamma = 20, 40, 60,$ and 80 %).

3.11 A horizontal plate (1 m $\times$ 1 m) is heated to 50 °C and exposed to ambient air at 30 °C at atmospheric pressure. Estimate the convective heat-transfer coefficient.

   Hint: Use $h = \frac{K}{L} \times 0.14 \times (Gr \cdot Pr)^{1/3}$, and evaluate Gr and Pr for thermal properties of the air at 30 °C (Appendix V) and $L = (L_1 + L_2)/2$.

3.12 Calculate the convective heat-transfer coefficient from a blackened surface to (a) water (base fluid) and (b) nano-fluid (TiO_2 nano-particles) of a passive double-slope solar still for the parameters given in Example 3.7. Properties of the TiO_2 nano-particles are given below:

   $C_{pp} = 697 (J/kg\ K)$, $\beta_p = 8.1 \times 10^{-6} (K^{-1})$, $\varphi_p = 0.004$ %, $\rho_p = 4.230 \times 10^3 (Kg/m^3)$, thermal conductivity of particle $k_p = 17.5 (W/m\ ^\circ C)$, diameter of Nan particle, $(d_p) = 15$ nm. Take temperature of the water $(T_w) = 60.25$ °C, and temperature of Nan fluid $(T_{nf}) = 61.65$ °C.

   Hint: See Example 3.7.

3.13 For the parameters given in Problem 3.12, evaluate the convective heat-transfer coefficient of a passive double-slope solar still from a blackened surface to (a) water (base fluid) and (b) nano-fluid (TiO_2 nanoparticles) for an 0.008 % and an 0.015 % volumetric concentration of nanoparticles.

   Hint: See Example 3.7.

References

1. E.K. Akpinar, A. Midilli, Y. Bicer, J. Food Eng. **72**(4), 320 (2006)
2. R. Petela, Sol. Energy **74**(6), 469 (2003)
3. J.T. Szargut, Energy **28**(11), 1047 (2003)
4. R. Battisti, A. Corrado, Energy **30**, 952 (2005)
5. G. Lewis, G. Keoleian, *National Pollution Prevention Center, School of Natural Resources and Environment* (University of Michigan, Ann Arbor, 1996)
6. G.N. Tiwari, *Solar Energy: Fundamental, Design, Modelling and Applications* (Narosa Publishing House, New Delhi and CRC Press, New York, 2004)
7. W.C. Mc Adams, *Heat Transmission*, 3rd edn. (McGraw Hill, New York, 1954)
8. H.Y. Wong, *Heat Transfer for Engineers* (Longman London art, New York, 1977)
9. J.P. Holman, *Heat Transfer* (McGraw Hill Int. (UK) Ltd, 1992)
10. J.C.A. Maxwell, *Treatise on Electricity and Magnetism*, II edn. (Clarendon Press, Oxford, UK, 1881)

11. D.A.G. Bruggeman, Ann. Phys. Leipzig **24**, 636 (1935)
12. R.L. Hamilton, O.K. Crosser, I&EC Fundam **1**, 182 (1962)
13. F.J. Wasp, Solid–liquid slurry pipeline transportation. Trans. Tech. 1977 (Berlin)
14. K. Khanafer, K. Vafai, Int. J. Heat Mass Transf. **54**, 4410 (2011)
15. A. Einstein, Ann. Phys. Leipzig **19**, 289 (1906)
16. H.C. Brinkman, J. Chem. Phys. **20**, 571 (1952)
17. G. Batchelor, J. Fluid Mech. **83**, 97 (1977)
18. T. Lundgren, J. Fluid Mech. **51**, 273 (1972)
19. S. Maiga, S.J. Palm, C.T. Nguyen, G. Roy, N. Galanis, Int. J. Heat Fluid Flow **26**, 530 (2005)
20. X. Wang, X. Xu, S.U.S. Choi, J. Thermophys. Heat Transfer **13**, 474 (1999)
21. J. Buongiorno, ASME J. Heat Transfer **128**, 240 (2006)
22. B.C. Pak, Y.I. Cho, Exp. Heat Transfer **11**, 151 (1999)
23. C.T. Nguyen, F. Desgranges, G. Roy, N. Galanis, T. Maré, S. Boucher, H.A. Mintsa, Int. J. Heat Fluid Flow **28**, 1492 (2007)
24. W.J. Tseng, K.C. Lin, Mater. Sci. Eng. A **355**, 186 (2003)
25. P.K. Namburu, D.P. Kulkarni, D. Misra, D.K. Das, Exp. Therm. Fluid Sci. **32**, 397 (2007)
26. P.K. Namburu, D.K. Das, K.M. Tanguturi, R.S. Vajjha, Int. J. Therm. Sci. **48**, 290 (2009)
27. W. Duangthongsuk, S. Wongwises, Int. J. Heat Mass Transf. **52**, 2059 (2009)
28. D.P. Kulkarni, D.K. Das, G. Chukwa, J. Nanosci. Nanotechnol. **6**, 1150 (2006)
29. D.P. Kulkarni, D.K. Das, S.L. Patil, J. Nanosci. Nanotechnol. **7**, 2318 (2007)
30. C.J. Ho, W.K. Liu, Y.S. Chang, C.C. Lin, Int. J. Therm. Sci. **49**, 1345 (2010)
31. Y. Xuan, W. Roetzel, Int. J. Heat Mass Transf. **43**, 3701 (2000)
32. R.S. Vajjha, D.K. Das, ASME **131** (2009)
33. K. Khanafer, K. Vafai, M. Lightstone, Int. J. Heat Mass Transfer **46**, 3639 (2003)
34. K.S. Wang, J.H. Lee, S.P. Jang, Int. J. Heat Mass Transfer **50**, 4003 (2007)
35. C.J. Ho, M.W. Chen, Z.W. Li, Int. J. Heat Mass Transfer **51**, 4506 (2008)
36. E.N. Seider, G.E. Tate, Ind. Eng. Chem. **28**(12), 1429 (1936)
37. B.C. Pak, Y.I. Cho, Exp. Heat Transfer **11**(2), 151 (1998)
38. Y. Xuan, Q. Li, Trans. ASME **125** (2003)
39. S.E.B. Maiga, C.T. Nguyen, N. Galanis, G. Roy, T. Mare, M. Coqueux, Int. J. Numer. Meth. Heat Fluid Flow **16**(3), 275 (2006)
40. S.M. Fotukian, M.N. Esfahany, Int. Comm. Heat Mass Transfer **37**, 214 (2010)
41. L. Qiang, X. Yimin, Sci. China (Series E) **45**(5), 408 (2002)
42. V. Gnielinski, Int. Chem. Eng. **16**, 359 (1976)
43. W. Duangthongsuk, S. Wongwises, Exp. Therm. Fluid Sci. **33**, 706 (2009)
44. J. Fernandez, N. Chargoy, Sol. Energy **44**(4), 215 (1990)

Additional References

45. P.K. Nag, *Engineering Thermodynamics*, 3rd edn. (McGraw-Hill Ltd, New York, 2005)
46. F. Kreith, *The CRC Handbook of Thermal Engineering* (CRC Press Springer, Berlin, 2000)
47. P. Incropera, F. DeWitt, P. David, *Fundamentals of Heat and Mass Transfer*, 4th edn. (Wiley (SEA) Pte Ltd, New York, 1998)
48. Y.A. Cengel, *Introduction to Thermodynamics and Heat Transfer* (McGraw-Hill companies, Inc, New York, 1997)
49. D.R. Pitts, L.E. Sissiom, *1000 Solved Problems in Heat Transfer* (McGraw-Hill, New York, 1991)
50. D. Rapp, *Solar Energy* (Prentice-Hall Inc, Engle Wood Cliffs, 1981)
51. W.M. Kays, M.E. Crawford, *Convective Heat and Mass Transfer*, 2nd edn. (McGraw-Hill, Inc., New York, 1980)
52. K.G.T. Holland, T.E. Unny, G.D. Raithby, L. Konicek, J. Heat Transfer **98**(2), 189 (1976)

Chapter 4
Solar Cell Materials, Photovoltaic Modules and Arrays

Abstract The photon energy (*hv*) of solar radiation in visible wavelengths creates ionization in the depletion region of the n–p junction of solar cells for generating direct (dc) power (current × voltage) to meet the basic high-grade energy demand of human beings in underdeveloped regions for rural applications. Rural applications include streetlights, calculators, water pumping, and mobile charging, etc.

Keywords Photovoltaic effect · Solar cell materials · PV modules · PV arrays · PVT system

4.1 Introduction

A photovoltaic (PV) cell transforms the solar energy incident on it into electricity due to the photovoltaic effect. Different technologies utilizing applications of solar cell constitute the field of photovoltaics. The solar radiation incident on the solar cell separates the charge carriers in the absorbing material. The electric fields present at the junctions or inhomogeneities in material provide the required EMF for the flow of electric current in the external circuit and hence the power generation.

Photovoltaic devices are driven by the flux of solar radiation and acts like a current source. Photovoltaic cells are mostly made of silicon semiconductor junction devices. Thus, knowledge of the basics of semiconductors is a prerequisite to understand photovoltaic cells, and this knowledge is outlined in subsequent sections of this book.

The rudimentary unit of a PV generator is the photovoltaic cell or solar cell. A PV generator is a system consisting of PV modules connected in different combinations (series connected, parallel connected, or connected in both configurations) depending on the requirements.

Depending on the nature of the electricity conduction, solids can be divided into three categories: conductors, semiconductors, and insulators. These can be differentiated on the basis of energy band gap between the valence band and the

Fig. 4.1 Semiconductor band structure of intrinsic material (i) Photon absorption $hv < E_g$, no photoelectric absorption. (ii) $(hv_1 - E_g)$ excess energy dissipated as heat and (iii) $hv_2 - E_g$ photon energy equals band gap (from Tiwari and Mishra [20])
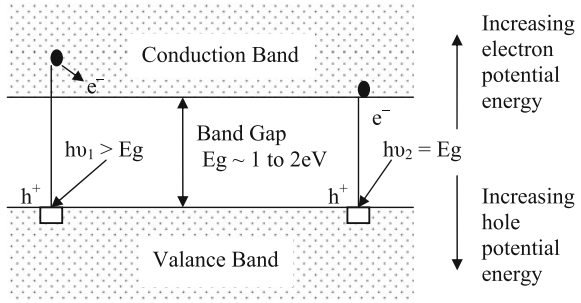
conduction band. The energy band gap in the case of insulators ($hv < E_g$, h is the Planck's constant, and v is the frequency), is very large. Thus, electrons in the valence band cannot reach the conduction band, which results in no conduction of current. For a semiconductor $(hv > E_g)$, this gap is less than that of the insulator, and the valence electron can cross this gap on acquiring thermal or light energy (Fig. 4.1). For conductors $(E_g \approx 0)$, no forbidden gap exists, and hence electron can easily move to the conduction band.

The variation of the band gap with temperature is given by the relation:

$$E_g(T) = E_g(0) - \frac{aT^2}{T + b} \tag{4.1}$$

where the value of a and b for different materials are given in Table 4.1. At $T = 0$, $E_g(T) = E_g(0)$, the materials behave as an insulator.

A variation of the band gap with temperature is shown in Fig. 4.2 for germanium, silicon, and gallium arsenide.

Example 4.1 Evaluate the band gap in a silicon crystal at 50 °C.

Solution
Substituting the appropriate values in the above equation, we obtain:

$$E_g(T) = 1.16 - \frac{7 \times 10^{-4} \times (323)^2}{323 + 1100} = 1.11 \text{ eV}$$

Table 4.1 The values of constants 'a' and 'b'

Material	$E_g(0)$ (eV)	a (eV K^{-1})	b (K)
Silicon (Si)	1.166	7×10^{-4}	636
Gallium arsenide (GaAs)	1.519	5.8×10^{-4}	204
Germanium (Ge)	0.7437	4.77×10^{-4}	235

Fig. 4.2 Temperature dependence of the energy band gap of germanium (*bottom curve*), silicon (*middle curve*), and GaAs (*top curve*)
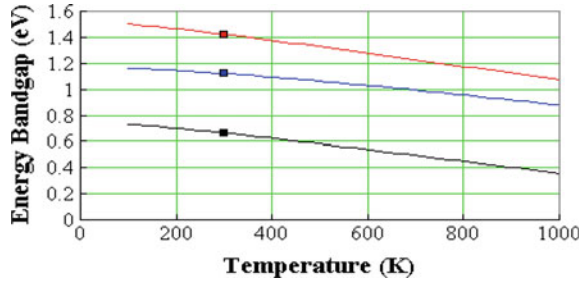
4.2 Fundamentals of Semiconductor and Solar Cells

In this section, the fundamental of the semiconductor will be discussed first and those of the solar cell second.

4.2.1 Doping

The conductivity of the intrinsic semiconductor can be increased by adding the controlled amount of specific impurity ions. The doped semiconductors are known as "extrinsic semiconductors." Impurity ions, having valency less than that of the semiconductor, produces electron acceptor sites, which trap free electrons. These traps have an energy level near that of the valence band in the forbidden energy band. These traps (vacancies) produce positively charged states called "holes," which contribute to the conduction of current through the material. Such a material is called p-type material having holes as majority carriers and electrons as minority carriers. The impurity ions, having valency greater than that of the semiconductor, produce an extra electron. In this case, electrons are the majority charge carriers, and holes are the minority charge carries. The resulting material is known as the "n-type" material.

The semiconductor can again be divided into two categories:

(i) **Intrinsic**

Intrinsic (pure) semiconductors have Fermi-level in the middle of the conduction and the valence band, i.e., the probability of a state being occupied is 0.5.

At thermal equilibrium, the concentration of electrons and holes is same and equal to the intrinsic carrier concentration for intrinsic semiconductors, i.e.,

$$n_e = n_h = n_i \tag{4.2}$$

Doping in a pure semiconductor affects the carrier concentration and other electrical properties of the semiconductor. According to Maxwell–Boltzmann statistics, the electron and hole concentration is given as follows:

$$n_e = N_c(T) \exp\left[\frac{(E_F - E_C)}{kT}\right] \tag{4.3}$$

$$n_h = N_V(T) \exp\left[\frac{(E_V - E_F)}{kT}\right] \tag{4.4}$$

where E_F is energy of the Fermi level; E_C is the energy at the bottom of the conduction band; and E_V is the energy at the top of the valance band as shown in Fig. 4.1. From Eq. (4.2), one can write an expression to relate them as follows:

$$n_i^2 = n_e \times n_h = N_V(T) \times N_C(T) \exp\left[\frac{-(E_C - E_V)}{kT}\right] \tag{4.5}$$

Equation (4.5) infers that the intrinsic carrier concentration depends on the energy band gap, which is independent of doping concentration.

The concentration factors $N_C(T)$ and $N_V(T)$ are given by

$$N_C(T) = N_C = \left[\frac{2\pi m_e kT}{h^2}\right]^{3/2} \tag{4.6a}$$

$$N_V(T) = N_V = \left[\frac{2\pi m_h kT}{h^2}\right]^{\frac{3}{2}} \tag{4.6b}$$

where m_e (9.11×10^{-31} kg) and m_h are the effective masses of electrons and holes, which are constant with temperature; and h is Plank's constant.

From Eq. (4.5), the ratio of probabilities that two states, namely, the conduction band and the valance band (separated by energy difference ΔE), will be occupied by an electron is equal to the Boltzmann factor $\left(= \exp\left(-\frac{\Delta E}{kT}\right)\right)$ where k is Boltzmann's constant. This is the ratio of the gas constant $R(8.314 JK^{-1}mole^{-1})$ and the Avogadro constant $N_A(6.022 \times 10^{22})$ and is expressed as $k = R/N_A$. The values of k in different units are given in Table 4.2.

Furthermore, the densities of free electrons in conduction (n_e) and free holes (n_h) in the valence band are equal ($n_e = n_h = n_i$) and can be obtained from Eq. (4.5) as

$$n_e = n_h = \sqrt{[N_V(T) \times N_C(T)]} \times \exp\left[-\frac{\Delta E}{2kT}\right] \tag{4.7}$$

which is proportional to $\exp(-E_g/2kT)$. Here $E_g = \Delta E = E_C - E_V$.

Table 4.2 Value of Boltzmann constant in various units	Value of k	Units
	1.38×10^{-23}	$J\ K^{-1}$
	8.62×10^{-5}	$eV\ K^{-1}$
	1.38×10^{-16}	$erg\ K^{-1}$

(ii) **Nonintrinsic**

For a nonintinsic or doped (low doping) semiconductor, if n_0, p_0 and n_i are the electron, the hole, and the intrinsic carrier concentrations, respectively, then at thermal equilibrium:

$$n_0 p_0 = n_i^2 \tag{4.8}$$

where the intrinsic carrier concentration n_i depends on the material characteristics and the operating temperature (for Si, $n_i \approx 1.08 \times 10^{10}$ cm^{-3} at 300 K) [1].

4.2.2   Fermi Level

The Fermi level is the energy level that resides in between the donor (or acceptor) level and the conduction (or valence) band of an extrinsic semiconductor. At a given temperature T, the probability for the majority charge carriers to become excited for conduction of the current varies as $\exp[-e\varphi/kT]$ where e is the electronic charge; and φ is the electric potential difference between the Fermi level and the valence or conduction band, k the Boltzmann constant (Table 4.2).

For n-type material,

$$E_F = E_C + kT \ \ln \frac{N_D}{N_C} \tag{4.9}$$

where E_F is the Fermi-energy level; E_C is the conduction band energy (Fig. 4.1); N_D is the donor concentration; and N_C is the effective density of states in conduction band (Eq. 4.6a) and is constant at a fixed temperature T.

For p-type material,

$$E_F = E_V - kT \ \ln \frac{N_A}{N_V} \tag{4.10}$$

where E_V is the valence band energy; N_A is the acceptor ion concentration; and N_V is the effective density of states in the valence band (Eq. 4.6b).

Example 4.2 Calculate the shift in Fermi energy level in a silicon crystal doped with a Vth-group impurity of concentration 10^{15} cm^3.

Given: the effective density of states in the conduction band $= 2.82 \times 10^{19}$ cm^{-3}; band gap $= 1.1$ eV; and room temperature $= 27$ °C.

Solution

From Eq. (4.9), one has

$$E_F = E_C + kT \ln (N_D/N_C)$$

If the valence band is taken as the reference level, then $E_C = 1.1$ eV. Substitution of the values gives

$$E_F = 1.1 + kT \ln (N_D/N_C)$$
$$E_F = 1.1 + \left[8.62 \times 10^{-5} \times 300 \times \ln \left(10^{15}/(2.82 \times 10^{19})\right)\right]$$
$$= 1.1 - 0.265 = 0.835$$

The shift is $0.835 - 0.55 = 0.285$

4.2.3 p–n Junction

The electronic inhomogeneity is the essential need for the conversion of solar energy into electricity. The electronic asymmetry is created by putting the p-type and n-type semiconductors in contact. At the junction between the p-type and n-type semiconductors, the majority charge carriers flow in the opposite direction, thus creating a positive charge in the n-region and a negative charge in the p-region. During the flow of charge carriers, the recombination process results in a region having no mobile charges; this region is known as the "depletion region." The steady state is achieved when the built-in potential across the junction opposes the flow of charge from either side.

The p–n junction (Figs. 4.3 and 4.4) is connected either in forward bias or in reverse bias per the required application. In the forward bias condition (Fig. 4.5a), the charge carrier faces reduced band potential difference V_B, whereas in reverse bias condition (Fig. 4.5b), the charge carriers must overcome increased band potential

Fig. 4.3 p–n junction energy levels in a p–n junction (from Tiwari and Mishra [20])
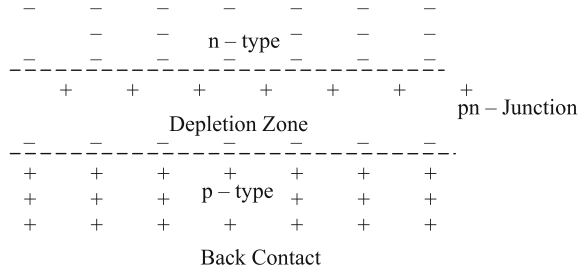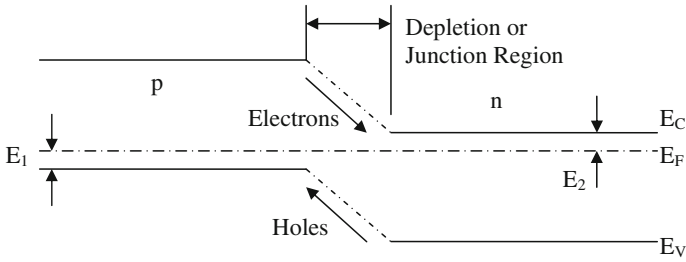
Fig. 4.4 Energy levels for a p–n junction (from Tiwari and Mishra [20])
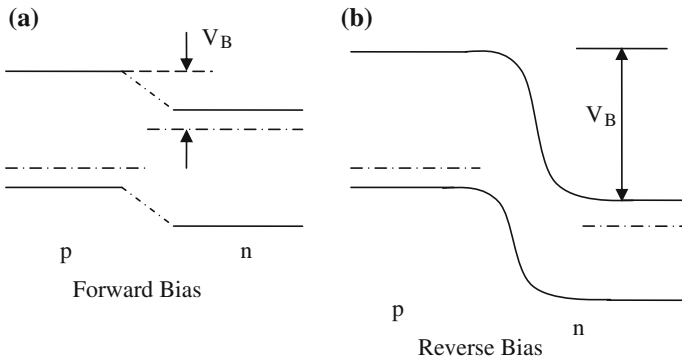
Fig. 4.5 Energy levels for p–n junction with **a** forward bias and **b** reverse bias (from Tiwari and Mishra [20])

difference V_B. The electrons and holes generated by any means recombine after moving a typical distance (diffusion length, L). The time difference between the generation and recombination of electron and holes is known as "relaxation time τ." The typical order of relaxation time for an intrinsic semiconductor is as long as 1 s, whereas for extrinsic semiconductors the order of relaxation time varies between 10^{-2} s and 10^{-8} s depending on the doping concentration as well as other factors.

Thermally or photo (light)-generated electrons and holes act as charge carriers in the semiconductor (Fig. 4.6). The potential difference across the junction pulls the minority charge carriers from the depletion region into the respective potential gradients, which in turn cause the generation current I_g. In the absence of illumination, the generation current is mainly controlled by temperature.

In an isolated junction, a reverse recombination current I_r of equal magnitude is produced from the bulk material to nullify the imbalance of current in the depletion region. The recombination current slightly reduces the band potential V_B. The recombination current can be controlled by external bias across the junction (Fig. 4.7).

Fig. 4.6 Generation and recombination currents at p–n junction (from Tiwari and Mishra [20])
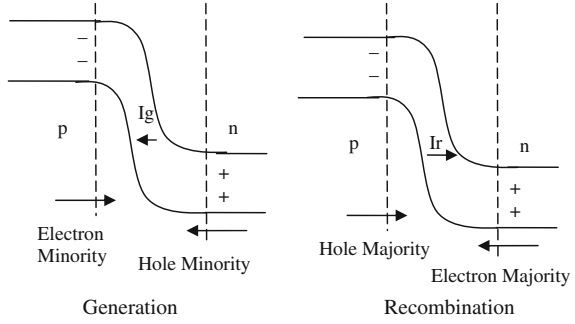
Fig. 4.7 Generation and recombination currents with external bias (from Tiwari and Mishra [20])
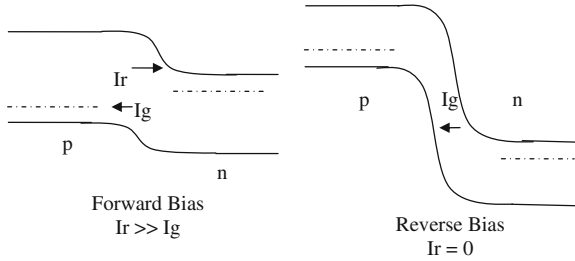
4.2.4   p–n Junction Characteristics

The p–n junction characteristics are given in Fig. 4.8.

In the absence of external bias $(V = 0)$

$$I_r = I_g \tag{4.11}$$

The recombination current will be increased. For a forward bias of voltage V, this is given as follows:

$$I_r = I_g \exp\left(\frac{eV}{kT}\right) \tag{4.12}$$

In the absence of illumination, the total current is given by the following equation:

$$I_D = I_r - I_g = I_g \left[\exp\left(\frac{eV}{kT}\right) - 1 \right] \tag{4.13}$$

Fig. 4.8 Dark characteristics for p–n junction (from Tiwari and Mishra [20])
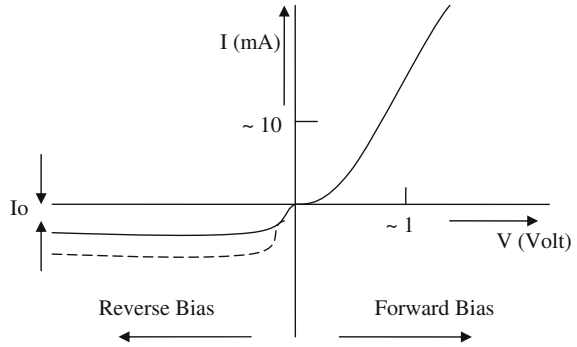
Equation (4.13) is the Shockley equation and can be written as follows:

$$I_D = I_0 \left[\exp\left(\frac{eV}{kT}\right) - 1 \right] \tag{4.14}$$

where $I_0(=I_g)$ is the saturation current under reverse bias before avalanche breakdown occurs. The reverse saturation current increases with increasing temperature (Fig. 4.8, dotted curve). The typical order of magnitude of I_0 is 10^{-8} A m^{-2}. This is also known as the "leakage current" or "diffusion current."

Example 4.3 Determine the value of the saturation current for silicon at 50 °C.

Solution

The dependence of the saturation current on temperature is given by the following relation:

$$I_0 = AT^3 \, \exp\left(E_g/kT\right)$$

Here, A is the non-ideality factor and its value is taken as 1:

$$E_g = 1.11 \text{ eV} = 1.11 \times 1.6 \times 10^{-19} \text{ J}$$

Substituting the known values in the above equation, we get

$$I_0 = (50 + 273)^3 \exp\left(-\frac{1.11 \times 1.6 \times 10^{-19}}{1.38 \times 10^{-23} \times 323}\right) = 1.67 \times 10^{-10} \text{A m}^{-2}$$

Example 4.4 Determine the value of dark current in the limiting case $V \rightarrow 0$.

Solution
From Eq. (4.14), one gets, as $V \to 0$, $\exp(eV/kT) \to 1$ and hence dark current $I_D \to 0$.

4.2.5 Photovoltaic Effect

The electron–hole pairs, generated in the depletion region due to the absorption of solar radiation, are driven by the internal electric fields producing a photo current (I_L). The direction of the photocurrent is in a direction opposite that of the forward dark current as shown in Fig. 4.8. This photocurrent flows continuously even in the absence of external applied voltage and is known as the "short circuit current"(I_{SC}). Absorption of more light produces more electron–hole pairs; hence, this current depends linearly on the light intensity. This effect is known as the **photovoltaic effect**. The p–n junction with this effect is referred to as a **solar cell**.

The overall solar cell current, I, is the difference of the light-induced current I_L and the diode dark current I_D.

$$I = I_D - I_L \tag{4.15}$$

Then,

$$I = I_0 \left[\exp \left(\frac{eV}{kT} \right) - 1 \right] - I_L \tag{4.16}$$

Example 4.5 Determine the value of the overall cell current in the limiting case $V \to 0$.

Solution
From Eq. (4.16), one gets, as $V \to 0$, $V \to 0$, $\exp(eV/kT) \to 1$, and hence, $I \to -I_L$.

Example 4.6 Determine the voltage for a zero overall solar cell current.

Solution
Substituting current $I = 0$ in Eq. (4.16), we have

$$I_0 \left[\exp \left(\frac{eV}{kT} \right) - 1 \right] - I_L = 0$$

or

$$\exp \left(\frac{eV}{kT} \right) = \frac{I_L}{I_0} + 1$$

or

$$V = \frac{kT}{e} \ln \left[\frac{I_L}{I_0} + 1 \right]$$

4.2.6 Solar Cell (Photovoltaic) Materials

Solar cells consist of various materials with different structures to reduce the initial cost and achieve maximum electrical efficiency. There are various types of solar cell materials, namely, (a) single crystal, (b) polycrystalline, (c) amorphous silicon, (d) compound thin-film material, as well as other semiconductor absorbing layers, which give highly electrical-efficient solar cells for specialized applications.

Crystalline silicon cells (c-Si) are expensive. However, they are most popular due to their easy availability. Amorphous silicon thin-film solar cells are less expensive. The amorphous silicon layer is used with both hydrogen and fluorine incorporated into the structure. The a-Si:F:H alloys are produced by the glow-discharge decomposition of Si F_4 in the presence of hydrogen. The efficiency of a-Si module lies between 6 and 8 %.

Thin-film solar cells can be manufactured by using a variety of compound semiconductors. These compound materials include (a) **copper–indium selenide** ($CuInSe_2$), (b) **cadmium sulphide** (CdS), (c) **cadmium telluride** (CdTe), (d) **copper sulphide** (Cu_2S), and (e) **indium phospate** (InP). The stability of the **copper–indium selenide** ($CuInSe_2$) solar cell appears to be excellent. Combinations of different band-gap materials in the tandem configurations lead to photovoltaic generators with greater efficiencies.

Silicon (Si)
Crystalline **silicon** (c-Si) is the most extensively used bulk material for the manufacturing of solar cells. Bulk silicon can be processed to obtain monocrystalline silicon, polycrystalline silicon, or ribbon silicon using advanced processing technologies.

(i) **Monocrystalline silicon (c-Si)**: Monocrystalline silicon is cut from cylindrical ingots made from the Czochralski process. The solar cells are cut in a pseudo-square shape to minimize the waste of processed monocrystalline silicon. Therefore, in a solar panel manufactured from monocrystalline silicon, some portion of the module area is uncovered from the cell.

(ii) **Polycrystalline or multicrystalline silicon (poly-Si or mc-Si)**: In polycrystalline or multicrystalline silicon, the crystal structure is not same throughout. Solar cells made from polycrystalline silica have grain boundaries. Polycrystalline silica is made from square ingots. The ingots are made by cooling and solidifying the molten silicon in a controlled environment. The wafers (of thickness approximately 180–350 μm) are cut from square ingots

and used for manufacturing polycrystalline solar cells. Polycrystalline solar cells are less expensive compared with monocrystalline solar cells, but these solar cells have lower efficiency due to the grain boundaries present in solar cells.

(iii) **Ribbon silicon**: Ribbon silicon is a thin film made from molten silicon. It is polycrystalline in nature. In the processing of ribbon silicon, there is no waste of processed silicon as well as no sawing requirement; therefore, solar cells manufactured from ribbon silicon are less expensive than polycrystalline solar cells.

Reflection losses are reduced by using an antireflection coating that allows higher absorbance of light into the solar cell. The antireflection coating is done by plasma-enhanced chemical vapour deposition (PECVD) technique. Previously titanium dioxide was used for an antireflection coating, but it is gradually being replaced by silicon nitride. Textured surfaces also reduce reflection losses; therefore, textured front surfaces can be used (for monocrystalline as well as polycrystalline solar cells) as an antireflection coating.

Silicon thin-films are grown by PECVD technique using silane and hydrogen gas. Deposition parameters decide the nature of thin film, namely, amorphous silicon, protocrystalline silicon, or nanocrystalline silicon.

The dangling and twisted bonds in thin-film silicon cause a deformation in the conduction and the valence band. These bonds also lead to the formation of energy levels in the band-gap region due to defects. The energy-conversion efficiency of solar cells made from these materials tends to be lower than those of bulk silicon solar cells. They are also less expensive to produce. Here the number of collected charge carriers per incident photon is less; the **quantum efficiency** of thin-film solar cells is also lower.

Amorphous silicon (band gap,1.7 eV) dominantly absorbs the visible portion of the solar spectrum. Nano-crystalline (nc-Si) and crystalline (c-Si) solar cells have nearly the same energy band gap. Therefore, the layered structure of these materials results in a layered structure of the solar cell, which is known as a "tandem solar cell." In theses solar cells, the upper layer (a-Si) mostly absorbs the visible part and the bottom layer mostly absorbs the infrared part of the solar spectrum.

To enhance the efficiency of thin-film solar cells, different techniques—such as light-trapping schemes—have been deployed to maximize the absorption of sunlight. At the same time, advanced thermal-processing techniques have been used to improve the crystallinity and hence the electrical properties of solar cells. Thin-film solar cells with improved crystallinity are known as "thin-film crystalline on glass" (CGS) [1]. These solar cells are low-cast solar cells, which utilizes the high-efficiency properties of bulk silicon.

Thin-film solar cells with transparent top and bottom cover are potentially used in building-integrated photovoltaic (BiPV) systems. These thin-film solar cells can be used in glazed portions of the building such as windows or the façade. Despite all of the present technologies (i.e., generations of solar cells), first-generation solar

cells abundantly fill the photovoltaic market; hence, efforts are being made to achieve a lowest cost per watt of solar cell.

Cadmium telluride (CdTe)

Amongst all the thin-film solar cells, CdTe thin solar cells have high light-absorbing efficiency. CdTe can be easily deposited on substrate and is suitable for large-scale production. The toxicity of these solar cells due to presence of cadmium is a major issue, which must be addressed for the use of this technology in the production of solar cells. Scientific research performed at different laboratories, particularly at National Renewable Energy Laboratories (NREL) in the USA, found that amount of cadmium released into the atmosphere during the processing of CdTe solar cells is comparatively lower than that of other solar-cell technologies [2].

Copper-indium selenide (CuInSe$_2$)

These thin-film solar cells are chemically resistant to the moisture and thermally stable at higher temperatures (approximately 500 °C). The high light-absorbing capacity, improved optical properties, and better electrical characteristics of CuInSe$_2$ make it a suitable option for the manufacturing of thin-film solar cells.

Gallium arsenide (GaAs) multijunction

The multijunction thin-film solar cell comprises thin films of different materials grown by molecular beam epitaxy. Different materials have different optical properties, and the materials are chosen in such a way that the multijunction solar cell absorbs the maximum incident solar radiation and converts it into electricity. An example of this type of solar cell is the multijunction of GaAs:Ge:GaInP$_2$ [3]. Gallium arsenide (GaAs) multijunction devices are the most efficient solar cells. The maximum achievable efficiency in the laboratory is 40.7 % [4].

Single crystal solar cell

Single-crystalline solar cells made from high-purity materials (solar grade) show excellent efficiencies and long-term stability, but they are expensive.

Figure 4.9 shows the diagram of the silicon solar cell structure and mechanism. The electric current generated in the semiconductor is extracted by contact to the front and rear of the cell. The cell is covered with a thin layer of dielectric material, an antireflective coating or ARC, to minimize reflection from the top surface.

The total series resistance of the cell can be expressed as:

$$R_s = R_{cp} + R_{bp} + R_{cn} + R_{bn} \tag{4.17}$$

where R_{cp} is the metal contact to p-type semiconductor resistance; R_{bp} the bulk p-type resistance (the bulk of p-type region is where the most electron–hole pairs are generated by the absorption of light and where minority carriers [electrons] are transported by diffusion and partially lost by recombination); R_{cn} is the contact to n-type semiconductor resistance; and R_{bn} is the bulk n-type resistance.
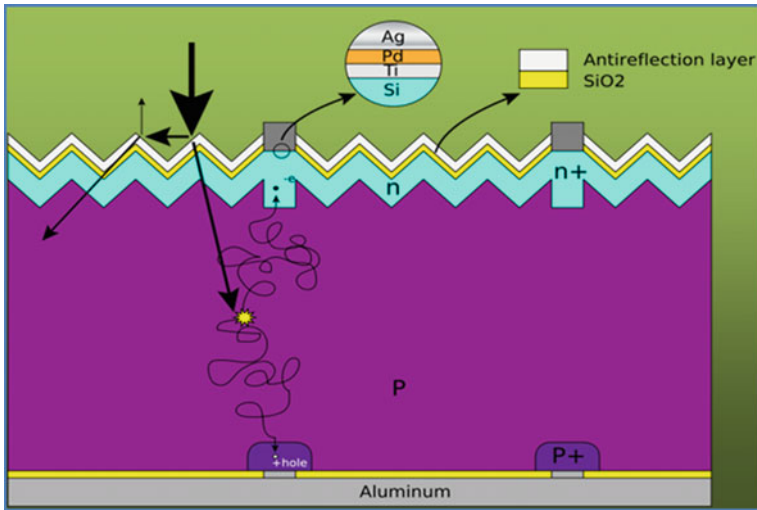
Fig. 4.9 The structure and working mechanism of silicon solar cells (from Tiwari and Mishra [20])

The idealized junction current is given as follows:

$$I = I_0 \left[\exp\left(\frac{e(V - IR_s)}{kT}\right) - 1 \right] \qquad (4.18)$$

In addition, a shunt path may exist for current flow across the junction due to surface effect or a poor junction region. This alternate path for current constitutes a shunt resistance R_p across the junction. Then,

$$I = I_L - I_0 \left[\exp\left(\frac{e(V - IR_s)}{AkT}\right) - 1 \right] - \left(\frac{V - IR_s}{R_p}\right) \qquad (4.19)$$

where A is an empirical non-idealist factor and is usually 1.

Light-absorbing dyes (DSSC)
The dye-sensitized solar cell (DSSC) consists of a metalorganic dye (light-absorbing material) and porous titanium dioxide (semiconducting material) in liquid or solid electrolyte [5]. The performance of DSSC strongly depends on the porous layer of titanium dioxide. Dye present in solar cell absorbs sunlight and generates electrons, which are transported to the anode TiO_2; photogenerated electrons are further transported through the external load, then to the electrolyte on the other side of the dye, and finally to the dye.

Most of the materials used in this type of thin-film solar cell have low cost. It can be manufactured by the less expensive roll-printing technique. The major

disadvantages of DSSC are instability, degradation, and use of platinum and ruthenium (expensive materials). Although the conversion efficiency of DSSC is low, the low cost has allowed this technology to grow on a commercial scale.

Organic/polymer solar cells
Organic solar cells are thin-film polymer solar cells. The polymer solar cell is made using organic semiconducting materials such as copper phthalocyanine, poly-phenylene vinylene, and carbon fullerenes [6]. These solar cells are less costly, have a high optical absorption coefficient, and the energy band gap can be tailored by changing the chain length of polymer. The energy-conversion efficiency of organic solar cells is low compared with inorganic solar cells. Lower stability, smaller life, and degradation are the major limitations of organic solar cells.

Nanocrystalline solar cells
Nanocrystalline solar cells consist of nanocrystals of semiconductor (Si, CIGS, CdTs porous metal oxide semiconductors) grown on a substrate (Si, conducting polymers, organic semiconductors, dyes). They are thin-film solar cells with a very high light-absorbing coefficient. The nano-size dimensions of these solar cells are responsible for their higher values of conversion efficiency. Earlier these solar cells were synthesized by molecular beam epitaxy, but now a day spin coating (a less costly technology) is used for the manufacturing of nanocrystalline solar cells.

Example 4.7 What is the condition for a zero idealized junction current ($I = 0$)?

Solution
Substituting $I = 0$ in Eq. (4.18), we get

$$\exp\left(\frac{eV}{kT}\right) = 1 \Rightarrow V = 0$$

4.2.7 Basic Parameters of the Solar Cell

In this section, some basic parameters essential for understanding the characteristics curve of the solar cell are discussed.

Overall current (I)
The overall current (I) flowing through a solar cell is given by the following equation:

$$I = I_D - I_L \tag{4.20}$$

or

$$I = I_0 \left[\exp\left(\frac{eV}{kT}\right) - 1 \right] - I_L \tag{4.21}$$

Where I_D is the diode dark current; and I_L is the light induced current I_0 leakage current.

Short circuit current (I_{SC})
The short-circuit current is the light-induced current that occurs when the load in the circuit is zero, i.e., both terminals (positive and negative) of the solar cell are connected together.

Open-circuit voltage (V_{oc})
The open-circuit voltage is the voltage across the solar cell when there is no current flowing in the circuit, i.e., there is infinite resistance between the terminals of the solar cell. This can be found from Eq. (4.21) and is expressed as follows:

$$V_\infty = \frac{kT}{e} \ln\left(\frac{I_L}{I_0} + 1\right) \tag{4.22}$$

The open-circuit voltage is the voltage of the maximum load in the circuit.

I–V characteristics
The I–V characteristics curve, with illumination and without illumination, is shown in Fig. 4.10. The I-V curve for both cases is plotted using $I = I_0 \left[\exp\left(\frac{e(V - IR_s)}{kT}\right) - 1 \right]$ [7]. For an ideal solar cell, the series resistance must be zero and the shunt resistance must be infinite. For better performance of a solar cell, the series resistance must be kept as minimum as possible and the shunt resistance must be as large as possible. In commercial solar cells, the shunt resistance is very large and is neglected compared with the forward resistance of the diode.

Fig. 4.10 *I–V* characteristics of a solar cell with and without illumination (from Tiwari and Mishra [20])
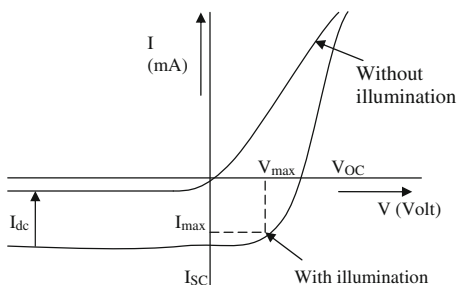
The optimum load resistance $R_L(P_{max}) = R_{pmax}$ corresponding to the maximum power delivered from the solar cell is obtained as follows:

$$P_{max} = V_{Pmax} I_{Pmax} \tag{4.23}$$

$$R_{Pmax} = \frac{V_{Pmax}}{I_{pmax}} \tag{4.24}$$

The efficiency is defined as

$$\eta = P/\phi \tag{4.25}$$

where $P = V \times I$ is the power delivered by the PV generator; $\phi = I_T \times A$ is the solar radiation falling on the PV generator; and I_T is the solar intensity; and A is the surface area irradiated.

Fill factor (FF)

The fill factor gives an idea of the maximum power output withdrawn from the solar cell for a given V_{oc} and I_{sc}. Mathematically it is given by Eq. (4.26). The value of FF under ideal conditions is unity. Deviation from the ideal value is due to defects and contact resistance. The lower the value of the FF, the less sharp will be the I–V curve (Fig. 4.11). For an Si solar cell, the maximum value of FF is 0.88.

$$\mathrm{FF} = \frac{P_{max}}{V_{oc} \times I_{sc}} = \frac{I_{max} \times V_{max}}{V_{oc} \times I_{sc}} \tag{4.26}$$

Maximum power (P_{max})

Output power from a solar cell is obtained by multiplying the output voltage and output current as given below:

$$P_{out} = V_{out} \times I_{out} \tag{4.27}$$

Fig. 4.11 Characteristic and power curve for determining the fill factor (FF) (from Tiwari and Mishra [20])
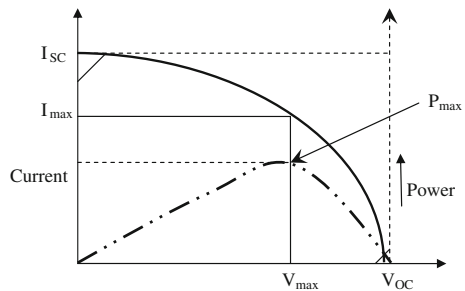
Similarly the maximum power is obtained by multiplying V_{max} and I_{max}. This corresponds to the maximum value of product IV on the characteristics curve. Hence,

$$P_{max} = V_{max} \times I_{max} \tag{4.28}$$

From Eq. (4.26) one can obtain:

$$P_{max} = V_{oc} \times I_{sc} \times FF \tag{4.29}$$

Solar cell efficiency (η_{ec})
The solar cell power conversion efficiency can be given as

$$\eta_{ec} = \frac{P_{max}}{P_{in}} = \frac{V_{max} \times I_{max}}{\text{Incident solar radiation} \times \text{Area of solar cell}} = \frac{V_{oc} \times I_{sc} \times FF}{I(t) \times A_c} \tag{4.30}$$

where I_{max} and V_{max} correspond to the given $(I(t))$.

Example 4.8 Calculate the fill factor for a solar cell that has the following parameters:

$$V_{OC} = 0.2 \text{ V}, I_{SC} = -5.5 \text{ mA}, V_{max} = 0.125 \text{ V}, I_{max} = -3 \text{ mA}$$

Solution
Substituting the appropriate values in Eq. (4.26), we get

$$\text{Fill factor} = \frac{V_{max} \times I_{max}}{V_{oc} \times I_{sc}} = \frac{0.125 \times 3}{0.2 \times 5.5} = 0.34$$

Example 4.9 Calculate the maximum power and electrical efficiency of a solar cell at an intensity of 200 W/m^2.
    Given: $V_{OC} = 0.24 \text{ V}, I_{SC} = -9 \text{ mA}, V_{max} = 0.14 \text{ V}, I_{max} = -6 \text{ mA}, A_C = 4 \text{ cm}^2$

Solution
From Eq. (4.28), we have

$$P_{max} = V_{max} \times I_{max} = 0.14 \times (-6) = -0.84 \text{ mW}$$

and from Eq. (4.30), we have

Solar cell electrical efficiency = output/input
$$= \left(0.14 \times 6 \times 10^{-3}\right) / \left(200 \times 4 \times 10^{-4}\right) = 0.0105 = 1.05 \ \%$$

Example 4.10 Calculate the power output from a solar cell under standard test conditions ($I(t) = 1000$ W/m^2 and $T_c = 25\,°$C), when $\eta = 16\,\%$, FF $= 0.782$, and the aperture area $= 4.02 \times 10^{-4}$ m^2.

Solution
Power output $= 0.16 \times 1000 \times 4.02 \times 10^{-4} \times 0.782 = 0.05$ W.

Effect of solar cell temperature on solar cell efficiency
A fraction of the total solar radiation incident on a solar cell produces electricity, and the remaining radiation is converted into thermal energy. A part of the produced thermal energy raises the temperature of solar cell, and the rest is dissipated from top and bottom of the solar cell [7]. The temperature of the solar cell deteriorates the electrical performance of the solar cell. For unit area, the energy balance can be written as follows:

$$\alpha\tau I(t) = \eta_c I(t) + U_L(T_c - T_a) \tag{4.31}$$

where τ is the transmittivity of the cover of the solar cell; α is the absorptivity of the solar cell; η_c is the electrical efficiency of the solar cell; and U_L is the overall loss coefficient, which is the sum of the top-loss coefficient and the bottom-loss coefficient. The top-loss coefficient is determined by taking into account the effect of both convection and radiation, and the bottom-loss coefficient includes the effect of the conductive heat transfer coefficient due to the bottom of solar cell as well as convective heat transfer coefficient from the back surface of the bottom to the ambient.

The nominal operating cell temperature (NOCT) is the temperature of the solar cell corresponding to 20 °C ambient temperature, 800 W/m^2 solar radiation, 1 m/s wind speed, and no-load conditions. It is defined as that cell or module temperature reached when the cells are mounted in their normal way at a solar radiation level of 800 W/m^2, a wind speed of 1 m/s, an ambient temperature of 20 °C, and no-load operation (i.e., with $\eta_c = 0$).

For no-load condition, $\eta_c = 0$; therefore from Eq. (4.31), one can have

$$\frac{\alpha\tau}{U_L} = \frac{T_{c,\text{NOCT}} - T_a}{I(t)_{\text{NOCT}}} \tag{4.32}$$

From Eq. (4.31), the solar cell temperature can be found as follows:

$$T_c = T_a + \frac{\alpha\tau}{U_L}\left(1 - \frac{\eta_c}{\alpha\tau}\right)I(t) \tag{4.33}$$

The value of $\frac{\alpha\tau}{U_L}$ calculated from Eq. (4.32) is substituted in Eq. (4.33) to calculate the solar cell temperature for a given solar radiation, ambient temperature, and wind speed.

The electrical efficiency (η_{ec}), as a function of temperature, is given by [8]

$$\eta_{ec} = \eta_0[1 - \beta_0[T_c - 298]] \tag{4.34a}$$

where η_0 is electrical efficiency of solar cell under the standard test conditions (STC) [solar flux of 1000 W/m^2 and surrounding temperature of 20 °C]; β_0 is the silicon efficiency temperature coefficient $(0.0045 \text{ K}^{-1} \text{ or } 0.0064 \text{ K}^{-1})$; and T_c is the solar cell temperature (K).

4.3 Generation of Solar Cell (Photovoltaic) Materials

Solar cell technologies are categorized into three generations. These generations are divided according to the time of evolution of respective technology. Presently, research and development activities for efficiency improvement and reduction in production costs for each generation of solar cell are being done in various research groups worldwide. Most of the solar cell market is covered by first-generation solar cells [9].

4.3.1 First Generation

First-generation solar cells are based on Si wafer technology. First-generation solar cells include monocrystalline and polycrystalline silicon solar cells. These solar cells are single-junction solar cells with 33 % theoretical efficiency [10]. The processing technology involved for the manufacturing of first-generation solar cell requires high energy and labour. The energy-conversion efficiency of first-generation solar cell is 15–20 %. These solar cells are widely used amongst all generations of solar cells.

4.3.2 Second Generation

Second-generation solar cells include the amorphous solar cells. The efficiency of these solar cells is low in comparison with the first-generation solar cells, but their production cost is low. This solar cell technology does not require high-temperature processing unlike first-generation solar cells. The second generation solar cell materials include CdTe, CIGS, a-Si, and micromorphous silicon. Second-generation solar cells are manufactured by depositing the thin film of the above materials on the substrates (Si, glass or ceramics) using chemical vapour deposition, molecular beam epitaxy, or spin-coating technique.

4.3.3 Third Generation

Third-generation technologies mainly focus on the improvement of the energy-conversion efficiency and light-absorption coefficient of second-generation solar cells while keeping the production cost close to that of second-generation solar cells. The enhancement in efficiency can be achieved by manufacturing multijunction solar cells, improving the light-absorption coefficients (concentrating solar cells), and using techniques to increase the carrier collection [11].

Here it is important to mention that there are two ways of defining solar cell electrical efficiency:

(a) Under standard test conditions (STC), i.e., indoor conditions

$$\left[I_o = \text{constant} = 1000 \text{ W/m}^2 \text{ and surrounding temperature} = 25 \text{ }^{\circ}\text{C}\right]$$

All electrical efficiencies of different solar cells reported earlier are under standard test conditions (STC) (Fig. 4.11a) NREL

(b) Under open-field conditions [for available variable solar radiation in terrestrial regions in wavelength range between 0.23 and 2.6 μm]

This is defined as

$$\eta = \frac{P_m}{I(t)} = \frac{I_m \times V_m}{I(t)} \tag{4.34b}$$

Here only energy of photons ($E = hc/\lambda = hv$) belonging to wavelength between 0.40 and 0.70 μm have sufficient energy greater than band-gap energy, E_g, Eq. (4.1), $\left(hv > E_g\right)$, which is responsible to carry electrons from the balance band to the conduction band and hence current is produced. Furthermore, the energy content from 0.40 to 0.70 μm is 47 %. This means that one cannot have an efficiency of solar cells produced from silicon (Si), gallium arsenide (GaAs), and germanium (Ge) materials that is more than 47 %. This is the reason that the electrical efficiency of such solar cells is much lower than 47 %.

4.4 Photovoltaic (PV) Module and PV Array

As discussed previously, solar cells convert solar energy in wavelengths of visible radiation into direct current (DC) electricity by way of the photovoltaic effect. Single solar cells cannot generate enough power for many of practical applications; therefore, solar cells are connected in series and sandwiched between top transparent and bottom opaque/transparent covers to protect them from adverse weather conditions. The series-connected packaged solar cells are known as photovoltaic modules (**PV modules**). PV modules are available in different sizes and shapes

depending on the required electrical output. The number and size of series-connected solar cells made from a particular material (wafer-based c-Si, thin-film CdTe, or crystalline silicon) primarily decides the output of the PV module. The electrical interconnections as well as weather and climatic conditions are some other factors that affect the output of a PV module. PV modules made of different materials are available on the market, but glass-to-Tedlar PV modules with 36 solar cells (each cell produces 0.5 V) connected in series (which can charge a typical 12-V battery) are widely used. In this type of PV module, the series-connected cells are sandwiched between a top glass cover and Tedlar and sealed with a metal frame. Most of the modules are rigid, but thin-film solar cell–based modules are flexible. The positive and negative terminals for interconnections are provided on the backside of PV module. PV modules are rated in terms of peak watts (W_p), which is the power produced at 1000 W/m^2. A typical panel with a 40 W_p rating may produce energy between 100 and 200 Wh/day.

A photovoltaic (PV) array is a collection series or parallel, or both series and parallel, connected photovoltaic (PV) modules. The size of a PV array depends on the requirement of electrical power. The DC power produced from a PV array is converted into AC power using an inverter and fed to the different electrical loads. PV modules are connected in series to achieve the desired voltage; then such series-connected strings are connected in parallel to enhance the current and hence power output from the array. The size of the PV array decides its capacity, which may be in watts, kilowatts, or megawatts.

The electrical output of a PV module depends on solar irradiance, solar cell temperature, electrical efficiency of solar cell, and load resistance. For a given size of solar cell, the current increases with increasing solar irradiance, and the current is marginally affected (marginal increase) due to temperature rise; however, a higher solar cell temperature decreases the voltage output of solar cell, which in turn decreases power output. Load resistance is decided by the operating point of module; the preferred operating is peak power point. Solar cell efficiency is governed by the manufacturing process and the solar cell material, and it varies from 9 to 20 %. Therefore, for better performance, the PV module in an array must operate at the peak power point; the array must be installed in an open place (no shading); and the PV module must be kept cool.

4.4.1 Single-Crystal Solar Cell Module

These type of module deploy series-connected crystalline solar cells sandwiched between a top glass cover (with high transmittivity, low-iron glass), an encapsulate (transparent and insulating; most commonly used is ethylene vinyl acetate (EVA)), and a back cover (Tedlar/Mylar/glass) as shown in Fig. 4.12. A series or parallel, or both series and parallel, combination of these modules forms the crystalline PV array.

Fig. 4.12 Typical arrangements of commercial Si solar cells: **a** cell, **b** module of 36 cells, and **c** array of PV module (from Tiwari and Mishra [20])
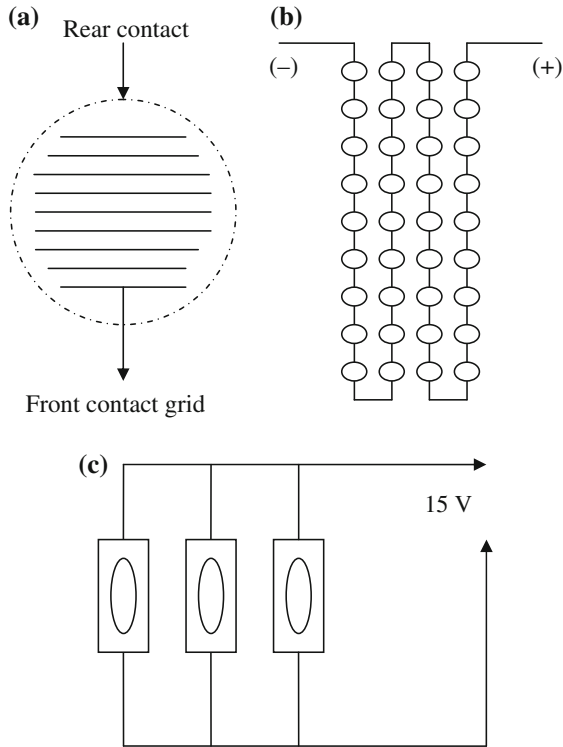
Crystalline PV modules are divided into two categories depending on the material of the back cover of the module. If the back cover of the module is made of opaque Tedlar, it is known as a "glass-to-Tedlar" or "opaque" PV module (Fig. 4.13a); if the back cover is made of glass, it is known as a "glass-to-glass" or "semitransparent" PV module (Fig. 4.13b, c). The amount of light transmitted from a semitransparent PV module depends on its packing factor. The lower the packing factor, the lower the area covered by the solar cell. Therefore, for electrical/thermal/day lighting application, the packing factor of the semitransparent PV module can be tailored (Fig. 4.13b, c) per the desired requirement (thermal/electrical/daylighting) from the system.

4.4.2 Thin-Film PV Modules

Thin-film PV modules are made of thin-film solar cells. Thin-film solar cells are manufactured at lower temperature compared with crystalline solar cells; hence, these technologies are less energy intensive. In addition, the production cost of thin-film solar cells is lower than that of crystalline solar cells. Furthermore, the thin
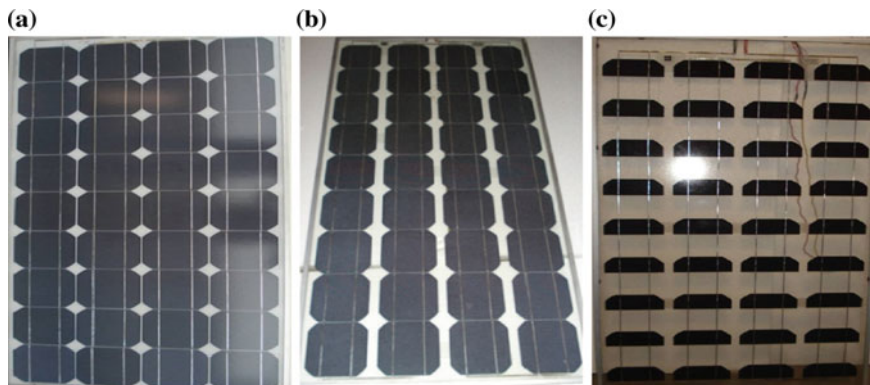
Fig. 4.13 a Opaque PV module of 75 Wp, **b** semitransparent PV module of 75 Wp, and **c** semitransparent PV module of 37 Wp

films can be easily deposited onto different substrates such as glass, metal, or even at plastic; this flexibility leads to greater interest in manufacturing of thin-film PV modules. Another advantage of thin-film PV modules is that they can bend; therefore, they can be used at different structures of the building facade and other glazing areas. The major drawback of this technology is low energy-conversion efficiency and degradation on exposure to adverse weather conditions (the Staebler-Wronski effect). The major challenge for this technology is improvement of the conversion efficiency of commercially made thin-film PV modules [12].

Initially amorphous silicon thin-film solar cells were used in thin-film PV modules because production cost are low and production processes are simpler than that of polycrystalline silicon [13]. However, the energy-conversion efficiency of amorphous silicon thin-film PV modules is only 6–7 % [14]. Other materials used for thin-film solar cell technology for manufacturing thin-film PV modules are copper–indium–diselenide (CIS), copper–gallium–diselenide (CGS), copper–indium–gallium–diselenide (CIGS), and cadmium telluride (CdTe). The energy-conversion efficiency achieved by these thin-film technologies is up to approximately 20 % (19.9 % for CIGS (NREL, USA), 16.5 % for CdTe (NREL, USA), and 13 % for CIGS (Wurth Solar, Germany)). Thin-film solar cell technology is gaining more interest, and large-capacity manufacturing plants are already in operation around the globe [15].

4.4.3 III–V Single Junction and Multijunction PV Modules

Multijunction solar cells utilize a wider range of solar spectra for electricity generation. In multijunction solar cells, different solar cells placed in a tandem arrangement have different band gaps. Therefore, a multijunction solar cell utilizes

a different range of spectra for electricity generation, which reduces absorption losses and improves efficiency. The thermodynamic performance limit of multi-junction solar cells is 68 %, which is further improved to 85 % for concentrating multijunction solar cells. The PV module manufactured from multijunction solar cells are very lightweight panels and are used particularly in space applications. The tandem arrangement can be made by mechanical stacking, by monolithic technique, or by both. The most commonly used dual-junction solar cells include the gallium-arsenide (GaAs) cell with efficiency of up to 30 % and the multijunction cell made of GaInP/GaInAs/Ge (gallium indium phosphide/gallium indium arsenide/germanium substrate). This multijunction solar cell has an efficiency (with concentrating sunlight) of 41.1 % (Fraunhofer Institute for Solar Energy Systems). GaAs solar cells are ideal for applications with concentrating sunlight, which allows the lesser quantity of gallium to further offset limited gallium resources [16].

4.4.4   Emerging and New PV Systems

This category of PV modules uses the recent and emerging technology of solar cells, namely, organic solar cells (OSC), dye-sensitised solar cells (DSSC), quantum-well solar cells (QWSC), etc. The major issues at the centre of recent research and development activities worldwide are reduced production cost and enhanced energy conversion efficiency. PV modules utilizing new and emerging solar cell technology are categorized on the basis of light-absorbing capacity and electricity-generation mechanism. The solar cell that contains only organic poly-mers is termed an "organic" solar cell; if it includes some inorganic material then it is known as a "hybrid organic" solar cell. Dye-sensitized solar cells contain porous nano-particles of titanium dioxide, which enhance the light-gathering capacity of the solar cell and hence its electrical efficiency. O'Regan and Gratzel [17] reported an efficiency of 10.4 % for these solar cells. DSSC has a low production cost because the processing mechanism is simpler and the material cost is also low. The quantum-well solar cell consists of a low-energy band-gap material sandwiched between relatively large-energy band-gap materials such as GaAs. Efficiencies of different modules utilizing different solar cells are given in Table 4.3. The move-ment of electrons is confined to in a plane in QWSC unlike the three-dimensional motion in other solar cells. The electrical efficiency of these solar cells is improved due to the confined motion in the quantum well. These solar cells are fabricated by chemical vapour deposition or molecular beam epitaxy techniques. Properties of different solar cell materials under standard test conditions are given in Appendix IV [18].

Photovoltaic generators, Fig. 4.14, consist of PV arrays. The rooftop-mounted PV array can meet the energy requirement of building such as daylighting, thermal

Table 4.3 Module efficiencies from National Renewable Energy Laboratories (NREL) survey of manufacturers' websites [20]

Module	Technology	Efficiency (%)
SunPower 315	Mono-Si, special junction (sp. j.)	19.3
Sanyo HIP-205BAE	CZ-Si, "HIT," sp. j.	17.4
BP7190	CZ-Si, sp. j.	15.1
Kyocera KC200GHT-2	MC-Si, standard junction (std.j.)	14.2
Solar World SW 185	CZ-Si, std. j.	14.2
BP SX3200	MC-Si, std. j.	14.2
Suntech STP 260S-24 V/b	MC or CZ-Si, std. j.	13.4
Solar World SW 225	MC-Si, std. j.	13.4
Evergreen Solar ES 195	String-ribbon-Si std. j.	13.1
Wu¨rthSolar WS11007/80	CIGS	11.0
First Solar FS-275	CdTe	10.4
Sharp NA-901-WP	a-Si/nc-Si	8.5
GSE Solar GSE120-W	CIGS	8.1
Mitsubishi Heavy MA100	a-Si, single-junction	6.3
Uni-Solar PVL136	a-Si, triple junction	6.3
Kaneka T-SC(EC)-120	a-Si single junction	6.3
Schott Solar ASI-TM86	a-Si/a-Si same bandgap tandem	5.9
EPV EPV-42	a-Si/a-Si same bandgap tandem	5.3

Fig. 4.14 Technical signs for various PV generator units (from Tiwari and Mishra [20])

PV generator

Solar cell diagram as electricity generator
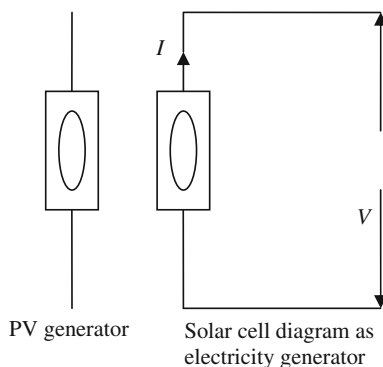
comfort, and electricity needed for different electrical appliances. In addition, these PV arrays can be connected to medium-scale decentralized grids. In grid-connected systems, surplus power is fed to the grid; under cloudy conditions, power can be fed from the grid.

4.4.5 Packing Factor (β_c) of the PV Module

The packing factor is defined as the ratio of total solar cell area to the total module area and can be expressed as:

$$\beta_c = \frac{\text{area of solar cells}}{\text{area of PV module}} \tag{4.35}$$

It is clear that β_c is less than unity (pseudo solar cell), and it has maximum value of one when all area is covered by the solar cell (e.g., rectangular solar cell).

4.4.6 Efficiency of the PV Module

The electrical efficiency of a PV module expressed as a percentage can be expressed as follows:

$$\eta_{em} = \tau_g \times \beta_c \times \eta_{ec} \tag{4.36a}$$

For $\beta_c = 1$, Eq. (4.36a) reduces to

$$\eta_{em} = \tau_g \times \eta_{ec} \tag{4.36b}$$

This shows that the electrical efficiency of a PV module (η_{em}) is less than the electrical efficiency of solar cell due to presence of glass over the solar cell (η_{ec}).

This is also expressed as:

$$\eta_{em} = \left(\frac{\text{FF} \times I_{sc} \times V_{oc}}{A_m \times I_p} \right) \times 100 \tag{4.37a}$$

where A_m = area of PV module; I_p = incident solar intensity on the PV module; and FF, I_{sc} and V_{oc} are the fill factor, the short-circuit current, and the open-circuit voltage, respectively, of the PV module. The maximum value of fill factor (FF) of an Si-based PV module is 0.88.

The temperature-dependent electrical efficiency of the PV module can be expressed as follows:

$$\eta_{em} = \eta_{mo}[1 - \beta_0[T_c - 298]] \tag{4.37b}$$

where η_{mo} is the electrical efficiency of the PV module under standard test conditions (STC).

The electrical load efficiency may be expressed as follows:

$$\eta_{\text{load}} = \left(\frac{I_{\text{L}} \times V_{\text{L}}}{A_{\text{m}} \times I_{\text{t}}}\right) \times 100 \tag{4.38}$$

4.4.7 Energy Balance Equations for PV Modules

In this section, we will consider the crystalline solar cell module generally known as the "PV module." There are two type of PV modules, namely, (a) the opaque PV module, Fig. 4.13a and (b) the semitransparent PV module, Fig. 4.13b.

The energy balance equations for PV modules have been written with following assumptions:

- One-dimensional heat conduction
- The system is in quasi-steady state
- The ohmic losses between solar cells in the PV module are negligible

(a) **For the opaque (glass-to-Tedlar) PV module (Fig. 4.13a) [19]**

In this case, solar radiation, $I(t)$, is transmitted by the glass of PV module as $\tau_{\text{g}}I(t)$, and furthermore it is absorbed by the solar cell of the PV module having area A_{m} and packing factor β_{c} as $\tau_{\text{g}}\alpha_{\text{c}}\beta_{\text{c}}I(t)A_{\text{m}}$. The remaining solar radiation $\tau_{\text{g}}(1 - \beta_{\text{c}})I(t)$ is absorbed by Tedlar (α_{T}) on the nonpacking portion of the PV module as $\tau_{\text{g}}\alpha_{\text{T}}(1 - \beta_{\text{c}})I(t)A_{\text{m}}$. The temperature of the solar cell increases; hence, there will be (i) the rate of overall upward heat loss $\left[U_{\text{t,ca}}(T_{\text{c}} - T_{\text{a}})A_{\text{m}}\right]$ and (ii) the rate of overall back heat loss $\left[U_{\text{b,ca}}(T_{\text{c}} - T_{\text{a}})A_{\text{m}}\right]$ in addition to electrical power generation as $\tau_{\text{g}}\eta_{\text{c}}\beta_{\text{c}}I(t)A_{\text{m}}$. This can be mathematically summarised as follows with the thermal circuit diagram shown in Fig. 4.15a

$$\tau_{\text{g}}[\alpha_{\text{c}}\beta_{\text{c}}I(t) + (1 - \beta_{\text{c}})\alpha_{\text{T}}I(t)] = \left[U_{\text{tc,a}}(T_{\text{c}} - T_{\text{a}}) + U_{\text{bc,a}}(T_{\text{c}} - T_{\text{a}})\right] + \tau_{\text{g}}\eta_{\text{c}}\beta_{\text{c}}I(t) \tag{4.39}$$

or

$$\tau_{\text{g}}[\alpha_{\text{c}}\beta_{\text{c}}I(t) + (1 - \beta_{\text{c}})\alpha_{\text{T}}I(t)] = \left[(U_{\text{tc,a}} + U_{\text{bc,a}})(T_{\text{c}} - T_{\text{a}})\right] + \tau_{\text{g}}\eta_{\text{c}}\beta_{\text{c}}I(t)$$

or

$$\tau_{\text{g}}[\alpha_{\text{c}}\beta_{\text{c}}I(t) + (1 - \beta_{\text{c}})\alpha_{\text{T}}I(t)] = U_{\text{Lm}}(T_{\text{c}} - T_{\text{a}}) + \eta_{\text{m}}I(t) \tag{4.40}$$

(a)

(b)
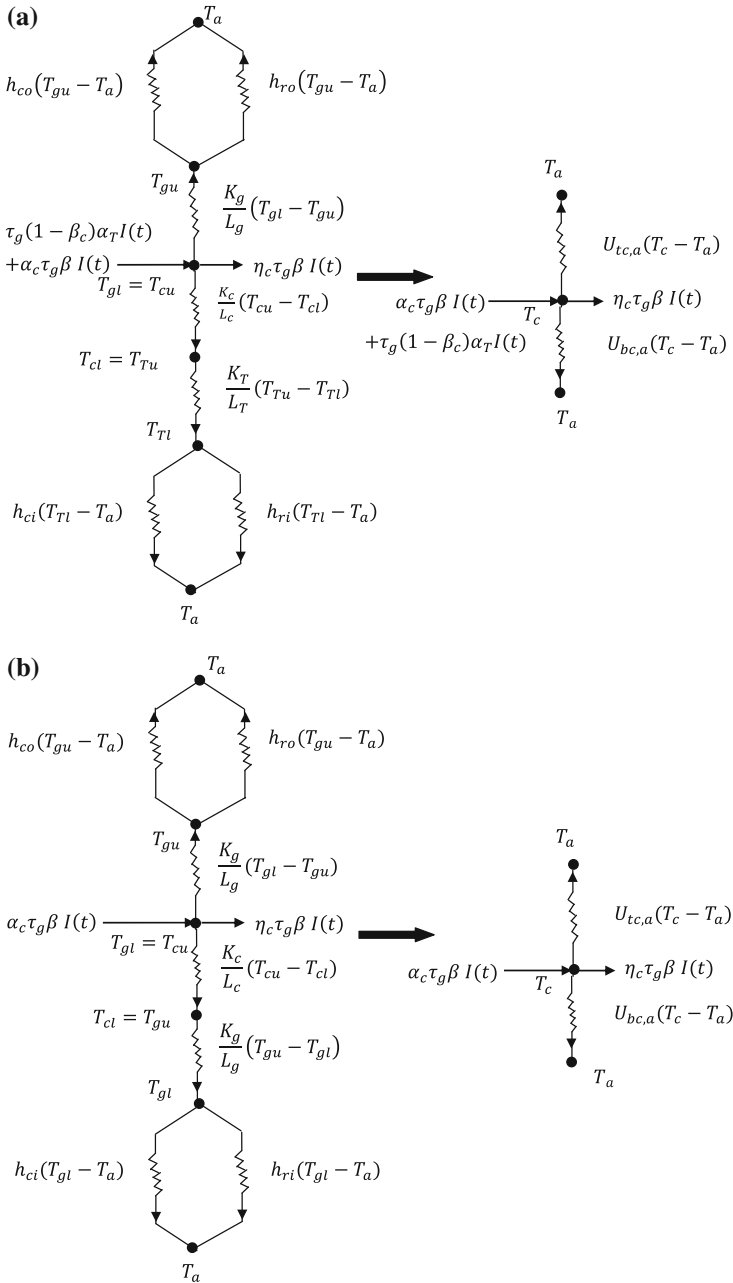
Fig. 4.15 **a** Thermal circuit diagram of opaque PV module shown in Fig. 4.13a. **b** Thermal circuit diagram of semitransparent PV module shown in Fig. 4.13b

where $U_{\mathrm{Lm}} = (U_{\mathrm{tc,a}} + U_{\mathrm{bc,a}})$ and $\eta_{\mathrm{m}} = \tau_{\mathrm{g}}\eta_{\mathrm{c}}\beta_{\mathrm{c}}$. In addition, A_{m} is eliminated from both sides of Eq. (4.39). From Eq. (4.40), one can get

$$T_{\mathrm{c}} - T_{\mathrm{a}} = \frac{\left[\tau_{\mathrm{g}}\{\alpha_{\mathrm{c}}\beta_{\mathrm{c}} + (1 - \beta_{\mathrm{c}})\alpha_{\mathrm{T}} - \eta_{\mathrm{c}}\beta_{\mathrm{c}}\}\right]I(t)}{U_{\mathrm{Lm}}} \tag{4.41}$$

or

$$T_{\mathrm{c}} - T_{\mathrm{ref}} = (T_{\mathrm{a}} - T_{\mathrm{ref}}) + \frac{\left[\tau_{\mathrm{g}}\{\alpha_{\mathrm{c}}\beta_{\mathrm{c}} + (1 - \beta_{\mathrm{c}})\alpha_{\mathrm{T}} - \eta_{\mathrm{c}}\beta_{\mathrm{c}}\}\right]I(t)}{U_{\mathrm{Lm}}} \tag{4.42}$$

The temperature-dependent electrical efficiency of the solar cell, Eq. (4.37b), is given as follows:

$$\eta_c = \eta_{\mathrm{ref}}[1 - \beta_{\mathrm{ref}}(T_{\mathrm{c}} - T_{\mathrm{ref}})] \tag{4.43}$$

where η_{ref} is the module's electrical efficiency at the reference temperature, T_{ref}, and at solar radiation of 1000 W/m². β_{ref} is the temperature coefficient. The values of η_{ref} and β_{ref} are given in Table 4.4 [20].

Using Eqs. (4.42) and (4.43), one obtains

$$\eta_{\mathrm{c}} = \eta_{\mathrm{ref}}\left[1 - \beta_{\mathrm{ref}}\left\{(T_{\mathrm{a}} - T_{\mathrm{ref}}) + \frac{\left[\tau_{\mathrm{g}}\{\alpha_{\mathrm{c}}\beta_{\mathrm{c}} + (1 - \beta_{\mathrm{c}})\alpha_{\mathrm{T}} - \eta_{\mathrm{c}}\beta_{\mathrm{c}}\}\right]I(t)}{U_{\mathrm{Lm}}}\right\}\right]$$

or

$$\eta_{\mathrm{c}} = \frac{\eta_{\mathrm{ref}}\left[1 - \beta_{\mathrm{ref}}\left\{(T_{\mathrm{a}} - T_{\mathrm{ref}}) + \frac{\left[\tau_{\mathrm{g}}\{\alpha_{\mathrm{c}}\beta_{\mathrm{c}} + (1 - \beta_{\mathrm{c}})\alpha_{\mathrm{T}}\}\right]I(t)}{U_{\mathrm{Lm}}}\right\}\right]}{\left[1 - \frac{\eta_{\mathrm{ref}}\beta_{\mathrm{ref}}\tau_{\mathrm{g}}\beta_{\mathrm{c}}}{U_{\mathrm{Lm}}}I(t)\right]} \tag{4.44a}$$

After determining the electrical efficiency of the solar cell by Eq. (4.44a), one obtains the electrical efficiency of the PV module as

$$\eta_{\mathrm{m}} = \tau_{\mathrm{g}}\eta_{\mathrm{c}}\beta_{\mathrm{c}} \tag{4.44b}$$

The threshold intensity $I(t)_{\mathrm{th}}$ can be obtained by putting the denominator of Eq. (4.44a) equal to zero and is given as follows:

$$I(t)_{\mathrm{th}} = \frac{U_{\mathrm{Lm}}}{\eta_{\mathrm{ref}}\beta_{\mathrm{ref}}\tau_{\mathrm{g}}\beta_{\mathrm{c}}} \tag{4.44c}$$

Table 4.4 Values of module electrical efficiencies and temperature coefficients [20]

$T_{ref}(°C)$	$\eta_{T_{ref}}$	β_{ref}	Comments	References
25	0.15	0.0041	Mono-Si	Evans and Florschuetz [21]
28	0.117 (average)	0.0038 (average)	Average of Sandia and commercial cells	OTA [22]
25	0.11	0.003	Mono-Si	Truncellito and Sattolo [23]
25	0.13	0.0041	PVT system	Mertens [24]
		0.005		Barra and Coiante [25]
20	0.10	0.004	PVT system	Prakash [26]
25	0.10	0.0041	PVT system	Garg and Agarwal [27]
20	0.125	0.004	PVT system	Hegazy [28]
25		0.0026	a-Si	Yamawaki et al. [29]
25	0.13	0.004	Mono-Si	RETScreen [30]
	0.11	0.004	Poly-Si	
	0.05	0.0011	a-Si	
25	0.178	0.00375	PVT system	Nagano et al. [31]
25	0.12	0.0045	Mono-Si	Chow [32]
25	0.097	0.0045	PVT system	Zondag et al. [33]
25	0.09	0.0045	PVT system	Tiwari and Sodha [34]
	0.12	0.0045	PVT system	
25	0.12	0.0045	PVT system	Assoa et al. [35]
25	0.127	0.0063	PVT system	Tonui and Tripanagnostopoulos [36]
	0.127 unglazed	0.006	PVT system	
	0.117 glazed	0.0054	PVT system	Othman et al. [37]

(b) **For the semitransparent (glass-to-glass) PV module** (Fig. 4.13b, c)

In this case, some fraction of solar radiation is transmitted through the bottom glass cover from the nonpacking area as $\tau_g^2(1 - \beta_c)I(t)A_m$. This can be mathematically summarised as follows with the thermal circuit diagram shown in Fig. 4.15b:

$$\alpha_c\tau_g\beta_c I(t) = \left[U_{tc,a}(T_c - T_a) + U_{bc,a}(T_c - T_a)\right] + \tau_g\eta_c\beta_c I(t) \qquad (4.45)$$

or

$$\alpha_c\tau_g\beta_c I(t) = (U_{tc,a} + U_{bc,a})(T_c - T_a) + \tau_g\eta_c\beta_c I(t) \qquad (4.46)$$

or

$$\alpha_c \tau_g \beta_c I(t) = U_{Lm}(T_c - T_a) + \eta_m I(t) \tag{4.47}$$

where $U_{Lm} = (U_{tc,a} + U_{bc,a})$ and $\eta_m = \tau_g \eta_c \beta_c$. In addition, A_m is eliminated from both sides of Eq. (4.45).

From Eq. (4.47),

$$T_c - T_a = \frac{(\alpha_c \tau_g \beta_c - \eta_m)I(t)}{U_{Lm}} \tag{4.48}$$

or

$$T_c - T_{ref} = (T_a - T_{ref}) + \frac{(\alpha_c \tau_g \beta_c - \eta_m)I(t)}{U_{Lm}} \tag{4.49}$$

With the help of Eq. (4.49), Eq. (4.43) becomes

$$\eta_c = \eta_{ref} \left[1 - \beta_{ref} \left\{ (T_a - T_{ref}) + \frac{(\alpha_c \tau_g \beta_c - \eta_c \tau_g \beta_c)}{U_{Lm}} I(t) \right\} \right]$$

or

$$\eta_c = \frac{\eta_{ref} \left[1 - \beta_{ref} \left\{ (T_a - T_{ref}) + \frac{\alpha_c \tau_g \beta_c}{U_{Lm}} I(t) \right\} \right]}{\left[1 - \frac{\eta_{ref} \beta_{ref} \tau_g \beta_c}{U_{Lm}} I(t) \right]} \tag{4.50a}$$

After determining the electrical efficiency of the solar cell by Eq. (4.50a), one obtains the electrical efficiency of the PV module as

$$\eta_m = \eta_c \tau_g \beta_c \tag{4.50b}$$

Similarly in this case also, the threshold intensity $I(t)_{th}$ is given as follows:

$$I(t)_{th} = \frac{U_{Lm}}{\eta_{ref} \beta_{ref} \tau_g \beta_c} \tag{4.50c}$$

Hourly variation of solar cell temperature and solar cell efficiency (Fig. 4.16a) reveals that the solar cell electrical efficiency decreases with increasing temperature, which is in accordance with the studies concluded by Evans [21].

Fig. 4.16 a Hourly variation of cell temperature and cell efficiency for a typical summer day (from Tiwari and Mishra [20]). **b** Series and parallel connection of modules in a solar panel (from Tiwari and Mishra [20])
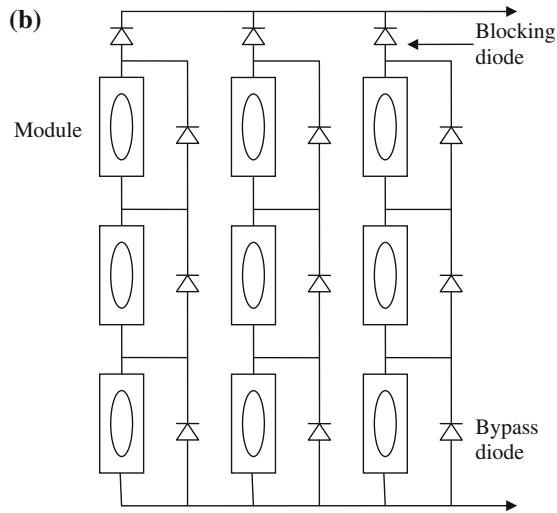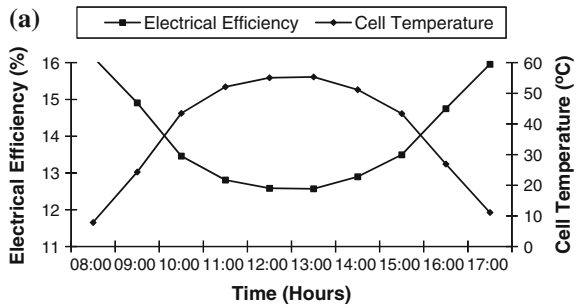
4.4.8 Series and Parallel Combination of PV Modules

PV modules are connected in series or in parallel to increase current and voltage ratings. When PV modules are connected in series/parallel, it is desired to have the maximum power production at the same current/voltage. A solar panel is a group of several modules connected in series/parallel combination in a frame that can be mounted on a structure.

Series and parallel connection of modules in a panel is shown in Fig. 4.16b. In parallel connection, blocking diodes are connected in a series with each series string of modules such that if any string should fail, the power output of the remaining series string will not be absorbed by the failed string. In addition, bypass diodes are installed across each module such that if one module should fail, the power output of the remaining modules in a string will bypass the failed module. Some modern PV modules come with such internally embedded bypass diodes. A large number of interconnected solar panels is known as solar PV array.

4.4.9 Applications of the PV Module/PV Array

There are many applications of the PV module/PV array such as street lights, water pumping, building, agriculture, transport, refrigeration, stand alone and roof top etc. These applications will be discussed in the chapter about solar power generation (Chapter XVI).

Example 4.11 Calculate the daily load for domestic use and determine the number of 40 W_p PV panels required in the array.

Solution
Consider the following domestic loads:
Four 40 W lamps + one 15 W television used 4 h per day: 700 Wh
Two 35 W fans used 6 h per day: 420 Wh.
One 60 W refrigerator used all day, compressor on 50 % of the time: 720 Wh.
Total daily domestic load = 1840 Wh
For 150 Wh per day energy production per PV module.
Number of panels required (in parallel connection) = 1840 Wh/150 Wh = 12.3.
Therefore, a 12 V system needs 13 PV modules connected in parallel.

4.5 Photovoltaic Thermal (PVT) Systems

From Eq. (4.34a), it is clear that an electrical efficiency of the photovoltaic (PV) module depends on the operating temperature of the PV module. If the operating temperature of the PV module is reduced, then the electrical efficiency of the PV module will be increased. In addition to increased electrical efficiency of the PV module, there can be additional thermal energy if thermal energy is properly collected by using a medium such as either water or air. Such a system is known as a **photovoltaic thermal (PVT) system.** Photovoltaic thermal (PVT) systems are broadly classified as follows.

4.5.1 PVT Water Collectors

In this case, water as a fluid can be flown either above or below the PV module as shown in Fig. 4.17a, b. One can get hot water in addition to enhanced electrical output. Hot water has many applications including domestic as well as industrial.

A thermal circuit diagram of an opaque PVT water collector and a semitransparent PVT water collector are shown in Fig. 4.18a, b, respectively.
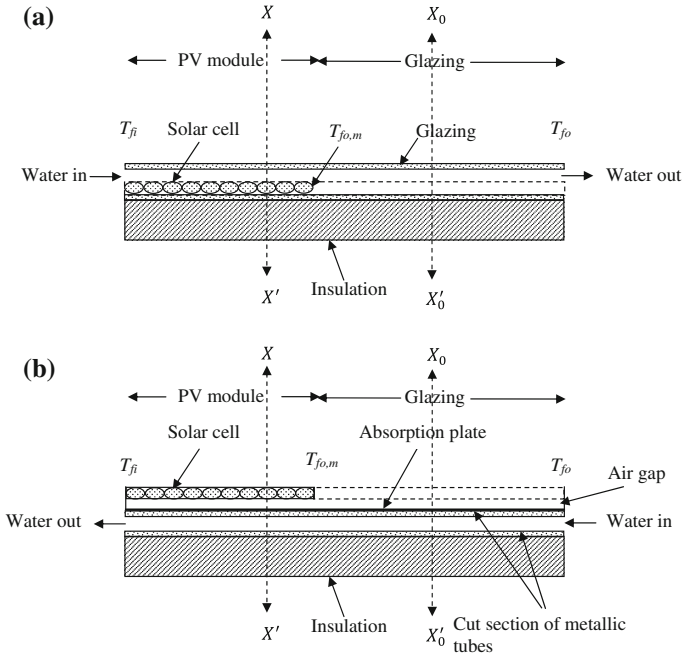
Fig. 4.17 **a** Cross-sectional view of PVT water collector with water flow above the PV module (*module at inlet*). **b** Cross-sectional view of PVT water collector with water flow below the PV module (*module at outlet*)

The semitransparent PVT water collector gives the better performance compared with the opaque PVT water collector. The expression of temperature-dependent electrical efficiency for a semitransparent PVT water collector can be obtained as follows [38]:

$$
\eta_{cN} = \frac{\eta_0 \left[1 - \beta_0 \left[\frac{1}{U_{tc,a}+U_{tc,p}} \left[\begin{array}{c} \left[\alpha_c \tau_g \beta + \frac{U_{tc,p}\{(\alpha\tau)_{2,eff}+PF_1\alpha_c\tau_g\beta\}}{U_{L1}+F'h_{pf}} + \frac{U_{tc,p}F'h_{pf}\{PF_{2}(\alpha\tau)_2,eff+PF_2PF_1\alpha_c\tau_g\beta\}A_mF_{Rm}}{2\dot{m}_fC_f(U_{L1}+F'h_{pf})} \right] I(t) \\ + \left[U_{tc,a} + \frac{U_{tc,p}U_{L1}}{U_{L1}+F'h_{pf}} + \frac{U_{tc,p}F'h_{pf}A_mF_{Rm}U_{L,m}}{2\dot{m}_fC_f(U_{L1}+F'h_{pf})} \right] T_a + \left[\frac{U_{tc,p}F'h_{pf}(1+K_m)}{2(U_{L1}+F'h_{pf})} \right] T_{fi} \end{array} \right] - T_0 \right] \right]}{\left[1 - \frac{\eta_0\beta_0 I(t)}{(U_{tc,a}+U_{tc,p})} \left[\tau_g\beta + \frac{U_{tc,p}}{U_{L1}+F'h_{pf}} PF_1\tau_g\beta + \frac{U_{tc,p}F'h_{pf}}{2\dot{m}_fC_f(U_{L1}+F'h_{pf})} PF_2PF_1\tau_g\beta A_mF_{Rm} \right] \right]}
$$

(4.51)

where $(\alpha\tau)_{2,eff} = \alpha_p(1-\beta)\tau_g^2$, $PF_1 = \frac{U_{tc,p}}{U_{tc,p}+U_{tc,a}}$, $PF_2 = \frac{h_{pf}}{F'h_{pf}+U_{L2}}$, $U_{L1} = \frac{U_{tc,p}U_{tc,a}}{U_{tc,p}+U_{tc,a}}$, $U_{L,m} = \frac{h_{pf}U_{L1}}{F'h_{pf}+U_{L1}}$, $A_mF_{Rm} = \frac{\dot{m}_fC_f}{U_{L,m}}\left[1 - \exp\left(\frac{-F'A_mU_{L,m}}{\dot{m}_fC_f}\right)\right] A_mF_{Rm} = \frac{\dot{m}_fC_f}{U_{L,m}}\left[1 - \exp\left(\frac{-F'A_mU_{L,m}}{\dot{m}_fC_f}\right)\right]$.

(a)

T_a

$h_{co}(T_{gu} - T_a)$ $h_{ro}(T_{gu} - T_a)$

T_{gu} $\dfrac{K_g}{L_g}(T_{gl} - T_{gu})$

$\tau_g(1 - \beta_c)\alpha_T I(t)$

$+\alpha_c \tau_g \beta\, I(t)$ $\eta_c \tau_g \beta\, I(t)$

$T_{gl} = T_{cu}$ $\dfrac{K_c}{L_c}(T_{cu} - T_{cl})$

$T_{cl} = T_{Tu}$ $\dfrac{K_T}{L_T}(T_{Tu} - T_{Tl})$

T_{Tl}

$\tau_g(1 - \beta_c)\alpha_T I(t)$

$+\alpha_c \tau_g \beta\, I(t)$ $\eta_c \tau_g \beta\, I(t)$

T_a

$h_{ci}(T_{Tl} - T_{pu})$ $h_{ri}(T_{Tl} - T_{pu})$ $U_{tc,a}(T_c - T_a)$

T_c

$U_{tc,p}(T_c - T_p)$

T_{pu} $\dfrac{K_p}{L_p}(T_{pu} - T_{pl})$

T_p $h_{pf}(T_p - T_f)$

$T_{pl} = T_{fu}$

$h_{pf}(T_{pl} - T_{fl})$ T_f $U_{bf,a}(T_f - T_a)$

$T_{fl} = T_{iu}$ T_a

$\dfrac{K_i}{L_i}(T_{iu} - T_{il})$

T_{il} T_a

$U_{tp,a}(T_p - T_a)$

$h'_{ci}(T_{il} - T_a)$ $h'_{ri}(T_{il} - T_a)$

$U_{tc,p}(T_c - T_p)$ T_p

T_a $h_{pf}(T_p - T_f)$

T_f
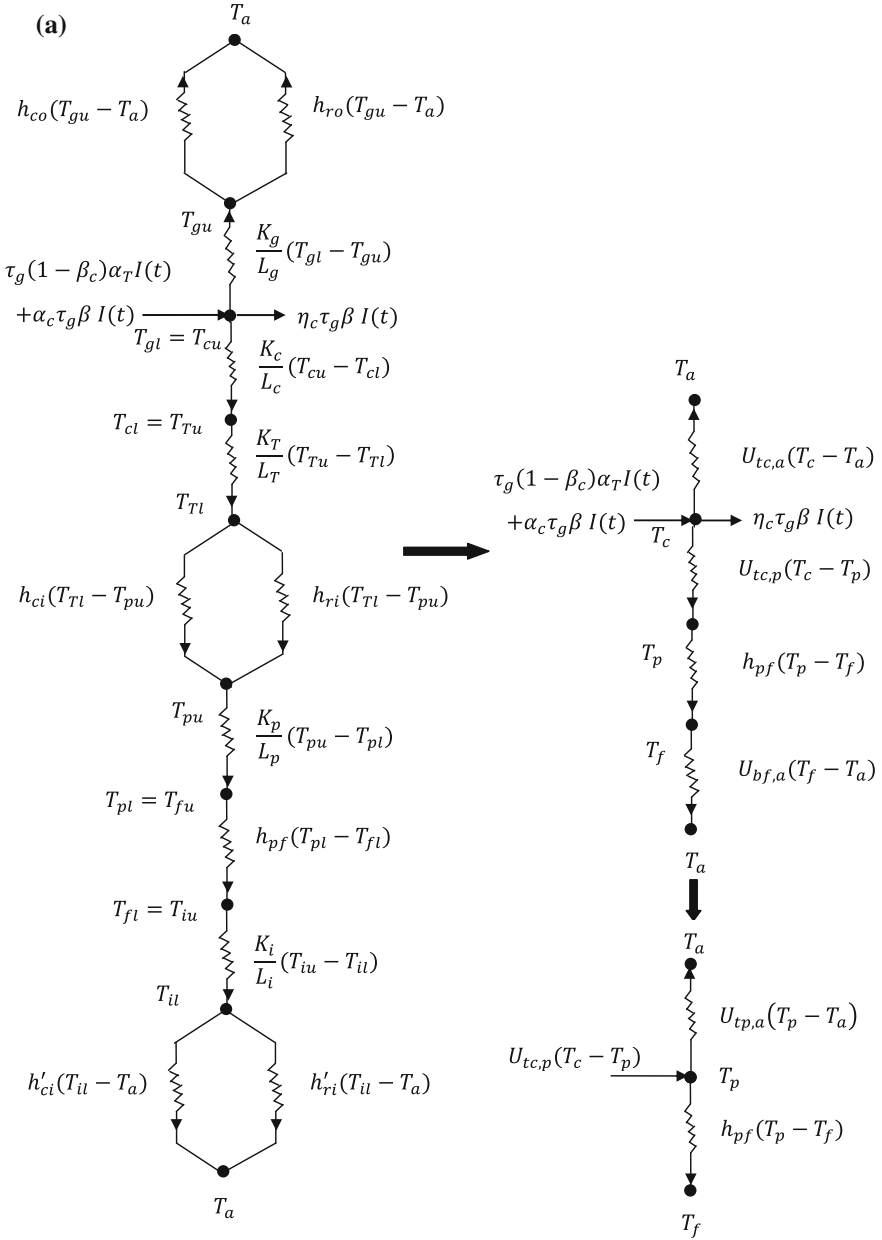
Fig. 4.18 **a** Thermal circuit diagram of opaque PVT water collector. **b** Thermal circuit diagram of semitransparent PVT water collector

(b)
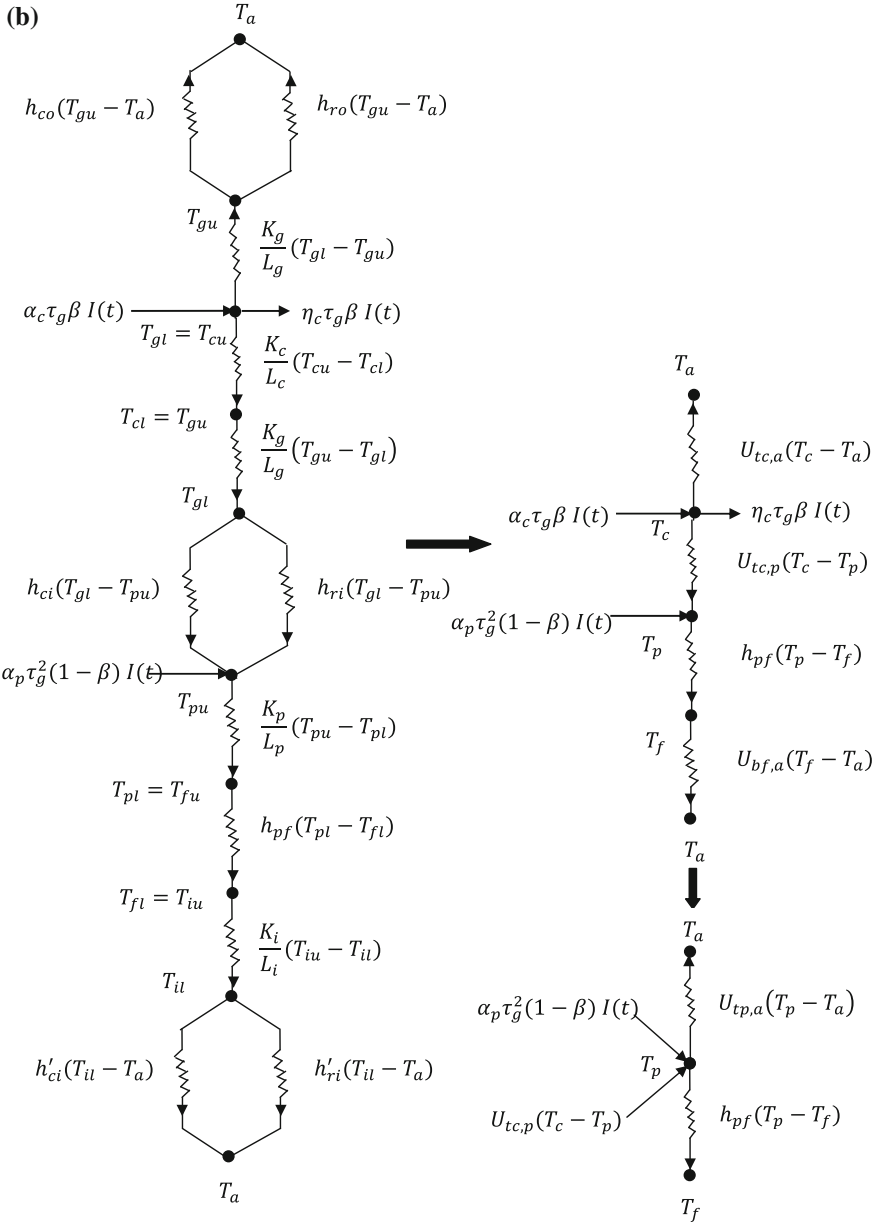
Fig. 4.18 (continued)

The threshold intensity in this case is obtained following the same procedure as adopted in Sect. 4.4.7. The threshold intensity for this case is given as follows:

$$I(t)_{\text{th}} = \frac{\left(U_{\text{tc,a}} + U_{\text{tc,p}}\right)}{\eta_0\beta_0\left[\tau_g\beta + \frac{U_{tc,p}}{U_{\text{L}1} + F'h_{\text{pf}}}\text{PF}_1\tau_g\beta + \frac{U_{\text{tc,p}}F'h_{\text{pf}}}{2\dot{m}_f C_f\left(U_{\text{L}1} + F'h_{\text{pf}}\right)}\text{PF}_2\text{PF}_1\tau_g\beta A_m F_{\text{Rm}}\right]}$$

(4.51a)

4.5.2   PVT Air Collectors

In this case, air as a fluid can be flown either above or below the PV module; one can get hot air in addition to enhanced electrical output. Hot air has also many applications such as solar crop drying and space heating.

The working principle of the PVT air collector can be explained as follows: There is an air duct with a proper channel below the PV module. There is a rate of overall heat transfer from the solar cell of the PV module, which flows air through the Tedlar, $U_{\text{tc,f}}(T_c - T_f)A_m$, which is used to heat the flowing air with a mass flow rate of

$$\dot{m}_a = \text{density of air}(\rho) \times \text{cross sectional area of air duct}(a = L \times b)$$
$$\times \text{flowrate}(u),$$

with specific heat of air as C_a. Once the temperature of the flowing air is increased, there is also a rate of overall heat loss from flowing air to ambient air through the bottom insulation, $U_{\text{bf,a}}(T_f - T_a)A_m$. Here it is important to mention that there is an indirect gain of thermal energy to the flowing air.

On the basis of energy balance of the solar cell of the PV module and the flowing air, an expression for the temperature-dependent electrical efficiency for the PVT air collector covered by opaque PV modules and semitransparent PV modules can be written as Eqs. (4.52a) and (4.52b) respectively.

$$\eta = \frac{\eta_0\left[1 - \frac{\beta_0\tau_g[\alpha_c\beta_c + \alpha_T(1-\beta_c)]I(t)}{U_T + h_T}\left\{1 + \frac{h_T h_{\text{p}1}}{h_t + U_{\text{tT}}} + \frac{h_T h_t h_{\text{p}1}h_{\text{p}2}}{(h_T + U_{\text{tT}})U_L}\left(1 - \frac{1-\exp(-X_o)}{X_o}\right)\right\}\right]}{1 - \frac{\beta_0\eta_0\tau_g\alpha_c\beta_c I(t)}{U_T + h_T}\left[1 + \frac{h_T h_{\text{p}1}}{h_t + U_{\text{tT}}} + \frac{h_T h_t h_{\text{p}1}h_{\text{p}2}}{(h_T + U_{\text{tT}})U_L}\left(1 - \frac{1-\exp(-X_o)}{X_o}\right)\right]}$$

(4.52a)

$$\eta = \frac{\eta_0\left[1 - \frac{\tau_g\beta_0 I(t)}{U_{\text{tc,a}} + U_{\text{Tc,f}}}\left\{\alpha_c\beta_c + \frac{U_{\text{Tc,f}}}{U_L}\left(h_{\text{p}1}\alpha_c\beta_c + h_{\text{p}2}\alpha_p(1 - \beta_c)\tau_g\right)\left(1 - \frac{1-\exp(-X_o)}{X_o}\right)\right\}\right]}{1 - \frac{\eta_0\beta_0\tau_g\beta_c\alpha_c I(t)}{U_{\text{tc,a}} + U_{\text{Tc,f}}}\left[1 + \frac{U_{\text{Tc,f}}h_{\text{p}1}}{U_L}\left(1 - \frac{1-\exp(-X_o)}{X_o}\right)\right]}$$

(4.52b)

where $X_o = \frac{bU_L L}{\dot{m}_a C_a}$;

$$(\alpha\tau)_{eff} = h_{p1}(\alpha\tau)_1, eff + h_{p2}(\alpha\tau)_2, eff;$$
$$(\alpha\tau)_{1,eff} = \tau_g \alpha_c \beta_c (1 - \eta) \text{ and } (\alpha\tau)_2, eff = \alpha_p (1 - \beta_c)\tau_g^2$$

h_{p1} and h_{p2} are the penalty factors due to the glass cover of the PV module and are defined as

$$h_{p1} = \frac{U_{Tc,f}}{U_{tc,a} + U_{Tc,f}} \quad \text{and} \quad h_{p2} = \frac{h_{p,f}}{U_{p,a} + h_{p,f}}$$

$$U_{tc,a} = \left[\frac{L_g}{K_g} + \frac{1}{h_o}\right]^{-1}; \quad U_{Tc,f} = \left[\frac{L_g}{K_g} + \frac{1}{h_i}\right]^{-1};$$

$$U_{tT} = \frac{U_{Tc,f} U_{tc,a}}{U_{Tc,f} + U_{tc,a}}; \quad U_T = \frac{U_{bp,a} h_{p,f}}{U_{bp,a} + h_{p,f}}; U_L = U_{tT} + U_T$$

$$h_o = 5.7 + 3.8 \, V, \quad V = 0.5 \text{ m/s};$$

$$h_{p,f} = h_i = 2.8 + 3 \text{ v}, \quad v = 2 \text{ m/s}.$$

The threshold intensities for opaque and semitransparent PVT air collectors are given as follows:

$$I(t)_{th} = \frac{(U_T + h_T)}{\beta_0 \eta_0 \tau_g \alpha_c \beta_c \left[1 + \frac{h_T h_{p1}}{h_t + U_{tT}} + \frac{h_T h_t h_{p1} h_{p2}}{(h_T + U_{tT})U_L}\left(1 - \frac{1-\exp(-X_o)}{X_o}\right)\right]} \quad (4.52c)$$

and

$$I(t)_{th} = \frac{(U_{tc,a} + U_{Tc,f})}{\eta_0 \beta_0 \tau_g \beta_c \alpha_c \left[1 + \frac{U_{Tc,f} h_{p1}}{U_L}\left(1 - \frac{1-\exp(-X_o)}{X_o}\right)\right]} \quad (4.52d)$$

The hourly variation of electrical efficiency of PV modules is shown in Fig. 4.19. It can be clearly observed that the semitransparent PV module has better solar cell efficiency because the radiation falling on the nonpacking area is transmitted to the blackened absorber plate. In the case of the opaque PV module, the radiation falling on the nonpacking area is absorbed by the tedlar resulting in a higher module temperature and hence lower solar cell efficiency.

The efficiency of the PVT system can be defined based on the following:

(a) The first law of thermodynamics, which will be referred to as the "overall thermal efficiency" of the PVT system; and
(b) the second law of thermodynamics, which will be referred as the overall exergy efficiency" of the PVT system.
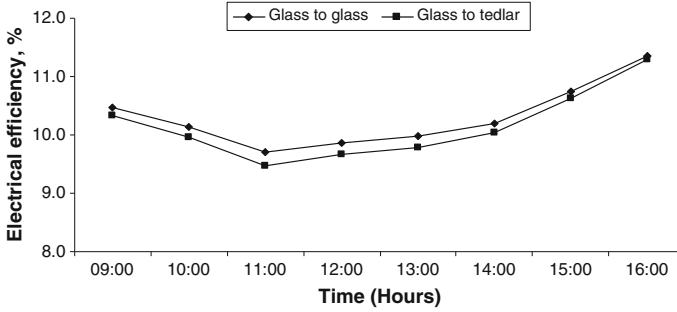
Fig. 4.19 Hourly variation of electrical efficiency of glass-to-glass and glass-to-Tedlar-type PV module (from Tiwari and Mishra [20])

Equations (4.37a) and (4.37b) gives the electrical efficiency of a PV module. If one needs to determine the equivalent thermal efficiency for a PV module in terms of percentage, it can be expressed as

$$\eta_{\text{eth}} = \frac{\eta_{\text{em}}}{0.38} \times 100 \tag{4.53}$$

where 0.38 is the conversion factor from thermal energy to electrical energy for the best coal available internationally. However, it varies from 0.20 to 0.40.

The overall thermal efficiency of the hybrid PVT system may be written as

$$\eta_{\text{ov,th}} = \eta_{\text{th}} + \frac{\eta_{\text{e}}}{0.38} \tag{4.54}$$

where η_{th} is the thermal efficiency of the PVT system.

The overall exergy efficiency of the hybrid PVT system is the sum of electrical efficiency and equivalent exergy efficiency of thermal energy, Eq. (3.6). The expression for this may be written as:

$$\eta_{\text{ov,ex}} = \eta_{\text{ex}} + \eta_{\text{e}} \tag{4.55}$$

where η_{ex} is exergy efficiency $= \eta_{\text{th}}\left(1 - \frac{T_{\text{sink}}}{T_{\text{source}}}\right)$; and T is the temperature in Kelvin.

Example 4.12 Calculate the packing factor of a PV module (36 solar cells) of area 0.605 m^2 with each pseudo solar cell having an area of 0.015 m^2.

Solution
From Eq. (4.35), we get $\beta_{\text{c}} = \frac{0.54}{0.605} \times 100 = 89.2\ \%$

Example 4.13 Calculate the efficiency of a PV module at an intensity of 400 W/m^2.

Given: FF $= 0.8$, $I_{\text{SC}} = 3.2$ A, $V_{\text{OC}} = 16$ V, $I_{\text{L}} = 1$ A, $V_{\text{L}} = 14$ V, and area of module $= 1$ m^2.

Solution
From Eq. (4.37a), we have

$$\eta_{\text{em}} = \frac{0.8 \times 3.2 \times 16}{400 \times 1} \times 100 = 10.24\ \%$$

Example 4.14 Using Example 4.11, calculate the load efficiency of a PV module.

Solution
From Eq. (4.37a), we have

$$\eta_{\text{em}} = \frac{1 \times 14}{400 \times 1} \times 100 = 3.5\ \%$$

4.6   Degradation of Solar Cell Materials [39]

4.6.1   Dust Effect

The deposition of dust on PV modules is a serious concern because it affects the performance of the PV systems. Dust deposition depends on the weather conditions and the local environment of the particular place. It also depends on the physical and chemical composition of the dust. The surface of the module also plays an important role for dust deposition because dust accumulation is higher for rough surfaces. The optical performance of a PV module is negatively affected due to dust deposition because dust blocks the solar radiation from coming into direct contact with the solar cells of the module.

Under outdoor conditions, the surface finish, tilt angle, humidity, and wind speed also affect dust accumulation. Tilted PV systems usually accumulate less dust compared with strictly horizontal systems.

4.6.2   Aging Effect

As time elapses, the performance of the PV modules degrades. This phenomenon of performance degradation is known as the "aging effect" of PV modules. The time period during which a PV module yields the rated power is closely connected to the life time of the PV module, which significantly depends on the materials and technology used for fabrication of the PV module. The aging effect is due to the weather conditions, fluctuation in ambient temperature, rain, dust deposition, etc. Decolouration and large strain formation affect the performance and life time of the module. It is suggested to optimize the effect of the environment on the operation of modules. By using UV-filtering glass superstrates, the modules can be made more resistant to degradation.

4.7 Additional Solved Examples

Example 4.15 Determine the Fermi energy level for a silicon crystal doped with an acceptor impurity of concentration 10^{17} cm^{-3} given that the effective density of states in the valence band at room temperature is 1.04×10^{19} cm^{-3}.

Solution
We have, $E_F = E_V - kT \ln \frac{N_A}{N_V}$.

If the conduction band is taken at the reference level, $E_V = 1.1$ eV. Substitution of value gives

$$E_F = 1.1 - \left[\left(\frac{8.62 \times 10^{-5}}{1.6 \times 10^{-19}} \right) \times 310 \times \ln \frac{10^{17}}{1.04 \times 10^{19}} \right]$$

$$E_F = 1.23 \text{ eV}$$

The shift is $1.23 - 0.55 = 0.68$ eV.

Example 4.16 Determine the band gap in a Ga-As crystal at 38 °C.

Solution
The variation of band gap with temperature is given by the relation (Eq. 4.1):

$$E_g(T) = E_g(0) - \frac{aT^2}{T+b}$$

Substituting values of a and b, we get

$$E_g(38) = 1.52 - \left[\frac{(5.84 \times 10^{-4}) \times (311)^2}{311 + 300} \right]$$

$$= 1.52 - 0.092$$

$$E_g(38) = 1.428 \text{ eV}$$

Example 4.17 Determine the saturation current value for silicon at 32 °C.

Solution
The dependence of the saturation current for silicon at 32 °C is given by the relation

$$I_0 = AT^3 \exp(E_g/kT)$$

Here, A is the non-ideality factor, and its value is taken as 1.

Substituting the known values in the previous relation, we get

$$I_0 = (305)^3 \exp\left[\frac{-1.776 \times 10^{-19}}{4.209 \times 10^{-21}}\right]$$

$$I_0 = +1.34 \times 10^{-11} \text{ A/m}^2$$

Example 4.18 Calculate the fill factor if a solar cell of area 4 cm^2 is irradiated with an intensity of 100 W/m^2.

Given $V_{OC} = 0.24$ V, $I_{SC} = -10$ mA, $V_{max} = 0.14$ V, $I_{max} = -6.5$ mA. Also calculate R_{OP}.

Solution

We have the expression for fill factor as

$$\text{Fill factor} = \frac{V_{max} \times I_{max}}{V_{oc} \times I_{sc}}$$

Substituting the appropriate values in above equation, we get

$$\text{Fill factor} = \frac{V_{max} \times I_{max}}{V_{oc} \times I_{sc}} = \frac{0.14 \times (-6.5)}{0.24 \times (-10)} = 0.37$$

and

$$R_{op} = \frac{V_m}{I_m} = \frac{0.14}{-6.5 \times 10^{-3}} = -21.53 \ \Omega$$

Example 4.19 What will be the solar cell current if the dark- and light-induced currents are equal?

Solution

The overall cell current is determined by subtracting the light-induced current I_L from the diode dark current I_D

$$I = I_D - I_L$$

if

$$I_D = I_L$$

then

$$I = 0$$

Thus, under this condition, the cell will not generate any current.

Example 4.20 Calculate the dark current for a solar cell for reverse and forward bias mode.

Solution
We have the expression for dark current as

$$\text{Dark current}, I_D = I_0 \left[\exp\left(\frac{eV}{kT}\right) - 1 \right]$$

For good solar cells,

$$I_0 = 10^{-8} \text{ A/m}^2 \text{ or } 10^{-5} \text{ mA/m}^2, e = 1.6 \times 10^{-19} \text{ J}, k = 1.38 \times 10^{-23} \text{ J/K}, T = 300 \text{ K}$$

Then

$$I_D = 10^{-5} \times \left[\exp\left(\frac{1.6 \times 10^{-19} \text{ V}}{1.38 \times 10^{-23} \times 300}\right) - 1 \right]$$

$$I_D = 10^{-5} \times [\exp(38.6 \text{ V}) - 1] \text{ mA}$$

Now, the previous equation is used to calculate I_D in forward- and reverse-bias modes

Variation of dark current with voltage in forward-bias mode		Variation of dark current with voltage in reverse bias mode (voltage is taken as negative in the reverse-bias mode)	
Voltage (V)	Dark current ID (mA)	Voltage (V)	Dark current ID (mA)
0.00	0.00	0.00	0.00
0.01	0.47×10^{-5}	0.01	-0.32×10^{-5}
0.02	1.16×10^{-5}	0.02	-0.53×10^{-5}
0.03	2.18×10^{-5}	0.03	-0.68×10^{-5}
0.04	3.68×10^{-5}	0.04	-0.78×10^{-5}
0.05	5.88×10^{-5}	0.05	-0.85×10^{-5}
0.06	9.10×10^{-5}	0.06	-0.89×10^{-5}
0.07	13.90×10^{-5}	0.07	-0.93×10^{-5}

(continued)

(continued)

Variation of dark current with voltage in forward-bias mode		Variation of dark current with voltage in reverse bias mode (voltage is taken as negative in the reverse-bias mode)	
Voltage (V)	Dark current ID (mA)	Voltage (V)	Dark current ID (mA)
0.08	20.90×10^{-5}	0.08	-0.97×10^{-5}
0.10	46.40×10^{-5}	0.09	-0.97×10^{-5}
0.50	2.40×10^{-5}	0.10	-0.97×10^{-5}
		0.50	-0.99×10^{-5}

Objective Questions

4.1. In what form can solar energy be used?
(a) Thermal energy (b) Electrical energy (c) Mechanical energy (d) All of these
Answer: (d)

4.2 What is the most common material used in making solar cells?
(a) Silver   (b) Iron   (c)   Aluminium   (d) Silicon
Answer: (d)

4.3 The electrical output of a solar cell depends on the
(a) Intensity of solar radiation   (b) Heat component of solar radiation
(c) Ultravoilet radiation   (d) Infrared radiation
Answer: (a)

4.4 Solar photovoltaic cells convert solar energy directly into
(a) Mechanical energy   (b) Electricity
(c) Heat energy   (d) Transportation
Answer: (b)

4.5 What does SPVT stand for with respect to solar energy?
(a) Solar photovoltaic thermal   (b) Solar platevoltaic thermal
(c) Solar platevoids thermal   (d) None of the above
Answer: (a)

4.6 Which of the following appliances use solar photovoltaic technology?
(a) Solar lantern   (b) Biogas plant
(c) Solar water heater   (c) Solar air heater
Answer: (a)

4.7 Which material has the highest reported solar cell efficiency?
(a) Amorphous silicon   (b) Thin-film silicon
(c) Polycrystalline silicon   (d) Single crystal silicon
Answer: (d)

4.8 At present, what is the maximum efficiency of a commercial solar cell?
(a) 3 %   (b) 12–30 %   (c) 50–65 %   (d) 65–70 %
Answer: (b)

4.9   Where is the world's largest solar power plant located?
      (a) Germany   (b) USA   (c) India   (d) UK
      Answer: (b)
4.10 Which of the following materials has the lowest reported solar cell
      efficiency?
      (a) Amorphous silicon   (b) Gallium arsenide
      (c) Polycrystalline silicon   (d) Single crystal silicon
      Answer: (b)
4.11 The exergy efficincy of PVT system
      (a) is less than thermal efficiency   (b) is more than thermal efficiency
      (c) is equal to thermal efficiency   (d) None of these
      Answer: (a)
4.12 The energy-production factor (EPF) on a life time basis
      (a) is more than 1   (b) is equal to 1
      (c) is less than 1   (d) None of these
      Answer: (c)
4.13 The life-cycle conversion efficiency (LCCE)
      (a) is more than 1   (b) is equal to 1
      (c) is less than 1   (d) None of these
      Answer: (c)
4.14 The energy payback time (EPBT) should be
      (a) more than the life of the PV system   (b) equal to the life of the PV
      system
      (c) no relation   (d) less than the life of the PV system
      Answer: (d)
4.15 A PVT system can be used for
      (a) air heating   (b) water heating   (c) air/water heating   (d) all of these
      Answer: (d)
4.16 A PVT system can also be used for
      (a) lighting   (b) underground water pumping   (c) building   (d) all of
      these
      Answer: (d)
4.17 A PV system is
      (a) a nonrenewable source of energy   (b) a renewable source of energy
      (c) a finite source   (d) all of these
      Answer: (b)
4.18 A PV system provides
      (a) clean power   (b) good environment   (c) sustainable climate   (d) all
      of these
      Answer: (d)
4.19 A PVT system is more economical
      (a) for building integration   (b) stand alone
      (c) for both (a) and (b)   (d) all of these
      Answer: (a)

4.20 The electrical efficiency of a semitransparent PV module is
    (a) more than an opaque PV module   (b) equal to an opaque PV module
    (c) less than an opaque PV module   (d) None of these
    Answer: (a)

References

1. J.D. Mondol, Y.G. Yohanis, B. Norton, Sol. Energy **80**, 1517 (2006)
2. B. Decker, U. Jahn, U. Rindelhardt, W. Vaaben, in *The German 1000-Roof-Photovoltaic-Programme: System Design and Energy Balance*. 11th European Photovoltaic Solar Energy Conference, Montreux, Switzerland (1992), pp. 1497–1500
3. M.H. Macagnan, E. Lorenzo, in *On the Optimal Size of Inverters for Grid Connected PV Systems*. 11th European Photovoltaic Solar Energy Conference, Montreux, Switzerland (1992), pp. 1167–1170
4. M. Jantsch, H. Schmidt, J. Schmid, in *Results of the Concerted Action on Power Conditioning and Control*. 11th Photovoltaic Solar Energy Conference, Montreux, Switzerland (1992), pp. 1589–1593
5. A. Louche, G. Notton, P. Poggi, G. Peri, in *Global Approach for an Optimal Grid Connected PV System Sizing*. 12th European Photovoltaic Solar Energy Conference, Amsterdam, The Netherlands (1994), pp. 1638–1641
6. N.K. Gautam, N.D. Kaushik, Energy **27**, 347 (2002)
7. P. Tsalides, A. Thanailakis, Solar Cells **14**, 83 (1985)
8. J. Kern, I. Harris, Solar Energy **17**(2), 97 (1975)
9. B. Pierce, *Very high efficient solar cells*, http://www.arpa.mil/sto/smallunitops/vhesc.html. Accessed 25 July 2008
10. J. Hance, *Breakthrough in solar energy*. http://news.mongabay.com/2008/0710-hance_solar.html. Accessed 18 Aug 2008
11. W. De Soto, S.A. Klein, W.A. Beckman, Solar Energy **80**, 78 (2006)
12. M. Fortman, T. Zhou, C. Malone, M. Gunes, R. Wronski, in *Deposition Conditions, Hydrogen Content and the Staebler-Wronski Effect in Amorphous Silicon*. Conference Record of the 21st Photovoltaic Specialist Conference (1990), pp. 1648–1652
13. A.M. Green, *Solar cells operating principles technology and system application*, 1st edn. (University of New South Wales, New South Wales, 1998)
14. B.V. Roedern, H.S. Ullal, in *The Role of Polycrystalline Thin Film PV Technologies in Competitive PV Module Markets*. 33rd IEEE Photovoltaic Specialists Conference Proceedings (2008), pp. 1–4
15. H. Schock, in *Chalcopyrite (CIGS) Based Solar Cells and Production in Europe*. Technical Digest 17th International Photovoltaic Science and Engineering Conference (PVSEC-17) (2007), pp. 40–43
16. Fraunhofer ISE, in *World Record: 41.1 % Efficiency Reached for Multijunction Solar Cells*. Fraunhofer ISE; press release (2009)
17. B. O'Regan, M. Gratzel, Nature **353**, 737 (1991)
18. G.N. Tiwari, S. Dubey, *Fundamentals of Photovoltaic Modules and Their Applications* (RSC publishing, UK, 2010)
19. A. Tiwari, M.S. Sodha, Renew. Energy **31**(15), 2460 (2006)
20. G.N. Tiwari, R.K. Mishra, in *Advanced Renewable Energy Sources* (RSC Publishing, London, 2012)
21. D.L. Evans, Solar Energy **27**, 555 (1981)

22. OTA—Office of Technology Assessment, Application of Solar Technology to Today's Energy Needs, in *Energy Conversion with Photovoltaic*, Princeton, 10, 406 (1978)
23. N.T. Truncellito, A.J. Sattolo, in *General Electric Advanced Energy Department* (1979)
24. R. Mertens, in *Proceedings of UK-ISES Conference on C21 Photovoltaic Solar Energy Conversion*, Sept 1979, p. 65
25. L. Barra, D. Coiante, Solar Energy **51**, 383 (1993)
26. J. Prakash, Energy Convers. Manag. **35**, 967 (1994)
27. H.P. Garg, R.K. Agarwal, Energy Convers. Manag. **36**(2), 87 (1995)
28. A.A. Hegazy, Energy Convers. Manag. **41**, 861 (2000)
29. T. Yamawaki, S. Mizukami, T. Masui, H. Takahashi, Sol. Energy Mater. Sol. Cells **67**, 369 (2001)
30. RET Screen International, in *Photovoltaic project analysis* (2001), PV 22
31. K. Nagano, T. Mochida, K. Shimakura, K. Murashita, S. Takeda, Sol. Energy Mater. Sol. Cells **77**, 265 (2003)
32. T.T. Chow, Solar Energy **75**(2), 143 (2003)
33. H.A. Zondag, D.W. de Vries, W.G.J. van Helden, R.J.C. van Zolingen, Solar Energy **74**(3), 253 (2003)
34. A. Tiwari, M.S. Sodha, Solar Energy **80**, 751 (2006)
35. Y.B. Assoa, C. Menezo, G. Fraisse, R. Yezou, J. Brau, Solar Energy **81**, 1132 (2007)
36. J.K. Tonui, Y. Tripanagnostopoulos, Renew. Energy **32**, 623 (2007)
37. M.Y. Othman, B. Yatim, K. Sopian, M.N. Abu, Bakar. Desalination **209**, 43 (2007)
38. Shyam, G.N. Tiwari, I.M. Al-Helal. Solar Energy **114**, 61 (2015)
39. Gaurav Kumar Singh, in *Analysis of Environmental Impacts on the Oerformance of PV Modules*, Ph. D. Thesis, I.I.T. Delhi New Delhi India (2013)

Additional References

40. J.A. Duffie, W. Beckman, *Solar Engineering of Thermal Processes* (Wiley, New York, 1991)
41. G.N. Tiwari, R.K. Mishra, S.C. Solanki, Appl. Energy **88**, 2287 (2011)
42. P. Dupeyrat, C. Ménézo, S. Fortuin, Energy Build. **68**, 751 (2014)
43. A. Makki, S. Omer, H. Sabir, Renew. Sustain. Energy Rev. **41**, 658 (2014)
44. N. Asim, K. Sopian, S. Ahmadi, K. Saeedfar, M.A. Alghoul, O. Saadatian, S.H. Zaidi, Renew. Sustain. Energy Rev. **16**(8), 5834 (2012)
45. B. Agrawal, G.N. Tiwari, *Building Integrated Photovoltaic Thermal Systems* (RSC Publishing, London, 2010)
46. B. Agrawal, G.N. Tiwari, in *Developments in Environmental Durability for Photovoltaics* (Pira International Ltd., London, 2008)

Chapter 5
Flat-Plate Collectors

Abstract A flat-plate collector (FPC) is a device to collect solar energy and transform it into thermal energy (low-grade energy) by using water as a working fluid. It is a heart of solar thermal devices that has many applications in a medium temperature range ≅100 °C from domestic to preheating to industrial sectors. The hot water available from flat-plate collectors (FPC's) can be also used to conserve fossil fuel.

Keywords Solar thermal collectors · PVT-FPC water collectors · Fin efficiency · Thermal losses · Instantaneous efficiency

5.1 Introduction

Solar radiation is considered to be in the form of electromagnetic waves as well as photon-carrying energy (hv). Solar energy can be used broadly by three technological processes, namely:

(i) **Heliochemical**: This process maintains life on Earth by producing food and converting CO_2 from the atmosphere into O_2 using photons through the process of photosynthesis, i.e., light and dark reaction.

(ii) **Helioelectrical**: In this process photons are used in a semiconductor to produce electricity (Chap. 4); these are known as "photovoltaic converters." They provide power for many applications including spacecraft.

(iii) **Heliothermal**: This process can be used to provide much of the thermal energy required for solar water/air heating and building heating. It is also referred as a "solar thermal system."

The most important part of the solar thermal system is the flat-plate collector (FPC), which will be discussed in this chapter.

5.2 Flat-Plate Collector

The FPC is the heart of any solar energy–collection system. It is designed for operation in the medium temperature range between 60 and 100 °C. It is used to absorb both the beam and the diffuse solar radiation (Chap. 1) after transmission from the glass cover. The absorber converts it into thermal energy (heat) and then transfers the absorbed thermal energy (heat) into a stream of liquid or gas (Fig. 5.1a). In the present case involves water. It does not require tracking of the Sun. It requires little operation and maintenance.

A conventional FPC generally consists of the following components, namely:

(a) **Glazing**: This is transparent material for the short wavelength range (0.23–2.6 μm) and opaque for the long wavelength range ≥2.6 μm. The number of transparent materials used can be more than one (Fig. 5.1a)

(b) **Tubes and fins**: The fluid is allowed to pass through tubes and fins for conducting or directing the heat transfer from absorber to the flowing fluid (Fig. 5.1b).
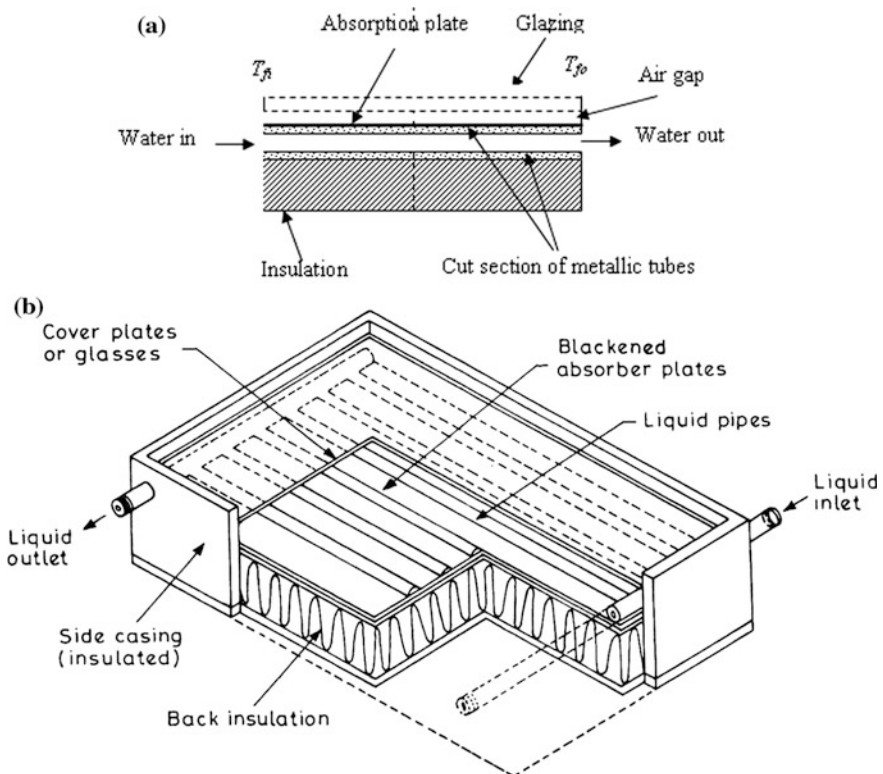
Fig. 5.1 a Side cross–section view of single glazed flat-plate collector. **b** Front and cut view of glazed flat-plate collector

(c) **Absorber plate**: This is a blackened conducting flat plate, corrugated or grooved, with tubes and fins for the absorption of short-wavelength solar radiation (Fig. 5.1b).

(d) **Header or manifolds**: There are two headers, namely, the lower header, which allows fluid to pass through, and upper header, which is used to discharge hot water after heating (Fig. 5.1b).

(e) **Insulation**: This is a nonconduting material at the bottom of tube and fins to minimize heat loss from the back and sides of the FPC (Fig. 5.1b).

(f) **Container or casing**: This surrounds the various components and protects them from dust and moisture, etc. (Fig. 5.1b).

It is important to mention that area of the glass cover and the absorber is equal.

5.2.1 Glazing Materials

The role of a glazing material is to transmit the maximum possible short-wavelength radiation and to minimize the upward loss of heat from the absorber to the ambient through the glazing. The most commonly used glazing material is glass. It can transmit up to 90 % of incident short-wavelength radiation, but it behaves as opaque for long-wavelength heat radiation (≥ 2.6 µm), which is emitted by the absorber plate. Plastic films and sheets may also be used for the purpose of glazing because they possess high transmittance to short-wavelength solar radiation.

The transmittance (τ)

The propagation of solar radiation through one non-absorbing cover is shown in Fig. 5.2a. Considering only the perpendicular component of polarization of incoming solar radiation, $(1 - \rho_\perp)$ of incident solar radiation reaches the second interface of the glass cover after reflection from the first interface of the glass cover. The $\rho_\perp$ part of $(1 - \rho_\perp) = \rho_\perp(1 - \rho_\perp)$ is again reflected back from second interface to first interface. The remaining solar radiation $= (1 - \rho_\perp) - \rho_\perp(1 - \rho_\perp) = (1 - \rho_\perp)^2$ passes through the second interface and so on. Summing the transmitted terms, one can obtain,

$$\tau_\perp = (1 - \rho_\perp)^2 \sum_{n=0}^{n=\infty} \rho_\perp^{2n} = \frac{(1 - \rho_\perp)^2}{(1 - \rho_\perp^2)} = \frac{1 - \rho_\perp}{1 + \rho_\perp} \tag{5.1}$$

The same expression can be obtained for the parallel component of polarization of incoming solar radiation. The $\rho_\perp$ and $\rho_\parallel$ are not equal except at normal incidence. The transmittance of initially unpolarised solar radiation is the average of the two components and it is expressed as

Fig. 5.2 a Propagation of
radiation through cover.
b Variation of transmittance
with incidence angle
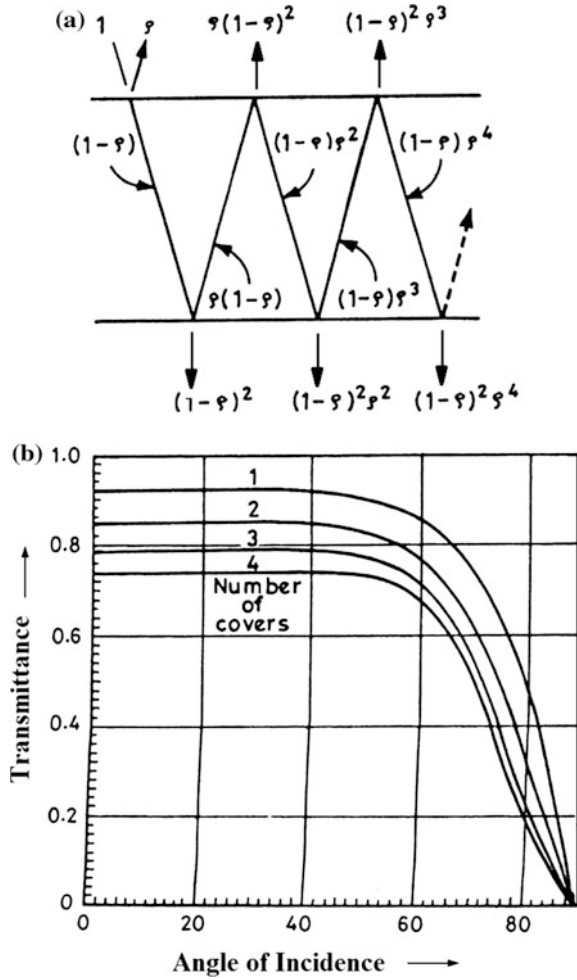
$$\tau_\rho = \frac{1}{2}\left[\frac{1-\rho_\|}{1+\rho_\|} + \frac{1-\rho_\perp}{1+\rho_\perp}\right] \qquad (5.2)$$

where the subscript ρ shows that only reflection losses are considered for the
transmission of solar radiation.

Similarly, an expression for $\tau_{\rho N}$ can be derived for a system of N covers, which
is written as follows:

$$\tau_{\rho N} = \frac{1}{2}\left[\frac{1-\rho_\|}{1+(2N-1)\rho_\|} + \frac{1-\rho_\perp}{1+(2N-1)\rho_\perp}\right] \qquad (5.3)$$

The variation of τ_ρ with angle of incidence is shown in Fig. 5.2b for a different glass covers. It shows that transmittance decreases as the number of glass covers increases.

Absorption by glazing

According to Bouguer's law, the absorbed solar radiation is proportional to the product of solar intensity and the distance travelled (x) in the medium. It can be expressed as follows:

$$dI = -KI\,dx \tag{5.4}$$

Here K is proportionality constant known as the "**extinction coefficient of glass**." It is assumed to be constant in the solar spectrum. The value of K varies from $4\,m^{-1}$ for "white-water" glass to $32\,m^{-1}$ for poor glass (greenish).

Integrating Eq. (5.4) from zero to the actual path length $(L/\cos\theta)$ in the medium, we obtained,

$$\frac{dI}{I} = -\int_0^{\frac{L}{\cos\theta}} K\,dx \tag{5.5}$$

which gives

$$\log I - \log I_i = -\frac{Kx}{\cos\theta}$$

or

$$\frac{I}{I_0} = \exp\left(-\frac{Kx}{\cos\theta}\right) \tag{5.6}$$

At $x = L$, the solar radiation transmitted through the glass cover, I_τ, is obtained as follows:

$$\frac{I_\tau}{I_i} = \exp\left(-\frac{KL}{\cos\theta}\right) \tag{5.7}$$

Equation (5.7) is a transmission due to absorption only and it is denoted as

$$\frac{I_\tau}{I_i} = \tau_a = \exp\left(-\frac{KL}{\cos\theta}\right) \tag{5.8a}$$

The subscript "a" indicates that the transmission is due to absorption only. The absorptance of a glass cover of the FPC can be written as
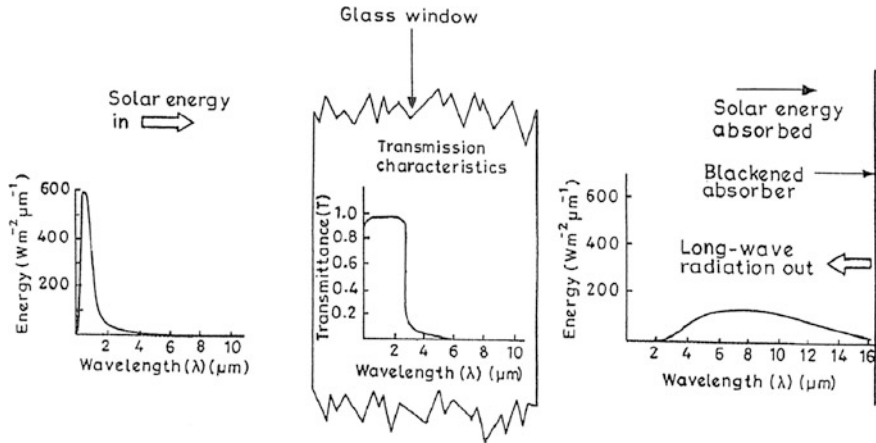
Fig. 5.3 Propagation of solar radiation through glass window

$$\alpha = 1 - \tau_a \qquad (5.8\text{b})$$

The reflectance of a single cover can also be written as

$$\rho = 1 - \alpha - \tau = \tau_a - \tau \qquad (5.8\text{c})$$

Now, the transmittance of single glass cover of a FPC becomes

$$\tau = \tau_\rho \times \tau_a \qquad (5.9)$$

The propagation of short-wavelength solar radiation (0.23–2.6 μm) through a glass window is shown in Fig. 5.3. The transmission characteristic of a window glass cover is also shown in the same figure.

5.2.2 Working Principle

The critical component of the FPC is to act as the absorber and tubes/duct for the flow of liquid/gas. In case of the water collector, water flowing in the tubes receives thermal energy from the absorber plate. The role of absorber of FPC is:

(i)   to absorb the maximum possible solar radiation incident on it through the glazing;

(ii)   to minimize heat losses from the absorber to the atmosphere from the top, bottom, and sides of the FPC; and

(iii) to transfer maximum heat to the fluid.

Fig. 5.4 Flat-plate collector inclined at an angle
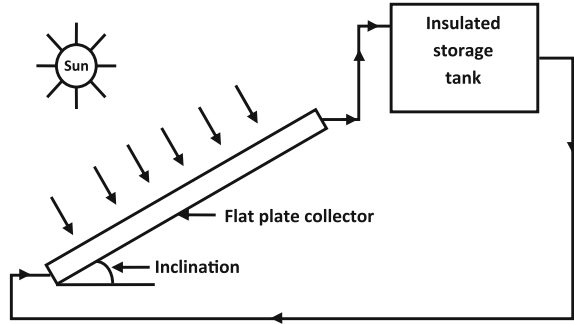
Materials generally used for collector absorber plates are copper, aluminum, and steel. For better performance and low maintenance, the cost and conductance should be properly chosen. The selective surface coating of the absorber plate must ensure high absorptivity (α) and low emissivity (ϵ) to retain maximum thermal (heat) energy. The role of selective surface is vital for high-temperature applications. For a domestic water-heating system, the absorber plate is normally painted black because the required temperature is low compared with the industrial demand. The solar energy absorbed by the absorber plate heats the absorber plate. The thermal energy from the absorber plate is transferred to the fluid circulating in the tubes in thermal contact with the absorber plate; or fluid can directly extract the heat if it is flowing on the absorbing plate. The sides and bottom of the FPC are properly insulated to reduce losses from the bottom- and sides. The flat-plate–collector assembly is inclined at the optimum angle (depending on the location of installation) to receive the maximum solar radiation throughout the year (Fig. 5.4).

5.2.3 Characteristic Curve of the Flat-Plate Collector

Under steady-state conditions, based on the first law of thermodynamics, the energy balance of a simple FPC will be as follows:

$$\dot{q}_{ab} = \dot{q}_u + \dot{q}_L \tag{5.10}$$

where $\dot{q}_{ab} = (\alpha\tau)I(t)$ and $\dot{q}_L = U_L(T_p - T_a)$.

Here $\dot{q}_{ab}$ is the rate of energy absorbed by the plate per unit area; $(\dot{q}_u)$ is the rate of useful energy transferred to the fluid; and $(\dot{q}_L)$ is the rate of energy lost per unit area by the absorber plate to the surroundings.

Equation (5.10) can be rewritten as follows:

$$\dot{q}_u = (\alpha\tau)I(t) - U_L(T_p - T_a) \tag{5.11a}$$

The rate of useful thermal energy for an FPC of area A_c can also be written as

$$\dot{Q}_u = A_c[(\alpha\tau)I(t) - U_L(T_p - T_a)] \tag{5.11b}$$

Furthermore, an instantaneous thermal efficiency can be defined as follows:

$$\eta_i = \frac{\dot{q}_u}{I(t)} = (\alpha\tau) - U_L\frac{T_p - T_a}{I(t)} \tag{5.11c}$$

where α and τ are the absorptivity and transmissivity of the glazing surface of the FPC, respectively; $I(t)$ is the incident total solar radiation in the plane of the absorber (W/m^2); T_p and T_a are the plate and the ambient temperature (°C), respectively; and U_L is an overall heat loss coefficient for the FPC (W/m^2 °C). Referring to Eq. (5.11a) and Fig. 5.2, the rate of useful energy decreases with increasing temperature difference. The thermal loss to the surroundings is an important factor in the determination of the performance of a FPC. The higher the rate of thermal losses ($\dot{q}_L$), the lower is the rate of useful energy output ($\dot{q}_u$). The rate of heat loss depends on $(T_p - T_a)$. Hence, for different ranges of temperature difference, different types of collectors are designed to minimize $\dot{q}_L$ and optimize $\dot{q}_u$.

Equation (5.11c) can be used to draw the curve between η_i and $\frac{(T_p - T_a)}{I(t)}$ as shown Fig. 5.5. This curve is known as the "characteristic curve of the flat-plate collector" (FPC).
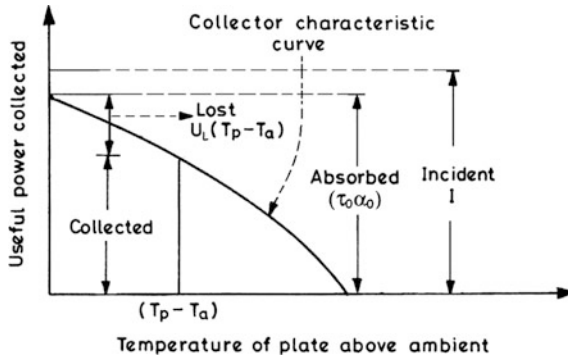
Fig. 5.5 Collector-characteristics curve

5.2.4   Classification of Flat-Plate Collectors (FPC)

In FPC's, heat loss by convection is important to determine its performance. The convective heat loss may be decreased by using double glazing, Fig. 5.6. However, solar radiation reaching the absorber is reduced due to double reflection. Hence, the use of single glazing gives better thermal efficiency than double glazing at low temperatures due to smaller loss. The use of double glazing is advisable for better performance at higher temperature differences. The classification of FPC's is shown in Table 5.1.

The schematic diagrams with single glazing are shown in Fig. 5.7 for all of the collectors. The types of FPC's used for water heating applications are as follows:

(a) Full pipe and fin: This type should be used with a fin made of a highly conducting material, namely, copper or aluminium. It is used for domestic water heating
(b) Full water sandwich type: In this case, both the wetted area and the water capacity are high. Because the thermal conduction is only across the skin thickness (short distance) of the materials, low-conductivity materials may be used. Both plastic and steel are used. It is commonly used for heating swimming pools with plastic panels.
(c) Semi-sandwich type: A medium-conductivity material, such as steel, is commonly used. In some case aluminium may also be used.

Fig. 5.6 Exposed cross-section through double-glazed flat-plate collector
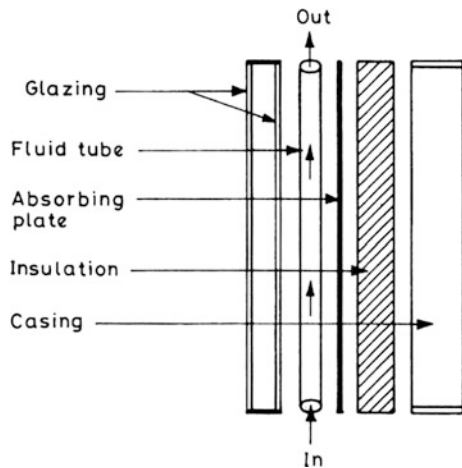
Table 5.1 Classification of flat-plate collectors

Flat-plate collectors							
Water or liquid collectors			Air collectors				
Pipe-and-fin type	Water-sandwich type	Semi-sandwich type	Finned plate	Metal matrix	Corrugated plate with selective surface	Miller LOF–type	Thermal trap
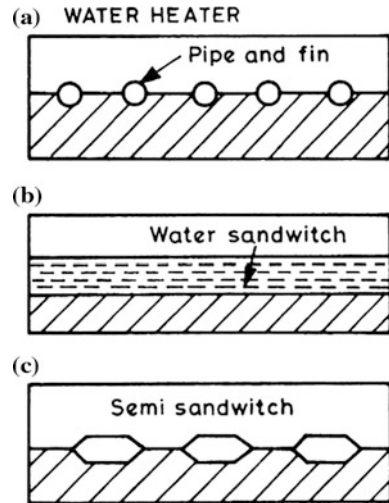
5.3   Flat-Plate Collector Testing

FPC performance can be determined from either

(a) controlled indoor tests by using a solar simulator; however, nonavailability of
a solar simulator matched to the solar spectrum limits the accuracy of indoor
tests; or

(b) carefully performed outdoor tests under steady-state conditions; in this case
weather variability limits that the accuracy of outdoor tests.

These tests are the ultimate check on FPC performance under field conditions.
The outdoor testing of FPC are described later in the text.

5.3.1   Orientable Test Rig [1]

The standard procedure for testing the FPC is to operate the collector under
steady-state conditions. This means the solar radiation and other conditions are
essentially constant for long-enough time to allow the outlet water temperature and
the rate of the useful gain $(\dot{Q}_u)$ to become steady.

To achieve the above conditions, water at constant temperature (T_{fi}) is allowed
at a constant flow rate $(\dot{m}_f)$ from a fixed head tank to the inlet of the FPC.
Furthermore, the FPC is rotated to face the Sun to reduce the angle of incidence and
capacitance effects as shown in Fig. 5.8. This adjustment feature extends for the
duration of the day available for constant steady input of solar radiation to the
system. Instantaneous thermal efficiency (η_i) is then calculated by measuring the

Fig. 5.8 Orientable test rig
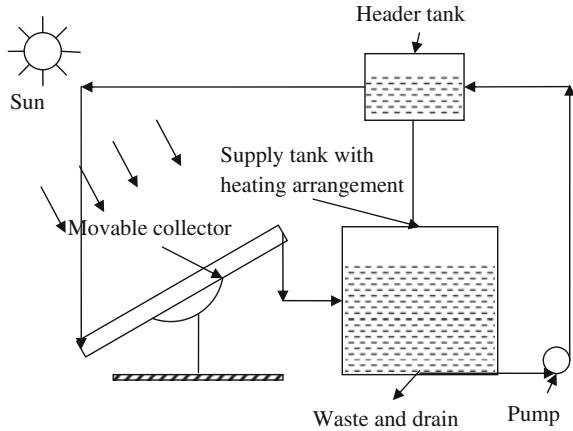
solar radiation $[I(t)]$, ambient temperature (T_a), mass flow rate of water $\dot{m}_f$, and inlet (T_{fi}) and outlet (T_{fo}) fluid temperature.

The rate of useful energy of the FPC in W can written as

$$\dot{Q}_u = \dot{m}_f C_f (T_{fo} - T_{fi}) \qquad (5.12)$$

where C_f is the specific heat of the fluid.

The instantaneous thermal efficiency (η_i) of the FPC of effective area of A_c is given by

$$\eta_i = \frac{\dot{Q}_u}{A_c I(t)} \qquad (5.13)$$

where A_c is the FPC area; and $I(t)$ is the incident radiation on the FPC (W/m^2).

After measuring $\dot{m}_f, T_{fo}, T_{fi}$ and $I(t)$ for given C_f and A_c, Eq. (5.13) can be used to evaluate η_i. Now a characteristic curve between η_i and $\frac{(T_p - T_a)}{I(t)}$ can be plotted.

5.3.2 Series-Connected Test Rig

For N-flat-plate collectors (FPC) connected in series and exposed to the same climatic operating conditions (Sect. 5.3.1), it is possible to carry out simultaneous testing of several FPC's under different operating conditions. In this case, inlet water temperature is maintained with a controlled flow rate. The inlet and outlet temperatures for each of the FPC's are continuously monitored separately. Although all FPC are exposed to the same environmental conditions. each one is at a successively higher operational temperature level. It is thus possible to create a

characteristic curve for each FPC for the mean radiant load during the test period by the same formulation given in Sect. 5.3.1.

5.3.3   Flat-Plate Collector with Intermittent Output

This method has been developed to overcome the limitations of previous methods of steady-state conditions (constant solar radiation and ambient temperature) for a longer time. In this model, the output water from the FPC is not continuous but intermittent. It is controlled by a thermal switch that operates only when the outflow temperature reaches a preset value. The outflow of hot water is driven by inlet cold water, which comes from a storage tank on the roof or a higher level under gravitational force.

The complete test set up is shown in Fig. 5.9, which consists of

(a) a cold-water tank from which the inlet water at temperature T_{fi} is fed to the FPC;

(b) a collector to be tested at some known inclination depending on the latitude of the testing place; and

(c) a pyranometer to measure the incident solar radiation on the collector, thermal switch, and storage tank.

The thermal switch controls the solenoidal valve with a thermal (mercury-type) sensor immersed inside the outflow header tube [2] of the FPC (T_{fo}). When the water inside the FPC attains a temperature equal to a preset value, the solenoidal valve opens, and hot water is forced out; when the temperature decreases below the preset value, cold water inflows into the tank, and the valve is closed. The solar water–heating process is repeated. The temperatures are measured with copper-constatan thermocouple wires. The thermal sensor is of mercury-type immersed inside the upper header tube [2]. The outflow temperature may differ from the preset value due to the natural convection inside the inclined collector.
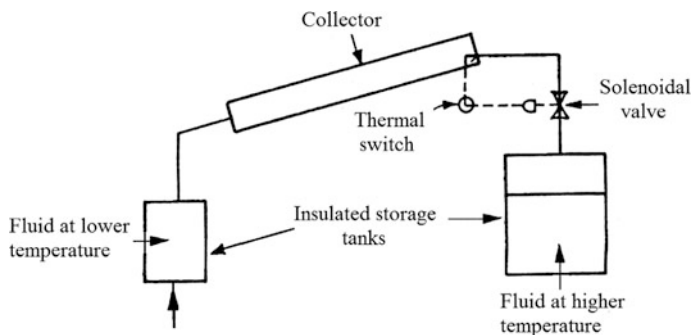
Fig. 5.9   Schematic diagrams of experimental apparatus

Therefore, during the discharging period, it is advised to measure the average temperature $\bar{T}_{\text{fo}}$, which is equal to the average temperature of the discharged and well-mixed fluid (inside the insulated storage tank).

Huang and Lu [2] measured the quantity of water discharged to the storage tank by graduated cylinder in each cycle. They found it to be different from the total fluid in the absorber. They correlated the quantity of discharged hot water in each cycle with a parameter Y as follows:

$$
M_{\text{fo}} = \left.
\begin{array}{l}
3.74\,Y^{-0.507} \pm 0.6\,\text{kg}\ (0 < \theta < 45°) \\
4.37\,Y^{-0.33} \pm 0.3\,\text{kg}(45° < \theta < 60°)
\end{array}
\right\}
\tag{5.14a}
$$

where $Y = \ln X$ and X is defined as

$$
X = \frac{E - (\bar{T}_{\text{fo}} - T_{\text{a}})/I(t)}{E - (\bar{T}_{\text{f}} - T_{\text{a}})/I(t)}
\tag{5.14b}
$$

where E is the equilibrium constant. The values of E are determined for different values of inclination and are found to be approximately independent of solar incident angle. The values of E for different ranges of incident solar angle are given in Table 5.2.

The average thermal efficiency of each FPC in each cycle is given by

$$
\eta_{\text{av}} = \frac{M_{\text{fo}}C_{\text{f}}(\bar{T}_{\text{fo}} - T_{\text{fi}})}{A_{\text{c}}\tau I(t)}
\tag{5.15}
$$

where τ is the time period of discharge of hot fluid M_{fo}.

The measured thermal efficiency has been correlated with X by Huang and Lu [2] as follows:

$$
\eta = \left.
\begin{array}{ll}
0.762X^{0.514} \pm 0.03 & (0° < \theta < 45°) \\
0.614X^{0.356} \pm 0.03 & (45° < \theta < 60°)
\end{array}
\right\}
\tag{5.16}
$$

Using Eqs. (5.15) and (5.16) along with Table 5.2, one can test the performance of a FPC.

Table 5.2 Determination of constant E

Angle	0–10°	10–20°	20–30°	30–40°	40–50°	50–60°
$E(°C - \text{m}^2/\text{kW})s$	87.8 ± 2.5	82.8 ± 2.7	79.3 ± 2.5	82.6 ± 3.0	78.1 ± 2.3	82.7 ± 1.7

5.3.4   The ASHRAE Method

There are three standard procedures for a liquid collector as given by ASHRAE 93–77. The essential requirements for all of the procedures are summarized below:

(i)   arrangement for the inlet of fluid at constant temperature with flexibility to set different values of inlet temperatures;
(ii) pyranometer to measure the solar radiation on the surface of the FPC;
(iii) provisions for recording mass flow rate and different temperatures; and
(iv) equipment for measuring pressure and pressure drop across the FPC.

The general test method is to operate the FPC in the test facility under nearly steady conditions as shown in Fig. 5.10. To determine $\dot{Q}_u$ (Eq. 5.12), the following data, namely, $I(t)$, T_{fo}, T_{fi} and T_a, are required to evaluate η_i from Eq. (5.13). Therefore, outdoor tests are performed preferably between 11 a.m. and 1 p.m. on
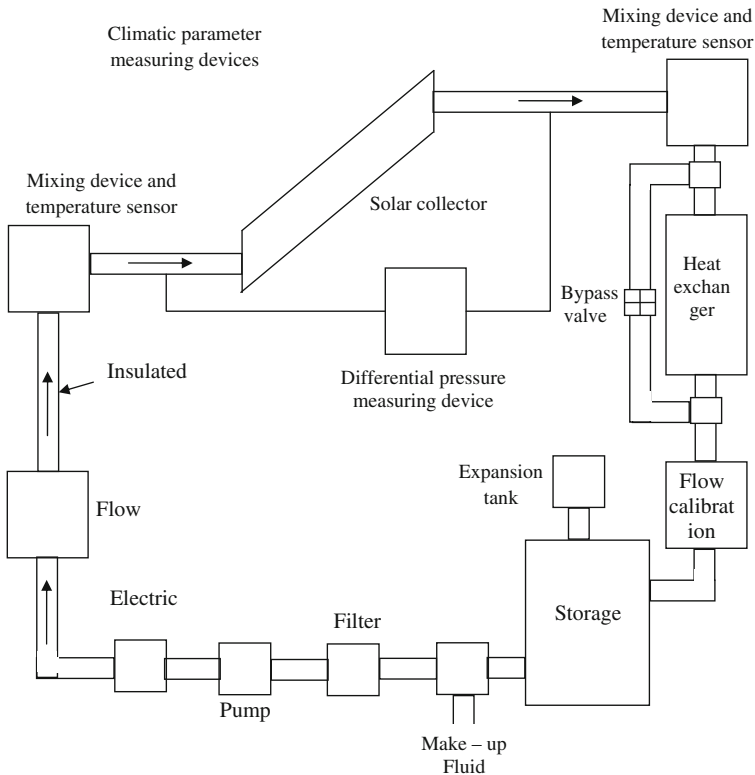
Fig. 5.10 Closed-loop test setup for liquid-heating flat-plate collectors

Fig. 5.11 Theoretical collector efficiency for liquid-heating flat-plate collector with one cover and a selective absorber
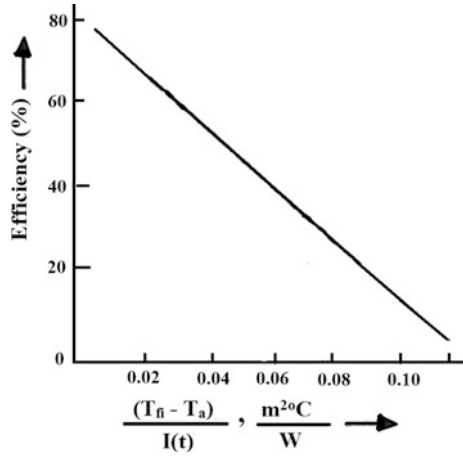
clear days. During this time period, the incident solar radiation falls perpendicularly on the surface of the FPC, and thus it contains maximum beam radiation. Therefore, the transmittance–absorptance product is approximately the normal incidence value. It is expressed as $(\alpha\tau)_n$ for N-glass cover if required.

Tests are performed for various values of the inlet fluid temperature. The effects of heat capacity of FPCs are minimized by conducting the tests in symmetrical pairs, i.e., before and after solar noon. Instantaneous thermal efficiencies (η_i) are determined from the expression given in Eq. (5.13) for the averaged pairs. These are plotted as a function of $(T_{fi} - T_a)/I(t)$. A sample plot of data taken for five test sites under ASHRAE 93–77 conditions is shown in Fig. 5.11.

For constant U_L, F_R and $(\alpha\tau)_n$, the plots of η_i versus $(T_{fi} - T_a)/I(t)$ would be straight lines with intercept $F_R(\alpha\tau)_n$ and slope $-F_R U_L$. U_L is a function of temperature and wind speed.

Even the data can be used to evaluate intercept $F_R(\alpha\tau)_n$, which is gain factor, and the slope $m = -F_R U_L = \tan\theta$, which is loss factor. This method can also be utilised to compare the performance of different designs of FPCs.

The curve represents the theoretical characteristics derived from points calculated for the test conditions [3].

The flow rate factor, F_R, and slope $-F_R U_L$, are weak functions of temperature. There can be variation of beam, diffuse, and ground-reflected components of solar radiation during the test period. Thus, scatter data from a straight line is to be expected due to these variations. Despite these deviations, FPCs can be characterized by the intercept $F_R(\alpha\tau)_n$ and slope $-F_R U_L$.

5.4   Heat-Transfer Coefficients

Thermal loss to the surroundings is an important factor in the study of the performance of an FPC. Thermal loss from an FPC to the surroundings can occur from:

(a) the absorber plate through the glass cover (referred to as "top loss"); and
(b) the absorber plate through the insulation (referred to as "bottom loss").

These thermal losses take place through conduction, convection, and radiation. These thermal losses are also shown in Fig. 5.12. The equivalent thermal losses in the terms of thermal resistance circuit are shown in Fig. 5.13. Here it is important to discuss that the thermal resistance (r) is inversely proportional to the heat-transfer coefficient (h). Knowledge of the heat-transfer coefficient is a main feature for analysis of the performance of the FPC. A discussion of these heat-transfer coefficients is given in the next sections.

5.4.1   Overall Top-Loss Coefficient

(a) **Convective heat-transfer coefficient**

(i) **From absorber plate to the glass cover ($h_{1c} = 1/r_3$):**

The convective heat-transfer coefficient between the absorber plate and the glass cover (inclined at an angle β to the horizontal), can be written as follows:

$$h_{1c} = \frac{1}{r_3} = \frac{Nu\, K_a}{d} \tag{5.17a}$$

Fig. 5.12 Various heat losses from absorber to ambient
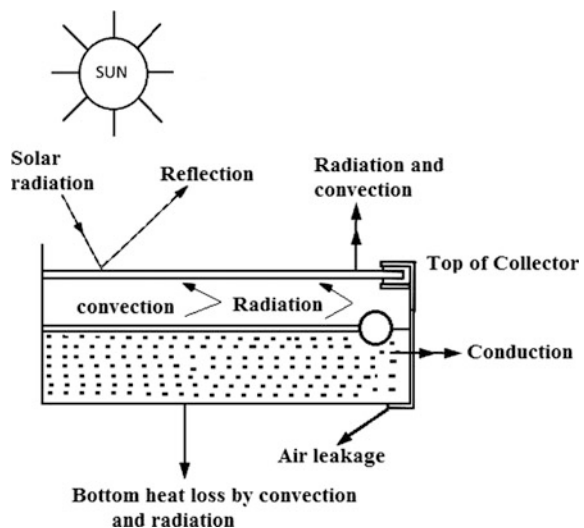
Fig. 5.13   a Equivalent
thermal-circuit diagram of
Fig. 5.12 with thermal
resistance of glass cover.
b Equivalent thermal-circuit
diagram of Fig. 5.13 without
thermal resistance of glass
cover
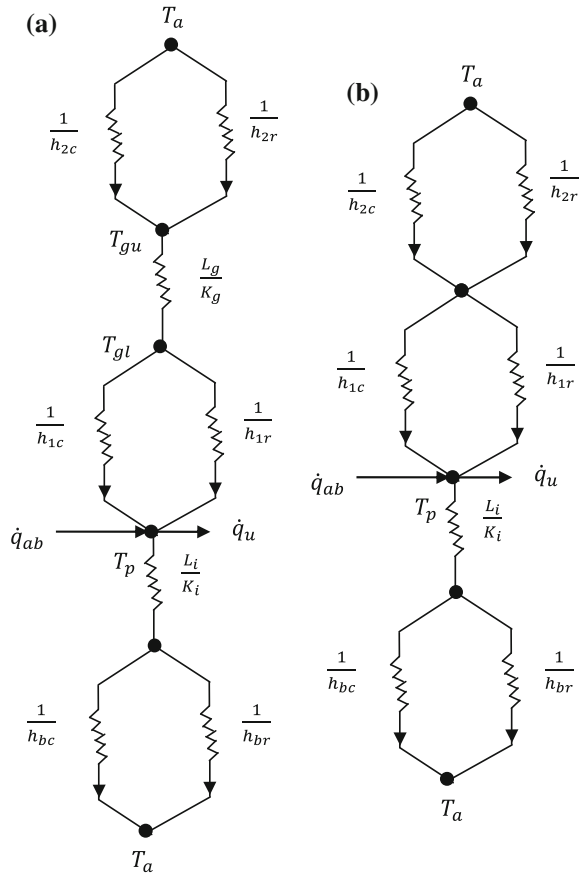
where Nu is the Nusselt number; K_a is the thermal conductivity of air between the
plate and the glass cover; and d is the spacing between the absorber plate and the
glass covers.

The expression for Nu can be obtained using the method given by Holland et al.
[4] for air as the medium between the absorber plate and the glass cover as follows:

$$Nu = 1 + 1.44 \left[1 - \frac{1708}{Ra \cos \beta} \right]^{+} \left(1 - \frac{\sin(1.8\beta)^{1.6} \times 1708}{Ra \cos \beta} \right) + \left[\left\{ \frac{Ra \cos \beta}{5830} \right\}^{1/3} - 1 \right]^{+} \tag{5.17b}$$

The '+' exponent means that only the positive value of the term in square
brackets is to be considered. The zero is to be used for negative value. The angle of
inclination, β, of the FPC can vary between $0°$ and $75°$, and Ra is the Rayleigh
number, which is given by:

$$Ra = Gr \cdot Pr = \frac{g\beta' \Delta T d^3}{v\alpha} \tag{5.17c}$$

If, $75° < \beta < 90°$, then

$$Nu = \left[1, \ 0.288\left(\frac{Ra \times \sin \beta}{A}\right)^{1/4}, \ 0.039(Ra \times \sin \beta)^{1/3}\right]_{max} \tag{5.18a}$$

where the subscript indicates that the maximum of the three quantities separated by commas should be taken for a given value of the Rayleigh number. A is the ratio of length of the flat plate inclined to spacing between the cover and the absorbing plate of the FPC (L/d).

The following three region correlations for convective heat-transfer losses for an inclined FPC were proposed by Buchberg et al. [5]:

$$Nu = 1 + 1.446\left[1 - \frac{1708}{Ra \cos \beta}\right] \quad \text{for } 1708 < Ra \cos \beta < 5900 \tag{5.18b}$$

$$Nu = 0.229(Ra \cos \beta)^{0.252} \quad \text{for } 5900 < Ra \cos \beta < 9.23 \times 10^4 \tag{5.18c}$$

$$Nu = 0.157(Ra \cos \beta)^{0.285} \quad \text{for } 9.23 \times 10^4 < Ra \cos \beta < 10^6 \tag{5.18d}$$

Example 5.1 Calculate the convective heat-transfer coefficient between two parallel plates. The plates are separated by 20 mm with an inclination of 40°. The lower and upper plates are at 50 and 30 °C, respectively.

Solution

At the mean air temperature of 40 °C, the air properties are as follows:

$K = 0.0272$ W/m °C, $T = 313$ K so $\beta = 1/T = 1/313$; $v = 1.70 \times 10^{-5}$ m^2/s; $\alpha = 2.40 \times 10^{-5}$ m^2/s (see Appendix V).

From Eq. (5.17c), one gets the value of the Rayleigh number as follows:

$$Ra = \frac{9.81 \times 20 \times (0.020)^3}{313 \times 1.70 \times 10^{-5} \times 2.40 \times 10^{-5}} = 1.23 \times 10^4$$

Now, from Eq. (5.17b), one can obtain the value of Nu as 2.123. The heat-transfer coefficient (h_{1c}) is obtained from Eq. (5.17a) as

$$h_{1c} = NuK_a/d = (2.12 \times 0.0272)/0.020 = 2.88 \text{ W/m}^2 \, °C$$

(ii) **From glass cover to ambient air ($h_{2c} = 1/r_1$):**

The convective heat-loss coefficient (W/m^2 °C) from the top of glazing to the ambient is given by [6],

$$h_{2c} = \frac{1}{r_1} = 2.8 + 3.0V \tag{5.19}$$

where V is the wind speed in m/s over the glass cover of the FPC.

(b) **Radiative heat-transfer coefficient**

(i) **From absorber plate to glass cover $h_{1r} = 1/r_4$:**

The rate of heat transfer from the absorber plate to the glass cover by radiation (W/m^2) can be written as

$$\dot{q}_{\mathrm{rad}} = h_{1r}\left(T_{\mathrm{p}} - T_{\mathrm{g}}\right) \tag{5.20a}$$

where T_{p} and T_{g} are the absorber plate and glazing temperatures in °C, respectively. The h_{1r} is the heat-transfer coefficient by radiation from the absorber plate to the glass cover, and it is expressed as

$$h_{1r} = \frac{1}{r_4} = \varepsilon_{\mathrm{eff}}\sigma\frac{\left[\left(T_{\mathrm{p}} + 273\right)^4 - \left(T_{\mathrm{g}} + 273\right)^4\right]}{T_{\mathrm{p}} - T_{\mathrm{g}}} \tag{5.20b}$$

where $\sigma = 5.67 \times 10^{-8}$ W/m^2 K^4 is Stefan's constant. The $\varepsilon_{\mathrm{eff}}$ is the effective emissivity of plate-glazing system, and it is given by

$$\varepsilon_{\mathrm{eff}} = \left[\frac{1}{\varepsilon_{\mathrm{p}}} + \frac{1}{\varepsilon_{\mathrm{g}}} - 1\right]^{-1} \tag{5.20c}$$

(ii) **From glazing cover to ambient ($h_{2r} = 1/r_2$):**

The heat-transfer coefficient by radiation from a glass cover to the ambient depends on the long-wavelength radiation exchange with the sky at sky temperature T_{sky}, which is given as

$$T_{\mathrm{sky}} = T_{\mathrm{a}} - 6 \tag{5.21a}$$

Thus, the radiative heat-transfer coefficient, h_{2r}, can be written as follows:

$$h_{2r} = \frac{1}{r_2} = \varepsilon_{\mathrm{g}}\sigma\frac{\left[\left(T_{\mathrm{g}} + 273\right)^4 - \left(T_{\mathrm{sky}} + 273\right)^4\right]}{T_{\mathrm{g}} - T_{\mathrm{a}}} \tag{5.21b}$$

(c) **Overall top-loss heat-transfer coefficient**

The total heat-transfer coefficient (a) from an absorber plate to a glass cover (h_1) i.e., the sum of h_{1c} and h_{1r}, Eqs. (5.17a) and (5.20b), can be expressed as follows:

$$h_1 = h_{1c} + h_{1r} = \frac{1}{r_3} + \frac{1}{r_4} \tag{5.22}$$

and (b) from a glass cover to the ambient air is the sum of Eqs. (5.19) and (5.21b) and is given by

$$h_2 = h_{2c} + h_{2r} = \frac{1}{r_1} + \frac{1}{r_2} \tag{5.23}$$

The conductive heat-transfer coefficient $(h_k = 1/r_k)$ is given by

$$h_k = \frac{1}{r_k} = \frac{K_g}{L_g} \tag{5.24}$$

where K_g and L_g are thermal conductivity and thickness of glass cover, respectively.

An overall top-loss heat-transfer coefficient (U_t) from the absorber plate to the ambient is an inverse of the sum of thermal resistance created by the total heat-transfer coefficient from the glass cover to the ambient air, Eq. (5.22), the glass-conductive heat-transfer coefficient, Eq. (5.24), and the total heat-transfer coefficient from the absorber to the glass cover, Eq. (5.23), and is given by

$$U_t = \left[\frac{1}{h_1} + \frac{1}{h_k} + \frac{1}{h_2} \right]^{-1} = \left[\left(\frac{1}{r_3} + \frac{1}{r_4} \right)^{-1} + \frac{L_g}{K_g} + \left(\frac{1}{r_1} + \frac{1}{r_2} \right)^{-1} \right]^{-1} \tag{5.25a}$$

It is important to mention here that the thermal resistance due to conduction $\left(r_k = L_g/K_g \right)$ in Eq. (5.25a) is not significant (Example 5.3), and hence it can be neglected. Then Eq. (5.25a) becomes

$$U_t = \left[\frac{1}{h_1} + \frac{1}{h_2} \right]^{-1} = \left[\left(\frac{1}{r_3} + \frac{1}{r_4} \right)^{-1} + \left(\frac{1}{r_1} + \frac{1}{r_2} \right)^{-1} \right]^{-1} \tag{5.25b}$$

The rate of heat loss through the top glass cover per unit area, $\dot{q}_t$, (W/m^2), can be written as

$$\dot{q}_t = U_t \left(T_p - T_a \right) \tag{5.26a}$$

The value of U_t is calculated by iteration due to the unknown value of T_g. For this, an arbitrary value of T_g is assumed, and the mean temperature and convective

(h_{1c}) and radiative (h_{1r}, h_{2r}) heat-transfer coefficients are calculated. Using these parameters, the top-loss coefficient is calculated. Substitution of a new value of U_t results in the following energy balance condition:

$$h_1 (T_p - T_g) = U_t (T_p - T_a)$$

and gives a new value of T_g:

$$T_g = T_p - \frac{U_t}{h_1} (T_p - T_a) \tag{5.26b}$$

With this new value of T_g, the above calculations are repeated until the two consecutive values of T_g become nearly the same. This refers to iterative methods that are described later in the text:

Step I: Choose an initial appropriate value of T_g.

Step II: Calculate the value of U_t for known value of T_p, T_g, and T_a as performed in Example 5.2.

Step III: After calculating the value of U_t, calculate the new value of T_g from the above equation.

Step IV: Repeat the same calculations with T_p, T_a, and new value of T_g until the two consecutive values of T_g obtained are nearly the same.

(d) **Back-loss coefficient**

Heat is lost from the absorber plate to the ambient air by conduction through the insulation. Then there is further loss from the bottom surface of the casing by convection and radiation. The bottom heat–loss coefficient (W/m^2 °C) is the sum of the insulating conductive heat-transfer coefficient and the total heat-transfer coefficient from the bottom to the ambient air. It is expressed as follows:

$$U_b = \left[\frac{L_i}{K_i} + \frac{1}{h_b} \right]^{-1} \tag{5.27a}$$

where h_b is the sum of convective heat-loss coefficient, h_{bc}, and radiative heat-loss coefficient, h_{br}, from the bottom of the casing to the ambient air. The value of h_{br} and h_{bc} can be calculated as in the case of the top cover. The magnitude of L_i/K_i and h_b are such that the second term in the Eq. (5.27a) is negligible compared with the first one; thus,

$$U_b \approx \frac{K_i}{L_i} \tag{5.27b}$$

The suffix 'i' indicates insulation.

(e) **Edge-loss coefficient**

Energy lost from the side of the collector casing is calculated exactly the same as performed Eq. (5.27a). Edge loss is generally expressed in terms of the area of collector and the back-loss coefficient, and the edge loss coefficient is given as:

$$U_e = U_b(A_e/A_c) \tag{5.28}$$

where A_e is the edge area in m^2.

5.4.2 Overall Heat-Loss Coefficient

The overall heat-loss coefficient, U_L, is the sum of the top, bottom, and edge loss coefficients, and it is given by

$$U_L = U_t + U_b + U_e \tag{5.29}$$

The overall rate of heat lost from the absorber to the ambient air through the glass cover and bottom insulation is given by

$$\dot{q}_L = U_L(T_p - T_a) \tag{5.30}$$

where $\dot{q}_L$ is the same as expressed in Eq. (5.10).

Example 5.2 Calculate the overall top-loss heat-transfer coefficient from the absorber to ambient through the glass cover of a FPC for the following specifications:

Absorber-to-glass cover spacing $(L) = 0.025 m$
Absorber-plate emittance $(\varepsilon_p) = 0.95$
Glass-cover emittance $(\varepsilon_g) = 0.88$
Inclination of FPC $(\beta) = 45°$
Convective heat-transfer coefficient due to wind $(h_{2c}) = 10 \, W/m^2 \, °C$
Ambient air temperature $(T_a) = 16 \, °C$
Thermal conductivity of glass cover $(K_g) = 0.78 \, W/m \, °C$
Thickness of glass cover $(L_g) = 0.003 \, m$
Mean absorber-plate temperature $(\bar{T}_p) = 100 \, °C$

Solution

Step I

ε_{eff} is determined by using Eq. (5.20c),

$$\varepsilon_{\text{eff}} = \left[\frac{1}{0.88} + \frac{1}{0.95} - 1 \right]^{-1} = 0.84$$

Using Eq. (5.21a), one can obtain $T_{\text{sky}} = 16 - 6 = 10\,^{\circ}\text{C}$
Let us assume $T_{\text{g}} = 35\,^{\circ}\text{C}$.

Now the radiative heat-transfer coefficient from the absorber plate to the cover, Eq. (5.20b), can be calculated as:

$$h_{1r} = \frac{0.84 \times 5.6697 \times 10^{-8} \left[(100 + 273)^4 - (35 + 273)^4 \right]}{100 - 35} = 7.496 \text{ W/m}^2\,^{\circ}\text{C}$$

The radiative heat-transfer coefficient from glass cover to the sky, Eq. (5.21b), can be calculated as:

$$h_{2r} = \frac{0.88 \times 5.6697 \times 10^{-8} \left[(35 + 273)^4 - (10 + 273)^4 \right]}{35 - 16} = 6.705 \text{ W/m}^2\,^{\circ}\text{C}$$

The average air temperature in the space between the glass and the plate is 67.5 °C. The physical properties of air at this temperature are (see Appendix V) as follows:

$$v = 1.96 \times 10^{-5}\,\text{m}^2/\text{s}; \quad K = 0.0293\,\text{W/m}\,^{\circ}\text{C};$$
$$g = 9.81\,\text{m/s}^2; \quad T = 340.5\,\text{K}; \quad Pr = 0.7$$

Then the Rayleigh number (Eq. 5.17c) can be calculated as follows:

$$Ra = Gr \cdot Pr = \frac{9.81 \times (100 - 35) \times (0.025)^3 \times 0.7}{340.5 \times (1.96 \times 10^{-5})^2} = 5.33 \times 10^4$$

For $Ra = 5.33 \times 10^4$ from Eq. (5.17b), the Nu is 3.19, and the convective heat-transfer coefficient has been calculated as follows:

$$h_{1c} = Nu \times \frac{K}{L} = 3.19 \times \frac{0.0293}{0.025} = 3.73\,\text{W/m}^2\,^{\circ}\text{C}$$

The conductive heat-transfer coefficient (h_k). can also be calculated from Eq. (5.24), as:

$$h_k = \frac{0.78}{0.003} = 260 \, \text{W}/\text{m}^2 \, °\text{C}$$

Using Eq. (5.25a), the overall top-loss coefficient is given by:

$$U_t = \left[\frac{1}{7.496 + 3.73} + \frac{1}{260} + \frac{1}{6.705 + 10}\right]^{-1} = \left[\frac{1}{11.226} + \frac{1}{260} + \frac{1}{16.705}\right]^{-1}$$

$$= [0.089 + 0.00385 + 0.0598]^{-1} = [0.15265]^{-1} = 6.551 \frac{\text{W}}{\text{m}^2} °\text{C}$$

Using Eq. (5.25b), the overall top-loss coefficient is given by:

$$U_t = \left[\frac{1}{7.496 + 3.73} + \frac{1}{6.705 + 10}\right]^{-1} = \left[\frac{1}{11.226} + \frac{1}{16.705}\right]^{-1}$$

$$= [0.089 + 0.0598]^{-1} = [0.1488]^{-1} = 6.72 \frac{\text{W}}{\text{m}^2} °\text{C}$$

Thus, the percentage of error can be calculated as:

$$\% \, \text{error in} \, U_t = \frac{6.72 - 6.551}{6.551} \times 100 = 2.58$$

Hence, the resistance created by the glass cover is neglected.

Step II

With this new value of $U_t = 6.72 \, \text{W}/\text{m}^2 \, °\text{C}$, a new value of T_g can be calculated from Eq. (5.20b) as follows:

$$T_g = 100 - \frac{6.714}{(7.496 + 3.73)} (100 - 10) = 49.76 \, °\text{C}$$

With this new value of $T_g = 49.76 \, °\text{C}$, the new values of h_{1r} and h_{2r} will be as follows:

$$h_{1r} = \frac{0.84 \times 5.6697 \times 10^{-8} \left[(100 + 273)^4 - (49.76 + 273)^4\right]}{100 - 49.76} = 7.96 \, \text{W}/\text{m}^2 \, °\text{C}$$

and

$$h_{2r} = \frac{0.88 \times 5.6697 \times 10^{-8} \left[(49.76 + 273)^4 - (10 + 273)^4\right]}{49.76 - 16} = 6.48 \, \text{W}/\text{m}^2 \, °\text{C}$$

There a new average air temperature in the space between the glass and the plate is 74.88–75 °C. The physical properties of air at this temperature are:

$$v = 2.076 \times 10^{-5} \, \text{m}^2/\text{s}; \quad K = 0.03 \, \text{W/m}\,^\circ\text{C};$$
$$g = 9.81 \, \text{m/s}^2; \quad T = 348.5 \, \text{K}; \quad Pr = 0.7$$

Then the Rayleigh number (Eq. 5.17c) can be evaluated as follows:

$$Ra = Gr.Pr = \frac{9.81 \times (100 - 49.76) \times (0.025)^3 \times 0.7}{348 \times (2.076 \times 10^{-5})^2} = 3.58 \times 10^4$$

For $Ra = 3.58 \times 10^4$ from Eq. (5.17b), the Nu number is 2.9, and the convective heat-transfer coefficient is calculated as:

$$h_{1c=Nu} \times \frac{K}{L} = 2.9 \times \frac{0.03}{0.025} = 3.48 \, \text{W/m}^2\,^\circ\text{C}$$

Using Eq. (5.25b), the overall top-loss coefficient is given by:

$$U_t = \left[\frac{1}{7.96 + 3.48} + \frac{1}{6.48 + 10}\right]^{-1} = \left[\frac{1}{11.44} + \frac{1}{16.48}\right]^{-1}$$
$$= [0.087 + 0.0606]^{-1} = [0.1488]^{-1} = 6.77 \, \frac{\text{W}}{\text{m}^2}\,^\circ\text{C}$$

With this new value of $U_t = 6.77 \, \frac{\text{W}}{\text{m}^2}\,^\circ\text{C}$, a new value of T_g can be calculated from (Eq. 5.20b) as follows:

$$T_g = 100 - \frac{6.75}{(11.44)}(100 - 10) = 50.4\,^\circ\text{C}$$

Step III

Now again, with this new values of $T_g = 50.4\,^\circ\text{C}$, the new values of h_{1r} and h_{2r} will be as follows:

$$h_{1r} = 7.98 \, \text{W/m}^2\,^\circ\text{C} \quad \text{and} \quad h_{2r} = 6.48 \, \text{W/m}^2\,^\circ\text{C}.$$

The new average air temperature in the space between the glass and the plate = 75.2 °C. At this temperature, Ra can also be calculated, as done earlier, as $Ra = 3.533 \times 10^4$.

For $Ra = 3.533 \times 10^4$ from Eq. (5.17b), the Nusselt number is 2.894, and the convective heat-transfer coefficient is calculated as:

$$h_{1c} = Nu \times \frac{K}{L} = 2.894 \times \frac{0.03}{0.025} = 3.47 \, \frac{W}{m^2} \, °C$$

Using Eq. (5.25b), the overall top-loss heat-transfer coefficient is given by:

$$U_t = \left[\frac{1}{7.98 + 3.47} + \frac{1}{6.47 + 10}\right]^{-1} = \left[\frac{1}{11.45} + \frac{1}{16.47}\right]^{-1}$$
$$= [0.087 + 0.0607]^{-1} = [0.1477]^{-1} = 6.76 \, \frac{W}{m^2} \, °C$$

With this new value of $U_t = 6.76 \, \frac{W}{m^2} \, °C$, a new value of T_g can be calculated from Eq. (5.20b) as:

$$T_g = 100 - \frac{6.76}{(11.45)}(100 - 10) = 50.4 \, °C$$

which is exactly similar to the values calculated in step II. Hence, the same values of U_t will be obtained if the calculations are repeated. This means that the exact value of U_t will be 6.76 $\frac{W}{m^2}$ °C.

Example 5.3 Determine the overall heat-transfer coefficient (U_L) for a FPC system inclined at 45 °C to the horizontal and facing due south for the following parameters:

- The average ambient air temperature for the day is 20 °C;
- The observed glass and absorber-plate temperatures are 45 and 69 °C, respectively;
- The system is provided with 6 cm—thick insulation (glass wool) at the bottom;
- The thermal conductivity of the insulation is 0.04 W/m °C;
- The air space between the absorber plate and the glass cover has an optimum thickness of 75 cm; and
- The emissivity of the glass and the plate is 0.88 and 0.95, respectively.

Solution
The average air temperature between the glass cover and the absorber plate is 57 °C. The physical properties of the air at this temperature (Appendix V) are as follows:

$$v = 1.88 \times 10^{-5} \, m^2/s; \quad \alpha = 2.69 \times 10^{-5} \, m^2/s; \quad K = 0.028 \, W/m \, °C;$$
$$\sigma = 5.67 \times 10^{-8} \, W/m^2 \, K^4; \quad g = 9.81 \, m/s^2; \quad T = 348.5 \, K; \quad Pr = 0.7$$

For, $\Delta T = 24 \, °C; L = 0.75 \, m; Pr = 0.7; \beta = 1/330 \, K^{-1}$, the Rayleigh number, is given by

$$Ra = \frac{9.81 \times 24 \times (0.075)^3 \times 0.7}{330 \times (1.88 \times 10^{-5})^2} = 5.961 \times 10^5$$

Substituting the values in following equation, one gets

$$Nu = 1 + 1.44\left[1 - \frac{1708}{5.961 \times 10^5 \cos 45}\right]^+ \left(1 - \frac{\sin(1.8 \times 45)^{1.6} \times 1708}{5.961 \times 10^5 \cos 45}\right)$$
$$+ \left[\left\{\frac{5.961 \times 10^5 \cos 45}{5830}\right\}^{1/3} - 1\right]^+ = 5.595$$

From Eq. (5.17a), we have

$$h_{1c} = \frac{5.595 \times 0.028}{0.075} = 2.089 \, \text{W/m}^2 \, ^\circ\text{C}$$

From Eq. (5.20c), we obtain $h_{2c} = 17.8 \, \text{W/m}^2 \, ^\circ\text{C}$ for $V = 5$ m/s. Furthermore, the new ε_{eff} will be

$$\varepsilon_{\text{eff}} = \left[\frac{1}{0.88} + \frac{1}{0.95} - 1\right]^{-1} = 0.841$$

The radiative heat-transfer coefficient from the absorber plate to the glass cover is given by

$$h_{1r} = \frac{0.841 \times 5.6697 \times 10^{-8}\left[(69 + 273)^4 - (45 + 273)^4\right]}{24} = 6.85 \, \text{W/m}^2 \, ^\circ\text{C}$$

The radiative heat-transfer coefficient from the glass cover to the sky is written as

$$h_{2r} = \frac{0.88 \times 5.6697 \times 10^{-8}\left[(45 + 273)^4 - (14 + 273)^4\right]}{45 - 20} = 6.885 \, \text{W/m}^2 \, ^\circ\text{C}$$

Now $h_1 = h_{1c} + h_{2c} = 2.089 + 6.85 = 8.939 \, \text{W/m}^2 \, ^\circ\text{C}$ [from Eq. (5.22)]
and $h_2 = h_{1r} + h_{2r} = 17.8 + 6.885 = 24.685 \, \text{W/m}^2 \, ^\circ\text{C}$ [from Eq. (5.23)].
The overall heat-transfer coefficient (W/m² °C) can be determined by using Eq. (5.25b) as follows:

$$U_t = \left[\frac{1}{8.939} + \frac{1}{24.685}\right]^{-1} = 6.536 \, \text{W/m}^2 \, ^\circ\text{C}$$

Bottom-loss coefficient [from Eq. (5.27b)] $U_b = 0.04/0.06 = 0.666 \, \text{W/m}^2 \, ^\circ\text{C}$

The overall heat-loss coefficient ($W/m^2\,°C$) from the absorber plate to the ambient air through the bottom insulation is given by

$$U_L = U_t + U_b = 6.536 + 0.666 = 7.202\,W/m^2\,°C$$

Example 5.4 For a FPC with a top-loss coefficient of 6.6 $W/m^2\,°C$, determine the overall loss coefficient by using following data:

Back insulation thickness = 0.045 m, insulation conductivity = 0.04 $W/m^2\,°C$
Collector bank length = 8 m, collector bank width = 2.5 m
Collector thickness = 0.08 m, edge insulation thickness = 0.02 m

Solution

From Eq. (5.27b), the bottom-loss coefficient is given by

$$U_b = \frac{K_{in}}{L_{in}} = \frac{0.04}{0.045} = 0.889\,W/m^2\,°C$$

From Eq. (5.28), the edge-loss coefficient (for 21-m perimeter) is given by

$$U_e = \frac{(0.04/0.02)(21)(0.08)}{8 \times 2.5} = 0.17\,W/m^2\,°C$$

The collector overall loss coefficient is written as

$$U_L = 6.6 + 0.889 + 0.17 \approx 7.7\,W/m^2\,°C$$

5.4.3 *Film Heat-Transfer Coefficient [7]*

To determine the film heat-transfer coefficient between the fluid in the collector tube and the inner tube wall (h_f), Fig. 5.14, the Nusselt number (Nu), is given by Baker [8]

$$Nu = 1.75 \left(\frac{\mu_\omega}{\mu'_\omega}\right)^{0.14} \left[Gz + 0.0083(Ra)^{0.75}\right]^{1/3} \tag{5.31}$$

where μ_w is the viscosity of the fluid at the mean system temperature; μ'_w is the viscosity of fluid at the temperature of the inner wall of the tube; and Gz is the Greatz number, which is given by

$$Gz = \frac{Re_D Pr}{x/D} \tag{5.32a}$$

where Re_D is the value of Reynolds number at the diameter D; and x is the characteristic dimension. If $x = D$, then

Fig. 5.14 Cross-section of
the tube of FPC with film-heat
transfer
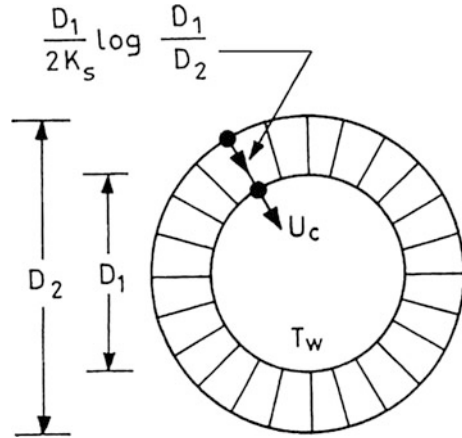
$$Gz = Re_D \times Pr \qquad (5.32b)$$

In general, the temperature of the water and the inner wall of the tube are time dependent. However, their average values may be used for the calculation of heat-transfer coefficients. The thermal conductance (i) from the inner wall of the heat exchanger to the cold water, U_c, as well as (ii) the thermal conductance from the hot water to the outer wall of the heat exchanger, U_h, can be evaluated from the following equation [9]:

$$Nu = \frac{U_h D_2}{K_w} = CRe^m Pr^n K_R \qquad (5.33)$$

where Re and Pr are the Reynold number and Prandtl numbers. respectively; and D_2 is the outer diameter of the tube.

For laminar flow and a long tube, $m = n = 0, K_R = 1$, and $C = 3.66$. On substituting the values, one gets

$$U_h = 3.66 K_w / D_2 \qquad (5.34)$$

Similarly,

$$U_c = 3.66 K_w / D_1 \qquad (5.35)$$

where D_1 is the inner diameter of the tube as shown in Fig. 5.15.

The overall heat conductance, U_k, can be evaluated from the following equation, $D = 2r$
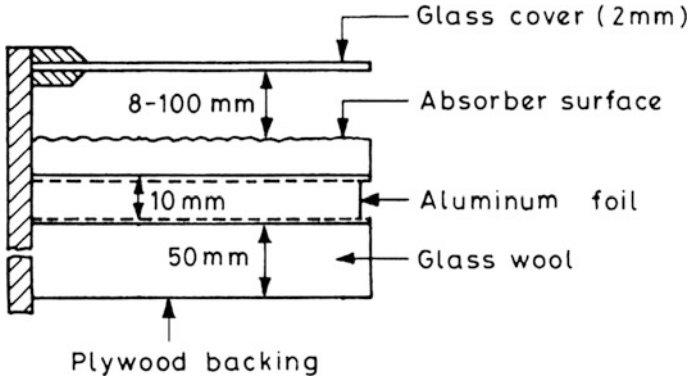
Fig. 5.15 Cross-section of collector assembly

$$\frac{1}{U_k} = \frac{1}{\frac{D_1}{D_2}(U_h)} + \frac{1}{U_c} + \frac{1}{\frac{2K_s}{D_2 \ln(D_2/D_1)}} \tag{5.36}$$

By assuming $D_2 \approx D_1$, the above equation becomes

$$\frac{1}{U_k} = \frac{1}{U_h} + \frac{1}{U_c} \tag{5.37}$$

If h_f is the heat-transfer coefficient per unit length of tube of length L_0, then h_f can be written as follows:

$$h_f = U_k/L_0 \tag{5.38}$$

5.5 Optimization of Heat Losses

There is approximately 33–50 % heat loss in most commercial FPCs, such as

  (i) 22–30 % convective losses and
 (ii) 5–7 % radiative loss.

These heat losses should be minimized to improve the collector's thermal efficiency. A highly reflective coating is used on the back surface of the FPC to minimize heat loss from the back surface. Furthermore, the bottom of the absorber plate is insulated with optimum-thickness glass wool, as shown in Fig. 5.15, to reduce losses from the bottom of the absorber plate, In the first step, radiation loss from the back surface of the absorber plate is minimized by the reflective coating. In the second step, loss is minimized due to the reflecting surface. From the front space of the absorbing plate, mainly convective and radiative losses take place. These two losses are minimized by (i) changing the spacing between the cover and the plate;

Fig. 5.16 Experimental setup in **a** normal configuration and **b** reverse configuration for flat-plate collector
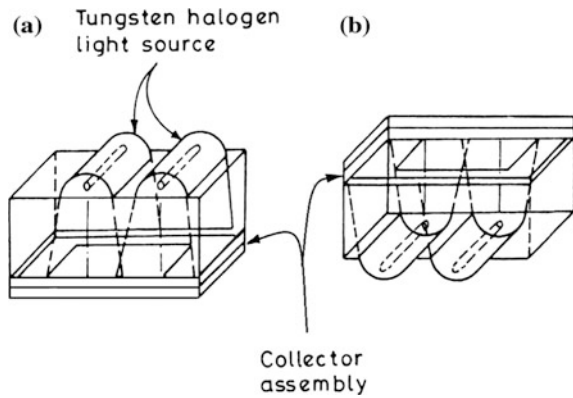
and (ii) using an absorbing surface with different emissivity. The optimum gap width is different for different absorbing surfaces. The convective thermal loss is further reduced to almost zero by illuminating the absorbing plate from below in the reverse flat-plate configuration. In this configuration, the hot air sticks to the plate due to a favourable density gradient; hence, convection losses are avoided.

A comparative study of the losses (i) from normal and (ii) from the reverse flat-plate absorber was performed by Madhusudan et al. [10]. In their study, the absorber plate was kept in a leak-proof cell (Fig. 5.16) uniformly illuminated by 1000-W cylindrical halogen lamps mounted in Phillips NV-51(2 × 15) reflectors. The illumination intensity on the absorber plate was measured using calibrated silicon solar cells. Various temperatures were recorded by a calibrated copper-constantan thermocouple and a multiple-strip chart recorder.

The theoretical and experimental values are compared (using black paint and cobalt oxide ($\alpha_s = 0.88, \varepsilon(100\,°C) = 0.15$) coating) in normal and reverse configurations of absorbing surfaces. The optimum gap width for the black-painted and the selective surface were ~ 2.5 and 5.0 cm, respectively, in normal and reverse configuration. No effect of radiation is observed on this gap width. The higher gap width shows equivalent or better performance in the case of selective surfaces. Smaller gaps are preferred to avoid shading of the absorber surface by the collector walls.

5.5.1 Transparent Insulating Material (Honeycomb)

When designing solar FPCs, the main objective is to reduce convective heat loss through the glass cover. Such studies of convection suppression have been performed by many researchers, particularly by Hollands [4], Buchberg et al. [5], Edwards [11], and Meyer et al. [12]. In their studies, the space between the top glass cover and the absorber plate is filled with a transparent/specularly reflecting honeycomb structure to reduce convective losses. In the absence of fluid motion, conduction and radiation will be the heat-transfer mechanism between the two plates.

Fig. 5.17 Hypothetical
selective surface with cut-off
wavelength at 3 μm
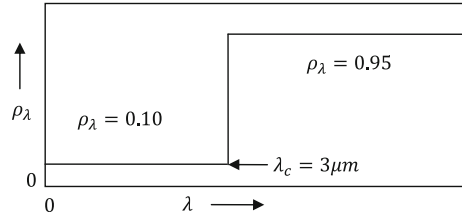
Inclusion of the honeycomb modifies the radiative characteristics of the solar FPC. The honeycomb structure reduces the amount of radiation reaching the absorber plate. The choice of the material for the honeycomb structure should be such that the material must be infrared-transparent or infrared–specularly reflecting. Specifically chosen materials do not affect the radiative characteristics of the solar FPC to a great extent. For infrared opaque material for the honeycomb structure, the radiative characteristics of solar FPC will be equivalent to a black body, which is undesirable.

5.5.2 Selective Surface

FPCs must have a high absorptance (α) for incident solar radiation. These collectors lose energy due to convection and radiation from the absorbing surface. For the reduction of radiation losses, an absorber surface with a lower value of long-wavelength emittance is desired. Both of the requirements, i.e., high absorbance and low long-wavelength emittance, can be achieved by choosing a selective absorber surface.

Figure 5.17 shows the variation of reflectance with wavelength for an ideal surface. The reflectance of this ideal surface is very low below a certain cut-off wavelength λ_c; however, for wavelengths greater than λ_c the reflectance is near unity, and emittance $(\epsilon_\lambda = \alpha_\lambda = 1 - \rho_\lambda)$ is low. The operating temperature of the solar FPC is low; hence, it emit at wavelengths greater than 3 μm.

5.6 Fin Efficiency

Figure 5.18 shows a dimension of one half- of one tube below the plate (absorber) configuration (Fig. 5.7). A bonding material has been used between the plate and the tube. The sheet above the bond is assumed to be at some local base temperature T_b. The distance between the centres of the two tubes is W, which is at the same as distance between centres of the two absorber sheets. Hence, the distance between the centres of the absorber sheet and the tube is $W/2$. If the outer and the inner-tube (riser) diameters are D and d, respectively, then solar radiation absorbed over
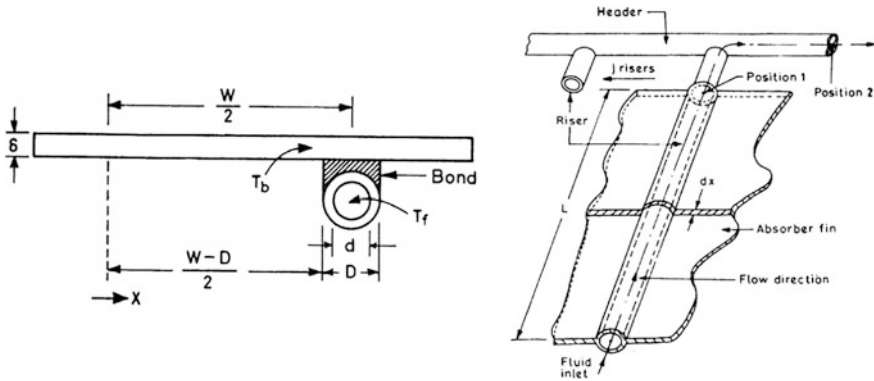
Fig. 5.18 Tube below plate (sheet) absorber: dimensions and configuration

$(W - D)/2$ length of absorber sheet will be performed toward the riser. The region between the centre line separating the tubes and the tube bond base can be considered as a fin problem. The absorber sheet has a thickness of δ. Because the sheet material is a good conductor, the temperature gradient through the thickness of sheet is negligible.

To see the effectiveness of a fin to transfer a given quantity of heat, a new parameter is defined, which is known as "**fin-efficiency factor**". It is expressed as follows:

$$\text{Fin efficiency}(F) = \frac{\text{Actual the rate of heat transferred to near bond}}{\text{Heat would have been transferred if entire fin area were at } T_b} \tag{5.39}$$

The fin, as shown in Fig. 5.18, is of the length $(W - D)/2$. An elemental region of width Δx and unit length in the flow direction is shown in Fig. 5.19.

Fig. 5.19 Energy flow on fin element
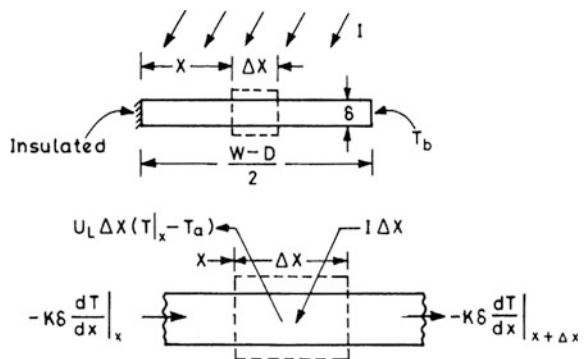
An energy balance on this element can be written as:

$$(\alpha\tau)I(t)\Delta x + U_L(T_a - T)\Delta x + \left\{-K\delta\frac{dT}{dX}\Big|_x\right\} - K\delta\frac{dT}{dX}\Big|_{x+\Delta x} = 0 \qquad (5.40)$$

where $I(t)$ is the absorbed solar energy. Dividing throughout by Δx and using the limit as $\Delta x \to 0$ yields:

$$\frac{d^2T}{dx^2} = \frac{U_L}{K\delta}\left(T - T_a - \frac{(\alpha\tau)I(t)}{U_L}\right) \qquad (5.41)$$

The two boundary conditions are required to solve the second-order differential equations. These are as follows:

$$\frac{dT}{dx}\Big|_{x=0} = 0 \quad \text{and} \quad T|_{x=(W-D)/2} = T_b \qquad (5.42)$$

If

$$m^2 = U_L/K\delta \quad \text{and} \quad \psi = T - T_a - [(\alpha\tau)I(t)]/U_L \qquad (5.43a)$$

Then

$$\frac{d^2\psi}{dx^2} = \frac{d^2T}{dx^2}; \frac{d\psi}{dx}\Big|_{x=0} = 0 \quad \text{and} \quad \psi|_{x=(W-D)/2} = T_b - T_a - \frac{(\alpha\tau)I(t)}{U_L} \qquad (5.43b)$$

With help of Eqs. (5.43a) and (5.43b), Eq. (5.41) becomes,

$$\frac{d^2\psi}{dx^2} - m^2\psi = 0 \qquad (5.44)$$

The general solution of the above equation can be given as:

$$\psi = C_1 \sinh mx + C_2 \cosh mx \qquad (5.45)$$

Now

$$\frac{d\psi}{dx}\Big|_{x=0} = mC_1 \cosh(m \times 0) + mC_2 \sinh(m \times 0) = 0 \Rightarrow C_1 = 0$$

Constants C_2 can be determined with the boundary conditions given by Eq. (5.43b) as follows:

$$T_b - T_a - \frac{(\alpha\tau)I(t)}{U_L} = C_2 \cosh m\frac{W-D}{2} \Rightarrow C_2 = \frac{T_b - T_a - \frac{(\alpha\tau)I(t)}{U_L}}{\cosh m\frac{W-D}{2}}$$

Now

$$\psi = \frac{T_b - T_a - \frac{(\alpha\tau)I(t)}{U_L}}{\cosh m\frac{W-D}{2}} \cosh mx;$$

thus,

$$\frac{T - T_a - [(\alpha\tau)I(t)]/U_L}{T_b - T_a - [(\alpha\tau)I(t)]/U_L} = \frac{\cosh mx}{\cosh m(W-D)/2} \qquad (5.46a)$$

or

$$T = \left(\frac{(\alpha\tau)I(t)}{U_L} + T_a\right) - \left[\frac{(\alpha\tau)I(t)}{U_L} - (T_b - T_a)\right]\frac{\cosh mx}{\cosh m(W-D)/2} \qquad (5.46b)$$

The energy conducted to the region of the tube per unit of length in the flow direction can be found by evaluating Fourier's law at the fin base.

$$\dot{q}_{\text{fin}} = -K\delta \frac{dT}{dx}\Big|_{x=(W-D)/2} = -K\delta\left[-\frac{1}{U_L}m\{(\alpha\tau)I(t) - U_L(T_b - T_a)\}\frac{\sinh\frac{m(W-D)}{2}}{\cosh\frac{m(W-D)}{2}}\right]$$

or

$$\dot{q}_{\text{fin}} = m\frac{K\delta}{U_L}[(\alpha\tau)I(t) - U_L(T_b - T_a)]\tanh\frac{m(W-D)}{2}$$

The above equation accounts for the energy collected on only one side of a tube; for both sides, the energy collection is

$$\dot{q}_{\text{fin}} = 2 \times m\frac{K\delta}{U_L}[(\alpha\tau)I(t) - U_L(T_b - T_a)]\tanh\frac{m(W-D)}{2} \qquad (5.47)$$

Equation (5.47) is the rate of heat conducted toward the tube by conduction due to fin per unit length can be written as

$$\dot{q}_{\text{fin}} = F(W-D)[(\alpha\tau)I(t) - U_L(T_b - T_a)] \qquad (5.48a)$$

where

$$F = \frac{\tanh m(W-D)/2}{m(W-D)/2} \quad \text{and} \quad m^2 = \frac{U_L}{K\delta} \qquad (5.48b)$$

The rate of heat conducted toward the tube by conduction due to the fin for length L_r can be written as

$$\dot{Q}_{\text{fin}} = F(W - D) \times L_r \times [(\alpha\tau)I(t) - U_L(T_b - T_a)] \tag{5.49}$$

5.7   Analysis of Flat-Plate Collectors

5.7.1   Basic Energy-Balance Equation

The rate of useful energy output of a FPC with area A_c is the difference between the rate of absorbed solar radiation, $\dot{q}_{ab}$ and the rate of thermal loss. It is given by:

$$\dot{Q}_u = A_c\dot{q}_u = A_c\left[\dot{q}_{ab} - U_L\left(T_p - T_a\right)\right] \tag{5.50a}$$

where

$$\dot{q}_{ab} = (\alpha\tau)I(t)$$

The instantaneous thermal efficiency η_i is given as:

$$\eta_i = \frac{\dot{Q}_u}{A_c I(t)} = \frac{\dot{q}_{ab}}{I(t)} - \frac{U_L\left(T_p - T_a\right)}{I(t)} = \alpha\tau - U_L\frac{\left(T_p - T_a\right)}{I(t)} \tag{5.50b}$$

where $I(t)$ is the incident solar radiation; τ and α are the transmissivity and absorptivity of the absorber, respectively. The expression for the overall heat-loss coefficient U_L is given in Sect. 5.4.

The overall collection of thermal efficiency is defined as the ratio of the useful gain to the incident solar energy over the same period of time. It is given by:

$$\eta_c = \frac{\int \dot{Q}_u \mathrm{d}t}{A_c \int I(t)\mathrm{d}t} \tag{5.51}$$

5.7.2   Effective Transmittance—Absorptance Product $(\tau\alpha)_e$

The value of $(\tau\alpha)_e$ is generally only 1–2 % greater than $(\tau\alpha)$. The equivalent transmittance—absorptance product can be approximated by Duffie and Beckman [3] as follows:

$$(\tau\alpha)_e = 1.02(\tau\alpha) \tag{5.52a}$$

Fig. 5.20 Variation of $(\tau\alpha)/(\tau\alpha)_n$ curves for different covers
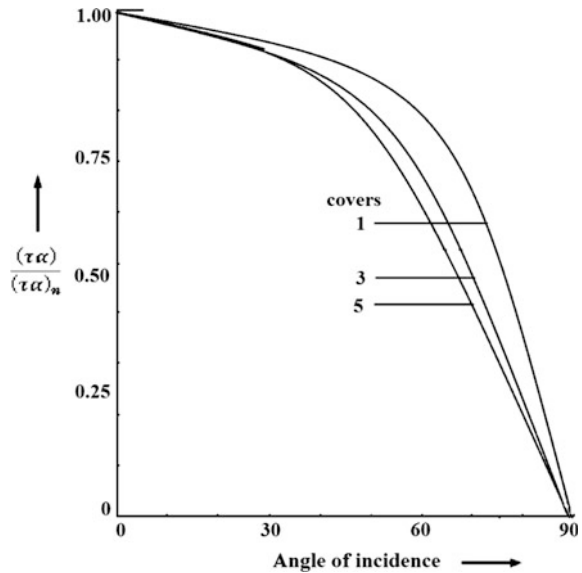
For a FPC with low-iron glass, $(\tau\alpha)_e$ and $(\tau\alpha)$ are nearly the same, i.e.,

$$(\tau\alpha)_e = 1.01(\tau\alpha) \tag{5.52b}$$

Klein [13] developed a relationship between $(\tau\alpha)/(\tau\alpha)_n$ and, θ where $(\tau\alpha)_n$ is the value of $(\tau\alpha)$ at normal incidence, to determine $(\tau\alpha)$ as a function of the incidence angle. The variation of $(\tau\alpha)/(\tau\alpha)_n$ with the incidence angle is shown in Fig. 5.20.

5.7.3 Flat-Plate Collector Efficiency Factor F'

The flat plate collector–efficiency factor F' is defined as the ratio of the actual rate of useful heat collection $(\dot{Q}_u)$ to the rate of useful heat collection when the collector's absorbing plate (T_p) is at the local fluid temperature (T_f), Eq. (5.11b). It is expressed as follows:

$$F' = \frac{\dot{Q}_u}{\dot{Q}_u\big|_{T_p=T_f}} = \frac{\dot{Q}_u}{A_c[\dot{q}_{ab} - U_L(T_f - T_a)]} \tag{5.53}$$

$$\dot{Q}_u = F'A_c[\dot{q}_{ab} - U_L(T_f - T_a)] \tag{5.54}$$

Fig. 5.21 a Schematic
representation of section
through typical finned tube.
b Thermal-circuit diagram of
FPC from bond to fluid
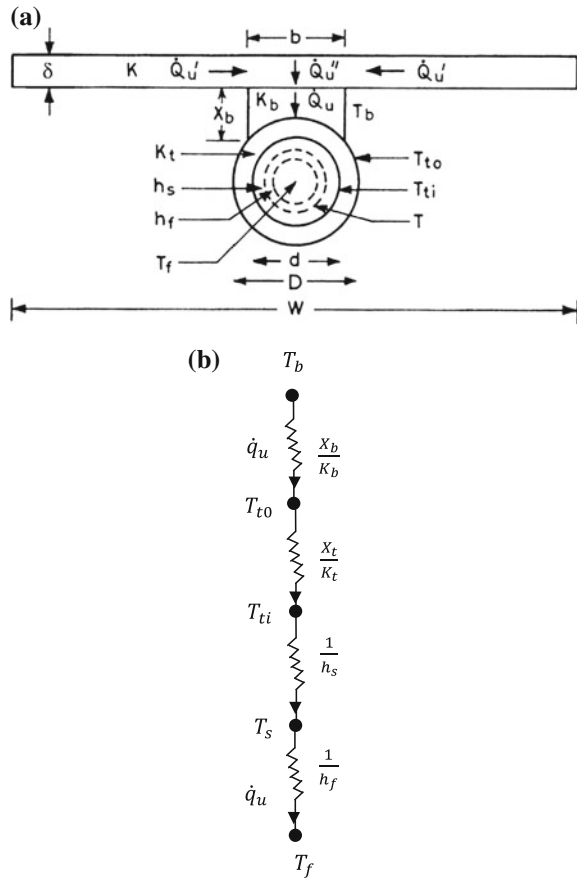
The following assumptions (Fig. 5.21a) are made to determine F' [7]:

(i)   the incident solar radiation is absorbed only by the absorber plate;
(ii) the bottom surface of the absorber plate and tubes are perfectly insulated;
(iii) the heat loss occurs only from the top surface of the plate;
(iv) the tubes are brazed onto the plate as shown in Fig. 5.21;
(v)   the bond has thermal conductivity K_b, which also accounts for the effects of a
      poor joint; and
(vi) the thermal inertia effects can be neglected under steady-state conditions.

According to Eq. (5.49), the rate of heat transfer from the base of the fin (T_b) to
the tube is written as:

$$\dot{Q}_u = (W - b) \times L_r \times F \times [(\alpha\tau)I(t) - U_L(T_b - T_a)] \tag{5.55}$$

where the fin-efficiency factor F (Eq. 5.48b) is given as follows:

$$F = \frac{\tanh m(W-D)/2}{m(W-D)/2} \quad \text{and} \quad m^2 = U_L/K\delta \tag{5.56}$$

where W is the tube pitch (m); b is the bond breadth (m); and L_r is the length of tube, which is also known as a "riser" (m).

The rate of heat transfer from the portion of the fin immediately above the tube bond, Eq. (5.50a), is given by:

$$\dot{Q}_u'' = bL_r[\dot{q}_{ab} - U_L(T_b - T_a)] \tag{5.57}$$

Here A_c is equivalent to $b \times L_r$.

The total rate of heat transfer from the absorber plate to the fluid in the tube can be written by summing Eqs. (5.55) and (5.57) as follows:

$$\dot{Q}_u = \dot{Q}_u' + \dot{Q}_u' = L_r[(W-b)F + b][\dot{q}_{ab} - U_L(T_b - T_a)] \tag{5.58a}$$

or

$$\dot{Q}_u = L_r[(W-b)F + b]U_L \times [(\dot{q}_{ab}/U_L) - (T_b - T_a)]$$

or

$$\dot{Q}_u = r_f'^{-1}[(\dot{q}_{ab}/U_L) - (T_b - T_a)] \tag{5.58b}$$

$$\dot{Q}_u r_f' = [(\dot{q}_{ab}/U_L) - (T_b - T_a)] \tag{5.58c}$$

where

$$r_f' = \{L_r[(W-b)F + b]U_L\}^{-1}$$

Under steady-state conduction and using Fourier's law of simple heat-conduction theory, the rate of heat transfer in W at different junction, Fig. 5.21b, is given by

$$\dot{Q}_{ub} = (T_b - T_{t0})bL_r(K_b/X_b) = (T_b - T_{t0})/r_b \text{ across flat bond}$$

or

$$\dot{Q}_{ub}r_b = (T_b - T_{t0}) \tag{5.59a}$$

$$\dot{Q}_{ut} = (T_{t0} - T_{ti})\pi A_{mw}L_r(K_t/X_t) = (T_{t0} - T_{ti})/r_t \text{ across tube wall}$$

or

$$\dot{Q}_{ut}r_t = (T_{t0} - T_{ti}) \qquad (5.59b)$$

$$\dot{Q}_{us} = (T_{ti} - T_s)\pi d_i L_r h_s = (T_{ti} - T_s)/r_s \text{ across scale}$$

or

$$\dot{Q}_{us}r_s = (T_{ti} - T_s) \qquad (5.59c)$$

$$\dot{Q}_{uf} = (T_s - T_f)\pi d_i L_r h_f = (T_s - T_f)/r_f \text{ across film}$$

or

$$\dot{Q}_{uf}r_f = (T_s - T_f) \qquad (5.59d)$$

The mean wall area A_{mw} is given by:

$$A_{mw} = \frac{D - d}{\ln(D/d)} \qquad (5.59e)$$

where T, K, X, D, d, r, and h are temperature, thermal conductivity, thickness, outer and inner diameter of riser, thermal resistance, and heat-transfer coefficient, respectively.

After adding Eqs. (5.58c) and (5.59a–5.59d), one obtains:

$$\dot{Q}_u\left(r_f' + r_b + r_t + r_s + r_f\right) = \frac{\dot{q}_{ab}}{U_L} - (T_f - T_a) \qquad (5.60)$$

The above equation can be rearranged as:

$$\dot{Q}_u = WL_r F'[\dot{q}_{ab} - U_L(T_f - T_a)] \qquad (5.61)$$

where F' is called the "collector-efficiency factor," which is given by

$$F' = \left\{U_L WL_r\left(r_f' + r_b + r_t + r_s + r_f\right)\right\}^{-1}$$

or

$$F' = \frac{1/U_L}{W\left[\frac{1}{U[(W-b)F+b]} + \frac{1}{(bK_b/X_b)} + \frac{1}{\pi A_{mw}K_t/X_t} + \frac{1}{\pi d h_s} + \frac{1}{\pi d h_f}\right]} \qquad (5.62)$$

Referring to Fig. 5.21b, it is clear that the denominator is the heat-transfer resistance from the fluid to the ambient air, given as $1/U_0$. The numerator is the heat-transfer resistance from the absorber plate to the ambient air.

Equation (5.62) can be further expressed as follows:

$$F' = \frac{1/U_L}{1/U_0} = \frac{U_0}{U_L} \tag{5.63}$$

If there is 'n' riser in one FPC, then Eq. (5.61) becomes:

$$\dot{Q}_u = nWL_rF'[\dot{q}_{ab} - U_L(T_f - T_a)]$$

Or

$$\dot{Q}_u = A_cF'[\dot{q}_{ab} - U_L(T_f - T_a)] \tag{5.64}$$

Equation (5.64) is the exactly same as Eq. (5.54).

The expression for instantaneous thermal efficiency (η_i) can be written as:

$$\eta_i = \frac{\dot{Q}_u}{A_cI(t)} = F'\left[\frac{\dot{q}_{ab}}{I(t)} - \frac{U_L(T_f - T_a)}{I(t)}\right] \tag{5.65}$$

or

$$\eta_i = F'\left[(\alpha\tau) - U_L\frac{(T_f - T_a)}{I(t)}\right] \tag{5.66}$$

The collector-efficiency factor, F', is essentially a constant for any collector design and fluid-flow rate. F' decreases with an increase in the centre-to-centre distance of the tube and increases with an increase in the material thickness and thermal conductivity. An increase in the overall loss coefficient decreases F', whereas an increase in the fluid-to-tube heat-transfer coefficient increases it. F' and F for some other configurations of collectors are shown in Fig. 5.22.

Example 5.4 A FPC has an aluminium absorber plate $(K_p = 211\,W/m\,°C)$ of thickness 0.35 mm and an area of 1.5 m^2, and it has two riser tubes each of diameter 0.025 m. The length of the tubes being 1 m, they determine the collector-efficiency factor F' for this collector if the convective heat-transfer coefficient from the inner-tube surface to the water is 50,100, and 500 W/m^2 °C. The overall loss coefficient is 7.2 W/m^2 °C.

Solution

The width of the spacing between the two riser tubes is calculated as follows:

$$W = (1.5 - 0.025 \times 10)/(10+1) = 0.114\,m$$

(a) $U_L = U_t + U_b$

$$F' = \cfrac{1}{\frac{WU_L}{\pi D_h} + \frac{WU_L}{C_{bond}} + \frac{W}{D+(W-D)F}}$$

$$F = \frac{\tanh[m(W-D)]/2}{[m(W-D)]/2}$$

$$m^2 = U_L/K\delta$$

$$U_L = U_t + U_b$$
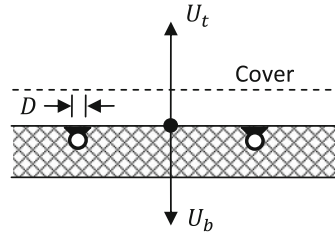
(b) $$F' = \cfrac{1}{\frac{WU_L}{\pi D_h} + \cfrac{1}{\frac{D}{W} + \cfrac{1}{\left(WU_L/C_{bond}\right)} + \frac{W}{(W-D)F}}}$$

$$F = \frac{\tanh[m(W-D)]/2}{[m(W-D)]/2}$$

$$m^2 = U_L/K\delta$$
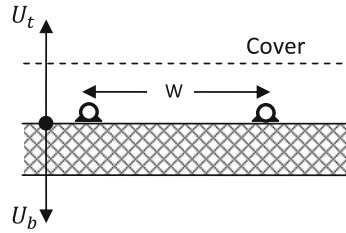
(c) $U_L = U_t + U_b$

$$F' = \cfrac{1}{\frac{WU_L}{\pi D_h} + \frac{W}{D+(W-D)F}}$$

$$F = \frac{\tanh[m(W-D)]/2}{[m(W-D)]/2}$$

$$m^2 = U_L/K\delta$$
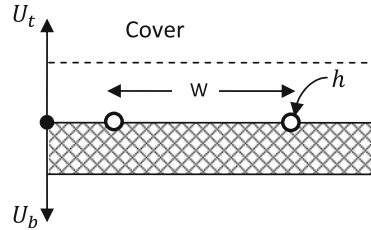
Fig. 5.22 Values of F' and F for various configurations of collector

The numerical value of m and the fin-efficiency factor F' can be obtained from Eq. (5.56) as follows:

$$m = \left(\frac{7.2}{211 \times 0.35 \times 10^{-3}}\right)^{1/2} = 9.87$$

and

$$F = \frac{\tanh[9.87 \times (0.114 - 0.025)/2]}{9.87 \times (0.114 - 0.025)/2} = \frac{\tanh 0.439}{0.439} = 0.9385$$

The collector-efficiency factor F' (Eq. (5.62)) for $h = 50\,\text{W/m}^2\,{}^\circ\text{C}$ is

$$F' = \frac{1}{\frac{0.114 \times 7.2}{3.14 \times 0.025 \times 50} + \frac{0.114}{0.025 + (0.114 - 0.025) \times 0.9385}} = 0.794$$

Similarly, for $h = 100\,\text{W/m}^2\,{}^\circ\text{C}$, $F' = 0.866$; for $h = 50\,\text{W/m}^2\,{}^\circ\text{C}$, $F' = 0.934$; and for $h = 1000\,\text{W/m}^2\,{}^\circ\text{C}$, $F' = 0.943$.

Example 5.5 Calculate the fin-efficiency factor and the collector-efficiency factor for the data given below:

Tube spacing $W = 100$ mm; tube diameter (inside) $d_i = 8$ mm; plate thickness $\delta = 0.45$ mm; plate thermal conductivity $K = 385\,\text{W/m}^2\,{}^\circ\text{C}$; and heat-transfer coefficient inside tubes $h = 300\,\text{W/m}^2\,{}^\circ\text{C}$. What will be the effect of the overall heat-transfer coefficient on F'?

Solution
For $U_\text{L} = 2\,\text{W/m}^2\,{}^\circ\text{C}$

From Eq. (5.56), one can obtain the value of m and F as follows:

$$m = \left(\frac{2}{385 \times 4.5 \times 10^{-4}}\right)^{1/2} = 3.40$$

and

$$F = \frac{\tanh[3.40 \times (0.10 - 0.008)/2]}{3.40 \times (0.10 - 0.008)/2} = 0.99$$

Furthermore, F' is given by Eq. (5.62). The value of F' comes out to be

$$F' = \frac{1/2}{0.10 \times \left[\frac{1}{2[(0.10 - 0.008) \times 0.99 + 0.008]} + \frac{1}{3.14 \times 0.008 \times 300}\right]} = 0.965$$

Similarly, for $U_\text{L} = 4\,\text{W/m}^2\,{}^\circ\text{C}$ $F' = 0.94$ and for $U_\text{L} = 8\,\text{W/m}^2\,{}^\circ\text{C}$ $F' = 0.893$.
Hence, we can see that increasing the overall loss coefficient (U_L) decreases the collector-efficiency factor F'.

5.7.4 Temperature Distribution in Flow Direction

The rate of net useful heat gain per unit length in W/m $(L_r = 1\,\text{m})$ available to the moving working fluid for one riser $(n = 1)$, Eq. (5.65), is given by:

$$\dot{q}'_u = WF'[\dot{q}_{ab} - U_L(T_f - T_a)] \tag{5.67}$$

The energy balance on the flowing fluid along x-direction (Fig. 5.23) through a single tube of length Δx can be written as follows:

$$\dot{q}'_u \Delta x = \frac{\dot{m}_f}{n} C_f T_f \big|_{x+\Delta x} - \frac{\dot{m}_f}{n} C_f T_f \big|_x = \frac{\dot{m}_f}{n} C_f \frac{dT_f}{dx} dx \tag{5.68}$$

where $\dot{m}_f$ is the total collector flow rate; n is the number of riser tubes; and C_f is the specific heat of the fluid. Substituting the value of $\dot{q}'_u$ from Eq. (5.68) into Eq. (5.69), one has the following equation:

$$\dot{m}_f C_f \frac{dT_f}{dx} - nWF'[\dot{q}_{ab} - U_L(T_f - T_a)] = 0 \tag{5.69}$$

Assuming F' and U_L to be constant during the operating temperature, the solution of Eq. (5.69) with the boundary condition $T_f = T_{fi}$ at $x = 0$ is given by

$$\frac{T_f - T_a - (\dot{q}_{ab}/U_L)}{T_{fi} - T_a - (\dot{q}_{ab}/U_L)} = \exp\left[-\frac{U_L n WF' x}{\dot{m}_f C_f}\right] \tag{5.70}$$

The outlet-fluid temperatures, T_{fo} at $x = L_r$, can be obtained as follows:

$$T_{fo} = T_f \big|_{x=L_r} = \left[\left(\frac{\dot{q}_{ab}}{U_L}\right) + T_a\right] + \left[T_{fi} - T_a - \frac{\dot{q}_{ab}}{U_L}\right] \exp[-A_c U_L F'/(\dot{m}_f C_f)] \tag{5.71a}$$

where $A_c(= nWL_r)$ is the FPC area; and L_r is the length of the riser in the flow direction.
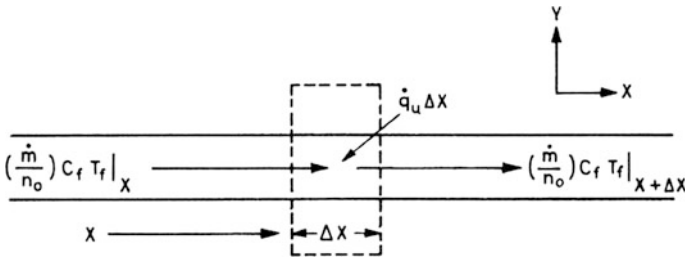
Fig. 5.23 Energy flow on water element

From Eq. (5.71a), one can also derive an expression for the rate of thermal energy available from one FPC as:

$$\dot{Q}_{\mathrm{u}} = \dot{m}_{\mathrm{f}}C_{\mathrm{f}}(T_{\mathrm{fo}} - T_{\mathrm{fi}}) = A_{\mathrm{c}}\frac{\dot{m}_{\mathrm{f}}C_{\mathrm{f}}}{A_{\mathrm{c}}U_{\mathrm{L}}}\left[1 - \exp\left(-\frac{A_{\mathrm{c}}U_{\mathrm{L}}F'}{\dot{m}_{\mathrm{f}}C_{\mathrm{f}}}\right)\right]\left[\dot{q}_{\mathrm{ab}} - U_{\mathrm{L}}(T_{\mathrm{fi}} - T_{\mathrm{a}})\right]$$

(5.71b)

5.7.5   Collector Heat-Removal Factor (F$_R$)

The **flat-plate heat removal factor ($F_{\mathbf{R}}$)** is defined as the ratio of the rate actual useful energy gain to the rate of useful energy gain if the entire collector were at the fluid-inlet temperature (T_{fi}) in a forced circulation mode. Mathematically it can be expressed as:

$$F_{\mathrm{R}} = \frac{\dot{Q}_{\mathrm{u}}}{A_{\mathrm{c}}[\dot{q}_{\mathrm{ab}} - U_{\mathrm{L}}(T_{\mathrm{fi}} - T_{\mathrm{a}})]}$$

(5.72a)

After substituting the expression for $\dot{Q}_{\mathrm{u}}$ from Eq. (5.71b) in the above equation, one gets an expression for F_{R} as:

$$F_{\mathrm{R}} = \frac{\dot{m}_{\mathrm{f}}C_{\mathrm{f}}(T_{\mathrm{fo}} - T_{\mathrm{fi}})}{A_{\mathrm{c}}[\dot{q}_{\mathrm{ab}} - U_{\mathrm{L}}(T_{\mathrm{fi}} - T_{\mathrm{a}})]}$$

(5.72b)

or

$$F_{\mathrm{R}} = \frac{\dot{m}_{\mathrm{f}}C_{\mathrm{f}}}{A_{\mathrm{c}}U_{\mathrm{L}}}\left[1 - \exp\left\{-\frac{F'A_{\mathrm{c}}U_{\mathrm{L}}}{\dot{m}_{\mathrm{f}}C_{\mathrm{f}}}\right\}\right]$$

(5.73)

Further, the flat-plate flow factor F'', in addition to F_{R}, can also be defined as follows:

$$F'' = \frac{F_{\mathrm{R}}}{F'} = \frac{\dot{m}_{\mathrm{f}}C_{\mathrm{f}}}{F'A_{\mathrm{c}}U_{\mathrm{L}}}\left[1 - \exp\left(-\frac{F'A_{\mathrm{c}}U_{\mathrm{L}}}{\dot{m}_{\mathrm{f}}C_{\mathrm{f}}}\right)\right]$$

(5.74)

The variation of the **flat plate collector–flow factor** (F'') with a **flow-rate factor** $\left[\frac{\dot{m}_{\mathrm{f}}C_{\mathrm{f}}}{F'A_{\mathrm{c}}U_{\mathrm{L}}}\right]$ is shown in Fig. 5.24. It is inferred that F'' becomes constant when the value of $\dot{m}_{\mathrm{f}}C_{\mathrm{f}}/F'A_{\mathrm{c}}U_{\mathrm{L}}$, the dimensionless collector capacitance rate, becomes >10.

From Eqs. (5.71b) and Eq. (5.72b), the rate of actual useful energy collected by fluid from the FPC is given by the following:

Fig. 5.24 Variation F'' with flow-rate factor, $\left[\frac{\dot{m}_f C_f}{NF'A_c U_L}\right]$
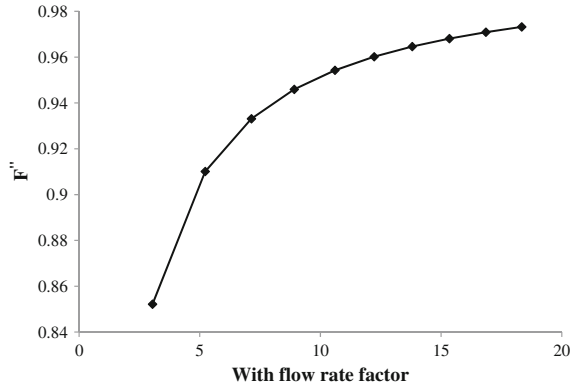
$$\dot{Q}_u = A_c F_R [\dot{q}_{ab} - U_L (T_{fi} - T_a)] \tag{5.75}$$

Example 5.6 Evaluate the net rate of useful energy per m^2 for the following parameters:

(i)   The overall heat loss coefficient $(U_L) = 6.0 \, \text{W/m}^2 \, ^\circ\text{C}$ and $F' = 0.8$ (Example 5.4)
(ii) $\dot{m}_f = 0.35 \, \text{kg/s}$ and $C_f = 4190 \, \text{J/kg} \, ^\circ\text{C}$
(iii) $I(t) = 500 \, \text{W/m}^2$ and $\alpha\tau = 0.8$
(iv) $T_{fi} = 60 \, ^\circ\text{C}$ and $T_a = 40 \, ^\circ\text{C}$

Solution
The heat-removal factor from Eq. (5.73) is calculated as follows:

$$F_R = \frac{0.35 \times 4190}{1 \times 6} \left[1 - \exp\left\{ -\frac{0.8 \times 1 \times 6}{0.35 \times 4190} \right\} \right] = 0.7986$$

The net rate of useful energy per m^2 can be calculated from Eq. (5.75) as

$$\dot{q}_u = 0.7986 \times [(0.8 \times 500) - 6 \times (60 - 40)] = 223.6 \, \text{W/m}^2$$

The factor F_R reduces the rate of useful energy gain from the expected value if the whole collector absorber plate has been at the fluid-inlet temperature. The temperature rise through the FPC decreases with an increase of the mass-flow rate. This results in fewer losses. Consequently, the actual rate of useful energy gain increases. The heat-removal factor, (F_R), can never become more than the FPC–efficiency factor, F'.

Another expression for F_R was derived by Hottel [14], Bliss [15], and Whiller [16] (HWB model), and it is given by

$$F_R = F'[1 - \exp(-N_0)]/N_0 \tag{5.76}$$

where $F' = (U_0/U_L)$ is the FPC–efficiency factor, Eq. (5.63), and $N_0 = A_c U_0/(\dot{m}_f C_f)$ is a dimensionless design parameter.

The analysis leading to Eq. (5.76) neglects the axial conduction in both the fluid and the absorber. In the case of the fluid, this assumption seems reasonable due to low conductivity of the fluids commonly used in FPCs. However, FPC absorber plates are of a good conducting material. Heat transfer due to axial conduction in the absorber plate is opposite to the heat transfer toward the fluid; hence, it decreases the fluid temperature and the overall thermal efficiency of the solar FPC. In some cases, the prediction made by the model of Hottel, Whiller, and Bliss (HWB) is as much as 30 % higher.

Taking the axial conduction of heat into consideration, Phillips [17] analytically derived an expression for F_R as follows:

$$F_R = F'[1 - \exp(-N_0)]/N_0 \quad \text{when } K = 0 \tag{5.77a}$$

and

$$F_R = \frac{F'[1 - \exp\{-N_0/1 - F'\}]}{N_0 + F'[1 - \exp\{N_0/1 - F'\}]} \quad \text{when } K = \infty \tag{5.77b}$$

For $N_0 = A_c U_0/(\dot{m}_f C_f) \sim \infty$, this implies a very small mass flow rate, Eqs. (5.77), which reduces to

$$F_R = F'/N_0 = \frac{F'\dot{m}_f C_f}{A_c U_0} \sim 0 \quad \text{(natural circulation mode of FPC)} \tag{5.78a}$$

and For $N_0 = 0$, this implies very large mass flow rate, Eqs. (5.77), which reduces to (Fig. 5.24)

$$F_R = F \quad \text{or} \quad \frac{F_R}{F'} \sim 1 \tag{5.78b}$$

Phillips has also developed an empirically expression for F_R over the full range of parameters N_0, F' and K as follows:

$$F_R = \frac{F'[1 - \exp\{-N_0/(1 - F'K')\}]}{N_0 + F'K'[1 - \exp\{-N_0/(1 - F'K')\}]} \tag{5.79}$$

where $K' = K/(K + 0.11)$

In the models by Hottel, Whiller, and Bliss (HWB), the error due to neglecting the axial conduction can be represented as a conduction error, and it is given as

$$\text{conduction error} = \frac{F''(N_0, 0) - F''(N_0, F', K')}{F''(N_0, F', K')} \tag{5.80}$$

where $F''(N_0, F', K') = F_R/F$.

The practical upper limit on the error for FPCs with $F'K' = 0.8$ that could result from neglecting axial conduction is approximately 22 %. For collectors having $F'K'$ products in the range of 0.1–0.5, the error is not more than 12 %.

From Eq. (5.75), an instantaneous thermal efficiency (η_i) of a FPC under forced mode can be defined as follows:

$$\eta_i = \frac{\dot{Q}_u}{A_c I(t)} = F_R \left[(\alpha\tau) - U_L \frac{T_{fi} - T_a}{I(t)} \right] \tag{5.81}$$

The variation of η_i with $(T_{fi} - T_a)/I(t)$ is shown in Fig. 5.12. Equation (5.81) is known as the Hottel-Whiller-Bliss (HWB) equation of a FPC. This is also known as the "characteristic equation of flat-plate collector."

5.7.6   Threshold Condition

The threshold radiation flux $(I_{th}(t))$ is the lowest amount solar radiation needed to allow the FPC to operate for thermal heating. The value of threshold radiation flux will be different for natural and forced modes as follows:

(a) **For natural mode:**
    From Eq. (5.64), one has

$$\dot{Q}_u = A_c F' [\dot{q}_{ab} - U_L (T_f - T_a)] \geq 0$$

This gives the expression for the threshold radiation flux $(I_{th}(t))$ as

$$I_{th}(t) = \frac{U_L (T_f - T_a)}{\alpha\tau} \tag{5.82a}$$

Here $\dot{q}_{ab} = \alpha\tau I(t)$.

(b) **For forced mode:**
    From Eq. (5.75), one has

$$\dot{Q}_u = A_c F_R [\dot{q}_{ab} - U_L (T_{fi} - T_a)] \geq 0$$

This gives the expression for the threshold radiation flux $(I_{th}(t))$ as

$$I_{th}(t) = \frac{U_L(T_{fi} - T_a)}{\alpha\tau} \qquad (5.82b)$$

Here also, $\dot{q}_{ab} = \alpha\tau I(t)$.

It is to be noted that $(T_f - T_a)$ in natural mode (Eq. 5.82a) will be higher than $(T_{fi} - T_a)$ for forced mode (Eq. 5.82b); hence, the threshold intensity in forced mode will have lower values. This means that the FPC will operate earlier under forced mode.

5.8 Combination of FPCs

A large bank of FPCs can be formed in the following ways:

(a) **Parallel connection**: In this case, the upper and lower headers of each FPC are connected to increase the volume of water to be heated. This makes a row and can be referred as "one module." The mass flow rate per FPC is the total mass flow rate divided by number of FPCs. The outlet-water temperature is the same at the outlet of each FPC. Such FPC modules can operate in natural as well as forced mode.

(b) **Series connection**: In this case, the outlet of one row of FPCs (the first module) is connected with the inlet to a second row of FPCs (second module) and so on. The mass-flow rates in such cases are the same for all rows. The outlet temperature depends on the number of rows of FPCs connected in series. Such series-connected FPC modules can only operate in forced mode.

(c) **Mixed-connection combination**: In this case, the first FPCs are connected in parallel for a given capacity of hot water to make one row (one module), and such modules formed are connected in series to increase the temperature per the requirement. This is generally referred to as "arrays." Here also the FPCs' arrays will only operate in forced mode.

5.8.1 M-FPC Connected in Parallel

Figure 5.25 show that m-FPCs are connected in parallel to from one module. As mentioned previously, the inlet and the outlet of each FPC are connected together. The mass-flow rate in each FPC will be $\dot{m}/m$ as shown in Fig. 5.25a. The rate of useful thermal energy of one FPC module will be expressed as follows:
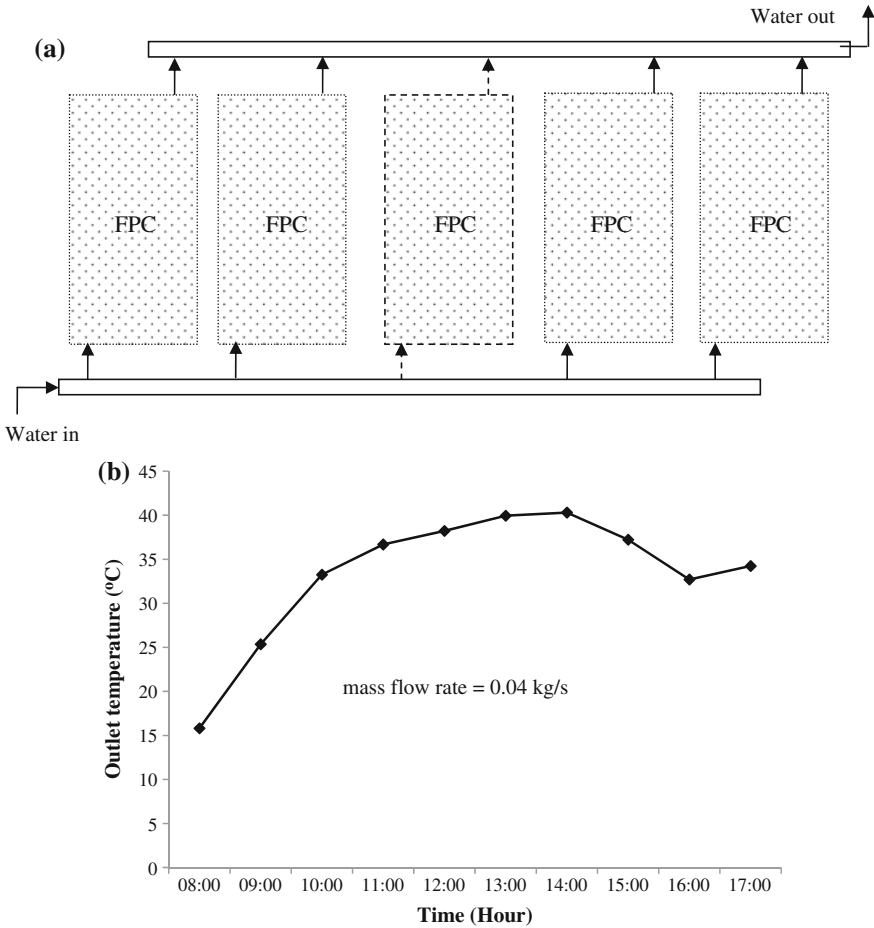
Fig. 5.25 **a** Flat-plate collectors connected in parallel makes one module. **b** Typical results for outlet temperature at different times of the day

(a)   Under natural mode

$$\dot{Q}_u = mA_c F'[\dot{q}_{ab} - U_L(T_f - T_a)] \tag{5.83a}$$

(b)   Under forced mode

$$\dot{Q}_u = A_{cm} F_{Rm}[\dot{q}_{ab} - U_{Lm}(T_{fi} - T_a)] \tag{5.83b}$$

where $A_{cm} = mA_c$ and $F_{Rm} = \frac{\dot{m}_f C_f}{A_{cm} U_{Lm}} \left[1 - \exp\left(-\frac{F' A_{cm} U_{Lm}}{\dot{m}_f C_f} \right) \right]$.

The combination of m-identical FPCs connected in parallel under forced mode are referred to as an "FPC module."

The outlet temperature in both cases will be same. The outlet temperature in forced mode can be evaluated from Eq. (5.71a). The typical results for $m = 12$ FPC (each 1.5 m^2) connected in parallel is shown in Fig. 5.25b. It is clear that the maximum temperature at the outlet depends on the magnitude of solar intensity. At 9 a.m., the outlet temperature is lowest due to low values of solar intensity. However, there is sharp increase in outlet temperature at 12 noon and 3 p.m., and then it starts decreasing due to heat losses. These results were recorded at IIT Delhi, New Delhi.

5.8.2 N-Collectors Connected in Series (Expression for T_{foN})

Equation (5.72a) can be rearranged for the outlet temperature from the first FPC as follows:

$$T_{fo1} = \left[\frac{\dot{q}_{ab}}{U_{L1}} + T_a\right] - \left[\frac{\dot{q}_{ab}}{U_{L1}} + T_a\right] \exp\left[-\frac{F_1' A_{c1} U_{L1}}{\dot{m}_f C_f}\right] + T_{fi} \exp\left[-\frac{F_1' A_{c1} U_{L1}}{\dot{m}_f C_f}\right]$$

(5.84)

For series-connected FPCs, the outlet temperature of a particular FPC will act as the inlet temperature for the next collector up to the Nth collector. Therefore, the outlet temperature from the Nth collector can be obtained in terms of inlet fluid temperature of the first collector.

Furthermore, according to Eq. (5.71a), the outlet fluid temperature of the second FPC collector T_{fo2} can be written in terms of the outlet temperature of the first FPC as follows:

$$T_{fo2} = \left[\frac{\dot{q}_{ab}}{U_{L2}} + T_a\right] - \left[\frac{\dot{q}_{ab}}{U_{L2}} + T_a\right] \exp\left[-\frac{F_2' A_{c2} U_{L2}}{\dot{m}_f C_f}\right] + T_{fi2} \exp\left[-\frac{F_2' A_{c2} U_{L2}}{\dot{m}_f C_f}\right]$$

(5.85)

where $T_{fi2} = T_{fo1}$ Eq. (5.85). After substituting T_{fo1} from Eq. (5.84) into Eq. (5.85), the expression for T_{fo2} becomes

$$\begin{aligned} T_{fo2} = &\left[\frac{\dot{q}_{ab}}{U_{L2}} + T_a\right]\left[1 - \exp\left\{-\frac{F_2' A_{c2} U_{L2}}{\dot{m}_f C_f}\right\}\right] \\ &+ \left[\frac{\dot{q}_{ab}}{U_{L1}} + T_a\right]\left[1 - \exp\left\{-\frac{F_1' A_{c1} U_{L1}}{\dot{m}_f C_f}\right\}\right]\exp\left\{-\frac{F_2' A_{c2} U_{L2}}{\dot{m}_f C_f}\right\} \\ &+ T_{fi1} \exp\left[-\frac{\left(F_1' A_{c1} U_{L1} + F_2' A_{c2} U_{L2}\right)}{\dot{m}_f C_f}\right] \end{aligned}$$

(5.86)

Similarly, the outlet fluid temperature for Nth collector can be given as:

$$
\begin{aligned}
T_{foN} = & \left[\frac{\dot{q}_{ab}}{U_{LN}} + T_a\right]\left[1 - \exp\left\{-\frac{F'_N A_{cN} U_{LN}}{\dot{m}_f C_f}\right\}\right] \\
& + \left[\frac{\dot{q}_{ab}}{U_{LN-1}} + T_a\right]\left[1 - \exp\left\{-\frac{F'_{N-1} A_{cN-1} U_{LN-1}}{\dot{m}_f C_f}\right\}\right] \\
& \times \exp\left\{-\frac{F'_N A_{cN} U_{LN}}{\dot{m}_f C_f}\right\} + \left[\frac{\dot{q}_{ab}}{U_{L1}} + T_a\right]\left[1 - \exp\left\{-\frac{F'_1 A_{c1} U_{L1}}{\dot{m}_f C_f}\right\}\right] \\
& \times \exp\left[-\frac{\left(F'_2 A_{c2} U_{L2} + \cdots + F'_N A_{cN} U_{LN}\right)}{\dot{m}_f C_f}\right] \\
& + T_{fi} \exp\left[-\frac{\left(F'_1 A_{c1} U_{L1} + \cdots + F'_N A_{cN} U_{LN}\right)}{\dot{m}_f C_f}\right]
\end{aligned}
\tag{5.87}
$$

If all of the FPCs are identical, then one has the following conditions:

$$
U_{L1} = U_{L2} = \cdots = U_{LN} = U_L
$$
$$
A_{c1} = A_{c2} = \cdots = A_{cN} = A_c
$$

and $F'_1 = F'_2 = \cdots = F'_N = F'$.

Then Eq. (5.87) reduces to:

$$
T_{foN} = \left[\frac{\dot{q}_{ab}}{U_L} + T_a\right]\left[1 - \exp\left\{-\frac{NF' A_c U_L}{\dot{m}_f C_f}\right\}\right] + T_{fi} \exp\left\{-\frac{NF' A_c U_L}{\dot{m}_f C_f}\right\}
\tag{5.88a}
$$

To obtain a constant outlet air temperature, i.e., $T_{foN} = T_0$ the mass flow rate of the fluid must be regulated for changing solar radiations and ambient temperature. After applying this condition in Eq. (5.88a), one can obtain an analytical expression for variable mass flow rate as

$$
\dot{m}_f = -\frac{NF' A_c U_L}{C_f}\left[\ln\frac{T_0 - \left(\frac{\dot{q}_{ab}}{U_L} + T_a\right)}{T_{fi} - \left(\frac{\dot{q}_{ab}}{U_L} + T_a\right)}\right]^{-1}
\tag{5.88b}
$$

For very large mass-flow rate, i.e., for $\dot{m} \sim \infty$, $\exp\left\{-\frac{NF' A_c U_L}{\dot{m}_f C_f}\right\} \sim 1$ and

$$
T_{foN} \approx T_{fi}
\tag{5.88c}
$$

Furthermore, the rate of thermal energy available at the outlet of the Nth FPC is obtained as

$$
\dot{Q}_{uN} = \dot{m}_f C_f (T_{foN} - T_{fi})
\tag{5.89a}
$$

or

$$\dot{Q}_{uN} = \frac{\dot{m}_f C_f}{U_L} \left[1 - \exp\left\{ -\frac{NF'A_c U_L}{\dot{m}_f C_f} \right\} \right] [\dot{q}_{ab} - U_L(T_{fi} - T_a)]$$

The above equation can also be rearranged as follows:

$$\dot{Q}_{uN} = NA_c \frac{\dot{m}_f C_f}{NA_c U_L} \left[1 - \exp\left\{ -\frac{NF'A_c U_L}{\dot{m}_f C_f} \right\} \right] [(\alpha\tau)I(t) - U_L(T_{fi} - T_a)]$$

or

$$\dot{Q}_{uN} = NA_c F_{RN}[(\alpha\tau)I(t) - U_L(T_{fi} - T_a)] \tag{5.89b}$$

where

$$F_{RN} = \frac{\dot{m}_f C_f}{NA_c U_L} \left[1 - \exp\left\{ -\frac{NF'A_c U_L}{\dot{m}_f C_f} \right\} \right]$$

The useful thermal energy increases with increasing flow rate factor and approaches a constant value for higher flow rate factor (Fig. 5.26). For large mass-flow rate, $T_{foN} = T_{fi}$ (Eq. 5.88a); then Eq. (5.89a) becomes

$$\dot{Q}_{uN} = 0 \tag{5.89c}$$

Fig. 5.26 Variation of $\dot{Q}_{uN}$ with flow-rate factor $\left(\frac{\dot{m}_f C_f}{NF'A_c U_L} \right)$ for a given $N = 5$
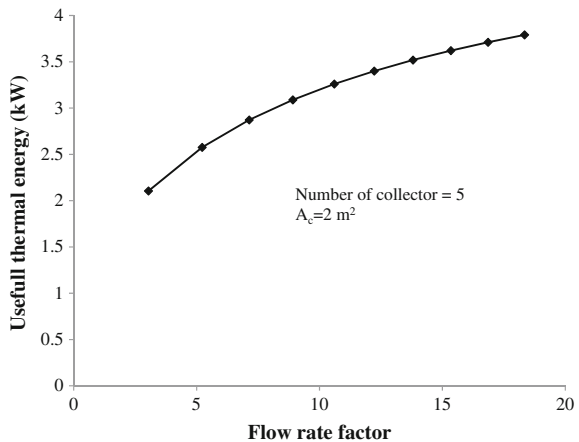
5.8.3 FPC Connected in Series and Parallel

Here it is important to mention the following:

(a) m-FPCs are connected in parallel under forced mode, which will be referred to as the "FPC module"; and
(b) N such modules are connected in series, which will be referred as FPC arrays as shown in Fig. 5.27.

For a two-FPC module, the rate of heat available in W can be written as follows:

$$\dot{Q}_{um1} = A_{m1}F_{Rm1}\left[(\alpha\tau)_1 I(t) - U_{Lm1}(T_{fim1} - T_a)\right] \tag{5.90a}$$

$$\dot{Q}_{um2} = A_{m2}F_{Rm2}\left[(\alpha\tau)_2 I(t) - U_{Lm2}(T_{fim2} - T_a)\right] \tag{5.90b}$$

where

$$F_{Rm1} = \frac{\dot{m}_f C_f}{A_{cm1}U_{Lm1}}\left[1 - \exp\left(\frac{F' A_{cm1} U_{Lm1}}{\dot{m}_{fC_f}}\right)\right] \tag{5.91a}$$

and

$$F_{Rm2} = \frac{\dot{m}_f C_f}{A_{cm2}U_{Lm2}}\left[1 - \exp\left(-\frac{F' A_{cm2} U_{Lm2}}{\dot{m}_f C_f}\right)\right] \tag{5.91b}$$

If a module with two sets of FPCs (each set having m collectors in parallel) are connected in series as shown in Fig. 5.27, the rate of useful heat output of the combination of two module is [from Eq. (5.90)]
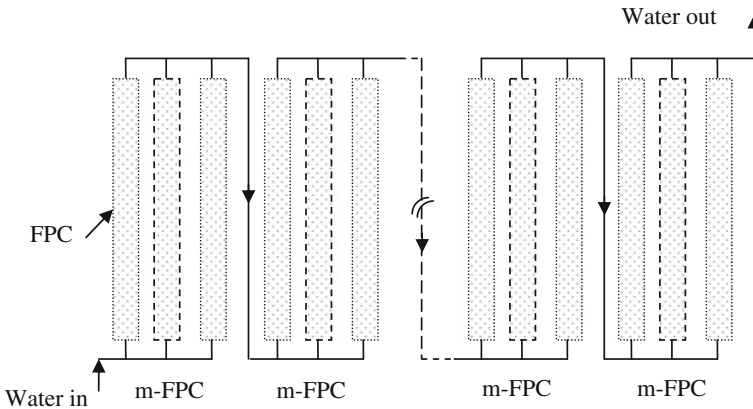
Fig. 5.27 N modules (m-FPC connected in parallel) connected in series (array)

$$\dot{Q}_{um1} + \dot{Q}_{um2} = A_{m1}F_{Rm1}\big[(\alpha\tau)_1 I(t) - U_{Lm1}(T_{fim1} - T_a)\big]$$
$$+ A_{m2}F_{Rm2}\big[(\alpha\tau)_2 I(t) - U_{Lm2}(T_{fim2} - T_a)\big] \tag{5.92}$$

A_{m1} and A_{m2} are the area of each set of collectors in the module, respectively; T_{fim1} is the inlet fluid temperature for the first set of collectors in the module; and T_{fom1} is the outlet temperature of the first set of collectors in the module, which is also the inlet temperature of the second set of collectors in the module $(T_{fom1} = T_{fim2})$.

Using Eq. (5.71b), one can obtain the outlet temperature of first set of collectors in the module as follows:

$$T_{fom1} = T_{fi} + \big[\dot{Q}_{um1}/\dot{m}_f C_f\big] \tag{5.93}$$

Substituting T_{fom1} from Eq. (5.93) for T_{fim2} into Eq. (5.92), the rate of useful heat output of the combination of the two sets of collectors in the module can be given as

$$\dot{Q}_{um1+2} = \big[A_{m1}F_{Rm1}(\alpha\tau)_1(1 - K_K) + A_{m2}F_{Rm2}(\alpha\tau)_2\big]I(t)$$
$$- \big[A_{m1}F_{Rm1}U_{Lm1}(1 - K_K) + A_{m2}F_{Rm2}U_{Lm2}\big](T_{fim1} - T_a) \tag{5.94}$$

where $K_K = (A_{m2}F_{Rm2}U_{Lm})/\dot{m}_f C_f$.

The form of Eq. (5.94) with the following values of, $F_{R2}(\alpha\tau)$, and $F_{R2}U_{L2}$ suggests that this series combination is equivalent to a single collector.

$$A = A_{m1} + A_{m2} \tag{5.95a}$$

and

$$F_{R2}(\alpha\tau) = \frac{A_{m1}F_{Rm1}(\alpha\tau)_1(1 - K_K) + A_{m2}F_{Rm2}(\alpha\tau)_2}{A} \tag{5.95b}$$

and

$$F_{R2}U_{L2} = \frac{A_{m1}F_{Rm1}U_{Lm1} + A_{m2}F_{Rm2}U_{Lm2}}{A} \tag{5.95c}$$

Then Eq. (5.94) becomes

$$\dot{Q}_{um2} = A\big[F_{R2}(\alpha\tau)_2 I(t) - F_{R2}U_{L2}(T_{fi} - T_a)\big] \tag{5.95d}$$

This procedure can be used to obtain the equivalent single collector for N-collectors connected in series.

If the two sets of collectors are identical, i.e., $A_{m1} = A_{m2} = A_{cm}$, then Eqs. (5.95d), (5.95b), and (5.95c) become

$$\dot{Q}_{\text{um2}} = 2A_{\text{cm}}\big[F_{\text{R2}}(\alpha\tau)_2 I(t) - F_{\text{R2}} U_{\text{L2}}(T_{\text{fi}} - T_{\text{a}})\big] \tag{5.96a}$$

$$F_{\text{R2}}(\alpha\tau) = F_{\text{Rm1}}(\alpha\tau)_1[1 - (K_{\text{K}}/2)] \tag{5.96b}$$

$$F_{\text{R2}} U_{\text{L2}} = F_{\text{Rm1}} U_{\text{Lm1}}[1 - (K_{\text{K}}/2)] \tag{5.96c}$$

For N-identical set of collectors in a module that are connected in series, the rate of useful thermal energy is given by

$$\dot{Q}_{\text{umN}} = NA_{\text{cm}}[F_{\text{RN}}(\alpha\tau)I(t) - F_{\text{RN}} U_{\text{LN}}(T_{\text{fi}} - T_{\text{a}})] \tag{5.97a}$$

where $F_{\text{RN}}(\alpha\tau)$ and $F_{\text{RN}} U_{\text{LN}}$ for N-identical set of collectors in a module that are connected in series are given by following, Oonk et al. [18], as

$$F_{\text{RN}}(\alpha\tau) = F_{\text{Rm1}}(\alpha\tau)_1\left[\frac{1 - (1 - K_{\text{K}})^N}{NK_{\text{K}}}\right] \tag{5.97b}$$

$$F_{\text{RN}} U_{\text{LN}} = F_{\text{Rm1}} U_{\text{Lm1}}\left[\frac{1 - (1 - K_{\text{K}})^N}{NK_{\text{K}}}\right] \tag{5.97c}$$

$$K_{\text{K}} = (A_{\text{m2}} F_{\text{Rm2}} U_{\text{Lm}})/\dot{m}_{\text{f}} C_{\text{f}} \tag{5.97d}$$

The cases of Eqs. (5.97a)–(5.97d) are as follows:

Case (i) for $N = 1$,

$$F_{\text{R1}}(\alpha\tau) = F_{\text{Rm1}}(\alpha\tau)_1\left[\frac{1 - (1 - K_{\text{K}})^N}{NK_{\text{K}}}\right] = F_{\text{Rm1}}(\alpha\tau)_1$$

$$F_{\text{R1}} U_{\text{L1}} = F_{\text{Rm1}} U_{\text{Lm1}}\left[\frac{1 - (1 - K_{\text{K}})^N}{NK_{\text{K}}}\right] = F_{\text{Rm1}} U_{\text{Lm1}}$$

$$K_{\text{K}} = (A_{\text{m2}} F_{\text{Rm2}} U_{\text{Lm}})/\dot{m}_{\text{f}} C_{\text{f}}$$

Equation (5.97a) with $A_{\text{m1}} = A_{\text{m2}} = mA_{\text{c}}$ reduces to

$$\dot{Q}_{\text{um}} = mA_{\text{c}} F_{\text{Rm1}}\big[(\alpha\tau)_1 I(t) - U_{\text{Lm1}}(T_{\text{fi}} - T_{\text{a}})\big] \tag{5.98}$$

where

$$F_{\text{Rm1}} = \frac{\dot{m}_{\text{f}} C_{\text{f}}}{mA_{\text{c}} U_{\text{Lm1}}}\left[1 - \exp\left\{-\frac{F' mA_{\text{c}} U_{\text{Lm1}}}{\dot{m} C_{\text{f}}}\right\}\right]$$

where 'm' is the number of FPC connected in parallel. For $m = 1$, Eq. (5.98) is same as Eq. (5.75).

Case (ii) for $N = 2$

$$\dot{Q}_{um2} = 2A_{cm}[F_{R2}(\alpha\tau)I(t) - F_{R2}U_{L2}(T_{fi} - T_a)] \qquad (5.99a)$$

$$F_{R2}(\alpha\tau) = F_{Rm1}(\alpha\tau)_1 \left[\frac{1 - (1 - K_K)^N}{NK_K}\right] = F_{Rm1}(\alpha\tau)_1[1 - (K_K/2)] \qquad (5.99b)$$

$$F_{R2}U_{L2} = F_{Rm1}U_{Lm1} \left[\frac{1 - (1 - K_K)^N}{NK_K}\right] = F_{Rm1}U_{Lm1}\left[1 - (K_{K/2})\right] \qquad (5.99c)$$

$$K_K = (A_{m2}F_{Rm2}U_{Lm})/\dot{m}_f C_f$$

These expressions are same as that of Eqs. (5.96a)–(5.96c).

Case (iii) For $K_K \ll 1$.

Because the specific heat of water, i.e., $C_f = 4190\,\text{J/kg}\,°\text{C}$ is very large, the value of K_K will be very small ($K_K \ll 1$); hence, the term

$$\frac{\left[1 - (1 - K_K)^N\right]}{NK_K} = \frac{[1 - (1 - NK_K)]}{NK_K} \sim 1 \qquad (5.100a)$$

and

$$F_{Rm1} = \frac{\dot{m}_f C_f}{A_{cm1}U_{Lm1}} \left[1 - \exp\left(-\frac{F'A_{cm1}U_{Lm1}}{\dot{m}_f C_f}\right)\right] = 0 \qquad (5.100b)$$

Then Eq. (5.97a) reduces to

$$\dot{Q}_{uN} = NA_{cm}F_{Rm}\left[(\alpha\tau)_1 I(t) - U_{Lm1}(T_{fi} - T_a)\right] = 0 \qquad (5.100c)$$

If N_0 such array is connected in parallel to increase the hot-water capacity, then the rate of heat available for the multiarray, Fig. 5.28, is given by

$$\dot{Q}_{uNN_0} = NN_0 A_{cm}F_{Rm}\left[(\alpha\tau)_1 I(t) - U_{Lm1}(T_{fi} - T_a)\right] \qquad (5.101)$$
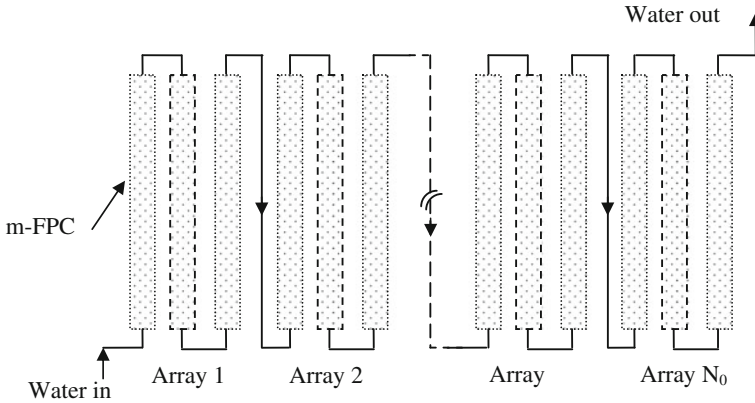
Fig. 5.28 N_0 arrays connected in series

5.9 Photovoltaic Thermal (PVT) Water Collector

5.9.1 Introduction

As discussed previously in Chap. 4, a photovoltaic thermal (PVT) water collector is a system that gives electrical as well as thermal energy with enhanced electrical power. Using this concept, a new PVT water collector is analysed in this section. PVT technology is the integration of a semitransparent PV module with a conventional solar water collector in a single unit. This can also be refesrred as the "hybrid PVT" concept. In this case, a semitransparent PV module converts a part (approximately 15–20 %) of incident solar radiation into electrical energy, whereas rest of the incident solar radiation (>80 %) is absorbed by PV module, and the absorber plate generates thermal energy. The thermal energy generated from the system is harnessed using water as the thermal energy carrier. Heating of the PV module lowers its electrical efficiency. Extraction of thermal energy from the system using water or air lowers the temperature, which in turn increases the efficiency of the system.

Conventional FPC require external source of electrical energy for operation in force mode. The electrical energy requirement is met from grid electricity, whereas in the PVT flat-plate water collector, the electrical energy needed for force-mode operation is supplied from the PV module of the integrated system.

The temperature profiles of the photovoltaic (PV) module under transient conditions was studied by Jones and Underwood [19]. They found that, corresponding to an ambient air temperature of 24.5 °C, the module temperature varies from 27 to 52 °C depending on the incident input solar radiation. They concluded that the electrical performance of the PV module is strongly affected by the (i) packing factor of module, (ii) ohmic losses, and (iii) module temperature. The electrical performance of a PVT FPC can be improved by increasing the packing factor and reducing the module temperature.

5.9.2 Partially Covered Photovoltaic Thermal (PVT) Water FPC [20, 21]

(a) **The lower portion of the FPC is partially covered by a semitransparent PV module**: In this case, the lower portion of the conventional FPC is replaced by the semitransparent PV module as shown in Fig. 5.29. The area covered by the semitransparent PV module is dependant on the desired requirement of electrical/thermal energy from the PVT system. The energy balance for different parts of the PVT-FPC is given as follows:

(i) **For solar cells of PV module (glass–glass):**

$$\alpha_c \tau_g \beta_c I(t) W\, dx = \left[U_{tc,a}(T_c - T_a) + U_{tc,p}(T_c - T_p) \right] W\, dx + \eta_c \tau_g \beta_c I(t) W dx$$

(5.102a)

where α_c is the absorptivity of the solar cell; τ_g is the transmissivity of the glass of the PV module; β_c is the packing factor of the module; $I(t)$ is the solar intensity; $W\, dx$ is the elementary section; η_c is the solar-cell electrical efficiency; $U_{tc,a}$ is the overall heat-transfer coefficient between the solar cell to ambient air through glass cover; $U_{tc,p}$ is the overall heat-transfer coefficient from the solar cell to the blackened absorber plate through the glass cover and air gap; T_c is the temperature of the solar cell; T_a is the ambient temperature; T_p is the temperature of the blackened absorber plate; and $\eta_m = \eta_c \tau_g \beta_c$ is the module efficiency.

Fig. 5.29 Lower portion of FPC is partially covered by semitransparent PV module
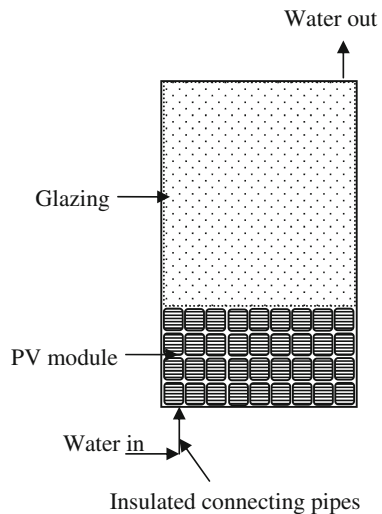
From Eq. (5.102a), the expression for the solar-cell temperature is given by

$$T_c = \frac{(\alpha\tau)_{1,\mathrm{eff}}I(t) + U_{\mathrm{tc,a}}T_a + U_{\mathrm{tc,p}}T_p}{U_{\mathrm{tc,a}} + h_{\mathrm{c,p}}} \tag{5.102b}$$

where $(\alpha\tau)_{1,\mathrm{eff}} = \tau_g(\alpha_c - \eta_c)\beta_c$

(ii) **For the blackened absorber plate temperature below the semitransparent PV module** (Fig. 5.29):

$$\alpha_p(1 - \beta_c)\tau_g^2 I(t)W\,dx + U_{\mathrm{tc,p}}(T_c - T_p)W\,dx$$
$$= F'h_{\mathrm{p,f}}(T_p - T_f)W\,dx + U_{\mathrm{tp,a}}(T_p - T_a) \tag{5.103}$$

where α_p is the absorptivity of the blackened plate; h_{pf} is the conductive heat-transfer coefficient from the absorber plate to the flowing fluid; and T_f is the temperature of the fluid.

From Eqs. (5.102) and (5.103), the expression for plate temperature (T_p) can be written as follows:

$$T_p = \frac{(\alpha\tau)_{2,\mathrm{eff}}I(t) + PF_1(\alpha\tau)_{1,\mathrm{eff}}I(t) + U_{L2}T_a + F'h_{\mathrm{p,f}}T_f}{U_{L2} + F'h_{\mathrm{p,f}}} \tag{5.104a}$$

where

$$(\alpha\tau)_{2,\mathrm{eff}} = \alpha_p(1 - \beta_c)\tau_g^2, \quad PF_1 = \frac{U_{\mathrm{tc,p}}}{U_{\mathrm{tc,a}} + U_{\mathrm{tc,p}}}$$

PF_1 can be referred as "penalty factor 1" for the absorber plate due to the semitransparent PV module; and U_{L1} is an overall heat-transfer coefficient from the blackened surface to the ambient air through the glass of the PV module. An expression for U_{L2} is given by

$$U_{L2} = U_{L1} + U_{\mathrm{tp,a}} \quad \text{and} \quad U_{L1} = \frac{U_{\mathrm{tc,p}}U_{\mathrm{tc,a}}}{(U_{\mathrm{tc,p}} + U_{\mathrm{tc,a}})} \tag{5.104b}$$

(iii) **For water flowing through an absorber pipe below the semitransparent PV module** (Fig. 5.29):

The flow pattern of water through the riser below the absorber is shown in Fig. 5.29.

The energy balance of flowing water through the riser (Fig. 5.29) is given by

$$\dot{m}_f C_f \frac{dT_f}{dx} dx = F' h_{p,f} (T_p - T_f) W dx \qquad (5.105)$$

where $\dot{m}_f$ is the mass of the fluid; C_f is the specific heat of the fluid; and F' is the collector-efficiency factor.

With the help of Eq. (5.104a), Eq. (5.105) can be rewritten as

$$\dot{m}_f C_f \frac{dT_f}{dx} dx = F' \left[PF_2 (\alpha\tau)_{m,eff} I(t) - U_{L,m} (T_f - T_a) \right] W dx \qquad (5.106a)$$

where $(\alpha\tau)_{m,eff} = PF_1 (\alpha\tau)_{1,eff} + (\alpha\tau)_{2,eff}, PF_2 = \frac{h_{p,f}}{U_{L2} + F' h_{p,f}}$, and PF_2 is the penalty factor 2 due to the absorber below the PV module; $(\alpha\tau)_{m,eff}$ is the effective absorptivity–transmissivity of the PV module; and $U_{L,m}$ is an overall heat-transfer coefficient from the fluid to the ambient air through the absorber and the PV module. An expression for $U_{L,m}$ is given by

$$U_{L,m} = \frac{U_{L2} h_{p,f}}{\left(U_{L2} + F' h_{p,f} \right)} \qquad (5.106b)$$

Integration of Eq. (5.106a) with initial conditions at $T_f|_{x=0} = T_{fi}$ and at $T_f|_{x=L} = T_{fo}$ gives,

$$\frac{T_{fo} - T_a - \left(\frac{PF_2 (\alpha\tau)_{m,eff} I(t)}{U_{L,m}} \right)}{T_{fi} - T_a - \left(\frac{PF_2 (\alpha\tau)_{m,eff} I(t)}{U_{L,m}} \right)} = \exp \left(-\frac{F' A_m U_{L,m}}{\dot{m}_f C_f} \right)$$

or

$$T_{fo} = \left[\frac{PF_2 (\alpha\tau)_{m,eff} I(t)}{U_{L,m}} + T_a \right] \left[1 - \exp \left(-\frac{F' A_m U_{L,m}}{\dot{m}_f C_f} \right) \right] + T_{fi} \exp \left(-\frac{F' A_m U_{L,m}}{\dot{m}_f C_f} \right) \qquad (5.107)$$

For $A_m = 0$, Eq. (5.107) reduces to $T_{fo} = T_{fi}$, which means that there is no semitransparent PV module.

The rate of thermal energy available at the end of the semitransparent PV module is given as

$$\dot{Q}_{u,m} = \dot{m}_f C_f (T_{fo} - T_{fi}) \qquad (5.108)$$

After substituting the expression for T_{fo} form Eq. (5.107) into Eq. (5.108), one gets

$$\dot{Q}_{u,m} = A_m F_{Rm} \left[PF_2 (\alpha\tau)_{m,eff} I(t) - U_{L,m}(T_{fi} - T_a) \right] \tag{5.109}$$

where,

$$A_m F_{Rm} = \frac{\dot{m}_f C_f}{U_{L,m}} \left[1 - \exp\left(-\frac{F' A_m U_{L,m}}{\dot{m}_f C_f} \right) \right]$$

or

$$F_{Rm} = \frac{\dot{m}_f C_f}{A_m U_{L,m}} \left[1 - \exp\left(-\frac{F' A_m U_{L,m}}{\dot{m}_f C_f} \right) \right] \tag{5.109a}$$

Here also for $A_m = 0$, Eq. (5.109) reduces to $\dot{Q}_{u,m} = A_m F_{Rm} = 0$, which means that there is no semitransparent PV module.

(iv) **The outlet water temperature at the end of the PVT water-first FPC:**

The expression of the outlet water temperature at the end of the collector can obtained according to a process [23] similar to that used with $T_{fi1} = T_{fo}$:

$$T_{fo1} = \left[\frac{(\alpha\tau)_{c1,eff} I(t)}{U_{L,c1}} + T_a \right] \left[1 - \exp\left(-\frac{F' A_{c1} U_{L,c1}}{\dot{m}_f C_f} \right) \right] + T_{fi1} \exp\left(-\frac{F' A_{c1} U_{L,c1}}{\dot{m}_f C_f} \right) \tag{5.110}$$

The rate of thermal energy available at the end of the conventional FPC with a glass–absorber combination can be written as follows:

$$\dot{Q}_c = \dot{m}_f C_f (T_{fo1} - T_{fi1}) = A_{c1} F_{Rc} \left[(\alpha\tau)_{c1,eff} I(t) - U_{L,c1}(T_{fi1} - T_a) \right] \tag{5.110a}$$

where the expression for F_{Rc} is given by

$$F_{Rc} = \frac{\dot{m}_f C_f}{A_{c1} U_{L,c1}} \left[1 - \exp\left(-\frac{F' A_{c1} U_{L,c1}}{\dot{m}_f C_f} \right) \right]$$

On substituting $T_{fi1} = T_{fo}$, one can have

$$
\begin{aligned}
T_{fo1} = {} & \left[\frac{(\alpha\tau)_{c1,eff} I(t)}{U_{L,c1}} + T_a \right] \left[1 - \exp\left(-\frac{F' A_{c1} U_{L,c1}}{\dot{m}_f C_f} \right) \right] \\
& + \left[\left[\frac{PF_2 (\alpha\tau)_{m,eff} I(t)}{U_{L,m}} + T_a \right] \left[1 - \exp\left(-\frac{F' A_m U_{L,m}}{\dot{m}_f C_f} \right) \right] \right. \\
& \left. + T_{fi} \exp\left(-\frac{F' A_m U_{L,m}}{\dot{m}_f C_f} \right) \right] \exp\left(-\frac{F' A_{c1} U_{L,c1}}{\dot{m}_f C_f} \right)
\end{aligned}
\tag{5.111}
$$

Equation (5.111) is discussed for the following cases:

Case (i): For $A_m = 0$ without a semitransparent PV module and $A_{c1} = A_c, (\alpha\tau)_{c1,\text{eff}} = (\alpha\tau), U_{Lc1} = U_L$ (only conventional FPC)

Equation (5.111) reduces to the following

$$T_{fo1} = \left[\frac{(\alpha\tau)I(t)}{U_L} + T_a\right]\left[1 - \exp\left(-\frac{F'A_cU_L}{\dot{m}_fC_f}\right)\right] + T_{fi}\exp\left(-\frac{F'A_cU_L}{\dot{m}_fC_f}\right) \quad (5.111a)$$

The above equation is exactly same as Eq. (5.72a) for a conventional FPC.

Case (ii): For $A_{c1} = 0$ without a conventional FPC, this means that the absorber is fully covered with a semitransparent PV module, and Eq. (5.111) reduces to the following:

$$T_{fo1} = \left[\frac{PF_2(\alpha\tau)_{m,\text{eff}}I(t)}{U_{L,m}} + T_a\right]\left[1 - \exp\left(-\frac{F'A_mU_{L,m}}{\dot{m}_fC_f}\right)\right] + T_{fi}\exp\left(-\frac{F'A_mU_{L,m}}{\dot{m}_fC_f}\right)$$
$$(5.111b)$$

The rate of thermal energy available from the PVT-FPC is given as

$$\dot{Q}_{u1} = \dot{m}_fC_f(T_{fo1} - T_{fi}) \quad (5.112)$$

The rate of thermal energy available from the semitransparent PVT-CPC can also be found by summing Eqs. (5.109) and (5.110a) as follows:

$$\dot{Q}_{u1} = \dot{Q}_{um} + \dot{Q}_{uc} = A_mF_{Rm}\left[PF_2(\alpha\tau)_{m,\text{eff}}I(t) - U_{L,m}(T_{fi} - T_a)\right]$$
$$+ A_{c1}F_{Rc}\left[(\alpha\tau)_{c1,\text{eff}}I(t) - U_{L,c1}(T_{fi1} - T_a)\right] \quad (5.113a)$$

Here from Eq. (5.109), we have

$$T_{fo} = T_{fi} + \frac{\dot{Q}_{um}}{\dot{m}_fC_f} \quad (5.113b)$$

On simplifying Eqs. (5.113a) and (5.113b), one can obtain

$$\dot{Q}_{u1} = \left[A_mF_{Rm}PF_2(\alpha\tau)_{m,\text{eff}}\left[1 - \frac{A_cF_{Rc}U_{L,c}}{\dot{m}_fC_f}\right] + A_{c1}F_{Rc}(\alpha\tau)_{c,\text{eff}}\right]I(t)$$
$$- \left[A_mF_{Rm}U_{L,m}\left[1 - \frac{A_cF_{Rc}U_{L,c}}{\dot{m}_fC_f}\right] + A_{c1}F_{Rc}U_{L,c}\right](T_{fi} - T_a) \quad (5.114)$$

Equation (5.114) can also be obtained by substituting Eq. (5.111) into Eq. (5.112).

Furthermore, Eq. (5.114) can be rewritten as

$$\dot{Q}_{u1} = (AF_R(\alpha\tau))_1 I(t) - (AF_R U_L)_1 (T_{fi} - T_a) \tag{5.115}$$

where

$$(AF_R(\alpha\tau))_1 = \left[A_m F_{Rm} PF_2(\alpha\tau)_{m,eff} \left[1 - \frac{A_c F_{Rc} U_{L,c}}{\dot{m}_f C_f} \right] + A_{c1} F_{Rc}(\alpha\tau)_{c,eff} \right]$$

and

$$(AF_R U_L)_1 = \left[A_m F_{Rm} U_{L,m} \left[1 - \frac{A_c F_{Rc} U_{L,c}}{\dot{m}_f C_f} \right] + A_{c1} F_{Rc} U_{L,c} \right]$$

An instantaneous efficiency can be obtained from the above equation as:

$$\eta_i = \frac{\dot{Q}_u}{I(t)}$$

or

$$\eta_i = (AF_R(\alpha\tau))_1 - (AF_R U_L)_1 \frac{T_{fi} - T_a}{I(t)} \tag{5.116}$$

Equation (5.116) is equivalent to the HWB equation of a conventional FPC (Eq. 5.81)

From Eq. (5.116), the gain factor and loss coefficient are given as

$$\text{Gain factor} = (AF_R(\alpha\tau))_1 \tag{5.117a}$$

and

$$\text{Loss coefficient} = (AF_R U_L)_1 \tag{5.117b}$$

(b) **Upper portion of the absorber is partially covered by the PV module**:

In this case, the upper portion of the conventional FPC is replaced by a semi-transparent PV module as shown in Fig. 5.30. The outlet water temperature at the end of the lower portion, i.e., at the start of the semitransparent PV module, is given as follows:

$$T_{fo} = \left[\frac{(\alpha\tau)_{c1,eff} I(t)}{U_{L,c1}} + T_a \right] \left[1 - \exp\left(-\frac{F' A_c U_{L,c1}}{\dot{m}_f C_f} \right) \right] + T_{fi} \exp\left(-\frac{F' A c U_{L,c1}}{\dot{m}_f C_f} \right) \tag{5.118}$$

Equation (5.118) is the same as Eq. (5.110).

Fig. 5.30 Upper portion of absorber is partially covered by PV module
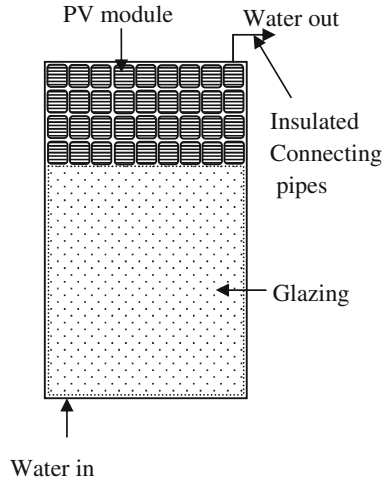
The rate of thermal energy available at the end of a conventional FPC with a glass–absorber combination (Lower portion of Fig. 5.30) can be written as

$$\dot{Q}_{c,1} = \dot{m}_f C_f (T_{fo} - T_{fi}) \tag{5.119}$$

The T_{fo} of the lower portion of the PVT FPC, as shown in Fig. 5.30, becomes the inlet to the PV module–absorber combination T_{fi}, i.e., the upper portion of the PVT FPC, as shown in Fig. 5.30.

Expression of the outlet of the water at the end of the upper portion of the PVT FPC, as shown in Fig. 5.30, is given by

$$T_{fo1} = \left[\frac{PF_2(\alpha\tau)_{m,eff} I(t)}{U_{L,m}} + T_a \right] \left[1 - \exp\left(-\frac{F' A_m U_{L,m}}{\dot{m}_f C_f} \right) \right] + T_{fi1} \exp\left(-\frac{F' A_m U_{L,m}}{\dot{m}_f C_f} \right) \tag{5.120}$$

The rate of thermal energy available at the end upper portion of Fig. 5.30 can be written as

$$\dot{Q}_{u,m} = \dot{m}_f C_f (T_{fo1} - T_{fi1}) \tag{5.121}$$

Here the T_{fi1} of Eq. (5.121) is equal to the T_{fo} of Eq. (5.118).

An expression for the rate of thermal energy available from the first PVT FPC is the sum of Eqs. (5.119) and (5.121), which can be written as follows:

$$\dot{Q}_{u,(c+m)} = \dot{Q}_{c,1} + \dot{Q}_{u,m} = \dot{m}_f C_f (T_{fo} - T_{fi}) + \dot{m}_f C_f (T_{fo1} - T_{fi1})$$

or

$$\dot{Q}_{u,(c+m)} = \dot{m}_f C_f (T_{fo1} - T_{fi}) \tag{5.122}$$

Here T_{fo1} is the outlet water temperature of the first PVT water FPC with a semitransparent PV module at the upper portion of the FPC, unlike the earlier PVT water collector.

According to Eqs. (5.113a)–(5.115), an expression for the total thermal energy available from the PV-integrated (upper side) FPC can be calculated as follows:

$$
\begin{aligned}
\dot{Q}_{u1} = {} & \left[A_c F_{Rc} (\alpha\tau)_{c,eff} \left[1 - \frac{A_m F_{Rm} U_{L,m}}{\dot{m}_f C_f} \right] + A_m F_{Rm} PF_2 (\alpha\tau)_{m,eff} \right] I(t) \\
& - \left[A_c F_{Rc} U_{L,c} \left[1 - \frac{A_m F_{Rm} U_{L,m}}{\dot{m}_f C_f} \right] + A_m F_{Rm} U_{L,m} \right] (T_{fi} - T_a)
\end{aligned}
\tag{5.123}
$$

Here it is important to mention that for first PVT water FPC, $A_{c1} = A_c$, $U_{L,c1} = U_{L,c}$, and $(\alpha\tau)_{c1,eff} = (\alpha\tau)_{c,eff}$.

The hourly variation of solar-cell temperature for the two cases is shown in Fig. 5.31. The configuration with a semitransparent PV module on the upper portion of the FPC has a higher solar-cell temperature. This is due to the fact that in this case, the water is preheated from the lower portion, and the temperature difference between the water and the solar cell is less, thus resulting in less heat transfer from the module to the water. A high solar-cell temperature reduces the solar-cell electrical efficiency (Fig. 5.32).

N-Photovoltaic thermal (PVT) water flat-plate collectors (FPCs) connected in series
The series connection of an N-photovoltaic–thermal water FPC is shown in Fig. 5.33.
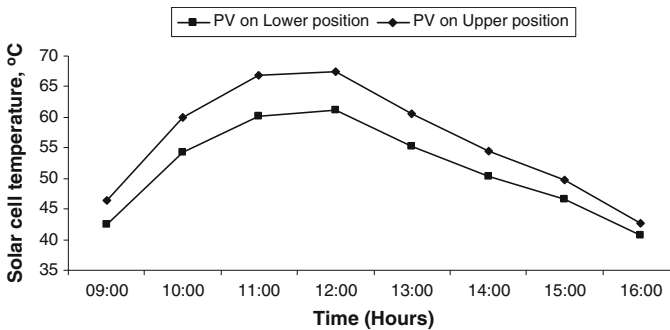
Fig. 5.31 Hourly variation of solar-cell temperature for both cases [21]
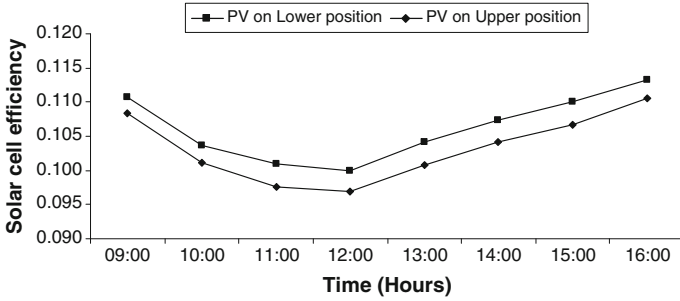
Fig. 5.32 Hourly variation of solar-cell efficiency and temperature for both cases [21]
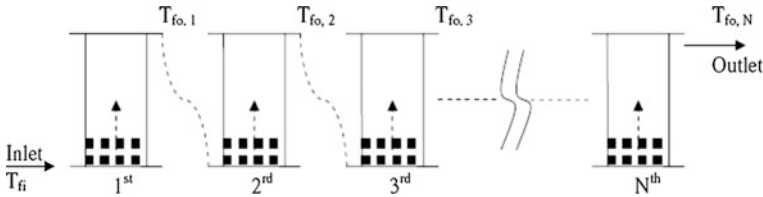
Fig. 5.33 Series connection of *N*-photovoltaic-thermal water FPCs [21]

According to Eq. (5.115), the rate of useful thermal output of the second PVT FPC (FPC) can also be written as

$$\dot{Q}_{u2} = (AF_R(\alpha\tau))_2 I(t) - (AF_R U_L)_2 (T_{fo1} - T_a) \tag{5.124}$$

Here

$$T_{fo1} = T_{fi} + \frac{\dot{Q}_{u1}}{\dot{m}_f C_f}$$

The rate of thermal energy at the end of second flate-plate collector in terms of inlet temperature of the first collector is obtained as follows:

$$\dot{Q}_{u1+2} = \dot{Q}_{u1} + \dot{Q}_{u2} = \left[(AF_R(\alpha\tau))_1 \left(1 - \frac{(AF_R U_L)_2}{\dot{m}_f C_f} \right) + (AF_R(\alpha\tau))_2 \right] I(t)$$
$$- \left[(AF_R U_L)_1 \left(1 - \frac{(AF_R U_L)_2}{\dot{m}_f C_f} \right) + (AF_R U_L)_2 \right] (T_{fi} - T_a) \tag{5.125}$$

For an identical PVT-FPC

$$(AF_R(\alpha\tau))_1 = (AF_R(\alpha\tau))_2 \quad \text{and} \quad (AF_R U_L)_1 = (AF_R U_L)_2$$

For an N identical PVT-FPC

$$\dot{Q}_{u,N} = NA_c\left[(\alpha\tau)_{\text{eff},N}I(t) - U_{L,N}(T_{\text{fi}} - T_a)\right] \tag{5.126}$$

Here

$$(\alpha\tau)_{\text{eff},N} = (F_R(\alpha\tau))_1\left[\frac{1 - (1 - K_{K,A})^N}{NK_{K,A}}\right] \quad U_{L,N} = (F_R U_L)_1\left[\frac{1 - (1 - K_{K,A})^N}{NK_{K,A}}\right]$$

where

$$K_{K,A} = \left[\frac{(AF_R U_L)_1}{\dot{m}_f C_f}\right]$$

Following the same procedure, one can obtain T_{fo1} using Eqs. (5.112) and (5.115)

$$T_{\text{fo1}} = \frac{(AF_R(\alpha\tau))_1}{\dot{m}_f C_f}I(t) + \frac{(AF_R U_L)_1}{\dot{m}_f C_f}T_a + \left(1 - \frac{(AF_R U_L)_1}{\dot{m}_f C_f}\right)T_{\text{fi}} \tag{5.127}$$

For second collector,

$$T_{\text{fo2}} = \frac{(AF_R(\alpha\tau))_2}{\dot{m}_f C_f}I(t) + \frac{(AF_R U_L)_2}{\dot{m}_f C_f}T_a + \left(1 - \frac{(AF_R U_L)_2}{\dot{m}_f C_f}\right)T_{\text{fi2}} \tag{5.128}$$

For N collectors connected in series, the outlet of a particular collector will be the inlet of the subsequent collector; therefore, on applying these initial conditions the fluid temperature at the outlet of the Nth PVT-FPC can be obtained as follows (for details see Sect. 5.8.2):

$$T_{\text{fo}N} = \frac{(AF_R(\alpha\tau))_1}{\dot{m}_f C_f}\left(\frac{1 - K_K^N}{1 - K_K}\right)I(t) + \frac{(AF_R U_L)_1}{\dot{m}_f C_f}\left(\frac{1 - K_K^N}{1 - K_K}\right)T_a + T_{\text{fi}}K_K^N \tag{5.129}$$

where

$$K_K = 1 - \frac{(AF_R U_L)_1}{\dot{m}_f C_f}$$
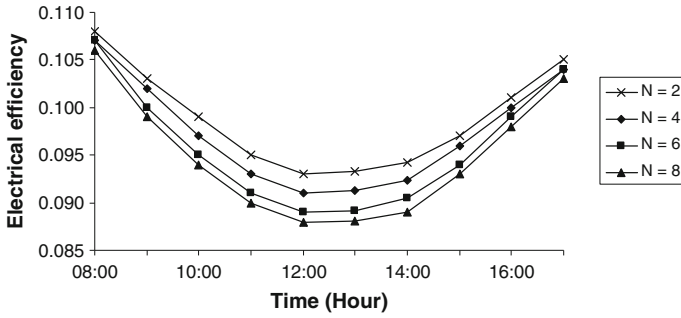
Fig. 5.34 Hourly variation of temperature-dependent electrical efficiency by varying the number of collectors at constant flow rate ($\dot{m} = 0.04\,\text{kg/s}$) [21]

The hourly variation of temperature-dependent electrical efficiency for a different number of collectors connected in series (the mass flow rate of water has been kept constant, i.e., $\dot{m} = 0.04\,\text{kg/s}$) is presented in Fig. 5.34. With an increasing number of collectors, the solar-cell temperature increases and hence its electrical efficiency decreases.

Different Cases

(i) **For fully covered with glass cover (conventional FPC)**

In this case, $A_\text{m} = 0$, and on substituting $A_\text{m} = 0$ one can obtain the expression of the rate of useful thermal gain as follows:

$$\dot{Q}_{\text{u,N}} = \left[NAF_\text{R}(\alpha\tau)_{\text{c,eff}} \left\{ \frac{1 - (1 - K_\text{K})^N}{NK_\text{K}} \right\} \right] I(t)$$
$$- \left[NAF_\text{R}U_{\text{L,c}} \left\{ \frac{1 - (1 - K_\text{K})^N}{NK_\text{K}} \right\} \right] (T_{\text{fi}} - T_\text{a}) \qquad (5.130)$$

where,

$$K_\text{K} = \left[\frac{AF_\text{R}U_{\text{L,c}}}{\dot{m}_\text{f}C_\text{f}} \right]$$

The gain and loss factors in this case are given as

$$\text{Gain factor} = F_R(\alpha\tau)_{c,\text{eff}} \left[\frac{1 - (1 - K_K)^N}{NK_K}\right]$$

$$\text{Loss factor} = F_R U_{L,c} \left[\frac{1 - (1 - K_K)^N}{NK_K}\right]$$

The outlet-fluid temperature

$$T_{\text{fo}N} = \left[\frac{(\alpha\tau)_{c,\text{eff}}I(t)}{U_{L,c}} + T_a\right]\left[1 - \exp\left(-\frac{NF'A_cU_{L,c}}{\dot{m}_fC_f}\right)\right] + T_{\text{fi}}\exp\left(-\frac{NF'A_cU_{L,c}}{\dot{m}_fC_f}\right) \tag{5.131}$$

Equations (5.130) and (5.131) are exactly same as Eq. (5.97a) for $m = 1$ and Eq. (5.88a).

(b) **For fully covered with PV modules**

In this case, $A_c = 0$, and on substituting $A_c = 0$ one can obtain the expression of the rate of useful thermal gain as follows:

$$T_{\text{fo}N} = \left[\frac{PF_2(\alpha\tau)_{m,\text{eff}}I(t)}{U_{L,m}} + T_a\right]\left[1 - \exp\left(-\frac{NF'A_mU_{L,m}}{\dot{m}_fC_f}\right)\right] + T_{\text{fi}}\exp\left(-\frac{NF'A_mU_{L,m}}{\dot{m}_fC_f}\right) \tag{5.132}$$

5.10   Effect of Heat Capacity in a Flat-Plate Collector

The effect of the heat capacity of the absorber plate $(mC)_p$ and glass cover $(mC)_p$ can be seen with the following assumptions, namely,

(i) The temperatures of the absorber plate, the water in the riser, and the back insulation are the same ($U_L \cong U_t$, back and edge losses are neglected); and
(ii) The glass cover is at uniform temperature across its thickness.

The energy balance of the absorber plate, water, and insulation from plate (T_p) to cover (T_c) can be written as follows:

$$(mC)_p \frac{dT_p}{dt} = A_c\left[\dot{q}_{ab} - h_1\left(T_p - T_g\right)\right] \tag{5.133}$$

where h_1 is the heat-transfer coefficient from the absorber plate to the glass cover (see Example 5.2).

Similarly, the energy balance equation for the glass cover can be written as

$$(mC)_{\mathrm{c}}\frac{\mathrm{d}T_{\mathrm{c}}}{\mathrm{d}t} = A_{\mathrm{c}}\left[h_1\left(T_{\mathrm{p}} - T_{\mathrm{g}}\right) - h_2\left(T_{\mathrm{g}} - T_{\mathrm{a}}\right)\right] \qquad (5.134)$$

where h_2 are the convective and radiative heat-transfer coefficients from the glass cover (T_{g}) to the ambient air (T_{a}).

Under steady-state conditions, if we have the following assumptions

$$U_{\mathrm{L}}(T_{\mathrm{p}} - T_{\mathrm{a}}) = h_2(T_{\mathrm{g}} - T_{\mathrm{a}}) \qquad (5.135)$$

Differentiating Eq. (5.135) with respect to time, one obtains

$$\frac{\mathrm{d}T_{\mathrm{g}}}{\mathrm{d}t} = \frac{U_{\mathrm{L}}}{h_2}\frac{\mathrm{d}T_{\mathrm{p}}}{\mathrm{d}t} \qquad (5.136)$$

Summing Eqs. (5.133) and (5.134) and substituting Eq. (5.135), we have following expression:

$$\left[(mC)_{\mathrm{p}} + \frac{U_{\mathrm{L}}}{h_2}(mC)_{\mathrm{c}}\right]\frac{\mathrm{d}T_{\mathrm{p}}}{\mathrm{d}t} = A_{\mathrm{c}}\left[\dot{q}_{\mathrm{ab}} - U_{\mathrm{L}}\left(T_{\mathrm{p}} - T_{\mathrm{a}}\right)\right] \qquad (5.137)$$

If the term in the square bracket is defined as an effective heat capacity, $(mC)_{\mathrm{e}}$, of the FPC, then Eq. (5.137) can be written as follows:

$$\frac{\mathrm{d}T_{\mathrm{p}}}{\left[\dot{q}_{\mathrm{ab}} - U_{\mathrm{L}}\left(T_{\mathrm{p}} - T_{\mathrm{a}}\right)\right]} = \frac{A_{\mathrm{c}}}{(mC)_{\mathrm{e}}}\mathrm{d}t \qquad (5.138)$$

or

$$\frac{\dot{q}_{\mathrm{ab}} - U_{\mathrm{L}}\left(T_{\mathrm{p}} - T_{\mathrm{a}}\right)}{\dot{q}_{\mathrm{ab}} - U_{\mathrm{L}}\left(T_{\mathrm{p0}} - T_{\mathrm{a}}\right)} = \exp\left(-\frac{A_{\mathrm{c}}U_{\mathrm{L}}}{(mC)_{\mathrm{e}}}t\right)$$

The solution of the above equation is

$$T_{\mathrm{p}} = \left[\frac{\dot{q}_{\mathrm{ab}}}{U_{\mathrm{L}}} + T_{\mathrm{a}}\right]\left[1 - \exp\left(-\frac{A_{\mathrm{c}}U_{\mathrm{L}}}{(mC)_{\mathrm{e}}}t\right)\right] + T_{\mathrm{p0}}\exp\left(-\frac{A_{\mathrm{c}}U_{\mathrm{L}}}{(mC)_{\mathrm{e}}}t\right) \qquad (5.139)$$

where T_{p0} is the plate temperature at $t = 0$.

The expression for the rate of energy stored in time $(\Delta t = t - 0)$ for the absorber plate, water, and insulation can be written as

$$\dot{Q}_{\mathrm{L}} = (mC)_{\mathrm{e}}(T_{\mathrm{p}} - T_{\mathrm{p0}}) = (mC)_{\mathrm{e}}\left\{\frac{\dot{q}_{\mathrm{ab}}}{U_{\mathrm{L}}} + T_{\mathrm{a}}\right\}\left[1 - \exp\left(-\frac{A_{\mathrm{c}}U_{\mathrm{L}}}{(mC)_{\mathrm{e}}}t\right)\right] \qquad (5.140)$$

5.11 Optimum Inclination of the Flat-Plate Collector

As we have seen in Chap. 1, there is a variation of solar radiation with (i) incli-
nation of the surface for a given latitude, (ii) orientation, (iii) the time of day, and
(iv) day of the year. Hence, there should be an optimum inclination to receive
maximum solar radiation. On the basis of a literature survey, a rule of thumb Indian
conditions has been made. Accordingly, an optimum inclination of the surfaces of
an FPC receiving maximum radiation is given by

$$\beta_{optimum} = \phi \pm 15° \tag{5.141}$$

where the +ve sign refers to winter conditions and −ve refers to summer conditions.

Because the design of the FPC is made from a water-heating point of view
during winter days, the optimum inclination of a collector for the region around
Delhi is $28°35' + 15 = 43°35' \approx 45°$. The surface should face the north direction in
the southern hemisphere due to the motion of the Sun. For year-round performance,
the optimum tilt is 0.9 times the latitude of the location.

5.12 Effect of Dust in the Flat-Plate Collector

Dust deposited on the transparent cover of an FPC deteriorates its performance.
This reduces the transmittance of the top cover, and it also increases scattering
losses. Dust deposition depends on various factors such as weather conditions of the
place, nature of soil of the place, type of cover, angle of incidence, etc. Due to the
dependency on various fluctuating parameters, the effect of dust deposition cannot
be generalized. For the northern region of India, it has been reported that trans-
mittance of the glass cover is decreased by 8–10 % for an inclined surface at 45°.

Objective Questions

  5.1 The window glass transmits the radiation of wavelengths between
      (a) $0.3 < \lambda < 3$ μm   (b) $0 < \lambda < 0.3$ μm
      (c) $3 < \lambda < 10$ μm   (d) none of these
      Answer: (a)
  5.2 The absorber emits the radiation of wavelengths
      (a) $0.3 < \lambda < 3$ μm   (b) $0 < \lambda < 0.3$ μm
      (c) $3 < \lambda < 10$ μm   (d) none of these
      Answer: (c)
  5.3 The window glass does not allow to the transmission of
      (a) short-wavelength radiation   (b) UV radiation

(c) Infrared radiation   (d) long-wavelength radiation
Answer: (d)

5.4   The transmittance of the window glass depends on
(a) reflectivity   (b) number of glass   (c) incidence angle   (d) all of these
Answer: (d)

5.5   Transmittance of window glass is maximum for
(a) zero angle of incidence   (b) 90° angle of incidence
(c) angle of incidence at latitude (φ) (d) None of these
Answer: (b)

5.6   Transmittance of the window glass depends on
(a) area of the glass cover   (b) length of the glass cover   (c) thickness of
the glass cover   (d) None of these
Answer: (c)

5.7   The fin efficiency of the plate absorber (F) in an FPC depends on
(a) thermal conductivity   (b) density   (c) specific heat   (d) none of these
Answer: (a)

5.8   The fin efficiency (F) of the absorber plate in a FPC depends on
(a) U-value   (b) U_t-value   (c) U_b-value   (d) none of these
Answer: (a)

5.9   The fin efficiency (F) of the absorber plate in a FPC depends on
(a) the length of the collector   (b) the breadth of the collector   (c) the
distance between the two risers   (d) none of these
Answer: (c)

5.10 The flow rate factor (F_R) is
(a) more than the FPC efficiency (F')
(b) less than the FPC efficiency (F')
(c) equal to the the FPC efficiency (F')
(d) none of these
Answer: (b)

5.11 The flow-rate factor (F_R) depends on
(a) mass flow rate   (b) an overall heat-transfer coefficient (U_L)
(c) area of the collector (A_c) (d) all of these
Answer: (d)

5.12 The flow-rate factor (F_R) is derived under
(a) natural flow   (b) turbulent flow   (c) streamline flow   (d) none of these
Answer: (c)

5.13 The total heat loss (U) in a double glazed FPC is
(a) increased   (b) unaffected   (c) decreased   (d) none of these
Answer: (c)

5.14 The heat gain in a double glazed FPC is
(a) unaffected   (b) decreased   (c) increased   (d) none of these
Answer: (c)

5.15 The outlet temperature in a double-glazed FPC

(a) decreases   (b) is unaffected   (c) increases   (d) none of these
Answer: (c)

5.16 The expression for threshold intensity for a natural-circulation FPC is
      (a) $> U_L \frac{T_{out} - T_a}{(\alpha\tau)}$ (b) $< U_L \frac{T_p - T_a}{(\alpha\tau)}$ (c) $= U_L \frac{T_{in} - T_a}{(\alpha\tau)}$ (d) none of these
      Answer: (b)

5.17 The expression for the threshold intensity for a forced-circulated FPC is
      (a) $> U_L \frac{(T_{fi} - T_a)}{(\alpha\tau)}$ (b) $< U_L \frac{(T_{fi} - T_a)}{(\alpha\tau)}$ (c) $= U_L \frac{(T_{fi} - T_a)}{(\alpha\tau)}$ (d) none of these
      Answer: (a)

5.18 For natural circulation, FPCs are connected in
      (a) series   (b) parallel   (c) series and parallel   (d) none of these
      Answer: (b)

5.19 For a forced-circulation solar water heater, the FPCs are connected
      (a) only in parallel   (b) only in series
      (c) in series and in parallel   (d) all of these
      Answer: (d)

5.20 The annually optimum inclination of a FPC conditions is
      (a) $\varphi + 15$ latitude   (b) $\varphi - 15$ (c) φ (latitude)   (d) none of these
      Answer: (c)

5.21 The optimum inclination of a FPC for winter conditions is
      (a) φ (latitude)   (b) $\varphi - 15$ (c) $\varphi + 15$ (d) none of these
      Answer: (c)

5.22 The optimum inclination of a FPC for summer conditions is
      (a) $\varphi - 15$ (b) $\varphi + 15$ (c) φ (latitude)   (d) all of these
      Answer: (a)

5.23 The heat capacity of an absorber (tube-in-plate) is neglected due to
      (a) low heat capacity   (b) low mass   (c) low density   (d) all of these
      Answer: (a)

5.24 The flow factor (F_{RN}) for an N-collector connected in series depends on
      (a) the number of collectors   (b) the flow rate   (c) the U_L-value   (d) all
      of these
      Answer: (d)

Problems

5.1 Draw the curve between the fin-efficiency factor (F) and the thickness of an
     absorber (δ) for a given diameter (D) of pipe and thermal conductivity (K)
     for a given flat-plate–collector specification.
     Hint: Use Sect. 5.6.

5.2 Determine the flat-plate–collector efficiency factor (F') with $(x_b = 0)$ and
     without $(x_b = 0)$ bond conductance for a given collector.
     Hint: Use Sect. 5.7.3.

5.3   Calculate the *U*-value for a double-glazed FPC. The spacing between the two glass covers is 5 cm.

   Hint: Apply $U = \left[\frac{1}{h_1} + \frac{1}{C} + \frac{1}{h_2}\right]^{-1}$, the air conductance for 5cm thickness $C = 5\,\text{W/m}\,^\circ\text{c}$.

5.4   What is the FPC's instantaneous thermal efficiency (η_i) and rate of heat collection $\dot{q}_u$ for the following specifications and climatic conditions: $(\alpha\tau) = 0.8$, $U = 6\,\text{W/m}^2\,^\circ\text{C}$, $I = 800\,\text{W/m}^2$, $T_p = 55\,^\circ\text{C}$, $T_a = 20\,^\circ\text{C}$, $W = 150\,\text{mm}$, $D_i = 7\,\text{mm}$, $D_o = 10\,\text{mm}$, $\delta = 0.5\,\text{mm}$, $x_b = 0$, $K = 385\,\text{W/m}\,^\circ\text{C}$, and $h_{fi} = 250\,\text{W/m}^2\,^\circ\text{C}$?

   Hint: Apply Eq. (5.64) and $\eta_i = \dot{Q}_{useful}/I(t)$.

5.5   How do you calculate the stagnation temperature of the FPC?

   Hint: Obtain $f_c = (T_p T_a)/I(t)$ at $\eta = 0$ in   and   evaluate $T_p(\text{stagnate}) = f_c I(t) + T_a$.

5.6   Derive an expression for total useful energy (Q_T) for a time interval of $\Delta T = 0 - t_T$.

   Hint: use $Q_T = \int_0^{t_T} \dot{Q}_u(t)dt$; with $\bar{I}(t) = \frac{\int_0^{t_T} I(t)dt}{t_T}$ and $\bar{T} = \frac{\int_0^{t_T} T_a(t)dt}{t_T}$.

5.7   Draw the curve between the flow-rate factor (F_R) and the flow rate $\dot{m}_f$ for a given collector area (A_c) and flat-plate–collector efficiency factor.

   Hint: Apply Eq. (5.73).

5.8   Derive an expression for the mean fluid temperature for a flat-plate solar collector.

   Hint: Apply $T_{fm} = \frac{1}{L}\int_0^L T_f(x)\,dx$.

5.9   Plot the curve between the collector flow factor $(F'' = F_R/F')$ and flow rate factor.

   Hint: Apply Eq. (5.74).

5.10 Determine the mean fluid and plate temperature for the collector in problem 5.4.

   Hint: See Problem 5.9.

5.11 Draw the curve between $F_R(\alpha\tau)$ and $F_R U_L$ and the number of FPCs connected in series.

   Hint: Apply Eq. (5.95d).

References

1. W.W.S. Charters, B.C. Window, Search **9(4)**, 123 (1978)
2. B.J. Huang, J.H. Lu, Sol. Energy **28**(5), 413 (1982)
3. J.A. Duffie, W.A. Beckman, *Solar engineering of thermal processes* (Wiley, New York, 1991)
4. K.G.T. Holland, T.E. Unny, G.D. Raithby, L. Konicek, J. Heat Transfer **98**(2), 189 (1976)
5. H. Buchberg, I. Catton, D.K. Edwards, J. Heat Transfer **98**(2), 182 (1976)
6. J.H. Watmuff, W.W.S. Charters, D. Proctor, Complex **2**, 56 (1977)
7. K.S. Ong, Sol. Energy **16**(3), 137 (1974)
8. L.K. Baker, Sol. Energy **11**(2), 78 (1967)
9. H.Y. Wong, *Heat transfer for engineers* (Longman London Art, New York, 1977)

10. M. Madhusudan, G.N. Tiwari, D.S. Hrizhikeshan, H.K. Sehgal, Energy Convers. Manag. **21**(3), 191 (1981)
11. D.K. Edward, Trans. ASME J. Heat Transfer **91**(1), 145 (1969)
12. B.A. Meyer, M.M. El-Wakil, J.W. Mitchell, *Natural convection heat transfer in small and moderate aspect ratio enclosures, in thermal storage and heat transfer in solar energy systems*, ed. by F. Kreith, R. Boehm, J. Mitchell and R. Bannerot (American Society of Mechanical Engineers, New York, 1978)
13. S.A. Klein, Sol. Energy **19**(4), 325 (1977)
14. H.C. Hottel, A. Whiller, *Evaluation of flat-plate collector performance*. Trans of the conference on the use of solar energy, vol. 2 (University of Arizona Press, Tucson, 1958), p. 74
15. R.W. Bliss, Sol. Energy **3**, 55 (1959)
16. A. Whiller, *Solar energy collection and its utilisation for house heating*, Sc.D. thesis MIT Michigan (1953)
17. W.E. Phillips, Sol. Energy **23**, 187 (1979)
18. R.L. Oonk, D.E. Jones, B.E. Cole-Apke, Sol. Energy **23**(6), 535 (1979)
19. A.D. Jones, C.P. Underwood, Sol. Energy **70**(4), 349 (2001)
20. G.N. Tiwari, R.K. Mishra, S.C. Solanki, Appl. Energy **88**, 2287 (2011)
21. G.N. Tiwari, R.K. Mishra, *Advanced renewable energy sources* (RSC Publishing, UK, 2012)

Additional References

22. G.N. Tiwari, *Solar energy: fundamental, design, modelling and applications* (Narosa Publishing House, New Delhi and CRC Press, New York, 2004)
23. A. Whillier, *ASHRAE* (1967)
24. N. Aste, C.D. Pero, F. Leonforte, Sol. Energy **102**, 98 (2014)
25. A. Ibrahim, M.Y. Othman, M.H. Ruslan, S. Mat, K. Sopian, Renew. Sustain. Energy Rev. **15**(1), 352 (2011)
26. M.J. Ahmed, G.N. Tiwari, Open Renew Energy J **2**, 19 (2009)
27. Y.D. Goswami, F. Kreith, J.F. Kreider, *Principles of solar engineering* (Taylor & Francis, London)
28. B. Norton, *Solar energy thermal technology* (Springer, New York, 2000)
29. F. Kreith, J.F. Kreider, *Principles of solar engineering* (McGraw-Hill Book Company, New York, 1980)
30. P.J. Lunde, *Solar thermal engineering (Chap. 7)* (Wiley, New York, 1980), p. 240
31. A.B. Meinel, M.P. Meinel, *Applied solar energy, an introduction* (Chap. 1) (Addison-Wesley Publishing Company, Reading, 1977)
32. S.I. Abdel-Khalik, Sol. Energy **18**(1), 59 (1976)

Chapter 6
Solar Concentrator

Abstract For the highest operating temperature range (≥300 °C) of solar thermal-energy applications in the industrial sector, the beam radiation of solar energy is concentrated at a low surface area of the receiver. This is referred to as the "concentrating system" and can be used for power generation by using a boiling-temperature fluid as a medium. Solar-power generation is economical for higher capacity of plants (≥1 MW) with grid power in a dust-free region for less cleaning of the reflecting sheet.

Keywords Solar concentrator · PVT concentrator · Solar tracking · Selective coating · Reflectors

6.1 Introduction

As we saw in Chap. 5, the flat plate collector (FPC) can provide a medium temperature range up to 150 °C with working fluid under steady-state conditions. However, for a temperature range >150 °C, we require a change in the design of the FPC. From Eq. (5.11b), one can observe that the rate of useful energy, $\dot{Q}_u$, in W is given by

$$\dot{Q}_u = A_c \left[(\alpha\tau)I(t) - U_L \left(T_p - T_a \right) \right] \qquad (6.1a)$$

where $U_L = U_t + U_b$.

In the above equation, the following should be noted:

(i) The first term is responsible for the rate of gain of thermal energy, whereas the second term is responsible for the rate of heat loss from the absorber to the ambient air from the top as well as the bottom of the FPC; and

(ii) the areas of the absorber, glass cover, and bottom insulation are equal.

The above equation can be written as

$$\dot{Q}_u = \left[A_c(\alpha\tau)I(t) - A_c U_L(T_p - T_a)\right] \tag{6.1b}$$

If the rate of heat loss from the absorber to the ambient air, $A_c U_L(T_p - T_a)$, can be reduced, then the numerical value of $\dot{Q}_u$ will increase; hence, the operating temperature of the absorber for the given collector area, A_c. This is only possible and practical if area involved in loss term, $A_c U_L(T_p - T_a)$, is reduced and referred as receiver area A_r. Now onward, A_c will be replaced by A_a as the aperture area.

In addition, U_L will be replaced by U_t because there will be only upward heat loss from the receiver to the ambient air through the glazed surface. Therefore, Eq. (6.1b) becomes

$$\dot{Q}_u = \left[A_a(\alpha\tau)I(t) - A_r U_t(T_p - T_a)\right] \tag{6.1c}$$

Because the beam radiation has the direction, hence it can be reflected by reflecting surface having reflectance, ρ, then Eq. (6.1c) becomes

$$\dot{Q}_u = \left[A_a \rho(\alpha\tau)I_b - A_r U_t(T_p - T_a)\right]$$

or

$$\dot{Q}_u = A_a \left[\rho(\alpha\tau)I_b - \frac{A_r}{A_a}U_t(T_p - T_a)\right]$$

or

$$\dot{Q}_u = A_a \left[S - \frac{A_r}{A_a}U_t(T_p - T_a)\right] \tag{6.1d}$$

where $S = \rho(\alpha\tau)I_b$ is the rate of absorbed beam radiation per m^2 unit area of unshaded receiver.

From the above equation, the rate of useful energy per m^2 in W/m^2 can be obtained as follows:

$$\dot{q}_u = \frac{\dot{Q}_u}{A_a} = \left[\rho(\alpha\tau)I_b - \frac{A_r}{A_a}U_t(T_p - T_a)\right]$$

or

$$\dot{q}_u = [\rho(\alpha\tau)I_b - \frac{1}{C}U_t(T_p - T_a)] \tag{6.1e}$$

where $C = \frac{A_a}{A_r}$ is the concentration ratio, which will be discussed later in the text.

A solar concentrator is a device that concentrates the solar radiation falling on a larger surface (aperture area, A_a) onto a smaller surface (receiver area, A_r) as shown in Eq. (6.1d). Appropriate reflecting or refracting components are used to increase the flux density on the absorber (receiver) surface compared with a FPC for higher concentration. For maximum concentration, tracking of beam radiation (the Sun's virtual motion) and an accurate focusing device is essential. Hence, a solar concentrator comprises a tracking arrangement, a focussing device and a receiver system. Temperatures up to 300 °C can be achieved by using solar concentrators. Therefore, concentrators are favourable for thermal as well as photovoltaic applications even at higher operating temperatures.

Solar-concentrating devices are used since as early as in 1695; a diamond was melted by solar energy in Florence. Lavoisier carried out a number of experiments with his double-lens concentrator. The knowledge of the concentrator dates back even to the time of Archimedes, whose book "On Burning Mirrors" is an evidence of this fact. Concentrators were predominantly used in heat engines and steam production in the eighteenth and nineteenth centuries.

Followings are the main advantages of a concentrator:

 (i) It increases the solar intensity (beam radiation) by concentrating the solar energy available over a large surface, A_a, onto a smaller surface, A_r, (absorber/receiver).
 (ii) Due to the concentration being on a smaller area, the heat-loss area is reduced as mentioned previously. Furthermore, the thermal mass is much smaller than that of a FPC and hence the transient effects are small.
 (iii) The delivery temperature is very high.
 (iv) It reduces the cost by replacing an expensive receiver (large glass-cover area) with a less-expensive reflecting or refracting surface.

However, a solar concentrator is an optical system. In this case, the optical loss terms become significant. Furthermore, it operates only on the beam radiation. It results in the loss of diffuse radiation. The basic concepts of FPCs are also applicable to solar-concentrating systems. A number of complications arise due to the following:

 (a) nonuniform flux on absorber/receiver;
 (b) wide variations in shape, temperature, and heat-loss behaviour of absorbers; and
 (c) optical considerations in the energy balance conditions.

As the requirement of higher-precision optics for a higher concentration of collector increases, the cost of the system also increases. In addition to the complexity of the system, the maintenance cost is also increased.

6.2   Characteristic Parameters

Definitions of the several terminologies that characterize concentrating solar collectors are given below.

Aperture area (A_a)
This is the area on the front of the solar concentrator that accepts the incident solar beam radiation as shown in Fig. 6.1.

Acceptance angle ($2\theta_c$)
This is the limiting angle over which the incident solar beam radiation path may deviate from normal to the aperture plane and reaches the absorber/receiver after reflection. For larger acceptance angles, solar concentrators are moved seasonally, whereas for smaller acceptance angles, solar concentrators must be moved continuously to track the Sun as shown in Fig. 6.1.

Absorber/receiver area (A_r)
This is the total area that receives the concentrated solar beam radiation. This area delivers the useful thermal energy to the system.

Geometric concentration ratio (C)
This is the ratio of the aperture area to the absorber/receiver area, Eq. (6.1e).

$$C = A_a/A_r \qquad\qquad (6.2a)$$

The value of C varies from unity (FPC) to several thousand (parabolic dish).

Fig. 6.1 Figure showing various characteristic parameters
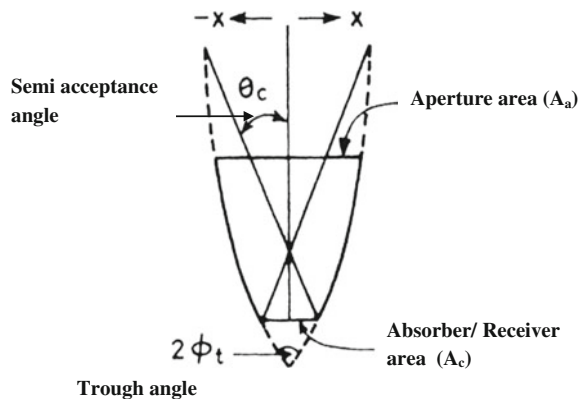
Local concentration ratio (brightness-concentration ratio)
The local concentration ratio is defined where the whole system is not uniformly illuminated; it is the ratio of the beam radiation at any point on the absorber/receiver to the incident beam radiation at the entrance of the solar concentrator.

Intercept factor (γ)
This is the fraction of focussed solar beam radiation intercepted by the absorber/receiver of a given size as shown in Fig. 6.1.

$$\gamma = \frac{\int_A^{B'} I_b(x)\,dx}{\int_{-\infty}^{+\infty} I_b(x)\,dx} \tag{6.2b}$$

The value of the intercept factor depends on the size of the absorber; for a typical concentrator/receiver design, it is >0.9. For normal incident (on aperture) radiation, it is unity.

Example 6.1 A linear parabolic solar concentrator is designed to intercept all of the specularly reflected beam radiation for normal incidence. It continuously rotates horizontally on an east–west axis and fitted with liquid-heating receiver unit of length 10.0 m. A strip of 0.21 m—wide reflector is shaded by the receiver. For the aperture, $a = 2.00$ m and focal length, $f = 1.00$ m, calculate the rate of useful energy in W for the following parameters.

(i) Normal beam radiation to the aperture = 950 W/m^2, (ii) here $\alpha\tau$ for the receiver = 0.78, (iii) $\rho = 0.84$, (iv) inlet-fluid temperature = 180 °C, (v) ambient air temperature = 20 °C, and (vi) $F_R = 0.85$.

Solution
For normal incidence, $\gamma = 1$, and a fraction of the reflector $0.21/2.00 = 0.10$ is shaded by the receiver; therefore, 0.90 of the reflector is effective.

The numerical value of product $\rho\gamma\tau\alpha$ is given by $\rho\gamma\tau\alpha = 0.84 \times 1 \times 0.78 = 0.655$.

The rate of absorbed thermal energy is given by

$$S = 950 \times 0.655 = 622.25 \text{ W/m}^2$$

For an estimated mean receiver-surface temperature of 200 °C, the overall heat-transfer coefficient (U_L) is 13.7 W/m^2 °C.

The concentration ratio $C = \frac{A_a}{A_r} = \frac{(2.00-0.21)}{0.21} = 8.5$.

The rate of useful thermal energy $(\dot{Q}_u)$ can be determined as

$$\dot{Q}_u = 0.85 \times 10.0(2.00 - 0.21)[622 - 13.7/8.5(180 - 20)]$$

or

$$\dot{Q}_{u} = 0.85 \times 10.0 \times 1.79 \times 364 = 5540 \text{ W} = 5.54 \text{ kW}$$

Optical efficiency (η_0)

This is defined as the ratio of the rate of net thermal energy available at the absorber/receiver to the incident beam radiation available at the absorber/receiver after absorption and transmission. It is mathematically expressed as

$$\eta_0 = \dot{q}_u / (\alpha \tau I_b) \tag{6.3}$$

The above equation includes the effect of the shape of mirror surface, different losses (reflection, transmission, and absorption), shading by the receiver, and the solar beam incident angle.

Instantaneous thermal efficiency (η_c)

This is the ratio of the rate of useful energy available at the absorber/receiver (A_r) to the beam energy incident on the aperture (A_a). It is given by

$$\eta_0 = \dot{q}_u / I_b \tag{6.4}$$

Concentration ratio (C)

From Eq. (6.2a), the concentration ratio is given by

$$C = A_a / A_r;$$

As shown in Fig. 6.2, let us consider the circular solar concentrator with aperture area A_a and receiver/absorber area A_r. It also views the Sun of radius r at a distance R. The half-angle subtended by the Sun is θ_s. For a perfect solar concentrator, the beam radiation from the Sun on the aperture is the fraction of the solar radiation emitted by the Sun that is intercepted by the aperture area A_a. The radiation (W) from the Sun to the aperture can be expressed as

$$Q_{s \to r} = A_a \frac{r^2}{R^2} \sigma T_s^4 \tag{6.5}$$

Fig. 6.2 Schematic of sun at T_s at a distance R from a concentrator with aperture area A_a and receiver area A_r
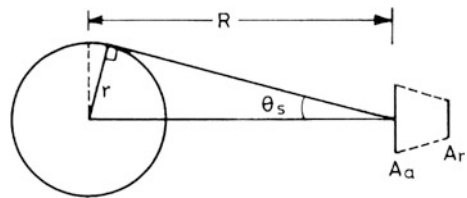
If $E_{r \to s}$ fraction of energy radiated from perfect receiver reaches the Sun, then

$$Q_{r \to s} = A_r \sigma T_r^4 E_{r \to s} \tag{6.6}$$

For the same T_r and T_s, $Q_{s \to r}$ will be equal to $Q_{r \to s}$ by the second law of thermodynamics. Thus, from Eqs. (6.5) and (6.6) one obtains
Thus

$$A_a \frac{r^2}{R^2} \sigma T_s^4 = A_r \sigma T_s^4 E_{r \to s} \tag{6.7}$$

The maximum possible value of $E_{r \to s}$ is unity, and the maximum concentration ratio for circular solar concentrators is written as

$$\left(\frac{A_a}{A_r} \right)_{max} = \frac{R^2}{r^2} = \frac{1}{\sin^2 \theta_s} \tag{6.8}$$

6.3 Classification of Solar Concentrators

Solar concentrators may be broadly classified as follows:

 (i) **Tracking type**: These types of solar concentrators are classified on the basis of tracking type (continuous, intermittent, one-axis, or two-axis) or on the basis of the moving device (focussing part or receiver or both) for tracking.
(ii) **Non-tracking type**: In this case, the axis of concentrator is fixed. There is no moving part.

Solar concentrators can also be classified on the basis of optical components. They may be (i) reflecting or refracting type, (ii) imaging or nonimaging type, and (iii) line-focussing or point-focussing type. The reflecting or refracting surface can be one piece or a composite surface. It may be either a single-stage– or two-stage–type system. It may be further classified as symmetric or asymmetric. In practice, however, hybrid and multistage systems occur frequently that incorporate various levels of the features.

6.4 Types of Solar Concentrator

There are a number of ways to measure flux of beam radiation on receivers. Some of them are discussed briefly in the following section.

6.4.1 Tracking Solar Concentrators

6.4.1.1 One-Axis Tracking Solar Concentrators

Solar concentrators are used to achieve moderate concentration with one-axis tracking. A few of them are discussed below:

(i) Fixed-mirror solar concentrator (FMSC)

The fixed-mirror solar concentrator consists of a (i) fixed mirror and (ii) a tracking receiver system as shown in Fig. 6.3. The fixed mirror consists of long, narrow flat strips arranged on a reference circular cylinder of a chosen radius R.

The width of the mirror strip is compatible with the diameter of a given absorber/receiver pipe. The angle of each element is adjusted in such a way that the focal distance of the array is twice the radius of the reference cylinder. The array produces a narrow focal line, which lies along the same circular path with the diurnal motion of the Sun. The focal line can be easily tracked by the movable receiver pipe. The pipe is made to rotate about the centre of curvature of the reflector module. Thus, the delicate part of the system comprises the rigidly fixed mirrors.

The image width is ideally the same as the projected width of the mirror element at the absorber/receiver. Thus, the concentration ratio is approximately the same as the number of mirror elements. For fixed and concave aperture, the mirror strips result in shading with very high or very low Sun altitude angles. Edge losses also occur during reflection due to the strips. However, the mirrors can be suitably designed for only 10 % loss of the total energy lost over a year's time. Fixed-mirror solar concentrator models have shown an overall thermal efficiency in the range of 40–50 %.

Fig. 6.3 View of fixed-mirror solar concentrator
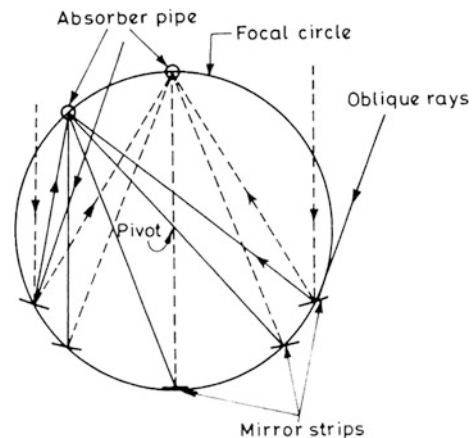
Fig. 6.4 View of cylindrical parabolic concentrator (CPC)
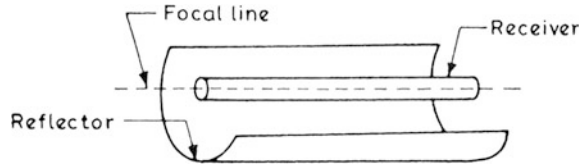
(ii) **Cylindrical parabolic solar concentrator (CPSC)**

A cylindrical parabolic trough solar concentrator comprises a cylindrical parabolic reflector and a metal tube receiver at the focal plane as shown in Fig. 6.4. The blackened receiver is covered by the concentrator and rotated about one axis to track the Sun. The heat-transfer fluid is heated as it flows through the absorber tube.

Such solar concentrators have been used for many years. The aperture diameter, rim angle, and absorber/receiver size and shape may be used to define the concentration. The absorber tube may be made of either mild (low carbon) steel or copper. It is coated with a heat-resistant black paint. Selective coatings on the absorber may be used for better performance. Depending on the temperature requirement, different heat-transfer liquids/fluids are is used. Reflectors may be made of anodized aluminum sheets, aluminized Mylar, or curved silvered glass. Because it is difficult to curve a very large glass, mirror strips are used in some cases. The reflecting part is fixed on a lightweight structure. The solar-concentration ratio (C) for a cylindrical absorber varies from 5 to 30.

The major thermal energy losses from a concentrator/receiver assembly for normal incidence are the losses that occur during reflection from the reflecting surface. There is convection loss from the absorber/receiver to the surroundings. Efforts are made to use high-reflecting materials to reduce losses. Twisted tapes are used in the absorber tube for large heat transfer from the absorber to the working fluid.

A cylindrical parabolic trough may be oriented in any of the three directions, namely, (i) east–west, (ii) north–south, or (iii) polar. The first two orientations have higher incidence-angle cosine losses. The polar configuration intercepts more beam radiation per unit area compared with other modes. Thus, it gives the better performance.

(iii) **Linear Fresnel lens/reflector**

A linear Fresnel lens solar concentrator, as shown in Fig. 6.5, consists of linear grooves on one surface of the refracting material. The groove angles are chosen with reference to a particular wavelength of incident beam radiation so that the lens acts as a converging one for the light, which is incident normally.

Both glass and plastic can be used as refracting materials for fabricating Fresnel lenses. Glass is seldom used because it is difficult to mould, and it also has large surface tension; on the other hand, plastic lenses are economical. Plastic moulding lasts for an appreciable time. Plastic Fresnel lenses with 20 grooves/mm are moulded.
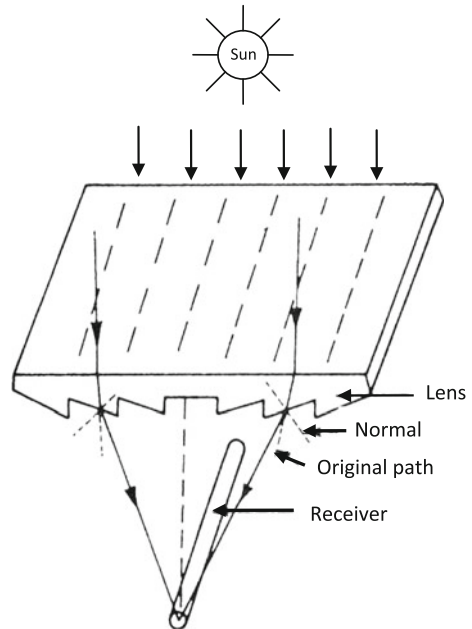
The Fresnel lens may be installed with either of the following:

(a) **Sun-facing grooves**: In this case, the ineffective facts of the grooves prevent a
    part of the input beam light from being transmitted to the focus. According to
    Snell's law, the refracted light is deviated away from the normal on moving
    from a denser to a rarer medium. Furthermore, the dust deposited in these
    grooves results in a poor performance.

(b) **Downward-facing grooves**: In this case, the solar concentrator has a high
    surface reflection loss and large off-axis aberrations. The reflection losses
    cause low thermal efficiency. Large off-axis aberrations give a low concen-
    tration ratio. In addition, the beam radiation is not incident normally, which
    affects the performance. The focal length of the lens varies rapidly with a
    change of the angle of incidence. The optical system needs to track the path of
    the Sun for a better performance.

Fresnel reflectors can also be used as concentrating devices as shown in Fig. 6.6.
They are made up of either smaller flat or curved components. They consist of a
number of mirror elements mounted suitably. All incident parallel rays of beam
radiation are focussed at a common point after reflection. Ideally, mirror elements
must be parabolic in shape. Flat mirrors are generally used to ameliorate manu-
facturing and assembling problems.

Fig. 6.6 View of Fresnel
reflectors
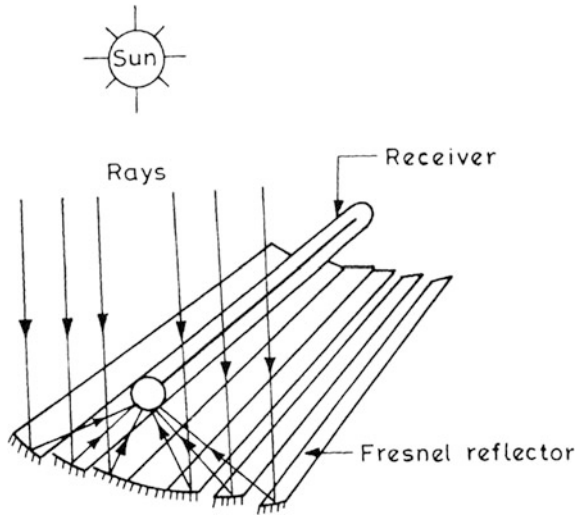
6.4.1.2   Two-Axes Tracking Concentrators

To achieve a high solar concentration for higher-temperature solar processes, concentrators with double curvatures are used. These require two-axes tracking of the Sun. Some of these are briefly discussed as follows:

(i) **Paraboloidal dish solar concentrator (PDSC)**

In a paraboloidal dish solar concentrator (PDSC), a parabola rotates about the optical axis as shown in Fig. 6.7. In this case, a higher concentration ratio (C) is achieved.

Considering the Sun as a point source of light, beam radiation is focussed at a point in a paraboloidal due to the compound curvature. However, an image is produced due to the finite angular substance of the Sun. Furthermore, the surface may not be strictly parabolic. This causes an enlarged image due to misdirection of the beam light rays because of misaligned surface elements. A degraded image is obtained for an off-axis object. The rays from the central region of the paraboloidal travel a shorter distance in arriving at the focus, and the rays from the edges travel a larger distance. Results spread of the image. Thus, a three-dimensional image of the Sun in the shape of an ellipsoid is formed as shown in Fig. 6.8.

The thermal losses from a paraboloidal are primarily radiative. They can be reduced by decreasing the absorber aperture area. However, this results in a smaller intercept factor. The optimum intercept factor is approximately 0.95–0.98. There should be large absorber size to achieve the optimum beam intercept.

High-collection thermal efficiency and high-quality thermal energy are the features of a paraboloidal or parabolic dish type of solar concentrator. These devices can be used as sources for a variety of purposes due to large delivery temperatures.
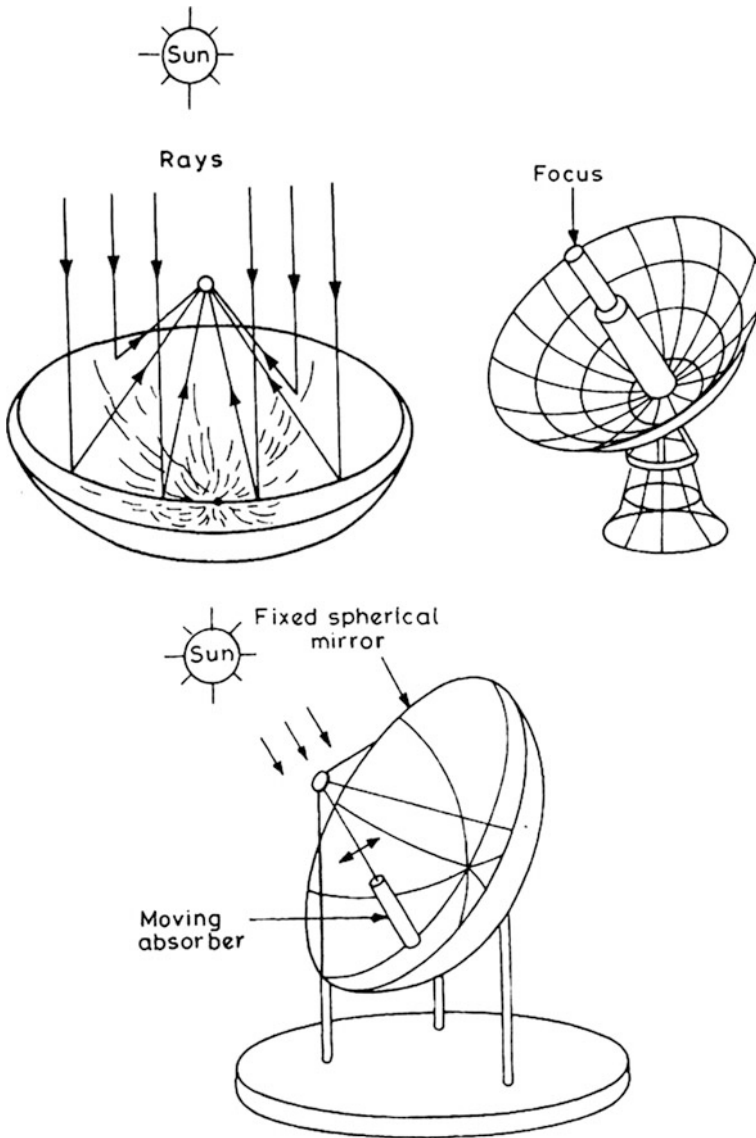
Fig. 6.7 Schematic view of a paraboloidal concentrator

(ii) **Central tower receiver (CTR)**

The central tower receiver (CTR) consists of (a) a central stationary receiver and (b) heliostats as shown in Fig. 6.9. A heliostat is composed of a large array of mirrors fixed to a supporting frame, which reflect the beam radiation toward receiver. This frame can be used to track the Sun as per requirement.

Fig. 6.8 Illustration of formation of an ellipsoid image in a paraboloid
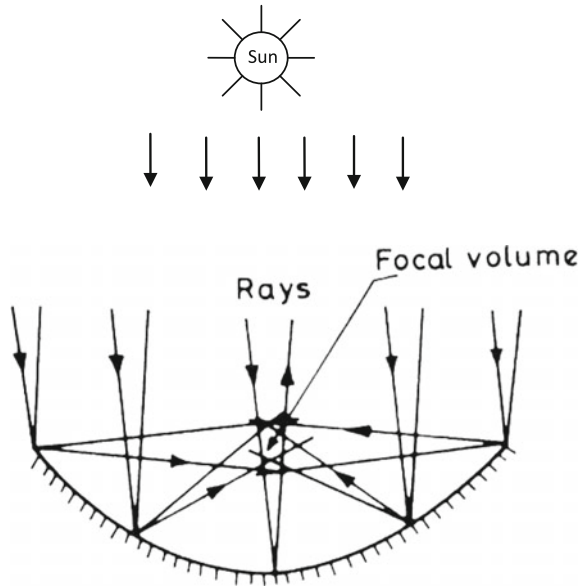
Fig. 6.9 Schematic view of central receiver–heliostat system
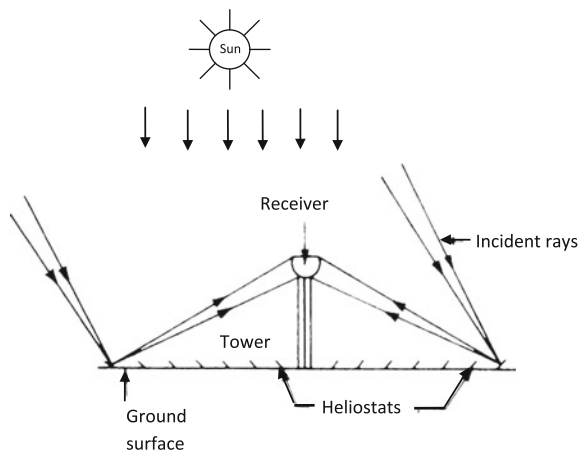
The heliostats are installed in the open space. Together they act like a dilute paraboloid. They focus beam radiation on a stationary central receiver. Concentration ratios (C) can be achieved ≤ 3000. The absorbed energy can be extracted from the receiver. This is delivered at a higher temperature and a pressure suitable for running the turbines for power generation.

The advantage of this system is to eliminate the need for carrying the working fluid over large distances. As a result, heat losses are reduced significantly to eliminate the need for insulation. However, many other problems are involved in the system. A majority of them are due to the heliostats and receiver. A large

number of heliostats are required to focus beam radiation, which requires a large free space. The heliostats may be provided with proper tracking arrangement. It may be arranged such that self-shading is avoided to achieve reasonable concentration. In addition to the cost, cleaning of the mirrors poses another problem. Furthermore, the heliostat arrangement must be strong enough to sustain extreme weather conditions. The receiver/absorber must be able to effectively intercept the focused beam radiation to absorb heat and transfer this energy to the working fluid with minimum heat loss. Several designs have been proposed for the receiver. Heat-transfer fluids, such as steam and liquid metals, have been suggested. Some problems arise due to reflection and transmission losses as well as thermal stress in the receiver.

(iii)   **Circular Fresnel lens (CFL)**

Lenses are not usually used in solar energy applications due to their high cost and weight. However, these are used for high-temperature requirements (solar furnace). Figure 6.10 shows the principle of Fresnel lens. Optically, the Fresnel lens is equivalent to a thin-lens approximation. It is divided into a number of zones. The zones are spaced at a few tenths of a millimetre. The space can also be few centimetres. Within each aperture zone, the tilt of the lens surface is adjusted such that its optical behaviour resembles that of the conventional spherical lens of the same focal length. The focus of the annulus does not need to be curved. However, it is required to have the correct tilt so as to refract the light to the focus. This is due to the large absorbing surface in comparison with the width of a Fresnel zone on the lens. Meinel [1] proposed the equation for the tilt of the facet as a function of the aperture zone and focal length.

The circular Fresnel lens provides a very good concentration ratio. For a precise plastic lens, the brightness concentration is as high as 2000. Hence, such concentrators are usually used with silicon and gallium arsenide solar cells for high flux. In solar-cell applications, the lens must track the Sun. It is required to keep the small solar image centred on the receiver. In this case, it may be noted that the brightness concentration is smaller in comparison with that of parabolic mirrors.

The transmitting system has an advantage over the reflecting system due to absorbing certain wavelength of incident beam. This may result in heating of the focus.

Fig. 6.10 Schematic diagram of a circular Fresnel lens
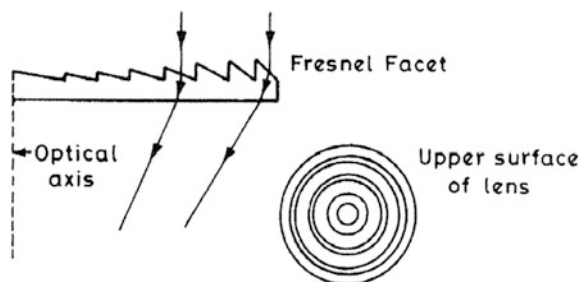
(iv) **Hemispherical bowl mirror**

Figure 6.11 shows a cross-sectional view of hemispherical mirror concentrator developed by Steward [2]. It has a fixed mirror and a moveable receiver-type concentrator. The major components of this concentrator are (a) a fixed hemispherical mirror, (b) a tracking linear absorber, and (c) a supporting structure.

The hemisphere produces a highly aberrant optical image. However, all rays entering into the hemisphere after reflection cross the paraxial line at some point between the focus and the mirror surface because of the symmetry of light. Therefore, an absorber pivots about the centre of the curvature of the hemisphere to intercept all reflected rays. The absorber/receiver is to be moved with axis, which is always aligned with solar rays passing through the centre of the sphere. This requires two-axes tracking. Although this motion can be set in a number of ways. One of the simplest ways is to use an equatorial mount, in which the absorber/receiver is driven around a polar axis at a constant angular speed of 15°/h during the day. It may be noted that this type of concentrator gives a lesser concentration than that in paraboloids due to the spherical aberration.

6.4.2   *Non-tracking Solar Concentrators*

Tracking solar concentrators provide high delivery temperatures due to an accurate tracking device and fine surface; and hence they are expensive. However,

Fig. 6.11 View of a hemispherical-mirror concentrator
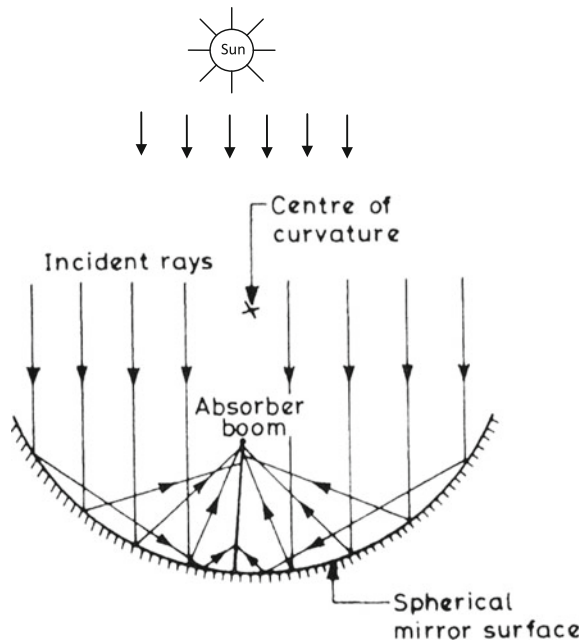
inexpensive concentrators are designed without tracking for medium-temperature operation. Some of these concentrators are discussed in brief as follows:

(i) **Flat receiver with booster mirror**

Figure 6.12 shows a conventional FPC receiver with plane reflectors at the edges to reflect additional radiation into the absorber/receiver. Flat mirrors are also called "booster mirrors." The concentration ratio of such a concentrator is relatively low, but it is higher than that of the conventional FPC. It has a maximum value <4. Booster mirrors become less effective due to the increase of the solar incidence angle. Booster mirrors can be used on all the four sides for a single collector. The mirror actually starts casting a shadow on the absorber for a Sun angle greater than the semi-angle of the booster mirrors. In case of an array of flat-plat collectors, plane booster mirrors can be used on only two sides.

The thermal efficiency of a boosted flat-plate system can be increased several times during the year with a change in the angle of the flat mirrors. The advantage of such a system is to use the diffuse radiation in addition to the beam radiation. In this case, the attainable temperature and collection thermal efficiency will be greater in comparison with those of a FPC with the same collection area.

(ii) **Tabor–Zeimer circular cylinder**

Figure 6.13 shows a view of a Tabor–Zeimer circular cylinder. It is a very simple cylindrical optical system. It consists of an inflated plastic cylinder with a triangular pipe receiver. The cylinder has a clear portion on the top to allow beam radiation to enter toward the rear portion, which is aluminized to act as a mirror. The incident beam radiation is reflected by the mirror and is focussed on the absorber/receiver near the bottom of the cylinder.

Without tracking, a concentration of approximately 3 can be achieved. It can be placed along an east–west axis. It requires only seasonal tracking. The concentrator

Fig. 6.12 Flat-plate collector with flat booster mirrors
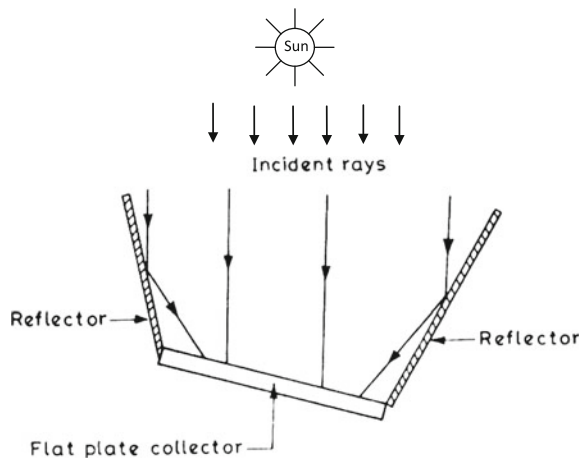
Fig. 6.13 Schematic view of
a Tabor–Zeimer cylindrical
concentrator
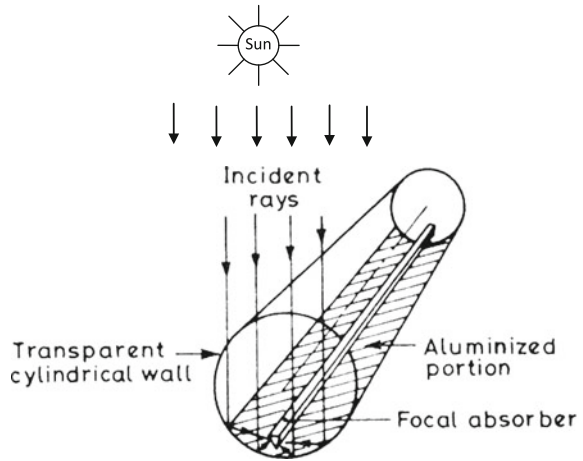
uses diffuse in addition to the beam component. The delivery temperatures and
collection thermal efficiencies are higher in comparison with those of the conventional FPC.

(iii)   **Compound parabolic solar concentrator (CPSC)**

This CPSC is a nonimaging one. It belongs to a family of concentrators with
maximum permissible concentration under thermodynamic limit for a particular
acceptance angle. Furthermore, it has a large acceptance angle. It needs to be
intermittently turned toward the Sun.

The first design of a CPSC was first made by Winston [3]. It consists of two
parabolic segments. It is oriented such that the focus of one is located at the bottom
end point of the other and vice versa as shown in Fig. 6.14. The axes of the
parabolic segments make an angle with the CPSC axis equal to the acceptance
angle. The slope of the reflector surfaces at the aperture plane is parallel to the

Fig. 6.14 Schematic
cross-section of a compound
parabolic concentrator (CPC)
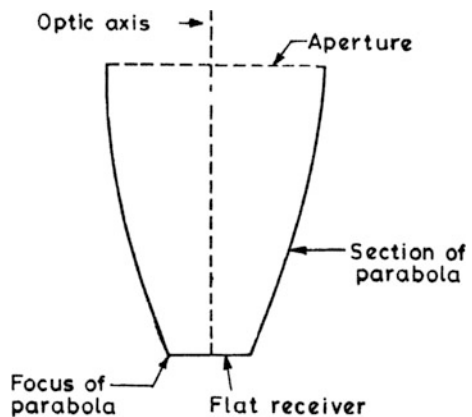
CPSC axis. The receiver is a flat surface parallel to the aperture joining the two foci of the reflecting surfaces.

Beam radiation (rays) incident in the central region of the aperture undergoes no reflection, whereas that near the edges undergoes one or more reflections. The numbers of reflections depend on (a) the incident angle, (b) the collector depth, and (c) the Concentration ratio [4].

To reduce the cost of the unit, the height of the CPC can be truncated by half from the bottom without any significant change in concentration ratio.

Extensive investigations have led to several modified designs of the ideal CPSC. The main modifications are mentioned as follows:

(i)   the use of receiver shapes like fins and circular pipes for better optical and thermal performance;
(ii) truncation of CPSC height to minimize the physical size and cost;
(iii) asymmetric orientation of source and aperture to provide seasonal varying outputs; and
(iv) design of the CPSC as a second-stage concentrator.

In view of the above modification, the reflecting surface of all resulting solar concentrators may not be parabolic. However, these still belong to the nonimaging group of concentrators.

The CPSC can be used in nontracking mode with a concentration ratios of approximately 6. However, for higher concentration ratios, the reflecting surface area becomes very large, and hence it cannot be used.

6.5   Theoretical Solar Image

In imaging-type concentrators, an image of the Sun is formed on the receiver/absorber. Because the Sun is not a point source, therefore even a perfect optical system produces an image of finite size. The Sun–Earth distance causes the solar disc to subtend an angle of $32'$ at a point on the Earth's surface (Fig. 6.17).

R_f is a reflector, and R_v is a plane receiver kept normal to the axis of the concentrator. Rays are shown to be incident at the edge from solar disc. After reflection, it forms the image on the receiver. If the distance between the point of incidence and the focus (mirror radius) is r, then the image size W is expressed as

$$W = \frac{2r(\tan 16')}{\cos \varphi} \tag{6.9}$$

where φ is the angle between the optical axis of the concentrator and the normal at the point of incidence (Fig. 6.15a).
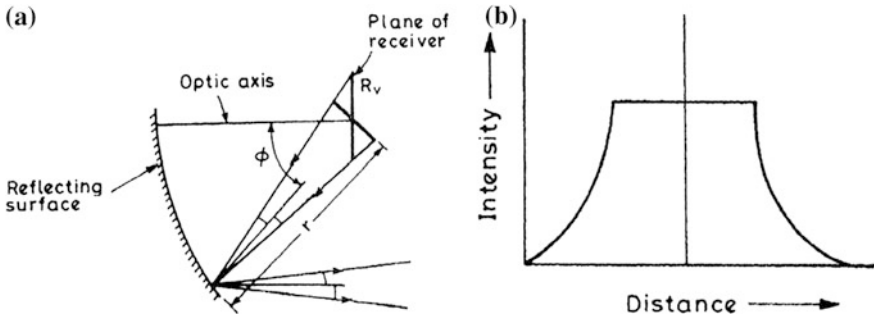
Fig. 6.15 Theoretical solar image schematic of **a** the compound parabolic concentrator's formation and **b** its cross-section

It may be noted that this theoretical image is subjected to modifications due to

(a) the solar disc is not uniformly bright with the centre being the brightest; and
(b) the actual concentrating systems are not precise optical systems.

6.6 Thermal Performance

Writing an energy balance to determine the performance of concentrator as shown in Figs. 6.1 and 6.14 is similar to writing one for FPC. Complications occur in the calculation of thermal losses from receiver/absorber due to the following reasons:

(i) Receiver shapes are widely variable and the beam radiation at the receiver is not uniform.
(ii) Due to the temperature being high, edge losses and conduction effects are significant.

The analytical expression for collection thermal efficiency will be discussed for following conditions: natural mode and forced mode.

6.6.1 Natural Mode

In this case, we follow the same procedure as done in the case of the FPC Sect. 5.7.

According to Eq. (5.50b), the instantaneous thermal efficiency, η_i, can be expressed as

$$\eta_i = (\dot{q}_u / I_b) \tag{6.10a}$$

where I_b is the incident beam radiation (Eq. 1.25); and $\dot{q}_u$ is the rate of useful thermal energy per unit aperture area given by Eq. (6.1e).

Equation (6.10a) can be rewritten as

$$\eta_i = \left[\rho(\alpha\tau) - \frac{1}{C} U_t \frac{(T_r - T_a)}{I_b} \right] \tag{6.10b}$$

Without thermal heat losses from the receiver, one has

$$\eta_i = \eta_0 = [\rho(\alpha\tau)] \tag{6.11}$$

Using Eq. (6.1d), the rate of useful thermal energy gain per unit length, in terms of the absorbed solar radiation per unit length, is obtained as

$$\dot{q}'_u = \frac{\dot{Q}_u}{L} = \left[\left(\frac{A_a}{L}\right) S - \left(\frac{A_r}{L}\right) U_t (T_p - T_a) \right] \tag{6.12}$$

where $S = \rho(\alpha\tau)I_b$ is the rate of absorbed beam radiation per unit area of unshaded receiver; and A_a and A_r are the aperture and receiver area of the concentrator, respectively.

Under steady-state conditions, the rate of useful thermal energy gain per unit collector length from the outer tube of the receiver/absorber (T_p) to the working fluid (T_f) can be written as

$$\dot{q}'_u = U_b \frac{A_r}{L} (T_p - T_f) \tag{6.13a}$$

where from Eq. (5.36), an expression for U_b is given by

$$\frac{1}{U_k} = \frac{1}{\frac{D_1}{D_2}(U_h)} + \frac{1}{U_c} + \frac{1}{\frac{2K_s}{D_2 \ln(D_2/D_1)}}$$

(a) **For a cylindrical copper tube** having inner and outer diameter as D_i and D_o, respectively

$$U_b = \frac{1}{\frac{D_o}{h_{fi}D_i} + \left(\frac{D_o}{2K} \ln \frac{D_o}{D_i}\right)} \tag{6.13b}$$

(b) **For a parallel flat-plate absorber/receiver**

$$U_b = \frac{1}{\left[\frac{1}{h_{fi}} + \frac{L_i}{K_i} + \frac{1}{h_i}\right]} \tag{6.13c}$$

Equations (6.12) and (6.13a)–(6.13c) can be rearranged as follows:

$$\dot{q}_u' / \left(\frac{A_r}{L} U_t \right) = \left[\left(\frac{A_a}{A_r} \right) \frac{1}{U_t} \rho(\alpha\tau) I_b - (T_p - T_a) \right] \tag{6.14a}$$

and

$$\dot{q}_u' / \left(\frac{A_r}{L} U_b \right) = (T_p - T_f) \tag{6.14b}$$

After addition of Eqs. (6.14a) and (6.14b), one gets

$$\dot{q}_u' \left[\frac{1}{\left(\frac{A_r}{L} U_t \right)} + \frac{1}{\left(\frac{A_r}{L} U_b \right)} \right] = \left[\left(\frac{A_a}{A_r} \right) \frac{1}{U_t} \rho(\alpha\tau) I_b - (T_f - T_a) \right] \tag{6.15a}$$

or

$$\dot{q}_u' = \left[\left(\frac{A_r}{L} U_t \right)^{-1} + \left(\frac{A_r}{L} U_b \right)^{-1} \right]^{-1} \left[\left(\frac{A_a}{A_r} \right) \frac{1}{U_t} \rho(\alpha\tau) I_b - (T_f - T_a) \right] \tag{6.15b}$$

Equation (6.15b) can also be written as

$$\dot{q}_u' = \frac{A_a}{L} F' \left[\rho(\alpha\tau) I_b - U_t \left(\frac{A_r}{A_a} \right) (T_f - T_a) \right] \tag{6.16}$$

where F' is the concentrator collection-efficiency factor, which is given by

$$F' = \frac{1/U_t}{\left[(U_t)^{-1} + (U_b)^{-1} \right]} = \frac{1/U_t}{1/U_L} \tag{6.17}$$

where the collector efficiency factor, F', is defined as the ratio between the thermal resistance from the receiver/absorber surface to the ambient air and the thermal resistance from the fluid to the ambient air (Sect. 5.7.3).

Equation (6.16) can further be written as the rate of thermal energy in W by

$$\dot{Q}_u = A_a F' \left[\rho(\alpha\tau) I_b - U_t \left(\frac{A_r}{A_a} \right) (T_f - T_a) \right] \tag{6.18}$$

The rate of thermal energy in W/m^2 is given by

$$\dot{q}_u = \frac{\dot{Q}_u}{A_a} = F' \left[\rho(\alpha\tau) I_b - U_t \left(\frac{A_r}{A_a} \right) (T_f - T_a) \right]$$

or

$$\dot{q}_u = \frac{\dot{Q}_u}{A_a} = F' \left[\rho(\alpha\tau)I_b - U_t \left(\frac{1}{C}\right)(T_f - T_a) \right] \tag{6.19}$$

where $C = \frac{A_a}{A_r}$ is the concentration ratio. Expressions for different geometries are discussed in the next section.

From Eq. (6.10a), one can obtain an expression for instantaneous thermal efficiency under the natural mode of operation of a CPC concentrator as follows:

$$\eta_i = \frac{\dot{q}_u}{I_b} = F' \left[\rho(\alpha\tau) - U_t \left(\frac{A_r}{A_a}\right) \frac{(T_f - T_a)}{I_b} \right]$$

or

$$\eta_i = \frac{\dot{q}_u}{I_b} = F' \left[\rho(\alpha\tau) - U_t \left(\frac{1}{C}\right) \frac{(T_f - T_a)}{I_b} \right] \tag{6.20}$$

6.6.2 Forced Mode

In the case of forced mode of operation of a CPC concentrator, the working fluid will flow through the circular tube and flat plate as shown in Fig. 6.16. The working fluid at inlet temperature T_{fi} is allowed to flow in the x-direction.

Let us consider an elemental length between 'x' and 'x + dx'. The fluid temperatures at 'x' and 'x + dx' are $T_f(x)$ and $T_f(x) + dT_f(x)$, respectively. Here the rate of heat available per unit length at fluid, Eq. (6.19), will be carried away by the working flowing fluid. Hence,

(a) **For circular conductive absorber/receiver tube**

$$\dot{q}'_u = \left(\frac{A_a}{L}\right) F' \left[\rho(\alpha\tau)I_b - U_t \left(\frac{A_r}{A_a}\right)(T_f - T_a) \right] = \dot{m} C_f \frac{dT_f}{dx} \tag{6.21a}$$

(b) **For parallel flat-plate conductive absorber/receiver**

$$\dot{q}'_u = \left(\frac{A_a}{L}\right) F' \left[\rho(\alpha\tau)I_b - (U_t + U_b) \left(\frac{A_r}{A_a}\right)(T_f - T_a) \right] = \dot{m} C_f \frac{dT_f}{dx}$$

Fig. 6.16 **a** Cross-sectional view of fluid flowing through a circular conducting pipe. **b** Cross-sectional view of fluid flowing through a parallel flat-plate glazed absorber/receiver
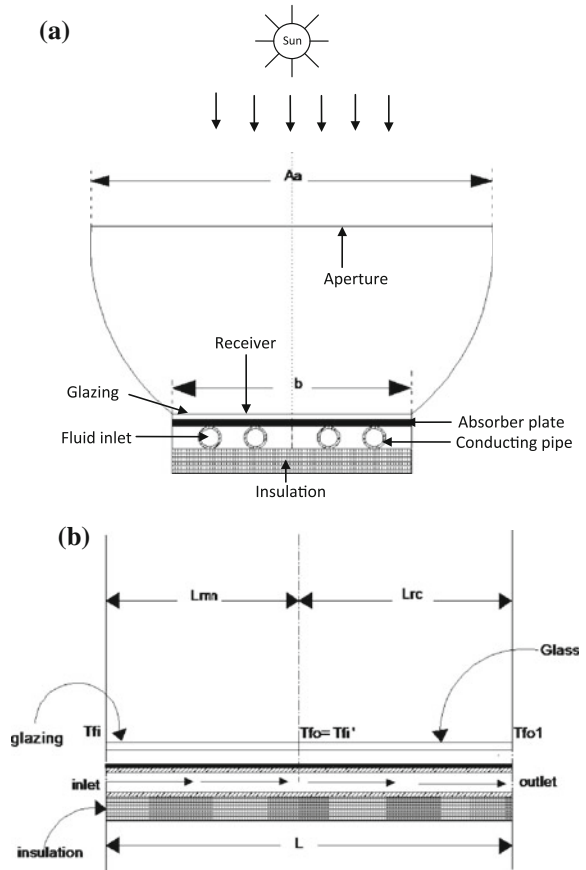
or

$$
\dot{q}'_u = \left(\frac{A_a}{L}\right) F' \left[\rho(\alpha\tau)I_b - U_L\left(\frac{A_r}{A_a}\right)(T_f - T_a) \right] = \dot{m}C_f \frac{dT_f}{dx} \tag{6.21b}
$$

where, $U_L = U_t + U_b$, T_f is the fluid temperature; $\dot{m}$ is the fluid mass-flow rate; T_a is an ambient temperature; and I_b is the beam radiation.

The difference in Eqs. (6.21a) and (6.21b) are as follows:

"U_t in the case of tube absorber is replaced by U_L for the absorber of the FPC"

After solving the one-order differential equation, the solution of Eqs. (6.21a) and (6.21b) becomes

$$\frac{\left[S - \left(\frac{A_r}{A_a}\right)U_t(T_{fo} - T_a)\right]}{\left[S - \left(\frac{A_r}{A_a}\right)U_t(T_{fi} - T_a)\right]} = \exp\left(-\frac{F'A_rU_t}{\dot{m}C_f}\right) \tag{6.22}$$

Here $S = \rho(\alpha\tau)I_b$ and the initial condition T_f at $x = 0$ are equal to T_{fi}. For derivation in details, see Sect. 5.7. Equation (6.22) can be also solved for an outlet-fluid temperature of the tube-type concentrator absorber/receiver, T_{fo}, as

$$T_{fo} = \left[\left(\frac{A_a}{A_r}\right)\frac{1}{U_t}S + T_a\right]\left\{1 - \exp\left(-\frac{F'A_rU_t}{\dot{m}C_f}\right)\right\} + T_{fi}\exp\left(-\frac{F'A_rU_t}{\dot{m}C_f}\right) \tag{6.23a}$$

An outlet-fluid temperature of a flat-type concentrator absorber/receiver, T_{fo}, can also be written as

$$T_{fo} = \left[\left(\frac{A_a}{A_r}\right)\frac{1}{U_L}S + T_a\right]\left\{1 - \exp\left(-\frac{F'A_rU_L}{\dot{m}C_f}\right)\right\} + T_{fi}\exp\left(-\frac{F'A_rU_L}{\dot{m}C_f}\right) \tag{6.23b}$$

The expression for the rate of heat transfer by the fluid under forced mode for a tubular absorber can be obtained using Eq. (6.23a) as

$$\begin{aligned}
\dot{Q}_u &= \dot{m}C_f(T_{fo} - T_{fi}) \\
&= \dot{m}C_f\left\{1 - \exp\left(-\frac{F'A_rU_t}{\dot{m}C_f}\right)\right\}\left[\left(\frac{A_a}{A_r}\right)\frac{1}{U_t}S - (T_{fi} - T_a)\right] \\
&= A_a\frac{\dot{m}C_f}{A_rU_t}\left\{1 - \exp\left(-\frac{F'A_rU_t}{\dot{m}C_f}\right)\right\}\left[S - U_t\left(\frac{A_r}{A_a}\right)(T_{fi} - T_a)\right]
\end{aligned}$$

or

$$\dot{Q}_u = A_aF_R\left[S - U_t\left(\frac{A_r}{A_a}\right)(T_{fi} - T_a)\right] \tag{6.24a}$$

where

$$S = \rho(\alpha\tau)I_b \quad \text{and} \quad F_R = \frac{\dot{m}C_f}{A_rU_t}\left\{1 - \exp\left(-\frac{F'A_rU_t}{\dot{m}C_f}\right)\right\}$$

which is known as the "mass flow–rate factor" for the concentrator.

The expression for the rate of heat transfer by the fluid under forced mode for a flat-plate absorber can be obtained using Eq. (6.23b) as

$$\dot{Q}_u = A_aF_R\left[S - U_L\left(\frac{A_r}{A_a}\right)(T_{fi} - T_a)\right] \tag{6.24b}$$

where

$$S = \rho(\alpha\tau)I_b \quad \text{and} \quad F_R = \frac{\dot{m}C_f}{A_r U_L}\left\{1 - \exp\left(-\frac{F'A_r U_L}{\dot{m}C_f}\right)\right\} \tag{6.24c}$$

The threshold intensity $(I_{b,th})$ for a single concentrator can be obtained as follows:

(a) **For a tube absorber**

To obtain the threshold intensity $(I_{b,th})$ for a single concentrator with a tube absorber/receiver, from Eq. (6.24a) one should have

$$\dot{Q}_u = A_a F_R\left[S - U_t\left(\frac{A_r}{A_a}\right)(T_{fi} - T_a)\right] \geq 0$$

which gives

$$I_{b,th} \geq \frac{U_t(T_{fi} - T_a)\left(\frac{A_r}{A_a}\right)}{\rho(\alpha\tau)} \tag{6.25a}$$

(b) **For a parallel flat absorber**

To obtain the threshold intensity $(I_{b,th})$ for single concentrator with a flat absorber/receiver, one should have the following from Eq. (6.24b)

$$\dot{Q}_u = A_a F_R\left[S - U_L\left(\frac{A_r}{A_a}\right)(T_{fi} - T_a)\right] \geq 0$$

which gives

$$I_{b,th} \geq \frac{U_L(T_{fi} - T_a)\left(\frac{A_r}{A_a}\right)}{\rho(\alpha\tau)} \tag{6.25b}$$

Because the numerical value of U_t is less than U_L, the threshold value for a tube-type absorber (Eq. 6.25a) is lower than that of the flat-type absorber (Eq. 6.25b).

Furthermore, an instantaneous thermal efficiency of the concentrator with tube absorber/receiver under forced mode can be obtained using Eq. (6.23a)

$$\eta_i = \frac{\dot{Q}_u}{A_b I_b} = F_R\left[\rho(\alpha\tau) - U_L\left(\frac{A_r}{A_a}\right)\frac{(T_{fi} - T_a)}{I_b}\right] \tag{6.26a}$$

In addition, an optical efficiency of the concentrator can be obtained as

$$\eta_i = \frac{\dot{Q}_u}{\rho(\alpha\tau)A_b I_b} = F_R \left[1 - U_L \left(\frac{A_r}{A_a} \right) \frac{(T_{fi} - T_a)}{I_b} \right] \tag{6.26b}$$

The optical efficiency will be greater than the thermal efficiency.

Example 6.2 A cylindrical parabolic concentrator having 2.0 m width and 8 m length has an absorbed radiation of 400 W/m^2. The absorber and the transparent envelope have a diameter of 55 and 85 mm, respectively. The inlet temperature of the fluid entering the absorber is 220 °C at a mass-flow rate of 0.04 kg/s. Calculate the useful gain and exit-fluid temperature for the following parameters:

$C_p = 3.26$ kJ/kg °C, $h_{fc} = 280$ W/m^2 °C, $U_L = 12$ W/m^2 °C, $K = 16$ W/m °C, $L = 5$ mm. $T_a = 22$ °C.

Solution
The area of the receiver $(A_r) = \pi DL = \pi \times 0.055 \times 8 = 1.382$ m^2:

The aperture area, by considering the shading of the central part of the collector, is given by

$$A_a = (2.0 - 0.085) \times 8 = 15.32 \text{ m}^2$$

The collector-efficiency factor is given by

$$F' = \frac{1/U_L}{\frac{1}{U_L} + \frac{D_2}{h_{fi}D_1} + \left(\frac{D_2}{2K} \ln \frac{D_2}{D_1} \right)}$$

or

$$F' = \frac{1/12}{\frac{1}{12} + \frac{0.055}{280 \times 0.045} + \frac{0.055}{2 \times 16} \ln \left(\frac{0.055}{0.045} \right)} = 0.946$$

The flow-rate factor F_R is given by Eq. (6.24c), and its value is calculated as

$$F_R = \frac{\dot{m}C_f}{A_r U_L} \left\{ 1 - \exp\left(-\frac{F'A_r U_L}{\dot{m}C_f} \right) \right\}$$

Here,

$$\frac{\dot{m}C_f}{F'A_r U_L} = \frac{0.04 \times 3.26 \times 10^3}{1.382 \times 12 \times 0.946} = 8.32$$

Substituting the above values into the expression for F_R, we obtain

$$F_R = 7.87 \left[1 - \exp\left(-\frac{1}{8.32} \right) \right] = 0.89$$

Now, the rate of useful gain is given by

$$\dot{Q}_u = A_a \times F_R \left[S - \frac{A_r \times U_L}{A_a} (220 - 22) \right]$$

$$= 15.32 \times 0.89 \left[400 - \frac{1.382 \times 12}{15.32} (220 - 22) \right] = 2531$$

and the exit fluid temperature is given by

$$T_0 = T_i + \frac{\dot{Q}_u}{\dot{m}_f C_f} = 220 + \frac{2531}{0.04 \times 3260} = 239 \,^\circ C$$

6.6.3 N-Solar Concentrators Connected in Series

(a) N-Solar Concentrators with a tube absorber/receiver

According to Sect. 5.8.2, the outlet-fluid temperature at Nth concentrator can be written as follows:

$$T_{foN} = \left[\left(\frac{A_a}{A_r} \right) \frac{1}{U_t} S + T_a \right] \left\{ 1 - \exp\left(-\frac{NF'A_r U_t}{\dot{m} C_f} \right) \right\} + T_{fi} \exp\left(-\frac{NF'A_r U_t}{\dot{m} C_f} \right)$$

$$(6.27a)$$

(b) N-Solar Concentrators with a flat-plate absorber/receiver tube

In this case, too, the outlet-fluid temperature at the Nth concentrator can be written as follows:

$$T_{foN} = \left[\left(\frac{A_a}{A_r} \right) \frac{1}{U_L} S + T_a \right] \left\{ 1 - \exp\left(-\frac{NF'A_r U_L}{\dot{m} C_f} \right) \right\} + T_{fi} \exp\left(-\frac{NF'A_r U_L}{\dot{m} C_f} \right)$$

$$(6.27b)$$

For constant collection temperature, i.e., $T_{foN} = T_0$, an expression for mass-flow rate can be obtained from the above equation as

$$\dot{m}_{\mathrm{f}} = -\frac{NF'A_{\mathrm{r}}U_{\mathrm{L}}}{C_{\mathrm{f}}} \left[\ln \frac{T_0 - \left(\frac{A_{\mathrm{a}}}{A_{\mathrm{r}}}\frac{S}{U_{\mathrm{L}}} + T_{\mathrm{a}}\right)}{T_{\mathrm{fi}} - \left(\frac{A_{\mathrm{a}}}{A_{\mathrm{r}}}\frac{S}{U_{\mathrm{L}}} + T_{\mathrm{a}}\right)} \right]^{-1} \tag{6.27c}$$

The expression for the rate of heat transfer by the fluid under forced mode can be obtained using Eq. (6.24a) as follows:

(a) **For a tubular absorber**

$$\dot{Q}_{\mathrm{uN}} = \dot{m}C_{\mathrm{f}}(T_{\mathrm{foN}} - T_{\mathrm{fi}})$$

$$\dot{Q}_{\mathrm{uN}} = NA_{\mathrm{a}}F_{\mathrm{RN}}\left[S - \left(\frac{A_{\mathrm{r}}}{A_{\mathrm{a}}}\right)U_{\mathrm{t}}(T_{\mathrm{fi}} - T_{\mathrm{a}})\right] \tag{6.28a}$$

where

$$S = \rho(\alpha\tau)I_{\mathrm{b}} \quad \text{and} \quad F_{\mathrm{RN}} = \frac{\dot{m}C_{\mathrm{f}}}{NA_{\mathrm{r}}U_{\mathrm{t}}}\left\{1 - \exp\left(-\frac{NF'A_{\mathrm{r}}U_{\mathrm{t}}}{\dot{m}C_{\mathrm{f}}}\right)\right\},$$

which is known as the "concentrator mass flow–rate factor."

(b) **For a parallel flat-plate absorber**

The expression for the rate of heat transfer by the fluid under forced mode for a flat-plate absorber can be obtained using Eq. (6.26b) as

$$\dot{Q}_{\mathrm{uN}} = NA_{\mathrm{a}}F_{\mathrm{RN}}\left[S - \left(\frac{A_{\mathrm{r}}}{A_{\mathrm{a}}}\right)U_{\mathrm{L}}(T_{\mathrm{fi}} - T_{\mathrm{a}})\right] \tag{6.28b}$$

where

$$S = \rho(\alpha\tau)I_{\mathrm{b}} \quad \text{and} \quad F_{\mathrm{RN}} = \frac{\dot{m}C_{\mathrm{f}}}{NA_{\mathrm{r}}U_{\mathrm{L}}}\left\{1 - \exp\left(-\frac{NF'A_{\mathrm{r}}U_{\mathrm{L}}}{\dot{m}C_{\mathrm{f}}}\right)\right\}$$

6.6.4 m-Solar Concentrators Connected in Parallel

The expression for the rate of heat transfer by the fluid under forced mode for an m-tubular absorber can be obtained using Eq. (6.24a) as

$$\dot{Q}_u = \dot{m}C_f(T_{fo} - T_{fi})$$

$$= mA_aF_R\left[S - U_t\left(\frac{A_r}{A_a}\right)(T_{fi} - T_a)\right] \tag{6.29}$$

where

$$S = \rho(\alpha\tau)I_b \quad \text{and} \quad F_R = \frac{\dot{m}C_f}{mA_rU_t}\left\{1 - \exp\left(-\frac{mF'A_rU_t}{\dot{m}C_f}\right)\right\},$$

which is known as the "mass flow–rate factor for m-concentrators connected in parallel."

6.6.5   Solar Concentrators Connected in Parallel and Series Combination

One can follow the procedure given in Sect. 5.8.3 to obtain an analytical expression for the rate of useful energy for a combination of series and parallel concentrators.

6.7   Solar Concentration Ratio (C)

To improve the performance of a solar concentrator, the rate of thermal losses from the receiver, namely, (a) $U_t(T_{fi} - T_a)$ for a tubular absorber and (b) $U_L(T_{fi} - T_a)$ for a flat-plate absorber/receiver, must be minimized. This implies that the area of absorber/receiver (A_r) should be small. However, smaller the size of the absorber implies a lower intercept factor. Thus, it leads to poor optical performance. Hence, a compromise must be made between optical and thermal performance of the solar concentrator to obtain a suitable concentration ratio. From the point of view of thermodynamic considerations, the upper limit of the concentration of any concentrating collector has been obtained by Rabl [4] and Rabl and Winston [5]. It is observed that the maximum possible concentration is the reciprocal of the radiation shape factor between the Sun and the solar concentrator. This limit is valid for a given acceptance angle $(2\theta_c)$ as shown in Fig. 6.1. Practical values of acceptance angle vary from a minimum value subtended by the disc of Sun approximately 0.5°–180°. This corresponds to a FPC receiving solar radiation from a full hemisphere.

Line focus or trough-like concentrators have the radiation shape factor (F_{A-S}) for two-dimensional geometries, which is given by

$$F_{A-S} = \sin \theta_c \tag{6.30a}$$

Hence, the thermodynamic concentration limit is given by

$$C = 1/\sin \theta_c \tag{6.30b}$$

A point-focus of dish-like concentrators has the shape factor and concentration limits for three-dimensional geometries, which are given by

$$F_{A-S} = \sin^2 \theta_c \tag{6.31}$$

and

$$C = 1/\sin^2 \theta_c \tag{6.32}$$

Example 6.3 Determine the solar-concentration ratio (C) for a two-dimensional geometry if the acceptance angle is 30° and compare the result with that of a three-dimensional geometry.

Solution
From Eq. (6.30b), for two-dimensional geometry we have $C = 1/\sin \theta_c$.
   For $\theta_c = 15°$, $C = 1/\sin 15° = 3.86$.
   From Eq. (6.32), for three-dimensional geometry we have $C = 1/\sin^2 \theta_c$.
   For θ_c, we get, $C = 1/\sin^2 15° = 14.93$.
   This shows that, for the same acceptance angle the concentration ratio is more in three dimension geometry.
   The maximum limit is determined from the minimum acceptance angle by considering the optical concepts. The solar concentrator is always facing the Sun; hence, the acceptance half-angle (θ_c) is equal to the half-angle of the solar disc (about 0.25°). Equations (6.30b) and (6.32) show that the concentration limit for a two-dimensional concentrator and three-dimensional concentrator is of the order of 200 and 40,000, respectively.
   However, in practice, solar concentrations are different due to the finite acceptance angles. Furthermore, the cosine effect reduces the energy gain at hours far from solar noon in nontracking collectors.
   The concentrations of some concentrators for different types of absorbers are discussed below.

6.7.1 Cylindrical Parabolic Solar Concentrator

The solar-concentration ratio for a flat-absorber (one-sided) is given by

$$C = \frac{\sin \phi \, \cos(\phi + \theta_c)}{\sin \theta_c} - 1 \tag{6.33}$$

The solar-concentration ratio (C) can be determined by using the relation for two-sided flat absorber,

$$C_{2-\text{sided}} = \frac{1}{2}[C_{1-\text{sided}} + 1] \tag{6.34}$$

The solar-concentration ratio (C) for a tube-absorber, is given by

$$C = (\sin \phi)/(\pi \, \sin \theta_c) \tag{6.35a}$$

The optimum value of rim angle (ϕ) for maximum geometrical concentration can be determined by the following condition:

$$\left.\frac{dt}{d\phi}\right|_{(\phi)_{\text{optimum}}} = 0 \tag{6.35b}$$

The $(\phi)_{optimum}$ and the corresponding solar-concentration ratio are given as follows:

(a) For a flat-plate absorber/receiver (one-sided)

$$(\phi)_{\text{optimum}} = (\pi/4) - (\theta_c/2) \tag{6.36}$$

and

$$C_{(\phi)_{\text{optimum}}} = (1/2)[(1/\sin \theta_c) - 3] \tag{6.37}$$

(b) For a cylindrical absorber

$$(\phi)_{\text{optimum}} = (\pi/2) \tag{6.38}$$

and

$$C_{(\phi)_{optimum}} = (1/\pi)(1/\sin\theta_c) \qquad (6.39)$$

We can see that if the optical limit is considered, i.e., $\theta_c = 0.25°$, then (a) for a cylindrical absorber, the solar concentration becomes 73 and (b) for a flat absorber (one-sided), it is 113. Thus, the highest possible solar concentrations and the practical values lie below these limits.

6.7.2 Three-Dimensional Concentrator

The solar-concentration ratio (C) for a flat absorber (one-sided) is given by

$$C = \frac{\sin^2\phi \, \cos^2(\phi + \theta_c)}{\sin^2\theta_c} - 1 \qquad (6.40)$$

and for a spherical absorber it is given by

$$C = \frac{\sin^2\phi}{4 \times \sin^2\theta_c} \qquad (6.41)$$

The optimum rim angle can also be determined as discussed previously. One can see that the condition of a flat-plate absorber (one-sided) remains the same, whereas for a spherical absorber its value is $(\phi)_{optimum} = \pi/2$. For $\theta_c = (1/4)°$, the maximum possible solar concentration is 1300 in both absorbers.

6.7.3 Hemispherical Bowl Mirror

The solar (C) solar concentration for a circular cylinder absorber is

$$C = \frac{\sin^2\phi}{\sin\theta_c} \qquad (6.42)$$

The optimum value of ϕ is $(\pi/2)$. For $\theta_c = (1/4)°$, the maximum possible solar concentration is 229. This concentrator cannot achieve the solar-concentration ratios of the paraboloid-type concentrator.

It may be noted that its aperture is not always normal to the Sun rays due to the fixed position. Hence the solar-concentration ratio (C) is decreased by the cosine factor and it is given by

$$C_{\text{eff}} = \frac{\sin^2 \phi}{\sin \theta_{\text{c}}} \cos \theta \tag{6.43}$$

where the angle of incidence of Sun's rays on the reflector is denoted by θ.

Example 6.4 Determine the solar-concentration ratio for a hemispherical bowl mirror for an acceptance half angle of $60°$. Compare the result with cylindrical parabolic concentrator and a spherical absorber.

Solution

From Eq. (6.42), we have $C = \frac{\sin^2 \phi}{\sin \theta_{\text{c}}}$.

For $\theta_{\text{c}} = 30°$ and $\phi = \pi/2$, $C = 2.0$.

Now, Eq. (6.35a) gives $C = (\sin \phi)/(\pi \sin \theta_{\text{c}}) = 0.637$.

Furthermore, for a spherical absorber, From Eq. (6.41), we have $C = \frac{\sin^2 \phi}{4 \times \sin^2 \theta_{\text{c}}} = 1$.

6.8   Solar Tracking

6.8.1   Three-Dimensional Solar Concentrators

For point-focus solar-concentrating systems, three-dimensional concentrators are required to continuously track the motion of the Sun for maximum brightness concentration and radiation balance. This is because their acceptance angles are small for the small absorber. Hence, solar collectors must be tracked along two axes to keep the Sun on the absorbers/receivers.

Geometries of fully tracking mountings are polar, azimuth, altitude–altitude, and horizontal yoke mountings etc. [6]. The simplest one is the polar mounting. In this case, one axis is placed parallel to the Earth's axis, and the second axis orthogonal. For the solar collector, if one axis is inclined with the horizontal at a latitude angle, then the axis is parallel to the Earth's axis, and the other axis is normal to it. This mounting is referred to as "polar mounting." The diurnal solar motion is required to track about the polar axis only.

Generally, two-axes tracking is required for all other configurations. A number of complications arise due to the nonlinear motion of the Sun. There are other mountings for mechanical motion. One such mounting for mechanical motion is the altitude–azimuth mounting. In this case, one axis is horizontal, and the other one is vertical. Being in the vertical plane of the concentrator, gravitational attractions are also minimized.

The mounting for heliostats results in the generalized case of nonlinear motion in two coordinates. The kinematics of the generalized heliostat is given by Meinel [1].

6.8.2 Two-Dimensional Solar Concentrators

Two-dimensional/line-focussing solar concentrators are moved only in one coordinate to track the motion of Sun. There are a number of feasible mounting configurations. The most commonly used mountings are with the long axis facing either north–south or east–west. For troughs oriented toward the north–south, the solar concentrators are moved to track the diurnal motion of the Sun. In this case, the long axis can be either horizontal or with an inclination equal to the latitude. The latter mounting is the polar mounting as discussed previously. If in addition to east–west tracking, north–south tracking is introduced; then the Sun always stays normal to the aperture for maximum availability of solar radiation on the aperture.

With east-west tracking, it must be noted that solar concentrators must be separated from each other in the north–south orientation so as to eliminate self shading. This problem is acute for the shallow Sun's angle during the morning and afternoon. In this case, more land area is required compared with the east–west orientation.

The east–west orientation is the most common for line-focussing solar concentrators. The motion of Sun then coincides with the long axis. Hence, the performance is similar to that of the FPC. It follows the pattern of solar intensity, i.e., maximum at noon and falling off on either side. As a result, these concentrators collect some diffuse energy from the Sun.

6.9 Materials for Solar Concentrators

The availability of suitable materials determines the effective use of solar energy. We briefly discuss the major material problems associated with the different components of solar concentrators.

6.9.1 Reflecting and Refracting Surfaces

Solar reflectors should have (a) high reflectivity and (b) good specular reflectance. No surface is perfectly specular due to either micro-roughness or surface undulation. For a low solar-concentration ratio, the reflector does not need to be highly specular. Glass silvered either on the rear or a second surface is usually used as mirror materials. Front-surface mirrors can also be used. Aluminium can also be used for the same purpose. It is protected by a coating of aluminium oxide, magnesium fluoride, or cerium oxide. Other materials, such as metalized plastic films and thin metal sheets, are also useful. Aluminium and silver with a total reflectivity

of approximately 85–90 and 95 %, respectively, are very good reflecting surfaces for solar energy applications. Silver is not adequate for front-surface mirrors.

Glass is the most durable material with low iron content. It can be used as a transmitting material. Currently plastics are used as refracting substances. Polymethyl methacrylate is generally used because it is weather resistant. Acrylic has been found to be an excellent material for Fresnel lenses because acrylic can be easily moulded or extruded.

For easy installation of reflectors and refractors, they should be light in weight. They should be able to withstand wind and extreme weather. Dust, sand, and other contamination strongly affect performance although the effect varies with the type of material used, collector configuration, exposure time, and site. The surfaces must be cleaned regularly.

6.9.2 Receiver Covers and Surface Coatings

A simple flat receiver is used in either parabolic concentrators or simple nonimaging-type (V-trough) concentrators, particularly at low-temperature applications. Glass and transparent plastic films are generally used as glazed materials for the receiver. Glass should have a low iron content to reduce absorption. Its surface should be etched to reduce reflection losses. A double-etching process can give better results with increased cost. Plastics are not suitable as cover materials due to low service temperature limit and ultraviolet degradation. Evacuated tube receivers have also been used to eliminate convection heat losses.

Coatings are required to have strong absorptivity and stability at high temperatures and are also cost effective. Black chrome appears to be the best among the selective coatings. It can be electroplated on steel, copper, and aluminium, etc. Other metal-oxide coatings, namely, black copper oxide and black nickel, are also used. Selective paints, such as lead sulphide particles in a silicon binder, can also be used.

6.9.3 Working Fluids

For effective heat transfer, the fluid should be (i) stable at high temperatures and (ii) noncorrosive and safe. It also should be cost-effective. Air is attractive for heating and cooling applications. However, the heat transfer is very poor. The most commonly used working fluids are pressurized water, liquid metals, therminol 55, and Mobile therm 603.

6.9.4   Insulation

Insulation is required to reduce heat losses from the unirradiated portions of the receiver. It is also used in the pipes carrying the working fluid. In addition to cost-effectiveness, the insulation should be strong enough to withstand high-temperature fluctuations. Commonly used insulations are fibre glass with and without binder, urethane foams, and mineral fibre blankets.

6.10   Photovoltaic Thermal (PVT) Concentrator

In a solar concentrator, the forced mode of operation is practical, which is going to be used for power generation. For such application, the fluid is chosen as per requirement. The receiver/absorber in a concentrator can be classified as follows:

(a) **Glazed tube–type**: In this case, the annular spacing between the selective coated copper tube and co-axial glazed tube can be evacuated for reducing convective heat loss between the annular spacing ($h_{1c} = 0$). There will be only radiative loss between annular spacing. It is not feasible to integrate a semi-transparent photovoltaic module with a glazed receiver/absorber.

(b) **Parallel flat-plate receiver/absorber**: In such configuration, it is possible to integrate a semitransparent photovoltaic (PV) module with a glazed receiver/absorber. However, fluid other than water flowing between two parallel receivers/absorbers is not practical due to high operating temperature (≈ 300 °C) and the leakage problem associated with this.

(c) **Tube-in-plate–type receiver/absorber**: In this case, the heat capacity of the fluid is reduced in comparison with parallel flat-plate absorber, and hence the operating temperature becomes greater. Furthermore, leakage of fluid due to high pressure is minimized. In addition, it is easier to integrate a semitransparent PV module with the glazed surface of receiver/absorber as has been done in the case of PVT FPC.

In this section, the tube-in-plate–type receiver/absorber configuration concentrator will be considered for thermal analysis.

6.10.1   Single Photovoltaic Thermal (PVT) Concentrator [7]

As shown in Fig. 6.17a, the tube-in-plate–type receiver/absorber base concentrator is considered. The energy balance equation for such a system will be same as in the case of a PVT water FPC with some modification, which will be discussed below.
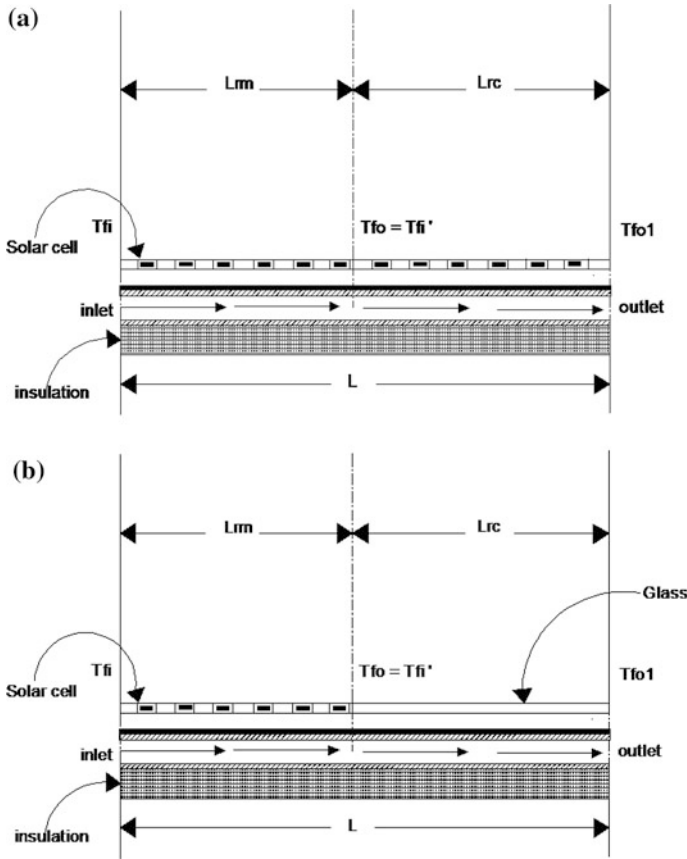
Fig. 6.17 a Cross-sectional side view of fully covered PVT-CPC water collector. **b** Cross-sectional side view of a proposed partially covered PVT-CPC water collector

(A) **Lower portion of the tube in a tube-in-plate–type receiver/absorber base concentrator up to length 'L' is covered by a semitransparent PV module (Fig. 6.17b)**

(a) **For semitransparent photovoltaic (PV) module**

$$\rho\alpha_c\tau_g\beta_c I_b A_a = \left[U_{tc,a}(T_c - T_a) + h_{p.c}(T_c - T_p)\right]A_{rm} + \rho\eta_m I_b A_a \qquad (6.44)$$

(b) **For blackened tube in plate-type receiver/absorber**

$$\rho\alpha_p\tau_g^2(1 - \beta_c)I_b A_a + h_{p.c}[(T_c - T_p)]A_{rm} = \left[F'h_{p.f}(T_p - T_f)\right]A_{rm} \qquad (6.45)$$

(c) **Flowing fluid through**

$$\dot{m}_\mathrm{f} C_\mathrm{f} \frac{\mathrm{d}T_\mathrm{f}}{\mathrm{d}x} \mathrm{d}x = F' \left[h_\mathrm{p,f} (T_\mathrm{p} - T_\mathrm{f}) \right] W \mathrm{d}x \tag{6.46}$$

where $A_\mathrm{rm} = WL$, W and L are the breath and length, respectively, of a blackened tube in a plate-type receiver/absorber below the PV module. The 'dx' is the elemental length along the length of the blackened tube in a plate-type receiver/absorber. An expression for F' is given by Eq. (5.62).

Equations (6.44) and (6.45) can be solved for T_c and T_p, which are given by

$$T_\mathrm{c} = \frac{(\alpha\tau)_{1,\mathrm{eff}} I_\mathrm{b} + U_\mathrm{tc,a} T_\mathrm{a} + h_\mathrm{c,p} T_\mathrm{p}}{(U_\mathrm{tc,a} + h_\mathrm{c,p})} \tag{6.47}$$

and

$$T_\mathrm{p} = \frac{(\alpha\tau)_{2,\mathrm{eff}} I_\mathrm{b} + PF_1 (\alpha\tau)_{1,\mathrm{eff}} I_\mathrm{b} + U_\mathrm{L1} T_\mathrm{a} + F' h_\mathrm{p,f} T_\mathrm{f}}{(U_\mathrm{L1} + F' h_\mathrm{p,f})} \tag{6.48}$$

where $(\alpha\tau)_{1,\mathrm{eff}} = \rho \left(\alpha_\mathrm{c} \tau_\mathrm{g} \beta_\mathrm{c} - \eta_\mathrm{m} \right) \frac{A_\mathrm{a}}{A_\mathrm{rm}}$; $(\alpha\tau)_{2,\mathrm{eff}} = \rho \alpha_\mathrm{p} \tau_\mathrm{g}^2 (1 - \beta_\mathrm{c}) \frac{A_\mathrm{a}}{A_\mathrm{rm}}$

$PF_1 = \frac{h_\mathrm{c,p}}{(U_\mathrm{tc,a} + h_\mathrm{c,p})}$ is the first penalty factor due to the PV module.

$U_\mathrm{L1} = \frac{h_\mathrm{c,p} U_\mathrm{tc,a}}{(U_\mathrm{tc,a} + h_\mathrm{c,p})}$ is an overall top heat-transfer coefficient from the receiver/absorber to the ambient air through the PV module.

Equation (6.42), with help of Eqs. (6.47) and (6.48), can be rewritten as follows:

$$\dot{m}_\mathrm{f} C_\mathrm{f} \frac{\mathrm{d}T_\mathrm{f}}{\mathrm{d}x} \mathrm{d}x = F' \left[PF_2 (\alpha\tau)_{\mathrm{m,eff}} I_\mathrm{b} - U_\mathrm{L,m} (T_\mathrm{f} - T_\mathrm{a}) \right] W \mathrm{d}x \tag{6.49}$$

where

$$(\alpha\tau)_{\mathrm{m,eff}} = PF_1 (\alpha\tau)_{1,\mathrm{eff}} + (\alpha\tau)_{2,\mathrm{eff}} \tag{6.50}$$

$PF_2 = \frac{F' h_\mathrm{p,f}}{(U_\mathrm{L,m} + F' h_\mathrm{p,f})}$ is the second penalty factor due to the PV module.

$U_\mathrm{Lm} = \frac{U_\mathrm{L1} F' h_\mathrm{p,f}}{(U_\mathrm{L1} + F' h_\mathrm{p,f})}$ is an overall top heat-transfer coefficient from the receiver/absorber to the ambient air through the PV module.

With the following initial condition, $T_\mathrm{f} = T_\mathrm{fi}$ at $x = 0$, the solution of Eq. (6.49) can be written as

$$\frac{T_\mathrm{f} - T_\mathrm{a} - \left(\frac{PF_2 (\alpha\tau)_{\mathrm{m,eff}} I_\mathrm{b}}{U_\mathrm{Lm}} \right)}{T_\mathrm{fi} - T_\mathrm{a} - \left(\frac{PF_2 (\alpha\tau)_{\mathrm{m,eff}} I_\mathrm{b}}{U_\mathrm{Lm}} \right)} = \exp\left(-\frac{F' U_\mathrm{L,m} W x}{\dot{m}_\mathrm{f} C_\mathrm{f}} \right) \tag{6.51}$$

or

$$T_f = \left[\left(\frac{PF_2(\alpha\tau)_{m,eff}I_b}{U_{Lm}} \right) + T_a \right] \left\{ 1 - \exp\left(-\frac{F'U_{L,m}Wx}{\dot{m}_f C_f} \right) \right\} + T_{fi} \exp\left(-\frac{F'U_{L,m}Wx}{\dot{m}_f C_f} \right)$$

(6.52)

The outlet-fluid temperature at the end of the PV module ($T_f = T_{fo}$ at $x = L$) is given by

$$T_{fo} = \left[\left(\frac{PF_2(\alpha\tau)_{m,eff}I_b}{U_{Lm}} \right) + T_a \right] \left\{ 1 - \exp\left(-\frac{F'U_{L,m}WL}{\dot{m}_f C_f} \right) \right\} + T_{fi} \exp\left(-\frac{F'U_{L,m}WL}{\dot{m}_f C_f} \right)$$

or

$$T_{fo} = \left[\left(\frac{PF_2(\alpha\tau)_{m,eff}I_b}{U_{Lm}} \right) + T_a \right] \left\{ 1 - \exp\left(-\frac{F'U_{L,m}A_{rm}}{\dot{m}_f C_f} \right) \right\} + T_{fi} \exp\left(-\frac{F'U_{L,m}A_{rm}}{\dot{m}_f C_f} \right)$$

(6.53)

The rate of thermal energy available at the outlet of the PV module can be written as

$$\dot{Q}_{um} = \dot{m}_f C_f(T_{fo} - T_{fi}) = A_{rm}F_{Rm}\left[PF_2(\alpha\tau)_{m,eff}I_b - U_{Lm}(T_{fi} - T_a) \right]$$

(6.54a)

where F_{Rm} is flow-rate factor for the PVT configuration of the concentrator, which is given by

$$F_{Rm} = \frac{\dot{m}_f C_f}{U_{L,m}A_{rm}} \left\{ 1 - \exp\left(-\frac{F'U_{L,m}A_{rm}}{\dot{m}_f C_f} \right) \right\}$$

(6.54b)

(B) **Upper portion of the tube in a plate-type receiver/absorber base concentrator up to length 'L_1' is covered by a glass cover**

In this case, the outlet-fluid temperature, T_{fo}, of the PV-covered portion of absorber will be the inlet temperature of the glass-covered upper portion of the absorber/receiver.

An expression for the outlet-fluid temperature at the end of the conventional FPC is similar to Eq. (5.110), which can be written as [7]

$$T_{fo1} = \left[\frac{A_{c1}}{A_{cr1}} \left(\frac{(\alpha\tau)_{c1eff,}}{U_{Lc1}} \right) I_b + T_a \right] \left\{ 1 - \exp\left(-\frac{F'U_{Lc1}A_{cr1}}{\dot{m}_f C_f} \right) \right\} + T_{fi} \exp\left(-\frac{F'U_{Lc1}A_{rc1}}{\dot{m}_f C_f} \right)$$

(6.55a)

The rate of thermal energy available at the end of glass-covered absorber/receiver at the upper portion will also be same as Eq. (5.110a) (conventional FPC). This can be written as

$$\dot{Q}_c = \dot{m}_f C_f (T_{fo1} - T_{fi1}) = A_{c1} F_{Rc}\left[(\alpha\tau)_{c1,eff} I_b - \frac{A_{cr1}}{A_{c1}} U_{L,c1}(T_{fi1} - T_a)\right] \quad (6.55b)$$

where

$$F_{Rm} = \frac{\dot{m}_f C_f}{U_{L,c1} A_{cr1}}\left\{1 - \exp\left(-\frac{F' U_{L,c1} A_{cr1}}{\dot{m}_f C_f}\right)\right\}$$

Here $T_{fi1} = T_{fo}$, (Eq. 6.53), the expression for final outlet temperature from the first semitransparent PVT flat-plate water collector, can be obtained as

$$
\begin{aligned}
T_{fo1} = &\left[\frac{A_{c1}}{A_{cr1}}\left(\frac{(\alpha\tau)_{c1eff.}}{U_{Lc1}}\right)I_b + T_a\right]\left\{1 - \exp\left(-\frac{F' U_{Lc1} A_{cr1}}{\dot{m}_f C_f}\right)\right\} \\
&+ \left[\left[\left(\frac{PF_2(\alpha\tau)_{m,eff} I_b}{U_{Lm}}\right) + T_a\right]\left\{1 - \exp\left(-\frac{F' U_{L,m} A_{rm}}{\dot{m}_f C_f}\right)\right\} + T_{fi}\exp\left(-\frac{F' U_{L,m} A_{rm}}{\dot{m}_f C_f}\right)\right]\exp\left(-\frac{F' U_{Lc1} A_{cr1}}{\dot{m}_f C_f}\right)
\end{aligned}
$$
$$(6.56)$$

According to Sect. 5.9.2, an expression for the rate of thermal energy available from the first semitransparent PVT concentrator can be written as,

$$\dot{Q}_{u1} = \left[\{AF_R(\alpha\tau)\}_1 I_b - \{AF_R U_L\}_1 (T_{fi} - T_a)\right] \quad (6.57)$$

where

$$\{AF_R(\alpha\tau)\}_1 = \left[A_{rm} F_{Rm} PF_2(\alpha\tau)_{m,eff}\left(1 - \frac{A_{c,1} F_{Rc} U_{Lm}}{\dot{m}_f C_f}\right) + \frac{A_{c1}}{A_{cr1}} F_{Rc}(\alpha\tau)_{c1eff}\right] \quad (6.58a)$$

and

$$\{AF_R U_L\}_1 = \left[A_{rm} F_{Rm} U_{Lm}\left(1 - \frac{A_{c,1} F_{Rc} U_{L,c1}}{\dot{m}_f C_f}\right) + A_{c,1} F_{Rc} U_{L,c1}\right] \quad (6.58b)$$

with

$$(\alpha\tau)_{m,eff} = \left[PF_1(\alpha\tau)_{1,eff} + (\alpha\tau)_{2,eff}\right] \quad (6.58c)$$

An instantaneous efficiency of the first semitransparent PVT concentrator can be defined and written as

$$\eta_i = \frac{\dot{Q}_{u1}}{(A_{rm} + A_{cr1})I_b}$$

or

$$\eta_i = \frac{1}{(A_{rm} + A_{cr1})}\left[(AF_R(\alpha\tau))_1 - (AF_R U_L)_1\frac{(T_{fi} - T_a)}{I_b}\right] \qquad (6.59)$$

Equation (6.59) is equivalent to the HWB equation of a conventional FPC (Eq. 5.82)

From the previous equation, the expression for the gain factor and loss coefficient can be obtained as

$$\text{Gain factor} = \frac{(AF_R(\alpha\tau))_1}{(A_{rm} + A_{cr1})} \qquad (6.60a)$$

and

$$\text{Loss coefficient} = \frac{(AF_R U_L)_1}{(A_{rm} + A_{cr1})} \qquad (6.60b)$$

(C) N-Photovoltaic thermal (PVT) concentrators connected in series

In this case, a similar expression for the outlet and the rate of thermal energy available at the Nth concentrator can be obtained as in the case of the FPC.

Objective Questions

6.1 The concentration ratio is maximal in the case of
    (a) flat-plate collector   (b) air heater
    (c) evacuated collector   (d) concentrator
    Answer: (d)
6.2 The concentration ratio is 1 in the case of
    (a) concentrator   (b) air heater
    (c) flat-plate collector   (d) air heater
    Answer: (c)
6.3 The concentration ratio for concentrator is
    (a) >1 (b) <1
    (c) $=1$ (d) none
    Answer: (a)

6.4 The absorber temperature in the case of the concentrator is
(a) more than the absorber temperature of the flat-plate collector
(b) less than the absorber temperature of the flat-plate collector
(c) equal to the absorber temperature of the flat-plate collector
(d) none of these
Answer: (a)

6.5 The fluid used in the concentrator has
(a) high boiling temperature   (b) low boiling temperature
(c) less than boiling temperature of water (d) equal to boiling temperature of water
Answer: (a)

6.6 The optical efficiency of the concentrator is
(a) less than the thermal efficiency   (b) more than the thermal efficiency
(c) equal to the thermal efficiency   (d) none of these
Answer: (b)

6.7 The concentration ratio (c) is defined as
(a) A_a/A_r (b) A_r/A_a
(c) A_r (d) $A_a/2$
Answer: (a)

6.8 The expression for the concentration ratio of a circular concentrator is
(a) $1/\sin\theta_s$ (b) $1/\sin^2\theta_s$
(c) $1/\sqrt{\sin\theta_s}$ (d) $\sin\theta_s$
Answer: (b)

6.9 The maximum concentration ratio occurs in the case of the
(a) central tower receiver   (b) paraboloidal concentrator
(c) cylindrical parabolic concentrator   (d) Fresnel concentrator
Answer: (a)

6.10 The expression for F_R for the concentrator is
(a) similar to F_R of the flat-plate collector   (b) different than F_R of the flat-plate collector
(c) similar to F_R of the air collector   (d) none of these
Answer: (a)

6.11 The outlet fluid temperature of the concentrator is
(a) less than the outlet fluid temperature of the flat-plate collector
(b) more than the outlet fluid temperature of the flat-plate collector
(c) equal to the outlet fluid temperature of the flat-plate collector
(d) none of these
Answer: (b)

6.12 The concentration ratio for a cylindrical absorber (C) is
(a) $1/\pi.\sin^2\theta_c$ (b) $\pi.\sin\theta_c$
(c) $\pi/\sin\theta_c$ (d) none of these
Answer: (a)

6.13   The concentration ratio for a circular cylindrical absorber is
        (a) $\sin\phi/\sin\theta_c$ (b) $\pi.\sin\theta_c$
        (c) $\pi/\sin\theta_c$ (d) none of these
        Answer: (c)
6.14   In a concentrator, the use of insulation is negligible compared with that of the
        (a) flat-plate collector   (b) air heater
        (c) evacuated tubular collector   (d) all of these
        Answer: (d)
6.15   The rate of useful energy is maximal for
        (a) no tracking   (b) presence of tracking
        (c) a horizontal absorber   (d) none of these
        Answer: (b)
6.16   The temperature of an absorber in a refracting concentrator is
        (a) greater than that of the reflecting concentrator   (b) less than that of the
        reflecting concentrator
        (c) equal to that of the reflecting concentrator   (d) none of these
        Answer: (a)
6.17   The absorber of a concentrating collector is
        (a) selective   (b) normal   (c) blackened   (d) none
        Answer: (a)

Problems

6.1   Derive an expression for the solar-concentration ratio for a circular
      concentrator.

$$Q_{s\to r} = \frac{4\pi r^2}{4\pi R^2}\sigma T_s^4, \quad Q_{r\to s} = A_r\sigma T_s^4 E_{r\to s}$$

      Hint: Since $Q_{s\to r} = Q_{r\to s}$ for $E_{r\to s} = 1$ (see Sect. 7.2, [8]).
6.2   What is the maximum solar-concentration ratio for a circular concentrator?
      Hint: Use $\theta_s = 0.27°$ in Problem 6.1.
6.3   A cylindrical receiver (70 mm diameter) has an emittance of 0.9 and a tem-
      perature of 250 °C. The absorber is covered with a tubular glass cover of
      100 mm diameter at 50 °C. The annular space is evacuated. Calculate the
      following GIVEN an ambient air temperature of 10 °C:
      (a) the convective heat-transfer coefficient $\left(h_{c,c-a}\right)$ from the cover tube to the
      ambient air
      (b) the radiative heat-transfer coefficient $\left(h_{r,c-a}\right)$ from the cover tube to the
      ambient air

(c) the radiative heat-transfer coefficient $\left(h_{r,r-c}\right)$ from the absorber (receiver) to the cover

(d) the overall heat-loss coefficient (U_L)

Hint: (a) $Nu = 0.40 + 0.54\,Re^{0.52}$ for $0.1 < Re < 1000$

and $Nu = 0.30\,Re^{0.6}$ for $1000 < Re < 50,000$

(b) $h_{r,c-a} = 4\varepsilon\sigma\bar{T}^3[\bar{T} = (50+10)/2]$

(c) $h_{r,r-c} = \dfrac{\sigma\left(T_2^2 + T_1^2\right)(T_2 + T_1)}{\frac{1-\varepsilon_1}{\varepsilon_1} + \frac{1}{F_{12}} + \frac{(1-\varepsilon_2)A_1}{\varepsilon_2 A_2}}$, $F_{12} = 1$ for the present case.

(d) $U_L = \left[\dfrac{A_r}{(h_{c,c-a} + h_{r,c-a})A_a} + \dfrac{1}{h_{r,r-c}}\right]^{-1}$

6.4 Prove that under steady-state conditions, the overall heat-transfer coefficient from the outer surface of cylindrical receiver to the flowing fluid is given by

$U = \left[\dfrac{D_o \ln(D_o/D_i)}{2K} + \dfrac{D_o}{D_i h_{fi}}\right]^{-1}$.

Hint: Use Sect. 6.7; $\dot{q}'_u = \dfrac{\dot{Q}_u}{L} = F'\left(\frac{A_a}{L}\right)\left[S - \left(\frac{A_r}{A_a}\right)U_L(T_f - T_a)\right]$.

6.5 Prove that the rate of useful energy per unit length $\dot{q}'_u$ for natural circulation is given by

$\dot{q}'_u = \frac{F'}{L}\left[A_a S - A_r U_L\left(T_p - T_f\right)\right]$ and also $\dot{q}'_u = \frac{U_L}{L}A_r\left(T_p - T_f\right)$

where $F' = \dfrac{1/U_L}{\left[\frac{1}{U_L} + \frac{D_o}{D_i h_{fi}} + \frac{D_o}{2K}\ln\frac{D_o}{D_i}\right]} = \dfrac{U_0}{U_L}$, $U_0 = \left[\frac{1}{U_L} + \frac{D_o}{D_i h_{fi}} + \frac{D_o}{2K}\ln\frac{D_o}{D_i}\right]^{-1}$

Hint: Under steady-state conditions, eliminate T_r from Eq. (6.12)

T_r to get the results.

6.6 Determine an expression for the rate of heat carried away from the solar concentrator under a forced circulation mode of operation. It is given by

$\dot{Q}_u = F_R A_a\left[S - \frac{A_r}{A_a}(T_{fi} - T_a)\right]$ with $F'' = \frac{F_R}{F'} = \frac{\dot{m}C_f}{F'A_r U_L}\left[1 - \exp\left(-\frac{F'A_r U_L}{\dot{m}C_f}\right)\right]$

Hint: Follow the same procedure given in Sect. 5.7.4 for a flat-plate collector.

6.7 Plot the curve between η_i and $(T_{fi} - T_a)/I_b(t)$.

Hint: $\eta_i = \dot{q}_u/I_b(t)$

6.8 The solar concentrator in Problem 6.3 has the following specifications:

$$S = 500\,\frac{W}{m^2}, K = 16\,\frac{W}{m\,°C}, C_f = 3.26\,\frac{kJ}{kg\,°C}, \dot{m} = 0.054\,\frac{kg}{s}, h_{fi}$$
$$= 200\,\frac{W}{m^2\,°C}.$$

Calculate the following parameters: (a) U_0 and F_R. (b) $\dot{q}_u$ and T_{fo}

Hint: See Problems 6.5 and 6.6, and use $T_{fo} = T_{fi} + \dot{Q}_u/\dot{m}C_f$

References

1. A.B. Meinel, Concentrating collectors Chap. 9, in *Solar Energy Engineering*, ed. by A.A.M. Sayigh (Academic press, New York, 1977)
2. W.G. Steward, A concentrating solar energy system employing a stationary spherical mirror and a movable collector, in *Proceedings of Solar Heating Cooling Building Workshop*, 1973, p. 17
3. R. Winston, Sol. Energy **16**(2), 89 (1974)
4. A. Rabl, Sol. Energy **18**(6), 497 (1976)
5. A. Rabl, R. Winston, Appl. Opt. **15**, 2880 (1976)
6. S. Vasilevskis, *Large Telescope Design Criteria in Telescope Design*, ed. by D.L. Crawford (Academic Press, New York, 1966)
7. D. Atheaya, A. Tiwari, G.N. Tiwari, I.M. Al-Helal, Sol. Energy **111**, 176 (2015)
8. J.A. Duffie, W.A. Beckman, *Solar Engineering of Thermal Processes* (Wiley, New York, 1991)

Additional Reference

9. A. Rabl, Sol. Energy **18**(2), 93 (1975)

Chapter 7
Evacuated Tubular Solar Collector (ETSC)

Abstract An evacuated tubular solar collector (ETSC) is another device to collect solar energy for thermal applications in the temperature range between 100 and 300 °C. In this case, an ETSC can be used for indirect space heating and crop drying through a heat exchanger. An ETSC can also be used for preheating of working fluid for power generation at lower capacity.

Keywords Evacuated tubular collector (ETC) · Natural mode · Force mode · Threshold intensity · Heat pipes

7.1 Introduction

In a flat-plate collector (FPC) (see Chap. 5) and solar concentrator (see Chap. 6), there are two thermal losses from the absorber/receiver to the glazing cover as follows:

(i) **The rate of convective heat transfer**: The rate of convective heat transfer depends on the temperature-dependent physical properties of the enclosed air between the absorber/receiver and the glazing cover. If enclosed air between the absorber/receiver and the glazing cover is evacuated to create a vacuum, then the rate of convective heat transfer is suppressed to a minimal value, and hence the upward rate of heat loss is minimized to have a maximum absorber/receiver temperature. In a glazed flat absorber/receiver surface, in both an FPC or a solar concentrator, it is difficult to have vacuum; it is also impractical for a larger-surface absorber/receiver. Because of such limitations, a vacuum is created between the coaxial glazed conductive tube absorber/receiver. The coaxial glazed conductive tube absorber/receiver is known as an "evacuated tubular absorber/receiver."

(ii) **The rate of radiative heat transfer**: The rate of radiative heat transfer depends on the emissivity (ϵ) of the blackened surface of the absorber/receiver. This can be achieved easily for smaller-surface absorber/receiver. It is also durable for a longer period compared with an FPC.

The above condition is achieved in an evacuated tubular collector (ETC). The evacuated tubular solar collector (ETSC) is always in solar concentrators (see Chap. 6). There is only a difference of the following:

(a) Only beam radiation is used in a solar concentrator due to the application of optical property; and
(b) total radiation is used in an ETSC.

The classification of an evacuated tubular collector is given as follows:
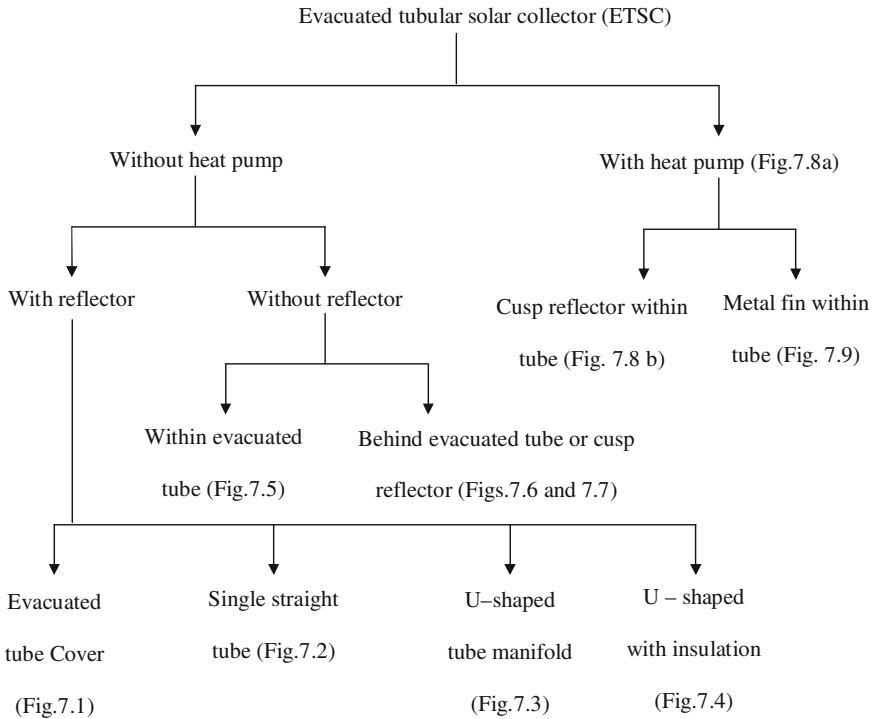
A brief description and working principle of each ETSC is discussed in the following sections.

7.2   Evacuated Tubular Solar Collectors (ETSC)

In an evacuated glazed tubular collector, a vacuum is created between the absorber and the transparent glass cover. There are many types of evacuated glazed tubular collectors, which will be discussed in the following sections.

7.2.1 Solaron Collector

Figure 7.1a shows a cross-sectional view of Solaron tubular collector with an evacuated transparent tube. In this case, the evacuated transparent tubes are arranged above the selective coating absorber. There should not be any space left between the consecutive tubes. The evacuated tubes provide a vacuum layer above the selective coating absorber. The vacuum layer suppresses convective heat loss from the absorber to the transparent glass cover. Incident solar radiation is absorbed by the selectively coated absorber after transmission from the transparent evacuated tubes. After absorption of solar radiation by the tube, most of the available thermal energy at the absorber will be first conducted and then convected to the working fluid below the absorber/receiver. The temperature of the working fluid will be increased. Afterward, there will be two types of heat losses from the working fluid to the ambient air as follows:

Fig. 7.1 **a** Cross-sectional view of a Solaron evacuated tubular solar collector (ETSC). **b** Cross-sectional view of a Phillips evacuated tubular solar collector (ETSC)
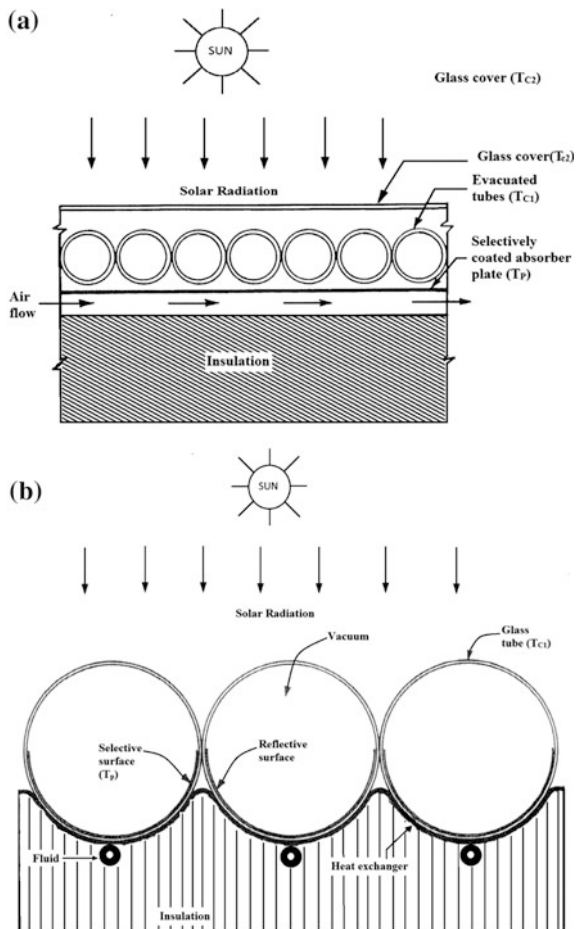
(a) **First loss**: The rate of heat loss from the working fluid to the ambient air through the evacuated tubes and glass cover, which is referred as "top-heat loss." The temperature of upper portion of evacuated tubes will be small; hence, there will be small heat losses. This top-heat loss will be minimum compared with that of an FPC.
(b) **Second loss**: The rate of heat loss from the working fluid to the ambient air through the bottom insulation is referred to as "bottom-heat loss."

The working fluid may be either air or any liquid (e.g., water). The temperature of the working fluid in this case will be greater compared with the fluid temperature of a conventional FPC due to decreased upward heat loss.

7.2.2   Phillips (Germany) Collector

The thermal performance of the Solaron collector with an evacuated tube with a single glass cover can be further increased. This can be achieved by increasing the convective heat transfer from the absorber tube to the working fluid through the surface area of the absorber/receiver (A_r) as shown in Fig. 7.1b. In this case, the working fluid passes through the conductive tubes attached at the bottom of the semicircular absorber/receiver. The heat capacity of the working fluid is also decreased. This results in a greater increase of the temperature of the working fluid. The curved selective surface absorber acts as a heat exchanger. The top surface of the evacuated tubes (T_{c2}) is directly exposed to solar radiation unlike to Solaron collector. Furthermore, the inner surface of the evacuated tubes (T_{c1}) is exposed to the absorber/receiver (A_r) through a vacuum.

Solar radiation, $I(t)$, is transmitted after reflection (ρ) from the outer curved portion of the glass tube inside the vacuum space. It is finally absorbed by the curved selective surface (α) after reflection. The reflected radiation is further transmitted to the atmosphere through the curved outer portion of the tube. Absorbed thermal energy is transferred to the working fluid through conduction and convection. The working fluid is then heated. After heating the working fluid, there is heat loss from the working fluid to the ambient air through the top as well as bottom insulation of area A_b.

7.2.3   Instantaneous Thermal Efficiency

The instantaneous thermal efficiency of an ETSC can be determined by assuming that the outside surface area of tube is equal to the overall dimensions of the collector, which is referred as the "aperture area" (A_a).

(a) **Natural mode**

The energy balance of a Phillips (Germany) collector under natural mode can be written (in Watts) as follows:

(i) **Without fluid**

The rate of net thermal energy in W at the absorber plate/receiver can be written as

$$\dot{Q}_u = \alpha(1 - \rho)A_a I(t) - \varepsilon\sigma\left(T_p^4 - T_c^4\right)A_r - U_b\left(T_p - T_a\right)A_b \qquad (7.1)$$

Here it is assumed that there is single glass cover. The first term on the right hand side of the above equation is the rate of thermal energy absorbed; the second term is the rate of radiative heat loss from the plate to the glass cover; and the last term is the rate of thermal energy lost from the plate to the ambient air through the bottom insulation.

The expression for U_b is given by

$$U_b = \left[\frac{L_i}{K_i} + \frac{1}{h_i}\right]^{-1} \qquad (7.1a)$$

where L_i and K_i are the thickness and thermal conductivity of bottom insulation, respectively, and $h_i = 5.7 + 3.8\,V$ for both convection and radiation losses and $h_i = 2.8 + 3\,V$ only for convection losses.

Now the rate of radiative heat loss from the absorber plate to the glass cover will be lost to the ambient air from the glass cover as follows:

$$\varepsilon\sigma\left(T_p^4 - T_c^4\right)A_r = h_o(T_c - T_a)A_a \qquad (7.2)$$

In terms of the radiative heat–transfer coefficient, the rate of radiative heat loss from the absorbing plate to the glass cover can be linearized as follows:

$$\varepsilon\sigma\left(T_p^4 - T_c^4\right)A_r = h_r\left(T_p - T_c\right)A_r \qquad (7.3)$$

Using Eqs. (7.3) and (7.1) becomes

$$\dot{Q}_u = \alpha(1 - \rho)A_a I(t) - h_r\left(T_p - T_c\right)A_r - U_b\left(T_p - T_a\right)A_b \qquad (7.4)$$

From Eqs. (7.2) and (7.3), one can have

$$h_r\left(T_p - T_c\right) = U_t\left(T_p - T_a\right) \qquad (7.5)$$

where, h_r and U_t are the radiative heat–transfer coefficient from the absorber plate to the glass cover and the overall heat-transfer coefficient from the absorber to the

ambient air through the glass cove, respectively. The expression for the same are given by

$$h_r = \varepsilon\sigma(T_p + T_c)\left(T_p^2 + T_c^2\right) \quad \text{and} \quad U_t = \frac{h_r h_o}{h_r + h_o} \tag{7.5a}$$

After substituting Eq. (7.5) into Eq. (7.4), one obtains

$$\dot{Q}_u = \alpha(1 - \rho)A_a I(t) - U_t\left(T_p - T_a\right)A_r - U_b\left(T_p - T_a\right)A_b \tag{7.6}$$

The above equation can further be written as

$$\dot{Q}_u = \alpha(1 - \rho)A_a I(t) - A_r U_{L,\text{eff}}\left(T_p - T_a\right) \tag{7.7}$$

where $U_{L,\text{eff}}$ is given by

$$U_{L,\text{eff}} = \left[U_t + U_b \frac{A_b}{A_r}\right] \tag{7.7a}$$

Now, an instantaneous thermal efficiency of the tubular collector can be written as

$$\eta_i = \frac{\dot{Q}_u}{A_a I(t)} = \alpha(1 - \rho) - \frac{A_r}{A_a} U_{L,\text{eff}} \frac{\left(T_p - T_a\right)}{I(t)} \tag{7.8}$$

Equation (7.8) is the characteristic equation for an evacuated collector.

(ii) **With fluid**

Absorber/receiver

The rate of thermal energy in W at the absorber/receiver can be written as

$$\dot{Q}_u = \alpha(1 - \rho)A_a I(t) - \varepsilon\sigma\left(T_p^4 - T_{c1}^4\right)A_r - U_{pf}\left(T_p - T_f\right)A_r \tag{7.9}$$

where U_{pf} is an overall heat-transfer coefficient from the absorber plate to the working fluid; T_p and T_f are the absorber and the fluid temperature, respectively; σ is the Stefan–Boltzman constant $\left(\sigma = 5.67 \times 10^{-8} \text{ W/m}^2 \text{ K}\right)$, and $\varepsilon = 0.3$ is the emittance of the absorbing selective surface at the collector temperature. An expression for U_{pf} is given by

$$U_{pf} = \left[\frac{D_o}{h_{fi}D_i} + \left(\frac{D_o}{2K}\ln\frac{D_o}{D_i}\right)\right]^{-1} \tag{7.10}$$

which is the same as Eq. (5.36).

Here D_o and D_i are the outer and inner diameters of the flowing tube; and K is the thermal conductive of the tube material.

Glass inner tube

The rate of thermal energy in W from the absorber/receiver surface to the inner tube can be written as

$$h_r(T_p - T_{c1})A_r = h_{1k}(T_{c1} - T_{c2})A_a \tag{7.11}$$

where h_r and h_{1k} are the radiative and convective heat-transfer coefficient from the inner tube to the outer tube, and its value can be approximated as 5.7 W/m^2 K.

Glass outer tube

The rate of thermal energy in W from the inner tube to an outer tube having approximately the same area of A_a can be written as

$$h_{1k}(T_{c1} - T_{c2})A_a = h_o(T_{c2} - T_a)A_a \tag{7.12}$$

Working fluid

The rate of thermal energy in W transferred from the absorber/receiver surface of area (A_r) to the working fluid can be written as

$$U_{pf}(T_p - T_f)A_r = U_b(T_f - T_a)A_b \tag{7.13}$$

where U_b is an overall heat-transfer coefficient from the fluid to the ambient air (T_a) through insulation having an area of A_b.

As performed previously, the radiative term in Eq. (7.9) can be linearized as follows:

$$\varepsilon\sigma\left(T_p^4 - T_{c1}^4\right) = h_r(T_p - T_{c1})$$

Then Eqs. (7.9) and (7.11) become as follows:

$$\dot{Q}_u = \alpha(1 - \rho)A_aI(t) - h_r(T_p - T_{c1})A_r - U_{pf}(T_p - T_f)A_r \tag{7.14}$$

$$h_r(T_p - T_{c1})A_r = h_{1k}(T_{c1} - T_{c2})A_a \tag{7.15}$$

Equation (7.14), with help of Eqs. (7.11)–(7.15), can be solved as

$$\dot{Q}_u = \alpha(1 - \rho)A_aI(t) - U_{L,eff}A_r(T_f - T_a) \tag{7.16}$$

where an expression for $U_{L,eff}$ is given by

$$U_{L,eff} = \left[U_{pa} \left\{ \frac{U_b}{U_{pf}} \frac{A_b}{A_r} + 1 \right\} + U_b \frac{A_b}{A_r} \right] \tag{7.16a}$$

where the expression for various heat transfer coefficients is given as

$$U_{pa} = \left[\frac{1}{h_r} + \frac{1}{U_{c1,a} \frac{A_a}{A_r}} \right]^{-1}; \quad U_{c1,a} = \left[\frac{1}{h_0} + \frac{1}{h_{1k}} \right]^{-1}; \quad h_{1k} = 5.7 \text{ W/m}^2 \text{ K} \tag{7.16b}$$

Now, an instantaneous thermal efficiency of a tubular collector with fluid can be written as

$$\eta_i = \frac{\dot{Q}_u}{A_a I(t)} = \alpha(1 - \rho) - \frac{A_r}{A_a} U_{L,eff} \frac{(T_f - T_a)}{I(t)} \tag{7.17}$$

Equation (7.17) is the characteristic equation for an evacuated collector with fluid similar to Eq. (5.50b) derived for a FPC.

Example 7.1 Derive an expression for F' for an evacuated flat-plate collector (Fig. 7.2).

Fig. 7.2 Sanyo evacuated tubular solar collector (ETSC). **a** Cross sectional view. **b** Front view. **c** Top view of ETSC
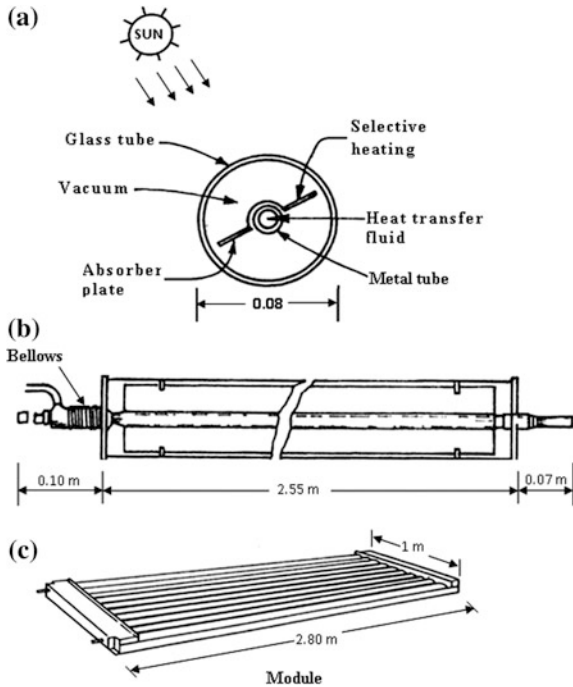
Solution

Under steady-state conditions, the energy balance of each component of Fig. 7.2 [with the help of Eqs. (7.11)–(7.15)], can be written as follows.

Absorber plate

$$\dot{Q}_u = \alpha(1 - \rho)A_a I(t) - U_{pa}A_r\left(T_p - T_a\right) - U_b A_b\left(T_p - T_a\right)$$

or

$$\dot{Q}_u = \alpha(1 - \rho)A_a I(t) - U_L A_r\left(T_p - T_a\right)$$

where

$$U_L = U_{pa}\left[1 + \frac{U_b A_b}{U_{pa} A_r}\right]$$

or

$$\frac{\dot{Q}_u}{U_L A_r} = \frac{\alpha(1 - \rho)A_a I(t)}{U_L A_r} - \left(T_p - T_a\right) \tag{E-1}$$

Fluid

$$\dot{Q}_u = U_{pf}\left(T_p - T_f\right)A_r$$

or

$$\frac{\dot{Q}_u}{U_{pf}A_r} = \left(T_p - T_f\right) \tag{E-2}$$

On addition of Eqs. (E-1) and (E-2), one obtains

$$\dot{Q}_u\left[\frac{1}{U_L A_r} + \frac{1}{U_{pf}A_r}\right] = \frac{\alpha(1 - \rho)A_a I(t)}{U_L A_r} - \left(T_f - T_a\right) \tag{E-3}$$

Equation (E-3) can be rewritten as

$$\dot{Q}_u = \left[\frac{1}{U_L A_r} + \frac{1}{U_{pf}A_r}\right]^{-1}\left[\frac{\alpha(1 - \rho)A_a I(t)}{U_L A_r} - \left(T_f - T_a\right)\right]$$

or

$$\dot{Q}_u = F'\left[\alpha(1 - \rho)I(t)A_a - U_L A_r(T_f - T_a)\right] \tag{E-4}$$

where

$$F' = \frac{1}{U_L A_r} \left[\frac{1}{U_L A_r} + \frac{1}{U_{pf} A_r} \right]^{-1} = \frac{\frac{1}{U_L}}{\frac{1}{U_L} + \frac{1}{U_{pf}}} = \frac{\frac{1}{U_L}}{\frac{1}{U_0}} = \frac{U_0}{U_L} \tag{E-5}$$

(b) Forced mode

In this case, the working fluid of specific heat of C_f is allowed to flow with the mass flow rate of $\dot{m}_f$ through the tube under forced mode by water pump. The rate of thermal energy of the tubular collector available under forced mode will be carried away by the fluid flowing through the tube under steady-state conditions.

From Example 7.1, one can obtain an expression for the rate of thermal energy per unit length of the tubular collector as

$$\dot{Q}'_u = \frac{\dot{Q}_u}{L} = \frac{1}{L} F'[\alpha(1 - \rho)I(t)A_a - U_L A_r(T_f - T_a)] \tag{7.18}$$

where L is the length of the tubular collector.

According to the section for the FPC, the rate of thermal energy carried away by the flowing fluid per unit length is given by

$$\dot{m}_f C_f \frac{dT_f}{dx} \tag{7.19}$$

Under steady-state conditions, one can write the energy balance of the flowing fluid by equating Eqs. (7.18) and (7.19) as follows:

$$\dot{m}_f C_f \frac{dT_f}{dx} = \frac{1}{L} F'[\alpha(1 - \rho)I(t)A_a - U_L A_r(T_f - T_a)] \tag{7.20}$$

The solution of Eq. (7.20) with initial condition of $T_f = T_{fi}$ at $x = 0$ is as follows:

$$-\frac{1}{U_L A_r} \ln \frac{[\alpha(1 - \rho)I(t)A_a - U_L A_r(T_f - T_a)]}{[\alpha(1 - \rho)I(t)A_a - U_L A_r(T_{fi} - T_a)]} = \frac{F'}{\dot{m}_f C_f L} x$$

or

$$\frac{[\alpha(1 - \rho)I(t)A_a - U_L A_r(T_f - T_a)]}{[\alpha(1 - \rho)I(t)A_a - U_L A_r(T_{fi} - T_a)]} = \exp\left(-\frac{F' A_r U_L}{\dot{m}_f C_f L} x \right)$$

or

$$T_f = \left[\frac{\alpha(1-\rho)I(t)}{U_L}\frac{A_a}{A_r} + T_a\right]\left\{1 - \exp\left(-\frac{F'A_rU_L}{\dot{m}_f C_f L}x\right)\right\} + T_{fi}\exp\left(-\frac{F'A_rU_L}{\dot{m}_f C_f L}x\right)$$
(7.21)

Furthermore, $T_f = T_{fo}$ at $x = L$; then Eq. (7.21) becomes as

$$T_{fo} = \left[\frac{\alpha(1-\rho)I(t)}{U_L}\frac{A_a}{A_r} + T_a\right]\left\{1 - \exp\left(-\frac{F'A_rU_L}{\dot{m}_f C_f}\right)\right\} + T_{fi}\exp\left(-\frac{F'A_rU_L}{\dot{m}_f C_f}\right)$$
(7.22a)

If an N-ETSC is connected in series, the outlet temperature at the Nth ETC is given by

$$T_{foN} = \left[\frac{\alpha(1-\rho)I(t)}{U_L}\frac{A_a}{A_r} + T_a\right]\left\{1 - \exp\left(-\frac{NF'A_rU_L}{\dot{m}_f C_f}\right)\right\} + T_{fi}\exp\left(-\frac{NF'A_rU_L}{\dot{m}_f C_f}\right)$$
(7.22b)

For constant collection temperature, i.e., $T_{foN} = T_0$, the expression for mass-flow rate is given by

$$\dot{m}_f = -\frac{NF'A_rU_L}{C_f}\left[\ln\frac{T_0 - \left\{\frac{\alpha(1-\rho)I(t)}{U_L}\frac{A_a}{A_r} + T_a\right\}}{T_{fi} - \left\{\frac{\alpha(1-\rho)I(t)}{U_L}\frac{A_a}{A_r} + T_a\right\}}\right]^{-1}$$
(7.22c)

Now the rate of thermal energy available at the end of the ETSC is given by

$$\dot{Q}_u = \dot{m}_f C_f(T_{fo} - T_{fi})$$
$$= \dot{m}_f C_f\left\{1 - \exp\left(-\frac{F'A_rU_L}{\dot{m}_f C_f}\right)\right\}\left[\frac{\alpha(1-\rho)I(t)}{U_L}\frac{A_a}{A_r} - (T_{fi} - T_a)\right]$$

or

$$\dot{Q}_u = \dot{m}_f C_f(T_{fo} - T_{fi}) = A_a F_R\left[\alpha(1-\rho)I(t) - \left(\frac{A_r}{A_a}\right)U_L(T_{fi} - T_a)\right]$$
(7.23a)

where an expression for F_R is given by

$$F_R = \frac{\dot{m}_f C_f}{A_r U_L}\left\{1 - \exp\left(-\frac{F'A_rU_L}{\dot{m}_f C_f}\right)\right\}$$
(7.23b)

Furthermore, according to Sect. 5.8.2, the rate of thermal energy available at the end of the Nth ETSC can be derived for the ETSC, and its expression is given by

$$\dot{Q}_u = \dot{m}_f C_f (T_{foN} - T_{fi})$$
$$= \dot{m}_f C_f \left\{ 1 - \exp\left(-\frac{NF'A_r U_L}{\dot{m}_f C_f} \right) \right\} \left[\frac{\alpha(1-\rho)I(t)}{U_L}\frac{A_a}{A_r} - (T_{fi} - T_a) \right]$$

or

$$\dot{Q}_u = \dot{m}_f C_f (T_{fo} - T_{fi}) = NA_a F_{RN} \left[\alpha(1-\rho)I(t) - \left(\frac{A_r}{A_a}\right) U_L (T_{fi} - T_a) \right] \quad (7.24a)$$

where

$$F_{RN} = \frac{\dot{m}_f C_f}{NA_r U_L} \left\{ 1 - \exp\left(-\frac{NF'A_r U_L}{\dot{m}_f C_f} \right) \right\} \quad (7.24b)$$

Now an instantaneous thermal efficiency for single and N-ETSC is given by

$$\eta_i = \frac{\dot{Q}_u}{A_a I(t)} = F_R \left[\alpha(1-\rho) - \left(\frac{A_r}{A_a}\right) U_L \frac{(T_{fi} - T_a)}{I(t)} \right] \quad (7.25a)$$

and

$$\eta_i = \frac{\dot{Q}_u}{A_a I(t)} = F_{RN} \left[\alpha(1-\rho) - \left(\frac{A_r}{A_a}\right) U_L \frac{(T_{fi} - T_a)}{I(t)} \right] \quad (7.25b)$$

One can observe that there is only a difference in the flow-rate factor. For higher N, the flow-rate factor will have a lower value and hence instantaneous thermal efficiency as per expectation.

Example 7.2 Determine threshold condition of tubular collector under natural and forced mode and compare their results.

Solution
For threshold intensity, one must obtain the following condition as follows:

$$\dot{Q}_u \geq 0$$

For natural mode, we have [from Example 7.1 and Eq. (E-4)] the expression for $\dot{Q}_u$ as

$$\dot{Q}_u = F'[\alpha(1-\rho)I(t)A_a - U_L A_r (T_f - T_a)] \geq 0$$

This gives the expression for the threshold intensity under natural mode as

$$I_{\text{threshold}} \geq \frac{U_L A_r (T_f - T_a)}{\alpha(1 - \rho)A_a}$$

For forced mode, From Eq. (7.23a), we have

$$\dot{Q}_u = \dot{m}_f C_f (T_{fo} - T_{fi}) = A_a F_R \left[\alpha(1 - \rho)I(t) - U_L \frac{A_r}{A_a}(T_{fi} - T_a) \right] \geq 0$$

The expression for the threshold intensity under forced mode can be obtained as follows:

$$I_{\text{threshold}} \geq \frac{U_L A_r (T_{fi} - T_a)}{\alpha(1 - \rho)A_a}$$

It is important to note that there is only a difference in the numerator of the threshold intensity for natural and forced mode. The numerical value of $(T_f - T_a)$ will be higher than $(T_{fi} - T_a)$, and hence the threshold intensity for the natural mode will be higher.

Example 7.3 Determine an overall heat-loss coefficient $U_{L,\text{eff}}$ for a single- and double-glazed cover of a tubular collector for the following parameters:

$T_a = 40\ °C$, $\quad T_p = 160\ °C$, $\quad T_{c1} = 140\ °C$, $\quad T_{c2} = 80\ °C$, $\quad L_i = 0.01$ m, $K_i = 0.04$ W/mK and $V = 1$ m/s, $\sigma = 5.67 \times 10^{-8}$ W/m^2 K, $\epsilon = 0.05$ (selective surface), $\frac{A_r}{A_a} = 0.01$, $\frac{A_b}{A_r} = 0.50$.

The conductance, the glass cover material can be neglected.

Solution

For single-glazed (Fig. 7.1b): $T_p = 160\ °C$ and $T_c = 80\ °C$.

From Eq. (7.5a), one has

$$
\begin{aligned}
h_r &= \varepsilon\sigma\left(T_p + T_c\right)\left(T_p^2 + T_c^2\right) \\
&= 0.05 \times 5.67 \times 10^{-8} \times (433 + 353) \times (18.74 + 12.46) \times 10^4 \\
&= 0.70\ \text{W/m}^2\ \text{K}
\end{aligned}
$$

and

$$h_o = 5.7 + 3.8\ V = 9.5\ \text{W/m}^2\ \text{K}$$

Furthermore, from Eq. (7.5a), one has

$$U_{\mathrm{t}} = \frac{h_{\mathrm{r}} h_{\mathrm{o}}}{h_{\mathrm{r}} + h_{\mathrm{o}}} = \frac{0.70 \times 9.5}{0.7 + 9.5} = 0.65 \text{ W/m}^2 \text{ K}$$

and from Eq. (7.1a), we have

$$U_{\mathrm{b}} = \left[\frac{L_{\mathrm{i}}}{K_{\mathrm{i}}} + \frac{1}{h_{\mathrm{i}}} \right]^{-1} = \left[\frac{0.10}{0.04} + \frac{1}{5.7} \right]^{-1} = 0.37 \text{ W/m}^2 \text{ K}$$

From Eq. (7.7a), we have

$$U_{\mathrm{L,eff}} = \left[U_{\mathrm{t}} + U_{\mathrm{b}} \frac{A_{\mathrm{b}}}{A_{\mathrm{r}}} \right] = 0.65 + 0.37 \times 0.50 = 0.835 \text{ W/m}^2 \text{ K}$$

Thus, $U_{\mathrm{L}} = U_{\mathrm{t}} + U_{\mathrm{b}} = 0.65 + 0.37 = 1.02$. The overall heat-loss coefficient in an evacuated solar collector is significantly decreased compared with the value of the overall heat-loss coefficient of a flat-plate collector (Example 5.2, $U_{\mathrm{L}} = 7.2$ W/m² K).

For double-glazed (Fig. 7.1b): $T_{\mathrm{p}} = 160$ °C and $T_{\mathrm{c}} = 140$ °C,

$$\begin{aligned}
h_{\mathrm{r}} &= \varepsilon \sigma \left(T_{\mathrm{p}} + T_{\mathrm{c}} \right) \left(T_{\mathrm{p}}^2 + T_{\mathrm{c}}^2 \right) \\
&= 0.05 \times 5.67 \times 10^{-8} \times (433 + 413) \times (18.74 + 17.06) \times 10^4 \\
&= 0.86 \text{ W/m}^2 \text{ K}
\end{aligned}$$

and

$$U_{\mathrm{t}1} = \frac{h_1 h_{\mathrm{c}}}{h_1 + h_{\mathrm{c}}} = \frac{5.8 \times 9.5}{5.8 + 9.5} = 3.6 \text{ W/m}^2 \text{ K}$$

Then

$$U_{\mathrm{t}} = \frac{h_{\mathrm{r}} U_{\mathrm{t}1}}{h_{\mathrm{r}} + U_{\mathrm{t}1}} = \frac{0.86 \times 3.6}{0.86 + 3.6} = 0.694 \text{ W/m}^2 \text{ K}$$

The overall heat-loss coefficient is obtained as $U_{\mathrm{L}} = U_{\mathrm{t}} + U_{\mathrm{b}} = 0.694 + 0.37 = 1.064$ W/m² K.

Thus, the overall heat-loss coefficient in the case of Fig. 7.1a is slightly higher.

7.3   Williams Evacuated Tubular Solar Collector (ETSC)

The working principles of various ETC are discussed in the following sections.

7.3.1   Sanyo Evacuated Tubular Solar Collector

Various views of the Sanyo ETSC are shown in Fig. 7.2. A cylindrical metal tube is fixed with a selectively coated conducting metal absorber as shown in Fig. 7.2a. The configuration is then inserted in a glass tube of 0.08-m diameter. The diameter of the tube and the thickness of the absorber depend on the material and its physical properties such as thermal conductivity and specific heat. Generally, copper material is used due to its high thermal conductivity. The effective length of the tube is approximately 2.8 m. The tube is evacuated to suppress the convective heat loss between the absorber and the tube cover. Hence, it comes under the ETSC. Bottom-heat loss is also decreased by proper insulating of the base of the ETSC. The absorber can also be rotated at the optimum angle to receive maximum solar radiation for a given latitude unlike other types of ETC. Ten tubes are connected in parallel to form one module with an effective area of 1 m × 2.8 m as shown in Fig. 7.2c.

7.3.2   Corning Evacuated Tubular Solar Collector

A cross-sectional view the top elevation of a Corning ETSC, as well as the module with an area of 2.65 m × 0.71 m, is shown in Fig. 7.3. In a Corning ETSC, a U-shaped copper tube is fitted with a selectively coated horizontal copper flat plate in a tube below the absorber configuration as shown in Fig. 7.3a. The assembly is inserted into a Pyrex (glass) tube with a diameter of 0.10 m and a length of 2.28 m. Furthermore, the U-shaped tubing is also supported by a plate strip. After creating a vacuum inside the tube, the other end of the tube is sealed. The tubes are connected in series to form one module as depicted in Fig. 7.3b. Six tubes connected in series for one module, which is known as a "Corning ETSC".

7.3.3   Phillips (Germany) Evacuated Tubular Solar Collector

The Phillips evacuated tube solar collector is an improved version of the evacuated tubular solar collector with a high operating temperature. The top elevation and cross-sectional view are shown in Fig. 7.4. In this case, too, a U-shaped copper tube is fitted into a glass tube. Each arm of the tube touches the inner glass wall as shown
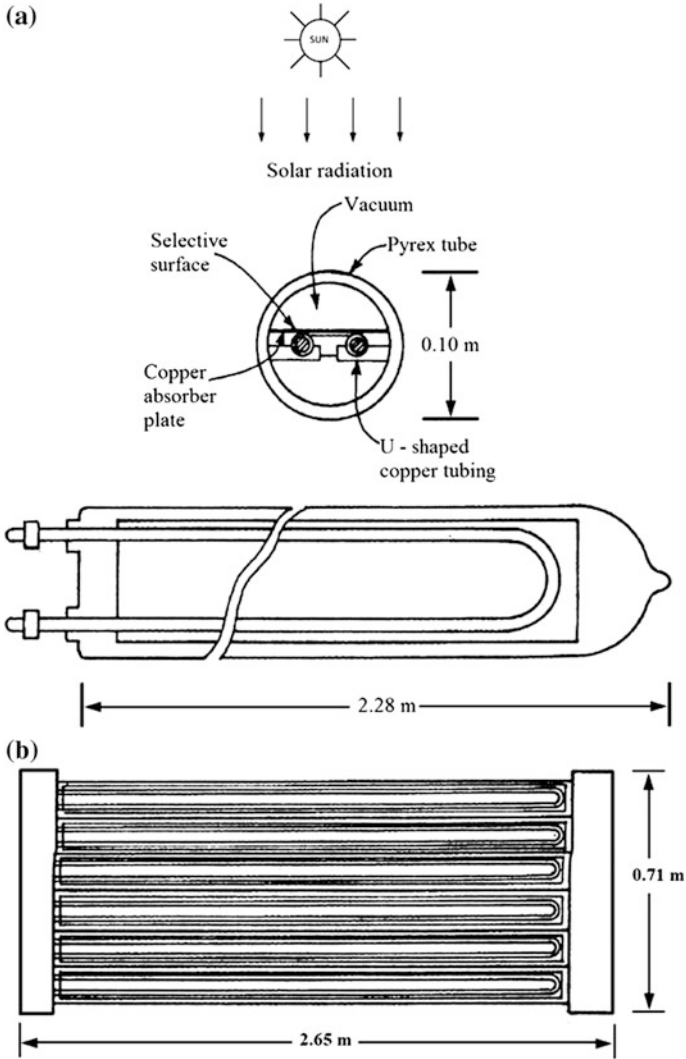
Fig. 7.3 Cross-sectional view of a Corning evacuated tubular solar collector (ETSC) and module.
a ETSC solar collector. **b** ETSC module

in Fig. 7.4b. The inner side of the tube is filled with polyurethane foam to avoid
heat exchanges between the tubes unlike a Corning evacuated tubular solar col-
lector. The outer side of the tube is selectively coated. This arrangement is further
inserted into another glass tube having a larger diameter. An annular space between
the inner and the outer tube is evacuated to decrease the upward convective heat
losses. In this case also, the tubes are connected in series to form a module of a
given area.
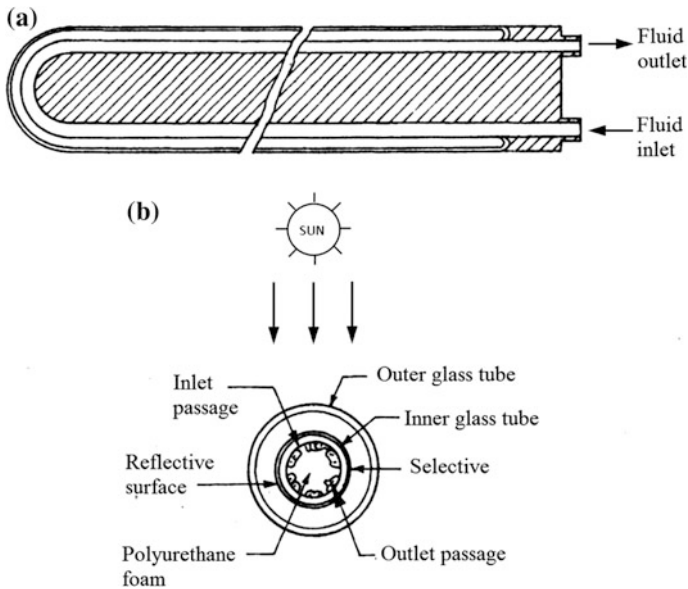
Fig. 7.4 Cross-sectional view of an improved Phillips evacuated tubular solar collector (ETSC).
a Top elevation. **b** Cross-sectional view

7.3.4   Roberts Evacuated Tubular Solar Collector

Figure 7.5 shows (a) a cross-sectional view and (b) the top elevation of a
Roberts ETSC. Here a concentric copper tube is centrally fitted with a flat steel
absorber plate. This arrangement is shown in Fig. 7.5a. There is an aluminum reflector
behind the absorber plate to reflect back all solar radiation falling on it toward the
absorber plate. The whole assembly is inserted into a glass tube with a diameter of
0.10 m. The glass tube is evacuated to minimize the convection top losses within the
tube. The open part of the tube is properly sealed to maintain a vacuum. The working
fluid is allowed to pass through the inner tube of the concentric copper tubes. The
working fluid is heated during its flow through an annular space of a concentric copper
tube as depicted in Fig. 7.5b. The outer portion of the concentric copper tube is
perfectly insulated to ensure minimum heat losses at the outlet.

7.3.5   General Electric (GE) TC-100 Evacuated Tubular
Solar Collector (ETSC)

A U-shaped copper tube is fitted inside a coaxial glass tube with an outer diameter
of 0.05 m and a length of 1.25 m as shown in Fig. 7.6a, b. This is referred to as
a "GE ETSC". The metal fin is fixed at the inner surface of a coaxial tube for better

Fig. 7.5 Cross-sectional view of a Robert evacuated tubular solar collector (ETSC). **a** Cross-sectional view. **b** Top elevation
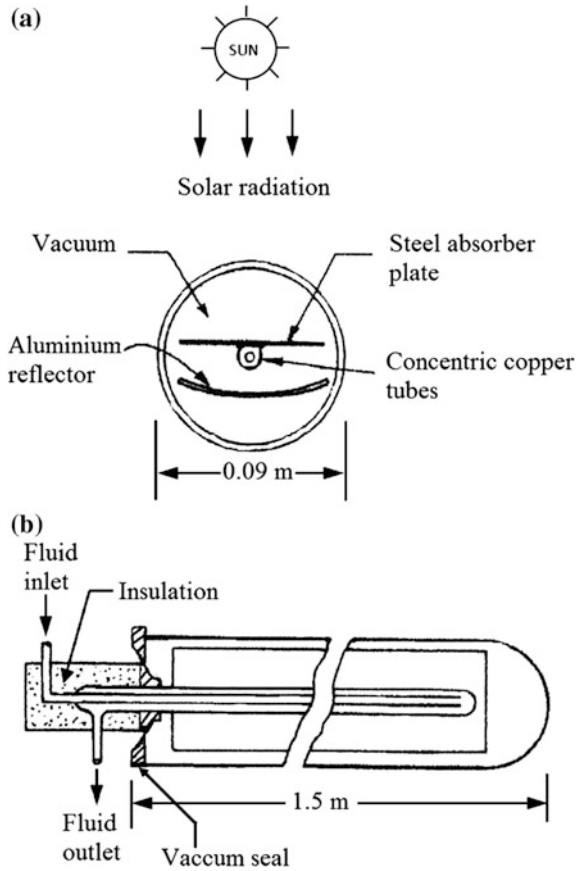
heat transfer from the surface of the inner tube to the working fluid. An annular space of the coaxial tube is evacuated to minimize convective heat loss from the surface of the inner tube to the outer tube. The outer surface of the inner tube is selectively coated for minimum radiation losses. The whole assembly is kept at a focal point of the cusp reflector as shown in Fig. 7.6a.

Solar radiation is reflected back to the outer glass of the coaxial tube from the cusp reflector. It is further transmitted after reflection. Finally it is absorbed by the inner tube. The absorbed thermal energy is transferred to the working fluid flowing through the U-shaped tube.

7.3.6   Owens–Illinois (OI) Evacuated Tubular Solar Collector (ETSC)

A cross-sectional view of the OI Sunpak ETSC is shown in Fig. 7.7. The working fluid passes through the glass delivery tube. The glass delivery tube is inserted into

(a)

(b)
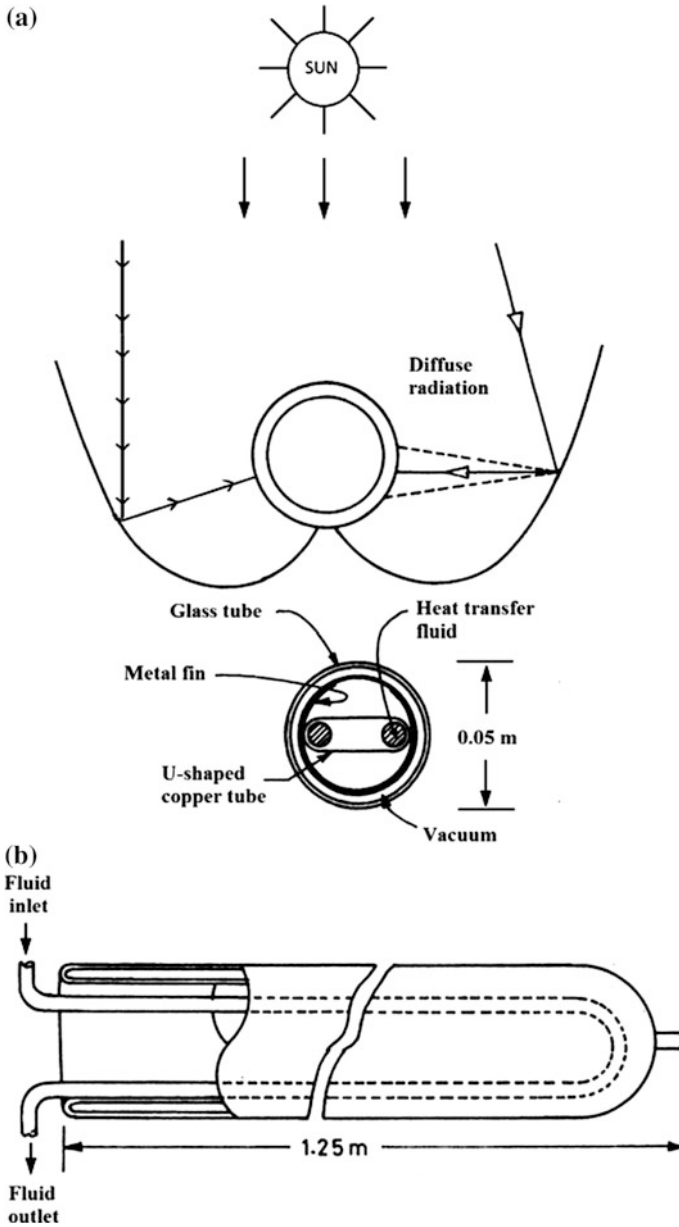
Fig. 7.6 Cross-sectional view of a General Electric (GE) evacuated tubular solar collector (ETSC). **a** Cross-sectional view. **b** Elevation view
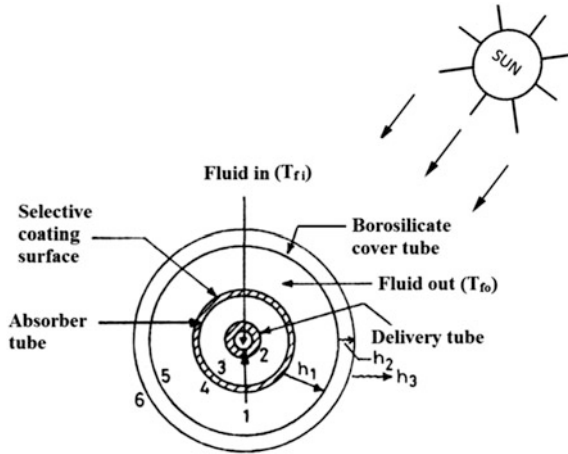
Fig. 7.7 Cross-sectional view of an Owens–Illinois (OI) Sunpak evacuated tubular solar collector (ETSC)

a selectively coated another tube of larger diameter. One end of the selectively coated tube is sealed. The working fluid is heated while it passes in a reverse flow through an annular space between the glass delivery tube and the selectively coated tube. The glass delivery tube and the selectively coated tube are further inserted into another borosilicate outer glass tube as shown in Fig. 7.7. To decrease convective losses from the inner tube, the annular space between the inner tube and the outer tube is evacuated. The collector tubes are often mounted above a white surface, which reflects sunlight onto the underside of the tubes.

7.4 Analysis of Owens–Illinois (OI) Tubular Solar Collector

Figure 7.7 shows a cross-sectional view of a single OI tubular solar collector. The glass cover tube is made of low-iron content glass for high transmittance. One end of the absorber tube is sealed. The other end is free to move in a flexible support to allow for differential thermal expansion between the two tubes.

The rate of useful heat $\left(\dot{Q}\right)$ made available by the tubular collector tube is given by Beekley and Mather [1]

$$\dot{Q} = \dot{m}_f C_f (T_{fo} - T_{fi}) = F_R A_c \left[(\alpha\tau) I_{eff} - U_L \left(\frac{A_L}{A_c} \right) (T_{fi} - T_a) \right] \qquad (7.26)$$

where

$$F_R = (\sinh \omega_2 \xi_1 / \{\omega_2 \xi_1 [\cosh \omega_2 \xi_1 + (\omega_1 \omega_2) \sin \omega_2 \xi_1]\}) F' \tag{7.27a}$$

$$\omega_1 = U_L P_L F' / 2 h_3 P_3 \tag{7.27b}$$

$$\omega_2 = U_L P_L F' [1 + 4(h_1 P_1 / U_L P_L F')]^{1/2} / 2 h_3 P_3 \tag{7.27c}$$

$$\xi_1 = h_3 P_3 l / \dot{m}_f C_f \tag{7.27d}$$

$$F' = 1/(1 + U_L P_L / h_3 P_3) \tag{7.27e}$$

The overall heat-loss coefficient can be obtained from

$$U_L = \left[\frac{1}{h_4} + \frac{1}{h_5} + \frac{1}{h_6} \right]^{-1} \tag{7.28}$$

where

$$h_4 = \frac{\sigma(T_4 + T_5)\left(T_4^2 + T_5^2\right)}{\{[(1 - \varepsilon_4)/\varepsilon_4] + [1/F_{45}] + [\{(1 - \varepsilon_5)/\varepsilon_5\}(A_4/A_5)]\}} \tag{7.29a}$$

$$h_5 = k/[(D_4/2)\ln(D_6/D_5)] \tag{7.29b}$$

$$h_6 = \left[h + \varepsilon_6 \sigma(T_6 + T_a)\left(T_6^2 + T_a^2\right)\right]/(A_6/A_4) \tag{7.29c}$$

$$h = 5.7 + 3.8\,V \tag{7.29d}$$

1   inner surface of the delivery tube
2   outer surface of the delivery tube
3   inner surface of the absorber tube
4   outer surface of the absorber tube (the selectively coated surface, in terms of which U_L is defined)
5   inner surface of the cover tube
6   outer surface of the cover tube (a = ambient air)
A_c absorber-tube diameter × collector length (l); $A_L = \pi A_c$
C_f specific heat of the fluid
F_{45} shape factor between the selective surface (4) and the inner surface of the cover tube (5)
h heat-transfer coefficient at the ith surface
I_{eff} effective solar radiation on the collector
$\dot{m}_f$ mass flow rate of the fluid
P_i perimeter of ith surface
P_L perimeter of the selectively coated surface
T_{fi} inlet-fluid temperature
T_{fo} outlet-fluid temperature
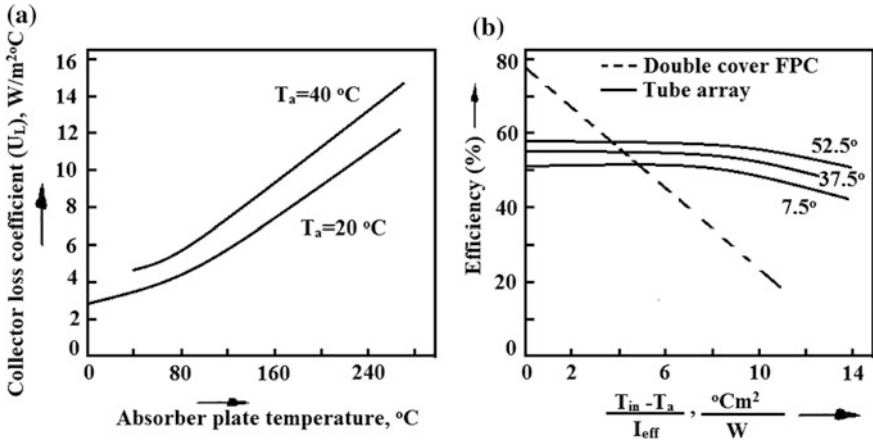
Fig. 7.8 **a** Variation of (U_L) with absorber temperature. **b** Characteristic curve

d is the centre-to-centre distance of the two tubes; and D_B is the distance of the centre of tube from the absorber (Fig. 7.8).

The expression for an instantaneous thermal efficiency (η_i) can be written as

$$\eta_i = \frac{\dot{Q}_u}{I_{eff}A_c} = F_R\left[(\alpha\tau) - \left(\frac{A_L}{A_c}\right)U_L\frac{(T_{fi} - T_a)}{I_{eff}}\right] \tag{7.30}$$

Referring to Fig. 7.8, the following observation can be made:

(a) There is variation of an overall heat-transfer coefficient (U_L) with the absorber temperature and

(b) There is a variation of η_i with $(T_{fi} - T_a)/I_{eff}$.

For comparison, the performance of a two-cover nonselective FPC is given in Fig. 7.8b. It can be seen that there insignificant variation in the value of an overall heat-transfer coefficient (U_L) with respect to the ambient air temperature (T_a). However, there is a sharp increase in the value of an overall heat-transfer coefficient (U_L) with respect to the absorber plate temperature (T_a).

Example 7.4 Determine the overall heat-transfer coefficient (U_L) for the following parameters of an OI collector:

Active-tube length (l) = 10.67 m; delivery-tube inner diameter (D_1) = 0.09 m; delivery-tube outer diameter (D_2) = 0.12 m; absorber-tube inner diameter (D_3) = 0.39 m; absorber-tube outer diameter (D_4) = 0.43 m; cover-tube inner diameter (D_5) = 0.49 m; and cover-tube outer diameter (D_6) = 0.09 m

$\sigma = 5.67 \times 10^{-8}$ W/m^2 K, $T_a = 40$ °C, $T_{fi} = 55$ °C, $T_4 = 160$ °C, $T_5 = 140$ °C, $T_6 = 110$ °C $F_{45} = 0.50$, $V = 1$ m/s, $\epsilon_4 = 0.05$ (selective surface), $\epsilon_5 = \epsilon_6 = 0.9$, K = thermal conductivity of glass cover = 1.09 W/m °C.

Solution

Here different areas used in this case is calculated as follows:

$$A_4 = 3.14 \times 0.43 \text{ m} \times 10.67 \text{ m} = 14.40 \text{ m}^2$$

$$A_5 = 3.14 \times 0.49 \text{ m} \times 10.67 \text{ m} = 16.42 \text{ m}^2$$

$$A_6 = 3.14 \times 0.53 \text{ m} \times 10.67 \text{ m} = 17.76 \text{ m}^2$$

$$A_4/A_5 = 0.8769; \ A_6/A_4 = 1.23 \text{ and } h = 5.7 + 3.8 = 9.5 \text{ W/m}^2 \text{ °C}$$

Furthermore, the denominator of Eq. (7.29a) $= \frac{1-0.05}{0.05} + \left(\frac{1}{0.5}\right) + \left[\frac{1-0.9}{0.9}\right] \times 0.8769 = 21.097$.

The various heat-transfer coefficients are as follows:

$$h_4 = \frac{5.67 \times 10^{-8}(433 + 413)\left[1.8749 \times 10^5 + 1.70569 \times 10^5\right]}{21.097} = 0.8098 \text{ W/m}^2 \text{ °C}$$

$$h_5 = \frac{1.09}{[0.215 \ln(1.0816)]} = \frac{1.09}{0.0168} = 64.88 \text{ W/m}^2 \text{ °C}$$

and

$$h_6 = \frac{9.5 + 0.9 \times 5.67 \times 10^{-8} \times (383 + 313) \times [1.4669105 + 0.9797105]}{1.23}$$
$$= 14.75 \text{W/m}^2 \text{ °C}$$

The overall heat-transfer coefficient in W/m^2 °C is calculated as

$$U_{\text{L}} = \left[\left(\frac{1}{0.8098}\right) + \left(\frac{1}{64.88}\right) + \left(\frac{1}{22.31}\right)\right]^{-1} = \frac{1}{1.295} = 0.77 \text{ W/m}^2 \text{ °C}$$

Example 7.5 Determine the convective heat transfer coefficients (h_1 and h_3) at an inner surface of case (i) the delivery and case (ii) an absorber tube for Example 7.4 with a water-flow rate of 3 m/s.

Solution

From Example 7.4:

An average temperature of water at the inner surface of the delivery tube is $T_1 > T_{\text{fi}} = 55$ °C (say $T_1 = 70$ °C) and

An average temperature of water at the inner surface of the delivery tube is

$$T_3 < T_4 = 55 \text{ °C (say } T_3 = 100 \text{ °C)}$$

Because $L/D_1 = 118.56$ and $L/D_3 = 27.36$, the convective heat-transfer coefficients in W/m^2 °C are calculated as follows:

$$Nu = 0.036 \, Re^{0.8} Pr^{1/3} \left(\frac{D}{L}\right)^{0.055} \quad \text{for } 10 < \frac{L}{D} < 400$$

From Appendix V we have

case (i) at $T_1 = 70$ °C, $Pr \cong 2.53$, $\mu = 4.01 \times 10^{-4}$ kg/m s, $\rho = 977.3$ kg/m^3, $v = \mu/\rho = 4.103 \times 10^{-7}$ m^2/s, $K = 0.669$ W/m °C and

$$Re = vD_1/v = \left(3 \times 0.09/4.103 \times 10^{-7}\right) = 6.58 \times 10^5,$$

then the convective heat-transfer coefficient for case (i) is determined as

$$h_1 = \frac{NuK}{D_1} = 0.036 \times \left(6.58 \times 10^5\right)^{0.8} (2.53)^{1/3} \left(\frac{0.09}{10.67}\right)^{0.055} \times \frac{0.665}{0.09}$$
$$= 12.583 \text{ kW/m}^2 \text{ °C}$$

case (ii) at $T_1 = 100$ °C, $Pr \cong 1.66$, $\mu = 2.67 \times 10^{-4}$ kg/m s, $\rho = 955.1$ kg/m^3, $v = \mu/\rho = 2.7955 \times 10^{-7}$ m^2/s, $K = 0.684$ W/m °C and

$$Re = vD_3vD_3/v = \left(3 \times 0.39/2.7955 \times 10^{-7}\right) = 41.85 \times 10^5,$$

then the convective heat-transfer coefficient for case (i) is determined as

$$h_3 = \frac{NuK}{D_3} = 0.036 \times \left(41.85 \times 10^5\right)^{0.8} (1.66)^{1/3} \left(\frac{0.39}{10.67}\right)^{0.055} \times \frac{0.684}{0.39}$$
$$= 12.356 \text{ kW/m}^2 \text{ °C}$$

There is not much difference in either case.

Example 7.6 Determine the collector efficiency (F') and flow-rate factors (F_R) for Examples 7.4 and 7.5, respectively.

Solution
Here various parameters are calculated as follows:

$$P_1 = 3.14 \times 0.09 = 0.2826 \text{ m}$$
$$P_3 = P_L = 3.14 \times 0.39 = 1.2246 \text{ m}.$$
$$h_1 P_1 = 12.583 \times 0.2826 = 3.556 \text{ kW/m °C}$$
$$h_3 P_3 = 12.356 \times 1.2246 = 15.131 \text{ kW/m °C}.$$

and

$$U_L P_L = 0.77 \times 1.2246 = 0.942 \text{ W/m } °C$$

The collector-efficiency factor F' is determined as

$$F' = \frac{1}{(1 + U_L P_L / h_3 P_3)} \approx 1$$

To calculate the flow-rate factor, one must compute the following parameters:

$$\omega_1 = U_L P_L F' / 2 h_3 P_3 = 0.943 \times 1 / (2 \times 15131) = 3.116 \times 10^{-5}$$

$$\omega_2 = \frac{U_L P_L F'}{2 h_3 P_3} [1 + 4 h_1 P_1 / U_L P_L F']^{1/2} = \frac{0.943 \times 1}{(2 \times 15131)} \left[1 + \frac{4 \times 3556}{0.943 \times 1}\right] = 3.83 \times 10^{-3} \text{ and}$$

$$\xi_1 = \frac{h_3 P_3 l}{\dot{m}_f C_f} = \frac{15131 \times 10.67}{3.14 \times (0.045)^2 \times 3 \times 1000 \times 4190} = 2.0199$$

Furthermore, $\omega_2 \xi_1 = 0.0077$, $\omega_1 \omega_2 = 1.19 \times 10^{-7}$.

After substituting the above values in the expression for F_R, one obtains

$$F_R = (\sinh \omega_2 \xi_1 / \{\omega_2 \xi_1 [\cosh \omega_2 \xi_1 + (\omega_1 \omega_2) \sin \omega_2 \xi_1]\}) F'$$

$$F_R = \frac{0.0077}{0.0077[1.00 + 1.17 \times 10^{-7} \times 0.0077]} \cong 1.0$$

This shows that the collector-efficiency factor F' and the flow-rate factor F_R in the case of evacuated collectors are the same. It is also equal to unity, which cannot be achieved in the case of the flat-plate collector.

7.5 Evacuated Tubular Solar Collector with Heat Pipe [2]

In this section, the design and working principle of a heat pipe and an ETSC will be discussed.

7.5.1 Heat Pipe

Figure 7.9 shows the schematic diagram of heat pipe. Heat pipes are used to transfer heat by a simple method. It consists of a perfectly insulated (to minimize losses from the fluid to the outside) circular pipe with an annular wick layer. Solar radiation incident on the evaporator end boils the fluid inside the pipe. The vapor

Fig. 7.9 Schematic view of heat pipe
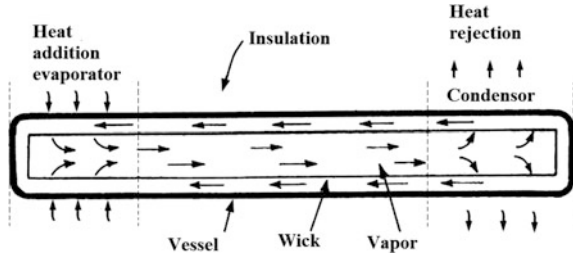
migrates to the condensing end, and transfers the heat of vaporization to the fluid loop at the condensing end. The heat created by the fluid loop is used at the end-use point. After thermal energy is released to the fluid, vapor is condensed and is returned to the boiler end by capillary action through the wicks (in case of horizontal pipes) or by gravitational force.

7.5.2 Corning Tubular Solar Collector with Internal Reflector

A cross-sectional view of a Corning tubular solar collector with (i) a heat pipe and (ii) an internal cusp reflector is shown in Fig. 7.10a. In this collector, there is a glass
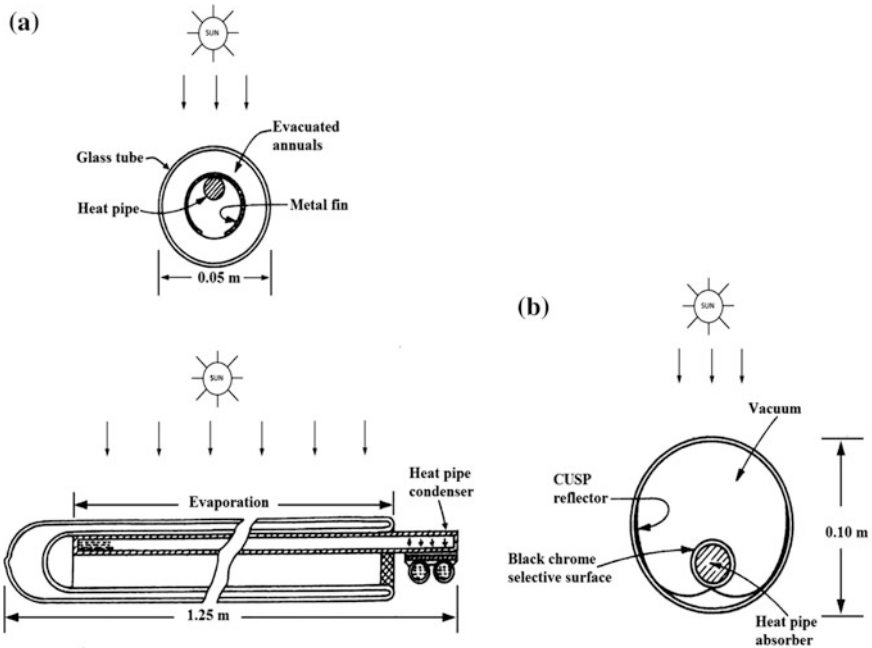
Fig. 7.10 a Cross-sectional view of a Corning evacuated tubular solar collector (ETSC) with heat pipe and internal cusp reflector. **b** Cross-sectional view of a Gumman evacuated tubular solar collector

tube with a diameter of 0.10 m and a length of 1.4 m. The position of the cusp reflector is in half of the tube. The heat pipe is placed at the focal point of the reflector. The outer surface of the evaporator of the heat pipe is a black chrome selective surface to minimize emittance. It also absorbs maximum solar radiation.

The evaporator of the heat pipe is covered with a glass tube along with the cusp reflector. The condenser is exposed to the end-point use. The end-point use may be immersed in working fluid either (i) directly or through (ii) the heat exchanger. This transfers the heat from the condenser to the working fluid.

7.5.3 Gumman Evacuated Tubular Solar Collector (ETSC)

A metal fin is used in the Gumman ETSC to maximize heat transfer from absorbed solar energy at the absorber. A cross-sectional view of the Gumman ETSC is shown in Fig. 7.10b. The position of the heat pipe evaporator and the condenser are also shown in same figure. The evaporator is exposed to solar radiation, and the condenser is attached with a tube in the plate-configuration plate. The working fluid flows through the tube flat plate of the condenser.

7.5.4 Thermal Analysis

A schematic view of an evacuated tubular solar collector with a selectively coated fin-absorber plate is shown in Fig. 7.11a. It comprises a heat pipe having an evaporator at one end and a condenser at the other end. The condenser is attached through a manifold, which transfers the heat of vaporization to the working fluid. The whole assembly is enclosed independently with an evacuated cylindrical envelope.

An electrical network for a system under consideration is shown in Fig. 7.11b for analysis. The figure also shows the thermal resistance at various points. The rate of energy transferred from one point to another is also shown.

Under steady-state conditions, the rate of useful energy $\left(\dot{Q}_u\right)$ available with the fin plate can be written by the following equation:

$$\dot{Q}_u = A_c \left[\dot{q}_{ab} - U_L \left(T_p - T_a\right)\right] \tag{7.31}$$

where $\dot{q}_{ab}$ is defined in Chap. 5. It is the rate of absorbed thermal energy in W/m^2.
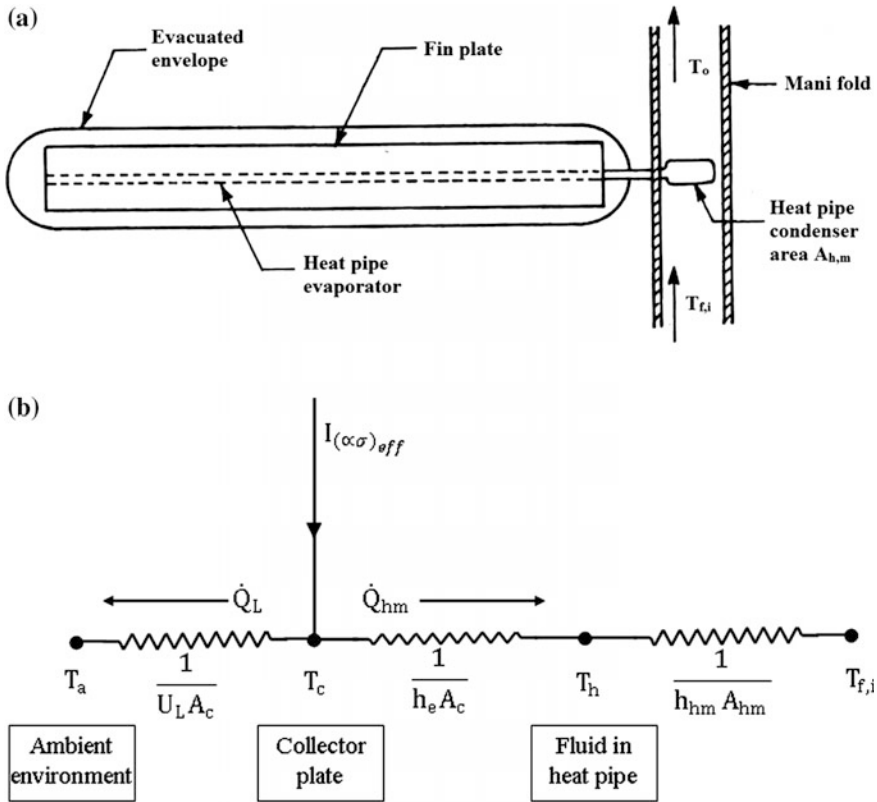
Fig. 7.11 a Cross-sectional view of evacuated tubular solar collector (ETSC) with heat pipe. **b** Thermal circuit diagram of (**a**)

The rate of thermal energy transferred from the fin-plate absorber to the working fluid in the evaporator heat pipe can be expressed as follows:

$$\dot{Q}_{p,h} = h_{ph}A_c\left(T_p - T_h\right) \tag{7.32}$$

After elimination of T_p from Eqs. (7.31) and (7.32), one gets

$$\dot{Q}_{p,h} = \frac{h_{ph}}{h_{ph} + U_L}A_c[\dot{q}_{ab} - U_L(T_h - T_a)] \tag{7.33}$$

It is assumed that there is no heat loss during heat transfer from the fin plate to the fluid of the evaporator under steady-state conditions. The rate of thermal energy transferred from the heat pipe fluid and manifold pipe can be written as follows:

$$\dot{Q}_{h,m} = h_{hm} A_{hm} (T_h - T_f) \tag{7.34}$$

For steady-state conditions $(\dot{Q}_{p,h} = \dot{Q}_{h,m})$, after eliminating T_h from Eqs. (7.33) and (7.34), one obtains

$$\dot{Q}_{h,m} = F' A_c [\dot{q}_{ab} - U_L (T_f - T_a)] \tag{7.35}$$

where

$$F' = \frac{1}{\left(\frac{U_L A_c}{h_{hm} A_{hm}}\right) + \left(\frac{U_L}{h_{ph}} + 1\right)} = \frac{1/U_L}{\left(\frac{A_c}{h_{hm} A_{hm}}\right) + \left(\frac{1}{h_{ph}} + \frac{1}{U_L}\right)} \tag{7.36}$$

where F' is one gets collector-efficiency factor similar to Eq. (5.62) obtained for a FPC.

An instantaneous thermal efficiency (η_i) of a tubular collector with a heat pipe can be written as follows:

$$\eta_i = \frac{\dot{Q}_u}{I A_c} = F'(\alpha\tau) - F' U_L \frac{(T_f - T_a)}{I} \tag{7.37}$$

The above equation is known as a characteristic equation of the tubular solar collector with a heat pipe. Equation (7.37) is same as the Hottel–Whiller–Bliss (HWB) equation of the flat-plate collector. A graph between η_i verses $(T_f - T_a)/I$ gives a straight line with intercept $F'(\alpha\tau)$ and slope $F' U_L$.

The heat collection–efficiency factor (F') depends on three ratios: (i) $U_L/h_{ph} = (0.001-0.50)$, (ii) $U_L/h_{hm} = (0.001-0.50)$, and (iii) $A_{hm}/A_c = (0.001-0.50)$. The effects of these parameters are shown in Fig. 7.12. It is clear from Fig. 7.12a that there is marginal effect of U_L/h_{ph} on F' for $U_L/h_{ph} > 0.01$ for evacuated tubular solar collector manufactured by Phillips, $U_L/h_{ph} (= 0.0038)$. Figure 7.12b shows the effect of U_L/h_{hm} on F' for $U_L/h_{ph} = 0.19$ for different A_{hm}/A_c. This shows that the value of F' is close to 0.8 for $A_{hm}/A_c > 0.1$ and $U_L/h_{hm} < 0.04$. Simultaneously, Fig. 7.12c shows that F' is nearly 0.8 for $A_{hm}/A_c > 0.02$, $U_L/h_{hm} = 0.001$ and $U_L/h_{ph} = 0.19$. The value of F' can go beyond 0.8 for $U_L/h_{ph} = 0.19$ for any value of ratio of resistances >17 (Fig. 7.12d).

It is important to note that this analysis is based on a single tubular module. The value of F' increases appreciably when a module with ≥ 20 tubes is used.

(a)

(b)

(c)

(d)
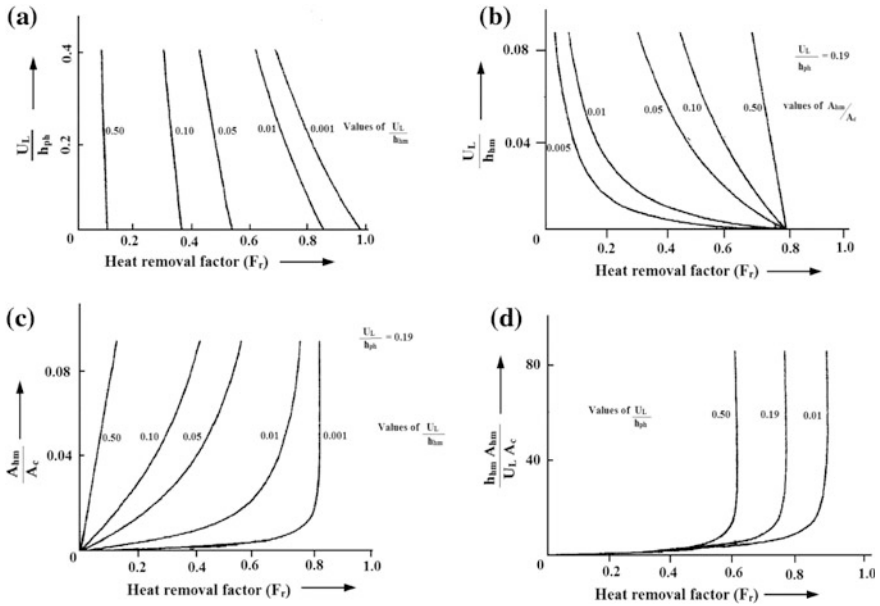
Fig. 7.12 Effect of collection-efficiency factor on various factors. **a–d** Heat removal factor (F_r)

Objective Questions

7.1. Convective heat loss between the absorber and the glass cover is decreased by
   (a) using fins   (b) creating a vacuum   (c) selective coating   (d) none of these
   Answer: (b)

7.2. Radiative heat loss between the absorber and the glass cover is decreased by
   (a) using a selective coating   (b) using a vacuum
   (c) using fins   (d) none of these
   Answer: (a)

7.3. The vacuum between absorber and glass cover can be maintained only in
   (a) a flat-plate collector   (b) a concentrating collector
   (c) a tubular collector   (d) none of these
   Answer: (c)

7.4. The outlet-fluid temperature is maximal in
   (a) a flat-plate collector   (b) an evacuated tubular collector
   (c) a fin-type flat-plate collector   (d) none of these
   Answer: (b)

7.5. The instantaneous thermal efficiency of an evacuated tubular collector at a higher operating temperature is
(a) greater than that of a flat-plate collector
(b) less than that of a flat-plate collector
(c) equal to that of a flat-plate collector
(d) none of these
Answer: (b)

7.6. The overall top-loss coefficient for an evacuated tubular collector (U_t) is
(a) less than that for a flat-plate collector
(b) greater than the value for a flat-plate collector
(c) equal to the value for a flat-plate collector
(d) none of these
Answer: (a)

7.7. The Phillips (Germany) evacuated tube collectors are connected in
(a) series   (b) parallel   (c) series and parallel   (d) none of these
Answer: (a)

7.8. The Sanyo evacuated tube collectors are connected in
(a) parallel   (b) series   (c) series and parallel   (d) none of these
Answer: (a)

7.9. In a Solaron air collector, the air passes through
(a) an evacuated tube   (b) below the evacuated tube
(c) above the evacuated tube   (d) none of these
Answer: (b)

7.10. In Phillips (Germany) water collector, the water passes
(a) below the evacuated tube   (b) above the evacuated tube
(c) through the evacuated tube   (d) none of these
Answer: (a)

7.11. Convective heat loss becomes negligible in a
(a) a flat-plate collector   (b) a concentrating collector
(c) an evacuated tube   (d) none of these
Answer: (c)

7.12. The absorber temperature in an evacuated tubular collector is
(a) less than that of a concentrating collector
(b) greater than that of a unglazed flat-plate collector
(c) greater than that of a glazed flat-plate collector
(d) all of these
Answer: (c)

7.13. The heat pipe transfers heat from a higher temperature to lower temperature by
(a) a flow of vapour   (b) convection   (c) conduction   (d) none greater than that of a
Answer: (a)

7.14. The performance of Corning evacuated collector with a heat pipe is more effective than

(a) a flat-plate collector   (b) an evacuated collector
(c) a heat pipe   (d) all of these
Answer: (b)

7.15. The expression of instantaneous thermal efficiency of a flat-plate collector
and an evacuated collector with and without a heat pipe are
(a) similar   (b) different   (c) unlike   (d) none greater than that of a
Answer: (d)

7.16. The value of the threshold intensity in the case of an evacuated collector is
(a) lower than the threshold intensity in the case of a flat-plate collector
(b) higher than the threshold intensity in the case of an FPC
(c) equal to the threshold intensity in the case of an FPC
(d) none of these
Answer: (a)

7.17. The value of the threshold intensity in the case of an evacuated collector is
lower due to
(a) decreased top-loss coefficient (U_t) (b) high operating temperature
(c) better design of collector   (d) none of these
Answer: (a)

7.18. The cost per m^2 of an evacuated tubular collector on a large scale is
(a) cheaper than the cost per m^2 of a flat-plate collector
(b) marginally equal to the cost per m^2 of an FPC
(c) higher than cost per m^2 of an FPC
(d) none of these
Answer: (a)

Problems

7.1. Write an expression (formula) for the rate of useful thermal energy $(\dot{Q}_{u,m})$ for
an m-ETSC connected in parallel under a natural mode of operation.
Hint: Multiply Eq. (E-4) (Example 7.1) by m.

7.2. Write an expression (formula) for the rate of useful thermal energy $(\dot{Q}_{u,Nm})$ for
an N-ETSC when connected in series and in parallel.
Hint: Multiply Eq. (7.24a) (Example 7.1) by m.

7.3. Write an energy-balance equation for a water-heating system of heat capacity
$(M_w C_w)$ integrated with m-ETSC connected in parallel without any heat losses
from of these storage tank under forced mode of operation.
Hint: Multiply Eq. (7.23a) by m and equate with $\left[M_w C_w \dfrac{dT_w}{dt} \right]$ and $T_{fi} = T_w$.

7.4. Determine an analytical expression for water temperature for Problem 7.3.

References

1. D.C. Beekley, G.R. Mather Jr., *Analysis and Experimental Test of High Performance Evacuated Tubular Collector*, DOE/NASA, CR-/50874 (1978)
2. B. Norton, *Solar Energy Thermal Technology* (Springer, London, 1992)

Additional References

3. G.N. Tiwari, *Solar Energy: Fundamentals, Design, Modeling and Applications* (Narosa Publishing House, New Delhi, India, 2004). (Also published by Alpha Science, UK and CRC Press, UK)
4. J.R. Williams, Am. Arbor Sci. **1**, 187 (1983)

Chapter 8
Solar Water-Heating Systems

Abstract A solar water-heating system is a device to store hot water available from a combination of flat-plate collectors (FPCs) and evacuated tubular solar collectors (ETSCs) at a moderate-temperature. Solar collectors can be connected in a combination of series and parallel per the requirement. Such a water heating system is mostly used during either off-sunshine hours or when there is a low level of solar radiation.

8.1   Introduction

The main component of a solar flat-plate collector (FPC), which is generally used for water heating, is the blackened absorber surface. Furthermore, the blackened absorber surface can be broadly classified as follows:

 (a) **Parallel flat plate**: In this case, the water can be stagnant either above the absorber or below the absorber for heating purposes. The water is heated by convective heat-transfer from the blackened absorber surface to the water. If the water depth (heat capacity, $M_w C_w$) is large, then such a water heater can also store the thermal energy due to reduced heat loss. This type of water heater is referred to as a "**collection-cum-storage water heater**." This can be used as a domestic-level application.
 (b) **Tube and plate**: In collection–cum-storage water heater, the temperature of water is lower due to the large heat capacity. To increase the temperature of the water, there should be least the heat capacity (lower water mass) of water. This condition can only be achieved in a tube-and-plate configuration. The flat-plate collector is generally used for large-scale water heating. The heated water in a flat-plate collector is then stored in an insulated storage tank. The mode of transfer of heated water from the FPC to an insulated storage tank can be either (i) natural circulation (thermo siphon) or (ii) forced-circulation mode.

Such a water heating system is referred to as a "**conventional water-heating system**." Furthermore, the transfer of heated water may be performed either directly or through a heat exchanger. These water solar heaters employ water as a transport fluid for energy transfer from the collection unit to the storage one. Water, apart from being a low cost and easily available fluid, has many advantageous thermo-chemical properties such as nontoxic, nonflammable, high specific heat, good heat-transfer and fluid dynamic characteristics, and suitable liquid–vapour equilibrium and temperature–pressure relationship for space-heating and cooling applications.

8.2 Collection-Cum-Storage Solar Water Heater

A collection-cum-storage solar water heater combines both collection and storage in the same unit. Thus there is no need of a separate insulated tank for the storage of hot water.

Collection-cum-storage water heaters can be classified as follows:

(i) **Built-in storage solar water heater** [1–4]
(ii) **Shallow solar pond (SSP) solar water heater** [4, 5]

Brief descriptions of the two are given below.

8.2.1 Built-in Storage Water Heater

In built-in storage water heaters, the water is below the absorber of the parallel flat-plate collector. It is compact in design, has a low cost, and is easy to install. In addition, they have a good collection efficiency and satisfactory overnight thermal storage.

A built-in storage water heater, as shown in Fig. 8.1, consists of a rectangular insulated tank. The tank is usually made of galvanized iron with dimensions of 1.12 m × 0.08 m × 0.1 m and is encased in a mild- iron or wooden box (1.22 m × 0.9 m × 0.2 m). The top surface of the tank is painted with blackboard paint. Furthermore, it is covered with one or two window-glass covers (3-mm thick) with approximately 4-cm air gaps between the absorbing surface and the glass cover. Due to the enormous water pressure, there is bulging of the tank; hence, braces are provided.

Cold water is fed through the inlet. Hot water is withdrawn from the outlet. In case there is no provision of piped water supply, hot water can be withdrawn by adding cold water into the inlet through a large funnel fixed at the top of the heater.

Fig. 8.1 Built-in storage water heater (from [12])
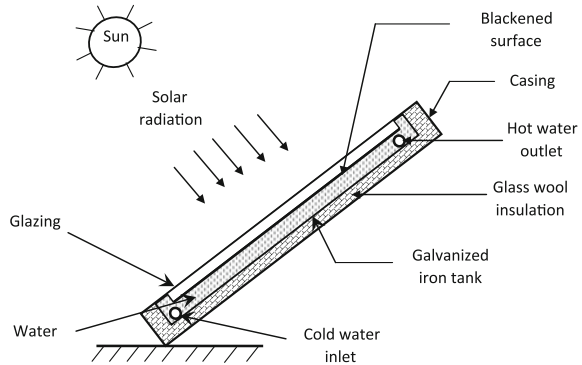
The major thermal losses in a built-in storage solar water heater are radiative and convective from the top surface during off sunshine hours. In this case, the solar heater cannot provide hot water in the early morning. To improve the night-time performance, the solar water heater should be covered with an adequate thickness of glass-wool insulation. The water is allowed to heat up during the day. The top of the tank is covered with insulation when the thermal collection reduces to zero (during off-sunshine hours).

Energy-balance equation:

To write an energy balance of a built-in storage solar water heater; it is fair to assume the same absorber and water temperature. Under this assumption, an energy balance can be written as

$$A_c[(\alpha\tau)I(t) - U_t(T_w - T_a)] = M_w C_w \frac{dT_w}{dt} + U_b(A_c + A_e)(T_w - T_a) \qquad (8.1)$$

where $U_t = \left[\frac{1}{h_1} + \frac{1}{h_2} + \frac{1}{h_{pw}}\right]^{-1}$, $U_b = \left[\frac{L_i}{K_i} + \frac{1}{h_i}\right]^{-1}$; and h_{pw} is the convective heat-transfer coefficient from the absorber plate to the water. Because the value of h_{pw} is very large, it can be neglected (see Example 8.1).

Equation (8.1) can be written as follows:

$$\frac{dT_w}{dt} + aT_w = f(t) \qquad (8.2)$$

where $a = \frac{\{A_c(U_t + U_b) + A_e U_b\}}{M_w C_w}$ and $f(t) = \frac{A_c(\alpha\tau)I(t) + \{A_c(U_t + U_b) + A_e U_b\}T_a}{M_w C_w}$

The solution of Eq. (8.2) can be obtained with following assumptions:

(a) $f(t)$ should be considered as $\overline{f(t)}$ for Δt time interval; and
(b) T_w is T_{wo} at $t = 0$.

Now the solution of Eq. (8.2) is given by

$$T_w = \frac{\overline{f(t)}}{a}[1 - \exp(-a\Delta t)] + T_{w0}\exp(-a\Delta t) \qquad (8.3)$$

or

$$\Delta t = -\frac{1}{a}\ln\left[\frac{T_w - \frac{\overline{f(t)}}{a}}{T_{w0} - \frac{\overline{f(t)}}{a}}\right] \qquad (8.4)$$

Example 8.1 Evaluate the convective heat-transfer coefficient (h_{pw}) from a blackened surface to a water mass (at $20\,°C$) for a built-in storage water heater for an effective area of 1 m × 1 m = 1 m².

Solution
From Appendix V, the properties of water at 20 °C are

$$v = 1.006 \times 10^{-6}\,m^2/s, \ K = 0.5967\,W/mK \text{ and } Pr = 7.02.$$

These values can be substituted in Eq. (3.22d), and the value of the Grashof number is calculated as

$$Gr = (9.8 \times 1 \times 0.1)/\left\{298 \times \left(1.006 \times 10^{-6}\right)^2\right\} = 3.2495 \times 10^9.$$

The value of the Nusselt number can be obtained from Eq. (3.24) using the values of $C = 0.15$ and $m = 1/3$ from Table 3.3.
Thus, $Nu = 425.4105$
Now $Nu = h_{pw}X/K$, where X is the characteristic dimension and is given by $(1 + 1)/2 = 1$.
Thus, $h_{pw} = 253.84\,W/m^2\,°C$

Example 8.2 Calculate an overall heat-transfer coefficient from water to the ambient (U_t) air through a blackened surface and glass cover, e.g., as in Example 8.1.

Solution
From Eq. (8.1) one has $U_t = \left[\frac{1}{h_1} + \frac{1}{h_2} + \frac{1}{h_{pw}}\right]^{-1}$

Here h_1 and h_2 are the heat-transfer coefficient from the absorber to the glass cover and from the glass cover to the ambient air, respectively. The values of h_1 and h_2 are given as

$$h_1 = 5.7\,W/m^2\,°C \text{ and } h_2 = 9.5\,W/m^2\,°C.$$

The values of $h_{pw} = 253.84\,\text{W/m}^2\,{}^\circ\text{C}$ (Example 8.1).

After substituting the corresponding values in the above equation, one obtains

$$U_t = \left[\frac{1}{5.7} + \frac{1}{9.5} + \frac{1}{253.84}\right]^{-1} \quad U_t = [0.175 + 0.105 + 0.0039]^{-1} = 3.57\,\text{W/m}^2\,{}^\circ\text{C}$$

Example 8.2 justifies our assumption of the water and the plate temperature being the same.

8.2.2 Shallow Solar Pond (SSP) Solar Water Heater

In this case, the water is placed between the absorber and the glass cover unlike the built-in-storage solar water heater. Such a solar water heater is referred to as a "shallow solar pond (SSP)." It is a simple and cost-effective device to harness solar energy for water heating.

A shallow solar pond (SSP) solar water heater consists of a blackened tray filled with water of small depth (say, approximately 0.10 m). The tray is properly insulated from the bottom and sides to reduce conductive heat losses. Evaporative cooling in a SSP solar water heater is suppressed by covering the water surface with a transparent glass/plastic sheet to avoid evaporation. Incident solar energy is absorbed at the blackened surface after transmission from the glass cover and the water mass, and absorbed energy is transferred to the water column by convection. Thus, the water is heated.

A compact SSP solar water heater consists of a pillow-type water bag placed in an insulated (from side and bottom) wooden box that is transparent on top with a blackened bottom to receive and absorb the maximum solar radiation for heating. It has a thermally insulated cover at the top, which can be used as a booster mirror during the day and as an insulation cover during off-sunshine hours, thus providing a means of overnight storage as shown in Fig. 8.2.

An efficient performance of the SSP solar water heater demands continuous withdrawal of hot water from the pond to reduce thermal losses.

Three modes of hot-water withdrawal from an SSP have been suggested

(a) **Batch withdrawal**: In the batch-withdrawal mode, the pond is filled early in the morning and is emptied into an insulated storage reservoir in the afternoon to achieve maximum water temperature.
(b) **Closed-cycle continuous flow**: In the closed-cycle mode, the water is circulated continuously at a constant flow rate between the SSP and the storage with or without the extraction of heat from storage by way of heat exchanger. In this case also, the pond water is transferred to storage in the afternoon.

Fig. 8.2 Schematic diagram
of a compact SSP (from [12])
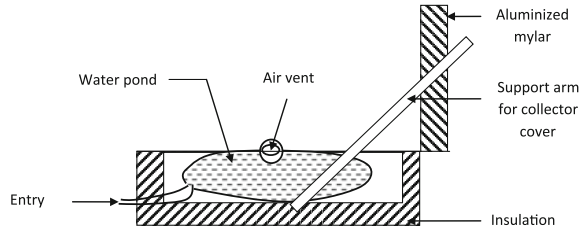
(c) **Open-cycle continuous flow**: In the open-cycle mode, water at an initial
temperature enters the pond, and the hot water flowing through the pond is
drained out continuously into storage or for some other end-use application.
The pond is emptied in the evening when the heat collection reduces to zero.

The solar heater can be designed to optimize performance. The water temper-
ature is observed to decrease with increasing water depth. Greater water depth
results in more water mass and hence a higher heat capacity per square meter.

Energy Balance:
To write an energy balance of an SSP solar water heater, it is fair to assume the
same absorber and water temperature. Under this assumption, an energy balance
can be written as

$$
A_c[(\alpha\tau)I(t) - U_t(T_w - T_a)] = M_w C_w \frac{dT_w}{dt} + U_b(A_c + A_e)(T_w - T_a) + \varepsilon \dot{M}_w C_w (T_w - T_a)
$$

$$(8.5)$$

where ε is the effectiveness of a heat exchanger placed in the storage tank for the
transfer of heat from the SSP water heater to the storage tank under a **closed-cycle
continuous (CCC) flow**, which is always <1 and $\dot{M}_w > 0$. The $\dot{M}_w = 0$ for **batch
withdrawal (BW)** and $\dot{M}_w > 0$ and $\varepsilon = 1$ for **open-cycle continuous (OCC) flow**.
The expression for U_t is given by

$$
U_t = \left[\frac{1}{h_1} + \frac{1}{h_2} + \frac{1}{h_{pw}}\right]^{-1}
$$

The solution of Eq. (8.5) can be obtained as done for a built-in storage water
heater.

The overall thermal efficiency of a collection-cum-storage solar water heater can
be defined as follows:

$$
\eta_{ov}(\%) = \frac{M_w C_w \left(T_{w(max)} - T_{in}\right)}{A_c \sum I_i(t)\Delta t} \times 100
$$

$$(8.6)$$

Fig. 8.3 Effect of storage-tank depth on storage temperature and efficiency (from [12])
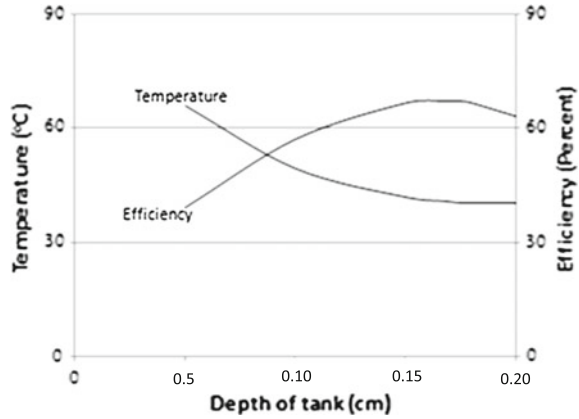
The effect of water depth on the maximum water temperature, as well as on the overall thermal efficiency, is shown in Fig. 8.3 for both built-in storage and SSP water heaters. It can be observed that the maximum water temperature in case of a SSP solar water heater is greater than that of a built-in storage water heater. This may be due to fact that the rate of thermal energy available for an SSP solar water heater is more. Furthermore, an overall thermal efficiency of an SSP solar water heater is less due to there being more thermal losses from the top cover unlike with a built-in storage solar water heater. As the water depth increases, the overall collection thermal efficiency increases due to the decrease in top thermal losses to the outside air. However, the thermal efficiency in both cases becomes stagnant up to a water depth of 10 cm; hence, one can conclude that a 10-cm water depth gives optimal thermal performance.

Losses from the top and bottom can be reduced by optimizing the thickness of the insulation. It has been seen that a 5.0-cm thickness of insulation is optimum for minimum heat loss from the bottom and top surfaces. The performance of the system can be improved by using a reflecting sheet (can be used as booster mirror) having 0.03 emissivity and a 5-cm air gap, which is equivalent to a 5 cm—thick layer of glass wool insulation.

Example 8.3 Calculate the convective heat-transfer coefficient from the blackened surface to the water $(60\,^\circ C)$ for an SSP solar water heater of area 1 m $\times$ 1 m.

Solution
From Appendix V, the properties of water at $60\,^\circ C$ are

$$v = 4.775 \times 10^{-7}\,\text{m}^2/\text{s},\ K = 0.6503\,\text{W/mK and } Pr = 3.02$$

From Eq. (3.22d), the Grashof number can be calculated as

$$Gr = (9.8 \times 1 \times 0.1)/\left\{333 \times \left(4.775 \times 10^{-6}\right)^2\right\} = 1.291 \times 10^{10}$$

From Eq. (3.24), the Nusselt number can be calculated using the values of C and m from Table 2.3 as follows:

$$Nu = 0.15 \times \left(3.898 \times 10^{10}\right)^{1/3} = 508.595$$

Thus, the convective heat-transfer coefficient from the blackened surface to water is calculated as

$$h = NuK/X = 330.74 \, \text{W/m}^2 \, °\text{C}$$

Example 8.4 Calculate the overall top-loss coefficient for a shallow solar pod (SSP) solar water heater if it is covered with 10 cm-thick glass wool insulation during off-sunshine hours.

Solution
The overall top-loss coefficient of an SSP solar water heater during off-sunshine hours is given by the following:
   For glass wool of thickness $(L_i) = 10 \, \text{cm} = 0.10 \, \text{m}$ and thermal conductivity $(K_i) = 0.0541 \, \text{W/mK}$

$$U = \left[\frac{1}{h_2} + \frac{L_i}{K_i}\right]^{-1}$$

The h_2 is the convective heat-transfer coefficient from the bottom of the glass wool to the ambient air, and its expression is given by Eq. (3.29a). The value of h_2 for $V = 3 \, \text{m/s} = 17.1 \, \text{W/m}^2 \, °\text{C}$.

$$U = \left[\frac{1}{17.1} + \frac{0.1}{0.0541}\right]^{-1} = 0.5247 \, \text{W/m}^2 \, °\text{C}$$

8.3   Solar Water-Heating System

A conventional solar water-heating system essentially consists of (a) the collection unit and (b) the insulated storage unit. The collection unit is a combination of flat-plate collectors (FPC) (Chap. 5, Sect. 5.2). The hot water, available at outlet (T_{fo}), is transferred to the insulated storage tank to reduce possible heat losses for the storage of hot water during off-sunshine hours (nighttime). Transportation of the hot water from the flat-plate collector (FPC) to the insulated storage tank can be performed by two modes, namely:

(i) **The thermo siphon/natural mode**: In this case, the hot water is circulated between the FPC to the insulated tank under gravitational force. To achieve this, an insulated storage tank should be placed above the flat-plate collector modules. This height should be at least 1 foot above the FPCs as shown in Fig. 8.4. There are three type of such water heater, namely

   (a) **Nonpressure type**: The schematic diagram of a nonpressure-type solar water heater with natural circulation is shown in Fig. 8.4a. In this case, an insulated storage tank is filled with cold water once in the morning, and hot water can be withdrawn per requirement at any time in the day or night.

   (b) **Pressure type**: The schematic diagram of pressure-type solar water heater with natural circulation is shown in Fig. 8.4b. In this case too, an insulated storage tank is filled with cold water once in the morning. However, hot water can only be withdrawn if main water line has water with sufficient pressure.

   (c) **Pressure type with heat exchanger**: The schematic diagram of pressure-type solar water heater with natural circulation with heat exchanger is shown in Fig. 8.4c. It is important to mention here that the heat exchanger is used only for the withdrawal of hot water from the insulated storage tank. For this, too, there should be sufficient pressure in the main line to withdraw hot water.

(ii) **Forced-circulation mode**: In this case, there is no need of placing an insulated storage tank above the FPC module due to the forced circulation of hot water between the FPC and the insulted tank. Here a water pump for a given capacity is required for the flow of water as shown in Fig. 8.5.

8.3.1 *Natural Circulation* [6]

A schematic diagram of a nonpressure-type solar water heater consists of m-FPCs connected in parallel under natural circulation mode. The storage tank of water heat capacity of $(MC)_w$ is an insulated cylinder with two inlets: One inlet is for the hot water coming from the outlet at mth FPC [T_{foN}, Eq. (5.88)], and the other inlet is to allow the cold water from the mains to reach the bottom of the insulated storage tank without it mixing with hot water. There are two outlets, namely, (i) for the withdrawal of hot water and (ii) to feed cold water to the inlet of first flat-plate collector. To reduce heat loss, the entire length of the connecting pipes is perfectly insulated. Solar radiation incident on the flat-plate collector modules heat the water inside. The hot water rises up the collector due to its lesser density. The vacuum created by this flow is filled up by the cold water from the insulated storage tank

Fig. 8.4 a Schematic
diagram of a nonpressure-type
solar water heater with natural
circulation. **b** Schematic
diagram of a pressure-type
solar water heater with natural
circulation. **c** Schematic
diagram of a pressure-type
solar water heater with natural
circulation and a heat
exchanger
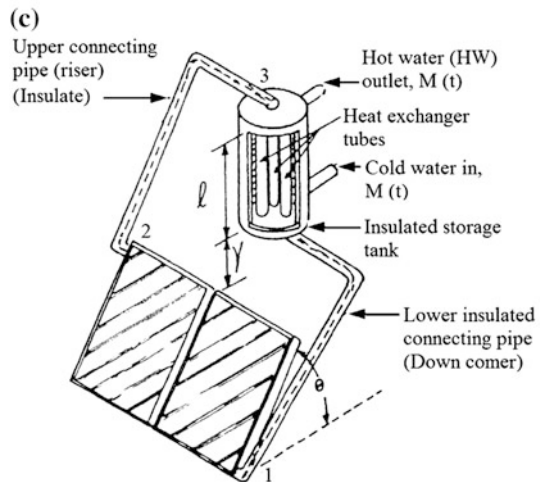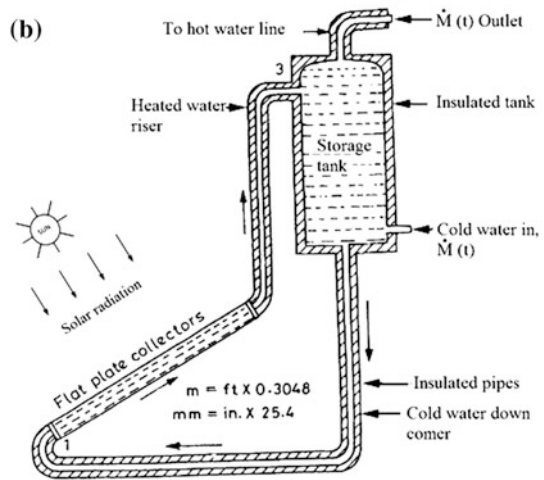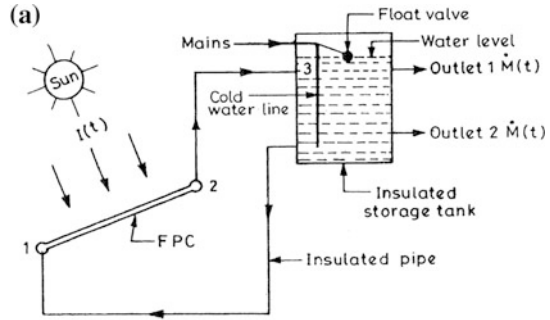
Fig. 8.5 Schematic diagram of a simple single-loop water-heating system
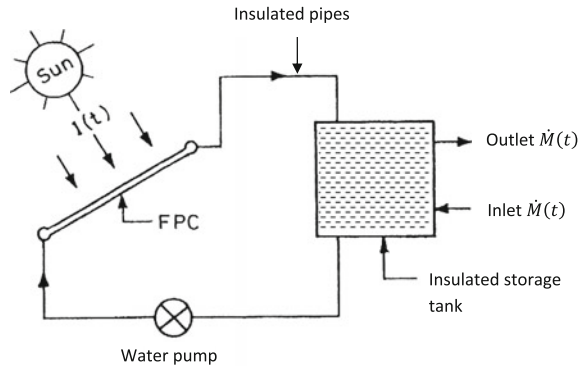
Fig. 8.6 View of m-FPCs connected in parallel to an insulated storage tank
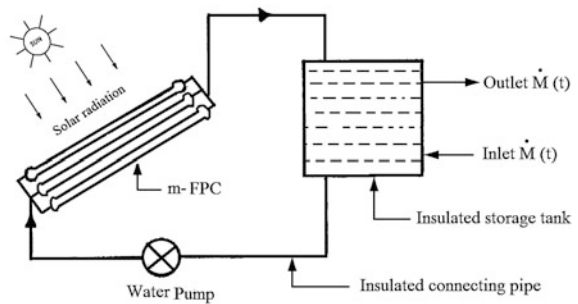
under gravity. Thus, the upper ends (2) of the collector modules have hot water, whereas the lower ends (1) have cold water. This hot water then enters the storage tank from inlet 3 as shown in Fig. 8.6.

Referring to Fig. 8.6, the energy balance for different components of a solar water-heating system can be written with the following assumptions:

- The heat capacity (mass × specific heat) of glass cover, connecting pipes, absorber plate, pipes, insulating materials, and storage materials are negligible compared with heat capacity of the water.
- The average temperature of the water in a solar FPC (between the upper and lower headers) and the storage tank (top and bottom water) is approximately the same.
- There are no heat losses from the insulating connecting pipes between the solar FPC and the storage tank.

The energy balances are as follows:

(i) **During sunshine hour**

Solar flat-plate collectors connected in parallel

From Eq. (5.84), the rate of thermal energy available from m-FPCs connected in parallel can be written as

$$\dot{Q}_{um} = A_{cm}F'[(\alpha\tau)I(t) - U_L(T_f - T_a)] = \dot{m}_f C_f(T_2 - T_1) \qquad (8.7)$$

where $A_{cm} = mA_c$; A_c is the effective area of one solar FPC; F' is the solar flat plate–collection efficiency factor; T_2 and T_1 are the outlet and inlet water temperature of the solar FPCs connected in parallel; $\dot{m}_f$ is the mass flow rate of water due to natural circulation, which depends on solar radiation; and T_f is the average temperature of the outlet and inlet water.

Storage tank

Because there is no losses occurring through the connecting pipes between the solar FPCs and the insulated storage tank, then the thermal energy available from the m-FPCs will be distributed as the (i) thermal energy stored in storage tank's water, (ii) the thermal energy lost to the ambient air from the storage tank, and (iii) the thermal energy withdrawn from the storage tank.

Now the energy balance of the storage tank can be written as

$$\dot{m}_f C_f(T_2 - T_1) = M_w C_w \frac{dT_w}{dt} + (UA)_t(T_w - T_a) + \dot{M}_w C_w(T_w - T_a) \qquad (8.8)$$

where M_w and $\dot{M}_w$ are the mass of water in the tank and the mass-flow rate of hot-water withdrawal; and $(UA)_t$ is an overall heat-transfer coefficient from the water of the storage tank to the ambient air through the insulation.

Equations (8.7) and (8.8) can be combined as follows:

$$A_{cm}F'[(\alpha\tau)I(t) - U_L(T_f - T_a)] = M_w C_w \frac{dT_w}{dt} + (UA)_t(T_w - T_a) + \dot{M}_w C_w(T_w - T_a)$$
$$(8.9)$$

Per one of assumptions, $T_f = T_w$, then Eq. (8.9) becomes

$$A_{cm}F'[(\alpha\tau)I(t) - U_L(T_w - T_a)] = M_w C_w \frac{dT_w}{dt} + (UA)_t(T_w - T_a) + \dot{M}_w C_w(T_w - T_a)$$
$$(8.10)$$

(ii) **Off-sunshine hours**

During off-sunshine hours, the FPC's modules are disconnected from the storage tank to avoid reverse flow of thermal energy from the storage tank to FPC's module. In this case, the energy balance will be as follows:

$$M_w C_w \frac{dT_w}{dt} + (UA)_t(T_w - T_a) + \dot{M}_w C_w(T_w - T_a) = 0 \tag{8.11}$$

Equations (8.10) and (8.11) can be written in the following form:

$$\frac{dT_w}{dt} + aT_w = f(t) \tag{8.12}$$

where

$$a = \frac{A_{cm}F'U_L + (UA)_t + \dot{M}_w C_w}{M_w C_w} \quad \text{during sunshine hours}$$

$$= \frac{(UA)_t + \dot{M}_w C_w}{M_w C_w} \quad \text{during off sunshine hours}$$

and

$$f(t) = \frac{A_{cm}F'(\alpha\tau)I(t) + \left[A_{cm}F'U_L + \{(UA)_t + \dot{M}_w C_w\}T_a\right]}{M_w C_w} \quad \text{during sunshine hours}$$

$$= \frac{\{(UA)_t + \dot{M}_w C_w\}T_a}{M_w C_w} \quad \text{during off sunshine hours}$$

The solution of Eq. (8.12) with the initial conditions $Tw = T_{w0}$ at $t = 0$ and $f(t) = \overline{f(t)}$ and constant 'a' within the interval Δt $(0 < t < \Delta t)$ can be written as

$$T_w = \frac{\overline{f(t)}}{a}\left(1 - e^{-a\Delta t}\right) + T_{w0}e^{-a\Delta t} \tag{8.13}$$

The overall thermal efficiency of the system can be defined in two cases:

(i) **Without hot-water withdrawal**

$$\eta = \frac{M_w C_w\left[T_{w,max} - T_{w0}\right]}{A_{cm}\int I(t)dt} \tag{8.14a}$$

(ii) **With hot-water withdrawal**

$$\eta = \frac{\sum_{i=1}^{n}\dot{M}_w C_w(T_w - T_{in})}{A_{CN}\int_0^T (t)dt} \tag{8.14b}$$

8.3.2 *Forced-Circulation Solar Water Heater [7–9]*

In this case, to transfer the hot water available at the upper header of the collector to the insulated storage tank, a water pump is used at the inlet of the collector between the solar flat-plate collector and the insulated storage tank. The solar FPCs can also be connected either in parallel, in series, or in a combination of both, as discussed in Sect. 5.8, for higher water temperature if required. Furthermore, it is important to mention here that for forced mode we need power; hence, PVT solar FPCs should be provided to make the system sustainable as shown in Fig. 8.7a.

A single- and double-loop water heating system will be discussed in the next section.

(i) **Single Loop** [8]

A line diagram of single-loop solar water-heating system is shown in Fig. 8.7b. It operates continuously until pump is switched off manually. This problem is automatically solved in the case of single-loop PVT solar water-heating system as shown in Fig. 8.7a. In this case, a DC pump operates only if there is solar radiation. Otherwise a controller with a sensor should be used as shown in Fig. 8.7c. The sensor is fitted at the outlet of the solar FPC. In this case, the pump operates at a desired set temperature. Furthermore, a coil-type heat exchanger with a controller is used in the collector loop inside the storage tank as shown in Fig. 8.7d. Antifreeze liquid is used in the collector loop. This is required in harsh cold climatic conditions where the temperature decreases beyond $0\,°C$. Another type of heat exchanger can also be used in a collector loop as shown in Fig. 8.7e. This is known as a "heating jacket used outside the tank." The maintenance of such a heat exchanger becomes easier. A detailed analysis of Figs. 8.7b to 8.8 will be discussed in the coming sections.

A complete set-up of a domestic solar water-heating system is shown in Fig. 8.8. Hot water can be withdrawn for a continuous supply of cold water at inlet under pressure. The nonreturn check valve is used. The controller with a sensor is connected to the absorber outlet and the storage tank. A back-up unit is also provided at the outside of the storage tank.

Energy Balance

In this case, water in the storage tank is allowed to pass through the inlet of the FPCs, i.e., $T_w = T_{fi}$. The flow of cold water from the insulated storage tank to the inlet of the collector is maintained by a pump as shown in Fig. 8.7b. An energy balance under forced mode for a simple and single-loop solar water heater can be written as

$$\dot{Q}_{uN} = M_w C_w \frac{dT_w}{dt} + (UA)_t (T_w - T_a) + \dot{M} C_w (T_w - T_a) \qquad (8.15)$$
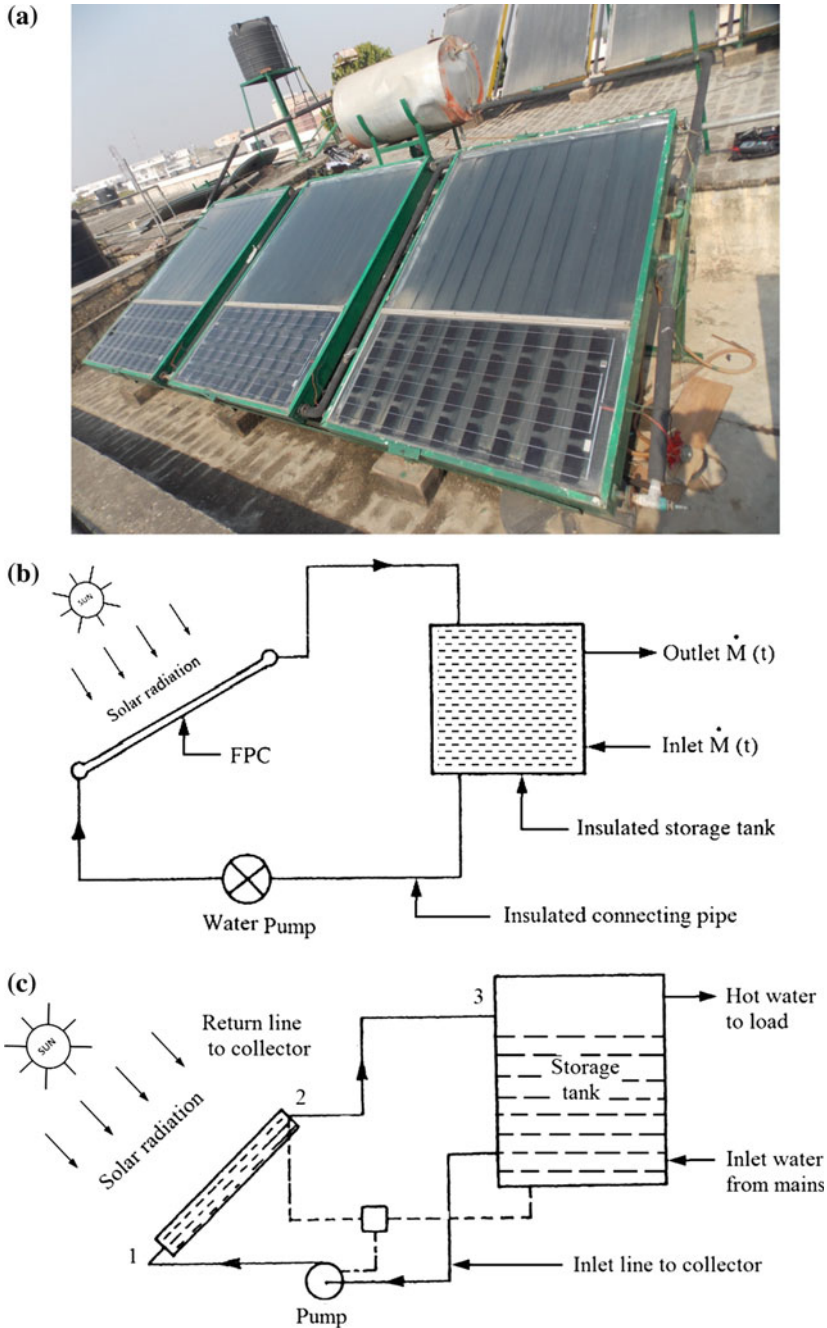
Fig. 8.7 **a** Photograph of a single loop of a PVT water-heating system at IIT Delhi. **b** Schematic diagram of a simple single-loop water-heating system. **c** Schematic diagram of a simple single-loop water-heating system with a sensor and a controller. **d** Schematic diagram of a simple single-loop water-heating system with s sensor, a controller, and a heat exchanger. **e** Schematic diagram of a simple single-loop water-heating system with a sensor, a controller, and a back-up

(d)

(e)
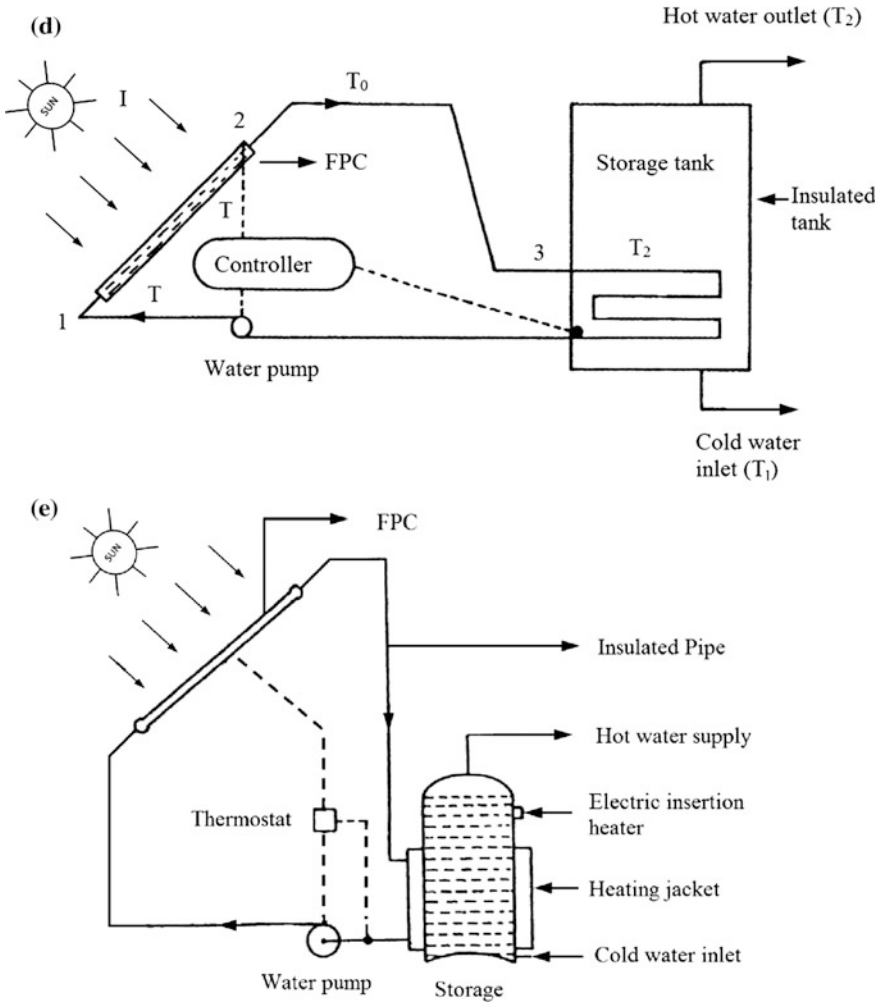
Fig. 8.7 (continued)

where an expression for $\dot{Q}_{uN}$ for the following conditions is as follows:

(a) For N-FPCs connected in series (Eq. 5.89b)

$$\dot{Q}_{uN} = NA_c F_{RN}[(\alpha\tau)I(t) - U_L(T_{fi} - T_a)] \tag{8.16}$$

where $F_{RN} = \frac{\dot{m}_f C_f}{NA_c U_L}\left[1 - \exp\left\{-\frac{NF'A_c U_L}{\dot{m}_f C_f}\right\}\right]$
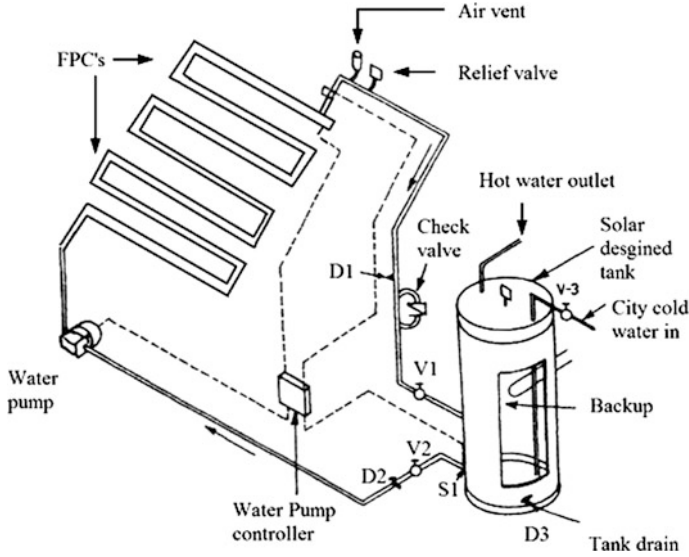
Fig. 8.8 Details of a simple single-loop water-heating system with a sensor, a controller, and a back-up

(b) M-FPCs connected in parallel (Eq. 5.83b)

$$\dot{Q}_{um} = A_{cm}F_{Rm}[\dot{q}_{ab} - U_{Lm}(T_{fi} - T_a)] \tag{8.17}$$

where $A_{cm} = mA_c$ and $F_{Rm} = \frac{\dot{m}_f C_f}{A_{cm}U_{Lm}}\left[1 - \exp\left(-\frac{F'A_{cm}U_{Lm}}{\dot{m}_f C_f}\right)\right]$

(c) For N-PVT FPCs connected in series (Eq. 5.126)

$$\dot{Q}_{u,N} = NA_c\left[(\alpha\tau)_{eff,N}I(t) - U_{L,N}(T_{fi} - T_a)\right] \tag{8.18}$$

here $(\alpha\tau)_{eff,N} = (F_R(\alpha\tau))_1\left[\frac{1-(1-K_{K,A})^N}{NK_{K,A}}\right]$ and $U_{L,N} = (F_RU_L)_1\left[\frac{1-(1-K_{K,A})^N}{NK_{K,A}}\right]$ where $K_{K,A} = \left[\frac{(AF_RU_L)_1}{\dot{m}_f C_f}\right]$

Even other collectors system, namely evacuated (Eq. 7.24a) and concentrating (Eq. 6.30a, b) collectors, can be considered depending on various applications.

Equation (8.15) can be solved with Eqs. (8.16 through 8.18) with $T_w = T_{fi}$.

Example 8.5 Derive an expression for Δt from Eq. (8.13).

Solution

Equation (8.13) can be written as

$$e^{-a\Delta t} = \frac{T_w - \frac{\overline{f(t)}}{a}}{T_{w0} - \frac{\overline{f(t)}}{a}}$$

Taking log on both the sides of the above equation, we obtain

$$-a\Delta t = \ln \frac{T_w - \frac{\overline{f(t)}}{a}}{T_{w0} - \frac{\overline{f(t)}}{a}}$$

or

$$\Delta t = -\frac{1}{a} \ln \frac{T_w - \frac{\overline{f(t)}}{a}}{T_{w0} - \frac{\overline{f(t)}}{a}}$$

The above equation can be used to determine the time interval (Δt) for raising the temperature from T_{w0} to T_w for a given $I(t)$.

(ii) **Double Loop**

Consider a solar water-heating system in which two heat exchanger loops have been used as shown in Fig. 8.9. First there is the heat exchanger between the collector and storage tank I for any fluid other than water, and there is the other heat exchanger between storage tanks I and II with forced circulation. There is water in storage tank II. Such a system is required when the temperature of frozen water goes into negative numbers.
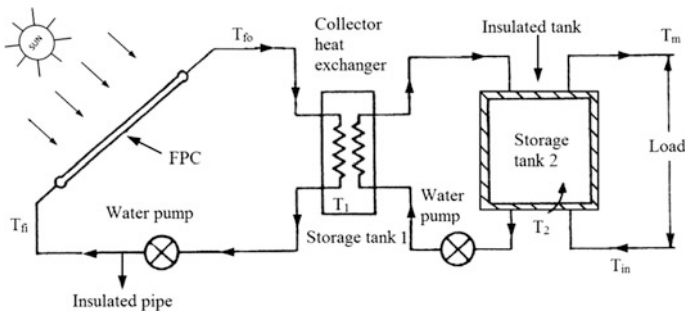
Fig. 8.9 Schematic of a double-loop solar water-heating system

The energy balance for the collector heat-exchanger storage tank (I) can be written as

$$W_I \frac{dT_I}{dt} = \dot{Q}_{gain,c} - \dot{Q}_{loss,I} \tag{8.19}$$

where $W_I(M_{f1}C_{f1})$ is the thermal capacity of liquid in storage tank I; and T_I is the mean temperature of storage tank I.

The rate of thermal energy transferred from the collector loop heat exchanger to storage tank I, $\dot{Q}_{gain,c}$, is given by

$$\dot{Q}_{gain,c} = hL(\bar{T}_f - T_I)$$

or

$$\dot{Q}_{gain,c} = \dot{m}_f C_f[1 - \exp(-\beta)](T_{fo} - T_I) \tag{8.19a}$$

where

$T_{fo} = \frac{1}{1-\exp(\beta\beta')}\left[(1 - \exp(-\beta'))\left[\frac{\alpha\tau}{U_L}I(t) + T_a\right] + T_I(1 - \exp(-\beta'))\exp(-\beta')\right]$

$\beta = \frac{hL}{\dot{m}_f C_f}$, and $\beta' = \frac{F'A_c U_L}{\dot{m}_f C_f}$

The rate of thermal energy transferred from the heat exchanger of storage tank I to the water in storage tank II is given by

$$\dot{Q}_{loss,I} = h_0 L'_0(T_I - T_w)$$

or

$$\dot{Q}_{loss,I} = \dot{m}_f C_f[1 - \exp(-\beta'')](T_I - T_{II})$$

where $\beta'' = \frac{h_0 L'_0}{\dot{m}_f C_f}$

The energy balance for the storage tank II can be written as

$$W_{II} \frac{dT_{II}}{dt} = \dot{Q}_{loss,I} - \dot{M}C_w(T_{II} - T_{in}) \tag{8.20}$$

here $T_{in} = T_w$.

Equations (8.19) and (8.20) can be rewritten in the following form:

$$\frac{dT_I}{dt} + a_1 T_I + a_2 T_{II} = f(t) \tag{8.21}$$

$$\frac{dT_{II}}{dt} + b_1 T_I + b_2 T_{II} = g(t) \tag{8.22}$$

where a_1, a_2, b_1, and b_2 depend on the design parameters of the FPC and the heat exchangers. The expression for $f(t)$ and $g(t)$ depends on the climatic and design parameters. These equations can be solved numerically as well as analytically.

Example 8.6 Determine an overall heat-transfer coefficient for an insulated storage tank with the following parameters:

(a) Cylindrical tank: $L = 0.10$ m, $K = 0.04$ W/m °C, $r_i = 0.02$ m, and $r_o = 0.025$ m; and (b) rectangular tank: $L = 0.10$ m, $K = 0.04$ W/m °C, $h_w = 100$ W/m °C.

Solution

The overall heat-transfer coefficient is given by

(a) For a cylindrical tank:

$$U = \left[\frac{1}{h_i} + \left(\frac{r_i}{K}\ln\frac{r_0}{r_i}\right) + \frac{1}{h_w}\right]^{-1} = \left[\frac{1}{11.8} + \left(\frac{0.02}{0.04}\ln\frac{0.025}{0.02}\right) + \frac{1}{100}\right]^{-1}$$
$$= 4.84\,\text{W}/\text{m}^2\,{}^\circ\text{C}$$

(b) For a rectangular tank:

$$U = \left[\frac{1}{h_i} + \frac{L_i}{K_i} + \frac{1}{h_w}\right]^{-1} = \left[\frac{1}{11.8} + \left(\frac{0.10}{0.04}\right) + \frac{1}{100}\right]^{-1} = 0.384\,\text{W}/\text{m}^2\,{}^\circ\text{C}$$

8.4   Detailed Analysis of a Double-Loop Solar Water-Heating System

The use of a heat exchanger mainly depends on (i) the quality of the water and (ii) the climatic condition of the location. In this section, it is assumed that all of the connecting pipes between (a) the collector and the heat exchanger loop and (b) the heat exchanger to an insulated storage tank loop are perfectly insulated to avoid heat loss, and hence there is no temperature drop for the hot water flowing through them.

The heat exchanger-based solar water-heating system, as shown in Fig. 8.10, works under forced-circulation mode. Pump no. 1 is used in a collector loop and is also known as "smaller stream" due to its low capacity of fluid. Pump no. 1 circulates the fluid through the collector. Pump no. 2 is used to circulate water in the outer loop between the storage tank and a heat exchanger and is also known as "larger stream" due to large heat capacity of the water in the storage tank.
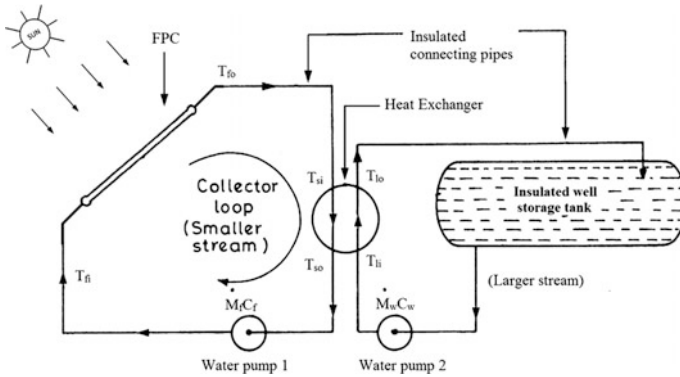
Fig. 8.10 Schematic view of solar water-heating system showing different components with a collector loop

8.4.1   Heat Exchanger [10]

The heat exchanger is essential only to avoid (a) corrosion due to poor quality of the water and (b) freezing of the water in the collector tubes due to harsh cold climatic conditions.

8.4.2   Choice of Fluid

Water is an ideal heat-transfer fluid for a flat-plate collector. Water is non-flammable, nontoxic, and noncorrosive, particularly in plastics as well as some metals (copper and stainless steel, etc.). It has high heat-transfer properties, high density, and high specific heat along with a reasonably high boiling temperature. It has also low viscosity. No heat exchanger is used for water. However, the problem, of course, is water's freezing point.

Some alternative fluids having a low freezing point are listed in Table 8.1. The freezing point of water can be lowered below 0 °C by the addition of some inorganic salts without affecting most of its other properties. Most of the fluids listed in Table 8.1 are noncorrosive, nonflammable, and nonfreezing. Except for water and air, the rest of the fluids are expensive with a high boiling point. Ethylene and propylene glycol are good choices and indeed are in general use (a 50 %-by-weight mixture approaches most of the properties of water). These are only used in a collector loop as shown in Fig. 8.10. Air, of course, does not have the problem of freezing. However, there is a penalty in terms of system performance due to air's poor heat-transfer properties.

Table 8.1 Physical properties of heat-transfer fluid

S. No.	Fluid	Temperature (°C)	Density (kg/m³)	Viscosity (g/ms)	Specific heat (kJ/kg °C)	Thermal conductivity (W/m °C)	Coefficient of thermal expansion (%/°C)
1	Water	38	993	0.684	4.166	0.628	0.037
		93	963	0.305	4.208	0.661	0.055
2	Ethylene glycol and water, 50 % by weight	38	1054	2.3	3.43	0.398	0.057
		93	1016	0.76	3.64	0.433	0.073
3	Propylene glycol and water, 50 % by weight	38	1025	3.1	3.64	0.389	0.066
		93	985	0.9	3.83	0.381	0.080
4	Silicone oil	38	935	14.98	1.55	0.144	0.0928
		93	889	6.40	1.63	0.138	0.0928
5	Air (relative humidity 50 % at sea level)	21	1.187	0.018	1.01	0.0260	
		66	1.033	0.021	1.02	0.0292	

8.4.3   Analysis of a Heat Exchanger

There are many kinds of liquid–liquid heat exchangers. However, only concentric tube and spiral heat exchangers in a tank, as shown in Fig. 8.11, are used in solar water-heating system. These are cost-effective, inexpensive, and easy to maintain locally.

Heat-exchanger performance is measured by effectiveness concept. In this section, an analysis of a counter-current heat exchanger will be briefly discussed. For simplification, a block diagram of Fig. 8.11a for a concentric tube exchanger for counter current is depicted in Fig. 8.12.

The outlet of a solar flat-plate collector (T_{fo}) becomes the inlet of small stream (T_{si}). It passes through an inner tube of the heat exchanger as shown in Fig. 8.11a. The cold water available from the storage tank at temperature T_{li} is allowed to pass in the opposite direction of the small stream for maximum heat transfer $(\dot{Q}_{max})$ from the small stream to the large stream. The inlet temperatures, $T_{si} = T_{fo}$ and T_{li}, to the heat exchanger are considered to determine outlet temperatures T_{so} and T_{lo}, respectively.

The maximum quantity of the rate of heat-transfer from the small stream to the large stream can be written as

$$\dot{Q}_{max} = \dot{M}_f C_f (T_{si} - T_{li}) \tag{8.23}$$
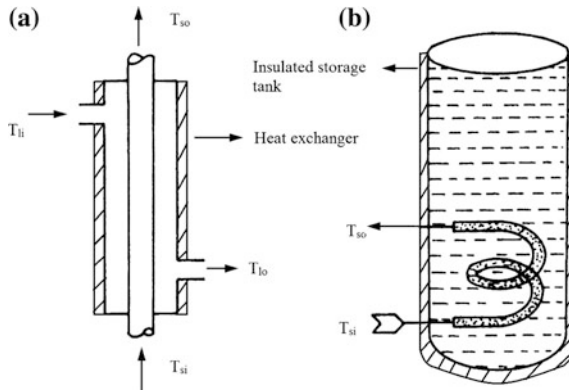
Fig. 8.11 Liquid–liquid heat-exchanger design showing **a** a concentric tube and **b** a within-tank heat exchanger
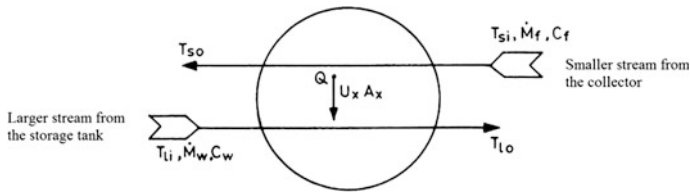
Fig. 8.12 Block diagram of counter-current heat exchanger

where $\dot{M}_f$ is the mass-flow rate of the hot fluid in kilograms per second available from the collector; and C_f is the specific heat of the working fluid. The actual heat exchange $(\dot{Q})$ between the hot fluid of the small stream and the water of the large stream can be expressed as a proportion ε of $\dot{Q}_{max}$. The 'ε' is referred to as "the effectiveness of the heat exchanger."

Now the actual heat exchange $(\dot{Q})$ between the hot fluid of the small stream and the water of the large stream is given by

$$\dot{Q} = \varepsilon \dot{M}_f C_f (T_{si} - T_{li}) \tag{8.24}$$

The effectiveness of the heat exchanger (ε) depends on its heat-transfer properties and the fluid flows. It is independent of the temperature level. Once these are fixed, the effectiveness (ε) can be used to determine the performance of heat exchanger in terms of inlet-fluid temperature.

The actual heat exchange $(\dot{Q})$ between the hot fluid of the small steam and the water of the large steam per unit area is given by

$$\dot{q} = \frac{\dot{Q}}{A_c} = \varepsilon \dot{m}_f C_f (T_{si} - T_{li}) \qquad (8.25)$$

where $\dot{m}_f = \dot{M}_f / A_c$

Referring to Fig. 8.12, the hot water available at T_{si} will cool down to T_{so} during its flow in a heat exchanger. Although the cold water available at T_{li} from the storage tank will be heated to T_{lo} during its flow in the opposite direction in the heat exchanger. If there is no heat loss, than the heat loss from the small stream (collector loop) will be a heat gain to the large stream (storage tank loop). Both will be equal and can be expressed as follows:

Heat lost by the small stream in W/m^2 (collector loop) $= \dot{m}_f C_f (T_{si} - T_{so})$ (8.26)

Heat gained by the large stream in W/m^2 (storage tank loop) $= \dot{m}_w C_w (T_{lo} - T_{li})$

$$(8.27)$$

By equating Eqs. (8.25) and (8.26), one has the following expression for the heat exchanger's effectiveness:

$$\text{Effectivness of the heat exchanger} = \varepsilon = \frac{T_{si} - T_{so}}{T_{lo} - T_{li}} \qquad (8.28)$$

The effectiveness (ε) is defined as the ratio of the actual temperature change achieved in the small and large steam, respectively.

The flow-capacity ratio is expressed as the ratio of temperature differences required for proper performance or the ratio of the temperature changes occurring in the two streams. It can be obtained by equating Eqs. (8.26) and (8.27), respectively, as follows:

$$\text{Flow capacity ratio} = \frac{\dot{m}_f C_f}{\dot{m}_w C_w} = \frac{T_{lo} - T_{li}}{T_{si} - T_{so}} \qquad (8.29)$$

Here it is important to note that the flow-capacity ratio should be <1, i.e.,

$$\frac{T_{lo} - T_{li}}{T_{si} - T_{so}} < 1 \qquad (8.29a)$$

For counter-current heat flow, an expression for the effectiveness of a heat exchanger in terms of its heat-transfer properties and the flow-capacity rates can be written as follows:

$$\text{Effectiveness of the heat exchanger} = \varepsilon = \frac{1 - \exp(-B)}{\left[1 - \frac{\dot{m}_f C_f}{\dot{m}_w C_w} \exp(-B)\right]} \qquad (8.30)$$

where $B = U_x a_x \left[\frac{1}{\dot{m}_f C_f} - \frac{1}{\dot{m}_w C_w}\right] = \text{NTU}\left[1 - \frac{\dot{m}_f C_f}{\dot{m}_w C_w}\right]; \text{NTU} = \frac{U_x a_x}{\dot{m}_f C_f} = \frac{U_x A_x}{\dot{M}_f C_f}$ with

$a_x = A_x/A_c$ and $\dot{m}_f = \dot{M}_f/A_c$

NTU is generally referred to as the "number of transfer units." For proper heat exchange, the value of NTU varies between 1 and 10.

Example 8.7 Determine an expression for the number of transfer units (NTU) in terms of 'ε'.

Solution

Equation (8.30) can be rearranged mathematically as follows:

$$\exp(-B) = \frac{1 - \varepsilon}{\left[1 - \varepsilon \frac{\dot{m}_f C_f}{\dot{m}_w C_w}\right]}$$

Taking the log of both side of above equation and solving for $B = \text{NTU}\left[1 - \frac{\dot{m}_f C_f}{\dot{m}_w C_w}\right]$, one gets an expression for the NTU as follows:

$$\text{NTU} = \frac{\ln\left(\frac{1 - \varepsilon \frac{\dot{m}_f C_f}{\dot{m}_w C_w}}{1 - \varepsilon}\right)}{\left(1 - \frac{\dot{m}_f C_f}{\dot{m}_w C_w}\right)}$$

If $\frac{\dot{m}_f C_f}{\dot{m}_w C_w} < 1$, the mean flow in the collector loop is very small, therefore, $\varepsilon \frac{\dot{m}_f C_f}{\dot{m}_w C_w}$ can be neglected due to the small value of ε; hence,

$$\text{NTU} = \frac{\ln\left(\frac{1}{1-\varepsilon}\right)}{\left(1 - \frac{\dot{m}_f C_f}{\dot{m}_w C_w}\right)}$$

Example 8.8 Derive an expression for the heat-transfer effectiveness (ε) and heat-transfer unit (NTU) for the following cases:

 (i) if the mass flow rate in the both stream are same; and
(ii) if one flow is much larger than the other.

Solution

Case (i) If $\dot{m}_f C_f = \dot{m}_w C_w = \dot{m} C$, then Eq. (8.30) is indeterminate due to $B = 0$. The following equation will be applied:
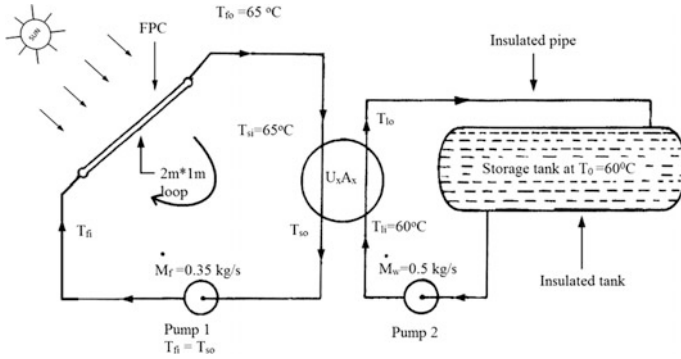
Fig. 8.13 Solar water-heating system showing the parameters of the collector, the heat exchanger, and the storage tank

$$\varepsilon = \frac{NTU}{1+NTU} \text{ and } NTU = \frac{U_x a_x}{\dot{m}C} = \frac{\varepsilon}{1-\varepsilon}$$

Case (ii) If $\dot{m}_f C_f = \dot{m}C \gg \dot{m}_w C_w$, this means that the flow in the collector loop is much higher. Equation (8.30) reduces to

$$\varepsilon = 1 - \exp(-NTU) \text{ and } NTU = (U_x a_x/\dot{m}C) = \ln[1/(1-\varepsilon)]$$

It is observed that $\dot{m}C$ is the mass-flow rate of a small stream.

Example 8.9 Determine the temperatures of the return (T_{lo}) to storage and to the collector (T_{so}) for the following parameters of a solar water-heating system as shown in Fig. 8.13.

  (i) Collector loop fluid (small stream): 50 % ethylene glycol with water, $C_f = 3.52\,\text{kJ/kg}\,°C$
 (ii) Outer loop fluid (large stream): water, $C_f = 4.19\,\text{kJ/kg}\,°C$
(iii) $U_x A_x = 5033\,\text{W}/°C$
 (iv) Number of collectors $= 30$.

Solution
For the total area of collectors, $A_c = 30 \times 2 = 60\,\text{m}^2$, let us first calculate the following normalized parameters:

$$\dot{m}_f C_f = \frac{\dot{M}_f C_f}{A_c} = \frac{0.35 \times 3520}{60} = 20.53 \, \text{W/m}^2 \, ^\circ\text{C}$$

$$\dot{m}_w C_w = \frac{\dot{M}_w C_w}{A_c} = \frac{0.5 \times 4190}{60} = 34.92 \, \text{W/m}^2 \, ^\circ\text{C}$$

$$U_x a_x = \frac{U_x A_x}{A_c} = \frac{5033}{60} = 83.88 \, \text{W/m}^2 \, ^\circ\text{C}$$

$$\text{NTU} = \frac{U_x a_x}{\dot{m}_f C_f} = \frac{83.88}{20.53} = 4.0857$$

$$B = U_x a_x \left[\frac{1}{\dot{m}_f C_f} - \frac{1}{\dot{m}_w C_w} \right] = 83.88 \left[\frac{1}{20.53} - \frac{1}{34.93} \right] = 1.6836$$

After substituting the above values in Eq. (8.30), one obtains

$$\text{Effectiveness of the heat exchanger} = \frac{1 - e^{-1.6836}}{1 - \frac{20.53}{34.93} e^{-1.6836}} = 0.9140$$

The rate of heat transfer $(\dot{q})$ from the small stream to the large stream is given by

$$\dot{q} = 0.914 \times 25.53 \times (65 - 60) = 93.82 \, \text{W/m}^2$$

The outlet temperature from the small-stream heat exchanger can be determined as follows:

$$T_{so} = T_{si} - \frac{\dot{q}}{\dot{m}_f C_f} = 65 - \frac{93.82}{20.53} = 60.43 \, ^\circ\text{C}$$

The outlet temperature from the large-stream heat exchanger can be determines as follows:

$$T_{lo} = T_{li} + \frac{\dot{q}}{\dot{m}_w C_w} = 60 + \frac{93.82}{34.93} = 62.69 \, ^\circ\text{C}$$

8.4.4   Heat-Exchanger Factor

In this section, a new flat-plate collector performance equation will be derived that directly incorporates the effect of the heat exchanger. Referring to Fig. 8.10, the basic equation for flat-plate collector performance for 1 m^2 a collector area (Chap. 5) can be rewritten as follows:

$$\dot{q} = \dot{m}_\mathrm{f} C_\mathrm{f}(T_\mathrm{fo} - T_\mathrm{fi}) = F_\mathrm{R}(\alpha\tau)I - F_\mathrm{R} U_\mathrm{L}(T_\mathrm{fi} - T_\mathrm{a}) \tag{8.31}$$

For a small collector flow-rate capacity, the outlet temperature from the solar flat-plate collector is given by

$$T_\mathrm{fi} = T_\mathrm{fo} - \frac{\dot{q}}{\dot{m}_\mathrm{f} C_\mathrm{f}} \tag{8.32}$$

Substituting T_fi from Eqs. (8.32) into (8.31), one gets

$$\dot{q} = F_\mathrm{R}(\alpha\tau)I - F_\mathrm{R} U_\mathrm{L}\left[\left(T_\mathrm{fo} - \frac{\dot{q}}{\dot{m}_\mathrm{f} C_\mathrm{f}}\right) - T_\mathrm{a}\right]$$

or

$$\dot{q} = \frac{F_\mathrm{R}(\alpha\tau)I - F_\mathrm{R} U_\mathrm{L}[T_\mathrm{fo} - T_\mathrm{a}]}{1 - \frac{F_\mathrm{R} U_\mathrm{L}}{\dot{m}_\mathrm{f} C_\mathrm{f}}} \tag{8.33}$$

From Eq. (8.24), one has the following relation:

$$T_\mathrm{si} = T_\mathrm{li} + \frac{\dot{q}}{\varepsilon \dot{m}_\mathrm{f} C_\mathrm{f}} \tag{8.34}$$

Because $T_\mathrm{fo} = T_\mathrm{si}$ due to negligible heat loss from the connecting pipe between the outlet of the solar flat-plate collector and the inlet to the heat exchanger, then Eq. (8.33) can be further rearranged as follows:

$$\dot{q} = \frac{F_\mathrm{R}(\alpha\tau)I - F_\mathrm{R} U_\mathrm{L}\left[T_\mathrm{li} + \frac{\dot{q}}{\varepsilon \dot{m}_\mathrm{f} C_\mathrm{f}} - T_\mathrm{a}\right]}{1 - \frac{F_\mathrm{R} U_\mathrm{L}}{\dot{m}_\mathrm{f} C_\mathrm{f}}} \tag{8.35}$$

The above equation can be solved for $\dot{q}$ as follows:

$$\dot{q} = \frac{F_\mathrm{R}(\alpha\tau)I - F_\mathrm{R} U_\mathrm{L}[T_\mathrm{li} - T_\mathrm{a}]}{1 + \frac{F_\mathrm{R} U_\mathrm{L}}{\dot{m}_\mathrm{f} C_\mathrm{f}}\left(\frac{1}{\varepsilon} - 1\right)} \tag{8.36}$$

For negligible heat loss in the connecting pipes, $T_\mathrm{li} = T_\mathrm{o}$, and Eq. (8.36) becomes

$$\dot{q} = \frac{F_\mathrm{R}(\alpha\tau)I - F_\mathrm{R} U_\mathrm{L}[T_\mathrm{o} - T_\mathrm{a}]}{1 + \frac{F_\mathrm{R} U_\mathrm{L}}{\dot{m}_\mathrm{f} C_\mathrm{f}}\left(\frac{1}{\varepsilon} - 1\right)} \tag{8.37}$$

The above equation can be rearranged as follows:

$$\dot{q} = F_x[F_R(\alpha\tau)I - F_R U_L(T_o - T_a)] \tag{8.38}$$

where

$$F_x = \left[1 + \frac{F_R U_L}{\dot{m}_f C_f}\left(\frac{1}{\varepsilon} - 1\right)\right]^{-1} \tag{8.39}$$

The above constant is known as the **de Winter heat-exchanger factor**. Equation (8.38) can further be rearranged as follows:

$$\dot{q} = F_x F_R[(\alpha\tau)I - U_L(T_o - T_a)] \tag{8.40}$$

or

$$\dot{q} = F_x'[(\alpha\tau)I - U_L(T_o - T_a)] \tag{8.41}$$

where $F_x' = F_x F_R$

Example 8.10 Evaluate the **de Winter heat exchanger factor** for $F_R U_L = 5.0\,\text{W/m}^2\,°\text{C}$ in Example 8.9.

Solution
From Eq. (8.39), one has the following relation:

$$F_x = \left[1 + \frac{F_R U_L}{\dot{m}_f C_f}\left(\frac{1}{\varepsilon} - 1\right)\right]^{-1} = \left[1 + \frac{5.0}{20.53}\left(\frac{1}{0.914} - 1\right)\right]^{-1} = 0.9776$$

8.4.5   Natural-Convection Heat Exchanger

The temperature difference between the circulating fluid in a heat exchanger and the water in the insulated storage tank, as shown in Fig. 8.14, depends on the flow rate of the fluid in the circulating collector loop. This temperature difference can be used to determine the heat-exchanger parameter $U_x A_x$. For a tank heating water with a given temperature difference, a convective heat-transfer coefficient can be calculated by using the following formula:

$$h = 142\left(\frac{\Delta T_x}{L_0}\right)^{0.25} \tag{8.42}$$

where h is in $\text{W/m}^2\,°\text{C}$; ΔT_x ($°\text{C}$) is the temperature difference; and $L_0(m)$ is the length of the characteristic path for natural convection. The above equation is valid
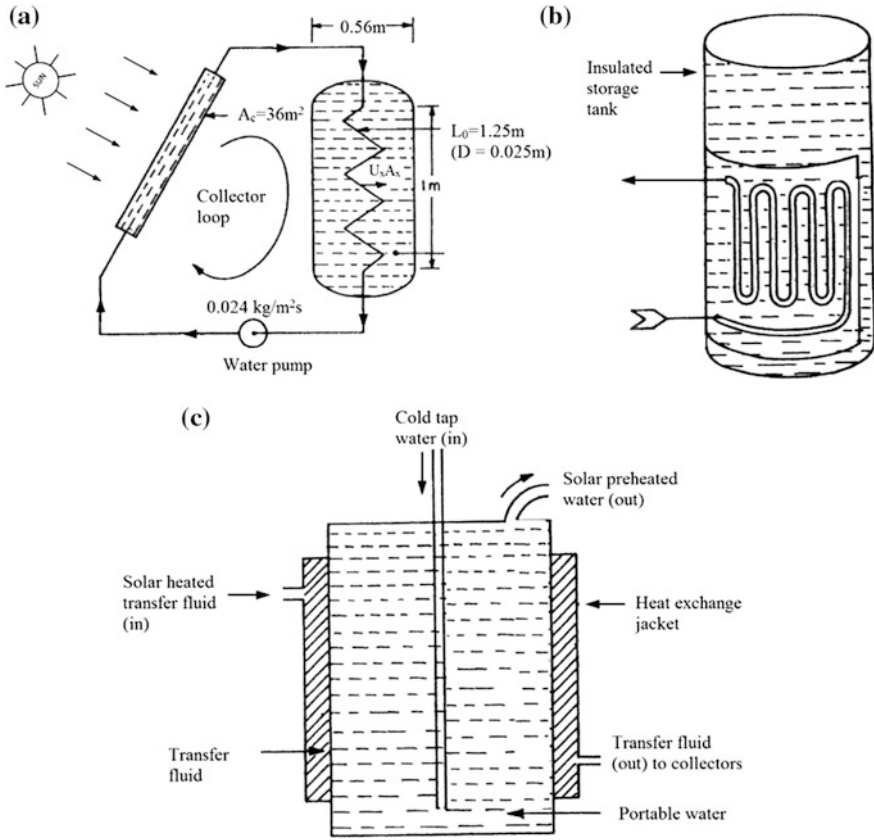
Fig. 8.14 Solar water-heating system with natural convection heat transfer from **a** the circulating fluid of the heat exchanger to the water in the storage tank, **b** a coil-type heat exchanger outside the tank, and **c** a heat-exchanger jacket outside tank

only for $\Delta T_x = 38\,°\text{C}$. For $\Delta T_x = 65\,°\text{C}$, multiply Eq. (8.42) by 1.15; for $\Delta T_x = 21\,°\text{C}$, divide Eq. (8.42) by 1.15. For higher ΔT_x, the flow rate should be small in the collector loop.

Example 8.11 Evaluate the effectiveness of the heat exchanger (ε) and the heat-exchanger factor (F_x) for the parameters given in Fig. 8.5. Other parameters are as follows:

(i) Circulating fluid: glycol solution with specific heat $C_f = 3.517\,\text{kJ/kg}\,°\text{C}$.
(ii) $F_R U_L = 5.069\,\text{W/m}^2\,°\text{C}$
(iii) Average net heat flux collected by the solar flat-plate collector $(\dot{q} = 230\,\text{W/m}^2)$
(iv) Surface area of the heat exchanger $= 10\,\text{m}^2$.
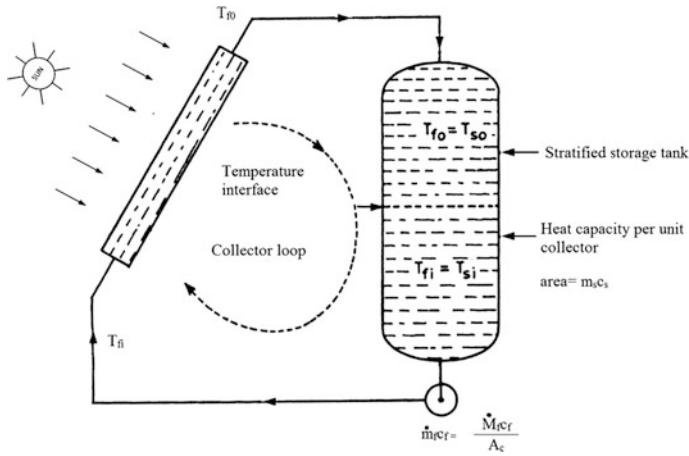
Fig. 8.15 Stratified storage tank with collector

Solution

Referring to Fig. 8.15, one can determine $\dot{m}_f C_f = 84.11\,\text{W/m}^2$ and $A_c/A_x = 3.6$.

If $\dot{q}$ is the net heat flux collected per unit area of the solar flat-plate collector, then the heat transfer through the heat exchanger to the water in the insulated tank is obtained as

$$\dot{q}A_c = U_x A_x \Delta T_x$$

In Eq. (8.42), $h = U_x$ and substituting ΔT_x from Eq. (8.42) in the above equation, one has

$$U_x^5 = \frac{142^4 \dot{q}(A_c/A_x)}{L_0}$$

or

$$U_x = 52.7 \left[\frac{\dot{q}(A_c/A_x)}{L_0} \right]^{1/5}$$

Substituting the required values in the above equation, one obtains

$$U_x = 52.7 \left[\frac{230 \times (3.6)}{125} \right]^{1/5} = 76.92\,\text{W/m}^2\,^{\circ}\text{C}$$

Now the number of transfer units (NTU) is calculated as

$$\text{NTU} = \frac{U_x a_x}{\dot{m}_f C_f} = \frac{76.92 \times (1/3.6)}{84.41} = 0.2531$$

Then from case (ii) of Example 8.9, one obtains the effectiveness of the heat exchanger as

$$\varepsilon = 1 - \exp(-\text{NTU}) = 1 - \exp(-0.2531) = 0.2236$$

From Eq. (8.39), one has

$$F_x = \left[1 + \frac{F_R U_L}{\dot{m}_f C_f}\left(\frac{1}{\varepsilon} - 1\right)\right]^{-1} = \left[1 + \frac{5.069}{84.41}\left(\frac{1}{0.2236} - 1\right)\right]^{-1} = 0.8138$$

8.5 Heat Collection in an Insulated Storage Tank [10]

The hot water from the outlet of a solar flat-plate collector is fed at the top of the insulated storage tank. If the insulated storage tank is in a horizontal position, as shown in Fig. 8.10, then there is quick mixing between the hot water of the solar flat-plate collector and the cold water of the insulated storage tank. In the case of a vertical position of the storage tank, as shown in Fig. 8.15 (without heat exchanger) and Fig. 8.14 (with heat exchanger), the mixing takes some time due to low density of the hot water at the top of the storage tank. The stratification generally takes place at a very low circulating-fluid flow rate in the collector loop. Hence, an analysis of a storage tank with and without stratification will be presented in the following section.

8.5.1 Heat Collection with a Stratified Insulated Storage Tank

Referring to Fig. 8.16 and Eq. (8.41), an expression for the total heat collected (q_T) over a time period, t_T, can be expressed as follows:

$$q_T = F'_x[(\alpha\tau)I_T - U_L(T_{si} - T_a)t_T] \tag{8.43}$$

where I_T is the total solar radiation over a time period, t_T, on a solar flat-plate collector.

The hot water available from a solar FPC is fed at the top of the storage tank. It does not affect the temperature of the fluid leaving the tank immediately; hence, the solar flat-plate collector operates at a constant thermal efficiency. After t_s time, the
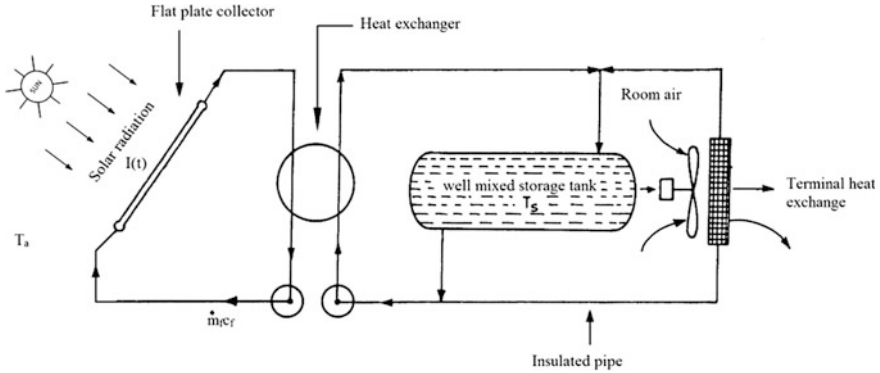
Fig. 8.16 Schematic of a solar water-heating system with a terminal heat exchanger

first-collected heat at the top of the solar FPC reaches the bottom of the tank and hence changes the temperature of the fluid leaving the tank. In this case, the performance of the flat-plate collector also changes due to the change in its inlet temperature. At this time, heat collected exactly equals the heat required to raise the temperature of the water storage in the tank from T_{si} to T_{so}. This can be mathematically expressed as follows:

$$Q_T = \dot{M}_f C_f (T_{fo} - T_{fi}) t_s = M_s C_s (T_{so} - T_{si}) \tag{8.44}$$

Because $T_{fo} = T_{so}$ and $T_{fi} = T_{si}$, as shown in Fig. 8.6, the above equation can be solved for t_s, which is expressed as

$$t_s = \frac{M_s C_s}{\dot{M}_f C_f} = \frac{m_s C_s}{\dot{m}_f C_f} \tag{8.45}$$

Here it is important to note that $t_T \leq t_s$.

The process can then be repeated with the flat-plate collector operating at new inlet temperature with a new constant thermal efficiency. After one turnover time of period t_s, a new storage tank temperature is calculated as

$$T_{so} = T_{si} + \frac{q_T}{m_s C_s} \tag{8.46}$$

Example 8.12 Evaluate the total heat collected (q_T) and the final storage temperature after 6 h operation for the following given parameters:

(i) $F'_x(\alpha\tau) = 0.75$ and $F'_x U_L = 5.0\,\text{W/m}^2\,°\text{C}$;

(ii) $\dot{m}_f C_f = 45\,\text{W/m}^2\,°\text{C}$ and $m_s C_s = 0.32\,\text{MJ/m}^2\,°\text{C}$;

(iii) average solar intensity $I(t) = 750\,\text{W/m}^2$; and

(iv) average ambient temperature $= 10\,°\text{C}$ and $T_{si} = 15\,°\text{C}$.

Solution

From Eq. (8.45), the storage turnover time can be calculated as

$$t_{\mathrm{s}} = \frac{m_{\mathrm{s}} C_{\mathrm{s}}}{\dot{m}_{\mathrm{f}} C_{\mathrm{f}}} = \frac{0.32}{45} = 0.0071\,\mathrm{Ms} \cong 2\,\mathrm{h}$$

Because the maximum value of t_{T} is equal to t_{s}, the total heat collected in 2 h is therefore calculated from Eq. (8.43) as

$$q_{\mathrm{t}} = F'_x[(\alpha\tau)I_{\mathrm{T}} - U_{\mathrm{L}}(T_{\mathrm{si}} - T_{\mathrm{a}})t_{\mathrm{T}}] = F'_x(\alpha\tau)\bar{I}t_{\mathrm{T}} - F'_x U_{\mathrm{L}}(T_{\mathrm{si}} - T_{\mathrm{a}})t_{\mathrm{t}}$$
$$= 0.75 \times 750.0 \times 0.0071 - 5.0(15 - 10) \times 0.0071 = 3.8163\,\mathrm{MJ/m^2}$$

After one turnover time, the temperature of entire storage tank can be calculated from Eq. (8.46) as

$$T_{\mathrm{so}} = T_{\mathrm{si}} + \frac{q_{\mathrm{T}}}{m_{\mathrm{s}} C_{\mathrm{s}}} = 15 + \frac{3.8163}{0.32} = 26.93\,^{\circ}\mathrm{C}$$

During the second turnover, the time collection will continue with the inlet temperature at 26.93 °C, hence the total heat collected in another two hours is calculated as

$$q_{\mathrm{T}} = 0.75 \times 750.0 \times 0.0071 - 5.0(26.93 - 10) \times 0.0071 = 3.3927\,\mathrm{MJ/m^2}$$

and $T_{\mathrm{so}} = T_{\mathrm{si}} + \frac{q_{\mathrm{T}}}{m_{\mathrm{s}} C_{\mathrm{s}}} = 26.93 + \frac{3.3927}{0.32} = 36.62\,^{\circ}\mathrm{C}$

Similarly, after a third turnover time, the total heat collected in 2 h is given as

$$q_{\mathrm{T}} = 0.75 \times 750.0 \times 0.0071 - 5.0(36.62 - 10) \times 0.0071 = 3..0486\,\mathrm{MJ/m^2}$$

and $T_{\mathrm{so}} = T_{\mathrm{si}} + \frac{q_{\mathrm{T}}}{m_{\mathrm{s}} C_{\mathrm{s}}} = 36.62 + \frac{3.0486}{0.32} = 46.15\,^{\circ}\mathrm{C}$

The total heat collected over period of 6 h is obtained as

$$q_{\mathrm{T}} = 3.8163 + 3.3927 + 3.0486 = 10.2576\,\mathrm{MJ/m^2}$$

8.5.2 Heat Collection with a Well-Mixed Insulated Storage Tank

In this case, fluid is circulated with a high flow rate in a horizontal storage tank as shown in Fig. 8.10. Due to higher fluid flow rate, one turnover time period, t_{T}, of the stratified storage tank is very small. A well-mixed insulate storage tank is less efficient due to the high temperature of the fluid leaving insulated storage tank. The large flow of fluid through the solar flat-plate collector gives a high heat-transfer

factor, which compensates for the loss due to the higher temperature. Under these circumstances, T_{si} should be replaced by $\bar{T}_s$ in Eq. (8.43) as follows:

$$q_t = F'_x[(\alpha\tau)I_T - U_L(\bar{T}_s - \bar{T}_a)t_T] \tag{8.47}$$

here

$$\bar{T}_s = (T_{so} + T_{si})/2 \tag{8.48}$$

also

$$q_T = m_s C_s (T_{so} - T_{si}) \tag{8.49}$$

Because $T_{fo} = T_{so}$ and $T_{fi} = T_{si}$ one gets the following after substituting T_{so} from Eq. (8.48) in the above equation:

$$\bar{T}_s = T_{si} + \frac{q_T}{2m_s C_s} \tag{8.50}$$

which can be substituted in Eq. (8.47). Furthermore, it is solved for q_T to give the integrated storage equation as follows:

$$q_T = \frac{F'_x[(\alpha\tau)I_T - U_L(T_{si} - \bar{T}_a)t_T]}{1 + \frac{F'_x U_L t_T}{2m_s C_s}} \tag{8.51}$$

Example 8.13 Evaluate the hourly temperature variation for a solar flat-plate collector with a well-mixed insulated storage tank for the following given parameters:
   (i) $F'_x = 1.0$, $\alpha\tau = 0.8$, $U_L = 5.0\,\mathrm{W/m^2\,°C}$ and $T_{si} = 45.0\,°C$; and
   (ii) $m_s C_s = 0.32\,\mathrm{MJ/m^2\,°C}$.
The Hourly variation of solar intensity and the ambient air are given below:

Time (h)	Solar intensity (I), $(\mathrm{W/m^2})$	Ambient temperature T_a ($°C$)	$q_t(\mathrm{MJ/m^2})$ using Eq. (5.26)	T_{so} ($°C$)	q_t ($\mathrm{MJ/m^2}$) using Eq. (5.23)
9	424	11.4	0.5994	46.87	0.5995
10	558	13.5	0.9789	46.87	0.5995
11	641	15.8	1.1980	49.93	0.9788
12	669	18.1	1.2513	53.67	1.1981
13	641	19.8	1.1342	57.58	1.2513
14	558	20.9	0.8589	61.12	1.1342
15	424	21.3	0.4437	65.19	0.4436
Average	559.28	17.26	0.9235	54.46	0.8864

Solution

Here $t_T = 1 \, h = 3600 \, s = 0.0036 \, Ms$.

For the first hour, $I = 424 \, W/m^2$ and $T_a = 11.4 \, °C$, so one gets q_T from Eq. (8.51) as

$$q_T = \frac{F_x'[(\alpha\tau)I_T - U_L(T_{si} - \bar{T}_a)t_T]}{1 + \frac{F_x'U_L t_T}{2m_s C_s}}$$

$$= \frac{0.8 \times 424 \times 0.0036 - 5.0 \times (45 - 11.4) \times 0.0036}{1 + \frac{5.0 \times 0.0036}{2 \times 0.32}} = \frac{0.6163}{1.0281} = 0.5994 \, MJ/m^2$$

From Eq. (8.49), one can also calculate T_{so} as

$$T_{so} = T_{si} + \frac{q_T}{m_s C_s} = 45 + \frac{0.5994}{0.32} = 46.87 \, °C$$

For the second hour, $I = 558 \, W/m^2$ and $T_a = 13.5 \, °C$, q_T is determined as

$$q_T = \frac{0.8 \times 558 \times 0.0036 - 5.0 \times (46.87 - 13.5) \times 0.0036}{1 + \frac{5.0 \times 0.0036}{2 \times 0.32}} = \frac{1.0064}{1.0281}$$

$$= 0.9789 \, MJ/m^2$$

and T_{so} as $T_{so} = T_{si} + \frac{q_t}{m_s C_s} = 46.87 + \frac{0.9789}{0.32} = 49.93 \, °C$

Similarly, for other hours, q_T and T_{so} can be also calculated as given in the above table. Furthermore, q_T can also be calculated from Eq. (8.47) as given in the same table, and it is inferred that the value of q_T calculated from both equation is the same for a 1-h time step.

Example 8.14 Estimate q_T and T_{so} for Example 8.13 for a 5-h time step.

Solution

In this case,

$$t_T = 5 \times 0.0036 = 0.018 \, Ms$$
$$I_T = (424 + 558 + 641 + 669 + 641) \times 0.0036 = 10.5588 \, MJ/m^2$$
$$\bar{T}_a = (11.4 + 13.5 + 15.8 + 18.1 + 19.8)/5 = 15.72 \, °C$$

From Eq. (8.51), one has q_T as

$$q_t = \frac{0.8 \times 10.5588 - 5.0 \times (45.0 - 15.72) \times 0.018}{1 + \frac{5.0 \times 0.018}{2 \times 0.32}} = \frac{5.81184}{1.140} = 5.0981 \, MJ/m^2$$

and T_{so} is calculated as

$$T_{so} = T_{si} + \frac{q_T}{m_s C_s} = 45.0 + \frac{5.0981}{0.32} = 60.93\,^\circ\text{C}$$

The above-calculated value of T_{so} is lower by $0.4\,^\circ\text{C}$ compared with a 1-h time step value of $T_{so} = 61.33$ (from the above table). This is due to the longer time step.

8.5.3 *Effect of Heat Load [11]*

In the previous section, the-FPC integrated storage equation was developed without considering any heat losses/thermal load. The effect of heating load to a room is shown in Fig. 8.16.

There can be two ways to determine room heating for a given load as follows:

(i) A noninsulated hot water-storage tank should be placed inside a room with provision of a fan at one end for fast heating.
(ii) There should be circulation of hot water between the insulated hot water-storage tank and the heat exchanger—fan arrangement, and hot air available at the exit of the fan is sent to the required room for space heating. In this case, there is no need of a hot water tank to be placed inside the room.

If l_T is the thermal load demand, which is expressed as the thermal head load per unit collector area, then it is defined as

$$l_T = \frac{(T_b - T_a)^+ (UA)_b}{A_c} \tag{8.52}$$

where the positive sign (+) indicates that only a positive value in the bracket should be considered for the thermal heating of a building. The $(UA)_b$ is the overall heat-loss coefficient from the room of a building to the ambient air through different walls, the roof, the floor, doors, windows, etc. The typical value of $[(UA)_b/A_c]$ is $0.01386\,\text{MJ/m}^2\,^\circ\text{C}\,\text{h}$. This can vary depending on the design of the building components. The base temperature of the room air (T_b) can be considered as $25\,^\circ\text{C}$ for the present case to analyze the system.

Now the expression for the net heat collected (q_N) can be written as

$$q_N = q_T - l_T \tag{8.53}$$

Similar to Eq. (8.50), the average temperature of a well-mixed insulated storage tank can be written as

$$\bar{T}_s = T_{so} + \frac{q_N}{2m_s C_s} \tag{8.54}$$

With help of Eqs. (8.47), (8.53), and (8.54), an expression for net heat collection (q_N) can be derived and is expressed as

$$q_N = \frac{F'_x[(\alpha\tau)I_T - U_L(T_{si} - \bar{T}_a)t_T] - l_T}{1 + \frac{F'_x U_L t_T}{2m_s C_s}} \tag{8.55}$$

The rise in temperature of the insulated storage tank during the daytime can be obtained from

$$T_{so} = T_{si} + \frac{q_N}{m_s C_s} = T_{si} + \frac{q_t - l_T}{m_s C_s} \tag{8.56}$$

Furthermore, an expression for total heat collected (q_T) can be obtained by substituting the above expression in Eq. (8.53) as follows:

$$q_T = \frac{F'_x[(\alpha\tau)I_T - U_L(T_{si} - \bar{T}_a)t_T]}{1 + \frac{F'_x U_L t_T}{2m_s C_s}} + \frac{l_T}{1 + \frac{2m_s C_s}{F'_x U_L t_T}} \tag{8.57}$$

Example 8.15 Evaluate the heating load for the climatic data of the table given in Example 8.13. In addition, determine (i) the total heat collected and (ii) the corresponding storage temperature by using hourly step.

Solution
From Eq. (8.52), first the calculation of heating load will be performed for the data given below:
   Thermal head–load calculation for the first time step:
   The thermal head load per unit of solar flat-plate collector area is obtained as

$$l_T = \frac{(T_b - T_a)^+(UA)_b}{A_c} = (25 - 11.4) \times 0.0139 = 0.1890\,\text{MJ/m}^2$$

Similarly, for the second time step, $l_t = 0.1599\,\text{MJ/m}^2$
   Storage-temperature calculation for the first time step:
   After calculating the heating load, the total heat collected can be obtained from Eq. (8.57) as

$$q_t = \frac{F'_x[(\alpha\tau)I_T - U_L(T_{si} - \bar{T}_a)t_T]}{1 + \frac{F'_x U_L t_T}{2m_s C_s}} + \frac{l_T}{1 + \frac{2m_s C_s}{F'_x U_L t_T}}$$

$$= \frac{1 \times [0.8 \times 424 - 5 \times (45 - 11.4)] \times 0.0036}{1 + \frac{1 \times 5 \times 0.0036}{2 \times 0.32}} + \frac{0.1890}{1 + \frac{2 \times 0.32}{1 \times 5 \times 0.0036}}$$

$$= \frac{0.6163}{1.0281} + \frac{0.1890}{36.5872} = 0.6046 \, \text{MJ/m}^2$$

The corresponding storage temperature, determined using hourly step, can be obtained from Eq. (8.56) as

$$T_{so} = T_{si} + \frac{q_T - l_T}{m_s C_s} = 45 + \frac{0.6046 - 0.1890}{0.32} = 46.30 \, °C$$

Similarly, for the second time step, $T_{so} = 46.30 + \frac{1.0159 - 0.1599}{0.32} = 48.98 \, °C$

Similar calculation can be performed for other time steps. The results have been tabulated below.

Time, (h)	Solar intensity (I), (W/m^2)	Ambient temperature T_a $(°C)$	l_t (MJ/m^2)	q_t (MJ/m^2) using Eq. (5.26)	T_{so} $(°C)$
9	424	11.4	0.1890	0.6046	46.30
10	558	13.5	0.1599	1.0159	48.98
11	641	15.8	0.1279	1.2879	52.61
12	669	18.1	0.0959	1.4057	56.70
13	641	19.8	0.0723	1.3564	60.71
14	558	20.9	0.0570	1.1427	64.10
15	424	21.3	0.0514	0.7742	66.36
Average	559.28	17.26	0.1076	1.0840	56.53

Example 8.16 Evaluate the rise in temperature of storage in Example 8.15 by using an entire-day time step.

Solution
For a entire-day time step, using data from the table in Example 8.15, one obtains the total heat collected (q_T) from Eq. (8.57) as

$$q_T = \frac{1 \times [0.8 \times 3915 \times 0.0036 - 5 \times (45 - 17.23) \times 7 \times 0.0036]}{1 + \frac{1 \times 5 \times 0.0036}{2 \times 0.32}} + \frac{0.7534}{1 + \frac{2 \times 0.32}{1 \times 5 \times 0.0036}}$$

$$= \frac{7.7762}{1.0281} + \frac{0.7534}{36.5872} = 7.5842 \, \text{MJ/m}^2$$

Using Eq. (8.57), the corresponding storage temperature is given by

$$T_{so} = 45.00 + \frac{7.5842 - 0.7534}{0.32} = 66.35\,^\circ\text{C}$$

which is nearly same as obtained by the 1-h time step in Example 8.15.

Objective Questions

8.1 In a collection-cum-storage water heater, there are
(a) separate heating and storing units   (b) the same heating and storing unit
(c) a heat exchanger in the storage tank   (d) none of these
Answer: (b)

8.2 In the northern hemisphere, built-in-storage water heat can be

(a) inclined to receive maximum solar radiation due south
(b) horizontal to receive maximum solar radiation
(c) inclined toward the east to receive maximum solar radiation
(d) none of these
Answer: (a)

8.3 A shallow solar pond water heater requires

(a) more maintenance compared with a built-in storage water heater
(b) less maintenance compared with a built-in storage water heater
(c) more maintenance compared with a conventional water heater
(d) none of these
Answer: (a)

8.4 The overall thermal efficiency of a collection-cum-storage water heater
(a) increases with an increase of water depth   (b) decreases with an increase
of water depth
(c) is unaffected by water depth   (d) none of these
Answer: (a)

8.5 The maximum temperature of water in a collection-cum-storage water heater

(a) increases with an increase of water depth
(b) decreases with an increase of water depth
(c) is unaffected by an increase of water depth
(d) none of these
Answer: (b)

8.6 In natural circulation mode of solar water heater, the position of storage tank
is
(a) above the upper header   (b) below the upper header
(c) below the lower header   (d) none.
Answer: (a)

8.7   In a forced circulation mode of a solar water heater, the position of the
      storage tank is
      (a) above the upper header   (b) below the upper header
      (c) below the lower header   (d) all of these
      Answer: (d)
8.8   A stratification in water temperature is observed in
      (a) natural-circulation mode   (b) forced-circulation mode
      (c) forced mode with a horizontal collector   (d) none of these
      Answer: (a)
8.9   A heat exchanger in a collector loop of a water heater is used in the case of
      (a) climate with freezing point   (b) location with bad water quality
      (c) space heating   (d) all of these
      Answer: (d)
8.10 A single- and double-loop heat exchanger water heater works under
      (a) natural mode   (b) forced mode
      (c) natural and forced mode   (d) none of these
      Answer: (b)
8.11 For a large-scale solar water-heating system, the FPCs should be connected
      in
      (a) series   (b) parallel
      (c) a combination of parallel and series   (d) all of these
      Answer: (c)

Problems

8.1   Determine the effectiveness of the heat exchange (ε) and the heat-exchanger
      factor for $\dot{q} = 500\,\text{W/m}^2$ for the parameters given in Example 8.11.
      Hint: See Example 8.11.
8.2   Repeat example 8.11 by assuming $\Delta T_x = 21$, 38, and 65 °C .
      Hint: Find U_x from $\dot{q}A_c = U_x A_x \Delta T_x$ and see Example 8.11.
8.3   Calculate the total heat collected and the final storage temperature after 4 h of
      operation of the system for the same parameters of Example 8.12.
      Hint: See Example 8.12, only the second turnover time-collection calculations
      are required.
8.4   Calculate the total heat collected after 10 h of operation of the system for the
      following parameters:
      (i) $F_x'(\alpha\tau) = 0.5$ and $F_x' U_L = 2.0\,\text{W/m}^2\,{}^\circ\text{C}$;
      (ii) $\dot{m}_f C_f = 45\,\text{W/m}^2\,{}^\circ\text{C}$ and $m_s C_s = 0.32\,\text{MJ/m}^2\,{}^\circ\text{C}$; and
      (iii) $\bar{I} = 500\,\text{W/m}^2$ and $T_a = 5\,{}^\circ\text{C}$.

References

1. G.N. Tiwari, H.P. Garg, U. Singh, M.S. Hussein, J. Thermal Eng. **4**(4), 12 (1984)
2. N.K. Dhiman, G.N. Tiwari, Appl. Energy **13**(4), 255 (1983)
3. J.K. Nayak, N.K. Dhiman, G.N. Tiwari, Appl. Energy **10**(3), 169 (1982)
4. M.S. Sodha, S.N. Shukla, G.N. Tiwari, Sol. Energy **32**(2), 291 (1984)
5. G.N. Tiwari, Energy Convers. Manag. **24**(2), 163 (1984)
6. M.S. Sodha, S.N. Shukla, G.N. Tiwari, J. Energy **7**(2), 107 (1983)
7. S.N. Shukla, G.N. Tiwari, Energy Convers. Manag. **23**(2), 77 (1983)
8. M.S. Sodha, S.N. Shukla, V. Ranjan, G.N. Tiwari, Energy Convers. Manag. **22**(2), 155 (1982)
9. M.S. Sodha, S.N. Shukla, G.N. Tiwari, Energy Convers. Manag. **22**(1), 55 (1982)
10. P.J. Lunde, *Solar Thermal Engineering, Chapter 7* (Wiley, New York, 1980), pp. 240–310
11. G.N. Tiwari, *Solar Energy: Fundamental, Design, Modelling and Applications,* Narosa Publishing House, New Delhi and CRC Press, New York, 2004
12. G.N. Tiwari, R.K. Mishra, *Advance Renewable Energy Sources*. RSC publishing, UK, 2012

Additional References

13. G.N. Tiwari, A.K. Singh, Energy Convers. Manag. **34**, 147 (1993)
14. M.S. Sodha, G.N. Tiwari, S.N. Shukla, *Thermal Model of Hot water System, 'Reviews of Renewable Energy Sources'*, ed. by Sodha et al. published by (Wiley Eastern Ltd., New Delhi, 1982), **I**, Chapter 3, p. 139
15. D.K. Dutt, S.N. Rai, G.N. Tiwari, Energy Convers. Manag. **27**, 303 (1987)
16. A.I. Kudish, D. Wolf, Sol. Energy **21**, 317 (1978)
17. K.S. Ong, Sol. Energy **18**, 137 (1974)
18. D.J. Close, Sol. Energy **6**, 33 (1962)

Chapter 9
Solar Flat-Plate Air Collectors

Abstract A solar flat-plate air collector has the application of space heating and crop drying under forced mode of operation with air as a working fluid. For space heating, hot air can be stored in a rock bed for night-time application. The electrical power consumed under forced mode can be met by integrating a PV module into an air collector panel.

Keywords Solar air collectors · Reverse absorber air heaters · PVT-FPC air collectors · Single pass air collector · Double pass air collector · Porous and non-porous air collectors · Fin effect

9.1 Introduction

A conventional solar air heater is essentially a flat-plate collector with a blackened absorber plate having α as absorptivity, a transparent cover having τ as a transmittivity at the top, and insulation at the bottom and on the sides. The whole assembly is encased in a sheet-metal container, and the system is referred to as a "**solar flat-plate air collector**." The working fluid is air, instead of water, which is blown either below or above the absorber plate. The description and analysis of various types of solar air heaters will be studied in this chapter. The **solar flat-plate air collector** is used for the heating of living spaces and drying of crops/vegetables.

Solar flat-plate air collectors are advantageous compared with other solar thermal collectors using liquid as working fluid. Solar flat-plate air collectors have following advantages:

(i) The system is compact and less complicated. The working fluid, i.e., air directly transfers heat to the living space or crops/vegetables; therefore, no additional (other than working fluid) heat-transfer medium is required.
(ii) The problem of corrosion is completely eliminated in the solar flat-plate air collector.
(iii) The leakage of air does not cause any serious problem.

 (iv) The working fluid does not freeze.
  (v) The pressure rise in the solar air collector is comparatively low.

   Thus, a solar air heater can be designed using less and cheaper material. Its operation and maintenance is simpler than those for solar water heaters. However, solar air heaters have certain following disadvantages as follows:

  (i) Poor thermo-physical properties of the working fluid (air) lead to a lesser amount of heat transfer from the absorber to the working fluid; therefore, specific additional arrangements are needed to enhance the heat transfer.
 (ii) A large volume of working fluid is required to be handled because of its low density.
(iii) The lower thermal capacity of air limits these systems to be used as thermal storage systems.
 (iv) The cost of an air heater can be very high due to improper design.

   The applicability of a solar air collector depends on various factors, namely, (a) thermal efficiency, (b) fabrication cost and installation, (c) operational and maintenance costs, and (d) the specific use. Solar air heaters have been extensively investigated both experimentally as well as theoretically. A variety of geometries have been proposed to enhance the heat-transfer properties of the system. Selcuk [1] has reported a comprehensive literature review on solar air heaters. It was concluded that technically solar air heaters are at a state-of-art-level, which should be addressed commercially to a greater extent.

9.2 Classification of Solar Air Heaters

Selective coating of the absorber plate, high absorptivity, α and low emissivity (ε) can be used to improve the collection thermal efficiency.
   Depending on the type of mechanism for transferring heat to air, the solar air heater can be classified as (a) nonporous solar air heaters or (b) porous solar air heaters. Figures 9.1 and 9.2 show the basic features of these solar air heaters.

9.2.1 Nonporous-Type Solar Air Heaters

In the nonporous-type solar air heater, an air stream flows as follows:

  (i) **Above the blackened absorber plate:** In this case, absorbed solar radiation, after transmission from the glass cover, heats the blackened absorber plate. Thermal energy from the blackened absorber plate is then convected to the flowing air above blackened absorber plate (hot surface facing upward), and then it is heated (Fig. 9.1a).
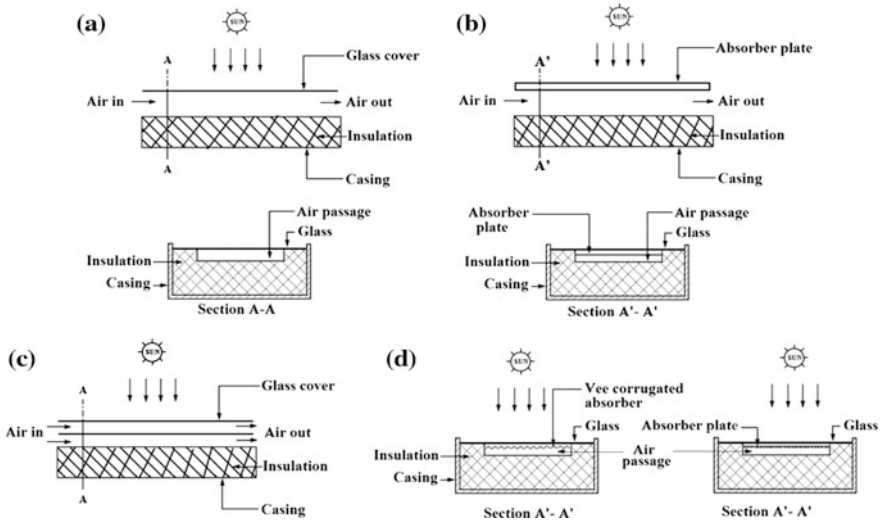
Fig. 9.1   a–d Schematic of nonporous absorber-type air heaters
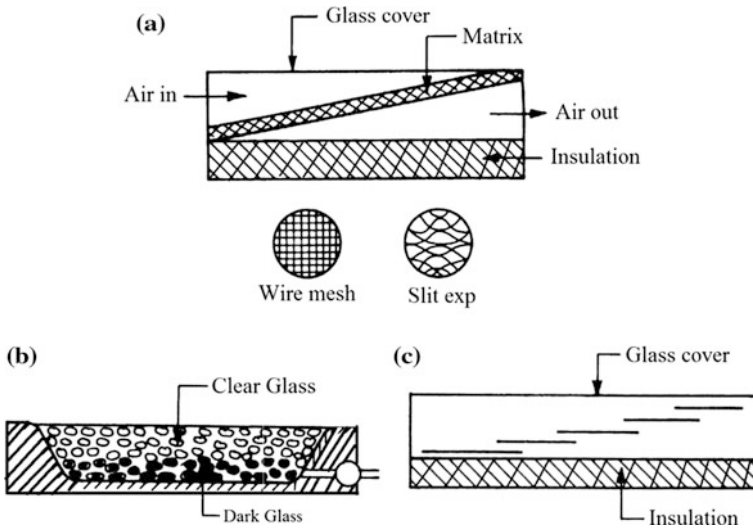
Fig. 9.2   a–c Schematics of porous absorber-type air heaters. (From [17])

(ii) **Below the blackened absorber plate:** In this case, absorbed solar radiation, after transmission from the glass cover, heats the blackened absorber plate. Thermal energy from the blackened absorber plate is then convected to the flowing air below the blackened absorber plate (hot surface facing downward), and then it is heated (Fig. 9.1b).

(iii) **Both sides of the blackened absorber plate:** In this case, air flows from both sides (above and below) of the blackened absorber plate (Fig. 9.1c). The temperature of hot air is much less compared with cases (i) and (ii) respectively.

Because there is more heat transfer in the case of the hot surface facing upward (double) compared with the hot surface facing downward (Chap. 3), the temperature of the hot air in case (i) is greater. Furthermore, the hot air in case (i) loses more heat to the ambient air through the glass cover due to high operating temperature. Therefore, thermal efficiency in case (i) has a lower value. Because of that, this configuration is not recommended compared with case (ii). In case (ii), there are provisions to increase the heat transfer by increasing the surface of the absorber as shown in Fig. 9.1c, d. In the case of Fig. 9.1d, a pressure drop also occurs, which requires greater consumption of electricity.

Because of low heat transfer between the blackened absorber plate and the air, the air collector has lesser thermal efficiency. However, the efficiency of the solar air heater can be improved by increasing the heat-transfer surface area or by increasing the turbulence. This can be achieved by roughing the surface of the blackened absorber plate or by using extended fin structures as shown in Fig. 9.1d. The turbulence caused by roughing the surface enhances the convective heat transfer between the blackened absorber plate and the air flowing through the solar air collector. For the nonporous-type solar air collectors, the losses from the blackened absorption plate due to radiation are considerable. In the absence of a selective coating, the collection thermal efficiency is low. Inclusion of a fin incurs the problem of an excessive pressure decrease, which restricts the use of this type of solar air heater.

9.2.2   Porous-Type Solar Air Heaters

In the porous absorber solar air heater, porous absorbers of different configurations—such as wire mesh, honeycomb, or glass plates—are used as shown in Fig. 9.2. The air heater with a porous-type absorber has the following advantages:

(i) The solar radiation penetrates through the porous absorber and is absorbed throughout the duct depth of the solar air heater. Consequently, loss is decreased in the porous-type absorber air heater. The air stream heats up as it passes through the porous absorber, which is also known as the "matrix."

(ii) The pressure decrease is usually lower than with the nonporous-type absorber.

The porosity and thickness of the absorber must be optimized for higher thermal efficiency. It should be optimized in such a way that it transfers more thermal energy to the air flowing in the solar air heater. Figure 9.2a shows the porous wire mesh along with its matrix. The absorber bed, formed by broken bottles (Fig. 9.2b) and an overlapped glass plate (Fig. 9.2c), is an examples of a porous-type absorbers.

9.3   Conventional Nonporous Solar Air Heaters

Figure 9.3a shows the various thermal losses in terms of percentage of the conventional nonporous solar air heater. It can be seen that the maximum thermal efficiency of a conventional nonporous solar air heater can be 60 %. This is also referred to as a "single-pass solar air heater." An equivalent thermal-resistance circuit diagram of a conventional nonporous solar air heater is shown in Fig. 9.3b.

The energy-balance equations in this chapter are written under quasi-steady state and transient conditions with the assumptions given as follows:

Fig. 9.3   a Thermal losses (in percentage) of a double-glazed conventional nonporous solar air heater. **b** Thermal losses through an equivalent thermal-resistance circuit diagram of a conventional nonporous solar air heater
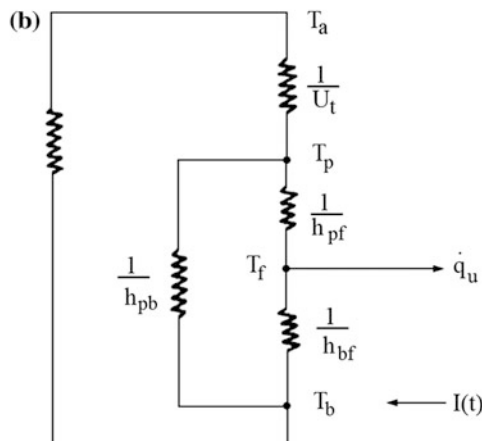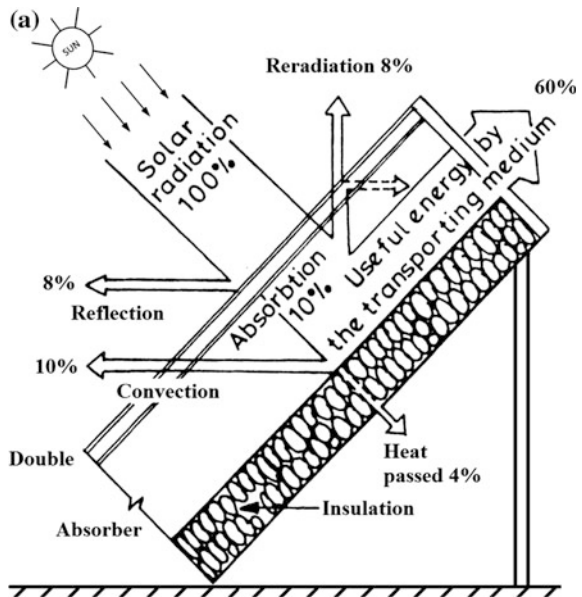
(i)   There is no temperature gradient along the thickness of the glass cover and the absorber plate.
(ii) The heat-transfer coefficients for the operating temperature range are assumed to be constant.
(iii) The mass-flow is stream-line flow and constant.
(iv) The side-heat losses are neglected.
(v)   The temperature gradient along the depth of the duct is negligible; average air temperature changes along the direction of flow.
(vi) The thermal/heat loss from the absorber plate through the bottom insulation is considered under steady-state conditions.
(vii) Absorptivity of solar radiation in a glass cover is negligible.

9.3.1 Steady-State Analysis for Natural Mode

(a) **First method**

Materials for the construction of solar air heaters are similar to those of liquid flat-plate collectors. Here the absorption of solar radiation in the absorber plate (α) takes place after the transmission of solar radiation (τ) through the glass cover system, which is identical to that of liquid flat-plate collectors. Hence, the rate of thermal energy at the absorber plate will be as follows:

$$\dot{Q}_u = A_c \big[(\alpha\tau)I(t) - U_L(T_p - T_a)\big] \tag{9.1a}$$

or,

$$\frac{\dot{Q}_u}{A_c U_L} = \left[\frac{(\alpha\tau)}{U_L}I(t) - (T_p - T_a)\right] \tag{9.1b}$$

where $I(t)$ is solar intensity; A_c is the area of the solar air heater; and T_p and T_a are the plate/absorber and ambient-air temperatures, respectively. The U_L is an overall heat-transfer coefficient from the absorber plate to the ambient air through glass cover as well as the bottom insulation.

If the working fluid as air can be either above or below the absorber plate, the rate of thermal energy transfer from the absorber plate to the air will be written as follows:

$$\dot{Q}_u = A_c \big[h_{pf}(T_p - T_f)\big] \tag{9.2a}$$

or

$$\frac{\dot{Q}_u}{A_c h_{pf}} = (T_p - T_f) \tag{9.2b}$$

where h_{pf} is the convective heat-transfer coefficient from the absorber plate to the fluid (air). Its value will be half in the case of fluid (air) below the absorber plate.

After the addition of Eqs. (9.1b) and (9.2b), one obtains

$$\dot{Q}_u \left[\frac{1}{A_c U_L} + \frac{1}{A_c h_{pf}} \right] = \frac{(\alpha\tau)}{U_L} I(t) - (T_f - T_a)$$

which can be written as

$$\dot{Q}_u = \frac{1/U_L}{\left[\frac{1}{U_L} + \frac{1}{h_{pf}} \right]} A_c [(\alpha\tau)I(t) - U_L(T_f - T_a)]$$

$$\dot{Q}_u = F'A_c[(\alpha\tau)I(t) - U_L(T_f - T_a)] \tag{9.3a}$$

where

$$F' = \frac{1/U_L}{\left[\frac{1}{U_L} + \frac{1}{h_{pf}} \right]} = \frac{1/U_L}{\frac{1}{U_0}} = \frac{U_0}{U_L} = \frac{h_{pf}}{(h_{pf} + U_L)} \tag{9.3b}$$

or,

$$F' = \frac{\dot{Q}_u}{[\dot{Q}_u]_{T_p=T_f}} = \frac{\dot{Q}_u}{A_c[(\alpha\tau)I(t) - U_L(T_f - T_a)]}$$

F' is the solar air heater–collection efficiency factor, which is always <1. It is defined as the ratio of the actual rate of useful energy to the rate of useful energy when the plate is placed at fluid (air) temperature. Equation (9.3b) was derived under the assumption that there is only heat transfer from the absorber to the fluid (air).

An instantaneous thermal efficiency of the conventional nonporous solar air heater can be obtained from Eq. (9.3a) as

$$\eta_i = \frac{\dot{Q}_u}{A_c I(t)} = F' \left[(\alpha\tau) - U_L \frac{(T_f - T_a)}{I(t)} \right] \tag{9.4}$$

The above equation is known as the "characteristic equation of solar air heater" similar to the HWB equation of the FPC Eq. (5.81).

Example 9.1 Two horizontal surfaces each having a temperature of 288 and 320 K, respectively, is separated by a 40 mm layer of air. Determine the rate of heat exchange per square meter (W/m^2) between the two surfaces.

Solution

In the given problem, $T_{avg} = (288 + 320)/2 = 304$ K. At this average temperature the properties of air are: $v = 1.61 \times 10^{-5} \, \text{m}^2/\text{s}$, $K = 0.026$ W/mK, $Pr = 0.708$ (Appendix V)

The Grashof number from Eq. (3.22d), is given by

$$Gr = (9.832) \times (0.04)^3 / \left(304 \times \left(1.61 \times 10^{-5}\right)^2\right) = 2.547 \times 10^5$$

The Nusselt number (Table 3.3) can be obtained as follows:

$$\bar{Nu} = (\bar{h}D/K) = (0.019)(Gr)^{1/4} = 4.38$$

The heat-transfer coefficient, $\bar{h}$, can be written as,

$$\bar{h} = (\bar{Nu}K/D) = (4.38 \times 0.026)/0.040 = 2.847 \, \text{W/m}^2 \, \text{K}$$

The rate of heat transfer per square meter (W/m^2) between two surfaces is determined as

$$\dot{q}/A = \bar{h}(T_h - T_c) = 2.847 \times 32 = 91.104 \, \text{W/m}^2$$

Example 9.2 An absorber of a conventional nonporous solar air heater at 44 °C is placed 5 cm below the glass cover, which is at a temperature of 10 °C. Calculate the following:

 (i)   convective and the radiative heat-transfer coefficients between the absorber plate and the glass cover;
 (ii) total heat-transfer coefficient between the absorber and the cover; and
 (iii) overall heat-transfer coefficient between the absorber and the ambient air.

Solution

(i) The convective and the radiative heat-transfer coefficients between the absorber plate and the glass cover

The average temperature of the absorber plate and the glass cover is determined by

$$T_{avg} = 27 \, °C = 300 \, \text{K}, \text{Thermal conductivity of air } (K) = 0.026 \, \text{W/mK}$$
$$v = 1.568 \times 10^{-5} \text{m}^2/\text{s}, Pr = 0.708, \beta = 1/300 \, (\text{Appendix V})$$

The Grashof number, Gr, is given by

$$Gr = \frac{g\beta(T_h - T_c)}{v^2}d^3 = \frac{9.8 \times 3.33 \times 10^{-3} \times (44 - 10) \times (0.05)^3(0.04)^3}{(1.568 \times 10^{-5})^2}$$
$$= 5.64 \times 10^5$$

The value of the Nusselt number (Table 3.3) can be calculated as follows:

$$\bar{Nu} = (h_{pf}d/K) = (0.068)(Gr)^{1/3} \quad \text{for, } 4 \times 10^5 < Gr$$
$$= (0.068)(82.623) = 5.618$$

or

$$h_{pf} = (5.618 \times 0.026)/0.05 = 2.921 \text{ W/m}^2 \text{ K}$$

Here a convective heat-transfer coefficient between the absorber plates to the fluid air is equal to the convective heat-transfer coefficient between the fluid air to the glass cover, i.e., $h_{fc} = h_{pf}$. Thus, the convective heat-transfer coefficient between the absorber plate to the glass cover $(h_{c,pc})$ is given by

$$h_{c,pc} = \left[\frac{1}{h_{pf}} + \frac{1}{h_{fc}}\right]^{-1} = \left[\frac{2}{2.921}\right]^{-1} = 1.46 \text{ W/m}^2 \text{ K}$$

The radiative heat-transfer coefficient [Eq. (3.34f)] is given by

$$h_{r,pc} = \frac{5.67 \times 10^{-8}\left[(44 + 273)^2 + (10 + 273)^2\right]\left[(44 + 273) + 10 + 273\right]}{\left[\frac{1}{0.8} + \frac{1}{0.8} - 1\right]}$$
$$= 4.095 \text{ W/m}^2 \text{ K}$$

(i) The total heat-transfer coefficient between the absorber and the cover and the total heat-transfer coefficient is $h_1 = h_{c,pc} + h_{r,pc} = 1.46 + 4.095 = 5.55 \text{ W/m}^2 \text{ K}$.

(ii) The overall heat-transfer coefficient between the absorber and the ambient air.

Here the convective and radiative heat-transfer coefficient from the glass cover to the ambient air Eq. (3.29b) is given by

$$h_2 = 5.7 \text{ W/m}^2 \text{ K (for, } V = 0 \text{ m/s).}$$

Thus the overall heat-transfer coefficient from the absorber to the ambient air is calculated as

$$U_t = \left[\frac{1}{h_1} + \frac{1}{h_2}\right]^{-1} = \left[\frac{1}{5.55} + \frac{1}{5.7}\right]^{-1} = 2.81 \text{ W/m}^2 \text{ K}$$

(b) **Second method**

In this method, the energy-balance equation under steady-state conditions for a conventional nonmatrix solar air heater with flow above the absorber (Fig. 9.3b) is written. The energy-balance equation of a conventional nonmatrix solar air heater with air flow above the absorber plate can be written as follows:

Absorber plate:

$$(\alpha\tau)I(t) = h_{pf}(T_p - T_f) + h_{rpc}(T_p - T_c) + U_b(T_p - T_a) \tag{9.5}$$

where T_p, T_c, T_f, and T_a are the temperature of the absorber plate, glass cover plate, fluid (air), and ambient air, respectively. The h_{pf} and h_{rpc} are the convective and the radiative heat-transfer coefficient between (i) the absorber plate and the fluid (air) and (ii) the absorber and the glass cover plate, respectively.

Glass cover:

$$h_{rpc}(T_p - T_c) + h_{fc}(T_f - T_c) = h_2(T_c - T_a) \tag{9.6}$$

where h_{fc} and h_2 are the convective and convective and the radiative heat-transfer coefficient between (i) the fluid (air) and the glass cover plate and (ii) the glass cover plate and the ambient air, respectively.

Working fluid (air):

The total rate of useful energy gain for the air is given as follows:

$$\dot{q}_u = h_{pf}(T_p - T_f) + h_{fc}(T_f - T_c) \tag{9.7}$$

After substituting T_p and T_c from Eqs. (9.5) and (9.6), respectively, in Eq. (9.7), one can derive an expression for $\dot{q}_u$ as follows:

$$\dot{q}_u = F'[(\alpha\tau)I(t) - U_L(T_f - T_a)] \tag{9.8a}$$

where the collector-efficiency factor (F') and the heat-loss factor (U_L), respectively, are given by

$$F' = \frac{B}{\left[h_{1f}(h_{pf} + U_b) + h_{pf}h_2 + h_{rpc}(h_{1f} + h_{pf} + U_b + h_2) + U_bh_2\right]} \tag{9.8b}$$

and

$$U_L = \frac{\left[h_{1f}\left(h_{pf}U_b + h_{pf}h_2 + U_bh_2\right) + h_{pf}U_bh_2 + h_{rpc}\left(h_{1f}U_b + h_{1f}h_2 + h_{pf}U_b + h_{pf}h_2\right)\right]}{B}$$

(9.8c)

where

$$B = h_{1f}h_{pf} + h_{pf}h_2 + h_{rpc}\left(h_{1f} + h_{pf}\right)$$

Furthermore, an instantaneous thermal efficiency of a conventional nonporous solar air heater can be obtained from Eq. (9.8a) as

$$\eta_i = \frac{\dot{q}_u}{I(t)} = F'\left[(\alpha\tau) - U_L\frac{(T_f - T_a)}{I(t)}\right]$$

(9.9)

Equations (9.4) and (9.9) are exactly the same with a change in expression for F' and U_L.

Example 9.3 Determine F' and U_L for the second method if a 5 cm—thick insulation of thermal conductivity 0.04 W/mK is placed below the absorber plate.

Solution
The bottom-loss coefficient with $h_i = h_2 = 5.7$ W/m² K for $V = 0$ m/s is given as

$$U_b = \left[\frac{L_i}{K_i} + \frac{1}{h_i}\right]^{-1} = [1.25 + 0.18]^{-1} = 0.699 \text{ W/m}^2 \text{ K}$$

Now, from Example 9.2, $h_{fc} = h_{pf} = 2.921$ W/m² K, $h_{rpc} = 1.46$ W/m² K, and $h_2 = 5.8$ W/m² K.

Substituting these values in Eq. (9.8), we obtain the values of $U_L = 3.088$ W/m² K and $F' = 0.689$.

9.3.2 Steady-State Analysis for Forced Mode

In this case, the heat capacity of the absorber plate, the glass cover, and the insulating material is neglected.

(a) **First Method**
In the forced mode of operation, a blower of known capacity is used to flow air with a mass-flow rate of $\dot{m}_f$ with a specific heat of C_f either above or below the absorber of a conventional nonporous solar air heater. According to Sect. 5.7.4, an energy-balance equation of flowing air for elemental area of 'bdx' can be written as

$$\dot{m}_f C_f \frac{dT_f}{dx} dx - F'[\dot{q}_{ab} - U_L(T_f - T_a)]bdx = 0 \tag{9.10}$$

where $\dot{q}_{ab} = (\alpha\tau)I(t)$.

Assuming F' and U_L to be constant during operating temperature Eqs. (9.3a), (9.3b) and (9.8a)–(9.8c), the solution of Eq. (9.10) can be obtained with initial condition $T_f = T_{fi}$ at $x = 0$, and it is given by

$$\frac{T_f - T_a - (\dot{q}_{ab}/U_L)}{T_{fi} - T_a - (\dot{q}_{ab}/U_L)} = \exp\left[-\frac{F'U_L bx}{\dot{m}_f C_f}\right] \tag{9.11}$$

The outlet-fluid air temperature T_{fo} at $x = L$ can be written by using Eq. (9.11) as

$$T_{fo} = T_f|_{x=L_r} = \left[\left(\frac{\dot{q}_{ab}}{U_L}\right) + T_a\right] + \left[T_{fi} - T_a - \left(\frac{\dot{q}_{ab}}{U_L}\right)\right] \exp\left(-\frac{F'A_c U_L}{\dot{m}_f C_f}\right) \tag{9.12}$$

where $A_c(=bL)$ is the flat-plate collector area; and L is the length of the conventional nonporous solar air heater in the flow direction.

Equation (9.12) can also be used to derive an expression for the rate of thermal energy available from one conventional nonporous solar air heater as

$$\dot{Q}_u = \dot{m}_f C_f(T_{fo} - T_{fi}) = A_c \frac{\dot{m}_f C_f}{A_c U_L}\left[1 - \exp\left(-\frac{F'A_c U_L}{\dot{m}_f C_f}\right)\right][\dot{q}_{ab} - U_L(T_{fi} - T_a)]$$

or

$$\dot{Q}_u = A_c F_R[\dot{q}_{ab} - U_L(T_{fi} - T_a)] \tag{9.13a}$$

where F_R is the flow-rate factor for one conventional nonporous solar air heater, and it is given by

$$F_R = \frac{\dot{m}_f C_f}{A_c U_L}\left[1 - \exp\left(-\frac{F'A_c U_L}{\dot{m}_f C_f}\right)\right] \tag{9.13b}$$

If N-conventional nonporous solar air heaters are connected in series, then an expression for an outlet-air temperature at the Nth conventional nonporous solar air heater is given by

$$T_{foN} = \left[\frac{\dot{q}_{ab}}{U_L} + T_a\right]\left[1 - \exp\left(-\frac{NF'A_c U_L}{\dot{m}_f C_f}\right)\right] + T_{fi}\exp\left(-\frac{NF'A_c U_L}{\dot{m}_f C_f}\right) \tag{9.14a}$$

In the above equation, one can determine the outlet-air temperature at N^{th} conventional nonporous solar air heaters connected in series for a constant mass-flow rate of air $(\dot{m}_f)$. In this case, there will be variation in the outlet-air

temperature. For industrial applications, sometimes a constant outlet-air temperature is required, in which case one must vary the mass-flow rate.

To obtain a constant outlet-air temperature, i.e., $T_{\text{foN}} = T_0$ in Eq. (9.14a). After applying this condition in Eq. (9.14a), one can obtain an analytical expression for variable mass-flow rate as

$$\dot{m}_{\text{f}} = -\frac{NF'A_{\text{c}}U_{\text{L}}}{C_{\text{f}}}\left[\ln\frac{T_0 - \left(\frac{\dot{q}_{\text{ab}}}{U_{\text{L}}} + T_{\text{a}}\right)}{T_{\text{fi}} - \left(\frac{\dot{q}_{\text{ab}}}{U_{\text{L}}} + T_{\text{a}}\right)}\right]^{-1} \tag{9.14b}$$

Furthermore, an expression for the rate of thermal energy available from N-conventional nonporous solar air heaters connected in series is given by

$$\dot{Q}_{\text{uN}} = \begin{cases} NA_{\text{c}}F_{\text{RN}}[(\alpha\tau)I(t) - U_{\text{LN}}(T_{\text{fi}} - T_{\text{a}})] & \text{for constant mass flow rate} \\ \dot{m}_{\text{f}}C_{\text{f}}(T_0 - T_{\text{fi}}) & \text{for constant collection temperature} \end{cases} \tag{9.14c}$$

where

$$F_{\text{RN}} = \frac{\dot{m}_{\text{f}}C_{\text{f}}}{NA_{\text{c}}U_{\text{L}}}\left[1 - \exp\left(-\frac{F'NA_{\text{c}}U_{\text{L}}}{\dot{m}_{\text{f}}C_{\text{f}}}\right)\right] \tag{9.14d}$$

Equations (9.14a) and (9.14c) are the same as Eqs. (5.88a) and (5.89b) but with changed values of F' and U_{L}.

Furthermore, an instantaneous thermal efficiency of N-conventional nonporous solar air heaters connected in series can be obtained as

$$\eta_{\text{i}} = \frac{\dot{Q}_{\text{uN}}}{NA_{\text{c}}I(t)} = F_{\text{RN}}\left[(\alpha\tau) - U_{\text{LN}}\frac{(T_{\text{fi}} - T_{\text{a}})}{I(t)}\right] \tag{9.14e}$$

(b) **Second Method**

The thermal performance of a conventional nonporous solar air heater, Fig. 9.3, was also studied analytically by Whillier [2].

For an infinitesimal small area $b\text{d}x$ along the flow direction at x (Fig. 9.4a), the thermal energy-balance equation for various components is given as follows:

(i) **The absorber plate:**

$$(\alpha\tau)I(t) = U_{\text{t}}(T_{\text{p}} - T_{\text{a}}) + h_{\text{pf}}(T_{\text{p}} - T_{\text{f}}) + h_{\text{rpb}}(T_{\text{p}} - T_{\text{b}}) \tag{9.15}$$

(ii) **Bottom plate:**

In this case, it can be written as:

$$h_{\mathrm{rpb}}(T_{\mathrm{p}} - T_{\mathrm{b}}) = h_{\mathrm{bf}}(T_{\mathrm{b}} - T_{\mathrm{f}}) + U_{\mathrm{b}}(T_{\mathrm{b}} - T_{\mathrm{a}}) \tag{9.16}$$

where b is the width of the absorber plate.

(iii) **Flowing fluid air:**

The rate of heat given by the bottom and the plate to the fluid is carried away, and it can be written as

$$\dot{m}_{\mathrm{f}} C_{\mathrm{f}} \frac{\mathrm{d}T_{\mathrm{f}}}{\mathrm{d}x} \mathrm{d}x = \left[h_{\mathrm{pf}}(T_{\mathrm{p}} - T_{\mathrm{f}}) + h_{\mathrm{bf}}(T_{\mathrm{b}} - T_{\mathrm{f}}) \right] b \mathrm{d}x \tag{9.17}$$

These equations can be solved for the outlet-fluid (air) temperature by the process of elimination and using the technique for a one-order differential equation in a way similarly performed in the first method.

According to Eqs. (9.15)–(9.17), the outlet-fluid air temperature T_{fo} at $x = L$ can be written as

$$T_{\mathrm{fo}} = T_{\mathrm{f}}|_{x=L_r} = \left[\left(\frac{\dot{q}_{\mathrm{ab}}}{U_{\mathrm{L}}} \right) + T_{\mathrm{a}} \right] + \left[T_{\mathrm{fi}} - T_{\mathrm{a}} - \left(\frac{\dot{q}_{\mathrm{ab}}}{U_{\mathrm{L}}} \right) \right] \exp\left(-\frac{F' A_{\mathrm{c}} U_{\mathrm{L}}}{\dot{m}_{\mathrm{f}} C_{\mathrm{f}}} \right) \tag{9.18}$$

According to the first method, the rate of useful heat gain of the conventional nonporous air collector can also be written as

$$\dot{q}_{\mathrm{u}} = F_{\mathrm{R}} A_{\mathrm{c}} [(\alpha\tau) I(t) - U_{\mathrm{L}}(T_{\mathrm{fi}} - T_{\mathrm{a}})] \tag{9.19}$$

where F_{R} is the collector heat-removal factor given by

$$F_{\mathrm{R}} = \frac{\dot{m}_{\mathrm{f}} C_{\mathrm{f}}}{A_{\mathrm{c}} U_{\mathrm{L}}} \left[1 - \exp\left(-\frac{F' A_{\mathrm{c}} U_{\mathrm{L}}}{\dot{m}_{\mathrm{f}} C_{\mathrm{f}}} \right) \right]$$

where

$$U_{\mathrm{L}} = U' + (1/F') \left[U_{\mathrm{b}} h_{\mathrm{bf}} / (h_{\mathrm{rpb}} + h_{\mathrm{bf}} + U_{\mathrm{b}}) \right]$$
$$U' = U_{\mathrm{t}} + \left[h_{\mathrm{rpb}} U_{\mathrm{b}} / (h_{\mathrm{rpb}} + h_{\mathrm{bf}} + U_{\mathrm{b}}) \right]$$

and the collector-efficiency factor (F') is given by

$$F' = \left[1 + \frac{U'}{h_{\mathrm{e}}} \right]^{-1} \text{ with } h_{\mathrm{e}} = h_{\mathrm{pf}} + \left[\frac{h_{\mathrm{bf}} h_{\mathrm{rab}}}{(h_{\mathrm{rbp}} + h_{\mathrm{bf}} + U_{\mathrm{b}})} \right]$$

Selcuk [1] reported the performance of nonporous type of air heaters as shown in Fig. 9.4b. It is inferred from the figure that transparent covers are not always

Fig. 9.4 **a** Heat-transfer process in a nonporous conventional solar air heater. **b** Optimum performance curve of solar air heaters
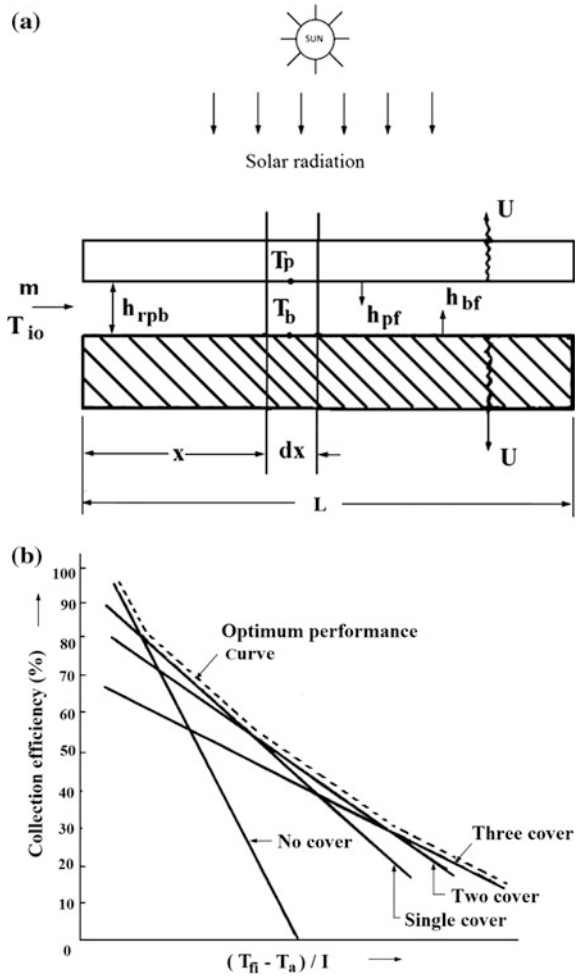
necessary for low-temperature applications. However, in a single glass cover, heat-loss reduction due to single glass compensates for the transmission losses and becomes beneficial beyond a certain temperature. However, the choice of the number of glass covers always confers economical constraints.

(c) **Photovoltaic thermal conventional nonporous air collector**

Here, N-photovoltaic thermal conventional nonporous air collectors are connected in series to produce thermal energy as well as DC electrical power to be used to run air blowers under forced mode to make the system sustainable. Here, a semitransparent PV module is integrated with a glass cover at the lower portion as performed in the case of the PVT flat-plate water collector (FPC) in Sect. 5.9.2.

According to Sect. 5.9.2, an analytical expression for the rate of useful thermal energy and the outlet-air temperature at the Nth photovoltaic thermal conventional nonporous air collector can be written with following modifications:

- The collector-efficiency factor (F') is given by Eqs. (9.3b) and (9.8a). respectively
- The values of h_{pf} should be taken for air

(i) The rate of thermal useful energy at the Nth photovoltaic thermal conventional nonporous air collector having area, $A = A_m + A_c$, is given by

$$\dot{Q}_{u,N} = NA\left[(\alpha\tau)_{eff,N}I(t) - U_{L,N}(T_{fi} - T_a)\right] \qquad (9.20a)$$

Here

$$(\alpha\tau)_{eff,N} = (F_R(\alpha\tau))_1\left[\frac{1 - (1 - K_{K,A})^N}{NK_{K,A}}\right]; U_{L,N} = (F_RU_L)_1\left[\frac{1 - (1 - K_{K,A})^N}{NK_{K,A}}\right]; K_{K,A} = \left[\frac{(AF_RU_L)_1}{\dot{m}_fC_f}\right]$$

$$(AF_R(\alpha\tau))_1 = \left[A_mF_{Rm}PF_2(\alpha\tau)_{m,eff}\left[1 - \frac{A_cF_{Rc}U_{L,c}}{\dot{m}_fC_f}\right] + A_cF_{Rc}(\alpha\tau)_{c,eff}\right]$$

$$(AF_RU_L)_1 = \left[A_mF_{Rm}U_{L,m}\left[1 - \frac{A_cF_{Rc}U_{L,c}}{\dot{m}_fC_f}\right] + A_cF_{Rc}U_{L,c}\right]$$

$$F_{Rm} = \frac{\dot{m}_fC_f}{A_mU_{L,m}}\left[1 - \exp\left(-\frac{F'A_mU_{L,m}}{\dot{m}_fC_f}\right)\right]; F_{Rc} = \frac{\dot{m}_fC_f}{A_cU_{L,c}}\left[1 - \exp\left(-\frac{F'A_cU_{L,c}}{\dot{m}_fC_f}\right)\right]$$

$$(\alpha\tau)_{m,eff} = PF_1(\alpha\tau)_{1,eff} + (\alpha\tau)_{2,eff}; (\alpha\tau)_{2,eff} = \alpha_p(1 - \beta_c)\tau_g^2; (\alpha\tau)_{1,eff} = \tau_g(\alpha_c - \eta_c)\beta_c$$

$$PF_1 = \frac{h_{c,p}}{U_{tc,p} + h_{c,p}}; PF_2 = \frac{h_{p,f}}{U_{L1} + F'h_{p,f}}; U_{L1} = \frac{h_{c,p}U_{tc,a}}{(h_{c,p} + U_{tc,a})}; U_{L,m} = \frac{U_{L1}h_{p,f}}{(U_{L1} + F'h_{p,f})}$$

The outlet-fluid temperature at the end of the Nth collector can be derived (see for details Sect. 5.9.2) as

$$T_{foN} = \frac{(AF_R(\alpha\tau))_1}{\dot{m}_fC_f}\left(\frac{1 - K_K^N}{1 - K_K}\right)I(t) + \frac{(AF_RU_L)_1}{\dot{m}_fC_f}\left(\frac{1 - K_K^N}{1 - K_K}\right)T_a + T_{fi}K_K^N \quad (9.20b)$$

where

$$K_K = 1 - \frac{(AF_RU_L)_1}{\dot{m}_fC_f}$$

Other expressions remain the same as in Sect. 5.9.2.

Different cases of the above equations will be same as in the case of the PVT water collector.

(d) **Single-pass nonporous PVT/nonporous solar air heater**

The configuration of a single-pass nonporous PVT conventional solar air heater is shown in Fig. 9.5. In this case, the rate of thermal energy available at the outlet can be obtained from Eq. (9.20a)–(9.20d) by substituting $A_c = 0$ and $N = 1$ as a special case, which is given by

$$\dot{Q}_{u,m} = A_m F_{Rm} \left[PF_2(\alpha\tau)_{m,eff} I(t) - U_{L,m}(T_{fi} - T_a) \right] \tag{9.20c}$$

Furthermore, the outlet-air temperature can be obtained from Eq. (9.20b) by substituting $A_c = 0$ and $N = 1$ as a special case, which can be written as

$$T_{foN} = \left[\frac{PF_2(\alpha\tau)_{m,eff} I(t)}{U_{L,m}} + T_a \right] \left[1 - \exp\left(-\frac{NF'A_m U_{L,m}}{\dot{m}_f C_f} \right) \right] + T_{fi} \exp\left(-\frac{NF'A_m U_{L,m}}{\dot{m}_f C_f} \right) \tag{9.20d}$$

Here $A_m = A = bL$, is the area of a single-pass nonporous PVT solar air collector.

Example 9.4 A fluid air at 28 °C blows over a flat-plate absorber at 40 °C having dimensions of 0.8 m × 0.8 m with an approach velocity of $V_\infty = 4$ m/s. Determine the total rate of heat transfer from the absorber plate to the flowing fluid air.

Solution

The viscosity of the fluid air at an average temperature of 32 °C is 1.578×10^{-5} (Appendix V). The Reynold number can be calculated using Eq. (3.22b) as

$$Re = \frac{v_\infty L}{v} = \frac{4 \times 0.8}{1.578 \times 10^{-5}} = 2.027 \times 10^5$$
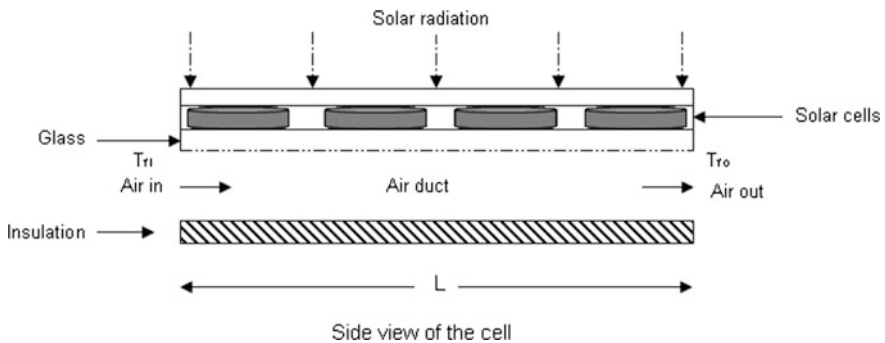
Fig. 9.5 Schematic diagram of a single-pass nonporous PVT conventional solar air heater. (From [9])

Because the flow is laminar, the heat-transfer coefficient can be calculated using Eq. (3.26) as follows:

$$\bar{h} = (K/L)\bar{Nu} = (K/L)\left(0.664 Re^{1/2} Pr^{1/3}\right)$$
$$= (0.026/0.8)\left(0.664 \times \left(2.027 \times 10^5\right)^{1/2}(0.713)^{1/3}\right) = 8.676 \text{ W/m}^2 \text{ K}$$

The total rate of heat transfer is given by

$$Q = \bar{h}A\,\Delta T = 8.676 \times 0.8 \times 0.8 \times 12 = 66.63 \text{ W}$$

Example 9.5 The following specifications for a conventional single-pass nonporous air heater are given below: Length $(L) = 2$ m, width $(b) = 1$ m, spacing $(d) = 10$ mm, plate temperature $(T_p) = 60\ °C$, glass temperature $(T_c) = 20\ °C$, flow rate $(\dot{m}_f) = 0.0017$ kg/s, ambient-air temperature $(T_a) = 9\ °C$, wind velocity $(V) = 3$ m/s, bottom-insulation thickness $(L_i) = 50$ mm, and thermal conductivity of the insulation $= 0.04$ W/mK.

Determine the heat-transfer coefficient between the absorber and the cover. In addition, calculate the following parameters:

(a) the overall top heat-transfer coefficient from the absorber to the ambient air (U_t);
(b) the total overall heat-transfer coefficient from the absorber to the ambient air (U_L) and the collection-efficiency factor (F'); and
(c) the mass-flow rate factor (F_R).

Solution
For an average fluid air temperature of 40 °C, the physical properties of fluid air are:

$v = 1.701 \times 10^{-5} \text{ m}^2/\text{s}$, $\rho = 0.1130 \text{ kg/m}^3$, $K = 0.0272$ W/mK, $Pr = 0.7051$, $Cp = 1005.867$ J/kg K (Appendix V)

The flow rate

$$(\dot{m}_f) = Lbd\rho/t$$

Thus,

$$L/t = v = \dot{m}_f/bd\rho = 0.0017/\left(1 \times 10^{-2} \times 0.1130\right) = 1.504 \text{ m/s}$$

The Reynold number can be calculated using Eq. (3.22b) as follows:

$$Re = Lv/v = (2 \times 1.504)/\left(1.701 \times 10^{-5}\right)$$
$$= 1.768 \times 10^5 < 5 \times 10^5 \text{(Laminar flow)}$$

The Nusselt number can be determined for laminar flow from the following relation

$$Nu = \frac{0.3387 Re_x^{1/2} Pr^{1/3}}{\left[1 + \left(\frac{0.0468}{0.7051}\right)^{2/3}\right]^{1/4}} \quad \text{for} Re \cdot Pr > 100$$

hence,

$$Nu = \frac{0.3387 \left(1.768 \times 10^5\right)^{1/2} \times (0.7051)^{1/3}}{\left[1 + \left(\frac{0.0468}{Pr}\right)^{2/3}\right]^{1/4}} = 122.02$$

The heat-transfer coefficient $\left(h_{pf}\right)$ from the absorber plate to the fluid air can be calculated by

$$h_{pf} = NuK/L = 1.659 \text{ W/m}^2 \text{ K}$$

The radiative heat-transfer coefficient can be calculated by

$$h_r = \varepsilon\sigma\left[\frac{\left(T_p + 273\right)^4 - \left(T_c + 273\right)^4}{T_p - T_c}\right]$$

$$h_r = 0.82 \times 5.67 \times 10^{-8}\left[\frac{(60 + 273)^4 - (20 + 273)^4}{60 - 20}\right] = 5.672 \text{ W/m}^2 \text{ K}$$

Total heat-transfer coefficient between the absorber plate and the glass cover is obtained as $h_1 = 1.659 + 5.726 = 7.385 \text{ W/m}^2 \text{ K}$.

The heat-transfer coefficient from the cover to ambient is given by Eq. (3.29a)

$$h_2 = 5.7 + 3.8 \quad V = 17.1 \text{ W/m}^2 \text{ K} \quad \text{for } V = 3 \text{ m/s}$$

(a) An overall top heat-transfer coefficient from the absorber to the ambient air (U_t) is given by

$$U_t = \left[\frac{1}{h_1} + \frac{1}{h_2}\right]^{-1} = \left[\frac{1}{7.385} + \frac{1}{17.1}\right]^{-1} = 5.158 \text{ W/m}^2 \text{ K}$$

An overall bottom-loss coefficient is given as

$$U_t = \left[\frac{L_i}{K_i} + \frac{1}{h_i}\right]^{-1} = 0.699 \text{ W/m}^2 \text{ K}$$

(b) From Eq. (9.20a), the value of U', F', and $U_L c$ an be calculated as follows:

$$U' = 5.158 + \frac{5.726 \times 0.699}{5.726 + 1.659 + 0.699} = 5.653 \text{ W/m}^2 \text{ K}$$

$$h_e = 1.659 + \left[\frac{1.659 \times 5.726}{5.726 + 1.659 + 0.699} \right] = 2.834 \text{ W/m}^2 \text{ K}$$

$$F' = \left[1 + \frac{U'}{h_e} \right]^{-1} = \left[1 + \frac{5.653}{2.834} \right]^{-1} = 0.334$$

Substituting these values, one obtains

$$U_L = 6.084 \text{ W/m}^2 \text{ K}$$

(c) The mass-flow rate factor, F_R, can also be determined as

$$F_R = \frac{0.0017 \times 1005}{6.0824 \times 2} \left[1 - \exp\left(-\frac{0.334 \times 6.0824 \times 2}{0.0017 \times 1005} \right) \right] = 0.1275$$

Various types of conventional air heaters have a nonporous-type absorber. The performance analyses of some of these have been discussed here.

9.3.3   Transient Analysis for Forced Mode

In this case, only the heat capacity of the absorber plate $(M_p C_p)$ is considered for simple analysis. Furthermore, one can also see the effect of the heat capacity of the absorber plate on the performance of a conventional nonporous solar air heater.

In view of the above, the transient analysis [3] of the configuration shown in Fig. 9.6 is performed.

In Fig. 9.6, an air gap with an air conductance of 'C' is introduced by inserting a reflecting sheet in between the absorber plate and the insulation. The inclusion of a

Fig. 9.6   Schematic view of conventional nonporous solar air heater with a reflecting sheet below the absorber
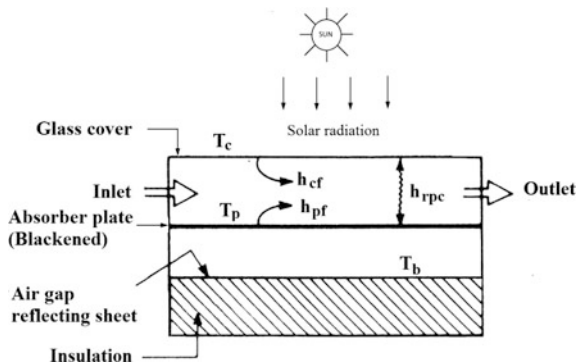
reflection sheet and an air gap reduces the overall bottom heat loss unlike shown Fig. 9.3a. However, analysis for conventional nonporous solar air heater air without an air gap and reflecting sheet can be considered as a special case similar to the earlier case.

The energy balance for the cover and the absorber plate can be written as follows:

Glass cover:

$$h_{fc}(T_f - T_c) + h_{rpc}(T_p - T_c) = U_t(T_c - T_a) \tag{9.21}$$

All terms were previously defined in Eq. (9.5).

Absorber plate:

$$(\alpha\tau)I(t) = h_{pf}(T_p - T_f) + h_{rpc}(T_p - T_c) + C(T_p - T_b) + M_p C_p(dT_p/dt) \tag{9.22}$$

where T_p is the temperature of the absorber plate.

Insulating cover:

Under steady-state conditions, the energy balance of the insulating bottom cover is given by

$$C(T_p - T_b) = U_b(T_b - T_a) \tag{9.23}$$

Flowing fluid air stream:

The energy balance of the air stream through the solar air collector is written for an elementary volume at a distance x from the inlet as shown in Fig. 9.12b.

$$\left[h_{cf}(T_c - T_f) + h_{pf}(T_p - T_f)\right]b\,dx = (\rho bd)C_f(dT_f/dt)dx + \dot{m}_f C_f(dT_f/dx)dx \tag{9.24}$$

Equations (9.21)–(9.24) can be solved by using Laplace transformation for T_f as a function of time 't' and 'x' for a given design and climatic parameters.

9.4 Double-Exposure Solar Air Heaters

The conventional nonporous solar air heater (Sect. 9.3) is also known as a "single-exposure air heater" due to fact that one side of blackened absorber plate is open for solar radiation exposure, whereas the other (bottom) side is insulated. A cross-sectional view of a double-exposure solar air heater is shown in Fig. 9.7. In this case, there is passage of fluid air between the two parallel blackened and glazed metallic absorber plates exposed to solar radiation. The fluid air stream in a double-exposure solar air heater receives thermal energy/heat from both of the

Fig. 9.7 Schematic sketch of
a double-exposure solar air
heater
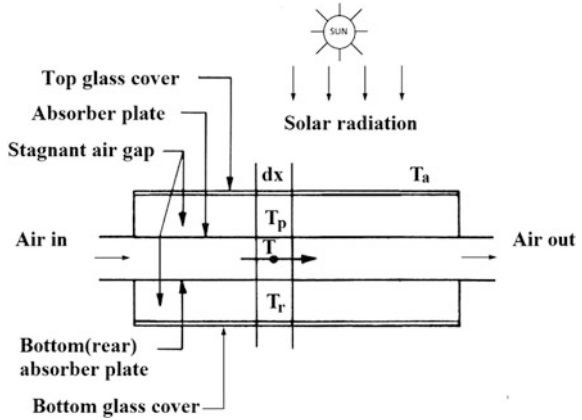
exposed absorber plates, thus forming the passage of fluid air. The thermal effi-
ciency of a double-exposure solar air heater, also nonporous, will certainly be
increased.

The double-exposure solar air heater can be studied according the similar pro-
cedure as performed in the case of the single-exposure solar air heater.

For an elemental area $'bdx'$ of a double-exposure solar air heater, the energy
balance for different elements is as follows:

Side 1:

$$(\alpha\tau)I_1(bdx) = U_t(T_p - T_a)(bdx) + h_{pf}(T_p - T_f)(bdx) + h_{rpb}(T_{pm} - T_{bm})(bdx) \tag{9.25}$$

Side 2:

$$(\alpha\tau)I_2(bdx) + h_{rpb}(T_p - T_b)(bdx) = h_{bf}(T_b - T_f)(bdx) + U_b(T_b - T_a)(bdx) \tag{9.26}$$

Flowing fluid air:

$$\dot{m}_f C_f \frac{dT_f}{dx}dx = h_{pf}(T_p - T_f)(bdx) + h_{bf}(T_b - T_f)(bdx) \tag{9.27}$$

where, I_1 and I_2 are the solar flux incident on side 1 and side 2 of the absorber plate
in W/m^2 respectively. These equations can be solved for an analytical expression
for outlet-air temperature as well as the rate of useful thermal energy as performed
previously.

9.5   Solar Air Heater with Flow on Both Sides of the Absorber

For a solar air heater with flow on both sides of the absorber (Fig. 9.8), the contact area between the absorber plate and the air stream is increased. For analysis of this type of solar air heater, it is assumed that the mass-flow rate and the heat-transfer coefficient (between absorber plate and air stream) in the upper and lower channels are the same. The analysis, which was discussed in the previous subsection, can easily be extended to study the thermal performance of this heater. Sodha et al. [4] have analyzed this solar air heater. The analysis is very approximate because it does not take into account the interaction of the cover and bottom plates with the air stream. The radiation exchanges between the absorber plate and the cover, and between the absorber plate and the bottom plate, have not been considered.

The steady-state heat-gain rate for the air stream can be written as follows [5]:

$$\dot{q}_u = h_{pf}\left(T_p - T_{ft}\right) + h_{pf}\left(T_p - T_{fb}\right) - h_{cf}(T_{ft} - T_c) - h_{cf}(T_{fb} - T_b) \qquad (9.28)$$

where T_{ft} is the air temperature in the top passage; and T_{fb} is the air temperature in the bottom passage.

The energy-balance equations for the cover, the absorber plate, and the bottom plate can be written. Furthermore, they are used to eliminate T_p, T_b, and T_c from Eq. (9.22). The two air temperatures (one above the plate and another below the plate) can be eliminated in the manner given below.

In general, the thermal loss from the top of absorber plate exceeds the heat loss from the bottom of the absorber plate. As a result of this, air temperature in the rear passage will be higher than in the top passage. The flow rates are the same on both sides. If T_f is the average of T_{ft} and T_{fb}, then the deviations of T_{ft} and T_{fb} from T_f must be same. The deviations between the fluid and the ambient-air temperatures
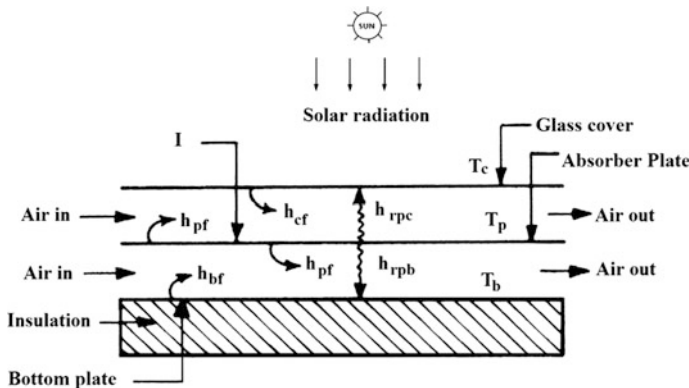
Fig. 9.8   Schematic view of a double-flow solar air heater

may also be used to indicate the deviations of T_{ft} and T_{fb} from T_{f}. Therefore, a fractional deviation 'n' is defined as follows:

$$(T_{\mathrm{f}} - T_{\mathrm{a}})(1 - n) = (T_{\mathrm{ft}} - T_{\mathrm{a}}) \tag{9.29}$$

and

$$(T_{\mathrm{f}} - T_{\mathrm{a}})(1 + n) = (T_{\mathrm{fb}} - T_{\mathrm{a}}) \tag{9.30}$$

These two equations can be used to express T_{ft} and T_{fb} in terms of T_{f}. Equation (9.22) can be expressed in terms of mean air temperature T_{f}.

On solving the equations, one can obtain the expressions for F' and U_{L} as follows:

$$F' = \frac{D}{\left\{2h_{\mathrm{cf}}h_{\mathrm{pf}}P + 2h_{\mathrm{pf}}U_{\mathrm{b}}h_2 + h_{\mathrm{rpc}}\left(h_{\mathrm{cf}} + h_{\mathrm{rpb}}\right)\left(P + 2h_{\mathrm{pf}}\right) + U_{\mathrm{b}}\left(2h_{\mathrm{pf}} + h_2\right) + h_{\mathrm{cf}}h_{\mathrm{rpb}} + h_{\mathrm{rpb}}\left[h_{1\mathrm{f}}\left(P + 2h_{\mathrm{pf}}\right) + 2h_{\mathrm{pf}}h_2 + U_{\mathrm{b}}h_2\right]\right\}}$$

$$U_{\mathrm{L}} = \frac{\left[\begin{array}{c} 4h_{\mathrm{cf}}h_{\mathrm{pf}}U_{\mathrm{b}}h_2 + 2h_{\mathrm{rpc}}\left[\left(h_{\mathrm{cf}} + h_{\mathrm{pf}}\right)\left(h_{\mathrm{rpb}}h_2 + U_{\mathrm{b}}h_2 + h_{\mathrm{rpb}}U_{\mathrm{b}}\right) + h_{\mathrm{cf}}h_{\mathrm{pf}}h_2\right] + 2h_{\mathrm{rpb}}U_{\mathrm{b}}\left(h_{\mathrm{cf}}h_{\mathrm{pf}} + h_{\mathrm{cf}}h_2 + h_{\mathrm{pf}}h_2\right) \\ + (1 - n)h_{\mathrm{cf}}h_2\left[h_{\mathrm{cf}}\left(2h_{\mathrm{pf}} + h_{\mathrm{rpc}}\right) + h_{\mathrm{rpb}}Q\right] + (1 + n)h_{\mathrm{cf}}U_{\mathrm{b}}\left[h_{\mathrm{cf}}\left(2h_{\mathrm{pf}} + h_{\mathrm{rpb}}\right) + h_{\mathrm{rpc}}Q\right] \end{array}\right]}{D}$$

where,

$$D = \left[2h_{\mathrm{cf}}h_{\mathrm{pf}}P + 2h_{\mathrm{pf}}U_{\mathrm{b}}h_2 + h_{\mathrm{rpc}}\left\{Q\left(h_{\mathrm{cf}} + h_{\mathrm{rpb}} + U_{\mathrm{b}}\right) + h_{\mathrm{cf}}h_{\mathrm{rpb}}\right\} + h_{\mathrm{rpb}}Q(h_{1\mathrm{f}} + h_2)\right]$$

$$P = h_{\mathrm{cf}} + U_{\mathrm{b}} + h_2 \text{ and } Q = h_{\mathrm{cf}} + 2h_{\mathrm{pf}}$$

It may be seen that although the method for calculating F' and U_{L} is the same, the expressions become complicated due to the configuration. Furthermore, the value of U_{L} changes with n. This indicates that neglecting the deviations of the top and bottom temperatures from the average fluid temperature may result in an appreciable error in the value of U_{L} [5].

9.6 Two-Pass Solar Air Heater

9.6.1 Nonporous Conventional Two-Pass Solar Air Heater

In this case, two types of flow pattern, as shown in Fig. 9.9, are described: (i) air flows between two glass covers in the upper channel, and then it flows in between the absorber plate and the insulated plate in the lower channel; and (ii) air flows in between the glass cover and the absorber plate in the upper channel, and then it flows in between the absorber plate and the insulated plate in the lower channel.

The concept of the two-channel solar air heater was proposed by Satcunanathan and Deonarine [6] and later studied by Caouris et al. [7]. Figure 9.9a shows the configuration of the air heater studied by Satcunanathan and Deonarine [6]. In this

Fig. 9.9 Schematic view of a
two-pass nonporous solar air
heater **a** air channels
separated by glass cover and
b air channels separated with
absorber metallic plate
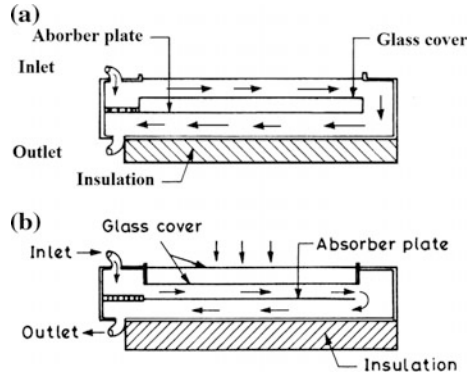
type of solar air heater, air flows between the glass cover, which reduces top heat
loss. Wijeysundera et al. [8] studied another configuration of two-channel solar air
heater as shown in Fig. 9.9b. They developed the thermal modeling of a
two-channel solar air heater and determined the performance of these solar air
heaters with experimental validation. They have reported improvement in the solar
air heater by 10–15 % with this configuration.

9.6.2   Comparison with Experimental Results

The experimentally observed results of Satcunanathan and Deonarine [6] have been
used by Wijeysundera et al. [8] to validate their theoretical model. They found a
good agreement between the experimental and modeled results. Figures 9.10 and

Fig. 9.10 Efficiency curve of
a solar air heater (*I* single pass
and *II* two pass)
$\dot{m} = 0.017\,\text{kg/s}$; $T_a = 303\,\text{K}$;
$A_c = 1.269\,\text{m}^2$;
gap $= 0.0381\,\text{m}$;
$V = 5.1\,\text{m/s}$
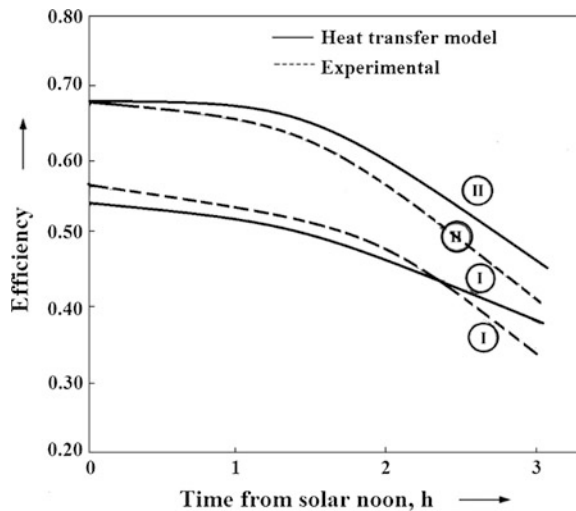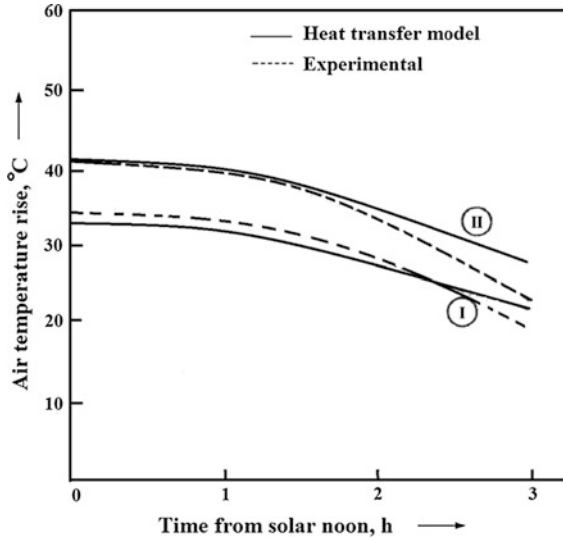
Fig. 9.11 Air temperature rise of a solar air heater (*I* single pass and *II* two pass) $\dot{m} = 0.017\,\mathrm{kg/s}$; $T_a = 303\,\mathrm{K}$; $A_c = 1.269\,\mathrm{m}^2$; gap $= 0.0381$ m; $V = 5.1\,\mathrm{m/s}$

9.11 depict the hourly variation of thermal efficiency and outlet-air temperature after solar noon for the single-channel and two-channel solar air heaters, respectively.

The figures infer that the two-channel solar air heater yields 10–15 % improved thermal efficiency compared with the single-channel solar air heater. The enhancement in thermal efficiency is due to the modification in the design of air passage of the solar air heater with nominal additional material and construction costs.

9.6.3 PVT Nonporous Conventional Two-Pass Solar Air Heater [9]

A schematic diagram of a semitransparent PVT nonporous conventional two-pass solar air heater/collector is shown in Fig. 9.12. In the PVT double-pass air collector, the air duct is divided into two parts by inserting the semitransparent PV module in the middle position in between the top glass cover and the blackened absorbing plate. The upper and lower air ducts are connected in series at the closed end of the solar air PVT collector. The upper and lower ducts are designed in such a way that there is a uniform air flow in both ducts. There is proper insulation on the sides and at the bottom of the PVT solar air heater to minimize side and bottom-losses.
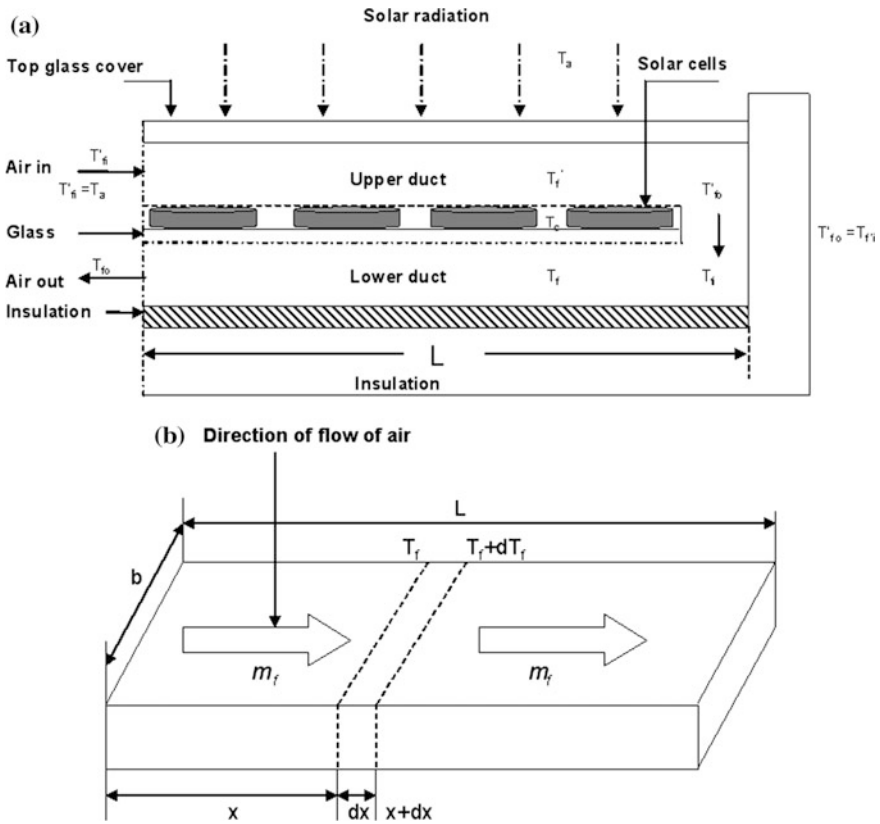
Fig. 9.12 **a** Schematic diagram of a semitransparent PVT nonporous conventional two-pass solar air heater/collector. (From [9]). **b** An elemental-length "dx" showing the air-flow pattern. (From [9])

Thermal modeling

Thermal modeling is performed for a semitransparent PVT nonporous conventional two-pass solar air heater/collector to determine the outlet-air temperature of the system and then use the obtained useful thermal energy for space heating during the winter season.

Assumption:

To write the energy-balance equations for various components of a semitransparent PVT nonporous conventional two-pass solar air heater/collector, the following assumptions are made:

(i)   Analysis is based on quasi steady-state conditions.
(ii)   Temperature variations along the depth and width of the duct are negligible.
(iii)   Heat capacities of the glass, PV module, and insulation are negligible.
(iv)   The width of the duct is equal to the width of the PV module.

(v)   Absorptivity of glass of PV module and the enclosed air is negligible.
(vi)   The ohmic losses in solar cells are negligible.
(vii)   Air is incompressible.
(viii)   Temperature of the glass cover and solar cell varies in the direction of fluid flow.

The energy-balance equations for different surfaces of the semitransparent PVT nonporous conventional two-pass solar air heater/collector in terms of W are written as follows:

(a) **For the top glass cover**

$$\left[\alpha_g I(t) + h_{crg}\left(T_c - T_g\right)\right] b\mathrm{d}x = \left[h_o\left(T_g - T_a\right) + h_{gf'}\left(T_g - T_f'\right)\right] b\mathrm{d}x \quad (9.31)$$

$$\begin{bmatrix} \text{The rate of thermal} \\ \text{enargy available} \\ \text{with the glass cover} \end{bmatrix} = \begin{bmatrix} \text{The rate of thermal energy} \\ \text{lost from the of glass} \\ \text{Cover to ambient} \end{bmatrix} + \begin{bmatrix} \text{The rate of thermal energy} \\ \text{lost from the of glass to the} \\ \text{flowing air} \end{bmatrix}$$

(b) **For the outer air duct (Fig. 9.12b)**
Referring to Fig. 9.12b, the energy balance for an elemental length 'dx' can be written as

$$\dot{m}_a C_a \frac{\mathrm{d}T_f'}{dx} dx = \left[h_{gf'}\left(T_g - T_f'\right) + h_{cf'}\left(T_c - T_f'\right)\right] b\mathrm{d}x \quad (9.32)$$

$$\begin{bmatrix} \text{The rate of thermal} \\ \text{energy carried away} \\ \text{by flowing air} \end{bmatrix} = \begin{bmatrix} \text{The rate of thermal} \\ \text{energy transferred by} \\ \text{convection from the} \\ \text{glass cover to the} \\ \text{flowing air} \end{bmatrix} + \begin{bmatrix} \text{The rate of thermal} \\ \text{energy transferred} \\ \text{from top of the solar} \\ \text{cell to the flowing} \\ \text{air by convection} \end{bmatrix}$$

(c) **For the solar cell**

$$\left[(1 - \alpha_g)\tau_g\alpha_c\beta_c I(t)\right] b\mathrm{d}x = \left[h_{crg}\left(T_c - T_g\right) + h_{cf'}\left(T_c - T_f'\right) + \eta_c\tau_g\beta_c\left(1 - \alpha_g\right)I(t)\right] b\mathrm{d}x$$
$$(9.33)$$

$$\begin{bmatrix} \text{The rate of} \\ \text{solar energy} \\ \text{absorbed by} \\ \text{the solar cell} \end{bmatrix} = \begin{bmatrix} \text{The rate of thermal} \\ \text{energy transferred from} \\ \text{the solar cell to the glass} \\ \text{by radiation} \end{bmatrix} + \begin{bmatrix} \text{The rate of thermal enargy} \\ \text{transferred by convection from} \\ \text{the solar cell to the flowing air} \end{bmatrix}$$
$$+ \begin{bmatrix} \text{The rate of thermal} \\ \text{energy converted into} \\ \text{electrical energy} \end{bmatrix}$$

(d) **For the inner air duct (Fig. 9.12b)**

An energy-balance for the inner duct will be similar to Eq. (9.32). Now, one has

$$\dot{m}_a C_a \frac{\partial T_f}{\partial y} dy = h_{bf}(T_b - T_f)bdy + h_{cf}(T_c - T_f)bdy \qquad (9.34)$$

$$\begin{bmatrix} \text{The rate of thermal energy} \\ \text{carried away by the flowing} \\ \text{air} \end{bmatrix} = \begin{bmatrix} \text{The rate of thermal energy} \\ \text{transferred by convection} \\ \text{from bottom insulation to} \\ \text{flowing air} \end{bmatrix} + \begin{bmatrix} \text{The rate of thermal energy} \\ \text{transferred from solar cell} \\ \text{to the flowing air by} \\ \text{convection} \end{bmatrix}$$

(e) **For the bottom insulation**

$$\left[\alpha_b \tau_g \tau_c^2 (1 - \alpha_g)(1 - \beta_c)I(t) \right] bdy = h_{bf}(T_b - T_f)bdy + h_{ba}(T_b - T_a)bdy \qquad (9.35)$$

$$\begin{bmatrix} \text{The rate thermal energy} \\ \text{absorbed by the bottom} \\ \text{insulation} \end{bmatrix} = \begin{bmatrix} \text{The rate thermal energy} \\ \text{transferred by convection} \\ \text{from bottom insulation to} \\ \text{flowing air} \end{bmatrix} + \begin{bmatrix} \text{The rate thermal energy} \\ \text{transferred from bottom} \\ \text{ambient by connection} \end{bmatrix}$$

Equations (9.31)–(9.35) can be solved for the solar cell, absorber, and fluid temperatures; hence, one can obtain an expression for electrical efficiency and the rate of thermal energy for a semitransparent PVT nonporous conventional two-pass solar air heater/collector.

Results and discussions

The hourly variation of solar cell temperature and electrical efficiency for a typical day is shown in Fig. 9.13. It shows that with the increase in solar-cell temperature, solar-cell efficiency decreases; it becomes constant at a constant solar-cell
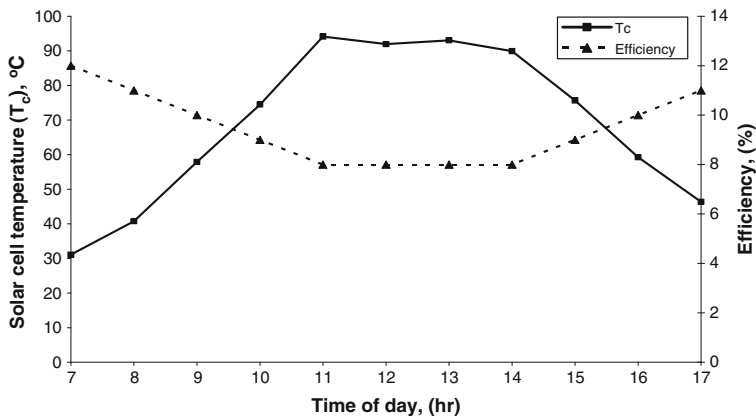
Fig. 9.13 Hourly variations of solar-cell temperature and efficiency with time for a typical day
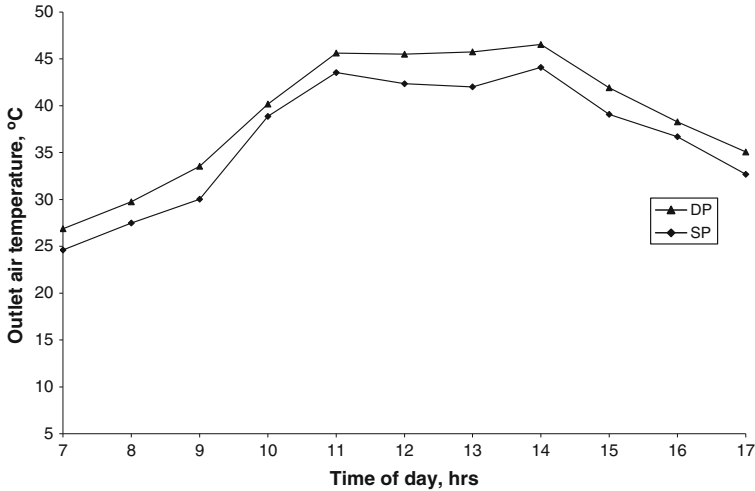
Fig. 9.14 Hourly variation of outlet solar air temperature for a typical day

temperature; and at the end of the day it again increases due to a decrease in cell temperature. This indicates the importance of solar-cell temperature. Based on this, electrical power can be determined on both an hourly and daily basis, and it can be extended to yearly electrical power.

The outlet-air temperature of single- and double-pass PVT air collectors for a typical winter day are shown Fig. 9.14. The outlet-air temperature varies from 26.9 to 46.6 °C for a double-pass air collector and from 24.6 to 43.2 °C for a single-pass air collector. It is seen that the outlet-air temperature of single-pass air collector is approximately 3–4 °C lower than that of the double-pass air collector due to low extraction of heat. These results show that the double-pass air collector has more utility than the single-pass air collector.

9.7   Effect of Fin

9.7.1   Air Heater with Finned Absorber

The heat-transfer rate (and hence the thermal efficiency of the solar air heater) from the fixed area of the absorber plate to the air stream can be increased by increasing the contact area between the air stream and the absorber plate. This can be achieved by introducing fins on the rear side of the absorber plate as shown in Fig. 9.1d. The inclusion of fines causes an additional pressure drop across the solar air heater. The number and design of additional fins are limited to the additional power requirement to run the fan for air circulation.

The thermal modeling of a solar air heater comprising additional fins can be developed by following similar approaches in convective heat-transfer problems.

However, the major constraint of this type of solar air heater is the unavailability of correlations for convective heat-transfer coefficients for various configurations of fin structures. Malik and Buelow [10] gave the correlation for the convective heat-transfer coefficient for a solar air heater used in solar crop-drying.

9.7.2 Air Heater with Vee-Corrugated Absorber

A Vee-corrugated absorber plate is shown in Fig. 9.15. Here the flat-plate absorber is replaced by a vee–corrugated absorber plate, which enhances the contact area in between the absorber plate and the air stream flowing inside the air duct. The increased surface area of the absorber plate also increases the loss from the absorber plate to the top cover, but this loss is overcome by the enhanced heat transfer from the absorber plate to the air stream inside the air duct.

   The acceptance angle for the vee-groove must be optimized in such a way that it compensates for the loss of solar radiation due to multiple reflections to the gain
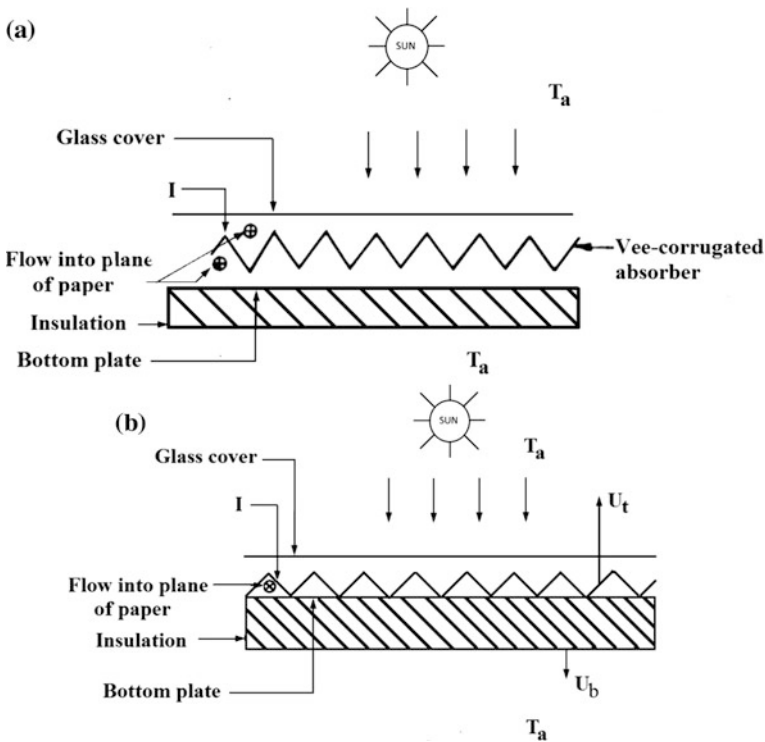
Fig. 9.15 a Schematic of a solar air heater with vee-corrugated absorber plate. b Schematic of solar air heater with triangular ducts

because of the increased heat transfer and improved efficiency. It should be properly designed. Inclusion of a vee–corrugated absorber plate increases the effective emissivity. The vee–corrugated absorber plate with selective coating and a 55° acceptance angle is suggested for this type of solar air heater.

Hollands [11] extensively analyzed the optical properties—such as absorptance, emittance, and directional selectivity—of the Vee-grooved specular surfaces.

A vee–corrugated absorber plate solar air heater may be designed for a single-pass as well as for a double-pass air flow through the upper and lower ducts. This type of solar air heater has the same values of collector thermal-efficiency factor (F') and overall heat-loss coefficient (U_L) as that of a flat-plate absorber solar air heater. The only difference is the improved value of the convective heat-transfer coefficient h_{pf} from the absorbing plate to the air stream [5].

When vee-grooves are extended to touch the bottom of the absorber plate, they form a triangular air duct as shown in Fig. 9.15b. The drawback of this type of solar air heater is that it resists the air flow through itself.

The triangular ducts are made of solid materials with high thermal conductivity. High thermal conduction provides a uniform temperature within the triangular duct. The lower temperature difference around the duct allows for neglecting the radiative heat transfer. The energy-balance for this type of solar air heater is written as follows (U_L is sum of the top and bottom overall heat-transfer coefficients):

$$(\alpha\tau)I(t) = \dot{q}_u + U_L(T_p - T_a)$$

or

$$\dot{q}_u = \left[(\alpha\tau)I(t) - U_L(T_p - T_a)\right] \tag{9.36}$$

where

$$U_L = U_t + U_b$$

Under steady-state conditions, the rate of heat transfer from the absorber plate to the ambient air is given by

$$\dot{q}_u = h_{pa}(T_p - T_a) \tag{9.37}$$

According to Sect. 9.3.1, the solar vee-corrugated collector-efficiency factor, F' can be derived as

$$\dot{q}_u = F'[(\alpha\tau)I(t) - U_L(T_f - T_a)] \tag{9.38}$$

where $F' = h_{pf}/(h_{pf} + U_L)$; which is the same as Eq. (9.3a) except for the greater numerical values of h_{pf}.

9.8   Reverse-Absorber Air Heater

A nonporous conventional air heater/collector can provide hot air at a temperature of 15–30 °C above the ambient temperature. Furthermore, the rise in temperature (say $\cong 100$ °C) can be obtained by reducing the convective and radiative top-heat losses from the absorber to the ambient air through the top glass cover. This is feasible in a new type of solar air collector known as a "reverse-absorber flat-plate collector" (RAFPC). It can collect solar energy at a high temperature of 200 °C. The working principle, energy-balance, and performance of RAFPC will be discussed in the following sections.

9.8.1   Working Principle

The schematic view of a reverse absorber flat-plate collector (RAFPC) is shown in Fig. 9.16 (a). Solar radiation is reflected by the polished curved cylindrical surface $\rho^N\{\tau I(t)\}$ after transmission from the glass cover $\{\tau I(t)\}$ toward the glazed reverse-absorber plate. After absorption, the absorber plate emits long-wavelength radiation. The long-wavelength radiation is then trapped between the absorber plate and the glazed cover. In this case, the convection and radiation heat losses are suppressed due to the hot absorber plate facing downward. An insulation thickness above the absorber plate reduces the top-heat loss due to conduction unlike the nonporous conventional air heater/collector. There is an air gap between absorber plate and the insulation to allow the air to flow above the absorber. The air passing above the absorber is heated. The aperture area of the RAFPC collector is equal to the absorber plate area. The concentration ratio is 1. other configurations of the RAFPC are shown in Fig. 9.16b–e.

9.8.2   Energy Balance

(a)   Steady-state conditions without airflow (First method)

According to Fig. 9.13a, the rate of thermal energy will be exactly same as Eq. (9.3a) as follows:

$$\dot{Q}_u = F'A_c[(\alpha\tau)I(t) - U_L(T_f - T_a)] \tag{9.39}$$

where

$$F' = \frac{1/U_L}{\left[\frac{1}{U_L} + \frac{1}{h_{pf}}\right]} = \frac{1/U_L}{1/U_o} = \frac{U_0}{U_L} = \frac{h_{pf}}{(h_{pf} + U_L)}$$
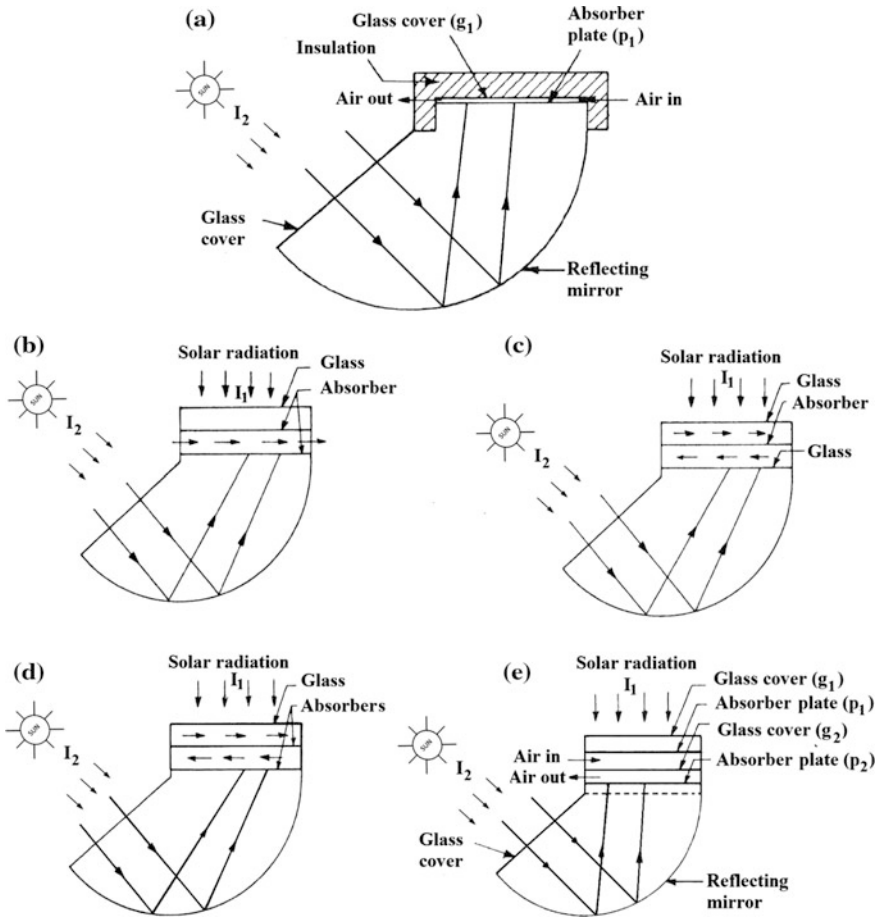
Fig. 9.16 Schematic view of various nonporous conventional solar air heaters/collectors reverse-absorber flat-plate air collectors (RAFPC): **a** Single pass, insulated on top **b** Single pass, glass cover on top, metallic absorber plates on bottom and middle **c** Double pass, glass cover on top and bottom, and metallic absorber plate as separator for air channels **d** Double pass, glass cover on top, metallic absorber plates on bottom and metallic absorber plate as separator for air channels **e** Double pass with two absorber plates and two glass plates

It is important to note here that the numerical value of h_{pf} will be half in the case of a nonporous conventional air heater/collector reverse-absorber flat-plate collector (RAFPC) with a reduced value of U_L.

(b) **Steady-state conditions with airflow**

First method:

In this case, an energy-balance for elemental length will be as follows:

$$\dot{m}_f C_f \frac{dT_f}{dx} dx - F'[(\alpha\tau)I(t) - U_L(T_f - T_a)]bdx = 0 \tag{9.40}$$

Second method:

Referring to Fig. 9.16a, the energy-balance equation at the reverse-absorber plate (T_p), the flowing fluid (T_f), and the glass cover (T_c) in the x-direction can be written as follows:

$$\tau I(t)\rho^N = h_{pf}(T_p - T_f) + h_{rpg}(T_p - T_c) \tag{9.41}$$

$$\dot{m}_f C_f \frac{dT_f}{dx} dx = \left[h_{pf}(T_p - T_f) - U_t(T_f - T_a)\right]bdx \tag{9.42}$$

Here U_t is the top-loss coefficient from the reverse-absorber to the ambient air through the top insulation, which is given by

$$U_t = \left[\frac{L_i}{K_i} + \frac{1}{h_o}\right]^{-1} \quad \text{with} \quad h_o = 5.7 + 3.8 \text{ V}$$

and

$$h_{rpg}(T_p - T_c) + h_{fc}(T_f - T_c) + U_b(T_c - T_a) \tag{9.43}$$

Here U_b is the bottom-loss coefficient from the reverse absorber to the ambient air through the top glazing cover of the reflector, which is given by

$$U_b = \left[\frac{1}{h_1} + \frac{1}{h_1'} + \frac{1}{h_o}\right]^{-1}$$

with h_1' being the convective and radiative heat-transfer coefficient between the glazed surface of the reverse absorber to the glass cover of the reflector.

The above equations can be solved for the rate of useful heat-gain rate of the RAFPC with a flow rate factor.

The energy-balance equations for other configuration (Fig. 9.16) can also be written in the similar ways.

9.8.3   Performance Study

Chandra et al. [12] compared the performance of a normal flat-plate collector (NFPC) with that of a reverse-absorber flat-plate collector (RAFPC) a for single-pass and double-pass solar air heating system. They concluded that the outlet-air temperature for the RAFPC is higher than that for the outlet-air temperature of an NFPC.

Fig. 9.17 Variation of an outlet air temperature with "x" for different N
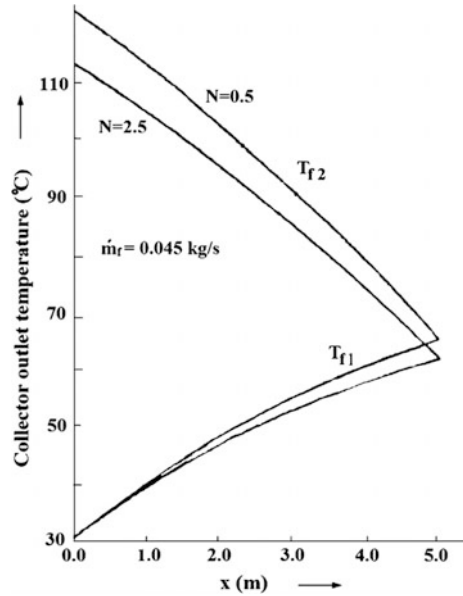
Fig. 9.18 Variation of outlet-air temperature with "x" for different $\dot{m}_f$
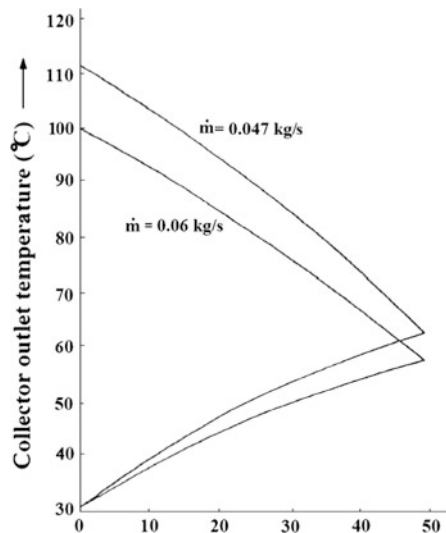
The effect of the number of reflections on the outlet-air temperature is shown in Fig. 9.17 for a two-absorber two-pass reverse flat-plate collector (Fig. 9.16e). It is observed that the outlet-air temperature deceases with an increase in the number of reflections (ρ^N) due to increase of reflection losses. Furthermore, the outlet-air temperature increases with a decrease in the mass-flow rate as shown in Fig. 9.17. In this case, the convective heat transfer is increased due to longer contact between the air and the hot absorber plate (Fig 9.18).

9.9   Solar Air Heaters with Porous Absorbers

Porous absorber increases the contact area between the absorber material and the air flowing through solar air heater. A higher contact area ensures higher heat exchange between the absorber material and the air; hence, the high temperature of the air. Therefore, these porous absorbers are most suited for high-temperature applications.

Generally blackened porous matrix with different structures, namely, honeycomb absorber, slit, expanded metal, and wire mesh, are used as the absorber in these solar air heaters.

9.9.1   Matrix Solar Air Heaters

Figure 9.19 shows a schematic view of a solar air heater that uses a porous matrix as the absorber. The degree of porosity and wire mess size is optimized per the end-use requirement of a particular solar air heater. Long-wavelength thermal radiation losses can be minimized by selectively coating the top surface of the absorber matrix. The upper surface of the porous absorber acts as a set of black cavities, which guarantee higher absorptivity. A different arrangement of air flow can be adopted for the heat-exchange mechanism between the air and the porous matrix as shown in Fig. 9.19. However, the arrangement depicted in Fig. 9.19b reduces the overall top-loss because the inlet cold air is always in contact with the cover of the solar air heater.

For a loosely packed porous matrix of semitransparent material, solar radiation is absorbed throughout the depth of the porous matrix; however, for the compact matrix the incident solar radiations are mostly absorbed by the upper surface of the porous absorber. Thermal analysis of this type of solar air heater is performed with the following assumptions:

  (i) Thermo-physical and transport properties of the porous absorber do not change with the temperature over the entire collector area.
 (ii) The flow of air stream and heat transfer is assumed to be one-dimensional and perpendicular to the bounding surfaces of the porous matrix.
(iii) It is assumed that there is no temperature gradient between the absorber matrix pores and the flowing air at any position inside the solar air heater.
 (iv) Radiation and convection losses from the sides and bottom of the solar air heater have been neglected.

The cost of these solar air heaters is strongly affected by the choice of matrix absorber material. To minimize the cost of the porous absorber, the use of screen doors, expanded metals, and black nylon in solar air heaters is avoided. Less costly
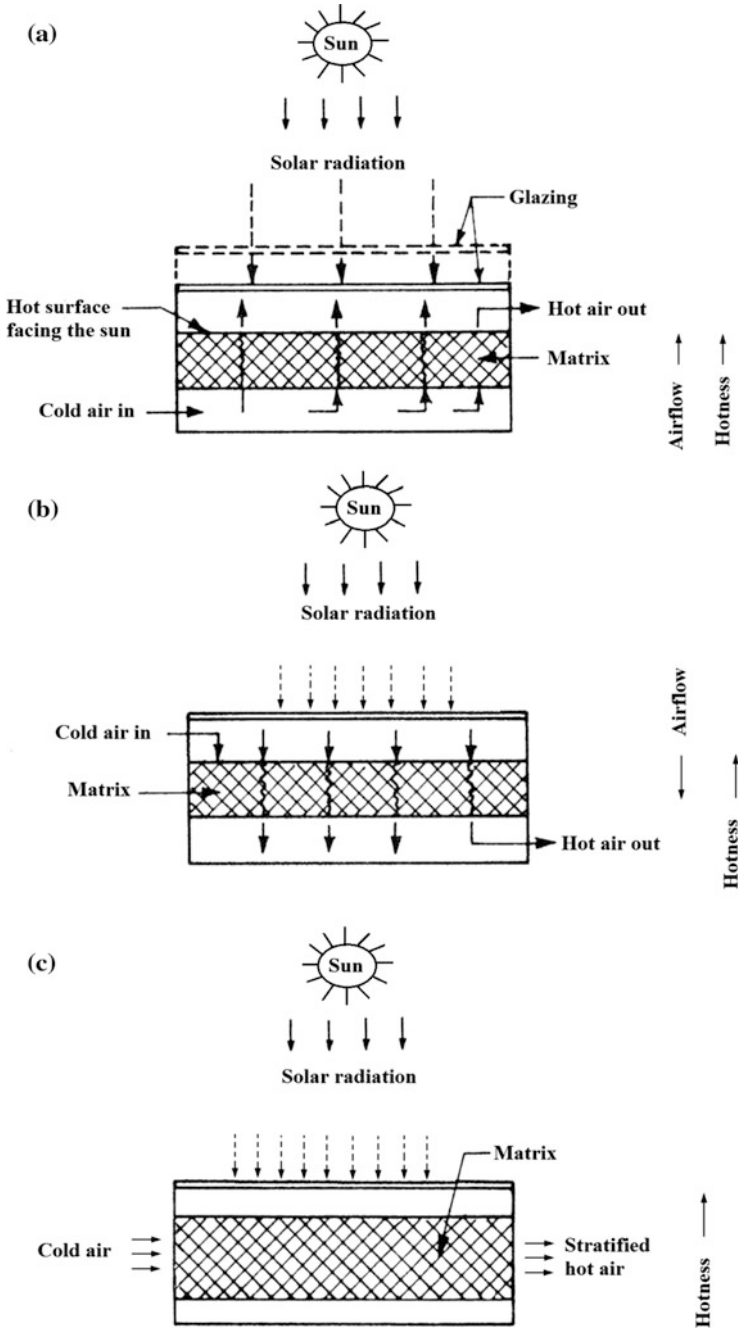
Fig. 9.19 Schematic view of different configurations of a matrix solar air heater: **a** Upward air flow through the matrix, air inlet near the hot surface **b** Downward air flow through the matrix, air inlet away from the hot surface **c** horizontal air flow through the matrix

materials—such as bronze, aluminum, stainless steel, and carbon steel—are preferred. Rusting of carbon steel is a major issue that limits the use of carbon steel in these solar air heaters. Blackened fiberglass insulation (FI) and dust filters can also be used as a porous matrix absorber.

9.9.2   Overlapped Glass-Plate Solar Air Heaters

A schematic diagram of an overlapped glass-plate solar air heater is shown in Fig. 9.20. This solar air heater comprises an overlapped set of glass plates. The overlapped portion of subsequent glass plates are painted black and the rest of the plate is left transparent. Solar radiation transmitted from the transparent portion of the glass plates falls on the blackened portion of lower glass plate and gets absorbed. This set of overlapped glass plates is covered by a glass cover on the top side, whereas the bottom side is insulated to reduce heat losses from the bottom side. This complete assemble is encased in a metal-sheet box. Solar radiation falling on the blackened portion of the glass plates are absorbed by the glass plates and thus heat them. The air flowing on either side of the glass plates receives thermal energy from the hot glass plates and thus becomes heated.

These solar air heaters provide a low pressure decrease and have high thermal efficiency for applications involving low and moderate temperatures. The requirement of a large area of glass plates make these solar air heaters costly. Parametric studies [1] have inferred that thermal efficiency is marginally affected by the variation of spacing between the plates and the use of multiple plates. The optimum glass thickness is approximately 3 mm, and the optimum spacing between the plates varies between 5 and 7 mm.
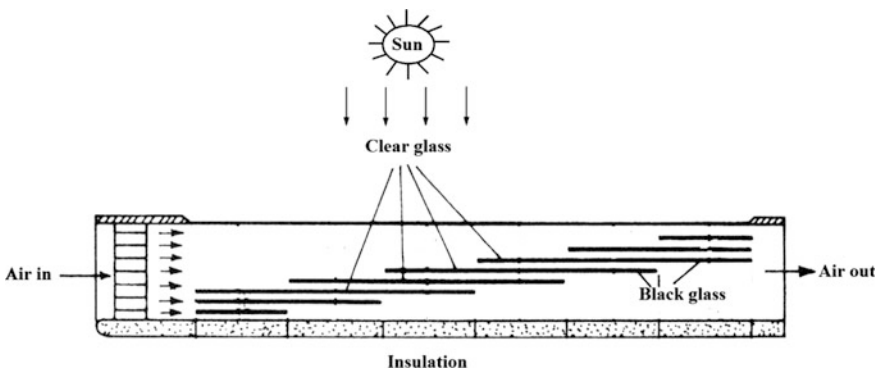
Fig. 9.20   Schematic of an overlapped-glass air heater

9.9.3   Solar Air Heater with Honeycomb Absorber

The use of honeycomb structures between the glass cover and the absorber plate is an established means of decreasing reduce top convective losses. A solar air heater can also be made by passing air through a honeycomb structure as shown in Fig. 9.21.

The honeycomb should be transparent. Different structure, e.g., hexagonal or rectangular, of honeycomb can be chosen per the desired requirement (Fig. 9.21). The convective and radiative heat losses from the absorber to the top glass cover can be reduced by adopting a porous matrix material for the honeycomb structure. Elaborated studies on honeycomb structure for use in solar air heater by Buchberg et al. [13] showed that reflecting walls coated with a thin lacquer film give a better performance compared with noncoated walls in solar air heaters.
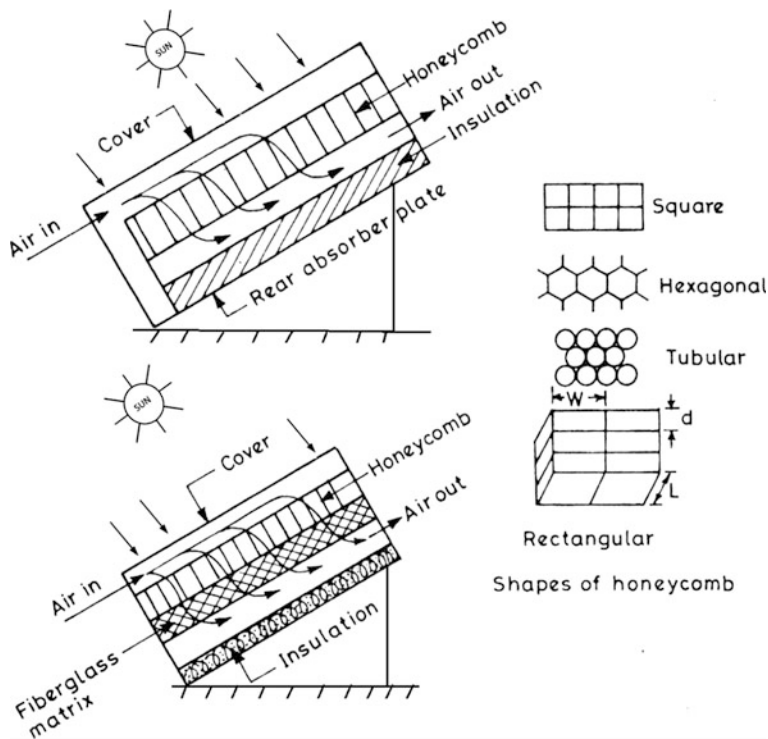
Fig. 9.21   Schematic of a transpired honeycomb solar air heater

9.10 Testing of a Solar Air Collector

A schematic view of a test facility developed at the University of Waterloo for testing solar air heaters is given in Fig. 9.22. The solar air collectors are tested at two different mass-flow rates viz. 7.5 and 10 L/m^2. The solar intensity $[I(t)]$ for the duration of testing is measured using a pyranometer mounted at the top of the solar air collector. The inlet air can be fed at the ambient temperature or at any other constant temperature. For constant inlet-air temperature, the inlet air is passed through a 2 kW–capacity thermostatically controlled electric heater.

The inlet air at constant temperature from the outlet of the electric heater is then fed to the solar air collector. Finally the hot air is passed through mixer duct—calibrated temperature—and flow rate–measuring devices.

The instantaneous thermal efficiency, η_i, can be calculated by using the following expression:

$$\eta_i = \frac{\dot{m}_f C_f (T_{fo} - T_{fi})}{A_c I(t)} \tag{9.44}$$

The variation of η_i with $\frac{(T_{fi} - T_a)}{I(t)}$ for two different mass-flow rates is shown in Fig. 9.23 [14]. One can observe clearly from the figure that solar air collectors give a better performance at a higher flow rate because of relatively low thermal losses.
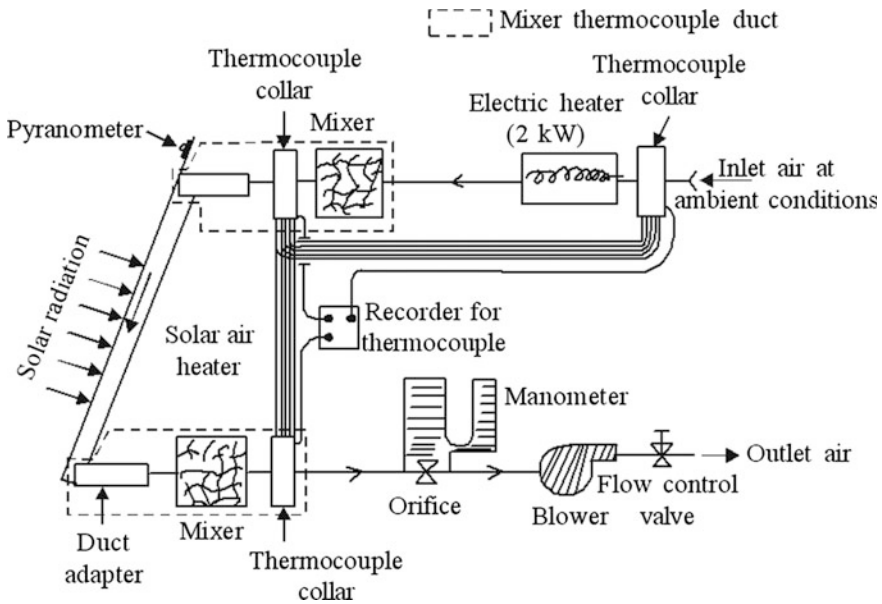
Fig. 9.22 Schematic of an air-heating solar collector testing apparatus (From [15])

Fig. 9.23 Comparison between a liquid and an air solar collector. (From [15])
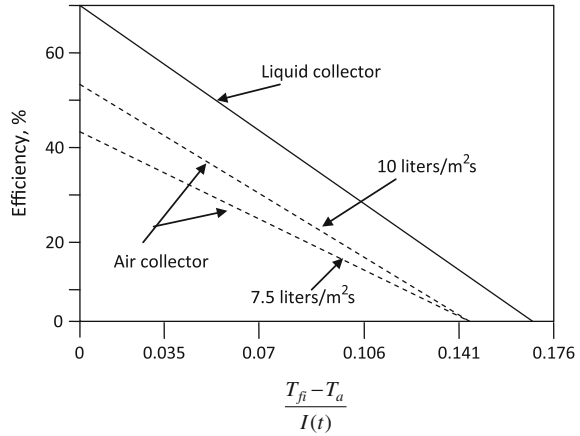
9.10.1 Performance of an Air Collector Versus that of a Liquid Collector

The characteristics curve for the flat-plate collector using liquid as a thermal energy carrier is also plotted in Fig. 9.23 for the purpose of comparison. Thermal performance in the case of a liquid collector is better than that of solar air collector, which can be credited to the high specific heat capacity of liquid. It can also be inferred from the figure that the air flow rate significantly affects the performance of the solar air heater, but at higher solar intensities a lesser influence of the flow rate is observed.

9.11 Parametric Studies

9.11.1 Effect of Air Leakage

Air leakage either from inside the solar air collector to the outside environment or within the solar air collector (i.e., between different flow channels at different temperatures) deteriorates the thermal performance of a solar air heater. The air leakage may occur due to various reasons viz. poor design and manufacturing, corrosion, vibrations and settlement, thermal expansion or contraction due to temperature variations, and poor handling of the solar air heater. Because the problem of air leakage cannot be solved completely, a small air leakage is generally ignored.

The instantaneous thermal efficiency is directly proportional to the mass-flow rate of air inside the solar air heater. For the same temperature difference in outlet and inlet air, the mass-flow rate measured at the inlet and outlet of the solar air heater will be different due to the small air leakage, which is ignored. The

mass-flow rate at the inlet will be higher than that at the outlet. Suppose mass-flow rates measured at inlet and outlet of the solar air collectors are $\dot{m}_{fi}$ and $\dot{m}_{fo}$. respectively.

For mass-flow rate measured at inlet the instantaneous thermal efficiency is given as follows:

$$\eta_i = \frac{\dot{m}_{fi} C_f \Delta T}{A_c I(t)} \tag{9.45}$$

The instantaneous thermal efficiency for the mass-flow rate measured at outlet is given as follows:

$$\eta_{iL} = \frac{\dot{m}_{fo} C_f \Delta T}{A_c I(t)} \tag{9.46}$$

The air-leakage flow rate is given as follows:

$$\dot{m}_L = \dot{m}_{fi} - \dot{m}_{fo} \tag{9.47}$$

The ratio of thermal efficiency with leakage to the thermal efficiency without leakage can be found using Eqs. (9.46) and (9.45) and is given as follows:

$$\frac{\eta_{iL}}{\eta_i} = 1 - \frac{\dot{m}_L}{\dot{m}_{fi}} \tag{9.48}$$

The above equation concludes that for no leakage, both of the efficiencies will be same. However, for a leakage, the leakage mass-flow rate ($\dot{m}_L$) will be greater than zero. Therefore, in case of leakage the instantaneous thermal efficiency is lower than that without leakage.

9.11.2 Effect of Particulate

Dust and the particulates in the air stream flowing through the solar air heater depreciate its performance. Dust and particulates are deposited on the inner walls of the air duct, which causes scaling on the inner surfaces of the duct. Due to the scaling effect, the rate of heat transfer decreases. Smaller particulates are deposited in the case of a laminar-flow condition due to molecular diffusion. Larger-size particulates, for example, fibrous dust, creates resistance to the air stream flowing inside the air duct. The denser particles present in the air stream are not in phase with the air flow inside the duct and are mainly deposited at the curved locations inside the duct.

The problem of particulate deposition can be overcome by using filters at the inlet of the solar air heater and designing the air duct with as minimum a number of bends as possible.

Objective Questions

9.1 The working fluid in solar air collector is
(a) air   (b) water   (c) oil   (d) none of these
Answer: (a)

9.2 The solar air collector is more effective and economical compared with the liquid collector due to
(a) freely available   (b) corrosion less   (c) no freezing   (d) all of these
Answer: (d)

9.3 The application of solar air collector is
(a) limited to space heating and crop drying
(b) unlimited such as a liquid flat-plate collector
(c) similar to that of a concentrating collector
(d) none of these
Answer: (a)

9.4 The conventional solar air collector is
(a) porous   (b) nonporous   (c) matrix   (d) all of these
Answer: (d)

9.5 The solar air collector is mostly operated
(a) under natural mode   (b) forced mode   (c) turbulent mode
(d) none of these
Answer: (b)

9.6 The collection-efficiency of a solar air collector is
(a) higher than that of a liquid collector
(b) equal to that of a liquid collector
(c) less than that of a liquid collector
(d) none of these
Answer: (c)

9.7 The collection-efficiency factor of a solar air collector (F') is
(a) lower than (F') that of a liquid collector
(b) higher than (F') that of a liquid collector
(c) equal to (F') that of a liquid collector
(d) none of these
Answer: (a)

9.8 Which solar air heater gives a better performance?
(a) single-exposure   (b) double-exposure
(c) single-exposure with fin   (d) none of these
Answer: (a)

9.9   The flow-rate factor (F_R) of a solar air collector is
    (a) equal to (F_R) that of a liquid collector
    (b) more than (F_R) that of a liquid collector
    (c) less than (F_R) that of a liquid collector
    (d) none of these
    Answer: (c)

9.10   The conventional solar air heater gives better performance if
    (a) the air flows above the absorber   (b) the air flows below the absorber
    (c) the air flows above and below the absorber   (d) none of these
    Answer: (b)

9.11   Which solar air heater gives a better performance?
    (a) single-exposure and single-pass
    (b) single-exposure and double-pass
    (c) double-exposure
    (d) none of these
    Answer: (b)

9.12   The performance of a solar air collector is better
    (a) at a high mass-flow rate   (b) at a low mass-flow rate
    (c) at a zero mass-flow rate   (d) none of these
    Answer: (a)

9.13   The reverse-absorber air collector is
    (a) better than a normal air collector
    (b) marginally better than a normal air collector
    (c) worse than a normal air collector
    (d) none of these
    Answer: (a)

9.14   The U_L-value of a reverse-absorber compared with normal air collector
    (a) higher value   (b) lower value   (c) equal value   (d) none of these
    Answer: (b)

9.15   The outlet-air temperature of a solar air collector
    (a) decreases with an increase of the mass-flow rate
    (b) increases with an increase of the mass-flow rate
    (c) is unaffected with an increase of the mass-flow rate
    (d) none of these
    Answer: (a)

9.16   The outlet-air temperature of a solar air collector
    (a) decreases with a decrease of the mass-flow rate
    (b) increases with a decrease of the mass-flow rate
    (c) is unaffected with a decrease of the mass-flow rate
    (d) none of these
    Answer: (b)

9.17   The mass-flow rate for a given cross-sectional area of duct
    (a) increases with an increase of air velocity in the air duct
    (b) decreases with an increase of air velocity in the air duct

(c) is unaffected with an increase of air velocity in the air duct

(d) none of these

Answer: (a)

9.18 The mass-flow rate for a given air velocity in an air duct

(a) increases with an increase of the cross-sectional area of the air duct

(b) decreases with an increase of the cross-sectional area of the air duct

(c) is unaffected by an increase of the cross-sectional area of the air duct

(d) none of these

Answer: (a)

9.19 The expression for mass-flow rate $(\dot{m}_f)$ is

(a) $\rho a u$ (b) $a u$ (c) ρu (d) none of these

Answer: (a)

9.20 Convection is only suppressed by evacuating the air in

(a) the flat-plate collector   (b) the solar air collector

(c) the evacuated collector   (d) the concentrating collector

Answer: (c)

9.21 The air leakage in a solar air collector affects the

(a) outlet-air temperature   (b) rate of useful energy

(c) thermal efficiency   (d) all of these

Answer: (a)

Problems

9.1 Determine the pressure drop (ΔP) across a single-pass solar air heater for the parameters in Fig. 9.10.

Hint: Given: $\Delta P = F(M_a^2/\rho)(L/D)^3$ where $F = F_0 + \gamma(D/L)$

For laminar flow $(Re < 2550)$; $F_0 = 24/Re$ and $\gamma = 0.9$

For transitional flow $(2550 < Re < 10^4)$; $F_0 = 0.0094$ and $\gamma = 2.92Re^{-0.15}$

For turbulent flow $(10^4 < Re < 10^5)$; $F_0 = 0.0599Re^{-0.2}$ and $\gamma = 0.73$

Mass flow rate per $m^2 = \dot{M}_a$

9.2 Determine the total pressure drop for a multi-pass air heater.

Hint: Calculate for each pass and then add to obtain the total pressure drop.

9.3 Determine the energy consumption for pumping the air through the air duct of a solar air collector.

Hint: $E = M(\Delta P/\rho_a)t$ (M in kg/m^2 s)

Take the value of ΔP, M, and ρ_a from Problem 9.1.

9.4 Calculate the convective heat-transfer coefficient (h_{pf}) from the absorber plate to the air flowing over it.

Hint: $h_{pf} = (NuK/D_h)$ where,

$$D_{\text{h}} = (4A/P); A = \text{cross sectional area and } P = \text{perimeter and } Nu$$
$$= Nu_0 + \beta_0(W/L)$$

(i)   For $Re < 2500$ (Laminar flow) $Nu_0 = 5.385; \beta_0 = 0.0148Re$

(ii) For $2500 < Re < 10^4$ (Transitional flow) $Nu_0 = 4.4 \times 10^{-4}Re^{1.2}; \beta_0 = 9.37Re^{0.471}$

(iii) For $10^4 < Re < 10^5$ (Turbulent flow) $Nu_0 = 0.03Re^{0.74}; \beta_0 = 0.788Re^{0.74}$

9.5 Determine the outlet-air temperature for a different-length collector (2m−10m) for the following parameters:

$$I = 350\,\text{W/m}^2; \quad T_{\text{a}} = 15\,^\circ\text{C}; \quad W = 1\,\text{m}; \quad \dot{m} = 0.02\,\text{kg/s}$$
$$U_{\text{t}} = 2.81\,\text{W/m}^2\,\text{K}; \quad 2h_{\text{pf}} = h_{\text{bf}} = 5.842\,\text{W/m}^2\,\text{K}; \quad h_{\text{rbp}} = 5.27\,\text{W/m}^2\,\text{K}$$

In addition, plot the curve between the outlet temperature and the length of the collector.
Hint: Use Eq. (9.12)

9.6 Calculate F' for Problem 9.5.
Hint: Use Eqs. (9.3) and (9.8).

9.7 Plot η_{i} versus $(T_{\text{fi}} - T_{\text{a}})/I(t)$ for Problem 9.5.
Hint: $\eta_{\text{i}} = \dot{q}_{\text{u}}/I(t); T_{\text{fi}} = (T_{\text{a}} + 2)\,^\circ\text{C}$.

9.8 Repeat Problems 9.5–9.7 of flat-plate solar air collector under steady-state conditions.
Hint: Use Eq. (9.14) and change the area of $A_{\text{c}} = b \times L$.

9.9 Calculate F' for a single-flow and a double-flow air heater, and compare the results.
Hint: Use Problem 9.6.

9.10 Write the energy-balance equation of the absorber considering the effect of conduction through the plate.
Hint: Use Eq. (9.4)

References

1. M.K. Selcuk, Solar air heaters and their applications, Chap. 8, in *Solar Energy Engineering*, ed. by A.A.M. Sayigh (Academic Press, New York, 1977)
2. A. Whiller, Sol. Energy **8**(1), 31 (1964)
3. V. Ranjan, N.K. Dhiman, G.N. Tiwari, Energy Convers. Manag. **23**(4), 211 (1983)
4. M.S. Sodha, N.K. Bansal, D. Singh, Appl. Energy **12**(4), 251 (1982)
5. B.F. Parker, Sol. Energy **26**(1), 27 (1981)
6. S. Satcunanathan, S. Deonarine, Sol. Energy **15**(1), 41 (1973)
7. Y. Caouris, R. Rigopoulos, J. Tripanagnostopoulos, P. Yianoulis, Sol. Energy **21**, 157 (1978)
8. N.E. Wijeysundera, L.L. Ah, L.E. Tjioe, Sol. Energy **28**, 363 (1982)

 9. D. Kamthania, Ph.D. thesis, IIT Delhi (2013)
10. M.A.S. Malik, F.H. Buelow, *Heat transfer characteristic of a solar dryer*. UNESCO Congress, The sun in the service of mankind, Paris 1973, Paper V, 55
11. K.G.T. Hollands, Sol. Energy **7**, 108 (1963)
12. R. Chandra, V.K. Goel, B.C. Raychaudhuri, Energy Convers. Manag. **23**, 177 (1983)
13. H. Buchberg, O.A. Lalude, D.K. Edwards, Sol. Energy **13**, 193 (1971)
14. F. Kreith, G.O.G. Log, A. Rabl, R. Winston, Prog. Energy Combust. Sci. **6**, 1 (1980)

Additional References

15. G.N. Tiwari, *Solar Energy: Fundamental, Design, Modelling and Applications* (Narosa Publishing House, New Delhi, CRC Press, New York, 2004)
16. S.C. Kaushik, G.N. Tiwari, J.K. Nayak, *Thermal Control in Solar Passive Building* (Geo Environ Academic Press, IBT Publisher, India, 1987)
17. G.N. Tiwari, R.K. Mishra, *Advance Renewable Energy Sources*. RSC publishing, UK, 2012

Chapter 10
Solar House

Abstract The thermal comfort inside solar houses can be met by using various concepts of cooling and heating technology by proper design of a building, which is known as a "passive house." In this case, a significant amount of high-grade energy of fossil fuel can be saved from an ecological and climatic point of view. Solar-passive heating of a building is more economical then solar-passive cooling.

10.1 Introduction

Each house on planet Earth is a **solar house**. In the modern days of building architecture, a solar house is an important concept that incorporates the motion of the Sun, the location of the building (latitude), climatic conditions, and locally available materials required for building construction. The concept of the solar house also includes the strong correlation between immensely available renewable sources of energy and building design. It ensures the use of naturally occurring sources as much as possible for the design and construction of the building as well as the day lighting and thermal comfort of the building. The solar house is not an entirely new concept. Socrates (400 B.C.) made a statement: "**Now in houses with south aspect, the Sun's rays penetrate into porticos in winter, but in summer the path of the Sun is right over our heads and above the roof. If then, this is the best arrangement one should build the south side loftier to keep out the cold winds, reflects this**." Ancient Iranian architecture used the following concepts.

(a) **Clustering of thick wall**: Clustering means decreasing the ratio of surface area to volume to reduce the thermal load of the building and the thick walls, which means there is large thermal storage capacity to reduce temperature fluctuations

(b) **Plantations**: Plantation provide shading on the building to reduce the solar flux incident on the building. During extreme heat, one can live in the basement.

(c) **Wind towers**: A wind tower makes the building comfortable in the summer due to cooling by the Earth and water evaporation.

The concept of clustering and mass walls was also used in medieval India. American Indians used passive solar techniques as long ago as 1100 A.D. However, the first scientific application of solar energy for the heating of a house with a blackened and glazed south wall was started in 1881 [1]. This concept, which is now referred to as a "**passive concept**," was granted a patent. This concept was not implemented for a long time until 1972. Trombe [2, 3] re-patented the concept and successfully applied it. Later on this concept of a blackened and glazed thick south wall was referred as a "**Trombe wall**."

However, in recent past years, people have chosen to abandon these long-standing considerations. They are increasingly relying on mechanical control of the indoor environment rather than exploiting climatic and other natural processes to satisfy their necessities. Such a system is referred as an "**active system**." As a result, even a minor power or equipment failure can make these buildings uninhabitable (i.e., uncomfortable). Furthermore, with the advent of the energy crisis in 1973, the effective use of renewable energy resources has become the basis for the design and planning of buildings. Now more emphasis is given to passive concepts for solar heating and cooling systems due to the energy availability in the immediate environment. It is simple in concept and requires little or no maintenance. Solar passive heating and cooling systems do not require any external source of energy. These systems also do not generate thermal pollution and produce no waste. Because these systems use energy resources available on site, transportation and distribution networks of conventional energy (i.e., nonrenewable energy) are eliminated.

There is strong need to add various passive solar concepts in the design of a building. An active solar heating/cooling system based on conventional energy is independent of the building architecture. It is difficult to include any passive concepts in a building designed based on active concepts. Thus, information regarding various passive concepts/systems must lead to a necessary degree of accuracy at each stage of building design. A judicious application of passive solar concepts provides thermal comfort in an economical way. Such thermal comfort is based on the following parameters:

(i) **Oxygen**
(ii) **Water**
(iii) **Air temperature**
(iv) **Relative humidity**

The thermal comfort chart, as shown in Fig. 10.1a, lists various factors influencing living thermal comfort.
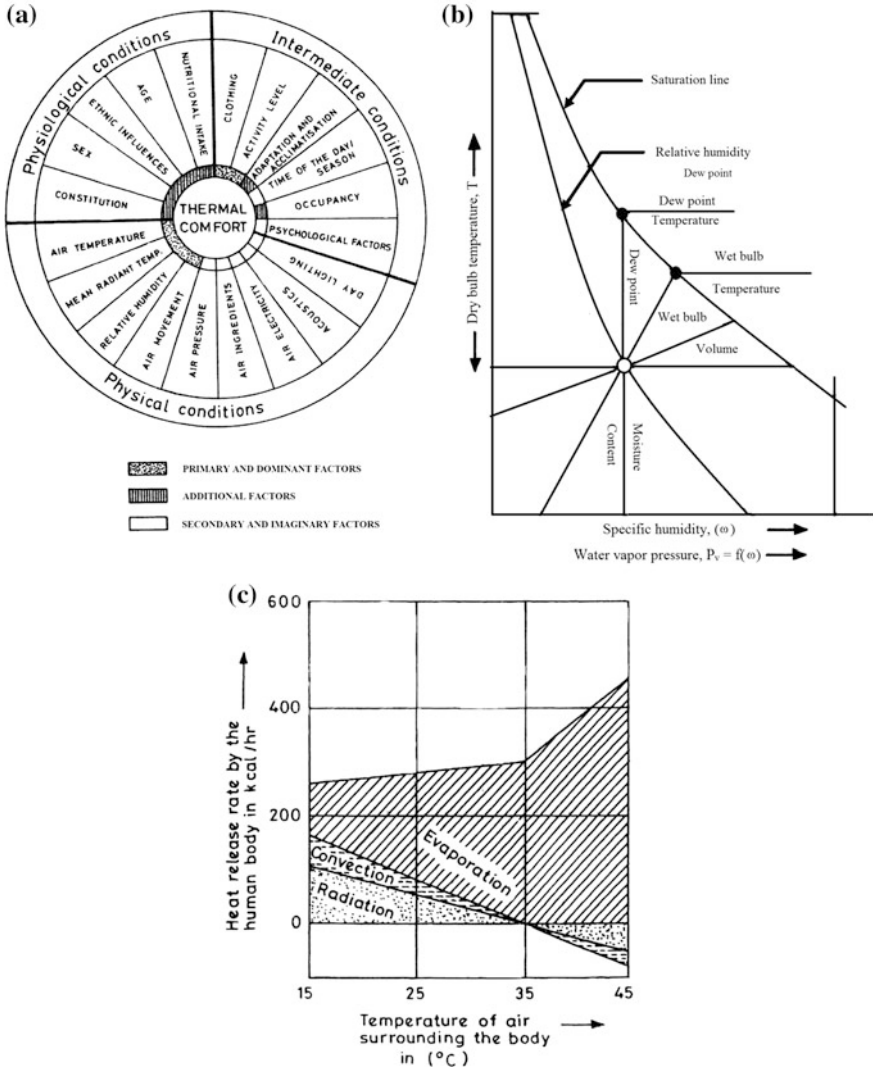
Fig. 10.1 a Thermal-comfort chart. **b** Psychometric chart. **c** Effect of surrounding temperature on the rate of heat released by the body

The thermal comfort factors have been divided into three categories:

(a) **Physical condition**: The primary and dominant factors are air temperature, mean radiant temperature, relative humidity, air movement, etc.
(b) **Physiological condition**: In this case, the additional factors are age, sex, and nutrition, etc.
(c) **Intermediate condition**: Here clothing and activity level are the dominant factors.

There can also be some additional factors such as secondary and imaginary factors. Similar to the physiological conditions, all of the factors are additional factors; in intermediate conditions, occupancy, adaptation, and acclimatization are additional factors.

10.2   Physical Parameters

10.2.1   Air Temperature

There are basically two temperatures:

(a) **Wet-bulb temperature (WBT)**: This is a temperature at which the vapour pressure of air is equal to the saturation pressure.
(b) **Dry-bulb temperature (DBT)**: This is the temperature of the air at atmospheric pressure, and it is measured by an ordinary thermometer. Dry-bulb temperature is always higher than wet-bulb temperature. It is dry-bulb temperature that is generally used to gauge thermal comfort.

The recommended dry-bulb temperature for thermal comfort for summer and winter are (25 ± 1) and $(20 \pm 1)\,°C$, respectively.

10.2.2   Relative Humidity

This is related to moist air. Moist air is a mix of dry air and water vapour. It can be defined as follows:

$$\textbf{Moist air} = \textbf{dry air}\,(\textbf{fixed part}) + \textbf{water vapour}\,(\textbf{variable part})$$

If the absorption of water reaches its maximum value in a given volume of dry air, then it is referred to as "saturated air."

Humidity or specific humidity (ω): This is defined as the ratio of water vapour mass (m_v) to dry air mass (m_a) in a given volume of moist air (mixture of dry air and water vapour). It is given by

$$\omega = \frac{m_v}{m_a} \tag{10.1}$$

The above equation shows that the numerical value of the humidity ratio or the specific humidity (ω) is always >1. The ratio of actual specific humidity to the specific humidity of saturated air at a given temperature is referred to as the "**degree of saturation**."

The relative humidity (γ) is the ratio of mass of the water vapour (m_v) in a given volume of moist air at a given temperature to the mass of water vapour (m_s) in the same volume of saturated air at the same temperature. It is expressed as

$$\gamma = \frac{m_v}{m_s} \qquad (10.2)$$

For thermal comfort, the recommended value of the relative humidity (γ) for both summer and winter condition is $(50 \pm 5)\,\%$. Its numerical value is always $<100\,\%$.

Figure 10.1b shows the variation of humidity ratio (specific humidity) with dry-bulb temperature for different relative humidities at atmospheric pressure. It is also known as a "psychometric chart."

10.2.3   Air Movement

The temperature of the body is constant between 36.9 and 37.2 °C. A body temperature $>40\,°C$ may be fatal. The thermal-comfort air temperature for a human being is approximately 20–25 °C for winter and summer, respectively. If air flows over a human body with a certain movement, there will be respiration (heat transfer) from the body to the environment. As the air movement over the body increases, the level of comfort increases. This is true only when the air temperature of the surroundings is lower than the body temperature. An increase of air movement over the body helps in the increase of heat transfer (respiration). The recommended value of air movement is approximately 0.2–0.4 m/s in winter and summer, respectively. This condition is obtained inside the room by operating a ceiling/table fan during the summer.

10.2.4   Mean Radiant Temperature

The body of loses heat by radiation (R), by convection (C), and by evaporation (E) (respiration) to the surroundings. The total heat loss (Q) from the body is given by

$$Q = (R + C) + E \qquad (10.3a)$$

where R and C are sensible heat loss (Q_S); and E is latent heat loss (Q_L).

Sensible heat loss (Q_S) mainly depends on the temperature difference (ΔT) between the surface of the body and the surrounding air. Latent heat loss (Q_L) depends on the difference in water-vapour pressure.

The heat transfer between humans and the environment can be expressed as follows:

$$M - W = Q + S \tag{10.3b}$$

where M is the metabolic rate; W is the work performed by a human; and S is the rate of heat storage.

In summer, body temperature increases due to the storage of energy (with S being positive). In such a situation, the blood flow rate increases through the extremities, and this is known as "vasodilation." In winter, the temperature of body tends to decrease (with S being negative), and hence the blood flow decreases, which causes shivering.

The rate of heat released by the human body given the surrounding temperature is shown in Fig. 10.1c.

Here the surrounding air temperature refers to the mean radiant temperature (MRT). This is the area-weighted average temperature of surfaces and can be defined as follows:

$$\text{MRT} = \frac{\sum_i T_i A_i}{\sum_i A_i} \tag{10.4}$$

where, T_i and A_i are the temperature and the respective area of the different surfaces of the living space, respectively.

10.2.5 Air Pressure

It is well known that a person feels more comfortable at atmospheric pressure. At higher altitudes, pressure is reduced and the person feels discomfort. This is due high pressure within the body.

10.2.6 Air Components

Each person requires $0.65 \, \text{m}^3/\text{h}$ of oxygen (O_2) under normal conditions. He or she produces $0.2 \, \text{m}^3/\text{h}$ of carbon-dioxide (CO_2). The human body requires at least this rate of oxygen for survival. It is also required to sustain the action of O_2 inside as well outside of the building. In open conditions this requirement is fulfilled by plants, which release oxygen to maintain the level of oxygen in the environment. Carbon dioxide, which is released by the human being, is consumed by plants to balance the ecosystem. However, the optimum levels of oxygen and carbon dioxide should also be maintained inside the building by either passive or active modes. To maintain this level, there should be provision of a roof vent (roshandan), ventilator,

exhaust fan, etc. in the building. In such a way, there is direct contact between the environment and the living space of the building.

10.2.7 Air Electricity

A person feels shock when a thin layer of air passes over the skin. This can be felt while rubbing the skin in the presence of thin layer of air. This is due to friction between the thin air layer and the skin.

10.2.8 Acoustics

A person feels more comfortable in effective working conditions up to maximum sound level of $120\,\mathrm{db}\left(0.01\,\mathrm{W/m^2}\right)$ in a living space. An average person can hear frequencies from 20 to 16,000 Hz. Unwanted sound creates a sense of irritation in a living space. It is termed "noise pollution."

10.2.9 Day Lighting

In the absence of natural lighting, artificial lighting is created by using electrical appliances such as an electric bulb, lamp, tube light, etc., in a building. By using an electric bulb, the thermal heat gain in a building is significant. In an electric lamp, only a fraction of the electrical energy is converted into light energy. The heating effect of day lighting of an electric lamp is 1 W per lumen.

10.3 Physiological Parameters

10.3.1 Nutritional Intake

Human comfort is influenced by physiological factors. It is determined by the rate of heat generated inside body and the rate of heat dissipated to the environment. The rate of heat produced by the human body is known as the "metabolic rate." A healthy person during sleep produces heat at the rate of 60 W $\left(\approx 35\,\mathrm{W/m^2}\right)$; during hard work it can increase to 600 W $\left(\approx 350\,\mathrm{W/m^2}\right)$.

It is well known that a person requires optimum nutritional intake. This depends on the composition of the body, which varies from person to person and from season to season. For example, nutritional intake (healthy food) for a person becomes greater during winter and it less during summer. Due to this, a person feels

more thermal comfort during the winter period after taking in higher-calorie food compared with summer.

10.3.2   Age

A person feels more cold in winter and warm in summer at an older age. This is due to following facts:

  (i)   the decrease of metabolic rate (the rate of heat generated within the body);
 (ii)   the change in food habits;
(iii)   the decrease in nutritional intake; and
(iv)   the change in activity level, etc.

10.3.3   Ethnic Influences

This deals with lifestyle of people living in a particular climatic condition. This includes food habits and clothing, etc.

10.3.4   Sex

Females produce more heat due energy generated within body compared with males. Hence, they feel more comfortable in cold climates.

10.3.5   Constitution

This refers to the physical constitution of an individual. It is well known that a weak person feels colder during winter than a healthy one and vice versa during the summer.

10.4   Intermediate Parameters

10.4.1   Clothing

Clothing intervenes with air movement across the skin. As a result, clothing decreases the potential of heat transfer [conduction, convection, and evaporation

(respiration)] from the body to the room air. The colour of the clothing is also important.

For example:

(i) In the desert, thin, loose-fitting, and light-colored clothing is more suitable. This gives lower absorption of solar radiation and heat transfer from the outside to the skin. It provides air movement across skin the due to the loose fit.

(ii) In hot and humid climates, loose, light-colored, and porous clothing is more suitable. Due to the porosity of the cloth, fast heat transfer takes place from skin to the air.

(iii) In cold climates, dark-colored, thick, and tight-fitting clothing is more suitable for higher absorption of solar radiation and minimum heat transfer from skin to the air.

10.4.2 Activity Level

As mentioned previously, the rate of heat transfer (dissipation) by a person depends on his or her activity. It varies from 60 W $(\approx 35 \text{ W/m}^2)$ to 600 W $(\approx 350 \text{ W/m}^2)$. Hence, the human body can be considered as a heat engine converting thermal energy (metabolic rate) into mechanical energy with an efficiency of 20%. A person's body dissipates energy at a rate of 335 KJ/h. To provide thermal comfort, the heat generated by a person can be removed by providing a ventilator in the room.

10.4.3 Adaption and Acclimatisation

This means that a person should first become accustomed to an artificial climate before he or she starts living in harsh climatic conditions.

10.4.4 Time of the Day/Season

The recommended thermal-comfort air temperature is 20 °C. It is known that ambient air temperature changes with the following:

(i) time of the day (due to changes in the level of solar intensity (insolation) with time); and

(ii) month of the year (from season to season).

For example, in a northern climatic condition there is variation of ambient air temperature from 5 to 15 °C in winter and from 30 to 45 °C in summer.

Therefore, the requirement of heating/cooling load depends on the time of day/season.

10.4.5   Occupancy

We know that a person can produce heat due to energy generated within the body (Sect. 10.4.2). For a given volume of an enclosed space, the total amount of heat produced increase depending on the number of people. This leads to an increase in the room air temperature, which affects the living as well working conditions.

10.4.6   Psychological Factors

Most of the time, by maintaining the levels of peak winter and summer conditions in a group, people feel comfortable by sharing their thoughts with others. This gives pleasure to the individual talking in a group due to psychological factors.

10.5   World Climatic Zone

The whole world can be divided into six climatic zones for the simplification of analysis in the solar energy system. The criterion for classification of these climatic zones is given in Table 10.1.

Table 10.1   Criteria for the classification of climates

Climate	Mean monthly temperature	Relative humidity (%)	Precipitation (mm) (rain/snow fall)	Number of clear days	Examples
Hot and dry (HD)	>30	<55	<5	>20	Jodhpur, Saudi Arabia
Warm and humid (WH)	>30	>55	>5	<20	Bombay, Pacific countries
Moderate (MO)	25–30	<75	<5	<20	Bangalore
Cold and cloudy (CC)	<25	>55	>5	<20	Srinagar, Europe
Cold and sunny (CS)	<25	<55	<5	>20	Leh, Singapore
Composite climate (CO)	This applies when ≥6 months do not fall within any of the above categories				New Delhi

   The heating/cooling requirement of a building can be determined if the solair temperature, defined below, is known.

10.6   Solair Temperature

There are three treatments of horizontal surfaces for various applications of heating and cooling of a building. Hence, there is need to define the solair temperature for all three cases: bare horizontal surface, wetted horizontal surface, and blackened and glazed horizontal surface.

10.6.1   Horizontal Bare Surface

Let us consider a horizontal surface that is exposed to solar radiation and an ambient air temperature with a wind velocity of V in m/s as shown in Fig. 10.2a.
   The energy balance for an exposed horizontal surface can be written as:

For a bare surface
Referring to Fig. 10.2a, the energy balance at $x = 0$ can be written as:

$$\alpha I(t) = -K\frac{\partial T}{\partial x}\bigg|_{x=0} + h_{\mathrm{ra}}\big(T|_{x=0}-T_{\mathrm{a}}\big) + \varepsilon\Delta R + h_{\mathrm{ca}}\big(T|_{x=0}-T_{\mathrm{a}}\big) \qquad (10.5)$$

where α and ε are the absorptivity and emissivity of the surface, respectively; K is the thermal conductivity; and $\Delta R = 60\,\mathrm{W/m^2}$ Eq. (3.34d). The value of ΔR is zero for a vertical wall.
   Equation (10.5) can be rewritten as follows:

$$-K\frac{\partial T}{\partial x}\bigg|_{x=0} = \alpha I(t) - h_{\mathrm{O}}\big(T|_{x=0}-T_{\mathrm{a}}\big) - \varepsilon\Delta R$$

where $h_{\mathrm{o}} = h_{\mathrm{ra}} + h_{\mathrm{ca}}$; $h_{\mathrm{ca}}(= 2.8 + 3V)$ and h_{ra} are given by Eqs. (3.29b) and (3.34f), respectively. Furthermore, h_{O} can also be considered as a combined convective and radiative heat-transfer coefficient and is given as $5.7 + 3.8\,V$, Eq. (3.29a).

   Furthermore, the above equation can also be rewritten as

$$\dot{q} = -K\frac{\partial T}{\partial x}\bigg|_{x=0} = h_{\mathrm{O}}\left[\frac{\alpha}{h_{\mathrm{O}}}I(t) + T_{\mathrm{a}} - \frac{\varepsilon\Delta R}{h_{\mathrm{o}}} - T|_{x=0}\right] = h_{\mathrm{O}}\big[T_{\mathrm{sa}} - T|_{x=0}\big] \qquad (10.6)$$

(a)

(b)

(c)
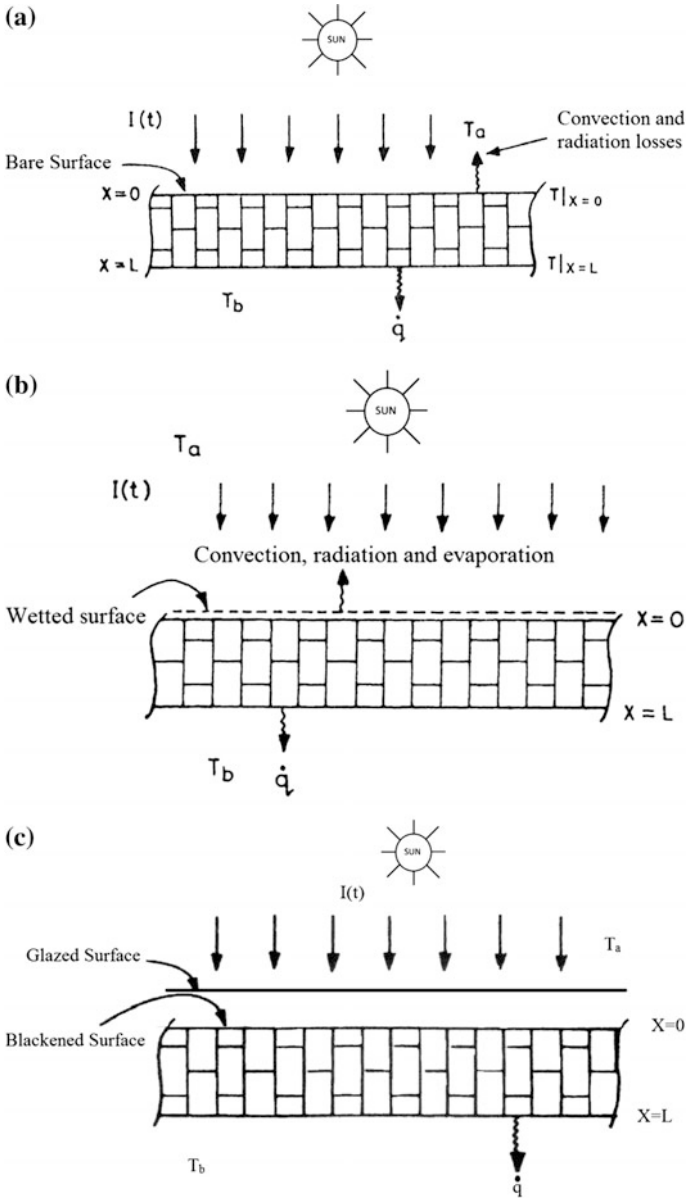
Fig. 10.2 **a** A bare surface exposed to solar radiation. **b** A horizontal wetted surface exposed to solar radiation. **c** Schematic view of a blackened and glazed surface

where

$$T_{sa} = \frac{\alpha}{h_O} I(t) + T_a - \frac{\varepsilon \Delta R}{h_o} \qquad (10.7a)$$

Equation (10.7a) is known as the "**solair temperature**" for a bare horizontal surface. It can be defined as follows:

"**The solair temperature is an effective ambient air temperature that includes the effect of solar and long-wavelength exchange radiation between the ambient air and the sky for a horizontal surface**."

Furthermore, Eq. (10.7a) can be discussed for the following cases:

Case (i): For $\frac{\alpha}{h_O} I(t) - \frac{\varepsilon \Delta R}{h_o} \geq 0$ or $\alpha I(t) - \varepsilon \Delta R \geq 0$, the solair temperature (T_{sa}) is greater than the ambient air temperature (T_a). In this case, heating is possible by solar energy from a horizontal roof surface.

Case (ii): For $\frac{\alpha}{h_O} I(t) - \frac{\varepsilon \Delta R}{h_o} \leq 0$ or $\alpha I(t) - \varepsilon \Delta R \leq 0$, the solair temperature (T_{sa}) is less than the ambient air temperature (T_a), i.e., $T_{sa} < T_a$. In this case, cooling is possible by solar energy from a horizontal roof surface.

Case (iii): For $\frac{\alpha}{h_o} I(t) - \frac{\varepsilon \Delta R}{h_o} = 0$ or $\alpha I(t) - \varepsilon \Delta R = 0$, the solair temperature (T_{sa}) is equal to the ambient air temperature (T_a). In this case, neither heating nor cooling is possible by solar energy from a horizontal surface.

For vertical surface, $\varepsilon \Delta R = 0$, the expression for solair temperature is given by

$$T_{sa} = \frac{\alpha}{h_O} I(t) + T_a \qquad (10.7b)$$

In this case, only heating of a room is possible through a vertical wall for $I(t) > 0$.

Under steady-state conditions, the rate of heat available at $x = 0$ will be same as the rate of heat available at $x = L$, and hence it will be transferred by conduction and can be written as

$$\dot{q} = \frac{K}{L}(T_{x=0} - T_{x=L}) \qquad (10.8)$$

This rate of heat is further transferred from $x = L$ to the living space by convection and radiation, and it can be expressed by

$$\dot{q} = h_i \left(T|_{x=L} - T_b \right) \qquad (10.9)$$

Equations (10.6), (10.8) and (10.9) can be rearranged as follows:

$$\frac{\dot{q}}{h_O} = T_{sa} - T|_{x=0} \qquad (10.10a)$$

$$\frac{\dot{q}}{\frac{K}{L}} = T_{x=0} - T_{x=L} \qquad (10.10\text{b})$$

$$\frac{\dot{q}}{h_i} = T|_{x=L} - T_{\text{b}} \qquad (10.10\text{c})$$

After adding the above three equations, we obtain an expression for $\dot{q}$ in W/m^2 given by

$$\dot{q} = U[T_{\text{sa}} - T_{\text{b}}] \qquad (10.11)$$

where $U = \left[\frac{1}{h_{\text{o}}} + \frac{L}{K} + \frac{1}{h_i}\right]^{-1}$

Equation (10.11) offers the rate of thermal energy that is being transferred during sunshine hours from an exposed horizontal surface to the living space kept at constant temperature T_{b}, which is known as an "**air-conditioned condition**" under steady-state conditions.

Equation (10.11) will be negative for case (ii) of Eq. (10.7a), i.e., $T_{\text{sa}} < T_{\text{a}}$. This means that only a horizontal bare surface can be used for cooling when it is exposed to direct sky conditions during either a low-intensity period or during night hours. In this case, reverse heat flow will take place.

The total energy gain for case (i), i.e., $T_{\text{sa}} > T_{\text{a}}$ through a horizontal roof per m^2 in terms of Joule during sunshine hours, t_{T}, can be obtained as

$$q_{\text{ud}} = \dot{q}_{\text{u}} \times t_{\text{T}} \times 3600 = U(T_{\text{sa}} - T_{\text{b}}) \times t_{\text{T}} \times 3600 \qquad (10.12)$$

If the horizontal bare surface is covered with insulation of thickness L_i during the night having a thermal conductivity of K_i, then the total energy per m^2 in terms of Joule during off-sunshine hours t'_{T} can be obtained as

$$q_{\text{un}} = \dot{q}_{\text{u}} \times t'_{\text{T}} \times 3600 = U(T_{\text{a}} - T_{\text{b}}) \times t'_{\text{T}} \times 3600 \qquad (10.13)$$

where $U = \left[\frac{1}{h_{\text{o}}} + \frac{L_i}{K_i} + \frac{L}{K} + \frac{1}{h_i}\right]^{-1}$ and $t = t_{\text{T}} + t'_{\text{T}} = 24\,h$

The net total daily energy per m^2 for an exposed horizontal surface available in terms of Joule during the day/night will be sum of the values obtained from Eqs. (10.12) and (10.13). This can be written as

$$q_{\text{T}} = q_{\text{ud}} + q_{\text{un}} \qquad (10.14)$$

10.6.2   Horizontal Wetted Surface

For this, a water film is maintained on a horizontal surface as shown in Fig. 10.2b.

In this case, there will be mass transfer (evaporation) from the exposed surface to the ambient air in addition to convection and radiation heat transfer; hence, Eq. (10.5) is modified as follows:

$$\alpha I(t) = -K\frac{\partial T}{\partial x}\bigg|_{x=0} + h_{ra}\big(T|_{x=0} - T_a\big) + \varepsilon\Delta R + h_{ca}\big(T|_{x=0} - T_a\big) + h_{ea}\big(T|_{x=0} - T_a\big)$$

or

$$\dot{q} = -K\frac{\partial T}{\partial x}\bigg|_{x=0} = h_1\big[T_{sa} - T|_{x=0}\big] \qquad (10.15)$$

where,

$$T_{sa} = \frac{\alpha}{h_1}I(t) + T_a - \frac{\varepsilon\Delta R}{h_1} \qquad (10.16)$$

where $h_1 = h_{ra} + h_{ea} + h_{ca}$ and $h_{ea}(= h_{ew})$ is given by Eq. (3.52). Furthermore, Eq. (10.16) is similar to Eq. (10.7a). However, the value of T_{sa} in the case of a wetted surface will be lower due to the higher value of h_1 compared with h_o of a bare surface.

Furthermore, Eq. (10.16) can be further discussed for the following limiting cases:

Case (i): For $\frac{\alpha}{h_1}I(t) - \frac{\varepsilon\Delta R}{h_1} \geq 0$ or $\alpha I(t) - \varepsilon\Delta R \geq 0$, the solair temperature (T_{sa}) is greater than the ambient air temperature (T_a). However, the values of T_{sa} in the case of a wetted surface will be lower compared with a bare surface; hence, in this case the heating level will be reduced.

Case (ii): For $\frac{\alpha}{h_1}I(t) - \frac{\varepsilon\Delta R}{h_1} \leq 0$ or $\alpha I(t) - \varepsilon\Delta R \leq 0$, the solair temperature (T_{sa}) is less than the ambient air temperature (T_a) i.e., $T_{sa} < T_a$. In this case, the cooling level will be increased with a wetted surface.

Case (iii): For $\frac{\alpha}{h_1}I(t) - \frac{\varepsilon\Delta R}{h_1} = 0$ or $\alpha I(t) - \varepsilon\Delta R = 0$, the solair temperature (T_{sa}) is equal to the ambient air temperature (T_a). In this case, the heating level will be reduced, whereas the cooling level is increased by solar energy from the horizontal wetted surface.

Also, in the case of a wetted surface, an expressions for the rate of heat conducted from $x = 0$ to $x = L$ by conduction and the rate of heat convected and radiated from $x = L$ to the living space (T_b) under steady-state conditions will be same as considered earlier, i.e., Equations (10.8) and (10.9).

According to Eqs. (10.10a–10.10c), an expression for the rate of heat transfer from an exposed horizontal wetted surface to the living space will be same as Eq. (10.11) except for the change in the numerical value of h_1 for the wetted surface.

$$\dot{q} = U(T_{sa} - T_b) \qquad (10.17)$$

where $U = \left[\frac{1}{h_1} + \frac{L}{K} + \frac{1}{h_i} \right]^{-1}$

Similarly, the expression for the net daily energy gain/loss during the day/night can also be obtained, Eq. (10.14).

Example 10.1 Calculate the total heat-transfer coefficient (h_1) for a wetted surface for the following parameters:

Temperature of the wetted exposed surface $T_s = 20\,°C$; ambient temperature $T_a = 12\,°C$; relative humidity $= 0.6$; wind velocity $= 3$ m/s; and emissivity $= 0.9$.

Solution

The total heat-transfer coefficient, h_1, is given by $h_1 = h_{ra} + h_{ca} + h_{ea}$.

h_{ra} can be determined as

$$h_r = \varepsilon\sigma \left[\frac{(T_s + 273)^4 - (T_a + 273)^4}{T_p - T_c} \right]$$

therefore,

$$h_{ra} = 0.9 \times 5.67 \times 10^{-8} \left[\frac{(20 + 273)^4 - (12 + 273)^4}{20 - 12} \right] = 4.867 \, \text{W/m}^2\,°C$$

In addition, h_{ca} can be obtained from Eq. (3.29b) as

$$h_{ca} = 2.8 + 3.0 \times 3 = 11.8 \, \text{W/m}^2\,°C$$

Now, $h_{ea} = h_{ew}$ can be obtained from Eq. (3.47) as

$$h_{ea} = 16.273 \times 10^{-3} \times 2.8 \left[\frac{2346.5 - 0.6 \times 1433.5}{20 - 12} \right] = 21.915 \, \text{W/m}^2\,°C$$

The total heat-transfer coefficient is given as

$$h_1 = 4.867 + 11.8 + 21.915 = 38.582 \, \text{W/m}^2\,°C$$

The rate of heat loss due to radiation, convection, and evaporation are as follows:

$$\dot{q}_{\mathrm{ra}} = 4.87(20 - 12) = 38.96\,\mathrm{W/m^2}$$
$$\dot{q}_{\mathrm{ca}} = 11.80(20.12) = 94.40\,\mathrm{W/m^2}$$
$$\dot{q}_{\mathrm{ea}} = 21.92(20 - 12) = 157.36\,\mathrm{W/m^2}$$

10.6.3   Blackened/Glazed Surface

For a blacked/glazed surface, the top of the bare surface is painted black, and the glass cover is placed on it at a proper distance as shown in Fig. 10.2c. In this case, the solar radiation after transmission $(\tau I(t))$ is absorbed $(\alpha\tau I(t))$ by the blackened surface. After absorption, there will be a rate of heat transfer from the blackened surface to the ambient air through the glass cover, and the rest is transferred by conduction through the bottom.

For a blackened and glazed surface, Eq. (10.5) becomes

$$\alpha\tau I(t) = -K\frac{\partial T}{\partial x}\bigg|_{x=0} + U_t\big(T|_{x=0} - T_a\big) \tag{10.18}$$

where U_t is the overall heat-loss coefficient from the blackened surface to the ambient air through the glass cover. It is given by

$$U_t = \left[\frac{1}{h_1} + \frac{1}{h_o}\right]^{-1} \tag{10.18a}$$

In Eq. (10.18), $\varepsilon\Delta R$ will be zero because the blackened and glazed surface is not directly exposed to the sky.

Equation (10.18) can be rearranged as follows:

$$\dot{q} = -K\frac{\partial T}{\partial x}\bigg|_{x=0} = U_t\big(T_{\mathrm{sa}} - T|_{x=0}\big) \tag{10.18b}$$

where the solair temperature T_{sa} is given by

$$T_{\mathrm{sa}} = \frac{\alpha\tau}{U_t}I(t) + T_a \tag{10.18c}$$

In Eq. (10.18c), the numerical value of U_t will be much lower compared with h_o (bare surface) and h_1 (wetted surface), and hence the value of the solar air temperature (T_{sa}) in the case of the blackened and glazed surface is significantly higher than in the other two cases, namely, the bare and wetted surfaces.

In this case, too, an expression for the rate of heat conducted from $x = 0$ to $x = L$ and the rate of heat convected from $x = L$ to the living space (T_b) will be same as that under steady-state conditions.

As done in Sect. 10.6.1, an expression for the rate of heat transfer from an exposed blackened/glazed horizontal surface to the living space (T_b) can be derived under steady-state conditions. The expression for the same is given by

$$\dot{q} = U(T_{sa} - T_b) \tag{10.19}$$

where

$$U = \left[\frac{1}{U_t} + \frac{L}{K} + \frac{1}{h_i} \right]^{-1}$$

The above-derived equation can be used to determine the rate of thermal energy gain for thermal heating of a building during the daytime.

10.7   Thermal Gain

To understand and analyse passive heating systems, there are three basic concepts to know: direct gain, indirect gain, and isolated gain. These are explained as follows.

10.7.1   Direct Gain

For direct gain, sunlight is admitted/transmitted through a glass window or a wall facing south (north for the southern hemisphere) to heat up the inside walls, floors, and objects (and, consequently, the air) in the room as shown in Fig. 10.3.

In this approach, the space becomes (i) a live-in solar collector, (ii) a heat-storage system; and (iii) a distribution system. Direct-gain systems are continuously working because they collect and use every bit of direct or diffuse radiation that passes through the glazing. To avoid overheating during the day and cooling at night, the floor and walls must be constructed of materials capable of storing heat for use during the night. The most commonly used materials for heat storage are masonry and water. Double-glazing is used to reduce the heat losses from the room to the outside air. The windows are covered by insulation at night for the same purpose.

The rate of net useful thermal energy gain into a room is given by

$$\dot{q} = \tau I(t) - U_t(T_b - T_a) \tag{10.20}$$
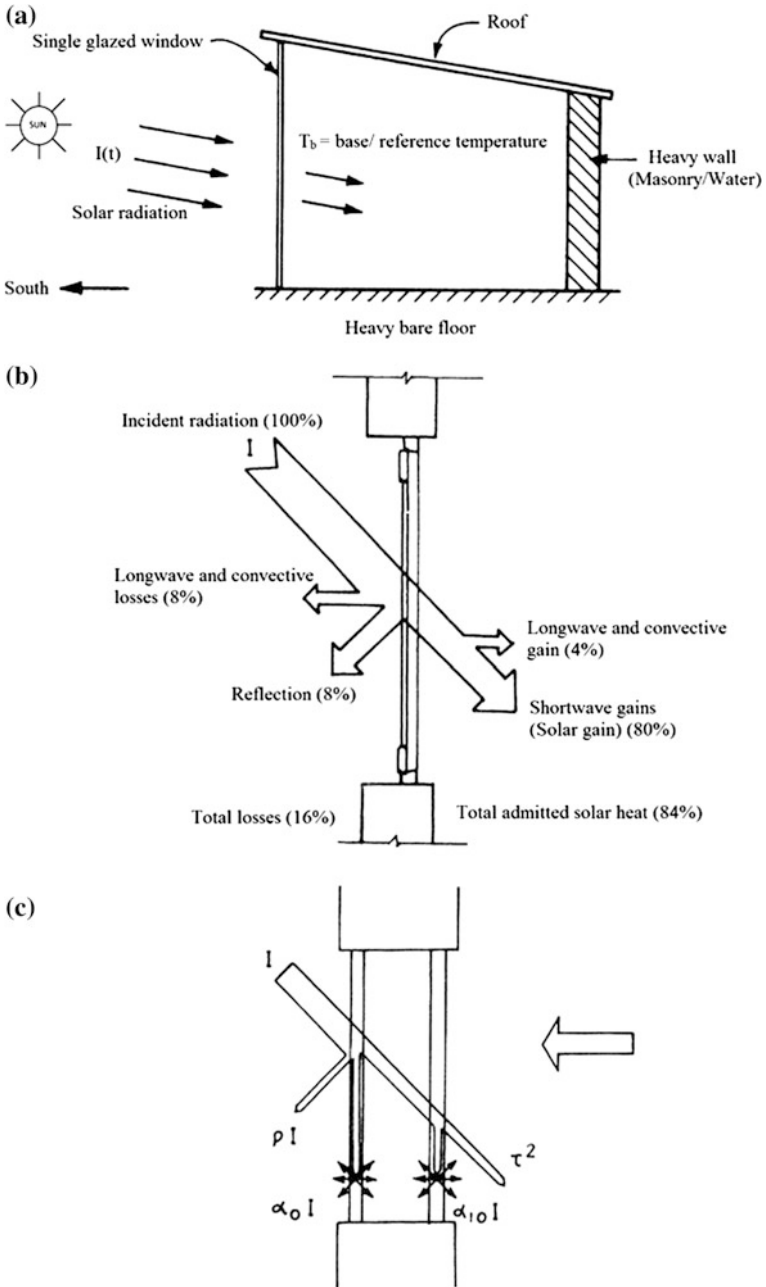
Fig. 10.3 Schematic representation of various direct gains

where τ is the transmissivity of a glass window/wall; U_t is the overall heat-transfer coefficient from the living room to the ambient air through the glass cover; T_b is the base or reference temperature in the building; and T_a is the ambient air temperature.

Equation (10.20) can be written as

$$\dot{q} = U_t \left[\frac{\tau}{U_t} I(t) + T_a - T_b \right] = U_t [T_{sa} - T_b] \tag{10.21}$$

where $T_{sa} = \frac{\tau}{U_t} I(t) + T_a$, which is the solair temperature of the glazed window and walls. The expression for U_t is given by Eq. (10.18a).

Equation (10.20) can also be used to determine the total net energy gain during sunshine hours (t_T is the total sunshine hours). This can be obtained as follows:

$$q_{ud} = \int_0^{t_T} \dot{q} dt = \left[\tau \int_0^{t_T} I(t) dt - U_t \left(T_b t_T - \int_0^{t_T} T_a dt \right) \right] \tag{10.22}$$

Now if average solar intensity $(\overline{I}(t))$ and ambient air temperature $(\overline{T}_a)$ are considered for $0 - t_T$ time interval, then

$$\overline{I}(t) = \frac{1}{t_T} \int_0^{t_T} I(t) dt \quad \text{and} \quad \overline{T}_a = \frac{1}{t_T} \int_0^{t_T} T_a dt$$

The accuracy of this assumption depends on the size of the time interval, say, approximately, a minimum of 1 h.

Furthermore, Eq. (10.22) becomes

$$q_{ud} = \left[\tau \overline{I}(t) - U_t (T_b - \overline{T}_a) \right] t_T \times 3600 \tag{10.23}$$

During off-sunshine hours/low-sunshine hours, the glazed window/walls are covered with movable insulation, which is generally a thick curtain to reduce losses from the enclosed space to the outside ambient air. In this case, the net daily loss can be calculated as follows:

$$q_{un} = U_t (T_b - \overline{T}_a)(24 - t_T) \times 3600 \tag{10.24}$$

The daily net heat/thermal energy gain is given by

$$q_T = q_{ud} + q_{un} \tag{10.25}$$

Example 10.2 Determine the total thermal energy gain q_{ud} in terms of kWh for a direct-gain system at a 20 °C base temperature and exposed to solar radiation of 800 W/m² for 4 h. Given parameters are ambient temperature = 12 °C, transmissivity = 0.9, and overall heat-loss coefficient = 6 W/m² °C.

Solution

From Eq. (10.23), q_{ud} is obtained as follows:

$$q_{ud} = [0.9 \times 800 - 6 \times (20 - 12)] \times 4 \times 3600$$
$$= (720 - 54) \times 4 \times 3600 = 2688 \times 3600 = 9.67 \times 10^6 \text{J}$$
$$= 2.69 \text{ kWh} \quad (\because 1 \text{ J} = 2.778 \times 10^{-7} \text{kWh})$$

10.7.2   *Indirect Gain*

In case of indirect gain, solar radiation first strikes a thermal mass located between the Sun and the living space. The solar radiation is first absorbed by the surface of the thermal mass. It is converted into thermal energy and then transferred into the living space. The advantage of indirect gain over direct gain is that a more uniform room-air temperature is achieved. The two basic indirect gain systems are (i) thermal storage walls generally known as "**Trombe walls**" and (ii) roof ponds.

The details of thermal storage walls/roof and roof ponds are discussed below under steady-state conditions.

(a) **Thermal storage walls/roof**

Both walls and roof can be used, but a south-facing wall is preferred to the roof because of the abundance of solar radiation on the south wall in winter and the difficulty of supporting a heavy roof. A thermal storage wall absorbs the Sun's radiation on its outer surface and then transfers this heat into the building through conduction. A thermal storage wall may be either masonry or water.

(i) **Simple glazed wall (Trombe wall without vents)**: To increase absorption, the outer surface of a Trombe wall is painted black and glazed as shown in Fig. 10.4.

Fig. 10.4 View of a Trombe wall
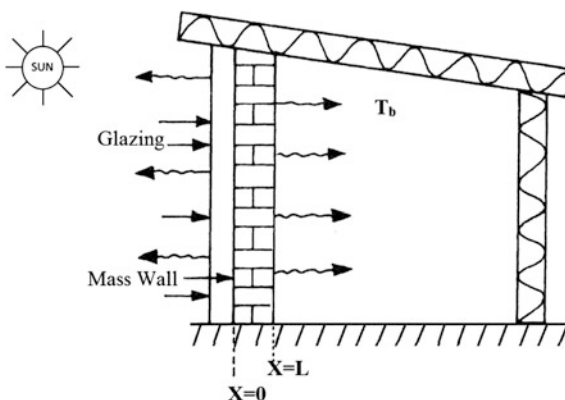
For a simple glazed wall of thickness L and thermal conductivity K, the heat flux available at the exposed surface for conduction into the inside room maintained at a temperature, T_b, can be written as

$$\dot{q} = \alpha\tau I(t) - U_t\left(T|_{x=0} - T_a\right) \tag{10.26}$$

where U_t is an overall heat-loss coefficient from the outer surface of the wall to the ambient air through the glazing. Under steady-state conditions, the amount of heat flux conducted and subsequently convected and radiated into the space remains the same as Eq. (10.19).

Example 10.3 Calculate the rate of heat flow through a south-facing concrete wall for the following parameters: (i) mean incident solar radiation $= 250\,\text{W/m}^2$, (ii) ambient air temperature $= 13\,°\text{C}$, (iii) wall thickness $= 30\,\text{cm}$, (iv) wall of thermal conductivity $= 0.72\,\text{W/m}°\text{C}$, (iv) mean room temperature $= 20\,°\text{C}$, $h_c = 8.7\,\text{W/m}^2\,°\text{C}$, $h_r = 3.8\,\text{W/m}^2\,°\text{C}$, $\alpha = 0.6$, $V = 1\,\text{m/s}$, and $h_i = 8\,\text{W/m}^2\,°\text{C}$.

Solution
Here, consider that $h_o = h_c + h_r = (8.7 + 3.8) = 12.5\,\text{W/m}^2\,°\text{C}$. The U value should be calculated as

$$\frac{1}{U} = \frac{1}{8.7 + 3.8} + \frac{0.30}{0.72} + \frac{1}{8} = 0.622$$

or,

$$U = 1.609\,\text{W/m}^2\,°\text{C}$$

From Eq. (10.7a), we have

$$T_{sa} = \frac{0.6 \times 250}{12.5} + 13 = 25\,°\text{C}$$

Here we have $R = 0$ for the south wall.

The rate of heat flow can be obtained from Eq. (10.11) as

$$\dot{q} = 1.609 \times (25 - 20) = 8.045\,\text{W/m}^2$$

The positive sign indicates that heat is gained from the environment to the living space. Heat must be removed from the living space at the above rate to maintain the space at $20\,°\text{C}$.

The same example, if performed with an ambient air temperature of $5\,^{\circ}\text{C}$, gives,

$$T_{\text{sa}} = \frac{0.6 \times 250}{12.5} + 5 = 17\,^{\circ}\text{C}$$

and

$$\dot{q} = 1.609 \times (17 - 20) = -4.827\,\text{W/m}^2$$

This indicates that heat must be added to the living space at this rate to maintain the space at $20\,^{\circ}\text{C}$.

Example 10.4 Determine the net heat flux into the room if the south wall (Example 10.3) is covered with a 4 cm—thick movable night insulation (NI) with $K = 0.025\,\text{W/m}\,^{\circ}\text{C}$.

Solution
With night insulation of $L = 0.04$ m, the overall heat-loss coefficient from the room to the ambient air can be calculated as follows:

$$U = \left[\frac{1}{12.5} + \frac{0.04}{0.025} + \frac{0.30}{0.72} + \frac{1}{8}\right]^{-1} = 0.45\,\text{W/m}^2\,^{\circ}\text{C}$$

The rate of heat loss from the room air to the ambient air during the night can be calculated as follows:

$$\dot{q} = 0.45(13 - 20) = 0.45 \times (-7) = -3.15\,\text{W/m}^2\,^{\circ}\text{C}$$

Comparing from the result of Example 10.3, we see that there are losses during the night; hence, the net rate of heat flux = $8.45 - 3.15 = 5.3\,\text{W/m}^2$.

This is true only when the duration of the day and the night is the same; otherwise, the gain and the loss should be multiplied by the duration of the day and the night, respectively, before adding.

Example 10.5 Consider a south-facing brick wall with $\alpha = 0.8$ and $\tau = 0.71$. Calculate the mean heat flux into a room through for a Trombe wall of 305 mm–thick concrete for the following parameters:

- room air temperature maintained = $18\,^{\circ}\text{C}$;
- external wall heat-transfer coefficient from glazed surface = $5\,\text{W/m}^2\,^{\circ}\text{C}$;
- $h_i = 8\,\text{W/m}^2\,^{\circ}\text{C}$;
- average ambient temperature = $14\,^{\circ}\text{C}$;
- mean solar radiation on south face = $310\,\text{W/m}^2$; and
- $K = 0.62\,\text{W/m}\,^{\circ}\text{C}$.

Solution

Using Eq. (10.19), we obtain the following:

$$\dot{q} = \left[\frac{1}{5.0} + \frac{0.305}{0.62} + \frac{1}{8}\right]^{-1}\left[\frac{0.8 \times 0.71 \times 310}{5} + 14 - 18\right]$$

$$= 1.224(35.22 + 14 - 18)$$

$$= 38.21 \text{ W/m}^2$$

Example 10.6 (a) For Example 10.5 and for an average ambient temperature of 8 °C, calculate the night loss for the above system if the inside temperature (T_b) is maintained at 18 °C, and also calculate the net heat flux into the room for the same duration of the day and the night.

Solution

For the Trombe wall described in Example 10.5 we have

The rate of night losses $= 1.22(8 - 18) = -1.22 \times 10 = -12.2 \text{ W/m}^2$

Because the duration of the day and night are same, i.e., 12 h each, then

The net heat flux $=$ the rate of heat flux gain $-$ the rate of night losses

$$= 38.21 - 12.2 = 26.01 \text{ W/m}^2$$

The net energy gain in terms of Joule $= 26.01 \times 12 \times 3600 \text{ J} = 1.12 \times 10^6$

$$= 0.31 \text{ kWh}.$$

Example 10.6 (b) Calculate the net energy in terms of *kWh* for Example 10.6 (a) when the Trombe wall is exposed to solar radiation for 8 and 4 h, respectively.

Solution

(a) For an 8-hour exposure:

$$\text{The net energy gain} = (38.21 \times 8 - 12.2 \times 16) \times 3600 \text{ J}$$

$$= 3.98 \times 10^5 \text{ J} = 0.11 \text{ kWh}$$

(b) For a 4-hour exposure:

$$\text{The net energy gain} = (38.21 \times 4 - 12.2 \times 20) \times 3600 \text{ J}$$

$$= -3.28 \times 10^5 \text{ J} = -0.091 \text{ kWh}$$

This means that some external thermal energy is required for a 4-hour exposure to maintain the living-space temperature.

Fig. 10.5 View of a water wall
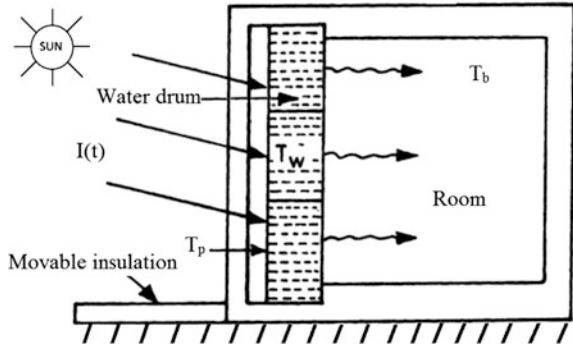
(ii) **Water Wall**: Here water drums are stacked vertically in between the solar thermal collector glazing wall and the living space as shown in Fig. 10.5. The water-wall has advantage of large heat capacity unlike the Trombe wall. It is used as a storage medium to release heat into the living space during the night.

If T_p is the temperature of the metallic surface of the drums, the energy- balance equations for the glazed water wall under steady-state conditions can be written as follows:

At a metallic surface:

$$\dot{q} = (\alpha\tau)I(t) - U_t\left(T_p - T_a\right) \tag{10.27}$$

Between a metallic surface and water:

$$\dot{q} = h_1'\left(T_p - T_w\right) \tag{10.28}$$

Between water and the back of a metallic surface:

$$\dot{q} = h_2'(T_w - T_{si}) \tag{10.29}$$

Between the back of metallic surface and the room air:

$$\dot{q} = h_{si}(T_{si} - T_b) \tag{10.30}$$

here, h_1' and h_2' are the convective heat-transfer coefficient from the absorber to the water and from the water to the other metallic surface.

Equations (10.27 through 10.30) can be solved for the rate of thermal energy transferred to living room as

$$\dot{q} = U(T_{sa} - T_b) \tag{10.31}$$

where,

$$\frac{1}{U} = \left[\frac{1}{U_t} + \frac{1}{h_1'} + \frac{1}{h_2'} + \frac{1}{h_{si}}\right] \tag{10.32}$$

and,

$$T_{sa} = \frac{\alpha\tau}{U_t}I(t) + T_a \tag{10.33}$$

Example 10.7 Consider a south-facing glazed water wall with the parameters given in Example 10.5 with $h_1' = h_2' = 206$ W/m^2 °C. Calculate the following parameters:

(a) the rate of mean heat flux into a room maintained at 18 °C;
(b) the rate of night losses from the system for an inside temperature maintained at 18 °C and an ambient temperature of 12 °C;
(c) the rate of net heat flux into the room for equal duration of day and night; and
(d) the rate of night losses for 3 cm—thick movable insulation during the night.

Solution

(a) The rate of mean heat flux into a room is given by

$$\dot{q} = \left[\frac{1}{5.0} + \frac{1}{206} + \frac{1}{206} + \frac{1}{8}\right]^{-1} \left[\frac{0.8 \times 0.71 \times 310}{5} + 14 - 18\right]$$
$$= 2.99(35.22 + 14 - 18) = 93.35 \text{ W/m}^2$$

(b) The night losses $= (2.99) \times (-6) = -17.94$ W/m^2
(c) The duration of the day and night is the same; hence

The net heat flux = the heat flux gain − the heat flux(night) loss
$$= 93.35 - 17.94 = 75.41 \text{ W/m}^2$$

(d) The rate of heat losses with insulation is

$$\dot{q} = \left[\frac{1}{5.0} + \frac{0.03}{0.025} + \frac{1}{206} + \frac{1}{206} + \frac{1}{8}\right]^{-1}(12 - 18)$$
$$= 0.65 \times (-6) = -3.90 \text{ W/m}^2$$

It is clear from the above calculation that there is a reduction in night losses due to the movable insulation from −17.94 to −3.90 W/m^2.

The net heat flux $= 93.35 - 3.90 = 89.45$ W/m^2

Fig. 10.6 View of a Transwall
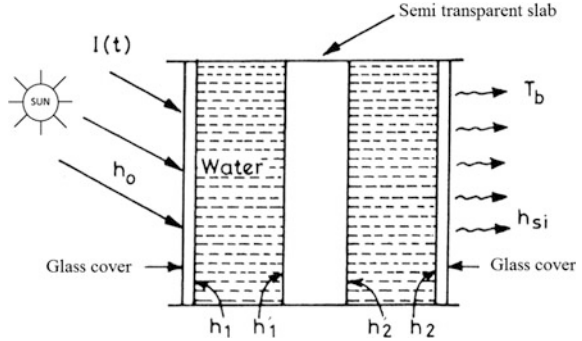
If the wall-exposure period is reduced from $12\,h$ to $8\,h$, then the net energy available with the movable insulation is

$$= (93.35 \times 8 - 3.9 \times 16) \times 3600 = 2.46 \times 10^6\,\text{J} = 0.68\,\text{kWh}$$

In this case, it is assumed that U_t is same for the glazed south wall with and without moveable insulation.

(iii) **Transwall**: A transwall, also known as a "translucent wall," is shown in Fig. 10.6. It is a transparent thermal storage wall admitting partial solar energy. Introduction of a layer of concrete wall behind the water mass decreases the average absorption of solar energy. It also reduces temperature fluctuations. Thus, a transwall absorbs marginally less energy compared with the pure Trombe wall. A transwall is more useful for heat transfer when the daytime-heating load is significant.

The rate of useful energy gain for a transwall can be written as:

$$\dot{q} = \tau I(t) - U_t(T_b - T_a) \tag{10.34}$$

where

$$U_t = \left[\frac{1}{h_o} + \frac{L_g}{K_g} + \frac{1}{h_1} + \frac{1}{h_1'} + \frac{L_t}{K_t} + \frac{1}{h_2} + \frac{1}{h_2'} + \frac{L_g}{K_g} + \frac{1}{h_{si}}\right]^{-1}$$

and

$$\tau = \left(1 - R_g\right)\left(1 - \alpha_g\right)(1 - \alpha_w)(1 - \alpha_t)(1 - \alpha_w)\left(1 - \alpha_g\right)$$

where α_g, α_w, α_t are, respectively, the absorptivity of the glass cover, the water, and the semitransparent material. R_g is the reflectivity of the glass cover.

(a)

(b)
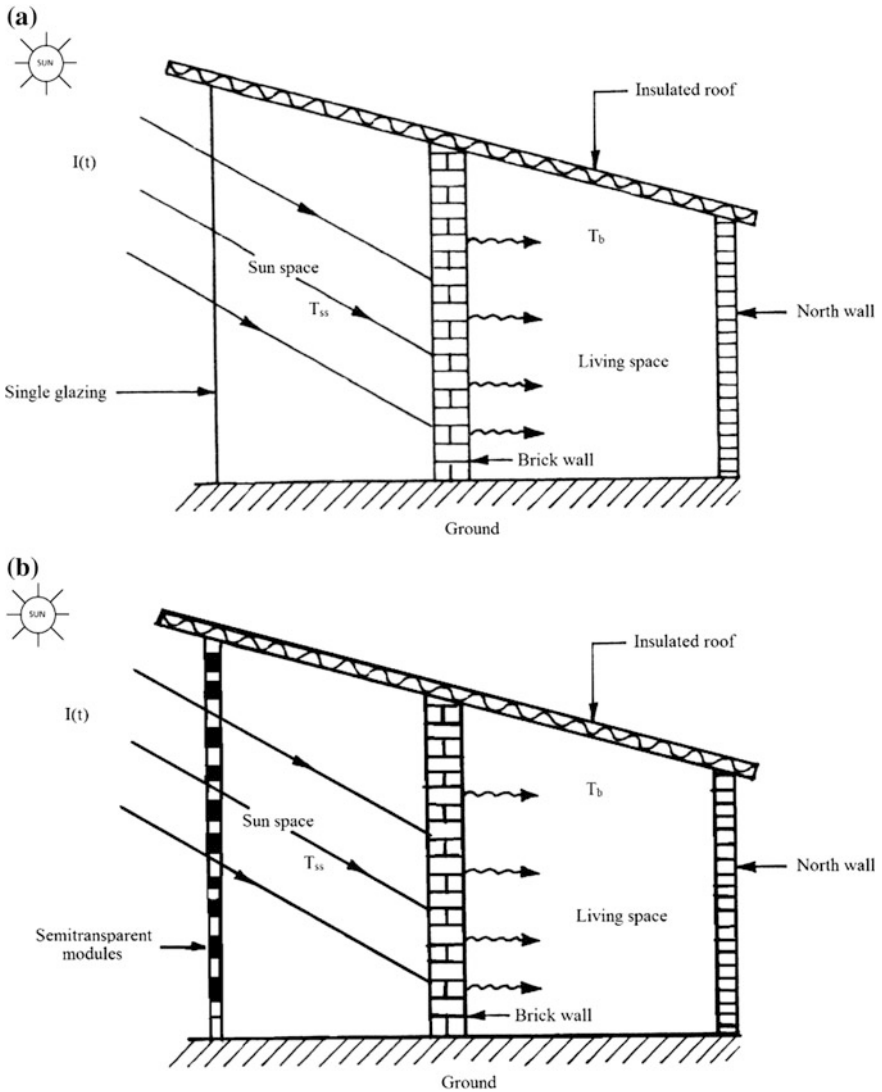
Fig. 10.7 a Schematic view of a solarium. **b** Cross-sectional view of semitransparent photovoltaic module wall

Equation (10.34) can be rewritten as follows:

$$\dot{q} = U_t \left[\frac{\tau}{U_t} I(t) + T_a - T_b \right] \tag{10.35a}$$

or

$$\dot{q} = U_t[T_{sa} - T_b] \tag{10.35b}$$

(iv) **Solarium**: A solarium, as shown in Fig. 10.7a, is an integration of direct-gain and thermal-storage concepts. It consists of a south-side sun space with thick-mass wall connecting the living space.

The thermal-storage mass link between the Sun and living space helps in heat retention and distribution. It also enhances the efficiency of the system. The overheating of the sunspace during the summer can be avoided by the use of shading. The use of movable insulation/shutters during the day to minimize heat gain.

There are two zones, namely, zone I and zone II, having temperatures T_s and T_b. These zones represent the sun space and the living space, respectively.

Solar radiation, after transmission (τ) from the glass cover of the sun space, is absorbed (α) by a blackened thermal-storage mass-link wall facing the south direction. Furthermore, there is convective heat transfer from the blackened thermal-storage mass-link wall to the sun space (T_s) and consequently from the sun space to the ambient air by an overall heat-transfer coefficient (U_0). At the same time, the rest of the heat is conducted to the living space. There is no direct heat transfer between the absorbing surface and the ambient air.

The energy-balance equations can be written as follows:

For zone I
The net heat-flux gain for a blackened thermal-storage mass-link wall is given by

$$\dot{q} = (\alpha\tau)I(t) - h_{TS}\left(T|_{x=0} - T_s\right) \tag{10.36}$$

Now, the rate of heat transfer from the blackened thermal-storage mass-link wall to the sun space will be lost to the ambient air, which can be represented by

$$U_0(T_s - T_a) = h_{TS}\left(T|_{x=0} - T_s\right) \tag{10.37}$$

In view of Eqs. (10.37), (10.36) can be further written as

$$\dot{q} = (\alpha\tau)I(t) - U_0(T_s - T_a) \tag{10.38}$$

From Eq. (10.37), one can have

$$U_0(T_s - T_a) = \frac{U_0 h_{bs}}{(U_0 + h_{bs})}\left[T|_{x=0} - T_a\right] = U_t\left[T|_{x=0} - T_a\right] \tag{10.39}$$

where

$$U_t = \left[\frac{1}{U_0} + \frac{1}{h_{bs}}\right]^{-1}$$

Now with the help of Eqs. (10.39), (10.38) can be as follows:

$$\dot{q} = (\alpha\tau)I(t) - U_t\left[T|_{x=0} - T_a\right] \tag{10.40}$$

Zone II
Under steady-state conditions, the energy balance for the blackened partition wall will be as follows:

$$\dot{q} = \frac{K}{L}\left(T|_{x=0} - T|_{x=L}\right) \tag{10.41}$$

Furthermore, the rate of heat transfer from the back of the blackened thermal-storage mass-link wall to the living space is given by

$$\dot{q} = h_i\left(T|_{x=L} - T_b\right) \tag{10.42}$$

According to Sect. (10.6.1), Eqs. (10.40 through 10.42) can be solved for $\dot{q}$ as

$$\dot{q} = U\left[\frac{(\alpha\tau)I(t)}{U_t} + T_a - T_b\right] \tag{10.43a}$$

or

$$\dot{q} = U[T_{sa} - T_b] \tag{10.43b}$$

where

$$U = \left[\frac{1}{U_0} + \frac{1}{h_{bs}} + \frac{L}{K} + \frac{1}{h_i}\right]^{-1}$$

and

$$T_{sa} = \frac{(\alpha\tau)I(t)}{U_t} + T_a \tag{10.44}$$

It may be noted that the expression for T_{sa} (Eq. 10.44) is similar to that in Eq. (10.18c).

(v) **Photovoltaic thermal (PVT) direct/indirect gain** [4]

In this case, a semitransparent photovoltaic module (see Sect. 4.4.1 in Chap. 4) is used in place of a window glass as shown in Fig. 10.7b. The solar radiation incident on the semitransparent photovoltaic module (facing south in the northern hemisphere) is used in two ways. The solar radiation incident on the packing factor is first converted into DC power, and the rest is lost to the ambient air and the enclosed room air (indirect gain). Furthermore, the solar radiation incident on the non-packing factor is directly transmitted to the room air, which represents a direct gain for the room air. Thus, one gets a direct as well as an indirect gain by using a semitransparent photovoltaic module. By such application, one gets thermal as well as electrical power, and hence it is referred as "photovoltaic thermal gain." It is also known as a PVT facade.

Referring to Fig. 10.7b, an energy-balance equation in W/m^2 for the PV module and the room air can be written as follows:

Semitransparent photovoltaic module wall

$$\tau_g \alpha_c \beta_c I(t) = \left[U_{t,ca}(T_c - T_a) + U_{t,cb}(T_c - T_b) \right] + \eta_m I(t) \tag{10.45}$$

where τ_g, α_c, β_c, and η_m are the transmittivity of the glass of the PV module, the absorptivity of the solar cell, the packing factor, and the electrical efficiency of the semitransparent PV module, respectively; $U_{t,ca}$ and $U_{t,cb}$ are an overall heat-transfer coefficient from the solar cell to the ambient air and from the solar cell to the room air, respectively.

Non-air conditioned room air

$$U_{t,cb}(T_c - T_b) + \tau_g^2(1 - \beta_c)I(t) = \dot{q}_u + U_{t,ba}(T_b - T_a) + 0.33NV(T_b - T_a) \tag{10.46}$$

where $U_{t,ba}$ is an overall heat-transfer coefficient from a non-air conditioned room to the ambient air; and $\dot{q}_u$ is the rate of useful energy in W. N and V are the number of air change and volume of the non-air conditioned room, respectively.

From Eq. (10.46), one obtains

$$T_c = \frac{\tau_g \alpha_c \beta_c I(t) - \eta_m I(t) + U_{t,ca}T_a + U_{t,cb}T_b}{U_{t,ca} + U_{t,cb}} \tag{10.47}$$

For a air-conditioned room, the values of T_b can be either 20 or 25 °C. Thus, for known T_b, T_c can be calculated and after knowing T_c; the temperature-dependent electrical efficiency, and hence the electrical power, can also be calculated from Eq. (4.37b).

After substituting the expression for T_c from Eq. (10.47) in Eq. (10.46), one can obtain an expression for $\dot{q}_u$ as $\dot{q}_u = \left[(\alpha\tau)_{\text{eff}} I(t) - U_{\text{eff}}(T_b - T_a) \right]$ or

$$\dot{q}_u = U_{\text{eff}}[T_{\text{sa}} - T_b] \qquad (10.48)$$

where $T_{\text{sa}} = \frac{(\alpha\tau)_{\text{eff}}}{U_{\text{eff}}} I(t) + T_a$ is the solair temperature of direct and indirect gain of the PVT non-air conditioned room as follows:

$$(\alpha\tau)_{\text{eff}} = \left[h_p \tau_g \alpha_c \beta_c + \tau_g^2 (1 - \beta_c) - \eta_m \right]; \ h_p = \frac{U_{\text{t,cb}}}{U_{\text{t,ca}} + U_{\text{t,cb}}};$$

$$U_{\text{eff}} = \left[U_{\text{ba}} + U_{\text{t,ba}} + 0.33 NV \right] \text{ and } U_{\text{ba}} = \frac{U_{\text{t,ca}} U_{\text{t,cb}}}{U_{\text{t,ca}} + U_{\text{t,cb}}}.$$

Furthermore, an instantaneous thermal efficiency as a function of design, climatic, and electrical parameters can be defined as follows:

$$\eta_i = \frac{\dot{q}_u}{I(t)} = \left[(\alpha\tau)_{\text{eff}} - \frac{(T_b - T_a)}{I(t)} \right] \qquad (10.49)$$

The above equation can be referred to as a characteristic equation of a PVT non-air conditioned room that has following limitation, and it is valid for

(i) $(T_b - T_a) > 0$ and
(ii) $h_p \tau_g \alpha_c \beta_c + \tau_g^2 (1 - \beta_c) - \eta_m > 0$

Now the threshold condition for a PVT non-air conditioned room is obtained as follows:

$$\dot{q}_u = \left[(\alpha\tau)_{\text{eff}} I(t) - U_{\text{eff}}(T_b - T_a) \right] > 0$$

or

$$I(t)_{\text{threshold}} > \frac{U_{\text{eff}}(T_b - T_a)}{(\alpha\tau)_{\text{eff}}} \qquad (10.50)$$

10.7.3   Isolated Gain

Isolating, the collection of the solar energy unit and the storage from the building, results in a greater flexibility of design and operation. The most common application of this concept is the natural convective loop with a thermo-syphoning water heater as shown in Fig. 10.8a. This figure represents the simplest version.

Figure 10.8b shows the working principle of the collector–cum–rock bed storage system integrated with a building. Hot air from the solar air collector is allowed to
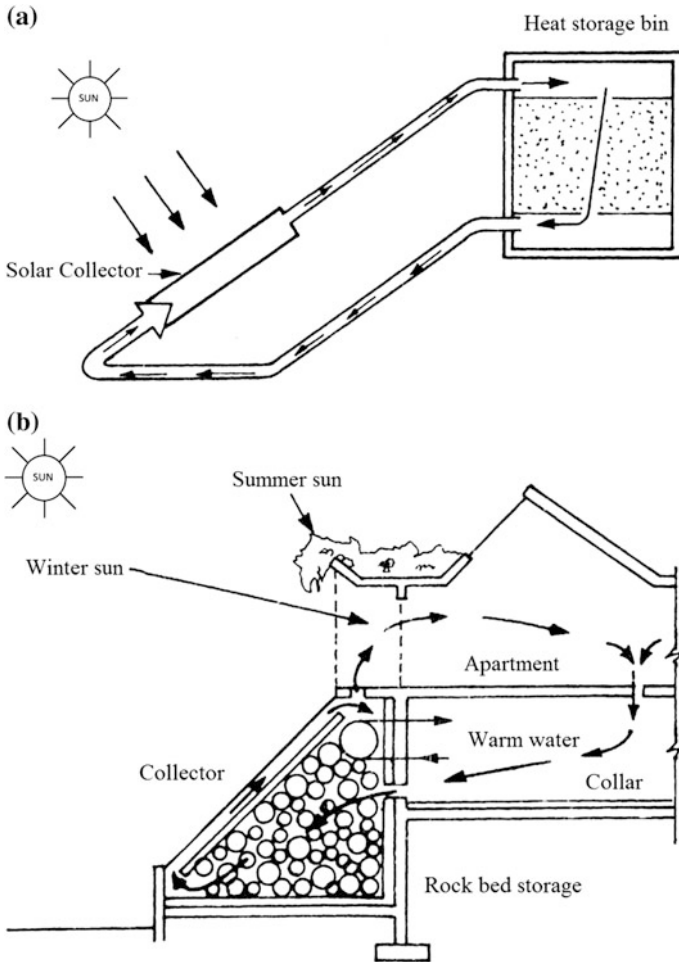
Fig. 10.8 a Isolated-gain convective loop. **b** View of Isolated gain rock bed-cum-collector loop

enter the building. The cooled air is returned to the solar collector through the basement and rock bed. In the case of hot air prevented from entering the building, it is allowed to enter the rock bed to be stored for later use, preferably at night.

10.8   Thermal Cooling

Thermal cooling of a building, which is the reduction of peak cooling power demand, utilizes a number of natural heat-rejection mechanisms, namely ventilation, evaporation, infrared radiations to the sky, and Earth-contact cooling, etc.

The first step in the direction of passive cooling is the reduction of unnecessary thermal loads.

(a) **Exterior load**: Climate-dependent loads involve the conduction of heat through the building skin, infiltration of the outside air, and direct penetration of short wavelength radiations. This is achieved by having optimized Trombe walls without ventilation during day and night.

(b) **Interior loads**: These are thermal emissions due to human activities/occupancy.

The cooling concepts may be divided into two categories as follows:

(I) **Direct cooling**: Direct-cooling concepts include (i) ventilation/infiltration/courtyard, (ii) wind tower/air vents and (iii) Earth shelter; and

(II) **Indirect cooling**: The indirect cooling concept include (i) evaporative cooling/roof pond (ii) shading/movable insulation and (iii) Earth air tunnel.

These concepts are described in subsequent sections.

10.8.1   Evaporative Cooling [5]

In a direct evaporative–cooling system, the room air should come into direct contact with the water surface. The relative humidity inside the room increases due to the evaporation of water. In such cases, it is possible to cool a small building by placing wetted pads in the windows or porches facing the wind direction.

Either water film or an intermittent spray of water or water flowing over the roof is another method of indirect evaporative cooling. As the water draws heat from the heated roof surface, it leaves a cooler ceiling surface. It acts as a radiative cooling panel for the space inside the room. The indoor temperature is lowered without elevating the humidity level as in the case of direct evaporative cooling. Indirect evaporative cooling by roof pond is more effective. The roof can also be covered with plants and movable insulation for indirect cooling.

The rate of reduction of thermal energy due to evaporation can be determined by Eqs. (10.7a), (10.7b).

10.8.2   Infiltration/Ventilation

Infiltration means the admittance of outside air into the living space through a door and/or window openings as well as cracks and interstices around the doors and windows. It can also be said that there is exchange of air between the room air and the outside air through infiltration/ventilation. The infiltration may be due to (i) the pressure difference generated by the difference in temperatures and the humidity of

the inside and the outside air of a building, (ii) wind pressure, and (iii) entry and exit of occupants.

Convective heat losses due to ventilation are attributable to the air-exchange rate, the temperature difference between the inside and the outside the building, and the heat capacity of the air.

The rate of infiltration/ventilation losses can be determined by the following relation:

$$\dot{Q}_v = 0.33NV(T_b - T_a) \tag{10.51}$$

where N is the number of air exchanges per hour and for **infiltration N < 10 and for ventilation N > 10** The V is the volume of the room of a building (m^3); and T_b is the temperature of the air inside the room of a building (°C).

Local topography and surface texture affect the wind conditions considerably. Spacing of buildings, at six times their height in a grid iron pattern, results in proper wind movement due to uniform flow and removal of stagnant zones.

Windows play a dominant role in inducing ventilation. The ventilation rate is affected by the parameters such as climate, wind direction, size of inlet and outlet, room volume, shading devices, and internal partitions.

10.8.3 Wind Tower

Wind towers are designed to harness cool air through the wind and circulate cool air inside the building. A wind tower provides heating or cooling depending on the time of the day as well as the presence or absence of wind. When ambient air at a higher temperature comes in contact with the walls of the wind tower during the day, it is cooled. The higher density of cool air creates a downdraft and settles down at the lower part of wind tower. The presence of a wind tower helps this downdraft. During the night, thermal energy stored in the wind tower during sunshine hour heats the air present in wind tower and works as a chimney. Higher temperatures in the upper part of the wind tower lower the pressure, and an updraft is created. The concept of a wind tower works well in individual units but not in multi-storey apartments unless it is designed accordingly.

10.8.4 Earth–Air Heat Exchanger (EAHE)

An Earth–air heat exchanger (EAHE) exploits the constant ground temperature a few meters below the Earth's surface. The ground temperature remains constant throughout the year at an appropriate depth. The depth along with temperature is given in Table 10.2. The constant temperature beneath the ground can be harnessed for cooling or heating during the winter or summer, respectively. The design

parameter (e.g., the depth below ground for installation of a heat exchanger, length of pipe, cross-sectional area for air flow, and air flow rate) and climatic parameter (such as humidity of inlet air, ambient temperature, and incident solar radiation) determines the heat exchange between the surrounding soil and the air flowing in the pipe.

Figure 10.9a shows a cross-sectional view of an Earth–air heat exchanger (EAHE) below the ground surface at 4-m depth. Air available from the atmospheric air temperature is allowed to pass through it. The shape of the EAHE is cylindrical having a radius of 'r' and length 'L'. As the air passes through the EAHE, there is heat transfer from the inner surface of the tunnel to the flowing air by forced convection. Depending on the air temperature, the air is either heated or cooled. If the temperature of the air is lower than the temperature of the inner surface of the EAHE, heat is transferred from the surface to the air for heating. This occurs in winter and vice versa for summer.

Referring to Fig. 10.9b, the energy balance for an elemental length 'dx' in terms of W can be written as [6]

$$\dot{m}_f C_f \frac{dT(x)}{dx} dx = 2\pi r h_c (T_0 - T(x)) \tag{10.52}$$

where h_c is a convective heat-transfer coefficient, which can be calculated by the formula given in Chap. 3. For a larger-diameter EAHE, one can approximate a heat-transfer coefficient considering it as $2.8 + 3V$ where V is the speed of air flowing through the EAHE; C_f is the mass-flow rate and specific heat of the air; and $T(x)$ is the temperature of air as a function of 'x'.

The solution of the above equation with the initial condition $T(x = 0) = T_{fi}$ can be written as

$$T(x) = T_0 \left[1 - \exp\left(-\frac{2\pi r h_c}{\dot{m}_f C_f} x \right) \right] + T_{fi} \exp\left(-\frac{2\pi r h_c}{\dot{m}_f C_f} x \right) \tag{10.53}$$

Now the outlet air temperature at the exit of the Earth–air heat exchanger can be obtained as follows:

$$T_{fo} = T(x = L) = T_0 \left[1 - \exp\left(-\frac{2\pi r h_c}{\dot{m}_f C_f} L \right) \right] + T_{fi} \exp\left(-\frac{2\pi r h_c}{\dot{m}_f C_f} L \right) \tag{10.54}$$

where L is the length of the EAHE.

Table 10.2 Ground temperatures for various surface conditions at a depth of ≥4 m

Surface condition	Ground temperature (°C)
Dry sunlit	27.5
Wet sunlit	21.5
Wet shaded	21.0
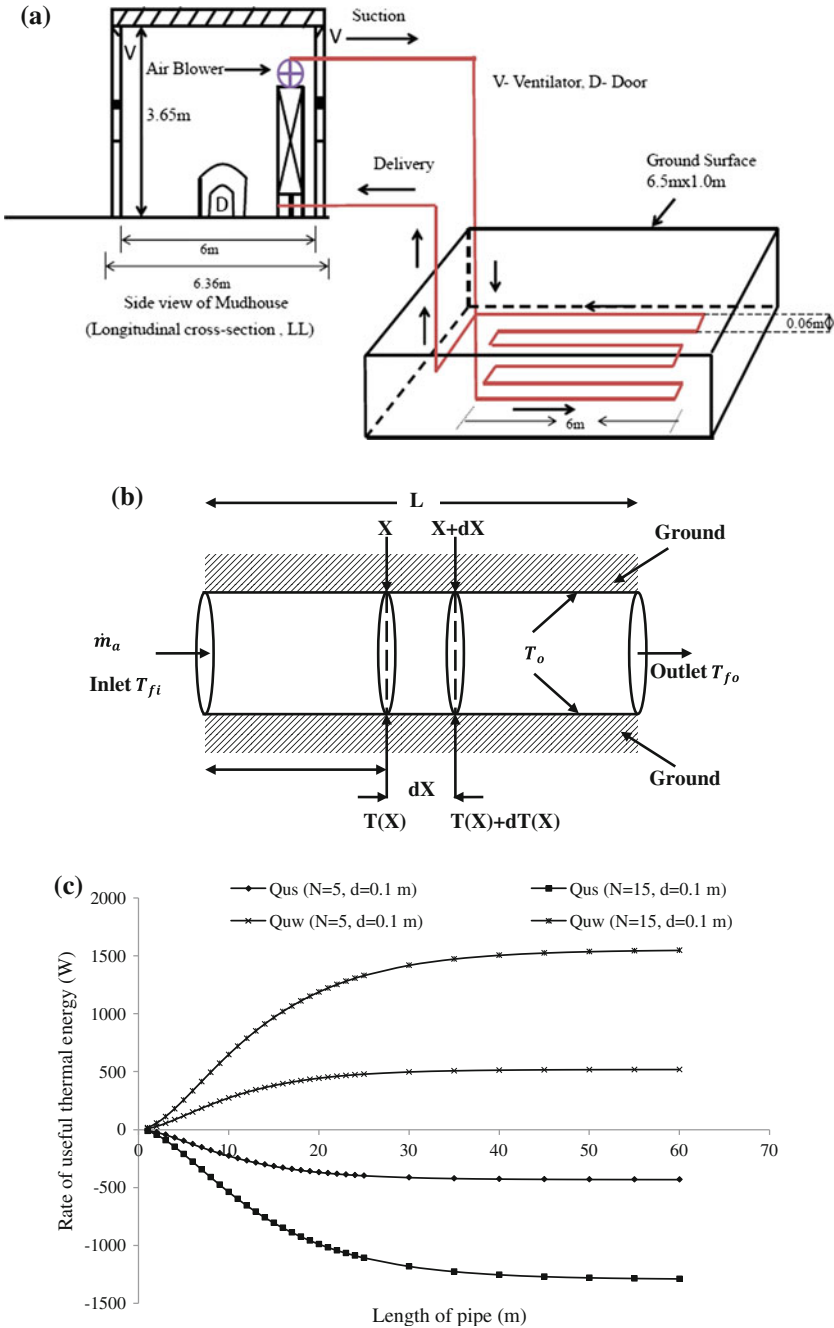
Fig. 10.9 a A combination of an underground stream and a wind tower. **b** Flow directions through a heat exchanger. **c** Variation of $\dot{Q}_u$ with the length of a heat exchanger

The rate of thermal energy in W carried away by the flowing air is given by

$$\dot{Q}_u = \dot{m}_f C_f (T_{fo} - T_{fi}) = \dot{m}_f C_f \left[1 - \exp\left(-\frac{2\pi r h_c}{\dot{m}_f C_f} L \right) \right] (T_0 - T_{fi}) \qquad (10.55)$$

The energy available in 1 h = $\dot{Q}_u \times 3600$ J.

The volume of hot air = $\pi r^2 V \times 3600$ m^3

If V_0 is the volume of a room to be heated, then the number of air change (N) per hour can be written as

$$N = (\pi r^2 V \times 3600)/V_0,$$

The following special cases should be discussed:

Case (i)

If either $L \Rightarrow \infty$ or $\dot{m}_f$ is very small, which indicates a very large tunnel length with very slow speed of air, then $T_{fo} = T_0$ and $\dot{Q}_u = \dot{m}_f C_f (T_0 - T_{fi})$.

This indicates maximum withdrawal of thermal energy to heat the living space.

Case (ii)

If $L \Rightarrow 0$ and $\dot{m}_f$ is very large, which indicates a small tunnel length with very large speed of air, then

$$T_{fo} = T_{fi} \text{ and } \dot{Q}_u = 0$$

This indicates no withdrawal of heat from tunnel, and hence there is a need to optimize the length, radius, and velocity of the air for thermal heating/cooling of a living space. The variation of $\dot{Q}_u$ with L for winter and summer conditions for a typical set of parameters is shown in Fig. 10.9c.

A combination of wind tower and Earth–air heat exchanger is effective in increasing the draft of air in the Earth–air tunnel to improve the cooling rate of the building air as shown in Fig. 10.9a.

Here it is important to mention that the depth in case of a wetted surface is greater than that of a dry surface. For a given depth, the ground temperature for a wetted surface will be lower than any other surface due to it high thermal conductivity.

10.8.5   Air Vent

Air vents are used due to the failure of a wind tower. A typical air vent is shown in Fig. 10.10. It consists of holes that have been appropriately optimized for size at the top of any cylindrical or domed roof. The hole is covered with a protective cap. When air passes through the openings of the protective cap, low pressure at top
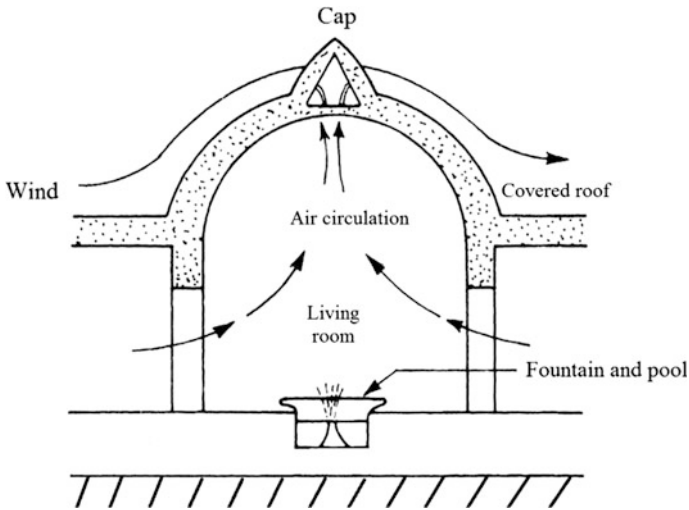
Fig. 10.10 Air vents under operation

of the curved roof is created. The low pressure created at the top directs the hot air inside the living space toward the upper vent, which results cooling of the living space. Thus, the air is kept circulating through the room. Air vents are usually placed over living rooms to cool air moving through the room. An air vent is suitable for hot and dry as well as warm and humid climatic conditions. Air vents are preferred for single-unit living/working spaces.

10.8.6 Shading

Another important building element is the glass window, which greatly influences the thermal environment. Glass window openings must be designed in relation to the sunlight, ventilation, and air movement. Window designing relating to sunlight can be performed by two methods as follows:

First method: In this case, one must design the shading devices to prevent radiation from entering the interior.
Second method: In this case, one must design the openings to permit the adequate natural lighting of the interior.

   There are also a number of options available for windows. These include the following:

 (i) **Self-inflating curtain**: The curtain consists of a number of thin layers of flexible material with high reflectivity and low emissivity. Solar radiation warms the air between the two layers, which increases the pressure and

decreases the density in the upper part of the layers. The pressure pushes the layers apart and creates fresh air intake of air from the bottom. Thus, the system of reflecting layers separated by air gaps provides good insulation. If insulation is not required between two layers, the air is evacuated from the sides.

The rate of thermal-energy transfer through a self-inflating curtain is written as follows:

$$\dot{q} = (1 - f)\tau I(t) - U(T_b - T_a) \tag{10.56}$$

where f is the shading factor; and the value of f is 1 for complete shading and < 1 for partial shading.

 (ii) **Window Quilt Shade**: The quilt consists of a sandwich of fine layers. It is assembled with an ultrasonic fibre welder. The quilt is enclosed in decorative polyester fibre.
(iii) **Venetian Blind between the glasses**: This is an effective system to reduce heat loss through a double-glazed window. In this case, the characteristic dimension of the unit is small; hence, the convective heat transfer is stopped. In this case, $\dot{q}$ is the same as that in Eq. (10.21) but with a lower value of τ and U.
 (iv) **Transparent Heat Mirrors**: This is a method to reduce heat loss from a glazed surface. In this case, the glass is coated by a film to reflect the infrared radiation from the surface a large extent. However, this coating also reduces the transmissivity of the glass window for solar radiation. A suitable compromise must be made as per requirement. The coating may consist of single or multiple layers of different substances deposited by vacuum evaporation or spray technique. The heat mirror gives much less heat loss and a higher transmission than a multi-pane system.
  (v) **Heat Trap**: A reasonable thickness of insulating material with good transmissivity may be used to reduce heat transfer.
 (vi) **Optical Shutter**: This consists of three layers of transparent sheets and one layer of cloud gel. It is opaque at high temperatures. It can be used for reducing air-conditioning loads and preventing overheating in green houses and solar-collector systems.

10.8.7   Rock Bed Regenerative Cooler

A cross-sectional view of a regenerative cooler is shown in Fig. 10.11. It consists of two rock beds set side by side. It also acts as a heat exchanger and is separated by an air space. A damper is used between the two rock beds to divert the incoming air from house toward the cooling rock bed by water spray. The rock beds are cooled

Fig. 10.11 Cross-sectional
view of a regenerative cooler
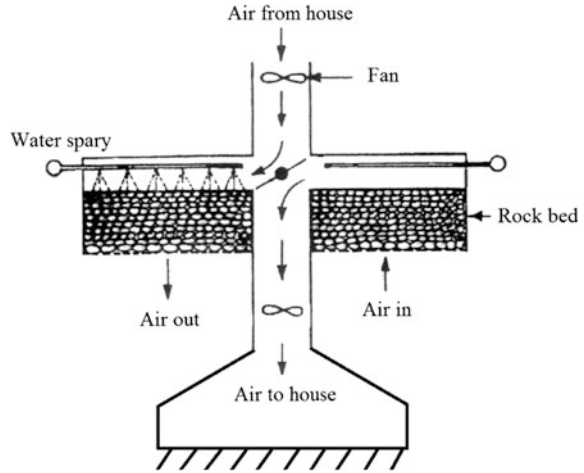
alternatively. It also absorbs water during cooling. The air passing through a cooled
dry rock bed in the first cycle gets cooled by transferring heat to the cooled rock
bed. The cooled air is allowed to pass into the room. Humid air is produced during
its evaporation cycle from the rock bed, and it is vented to the outside. After getting
the rock bed warm, the damper is reversed for further cooling. In the meantime,
another cooled rock bed is used similarly for cooling.

10.8.8 Radiative Cooling

The sky temperature is always lower than the ambient air temperature by 12 °C
under clear night sky conditions. The northern sky in the northern hemisphere is
often cool enough even during the day. It acts as a cooler heat sink with respect to
ambient air during the day/night. A horizontal surface is the most effective radiative
configuration.

Exposed horizontal surface loses heat to the ambient air by convection until its
temperature is equal to the dry-bulb air temperature. In addition, there is heat loss
from the ambient air/surface to the sky by long-wavelength radiation exchange. If
the net heat exchange between the surface and the sky reduces the roof surface
temperature to the wet-bulb temperature of the surrounding air, condensation of
moisture of the air starts taking place on the roof. The condensation will further cool
the roof due to fast heat loss from the enclosed room to the surface of the roof.
(Case (ii) of Eq. 10.16)

If a surface is inclined as shown in Fig. 10.12, then the cooled air will trickle
down toward an internal courtyard from the inclined surface due to its high density.
Then the trickled cooled air enters the room, as shown in the figure, through the
openings at lower level. However, this does not work in windy conditions because

Fig. 10.12 Cooling by
radiation through an
open-roof loop
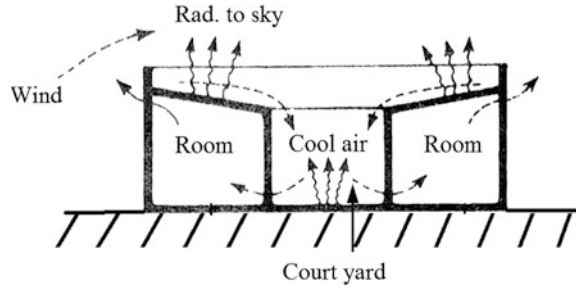
Fig. 10.13 Cooling by
radiation through a
closed-roof loop
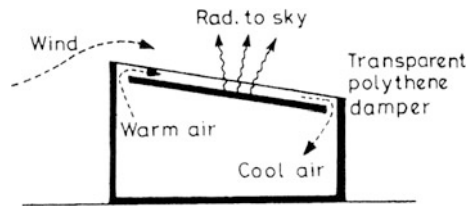
the wind becomes the carrier of cooled air. To avoid this, the roof should be
covered with a transparent polyethylene sheet which has a limited life time. This
problem can be solved by covering the roof with a corrugated metallic sheet with
the provision of openings at the lower and upper end from inside the roof as shown
in Fig. 10.13.

10.8.9   Green/Cool Roof

A "green" roof or "cool" roof is a concept in which there is vegetation and gar-
dening [7] on the roof of the building to decrease the heat flux inside the building
from the top. In addition to the vegetation, there are some other concepts that are
used such as colouring of the roof [8, 9] evaporative cooling, and solar ponds [10,
11]. There are also some selective coatings on the roof of the building that reflect
radiation and cool the roof. In some cases, roof ventilation has also been used to
cool the roof. Green roofs are a passive cooling technique, which does not have any
ill effect on environment or on human health.

10.8.10   Heating and Cooling

Figure 10.14 shows a schematic view of a roof pond integrated with a
water-circulating column working under natural circulation mode. The roof pond is
covered permanently with a thin-layer exchange membrane. There is a louvered
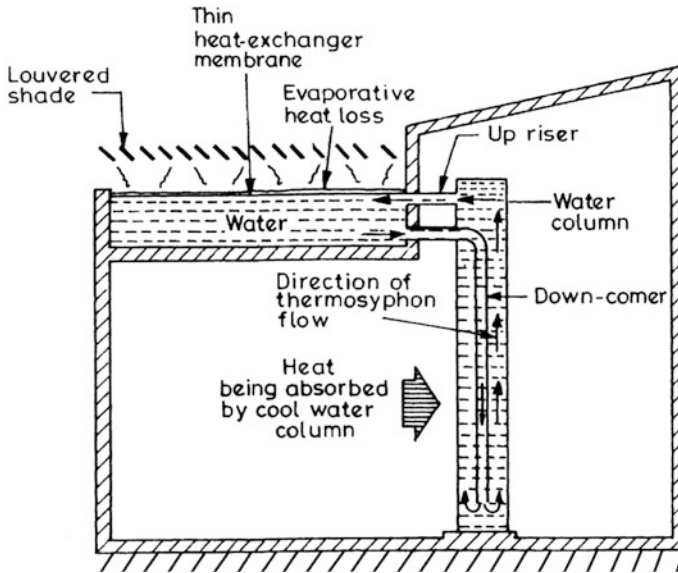
Fig. 10.14 Schematic view of a roof pond with natural flow

shade above the membrane. The louvered shade is closed to reduce heat loss during the night. It is opened to allow solar radiation to be incident on the roof pond during the day. This is precisely performed for thermal heating. In this case, the water of the roof pond is heated. The hot water is allowed to pass through the downcomer. During passes through the downcomer, thermal energy is released to the water outside and cooled down toward the lower ends due to high density.

For thermal cooling, the louvered shade is opened to increase heat loss during night time. There will be evaporation from the water surface; it cools the water. It is closed during the day to minimize solar radiation to incident on the roof pond. The cooled water is allowed to pass through the downcomer. The thermal energy gained from the room air during passes through the downcomer. Thus room is then cooled.

10.9 Time Constant

For most of the commonly encountered thermal structures, the boundary conditions change constantly. The steady-state methods gives only approximate solutions. The exact analyses of the heat transmission under transient conditions are complex. An approximate estimation of the time-dependent response of the thermal structures can be performed by assuming a constant temperature throughout the structure at any instant. If there is a small change in temperature dT in time dt, the change in the

internal energy is equal to the net heat flow rate across the boundary, which is represented by

$$\rho CV dT = h'A(T - T_a) dt \qquad (10.57)$$

where h' is the convective heat-transfer coefficient from the building surface to the ambient air.

The solution of Eq. (10.57) can be written with the initial condition that $T = T_0$ at $t = 0$ as:

$$\left[\frac{T(t) - T_a}{T_0 - T_a}\right] = \exp\left\{-\frac{h'A}{\rho CV}t\right\} \qquad (10.58)$$

If the quantity $(h'L/K)$, i.e., the Biot number, is <0.1, the error introduced by assuming that the temperature is uniform throughout the structure at any instant is <5 %.

For a multi-layered structure, the time constant is defined as

$$\text{Time constant} = \frac{\text{heat stored}}{\text{heat transmitted}} = \sum_i \left[\frac{\dot{q}}{U}\right]_i = \sum_i \left(R_{s0} + \frac{L_i}{K_i}\right)(L_i \rho_i C_i) \quad (10.59)$$

The value of the time constant depends significantly on the position of the insulating layer in the element of the building.

10.10 Approximate Methods

These methods are used to determine the average requirements for the heating/cooling of a building. They are used during the planning stage. The approximate methods include the degree day (DD) under steady-state conditions. The degree-day (DD) method is commonly practiced by architects.

The rate of heat losses from inside the building to the ambient air can be expressed as:

$$\dot{q} = (UA)(T_b - T_a) \qquad (10.60)$$

where T_b is referred to as the "temperature base" (room air) for heat-loss calculations.

Integration of Eq. (10.60) over an entire day (T) gives the total daily heat losses from a building surface as

$$Q_{\mathrm{T}} = \int_0^T \dot{q}\mathrm{d}t(UA)(T_{\mathrm{b}} - \overline{T}_{\mathrm{a}})T \tag{10.61}$$

where $\overline{T}_{\mathrm{a}}$ is the average daily ambient air temperature (Eq. (10.22)).

The term over the entire day period is determined only for $T_{\mathrm{a}} < T_{\mathrm{b}}$.

The numbers of degree-days (DD) per month are defined as follows

$$\mathrm{DD} = (T_{\mathrm{b}} - \overline{T}_{\mathrm{a}})Tn_{\mathrm{d}}' \tag{10.62}$$

where n_{d}' is the number of days in a month for which thermal heating is a requirement.

The monthly space-heating load (Q_{m}) is calculated using the following formula:

$$Q_{\mathrm{m}} = Q_{\mathrm{T}} \times n_{\mathrm{d}}' = (UA)\mathrm{DD} \tag{10.63}$$

The product of the building's overall energy-loss coefficient and the area, (UA), can be determined as follows:

For structures whose conventional fossil-fuel requirements are known, UA can be calculated as the ratio of an amount of energy required to heat the building for a given period (considering the heating value of fuel and the furnace efficiency) for the total number of degree-days during that period as

$$UA = (M_{\mathrm{F}} \times H_{\mathrm{F}} \times \eta_{\mathrm{F}})/\mathrm{DD} \tag{10.64}$$

where M_{F}, H_{F}, and η_{F} are the mass-heating value and the burning efficiency of fossil fuel (Appendix VII).

Example 10.8 Determine an overall heat-loss coefficient of a building (UA) if the number of DD in the month of January is 750. Ninety litres of oil must be used to keep the space comfortable.

Solution
From Eq. (10.64),

$$UA = (M_{\mathrm{F}} \times H_{\mathrm{F}} \times \eta_{\mathrm{F}})/\mathrm{DD}$$

After substituting the known parameters of H_F and η_F from Appendix VII in the above equation, we obtain

$$UA = (90 \times 43000 \times 80)/(750 \times 100 \times 24)$$
$$= 172 \, \text{kJ/h} \, ^\circ\text{C} = 47.8 \, \text{W}/^\circ\text{C}$$

Example 10.9 A building at Leh has $(UA) = 500 \, \text{W}/^\circ\text{C}$. If the DD for January are 750, calculate the total space-heating load for January.

Solution
The total heating load can be calculated as

$$\text{Space heat load} = 500 \times 750 \times 24 \times 3600 \, \text{J} = 32.4 \, \text{GJ}$$

10.11   Solar Load–Ratio Method

This method determines the yearly requirements for supplementary energy in a building. The solar load–ratio method was put forward by Balcomb et al. [12]. It is extensively applied for designing sunspace, solar collector/storage, and direct gain in buildings. This method employs simulation techniques of passive-heating systems. The solar load–ratio method requires knowledge of some basic terms. The important definitions of each one of them are as follows:

Solar Wall: A glazed wall of a building that absorbs solar radiation and transfer thermal energy to the living space of a building is known as a "solar wall."
Solar Aperture: The glazed area of the wall that transmits solar radiation into the living space for direct thermal gain and day lighting is termed a "solar aperture." SLR correlations assume the negligible losses through the solar aperture. Hence, losses through the solar aperture are neglected.
Net Glazing Area (A_r): A_r is the area obtained after excluding the area of mullions, framing, etc., from the solar aperture.
Projected Area (A_{rp}): A_{rp} is the projection of the net glazing area on a vertical plane normal to the azimuth of the glazing. Net glazing area and projected area are equal for a collector storage wall and direct gain portions of the building, whereas the net glazing area for a sunspace is significantly higher than projected area (Fig. 10.7a).
Net Reference Load (L_{ns}): L_{ns} is the thermal losses incurred from the nonsolar components of the building in 1 month.

The net reference load (in Wh) is given by

$$L_{ns} = 24(UA)_{ns}(\text{DD}) \qquad (10.65)$$

where $(UA)_{ns}$ is in $W/^\circ\text{C}$, and DD is the number of DD in the month.

Net-Load Coefficient: Net-load coefficient is the ratio of net reference load to the temperature difference between living space and the outdoor of a building.

Gross Reference Load: L is the sum of heat losses from the solar and nonsolar components of the building.

Total-Load Coefficient: Total-load coefficient is ratio of the gross reference load to the temperature difference between the living space and the outdoors of a building. It can be expressed as follows:

$$L = 24(UA)(\text{DD}) \tag{10.66}$$

Solar-Savings Fraction: (f_{ns}) is the fraction of energy requirement in the building that is met by solar components installed in the building. It can be expressed as

$$f_{ns} = \frac{L_{ns} - L_A}{L_{ns}} = 1 - \frac{L_A}{L_{ns}} \tag{10.67}$$

where L_A is the auxiliary energy required for each month given by

$$L_A = L_{ns}(1 - f_{ns}) \tag{10.68}$$

Load-Collector Ratio: (LCR) is defined as the net-load coefficient per unit of projected area of solar aperture in a building. It is expressed as

$$\text{LCR} = 24(UA)_{ns}/A_{rp} \tag{10.69}$$

Load-Collector Ratio for the Solar Aperture: (LCR_s) is defined as the loss coefficient per unit of projected area of the aperture.

The "unutilizability" method (double-U method) assumes a passive building as a collector with a finite heat capacity for designing the direct gain and solar collector and storage wall of the building. Two limiting cases are considered for the estimation of required auxiliary energy.

(i) **For an infinite-capacitance structure**: An infinite capacitance structure has a very large heat capacity. This structure allows the storage of excess energy (excess of loads) met from the solar elements of the building for later time.

(ii) **For a zero-capacitance structure**: In this case, excess energy from the loads is not stored for later use.

Therefore, all of the correlations used for the estimation of the auxiliary energy of a building fall in between these two limits. Figure 10.15 presents the input and output energy streams from a direct-gain component in 1 month.

Solar energy absorbed in the room is given by the following expression:

$$\bar{I}_t N(\overline{\alpha\tau})A_r = N\bar{S}A_r \tag{10.70}$$

where N is the number of days of the month and $\bar{S} = (\overline{\alpha\tau})\bar{I}_t$.

Fig. 10.15 Monthly energy streams for a direct-gain building
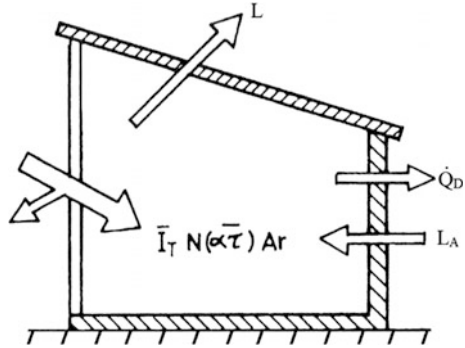
"Load" is defined as the energy lost through the building shell by conduction, infiltration, etc. There are two possibilities as follows

(i) when energy from solar components is unable to meet loads, i.e., the requirement of auxiliary energy L_A; and

(ii) when there is excess absorption of solar energy compared with load, this energy cannot be stored from a thermal-comfort point of view; in this case, excess heat Q_D must be vented or "dumped."

For nonzero thermal capacitance, there will be a sensible amount of heat, which may be removed from or stored in any structure in 1 month. Thermal energy stored is not shown in Fig. 10.15.

For a building having infinite storage capacity, the excess energy of the loads is stored, which gives a constant temperature. In this case, the energy balance (for 1 month) for the auxiliary energy requirement $L_{A,i}$ is given as follows:

$$L_{A,i} = \left(L - N\overline{S}A_r\right)^+ \tag{10.71}$$

where L is the load for the entire building. The '+' sign indicates that only positive values of the bracket are considered.

For a zero storage–capacity building, the excess energy of the loads is dumped, and the deficit energy is given by auxiliary energy. The temperature inside the building is constant in this case, too, but at the cost of the addition or removal of energy instead of storage.

The instantaneous rate of energy removal $\dot{Q}_D$ from the structure is given as following:

$$\dot{Q}_D = \left[I(t)(\alpha\tau)A_r - (UA)_h(T_b - T_a)\right]^+ \tag{10.72}$$

A critical solar radiation level (threshold level) may be defined at the point at which the gains simply offset the losses:

$$I_{TC} = (UA)_h(T_b - T_a)/(\alpha\tau)A_r \qquad (10.73)$$

Absorbed solar radiation above this value is "unutilizable," and it must be dumped. The dumped energy for the month, Q_D, can be obtained by integrating Eq. (10.72) over time as

$$Q_D = A_r(\bar{\alpha}\,\bar{\tau}) \int (I_T - I_{TC})^+ \, dt \qquad (10.74)$$

Over a month, I_{TC} is considered to be constant. The monthly average value is given by

$$I_{TC} = (UA)_h(T_b - \overline{T}_a)/(\bar{\alpha}\,\bar{\tau})A_r \qquad (10.75)$$

Energy below I_{TC} is useful; otherwise it must be dumped.

In terms of monthly average unutilizability $\bar{\phi}$, Eqs. (10.70) and (10.74) can be expressed as follows:

$$Q_D = N\overline{S}A_r\bar{\phi} \qquad (10.76)$$

or

$$\bar{\phi} = \frac{Q_D}{N\overline{S}A_r} = \frac{1}{\overline{I}_T N}\sum_{\text{days}}\sum_{\text{hours}}(I_T - I_{TC})^+ \qquad (10.77)$$

For zero capacitance building, required auxiliary energy is obtained by subtracting the absorbed solar energy from the sum of the load of the building and energy dumped from the building.

Thus,

$$L_{A,Z} = (L + \bar{\phi}N\overline{S}A_r) - N\overline{S}A_r = L - (1 - \bar{\phi})N\overline{S}A_r \qquad (10.78)$$

Equations (10.71) and (10.78) give the bounds on the auxiliary-energy requirements. Correlations have been developed in terms of the fraction of the load supplied by solar energy as

$$f = 1 - L_A/L \qquad (10.79)$$

A solar-load ratio (SLR $= X$) is expressed as follows:

$$X = \frac{\overline{I}_T N(\bar{\alpha}\,\bar{\tau})A_r}{L} = \frac{N\overline{S}A_r}{L}. \qquad (10.80)$$

For infinite-capacitance system, X is the solar fraction f_i

$$f_i = X = \left(1 - L_{A,i}/L\right) \tag{10.81}$$

For a zero-capacitance building (10.82)

$$= (0.4898 - 0.1218) \times 1367 = 0.36947 \times 1367 = 503.06 W/m^2 \tag{10.82}$$

The storage-dump ratio (Y) is expressed as follows:

$$Y = \frac{C_b \Delta T}{\bar{I}_T(\bar{\alpha}\,\bar{\tau})A_r\bar{\phi}} = \frac{C_b \Delta T}{\overline{S}A_r\bar{\phi}} = \frac{NC_b \Delta T}{Q_D} \tag{10.83}$$

where C_b is the effective thermal capacitance; ΔT_b is the difference in the upper and lower temperatures; and Y is dimensionless. $\bar{\phi}$ can be calculated from Eq. (10.77).

Objective Questions

10.1 The optimum temperature of thermal comfort in the winter/summer is
      (a) 0 °C   (b) 20 °C   (c) 25 °C   (d) 15 °C.
      Answer: (b)

10.2 The primary and dominant factors for thermal comfort are
      (a) air temperature   (b) relative humidity   (c) air movement   (d) all of these
      Answer: (d)

10.3 The additional factors for thermal comfort are
      (a) nutritional intake (food)   (b) occupancy and age   (c) sex   (d) all of these
      Answer: (d)

10.4 The secondary and imaginary factors for thermal comfort are
      (a) time of day/season   (b) psychological factor   (c) day lighting   (d) all of these
      Answer: (d)

10.5 The rate of heat produced by a healthy person during sleep is
      (a) 60 W   (b) 600 W   (c) 6 W   (d) none of these
      Answer: (a)

10.6 The rate of heat produced by a healthy person during hard work is
      (a) 60 W   (b) 6 W   (c) 600 W   (d) none of these
      Answer: (c)

10.7 A person feels more cold in winter and warm in summer in old age due to
      (a) an increase of metabolic rate   (b) a decrease of metabolic rate
      (c) a decrease in nutritional intake   (d) both (b) and (c)
      Answer: (d)

10.8 The maximum rate of heat release by the human body occurs by
     (a) evaporation   (b) convection   (c) radiation   (d) none
     Answer: (a)

10.9 The rate of heat release by the human body by evaporation

     (a) increases with surrounding air temperature
     (b) decreases with surrounding air temperature
     (c) is unaffected by surrounding air temperature
     (d) none of these

     Answer: (b)

10.10 The optimum recommended values of relative humidity for thermal comfort
      is
      (a) 25 %   (b) 50 %   (c) 100 %   (d) 75 %
      Answer: (b)

10.12 The temperature of the body remains constant and is given by
      (a) 37 °C   (b) 47 °C   (c) 17 °C   (d) none of these
      Answer: (a)

10.13 The optimum level of carbon dioxide in atmosphere should be
      (a) 320 ppm   (b) 640 ppm   (c) 180 ppm   (d) none of these
      Answer: (a)

10.14 The optimum level of illumination for the eyes due to day lighting is
      (a) 500 lx   (b) 1000 lx   (c) 250 lx   (d) none of these
      Answer: (a)

10.15 The conversion factor from $1 W/m^2$ to lux is
      (a) 100   (b) 1000   (c) 750   (d) 10
      Answer: (a)

10.16 The climatic condition of India is classified into
      (a) 3 climates   (b) 6 climates   (c) 12 climates   (d) 5 climates
      Answer: (b)

10.17 The solair temperature for a horizontal bare surface depends on
      (a) solar intensity   (b) ambient air temperature
      (c) long-wavelength radiation exchange between ambient and sky
      (R)   (d) all of these
      Answer: (d)

10.18 For a vertical wall, the long-wavelength radiation exchange between
      ambient and sky is
      (a) zero   (b) one   (c) $60 W/m^2$ (d) none of these
      Answer: (a)

10.19 For a blackened and glazed surface, the long-wavelength radiation
      exchange between ambient and sky is
      (a) one   (b) $60 W/m^2$ (c) zero   (d) none of these
      Answer: (c)

10.20 The solair temperature is maximum in the case of
       (a) a bare surface   (b) a wetted surface
       (c) a blackened and glazed surface   (d) a reflecting surface
       Answer: (c)
10.21 The solair temperature is minimum in the case of
       (a) a bare surface   (b) a reflecting surface
       (c) a wetted surface   (d) a blackened and glazed surface
       Answer: (c)
10.22 The rate of net useful gain per m^2 is maximum in the case of
       (a) a direct gain   (b) an indirect gain   (c) an isolated gain   (d) none of
       these
       Answer: (a)
10.23 The overall heat-transfer coefficient (U_L) is maximum in the case of
       (a) a wetted surface   (b) a blackened and glazed surface
       (c) a bare surface   (d) none of these
       Answer: (a)
10.24 For thermal heating through Earth–air heat exchanges, the heat gain is
       (a) positive   (b) negative   (c) zero   (d) none of these
       Answer: (a)
10.25 The time constant of a building is
       (a) inversely proportional to heat capacity   (b) proportional to heat
       capacity
       (c) constant   (d) none of these
       Answer: (b)
10.26 The solar-saving faction (f_{ns}) is
       (a)>1   (b) <1   (c) zero   (d) none of these
       Answer: (b)

Problems

10.1   Name the three most important parameters to determine thermal comfort.
       Hint: Use Fig. 10.1.
10.2   What is the unit of illumination?
       Hint: Lux, 1 lx $= 10^{-2}$ W/m^2.
10.3   Determine U value for a multi-layered exposed wall for the following given
       specifications:

$$L_1 = L_2 = L_3 = 5\,\text{cm}, \; K_1 = K_2 = K_3 = 0.67\,\text{W/m}\,^\circ\text{C}, \; h_i$$
$$= 5.7\,\text{W/m}^2\,^\circ\text{C}, \text{ and } h_o = 9.5\,\text{W/m}^2\,^\circ\text{C}.$$

10.4   Determine the U value for the following wall configurations:

   (a) glass wall: $L_g = 5\,\text{mm}$, $K_g = 0.78\,\text{W/m}\,°\text{C}$
   (b) brick wall: $L = 15\,\text{cm}$, $K = 0.67\,\text{W/m}\,°\text{C}$
   (c) glazed brick wall: $L = 15\,\text{cm}$, $K = 0.67\,\text{W/m}\,°\text{C}$
   (d) water wall: $h_1' = h_2' = 100\,\text{W/m}^2\,°\text{C}$
   (e) transwall: $h_1 = h_1' = h_2 = h_2' = 100\,\text{W/m}^2\,°\text{C}$

   $h_o = 15\,\text{W/m}^2\,°\text{C}$ for a bare wall and $7\,\text{W/m}^2\,°\text{C}$ for a glazed wall and $h_i = 5.7\,\text{W/m}^2\,°\text{C}$.
   Hint: Use Eqs. (10.11), (10.17), (10.19), and (10.32).

10.5   Determine the total heat-transfer coefficient (h_1) for a wetted surface at temperature $35\,°\text{C}$ and exposed to ambient air temperature of $32\,°\text{C}$ and relative humidity of 50 %.

$$P(T) = \exp\left(25.317 - \frac{5144}{T + 273}\right)$$

   Hint: Given $\varepsilon_1 = \varepsilon_2 = 0.9$, $\sigma = 5.67 \times 10^{-8}\,\text{W/m}^2\text{K}^4$,   and $h_{ca} = 2.8\,\text{W/m}^2\,°\text{C}$; see Example 10.1

10.6   Determine the solair temperature for a wetted and glazed roof for $I(t) = 300\,\text{W/m}^2$ given $\alpha(\text{wetted}) = 0.9$, $\alpha\tau(\text{glazed}) = 0.8$
   Hint: Take h_1 for a wetted surface from problem 10.5 and U_t for a glazed surface from Example 10.2.

10.7   Calculate the rate of heat lost from a room maintained at $20\,°\text{C}$ through different walls of Problems 10.3 and 10.4 exposed to an ambient air temperature of $10\,°\text{C}$.
   Hint: Use $\dot{q} = U(20 - 10)$.

10.8   Determine the net rate of energy saved through different walls of Problems 10.3 and 10.4 exposed to an average solar intensity of $350\,\text{W/m}^2$ for a duration of 8 h given $\alpha = \tau = 0.9$, $T_b = 20\,°\text{C}$, $T_a = 10\,°\text{C}$.
   Hint: See Example 10.2.

10.9   Write down an expression for an overall heat-transfer coefficient for a double-glazed wall with an air gap of air conductance C.
   Hint: $U = \left[\frac{1}{h_o} + \frac{L_{g1}}{K_{g1}} + \frac{1}{C} + \frac{L_{g2}}{K_{g2}} + \frac{1}{h_i}\right]^{-1}$

10.10 Derive an expression for the rate of net heat transferred into a room having a south wall as a water wall or brick wall.
   Hint: See Sects. 10.7.1.

References

 1. E.L. Morse, US Patent, 1881, 246, 626
 2. F. Trombe, US Patent, 3, 832, 992, 1972
 3. F. Trombe, Maison Salaires Techniques de Inginiear **3**, 777 (1974)
 4. B. Agrawal, G.N. Tiwari, *Building Integrated Photovoltaic Thermal Systems* (RSC Publishing, UK, 2010)
 5. G.N. Tiwari, A. Kumar, M.S. Sodha, Energy Convers. Manag. **22**(2), 143 (1982)
 6. G.N. Tiwari, V. Singh, P. Joshi, Shyam, A. Deo, Prabhakant, A. Gupta, Open Environ. Sci. **8**, 18 (2014)
 7. P.J. Rosado, D. Faulkner, D.P. Sullivan, R. Levinson, Energy Build. **80**, 57 (2014)
 8. A.R. Gentle, J.L.C. Aguilar, G.B. Smith, Sol. Energy Mater. Sol. Cells **95**(12), 3207 (2011)
 9. M.S. Sodha, A. Kumar, U. Singh, G.N. Tiwari, Appl. Energy **7**(4), 305 (1980)
10. M.S. Sodha, U. Singh, A. Srivastava, G.N. Tiwari, Build. Environ. **16**(2), 93 (1981)
11. M. Zinzi, S. Agnoli, Energy Build. **55**, 66 (2012)
12. J.D. Balcomb, R.W. Jones, R.D. McFarland, W.O. Wray, Passive Solar J. **1**, 67 (1983)

Additional References

13. S.C. Kaushik, G.N. Tiwari, J.K. Nayak, *Thermal Control in Solar Passive Building* (Indian Academy of Sciences, Bangalore, 1987)
14. B. Givoni, Energy Build. **1**(2), 141 (1977)

Chapter 11
Solar Cooling

Abstract A flat-plate collector, if operated at low temperature by using working fluid refrigerant, is known as a "solar-cooling device." The concepts of vapor absorption and compression (refrigeration) are used. This device is used for household refrigerators and air conditioning, etc. Solar collectors are the main part that heats the working fluid.

Keywords Solar cooling technology · Solar air conditioning · Solar photovoltaic cooling · Instantaneous efficiency · Overall system efficiency

11.1 Introduction

Solar cooling has the following advantages:

- It saves the conventional primary energy source based on electricity.
- It leads to a reduction of peak electricity demand for cost saving.
- It is environmentally sound without ozone depletion to sustain global warning.
- The demand and supply matches, i.e., the hottest period has sufficient maximum solar energy.

Solar energy is used in cooling cycles for the following cases:

(i) **Thermal-comfort cooling**:

In hot climates, thermal-comfort cooling is important for space conditioning of buildings. The feasibility of solar insolation and cooling load exists nearly in a similar phase. Solar air conditioning can be attained by (a) absorption cycles, (b) desiccant cycles, and (c) solar-mechanical processes. A continuous or intermittent cycle, hot- or cold-side energy storage, diverse control strategies, various temperature ranges of operation, different collectors, etc., can be possible under the above-mentioned categories. Theoretically, numerous thermal efficiencies of solar-cooling processes can be achieved. The temperature constraints of a mechanism of solar collectors restricts their thermal efficiencies. Compared with the

provision of additional cooling, minimization of cooling loads through cautious building design and insulation are much cheaper, which makes them more preferable (Chap. 10). Proficient design and construction of a building can minimize the load on any air-conditioning or heating system, but we are concerned about cooling loads that should really be considered in an effective building design.

(ii) **Refrigeration cooling**:

Refrigeration is a process in which work is carried out to convey heat from one point to another. The conveyance of heat is done by mechanical work. Refrigeration has numerous applications such as household refrigerators, industrial freezers, cryogenics, and air conditioning.

Refrigeration cyclic can be categorized as follows: a vapor cycle and a gas cycle.

Vapor cycle refrigeration can further be categorized as follows:

(I) Vapor-compression refrigeration
(II) Vapor-absorption refrigeration.

11.2   Solar Air Conditioning

Different aspects of solar air-conditioning will be discussed in the following sections.

11.2.1   Solar-Absorption Process [1]

The solar-absorption process utilizes the difference in the binding of a fluid, known as a "refrigerant," into two vessels at different temperatures. The fluid (refrigerant) can be bound by a liquid or a solid solvent known as an "absorbent." The solar-absorption process takes place as follows:

The solar-absorption process is shown in Fig. 11.1. Vessel I contains the refrigerant (R) bound with the absorbent (A), and vessel II contains the pure refrigerant. The valve between the two vessels is closed for the same temperature. The vapour pressure in vessel II will be higher than that in vessel I ($P_{II} > P_I$ with $T_I = T_{II}$). If the valve opens, the refrigerant gas flows from vessel II to I vessel due to the existing pressure difference. The vapour pressure in I becomes higher than the equilibrium vapour pressure, and the vapour condenses in it. The temperature in vessel I increases due to the latent heat of condensation. The reverse process taking place in vessel II decreases its temperature.

Due to mass transfer from vessel II to vessel I, the vapour pressure tends to equalize in the two vessels. This causes a temperature difference between them ($P_I = P_{II}$ with $T_I > T_{II}$). Now the heat is supplied to the cold vessel II from the surroundings, and the pressure equilibrium is disturbed. The vapour pressure in

Fig. 11.1 Basic working
principle of the absorption
process
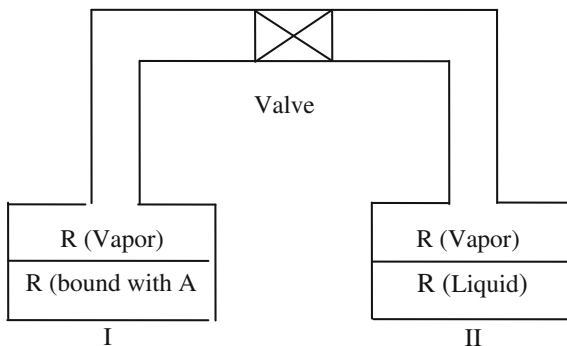
vessel II exceeds the vapour pressure in vessel I, which causes mass transfer from vessel II to vessel I; hence, the flow of heat/thermal energy from vessel II to I. Thus, heat is transferred (pumped) from the lower temperature of vessel II to the higher temperature of vessel I. The absorption process may be utilized for the following:

(a) **For cooling**: In this case, the cold vessel takes the heat from the surrounding; or
(b) **For heating**: In this case, the heat developed in the warm vessel is utilized.

The heat-pumping ability of the device is thus consumed; to restore it, the system must be regenerated by reversing the mass transfer/heat transfer from vessel I to vessel II. In between the phases of heat pumping and regeneration, energy can be stored. Therefore, an absorption process has three main characteristics viz. cooling, heating, and energy storage. The success of the absorption process depends on the selection of a suitable pair of refrigerant and absorbent.

The selection of suitable pair of refrigerant and absorbent is generally based on the following criteria:

(i) Chemical and physical properties of the fluid; and
(ii) Acceptable range in particular for the thermo-physical and thermodynamic properties of the fluid.

For an absorption system, the preferable features of a refrigerant/absorbent mixture are (i) low viscosity of the solution under operating conditions to minimize the pump work; (ii) freezing point of the liquid lower than the lowest temperature in the cycle; (iii) good chemical thermal stability; and (iv) noncorrosive, nontoxic, and nonflammable components.

The thermodynamic properties of the solutions of refrigerant and absorbent are critical in determining its suitability for absorption systems. The combination of refrigerant and absorbent should satisfy two primary thermodynamic requirements: (a) high equilibrium solubility of the refrigerant in the absorber; and (b) a larger difference in boiling points of the absorbent and the refrigerant. The combinations of lithium–bromide–water ($LiBr–H_2O$) and ammonia–water ($NH_3–H_2O$) are often used. Solar energy-based absorption coolers can operate in two ways: (i) the use of

continuous coolers having the same construction and operation as conventional gas or steam-fired units (in this case, energy supplied to the generator from the solar-collector/storage auxiliary system); and (ii) the use of intermittent coolers. A diagram of one of the possible arrangements for continuous-absorption cycles is shown in Fig. 11.2.

Temperature limitations of flat-plate collector limit the consideration of commercial machines for lithium–bromide–water (LiBr–H_2O) systems. The principle advantages of lithium–bromide–water (LiBr–H_2O) systems are as follows:

(i)   Water as a refrigerant has a very high latent heat of vaporization.
(ii) The absorbent is nonvolatile.
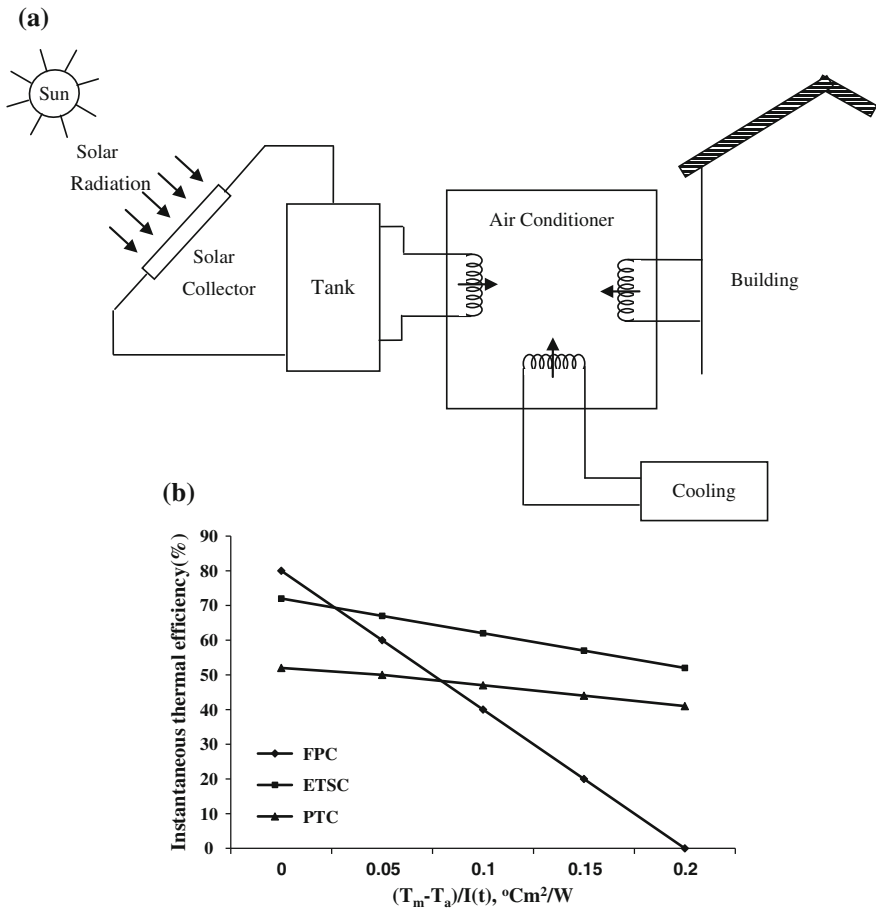
Fig. 11.2 a Schematic diagram of a solar-absorption air-conditioning system with a flat-plate collector (FPC) [1]. **b** Characteristic curve of (i) a flat-plate collector (FPC) with a selective surface, (ii) concentrating solar collectors (CSC), and (iii) an evacuated tubular collectors (ETC) [2]

(iii) Lithium–bromide–water (LiBr–H$_2$O) systems operate at low pressure and hence have a low pumping-power requirement.

(iv) The material is nontoxic and nonflammable.

Lithium–bromide–water (LiBr–H$_2$O) machines require water to cool the absorber and condenser, and in most of the applications a cooling tower is required. The disadvantage of using water as the refrigerant is that a water-cooled condenser is required to attain temperatures corresponding to those of air conditioning. The temperatures corresponding to refrigeration cannot, however, be reached even with a water-cooled condenser. This is due to the fact that LiBr is not sufficiently soluble in water to permit the absorber to be air-cooled. The combination is corrosive to the materials of construction of the cycle (hydrogen, which is the product of the corrosion reaction, increases the system pressure and hence decreases the efficiency of the cycle). In addition, during the system operation the combination produces salt crystallization and thus cannot be used for a long period. Ammonia–water (NH$_3$–H$_2$O) system is mostly used for industrial absorption air conditioning and refrigeration.

Solar-assisted desiccant-cooling systems generally use the solar thermal flat-plate collector (FPC) with a selective-surface/concentrating-collector/evacuated tubular solar collector (ETSC) as a heating system. The solar thermal system consists of a solar flat-plate collector (FPC)/concentrating collector with a selective-surface/evacuated tubular solar collector (ETSC) using water as the fluid and an insulated water storage tank operating under forced mode to increase exploitation of the solar energy. However, to connect the solar and air systems together, a supplementary water/air heat exchanger is needed.

The thermal instantaneous efficiency of a solar flat-plate collector (FPC) with a selective-surface/concentrating collector/evacuated tubular solar collector (ETSC) [2] can be defined as follows:

$$\eta_{i,th} = \eta_o - a_1 \frac{(T_m - T_a)}{I(t)} - a_2 \frac{(T_m - T_a)^2}{I(t)} \tag{11.1}$$

where η_o is the optical instantaneous efficiency. It is given by

$\eta_o = (\alpha\tau)$ selective coated flat-plate collector (FPC)

$\quad = (\rho\alpha\tau)$ concentrating solar collector (CSC)/parabolic-trough concentrator (PTC)

$\quad = [(\alpha\tau)(1 - \rho)]$ evacuated tubular solar collector (ETSC)

where α, τ and ρ are the absorptivity, transmissivity, and reflectivity of respective selective absorber, glazing, and reflective surfaces; T_{fo}, T_{fi} and T_a are the outlet, inlet fluid, and ambient air temperatures, respectively; and $I(t)$ is the incident solar radiation on an inclined surface at latitude = 30° [Chap. 1].

Table 11.1 Numerical values of η_o, a_1 and a_2

Parameters	FPC	CSC (PTC)	ETC	Units
η_o	0.79	0.52	0.720	Nil
a_1	3.94	0.475	0.974	W/m^2 K
a_2	0.012	0.0031	0.005	W/m^2 K

Furthermore,

$$T_{\mathrm{m}} = T_{\mathrm{fi}} + \frac{(T_{\mathrm{fo}} - T_{\mathrm{fi}})}{2} = \frac{(T_{\mathrm{fo}} + T_{\mathrm{fi}})}{2}$$

The numerical values of η_o, a_1, and a_2 are given in Table 11.1. The value of a_2 plays an important role at a high operating temperature; otherwise one can consider it as zero.

The variation of instantaneous thermal efficiency of (i) a solar flat-plate collector (FPC) with a selective surface, (ii) a concentrating collector, and (iii) an evacuated tubular solar collector (ETSC) with $\frac{(T_{\mathrm{fi}} - T_{\mathrm{a}})}{I(t)}$ is shown in Fig. 11.2b.

An overall instantaneous thermal efficiency of a solar-cooling system can be defined as the ratio of the specific cooling effect (q_0) to the incident solar radiation. This can be expressed as follows:

$$\text{Overall System Efficiency (OSE)} = \frac{q_0}{I(t)} \tag{11.2}$$

The above OSE can be calculated for a specific time period, e.g., 1 day, 1 month, or 1 year.
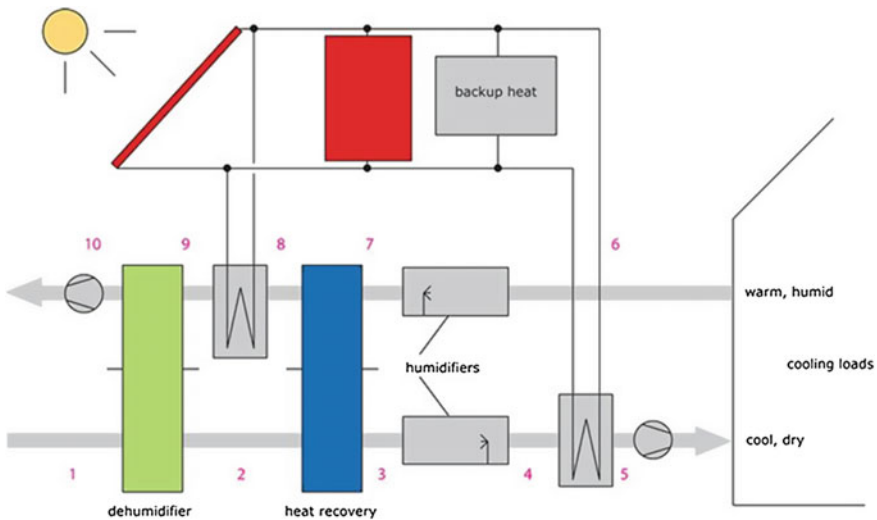
Fig. 11.3 A schematic diagram of a solar desiccant-cooling system

Equation ([11.2](#)) can also be rewritten as

$$\text{OSE} = \frac{q_0}{q_{\text{thi}}} \frac{q_{\text{thi}}}{I(t)} \tag{11.3}$$

where q_{thi} is the thermal energy obtained from either (i) the solar flat-plate collector (FPC) with a selective surface; (ii) a solar-concentrating collector or (iii) an evacuated tubular solar collector (ETSC), which is the input to drive the chiller.

The term $\text{TR} = \frac{q_0}{q_{\text{thi}}}$ is defined as the thermal ration between the cooling effect and the input thermal power. The TR can be also referred as the "coefficient of performance" (COP).

Equation ([11.3](#)) can be expressed as

$$\text{OSE} = \text{TR} \times \eta_{\text{i,th}} = \text{COP} \times \eta_{\text{i,th}} \tag{11.4}$$

Example 1.1 Determine the optical efficiency (η_{o}) of a solar flat-plate collector and an evacuated tubular solar collector (ETSC) for $\alpha = 0.9$, $\tau = 0.9$, and $\rho = 0.6$.

Solution
From Eq. ([11.1](#)) we have

$\eta_{\text{o}} = \alpha\tau = 0.9 \times 0.9 = 0.81 \text{ for a solar flat}-\text{plate collector}$
$\eta_{\text{o}} = \rho\alpha\tau = 0.6 \times 0.9 \times 0.9 = 0.486 \text{ for a solar}-\text{concentrating collector}$
$\eta_{\text{o}} = \alpha\tau(1 - \rho) = 0.9 \times 0.9 \times 0.4 = 0.329 \text{ for an evacuated tubular solar collector}$

One can see that η_{o} is lowest for an evacuated tubular solar collector (ETSC).

Example 1.2 Write down an expression for an instantaneous thermal efficiency of a solar flat-plate collector/evacuated tubular solar collector/parabolic-trough solar concentrator at a low operating temperature.

Solution
At a low operating temperature, the numerical value of a_2 will be negligible; hence, Eq. ([11.1](#)) reduces to

$$\eta_{\text{i}} = \eta_{\text{o}} - a_1 \frac{(T_{\text{m}} - T_{\text{a}})}{I(t)}$$

which is similar to the characteristic equation (Eq. ([5.81](#))) known as the HWB equation.

11.2.2   Solar-Desiccant Cooling

Solar-desiccant cooling is an open-cycle system in which water acts as a refrigerant and is in direct contact with air unlike the solar-absorption process. The water is easily available. A combination of evaporative cooling with air dehumidification using a desiccant (a hygroscopic material) constitutes the thermally driven cooling. A liquid or solid material can be used for this. The term "open" signifies that the refrigerant is not reused after accomplishing the cooling effect. Therefore, water is the only possible medium that can act as a coolant with direct contact to the neighbouring air for evaporation. Currently frequently applied technology uses rotating desiccant wheels equipped either with silica gel or lithium–chloride (Li–Cl) as sorption material.

There are two type of solar-desiccant cooling, which will be discussed as follows:

(a) **Solid-desiccant cooling**

The principle components of a solar-assisted **solid-desiccant cooling** system are given in Fig. 11.3. The basic working principle is given below.

Warm and humid air is passed above the slowly revolving desiccant wheel where it is dehumidified due to the adsorption of water (1 and 2). The hot air is then passed through the heat-recovery wheel (2 and 3) where it is cooled. This precooled air is fed to the humidifier and further cooled and humidified up to the desired value of humidity and temperature (3 and 4). Now the cool, dried air is fed inside the building. The warm, humid air from the room is passed through the humidifier (6 and 7) and humidified to the saturation level to utilize the maximum cooling potential. Then it is fed to the heat-recovery unit (7 and 8). Thereafter this air is passed through the dehumidifier (9 and 10) and exited. For continuous operation of the cooling process, the sorption unit is regenerated by heating it in a low temperature range (50 °C–75 °C).

For critical outdoor weather conditions, such as high-humidity weather for coastal areas, one needs an advanced design of desiccant cycle that is capable enough to reduce the humidity level up to a certain minimum level favourable for direct evaporative cooling. In this specific case, an extra heat-recovery wheel or additional air coolers can achieve the desired requirement. An innovative approach may be the simultaneous dehumidification (using sorptive coating on a heat-exchanger wall) and cooling of air (through returning humidified air) by using air-to-air heat exchanger. This approach improves the thermal efficiency of the system. The sorptive coating material becomes saturated after some time; hence, two such heat exchangers can be used intermittently with one in operation and the other regenerated (i.e., ready to use if one becomes saturated).

(b) **Liquid-desiccant cooling**

A liquid desiccant-cooling system is a novel technology in which a liquid water–lithium chloride (H_2O–Li–Cl) solution is used as sorption material. Such systems have numerous benefits as follows:

 (i) It has higher air dehumidification compared with a solid-desiccant cooling system for the same temperature range.
(ii) It has a higher energy-storage capacity with concentrated solutions.

   For air conditioning, based on solar thermal systems, **liquid-desiccant cooling** can raise the utilization of solar thermal systems significantly.

11.2.3 *Solar Mechanical Cooling*

There is another cooling method that involves the coupling of a solar-powered Rankine-cycle engine with a conventional air-conditioning system. The major limitations of a solar-assisted conventional air-conditioning system include (i) the production of mechanical energy from solar energy; and (ii) the modification of an existing air-conditioning system for variable-load operation.

   A simple Rankine-cycle cooling system is presented in Fig. 11.4. The heat engine in this cooling system produces mechanical work by utilizing the thermal energy available in insulated storage water tank through a heat exchanger. It is a well-known fact that the efficiency of solar thermal systems decreases with increasing temperature, which is in contrast to the heat engine where higher temperatures result in higher efficiency. A typical variation of solar thermal collector efficiency versus engine efficiency with temperature is shown in Fig. 11.5a. The overall system efficiency is shown in Fig. 11.5b.
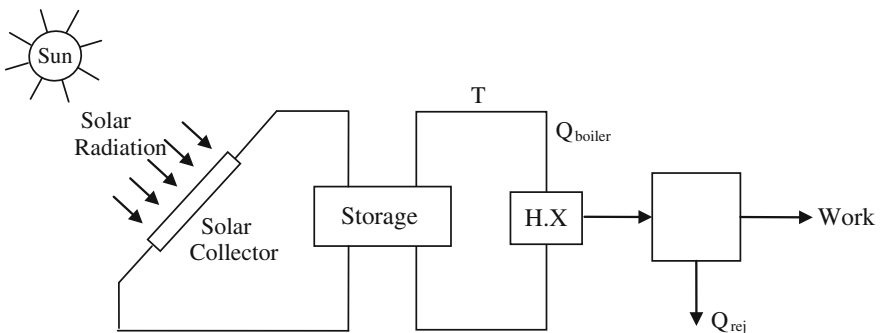
Fig. 11.4 Schematic of a solar-operated rankine cycle cooler
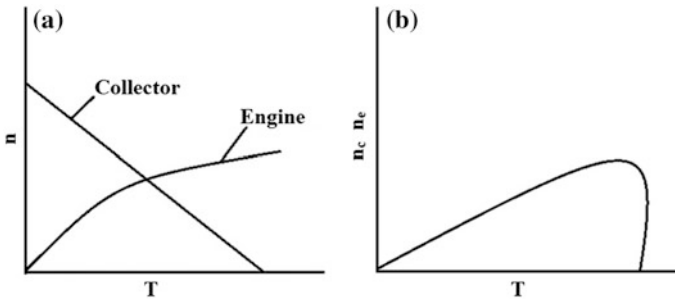
Fig. 11.5 Solar thermal collector and power-cycle efficiencies as a function of **a** operating temperature and **b** overall system efficiency

11.2.4 Solar Photovoltaic Cooling

Solar photovoltaic is used to provide electrical power to a absorption/adsorption-based vapour compressor as shown in Fig. 11.6a. In the absorption/adsorption-based vapour compressor process, energy is transferred through a phase-change process. For small residential/commercial cooling (≤ 5 MWh/year), solar photovoltaic-power cooling is the most suitable/successful solar cooling technology. The reason for this may be the incentive provided by government agencies. The cost of solar photovoltaic-power cooling effectiveness mainly depends on the cooling system and the use of electrical processes. Partially replacing the grid supply for air conditioning with PV systems can be significantly cost-effective. This also limits carbon emission in the atmosphere.

Vapor-compression refrigeration system
A circulating liquid (refrigerant) is used in the **vapor-compression refrigeration system**. The refrigerant works as a medium that absorbs the heat from the space to be cooled and discards that heat somewhere else. Figure 11.6b shows a typical single-stage vapor-compression system that has four components: (i) a vapour compressor, (ii) a condenser, (iii) a thermal-expansion valve (throttle valve), and (iv) an evaporator. The circulating refrigerant first enters the vapour compressor (i) in the thermodynamic state known as "saturated vapor." [2] It is then compressed to a higher pressure, which causes an increase in temperature. In a thermodynamic state, the hot and compressed vapor is known as "superheated vapour." The superheated vapour is allowed to pass through the condenser, and (ii) cool water or cool air streaming across the coil or tubes can make the saturated heat condensed into a saturated liquid flowing by way of the same coil or tubes. The rejected heat from the condenser is carried away by either the water or the air. This route is considered as the high-pressure side (hot refrigerant) as shown in Fig. 11.6a. In solar-assisted refrigeration systems, the electricity provided to the compressor is met by photovoltaic (PV) systems.
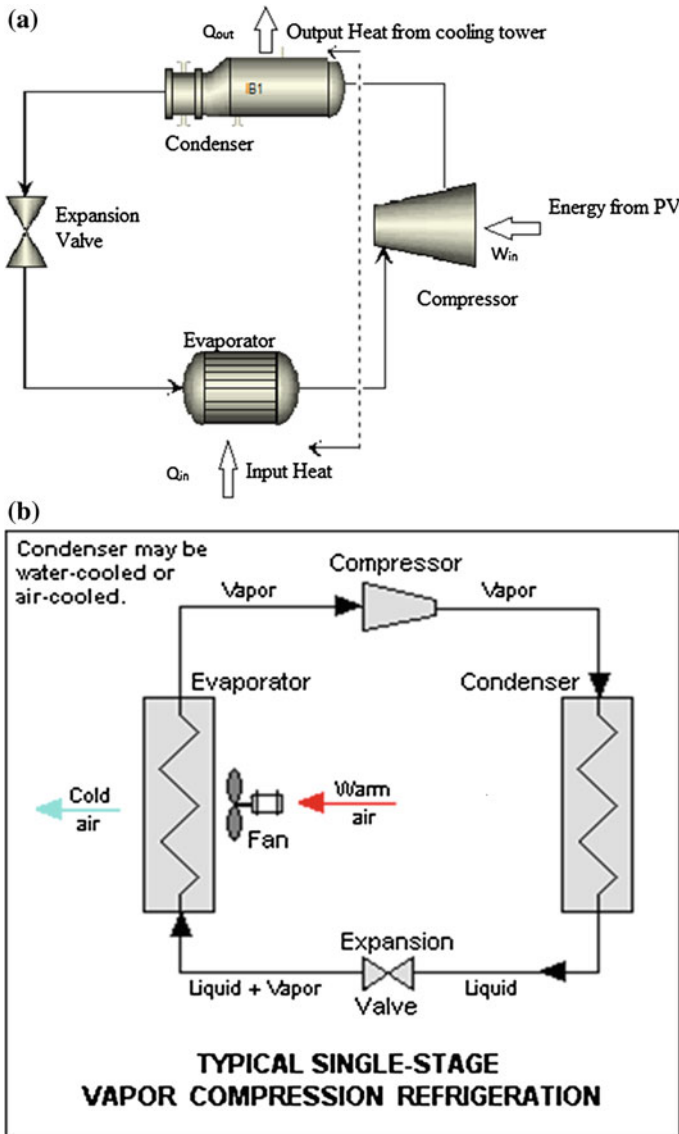
Fig. 11.6   a Schematic diagram of solar photovoltaic cooling. **b** Vapor compression-refrigeration system

The condensed liquid refrigerant, after condensation, is known as "saturated liquid" in the thermodynamic state. The saturated liquid is next allowed to pass through an expansion valve (iii) for an abrupt reduction in pressure. Due to pressure reduction, one obtains the following:

(i)   A part of the liquid refrigerant is evaporated.
(ii)   It lowers the temperature of the vapor–liquid mixture by the auto-refrigeration effect of the adiabatic flash evaporation.
(iii) The vapour–refrigerant liquid mixture is cooler than the temperature of the living space (v) in the building to be cooled.

The cold mixture moves through the coil or tubes in the evaporator (iv). The warm air is circulated by a fan in the enclosed room air (v) to be cooled across the coil or tubes carrying the cold refrigerant liquid–vapor mixture. That warm air from the enclosed room of a building evaporates the liquid part of the cold refrigerant mixture in the coil of evaporator. Instantly the circulating air becomes cooler and hence lowers the temperature of the enclosed room to the desired temperature.

For completing the refrigeration cycle, the refrigerant vapor from the evaporator (iv) is again a saturated vapour and is further allowed to pass through the vapour-compressor (i).

In this case, an electrical efficiency of crystalline silicon solar cell (η_e) of PV [2] module can be considered as

$$\eta_e = \eta_o \left[1 - \beta_0(T_c - T_0) - \frac{\beta_0 \alpha \tau I(t)}{U_L} \right] \tag{11.5}$$

where η_o is an electrical efficiency of the crystalline silicon solar cell under standard test conditions with T_0 as the reference temperature. The values of β_0 is $0.0045 \, \text{K}^{-1}$. $U_L = 20 \, \text{W/m}^2 \, ^\circ\text{C}$ is a total overall heat-transfer coefficient from solar cell to the ambient air through the top and bottom of the solar cell.

For a PV-operating cooling system, Eq. (11.2) can be written as

$$\text{Overall System Efficiency (OSE)} = \frac{q_0}{E} \frac{E}{I(t)} \tag{11.6}$$

where E is the electrical output of the PV system used as input to drive the chiller unit.

Furthermore, Eq. (11.6) can also be written as

$$\text{Overall System Efficiency (OSE)} = \text{COP} \times \eta_e \tag{11.7}$$

where η_e is given by Eq. (11.5); and COP is the coefficient of performance of the chiller unit.

11.2.5 *Difference Between Basic Vapour Compression and the Absorption Cooling Cycle*

The vapour-compression system, as shown in Fig. 11.6, is an electrically driven compressor based on a photovoltaic system, whereas in case of absorption cooling,

an electrically driven compressors based on a photovoltaic system is replaced by a chemical cycle taking place between the absorber, the pump, and the regenerator [3].

Basically, instead of compressing the refrigerant vapour in compression cycle, the absorption cycle dissolve as follows:

(i)   The vapour in a liquid known as the "absorbent."
(ii) The cycle can pump the liquid to a high pressure with much less work input compared with a vapour compressor.
(iii) Heat input is used to evaporate part of the liquid into refrigerant vapour.

Hartmann et al. [4] investigated the investment cost for solar thermal and solar electrical heating and cooling in Freiburg in Germany. They observed that the primary energy saving was 36 %. Corresponding to 36 % primary energy saving, the optimized solar thermal and solar electrical systems are as follows:

(i)   The optimum solar thermal collector area is 160 m^2 with a storage tank of 40 l/m^2.
(ii) There is a photovoltaic module of 24 m^2.

The cumulated investment cost for a solar electric system is 73 % lower than that of a solar thermal system because of the low-utilization factor and low COP of solar thermal system.

11.3 Comparison of Different Solar Cooling Technologies

In this section, a comparison of performance the following solar based-cooling technologies will be discussed as follows:

(i)   Selective solar flat-plate collector (FPC);
(ii) Parabolic-trough collector (PTC);
(iii) Evacuated tubular solar collector (ETC); and
(iv) Photovoltaic (PV) collector (Fig. 11.6).

The performance of these technologies was carried out by Lazzarin [2] for the following **constant-collection temperature** conditions:

(a) Adsorption at 70 °C.
(b) Single-effect absorption at 90 °C.
(c) Double-effect absorption at 160 °C.
(d) GAX ammonia-absorption air cooled at 160 °C.

Here it important to note that to maintain a **constant-collection temperature** for a given hourly variation of climatic condition (solar intensity and ambient air temperature), the mass flow rate should be varied to determine the daily useful thermal energy (kWh/m^2/day) given in Table 11.2.

Table 11.2 The daily useful thermal energy $(kWh/m^2/day)$ available at different operating constant temperatures

Temperature (°C)	Selective FPC	Parabolic trough concentrator (PTC)	Evacuated tubular collector (ETC)	Unit
70	3.63	4.50	3.34	$kWh/m^2/day$
90	2.98	4.29	3.23	$kWh/m^2/day$
160	0.89	3.54	2.87	$kWh/m^2/day$

The analytical expression for a variable mass-flow rate as a function of time can be obtained by considering $T_{foN} = T_0$. The expressions are as follows:

$$\dot{m}_f = -\frac{NF'A_c U_L}{C_f} \left[\ln \frac{T_0 - \left(\frac{\dot{q}_{ab}}{U_L} + T_a \right)}{T_{fi} - \left(\frac{\dot{q}_{ab}}{U_L} + T_a \right)} \right]^{-1} \tag{11.8}$$

For selective FPC (Eq. (5.88b))

$$\dot{m}_f = -\frac{NF'A_r U_L}{C_f} \left[\ln \frac{T_0 - \left(\frac{A_a}{A_r} \frac{S}{U_L} + T_a \right)}{T_{fi} - \left(\frac{A_a}{A_r} \frac{S}{U_L} + T_a \right)} \right]^{-1} \tag{11.9}$$

For parabolic-trough concentrators (Eq. (6.29c))

$$\dot{m}_f = -\frac{NF'A_r U_L}{C_f} \left[\ln \frac{T_0 - \left\{ \frac{\alpha(1-\rho)I(t)}{U_L} \frac{A_a}{A_r} + T_a \right\}}{T_{fi} - \left\{ \frac{\alpha(1-\rho)I(t)}{U_L} \frac{A_a}{A_r} + T_a \right\}} \right]^{-1} \tag{11.10}$$

For ETSC (Eq. (7.22c)).

Equations (11.8 through 11.10) can be used to calculate the daily useful thermal energy $(kWh/m^2/day)$ for each case as follows:

$$Q_{daily} = \sum \dot{m}_f(t) C_f (T_0 - T_{fi}) \times \frac{2.27 \times 10^{-7}}{N \times \text{area}} \text{ kW} \tag{11.11}$$

The values of $\dot{m}_f(t)$ can be obtained from Eqs. (11.8 through 11.10) for a given hourly variation of solar intensity and ambient air temperature. The results are summarised in Tables 11.2, 11.3 and 11.4.

Table 11.3 Coefficient of performance (COP) for different sorption technology

Different sorption technology	Coefficient of performance (COP)
Single effect adsorption (Li–Br), thermal energy	0.80
Double effect absorption (Li–Br), thermal energy	1.2
GAX NH_3 absorption air cooled, thermal energy	0.6
Adsorption, electrical energy (PV)	0.4

Table 11.4 Cost for different sorption technology per m^2 and per kW

Collector type	Cost/m^2 (ϵ/m^2)	Cost/kW (ϵ/kW)	Chiller
FPC	350	400	Single effect
PTC	450	300	Double effect
ETC	650	700	Vapor-compression
PV	650	600	Adsorption

Objective Questions

11.1 The optical instantaneous efficiency is maximal for
    (a) a concentrating solar collector   (b) a selective-coated FPC
    (c) a parabolic-trough concentrator   (d) an evacuated tubular solar collector (ETSC)
    Answer: (a) and (c)

11.2 The optical instantaneous efficiency is minimal for
    (a) a concentrating solar collector   (b) a selective-coated FPC
    (c) a parabolic-trough concentrator   (d) an evacuated tubular solar collector (ETSC)
    Answer: (d)

11.3 Instantaneous thermal efficiency is linear
    (a) at low operating temperature   (b) at high operating temperature
    (c) at ambient air temperature   (d) at all temperatures
    Answer: (a)

11.4 Instantaneous thermal efficiency is nonlinear
    (a) at low operating temperature   (b) at high operating temperature
    (c) at ambient air temperature   (d) at all temperatures
    Answer: (b)

11.5 The thermal ratio is equal to
    (a) the coefficient of performance (COP)   (b) the thermal efficiency
    (c) the electrical efficiency   (d) none of these
    Answer: (a)

11.6 Thermal ratio/coefficient of performance (COP) is
    (a) equal to the overall system efficiency (OSE)
    (b) higher than the overall system efficiency (OSE)

(c) lower than the overall system efficiency (OSE)

(d) none of these

Answer: (c)

11.7 The coefficient of performance (COP) of single-effect absorption (Li–Br) (thermal energy) is

(a) =1   (b) <1   (c) >1   (d) none of these

Answer: (b)

11.8 The coefficient of performance (COP) of double-effect absorption (Li–Br) (thermal energy) is

(a) =1   (b) <1   (c) >1   (d) none of these

Answer: (c)

11.9 The Cost of sorption technology is maximal for

(a) ETC   (b) PTC   (c) FPC   (d) PV

Answer: (a) and (d)

11.10 The Cost/m^2 of sorption technology is minimal for

(a) ETC   (b) PTC   (c) FPC   (d) PV

Answer: (c)

11.11 The Cost/kWh of sorption technology is minimal for

(a) ETC   (b) PTC   (c) FPC   (d) PV

Answer: (c)

Problems

11.1 Plot the curve between instantaneous thermal efficiency ($\eta_{i,th}$) and $\frac{(T_m - T_a)}{I(t)}$ for a_1.

Hint: Use Eq. (11.1), Table 11.1, and Fig. 11.2b.

11.2 Plot the curve between instantaneous thermal efficiency (η_i) and $\frac{(T_m - T_a)}{I(t)}$ for a_1 and a_2.

Hint: Use Eq. 11.1, Table 11.1, and Fig. 11.2b.

11.3 Compare the results of Problems 11.1 and 11.2 and discuss in brief.

11.4 Calculate the overall system efficiency (OSE) for different sorption technologies (Table 11.3).

Hint: Use Table 11.3 and the results of Problems 11.1 and 11.2.

11.5 Calculate the electrical efficiency of a crystalline solar cell (η_e) using the data of Chap. 4.

11.6 Plot the curve between $\dot{m}_f$ and $I(t)$ for FPC, PTC, and ETSC.

Hint: See chapters on FPC, PTC, and ETSC.

References

1. G.N. Tiwari, *Solar Energy: Fundamental, Design, Modelling and Applications* (Narosa Publishing House, New Delhi and CRC Press, New York, 2004)
2. R.M. Lazzarin, Int. J. Refrig **39**, 38 (2014)
3. CHP group, CIBSE, Annon, Absorption cooling, Data sheet 7, 2012

Additional Reference

4. N. Hartman, C. Glueck, F.P. Schmidt, Renew. Energy **36**(5), 1329 (2011)
5. A. Caglar, C. Yamali, Energy Build. **54**, 22 (2012)
6. X. Zhang, X. Zhao, J. Shen, X. Hu, X. Liu, J. Xu, Sol. Energy **97**, 551 (2013)
7. S. Ishaya, ASHRAE Trans. **116** part 2 (2010)

Chapter 12
Solar Crop Dryers

Abstract A solar crop dryer is used to reduce crop losses during in-season harvesting periods. A solar-dried crop is hygienic and preserves nutritional value. A solar crop dryer reduces drying time with protection from external disturbances such as rain and strong wind.

12.1 Importance of Solar-Drying

The primary requirement for survival of human beings is food after air and water. The Food and Agriculture Organization (FAO) estimated that >852 million people worldwide were undernourished in the year 2000–2002 [1]. The projected figure of the world's population is >7.6 billion up to the year 2020. Hence, agricultural production should be increased to meet the food demand of the fast-growing population across world. In the next 25 years, approximately 50 % more food must be produced, particularly in developing countries. The gap between the supply and demand for food can be challenged (i) by increasing crop/food productivity (ii) by controlling population growth (iii) by reducing food losses, or (iii) a combination of both. In this chapter, we will address the problem of decreasing food losses before/after harvesting using solar drying.

Solar drying of agricultural product is one of the important postharvest operations to save grain from postharvest losses. Solar drying is the process of removing moisture from produce to attain optimum moisture content for its long-term storage (Table 12.1).

Solar drying of crops helps with the following: (i) facilitating early or preharvest activities, (ii) planning the harvest season, (iii) providing long-term storage, (iv) fetching better returns for farmers, (v) maintaining the viability of seeds, (vi) selling a better-quality product, (vii) the handling, transport, and distribution of crops, and (viii) reduction of the requirement for storage space [2].

Table 12.1 Initial and final moisture contents and maximum allowable temperature for drying of some crops [26]

Sl. no.	Crop	Initial moisture content (%w.b.)	Final moisture content (%w.b.)	Maximum allowable temperature (°C)
1	Apple	80	24	70
2	Apricot	85	18	65
3	Bananas	80	15	70
4	Brinjal	95	6	60
5	Cabbage	80	4	55
6	Carrots	70	5	75
7	Cauliflower	80	6	65
8	Chilies	80	5	65
9	Corn	24	14	50
10	Garlic	80	4	55
11	Grapes	80	15–20	70
12	Green beans	70	5	75
13	Green peas	80	5	65
14	Guavas	80	7	65
15	Maize	35	15	60
16	Oil seeds	20–25	07–09	40–60
17	Okra	80	20	65
18	Onion	80	4	55
19	Paddy (parboiled)	30–35	13	50
20	Paddy (raw)	22–24	11	50
21	Pineapple	80	10	65
22	Potatoes	75	13	75
23	Pulses	20–22	09–10	40–60
24	Rice	24	11	50
25	Sweet potato	75	7	75
26	Tomatoes	96	10	60
27	Wheat	20	16	45

Conventional drying of agricultural products is an energy-intensive operation. For conventional drying processes, large amounts of energy are consumed by various industries. In developed countries, nearly 8–12 % of primary energy demand is consumed by drying purposes. The use of conventional sources of energy for drying agricultural products substantially affects the environment. The rise in the price of conventional fuels directly affects the market price of the products dried by using conventional sources of energy [3].

12.2 Solar Crop-Drying

Solar energy available in the terrestrial region can be converted into either thermal energy or DC electricity, or both, by photovoltaic (PV) cells. Solar crop-drying utilizes thermal energy available from the Sun for drying agricultural products. Solar crop-drying is categorized on the basis of the methodology for solar-energy collection and conversion of solar energy into useful thermal energy.

Open-Sun drying (OSD) was used for drying fruits, vegetables, and other products from ancient times. Worldwide a large share of dried products are dried using OSD without any advanced technology [4]. OSD, as adopted by a large number of farmers, has inherent challenges: (i) It requires a large space and more time for drying; (ii) it poses considerable loss due to rodents, birds, insects, microorganisms as well as hostile weather conditions, e.g., unexpected rain or storms; (iii) crops can be contaminated by foreign materials such as dust, dirt etc.; (iv) there is a risk of overdrying/insufficient drying as well as discoloring by UV radiation; (v) and there can be a degraded quality of dried products (due to the readsorption of moisture. Thus, OSD results in a product of degraded quality. If the quality of products is lower, then they are not marketable for their reference value [5–11].

Therefore, to overcome the limitations and disadvantages owing to OSD, a more advanced and controlled method of solar-energy harvesting was adopted for crop-drying. The advanced method is known as controlled solar drying; it uses a combination of a solar thermal energy-collection system and a drying chamber. Solar energy may be collected separately using (1) a solar thermal-collector unit and be fed to the drying chamber or (2) a solar thermal energy collection unit can also be integrated with the drying chamber in a single unit. Controlled solar drying is more efficient, healthier, more hygienic, faster, and more economical than OSD [12–15].

Figure 12.1 shows the classification of solar dryers. Solar dryers are differentiated on the basis of methods adopted for the collection of solar energy as thermal energy and the transfer of this thermal energy from the solar collector to the drying unit. Broadly there are two types of solar dryers, namely, passive solar dryer (utilizes natural convection for the transfer of thermal energy to the drying products) and active solar dryer (utilizes natural forced convection for transfer of thermal energy to the drying products).

In passive solar dryers, air inside the drying chamber receives thermal energy from the solar collector surface and transfers it to the adjacent layer of air due to the temperature gradient between layers. The hot air is circulated to the crop surface either due to buoyancy of the pressure difference or due to the combined effect of both. In active solar dryers, hot air from the solar thermal collector unit is circulated using external source such as fans or blowers. Furthermore, these dryers are classified into three major subgroups, namely, direct mode, indirect mode, and mixed mode [16, 17]. A solar thermal energy-collection unit is integrated to the roof or walls of the drying chamber in direct-mode type of solar dryers, whereas the solar
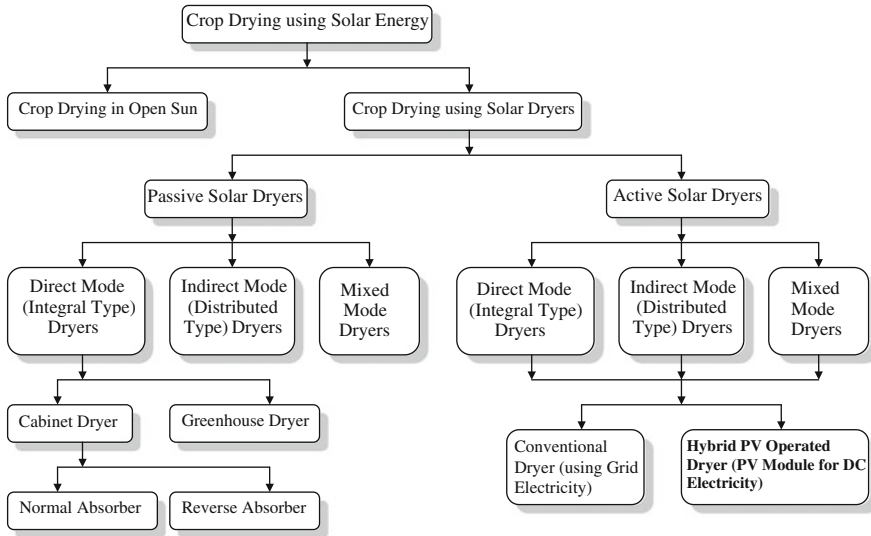
Fig. 12.1 Classification of crop dryers using solar energy

thermal energy-collection unit and drying chamber are separately operated in the indirect-mode type of solar dryers. The mixed-mode type of solar dryer uses some features of the direct-mode type of solar dryer and some features of the indirect-mode type of solar dryer in a single unit.

The energy needed for the forced circulation of air is provided by external electrical sources, but in the case of solar dryers integrated with a PV module, the DC electrical energy generated from the PV modules is used to operate the fan or blower. Active solar dryers are more controlled and flexible because they can be regulated to a desired drying rate for faster and better drying compared with passive solar dryers [18–20].

12.2.1 Open-Sun Drying (OSD)

In open-Sun drying (OSD), some part of incoming solar energy $I(t)$ in the form of short-wavelength radiation is reflected back to the atmosphere, and the remaining radiation is selectively (different absorptivity (α_c) of a crop surface pertains to the color of crop) absorbed by the crop surface. A fraction of absorbed radiation increases the temperature of crop surface and rest is performed inside the interior of crop. Due to temperature rise, thermal energy is transfer from the crop surface to the ambient air by way of radiation (long wavelength) and convection in addition to mass transfer due to evaporation. The rate of convective heat transfer depends on the velocity of wind blowing above the crop surface (Fig. 12.2): The greater the
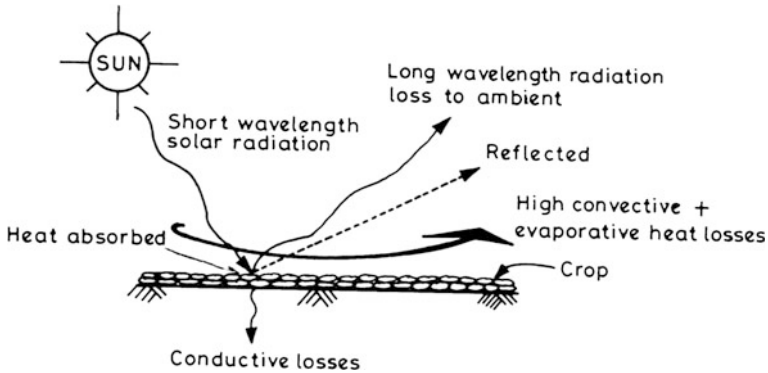
Fig. 12.2 Open-sun drying

velocity of the wind, the greater the convective heat transfer. The evaporation process removes moist air from the crop surface and is responsible for crop-drying. The thermal energy conducted inside the crop raises the temperature of the interior of the crop resulting vapor formation inside the crop. Water vapors diffuse from the interior toward the outer surface of the crop and evaporate to the ambient air. Initially, moisture removal from the crop surface is higher due to the wet crop surface, but when moisture is removed from the outer layer of the crop, the rate of drying depends on diffusion (which depends on the type of crop) of water vapor from the interior toward the outer crop surface [5, 21].

Thermal modeling

(a) **Analysis in quasi-steady state**

The following assumptions are made for OSD:

- The heat capacity of a tray of area, A_t, and moist air are negligible.
- There is no heat conduction between particles.
- Heat flow is one dimensional.
- There is an approximation of thin-layer drying.

The energy balance on a crop surface

$$\alpha_c I(t) A_t - h_{rc}(T_c - T_e)A_t - 0.016 h_c [P(T_c) - \gamma P(T_e)]A_t - h_i(T_c - T_a)A_t$$
$$= M_c C_c \frac{dT_c}{dt} \tag{12.1}$$

where the third term on the right-hand side is the rate of moisture evaporated from the crop surface to air of a relative humidity, γ, just above the crop surrounding; T_e is the temperature of the immediate surroundings of the crop; T_a is the ambient air

temperature; h_{rc} is the sum of a radiative h_r and convective h_c heat-transfer coefficient from the crop surface; h_i is the overall bottom heat-loss coefficient from the crop to the ambient air; and C_c is the specific heat of the crop.

Equation (12.1) can also be defined as

$$\dot{Q}_u = \alpha_c I(t) A_t - h_{rc}(T_c - T_e)A_t - h_{ev}(T_c - T_e)A_t - h_i(T_c - T_a)A_t$$
$$= M_c C_c \frac{dT_c}{dt} \tag{12.1a}$$

According to Eq. (3.47), an expression for h_{ev} is given by

$$h_{ev} = \frac{0.016 h_c \left[P(\overline{T}_c) - \gamma P(\overline{T}_e)\right]}{(\overline{T}_c - \overline{T}_e)} \tag{12.1b}$$

where $\overline{T}_c$ and $\overline{T}_e$ are an average crop and the surrounding temperatures over the daily drying period.

An energy-balance equation of moist air is

$$h_{rc}(T_c - T_e)A_t + 0.016 h_c[P(T_c) - \gamma P(T_e)]A_t = h_2(T_e - T_a)A_t \tag{12.2}$$

where $h_2 = 5.7 + 3.8V$ is a convective and radiative heat-transfer coefficient from moist air to ambient air; and V is the wind velocity above the crop surface.

According to Eqs. (12.1a) and (12.2) can also be written as follows:

$$h_{rc}(T_c - T_e)A_t + h_{ev}(T_c - T_e)A_t = h_2(T_e - T_a)A_t \tag{12.2a}$$

Moisture evaporated (m_{ev}) in time 't' can be determined as

$$m_{ev} = \frac{0.016 h_c}{L}[P(T_c) - \gamma P(T_e)]A_t t \tag{12.3}$$

where L is the latent heat of evaporation.

The variation of temperature-dependent partial pressure can be assumed to be linear due to the low operating-temperature range (35–50 °C) of OSD. Under this assumption, the expression for temperature-dependent partial pressure can be given follows:

$$P(T) = R_1 T + R_2 \tag{12.4}$$

where the constants R_1 and R_2 can be obtained using data in Appendix VIII. The $R_1 = 293.4$ and $R_2 = -3903.3$ for the operating-temperature range of 15–50 °C.

By substituting Eq. (12.4) into Eqs. (12.1) and (12.2), we obtain

$$\alpha_c I(t)A_t - h_{rc}(T_c - T_e)A_t - 0.016h_c[(R_1 T_c + R_2) - \gamma(R_1 T_e + R_2)]A_t - h_i(T_c - T_a)A_t$$
$$= M_c C_c \frac{dT_c}{dt}$$

(12.5)

and

$$h_{rc}(T_c - T_e) + 0.016h_c(R_1 T_c + R_2) - 0.016h_c\gamma(R_1 T_e + R_2) = h_2(T_e - T_a) \quad (12.6)$$

From Eq. (12.6), one gets an expression for surrounding moist air temperature as

$$T_e = \frac{(h_{rc} + 0.016R_1 h_c)T_c + R_2[0.016h_c(1 - \gamma)] + h_2 T_a}{h_{rc} + 0.016h_c\gamma R_1 + h_2}$$

(12.7)

and Eq. (12.5) can also be rewritten with the help of Eq. (12.4)

$$\alpha_c I(t)A_t + h_i A_t T_a - [(h_{rc} + h_i)A_t + 0.016h_c R_1 A_t]T_c$$
$$+ (h_{rc} + 0.016h_c R_1 \gamma)A_t T_e - 0.016h_c R_2 A_t (1 - \gamma) = M_c C_c \frac{dT_c}{dt}$$

(12.8)

By substituting Eq. (12.7) in Eq. (12.8), one has the following expression to determine the crop temperature:

$$\alpha_c I(t)A_t + h_i A_t T_a - [(h_{rc} + h_i)A_t + 0.016h_c R_1 A_t]T_c + [(h_{rc} + 0.016h_c R_1 \gamma)A_t]$$
$$\times \left[\frac{(h_{rc} + 0.016R_1 h_c)T_c + R_2[0.016h_c(1 - \gamma)] + h_2 T_a}{h_{rc} + 0.016h_c\gamma R_1 + h_2}\right]$$
$$- 0.016h_c R_2 A_t (1 - \gamma) = M_c C_c \frac{dT_c}{dt}$$

After rearranging and simplification, the above equation becomes as follows:

$$\frac{dT_c}{dt} + aT_c = f(t)$$

(12.9)

where

$$a = \frac{[(h_{rc} + h_i)A_t + 0.016h_c R_1 A_t] - \frac{(h_{rc} + 0.016h_c R_1 \gamma)A_t(h_{rc} + 0.016R_1 h_c)}{h_{rc} + 0.016h_c\gamma R_1 + h_2}}{M_c C_c}$$

$$f(t) = \frac{\alpha_c I(t)A_t + h_i A_t T_a + \left[\frac{h_2(h_{rc} + 0.016h_c R_1 \gamma)A_t}{h_{rc} + 0.016h_c\gamma R_1 + h_2}\right]T_a + \frac{(h_{rc} + 0.016h_c R_1 \gamma)A_t R_2[0.016h_c(1 - \gamma)]}{h_{rc} + 0.016h_c\gamma R_1 + h_2}}{M_c C_c}$$

Equation (12.9) is a one-order differential equation that can be solved using the initial condition namely $T_c = T_{co}$ at $t = 0$. The analytical solution of the Eq. (12.9) is

$$T_c = \frac{f(t)}{a}(1 - e^{-at}) + T_{co}e^{-at} \tag{12.10}$$

After determining the crop temperature, T_c, the surrounding temperature, T_e, can be determined from Eq. (12.7). Furthermore, after knowing T_c and T_e, the amount of moisture evaporated, m_{ev}, can be determined by Eq. (12.3), which can be rewritten as

$$m_{ev} = \frac{0.016h_c}{L}[(R_1T_c + R_2) - \gamma(R_1T_e + R_2)]A_t t \tag{12.11}$$

(b) Analysis for steady-state conditions

Under steady-state conditions, $\frac{dT_c}{dt} = 0$; then Eqs. (12.1a) and (12.2a) become as

$$\alpha_c I(t)A_t - h_{rc}(T_c - T_e)A_t - h_{ev}(T_c - T_e)A_t - h_i(T_c - T_a)A_t = 0$$

or

$$\alpha_c I(t)A_t - h_1(T_c - T_e)A_t - h_i(T_c - T_a)A_t = 0 \tag{12.12}$$

where

$$h_1 = h_{rc} + h_{ev}$$
$$h_1(T_c - T_e)A_t = h_2(T_e - T_a)A_t \tag{12.13}$$

Now the above equations can be solved for the crop (T_c) and the surrounding temperatures (T_e) as

$$T_c = \frac{\alpha_c I(t) + h_1 T_e + h_i T_a}{(h_1 + h_i)} \tag{12.14}$$

and

$$T_e = \frac{h\alpha_c}{U_L}I(t) + T_a \tag{12.15}$$

where

$$h = \frac{h_1}{(h_1 + h_i)} \quad \text{and} \quad U_{\mathrm{L}} = \left[\frac{h_1 h_i}{(h_1 + h_i)} + h_2\right]$$

Equation (12.15) is an expression of equivalent solair temperature (T_{sae}) as defined in Sect. 10.6. It is also important to mention that the numerical values of the surrounding moist temperature may or may not be higher than the crop temperature. It will depend on the hardness of the crop.

After knowing T_c and T_e from Eqs. (12.14) and (12.15), the amount of mass evaporated can be determined either from Eq. (12.3) or (12.11).

Evaluation of Convective Heat Transfer (h_c)

According to Sect. 3.3.3, the convective heat-transfer coefficient (h_c) from the crop surface and the surrounding moist air in OSD (Eq. 12.3) can be determined as follows:

$$Nu = \frac{h_c X}{K_v} = C(Gr.Pr)^n$$

or

$$h_c = \frac{K_v}{X} C(Gr.Pr)^n \tag{12.16}$$

where Nu, Pr and Gr are the Nusselt, Prandtl, and Grashof numbers defined in Chap. 3 (Eqs. 3.22a, c, and d). The numerical values of C and n depend of the type of crop to be dried, and these are constants for a given crop. K_v and X are the thermal conductivity of humid air and the characteristic dimension, respectively.

The amount of moisture evaporated (m_{ev}) in time 't' and a given tray area A_t can be obtained from Eq. (12.3). After the substitution of Eq. (12.16) in Eq. (12.3), one gets

$$m_{ev} = \frac{0.016}{L} \frac{K_v}{X} C(Gr.Pr)^n [P(T_c) - \gamma P(T_e)] A_t t \tag{12.17}$$

Let

$$\frac{0.016}{L} \frac{K_v}{X} [P(T_c) - \gamma P(T_e)] A_t t = Z$$

Now Eq. (12.17) can be rearranged as

$$\frac{m_{ev}}{Z} = C(Gr.Pr)^n \tag{12.18}$$

After taking the logarithm of both sides of Eq. (12.18), one gets

$$\ln\left[\frac{m_{ev}}{Z}\right] = \ln C + n\ln(Gr.Pr) \tag{12.19}$$

Equation (12.19) is in the form of a linear equation as follows:

$$Y_0 = mX_0 + C_0 \tag{12.20}$$

where

$$Y_0 = \left[\frac{m_{ev}}{Z}\right], \quad \text{and } X_0 = \ln(Gr.Pr)$$

Furthermore, linear regression analysis gives

$$n = m = \frac{N\sum X_0 Y_0 - \sum X_0 \sum Y_0}{N\sum X_0^2 - (\sum X_0)^2} \quad \text{and} \quad C_0 = \frac{\sum X_0 \sum Y_0 - \sum X_0 Y_0}{N\sum X_0^2 - (\sum X_0)^2} \tag{12.21}$$

In addition, from Eqs. (12.20) and (12.21), $C_0 = \ln C$.
Thus,

$$C = e^{C_0} \tag{12.22}$$

After knowing C and n and substituting the numerical values of K_v, X, Gr, and the Pr number, one can obtain the values of the convective mass-transfer coefficient (h_c) from Eq. (12.16).

Here, mass evaporated m_{ev}, crop temperature T_c, surrounding air temperature T_e, and relative humidity of moist air γ are experimentally recorded. Furthermore, it is to be noted that for N set of experimental data for m_{ev}, T_c, T_e, and γ, one must take $(N+1)$.

Experimental observations for open-sun drying (OSD)
For drying of the various crops, a wire mesh (porous) tray of 0.45×0.19 m size was constructed and placed on an electronic balance with the same of space below the tray to flow the air from the bottom of tray through the crop to the ambient air. A digital temperature indicator with a least count of 0.1 °C with a copper-constantan thermocouple was used to measure (i) the crop temperature (T_c), the surrounding moist temperature (T_e), and the ambient air (T_a) at different time points at interval of 15 min. The relative humidity of moist air just above the crop surface was measured with a dial-type hygrometer (least count of 1). The mass evaporated

Table 12.2 Design parameters of a drying tray

Parameters	Values
A_t	0.45×0.19 m^2
g	9.81 m/s^2
X	$[(0.45 + 0.19)/2$ m$]$
L	2.26×10^6 J/kg
ε	0.9
σ	5.67×10^{-8}
t	15×60
h_i	5.7

was estimated using an electronic balance (least count 0.1 g). The design parameters of the drying tray to determine convective the mass transfer is given in Table 12.2.

The crop was placed above the wire mesh tray with different copper–constantan thermocouples to measure the various temperatures, and the whole system was further kept on the electronic balance. A hygrometer was kept above the crop surface with a sensing element facing the crop surface. For every observation, the hygrometer was kept over the crop surface for 2 min to record the humidity of moist vapor. The whole experimental assembly was kept in the open Sun. The effect of wind velocity was neglected during the experiment. For consecutive observations, the difference between the crops' mass gives the amount of evaporated water during that specified time period. The experiment was repeatedly performed to obtain the most accurate results. Different treatments were given for different crops before performing the experiment. Various treatments and the densities of different crops are listed in Table 12.3.

The other parameters, including the physical properties of the various crops, are given in Table 12.4.

Experiments were performed during the summer months in the year 1999.

Table 12.3 Various treatments given to crops before drying and their final bulk density

No.	Crop	Treatment given	Bulk density (kg/m^3)
1	Green chilies	No treatment	280
2	Green peas	No treatment	575
3	Kabuli chana	Soaked in water for 6 h to raise the moisture content ≤30 (w.b.)	550
4	Onion	Peeled and cut with the help of a slicer in the form of flakes of 2-mm thickness	450
5	Potato	Peeled and cut with the help of a slicer in the form of slices of 2-mm thickness (average diameter 35 mm)	500
6	Cauliflower	Cut into small pieces of 2-cm size	415

Table 12.4 Input initial values of various crops used for modeling

Parameter	Green chilies	Green pea	Kabuli chana	Onion flakes	Potato slices	Cauliflower
α	0.65	0.8	0.8	0.7	0.8	0.65
C	1.3158	0.9769	1.3105	1.0064	1.0200	0.9784
n	0.1556	0.2196	0.2098	0.2579	0.2965	0.2323
C_c	3950	3060	3060	3810	3520	3900
γ	0.35	0.362	0.371	0.3825	0.371	0.337
T_c	38.21	38.83	36.89	33.91	43.61	33.03
T_e	40.23	46.40	38.23	38.23	38.33	39.00
M_c	0.607	0.6157	0.6135	0.6029	0.6246	0.6246

Table 12.5 Experimental data for green pea

Time (min)	$\overline{T}_c$ (°C)	$\overline{T}_e$ (°C)	T_i (°C)	$\dot{m}_{ev}$ (g)	$\overline{\gamma}$	$Gr \times 10^5$	Pr
15	39.39	46.95	43.170	12.4	0.380	17.38	0.7057
30	41.14	47.97	44.555	15.1	0.395	14.98	0.7058
45	42.22	47.65	44.935	22.2	0.380	11.76	0.7058
60	42.34	47.25	44.795	18.4	0.355	10.68	0.7058
75	42.76	47.55	45.155	32.7	0.350	10.30	0.7058
90	43.07	47.38	45.225	21.2	0.350	9.24	0.7058
105	43.21	47.30	45.255	19.6	0.350	8.76	0.7058
120	43.71	47.24	45.475	15.1	0.350	7.51	0.7058
135	44.67	47.98	46.325	14.1	0.350	6.85	0.7059
150	45.40	49.03	47.215	14.3	0.350	7.29	0.7059

The measured experimental data for a typical crop, namely, green peas, is reported in Table 12.5.

The experiment was performed on June 15, 1999, between 11.00 and 13.30 h for the climatic conditions of Delhi. The variation of the solar intensity was found to be between 990 and 1020 W/m^2. The T_i is an average temperature of the crop surface and the surrounding moist temperatures, which was used to determine Gr (3.22d) and Pr (3.22c), respectively. Using Eqs. (12.21) and (12.22) and the data in Table 12.5, the values of C and n can be determined and are given in Table 12.6 for green peas. In addition, the convective mass-transfer coefficient is also given in the same figure. Different crops have different thermo-physical properties resulting different heat- and mass-transfer coefficients for different crops.

The average values of C and n of Table 12.6 for green peas, along with data of other crops, is also given in Table 12.4.

According to Anwar and Tiwari [22], Eqs. (12.7), (12.10), and (12.11) are computed by using the data in Tables 12.2, 12.3, 12.4, 12.5 and 12.6 for the crop

Table 12.6 C, n, and h_c for green pea

Time (min)	C	N	h_c
15	1.0000	0.2102	7.78
30	1.0007	0.2148	8.19
45	1.0057	0.2220	8.92
60	1.0050	0.2214	8.68
75	1.0131	0.2281	9.50
90	1.0125	0.2278	9.34
105	1.0102	0.2268	9.10
120	0.9999	0.2243	8.61
135	0.9866	0.2219	8.13
150	0.9769	0.2196	7.75

Fig. 12.3 Prediction of crop temperature (T_c) and mass (M_c) under open sun-drying conditions for green pea
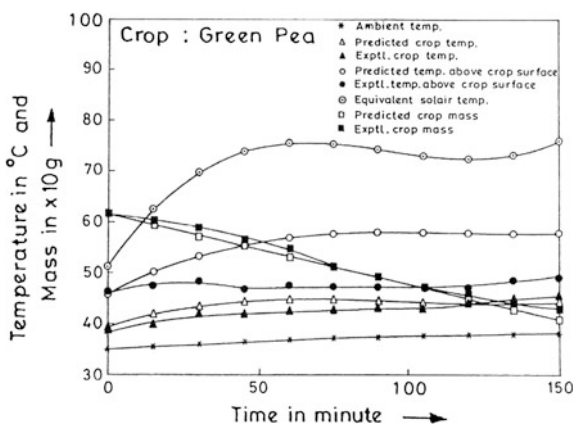
and surrounding moist temperatures and the mass evaporated, and the results are shown in Fig. 12.3. It was observed that except for the surrounding temperature, there is good agreement between experimental and theoretical prediction. In the case of the surrounding temperature, there is possibility of error due to improper position of the sensor to measure the surrounding moist temperature.

Example 12.1 Determine C and n for green chilies for given following data:

Time (min)	$\overline{T}_c$ (°C)	$\overline{T}_e$ (°C)	T_i (°C)	m_{ev} (g)	$\overline{\gamma}$	$Gr(\times 10^5)$	Pr
15	39.34	40.80	40.070	5.9	0.365	3.74	0.7055
30	42.66	42.67	42.665	8.7	0.360	0.02	0.7056
45	45.54	44.43	44.985	10.9	0.360	2.40	0.7058
60	47.39	45.06	46.225	13.2	0.355	4.83	0.7058
75	48.79	45.29	47.040	12.7	0.355	7.07	0.7059
90	49.49	45.60	47.545	15.3	0.355	7.73	0.7059

Solution

To determine C and n for the above data, first X_0 and Y_0 should be calculated for each observation from Eq. (12.21). The calculated values of X_0 and Y_0 are given below:

Time (min)	$X_0 = \log(Gr.Pr)$	Z	$Y_0 = m_{ev}/Z$
15	12.48	0.0009	1.8929
30	7.409	0.0011	2.0474
45	12.04	0.0013	2.0892
60	12.74	0.0015	2.1478
75	13.12	0.0017	2.0117
90	13.21	0.0018	2.1541

The value of C_0 and n can be obtained from Eqs. (12.21) and (12.22) after substituting the values of X_0 and Y_0 from the above table; they are given by

$$C_0 = 0.2910 \quad \text{and} \quad C = \exp C_0 = 1.3378 \quad \text{and} \quad n = 0.145$$

12.2.2   *Direct Solar Drying (DSD)*

Open-Sun drying is not hygienic due to dust and insects and losses due to birds, etc. It is also a slow drying process. To solve these problems, the concept of the greenhouse effect was used. It is the first scientific step for crop-drying using solar energy. In this case, the crop is placed inside a cabinet box covered with an inclined glazed roof. The cabinet box has openings at its base and at the top of the large vertical wall for air inlet and outlet, respectively. Thus, it is also referred to as "cabinet drying" as shown in Fig. 12.4. Some part of the short-wavelength solar radiation transmitted from the glazed cover of the cabinet is reflected back, and the rest is absorbed by the crop surface. The absorbed solar radiation heats the crop surface and crop start emitting long-wavelength radiation, which is trapped by the glazed cabinet covers. The blocked radiation further raises the crop temperature, which results in faster drying compared with OSD. In addition to creating a greenhouse effect inside the cabinet dryer, the glazed covers also reduces convective losses to the ambient air. The moisture formed due to evaporation is taken away by the air. The air enters from the bottom of the cabinet dryer and takes away the moisture from the opening provided at the top of the vertical wall. This phenomenon is referred to as "natural convection drying" without any use of additional source of energy.

Thermal analysis

The energy-balance equations of a cabinet dryer (Fig. 12.4) can be written with the following assumptions:

Fig. 12.4 The cabinet dryer

- Heat capacities of different components (glass cover, tray, drying chamber wall) and the air are negligible.
- The volume of crop is assumed to be constant.
- The conduction between particles is negligible.
- There is no heat flow and stratification inside the crop.
- Moisture is immediately removed from the chamber, i.e., condensation inside the chamber is negligible.

The energy-balance equations are as follows:

For the crop surface
Using the first law of thermodynamics, the rate of thermal energy available to the crop is equal to the rate of thermal energy stored inside the crop and the rate of thermal energy lost to chamber by radiation, convection, and evaporation.

$$[\alpha_c \tau I(t)]A_c = M_c C_c \frac{\mathrm{d}T_c}{\mathrm{d}t} + h(T_c - T_{ch})A_c \qquad (12.23)$$

where $h = h_{rc} + h_{ev}$ is the sum of the radiative, convective, and evaporative heat-transfer coefficients (Eq. 12.1a).

For the drying chamber
Furthermore, the rate of thermal energy lost from the crop to the inside of the chamber by radiation, convection, and evaporation is transferred outside through

the vent provided at the top of the vertical wall by natural mode due to a pressure difference, and the rest is lost to the outside by conduction through the side walls.

$$h(T_c - T_{ch})A_c = V_1(T_{ch} - T_a) + h_s A_s(T_{ch} - T_a) \qquad (12.24)$$

where $V_1 = \frac{NV}{3}$, V, and N are the volume of the drying chamber and the number of air change per hour, which is very small; its value is always <1.

12.2.3   Indirect Solar Drying (ISD) [23]

This is also referred to as a "conventional drying unit." In this case, there are two units, namely, a heating unit and a drying unit as shown in Fig. 12.5a. In this case, drying is more controlled and homogeneous (resulting in a better quality of dried product) because the crops are not directly exposed to solar radiation. Here solar energy is collected and converted into thermal energy by the use of solar air heater. The solar air heater is further integrated with the drying chamber. The hot air from the inclined solar air heater is allowed to flow in a natural mode through a wet crop placed inside the drying chamber. Here, the heated air passes through the crop after transferring the heat to the crop, thus heating it. The water inside the crop gets evaporated and is allowed to pass through the vent provided at the top of the drying chamber.

   In a natural ventilated indirect solar dryer (ISD), the drying time is longer due to the fact that the rate of moisture evaporated from the crop is not immediately transferred from the drying chamber to the ambient air through the vent, particularly at noon, and hence the drying time is significantly affected. Therefore, an indirect solar-dryer (ISD) system operating under forced mode of operation is most appropriate. For the forced mode of operation, an photovoltaic thermal (PVT) integrated with mixed-mode dryer was developed as shown in Fig. 12.5b.

   In this case, too, there are two components, namely, a PVT solar air collector (Chap. 9) and a drying chamber. A PVT solar air heater consists of semitransparent PV modules [35 W and (0.65 m × 0.55 m)] integrated with a conventional flat-plate air collector. Solar radiation falling on the packing area (solar cells) of a semitransparent PV module generates electricity. Solar radiation falling on the nonpacking area of the semitransparent PV module is absorbed by the blackened absorber plate of the solar air-collector unit. Air inside the duct of a solar air heater receives thermal energy from the blackened absorbing plate and is thus heated. The hot air is fed to the drying chamber (for drying the crop) by the DC fan at the outlet of the solar air heater. The DC fan is operated by the electricity produced from the semitransparent PV module. Here it important to mention that the speed of fan (and thus the rate of withdrawal of moisture) depends on the level of solar radiation, which is a required condition of such sustainable dryer. In this case, the rate of removal of moisture from the drying chamber will match with rate of removal of moisture from the crop.
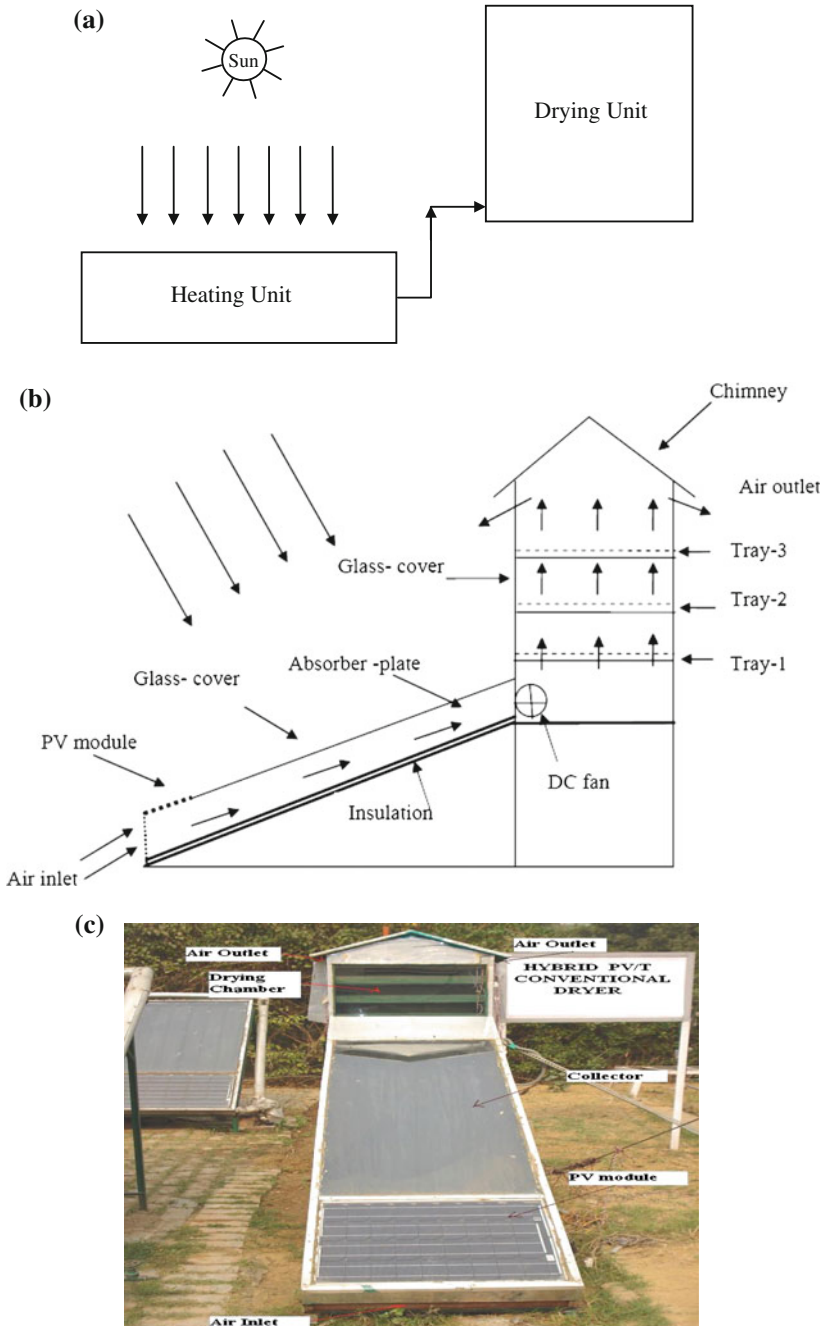
Fig. 12.5   a Schematic of indirect solar drying. **b** Schematic diagram of PVT mixed-mode dryer. **c** Photograph of conventional PVT mixed-mode dryer

Table 12.7   Design specifications of a PVT mixed-mode dryer

Sl. no.	Details of particulars	Specification
1	Air duct	Size: 2.2 m × 0.65 m × 0.05 m
2	PV module	Size: 0.65 m × 0.55 m; 35 W
3	Spacing between absorber and glass	0.10 m
4	DC fan	12 V, 1.3 A
5	Chimney	Size: 0.65 m × 0.26 m × 0.60 m
6	Number of trays	3
7	Spacing between two trays	0.15 m
8	Inclination of absorber (air duct) with horizontal	30°

A drying chamber [with dimensions (0.65 m × 0.30 m × 0.66 m)] is made of a wood, but the front side is glazed [with plain glass of dimensions (4 mm thickness, 0.65 m × 0.4 m in size)], which allows solar radiation to fall directly on the crop surface. There are three layers of trays [with dimensions (0.65 m × 0.26 m × 0.04 m)] are stacked at equal spacing (0.15 m) inside the drying chamber. The products to be dried are kept on theses trays.

The above-mentioned components are integrated with each other as shown in Fig. 12.5c.

The design parameters of PVT mixed mode dryer are given in Table 12.7.

12.2.4   PVT Greenhouse Dryer [24]

A PVT greenhouse dryer consists of eight semitransparent PV modules with each having a packing factor of 0.425 and power of 35 W_p with an effective area of 1.2 m × 0.54 m. Each PV module is connected in series to produce 280 W_p of electricity, which is used to operate four fans for forced mode of operation. Solar radiation transmitted through non-packing area is a direct gain received by the crop placed on the top tray for heating. Thermal energy associated with the solar cell is convected to the inside enclosure of a PVT dryer for indirect heating of the crop. A clean PVT dryer is shown in Fig. 12.6. The PVT dryer was installed at top of wind tower of the SODHA BERS' complex, (Varanasi, India) so that preheated air can circulate from the bottom of the dryer to the upper vent through crops placed on different trays. This helps cause faster drying.

The design parameters of a PVT dryer are given in Table 12.8. There are four AC fans of rating (20 W, 1100 rpm) that are at the top of the north side to remove moist air from inside the dryer for fast evaporation from the crop placed on different trays. There is also provision of two glass doors at the east side through which the removal of trays, as per requirement at regular intervals, to determine the loss of
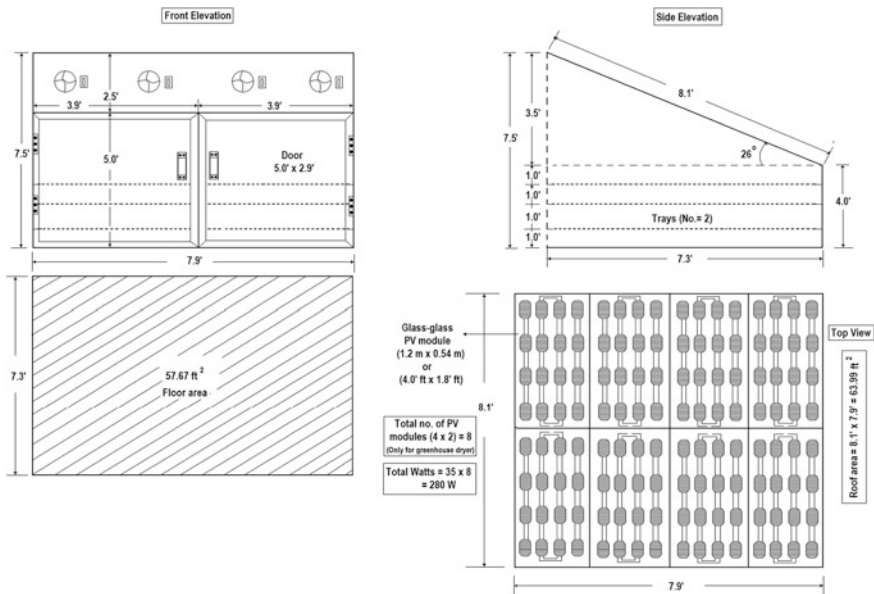
Fig. 12.6 Schematic view of a PVT greenhouse dryer

Table 12.8 Design specification of a PVT greenhouse dryer

Sl. no.	Components	Dimensions
1	Vertical upper height	2.25 m
2	Vertical lower height	1.2 m
3	Inclination	28°
4	Floor area	5.2 m^2
5	Roof area	5.75 m^2
6	No. of trays	12
7	Area of tray	0.54 m^2
8	No. of layers	3
9	Distance between two layers of trays	0.3 m
10	Cross section of Al. channel	(0.025 × 0.025) m^2
11	Rubber gasket	5 mm
12	Glass	5 mm

weight of crop on different trays. Five-millimetre glass was fitted with an Al frame with the help of a 5-mm U rubber gasket of. Porous cotton was placed inside each tray to avoid the losses of medicinal plant during the drying process. A space of approximately 30 mm was provided at the bottom of the structure to allow cold air passage from bottom to top through each tray of area 0.54 m^2 along with hot air available from the wind tower at the base of the dryer.

(a)

(b)
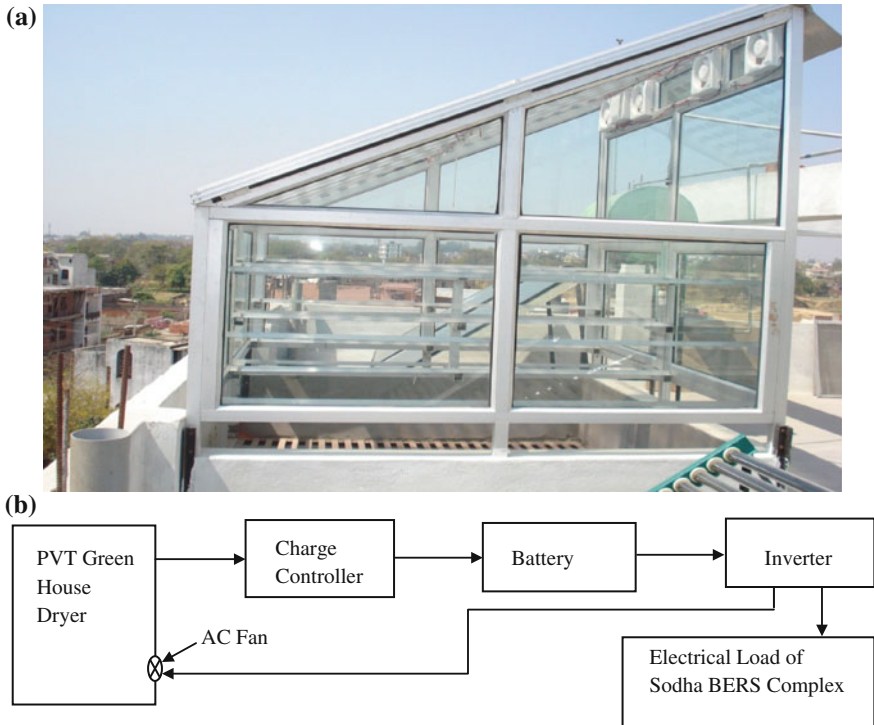
Fig. 12.7 a East pictorial view of the PVT greenhouse dryer. **b** Block diagram of a PVT greenhouse dryer

The structure of the PVT dryer is permanently fixed at a vertical foundation wall with a galvanized iron angle fitted with nuts and bolts. Furthermore, a semitransparent PV module is fixed at the top of the structure with an aluminum L-strip, nut, and bolts to have minimum resistance. The output of the PV module is connected to an 18 V battery through a solar-charge controller. The output of the battery is further connected to the fan through an inverter. The charge controller and inverter are packed in one box for simple operation. The trays are provided with side support in each layer. The proposed system can be used to dry a minimum of 12 items at a time. The east view of a clean hybrid PVT dryer is shown in Fig. 12.7a.

A block diagram of whole assembly of a PVT greenhouse dryer, including a photograph of the charge controller, battery, and inverter, is shown in Fig. 12.7b. It is also necessary to mention that the additional electrical power used for lighting of the SODHA BERS complex when greenhouse dryer is not employed.

12.2.5   *Reverse-Absorber Cabinet Dryer*

A cross-sectional view of a reverse-absorber cabinet dryer (RACD) is shown in Fig. 12.8. This can also be an indirect (Fig. 12.8a) or mixed-mode (Fig. 12.8b) solar dryer. If the top inclined surface is metallic, then it is an indirect solar dryer; it becomes mixed-mode if the top inclined surface is glazed. Goyal and Tiwari [25] proposed and analyzed the RACD for drying purposes. The drying chamber in a RACD is similar to that of conventional cabinet dryer, but it receives direct radiation from the top glazing cover as well as thermal energy from the bottom of the dryer using a reverse-absorber flat-plate air collector. A reverse absorber flat-plate air collector is fixed below an optimized depth ($\cong 0.05$ m) from the bottom of the drying chamber. The air gap between the bottom of the drying chamber and the top of the reverse-absorber flat-plate air collector serve as the air duct for the heating of air. Hot air passes through the crop placed on wire mess or trays and thus dries the
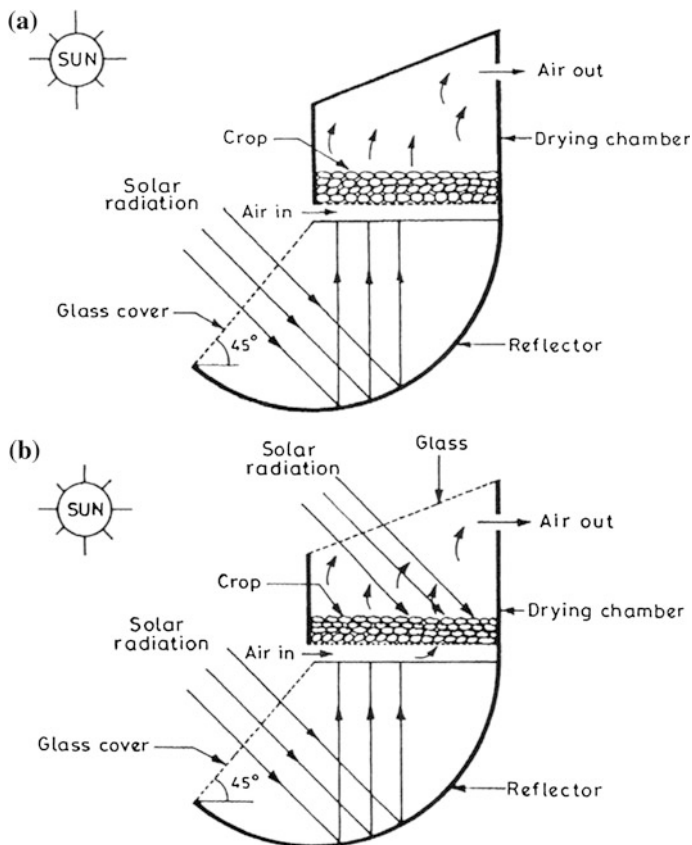
Fig. 12.8 Schematic view of a reverse-absorber cabinet dryer **a** Indirect solar dryer **b** Mixed mode solar dryer

crop. Solar radiation is collected using a glass aperture fitted with a cylindrical reflector. The aperture is inclined at an angle equal to the latitude to receive maximum annual solar radiation throughout the year. The area of the glass cover and absorber are kept the same as area of the bottom surface of the drying chamber. The working principle of this RACD is different from that of a conventional cabinet dryer because in this case solar radiation is transmitted from the inclined glass cover and then reflected to the selectively-coated reverse-absorber plate. The radiation absorbed by the absorber plate is converted into thermal energy. Air in between the absorber plate and the bottom of the cabinet dryer receives thermal energy by convection and heats the crop surface. Thereafter, air leaves the drying chamber by removing moist air from the upper vent at the top of the drying chamber.

Thermal modeling

Referring to Fig. 12.8, the energy-balance equations for different components of an indirect inverse absorber cabinet dryer for thin layer are as follows:

At the absorber plate

$$\tau \rho' \alpha_p I' = h_{pf}(T_p - T_f) + h_{rpc}(T_p - T_c) + U_t(T_p - T_a) \tag{12.25}$$

where τ, ρ', α_p, and I' are the transmittivity of the inclined glass, the reflectivity of the reflector or absorptivity of the selective blackened plate, and the solar radiation falling on the inclined glass cover, respectively. h_{pf} and h_{rpc} are the convective and radiative heat-transfer coefficient between the plate (T_p) and the fluid (T_f) and between the plate (T_p) and the crop (T_c) respectively. U_t is an overall heat-transfer coefficient from the plate to the ambient air (T_a) through the inclined glass cover.

At the working fluid (Air)

$$h_{pf}(T_p - T_f) = h_{fc}(T_f - T_c) \tag{12.26}$$

where h_{pf} and h_{fc} are the heat-transfer coefficient from the plate to the fluid and the heat-transfer coefficient from the fluid to the crop, respectively.

At the crop surface

$$\left[h_{fc}(T_f - T_c) + h_{rpc}(T_p - T_c)\right]A_c = M_c C_c \frac{dT_c}{dt} + h(T_c - T_{ch})A_c \tag{12.27}$$

where $h = h_{rc} + h_{cc} + h_{ec}$ is the total (the sum of radiative, convective, and evaporative) heat-transfer coefficient from the crop surface.

At chamber

$$h(T_c - T_{ch})A_c = V_1(T_{ch} - T_a) + h_s A_s(T_{ch} - T_a) \qquad (12.28)$$

where $V_1 = NV/3$ and h_s is the conductive heat-transfer coefficient from the drying chamber to the ambient air; and A_s is the surface area of the drying chamber.

The overall thermal efficiency of the conventional and the RACD is shown in Fig. 12.9. From this figure, one can conclude that there is an improvement of approximately 10 % in the performance of a RACD due to a reduction in heat losses.

Example 12.2 Determine the expression for the rate of heat transfer from the air to the crop for RACD.

Solution
The plate temperature can be obtained using Eq. (12.25):

$$T_p = \frac{\tau \rho' \alpha_p I' + h_{pf} T_f + h_{rpc} T_c + U_t T_a}{h_{pf} + h_{rpc} + U_t}$$

also

$$T_p - T_f = \frac{\tau \rho' \alpha_p I' - h_{rpc}(T_f - T_c) - U_t(T_f - T_a)}{h_{pf} + h_{rpc} + U_t}$$

Fig. 12.9 Overall thermal efficiency of a conventional versus reverse-absorber cabinet dryer
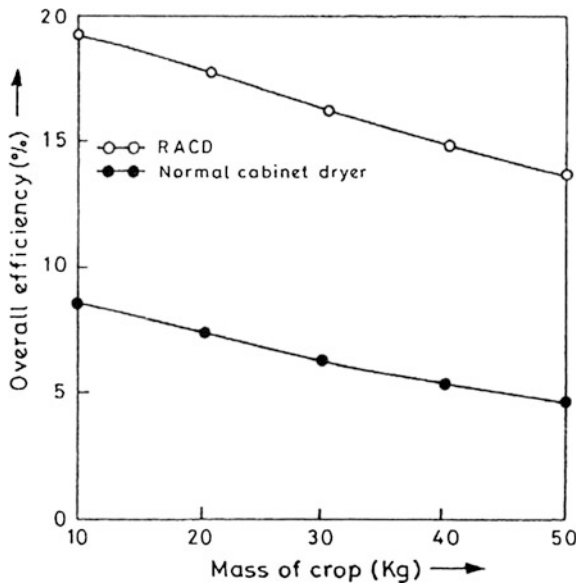
furthermore,

$$h_{\text{pf}}(T_{\text{p}} - T_{\text{f}}) = h\tau\rho'\alpha_{\text{p}}I' - U_{\text{fc}}(T_{\text{f}} - T_{\text{c}}) - U_{\text{fa}}(T_{\text{f}} - T_{\text{a}})$$

where

$$h = \frac{h_{\text{pf}}}{h_{\text{pf}} + h_{\text{rpc}} + U_t}, \quad U_{\text{fc}} = \frac{h_{\text{pf}} h_{\text{rpc}}}{h_{\text{pf}} + h_{\text{rpc}} + U_t}, \quad U_{\text{fa}} = \frac{h_{\text{pf}} U_t}{h_{\text{pf}} + h_{\text{rpc}} + U_t}$$

T_{p} can be eliminated from Eq. (12.26) by putting the value of $h_{\text{pf}}(T_{\text{p}} - T_{\text{f}})$ into Eq. (12.26),

$$h\tau\rho'\alpha_{\text{p}}I' - U_{\text{fc}}(T_{\text{f}} - T_{\text{c}}) - U_{\text{fa}}(T_{\text{f}} - T_{\text{a}}) = h_{\text{fc}}(T_{\text{f}} - T_{\text{c}})$$

This gives

$$T_{\text{f}} = \frac{h\tau\rho'\alpha_{\text{p}}I' + U_{\text{fc}}T_{\text{c}} + h_{\text{fc}}T_{\text{c}} + U_{\text{fa}}T_{\text{a}}}{U_{\text{fc}} + h_{\text{fc}} + U_{\text{fa}}}$$

Finally, on substituting T_{f} into $h_{\text{fc}}(T_{\text{f}} - T_{\text{c}})$, the rate of heat transfer from the fluid to the crop surface can be obtained as follows:

$$\dot{q}_{\text{fc}} = h_{\text{fc}}(T_{\text{f}} - T_{\text{c}}) = H\tau\rho'\alpha_{\text{p}}I' - U_{ca}(T_{\text{c}} - T_{\text{a}})$$

where

$$H = \frac{h_{\text{fc}}h}{U_{\text{fc}} + U_{\text{fa}} + h_{\text{fc}}} \text{ and } U_{ca} = \frac{h_{\text{fc}}U_{\text{fa}}}{U_{\text{fc}} + U_{\text{fa}} + h_{\text{fc}}}$$

12.3   Deep-Bed Grain Drying

In Sect. 12.2, the thermal model is based on thin-layer drying. Now the thermal model for deep-bed drying will be discussed in the following section.

The energy-balance equation for an absorber for deep-bed drying will be same as Eq. (12.25). In addition, general equations for deep-bed drying are given by Brooker et al. [26].

The rate of drying is given as follows:

$$\frac{\partial M}{\partial t} = -K_d(M - M_{\text{e}}) \tag{12.29}$$

where M and M_e are the moisture content and equilibrium moisture content (decimal on dry basis), respectively, $K_d = a \exp(-b/T_c)$ and $M = 0.01[\ln(-\gamma)/\{2.31 \times 10^{-5}(T_f + 55.815)\}]^{\frac{1}{2.99}}$. For rough rice, $a = 13.88 \, \mathrm{s}^{-1}$ and $b = 3818.2 \, \mathrm{K}$; Verma et al. [27].

Mass-balance equation

$$M\frac{\partial H}{\partial Y} = -\rho_c \frac{\partial M}{\partial t} \tag{12.30}$$

Energy-balance equation

In equilibrium, the thermal exchange between the air and crop is given as follows:

$$\dot{M}(C_f + C_v H)\frac{\partial T_f}{\partial Y} = \rho_c C_v (T_f - T_c)\frac{\partial M}{\partial t} - \rho_c(C_c + C_1 M)\frac{\partial T_c}{\partial t} + \rho_c \lambda \frac{\partial M}{\partial t} \tag{12.31}$$

Heat-transfer rate equation

The rate of heat transfer between air and grain can also be written as

$$\rho_c(C_c + C_1 M)\frac{\partial T_c}{\partial t} = h_v(T_f - T_c) + \rho_c \lambda \frac{\partial M}{\partial t} \tag{12.32}$$

Heat-utilization factor

The quantity of heat used in any process is governed by the heat-utilization factor (H.U.F), which is defined as the ratio of heat used to the heat supplied. Mathematically H.U.F. is expressed as follows:

$$\mathrm{H.U.F} = \frac{\text{Heat utilized}}{\text{Heat supplied}} = \frac{T_f - T_c}{T_f - T_a} \tag{12.33}$$

Coefficient of performance

The coefficient of performance (C.O.P.) of a deep-bed dryer is given as follows:

$$\mathrm{C.O.P} = \frac{T_c - T_a}{T_f - T_a} \tag{12.34}$$

The hourly variation of coefficient of performance (C.O.P.) and heat-utilization factor (H.U.F.) is shown in Fig. 12.10a. H.U.F. first increases rapidly and is then

Fig. 12.10 a Variation of the heat-utilization factor (H.U.F.) and coefficient of performance with time of the day. **b** Variation of the drying rate with moisture content
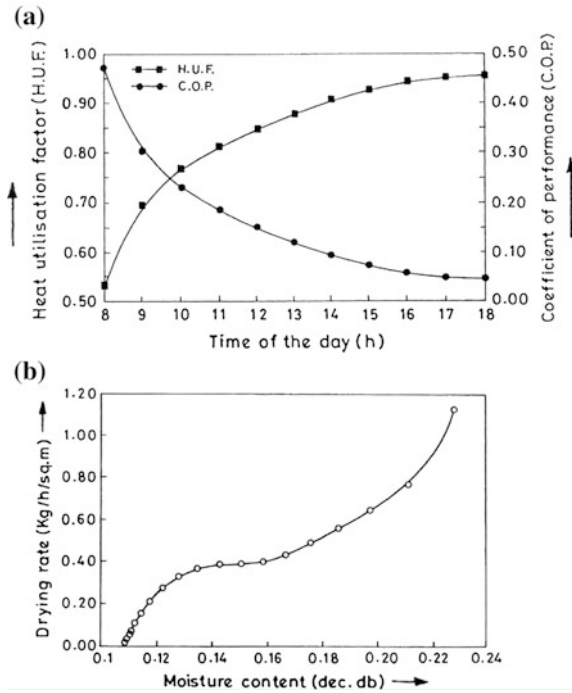
saturated by afternoon due to the fact that in the morning hours more moisture content results in more heat transfer from the fluid to the crop, whereas in afternoon it is decreased. The C.O.P. decreases as the time of the day progresses owing to the lesser level of solar radiation [resulting in a lesser value of $(T_f - T_a)$] in the later hours of the day.

Thermal efficiency

An instantaneous thermal-drying efficiency (η_i) of the system is defined as follows:

$$\eta_i = \frac{\dot{M}_{ev} \times \lambda}{3600 \times I'(t)} \times 100 \qquad (12.35)$$

The overall daily thermal efficiency can be obtained by taking the ratio of thermal energy utilized in evaporating the moisture content of the crop to the solar energy received by absorber. Mathematically it is expressed as:

$$\eta_0 = \frac{\lambda \sum_{t=1}^{t=24} \dot{M}_{ev}(t)}{(3600) \sum_{t=1}^{t=24} I'(t)} \qquad (12.36)$$

The overall daily thermal efficiency also determines the drying rate and time. The greater the overall daily thermal efficiency, is the greater the drying rate and the less the drying time. The variation of drying rate with moisture content is shown in Fig. 12.10b. This shows that the drying rate is greater for greater moisture content as desired.

12.4 Energy Balance for Indirect Solar Drying (ISD) Systems

An indirect solar drying system consists of a solar air heater and a drying chamber. The energy balance for a solar air heater and drying chamber are given as follows:

In a conventional ISD, the PV module area is zero for Fig. 12.5b.

A. Solar Air Heater

Absorber Plate

$$\tau\alpha_p IW dx = U_t(T_p - T_a)W dx + h_{pf}(T_p - T_f)W dx \tag{12.37}$$

Working Fluid

$$h_{pf}(T_p - T_f)W dx = \dot{m}C_f \frac{dT_f}{dx} dx + U_b(T_f - T_a)W dx \tag{12.38}$$

where

$$U_b = \left[\frac{1}{h_{pg}} + \frac{1}{h_{ga}}\right]^{-1}$$

B. Drying Chamber

$$\dot{m}C_f(T_{fo} - T_{fi}) = M_c C_c \frac{dT_c}{dt} + h(T_c - T_{ch})A_{ch} \tag{12.39}$$

$$h(T_c - T_{ch})A_{ch} = 0.33NV(T_{ch} - T_a) + h_s A_s(T_{ch} - T_a) \tag{12.40}$$

Equations (12.37)–(12.40) can be solved for plate temperature (T_p), fluid temperature (T_f) and crop temperature (T_c), and change temperature (T_{ch}).

Objective Questions

12.1. Solar crop-drying is better
  (a) in open-Sun drying   (b) in shadow drying
  (c) in controlled drying   (d) all of these
  Answer: (c)
12.2. In solar crop-drying, one of the following heat transfers is dominant
  (a) radiation   (b) convection
  (c) conduction   (d) evaporation (mass transfer)
  Answer: (b) and (d)
12.3. In solar crop-drying, there is relation between
  (a) radiation and evaporation   (b) convection and evaporation
  (c) conduction and evaporation   (d) none of these
  Answer: (b)
12.4. The drying time increases with
  (a) an increase of moisture content   (b) a decrease of moisture content
  (c) an increase of solar radiation   (d) none of these
  Answer: (a)
12.5. The direct drying of crops takes place in
  (a) a cabinet dryer   (b) a greenhouse dryer
  (c) open-Sun drying (d) all of these
  Answer: (d)
12.6. The final moisture content of a vegetable crop after drying should be
  between
  (a) 4 and 10 %   (b) 10 and 50 %   (c) zero   (d) none of these
  Answer: (a)
12.7. The maximum allowable temperature range for a vegetable crop to be dried
  by a dryer is between
  (a) 65–75 °C   (b) 100 °C   (c) 0 °C   (d) none of these
  Answer: (a)
12.8. The drying time in a solar dryer is
  (a) more than with open-Sun drying   (b) less than with open-Sun drying
  (c) equal to that of open-Sun drying   (d) none of these
  Answer: (b)
12.9. Equivalent solair temperature in the case of open-Sun drying of a crop is
  similar to
  (a) the solair temperature of a bare surface   (b) the solair temperature of
                                                                        a wetted surface
  (c) the solair temperature of a glazed surface (d) none of these
  Answer: (b)
12.10. A RACD is better than
  (a) a normal cabinet dryer   (b) a conventional dryer
  (c) an open-Sun dryer   (d) none of these
  Answer: (a)

12.11. Thin-layer drying of a crop is
    (a) better than deep-bed drying   (b) equal to deep-bed drying
    (c) worse than open-Sun drying   (d) none of these
    Answer: (a)
12.12. The heat-utilization factor (H.U.F.) is
    (a) proportional to the coefficient of performance (COP)
    (b) inversely proportional to the coefficient of performance (COP)
    (c) equal to the coefficient of performance (COP)
    (d) none of these
    Answer: (d)

Problems

12.1. Determine the rate of convective and evaporative heat losses from the green
    chilies of Example 12.1.
    Hint: Use Eqs. (12.16) and (12.1b), and the results of Example 12.1.
12.2. Derive an expression for T_p, T_f, T_c, and T_{ch} for indirect solar drying.
    Hint: Eliminate T_p between Eqs. (12.37) and (12.38) and also T_{ch} between
    Eqs. (12.39) and (12.40).
12.3. Determine the evaporative heat-transfer coefficient for green peas.
    Hint: Use Eq. (12.1b) and data from Tables 12.5 and 12.6.

References

 1. Anon, *The state of food insecurity in the world 2004. Food and agriculture organization of the United Nations.* Rome, 2004
 2. G.N. Tiwari, *Solar Energy: Fundamental, Design, Modelling and Applications* (Narosa Publishing House, New Delhi and CRC Press, New York, 2004)
 3. L. lmre, C. Palaniappan, Drying Technol. Int. J. **14**(6), 1381 (1996)
 4. W. Szulmayer, Food Technol. Aust. **23**, 440 (1971)
 5. M.S. Sodha, A. Dang, P.K. Bansal, S.B. Sharma, Energy Convers. Manage. **25**(3), 263 (1985)
 6. M.S. Sodha, R. Chandra, Energy Convers. Manage. **35**(3), 219 (1994)
 7. A. Esper, W. Mühlbauer, Renew. Energy **15**, 95 (1998)
 8. K. Lutz, W. Muhlbauer, J. Muller, G. Reinsinger, Solar Wind Technol. **4**(4), 417 (1987)
 9. A. Mulet, A. Berna, C. Rossello, J. Canellas, Drying Technol. Int. J. **11**(6), 1385 (1993)
10. S. Oztekin, A. Bascetincelik, Y. Sosyal, Renew. Energy **16**, 789 (1999)
11. T. Koyuncu, Renew. Energy **31**(7), 1055 (2006)
12. M.A. Zaman, B.K. Bala, Solar Energy **42**(2), 167 (1989)
13. A. Arata, V.K. Sharma, G. Spagna, Energy Convers. Manage. **34**(5), 417 (1993)
14. R. Budin, A. Mihelic-Bogdanic, Energy Convers. Manage. **35**(2), 97 (1994)
15. K.J. Chua, S.K. Chou, Trends Food Sci. Technol. **14**(12), 519 (2003)
16. O.V. Ekechukwu, B. Norton, Energy Convers. Manage. **40**, 593 (1999)
17. G.N. Tiwari, M.K. Ghosal, *Renewable Energy Resources: Basic Principles and Applications* (Narosa Publishing House, New Delhi, 2005)

18. G.N. Tiwari, S. Kumar, O. Prakash, J. Food Eng. **63**, 219 (2004)
19. K.R. Manohar, P. Chandra, Int. Agric. Eng. J. **9**(3), 139 (2000)
20. D. Jain, G.N. Tiwari, Energy Convers. Manag. **45**, 765 (2004)
21. G.N. Tiwari, R.K. Mishra, *Adv. Renew. Energy Sources* (RSC Publishing, UK, 2011)
22. S.I. Anwar, G.N. Tiwari, Energy Convers. Manage. **42**, 627 (2001)
23. A.K. Singh, *Performance evaluation of mixed mode and greenhouse PVT dryer*, Ph.D. thesis, IIT Delhi, New Delhi, India, 2012
24. A. Kumar, *Drying of medicinal/vegetables products by PVT greenhouse dryer*, Ph.D. thesis, IIT Delhi, New Delhi, India, 2012
25. R.K. Goyal, G.N. Tiwari, Energy Convers. Manage. **40**, 385 (1999)
26. D.B. Brooker, A.F.W. Bakker, C.W. Hall, *Drying Cereal Grain* (The AVI Publishing Co. Inc, Western Port, 1978)
27. L.R. Verma, R.A. Bucklin, J.B. Edan, F.T. Wratten, Trans. ASAE **28**, 296 (1985)

Additional References

28. G.N. Tiwari, P. Barnwal, *Fundamentals of Solar Dryers* (Anamaya Publisher, New Delhi, 2008)
29. S.V.V. Raman, S. Iniyan, R. Goic, Renew. Sustain. Energy Rev. **16**(5), 2652 (2012)

Chapter 13
Solar Distillation

Abstract Solar distillation is a process used to purify brackish/saline water into potable water using solar energy in underdeveloped region with hard ground water. The system gives a better performance under forced (active) mode of operation. Passive and active solar stills are economical from the point of view of potable water and industry.

Keywords Solar distillation · Passive solar distillation · Active solar distillation · Internal heat-transfer coefficients · External heat-transfer coefficients

13.1 Importance of Solar Distillation

Potable (drinking) water, along with food and air, is a basic necessity for human beings for survival. Potable water shortage is a serious problem in developing and underdeveloping countries due to either a lack of water or polluted underground water. Human beings, along with all animals, birds, and fish, etc., are dependent on rivers, lakes, and underground water reservoirs for potable water. However, the pollution of rivers, lakes, and underground water by industrial waste has caused a scarcity of fresh/potable water near lakes and rivers. Global surveys show that approximately 79 % of water available on Earth is salty as seawater. Approximately 20 % of underground water is brackish, and only 1 % is freshwater. Many developing and underdeveloping countries have a prime objective to provide potable water supply to each and every citizen. For example, in India, the Rajiv Gandhi National Drinking Water Mission is actively involved in promoting projects aimed at supplying drinking water in remote villages where people travel <30 km for freshwater.

Unlike conventional distillation techniques, solar distillation uses abundantly available solar energy for the distillation of brackish or saline water to obtain potable water. Conventional distillation techniques generally used fossil fuels for distillation process and are energy intensive. Solar distillation is a simple technology that uses nonpollutant solar energy as input energy. This technology does
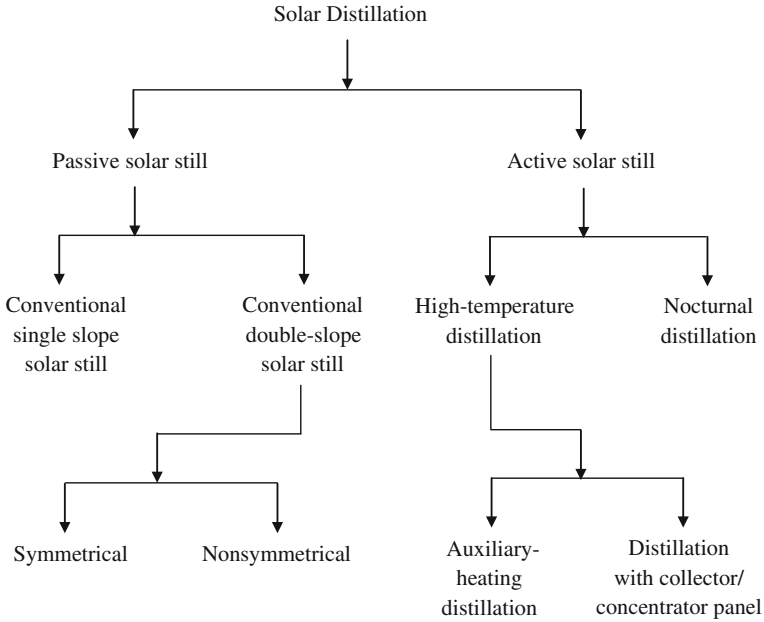
Fig. 13.1   Classification of a solar-distillation unit

not require very skilled labour and requires very little maintenance. It can be used at any place without much difficulty.

A classification of published literature on solar distillation is given in Fig. 13.1 [1–3]. The details of some designs of solar stills are discussed along with their performance in following sections.

13.2   Working Principle of Solar Distillation

Figure 13.2 shows the various energy losses at different components in a conventional double-slope **passive solar distiller unit**. It has an airtight basin. The basin with a rectangular base is currently constructed using (i) concrete/cement for a larger plant and (ii) fibre-reinforced plastic (FRP) for a smaller plant. There is a top cover of transparent material such as glass, plastic, etc. The inner portion of the rectangular basin is blackened to efficiently absorb short-wavelength solar radiation after transmission through the transparent cover. There is a provision to collect the distillate output (yield) at the lower end of the transparent cover. Following is the working principle of the solar double-slope distiller unit.

The short-wavelength solar radiation $[I(t)]$ is transmitted through the transparent cover inside an enclosure of a solar still. The transmitted solar radiation $\tau_g[I(t)]$ is partially reflected $[R'_w I(t)]$ and partially absorbed $[\alpha'_w I(t)]$ by the water mass in the
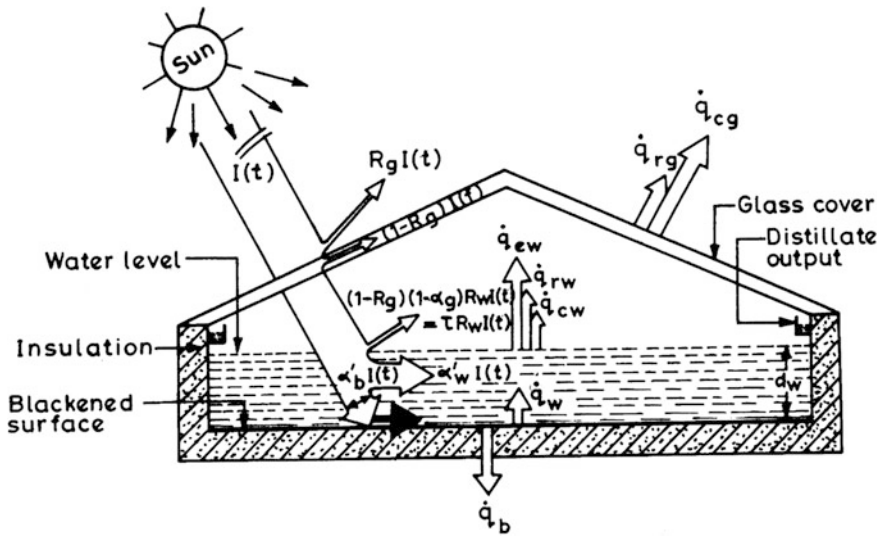
Fig. 13.2 Energy-flow diagram in a conventional double-slope passive solar still [from Tiwari and Mishra [16]]

basin. The remaining solar radiation reaches to the blackened absorber/basin liner where it is absorbed and heats the blackened absorber plate. Most of the thermal energy from the blackened absorber plate is transferred to the water mass through convection, and a small fraction is lost to the ambient air through the insulation on the bottom of the solar still. As the water temperature increases, heat is transferred from the water to the glass cover by (i) radiation ($\dot{q}_{rw}$), (ii) convection ($\dot{q}_{cw}$), and (iii) evaporation ($\dot{q}_{ew}$). The evaporated water (without impurity) first saturates the enclosure and then condenses on inner glass cover by releasing the heat of condensation to the glass cover. The glass cover loses thermal energy from the top surface to the ambient air by way of convection and radiation. The condensed droplets on the top glass cover trickle down to the lower ends of the inclined glass cover due to gravity and are stored in containers.

The fraction of short-wavelength solar radiation is shown in Fig. 13.2 at different components of the east distiller unit. These fractions can be mathematically expressed as follows [4]:

The fraction of incoming solar radiation absorbed by glass cover is given as follows:

$$\alpha_g' = (1 - R_g)\alpha_g \tag{13.1a}$$

The fractions of incoming solar radiation reflected and absorbed by water mass are given by Eqs. (13.1b) and (13.1c), respectively:

$$R'_{\mathrm{w}} = (1 - R_{\mathrm{g}})(1 - \alpha_{\mathrm{g}})R_{\mathrm{w}} \tag{13.1b}$$

$$\alpha'_{\mathrm{w}} = (1 - \alpha_{\mathrm{g}})(1 - R_{\mathrm{g}})(1 - R_{\mathrm{w}})\alpha_{\mathrm{w}} \tag{13.1c}$$

Further fractions of incoming solar radiation absorbed by basin liner and lost through water mass and the glass cover are given by Eqs. (13.1d) and (13.1e), respectively:

$$\alpha'_{\mathrm{b}} = (1 - R_{\mathrm{g}})(1 - \alpha_{\mathrm{g}})(1 - R_{\mathrm{w}})(1 - \alpha_{\mathrm{w}})\alpha_{\mathrm{b}} \tag{13.1d}$$

$$(1 - \alpha_{\mathrm{b}})(1 - R_{\mathrm{g}})(1 - \alpha_{\mathrm{g}})(1 - R_{\mathrm{w}})(1 - \alpha_{\mathrm{w}}) \tag{13.1e}$$

If attenuation of the solar radiation through the water mass is taken into account, then Eqs. (13.1c)–(13.1e) are given by Eqs. (13.2a)–(13.2c), respectively:

$$\alpha'_{\mathrm{w}} = (1 - R_{\mathrm{g}})(1 - \alpha_{\mathrm{g}})(1 - R_{\mathrm{w}})\left[1 - \sum \mu_j \exp(-\eta_j d_{\mathrm{w}})\right] \tag{13.2a}$$

$$\alpha'_{\mathrm{b}} = \alpha_{\mathrm{b}}(1 - R_{\mathrm{g}})(1 - \alpha_{\mathrm{g}})(1 - R_{\mathrm{w}})(1 - \alpha_{\mathrm{w}})\sum \mu_j \exp(-\eta_j d_{\mathrm{w}}) \tag{13.2b}$$

$$(1 - \alpha_{\mathrm{b}})(1 - R_{\mathrm{g}})(1 - \alpha_{\mathrm{g}})(1 - R_{\mathrm{w}})(1 - \alpha_{\mathrm{w}})\sum \mu_j \exp(-\eta_j d_{\mathrm{w}}) \tag{13.2c}$$

The numerical values of μ_j and η_j for different j are given in Table 13.1. The variation of attenuation factor with water depth is given in Table 13.2, and a variation of (α'_{b}) for different absorptivity (α_{w}) is reported in Table 13.3.

Example 13.1 Determine the attenuation factor for water depth of 0.15 m.

Solution
Attenuation factor $= \sum \mu_j \exp(-\eta_j d_{\mathrm{w}})$.

Substituting the different values of j, and μ_j, η_j from Table 13.1 in the above expression for $d_{\mathrm{w}} = 0.15$, one gets.

For $j = 1; \mu_j = 0.237$ and $\exp(-\eta_j d_{\mathrm{w}}) = 0.9952$; attenuation factor = 0.2359.

Similarly for $j = 2$ the attenuation factor = 0.1804; for $j = 3$ the attenuation factor = 0.106.

Table 13.1 Values of μ_j and η_j	j	μ_j	$\eta_j (m^{-1})$
	1	0.237	0.032
	2	0.193	0.45
	3	0.167	3.0
	4	0.179	35.0
	5	0.124	255.0

Table 13.2 Variation of attenuation factor with water depth

d_w	$\sum \mu_j \exp(-\eta_j d_w)$
0.20	0.51
0.10	0.5492
0.08	0.5648
0.06	0.5858
0.04	0.6185
0.02	0.6756
0.01	0.7344
0.008	0.7565
0.004	0.831
0.0	1.0

Table 13.3 Variation of α'_b with α_w (with dye) for $d_w = 0.10$, $R_g = R_w = 0.05$, $\alpha_g = 0.0$, and $\alpha_b = 0.8$

α_w	α'_b without attenuation
0.0	0.7220
0.2	0.5776
0.4	0.4332
0.6	0.2888
0.8	0.1444
1.0	0

For $j = 4$ the attenuation factor $= 0.939 \times 10^{-3}$; and for $j = 5$ the attenuation factor $= 0.939 \times 10^{-18}$.

Hence, the effective attenuation factor is $\sum \mu_j \exp(-\eta_j d_w) = 0.523$.

13.3 Thermal Efficiency

The thermal efficiency of a solar-distillation unit is defined as the ratio of distilled water to the input of solar energy. This efficiency can be classified as follows.

13.3.1 Instantaneous Thermal Efficiency

(a) **Passive solar still**

It is ratio of the rate of heat transfer due to mass transfer (evaporation) from the passive solar still $(\dot{Q}_{ew} = \dot{M}_{ew} \times L)$ to the rate of incident solar radiation $(I(t)A_s)$ on the glass cover. Mathematically it is defined as

$$\eta_{\mathrm{i}} = \frac{\dot{Q}_{\mathrm{ew}}}{I(t)A_{\mathrm{s}}} = \frac{\dot{M}_{\mathrm{ew}} \times L}{I(t)A_{\mathrm{s}}} = \frac{h_{\mathrm{ew}}(T_{\mathrm{w}} - T_{\mathrm{g}})}{I(t)} \qquad (13.3\mathrm{a})$$

where L and A_{s} are the latent heat of condensation (J/kg °C) and the area of the solar still (m^2), respectively. The rate of distilled water ($\dot{M}_{\mathrm{ew}}$) will depend on the difference between the temperatures of the water (T_{w}) and the glass cover (T_{g}), i.e., ($T_{\mathrm{w}} - T_{\mathrm{g}}$). The h_{ew} is an evaporative (mass) transfer coefficient (W/m^2 °C).

(b) **Active solar still**

It is important to mention here that the rate of distilled water yield will depend on the temperature difference between the water and the glass cover, i.e., ($T_{\mathrm{w}} - T_{\mathrm{g}}$). One of the methods to increase the temperature difference between the water and the glass cover is to increase the water temperature by feeding some additional thermal energy into the basin of the solar still. Such a solar-distillation unit is referred to as an "active solar still."

In the present chapter, we describe an external thermal energy fed by flat-plate collectors integrated with the basin of the solar-distillation unit. In this case, an instantaneous thermal efficiency can be written as follows:

$$\eta_{\mathrm{i}} = \frac{\dot{Q}_{\mathrm{ew}}}{I(t)A_{\mathrm{s}}} = \frac{\dot{M}_{\mathrm{ew}} \times L}{I(t)A_{\mathrm{s}} + NA_{\mathrm{c}}I'(t)} = \frac{h_{\mathrm{ew}}(T_{\mathrm{w}} - T_{\mathrm{g}})A_{\mathrm{s}}}{I(t)A_{\mathrm{s}} + NA_{\mathrm{c}}I'(t)} \qquad (13.3\mathrm{b})$$

It is to be noted that the operating temperature of the water in the basin of active solar still will be higher than the operating temperature of that in a passive solar still; hence, an instantaneous thermal efficiency of the active solar still will be lower compared with that of the passive solar still, i.e.,

$$\eta_{\mathrm{i,active}} < \eta_{\mathrm{i,passive}} \qquad (13.3\mathrm{c})$$

13.3.2   An Overall Thermal Efficiency

The overall thermal efficiency of the passive and active solar-distillation unit can be mathematically expressed as follows:

(a) **Passive solar still**

$$\eta_{\mathrm{i,passive}} = \frac{\sum \dot{M}_{\mathrm{ew}}L}{A_{\mathrm{s}} \int I(t)\mathrm{d}t} \times 100 \qquad (13.4\mathrm{a})$$

(b) **Active solar still**

$$\eta_{i,active} = \frac{\sum \dot{M}_{ew} L}{\left[A_s \int I(t)dt + NA_c \int I'(t)dt\right]} \times 100 \qquad (13.4b)$$

where N is the numbers of collectors connected either in series or parallel. The temperature-dependent latent heat of vaporization (L) is given as follows [5]:

(a) For temperature $> 70\,°C$

$$L = 3.1615 \times 10^6 \left[1 - 7.616 \times 10^{-4} T\right] \qquad (13.5a)$$

(b) For operating temperature $< 70\,°C$.

$$L = 2.4935 \\ \times 10^6 \left[1 - 9.4779 \times 10^{-4} T + 1.3132 \times 10^{-7} T^2 - 4.7974 \times 10^{-9} T^3\right] \qquad (13.5b)$$

13.4 Basic Heat Transfer

The basic heat-transfer process in a solar-distillation unit (Fig. 13.2) is classified as follows:

(a) **External**: External heat transfer includes heat transfer from the outer surfaces of the solar still to the ambient air. The mutually independent mechanisms involved in external heat transfer are conduction, convection, and radiation.

(b) **Internal**: The heat transfer tacking place between the water's top surface and the glass cover falls under the category of "internal heat transfer." Internal heat-transfer mechanism involve convection, evaporation, and radiation. Evaporative heat transfer depends on convection heat transfer, but radiative heat transfer is independent from both convective and evaporative heat transfer.

13.4.1 External Heat Transfer

According to Chap. 5, external heat transfer consists of (a) transfer from the inner glass cover to the ambient air mainly due to conduction, convection, and radiation' and (b) transfer from the basin liner to the ambient air through the bottom and side insulation.

From the inner glass to the ambient air

In this case, it is important to mention that heat transfer due to conduction through the glass cover can be neglected as proven in Chap. 5 (Sect. 5.5.4); hence, there will be only convective and radiative heat transfer in W/m^2 from the outer glass cover to the ambient air, which can be expressed as

$$\dot{q}_{ga} = h_2(T_g - T_a) \tag{13.6}$$

where $h_2 = 5.7 + 3.8$ is similar to Eq. (3.29a).

From the bottom insulation to the ambient air

In this case, an expression for a convective heat-transfer coefficient from the bottom insulation to the ambient air can be considered by

$$h_b = 2.8 + 3V \tag{13.7}$$

similar to Eq. (3.29b).

In the above equation, radiative heat transfer is neglected because the bottom of the insulation faces the surface of the ground.

13.4.2   Internal Heat Transfer [2]

This section covers in detail internal heat-transfer processes, which includes radiation, convection, and evaporation.

Radiative heat transfer

In this case, the water surface and the glass cover are considered to be parallel planes to take the radiation shape factor as 1. This approximation requires a small inclination of the glass cover of the solar-distillation unit. The rate of radiative heat transfer ($\dot{q}_{rw}$) (Eq. 3.34a) from the water surface to the glass cover is given by

$$\dot{q}_{rw} = \varepsilon_{eff}\sigma\left[(T_w + 273)^4 - (T_g + 273)^4\right] \tag{13.8a}$$

or

$$\dot{q}_{rw} = h_{rw}(T_w - T_g) \tag{13.8b}$$

where h_{rw} is the radiative heat-transfer coefficient from the water surface to the glass cover (Eq. 3.34f), which is expressed as

$$h_{rw} = \varepsilon_{eff}\sigma\left[(T_w + 273)^2 + (T_g + 273)^2\right]\left[T_w + T_g + 546\right] \tag{13.8c}$$

Convective heat transfer

Convective heat transfer occurs between the water surface and the humid air inside the solar still. It depends on buoyancy, density gradient of the humid air, and temperature gradient in the different layers of air:

The rate of heat transfer from the water surface to the glass cover $(\dot{q}_{cw})$ in (W/m^2) by convection can be determined by

$$\dot{q}_{cw} = h_{cw}(T_w - T_g) \tag{13.9a}$$

where the convective heat-transfer coefficient, h_{cw}, can be determined by the relation

$$Nu = \frac{h_{cw}d_f}{K_f} = C(GrPr)^n$$

or

$$h_{cw} = \frac{K_f}{d_f}C(GrPr)^n \tag{13.9b}$$

where an expression for the Grashof and Prandtl numbers (Chap. 3) depends on the physical properties of moist air; and K_f and d_f are thermal conductivity of water in the basin and characteristic dimension of the basin in the solar still, respectively.

In the Grashof number, the following expression of $\Delta T'$ should be used [1]

$$\Delta T' = \left[\Delta T + \frac{(P_{w0} - P_{g0})(T_{w0} + 273)}{268.9 \times 10^3 - P_{w0}}\right] \tag{13.9c}$$

For a normal operating-temperature range, say $50\,°C$ and $\Delta T' = 17\,°C$, the expression for the Grashof number is reduced to

$$Gr = 2.81 \times 10^7 d_f^3 \tag{13.9d}$$

As can be seen from Eq. (13.9d), the Grashof number depends on the average gap between the glass cover and the water surface (Table 13.4) for a typical operating-temperature range. The values of C and n for different ranges of Grashof number are given in Table 3.5. For the typical operating-temperature range and

Table 13.4 Value of the Grashof number (Gr) for different average spacing (d_f)

d_f (m)	Gr	C	n
0.15	0.948×10^5	0.21	1/4
0.20	2.248×10^5	0.21	1/4
0.25	4.39×10^5	0.075	1/3

Table 13.5 The values of C and n for different Grashof number ranges

Case	C	n	Grashof number	Source
I	1.00	0	$Gr < 10^3$	Mull and Reiher [17]
	0.21	1/4	$10^4 < Gr < 3.25 \times 10^5$	
	0.075	1/3	$3.2 \times 10^5 < Gr < 10^7$	
	0.07477	0.36	$2.5 \times 10^3 < Gr < 6 \times 10^4$	
II	0.05238	0.36	$2.5 \times 10^5 < Gr < 10^7$	Held [18]
	0.05814	0.4	$2 \times 10^3 < Gr < 5 \times 10^4$	
III	3.8	0.0	$5 \times 10^4 < Gr < 2 \times 10^5$	De Graaf and Held [19]
	0.04836	0.37	$2 \times 10^5 < Gr$	
IV	0.3	1/4	$2.8 \times 10^3 < Gr < 2.1 \times 10^5$	Jakob and Gupta [20]
	0.1255	1/3	$4.2 \times 10^5 < Gr < 4.2 \times 10^9$	

$d_f = 0.25$ m ($C = 0.075$ and $n = 1/3$), Dunkle [6] obtained the following expression for h_{cw} in (W/m^2) :

$$h_{cw} = 0.884 \left[T_w - T_g + \frac{(P_w - P_g)(T_w + 273)}{268.9 \times 10^3 - P_w} \right]^{1/3} \tag{13.9e}$$

Evaporative heat transfer

According to Sect. 3.3.5, the rate of heat transfer per unit area from the water surface to the glass cover is given by

$$\dot{q}_{ew} = 0.0162 \times h_{cw} \times \left(P_w - P_g \right) \tag{13.10a}$$

or

$$\dot{q}_{ew} = h_{ew} \times (T_w - T_g) \tag{13.10b}$$

where

$$h_{ew} = 16.273 \times 10^{-3} h_{cw} \times \left[\frac{P_w - P_g}{T_w - T_g} \right] \tag{13.10c}$$

(Cooper [7]) The value of h_{ew} is closer for the higher value of $(T_w - T_g)$. In addition, it gives the real values only for the positive values of $(T_w - T_g)$; otherwise the theoretical values for the distillate output is a complex number. The values of P_w and P_g (Eq. 13.10c) for the operating-temperature range of 10–90 °C can be expressed as follows:

$$P(T) = \exp\left(25.317 - \frac{5144}{T + 273}\right) \tag{13.10d}$$

The total internal heat-transfer coefficient can be obtained by combining Eqs. (13.8c), (13.9e), and (13.10c), and is given as

$$h_1 = h_{rw} + h_{cw} + h_{ew} \tag{13.10e}$$

Now the internal heat transfer from the water surface to the inner glass cover is given by

$$\dot{q}_{wg} = \dot{q}_{rw} + \dot{q}_{cw} + \dot{q}_{ew} = h_1(T_w - T_g) \tag{13.10f}$$

Basin-liner convective heat transfer
The rate of convective heat transfer from the basin liner (blackened surface) to the water mass can be estimated by

$$\dot{q}_{bw} = h_{bw}(T_b - T_w) \tag{13.11a}$$

where the convective heat-transfer coefficient, h_{bw}, from the basin liner (blackened surface) to the water mass can be determined by the following expression:

$$Nu = \frac{h_{bw}X}{K_w} = C(GrPr)^n$$

or

$$h_{bw} = \frac{K_w}{X}C(GrPr)^n \tag{13.11b}$$

For a hot surface facing upward, $C = 0.54$ and $n = 0.25$ (Table 3.3). The Gr and Pr can be determined at the average water temperature in the basin. The numerical values of h_{bw} will be on the order of three digits, and one can consider the value as ≥ 100 W/m^2 °C.

13.4.3   Overall Heat-Transfer Coefficient

There are basically two overall heat-transfer coefficients: the overall top-loss coefficient and the overall bottom-loss coefficient, which can be expressed using the thermal circuit diagram shown in Fig. 13.3.

(a) **Overall top-loss coefficient**
    The top-loss coefficient (U_t) from the water surface to the ambient air through the condensing glass cover can be written as

Fig. 13.3 Thermal-circuit diagram of a solar-distillation unit
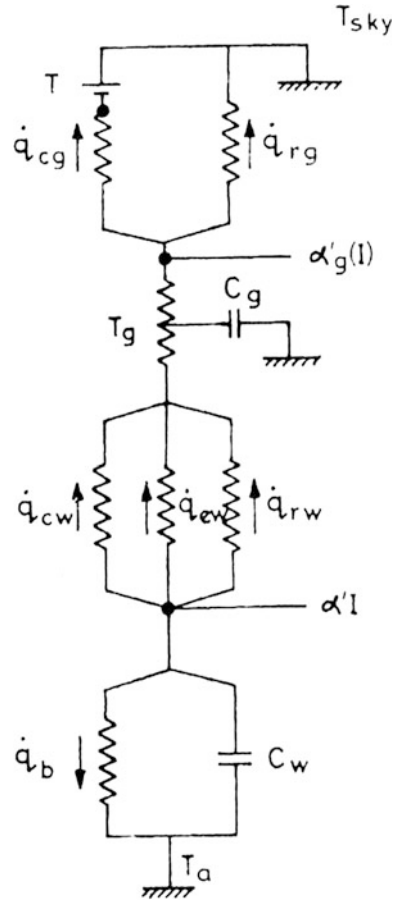
$$U_t = (r_1 + r_2)^{-1} = \left[\frac{1}{h_1} + \frac{1}{h_2} \right]^{-1} \tag{13.12a}$$

Here the conductive heat-transfer coefficient can be neglected as done in Sect. 5.5.4.

Hence, the rate of heat lost in the upward direction from the distillation system through the condensing cover is given by

$$\dot{q}_t = U_t (T_w - T_a) \tag{13.12b}$$

(b) **Overall bottom-loss coefficient**

Using the definition of an overall heat-transfer coefficient, an overall bottom-heat transfer from the basin liner to the ambient air through the bottom insulation in W/m² can be written as

$$\dot{q}_b = U'_b(T_b - T_a) \tag{13.13a}$$

where U'_b is an overall bottom heat–transfer coefficient in W/m^2 °C, which is expressed as

$$U'_b = (r_i + r_b)^{-1} = \left[\frac{L_i}{K_i} + \frac{1}{h_b}\right]^{-1} \tag{13.13b}$$

where L_i and K_i are the thickness and thermal conductivity of the bottom and side insulation, respectively.

If side losses are considered, then an overall edge-loss coefficient can be considered as

$$U'_e = U'_b \frac{A_{ss}}{A_s} \tag{13.13c}$$

Thus, the total bottom$-$loss coefficient $= U'_{be} = U'_b + U'_e$

For small water depth, $U'_e = 0$.

Furthermore, an overall bottom-heat transfer from the water mass to the ambient air through the bottom insulation in W/m^2 °C can be written as

$$\dot{q}_b = U_b(T_w - T_a) \tag{13.14a}$$

Where U_b is an overall bottom heat–transfer coefficient in W/m^2 °C, which is expressed as

$$U_b = (r_{bw} + r_i + r_b)^{-1} = \left[\frac{1}{h_{bw}} + \frac{L_i}{K_i} + \frac{1}{h_b}\right]^{-1} \tag{13.14b}$$

Overall total loss coefficient

From Eqs. (13.12a) and (13.14b), an overall total heat-transfer coefficient from the water mass to the ambient air through the glass and bottom insulation can be written as

$$U_L = U_t + U_b \tag{13.15}$$

Example 13.2 Determine an overall bottom-loss coefficient (U_b) from a solar still with 5 mm–thick insulation $K_i = 0.04$ W/m^2 °C given $h_{bw} = 100$ and 1000 W/m^2 °C.

Solution

From Eq. (13.14b), an overall bottom-loss coefficient from the water to the ambient air is given by

$$U_b = \left[\frac{1}{h_{bw}} + \frac{L_i}{K_i} + \frac{1}{h_b}\right]^{-1}$$

Here $h_b = 5.7\,\text{W/m}^2\,^\circ\text{C}$ (Eq. 9.14a), $h_{bw} = 100\,\text{W/m}^2\,^\circ\text{C}$, $K_i = 0.04\,\text{W/m}\,^\circ\text{C}$, and $Li = 5\,\text{mm} = 0.005\,\text{m}$ (given). Then

$$U_b = \left[\frac{1}{100} + \frac{0.005}{0.04} + \frac{1}{5.7}\right]^{-1} = 3.22\,\text{W/m}^2\,^\circ\text{C}$$

Similarly, U_b can be found for $h_{bw} = 1000\,\text{W/m}^2\,^\circ\text{C}$.

Example 13.3 Determine an overall top-loss coefficient from a water surface at $20\,^\circ\text{C}$ to the ambient air at $8.5\,^\circ\text{C}$ through glass cover given that the temperature of the glass cover is $12\,^\circ\text{C}$.

Solution
The radiative, convective, and evaporative heat-transfer coefficients from the water to the glass are given by Eqs. (13.8c), (13.9e), and (13.10c), respectively.
Here in the given problem

$$\varepsilon_{\text{eff}} = \left[\frac{1}{0.9} + \frac{1}{0.9} - 1\right]^{-1} = 0.82 \text{ for } \varepsilon_g = \varepsilon_w = 0.9$$

Now the radiative heat-transfer coefficient (Eq. 13.8c) is

$$h_{rw} = 0.82 \times 5.67 \times 10^{-8}\left[(20+273)^2 + (12+273)^2\right][20+12+546]$$
$$= 4.49\,\text{W/m}^2\,^\circ\text{C}$$

In addition $P_w = 2367.69\,\text{N/m}^2$ and $P_g = 1447.18\,\text{N/m}^2$. Furthermore, the convective mass transfer coefficient is given by

$$h_{cw} = 0.884\left[(20-12) + \frac{(2367.69 - 1447.18)(293)}{268.9 \times 10^3 - 2367.69}\right]^{1/3} = 1.84\,\text{W/m}^2\,^\circ\text{C}$$

An evaporative heat-transfer coefficient is given by

$$h_{ew} = 16.273 \times 10^{-3} \times 1.84 \times \left[\frac{920.5}{8}\right] = 3.445\,\text{W/m}^2\,^\circ\text{C}$$

Now the total internal heat-transfer coefficient can be obtained as

$$h_1 = 3.445 + 1.84 + 4.49 = 9.775 \, \text{W/m}^2 \, {}^\circ\text{C}$$

and the upward external heat-transfer coefficient is given by

$$h_2 = 17.1 \, \text{W/m}^2 \, {}^\circ\text{C}$$

The overall top-loss coefficient from the water surface to the ambient air through the glass cover can determined (Eq. 13.12b) as

$$U_t = \left[\frac{1}{17.1} + \frac{1}{9.775} \right]^{-1} = [0.058 + 0.102]^{-1} = 6.25 \, \text{W/m}^2 \, {}^\circ\text{C}$$

13.4.4 Distillate Yield

The hourly distillate yield per m^2 from a solar-distillation unit can be written as

$$\dot{m}_{ew} = \frac{\dot{q}_{ew}}{L} \times 3600 = \frac{h_{ew}(T_w - T_g)}{L} \times 3600 \qquad (13.16a)$$

After knowing the hourly yield ($\dot{m}_{ew}$), the daily yield can be determined by adding all hourly yields in a day as

$$M_{ew} = \sum \dot{m}_{ew} \qquad (13.16b)$$

13.5 Other Designs of Passive/Active Solar Stills [1, 2]

It is important to note from Eq. (13.16a) that the hourly yield ($\dot{m}_{ew}$) can be increased by increasing either the numerical value of h_{ew} or the difference between the water and glass temperatures i.e., $(T_w - T_g)$. These conditions can be achieved by any one of the below methods as follows:

(i) Decrease the condensing glass cover temperature.
(ii) Increase the water temperature in the basin.
(iii) Achieve both conditions (i) and (ii).

13.5.1   Passive Solar Still

In this case, generally the condensing cover temperature is reduced by changing the design of solar still as follows:

(a) **Solar still with passive condenser**

In a conventional passive solar still, the condensing glass cover acts as the input (solar radiation) as well as output surface (hourly yield). The latent heat of condensation released by the evaporated water to the glass condensing cover increases the condensing-surface temperature. If the rate of release of the latent heat of condensation is not equal to the rate of release of heat from the condensing cover to the ambient air, then the temperature of the condensing cover starts increasing, which reduces the temperature difference between the water and the condensing cover and hence decreases the hourly yield. In this design, the condensing chamber is separated from the evaporated water chamber in the basin as shown in Fig. 13.4. In this case, the condensing chamber is made of conducting material to release the latent heat of condensation as quickly as possible to have a minimum condensing-cover temperature. There is very little condensation on the sloped glass surface; condensation mainly takes place in the attached passive condenser. This is due to the purging of vapor into the condenser. Because most of the latent heat of condensation is given to the passive condenser, the temperature difference between condenser and the water is greater, which causes faster evaporation and increases distillate output.

To further increase hourly yield, a provision for the natural circulation of vapor can be made between the condensing chamber and the evaporating chamber.
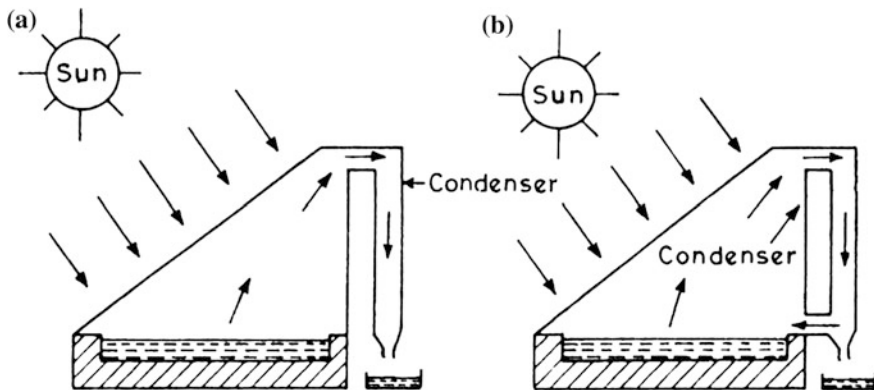
Fig. 13.4 Single-slope solar still with a passive condenser. **a** Purging. **b** Natural circulation

(b) **Double-condensing chamber solar still**

The design of the solar still with a passive condenser was modified by Agrawal and Tiwari [8], and the modified design is known as a "double-condensing chamber" (DCS). A schematic view of a double-condensing chamber solar still (DCS) is shown in Fig. 13.5. The double-condensing chamber (DCS) has two chambers: chamber I and chamber II. They are separated by an insulating partition wall. The condensing cover for chamber II is made of stainless steel. The shading of chamber II is performed with cardboard covered with black plastic so that it does not receive solar radiation directly. A mirror is also fitted on the partition wall facing chamber I to reflect most of the solar radiation falling on it toward the water surface in the basin. A double-glass cover is used to ensure minimum upward heat loss and maximum vapor temperature for maximum pressure difference between the two chambers.

For faster discharge of heat from the metallic condensing cover, a water-flow arrangement over it was also made.

(c) **Conical solar still**

In a conical solar still, the condensing surface area is significantly greater compared with that of a conventional passive solar still (Fig. 13.6); hence, the rate of heat loss from the condensing surface area to the ambient air is more for the lower temperature of the condensing cover (T_g). There will be higher hourly yield in this solar still. Brackish water is fed in a transparent twin-cone arrangement. Solar radiation is transmitted through the transparent enclosure to heat the water. It causes evaporation and then condensation on the inner
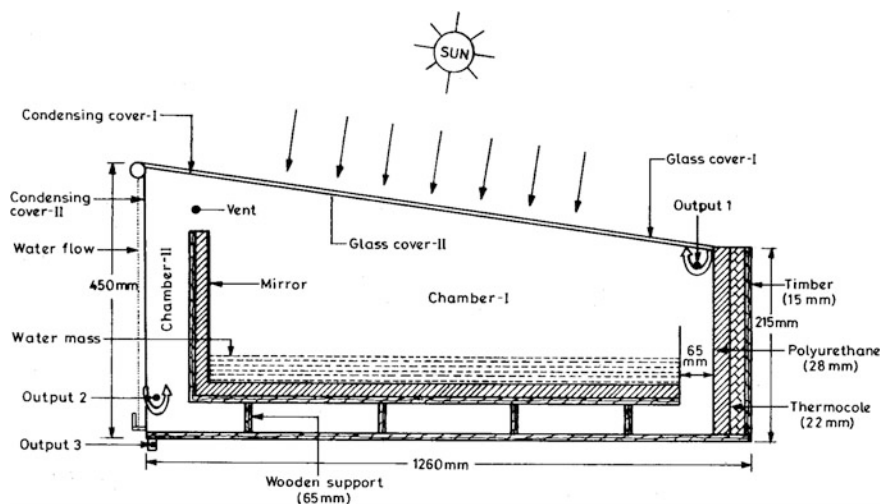
Fig. 13.5 Schematic view of a double condensing–chamber solar still
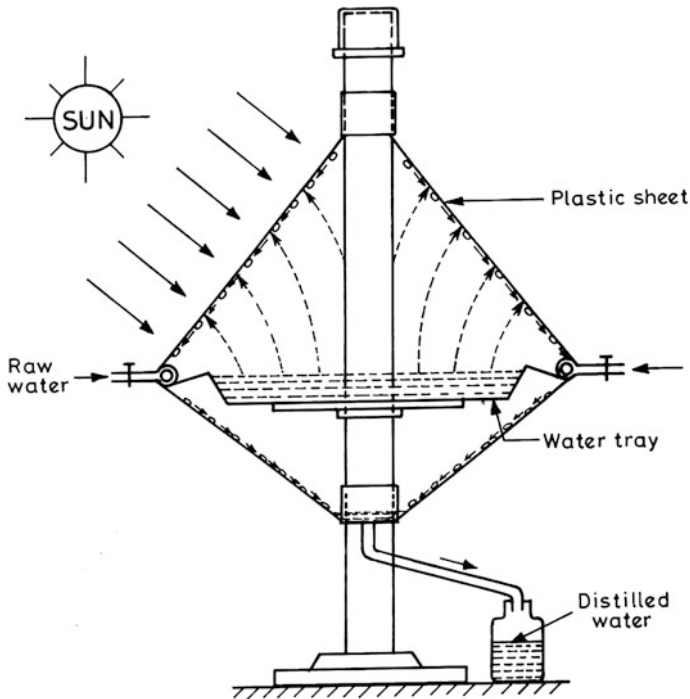
Fig. 13.6 Schematic diagram of a conical solar still

face of the transparent cone. Condensed water droplets slide past in the water pan and are collected in the bottom cone.

(d) **Inverted-absorber solar still**

The schematic view of an inverted-absorber solar still is shown in Fig. 13.7. In this type of solar still, the surface receiving the input energy (solar radiation) is separated from the condensing surface unlike a conventional solar still. Solar radiation is received from below the absorbing plate, and condensation takes place on the inner surface of the metallic condensing cover. The metallic condensing cover can also be replaced by a transparent condensing cover. The absorbing surface area can be a selective surface for high absorbtion and low emissivity to minimise heat losses from the bottom. For a metallic condensing cover in an inverted-absorber solar still, there is an additional advantage of increased upward heat transfer to the atmosphere as well as low maintenance costs. A HIGH absorptive surface and increased upward heat transfer to the atmosphere results in a higher yield. This design consists of a cylindrical reflector integrated with the solar still. It is based on the concept of an inverted-absorber flat-plate collector.

As shown in Fig. 13.7, solar radiation after transmission and multiple reflections by the reflecting surface reaches the selective absorber plate
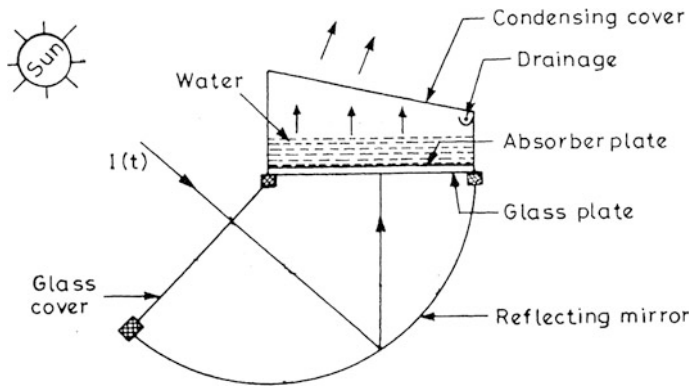
Fig. 13.7 Schematic diagram of an inverted-absorber solar still

through the glass plate G_2. Most of the solar radiation is absorbed by the selective surface, and then it is converted into thermal energy. Most of the thermal energy is transferred to the water mass above the absorber plate where the water is heated. A very small part of it is lost to the atmosphere through the glass plate G_1. Furthermore, heat from the water mass is lost to the metallic condensing cover in the form of radiation, convection, and evaporation. The evaporated water releases it's latent heat of vaporaization to the glass cover and condenses. The condensed droplets trickle down under gravitational force and collect through the channel at the lower end of the inclined glass cover. The heat transferred to the condensing cover is lost to the ambient air through radiation and convection at a faster rate compared with a conventional solar; this is still due to the metallic cover rather than the glass.

(e) **Multi-wick solar still [9]**

A cross-sectional view of multi-wick solar still is shown in Fig. 13.8. The structure of this type of solar still is made of an insulated fibre–reinforced plastic (FRP) material. It can also be any light-insulating material. There is water storage tank at one end. Furthermore, a flat surface made of the same material, with optimum inclination, is attached to it to support the multi-wick system as shown in the figure. One end of the blackened multi-wick system is dipped in the water of the storage tank, and the other ends are spread over the flat surface. Each layer of blackened jut cloth wick is separated by a thin plastic sheet so that each jute cloth acts independently. Before arranging the blackened multi-wick jute cloth over a flat surface, it should be wetted so that capillary action starts immediately. In this design, the storage effect due to the water film over the jute cloth is neglected. The inclined-wick solar still has black porous fabric that acts as an absorber. Water is fed at a slow rate through the porous absorber by capillary action of the jute cloth placed in the water-storage tank. There is a glass cover over the jute cloth, which acts as a condensing cover. The water in the absorber (jute cloth) is evaporated
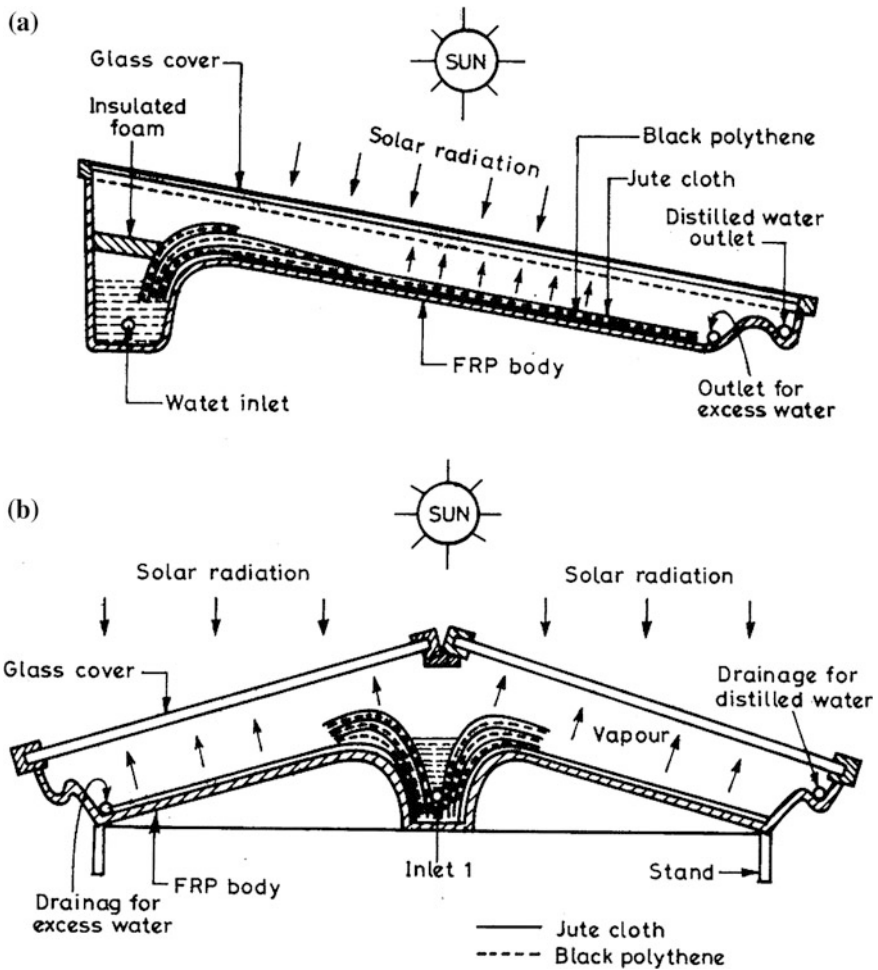
Fig. 13.8 Cross-sectional view of **a** an FRP multi-wick solar still and **b** an FRP double-slope multi-wick solar still

immediately after receiving solar radiation and condenses on the inner surface of the glass cover. Such a solar still even works under diffuse climatic conditions.

(f) **Multiple-effect solar still**

The latent heat of condensation released to the condensing cover is lost to the ambient air by convection and radiation in the passive solar still. If the latent heat of condensation released to the condensing cover is used further for distillation purpose, as performed in the double-basin solar still, then the overall yield is increased. This process can be repeated a number of times. In contrast, the rate of solar radiation reaching the basin is also affected

significantly. In addition, there will be a problem of maintenance in this type of solar still; hence, it is never recommended for producing distilled water. The multi-effect solar still has more than two basins.

13.5.2 Active Solar Still [10]

As mentioned previously, the hourly yield is directly proportional to the temperature difference between the water and the internal glass cover (condensing cover). The temperature of the water mass can be increased by supplying thermal energy from the external active thermal-energy source. Such a solar still is referred to as an "active solar still."

The different arrangements for feeding thermal energy from the external sources are classified as follows:

(a) **Nocturnal production**: In this case, the waste hot water available from industries is fed into the basin once in a day.
(b) **Preheated water applications**: The feeding of hot water available from industries is fed into the basin at a constant flow rate.
(c) **Distillation with a collector panel**: The feeding of hot water from a flat-plate collector is fed into the basin by integration. It can be either a **flat plate** or **concentrator**.

The methodologies and performance of the active solar still will be briefly discussed in the following subsections.

(a) **Nocturnal production**
The hourly yield from any solar still in the absence of solar radiation is known as "nocturnal production." A conventional passive solar still with large water depth in the basin stores a large amount of thermal energy from solar radiation during the day due to its large heat capacity. During low solar radiation, the hot water (heated from a source other than solar radiation, i.e., nocturnal production) can be supplied to the basin for higher yield. The first parametric studies were performed by Malik and Tran [11] with a mathematical model for predicting nocturnal distillate under controlled environment conditions. Madhuri and Tiwari [12] studied the effect of feeding hot water in the morning (once in a day) on the performance of a conventional passive solar still. They reported that the daily distillate output increases with water depth in the basin due to the nocturnal effect. This is the reverse of the performance of a passive solar still (passive).

(b) **Preheated water application**
Preheated waste hot water available from industries/thermal-power plants can be used in the basin as raw water. The use of preheated waste hot brine water in a tubular solar still is fed at a constant flow rate; this was studied by Tiwari

and Kumar [13], the researchers found that the solar still with low water depth acts in the passive mode even during the daytime. Such a condition is not effective during the night hours due to there being no storage effect. Therefore, the solar-distillation unit can be used under both passive as well as active mode depending on the water depth in the basin under nocturnal mode. Intermittent as well as continuous feeding of preheated hot water is used by many scientists.

(c) **Distillation with a collector panel**

In this case, additional hot water from a collector panel is fed into the basin of a passive-mode solar still to obtain a higher water temperature. In this case, the collector panel is integrated with the basin of a solar-distillation unit. The collector panel may be either a conventional /PVT water collector (Chap. 5) or a CPC-PVT collector (Chap. 6). Furthermore, integration of the collector panel may be done either directly or through a heat exchanger depending on the type of fluid used in the closed loop. As shown in Fig. 13.9, a PVT water-collector panel is integrated with a basin-type single-slope solar still. The connecting pipes are completely insulated so that there is no heat loss to the ambient air during water circulation. The water in the basin is heated by solar energy through the inclined glass cover as explained in the working principle (previous text). The water in the basin is additionally heated by the flat-plate collector. This results in higher evaporation and more distillate output. Water circulation through the collector panel is performed during sunshine hours. It is closed during off-sunshine hours to avoid heat losses.

As shown in Fig. 13.10, a collector panel consists of a number of collectors integrated with the basin of solar still. The water temperature in the basin can be further increased, hence the increase in distillate output. The optimum number of

Fig. 13.9 A schematic view of an active solar still coupled with a PVT flat-plate collector
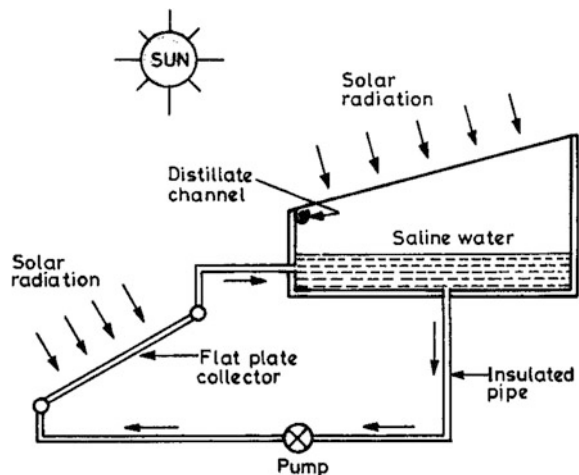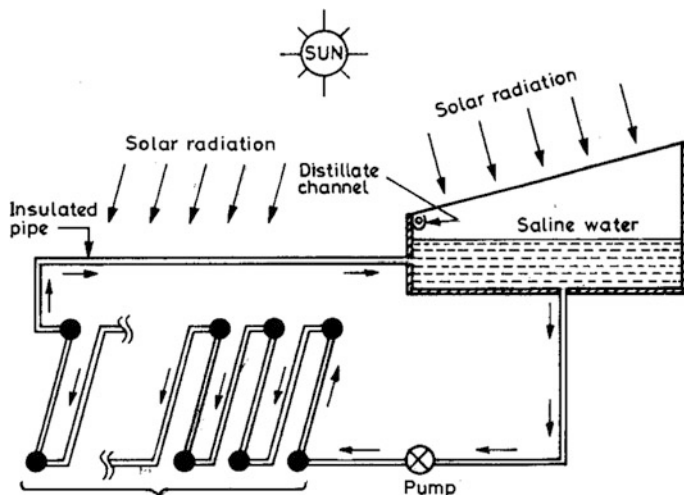
Fig. 13.10 A schematic view of a solar still coupled with a flat plate–collector panel

collectors for maximum distillate output depends on the number of parameters as follows:

(a) water mass in the basin;
(b) mass-flow rate in the collector loop'
(c) climatic conditions; and
(d) number of effects, etc.

Distillation unit with a hybrid system
In this case, distillate yield can be increased by exhausting moist air from the basin enclosure to the condensing chamber using an electrically operated fan. Figure 13.11 shows a solar still (single slope) integrated with an active component. Electricity runs the active components (blower and condenser), which can be met using a photovoltaic system or integration of a photovoltaic system with a solar-distillation system to make it a hybrid system.

13.6 Heat and Mass Transfer: A New Approach [14]

In Sect. 13.4, basic heat and mass transfer in relation to the solar-distillation system is discussed. However, most transfer of heat and mass has the following limitations:

(a) The inclination of the condensing cover is small to make parallel the evaporating and condensing cover; and
(b) the operating temperature range is approximately $50\,^\circ\mathrm{C}$.
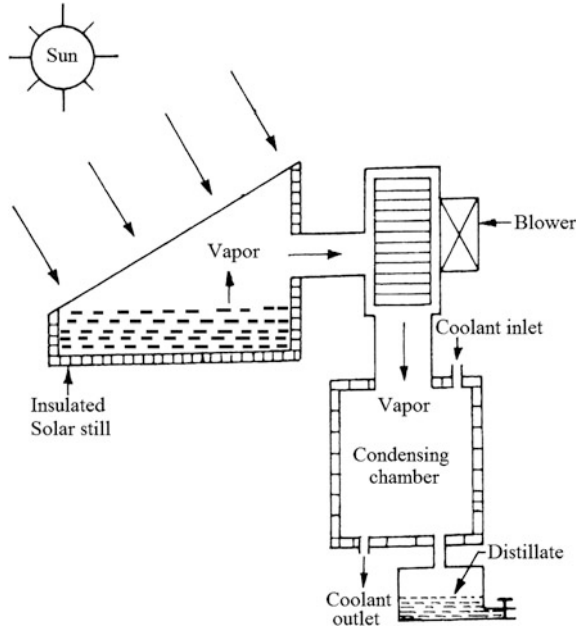
It is well known that evaporative heat transfer plays a dominant role compared with other modes of internal heat transfer; hence, we will discuss only evaporative heat transfer in this section. Furthermore, evaporative heat transfer directly depends on an internal convective heat-transfer coefficient. It is important to mention here that the evaporating/condensing cover may not be parallel as can be seen in other solar-still designs (Sect. 13.5). Therefore, there is need for further study into an internal convective heat transfer without any limitations.

According to Eq. (13.10a), the hourly distillate output per square metre from a solar-distillation unit can be written as follows:

$$\dot{m}_{ew} = \frac{\dot{q}_{ew} \times 3600}{L} = \frac{0.0162 \times h_{cw} \times (P_w - P_g) \times 3600}{L} \tag{13.17}$$

where an expression for h_{cw} is given by Eq. (13.9b).

After substituting an expression from Eq. (13.9b) for h_{cw} in Eq. (13.17) and rearranging, one gets

$$\frac{\dot{m}_{ew}}{R} = C(Gr.Pr)^n \tag{13.18}$$

where

$$R = \frac{0.0162 \times (P_w - P_g) \times k_f \times 3600}{L \times d_f}$$

Now Eq. (13.18) can be written in the following form:

$$y = ax^b \tag{13.19}$$

where $y = \frac{\dot{m}_{ew}}{R}$; $x = Gr.Pr$; $a = C$ and $b = n$.

By considering log on both the sides of the Eq. (13.19), it can be written in the form of a straight-line equation as

$$y' = b'x' + a' \tag{13.20}$$

where

$$y' = \ln y;\ b' = b;\ x' = \ln x;\ a' = \ln a$$

Using the linear regression analysis method, coefficients a' and b' in Eq. (13.20) can be obtained as

$$a' = \left(\frac{\sum y'}{N}\right) - b'\left(\frac{\sum x'}{N}\right)$$

and

$$b' = \frac{N(\sum x'y') - (\sum x')(\sum y')}{N(\sum x'^2) - (\sum x')^2}$$

where N is the number of experimental observations under steady-state conditions. Under a quasi steady-state conditions, N becomes $N + 1$ (Example 13.1).

After determining a' and b' from the above equation, C' and n' can be obtained by the following expression:

$$C = \exp(a') \text{ and } n = b'$$

Once the value of C and n are known, a convective heat-transfer coefficient can be obtained from Eq. (13.9b).

The procedure for evaluating an evaporative heat-transfer coefficient is the same as discussed in Sect. 13.4.

It should be noted that if the hourly rate of distillate output ($\dot{m}_{ew}$), water, and condensing cover temperature is known experimentally for any design of solar still as discussed in Sect. 13.5, then the internal convective and evaporative heat-transfer coefficient can be determined without any limitation of shape of the condensing cover and operating temperature.

13.7 Thermal Modelling

Here it important to mention that the passive solar still is a special case of active solar still if the feeding of external thermal energy is made to be zero. Hence, we will discuss the thermal modelling of active solar-distillation unit,which can also be used for a passive solar still. Furthermore, it is observed that in an active solar still the rate of condensation is much higher than the rate of heat loss from the condensing cover to the ambient air, and the glass cover temperature becomes significantly greater in case of an active solar still. Thus, the inner glass-cover temperature is greater than that of the outer glass-cover temperature. In thermal modelling, we make one of most important assumptions for the same inner and outer condensing cover temperature. The schematic diagram of a single-slope active solar still is shown in Fig. 13.9.

Energy balances: Heat fluxes at various component of a double-slope passive solar still facing east–west are shown in Fig. 13.2. The fluxes are the same for a single-slope south-facing solar still. The only difference will be the rate of incident solar radiation in each case.

The energy-balance equations (in W/m^2) for different components of a solar still have been written with the following assumptions:

  (i)   The inclination of the glass condensing cover is very small.
 (ii)   The thermal heat capacity of the different components (glass cover, absorbing blackened surface, side insulation, and bottom insulation) is very small.
(iii)   The active solar-distillation unit is airtight.

For the glass Cover: The glass cover receives energy from the absorbed solar radiation and from the hot water in the basin. Under steady-state conditions, this energy will be balanced by energy lost to the air by radiation and convection.

$$\alpha'_g I(t) + [\dot{q}_{rw} + \dot{q}_{cw} + \dot{q}_{ew}] = \dot{q}_{rg} + \dot{q}_{cg} \qquad (13.21)$$

For the water Mass: The water receives energy from the absorbed solar radiation, energy convected from the basin liner, and useful energy from external sources (FPC, PVT-FPC, CPC-PVT). The energy received by the water is distributed in raising the temperature of the water and in losses due to radiation, convection, and evaporation

$$A_s\left[\alpha'_w I(t) + \dot{q}_b\right] + \dot{Q}_{u,N} = (MC)_w \frac{dT_w}{d}t + A_s[\dot{q}_{rw} + \dot{q}_{cw} + \dot{q}_{ew}] \qquad (13.22)$$

An expression for $\dot{Q}_{u,N}$ is given by

$$\dot{Q}_{u,N} = 0 \;\; \text{For a passive solar still}$$

where $\dot{Q}_{u,N}$ for conventional flat-plate, PVT flat-plate and CPC-PVT collectors are given as follows:

For conventional N flat-plate collectors connected in series:

$$\dot{Q}_{uN} = NA_c F_{RN}[(\alpha\tau)I(t) - U_L(T_{fi} - T_a)] \quad \text{(Section 5.8.2, Eq.(5.89b))}$$

For N-PVT flat-plate collectors connected in series:

$$\dot{Q}_{u,N} = NA_c \left[(\alpha\tau)_{eff,N} I(t) - U_{L,N}(T_{fi} - T_a) \right] \quad \text{(Section 5.9.2, Eq.(5.126))}$$

For a single CPC-PVT collector:

$$\dot{Q}_{u1} = \left[\{AF_R(\alpha\tau)\}_1 I_b - \{AF_R U_L\}_1 (T_{fi} - T_a) \right] \quad \text{(Section 6.10.1, Eq.(6.57))}$$

Furthermore, here $T_{fi} = T_w$ due to the recirculation of water between the solar still and the collector panel.

For the basin Liner: One part of the energy absorbed by the basin liner is transferred to the water, and the other is lost by conduction through the bottom and sides.

$$\alpha'_b I(t) = \dot{q}_b + \left[\dot{q}_{bg} + \dot{q}_s (A_{ss}/A_s) \right] \tag{13.23}$$

where α'_g, α'_w and α'_b are defined in Sect. 13.2. The various expressions for $\dot{q}$ are discussed in Sect. 13.4.

For small water depth, $A_{ss}/A_s \approx 0$.

On substituting the expressions for all $\dot{q}$ from Sect. 13.4, Eqs. (13.21–13.23) become

$$\alpha'_g I(t) + h_1(T_w - T_g) = h_2(T_g - T_a) \tag{13.24}$$

$$\dot{Q}_{u,N} + A_s \left[\alpha'_w I(t) + h_{bw}(T_b - T_w) \right] = A_s (MC)_w \frac{dT_w}{d}t + A_s h_1(T_w - T_g) \tag{13.25}$$

$$\alpha'_b I(t) = h_{bw}(T_b - T_w) + U'(T_b - T_a) \tag{13.26}$$

The value of $(MC)_w$ for water mass is taken per unit area.

Equation (13.25), after elimination of T_g and T_b from Eqs. (13.24) and (13.26) for a passive solar still, becomes

$$\frac{dT_w}{d}t + aT_w = f(t) \tag{13.27}$$

where for a passive solar still, $a = \frac{U_L}{(MC)_w}$; $f(t) = \frac{(\alpha\tau)_{eff}I(t) + U_L T_a}{(MC)_w}$;

$(\alpha\tau)_{eff} = \alpha'_w + \frac{h_{bw}}{h_{bw} + U'}\alpha'_b + \frac{h_1}{h_1 + h_2}\alpha'_g$; $U_L = U_b + U_t$; $U_b = \frac{h_{bw}U'}{h_{bw} + U'}$; $U_b = \frac{h_{bw}U'}{h_{bw} + U'}$; $U_t = \frac{h_1 h_2}{h_1 + h_2}$

Approximate solution of Eq. (13.27)
An approximate solution of Eq. (13.27) can be obtained with the following initial conditions:

 (i) The time interval $\Delta t (0 < t < \Delta t)$ is infinitesimally small.
 (ii) The function $f(t)$ (i.e., $f(t) = \overline{f(t)}$) and 'a' are constant for the time interval Δt, and h_1 can be computed by finding the water temperature $T_w = T_{w0}$ and glass-cover temperature $T_g = T_{g0}$ at $t = 0$.

The solution of Eq. (13.27) can be written as

$$T_w = \frac{\overline{f(t)}}{a}[1 - \exp(-a\Delta t)] + T_{w0}\exp(-a\Delta t) \tag{13.28}$$

where T_{w0} is the temperature of the basin water at $t = 0$; and $\overline{f(t)}$ is the average value of $f(t)$ for the time interval between 0 and t.

The average temperature of water $\overline{T}_w$ is given by

$$\overline{T}_w = \frac{1}{t}\int_0^t T_w dt = \frac{\overline{f(t)}}{a}\left[1 - \frac{\left(1 - e^{-a\Delta t}\right)}{a}\right] + T_{w0}\frac{\left(1 - e^{-a\Delta t}\right)}{a} \tag{13.29}$$

After substituting the average water temperature, one can obtain average glass temperature using Eq. (13.24):

$$\overline{T}_g = \frac{\alpha'_g I(t) + h_1 \overline{T}_w + h_2 \overline{T}_a}{h_1 + h_2} \tag{13.30}$$

The thermo-physical properties of water are estimated after knowing the water temperature (T_w) and the glass temperature (T_g). Furthermore, the heat-transfer coefficient (h_1) can be computed using the estimated thermo-physical properties. The temperature obtained for a particular time interval will serve as the initial temperature for the next time interval for the calculation of thermo-physical properties and heat-transfer coefficients. The accuracy of the estimated values depends on the time interval; for a smaller time interval the accuracy is high. In present the chapter, generally the time interval taken is 1 h.

Hourly evaporative heat loss and the hourly yield of the solar still are obtained by following expressions:

$$\dot{q}_{ew} = h_{ew}(T_w - T_g) \tag{13.31}$$

$$\dot{m}_{ew} = \frac{h_{ew}(T_w - T_g)}{L} \times 3600 \, \text{kg/m}^2 h \tag{13.32}$$

For the next time interval,
the new value of $(MC)_w$ will be

$$(MC)_w - (\dot{m}_{ew}C) \tag{13.33}$$

The instantaneous thermal efficiency of the solar still is obtained as follows:

$$\eta_i = \frac{\dot{q}_{ew}}{I(t)} = \frac{h_{ew}(T_w - T_g)}{I(t)} \tag{13.34a}$$

From Eq. (13.30), the above equation becomes

$$\eta_i = \frac{h_{ew}h_2}{h_1 + h_2} \frac{(\overline{T}_w - \overline{T}_a)}{I(t)} - \frac{h_{ew}\alpha_g'}{h_1 + h_2}$$

Because α_g' is very small, the second term can be neglected; thus, have

$$\eta_i = \frac{h_{ew}h_2}{h_1 + h_2} \frac{(\overline{T}_w - \overline{T}_a)}{I(t)} \tag{13.34b}$$

The above equation can be rewritten by substituting the value of $\overline{T}_w$ from Eq. (13.29) as follows:

$$\eta_i = \frac{h_{ew}h_2}{h_1 + h_2} \frac{1}{U_L} \times \left[(\alpha\tau)_{\text{eff}}(1 - e^{-a\Delta t}) + U_L \frac{(T_{w0} - T_a)}{I(t)} e^{-a\Delta t} \right] \tag{13.35}$$

The variation of η_i with $(T_{w0} - T_a)/I(t)$ is depicted in Fig. 13.12. The slope of Fig. 13.12 is positive (Eq. 13.35). It is opposite to the slope in Fig. 5.5 (flat-plate collector). The reason for this variation is that in the case of a solar still, the higher top loss to the ambient air results in a higher yield (hence higher efficiency), whereas for FPC, less loss from the top results in a higher efficiency. The nonlinear behavior of Fig. 13.12 is due to the high temperature dependence of the evaporative heat-transfer coefficient (h_{ew}).

Fig. 13.12 Characteristic
curve of a single-slope solar
still
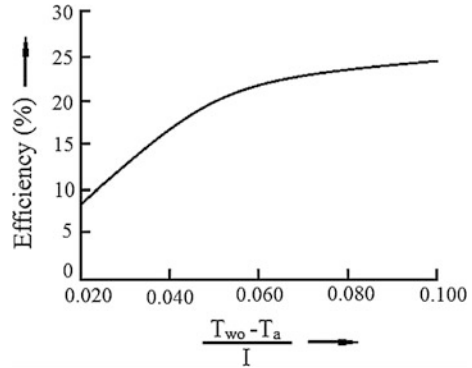
Example 13.4 Determine the amount of time it takes (Δt) for the water temperature
in the basin to be heated to $40\,^{\circ}\text{C}$ from an initial value of $20\,^{\circ}\text{C}$ given the following
parameters:

$$(\alpha\tau)_{\text{eff}} = 0.65, I(t) = 900\text{W/m}^2; T_a = 8.5\,^{\circ}\text{C}; U_L = 9.48\ \text{W/m}^2\,^{\circ}\text{C}.$$

Solution
From Eq. (13.28), one can obtain an expression for Δt as

$$\Delta t = -\frac{1}{a}\ln\left[\frac{T_w - \frac{\overline{f(t)}}{a}}{T_{w0} - \frac{\overline{f(t)}}{a}}\right]$$

with

$$a = \frac{U_L}{\text{MC}} = \frac{9.48}{41900} = 2.26 \times 10^{-4}$$

and

$$\overline{f(t)} = \frac{0.65 \times 900 + 9.48 \times 8.5}{4190} = 0.0159$$

Hence, we have

$$\Delta t = -\frac{1}{2.26 \times 10^{-4}}\ln\left[\frac{40 - \frac{0.0159}{2.26\times10^{-4}}}{20 - \frac{0.0159}{2.26\times10^{-4}}}\right] = 2239\,\text{s}$$

$$\Delta t = 37\,\text{min}$$

13.8   Effect of Design and Climatic Parameters

The hourly output (yield) from a solar-distillation unit depends on the temperature difference between the evaporating (water) and the condensing surfaces. One can see from Eq. (13.16a) that the higher the value of $(T_w - T_g)$, the higher the yield.

Effect of wind velocity
Wind flowing over the outer condensing cover creates a faster rate of heat loss from it. This reduces the condensing-cover temperature and hence increases $(T_w - T_g)$ for a higher yield. This has a significant effect at a larger water depth in the basin unlike a smaller one. After a typical maximum wind velocity (5 m/s), the yield is not much affected [7].

Effect of ambient air temperature
With higher ambient air temperature, there is lower rate of heat loss due to smaller $(T_g - T_a)$; hence,the glass condensing-cover temperature increases. This decreases $(T_w - T_g)$ and hence the hourly yield.

Effect of solar radiation
Solar radiation is one of the sensitive parameters in solar distillation. It is an important input parameter that determines yield from a solar still. As solar intensity increases, the yield also increases until the rate of heat released to the inner condensing cover due to condensation is equal to the rate of release of heat from the outer surface of condensing surface to the ambient air for a given water depth. After a certain level of solar radiation, if the rate of heat released to the inner condensing cover due to condensation becomes greater than the rate of release of heat from the outer surface of the condensing surface to the ambient air, then the yield starts decreasing.

Effect of bottom loss
Water depth plays an important role in terms of the thickness of insulation, which determines an overall bottom heat-transfer coefficient (U_b), Eq. (13.14b). At lower water depth, the water temperature is significantly higher and hence the bottom heat loss due to larger values of $(T_w - T_a)$; this causes a lower yield. However, there has been no significant effect of this in studies of larger depth performed by many researchers.

Effect of a double-glazed condensing cover
As mentioned in Sect. 13.7 (Eq. 13.12a), the upward top-heat loss in a solar-distillation unit should be maximum unlike in a flat-plate collector for higher yield. If the upward top-heat loss in a solar-distillation unit is reduced due to the presence of a double-glazed condensing cover, then the yield will be significantly reduced. In this case, the water temperature in the basin will be also increased as in the case of a flat-plate collector. In addition, the rate of evaporation will be increased. In such a case, vapour is transported to another condensing chamber.

Effect of condensing-cover inclination [2]

Because there is a relation between condensing-cover inclination and solar radiation, and this effect cannot be discussed in isolation. It is well known that annual solar radiation on a surface is highest for the surface inclined at the latitude of place. Furthermore, the condensing cover should also be inclined to draw the condensed water, under the force of gravity, into the collecting bottle at the lower end of the condensing cover. The optimum inclination of solar distillation should be performed from an annual point of view for different. For New Delhi climatic conditions, the optimum inclination is $30°$. Cooper [7] found that the evaporation rate decreases with condensing-cover inclination variation from $0°$ to $45°$ and increases at approximately $60°$ and decreases again beyond $75°$.

Effect of salt concentration [1]

With an increase of salt concentration, the heat capacity of the water mass also increases for a given water depth. This causes a lower water temperature and hence lowers $(T_w - T_g)$. Finally the yield is reduced. There is another problem with high salt concentration, which causes high scaling in the basin liner, which increases maintenance costs. This reduces the absorption coefficient of solar radiation in the basin. On the basis of this observation, the purification of seawater (salinity approximately 40,000 ppm) is never recommended for solar distillation.

Seawater also causes high corrosion of the metallic sheet, which can be solved by using a noncorrosive metal for the basin construction.

Effect of water depth [1]

It can be seen that there is no effect of water depth without insulation. However, the yield decreases with water depth in an insulated basin. This finding has been verified by many researchers. The optimum depth for a passive and an active solar still is considered 0.02 and 0.05 m, respectively.

Effect of black dye [15]

To increase the yield, there have been many attempts to use black dye, charcoal etc. It has been observed that there is no marginal effect at lower water depth.

Objective Questions

13.1. Thermal efficiency of an ideal solar still is
    (a) 60 %   (b) 100 %   (c) 10 %   (d) none
    Answer: (a)

13.2. Compared with that of an active solar still, the thermal efficiency of a passive solar still is
    (a) lower   (b) higher   (c) equal   (d) none of these
    Answer: (b)

13.3. The thermal efficiency of multi-effect solar still compared with a single-effect one is
    (a) lower   (b) higher   (c) equal   (d) none compared with an active solar still
    Answer: (b)

13.4. An active solar still operates at
(a) low temperature   (b) high temperature   (c) medium tempera-
ture   (d) all compared with an active solar still
Answer: (d)

13.5. Evaporative heat transfer depends on
(a) the radiative heat-transfer coefficient   (b) the convective heat-transfer
coefficient
(c) the mass-transfer coefficient   (d) none compared with an active solar
still
Answer: (b)

13.6. The evaporative heat-transfer coefficient is
(a) linear   (b) nonlinear   (c) both linear and nonlinear   (d) all of these
Answer: (d)

13.7. Bottom insulation has no effect on yield at
(a) lower water depth   (b) large water depth   (c) water film   (d) none
of these
Answer: (b)

13.8. The effect of dye plays an important role at
(a) lower water depth   (b) large water depth   (c) water film   (d) none
of these
Answer: (b)

13.9. A double-slope solar still compared with single-slope solar still is
(a) economical   (b) not economical   (c) better   (d) none of these
Answer: (a) and (c)

13.10. The characteristic curve of a solar still is
(a) linear   (b) nonlinear   (c) both linear and nonlinear   (d) all of these
Answer: (b)

13.11. The characteristic equation of a solar still compared with that of FPC is
(a) similar   (b) opposite   (c) a straight line   (d) none of these
Answer: (b)

Problems

13.1 Determine the value of α'_w at a water depth of 0.10 m for a given $\alpha_w = 0.2$.
The values of R_g and R_w are 0.05, and the value of $\alpha_b = 0.075$ and $\alpha_g = 0.0$
Hint: Use Eq. (13.2a).

13.2 Calculate the value of the latent heat of vaporization (L) at $40\,°C$.
Hint: Use Eq. (13.5b).

13.3 Calculate the saturated vapor pressure at $30\,°C$ and $90\,°C$.
Hint: Use Eq. (13.10d).

13.4 Calculate the rate of evaporative heat loss from the solar still given in
Example 13.3.
Hint: See Example 13.3 and use Eq. (13.31).

13.5 Calculate the hourly output from the still given in Example 13.3.
Hint: See Example 13.3 and use Eq. (13.32).

13.6 Calculate the instantaneous efficiency of the distillation unit given in Example 13.3.
Hint: Use Eq. (13.34a).

13.7 Plot the curve between the fraction of energy absorbed by a basin liner (α'_b) and the depth of water in the basin.
Hint: Refer to Table 13.2b. $R_g = \alpha_g = R_w = \alpha_w = 0.05$ and $\alpha_b = 0.8$.

13.8 Plot the curve between the rate of radiative $(\dot{q}_{rw})$, convective, $(\dot{q}_{cw})$ and evaporative $(\dot{q}_{ew})$ heat transfer at water temperature T_w for $T_w - T_g = 10$ and $30\,°C$.
Hint: Consider $T_w = 20, 30, 40, 50, 60, 70$ and $80\,°C$.

13.9 Write the energy balance equation for a double-slope solar still.
Hint: Assume the water temperature is the same for east (T_{gE}) and west (T_{gW}). Glass temperatures and h_{1E} and h_{2w} will be different.

13.10 Discuss Eq. (13.29) for the two limiting cases of $\Delta t \to 0$ and ∞.
Hint: See Eq. (13.29).

13.11 How is the energy balance for a nonsymmetrical double-slope solar still different from that of symmetrical double-slope solar still?
Hint: Through the glass cover area $(A_{g1} \neq A_{g2})$.

13.12 Write the energy-balance equation for a reverse-absorber solar still (Fig. 13.7a).
Hint: The energy balance for a reverse-absorber solar still is $\alpha_b \rho^N I(t) = h_3(T_b - T_w) + U'_t(T_b - T_a)$, ρ reflectivity, and N number of reflections.

13.13 Write the energy-balance equation for a multi-wick solar still (Fig. 13.8a).
Hint: Use $\dot{m}_w C_w \dfrac{dT_w}{dx}$ in place of $(MC)_w \dfrac{dT_w}{dx}$.

13.14 Derive an expression for T_w and $\overline{T}_w$ as a function of x for Problem 13.13.
Hint: Follow the similar procedure as done in Sect. 13.7 by considering x as a variable.

References

1. M.A.S. Malik, G.N. Tiwari, A. Kumar, M.S. Sodha, *Solar Distillation* (Pergamon Press Ltd., UK, 1982)
2. G.N. Tiwari, A.K. Tiwari, *Solar Distillation Practice for Water Desalination Systems* (Anamaya Publisher, New Delhi, 2007, and Anshan Publisher, UK, 2008)
3. G.N. Tiwari, M.A.S. Malik, *Solar Distillation in Reviews of Renewable Energy Sources*, ed. by Sodha et al. vol. 1, Chap. 5 (Wiley Eastern Ltd., New Delhi, 1982), pp. 324–358
4. G.N. Tiwari, *Solar Energy: Fundamental, Design, Modelling and Applications* (Narosa Publishing House, New Delhi and CRC Press, New York, 2004)
5. J. Fernandez, N. Chargoy, Sol. Energy **44**, 215 (1990)
6. R.V. Dunkle, ASME, Proc. Int. Heat Transfer. **V**, 895 (1961)

7. P.I. Cooper, The transient analysis of glass covered solar still. Ph.D. Thesis, University of Western Australia, Australia, 1970
8. S. Agrawal, G.N. Tiwari, Energy Convers. Manag. **40**, 97 (1999)
9. M.S. Sodha, A. Kumar, G.N. Tiwari, R.C. Tyagi, Sol. Energy **26**(2), 127 (1981)
10. S.N. Rai, G.N. Tiwari, Energy Convers. Manag. **23**, 145 (1982)
11. M.A.S. Malik, V.V. Tran, Sol. Energy **14**, 271 (1973)
12. Madhuri, G.N. Tiwari, Desalination. **52**, 345 (1985)
13. G.N. Tiwari, A. Kumar, Desalination **69**, 309 (1988)
14. S. Kumar, G.N. Tiwari, Sol. Energy **57**, 459 (1996)
15. M.S. Sodha, A. Kumar, G.N. Tiwari, G.C. Pandey, Appl. Energy **7**, 147 (1980)
16. G.N. Tiwari, R.K. Mishra, Advance Renewable Energy Sources. RSC   publishing, UK, 2012
17. W. Mull, M. Rehier, Gesundh, Ing. Beihoffe, Reiher, **28**, (1930)
18. E.F.M. Van Der Held, Z. Phys. **70**, 508(1931)
19. J.G.A. De Graaf, E.F.M. Van Der Held, Appl. Sci. Res. **A3**, 393 (1953)
20. M. Jakob, P.C. Gupta, Chem. Eng. Prog., Symp. **9**, 15 (1954)

Additional References

21. M.S. Sodha, J.K. Nayak, G.N. Tiwari, A. Kumar, Energy Convers. Manag. **20**(1), 23 (1980)
22. J.K. Nayak, G.N. Tiwari, M.S. Sodha, Energy Res. **4**(1), 41 (1980)
23. M.S. Sodha, U. Singh, A. Kumar, G.N. Tiwari, Energy Res. **5**(4), 341 (1981)
24. M.S. Sodha, J.K. Nayak, U. Singh, G.N. Tiwari, J. Energy **5**, 331 (1981)
25. M.S. Sodha, A. Kumar, G.N. Tiwari, Desalination **37**(3), 325 (1981)
26. S.N. Rai, G.N. Tiwari, Energy Res. **8**, 281 (1984)
27. G.N. Tiwari, S.B. Sharma, M.S. Sodha, Energy Convers. Manag. **24**, 155 (1984)
28. G.N. Tiwari, Energy Convers. Manag. **24**, 313 (1984)
29. K.R. Ranjan, S.C. Kaushik, Renew. Sustain. Energy Rev. **27**, 709 (2013)
30. P.T. Tsilingiris, Sol. Energy **86**(11), 3288 (2012)
31. 31. A.M. Manokar, K.K. Murugavel, G. Esakkimuthu, Renew. Sustain. Energy Rev. **38**, 309 (2014)
32. A.F. Muftah, M.A. Alghoul, A. Fudholi, M.M. Abdul-Majeed, K. Sopian, Renew. Sustain. Energy Rev. **32**, 430 (2014)
33. S.A. Abdul-Wahab, A.M. Al-Damkhi, H. Al-Hinai, R. Dev, G.N. Tiwari, Desalin. Water Treat. **19**, 249 (2010)
34. G.N. Tiwari, H.N. Singh, *Solar Distillation Encyclopedia of Life Support System (ELOSS) under UNESCO* (2005)
35. R.N. Morse, W.R.W. Read, Energy Convers. Manag. **26**, 155 (1986)
36. E.E. Delyannis, A. Delyannis, Desalination **52**, 167 (1985)
37. G.O.G. Löf, Sol. Energy **5**, 35 (1961)
38. H.E.S. Fath, Desalination **116**, 45 (1998)
39. M. Abu-Qudais, B.A. Abu-Hijleh, O.N. Othman, Energy **21**(10), 851 (1996)

Chapter 14
Energy Analysis

Abstract Energy analysis of a solar energy thermal and PV system is based first on the law of thermodynamics by considering the overall life and annual performance of individual system. The analysis gives information for the cost-effectiveness of the system.

Keywords Energy density · Embodied energy · Energy matrices · Energy payback time · Energy production factor · Life cycle conversion efficiency

14.1 Introduction

After air, water, and food, energy is the fourth basic need of human beings. It is the most essential and secure accessible supply of energy for modern societies with a persistent demand as human needs evolve. Now energy plays a vital role in human life for nearly all activities including domestic, transport, industrial, medical, etc. Thus, energy security for the worthwhile growth of the world population is very necessary. Continued use of conventional energy sources (fossil fuels) is set to face multiple challenges including (i) depletion of fossil fuel reserves, (ii) global warming and other environmental concerns, (iii) geopolitical and military conflicts, and (iv) continuing increases in fuel prices. These problems will eventually create an unsustainable situation. Solar energy is one of many solutions to the growing energy challenges/crisis. Fossil fuels impose a huge detrimental impact on the environment. Human activities causing climate changes result in the production of greenhouse-gas emissions (GHG), which negatively affect the environment directly. Per the report of the World Health Organization (WHO), as many as 160,000 people die each year due to the side effects of climate change. This figure could approximately double by 2020. The energy supply, in the form of energy derived directly or indirectly from the Sun, comprises the total energy demand, without exception, of every human being and living organism on Earth. Energy requirements for humans include the heating, cooling, transport, and manufacture of goods and agriculture. Solar energy is renewable and eco-friendly, free of contamination,

and easily and freely obtainable. **Basically, solar energy is both a direct renewable source and an indirect nonrenewable source of energy**. In this perception, solar-energy systems have been growing fast globally during the last two decades. Most of the world receives a high level of solar radiation. Energy analysis of solar thermal and PVT systems can calculate their environmental impact [1, 2]. Both thermal and electrical energy can be achieved through solar energy. In view of the above, solar-energy technology must meet the following two chief criteria:

 (i) cost-effectiveness; and
(ii) utmost annual energy savings.

   In the present chapter, annual energy savings will be evaluated using the first law of thermodynamics (Chap. 3).

14.2   Embodied-Energy Analysis

To perform an analysis of life-cycle energy and environmental impact for any system, an embodied-energy analysis is an important and relatively new concept. **Embodied energy is defined as: "the quantity of energy required by all of the activities associated with a production process, including the relative proportions consumed in all activities upstream to the acquisition of natural resources and the share of energy used in making energy equipment and in other supporting functions i.e. direct energy plus indirect energy"** [3]. Embodied-energy analysis quantitatively assesses the energy required to manufacture the system including raw-material extraction, fabrication of every component, and assembly and maintenance of each component. Embodied-energy analysis also includes quantitative analysis of the components (construction, operation, and maintenance) of any system on a life-cycle basis.

   The embodied energy of any system indicates the amount of energy consumed to get the system into operational condition starting from raw-material extraction to fabrication and the installation of each component. Operational energy consumption can be reduced by improving the design and efficiency of the system. However, embodied energy is neglected in theses analysis. Embodied energy is ignored due to the unavailability of data, the unavailability of techniques for the assessment of embodied energy of components and processes, and the common assumption that determining the embodied energy of different components and processes is insignificant. However, in the recent past these limitations of data and techniques have been conquered, and it has been found that embodied energy can be as much as 20 times the annual operational energy [4].

   In embodied-energy analysis, the energy consumed for the fabrication of each component is calculated and summed to obtain the embodied energy of the system. For this, the energy densities (available in literature and provided by the manufacturer) of the materials of each component are multiplied by the quantity of

materials used in fabricating the component. For life-cycle analysis as well as embodied-energy analysis, some environmental factors—such as CO_2 emission—are considered in fabricating all components of the system.

14.3 Energy Density (Intensity)

The energy densities (intensities) can be procured from various national and international studies of energy analysis. The difficulty experienced in using a broad range of sources to confirm the values is necessary to explicate the definitions of technique boundaries or to determine whether the values are presented in terms of primary energy or delivered energy.

It is a huge task to obtain an exact and authentic energy database for the materials used in PVT systems. An extensive comparison of materials is needed. Acquiring the exact and useable quantities of materials is the most essential requirement in the calculation of embodied energy at the design stage. Inclusion of the same with current available energy-intensity values is also important [4].

To execute energy analyses, the following methods are given:

- **Process analysis**: This is a frequently used method, which identifies the system periphery around a meticulous process. This process evaluates the needs for direct and indirect energy by determining the condition of other goods and services, as well as capital equipment and buildings, that cross the system's periphery. In process analyses, definition of the system periphery is a crucial facet. The proper selection of different system peripheries gives a significant range of results. In a system periphery, a meticulous manufacturing process may consist of the needs "upstream" for the provision of natural resources where the system periphery may be the factor hedge.
- **Input–output analysis**: This analysis can trace the economic flows of goods and services in different sectors of the economy. Government economists have collected data for the compilation of input–output matrices used for input–output analysis, which was developed for economic analysis. Input–output matrices for 109 economic sectors are published by the Australian Bureau of Statistics every fifth year in Australia. The matrix row indicates all of the sales of a sector, and the matrix column indicates all of the purchases in dollars of input per \$100 of output. Thus, the energy intensity of a sector can be derived by dividing purchases from the individual energy supply sectors by the suitable tariffs, which is expressed in gigajoules (10^9 J) of energy per \$100 of sector output (GJ/\$100).
- **Hybrid analysis**: A crucial facet of concern involves the direct energy and quantities of goods and services acquired by process analysis. This analysis examines and quantifies in detail the production process for materials in which the manufacture represents the main bulk of the overall environmental impact. Then the energy intensities of goods and services further upstream are acquired

by input–output analysis. This approach reduces the errors involved with input–output analysis to a great extent, but the energy intensities derived can be applied to materials and products manufactured by the specific process(es) audited. It does not apply globally.

To derive the embodied-energy intensities, input–output analysis is often used, but net energy intensities were found to rival those derived from process analysis. The precision of input–output analyses is intrinsically untrustworthy, but it gives a general base for comparison purposes. This method is judged as the most preferred one for embodied-energy analysis because it can minimize to a large extent the errors associated with input–output analysis. The energy densities of different materials generally used to manufacture solar energy technology are given in Appendix VI.

14.4 Overall Thermal Energy

As we have seen, two types of energy are available from the solar system, namely, thermal and electrical energy. Because thermal energy is low-grade energy and electrical energy is high-grade energy, they cannot be added directly for energy analysis, which is based on the first law of thermodynamics. For this, electrical energy is first converted to the equivalent thermal energy, and then it is added to the thermal energy to obtain the overall thermal energy available from any system. Mathematically, overall thermal energy is expressed as follows:

$$Q_{\text{overall, thermal}} = Q_{\text{thermal}} + \frac{E_{\text{electrical}}}{\eta_{\text{cp}}} \tag{14.1}$$

where η_{cp} is the electric power–generation efficiency. Its value depends on the quality of the coal. For good-quality coal with low ash content, $\eta_{\text{cp}} = 0.38$. The value of η_{cp} varies between 0.20 and 0.40 for different types of coal used in power plants.

14.5 Energy-Payback Time (EPBT)

In this section, the energy-payback time (EPBT) of a solar system will be discussed based on the first law of thermodynamics. It is defined as the recovery period of embodied energy. Mathematically, it is expressed as follows:

$$\text{EPBT} = \frac{E_{\text{in}}}{Q_{\text{annual}}} \qquad (14.2)$$

where E_{in} is the embodied energy of the solar-energy system.

Calculation of the embodied energy of solar thermal technology is straightforward except for a PV module, which goes through various high-technological processes.

Calculation of the embodied energy of a particular solar thermal energy technology can be achieved as follows:

(i) Multiply the mass of the different materials (m_i) used for manufacturing the solar-energy technology by the corresponding energy density (e_i) given in Appendix A.4, which gives $m_i e_i$.
(ii) Summing each numerical product gives the total embodied energy, i.e., summation of each $m_i e_i$.

14.6 Embodied Energy and Payback Time of Solar Systems

14.6.1 PV Module

Calculation of the total embodied energy of a PV module per m^2 is difficult. It requires the manufacturing energy requirement for the individual components. The energy requirements for different processes involved in the production of a PV module are given in Table 14.1.

Table 14.1 Energy need for the production of a PV module (from Tiwari and Mishra [5])

Process		Energy requirement
Silicon purification and processing		
(a)	Metallurgical-grade silicon (MG-Si) production from silicon dioxide (quartz, sand)	20 kWh per kg of MG-Si
(b)	Electronic-grade silicon (EG-Si) production from MG-Si	100 kWh per kg of EG-Si
(c)	Czochralski silicon (Cz-Si) production from EG-Si	290 kWh per kg of EG-Si
Solar-cell fabrication		120 kWh per m^2 of silicon cell
PV-module assembly		190 kWh per m^2 of PV module
Rooftop-integrated PV system		200 kWh per m^2 of PV module

The embodied energy of a PV module for 1 m^2 for the following specifications is given as follows:

Process	MG-Si (kWh)	EG-Si (kWh)	Cz-Si (kWh)	Cell fabrication (kWh)	Module assembly (kWh)	Total (kWh)
Case (i)	48	230	483	120	190	1071
Case (ii)	26.54	127.30	267.33	60.3	125.4	607
Case (iii)	4.80	23.00	48.30	90.0	95.0	261

The above data of case (i) were generated using the high-grade energy used at different processes excluding the embodied energy of the balance of system (BOS) of a PV system.

The basis of the data generated above is due to the following reasons:

(i)   Reduction of mass of the solar cell, which may occur due to development of new materials. Case (iii) is considered as 10 % of case (i)
(ii) Cell-processing energy: This is reduced by 75 % from case (i) to (iii)
(iii) Cell efficiency: This is increased by 4 %
(iv) Elimination of wafer trimming and packaging
(v)   Reduction of embodied energy of the module assembly by 50 %.

Case (ii) is based on the average value of case (i) and (ii), respectively. For details on the above calculations, refer the books by Tiwari and Ghosal [6], Agrawal and Tiwari [7], and Tiwari and Dubey [8]. The above results show that the embodied energy of a PV module decreased significantly from 1071 to 261 kWh/m^2 due to the reasons described above.

If the embodied energy for an open field (stand alone) and a rooftop per m^2 is considered to be 500 and 200 kWh, respectively, then the total embodied energy of a PV module per m^2 with installation for an open field and rooftop integration to a building will be 1571 and 1271 kWh, respectively, for case (i).

$$\text{Annual output of PV module} = \eta_m \times \bar{I} \times A_m \times N \times n_0$$

Where η_m and A_m are electrical efficiency and the area of the PV module; N and n_0 are the number of sunshine hours and clear days in a year; and $\bar{I}$ is the annual average values of solar intensity, which vary from place to place, e.g., its value for Port Hedland (NW Australia, Sydney, and India are 2494, 1926, and 1800 kWh/m^2/year, respectively. This indicates that the annual electrical output for Port Hedland (NW Australia) will be maximum.

For the following parameters, namely, $\eta_m = 0.12$, $A_m = 1$ m^2 and for **Port Hedland (NW Australia)** climatic condition, calculate the

Annual output of PV module for 1 m^2 $= 0.12 \times 2494 \times 1 = 299.28$ kWh

Similarly, for Sydney and Indian climatic condition for the same design parameters, we calculate the following:

$$\text{Annual output of PV module for 1 m}^2 = 0.12 \times 1926 \times 1 = 231.12 \text{ kWh}$$

and the

$$\text{Annual output of PV module for 1 m}^2 = 0.12 \times 1800 \times 1 = 216 \text{ kWh}$$

If the life of a PV module is considered as $T = 30$ years, then the matrices of the PV module can be obtained as follows:

City	Port Hedland			Sydney			India		
Cases	EPBT	EPF	LCCE	EPBT	EPF	LCCE	EPBT	EPF	LCCE
Case (i)	3.60	8.30	0.105	4.64	6.47	0.101	4.96	6.05	0.100
Case (ii)	2.00	15.0	0.112	2.62	11.45	0.109	2.81	10.68	0.109
Case (iii)	0.87	34.5	0.116	1.13	26.55	0.115	1.21	24.79	0.115

From the above table, one can conclude the importance of embodied energy (E_i), annual electrical output (E_{out}), and the life of renewable energy technology (T). This shows that the PV module is best suited for Port Hedland (NW Australia) due to the lowest value of EPB and the highest values of EPF and LCCE.

14.6.2 Flat-Plate Collector

(a) **Copper plate and tube**

First Method

The embodied energy for two flat-plate collectors each having an area of 2 m^2 is given in Table 14.2. The value of embodied energy for two flat-plate collectors is 2315.10 kWh.

$$\text{Embodied energy for flat plate collector (FPC) of 2 m}^2 = 1157.11 \text{ kWh}$$

For clear-sky (blue sky) conditions for 268 days/year in New Delhi, 8 sunshine hours/day, and average solar radiation of 400 W/m^2, the following is calculated:

$$\text{Annual input solar radiation on FPC of 2 m}^2 = 400 \times 8 \times 2 \times 268 \text{ Wh}$$
$$= 1715 \text{ kWh}$$

Table 14.2 Embodied energy of different components of a PVT active solar still (from Tiwari and Mishra [5])

Components	Items	Quantity	Total weight (kg)	Embodied energy (MJ/kg)	Total embodied energy MJ	kWh
Solar still (1 m²)	GRP body	1	21.17	92.3	1954.0	542.8
	Glass cover 4 mm	1	1.16	40060 MJ/m³	185.9	51.6
	MS clamping frame	1	5	34.2	171.1	47.5
	MS clamp	8	2	34.2	68.4	19.0
	Mild-steel stand	1	14/20	34.2	478	133
	Inlet/outlet nozzle	2	0.100	44.1	4.4	1.2
	Gaskets 8.9 m	1	2.1	11.83	24.8	6.9
Subtotal						802
Flat-plate collector quantity 2	Copper riser	20 × 1.8 = 36 m	8.2	81.0	664.2	184.5
	Header	4 × 1.15 = 4.6 m	3.8	81.0	307.8	85.5
	Al box	2	10	199.0	1990.0	552.0
	Cu sheet	2	11	132.7	1460	405.6
	Glass cover toughened 4 mm	2 (3.75 m²)	0.01464 m³	66020 MJ/m³	966.5	268.3
	Glass wool	13 m²	0.064 m³	139 MJ/m³	8.89	2.5
	Nuts/bolts/screws	32	1	31.06	31.06	8.6
	Union/lbow	8	1.5	46.8	70.2	19.5
	Nozzle/flange	8	1	62.1	62.1	17.3
	Mild-steel stand	1	40	34.2	1368	380
	Paint	1 L	1 L	90.4	90.4	25.1
	Rubber gasket	18 m	4.2	11.83	49.7	13.8
	GI pipes 1/2″		9.5	44.1	418.9	116.4
	Al frame 1″	12 m	2.5	170	425	118
	Al sheet 24 gauge		2.5	170	425	118
Subtotal						2315.1
PV module	Glass to glass	1	0.605 m²	3612/m²	2185.2	607
	BOS			475.2	475.2	132
Subtotal						739
Water pump	Copper wire		0.150	110.19	16.5	4.6
	Copper commuter	2	0.04	70.6	2.8	0.78
	Si–steel armature	1	0.05	*	*	*
	Wire insulation	2	0.01	*	*	*
	Motor body (SS)	1	0.100	36.1	3.61	1.0
	Casing (brass)	1	0.300	62.0	18.6	5.2
	Bearings	2	0.030	*	*	*
	Steel shaft	1	0.050	12.5	0.625	0.17
	Impellers (plastic)	1	*	*	*	*
	Nuts/screws/flange		0.100	31.06	3.1	0.86
Subtotal						12.61
Total embodied energy of hybrid active still						3868.6

For $\eta_c = 0.70$ (efficiency of FPC),

An annual thermal energy of 2 m² FPC = $0.7 \times 1715\,\text{kWh} = 1205.5\,\text{kWh}$

The energy-payback time of one flat-plate collector of 2 m² is given by

$$\text{Energy pay back time (EPBT)} = \frac{1157.11}{1202.5} = 0.96\,\text{years}$$

The above calculated energy-payback time is based on the annual thermal energy of an FPC. Hence, the use of an FPC is economical.

Second Method

For natural mode, $F' = 0.9, A_c = 2$ m², $\alpha\tau = 0.8, I(t) = 400$ W/m² and $T_a = 25$ °C (annual average values), $U_L = 6$ W/m² °C and $T_f = 60$ °C and $n = 268$ clear days in 1 year and 8 sunshine hours per day, the annual thermal energy available can be calculated from Eq. (5.54) as follows:

Annual thermal energy under natural mode (Q_{annul})
$$= 0.9 \times 2 \times [0.8 \times 400 - 6 \times (60 - 25)] \times 8 \times 3600 \times 268\,\text{J}$$
$$= 1.528 \times 10^9\,\text{J} = 425\,\text{kWh}$$

For forced mode, a pump of 20 W is required to circulate the water through the flat-plate collector, and it is the only change in $F_R = 0.8$ and $T_{fi} = 30$ °C in the above calculation; the annual thermal energy available can be calculated from Eq. (5.75) as follows:

Annual thermal energy $Q_{\text{annul}} = 0.8 \times 2 \times [0.8 \times 400 - 6 \times (30 - 25)] \times 8 \times 3600 \times 268\,\text{J}$
$$= 9.94 \times 10^9\,\text{J} = 994\,\text{kWh}$$

Annual electrical energy required to operate the pump = $20 \times 8 \times 286$ W = 42.88 kWh
Net annual energy saved for forced mode of operation = $(994 - 42.88)$ kWh
$$= 951.12\,\text{kWh}$$

This calculation indicates that the net annual energy saved for forced mode of operation is higher than the annual thermal energy available in natural circulation mode of operation.

For natural-circulation mode,

$$\text{Energy pay back time (EPBT)} = \frac{1157.11}{425} = 2.72\,\text{years}$$

For forced-circulation mode,

$$\text{Energy pay back time (EPBT)} = \frac{1157.11}{951} = 1.2 \, \text{years}$$

This shows that the EPBT is less than the life of the flat-plate collector, i.e., 10–15 years. However, increasing the annual energy saving can further reduce the EPBT of the flat-plate collector. This can be achieved as follows:

(i) increase the amount of insolation;
(ii) increase the number of sunshine hours; and
(iii) decrease the overall heat loss, etc.

14.6.3 Hybrid Flat-Plate Collector

The embodied energy for one hybrid flat-plate collector (FPC) of 2 m^2 will be approximately the sum of the embodied energy for one flat-plate collector (FPC) at 2 m^2 (1157.11 kWh) and the embodied energy for one PV module at 0.605 m^2 (607 kWh). From Table 14.2, this value will be approximately 1764.11 kWh. Now, the energy-payback time for one hybrid flat-plate collector is given as

$$\text{Energy pay back time (EPBT)} = \frac{1764.11}{994} = 1.77 \, \text{years}$$

In this case, the electrical energy needed to operate the pump is taken from the PV module. Furthermore, such system is self-sustaining. In this case, the EPBT is higher due to an increase in the embodied energy by the PV module.

14.6.4 Hybrid Air Collector

The calculation of total embodied energy for two hybrid air collectors connected in series is given in Table 14.3. The embodied energy for two hybrid air collectors of 2.64 m^2 (fully covered opaque) is 3297.7 kWh. In this case, the embodied energy of a PV module is 2587.2 kWh, and the remaining (710.5 kWh) is embodied energy for the BOS. The embodied energy for two hybrid air collectors connected in series, as done in the case of the PV module, will be as follows:

Case (i)   Embodied energy $= (2.64 \times 980 + 710.5) = 3298 \, \text{kWh}$
Case (ii) Embodied energy $= (2.64 \times 607 + 710.5) = 2313 \, \text{kWh}$
Case (iii) Embodied energy $= (2.64 \times 261 + 710.5) = 1399 \, \text{kWh}$

Table 14.3 Embodied energy of different components of a PVT air collector (from Tiwari and Mishra [5])

S. no.	Component	Quantity	Energy density (kWh/kg)	Total embodied energy (kWh)
1.	MS support structure	60 kg	8.89	533.4
2.	Wooden duct	10 kg	2.89	28.9
3.	PV module (glass–tedlar type)	2.64 m^2	980 kWh/m^2	2587.2
4.	Battery	One	–	121.4
5.	DC fan (one) (i) Aluminium	0.390 kg	55.28	21.56
	(ii) Iron	0.220 kg	8.89	1.96
	(iii) Plastic	0.120 kg	19.44	2.33
	(iv) Copper wire	0.050 kg	19.61	0.98
			Total	3297.7

The annual thermal and electrical energy of the hybrid air collector (2.64 m^2) is evaluated as 987 and 292 kWh, respectively. Using conversion factor, Eq. (14.1), we get the following:

Overall annual thermal energy for two hybrid air collectors $= 987 + \frac{292}{0.38} = 1755$ kWh.

If the conversion factor has not been considered, then we get the following:

Overall annual thermal energy for two hybrid air collectors $= 987 + 292 = 1279$ kWh.

For clear-sky conditions 268 days/year, 8 sunshine hours/day, and an annual average solar radiation of 400 W/m^2, the annual solar radiation on two hybrid air collectors of 2.64 m^2 is given by

$$\text{Annual solar radiation} = 400 \times 8 \times 2.64 \times 268 = 2,264,064 \, \text{Wh} = 2264 \, \text{kWh}$$

The EPBT for both cases is given below:

Basis	Overall thermal energy			Overall exergy			Direct sum of thermal and electrical energy		
Cases	EPBT	EPF	LCCE	EPBT	EPF	LCCE	EPBT	EPF	LCCE
Case (i)	1.88	15.96	0.726	9.87	3.04	0.099	2.58	11.62	0.516
Case (ii)	1.32	22.72	0.740	6.93	4.33	0.114	1.81	16.57	0.531
Case (iii)	0.80	37.50	0.754	4.19	7.15	0.127	1.09	27.52	0.544

From the above results, one can infer that case (iii) gives the most favorable energy results from the user's point of view per expectation for all conditions mentioned previously. This shows that there is strong need to produce fewer materials that consume high-grade energy to produce a PV module or any other renewable-energy system.

14.6.5   Solar Still

Passive Solar Still

To determine the payback period (EPBT) for a single-slope passive solar still, one needs the embodied energy with an effective area of $1m^2$ and the annual yield from the solar still.

The embodied energy of a fibre reinforced–plastic passive solar still can be calculated as follows:

$$\text{Embodied energy of } 1.2 \text{ m}^2 \text{ glass cover} = \text{Area} \times \text{thickness} \times \text{density} \times \text{energy density}$$
$$= 1.2 \times 0.003 \times 2350 \times 8.72 = 73.77 \text{kWh}$$

Embodied energy of a fiber glass material of 3 mm $= 10 \times 25.64 = 256.4$ kWh
Embodied energy of a galvanized-iron angle stand $= 8 \times 13.88 = 11.04$ kWh
Total embodied energy for the solar still $= 441.21$ kWh

If the annual yield/m^2 (output) is assumed to be 2 kg and the number of sunshine hours per day per year is considered as 268, then the annual energy available from solar still will be

$$\text{Annual energy} = 2 \times 268 \times 2.50 \times 10^6 = 13.50 \times 10^8 \text{ J} = 375.2 \text{ kWh}$$

Thus, the energy-payback time is given by $\text{EPBT} = \dfrac{441.21 \text{ kWh}}{375.1 \text{ kWh per year}} =$ 1.18 years.

This indicates that the energy-payback time (EPBT) for a passive solar still is much less than the expected life of a passive solar still (by 25–30 years).

Active Solar Still

Embodied energy for an active solar still (Fig. 13.9b) is the sum of the embodied energy of the passive solar still plus the 2 m^2 area of the flat-plate collector and is given by

$$\text{An embodie energy for active solar still} = \text{Embodied energy of passive solar still}$$
$$+ \text{Embodied energy for 2 m}^2 \text{ FPC area}$$

According to Sect. 14.6.2, an embodied energy for 2 m^2 FPC area $= 1724$ kWh, then an embodied energy for the active solar still $= 441.21 + 1724 = 2165.21$ kWh.

If the daily yield per 1 m^2 of an active solar still is 5 kg, then Annual energy $= 5 \times 268 \times 2.50 \times 10^6 = 33.5 \times 10^8$ J $= 930$ kWh.

Thus,

$$\text{EPBT} = \frac{2165.21 \text{ kWh}}{930 \text{ kWh per year}} = 2.32 \text{ years}.$$

It is necessary to observe that the energy-payback time (EPBT) for an active solar still is significantly higher than that for passive a solar still by 96 %. This is due to fact that an overall thermal efficiency of an active solar still is reduced due to high operating temperature range. Hence, an active solar still is recommended for commercial applications having a high quality of water, and a passive solar still should be used for domestic applications.

14.6.6   Solar Dryer

Cabinet Dryer

The embodied energy for different materials used in a cabinet dryer (Fig. 12.5) having 0.5 m^2 effective area is as follows:

(a) *Mass of glass cover* = 4 kg,

$$\text{Embodied energy} = \text{mass} \times \text{energy density} = 4 \times 8.72 = 34.88$$

(b) *Mass of wood material* = 10 kg,

$$\text{Embodied energy} = \text{mass} \times \text{energy density} = 10 \times 4.95 = 49.5 \text{ kWh}$$

(c) *Mass of galvanized iron* = 1 kg,

$$\text{Embodied energy} = \text{mass} \times \text{energy density} = 1 \times 13.88 = 13.88 \text{ kWh}$$

$$\text{The total embodied energy used for a } 0.5 \text{ m}^2 \text{ cabinet dryer} = (34.88 + 49.5 + 13.88) \text{ kWh}$$
$$= 98.26 \text{ kWh}$$

The annual energy produced by a cabinet dryer $= \eta \times \alpha_c \times \tau \times \bar{I} \times A_c \times N \times n \times 10^{-3}$ kWh.

The values of the different parameters are as follows: $\eta = 0.50, \alpha_c \tau = 0.40 \times 0.8 = 0.32, A_c = 0.5 \text{ m}^2, \bar{I} = 500 \text{ W/m}^2, N = 5$ and $n = 268$ clear days/year.

The useful energy produced by a cabinet dryer in 1 year $= 0.5 \times 0.32 \times 400 \times 0.5 \times 5 \times 268 \times 10^{-3}$ kWh = 42.8 kWh.

Thus, the energy-payback time (EPBT) is given by EPBT $= \dfrac{98.26 \text{ kWh}}{42.8 \text{ kWh per year}} =$ 2.29 years.

Greenhouse Dryer

The embodied energy for the different materials used in a greenhouse dryer for an effective area of 0.96 m^2 is given as follows:

(a) *Mass of PVC pipe of diameter* $1'' = 0.25$ kg,

Embodied energy = mass × energy density = $0.25 \times 18.9 = 7.225$ kWh

(b) *Mass of wood material* = 0.5 kg,

Embodied energy = mass × energy density = $0.5 \times 25.64 = 12.82$ kWh

(c) *Mass of galvanized iron* (*nails*) = 0.100 kg,

Embodied energy = mass × energy density = $0.100 \times 13.88 = 1.388$ kWh

The total embodied energy of greenhouse dryer of 0.96 m^{2}area = $(7.23 + 12.82 + 1.388)$ kWh
$$= 21.50 \text{ kWh}$$

The useful energy for greenhouse dryer in 1 year = $\eta \times \alpha_c \times \tau \times \bar{I} \times A_c \times N \times n \times 10^{-3}$ kWh.

The values of different parameters are $\eta = 0.10, \alpha_c \tau = 0.40 \times 0.8 = 0.32, A_c = 0.96$ m$^2, \bar{I} = 500$ W/m$^2, N = 5$ and $n = 268$.

The useful energy produced in 1 year = $0.1 \times 0.32 \times 500 \times 0.96 \times 5 \times 268 \times 10^{-3}$ kWh
$$= 20.6 \text{ kWh}$$

Thus, the energy-payback time is EPBT $= \dfrac{21.50 \text{ kWh}}{20.6 \text{ kWh per year}} = 1.04$ years

It is observed that the energy-payback time (EPBT) for a greenhouse crop dryer is much less than that for a cabinet dryer. However, the life of a cabinet dryer (10 years) is longer than that of a greenhouse crop dryer (by 4–5 years).

Reverse-Absorber Cabinet Dryer (RACD)

The embodied energy of different materials for a reverse-absorber cabinet dryer of 1 m^2 area is given as follows:

(a) *Mass of glass cover* = 8 kg,

Embodied energy = mass × energy density = $8 \times 8.72 = 69.76$ kWh

(b) *Mass of wooden structure* = 25 kg,

Embodied energy = mass × energy density = $25 \times 4.95 = 123.75$ kWh

(c) *Mass of galvanized iron with stand* $= 15 \, \text{kg}$,

$$\text{Embodied energy} = \text{mass} \times \text{energy density} = 15 \times 13.88 = 208.20 \, \text{kWh}$$

$$\text{The total embodied energy of RACD} = (69.76 + 123.75 + 208.20)$$
$$= 451.71 \, \text{kWh}$$

The useful energy produced in 1 year $= \eta \times \alpha_c \times \tau \times \bar{I} \times A_c \times N \times n \times 10^{-3} \, \text{kWh}$

In this case, the thermal efficiency of the system will be the product of thermal efficiency of the air heater and the efficiency of the drying chamber. For 50 % efficiency of each, the values of the efficiency of the system and other parameters are given as follows: $= 0.25 \, \alpha_c \tau = 0.90 \times 0.8 = 0.72, A_c = 1.0 \, \text{m}^2, \bar{I} = 500 \, \text{W/m}^2$, and $n = 268$.

$$\text{The useful energy produced by RACD} = 0.25 \times 0.72 \times 500 \times 1.0 \times 5 \times 268 \times 10^{-3} \, \text{kWh}$$
$$= 120.6 \, \text{kWh}$$

Thus, the energy-payback time is EPBT $= \dfrac{471.71 \, \text{kWh}}{120.6 \, \text{kWh per year}} = 3.91 \, \text{years}$

The EPBT for RACD is more because of more materials were used in its fabrication, which can be reduced by using wooden material for the stand and fiber-reinforced plastic (FRP) material for the other structures.

Active Solar Dryer

The embodied energy of different materials used in an active solar drying system of $0.5 \, \text{m}^2$ area is calculated as follows:

(a) *Mass of glass cover* $(1 \, \text{m}^2) = 8 \, \text{kg}$,

$$\text{Embodied energy} = \text{mass} \times \text{energy density} = 8 \times 8.72 = 69.76 \, \text{kWh}$$

(b) *Mass of wooden structure in air collector* $(1 \, \text{m}^2)$ *and dryin chamber* $= 35 \, \text{kg}$,

$$\text{Embodied energy} = \text{mass} \times \text{energy density} = 35 \times 4.95 = 173.25 \, \text{kWh}$$

(c) *Mass of galvanized iron stand for collector and drying chamber* $= 35 \, \text{kg}$,

$$\text{Embodied energy} = \text{mass} \times \text{energy density} = 35 \times 13.88 = 485.80 \, \text{kWh}$$

(d) *Black paint and other paint* $= 1 \, \text{kg}$

$$\text{Embodied energy} = \text{mass} \times \text{energy density} = 1 \times 40 = 40 \, \text{kWh}$$

The total embodied energy of active solar dryer is $= (69.76 + 173.25 + 485.80 + 40) = 768.81$ kWh.

The useful energy produced by active solar dryer in 1 year $= \eta \times \alpha_c \times \tau \times \bar{I} \times A_c \times N \times n \times 10^{-3}$ kWh.

In this case also, the thermal efficiency of an active solar dryer is the product of the thermal efficiency of the active air collector and the efficiency of the crop chamber. For a 70 % efficient active air collector and a 50 % efficient drying chamber, values for the thermal efficiency and other parameters of the active solar drying system are given as follows: $\eta = 0.35, \alpha_c\tau = 0.90 \times 0.8 = 0.72$, $A_c = 1.0$ m$^2, \bar{I} = 400$ W/m$^2, N = 5, n = 268$.

The useful energy produced by an active solar dryer

$$= 0.35 \times 0.72 \times 400 \times 1.0 \times 5 \times 268 \times 10^{-3} \text{ kWh}$$
$$= 135.0 \text{ kWh}$$

Thus, the energy-payback time is EPBT $= \dfrac{768.81 \text{ kWh}}{135.0 \text{ kWh per year}} = 5.69$ years.

The above calculations do not include the effect of the electrical energy used to operate the air blower.

The energy-payback time can be further reduced by using wooden material for the stands and fiber-reinforced plastic (FRP) materials for the other structures.

The above analysis shows that the EPBT strongly depends on the design of and the material used for the fabrication of solar dryers. Therefore, a solar dryer must be designed and fabricated in such a way that it utilizes low energy density material with longer life time. Solar dryers should operate at a maximum throughout the year and require less maintenance.

14.6.7 Evacuated Tubular Collector

For following parameters,

$A_c =$ Absorber tube diameter times collector length $= 0.043$ m $\times 1.067$ m $= 0.0458$ m^2

$A_L = A_c = 0.1440$ m^2

$U_L =$ The overall heat loss coefficient $= 0.77$ W/m^2 °C

$F_r =$ The flow rate factor $= 1.0$

$\alpha\tau =$ The product of absorptivity and transmitivity of glass tube $= 0.81$

For $I(t) = 400$ W/m^2 and $T_a = 25$ °C (annual average values), $n = 268$ clear days in 1 year, and 8 sunshine hours/day, then

$$\text{Annual thermal energy } (Q_{\text{annul}}) = 0.0458 \times 1 \times [0.8 \times 400 - 0.77 \times 3.14$$
$$\times (30 - 25)] \times 8 \times 3600 \times 268$$
$$= 0.13 \times 10^9 \text{ J} = 30.24 \text{ kWh}$$

The total embodied energy for a 3 mm(0.003 m) thickness of copper and glass tubes with an effective surface area of 0.144 m^2 (density $= 8795$ kg/m^3 and energy density $= 36.87$ kWh/kg) and 20.5 m^2 (density $= 2700$ kg/m^3 and energy density $= 8.72$ kWh/kg) for an evacuated tubular collector is 152.62 kWh. Out of total embodied energy, 8.25 % is from the glass cover, and the remaining 91.75 % is from the copper.

The energy-payback time (EPBT) for an evacuated tubular collector can be evaluated as

$$\text{EPBT} = \frac{152.62 \text{ kWh}}{30.24 \text{ kWh per year}} = 5.1 \text{ years}$$

The energy-payback time (EPBT) for an evacuated tubular collector is longer than that for a flat-plate collector. The evacuated tubular collector is generally used for industrial applications, unlike a flat-plate collector. However, either increasing the annual energy savings or decreasing the total embodied energy of an evacuated tubular collector can further reduce the EPBT for an evacuated tubular collector.

Annual energy savings can be increased by

(i) increasing the insolation; and
(ii) increasing the number of sunshine hours, etc.

The total embodied energy of an evacuated tubular collector can be reduced by

(i) decreasing the thickness of the copper tubes; and
(ii) changing the design for minimum use of copper.

Objective Questions

14.1 The Sun is a direct/indirect source of
      (a) renewable energy   (b) nonrenewable energy
      (c) both of these   (d) all of these
      Answer: (d)
14.2 The energy density of a solar thermal system is
      (a) greater than that of a PV module   (b) less than that of a PV module
      (c) equal to that of a PV module   (d) none of these
      Answer: (b)
14.3 Thermal energy is
      (a) high-grade energy   (b) low-grade energy
      (c) both low- and high-grade energy   (d) all of these
      Answer: (b)

14.4 The energy-payback time (EPBT) of a solar thermal system is
       (a) less than that of a PV module   (b) greater than that of a PV module
       (c) equal to that of a PV module   (d) none of these
       Answer: (a)
14.5 Energy-payback time (EPBT) should be calculated under
       (a) standard test conditions (STC)   (b) real weather conditions
       (c) both conditions   (d) all of these
       Answer: (b)
14.6 Energy matrices consist of the following:
       (a) energy-payback time (EPBT)   (b) energy-production factor (EPF)
       (c) life cycle–conversion efficiency (LCCE)   (d) All of these
       Answer: (d)
14.7 The energy-payback time (EPBT) of an active solar still is
       (a) higher than that of a passive solar still   (b) lower than that of a passive solar still
       (c) equal to that of a passive solar still   (d) none of these
       Answer: (a)
14.8 The energy-payback time (EPBT) of an active solar dryer is
       (a) lower than that of a passive solar dryer   (b) higher than that of a passive
                                                            solar dryer
       (c) equal to that of a passive solar dryer   (d) none of these
       Answer: (b)

References

1. P. Frankl, A. Masini, M. Gamberale, D. Toccaceli, Prog. Photovolt. Res. Appl. **6**(2), 137 (1998)
2. G.N. Tiwari, R.K. Mishra, *Advanced Renewable Energy Sources* (RSC Publishing, London, 2011)
3. G.J. Treloar, *Energy analysis of the construction of office buildings*, Master of Architecture Thesis, Deakin University, Geelong (1994)
4. I. Boustead, G.F. Hancock, *Handbook of Industrial Energy Analysis*, (Ellis Horwood Publishers, 1979), p. 309
5. G.N. Tiwari, R.K. Mishra, *Advance Renewable Energy Sources*. RSC publishing, UK, 2012
6. G.N. Tiwari, M.K. Ghosal, *Renewable Energy Resources: Basic Principles and Applications* (Narosa Publishing House, New Delhi, India, 2005)
7. B. Agrawal, G.N. Tiwari, *Building Integrated Photovoltaic Thermal Systems* (RSC Publishing, London, 2010)
8. G.N. Tiwari, S. Dubey, *Fundamentals of Photovoltaic Modules and Their Applications* (RSC Publishing, London, 2010)

Additional References

9. G.N. Tiwari, *Solar Energy Technology Advances* (Nova Science Publishers Inc., New York, 2006)
10. C. Lamnatou, G. Notton, D. Chemisana, C. Cristofari, Energy Build. **84**, 378 (2014)

Chapter 15
Energy Storage

Abstract Due to the intermittent nature of solar energy, storage of energy is required for night application. Both thermal and electrical energy can be stored for short and long periods of time for the betterment of human life and needs. The solar system is most economical without storage of energy and has many applications, particularly in PVT technology.

Keywords Solar energy storage · Sensible heat storage · Latent heat storage · Phase change materials · Solar battery

15.1 Introduction

A medium that stores all forms of energy to perform useful functions after some time is known as "**energy storage**." Forms of energy can be classified as follows:

 (i) **Potential energy**: This takes the form of chemical, gravitational, electrical, temperature differential, latent heat. etc.
(ii) **Kinetic energy**: This takes the form of momentum.

Furthermore, there can be short- and long-term storage as follows:

Short-term storage: Some technologies, such as an insulated storage tank through sensible heat, directly store solar energy in the form of short-term energy. Even food, through the photosynthesis process, is a form of energy stored in chemical form. Solar energy is an intermittent and a time-dependent energy resource. It is available during sunshine hours (Chap. 1). It can be stored for off-sunshine hours if required. It is stored for the use of energy requirements in day-to-day life.

Long-term storage: Other technologies, such as fossil fuels (coal, petroleum, natural gas), deep aquifers and bedrock, can store energy long-term. Fossil fuels indirectly store solar energy received by organisms and plants (dead and buried over a long period of time).

Solar thermal energy storage can be classified as follows:
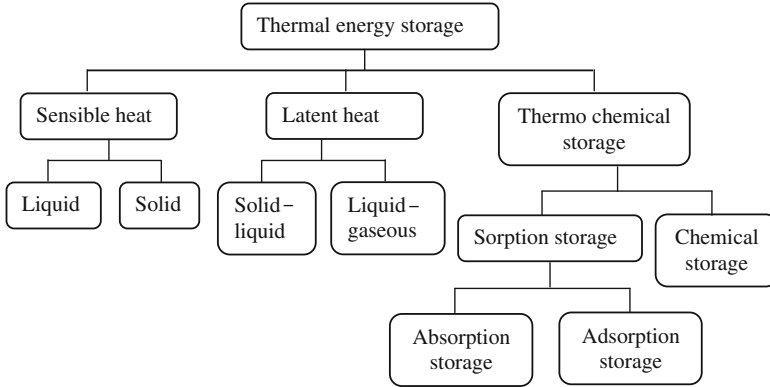
15.2 Sensible Heat Storage [1]

Thermal energy may be stored as

- sensible heat in liquid or solid; and
- latent heat in melting or vapour condition.

The level of sensible heat-storage systems depends on the heat capacity (MC_p) and temperature difference during heating (charging) or cooling (discharging).

The first law, i.e., sensible heat is stored (Q) during charging operations by a storage medium from T_1 to T_2 (the maximum temperature at end of charging period), is expressed as

$$Q = M \int_{T_1}^{T_2} C_p dT = V \int_{T_1}^{T_2} \rho C_p dT \qquad (15.1)$$

where M, ρ, and C_p are the mass (kg), the density (kg/m^3), and the specific heat (J/kg °C) of the storage medium; and V is the volume (m^3).

For a temperature independent of C_p, Eq. (15.1) becomes

$$Q = MC_p(T_2 - T_1) \qquad (15.2)$$

It is important to mention that that T_1 is a time-dependent temperature.

The amount of sensible-heat storage depends on the following parameters:

(i)   higher specific heat;
(ii) higher thermal diffusivity, $\alpha = \frac{K}{\rho C_p}$, with K being thermal conductivity;

(iii) charging/discharging without loss of energy;
(iv) low cost and maintenance; and
 (v) Stability.

The physical properties of some sensible-heat storage materials are given in Table 15.1.

Using the second law of thermodynamics, the exergy change in terms of sensible-heat storage can be expressed as [2]

$$\Delta E_{12} = MC_p(T_2 - T_1) - MC_p(T_a + 273) \ln \frac{T_2 + 273}{T_1 + 273} \tag{15.3}$$

It can be seen that the exergy change is nonlinear unlike the energy of sensible-heat storage.

In the case of sensible-heat storage, thermal-energy efficiency is defined as the ratio of energy used from storage to the energy available for storage. Mathematically, it is expressed as

$$\eta_{th} = \frac{MC_p(T_2 - T_0)}{MC_p(T_2 - T_1)} = \frac{T_2 - T_0}{T_2 - T_1} < 1 \tag{15.4}$$

where T_2 is the maximum temperature at the end of charging; and T_0 is the minimum temperature during discharge.

Accordingly, the second law exergy efficiency is given by

$$\eta_{ex} = \frac{MC_p\left[(T_2 - T_1) - (T_a + 273) \ln\left\{\frac{T_2 + 273}{T_1 + 273}\right\}\right]}{Ex_{in}} \tag{15.5}$$

Table 15.1 Properties of salt-hydrates as PCM materials

Material	Melting point (°C)	Heat of fusion (kJ/kg)	Specific heat (J/kg °C)		Thermal conductivity (W/m K)
			Solid	Liquid	
Mg (NO₃)₂·6H₂O	89.9	167	1.84	2.51	0.490 at 95 °C
MgCl₂·6H₂O	115.0	165–169	1.72	2.82	0.570 at 120 °C
Zn(NO₃)₂·6H₂O	36.1	134–147	1.34	2.26	0.464 at 39.9 °C
Na₂ S₂O₃·5H₂O	48.5	210	1.46	2.38	0.57 at 40 °C
CaCl₂·6H₂O	29.7	170	1.46	2.13	0.540 at 38.7 °C
Na₂SO₄·10H₂O	32.4	251–254	1.76	3.30	0.544 at 38.7 °C
LiBr·2H₂O	34.0	124	–	–	–

Furthermore, sensible heat-storage technology is categorized on the basis of storage media. It can be liquid-media storage, solid-media storage, or dual-media storage.

Example 15.1 Calculate the thermal energy lost from an insulated tank filled with 1000 l olive oil for a temperature drop of 100 °C from the boiling point ($T_{boiling} = 570$ K).

Solution
From Appendix IX, the density and specific heat capacity of olive oil are $\rho = 920$ kg/m^3 and $C = 1970$ J/kg K, respectively.

Using Eq. (15.2), we have

$$Q = 1000 \times 920 \times 1970 \times 373 = 6.76 \times 10^{11} \text{ J}$$

15.2.1   Liquid-Media Storage

Many liquid can be used for thermal storage. However, the water is most economically freely available with high heat capacity in abundant liquid for the short-term storage of thermal energy <100 °C.

Water has the following advantages:

(a) It is nontoxic and noncombustible.
(b) It has low thermal conductivity and viscosity.
(c) The charging and discharging of energy can occur simultaneously.

Apart from the abovementioned advantages, water has some disadvantages. These are as follows:

(a) It freezes below 0 °C and boils over 100 °C.
(b) It is a corrosive medium.
(c) It has low surface tension and hence leaks easily.

Liquid-storage tank without stratification (well-mixed) and no heat exchanger
The analysis presented here is widely used for water storage, but is also valid for other liquids.

In this case, one can consider a solar water-heating system under forced mode of operation. According to Eqs. (8.15 and 8.17), one can write an overall energy balance as follows:

$$A_{cm}F_{Rm}[(\alpha\tau)I(t) - U_L(T_w - T_a)] = M_wC_w\frac{dT_w}{dt} + (UA)_t(T_w - T_a) + \dot{M}_wC_w(T_w - T_a)$$

$$(15.6)$$

The above equation can also be written as

$$M_w C_w \frac{dT_w}{dt} = \dot{Q}_C - \dot{Q}_L - (UA)_t (T_w - T_a) \tag{15.7}$$

where $\dot{Q}_C = \dot{Q}_{um} = \dot{m}_f C_f (T_{fo} - T_w) = A_{cm} F_{Rm}[(\alpha\tau)I(t) - U_L(T_w - T_a)]$ is the rate of charging energy from the source (FPCs connected in parallel) in W without a heat exchanger within the storage tank. It is important to mention that the inlet temperature of a flat-plate collector (FPC), (T_{fi}), is equal to the storage water temperature (T_w). In this case, solar energy is the source, but it can be any source of charging, and $\dot{Q}_L = \dot{M}_w C_w (T_w - T_a)$ is the rate of heat removal by the load (W) without a heat exchanger as shown in Fig. 15.1.

For a constant rate of heat addition and removal and for a given finite time interval, Δt, a new water temperature in the storage tank can be determined as follows:

$$T_{w,new} = T_{w,old} + \frac{\Delta t}{M_w C_w \left[\dot{Q}_C - \dot{Q}_L - (UA)_t (T_w - T_a) \right]} \tag{15.8}$$

Equation (15.8) can be used for the estimation of hourly storage water temperature for a known hourly heat addition and withdrawal.

For a known time variation of $\dot{Q}_C = \dot{Q}_{um}$ and $\dot{Q}_L$, the new storage water temperature, $T_{w,new}$, can be determined as a function of time.

Example 15.2 An insulated water-storage tank with a heat capacity of 900 J and a surface area of 10 m^2 is at a temperature of 30 °C. Determine the temperature of the tank after 2 h with $\dot{Q}_C = 100$ W and $\dot{Q}_L = 0$ for an ambient air temperature of 12 °C. The overall heat-transfer coefficient between the liquid in the tank and the ambient air is 6 W/m^2.

Fig. 15.1 Cross-sectional view of a well-mixed water/liquid storage tank
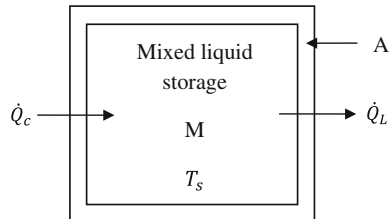
Solution

Given: $T_{w,old} = 30\,°C, \Delta t = 2\,h, M_w C_w = 900\,J$

After substituting the above values in Eq. (15.8), one gets

$$T_{w,new} = 30 + \frac{2}{900}[100 - 60 \times (30 - 12)] = 27.82\,°C$$

Liquid storage tank without stratification (well mixed) and with heat exchanger in collector as well open loop

A well-mixed liquid-storage tank with heat exchanger for both charging **a collector loop** and discharging an **open loop (load loop)** is shown in Fig. 15.2.

In this case, the inlet temperature of the flat-plate collector (FPC), T_{fi} is not the same as the storage temperature T_w in a collector loop as mentioned earlier. The outlet of flat-place collector, T_{fo}, becomes the inlet of the collector-loop heat exchanger and the outlet of the collector-loop heat exchanger becomes the inlet of the FPC, T_{fi}.

The energy balance for an elemental length dx in W of the heat exchanger in the collector loop, Fig. 15.3, can be written as

$$-(\dot{m}_f C_f)_c \frac{dT_f}{dx} dx = (2\pi r dx. U)(T_f - T_w)$$

or

$$\frac{dT_f}{(T_f - T_w)} = -\frac{(2\pi r.U)}{(\dot{m}_f C_f)_c} dx \qquad (15.9)$$
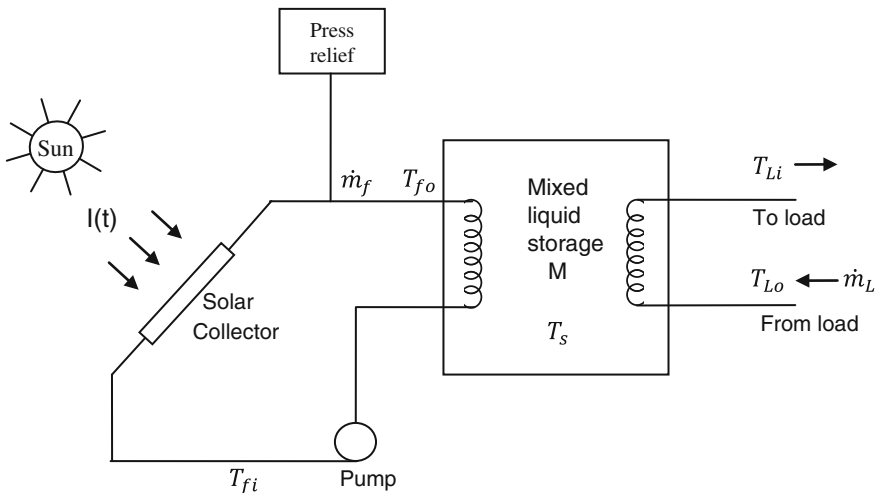
Fig. 15.2 Cross-sectional view of a stratified water/liquid storage tank
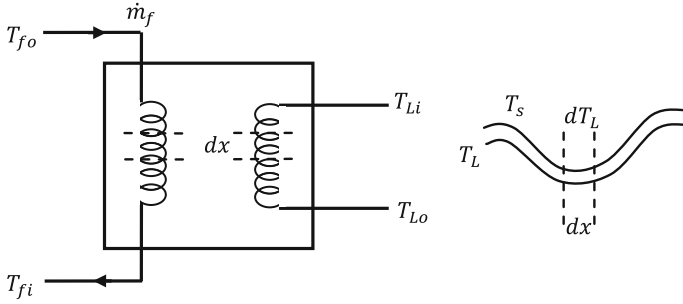
Fig. 15.3 View of a heat exchanger with elemental length "dx"

By using the initial condition (T_f at $x = 0 = T_{fo}$), i.e., the outlet of flat-place collector, T_{fo}, becomes the inlet of the collector-loop heat exchanger, and the solution of Eq. (15.9) becomes

$$\ln \frac{(T_f - T_w)}{(T_{fo} - T_w)} = -\frac{(2\pi r.U)}{(\dot{m}_f C_f)_c} x$$

or

$$\frac{T_f - T_w}{T_{fo} - T_w} = \exp\left[-\frac{2\pi r.U}{(\dot{m}_f C_f)_c} x\right] \tag{15.10}$$

Furthermore, T_f at $x = L$ is T_{fi} i.e., outlet of collector loop heat exchanger becomes the inlet of FPC, T_{fi}. Equation (15.10) becomes as

$$\frac{T_{fi} - T_w}{T_{fo} - T_w} = \exp\left[-\frac{2\pi r.U}{(\dot{m}_f C_f)_c} L\right]$$

From the above equation, one can obtain the rate of charging to the fluid inside the storage tank as follows:

$$\dot{Q}_C = (\dot{m}_f C_f)_c (T_{fo} - T_{fi}) = (\dot{m}_f C_f)_c \left[1 - \exp\left(-\frac{2\pi r.U}{(\dot{m}_f C_f)_c} L\right)\right] (T_{fo} - T_w)$$

$$= (\dot{m}_f C_f)_c \left[1 - \exp\left(-\frac{(UA)_c}{(\dot{m}_f C_f)_c}\right)\right] (T_{fo} - T_w)$$

$$\tag{15.11}$$

with $(UA)_c = U.2\pi rL$, and the factor $\varepsilon = \left[1 - \exp\left(-\frac{(UA)_c}{(\dot{m}_f C_f)_c}\right)\right]$ is known as the "penalty factor" for the heat exchanger in the collector loop as shown in Fig. 15.3.

Equation (15.11) can be discussed in terms of the following cases:

Case (i): For $L \sim$ very large, the length of the heat exchanger in the collector loop is very large, so then the penalty factor $\varepsilon \sim 1$. In this case,

$$\dot{Q}_C = (\dot{m}_f C_f)_c (T_{fo} - T_w)$$

which is same as $\dot{Q}_C$ of Eq. (15.7). This indicates that most of thermal energy available at the outlet of the FPC is transferred to the liquid/water in the storage tank.

Case (ii): For $\dot{m}_f \sim$ very small, then the penalty factor $\varepsilon \sim 1$. In this case, too,

$$\dot{Q}_C = (\dot{m}_f C_f)_c (T_{fo} - T_w)$$

which is same as $\dot{Q}_C$ of Eq. (15.7). This also indicates that most of thermal energy available at the outlet of the FPC is transferred to the liquid/water in the storage tank.

Case (iii): For $\dot{m}_f \sim$ very large, then the penalty factor $\varepsilon \sim 0$. In this case,

$$\dot{Q}_C = 0$$

This means that there is no transfer of heat to the liquid/water in storage tank. This indicates that the hot fluid is passed through collector-loop heat exchanger without transferring the heat into the tank.

Similarly, the rate of withdrawal of hot water through load loop, $\dot{Q}_L$, can be derived as

$$\dot{Q}_L = (\dot{m}_f C_f)_L (T_{Lo} - T_{Li}) = (\dot{m}_f C_f)_L \left[1 - \exp\left(-\frac{(UA)_L}{(\dot{m}_f C_f)_L} \right) \right] (T_{Lo} - T_w)$$

$$(15.12)$$

Equation (15.12) can also be discussed in a similar way as performed for Eq. (15.11).

After knowing $\dot{Q}_C$ and $\dot{Q}_L$ from Eqs. (15.11) and (15.12), Eq. (15.8) can be used to determine the temperature profile of a storage tank with a heat exchanger.

Liquid storage tank with stratification

In a solar water-heating system, this can be achieved as follows:

(a) Natural-circulation mode without a heat exchanger in the collector loop, Eq. (8.10)

$$\dot{Q}_C = \dot{Q}_{um} = A_{cm} F'[(\alpha\tau)I(t) - U_L(T_w - T_a)]$$

(b) Forced-circulation mode with a heat exchanger in the collector loop

In both cases, hot-water withdrawal (i.e., the rate of discharging, $\dot{Q}_L$) can occur either directly, Eq. (15.16), or through a heat exchanger in the open loop.

15.2.2 Solid-Media Storage

Thermal energy (heat) can be stored in loosely, abundant available packed rock-bed material either in insulated box or underground for a temperature range of 100 °C with a solar air heater for space heating. It can also be used for much higher temperature ranges. The packed rock-bed material is simple in design with size ranging from 1 to 5 cm, is relatively low cost, and has a longer life. It is porous with a large surface area and facilitates fast heat transfer with a working fluid (water/air) as medium with minimum internal conductive loss. The amount of energy stored in a rock bed mainly depends on the thermo-physical properties of the rock bed, rock size and shape, rock porosity, etc.

Packed rock-bed storage material has following advantages:

(a) It is nontoxic and noncombustible.
(b) Use of a heat exchanger can be avoided.
(c) It lacks freezing and corrosion problems.

The system has also some disadvantages as follows:

(a) The storage capacity is large.
(b) There is a high pressure drop.
(c) Simultaneous charging and discharging is not possible.

Abundantly available packed rock-bed material can also be used in a wall, which can be considered a Trombe wall. Figure 15.4 shows a cross-sectional view of an insulated packed rock-bed storage system with an N-segment in the vertical direction if air flow is from the top.

The energy-balance equations have been written considering a one-dimensional heat flow without axial conduction. It has also been assumed that the physical properties of solid storage are the same throughout the rock bed, i.e., there is no mass transfer; the temperature gradient between the solid particles is similar within the elemental distance dx; and the rock bed is thermally insulated from the environment.

The energy balances for flowing fluid (water/air) and rock-bed storage media are as follows:

Flowing fluid:

$$\left(\rho C_{\mathrm{p}}\right)_{\mathrm{f}} \varepsilon \frac{\partial T_{\mathrm{f}}}{\partial t} = -\frac{\left(\dot{m} C_{\mathrm{p}}\right)_{\mathrm{f}}}{A} \frac{\partial T_{\mathrm{f}}}{\partial x} + h_{\mathrm{v}}(T_{\mathrm{b}} - T_{\mathrm{f}}) \tag{15.13}$$

Rock-bed storage:

$$\left(\rho C_{\mathrm{p}}\right)_{\mathrm{b}}(1 - \varepsilon) \frac{\partial T_{\mathrm{b}}}{\partial t} = -h_{\mathrm{v}}(T_{\mathrm{b}} - T_{\mathrm{f}}) \tag{15.14}$$

where ε is the porosity of the rock bed; h_{v} is the volumetric heat-transfer coefficient between the rock bed and the fluid (W/m^2 °C); and $\left(\rho C_{\mathrm{p}}\right)_{\mathrm{f}}$, and $\left(\rho C_{\mathrm{p}}\right)_{\mathrm{b}}$ are the heat capacity, respectively, per unit volume, (J/m^3 °C), of the fluid and the rock bed.

Fig. 15.4 Cross-sectional view of an insulated packed rock-bed storage system
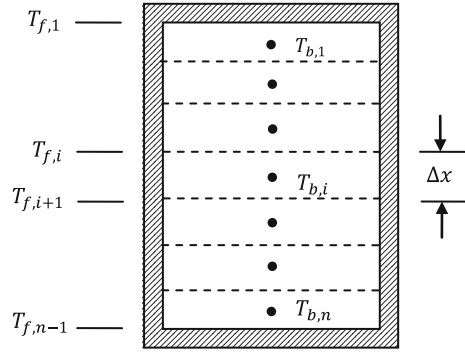
Equations (15.13) and (15.14) can be rearranged as follows:

$$\frac{\partial T_f}{\partial (X/L)} = \text{NTU}(T_b - T_f) \tag{15.15}$$

and

$$\frac{\partial T_b}{\partial \theta} = -\text{NTU}(T_b - T_f) \tag{15.16}$$

where NTU number of the transfer unit and dimensionless time are given by

$$\text{NTU} = \frac{h_V A L}{(\dot{m} C_p)_f} \quad \text{and} \quad \theta = \frac{t(\dot{m} C_p)_f}{(\rho C_p)_b (1 - \varepsilon) A L}$$

where A is the cross-sectional area (m^2) of the rock bed top; and L is the bed length (m).

With the initial condition, i.e., T_f at $\frac{X}{L} = 0 = T_{f,i}$ and T_f at $\frac{X}{L} = \frac{\Delta x}{L} = T_{f,i+1}$, the solution of Eq. (15.15) is given by

$$\frac{T_{f,i+1} - T_{b,i}}{T_{f,i} - T_{b,i}} = \exp\left[-\text{NTU}\frac{\Delta x}{L}\right] \tag{15.17}$$

Equation (15.16) can also be discussed as follows:

Case (i): If Δx is very small, then $\exp\left[-\text{NTU}\dfrac{\Delta x}{L}\right] = 1$ and $T_{f,i+1} = T_{f,i}$.

Case (ii): If L is very large then $\exp\left[-\text{NTU}\dfrac{\Delta x}{L}\right] = 1$ and $T_{f,i+1} = T_{f,i}$.

For elemental distance, ΔX, the energy transfer from air to the bed is expressed as

$$(\dot{m}C_p)_f(T_{f,i+1} - T_{b,i}) = (\dot{m}C_p)_f(T_{f,i} - T_{b,i})\exp\left[-\mathrm{NTU}\frac{\Delta x}{L}\right] \qquad (15.18)$$

For the rock bed, the energy balance within ΔX is as follows:

$$\frac{dT_b}{d\theta} = \eta N(T_{f,i} - T_{b,i}) \qquad (15.19)$$

where $\eta = 1 - e^{-\mathrm{NTU}/N}$ and $N = L/\Delta X$.

The above equation represents N differential equations for N bed temperatures. An extension of the above equation by considering the losses to the environment at an ambient temperature (T_a) will result in

$$\frac{dT_b}{d\theta} = \eta N(T_{f,i} - T_{b,i}) - \frac{(U\Delta A)_i}{(\dot{m}C_p)_f}(T_{b,i} - T_a) \qquad (15.20)$$

where $(U\Delta A)_i$ is the loss area-loss coefficient product for node i.

Example 15.3 Determine the volumetric heat-transfer coefficient (h_v) between a rock bed having dimensions of 2 cm diameter and volume (V) 3.5 m × 3.0 m × 1.5 m and air with a mass velocity of 258.5 kg/h.

Solution

The volumetric heat-transfer coefficient between the bed and the air (h_v) is given by

$$h_v = 824(G_0/D_s)^{0.92},$$

where G_0 is the mass velocity in kg/m^3 s; and D_s is the particle diameter in m.

Given the parameters:

$$G_0 = 258.5/(3.5 \times 3.0 \times 1.5 \times 3600) = 4.56 \times 10^{-3} \text{ kg/m}^3 \text{ s}, \quad D_s = 0.02 \text{ m}$$

After substituting the above values in the above relation, one gets

$$h_v = 824 \times (4.56 \times 10^{-3}/0.02)^{0.92} = 211.46 \text{ W/m}^2 \text{ °C}$$

Example 15.4 Determine the number of heat-transfer units (NTU) for air passing through a pebble rock bed with area 3.5 m × 3.0 m with mass velocity of 1782 kg/h given that the heat-transfer coefficient between the bed and the air is 225 W/m^2 °C and $C_p = 1006$ J/kg K..

Solution

The number of heat-transfer units NTU $= \frac{h_v A L}{(\dot{m}C_p)_f} = \frac{225 \times 3.5 \times 3.0 \times 3.5 \times 3600}{1782 \times 1006} = 17.12$.

15.2.3   Dual-Media Thermal Energy Storage (TES)

Solid and liquid heat-sensible thermal-energy storage (TES) materials can be combined in the following ways:

Hybrid thermal energy storage
In this case, a water tank is surrounded by a rock bed and can be used for room and greenhouse space heating. Flat-place collectors connected in series are mounted on the inclined roof of a building/greenhouse that is connected to a system of water and a rock bed by water motor P_1. The rock-bed water system is placed below the building/greenhouse in the basement as shown in Fig. 15.5. A hot-air blower is fitted between the room and the top of rock bed, which is porous. Furthermore there is connection between the floors of the building/greenhouse to the bottom of the rock bed to pass cold air of the building/greenhouse to the base of the rock bed.

Furthermore, rocks and oil can be placed in a single insulated vessel. In this case, the thermal energy produced by the concentrating collector at high temperature and pressure can be stored during the day, and power can be produced during the night. Such a system has been used for off-grid solar thermal-power applications.

Concrete thermal energy storage
Figure 15.6 shows a cross-sectional view of a floor of a building. It consists of a concrete floor, a concrete block, and packed gravel. There is provision of air flow thorough the concrete block for charging hot air and discharging cold air in the room. In the case of charging, hot air is circulated between the solar air collector and the concrete block. There is transfer of thermal energy from hot air to the packed gravel during charging (sunshine hours) and vice versa during discharging (off-sunshine hours). The packed gravel is porous to increase the surface area for maximum heat transfer. During discharging, the room air is allowed to flow between the room and the concrete block to the heat room as shown in Fig. 15.6b.

Ground thermal energy storage [3]
It is well established that soil in the ground has a large thermal capacity and can act as a large reservoir of solar energy. It has insulating properties as well. Therefore, the ground can be potentially used for the storage of hot water available from solar energy at low temperature ranges.

The system, a combination of a water tank and a rock bed, as discussed in the section on hybrid systems, is buried at an appropriate depth for long-term storage for space heating of a building as well as a greenhouse by heat pump. In this case, surplus heat in the summer can be stored and used later in the winter.

The above combination of a water tank and a rock bed is expensive and can also be used for short-term storage. To reduce the cost and for long-term storage, is necessary to use naturally existing confined underground aquifers containing water as shown in Fig. 15.7. In this case, excessive hot water available from the flat-place collector panel during summer is fed into the aquifer for long-term storage. It can be used on demand during the winter by withdrawing it using a water pump.

Fig. 15.5 Water tank and rock-bed storage system
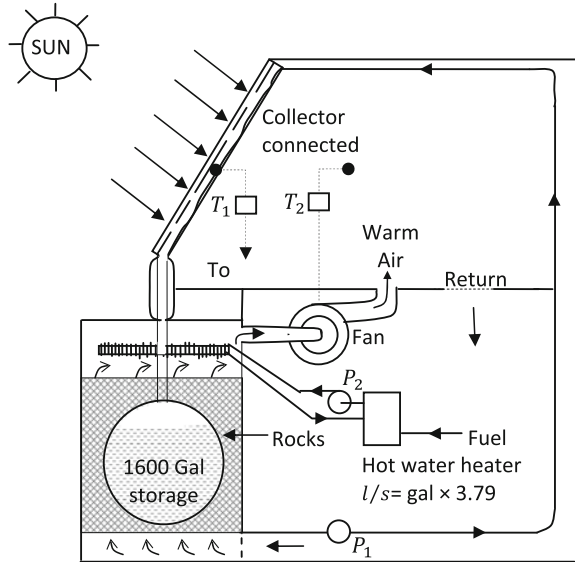
Fig. 15.6 View of a concrete block and hot air-storage system. **a** End view of floor. **b** Side view of floor
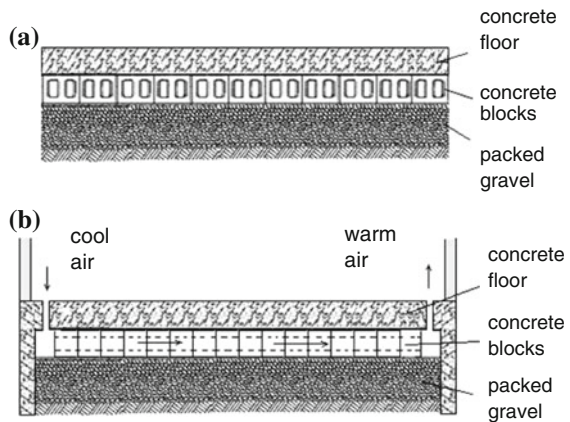
15.3 Latent-Heat Storage (LHS)

Latent heat is thermal energy either absorbed (solar energy) or released by a substance during a phase change at constant temperature. The substance can be a solid or a liquid. Examples of phase change include the melting of ice (solid) into water (liquid) or the evaporation of water (liquid) into vapor (gas). In both examples, the temperature is constant. Most phase-change materials (PCM) have high thermal energy storage densities compared with sensible-heat storage materials.

The classification of latent-heat storage is given below [4].

Fig. 15.7 View of
ground-aquifer storage
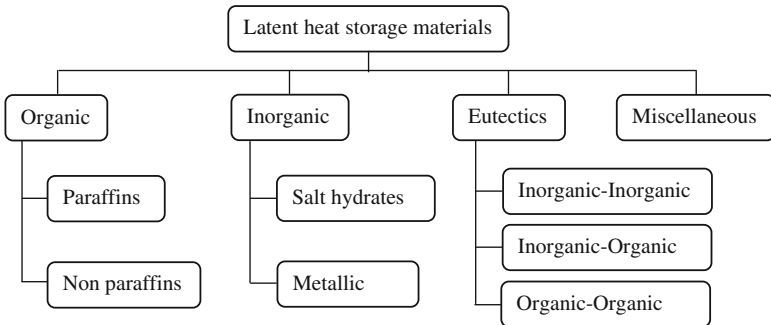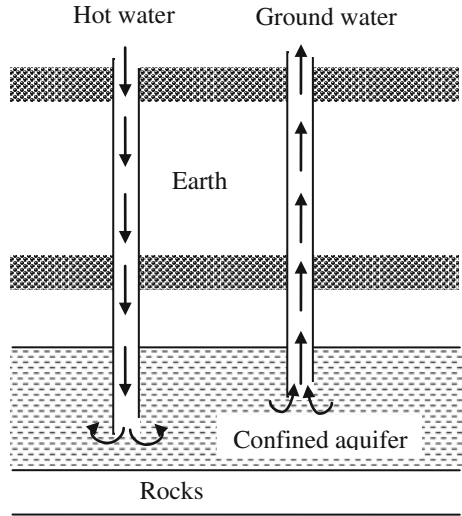
In this section, only solid–liquid phase-change materials will be discussed.

For a latent-heat thermal-energy storage system, there are mainly three components as follows:

(a) a PCM for heat storage in a specific temperature range;
(b) a PCM container; and
(c) a heat exchanger for transferring heat between the working fluid and the PCM.

Latent-heat storage (LHS) systems are more expensive than sensible heat-storage media.

15.3.1 *Energy Analysis [1]*

Figure 15.8 shows a glazed PCM slab exposed to solar radiation, $I(t)$, and ambient air temperature, T_a. After the absorption of solar radiation by the top of the PCM slab, the slab starts melting at the melting point with the latent heat of fusion of the PCM. For given $I(t)$ at time 't', a portion of the PCM will be in liquid state, and the rest of the PCM will be in a solid state. We will assume that at $x = 0$ is the interface of the liquid and solid PCM.

If $\dot{m}$ is the mass-flow rate of fluid flowing at the interface having temperature T_o, then the rate of thermal energy withdrawn from interface is given by

$$\dot{Q}_u = \dot{m}_f C_f (T_{fo} - T_{fi}) \tag{15.21}$$

where C_f and T_{fi} are specific heat (J/kg °C) and inlet temperature (°C), respectively, of the fluid flowing through the interface of the PCM fluid.

Following is the energy-balance equation at different boundaries for such a glazed PCM slab:

$$-K_1 \frac{\partial T_1}{\partial x}\bigg|_{x=-L_1} = U_t \left(T_{sa} - T_1|_{x=-L_1} \right) \tag{15.22}$$

where

$$T_{sa} = \frac{\alpha\tau}{U_t} I(t) + T_a \quad \text{and} \quad U_t = \left[\frac{1}{h_1} + \frac{L_g}{K_g} + \frac{1}{h_0} \right]^{-1}$$

again

$$T_1|_{x=0} = T_s|_{x=0} = T_f \tag{15.23}$$

$$-K_1 \frac{\partial T_1}{\partial x}\bigg|_{x=0} b dy = -K_s \frac{\partial T_s}{\partial x}\bigg|_{x=0} b dy + \dot{m}_f C_f \frac{dT_f}{dy} dy \tag{15.24}$$

Fig. 15.8 Glazed phase-change material (PCM) slab
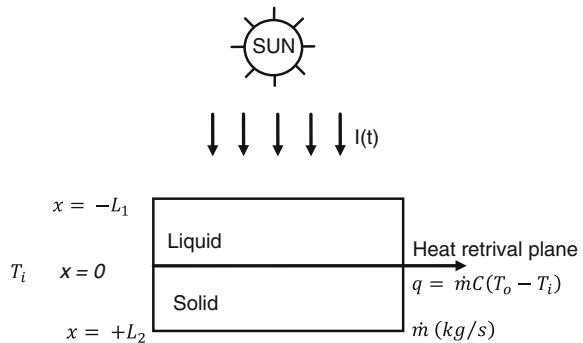
$$-K_s\frac{\partial T_s}{\partial x}\bigg|_{x=L_2} = h_i\left(T_s|_{x=L_2}-T_a\right) \qquad (15.25)$$

Under steady-state conditions, there will be linear variation of temperature in the liquid and solid PCM as follows:

$$T_l = A_1x + B_1 \quad\text{and}\quad T_s = A_2x + B_2 \qquad (15.26)$$

Furthermore, $T_{sa} = T_{sa0}$, a constant.

After substitution of an expression for T_l and T_s from Eq. (15.26) in Eqs. (15.22)–(15.25), one gets

$$-K_1A_1 = U_t[T_{sa0} - (-A_1L_1 + B_1)] \qquad (15.27)$$

$$B_1 = B_2 = T_f \qquad (15.28)$$

$$-K_1A_1b\,dy = -K_sA_2b\,dy + \dot{m}_fC_f\frac{dT_f}{dy}\,dy \qquad (15.29)$$

$$-K_sA_2 = h_i(A_2L_2 + B_2 - T_a) \qquad (15.30)$$

From Eqs. (15.27) and (15.30), with help of $B_1 = B_2 = T_f$, Eq. (15.28), one has

$$A_1 = -\frac{(T_{sa0} - T_f)}{K_1 + U_tL_1} \quad\text{and}\quad A_2 = -\frac{(T_f - T_a)}{K_s + h_iL_2}$$

With help of the above equations, one can rearrange Eq. (15.29) as

$$\frac{dT_f}{dy} + \frac{b}{\dot{m}_fC_f}\left[\frac{K_1}{K_1 + U_tL_1} + \frac{K_s}{K_s + h_iL_2}\right]T_f = \frac{b}{\dot{m}_fC_f}\left[\frac{K_1T_{sa0}}{K_1 + U_tL_1} + \frac{K_sT_a}{K_s + h_iL_2}\right] \qquad (15.31)$$

With the help of initial conditions, i.e., $T_f|_{y=0} = T_{fi}$, the solution of the above Eq. (15.31) is given by

$$T_f = \frac{f(t)}{a}\left(1 - e^{-ay}\right) + T_{fi}e^{-ay}$$

The outlet-fluid temperature is given by

$$T_{fo} = T_f|_{y=L} = \frac{f(t)}{a}\left(1 - e^{-aL}\right) + T_{fi}e^{-aL} \qquad (15.32)$$

where $a = \frac{b}{\dot{m}_fC_f}\left[\frac{K_1}{K_1 + U_tL_1} + \frac{K_s}{K_s + h_iL_2}\right]$ and, $f(t) = \frac{b}{\dot{m}_fC_f}\left[\frac{K_1T_{sa0}}{K_1 + U_tL_1} + \frac{K_sT_a}{K_s + h_iL_2}\right]$.

From Eqs. (15.21) and (15.32), the rate of thermal energy withdrawn from the interface of the glazed PCM slab is obtained as

$$\dot{Q}_u = \dot{m}_f C_f (T_{fo} - T_{fi}) = \dot{m}_f C_f \left(1 - e^{-aL}\right)\left[\frac{f(t)}{a} - T_{fi}\right] \qquad (15.33)$$

After knowing these constants, an average temperature of the PCM can be obtained as

$$\bar{T} = \frac{1}{L}\left[\int_{-L_1}^{0} T_1(x)\mathrm{d}x + \int_{0}^{L_2} T_s(x)\mathrm{d}x\right]$$

Then, the effective thermal properties of PCM can be obtained from the following expression:

$$C_{eff} = C_s + \left(\frac{H_0}{\bar{T} - T_a}\right)\left(\frac{L_1}{L}\right) \qquad (15.34)$$

where C_s is the specific heat of the solid phase of the PCM; and H_0 is the latent heat of fusion.

Similarly, the expression for effective thermal conductivity, K_{eff} can be written as

$$K_{eff} = K_s\left(1 - \frac{L_1}{L}\right) + K_1\frac{L_1}{L} \qquad (15.35)$$

The properties of some of the salt hydrates acting as PCM are given in Table 15.1.

15.3.2   Exergy Analysis

The exergy of sensible-heat storage during charging can be expressed as follows:

$$\mathrm{Ex}_C = M_p C_p\left[(T_2 - T_1) - (T_a + 273)\ln\frac{T_2 + 273}{T_1 + 273}\right] \qquad (15.36)$$

where M_p and C_p are the mass and the specific heat, respectively, of sensible-heat storage that has been charged from temperature T_1 to T_2.

One can see that exergy does not behave linearly as does the energy relation (Eq. 15.33).

Similarly, the exergy of sensible-heat storage during discharging can be expressed as follows:

$$\text{Ex}_D = M_p C_p \left[(T_2 - T_0) - (T_a + 273) \ln \frac{T_2 + 273}{T_0 + 273} \right] \qquad (15.37)$$

During discharging, the temperature of sensible heat-storage material is brought down from T_2 to T_0.

Now an overall exergy efficiency of discharging sensible heat-storage material is given by

$$\varepsilon = \frac{\text{Ex}_D}{\text{Ex}_C} \qquad (15.38)$$

Furthermore, the rates of exergy of charging and discharging sensible heat-storage material are given, respectively, by [5]

$$\dot{\text{Ex}}_C = \dot{m}_p C_p \left[(T_2 - T_1) - (T_a + 273) \ln \frac{T_2 + 273}{T_1 + 273} \right] \qquad (15.39)$$

and

$$\dot{\text{Ex}}_D = \dot{m}_p C_p \left[(T_2 - T_0) - (T_a + 273) \ln \frac{T_2 + 273}{T_0 + 273} \right] \qquad (15.40)$$

An instantaneous exergy efficiency of discharging sensible-heat storage material is given by

$$\varepsilon_i = \frac{\dot{\text{Ex}}_D}{\dot{\text{Ex}}_C} \qquad (15.41)$$

15.3.3 *Applications of PCM Materials* [6]

(a) **Solar cooker**

A cylindrical solar-cooker vessel is surrounded by PCM (with erythritol having a melting point of 118 °C and a latent heat of fusion approximately 339.8 kJ/kg) material. The PCM material is filled between the annular space between the outer surface of the cooking vessel and another cylindrical vessel. The outer surface is attached by a heat exchanger, which is connected to an evacuated tubular collector (ETC) through an insulated pipe. The flow of water between the ETC and the heat exchanger is under forced mode of operation. The cooking vessel has two hollow concentric aluminum cylinders having a diameter of 30.4 and 44.1 cm, respectively, and a height of 42.0 cm. The thickness of the aluminum sheet used for fabrication of the cooking vessel is 9 mm. The hot water circulated through the heat exchanger placed in the PCM transfers its thermal energy to the PCM, which is

melted at 118 °C by the latent heat of fusion, and the thermal energy is stored for cooking at the required time.

All sides and the base of the conventional solar cooker can be surrounded by PCM materials to maintain a uniform temperature inside the cooking vessel. Even fluctuation of the temperature inside the cooking vessel is reduced.

(b) **Greenhouse heating**

The floor of the greenhouse is constructed in a similar way except the packed gravel is replaced by the appropriate PCM material having a melting temperature of approximately the greenhouse temperature. In this case, thermal heating (charging) can be performed as follows.

 (i) Hot air is passed from the solar flat-plate collector through a concrete porous block at a slow flow rate to enable maximum heat transfer between the hot air and the PCM material. In this case, the PCM material is melted when the passing hot air has a temperature greater than the melting temperature of the PCM material.
(ii) The hot water from a solar flat-place collector is passed at a slow flow rate through a heat exchanger placed between the concrete floor and the PCM material. The charging takes place in similar way as mentioned above.

(c) **Space heating**

In this case, thermal heating of room can be performed either through floor or facade heating. The design and construction of the floor and the facade of building depend on the level of heating needed and the size of the room.

(d) **Solar water heating**

In this case, a suitable PCM material with proper thickness and melting temperature is placed between the absorber and the back insulating sheet. This can be a collection-cum-storage water heater/flat-plate water and air collector/evacuated tubular collector/concentrating collector. For such system, there will be no flow of fluid during sunshine hours due to the transfer of thermal energy from the absorber to the PCM material for the storage of heat (charging). Flow of fluid is required at the time of heating during night time (discharging).

(e) **Waste-heat recovery**

There is wastage of hot air (thermal energy) from an air conditioning unit; and wastage of hot water (thermal energy) from industries.

A novel design of heat exchanger with a shell and a tube for low-temperature waste-heat recovery using PCM can be a good solution. The stearic acid (PCM material), which has melting temperature of 59 °C, fills the shell of the heat

exchanger for thermal-energy storage. Hot waste fluid is used to flow through the tubes for the transfer of heat from the tubes to the shell during charging. During discharging, cold fluid is allowed to flow through tube, and heat is transferred from the PCM in the shell to the fluid.

15.4   Chemical-Energy Storage (CES)

Chemical energy is a form of potential energy. The storage capacity depends on its source. In this concept, energy is stored in the form of heat from chemical reactions. It is often of a larger magnitude than latent-heat storage. The idea of storing solar energy by the use of chemical reactions is not a new concept. Nature sores energy by the use of chemical reactions in photosynthesis.

Chemical-energy storage (CES) is a two-step process, namely:

Endothermic (charging) mode: This describes a process or reaction in which the system absorbs thermal energy from its surroundings in the form of heat. Absorbed energy occurs either in the breaking or rearranging of chemical bonds. This produces more energetic species, which are stored.

Exothermic (discharging) mode: In this case, the reaction is reversed to produce thermal energy and regenerate the starting material.

A chemical-energy storage (CES) system has following advantages:

 (i) The energy storage density of these systems are high.
 (ii) These systems are suitable for high-temperature applications.
(iii) The chemical-reaction rate is fast.
(iv) These systems have fewer energy losses.
 (v) It has easy transportability and an unlimited life.

Apart from these advantages, chemical energy storage (CES) has the following disadvantages:

 (i) The underlying technology for CES is much more complex than the other two energy storage systems.
 (ii) CES may have a hazardous affect on the environment.

The following CESs have been suggested:

 (i) **Hydrogen**: This is colorless, odorless, tasteless, and nontoxic gas and has potentials as a source of energy. It can be produced by the electrolysis of water (DC power from a PV module can be used for electrolysis). The produced H_2 gas can then be burnt to release heat, or it can be stored and/or distributed to the desired location. The enthalpy of change is $\Delta H = -242$ kJ mol^{-1}, i.e., 242 kJ are released for every mole (18 g) of H_2O formed.

(ii) **Ammonia**: Ammonia can also be dissociated at realizable temperatures. Along with a heat engine, these reactions may form the basis of an efficient way to generate continuous electrical power from solar energy.

(iii) **Liquid nitrogen**: Just like hydrogen, liquid nitrogen shows potential as a source of energy. It can be used to generate electricity or for refrigeration and cooling.

(iv) **Oxy-hydrogen**: This is a mixture of oxygen and hydrogen. It releases high-pressure and high-temperature steam after ignition, which can be used to generate electricity.

(v) **Biofuels and biomass**: This is another example of indirect solar energy chemical storage. It releases thermal energy after the burning of biofuels/biomass, which is stored in the bonds of molecules and atoms from photons of solar energy.

15.5 Solar Battery

A solar battery is very useful. It delivers electric power for a multitude of purposes with no moving parts and gives no visual evidence of its operation. The advantages of solar batteries areas follows:

(i) It is a portable source of electric power.

(ii) It is capable of delivering large quantizes of power for short periods and can be recharged at low rates over an extended period of time.

(iii) It provides the most reliable source known of emergency power, instantaneously, when normal power sources fail.

(iv) It provides a source of pure direct current for laboratory and other specific purposes either as a separate and independent supply or by acting as filter in a normal supply system.

15.6 PV Pumped-Storage Hydroelectricity

Pumped-storage hydroelectricity (PSH) is a type of hydroelectric-power generation. It is generally used by some power plants for load balancing during peak demand. The water from a lower elevation reservoir is pumped by PV arrays to a higher elevation. This method stores energy in the form of the potential energy of water. The water stored at a higher elevation is released through turbines to produce electric power during periods of high electrical demand. These system can met the peak demand and generate more revenue.

Objective Questions

15.1 The sensible-heat storage of solar energy depends on
      (a) the mass of the material   (b) the specific heat of the material
      (c) temperature difference   (d) all of these
      Answer: (d)
15.2 Sensible-heat storage can be performed by
      (a) liquid media   (b) solid media   (c) liquid/solid media   (d) all of these
      Answer: (a)
15.3 The cheapest and most freely available liquid medium for sensible-heat
      storage of solar energy is
      (a) water   (b) oil   (c) seawater   (d) none of these
      Answer: (a)
15.4 The penalty factor of a heat exchanger depends on
      (a) the mass-flow rate   (b) (UA) values
      (c) temperature difference   (d) the mass flow rate and the (UA) value
      Answer: (d)
15.5 For space heating, the type of heat exchanger used is
      (a) coil type   (b) tube-in-tube type   (c) shell type   (d) none of these
      Answer: (a)
15.6. The penalty factor of a heat exchanger for a very large mass-flow rate is
      (a) 0   (b) <1   (c) >1   (d) none of these
      Answer: (a)
15.7 The penalty factor of a heat exchanger for very small mass-flow rate is
      (a) 1   (b) <1   (c) >1   (d) none of these
      Answer: (a)
15.8 The following fluid is used for packed rock-bed storage:
      (a) air   (b) water   (c) oil   (d) none of these
      Answer: (a)
15.9 For packed rock-bed storage media, there is
      (a) a stratification in temperature   (b) no stratification in temperature
      (c) a constant temperature   (d) none of these
      Answer: (a)
15.10 For packed rock-bed storage media, there is
      (a) a pressure gradient   (b) no pressure gradient
      (c) a constant flow of air   (d) none of these
      Answer: (a)
15.11 For packed rock-bed storage media, the unit of heat-transfer coefficient from
      the packed rock-bed storage to the air is
      (a) W/m^2 K   (b) W/m^3 K   (c) W/m K   (d) none of these
      Answer: (b)
15.12 The value of a bed void fraction (ε) is
      (a) <1   (b) >1   (c) 1   (d) none of these
      Answer: (a)

15.13 The number of transfer units (NTU) depends on
(a) the volumetric heat transfer   (b) the dimension of the packed rock
                                               bed (volume)
(c) the mass-flow rate   (d) all of these
Answer: (d)

15.14 The value of the volumetric heat-transfer coefficient between a packed rock
bed and flowing air can be on the order of
(a) 3–30 W/m^2 °C   (b) 150–200 W/m^3 °C   (c) 1000 W/m^3 °C
(d) none of these
Answer: (b)

15.15 The value of the number of heat transfer units (NTU) for a packed
rock-bed/air-flow combination is
(a) 1   (b) <1   (c) >1   (d) none of these
Answer: (c)

15.16 A ground heat source is used for
(a) space heating   (b) water heating   (c) drying   (d) (a) and (b)
Answer: (d)

15.17 The specific heat of a liquid phase-change material (PCM) is
(a) higher than the specific heat of a solid phase-change material
(b) lower than the specific heat of a solid-phase change material
(c) equal to the specific heat of a solid phase-change material
(d) none of these
Answer: (a)

15.18 The thermal conductivities of a liquid versus solid phase-change material
(PCM) are
(a) the same   (b) different   (c) insulating   (d) none of these
Answer: (a)

15.19 The melting point of different PCM materials
(a) varies   (b) is constant   (c) is 25 °C   (d) none of these
Answer: (a)

15.20 The following gas can be used as a storage medium:
(a) hydrogen   (b) air   (c) O$_2$ (d) none of these
Answer: (a)

Problems

15.1   Determine an expression for total energy loss/gain (Q) for constant thermal
and physical properties of a solid/liquid storage material.
Hint: Integrate Eq. (15.1) between T_1 and T_2 with constant ρ and C.

15.2   Determine the temperature of paraffin for 75 J of energy lost from boiled oil.
Hint: See Problem 15.1 and Appendix IX.

15.3   Determine (UA) for an insulated 100 l cylindrical tank having a length of 1 m filled with acetic acid for a drop of oil temperature from 300 to 150 °C in 1 h.

Hint: $(UA)(T_2 - T_1) \times 3600 = Q$ (Eq. 15.1).

15.4   Obtain an expression for an overall heat-loss coefficient (U) in terms of the physical properties of an insulated storage tank.

Hint: $(UA)(T_2 - T_1) \times 3600 = Q$ (Eq. 15.1)   for   constant   physical properties.

15.5   Determine the boiling temperature of seawater for a given Q and T_1.

Hint: $Q = MC(T_2 - T_1)$.

15.6   Calculate the temperature drop when 8×10^{11} J of thermal energy is lost from an insulated tank filled with 1500 l of olive oil.

Hint: See Example 15.1.

15.7   Calculate the time required for the temperature of a storage tank of heat capacity 1000 l, at a temperature of 35 °C, to change by 5 °C if there is no charging from the source and the rate of heat removal by the load is zero and given that ambient air temperature is 15 °C, the area of storage is 15 m², and the overall heat-transfer coefficient between the liquid in the tank and ambient air is 7 W/m² °C.

Hint: See Example 15.1.

15.8   Water, at 50 °C, flows at a rate of 5 kg/s through an 8 m long pipe buried at a depth of 4 m. Calculate the outlet temperature for (i) the wetted surface and (ii) the glazed surface.

Hint: See Sect. 10.8.4 and use the properties of water.

References

1. G.N. Tiwari, *Solar Energy: Fundamental, Design, Modelling and Applications* (Narosa Publishing House, New Delhi and CRC Press, New York, 2004)
2. E. Hahne, *Storage of Sensible Heat, Energy Storage Systems, vol. I, Encyclopedia of Life Support Systems (EOLSS)*, http://www.eolss.net/Eolss-sampleAllChapter.aspx
3. O.E. Ataer, *Storage of Thermal Energy, Energy Storage Systems, Encyclopedia of Life Support Systems (EOLSS)*, http://www.eolss.net
4. S.D. Sharma, K. Sagara, Int. J. Green Energy **2**, 1 (2005)
5. G.N. Tiwari, R.K. Mishra, *Advanced Renewable Energy Sources* (RSC, UK, 2011)

Additional References

6. H. Shabgard, C.W. Robak, T.L. Bergman, A. Faghri, Sol. Energy **86**, 816 (2012)
7. G.N. Tiwari, *Solar Energy Technology Advances* (Nova Science Publishers Inc, New York, 2006)

8. B. Agrawal, G.N. Tiwari, *Building Integrated Photovoltaic Thermal Systems* (RSC Publishing, UK, 2010)
9. K. Pielichowska, K. Pielichowski, Prog. Mater Sci. **65**, 67 (2014)
10. M. Pomianowski, P. Heiselberg, Y. Zhang, Energy Build. **67**, 56 (2013)
11. N. Soares, J.J. Costa, A.R. Gaspar, P. Santos, Energy Build. **59**, 82 (2013)
12. N. Kumari, G.N. Tiwari, M.S. Sodha, Int. J. Energy Res. **30**, 221 (2006)

Chapter 16
Solar-Power Generation

Abstract Solar-power generation means the generation of electrical (high-grade) power, and it is achieved from a solar-concentrator device and photovoltaic system. DC-power generation is converted/transferred to AC power by means of suitable generators through a charge controller. It works on the basis of the second law of thermodynamics, and it can partially replace grid power.

Keywords Solar-power generation · Concentrated solar power · Charge controller · DC–AC inverter · Grid-connected systems

16.1 Introduction

Solar power is generated by converting solar radiation (sunlight) into electricity by the following methods:

(i) **Photovoltaic (PV) method**: In this case, photons of the visible wavelength of solar radiation is responsible for the direct generation of electricity (Chap. 4). The PV method is economical at small (off-grid) as well as large (grid-connected) scale capacity. The small scale can be classified as $\leq 1000\,\mathrm{kW_p}$. This includes solar calculators, solar battery charging for remote application, solar street lighting, water pumping, telecommunications, and solar home lighting for energy security, etc.

(ii) **Concentrated solar power (CSP) method**: In this case, lenses or mirrors and tracking systems are used to focus a large area of solar radiation (sunlight) into a smaller area to have more temperature to operate turbine for power generation (Chap. 6). It is an indirect method for power generation. The CSP method is viable and economical at large (grid-connected) scale, which can be on the scale of $\mathrm{MW_p}$.

16.2   Power Generation by PV Modules

Because there is global market of approximately 80 % production of crystalline-base PV modules, we will consider only power generation from a single (mono) pseudo-shape and multi-crystalline rectangular-shape PV modules in this chapter.

16.2.1   PV Arrays

Thirty-six mono-crystalline silicon (Si) solar cells are interconnected in series to give 18 V and 4.17 A current under standard test conditions ($I = 1000\,\text{W/m}^2$ and an ambient air temperature of 25 °C). It is encapsulated between hardened glass and Tedlar or Mylar with ethyl vinyl acetate (EVA) to form an air-proof PV module as shown in Fig. 4.13. The Tedlar or Mylar may be opaque or transparent depending on the application. An aluminium frame surrounds the PV module to prevent any leakages. Such rated PV modules are available everywhere in the world.

Individual PV modules are connected in series to increase the required voltage to charge a battery of 24 and 48 V with the same current for a higher rated output. This series combination of PV modules is known as a "PV array." Furthermore, PV arrays can be connected in parallel to increase the current to achieve the given voltage for a required rated power (Chap. 4).

16.2.2   Applications of PV Cells

(a) **Solar calculator**

Solar calculators were introduced at the end of the 1970s. Hand-held calculators are powered by a solar cell in the low voltage range of 1.5–2 V. They have liquid crystal displays and can be operated at a very illumination level of 500 lx. They do not require any battery back-up and are very economical and useful for remote rural area.

(b) **Street light**

Street light is powered by a PV module (Fig. 4.13) of high rated power compared with a single solar cell. The module is mounted on the light structure. In this case, the PV module charges a rechargeable battery. The charged battery powers a compact fluorescent light (CFL)/light-emitting diode (LED)/lamp during the night. A LED consumes 50 % less power. Mono-crystalline Si solar cells are used in PV modules, which convert solar energy into DC power during the day to charge the battery (gel cell deep-cycle battery and lead-acid battery). A PV-based street light is generally used as yard lighting, peripheral lighting for industries, street lights in layouts, compound lights, etc. A PV module of a

street light turns on and turns off automatically by sensing the outdoor light using a light source. The module can also be mounted on a roof to minimize the cost of the street light.

(c) **Stand-alone off-grid PV system**

In a stand-alone system, PV arrays are used to generate more power compared with single PV modules to operate high rated-capacity electronics instruments including the following:

(i) **Domestic light/fan**

In this case, the PV array design depends on the total load (kWh) of the house for light during the night and cooling by fan during day/night. Accordingly, the charge controller, battery, and inverter (next section) should be specially designed.

(ii) **Water pumping**

A water well is a solid structure that is created manually in the ground by digging, driving, boring, or drilling to access groundwater for human use. In the past, water from a well was drawn either by mechanically or by hand using buckets. However, this was feasible only up to a certain depth. At larger depths, a water pump is used depending on the flow rate and depth of the underground water well. In the case of solar photovoltaic (SPV) water pumping, underground water at larger depths is pumped at ground level by a stand-alone PV system for many applications, namely, livestock, plants, or human use, etc. The water requirement during dry conditions is in phase with the solar insolation (higher values of solar insolation); hence, SPV water pumping is a suitable option. A 200 Wp PV system on a clear-sky day can deliver at least 15,000 L/day from a 7-m depth and/or 10-m head.

(iii) **Medical refrigeration**

It has been strictly recommended by the World Health Organization (WHO) that vaccines must be kept in the temperature range suggested by the manufacturer until their end use. Vaccines need to be refrigerated for 24 h. The PV-operated refrigeration system is a suitable option for medical refrigeration at places where fossil fuel-based power is not available. The rated power of a stand-alone system, including all components, namely, charge controller, battery, and inverter, depends on the capacity of the refrigeration system.

(iv) **Transport carrier**

Photovoltaic (PV) power was initially used for power generation in space applications. PV technologies are also in used in the following area of transport:

(a) Power boats: These are battery operated and used as ferries in rivers/canals mostly during sunshine hours.

(b) Cars: There have been many driving tests of solar-operated cars throughout world.

(c) Rickshaws: Battery-operated rickshaws are used to transport people from one place to another by road.

(d) Generation of hydrogen: Hydrogen power is also being used in cars.

(e) Air carrier: Recently, Switzerland successfully tested a solar-based aeroplane.

In all cases, a battery bank is used, which is charged by arrays of PV modules through a charge controller.

The PV system discussed so far is an off-grid system. However, grid-connected PV systems without a battery operating on the basis of MW-rated capacity also exist.

(v) **Building-integrated photovoltaic (BiPV) systems**

In this case, no land is required for the installation of a PV system to supply electrical power to a building. The PV is an integral part of the roof of a building, and the space below the rooftop PV roof can be used for many purposes; hence, it is referred as a "building-integrated photovoltaic (BiPV) system." If thermal energy associated with a PV is used for thermal heating of the space below the roof, then it is referred to as a "building-integrated photovoltaic thermal (BiPVT) system." As discussed in Chap. 4, there are two type of PV modules, namely, opaque and semitransparent. In a BiPVT system, a semitransparent PV module is used on the rooftop of a building. In this case, the advantages are as follows:

(i) The electrical efficiency of a semitransparent PV module is higher than that of an opaque PV module.

(ii) Solar radiation transmitted through a nonpacking-factor area is used for thermal heating of the space below the rooftop PV.

(iii) The semitransparent roof can provide sufficient day lighting into various rooms.

(iv) The space below a semitransparent PV module can be used for drying crops/vegetables drying, sun bathing, crop-pot cultivation during off season, etc.

(v) The heating of various rooms in a building can be performed by providing an air duct connected to the roof of a building.

The integration of such PV systems into buildings usually requires experts from civil engineering, architecture, and PV-system design. The semitransparent PV module should face south with optimum inclination (generally at latitude) on the roof to receive the maximum yearly solar radiation.

Electrical power obtained by a BiPVT system can be used either to provide electrical energy to a building or to transport it to the same locality if needed. Electrical power from a BiPVT system can be regulated through a charge controller for DC back-up and a charge controller, battery, and inverter for AC back-up.

Such a system is most suitable to localities not having access to grid power, and it is economical from the point of view of energy conservation as well as carbon credits.

A photograph of the BiPVT roof of the SODHA BERS COMPLEX (SBC), Varanasi, is shown in Fig. 16.1.
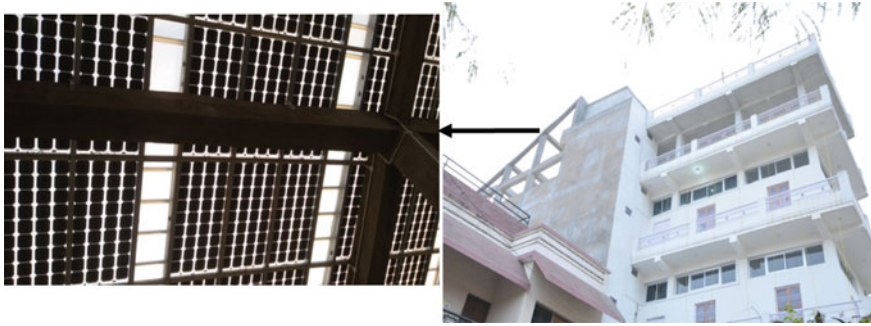
Fig. 16.1 Photograph of the SODHA BERS complex

16.2.3 Charge Controller

At peak sunshine hour, maximum voltage is produced by a PV module; excessive voltage can damage the batteries. A solar charge controller regulates the DC voltage from a PV module for charging the batteries to a given voltage. It is also referred to as a "battery regulator." It prevents overcharging the batteries and can also protect against overvoltage. This increases the life span of the batteries. It also prevents complete draining of a battery. The term "**solar-charge controller/regulator**" generally refers to either a stand-alone device or a battery recharger. A "**series-charge controller/regulator**" stops the current flow in a fully charged battery.

Solar-charge controllers are specified by the system voltage, which is generally 12, 24, and 48 V. In this case, PV modules are connected in series to form arrays. The maximum current is determined by connecting such arrays in parallel.

A single conventional PV module of 75 W_p requires a solar-charge controller of approximately 4–6 A rating. A larger PV array may need solar controllers ≥40 A. Figure 16.2 shows a basic solar-charge controller circuit with ratings of 8, 12, 20, and 30 A, which automatically selects between 12 and 48 V.

16.2.3.1 Working Principle

A solar-charge controller monitors voltage across the battery and disconnects the battery from the PV array or diverts the power away from the battery when it is fully charged. This can be achieved by short circuiting the PV array (**shunt regulator**) or by disconnecting the positive and negative terminals (open-circuited **series regulator**). In addition to a shunt/series regulator, an auto cut switch is also provided, which disconnects the electrical load for very low battery voltage. This is referred to as a "low-voltage disconnect function." The solar-charge controller (SCC) is provided between the solar PV panel and the batteries.
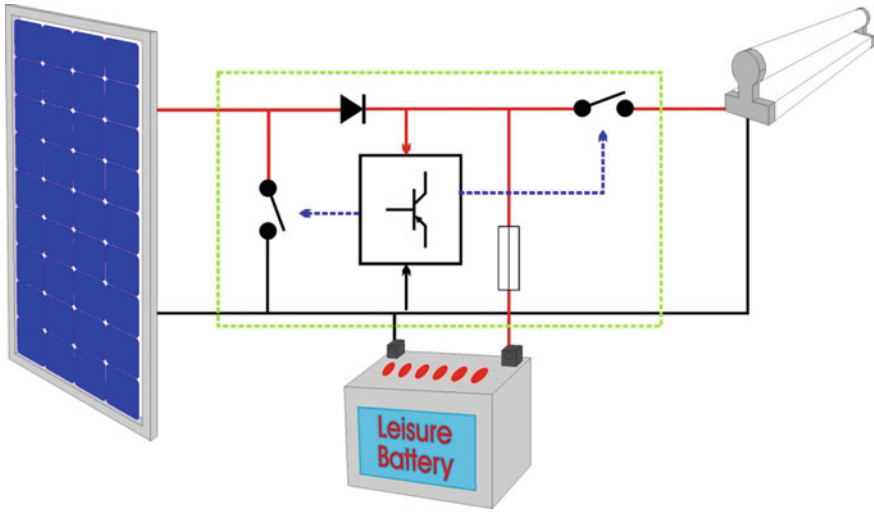
Fig. 16.2 Circuit diagram of a solar-charge controller

16.2.4   PV Battery

Generally a lead-acid automotive battery is used for the storage of electrical energy generated from a PV array. Other suitable batteries used in a PV system for energy storage are alkaline batteries, nickel–cadmium batteries, and sealed batteries.

To avoid accidents, a solar battery for PV application is installed in a separate room with proper ventilation and a moderate temperature range as suggested by the manufacturer. Sealed batteries can be placed in usual working places with normal ventilation. Battery manufacturers and suppliers provides specific guidelines for stacking batteries and designing rooms for battery installation. These guidelines vary by battery type and construction. Generally batteries are designed for floor placement over a wooden or plastic platform. In some specific cases, they may be installed in steel step or slotted iron stands. For long life and better performance, these batteries are charged using a charge controller as discussed previously.

16.2.5   DC–AC Converter and Inverter

A **power inverter**, also known as an "**inverter**," is an electronic device/circuitry that converts DC current into AC current as shown in Fig. 16.3.

The power inverter can also charge batteries if it is connected to an AC utility grid or, in the case of a stand-alone system, one's own AC generator.
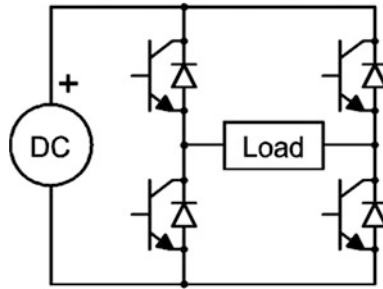
Fig. 16.3 Circuit diagram of a DC–AC converter and inverter

16.2.6   Off Grid–Connected PV Power Systems

Figure 16.4 shows a view of grid-connected PV power systems.

16.3   Concentrated Solar Power (CSP)

16.3.1   Solar Stirling Engine

A **solar-powered stirling engine** is a solar dish collector/heat engine operated by cyclic compression and expansion of air/working fluid at different temperature levels to produce electricity. It consists of a large spherical dish focused toward the
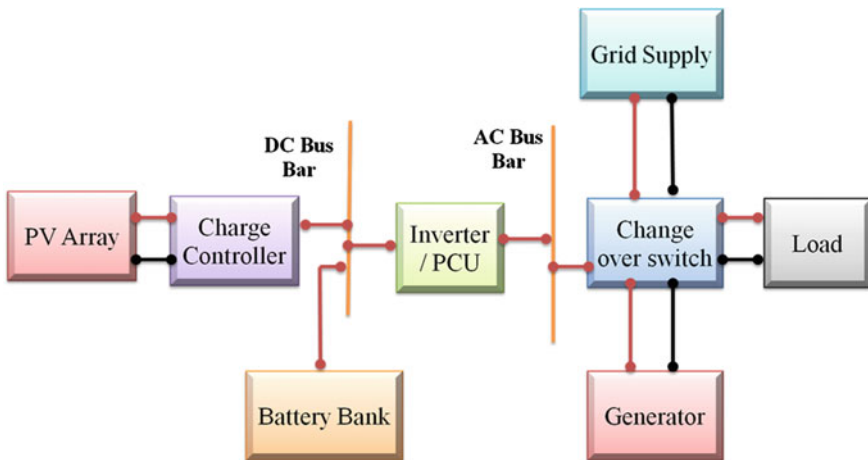
Fig. 16.4 Grid-connected PV power systems

Fig. 16.5 Photograph of a stirling solar engine

Sun to reflect its rays into the focus point as shown in Fig. 16.5. Solar radiation is collected in the form of heat to fuel the Stirling cycle engine. The heat engine operates by allowing heat flow from a heat source to a cold sink. The work output of the Stirling cycle is then used to drive a generator and create electric power. If solar power is used as a heat source, there is need of regulation (tracking) of solar disk to have continuous maximum solar radiation. In some applications, Fresnel lenses and mirrors are used for solar-power generation. The solar-powered Stirling engine eliminates the use of fossil fuels for power generation; therefore, they have fewer detrimental effects on the environment. The Stirling engine has been found to have high efficiency compared with steam engines.

16.3.2 Concentrating Linear Fresnel Reflector (CLFR)

A concentrating linear Fresnel reflector is also known as a "**compact linear Fresnel reflector**: (**CLFR**)". This **linear Fresnel reflector** (LFR) system consists of various long, thin strips of mirror. These mirrors reflect and focus solar radiation on a fixed absorber that is placed on a common focal point as shown in Fig. 16.6.

The reflecting mirrors can concentrate the incident solar radiation up to 30 times. The energy absorbed by the linear absorber heats the fluid (high boiling temperature). The fluid flowing through the absorber tubes powers the steam generator using a heat exchanger. The CLFR utilizes multiple flat-plate absorbers within the vicinity of the mirrors unlike a traditional LFR.

16.3.3 Solar Steam Turbine

A steam turbine is a device that extracts thermal energy from pressurized steam of high temperature fluid obtained from concentrating solar collectors. It converts
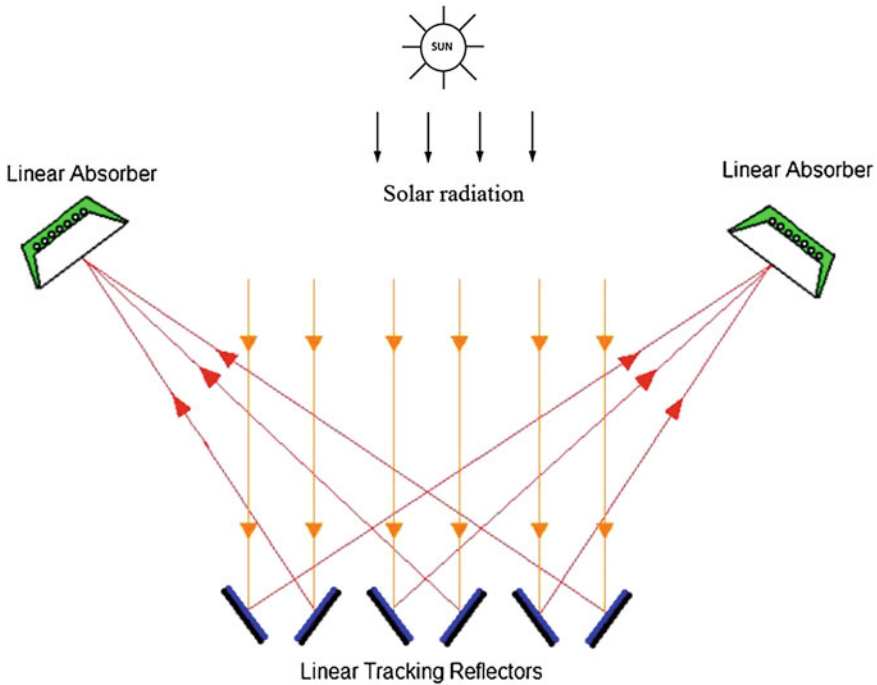
Fig. 16.6 Solar-concentrating linear fresnel reflector

thermal energy into mechanical energy by rotating the output shaft. A steam turbine generates a rotary motion to drive an electrical generator. The electrical power generated by this process can be used for many applications. There are two type of steam turbine as follows:

(a) **Impulse turbines**

An impulse turbine works on the principle of the law of moments/law of the conservation of momentum or a direct push or impulse. The fixed nozzles of an impulsive turbine increase the speed of the incoming steam. The high-speed jet of steam from the fixed nozzles falls on the bucket, such as blades, and rotates the shaft, which is connected to the electrical generator.

(b) **Reaction turbines**

A reaction turbine works on the principle of action and reaction (reactive force). In reaction turbines, there are no nozzles like in an impulse turbine. In this case, the blades, also known as "rotor blades," are mounted on the revolving rotor, and they are arranged to form convergent nozzles. The rotor blades are called "moving blades." The steam enters from the **stator blade** to the rotor blade through the nozzle created by the rotor blade geometry. As the

steam jet leaves the rotor blade, the pressure decreases across both blades. As the steam jet moves through rotor blade, it creates a reaction force, which further creates turning moment.

Performance of a reaction turbine depends on three main forces as follows:

  (i)   the reactive force on the rotor blades due to an increase in velocity;
 (ii)   the reactive force on the rotor due to the changing direction of gas; and
(iii)   the impulsive force of gas on the rotor blades

16.3.4   Parabolic-Trough Concentrator Power

Concentrated solar power (**CSP**) is also known as a "**concentrating solar power/ concentrated solar thermal** system." It uses mirrors or lenses to concentrate a large area of solar thermal energy onto a small focal area of a parabolic-trough mirror/lenses, etc. Electrical power is produced when the concentrated solar energy (beam radiation) at the focal point is converted to thermal energy by fluid flowing through the heat exchanger as shown in Fig. 16.7a. The thermal energy drives a solar-heat engine. The heat engine, also referred to as a "steam turbine," is connected to an electrical power generator to produce electrical power supplied to the grid.

Referring to the chapter on concentrating solar collectors, the rate of solar radiation available at a receiver of area, A_r, and a concentration ratio of C for beam radiation, I_b incident over the concentrator is given by

$$\dot{Q}_{ab} = \alpha \tau \eta_o C I_b A_r \tag{16.1}$$

where α and τ are the absorptivity and transmittivity of the evacuated glazed receiver, respectively; and η_o and C are the optical efficiency and concentration ratio of the concentrating collector, respectively.

At a high operating temperature of the solar concentrator, only radiative heat loss can be dominant from a receiver having temperature T_r; hence, the rate of thermal energy lost by radiation can be expressed as

$$\dot{Q}_L = \varepsilon \sigma A_r T_r^4 \tag{16.2}$$

where ε and σ are the emissivity of receiver and Stefan–Bloltzmann constant, respectively. In this case, radiation exchange between ambient air and receiver has been neglected due to the very small value compared with the radiative heat loss from the receiver to the ambient air due to very high operating temperature. Hence,

(a)
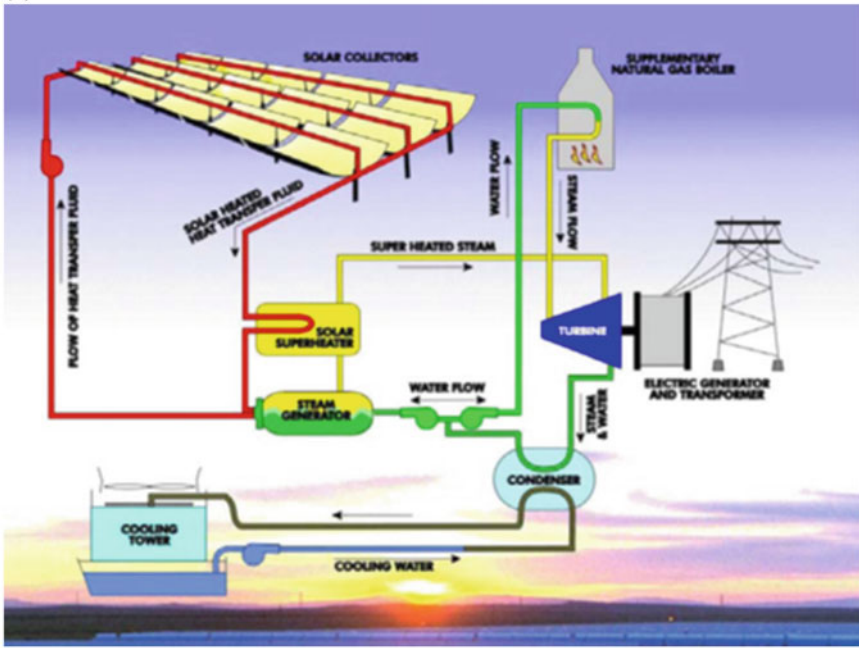
(b)
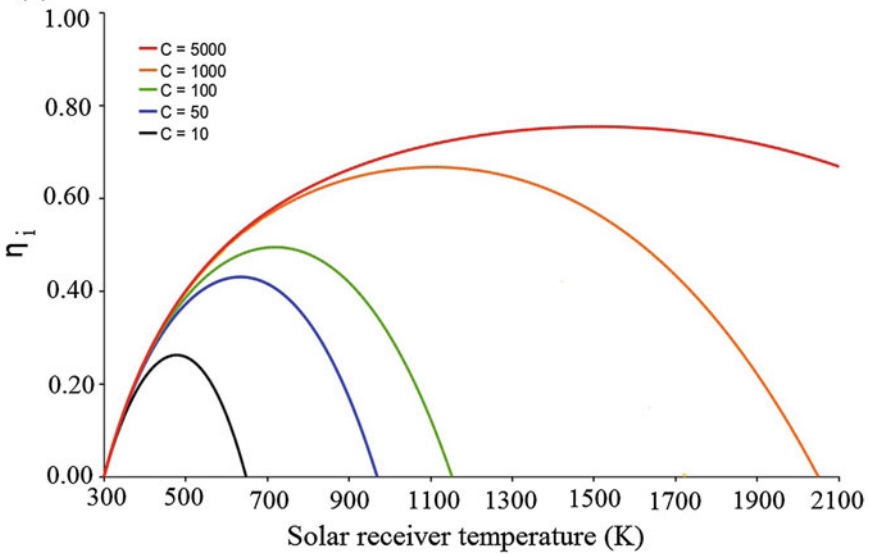
Fig. 16.7 **a** Solar parabolic-trough concentrator power. **b** Variation of overall instantaneous efficiency η_i with solar-receiver temperature (T_r)

the net rate of thermal energy available for heating of the working fluid for power generation is given as

$$\dot{Q}_{TH} = \dot{Q}_{ab} - \dot{Q}_{L} \tag{16.3}$$

An instantaneous optical thermal efficiency of the receiver is expressed as

$$\eta_{i,th} = \frac{\dot{Q}_{ab} - \dot{Q}_{L}}{\dot{Q}_{ab}} \tag{16.4}$$

After substituting the values of known parameters, the above equation can also be written as

$$\eta_{i,th} = \left[1 - \frac{\varepsilon \sigma T_r^4}{\alpha \tau \eta_o C I_b} \right] \tag{16.5}$$

For ideal conditions, one can assume that

$$\alpha = \tau = \eta_o = \varepsilon = 1 \tag{16.6}$$

An instantaneous optical thermal efficiency of the receiver becomes

$$\eta_{i,th} = \left[1 - \frac{\sigma T_r^4}{C I_b} \right] \tag{16.7}$$

This is an instantaneous thermal efficiency of a solar receiver for converting beam radiation into thermal energy. For thermodynamic solar systems, one is interested to have the maximum solar-to-work (electricity) efficiency, η, which can be obtained by multiplying Eq. (16.7) by Carnot's efficiency as follows:

$$\eta_i = \left[1 - \frac{\sigma T_r^4}{C I_b} \right] \left[1 - \frac{T_a}{T_r} \right] \tag{16.8}$$

Here all temperatures are expressed in Kelvin.

The plot of η_i and T_r for different concentration ratio, C, is shown in Fig. 16.7b. One can see that an overall instantaneous efficiency of solar-to-work (electricity) efficiency significantly depends on concentration ratio and operating receiver temperature, T_r. One can conclude that instantaneous efficiency does not simply increase monotonically with the receiver temperature.

Example 16.1 Evaluate an instantaneous thermal efficiency of a solar receiver having temperature (T_r) of 300 °C, beam radiation (I_b) of 500 W/m², and concentration ratio (C) of 15.

Solution

Given $T_r = 300 + 273 = 573$ K, $I_b = 500$ W/m^2, $C = 15$.

Using Eq. (16.7), one gets

$$\eta_{i,th} = \left[1 - \frac{5.67 \times 10^{-8} \times (573)^4}{15 \times 500} \right] = 0.19(19\%)$$

Example 16.2 Calculate an overall instantaneous thermal efficiency of a solar receiver according to the work of Example 16.1.

Solution

Given an ambient air temperature of 25 °C, then $T_a = 25 + 273 = 298$ K.

Then using Eq. (16.8), we have

$$\eta_i = 0.19 \times \left[1 - \frac{298}{573} \right] = 0.19 \times 0.47 = 0.09(9\%)$$

16.3.5 *Latent-Heat Storage Concentrating Solar Power [1]*

In parabolic-trough concentrator, power generated can either be used immediately or transferred to a grid. However, in the case of latent-heat storage concentrating solar power, power can be generated at a later stage due to the storage of thermal energy in the phase-change materials.

Latent-heat thermal energy storage (LHTES) consists of three individual phase-change materials (PCM) units connected in series as shown in Fig. 16.8.

A gravity-assisted heat pipe is buried inside the PCM unit (Fig. 16.9) to increase the heat-transfer rate by decreasing thermal resistance between the heat-transfer

Fig. 16.8 Cascade of latent heat thermal-energy storage systems
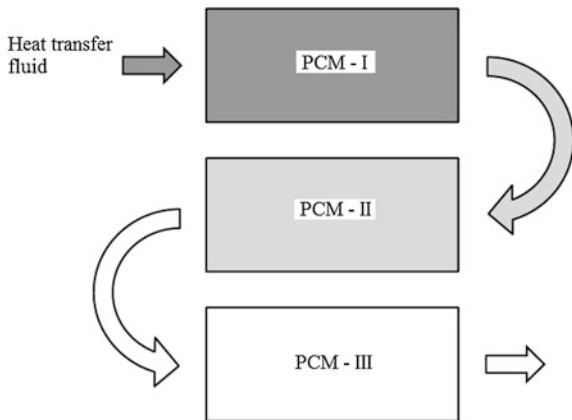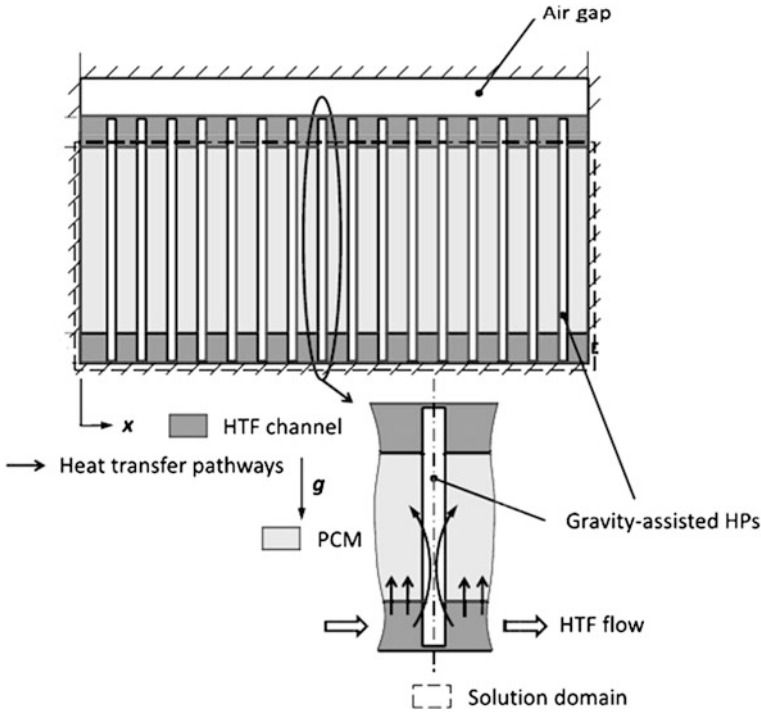
Fig. 16.9 Charging of PCM unit

fluids (HTF) and the PCM. The gravity-assisted heat pipe serves as a wick to maintain uniform distribution on the interiors walls of the heat pipe. Furthermore, the condensate returns to the evaporator section due to gravitational force. The thermal energy available from the solar concentrators is allowed to pass through the HTF during charging. The flow direction of the transfer of thermal energy through PCM and gravity-assisted heat pipe during charging.

The thermal properties of some PCM materials used for power generation are given in Table 16.1 [2].

There are three stages during the charging of a PCM as follows:

- less-than-melting temperature;
- melting temperature; and
- completely molten.

The above-mentioned stages depend on the size of the solar concentrator and the time of charging. The operating temperature of LHTES can vary between 280 and 390 °C. This corresponds to the working-fluid temperature in a parabolic-trough solar power plant.

Table 16.1 Properties of some PCM materials

S. no.	PCM composition (wt%)	Melting point (°C)	Heat of fusion (kJ/kg)	Thermal conductivity (W/mK)	Density (kg/m^3)	Specific heat (kJ/kg K)
1	NaOH(73.3)–NaCl (26.7)	370	370	0.79	1960	1850
2	KCl(22.9)–MnCl$_2$ (60.6)–NaCl(16.5)	350	215	0.95	2250	960
3	NaOH(65.2)–NaCl (20)–Na$_2$CO$_3$(14.8)	318	290	1.0	2000	1850
4	MgCl$_2$·6H$_2$O	115–117	165–169	0.57–0.70	1450–1570	NA
5	Mg(NO$_3$)·H$_2$O	89–90	162–167	0.49	1550–1636	NA

The exergy of charging PCM material is expressed as

$$Ex_{c,in} = \dot{m}_{fc}C_f \int_0^{t_c} \left[T_{c,in} - T_a - (T_a + 273) \ln \frac{T_{c,in} + 273}{T_a + 273} \right] dt$$

Or

$$Ex_{c,in} = \dot{m}_{fc}C_f \left[T_{c,in} - T_a - (T_a + 273) \ln \frac{T_{c,in} + 273}{T_a + 273} \right] t_c \qquad (16.9)$$

It is important to note that $T_{c,in}$ is the inlet temperature of the HTF, which is equal to the temperature of the fluid coming from the parabolic-trough solar concentrator, Eq. (6.25). The $\dot{m}_{fc}$ and C_f are the mass-flow rate and specific heat of the working fluid, respectively; and T_a is the environment air temperature.

The flow direction of the transfer of thermal energy through the PCM and the gravity-assisted heat pipe during discharging is shown in Fig. 16.10. Furthermore, it is to be noted that charging and discharging should not be performed simultaneously. Hence, charging is only performed during sunshine hours, and discharging is performed at the time of power requirement; hence, this case shows the storage effect in a power-generating system unlike in the case of conventional power production.

The exergy of discharging PCM material is expressed as follows:

$$Ex_{d,in} = \dot{m}_{fd}C_f \int_0^{t_d} \left[T_{d,out} - T_{d,in} - (T_a + 273) \ln \frac{T_{c,in} + 273}{T_{d,in} + 273} \right] dt$$

or

$$Ex_{d,in} = \dot{m}_{fd}C_f \left[T_{d,out} - T_{d,in} - (T_a + 273) \ln \frac{T_{c,in} + 273}{T_{d,in} + 273} \right] t_d \qquad (16.10)$$
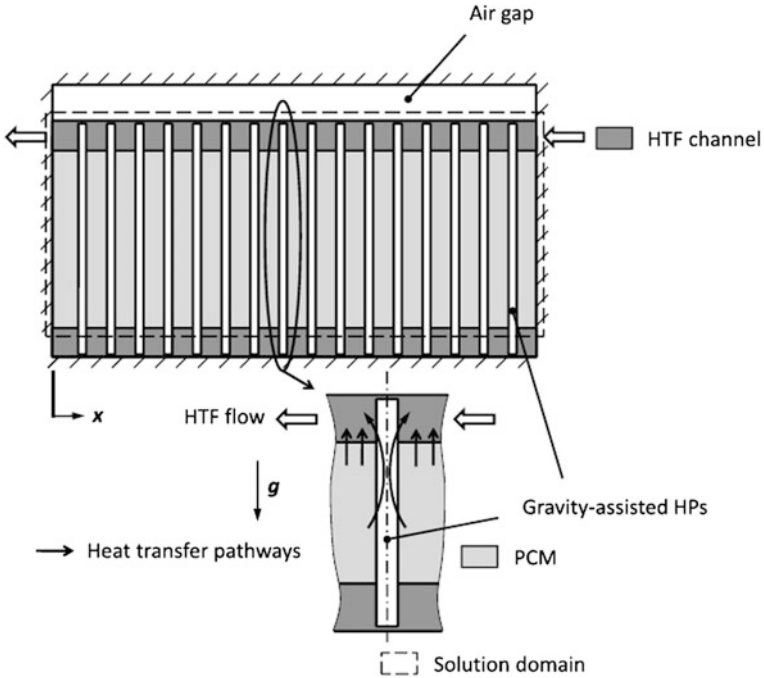
Fig. 16.10 Discharging of PCM unit

Here, $T_{d,out}$ and $T_{d,in}$ are the outlet and inlet temperatures, respectively, of the HTF during discharge; and $\dot{m}_{fd}$ is the mass-flow rate of the working fluid during discharging.

An exergy efficiency of LHTES is defined as the ratio of exergy recovered by the heat-transfer fluid during discharging in time, t_d, to the total exergy of the heat-transfer fluid at the inlet to the LHTES system in time, t_c, which is expressed as

$$\varepsilon = \frac{Ex_{d,in}}{Ex_{c,in}} \qquad (16.11)$$

It has been observed that cascaded (series-connected) LHTES units recover maximum energy during charging and discharging in a 24-h cycle.

Objective Questions

16.1   If solar cells are connected in series for a PV module, the electrical efficiency
       of the PV module is
       (a) greater than that of a solar cell
       (b) less than that of a solar cell
       (c) equal to that of a solar cell
       (d) none of these
       Answer: (b)

16.2   The electrical efficiency of a PV arrays is
       (a) greater than that of a PV module
       (b) less than that of a PV module
       (c) equal to that of a PV module
       (d) none of these
       Answer: (b)
16.3   In concentrated solar power, only the following is used:
       (a) total solar radiation   (b) beam radiation   (c) direct radiation   (d) all
       of these
       Answer: (b) and (c)
16.5   An overall instantaneous thermal efficiency of a solar receiver-to-work (η_i) is
       (a) less than that of a solar receiver $(\eta_{i,th})$
       (b) higher than that of a solar receiver $(\eta_{i,th})$
       (c) equal to that of a solar receiver $(\eta_{i,th})$
       (d) none of these
       Answer: (a)
16.6   An overall instantaneous thermal efficiency of a solar receiver-to-work (η_i)
       for a lower value of C
       (a) increases with the solar-receiver temperature (T_r)
       (b) decreases with the solar-receiver temperature (T_r)
       (c) first increases and then decreases with the solar-receiver temperature (T_r)
       (d) is not affected by the solar-receiver temperature (T_r)
       Answer: (c)
16.7   An overall instantaneous thermal efficiency of a solar receiver-to-work (η_i)
       for a higher value of C
       (a) increases with the solar-receiver temperature (T_r)
       (b) decreases with the solar-receiver temperature (T_r)
       (c) first increases and then decreases with the solar-receiver temperature (T_r)
       (d) has no effect with the solar-receiver temperature (T_r)
       Answer: (a)
16.8   For solar-power generation, the melting point of PCM material is generally
       most suitable at
       (a) >300 °C   (b) <200 °C   (c) equal to 300 °C   (d) all of these
       Answer: (a) and (c)

Problems

16.1   Plot the curve between an instantaneous thermal efficiency of a solar receiver
       $(\eta_{i,th})$ and a receiver temperature (T_r) for a different concentration ratio (C).
       Hint: Use Eq. (16.7) for the data of Fig. 16.7.
16.2   Plot the curve between an instantaneous thermal efficiency of a solar receiver
       $(\eta_{i,th})$ and concentration ratio (C) for a different receiver temperature (T_r).
       Hint: Use Eq. (16.7) for the data of Fig. 16.7.

16.3   Plot the curve between an overall instantaneous thermal efficiency of a solar receiver to work (η_i) and a concentration ratio (C) for a different receiver temperature (T_r).

Hint: Use Eq. (16.8) for the data of Fig. 16.7 and Example 16.2.

References

1. H. Shabgard, C.W. Robak, T.L. Bergman, A. Faghri, Sol. Energy **86**(3), 816 (2012)
2. S.D. Sharma, K. Sagara, Int. J. Green Energy **2**, 1 (2005)

Additional References

3. D.A. Baharoon, H.A. Rahman, W.Z.W. Omar, S.O. Fadhl, Renew. Sustain. Energy Rev. **41**, 996 (2014)
4. O. Behar, A. Khellaf, K. Mohammedi, Renew. Sustain. Energy Rev. **23**, 12 (2013)

Chapter 17
Other Applications of Solar Energy

Abstract Low-temperature operating solar passive and active devices, namely, solar cookers, greenhouses, swimming pool heating, solar ponds, and biogas plants, etc., have been an important topic from the point of view of energy savings, a clean environment, and climate change.

17.1 Introduction

The Sun is the primary source of energy for all living organisms on Earth. Solar radiation comes from the Sun.

As discussed in earlier chapters, solar radiation is considered as follows:

(i) **A wave (electromagnetic radiation)**: This is used for many applications such as day lighting, water/air heating, crop drying, solar houses, solar cooling, solar distillation, etc. Solar energy reaches the Earth with a spectrum of wavelengths ranging from approximately 0.3 to 3 μm.

(ii) **A photon**: The energy association with a *quantum* of light (**photon**) is hv. The h is the Planck's constant, and v is the frequency of the light. The energy per photon is 1.7 eV. It is used to generate electricity through solar cells (Chap. 4).

17.2 Fossil Fuel [1]

In addition to producing electricity, photons are also directly used for photosynthesis, which refers to a chemical reaction occurring in green plants in the form of chemical energy. "Photo" means "light," and "synthesis" means "making." In the

photosynthesis process, solar energy is absorbed by green plants, which sythesize organic compounds from low-energy carbon dioxide (CO_2) and water (H_2O). This same photosynthesis process converted solar energy into living organisms millions of years ago to create **fossil fuels**.

Photons in the visible portion of the spectrum have sufficient energy to ionize atoms of H_2O into hydrogen and oxygen during sunshine hours. This is generally referred to as a "**light reaction**." Hence, green plants discharges oxygen during day, which is required by humans.

Hydrogen ions combine with CO_2 in the atmosphere, which is released by humans, to form hydrocarbon during off-sunshine hours. This is also known as a "**dark reaction**." The overall photosynthetic process is shown in the following equations:

$$CO_2 + 2H_2O \xrightarrow{\text{light}} CH_2O + H_2O + CO_2 + O_2 \tag{17.1}$$
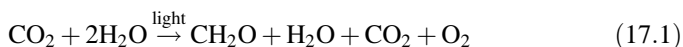
In the above equation, the light energy required to produce one mole (30 g) of CH_2O is 112 kcal.

Solar energy also contains vitamin D, which is basic need of humans. Hence, people are advised to be exposed directly to the Sun during early morning hours to absorb vitamin D. Living organisms also utilizes light energy indirectly. Sunlight energy is converted into usable chemical energy for the origin of biomass through a photosynthetic process. Humans depend on the chemical energy (food) formed by the plants (biomass) during the photosynthesis process. Human beings eat the food produced. The human body oxidizes or burns the carbohydrates with oxygen from the air and releases carbon dioxide. One of the carbohydrates resulting from photosynthesis is cellulose. The burning of wood results in the decomposition of cellulose into water and carbon dioxide, which is similar to the oxidation process of food in the human body. In this process, the stored energy is released as heat. Therefore, biomass is also referred to as "biofuel."

The amount of biomass that can be grown certainly depends on the availability of sunlight to drive the conversion of CO_2 and H_2O into carbohydrates (CH_2O), Eq. (17.1). Let us examine the overall conversion efficiency from sunlight to biomass. The average solar energy per unit of horizontal area per unit of time in the extraterrestrial region is approximately 0.5 cal/min cm^2 (Example 17.1). For the purposes of evaluating plant production, it is easier to determine the number of calories in a day per square centimeter. Of the available solar energy available for biomass production, 47 % comes from photosynthesis in the terrestrial region. Thus, the energy available for food production (biomass) is

$$= 0.5 \frac{\text{cal}}{\text{min cm}^2} \times (0.47) \times \frac{60 \text{ min}}{1 \text{ h}} \times \frac{24 \text{ h}}{1 \text{ day}} = 338 \frac{\text{cal}}{\text{cm}^2 \text{ day}} \left(1420 \text{ J/cm}^2 \text{ day}\right)$$

$$\tag{17.2}$$

The overall conversion efficiency of photosynthesis is as follows:

(i) Plants use visible light (0.4–0.7 µm), i.e., 50 % of the solar spectrum (Example 1.1).
(ii) Chloroplasts absorb 80 % of visible light.
(iii) The theoretical photon-to-glucose efficiency for the absorption process is 35 % (8 hf for each CO_2).
(iv) Dark respiration (metabolism) uses 50 % of visible light; therefore, 50 % remains.

Taking all of these factors into account,

$$\text{overall efficiency} = 0.5 \times 0.8 \times 0.35 \times 0.5 \times 100 = 7 \% \qquad (17.3)$$

The amount of energy stored per carbohydrate unit synthesized is approximately 5 eV.

Example 17.1 Evaluate the average solar energy available in the extraterrestrial region per unit area and time (cal/min cm^2).

Solution
The value of the solar constant in the extraterrestrial region is 1367 W/m^2 (Chap. 1).
Hence, the energy associated with the solar constant per minute

$$= 1367 \frac{W \times 60\,s}{m^2 \times 60\,s} = 1367 \times 60 \frac{J}{m^2\,min}$$

$$= 1367 \times 60 \frac{J}{m^2\,min} \times \frac{1\,cal}{4.187\,J} \times \frac{1\,m^2}{10^4\,cm^2} = 1.96 \frac{cal}{min\,cm^2} \approx 2 \frac{cal}{min\,cm^2}$$

Here 1 cal = 4.187 J and 1 $m^2 = 10^4$ cm^2.
The Earth appears to be a disk with surface area of πr_e^2 with a total surface area of $4\pi r_e^2$.
The average solar energy per unit area per minute

$$= \frac{2\frac{cal}{min\,cm^2} \times \pi r_e^2}{4\pi r_e^2} = 0.5 \frac{cal}{min\,cm^2}$$

Example 17.2 Evaluate the energy associated with photons having a wavelength λ of 700 nm (0.7 µm) (red end of the visible solar spectrum).

Solution

The energy associated with one photon (E) is given by

$$E = h\nu$$
$$= \frac{hc}{\lambda}, \text{ where } c \text{ is the velocity of light.}$$

For the value of Plank's constant $(h) = 6.63 \times 10^{-34}$ J s and $c = 3 \times 10^8$ m/s, we have

$$E = \frac{6.63 \times 10^{-34} \text{ J s} \times 3 \times 10^8 \text{ m/s}}{700 \times 10^{-9} \text{ m}}$$
$$= 2.84 \times 10^{-19} \text{ J}$$

The value of E in terms of eV is given by

$$E = \frac{2.84 \times 10^{-19} \text{ J}}{1.60 \times 10^{-19} \text{ J/eV}} = 1.7 \text{ eV} \left(1 \text{ eV} = 1.6 \times 10^{-19} \text{ J}\right)$$

17.3 Box-Type Solar Cooker

A schematic view of box-type solar cooker is shown in Fig. 17.1. It is suitable for a nonpressure boiling type of cooking. The maximum cooking temperature is approximately 100 °C. It consists of double-walled insulated rectangular box with double-glazing at the top to reduce heat loss from the exposed surface. The inner area of the box may be 0.36 m². The body is made of lightweight fiber-reinforced plastic (FRP) material. There is a reflector on one side with the same effective area to reflect more solar radiation toward the cooking vessel. The cooking period is generally between 11 am and 2 p m under clear-sky conditions throughout the year.

Fig. 17.1 Box-type solar cooker (from Tiwari and Mishra [1])

The components of a solar cooker are as follows:

(1) double-glass lid; (2) aluminium cooking pot; (3) inner tray made of an aluminium sheet; (4) outer box of teakwood with glass wool insulation and (5) a booster mirror.

Working Principle
As shown in Fig. 17.1, the double-glazed surface of the solar cooker receives incident $[I(t)]$ and reflected $[\rho I(t)]$ solar radiation. The resultant incident radiation $[I_T(t)]$ can be given as the sum of the two. The total solar radiation is transmitted inside the solar cooker and is absorbed by the blackened cooking pot and inside surfaces. The absorbed solar radiation inside the solar cooker is transferred by convection to the inside cooking pot to heat the water to cook the food. During the cooking time, there is an overall heat loss through the top, side, and bottom of the solar cooker. The quantity of heat required for the physical/chemical changes involved in cooking are small compared with the sensible heat of the increasing water/food temperature.

Thermal Analysis
In a solar cooker, the initial operation is transient before attaining a stagnation temperature of 100 °C. Hence, quasi–steady state thermal modeling is performed.

To simplify the thermal analysis of the solar-cooker system, the overall energy balance is written with following assumptions:

- There is no stratification in the water column.
- The bottom of the cooking pot is in contact with the inner surface of the cooker.
- The physical properties of the cooking material and the water are the same.

The energy balance of solar cooker can be written as

$$(MC)_w \frac{dT_w}{dt} = F'A_p[(\alpha\tau)I_T(t) - U_L(T_w - T_a)] \qquad (17.4)$$

where F' is the solar-cooker efficiency factor, which is considered to be 0.85.
The above equation can be rearranged as follows

$$\frac{dT_w}{[(\alpha\tau)I_T(t) - U_L(T_w - T_a)]} = \frac{F'A_p}{(MC)_w} dt$$

After integration of the above equation with the initial conditions of $t = 0$, $T_w = T_{w0}$ one obtains

$$e^{-t/t_0} = \frac{(\alpha\tau) - \frac{U_L(T_w - T_a)}{I_T(t)}}{(\alpha\tau) - \frac{U_L(T_{w0} - T_a)}{I_T(t)}} \qquad (17.5)$$

where t_0 is the time constant and is given by $t_0 = \frac{(MC)_w}{F'A_p U_L}$.

The above equation can also be written as

$$t = -t_0 \ \ln \left[\frac{(\alpha\tau) - \frac{U_{\mathrm{L}}(T_{\mathrm{w}} - T_{\mathrm{a}})}{I_{\mathrm{T}}(t)}}{(\alpha\tau) - \frac{U_L(T_{\mathrm{w0}} - T_{\mathrm{a}})}{I_{\mathrm{T}}(t)}} \right] \tag{17.6}$$

Example 17.3 Calculate the time taken for the water at 40 °C to boil in a solar cooker with the following given specifications:

$(\alpha\tau) = 0.7;\ F' = 0.85;\ U_{\mathrm{L}} = 6\ \mathrm{W/m^2\ °C};\ A_{\mathrm{p}} = 0.36\ \mathrm{m^2}(\mathrm{MC})_{\mathrm{w}} = 4 \times 4190\ \mathrm{J/°C};\ T_a = 15\ °\mathrm{C};$

$T_{\mathrm{w0}} = 40\ °\mathrm{C};\ T_{\mathrm{w}} = 100\ °\mathrm{C};\ I_{\mathrm{T}}(\mathrm{with + without\ reflector}) = (400 + 600) = 1000\ \mathrm{W/m^2}$

Solution
Here

$$t_0 = \frac{(\mathrm{MC})_{\mathrm{w}}}{F'A_{\mathrm{p}}U_{\mathrm{L}}} = 9129\ \mathrm{s}$$

$$t = -9129 \times \ln \left[\frac{0.7 - \frac{6 \times (100 - 15)}{1000}}{0.7 - \frac{6 \times (40 - 15)}{1000}} \right] = 9676.7\ \mathrm{s} = 161\ \mathrm{min}$$

17.4   Swimming Pool Heating

Solar energy can also be used for heating either an open or indoor swimming pool at a low temperature. The heating may be either passive or active.

17.4.1   Passive Heating

In this case, a transparent floatable plastic cover is used over the water surface in the swimming pool during peak sunshine hours. The incoming solar radiation is transmitted through the plastic cover on the water surface and is then attenuated through the water column and finally absorbed by the blackened bottom surface. Most of the absorbed solar radiation is transferred by convection to the water in the pool, and the remaining is lost to the ground. The loss can be minimized by using a layer of insulating material beneath the bottom surface. Finally, the water of the swimming pool gets heated and moves upward due to its low density. To minimize these losses at night, the top pool surface is covered with waterproof insulating

material. To use the swimming pool, the transparent cover sheet is removed. By passive heating, the temperature of the swimming pool is raised marginally.

17.4.2 *Active Heating of a Swimming Pool [3]*

For increasing the temperature of the swimming pool, additional thermal energy from another heating source, say flat-plate collectors, should be integrated with the basin of the swimming pool. The integration of a collector system can performed by connecting a panel of collectors to the pool either directly or through a heat exchanger depending on the climatic conditions. The area of the collectors depends on the capacity of the pool. Such heating is desirable for indoor swimming pools in harsh climatic conditions.

An indoor swimming pool has following advantages:

- It is protected from dust, birds, the climate etc.
- It is an integral part of the building.
- It is easy to clean.
- It has a lower maintenance cost.
- It can be used in extreme cold climatic conditions.

Active swimming pool heating, as shown in Fig. 17.2, has mainly three components as follows:

(a) Flat-plate collectors;
(b) A fluid circulation system between the FPC and the swimming pool; and
(c) A control system integrated with the panel of collectors and the pool water.

The cost of an active indoor swimming pool system depends on the type of flat-plate collectors used, which can include the following:

(i) Unglazed flat-plate collectors (small temperature range) including

    (a) plastic panels;
    (b) strip collectors;
    (c) plastic pipe collectors; and
    (d) permanent collectors.

(ii) Glazed collectors (large temperature range) including

    (a) boxed collectors; and
    (b) an integrated collector, i.e., an integral part of the roof of a building.

Unglazed and glazed flat-plate collectors are preferred for heating outdoor and indoor swimming pools. Unglazed flat-plate collectors are more cost-effective than any conventional flat-plate collector system.
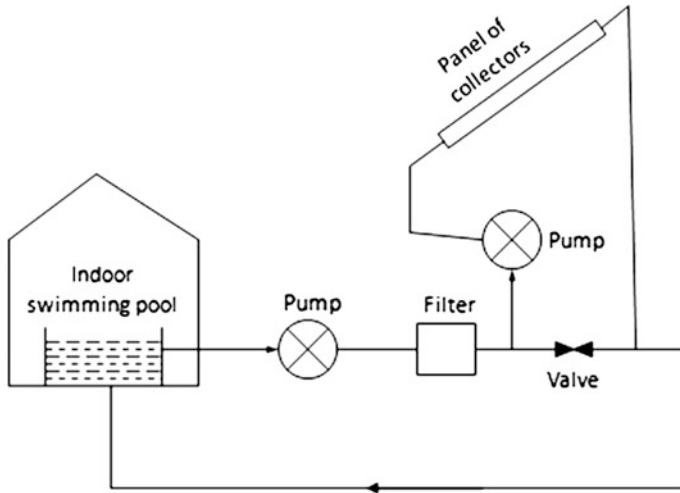
Fig. 17.2 Schematic diagram of an active indoor swimming pool (from Tiwari and Mishra [1])

17.5   Solar Heating of Biogas Plant [4]

Solar heating of biogas plants have gained importance for use in cold climatic conditions in rural areas. The optimum temperature for biogas production is approximately 37 °C, which can be achieved by using solar thermal collectors. An abundance of animal dung is a favorable factor for the production of biogas in rural areas. The biogas plant supplies biogas for cooking, lighting, and other small-scale industrial applications. The byproduct of a biogas plant (manure) serves as a good quality of fertilizer for organic farming resulting in increased production.

Biogas consists of 70 % methane (CH_4) and 30 % carbon dioxide (CO_2). It has a calorific value of 20 MJ/m^3. Biogas is produced from the slurry (50 % water + 50 % dung) by anaerobic fermentation.

The quantity of gas produce from a biogas plant depends on the type of dung (Table 17.1) and type of biogas plant (Table 17.2). After feeding the slurry into the digester of a biogas plant, the optimum temperature is achieved after a certain number of days for the maximum production of biogas. This is referred to as the "retention period." The retention period depend on the type of dung and the operating temperature. The retention period can be reduced by heating the slurry to the optimum temperature.

Solar heating is performed as follows:

Passive Mode
This is performed by erection of a greenhouse over the dome as shown Fig. 17.3. The slurry (50 % water + 50 % dung) reaches the digester from the inlet and is heated through the greenhouse effect. Biogas is produced through a biochemical

Table 17.1 Potential biogas gas production from different manure (from Tiwari and Mishra, [1])

Type of feedstock (dung)	Gas yield/kg (m^3)	Normal manure availability/animal/day	Gas yield/day (m^3)
Buffalo	0.036	15.00	0.54
Cattle	0.036	10.00	0.36
Chicken	0.062	0.18	0.01
Human (adult)	0.070	0.40	0.028
Pig	0.078	2.25	0.18

Table 17.2 Important comparison of biogas plants (from Tiwari and Mishra, [1])

Floating gas holder type	Fixed-dome type
Constant pressure	Variable pressure
High maintenance cost	Low maintenance cost
High initial cost	Low initial cost
Low temperature in winter	High temperature in winter
Life span is short	Life span is long
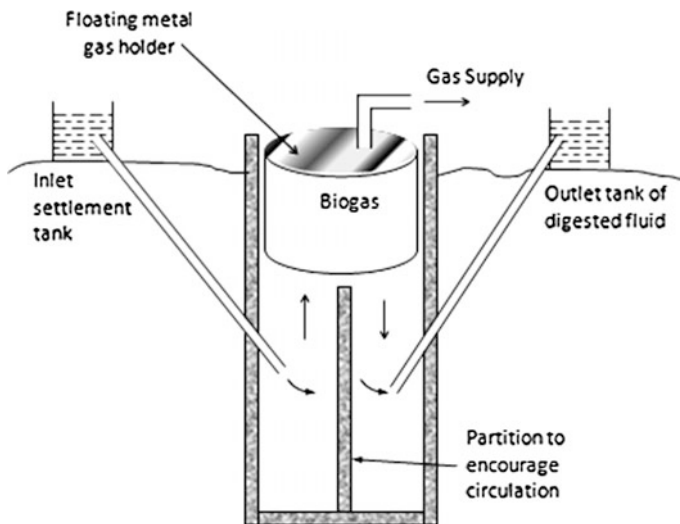
Fig. 17.3 Floating-type greenhouse-heating biogas plant (from Tiwari and Mishra [1])

process, and it comes out through the pipe provided for gas supply. The digested fluid comes out to the outlet. A partition is provided in the digester to encourage proper circulation. The floating gas holder provided at the top of the digester helps keep the pressure constant. It rises when the pressure is increased.

17.5.1   Active Mode

This is performed by integrating flat-plate collectors with a digester through a heat exchanger as shown in Fig. 17.4.

In this case, the dome is fixed inside the ground. With an increase of biogas production, the pressure inside digester increases. The process is identical to the floating dome–type except that the pressure in the digester varies.

Thermal active heating is the same as discussed for swimming pool heating in Sect. 17.4.2.

The heating mode also depends on the climatic conditions (Chap. 1) including ambient air temperature. For higher thermal heating, the active mode is most preferable. The slurry in the digester in active mode is heated through the heat exchanger.

Biogas is produced at optimum temperature, say, approximately 37 °C, by the decomposition of decaying biomass and animal wastes in presence of fungi and anaerobic bacteria under dark conditions (i.e., no oxygen). Aerobic bacteria flourish in the presence of oxygen. Dark reactions, in the presence of anaerobic bacteria (microorganisms) are called "fermentations." The term "digestion" is also often used with anaerobic conditions, which leads to methane. The use of biogas is less hazardous to human health than the input material. Biogas is used for both small- as well as large-scale operations; it can also be attractive for an integrated farming system.

The general equation for anaerobic digestion can be written as

$$(C_6H_{10}O_5)_n + nH_2O \rightarrow 3nCO_2 + 3nCH_4 \tag{17.7}$$
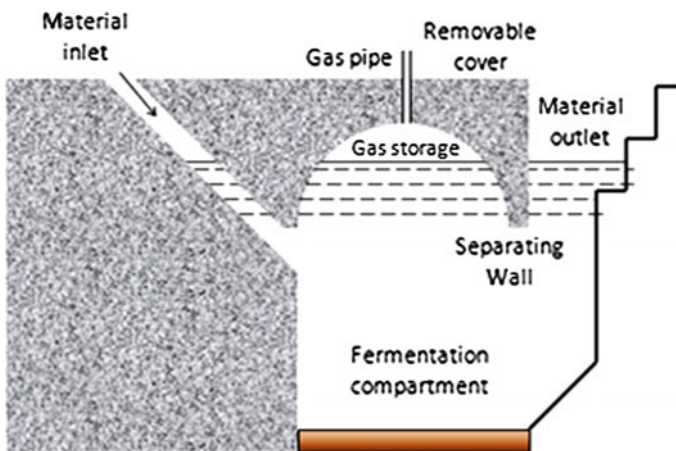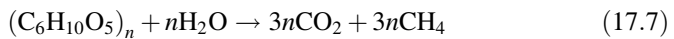
Fig. 17.4 Fixed dome-type active heating of a biogas plant (from Tiwari and Mishra [1])

17.5.2   Design Digester

The thermal energy available (E) from a biogas digester can be written as

$$E = \eta H_b V_b \tag{17.8}$$

where η is the combustion efficiency of the burners/boilers (approximately 60 %); H_b is the heat of combustion per unit volume of biogas; and V_b the volume of the biogas produced.

Equation (17.8) can be further written as

$$E = \eta H_m f_m V_b \tag{17.9}$$

where H_m is the heat of methane combustion; and f_m is the fraction of methane in the biogas.

The volume of biogas (V_b) is given by

$$V_b = C M_0 \tag{17.10}$$

where C and M_0 are the biogas yield per unit dry mass and the mass of dry input, respectively.

The volume of fluid (V_f) in the digester is given by

$$V_f = m_0 / \rho_m \tag{17.11}$$

where ρ_m is the density of dry matter in the fluid.

The volume of the digester (V_d) is given by

$$V_d = \dot{V}_f t_r \tag{17.12}$$

where $\dot{V}_f$ and t_r are the flow rate of the slurry and the retention time in the digester, respectively.

Example 17.4 Evaluate the volume of a biogas digester and the power suitable for the manure output of six cows for the following parameters:

Retention time (t_r) $= 14$ days; operating temperature $= 30\,^{\circ}$C; dry matter consumed (m_0) $= 2.5$ kg day^{-1}; biogas yield $= 0.24$ m^3 kg^{-1} per cow; burner efficiency $= 0.6$; methane proportion $= 0.7$; and density of dry matter $= 50$ kg/m^3.

Solution

Known: m_0 for six cows $= (2.5$ kg day$^{-1})(6) = 15$ kg day^{-1}.

From Eq. (17.11), one gets, fluid volume (V_f) $= m_0/\rho_m = 15$ kg day$^{-1}/$ 50 kg/m$^3 = 0.3$ m^3 day^{-1}.

From Eq. (17.12), one obtains, digester volume, $V_d = \dot{V}_f t_r = 0.3 \times 14 = 4.2$ m^3.

From Eq. (17.10), we have, $V_b = 0.24 \times 15 = 3.6$ m^3.

Equation (17.9) gives $E = 0.6 \times 28 \times 0.7 \times 3.6 = 42.336$ MJ day^{-1} = 11.57 kWh day^{-1}.

17.6 Greenhouse [5]

A greenhouse is also known as "glass house." It works on the principle of the greenhouse effect and is generally made of an ultraviolent (UV)-resistant plastic cover. This is available in various shapes and sizes depending on the climatic conditions at the location of the greenhouse. There are many application of greenhouse including the following:

- Crop cultivation.
  For cultivation inside the greenhouse, four parameters are to be monitored on a regular basis including the amount of CO_2, the temperature, the relative humidity and the inside solar lighting. In addition to these four parameters, root media plays an important role. This depends on type of crop to be grown. Here, it is important to note that high relative humidity (say, approximately 80 %) plays a significant role for maximum plant survival unlike humans. A well-designed greenhouse always maintains the inside environment to be favorable for healthy plant growth.
- Drying of crops/vegetables/fruits
  In this case, two parameters (temperature and relative humidity) are to be maintained for a particular crop/vegetable/fruit. In solar drying, the relative humidity should be maintained as low as possible for maximum respiration unlike for crop cultivation.
- Sun bath/storage in solarium
  In this case, temperature is important.

17.6.1 Working Principle of a Greenhouse

A schematic view of an evenly shaped greenhouse is shown in Fig. 17.5. It has an east–west orientation. It has centrally raised roof with a door on the north side. The support structure can be bamboo/galvanized pipe with a covering of a single layer of UV-stabilized polyethylene sheet. For heating, it has maximum transmissivity, and for cooling it has a low value. Inside the greenhouse, plants can be grown either in pots or fields.
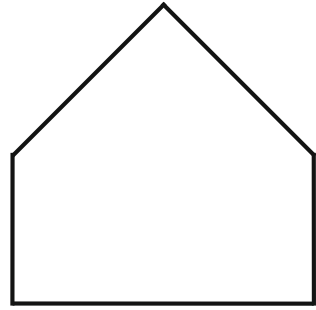
The incident solar radiation on a UV-stabilized polyethylene cover in a greenhouse is the first radiation transmitted inside the greenhouse. A part of the solar radiation is absorbed by the plant as well as the floor after reflection. The reflected solar radiation from the plant and floor is further transmitted through the UV-stabilized polyethylene cover into the atmosphere. The energy absorbed by the plant and floor is transferred to the enclosed air by convection, and hence the room air is heated. In case of overheating of the enclosed air, different cooling arrangements are adopted to achieve a favorable temperature inside the greenhouse. The loss/gain of thermal energy from the enclosure room air to the ambient air depends on the temperature difference between the two.

There are different cooling and heating methods are as follows.

17.6.2 Different Cooling Methods

(a) **Natural convection through roof vents**

A roof vent is a passive method to transfer a thermal energy trap inside a greenhouse to the outside environment. The area and number of roof vents depends on size and volume of the greenhouse. The rate of transfer of thermal energy from inside the greenhouse to the outside environment depends on the pressure difference created between the inside of the greenhouse and the outside environment. The uneven-shaped greenhouse has such a roof vent at the top across its length as shown in Fig. 17.6. The rate of heat loss (W) by natural convection through the roof vent is given by

$$\dot{Q}_{\text{loss}} = C_{\text{d}} A_{\text{v}} \sqrt{\frac{2\Delta P}{\rho}} \Delta P \qquad (17.13)$$

where C_{d} is the coefficient of diffusion; P is the partial pressure $\left(\text{N/m}^2\right)$ at temperature $T(^{\circ}\text{C})$; Eq. (3.48), A_{v}, and ρ are the area of the vent (m^2) and the air density $\left(\text{kg/m}^3\right)$; and $\Delta P = P(T_{\text{r}}) - \gamma P(T_{\text{a}})$.
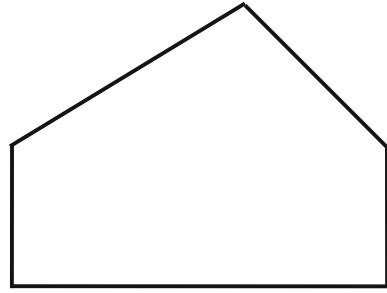
(b) **Forced convection**

This can also be considered a passive method due to the low consumption of
power to operate the fan. The capacity of the fan also depends on the volume
of the greenhouse. The size and number of fans can be calculated for a given
number of air changes (N). The position of fans should be at either the east or
the west side of the greenhouse so that air moves along the length of green-
house. The exhaust fan is usually used when there is insufficient heat transfer
due to natural convection through the roof vent. Incoming solar radiation can
also be reduced by using a movable insulating cover over the greenhouse
during high-sunlight periods. If insulating cover is a white color, it will be
more appropriate. The rate of heat loss by forced convection is given as

$$\dot{Q}_{\text{loss}} = 0.33\ NV(T_{\text{R}} - T_{\text{a}}) \tag{17.14}$$

where N is the number of air changes; V is the volume of greenhouse; and T_{R}
and T_{a} are the room and the ambient air temperatures (°C), respectively.

Example 17.5 Calculate the rpm of fan/power for a given N the same as EAHE.

Solution

If v is the velocity of air inside the EAHE and V is the volume of the room, then the
number of air changes (N) per hour is given as

$$N = \frac{\pi r^2 v \times 3600}{V}$$

The pressure difference and the power required to pump the air through the
Earth–air heat exchanger is given by

$$\Delta P = F\left(\frac{\dot{M}_{\text{a}}}{\rho}\right)\left(\frac{L}{D}\right)^3,$$

where $F = F_0 + \gamma\left(\frac{D}{L}\right)$ (see Problem 9.1)

$$\text{Power} = \dot{m}_a \frac{\Delta P}{\rho}$$

The RPM (N_0) of the fan is expressed as

$$N_0 = \frac{60 \times v}{\pi \times D}$$

(c) **Evaporative cooling**

In this case, a cooling-arrangement pad is fitted opposite a fan side as shown in Fig. 17.7. The cooling pad is made of a wire mesh, wood ash, and aluminium (Al) frame. There is provision of water flow at a constant flow rate with a minimum speed over the cooling pad to cool the air entering the greenhouse. The evaporative-cooling arrangement is used during peak sunshine hours in extreme climatic conditions. If possible, the movable cover should also be used for reducing heat flux during peak hours. The air passing through the cooling pad is cooled and then propagates inside the greenhouse over and along the length of greenhouse by forced convection. Due to the movement of cool air over the plants, the hot air inside the greenhouse is carried away by forced convection. The rate of heat removal by cool water is given by

$$\dot{Q}_{\text{loss}} = 0.33 \, NV(T_R - T_w) \tag{17.15}$$
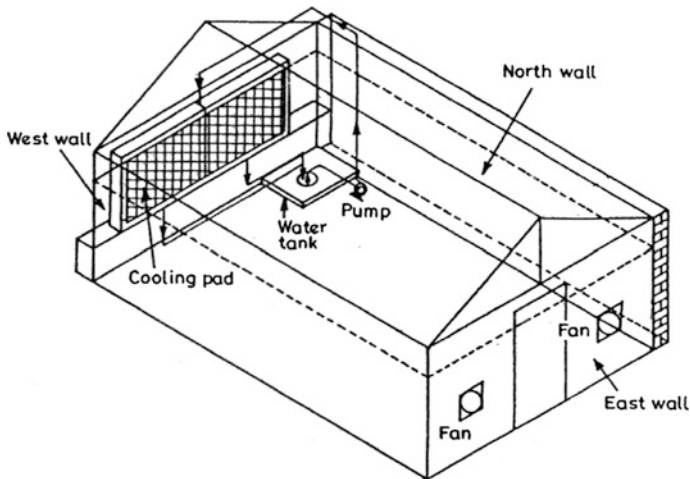
Fig. 17.7 View of evaporative cooling for a greenhouse

where T_w is the water temperature (°C) of the cooling pad. The fan speed should be very low to have maximum contact between the hot ambient airs and the cooled water in the pad.

(d) **Misting arrangement**

A misting arrangement is another way to increase the relative humidity to prevent plants from dying. This can also be referred to as a "cooling arrangement" inside greenhouse. There is a lateral hard plastic pipe along the length of the greenhouse. Water from the storage tank is pumped inside the pipe through a filter by a water pump. The foggier is fitted to the pipe at appropriate places to provide complete fog inside. Both a misting and an evaporative-cooling arrangement are used in extremely hot climatic conditions.

A greenhouse provides an excellent environment to maximize the yield of vegetables, fruits, and flowers.

Example 17.6 Determine an overall heat-transfer coefficient in W/m² °C from the enclosed room air of a greenhouse to the ambient air through a canopy cover with and without movable insulation.

Solution

(a) Without insulation cover

The overall heat-transfer coefficient, U in W/m² °C, is given by

$$U_t = \left[\frac{1}{h_o} + \frac{1}{h_i} \right]^{-1}$$

where h_i is the inside heat-transfer coefficient; the convective and radiative heat transfer coefficient from the top greenhouse cover to the ambient air is given by

$$h_o = 5.7 + 3.8 \, V = 5.7 \, \text{W/m}^2 \, °C \quad \text{for } V = 0 \text{ m/s}$$

thus,

$$U_t = \left[\frac{1}{5.7} + \frac{1}{9.5} \right]^{-1} = 4.0 \, \text{W/m}^2 \, °C$$

(b) With insulation cover

The overall heat-transfer coefficient, U in W/m² °C, is given by

$$U_t = \left[\frac{1}{h_o} + \frac{L_i}{K_i} + \frac{1}{h_i} \right]^{-1}$$

here $L_i = 0.001$ m and $K_i = 0.04$ W/m °C thus, $U_t = \left[\frac{1}{5.7} + \frac{0.001}{0.04} + \frac{1}{9.5}\right]^{-1} = 3.2$ W/m² °C.

However, in this case the transmissivity of cover is reduced significantly to reduce the solar radiation inside the greenhouse.

Example 17.7 Determine the number of air changes per hour (N) for a greenhouse of volume 60 m³ by a fitted exhaust fan (capacity 1440 rpm).

Solution
For the diameter of the fan $(D) = 0.45$ m and its rpm $(N) = 1440$, we have

Velocity of air $(V) = (\pi DN)/60 = 33.92$ m/s
Cross-section area of fan $A = (\pi D^2)/4 = 0.159$ m²
Thus, the volume of air sucked out $= V \times A = 33.92 \times 0.159 = 5.3947$ m³/s
Number of air changes per second $= \frac{5.3947}{60}$ and
Number of air change per hour $= \left(\frac{5.3947}{60}\right) \times 3600 = 324$
For two fans, the number of air changes $= 324 \times 2 = 648$.

(e) **Earth–air heat exchanger (EAHE)**
An Earth–air heat exchanger utilizes the constant ground temperature beneath the Earth surface throughout the year. This constant ground temperature can be used to condition the any living space or the greenhouse in summer or winter. This concept is discussed in Chap. 10 for both heating and cooling purposes.

(f) **Shading effect**
In this case, one must use either an ultraviolent (UV)-resistant plastic cover with low transmittivity or a greenhouse cover made of opaque green flexible material during sunshine hours. The opaque flexible material does not allow solar radiation to pass into the greenhouse, thereby achieving a cooling effect inside the greenhouse.

17.6.3 Different Heating Methods

(a) **Partially underground greenhouse**
Partially underground greenhouses are conditioned by the constant ground temperature beneath the Earth's surface. The inside of the underground greenhouse can be made of a dense natural material that absorbs more heat such as stones mud brick, etc. The glazing from the upper portion and the roof creates the greenhouse effect. Because the greenhouse is partially underground, crops inside the greenhouse are safe from harsh climatic conditions.

(b) **Earth–air heat exchanger**

   The Earth–air heat exchanger can also be used for heating of the living space during the winter season in composite climates. For the cold climatic condition the EAHE are used throughout the year for heating. The use of EAHE eliminates or reduces the load of heating performed by the conventional fuels.

(c) **Ground air collector**

   The ground air collector utilizes thermal energy stored in the ground. The absorptivity and hence the thermal storage of the ground can be increased by making the surface of the ground black. In a ground air collector, there is a glazing above the ground surface. The air in between the ground and the glazing is heated by the solar energy absorbed by the ground. There is a provision to couple the ground air collector with the living space. The main drawback of a ground air collector is the requirement of a large open area for heating of the living space.

(d) **Active heating**

   Active heating involves the use of an active source for heating of the living space. To use solar energy for active heating, it is necessary to use photovoltaic modules for the generation of electricity to circulate hot air inside the living area. In addition, DC power can be converted in AC power by means of a charge controller and an inverter; then this AC power can be used to heat the living space. The use of semitransparent photovoltaic module enables one to use the direct thermal gain, the indirect thermal gain, and the generation of electricity.

17.7   Solar Ponds [2]

(a) **Shallow solar pond** (Sect. 8.8.2): This is pool of fresh stagnant water filled in a rectangular insulated box with glass cover at top to minimize top-heat loss. The box is blackened from the inside to absorb solar radiation. The heat from the bottom to the top is transfer by convection. The hot water is at the top surface. It is used for the short-term storage of thermal energy. In this case only is convection dominant.

(b) **Nonconvective solar pond**: This is a pool of stagnant salty water in a very large pond as shown in Fig. 17.8. In this case, convection from the bottom to the top is suppressed due to the salt gradient. The bottom layer is hot unlike a convective solar pond. It is used for the long-term storage of thermal energy. In this case, heat loss from the top surface is minimized due to the salt-density gradient, i.e., the density increases with depth. In this case, warmer water at the bottom may not acquire low density and rise to the top by convection. It has many applications. The convective pond has lower thermal efficiency due to higher top loss compared with a nonconvective solar pond.
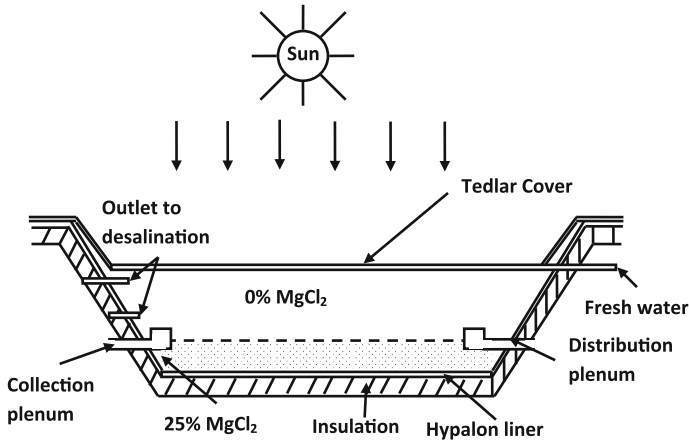
Fig. 17.8 Cross-sectional view of nonconvective solar pond

17.7.1 Stability Criteria for a Nonconvective Solar Pond

Salt is the most expensive component of a nonconvective solar pond. For efficient operation of a nonconvective solar pond, knowledge of the salt-gradient requirement and the technology is required along with maintenance.

In a nonconvective solar pond, the density (ρ) of the fluid is a function of salt concentration, S, and temperature, T. In this case, stability against vertical convection, i.e., the magnitude of the salt-density gradient $\left(\frac{\partial \rho}{\partial S}\right)$ due to the salt-concentration gradient $\left(\frac{\partial S}{\partial x}\right)$, must be greater than the negative-density gradient $\left(\frac{\partial \rho}{\partial T}\right)$ produced by the temperature gradient $\left(\frac{\partial T}{\partial x}\right)$.

If the x-axis is positive along with vertical depth, the equilibrium state of a nonconvective solar pond can be expressed as

$$\frac{\partial \rho}{\partial S} \cdot \frac{\partial S}{\partial x} \geq -\frac{\partial \rho}{\partial T} \cdot \frac{\partial T}{\partial x}$$

or

$$\frac{\partial S}{\partial x} \geq \frac{\alpha_c}{\beta} \frac{\partial T}{\partial x} \tag{17.16}$$

where $\alpha_c = \frac{1}{\rho}\frac{\partial \rho}{\partial T}$ is the thermal-expansion coefficient, and $\beta = \frac{1}{\rho}\frac{\partial \rho}{\partial S}$ is the salt-expansion coefficient.

Equation (17.16) gives the "static stability criterion" as

$$(\Delta S)_{\min} = \frac{\alpha_c \Delta T}{\beta} \qquad (17.17)$$

Equation (17.17) gives an idea of the minimum concentration difference required $(\Delta S)_{\min}$ or the fluid to be stable against vertical convection occurring due to a temperature difference (ΔT) between the two layers.

Basically, there are three methods to accomplish the nonconvecting mode of the solar pond. They are as follows:

(a) salt-stabilized;
(b) partitioned or membrane; and
(c) viscosity stabilized.

Based on past experience, there are not many existing nonconvective ponds, and hence we will discuss only salt-stabilized ponds.

17.7.2   Salt-Stabilized Nonconvective Solar Pond

As shown in Fig. 17.9, a salt-stabilized solar pond consists of a nonconvective fluid contained with an impervious bottom liner. The density gradient (salt solution) is created by superimposing layers of decreasing salinity without disturbing the fluid layers. Brine (salt + water) with different concentrations (S) is prepared in a small evaporation pond. The nonconvective zone is created by pumping batches of brine into the solar pond through a horizontal diffuser. The brine with high concentration is fed at the bottom of a large solar pond. The solar radiation falling on the water surface penetrates the **nonconvective solar pond**. Because solar radiation travels
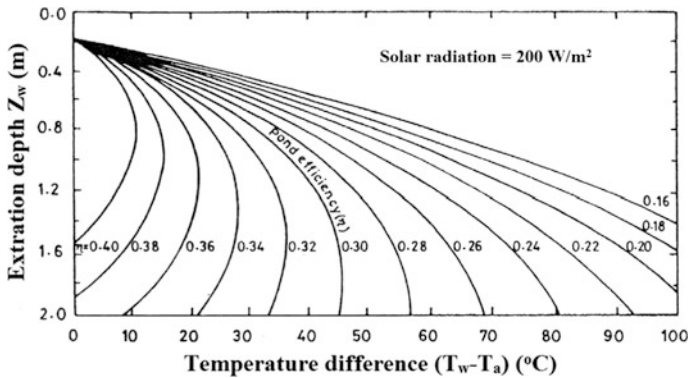
Fig. 17.9 Variation of working temperature increment $(T_w - T_a)$ with an extraction depth Z_w for a range of output thermal efficiencies η

through the layers of different density, it is absorbed, and only a fraction of solar radiation reaches the bottom and is trapped there due to the opaqueness of the water for long-wavelength radiations. The trapped solar radiation at the bottom is not moved toward the top layer due to the relatively poor thermal conductivity of the still water and the stabilizing influence of the gradient. Stored thermal energy at the bottom of the solar pond is withdrawn through a heat exchanger without disturbing the concentration of the various layers. After using the thermal energy, extra thermal energy associated after delivery is again fed to the bottom of the pond.

Figure 17.9 shows the variation of working-temperature increment, $(T_w - T_a)$ with extraction depth Z_w for a range of output thermal efficiencies η.

From Fig. 17.9, one can predict the heat-collection thermal efficiency of an idealized nonconvective solar pond. An instantaneous thermal performance of a solar pond cannot be defined due the excessive thermal mass (storage capacity). It gives an average collection thermal efficiency for an average annual insulation level of 200 W/m^2 for various extraction depths. Figure 17.9 also shows that **the temperature rise of the pond** $(T_w - T_a)$ **should be directly proportional to the insulation level (I)** for average flux intensities other than 200 W/m^2.

A salt-stabilized solar pond also suffers from some drawbacks. A few of them are as follows:

(i)   Salt is expensive.
(ii) The pond suffers from energy-withdrawal problems without a heat exchanger
(iii) Establishing the necessary salt gradient constitutes major operational and maintenance problems.

17.7.3   Applications

- **Space heating**

Thermal-energy extraction through a heat exchanger, as mentioned previously, can be used for providing thermal energy at a reasonable operating temperature of approximately 25 °C by regulating the mass-flow rate of the water. This can be performed for a 24-h cycle due to the large heat-storage capacity.

- **Crop drying**

In this case also, the temperature of a drying chamber can be maintained at a drying temperature (50 °C) by regulating the flow rate in the heating plate placed inside the drying chamber. The drying can also be performed during off-sunshine hours unlike a conventional solar drying system.

- **Greenhouse heating**

Greenhouse heating can be performed on a 24-h cycle to provide constant greenhouse room air temperature with minimum fluctuation inside a greenhouse. This is a required condition for floriculture.

Electricity Generation
Electricity can be generated at a higher temperature by using an organic Rankle cycle converter. A nonconvective solar pond can also be used for salt and mineral production, solar-absorption refrigeration, heating an indoor/outdoor swimming pool, hot-water production, distillation, industrial drying of laundry, and processed food, etc.

Objective Questions

17.1 For cooking food in a solar cooker, the temperature of the water is
       (a) 100 °C   (b) 150 °C   (c) <100 °C   (d) none of these
       Answer: (c)
17.2 The best time period for cooking by a solar cooker under clear-sky conditions is
       (a) 11 am to 1 pm   (b) 9 am to 12 noon   (c) 12 noon to 3 pm
       (d) none of these
       Answer: (a)
17.3 Indoor swimming pool heating is more economical with the use of
       (a) an unglazed plastic collector   (b) a glazed plastic collector
       (b) a convectional metallic collector   (d) none of these
       Answer: (a)
17.4 The optical properties of the atmosphere with respect to short and long wavelength radiation is the same as
       (a) a window glass   (b) a transparent plastic sheet
       (c) a transparent toughened glass   (d) all of these
       Answer: (d)
17.5 The heat transfer during the operation of swimming pool is
       (a) radiation   (b) convection   (c) evaporation   (d) all of these
       Answer: (d)
17.8 There is no stratification in the temperature of swimming pool heating due to
       (a) forced mode   (b) use of pool   (c) heat storage   (d) all
       Answer: (a)
17.9 The solar heating of swimming pool is economical only for
       (a) indoor conditions   (b) outdoor conditions
       (c) both indoor and outdoor conditions   (d) all of these
       Answer: (d)
17.10 The solar heating of a swimming pool is known as
       (a) passive   (b) active   (c) passive/active   (d) all of these
       Answer: (b)
17.11 The optimum temperature range of swimming pool is approximately
       (a) 20 °C   (b) 30 °C   (c) 0 °C   (d) 15 °C
       Answer: (a)

17.12 Slurry used in biogas has the following composition
   (a) 50 % water and 50 % dung   (b) 25 % water and 75 % dung
   (c) 75 % water and 25 % dung   (d) none of these
   Answer: (a)
17.13 Biogas has the following composition of gases
   (a) 70 % CH_4 and 30 % CO_2 (b) 30 % CH_4 and 70 % CO_2
   (c) 50 % CH_4 and 50 % CO_2 (d) none of these
   Answer: (a)
17.14 The optimum temperature for the production of biogas in a digester is
   (a) 15 °C   (b) 37 °C   (c) 50 °C   (d) all of these
   Answer: (b)
17.15 The production of biogas in winter is reduced due to
   (a) a reduction in the temperature of slurry
   (b) an increase in the temperature of slurry
   (c) reduction in the ambient air temperature
   (d) (a) and (c)
   Answer: (d)
17.16 The floating type of biogas plant is more suitable for
   (a) a composite climate   (b) a cold climate
   (c) warm and humid climate   (d) none of these
   Answer: (a)
17.17 The fixed-dome biogas plant is more suitable for
   (a) a warm and humid climate   (b) a cold climate
   (b) a composite climate   (d) none of these
   Answer: (a)
17.18 Biogas production is based on
   (a) a chemical reaction
   (b) a biological reaction
   (c) a thermal reaction
   (d) all of these
   Answer: (d)
17.19 The retention time of biogas production is high in the case of
   (a) winter conditions   (b) summer conditions
   (c) monsoon conditions   (d) none of these
   Answer: (a)
17.20 The heating of slurry can be achieved during winter months by
   (a) erecting a greenhouse over a dome
   (b) heating the slurry by solar collector
   (c) charging the slurry by hot water
   (d) all of these
   Answer: (d)
17.21 The orientation of a greenhouse should be
   (a) east–west   (b) north–south   (c) south only   (d) none of these
   Answer: (b)

17.22   For large-scale greenhouse cultivation in a composite climate, the following
        design of greenhouse is preferred:
        (a) uneven shape   (b) even shape   (c) quonset shape   (d) none of these
        Answer: (c)
17.23   The north wall of a greenhouse oriented east–west doe s the following:
        (a) increases greenhouse room-air temperature
        (b) decreases greenhouse room-air temperature
        (c) has no effect on greenhouse room-air temperature
        (d) none of these
        Answer: (a)
17.24   Greenhouse room-air temperature can be reduced by
        (a) roof ventilation   (b) forced convection
        (c) misting water inside the greenhouse room   (d) all of these
        Answer: (d)
17.25   Greenhouse room-air temperature can be reduced by the use of
        (a) evaporative cooling   (b) movable insulation at night
        (c) a ground air collector (d) a north wall
        Answer: (a)
17.26   Greenhouse room-air temperature can be cooled/heated by
        (a) an Earth–air heat exchanger   (b) movable insulation during day/night
        (c) both (a) and (b)   (d) all of these
        Answer: (c)
17.27   In a nonconvective solar pond, the maximum temperature available is at
        (a) the bottom surface   (b) the top surface   (c) the middle position
        (d) none of these
        Answer: (a)
17.28   The convection heat loss in a nonconvective solar pond is
        (a) increased   (b) decreased   (c) unaffected   (d) none of these
        Answer: (b)
17.29   A nonconvecting solar pond can be used for
        (a) space heating   (b) greenhouse heating
        (c) industrial drying   (d) all of these
        Answer: (d)

Problems

17.1   Evaluate the total time required (t) to boil the water in a solar cooker of mass
       2 and 4 kg for initial temperatures of 40, 60 and 80 °C for the parameters of
       Example 17.3.
       Hint: Consider $T_w = 100$ °C and use Eq. (17.6).
17.2   Evaluate the total time required to boil the water in a solar cooker from 60 °C
       for 6 and 8 kg of water for the parameters of Example 17.3 without using a
       reflector.
       Hint: Consider $T_w = 100$ °C, and use Eq. (17.6) with $I_T = 400$ W/m^2.

17.3 Write down an overall energy balance of active heating of an indoor swimming pool.

Hint: $\dot{Q}_{uN} = M_w C_w \dfrac{dT_w}{dt} + h_1(T_w - T_a)$; h_1 is sum of the radiative, convective, and evaporative heat-transfer coefficients from the water surface to the ambient air, Eq. (3.52). An expression for $\dot{Q}_{uN}$ can be obtained from Chap. 5.

17.4 Evaluate the power available from a biogas digester suitable for the output of one dozen cows for 10 days' retention time for the parameters of Example 17.4.

Hint: See Example 17.4.

17.5 Write down an overall energy balance of active heating of a biogas plant.

Hint: See Problem 17.3 but without evaporation.

17.6 Derive an expression for the temperature of the water in a swimming pool and the slurry in biogas plant of Problems 17.3 and 17.4, respectively.

Hint: See Sect. 17.3.

17.7 Determine the rate of air flow in terms of the number of air changes.

Hint: $\dot{m} = NV/3600$.

References

1. G.N. Tiwari, R.K. Mishra, in *Advanced Renewable Energy Sources* (RSC Publishing, London, 2012)
2. G.N. Tiwari, in *Solar Energy: Fundamental, Design, Modelling and Applications (*Narosa Publishing House, New Delhi and CRC Press, New York, 2004)
3. G.N. Tiwari, S.P. Gupta, S.A. Lawrence, Y.P. Yadav, S.B. Sharma, RERIC Int. Energy J. **10** (1), 7 (1988)
4. G.N. Tiwari, S.K. Singh, L.M. Srivastava, Int. J. Solar Energy **10**, 115 (1991)
5. G.N. Tiwari, *Greenhouse Technology for Controlled Environment* (Narosa Publishing House, New Delhi, also published by Alpha Science, London 2003)

Additional References

6. F. Yettou, B. Azoui, A. Malek, A. Gama, N.L. Panwar, Renew. Sustain. Energy Rev. **37**, 288 (2014)
7. E. Cuce, P.M. Cuce, Appl. Energy **102**, 1399 (2013)
8. G. Zsembinszki, M.M. Farid, L.F. Cabeza, Sol. Energy **86**(1), 567 (2012)
9. T.T. Chow, Y. Bai, K.F. Fong, Z. Lin, Appl. Energy **100**, 309 (2012)
10. G.N. Tiwari, Bikash Sarkar, *Fundamentals of Aquaculture Greenhouse* (Anamaya Publisher, New Delhi, 2007)
11. G.N. Tiwari, *Greenhouse Technology for Controlled Environment* (Narosa Publishing House, New Delhi, also published by Alpha Science, London 2003)
12. G.N. Tiwari, Y.P. Yadav, Energy Convers. Manage. **26**(1), 41 (1986)

Chapter 18
Energy Conservation

Abstract Energy conservation gives an opportunity to human beings to minimally use fossil fuel for the future generation to create a better ecological balance for healthy life on Earth.

18.1 Introduction

The meaning of energy conservation is to reduce the quantity of fossil fuel-based conventional energy used for different applications in human life. Individuals, private parties/governments, and industrial/commercial organizations are the prime users of conventional energy sources. Conservation of such resources reduces the cost of using conventional energy, which leads to economic, political, and environmental sustainability by incorporating the CO_2 credit.

On a national level, energy conservation reduces annual conventional energy consumption; it also reduces energy demand per capita. With conservation, the use of conserved conventional energy can be extended to a need-based requirement from the point of view of energy security, particularly in underdeveloped/developing countries.

Energy saving/conserving is equivalent to producing energy and saving money
In this chapter, we will consider the conservation/saving of energy (conventional/nonrenewable fuel) by using solar energy (renewable energy sources) in different sectors. Energy conservation is also an important tool to minimize climate change due to CO_2 emissions, which are produced during conventional power generation

using fossil fuels. In the present scenario, the reduction of CO_2 emission in the energy sector by using energy-efficient equipment is the most important area of study. Energy conservation is the most economical solution to energy shortages in underdeveloped/developing countries. Energy conservation reduces stables energy cost as well as energy import and eliminates the requirement of new power plants.

Any form of conventional energy may be conserved. Saving fossil fuel-based electrical energy is commonly referred to as "energy conservation," which is the act of using energy in a more efficient and effective manner.

Fossil fuel will be depleted very quickly in the near future without energy conservation. Finally we will have nothing to use for energy and will be forced to live our lives uncomfortably. Furthermore, energy conservation is crucial when it comes to energy security for environmental and climate change for future generations. In the present scenario, frequent erratic climates and climatic changes caution us to conserve energy as much as possible. The importance of energy conservation is clear from the fact that every year December 14th is celebrated as **World Energy Conservation Day**.

Energy conservation can be achieved as follows:

- less use of fossil fuel-based energy;
- use of energy-efficient electronic equipment; and
- development of new renewable energy-based technology.

18.2   Energy Efficiency

Energy efficiency is also simply known as "efficient energy use" in day-to-day activity. It is a goal to provide all kind of products and services using the minimum amount of required energy. Following are some examples to conserve the energy:

Insulating a home
For an air-conditioned room, the inner floor, walls, and roof should be insulated. It requires less heating and cooling by fossil-fuel energy to achieve and maintain thermal comfort.

Compact fluorescent lights (CFL)
These reduce the amount of energy required to maintain the same illumination level compared with conventional incandescent light bulbs. Furthermore, they consume one third of the energy of incandescent lights and last 6–10 times longer.

Natural skylights
In this case, there is no need for any conventional energy for illumination as discussed in Chap. 2. This approach is most suitable for use in building academic institutions. Energy can be saved by installing a smart sensor, which monitors the illuminance level during the day with natural light and switches the artificial light on or off as per the requirement.

Turning off all electronic devices
This is one of the best ways of conserving fossil fuel energy. Replacing or repairing leaky faucets helps to save a lot of water.

Using sensors
The sensor should be used to control the air conditioner with closed doors and vents to keep optimum room comfort level.

In many countries, particularly in underdeveloped and developing countries, the energy efficiency of electronic equipment is also seen to confer a national energy-security benefit. The use of energy-efficient equipments reduces energy import and depletion rate of domestic-energy resources.

According to the International Energy Agency (IEA), improved energy efficiency in buildings, industrial processes, and transportation could reduce the world's energy needs in 2050 by one third, which can help control global emissions of greenhouse gases [1].

From the point of view of energy conservation, the following home appliances should have at least five-star energy rating:

- home electronics (TV, computer, mobile, fans, etc.);
- kitchen appliances;
- laundry appliances;
- refrigeration; and
- space conditioning (air conditioner, geyser, cooler, etc.).

18.3 Solar Fraction [2]

This is a term generally used to refer to the conservation of fossil fuel in different sectors in day-to-day life. For example, the daily auxiliary energy needed in supplementing the supply of hot water at a fixed temperature T_d (required water temperature) is given by

$$\text{Auxiliary energy, } AE_{FPC} = \int_0^{24\,h} \dot{m}_w C_w (T_d - T_w)^+ \, dt \qquad (18.1)$$

where dt is the time interval (generally 1 h); T_w is the water temperature from the flat-plate collector (FPC); $(T_d - T_w)^+$ means $T_d > T_w$ (hence only auxiliary [fossil-fuel] energy is needed; and $T_d < T_w$ means that no auxiliary (fossil-fuel) energy is needed (hence fossil fuel is conserved). The calculations for T_w are made for an average day of each month.

Without a FPC, the daily auxiliary energy needed in supplementing the supply hot water at a fixed temperature T_d (required water temperature) is given by

$$\text{Auxiliary energy, } \text{AE} = \int_0^{24\,\text{h}} \dot{m}_w C_w (T_d - T_{in}) \mathrm{d}t \qquad (18.2)$$

where T_{in} is the inlet-water temperature available from the main supply.

The solar fraction (f), which can be used to optimize the area of the FPC for a given fixed temperature requirement, is defined as follows

$$f = 1 - \frac{\int_0^{12\,\text{month}} \text{AE}_{FPC} n_d}{\int_0^{12\,\text{month}} \text{AE} n_d} \qquad (18.3)$$

where n_d is the number of days in a particular month for a hot water requirement.

Equation (18.3) can be discussed as follows:

Case (i): For $T_d < T_w$, i.e., the desired temperature is less than the outlet temperature from the FPC i.e., $(T_d - T_w)^+$ is negative; hence from Eq. (18.1) we have

$$\text{Auxiliary energy, } \text{AE}_{FPC} = 0$$

Then from Eq. (18.3), one gets $f = 1$, i.e., no auxiliary (fossil-fuel) heating is required.

Case (ii): For $T_d > T_w$, i.e., the desired temperature is more than the outlet temperature from the FPC, i.e., $(T_d - T_w)^+$ is positive; hence, from Eq. (18.1) we have

$$\text{Auxiliary energy, } \text{AE}_{FPC} = \text{positive}$$

Then from Eq. (18.3) one gets $f < 1$, i.e., auxiliary (fossil-fuel) heating is required. The amount of fossil fuel depends on the following parameters:

- combustion (burning) efficiency;
- heating value;
- losses through piping; and
- conversion factor.

18.4   Energy Conservation in Building

The solar-load ratio (SLR) method is widely used to design glass windows (direct gain), collector-cum-storage walls (indirect gain), and sunspace systems to save fossil fuel for thermal heating for cold climatic conditions. Energy conservation in buildings has already been discussed in Chap. 10 (Sect. 10.11).

18.5   Energy Conservation in Cooking

It is a well-established fact that slow cooking is the best way to cook because it retains most of bacteria needed by human beings to maintain good health. In ancient times, most cooking was performed using biomass (renewable energy), which is also a byproduct of solar energy (Chap. 15). Even today, people use biomass in underdeveloped/ developing countries. For them, it is suggested to use the most efficient cook stove to reduce the cost of biomass to save the ecological system.

In this section, we will mostly discuss how to conserve fossil fuels (electricity and petroleum products), e.g., pressurized natural gas (PNG), liquefied petroleum gas (LPG), etc., by using solar energy for cooking if sufficient exposed working space is available either on the roof or in the corridor. As discussed in Chap. 17, one can cook using a solar cooker. It is also known that a solar cooker can only be used in the presence of sufficient solar energy. However, a solar cooker can be used to conserve some part of fossil fuel. There are many type of solar cookers. A properly designed solar cooker should be used for cooking a meal of a given capacity.

There are many ways to improve cooking to conserve fossil fuels and save money. These are as follows:

The cooking method
This means choosing the appropriate size of cooking pot for a food/meal. It is suggested that the box-type solar cooker is the best size for cooking a small meal for two to three people. Rice, lentils, and beans, etc., can be cooked in a box-type solar cooker once a day for lunch. In each cooking process, food should be rinsed with hot water and kept for some time before placing in the solar cooker. Cooking will take less time in sunny conditions; sometimes cooking twice is also possible. For a small family, a concentrated pressurized solar cooker should not be used. It is always better to use this type of cooker for a large-size family meal. One can also cook food more efficiently using specialized appliances such as a pressure cooker/rice steamer for rice and lentils, etc.

Cooking pot
The outer surface of a cooking pot and the inner surface of a solar cooker should be regularly painted black to absorb maximum solar radiation. This will help in reducing the cooking time. The mirror should also be adjusted according to the season to reflect the solar radiation accordingly.

Solar water heating
There are many application for a solar water heater in the kitchen. First, hot water from a solar water heater, if available, can be used to preheat water for cooking meals. This will save conventional energy, which will help in reducing the monthly energy bill. It is also environmentally friendly. Furthermore, the hot water can also be used to clean kitchen utensils with less use of cleaning powder.

Solar cooker as hot oven
This is most suitable for office workers. A solar heater can be used to warm cooked food for before consumption to retain its taste. This will also save electricity during the lunch period.

Fried vegetables
Vegetables can be flash-fried in a pot using conventional fuel (LPG, PNG) and then cooked in a concentrated pressurized pot to save conventional fuel. However, it is recommended for use in cooking for large group.

18.6 Energy Conservation in Transportation

There has been a s significant increase in petroleum products used in the transport sector due to the increase in the population and the need of individuals. This increase in the demand for petroleum products causes concern regarding a possible increase in the local pollution level, which ultimately will increase pollution globally. This also affects the climate. These concerns can be partially solved as follows:

- **Use of efficient automobile engine**: This gives better mileage and energy savings.
- **Battery-operated engine**: In this case, photovoltaic (PV) system can be used to charge the battery. This is most feasible and practical in underdeveloped/ developing countries through the use of solar rickshaws/small cars. Such rickshaws/small cars have mileage of 50–80 km on just one battery charging and sizing.
- **Solar car**: Some countries have also developed solar cars, which are on trial and will soon be launched in the market.
- **Aeroplane**: There have been attempts to develop solar aeroplanes, particularly by Switzerland, for public transport. This is also in the trial stage.
- **Solar cycle**: This also means operated by a solar-charged battery. By using this mode of transportation, working efficiency is increased.
- **Hydrogen vehicle**: Recently, hydrogen has been used as a fuel for transportation, particularly in small cars. There are many methods for producing hydrogen using solar energy. However, we will discuss the two most important methods for doing so by splitting H_2O into hydrogen.

  (i) **Water-splitting process**: This is performed by using photons in the visible length of solar energy to achieve clean hydrogen, which is a renewable energy in nature. The process is known as "photocatalytic water splitting."
  (ii) **Electrolytic hydrogen production**: Electrolysis is a process for breaking water (H_2O) into its constituent elements, hydrogen (H_2) and oxygen (O_2), by supplying electrical energy from a PV system. An electric current from

WORK TO EXPAND GASES PRODUCED
PΔV=3.7 KJ

ΔG=237.13 KJ
INPUT
ELECTRICAL ENERGY

ENERGY
EXCHANGE
PROCESSES
FOR
ONE
MOLE
OF
WATER
ΔH=285.83 KJ

−

+

+

−

BATTERY

ELECTROLYSIS OF WATER

$H_2O \rightarrow H_2 + \frac{1}{2}O_2$

FORMS
HYDROGEN
BUBBLES

FORMS
OXYGEN
BUBBLES

ENERGY FROM ENVIRONMENT
PΔS=48.7 KJ
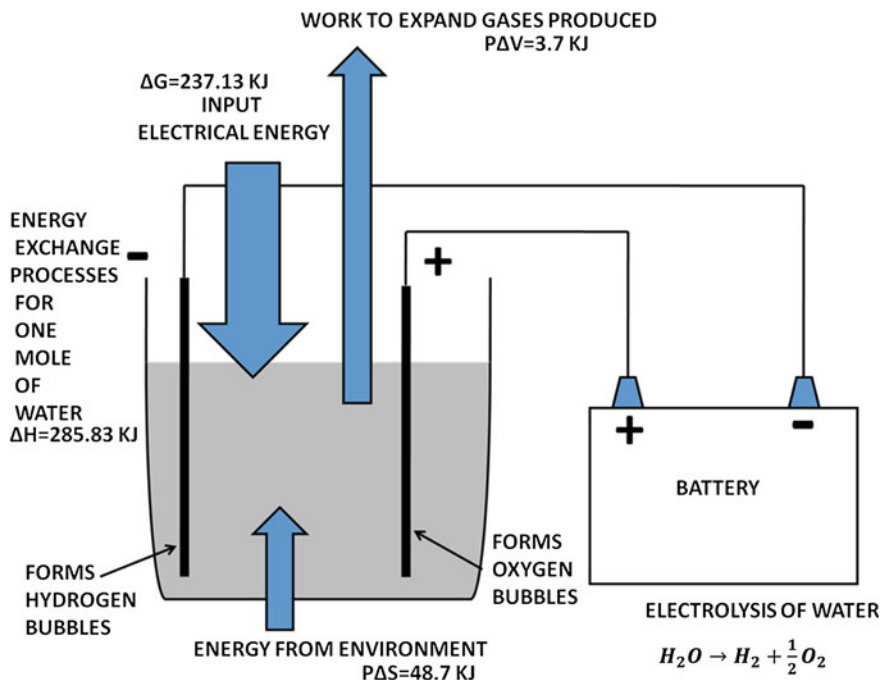
Fig. 18.1 Electrolysis process for breaking water (H_2O)

a PV system is passed through an anode and a cathode immersed in water as shown in Fig. 18.1. The following reaction takes place:

$$2H_2O \text{ liquid} + \text{electricity} \rightarrow 2H_2 + O_2 \qquad (18.4)$$
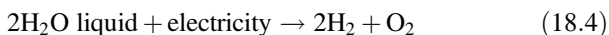
The chemical reaction in Eq. (18.4) needs 39 kWh of electricity to produce 1 kg of hydrogen at 25 °C under 1 atmospheric pressure. Presently water electrolysis is foreseeable in the future. Hydrogen production using PV technology has a lower share (0.1–0.2 %) of total hydrogen production, which may increase in the near future. Hydrogen produced by this technique, a low-pressure electrolysis method, is free from sulphur and carbon impurities.

18.7 Commercial Sector

The commercial sector mainly consists of (i) retail stores, (ii) offices (business and government), (iii) restaurants, (iv) schools, and (v) other working places that operate mostly during the day and late evening. In these sectors, PV technology can be most economical and environmentally friendly compared with other fossil fuels

such as petroleum-based electricity (generator) in the absence of power from a grid in rural areas. Sometimes it is also referred to as an "oil saver." In such a case, sizing of the battery becomes minimal due to less need during the late evening. Lights and fans are more frequently used in these sectors. In addition, commercial buildings can allow centralized control and coordination of energy-conservation efforts in the case of PV systems.

18.8   Industrial Sector

Many industries save traditional power by using solar energy as follows:

- water pumping through a PV system during peak sunshine hours for agriculture and other industries
- use of a PV lighting system during off-sunshine hours;
- use of preheated hot water in the cotton and power industries;
- purification of wastewater by a chemical–solar system;
- use of waste hot water for the purification of saline water by a distillation process through a heat exchanger; and
- use of a PV telecommunications system in remote areas.

Objective Questions

18.1   To conserve energy in a building during the summer, the exterior (exposed) wall should be insulated from
(a) the outside   (b) the inside   (c) both sides   (d) none of these
Answer: (a)

18.2   To conserve fossil fuel for thermal heating of a building in the winter, the exterior (exposed) wall should be insulated from
(a) the outside   (b) the inside   (c) both sides   (d) none of these
Answer: (b)

18.3   For lighting inside a building, which option among following is best?
(a) day lighting   (b) LED lighting   (c) both a and b   (d) none of these
Answer: (b)

18.4   Fossil fuel can be conserved in cooking by using
(a) an improved biomass burner   (b) a solar cooker   (c) both a and b   (d) all of these
Answer: (d)

18.5   The energy generated by PV module can be stored as
(a) potential energy during water pumping   (b) kinetic energy
(c) gravitational energy   (d) none of these
Answer: (a)

References

1. S. Hebden (22 June 2006), *Invest in clean technology says IEA report*. Scidev.net. Retrieved 16 July 2010)
2. G.N. Tiwari, *Solar energy: fundamental, design, modelling and applications.* (Narosa Publishing House, New Delhi and CRC Press, New York, 2004)

Additional References

3. F. Kreith, Y.D. Goswami, *Energy management and conservation handbook* (CRC Press, Taylor and Francis, Boca Raton, 2008)

Chapter 19
Exergy Analysis

Abstract Exergy as an available useful work needs to be analyzed from the point of view of the second law of thermodynamics. It derives from Carnot's thermal efficiency, which is responsible for high-grade energy. Exergy plays an important role in life-cycle cost analysis (LCCA).

Keywords Energy analysis · Exergy analysis · Energy matrices · CO_2 emission · Carbon credit

19.1 Introduction

Current progress in the concepts, design, developments, and manufacture of solar energy technologies is very rapid. New solar-energy technologies are now predicted to play a major role to meet the energy demand by human being for good living comfort. This is most important areas in undeveloped/developing countries.

The energy output from solar-energy technologies can be classified as follows:

(i) **Thermal energy(low-grade energy)**: Solar thermal systems

The energy analysis of thermal energy (low-grade energy) output is based on the first law of thermodynamics as performed in Chap. 14. However, the concentrating collector operating at high temperature should be analyzed on the basis of the second law of thermodynamics.

(ii) **Electrical energy(high-grade energy)**: Photovoltaic systems

The energy analysis of high-grade energy (photovoltaic) is based on the second law of thermodynamics and is known as "exergy analysis."

(iii) **Both thermal (low-grade energy) and electrical energy (high-grade energy)**: Photovoltaic thermal systems

In this case, either thermal energy is converted into high-grade energy using the concept of Carnot's efficiency, or electrical energy is converted into low-grade

energy by dividing it by power plant–conversion factor (Eq. 14.1) as performed in Chap. 14.

19.2   Exergy Analysis

As mentioned in Chap. 3, an exergy analysis of any system incorporates all of the irreversibilities and inefficiencies that lead to the destruction of exergy.

In this chapter, since we are dealing with exergy analysis, thermal energy (low-grade energy) will be converted into exergy (high-grade energy) as follows.

First method

If the operating temperature is very high, say, approximately 400–500 °C in the case of a concentrating system for power generation, then thermal energy will be converted into exergy as

$$\dot{E}x = \dot{Q}_u\left[1 - \frac{T_{fi} + 273}{T_{fo} + 273}\right] \tag{19.1}$$

where $\dot{Q}_u = \dot{m}_f C_f(T_{fo} - T_{fi})$ is the rate of thermal energy (low-grade energy) at temperature T_{fo} (°C); and T_{fi} (°C) is the inlet temperature at the surrounding air temperature.

Second method

Unlike a solar concentrator, the flat-plate collector operates at medium temperature range, say, approximately 100–150 °C. The second method of exergy analysis incorporates entropy losses in the system. For a solar thermal collector system, if T_{fo} and T_{fi} are, respectively, the outlet and inlet fluid temperature (K), and $\dot{m}_f$ is the mass flow rate (kg/s) of fluid, then the exergy ($\dot{E}x_c$) of the system is expressed as follows:

$$\dot{E}x_c = \dot{m}_f C_f(T_{fo} - T_{fi}) - \dot{m}_f C_f(T_a + 273)\ln\frac{T_{fo} + 273}{T_{fi} + 273} \tag{19.2a}$$

Exergy efficiency is the ratio of exergy available from the solar thermal system to the exergy of the Sun and is expressed as

$$\varepsilon_c = \frac{\dot{E}x_c}{\dot{E}x_{sun}} \tag{19.2b}$$

where $\dot{E}x_{sun}$ is given by Eq. (3.15).

The exergy efficiency can be improved by reducing the reversibility at every component as well as the inefficiency of each critical component of the system.

Example 19.1 Calculate the exergy (maximum work available) from the collector system operating at 60 °C and 600 °C and an ambient air temperature at 20 °C for producing thermal energy at a rate of 150 kW.

Solution
First method

Using Eq. (19.1), one can obtain

$$\dot{Ex} = 150\left[1 - \frac{20 + 273}{60 + 273}\right] = 18\,\text{kW}$$

and

$$\dot{Ex} = 150\left[1 - \frac{20 + 273}{600 + 273}\right] = 98.8\,\text{kW}$$

It can be observed that the exergy (maximum work available), which is high-grade energy, will be reduced significantly. It is also to be noted that exergy is higher at high temperatures as expected.

Example 19.2 Calculate the exergy output from a flat-plate collector when $T_{fo} = 60\,°C$ and $T_{fi} = T_a = 25\,°C$ for a mass-flow rate of 0.06 kg/s and $C = 4190$ J/kg K.

Solution
First method

From Eq. (19.1), we obtain

$$\dot{Ex} = 0.06 \times 4190 \times 35 \times \left[1 - \frac{25 + 273}{60 + 273}\right] = 924.8\,\text{W} = 0.924\,\text{kW}$$

Second method

From Eq. (19.2a), we obtain

$$\dot{Ex}_c = \left[0.06 \times 4190 \times 35 - 0.06 \times 4190 \times (298)\ln\frac{60 + 273}{25 + 273}\right] = 5188\,\text{W}$$
$$= 5.19\,\text{kW}$$

In this example, calculating exergy by the second method has a significantly higher result than by the first method at a medium temperature range.

The following conclusions have been made

(i) For high operating temperature, Eq. (19.1) should be used to covert thermal energy into exergy,

(ii) For low operating temperature, Eqs. (19.2a, b) should be used to covert thermal energy into exergy,

To obtain an overall exergy, the exergy of thermal energy should be added to the electrical energy as in the case of a photovoltaic thermal system (Sect. 4.2.7).

It is also important to note that energy (generally high grade) used in the manufacturing of solar systems should be less than they can produce in their whole lifetime; otherwise, it makes no sense.

If solar thermal energy (low-grade energy), solar water heating, or replacement of thermal energy is produced by high-grade energy, e.g., a water geyser, then it is considered as the conservation of high-grade energy. In this case, low-grade energy can be placed on par with high-grade energy as far as exergy analysis is considered. Otherwise, it should be multiplied by Carnot's efficiency to make it high-grade energy.

19.3 Energy Matrices

Energy matrices are most important parameters for renewable technologies. In this chapter, we will discuss the energy matrices of solar-energy technologies, which are basically the source of all renewable energy sources. The energy-payback time (EPBT) (Eq. 14.2), as defined in Chap. 14, is always be one of the criteria used for comparing the viability of solar-energy technologies. The EPBT in Chap. 14 was calculated on the basis of the first law of thermodynamics. In this chapter, we will discuss the EPBT on the basis of the second law of thermodynamics.

For example, a photovoltaic unit gives DC electricity, which is considered high-grade energy. The embodied energy of a PV system is also high-grade energy. Hence, the EPBT in this case will be based on high-grade energy unlike as discussed in Chap. 14.

The energy analysis of a PV module was investigated by Hunt [1]. In his studies, the EPBT of a PV module was found to be 12 years, which is in accordance with the results of the study by Kato et al. [2]. Furthermore, many researchers have studied the EPBT of PV modules using different solar-cell technologies with different encapsulating materials operating under different climatic conditions and different applications [3–7]. In these studies, it was found that the EPBT varies from 2 to 8 years depending on the solar-cell technology, the material used for module manufacturing, and the operating and climatic conditions.

To reduce the EPBT, the following considerations should be adopted:

  (i)   increase overall efficiency;
 (ii)   use cost-effective materials with low energy densities with longer life; and
(iii)   minimize annual maintenance.

19.3.1   Energy-Payback Time (EPBT)

As defined in Chap. 14, the EPBT is the ratio of embodied energy in kWh and the annual energy output in kWh from a solar system. It can be mathematically expressed as

$$\text{EPBT}\left(T_{\text{epb}}\right) = \frac{\text{Embodied Energy }(E_{\text{in}})}{\text{Annual Energy Output }(E_{\text{out}})} \tag{19.3}$$

In Eq. (19.3), the annual energy output in kWh is high-grade energy (exergy). Furthermore, the numerical values of EPBT should be as minimum as possible to make the solar-energy technologies cost-effective.

19.3.2   Energy-Production Factor (EPF)

The energy-production factor is based on the first law of thermodynamics. However, it becomes the electricity-production factor (EPF) if the annual energy output in kWh is high-grade energy (exergy). It is used to predict the overall performance of the solar system. It is defined in two ways as follows.

 (a)   **On an annual basis**

In this scenario, it is defined as the ratio of the output energy to the input energy (embodied energy). In this case, it can also be expressed as the inverse of the EPBT.

$$\chi_{\text{a}} = \frac{E_{\text{out}}}{E_{\text{in}}} \tag{19.4}$$

or

$$\chi_{\text{a}} = \frac{1}{T_{\text{epb}}} \tag{19.4a}$$

If $\chi_{\text{a}} \to 1$, for $T_{\text{epb}} \to 1$, the solar system is worthwhile; otherwise, it is not worth it from energy/exergy point of view.

(b) **On a lifetime basis**

In this case, it is defined as the ratio output energy during the whole lifetime to the input energy (embodied energy). Mathematically it can be expressed as follows:

$$\chi_a = T \frac{E_{\text{out}}}{E_{\text{in}}} \tag{19.4b}$$

In this case, χ_a should be as maximum as possible, at least >1, to the make solar system cost-effective from an exergy point of view.

19.3.3 *Life Cycle Conversion Efficiency (LCCE)*

The LCCE is the net energy productivity of the system with respect to the solar input (radiation) over the lifetime of the system, (*T* years). Mathematically it can be expressed as follows:

$$\phi(t) = \frac{E_{\text{out}} \times T - E_{\text{in}}}{E_{\text{sol}} \times T} \tag{19.5}$$

The numerical value of the LCCE is always less than one. However if the value of the LCCE approaches one, it is the best technology from an energy point of view.

One can observe that the embodied energy (E_i), the annual electrical output (E_{out}), and the life of solar-energy technology all play a very important role in evaluating the energy matrices [Eqs. (19.3)–(19.5)].

Energy matrices can be studies in the following ways:

 (i) annual output based on thermal energy (first law of thermodynamics); and
(ii) annual output based on exergy (second law of thermodynamics).

19.4 **Energy Matrices of Different Solar Systems**

19.4.1 *Flat-Plate Collector*

(a) **Based on thermal energy**

The embodied energy for two flat-plate collectors each having an area of 2 m^2 is given in Table 14.1. The value of embodied energy for the two flat-plate collectors is 2315.10 kWh.

Embodied energy for a flat-plate collector (FPC) of $2\,\text{m}^2 = 1157.11\,\text{kWh}$.

Annual solar radiation incident on the FPC of $2\,\text{m}^2 = 400 \times 8 \times 2 \times 268\,\text{Wh} = 1715\,\text{kWh}$.

For the following parameters, namely, $\eta_c = 0.70$ (efficiency of the FPC), $A_m = 2\,\text{m}^2$, and 1715 kWh for New Delhi clear-sky (blue-sky) conditions, T_{fo} and $T_{fi} = T_a$ are 60 °C and 25 °C, respectively, and $\dot{m}_f = 0.004\,\frac{\text{kg}}{\text{s}}$.

An overall annual thermal energy for one FPC $= 0.7 \times 1715\,\text{kWh} = 1205.5\,\text{kWh}$.

The energy matrices of one flat-plate collector have been calculated for $T = 15$ years using Eqs. (19.3)–(19.5) as follows:

$$\text{Energy payback time (EPBT)} = \frac{1157.11}{1205.5} = 0.96 \text{ years}$$

$$\text{Energy production factor (EPF)} = \frac{1205.5 \times 15}{1157.11} = 15.63$$

$$\text{Life cycle conversion efficiency (LCCE)} = \frac{1205.5 \times 15 - 1157.11}{1715 \times 15} = 0.66$$

The above calculated energy matrices are based on the annual thermal energy of the FPC, and they satisfy all conditions mentioned in Sect. 19.3. Hence, the use of an FPC is economical.

(b) **Based on exergy**

Because a flat-plate collector operates at a medium temperature range, using Eq. (19.2a) the exergy of a flat-plate collector output is given by

$$\dot{\text{Ex}}_c = \left[0.004 \times 4190 \times 35 - 0.004 \times 4190 \times (25 + 273)\ln\frac{60 + 273}{25 + 273}\right]$$
$$\times 8 \times 268 = 827 \text{ kWh.}$$

The energy matrices of one flat-plate collector have been calculated based on exergy for $T = 15$ years using Eqs. (19.3)–(19.5) as follows:

$$\text{Energy payback time (EPBT)} = \frac{1157.11}{827} = 1.4 \text{ years}$$

$$\text{Energy production factor (EPF)} = \frac{827 \times 15}{1157.11} = 10.7$$

$$\text{Life cycle conversion efficiency (LCCE)} = \frac{827 \times 15 - 1157.11}{1715 \times 15} = 0.44$$

The exergy-based calculated energy matrices also satisfy all conditions mentioned in Sect. 19.3. Hence, the use of an FPC is economical.

A flat-plate collector is an economical device both from the thermal as well the exergy point of view.

19.4.2   Solar Cooker

A solar cooker, which is made of fiber-reinforced plastic, is used to cook rice. 4 kg/day, in summer at 100 °C with an ambient air temperature of 40 °C under clear climatic conditions for 268 days in 1 year. It takes approximately 2.5 hour to cook the rice each time. If the embodied energy of a solar cooker is 125 kWh and 600 kWh solar energy used in one year for cooking, calculate its energy matrices.

First, the exergy is calculated as follows:

First method

From Eq. (19.1), we obtain

$$\dot{Ex}_c = 4 \times 4190 \times 60 \times \left[1 - \frac{40 + 273}{100 + 273}\right] \times 2.5 \times 268 = 30 \text{ kWh}$$

Second method

From Eq. (19.2a), we obtain

$$\dot{Ex}_c = \left[4 \times 4190 \times 60 - 4 \times 4190 \times (40 + 273) \ln \frac{100 + 273}{40 + 273}\right] \times 2.5 \times 268$$
$$= 112.5 \text{ kWh}$$

One can observe from the above calculations that the second method is as reasonable as the first method; hence, we will consider annual exergy savings of 45 kWh for the energy matrices.

Using Eqs. (19.3)–(19.5), the energy matrices of a solar cooker (life approximately 10 years) are calculated as follows:

$$\text{Energy payback time (EPBT)} = \frac{125}{112.5} = 1.11 \text{ years}$$
$$\text{Energy production factor (EPF)} = \frac{112.5 \times 10}{125} = 9$$
$$\text{Life cycle conversion efficiency (LCCE)} = \frac{112.5 \times 10 - 125}{600 \times 10} = 0.17$$

This indicates that the solar cooker is also viable for its application from an exergy point view.

19.4.3   Solar Still

From Sect. 14.6.5, we have the following parameters of a solar still.

Passive solar still
The total embodied energy of a passive solar still of $1 \text{ m}^2 = 441.21$ kWh and annual solar radiation $= 857.5$ kWh.

For $h_{ew} = 5.83 \text{ W/m}^2 \, ^\circ\text{C}$, $T_w = 60 \, ^\circ\text{C}$ and $T_g = T_a = 25^\circ \text{C}$, an annual yield/m^2 (output) will be 2 kg. For 268 number of clear days, exergy in W/m^2 can be calculated from the following expression:

$$\dot{\text{E}}\text{x}_{ps} = h_{ew}\left(T_w - T_g\right) - h_{ew}(T_a + 273) \ln \frac{T_w + 273}{T_g + 273}$$

The annual exergy of a passive solar still is given by

$$\dot{\text{E}}\text{x}_{ps} = \left[5.83 \times (60 - 25) - 5.83 \times (25 + 273) \ln \frac{60 + 273}{25 + 273} \right]$$
$$\times 8 \times 268 = 257 \text{ kWh}$$

Using the energy matrices of a passive solar still for $T = 30$ years using Eqs. (19.3)–(19.5), we obtain

$$\text{Energy payback time (EPBT)} = \frac{441.21}{257} = 1.7 \text{ years}$$
$$\text{Energy production factor (EPF)} = \frac{257 \times 15}{441.21} = 8.74$$
$$\text{Life cycle conversion efficiency (LCCE)} = \frac{257 \times 30 - 441.21}{857.5 \times 30} = 0.28$$

This shows that the EPBT for a passive solar still on the basis of exergy becomes greater. However, it is still economical.

Active solar still
The embodied energy for an active solar still $= 441.21 + 1724 = 2165.21$ kWh.

For $h_{ew} = 9.72 \text{ W/m}^2 \, ^\circ\text{C}$, $T_w = 80 \, ^\circ\text{C}$, and $T_g = 65 \, ^\circ\text{C}$ and $T_a = 25 \, ^\circ\text{C}$, an annual yield/m$^2 = 5$ kg. For 268 number of clear days, the exergy in W/m^2 can be calculated as

$$\dot{\text{E}}\text{x}_{as} = h_{ew}\left(T_w - T_g\right) - h_{ew}(T_a + 273) \ln \frac{T_w + 273}{T_g + 273}$$

The annual exergy of an active solar still is given by

$$\dot{Ex}_{as} = \left[9.72 \times (80 - 65) - 9.72 \times (25 + 273) \ln \frac{80 + 273}{65 + 273}\right]$$
$$\times 8 \times 268 = 195.48 \text{ kWh}$$

Using Eqs. (19.3)–(19.5), the energy matrices of an active solar still for $T = 30$ years and an annual solar radiation of 2572.5 W/m^2 are as follows:

$$\text{Energy payback time (EPBT)} = \frac{2165.21}{195.48} = 11 \text{ years}$$
$$\text{Energy production factor (EPF)} = \frac{195.48 \times 30}{2165.21} = 2.71$$
$$\text{Life cycle conversion efficiency (LCCE)} = \frac{195.48 \times 30 - 2165.21}{2572.5 \times 30} = 0.047$$

This indicates that the EPBT for an active solar still is significantly higher compared with that of a passive solar still on the basis of exergy; however, it can still be considered as economical viable.

19.4.4   Evacuated Tubular Solar Collector

An evacuated tubular solar collector mainly consists of cooper pipes and glass tubes in addition to stainless steel material for the framing, etc. In this case, the embodied energy of an evacuated tubular solar collector will be approximately 75 % of that of a flat-plate collector (FPC) of 2 m^2 is 867 kWh.

For New Delhi clear-sky (blue-sky) conditions:

$$\text{Annual solar radiation incident on ETSC of } 2\,\text{m}^2 = 400 \times 8 \times 2 \times 268 \text{ Wh}$$
$$= 1715 \text{ kWh}$$

In ETSC, T_{fo} and $T_{fi} = T_a$ are 80 and 25 °C, respectively, and $\dot{m}_f = 0.004 \frac{\text{kg}}{\text{s}}$.

Because a flat-plate collector operates at medium temperature range, by using Eq. (19.2a) the exergy of a flat-plate collector's output is given by

$$\dot{Ex}_c = \left[0.004 \times 4190 \times 55 - 0.004 \times 4190 \times (25 + 273) \ln \frac{80 + 273}{25 + 273}\right]$$
$$\times 8 \times 268 = 195.48\,\text{kWh}$$

The energy matrices of one-flat plate collector have been calculated based on exergy for $T = 15$ years using Eqs. (19.3)–(19.5) as follows:

$$\text{Energy payback time (EPBT)} = \frac{867}{1228} = 0.71 \text{ years}$$

$$\text{Energy production factor (EPF)} = \frac{1228 \times 15}{867} = 21.2$$

$$\text{Life cycle conversion efficiency (LCCE)} = \frac{1228 \times 15 - 867}{1715 \times 15} = 0.68$$

The use of an evacuated tubular solar collector is more viable compared with a flat-plate collector from an exergy point of view.

19.4.5   PV Module

An electrical output is high-grade energy (electricity), which can be treated as exergy. If the life of a PV module is considered to be $T = 30$ years, then the matrices of a PV module can be obtained from Eqs. (19.2a)–(19.4b) for different cities. The results are discussed in Sect. 14.6 of Chap. 14.

19.4.6   Hybrid Flat-Plate Collector

The embodied energy for one hybrid flat-plate collector (FPC) of 2 m^2 will be approximately the sum of embodied energy for one flat-plate collector (FPC) of 2 m^2 (1157.11 kWh) and the embodied energy for one PV module of 0.605 m^2. From Table 14.2, this value will be approximately 1764.11 kWh.

19.4.7   Hybrid Air Collector

The calculation of total embodied energy for two hybrid air collectors connected in series is given in Table 14.3. AN elaborate analysis is given on Sect. 14.6.4.

19.4.8   PVT Greenhouse Dryer

The embodied energy of a PVT greenhouse dryer of a given design at SODHA BERS complex Varanasi was found to be 4816.13 kWh. The EPBT was found to be 9.31 years; and for a lifetime of 30 years the energy-production factor and the life-cycle conversion efficiency was found to be 3.22 and 0.038, respectively.

19.4.9 PVT Solar Concentrators

The embodied energy of a PVT solar concentrator is higher than that of a flat-plate PVT solar collector due to the inclusion of the concentrating device. In addition, the thermal efficiency of a solar PVT concentrator is lower than that of a PVT solar collector. The payback time is also more for a PVT solar concentrator.

19.5 CO_2 Emissions

Energy consumption is one of the indicators of the socioeconomic development of a country. Socioeconomic development (which depends on the GDP, literacy, life expectancy, industrialization, advanced technologies, and level of employment) increases the quantity of per-capita energy used. The use of conventional sources of energy to fulfill energy demands will lead to a heavy amount of CO_2 emissions into the atmosphere, it will also exhaust the conventional sources of energy [8].

Greenhouse gases (GHG) are gases present in the earth's atmosphere in terrestrial region. They reduce the loss of thermal energy emitted from Earth into space. GHG are essential to maintaining the temperature of the Earth and its terrestrial region. However, an excess of GHG can raise the temperature of a planet. GHG are produced mainly by many natural and industrial processes. Currently they result in CO_2 levels of >400 ppm in the atmosphere. Carbon emissions from various global regions during the period 2010–2040 are shown in Fig. 19.1a.

The average carbon dioxide (CO_2) emitted for electricity generation from the best quality of coal is approximately 0.98 kg of CO_2/kWh [9]. The CO_2 emissions per year by each component of a PV module during its entire life can be calculated as

$$CO_2 \text{ emission per year} = \frac{\text{Embodied energy} \times 0.98}{\text{Life time}} \qquad (19.6)$$

The CO_2 emissions per year for a PV module (glass to glass) (effective area = 0.605 m^2 and size = 1.20 m × 0.55 m × 0.01 m) and a 35-year life under present conditions is given in Table 19.1. The CO_2 emissions for different PV/T systems are shown in Fig. 19.1b.

Example 19.3 Calculate the carbon dioxide emission per year from a solar water heater with a lifetime of 10, 20, and 30 years when the total embodied energy required for manufacturing the system is 3550 kWh.

Solution
Using Eq. (11.6), we have

For lifetime = 10 years, CO_2 emission per year $= \dfrac{3550 \times 0.98}{10} = 347.9$ kg.
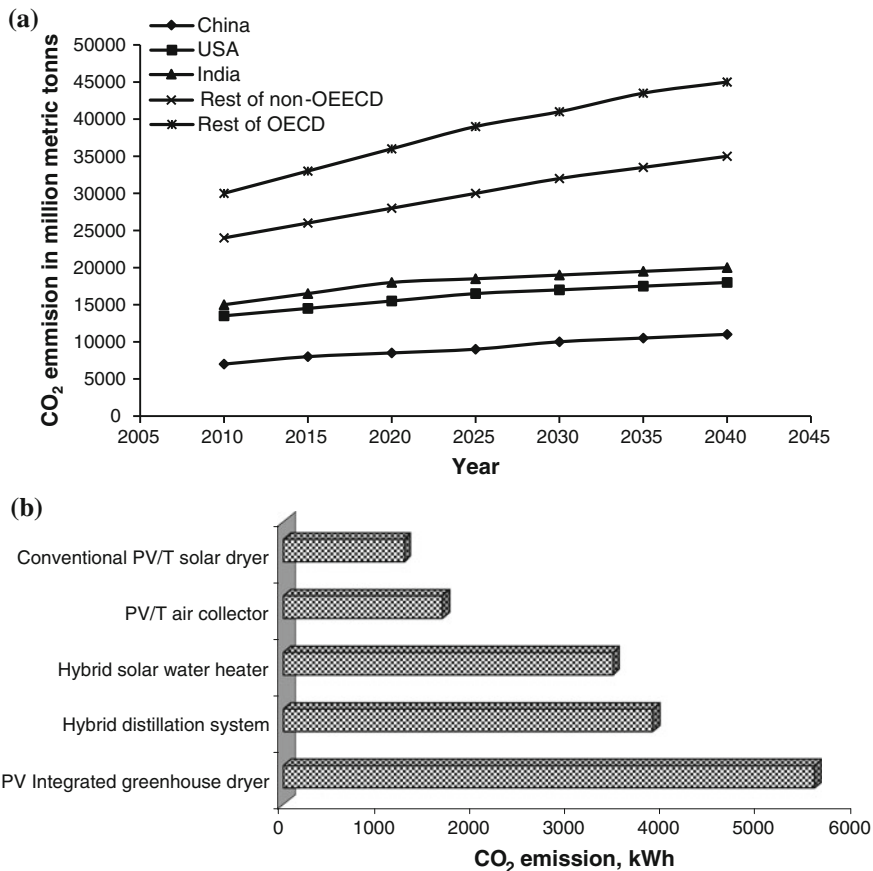
Fig. 19.1 **a** Carbon emissions from various global regions during the period 2010–2040. **b** CO$_2$ emissions for different PVT systems (from [20])

Table 19.1 CO$_2$ emissions/year from a PV module (glass to glass) (effective area = 0.60534 m^2) (from Tiwari and Mishra 2012)

S. no.	Components	Embodied energy (kWh)	CO$_2$ emissions (kg)
1	MG-Si	26.54	0.74
2	EG-Si	127.30	3.56
3	Cz-Si	267.33	7.49
4	Solar-cell fabrication	60.29	1.69
5	PV module assembly	125.40	3.51
Total		606.86	16.99

Similarly, for lifetime = 20 and 30 years, CO$_2$ emissions per year is 173.9 and 115.9 kg of CO$_2$, respectively.

19.6   Carbon Credit (C-Credit [CC]) [10]

The business of carbon credits (CC) was created to reduce the effect of GHG emission into atmosphere by reducing the carbon footprint. CC are defined as "a key component of national and international carbon emissions trading schemes that have been implemented to mitigate CO_2 to reduce global warming.' It is based on an industrial scale by capping the total annual emissions. C-Credits can be exchanged between businesses or bought and sold in international markets at the prevailing market price fixed by international agreement. C-Credits can be used to finance carbon reduction schemes in the atmosphere between trading partners (as well countries) around the world.

19.6.1   Formulation

If a unit power (kWh) is used by a consumer, the Lais electrical loss due to poor domestic appliances, namely, tube lights, fans, water pumps, and refrigerators, then the transmitted power should be $\frac{1}{1-L_a}$ units. For L_{td} (transmission and distribution), the generated power at the power-plant site is $\frac{1}{1-L_a} \times \frac{1}{1-L_{td}}$ units.

The average CO_2 emission for electricity generation of a unit of energy (1 kWh) from coal at the site (source) is approximately 0.98 kg of CO_2. Thus, the amount of CO_2 emission is $\frac{1}{1-L_a} \times \frac{1}{1-L_{td}} \times 0.98$ per unit of power consumption by the user.

The annual CO_2 emission from a solar system can be expressed as:

$$CO_2 \text{ emission per year from solar system} = \frac{\text{total } CO_2 \text{ emission by embodied energy}}{\text{Life of solar system}}$$

$$= \frac{E_{in}}{n_{sys}} \times \frac{1}{1-L_a} \times \frac{1}{1-L_{td}} \times 0.98 \text{ kg}$$

$$(19.7)$$

where E_{in} and n_{sys} are the embodied energy and lifetime of the solar system.

The net CO_2 mitigation over the lifetime of the system

$$= \text{Total } CO_2 \text{ mitigation} - \text{total } CO_2 \text{ emission}$$

$$= (E_{aout} \times T_{LS} - E_{in}) \times \frac{1}{1-L_a} \times \frac{1}{1-L_{td}} \times 0.98 \text{ kg}$$

$$(19.8)$$

where E_{aout} is an overall annual exergy gain.

The net CO_2 mitigation over the lifetime in tonnes of CO_2

$$= (E_{aout} \times n_{Sys} - E_{in}) \times \frac{1}{1 - L_a} \times \frac{1}{1 - L_{td}} \times 0.98 \times 10^{-3}$$

$$(19.9)$$

19.6.2   A Case Study with the BIPVT System

For Indian conditions, the transmission and distribution losses are nearly 40 %, and losses due to domestic appliances are 20 %. If these losses are considered for 1 U of electricity used by the consumer, then 2.08 U of electricity must be produced at the power plant, which emits 2.04 kg of CO_2. For the BIPVT system, the annual CO_2 mitigation in tonnes of CO_2 is given by

$$\left(E_{aout} - \frac{E_{in}}{n_{Sys}}\right) \times 2.04 \times 10^{-3} \qquad (19.10)$$

Assume that the overall embodied energy for technological BiPVT systems based on monocrystalline silicon (c-Si, $n_{Sys} = 30$ years), multi-crystalline silicon (p-Si, $n_{Sys} = 30$ years), ribbon silicon (r-Si, $n_{Sys} = 25$ years), amorphous silicon (a-Si, $n_{Sys} = 25$ years), cadmium telluride (CdTe, $n_{Sys} = 15$ years), and copper indium gallium selenide (CIGS, $n_{Sys} = 15$ years) are 607,613, 540,628, 409,716, 272,324, 211,984, and 63,937 MJ, respectively. The overall exergy calculations for the climatic conditions of New Delhi show that c-Si, p-Si, r-Si, a-Si, CdTe, and CIGS BIPVT systems covering 45 m^2 of roof area generate 16,224, 14,352, 12,512, 7790, 9547, and 11,037 kW of overall exergy output, respectively. Thus, the annual CO_2 mitigation for c-Si, p-Si, r-Si, a-Si, CdTe, and CIGS systems is 77.83, 68.64, 58.45, 29.44, 41.29, and 54.97 tonnes, respectively. If CO_2 emissions are being traded at USD20/tonnes of CO_2 mitigation, then the carbon credit earned by the BiPVT system with the c-Si, p-Si, r-Si, a-Si, CdTe, and CIGS technologies are USD $1557, USD$1373, USD$1169, USD$589, USD$826, and USD$1099, respectively. This shows that the monocrystalline silicon BiPVT system gives the highest earnings through carbon-credit trading.

Objective Questions

19.1   The 1 kWh is
   (a) 36 MJ   (b) 3.6 MJ   (c) 0.36 MJ   (d) 360 MJ
   Answer: (b)
19.2   Energy density is maximal for
   (a) nonmetal   (b) metal   (c) glass   (d) none of these
   Answer: (b)

19.3 Energy-payback time (EPBT), if possible, should preferably be
       (a) <1   (b) >1   (c) =1   (d) =0
       Answer: (a)
19.4 For zero embodied energy, CO_2 emission is
       (a) <1   (b) >1   (c) =1   (d) =0
       Answer: (d)
19.5 At source of coal-based power generation, 1 kWh, is equivalent to
       (a) 0.98 kg CO_2 emission   (b) 9.8 kg CO_2 emission
       (c) 0.098 kg CO_2 emission   (d) none of these
       Answer: (a)
19.6 The energy-payback time (EPBT) for a flat-plate collector (FPC) mainly
       depends on
       (a) ambient air   (b) wind velocity   (c) solar intensity   (d) all of these
       Answer: (d)
19.7 The energy-payback time (EPBT) for a PV module with BOS is
       (a) reduced   (b) increased   (c) unaffected   (d) none of these
       Answer: (b)
19.8 The energy-payback time (EPBT) for a PV module at present is
       (a) <1   (b) >1   (c) =1   (d) =0
       Answer: (b)
19.9 Energy-payback time (EPBT) is
       (a) the ratio of embodied energy to annual energy output
       (b) the ratio of annual energy output to embodied energy
       (c) the ratio of annual energy output to annual input energy
       (d) None of these
       Answer: (b)

Problems

19.1 Calculate the rate of exergy loss by convection and radiation for the
       parameters of Sect. 19.4.3 and $h_{\text{cw}} = 2.8\,\text{W/m}^2\,{}^\circ\text{C}$ and $h_{\text{rw}} = 2.8\,\text{W/m}^2\,{}^\circ\text{C}$.
       Hint: Use the following expression

$$\dot{\text{Ex}}_{\text{LC}} = h_{\text{cw}}\left(T_{\text{w}} - T_{\text{g}}\right) - h_{\text{cw}}(T_{\text{a}} + 273)\ln\frac{T_{\text{w}} + 273}{T_{\text{g}} + 273}$$

$$\text{and}\quad \dot{\text{Ex}}_{\text{LR}} = h_{\text{rw}}\left(T_{\text{w}} - T_{\text{g}}\right) - h_{\text{rw}}(T_{\text{a}} + 273)\ln\frac{T_{\text{w}} + 273}{T_{\text{g}} + 273}$$

19.2 Write an expression for exergy loss due to the storage of thermal energy in a
       water mass in the basin
       Hint: The expression is given by

$$\dot{E}x_{LS} = M_w C_w(T_{wf} - T_{wi}) - \frac{M_w C_w(T_a + 273)\ln(T_{wf} + 273)}{T_{wi} + 273}$$

where T_{wf} and T_{wi} are the final and initial water temperatures in the basin, respectively.

19.3 Calculate total exergy loss for Problem 19.1 and 19.2.

Hint: For the known parameters of a passive solar still (Chap. 8), the sum of exergy of Problem 19.1 and 19.2 will be the total exergy loss in W/m^2.

References

1. L.P. Hunt, *IEEE PV specialists conference*. Piscataway, NJ, 1986, pp. 347–352
2. K. Kato, A. Murata, K. Sakuta, Prog. Photovolt. Res. Appl. **6**(2), 105 (1998)
3. H.A. Aulich, F.W. Schulz, B. Strake, *IEEE PV specialist conference*. Piscataway, NJ, 1986, pp. 1213–1218
4. R. Prakash, N.K. Bansal, Energy Sources **17**(6), 605 (1995)
5. G. Lewis, G. Keoleian, *National Pollution Prevention Center, School of Natural Resources and Environment*. University of Michigan (1996)
6. K.S. Srinivas, M. Vuknic, A.V. Shah, R. Tscharner, *6th international photovoltaic science and engineering conference (PVSEC-6)*. New Delhi, India, 1992, pp. 403–413
7. R. Battisti, A. Corrado, Energy **30**, 952 (2005)
8. R. Kalshian, *Energy versus emissions: the big challenge of the new millennium, by Info Change News & Features*. www.infochangeindia.org/agenda5_01.jsp. Accessed 21 Mar 2008
9. M. Watt, A. Johnson, M. Ellis, H.R. Outhred, Prog. Photovolt. Res. Appl. **6**(2), 127 (1998)
10. B. Agrawal, G.N. Tiwari, *Building integrated photovoltaic thermal systems* (RSC Publishing, UK, 2010)

Additional References

11. S.Z. Farooqui, Renew. Sustain. Energy Rev. **31**, 439 (2014)
12. E. Saloux, A. Teyssedou, M. Sorin, Energy Build. **67**, 275 (2013)
13. K.R. Ranjan, S.C. Kaushik, Renew. Sustain. Energy Rev. **27**, 709 (2013)
14. R. Saidur, G. BoroumandJazi, S. Mekhlif, M. Jameel, Renew. Sustain. Energy Rev. **16**(1), 350 (2012)
15. S. Agrawal, G.N. Tiwari, Solar Energy. **85**(2), 356 (2011)
16. B. Prabhakant Agrawal, G.N. Tiwari, Appl Solar Energy. **46**(1), 33 (2010)
17. I. Dincer, M.A. Rosen, *Exergy energy, environment and sustainable development*, 2nd edn. (Elsevier Ltd., Amsterdam, 2007)
18. G.N. Tiwari, *Advances in solar energy technology* (Nova Science Publishers, New York, 2005)
19. H.H. Öztürk, Sol. Energy **77**(1), 67 (2004)
20. G.N. Tiwari, R.K. Mishra, *Advance Renewable Energy Sources* (RSC publishing, UK, 2012)

Chapter 20
Life-Cycle Cost Analysis

Abstract Life-cycle cost analysis (LCCA) of any system is the most important analysis for the success of any technology. It gives an idea to accept or reject the system for its implementation. The LCCA should be done by considering annual energy and exergy analysis of any technology.

20.1 Introduction

Techno-economic analysis is a fundamental subject of life-cycle cost analysis (LCCA). This is field of study where the cost of the system is optimized utilizing the engineering skills and experience in the particular field. Cost analysis is used for project-cost control through benefit–cost analysis, profitability analysis, planning, scheduling, and optimization of operational research, etc. In the case of solar-energy technology, it is necessary to determine its economic viability so that the users of the technology may know the importance.

LCCA of solar-energy technology primarily depends on some critical parameters listed below:

- initial investment (present value/first cost) for construction of solar-energy technology (P);
- annual operating cost (O);
- annual maintenance cost (M);
- annual energy output in term of either thermal energy or exergy (AEC);
- interest rate (i);
- CO_2 credit (C–C);
- impact on the environment due to CO_2 emission by embodied energy;
- overhauling cost of renewable-energy system, if any, during life of the system (OC);

- energy-payback time (EPBT); and
- life (n) and salvage value (s) of the system.

In the forthcoming section, definitions of different terms, such as "energy-payback time," "cash-flow diagram," "inflation," and "taxation," etc., will be discussed.

20.2 Cost Analysis

Financial evaluation of solar-energy technologies depends on various parameters, which will be discussed briefly with the required formulation. There are as follows.

20.2.1 Future Value Factor or Compound-Interest Factor (CIF)

Let P be the initial investment (present value/first cost) of a solar-technology system at zero time ($n = 0$) at the interest rate of i per year. If the future value of the solar technology at the nth year is S_n, then based on the following cash flow,
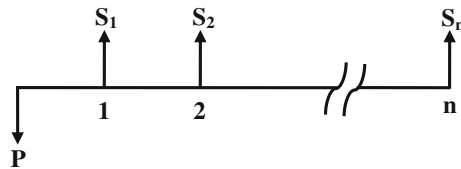
the future value (S_n) in the term of present value at the nth years can be obtained as

$$\text{Future value } (S_n) = \text{Present value } (P) \times \text{Future value factor } (F_{PS}) \qquad (20.1)$$

where F_{PS} is the conversion factor for the present value to the future value, which is expressed as

$$F_{PS,i,n} = (1+i)^n \qquad (20.2)$$

If analysis is done for time <1 year, say, p equal units of time, then n will be replaced by np, and i will be replaced by i/p; then

$$S = P\left(1 + \frac{i}{p}\right)^{np} = P\left[\left(1 + \frac{i}{p}\right)^p\right]^n \qquad (20.3)$$

where $\left(1 + \frac{i}{p}\right)^p = 1 + \text{effective rate of return}$.

20.2.2 Present-Value Factor

If the future value (S_n) needs to be converted to the present value (P), then

$$\text{Present value } (P) = \text{Future value } (S_n) \times \text{Present value factor } (F_{SP}) \qquad (20.4)$$

where F_{SP} is the conversion factor for the future value to the present value, which is expressed as

$$F_{SP,i,n} = (1+i)^{-n} \qquad (20.5)$$

F_{SP} is also known as the "**compound-interest factor**," which is always less than unity. This method is known as the "**discounted cash-flow (DCF) method**," and most of time it is also referred as the "**present value**" (**PV**) or "**net present value**" (**NPV**).

Furthermore,

$$F_{PS} = \frac{1}{F_{SP}} \quad \text{or} \quad F_{PS} \cdot F_{SP} = 1 \qquad (20.6)$$

20.2.3 Uniform Annual Cost (Unacost)

In solving solar-engineering economic problems, expenditures (debits) and receipts (credits) can be considered to be in opposite directions in the cash-flow diagram. Using this concept, a cash-flow diagram based on Sect. 20.2.1 is shown below:
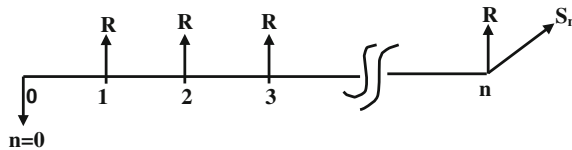
where R is the uniform annual cost (Unacost) at end of each year. This can be expenditures (debits), such as annual operating and maintenance for a solar system, and it can be shown below the line. If R is receipts (credits), such as cost of annual energy saving and carbon credit (CC), from the solar system, then it can be shown above the line of cash flow.

In a cash-flow diagram, the present value/expenditure at $n = 0$ can be converted into the uniform annual cost (unacost) using the following formula as follows:

$$\text{Unacost} = (\text{Present value}) \times (\text{Capital recovery factor}) \qquad (20.7)$$

where, $F_{PR,i,n}$ is known as the "**capital-recovery factor**" (CRF), which is given by

$$F_{PR,i,n} = \left[\frac{i(1+i)^n}{(1+i)^n-1}\right] = \text{CRF} \tag{20.8}$$

Furthermore, to convert uniform annual cost (unacost) (either an expenditures [debits] or receipts [(credits]) to the present value, the following expression is used:

$$\text{Present value} = (\text{Unacost}) \times (\text{Unacost present value factor}) \tag{20.9}$$

where $F_{RP,i,n}$ is the **equal-payment series present-value factor** or the **annuity present-value factor (APVF)**, and its expression is given by

$$F_{RP,i,n} = \left[\frac{(1+i)^n-1}{i(1+i)^n}\right] \tag{20.10}$$

Equations (20.8) and (20.10) can be combined to obtain the relation between the **equal-payment series present value factor** and **the capital-recovery factor**

$$F_{RP,i,n} = \left[\frac{1}{F_{PR,i,n}}\right] \tag{20.11}$$

20.2.4 Sinking-Fund Factor (SFF)

The future value S_n is generally known as a salvage value. It is also known as scrap value/residual value. It can be equally distributed for n years similar to unacost, R. It is also known as the "***uniform end-of-year annual amount***," but it will correspond to the future value S_n.

The **uniform end-of-year annual amount** equivalent to the unacost for a future value can be obtained from the following expression:

$$\text{Unacost} = (\text{Future amount}) \times (\text{Sinking fund factor}) \tag{20.12}$$

where

$$(\text{sinking fund factor SFF}) = F_{SR,i,n} = \left[\frac{i}{(1+i)^n-1}\right] \tag{20.13}$$

SFF is a factor used to calculate the **uniform end-of-year annual amount** for the salvage value of the system.

For a known unacost, the future value can also be calculated as

$$\text{Future amount} = (\text{Unacost}) \times (\text{Equal payment series future value factor}) \tag{20.14}$$

where

$$\text{equal payment series future value factor} = F_{RS,i,n} = \left[\frac{(1+i)^n - 1}{i}\right] \qquad (20.15)$$

The **sinking-fund factor** is reciprocal of the equal-**payment series future value factor**.

20.3   Cash Flow

With cash flow, one can represent all parameters mentioned in Sect. 20.1 graphically on time scale to understand the engineering economics of a solar-technology system. A cash-flow diagram is the most important element for performing a cost analysis of the system. It represents the amount of money inflow into the system and the amount of money outflow from the system.

As mentioned previously, the net cash flow can be represented by a cash-flow diagram as shown below:
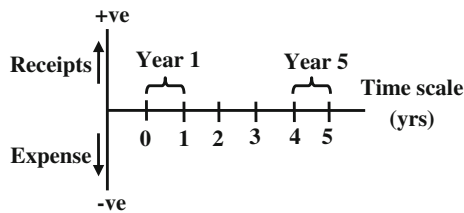
In the above cash-flow diagram, all annual receipts (e.g., the cost of annual energy savings, C-credit (CC), salvage value at the nth year, etc.) as well as expenditures (e.g., annual operating and maintenance [O&M], overhaul cost of the system at any time, etc.) have been converted into the present value.

The net cash flow is calculated as

$$\text{Net cash flow} = \text{Receipts (Credits)} - \text{Expenditures (Debits)} \qquad (20.16)$$

For economical viability, the net cash flow should be positive for any solar-technology system.

In the above cash-flow diagram, a finite time scale has been assumed. It is based on a **uniform end-of-year annual amount (R)** at the end of each year.

20.4   Capitalized Cost

In Sect. 20.3, cash flow is based on a finite time scale. After determining the net cash flow, each net cash flow is repeated on an infinite time scale as shown in the diagram below.

Capitalized cost is the present value on an infinite time basis. For a system costing P_n and lasting n years, the present value replacing out to infinity is as follows:

$$K = P_n \left[1 + \frac{1}{(1+i)^n} + \frac{1}{(1+i)^{2n}} + \cdots \right] = P_n \sum_{x=0}^{\infty} \frac{1}{(1+i)^{xn}} = P_n \frac{(1+i)^n}{(1+i)^n - 1}$$

$$(20.17)$$

Equation (20.17) can also be expressed as

$$\text{Capitalized cost} = \text{net present value (cash flow) on basis } n \text{ years time scale}$$
$$\times \text{ (capitalized cost factor)}$$

where the capitalized cost factor $F_{PK,i,n}$ is given by

$$F_{PK,i,n} = \frac{(1+i)^n}{(1+i)^n - 1} \tag{20.18}$$

From Eq. (20.8), one can write

$$F_{RP,i,n} = iF_{PK,i,n} \tag{20.19}$$

or,

$$\text{Capital recovery factor (CRF)} = \text{rate of return}$$
$$\times \text{ capitalized cost factor (CCF)}$$

Uniform end-of-year annual amount (R) and capitalized cost (K) are expressed as

$$R = iK \tag{20.20}$$

or

$$\text{Unacost} = \text{rate of return} \times \text{(capitalized cost factor)}$$

Example 20.1 Two solar-energy systems have the following cost comparison. By using the capitalized method, determine which system is economical.

Cost components (USD $)	System (A)	System (B)
First cost	20,000	30,000
Uniform end-of-year maintenance	4000	3000
Salvage value	500	1500
Service life (years)	2	3
Rate of interest (i) (%)	10	10

Solution

In this case, the net present value (NPV) for both systems should be calculated using Eqs. (20.5) and (20.9) and with help of cash-flow diagrams. One can obtain the following:

$$\text{NPV of system A}(P_{A2}) = \text{USD\$26,529} \quad \text{and}$$
$$\text{NPV of system B}(P_{B3}) = \text{USD\$36,334.}$$

Furthermore, by using the capitalized-cost method (Eq. 20.17), we get

$$K_A = P_{A2}, F_{PK,10\%,2} = 26,529 \times 5.7619 = \text{US\$152,857.45}$$
$$K_B = P_{B3}, F_{PK,10\%,2} = 36,334 \times 4.0211 = \text{US\$146,102.65}$$

The ratio of the capitalized cost is obtained as

$$\frac{K_A}{K_B} = \frac{152,857.45}{146,102.65} = 1.0462$$

It is clear from the above calculation that system B is more economical than system A.

20.5 Net Present Value (NPV)

For NPV, the following cash-flow diagram should be prepared based on available expenditure (debits) or receipt (credits) data as follows:
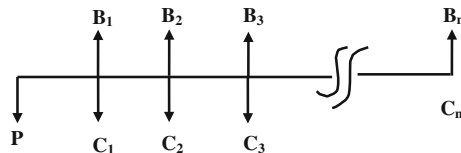
Here, receipts (credits) and expenditures (debits) are denoted as B_j and C_j, respectively, at the jth year. The numerical values of B_j include all credits such as

annualized salvage value, annual C-credit, cost of annual energy savings, etc. In the same way, C_j includes annual O&M and annual overhauling cost (if any). The initial investment (P) will be always negative. NPV of the investment is mathematically given as follows:

$$NPV = -P + \sum_{j=1}^{n} \frac{B_j - C_j}{(1+i)^j}$$

For $(B_j - C_j)$ constant and for all j except for $j = 0$

$$NPV = -P + (B - C) \sum_{j=1}^{n} \frac{1}{(1+i)^n} = -P + (B - C)\left[\frac{(1+i)^n - 1}{i(1+i)^n}\right] \quad (20.21)$$

The above equation is valid for a constant rate of interest per year and $(B_j - C_j)$. For an unequal rate of interest and $(B_j - C_j)$, Eq. (20.21) becomes

$$NPV = P + \frac{B_1 - C_1}{(1+i_1)} + \frac{B_2 - C_2}{(1+i_1)(1+i_2)} + \cdots + \frac{B_j - C_j}{(1+i_1)(1+i_2)\cdots(1+i_j)}$$
$$+ \cdots + \frac{B_n - C_n}{(1+i_1)(1+i_2)\cdots(1+i_n)}$$

$$(20.22)$$

The NPV of any project determines whether a particular project should be accepted or rejected: If **NPV > 0, accept the project**; if **NPV = 0, remain indifferent**; and if **NPV < 0, reject the project**.

Example 20.2 A PV system for water pumping has the following input data for a life of 30 years:

$P = US\$10,000$; $B_j = US\$1200$ worth of diesel fuel annual saving; annual maintenance cost estimated at $C_j = US\$100$ Calculate the NPV of the investment at an interest rate of 8 %.

Solution
The net annual benefits of using a PV system $(B - C) = 1200 - 100 = US\$1100$.
For constant net annual benefits, Eq. (20.21) can be used for determining the NPV as follows:

$$NPV = -P + (B - C)\left[\frac{(1+i)^n - 1}{i(1+i)^n}\right]$$
$$= -10,000 + 1100\left[\frac{(1+0.08)^{30} - 1}{0.08(1+0.08)^{30}}\right]$$
$$= -10,000 + 12,384 = US\$2384$$

Therefore, an investment in the PV system is a financially viable for a farmer.

20.6   Analytical Expression for Payout Time

The payback period (n) is defined as the number of years to recover the initial investment P. This can be obtained by making the NPV Eq. (20.21) for $\left(B_j - C_j\right)$ constant for all j except for $j = 0$ is zero as follows:

$$\text{NPV} = -P + (B - C)\left[\frac{(1+i)^n - 1}{i(1+i)^n}\right] = 0$$

where $(B - C)$ is the net cash flow (CF) at the end of every year:
  For $i = 0$, $n = \frac{P}{\text{CF}}$.
  For the unequal saving in every year, the expression of n can be given as
  or

$$n = \frac{\ln\left[\frac{\text{CF}}{\text{CF} - P \times i}\right]}{\ln[1 + i]} \tag{20.23}$$

20.7   Benefit–Cost Analysis

For mutually exclusive projects, the B/C ratio gives a method to compare them against each other. We will define some terminology that is going to be used for B/C analysis as follows.

Owner (Public/users): This is the entity that incurs the costs.
Benefits (B): Benefits are the advantages to the owner. These will be positive in the cash-flow diagram. All benefits, such salvage value, annual C-credit, cost of annual energy savings, etc., should be converted into present value as follows:

$$B = \sum_{j=1}^{n} \frac{B_j}{(1+i)^j}$$

Costs (C): These are the anticipated expenditures for annual O&M, annual over-hauling cost, etc., and should be converted into the present value and then added to the construction cost (P) as follows:

$$C = \sum_{j=1}^{n} \frac{C_j}{(1+i)^j} + P$$

For a larger project, the initial investment (P) is required in the first M-period.

$$P = C_0 = \sum_{j=0}^{m} \frac{C_j}{(1+i)^j}$$

After the M-period, the annual costs for annual O&M, annual overhauling cost, etc., accrue in each of the following periods until the end of the useful life of n periods; then

$$C'' = \sum_{j=m+1}^{n} \frac{C_j}{(1+i)^j}$$

Disbenefits (D): The project involves disadvantages/loss per year to the owner. This should be also converted into present value.

A project is considered to be attractive when the benefits derived from its execution exceed its associated costs.

The conventional B/C ratio is calculated as

$$B/C = (\text{Benefits} - \text{Disbenefits})/\text{cost} = (B - D)/C \qquad (20.24)$$

The B/C ratio influences the decision on the project approval.
If

$$B/C > 1, \quad \text{accept the project}$$
$$B/C < 1, \quad \text{reject the project}$$

Example 20.3 The building regulation in a city stipulates that all new student hostels must use a solar-energy hot-water system. There are two options available, namely:

Alternative X: Double-glazed flat-plate collectors; and
Alternative Y: Evacuated tubular collectors.

The associated costs and benefits are tabulated below:

Cost and benefits	Amount (USD$)	
	Alternative X	Alternative Y
Capital cost	32,00,000	27,00,000
Annual maintenance cost	50,000	80,000
Annual benefits due to fuel savings	6,00,000	5,60,000
Life, Years (N)	20	20
Interest ratio (i)	10	10
Salvage value (S)	0	0

Which option should be preferred on the basis of incremental net benefit–cost ratio?

Solution

As a stipulated by the latest building regulations in the city, one of the two alternatives should be chosen. Thus, the lower (alternative Y) need not be compared with the do-nothing alternative. Instead, alternatives X and Y are compared with each other in terms of their incremental costs and benefits. The incremental capital cost of alternative X compared with alternative Y is USD500,000(US\$3,200,000 − US\$2,700,000); similarly the incremental net annual benefits of alternative X compare with the net annual benefits of alternatives Y are

$$(600{,}000 - 50{,}000) - (560{,}000 - 80{,}000) = 550{,}000 - 480{,}000 = \text{US\$70,000}$$

The cumulative present worth of the incremental benefits over 20 years of useful life of alternative X compared with alternative Y is

$$= \sum_{j=1}^{n} \frac{70{,}000}{(1+i)^j} = 70{,}000 \left[\frac{(1+0.1)^{20} - 1}{0.1(1+0.1)^{20}} \right] = 70{,}000 \times 8.51 = \text{US\$595,949.4}$$

Thus, the net incremental benefit–cost ratio $= 595{,}949.4/500{,}000 \approx 1.19$.

A value greater than one for the ratio of net incremental benefits to incremental capital cost implies that the additional discounted benefits more than justify the extra capital cost of alternative X compared with alternative Y. Therefore, alternative X should be selected for installation on the hostel.

The computation for the net benefit–cost ratio for each alternative independent of each other is given below.

The net benefit–cost ratio for alternative X is

$$= \frac{(600{,}000 - 50{,}000) \left[\frac{(1+0.1)^{20} - 1}{0.1(1+0.1)^{20}} \right]}{3{,}200{,}000} = \frac{550{,}000 \times 8.51}{3{,}200{,}000} = 1.463$$

Similarly, the net benefit–cost ratio for alternative Y is

$$= \frac{(560{,}000 - 80{,}000) \left[\frac{(1+0.1)^{20} - 1}{0.1(1+0.1)^{20}} \right]}{3{,}200{,}000} = \frac{480{,}000 \times 8.51}{2{,}700{,}000} = 1.513$$

It may be noted that an appraisal of the two alternatives using their net benefit–cost ratios would suggest that alternative Y is selected.

Because the results obtained with the two methods do not match, the NPVs of both alternatives are determined to identify the correct method.

The NPV of alternative X is

$$\text{NPV}_X = -3{,}200{,}000 + (600{,}000 - 50{,}000)\left[\frac{(1+0.1)^{20}-1}{0.1(1+0.1)^{20}}\right]$$

$$= -3{,}200{,}000 + 550{,}000 \times 8.51 = \text{US}\$1{,}480{,}500$$

The NPV of alternative Y is

$$\text{NPV}_Y = -2{,}700{,}000 + (560{,}000 - 80{,}000)\left[\frac{(1+0.1)^{20}-1}{0.1(1+0.1)^{20}}\right]$$

$$= -2{,}700{,}000 + 480{,}000 \times 8.51 = \text{US}\$1{,}384{,}800$$

i.e., $\text{NPV}_X > \text{NPV}_Y$

Thus, the appraisal based on incremental costs and benefits is correct.

20.8   Internal Rate of Return (IRR)

The internal rate of return (IRR) of an investment, P, is the discount rate at which the NPV of costs (negative cash flows, Figure, Sect. 20.3) of the investment equals the NPV of the benefits (positive cash flows, Figure, Sect. 20.3) of the investment. Mathematically, it is expressed as

$$P + \sum_{j=1}^{n}\frac{C_j}{(1+i_{\text{IRR}})^j} = \sum_{j=1}^{n}\frac{B_j}{(1+i_{\text{IRR}})^j} \quad \text{or}$$

$$\sum_{j=1}^{n}\frac{B_j}{(1+i_{\text{IRR}})^j} - \left[P + \sum_{j=1}^{n}\frac{C_j}{(1+i_{\text{IRR}})^j}\right] = \left[\sum_{j=0}^{n}\frac{B_j - C_j}{(1+i_{\text{IRR}})^j}\right] = 0 \qquad (20.25)$$

Because at $j = 0$, $C_0 = P$ and $B_0 = 0$.

Equation (20.21) gives the present value of a series of cash flows $(B_j - C_j)$ to zero at the IRR.

The IRR is widely used in the appraisal of projects due to following facts;

- The IRR on a project is its expected rate of return,
- It employs a percentage rate of return as the decision variable, which suits the banking community.
- For situations in which (IRR) exceeds the cost of the funds used to finance the project, a surplus would remain after paying for the capital investment, P.

Iterative method to compute IRR in Eq. (20.25)
The following steps are suggested:

- Step 1: Make a guess at a trial rate of interest as follows:
  For constant net cash flow, i.e., $(B_j - C_j) = (B - C)$ and for all j except for $j = 0$ and following Eq. (20.21), Eq. (20.25) becomes

$$\sum_{j=1}^{n} \frac{B_j}{(1 + i_{IRR})^j} - \left[P + \sum_{j=1}^{n} \frac{C_j}{(1 + i_{IRR})^j} \right] = -P + \sum_{j=1}^{n} \frac{B_j - C_j}{(1 + i_{IRR})^j}$$

$$= -P + (B - C) \sum_{j=1}^{n} \frac{1}{(1 + i_{IRR})^j} = 0$$

For infinite series, i.e., $n \to \infty$, above the equation becomes

$$-P + \frac{(B - C)}{i_{IRR}} = 0 \quad \text{or} \quad i_{IRR} = \frac{(B - C)}{P} \tag{20.26}$$

- Step 2: Using the greater value of the interest rate calculated in step 1, calculate the

$$\text{Net NPV} = \sum_{j=1}^{n} \frac{B_j}{(1 + i_{IRR})^j} - \left[P + \sum_{j=1}^{n} \frac{C_j}{(1 + i_{IRR})^j} \right] \tag{20.27}$$

- Step 3: If the above-calculated value is positive, then repeat the calculation until it becomes negative.
- Step 4: Proceed with steps 2 and 3 again until one value of $i(=i_1)$ is found at a positive (+) NPV and the next higher value of $i(=i_2)$ is found with a negative NPV.
- Step 5: Solve for the value of IRR $= i_{IRR}$ by using the following:

$$i_{IRR} = i_1 - \text{NPV}_1 \frac{(i_2 - i_1)}{\text{NPV}_2 - \text{NPV}_1} \tag{20.28}$$

The IRR is a measure of profitability for the assessment of the project.

Example 20.4 Evaluate the IRR for the initial investment (P) of US$500,000 in a PV plant with a life (n) of 10 years. From the PV plant, an annual income (B) of USD$145,000 has been generated without any salvage value ($S = 0$) or annual operating and maintenance cost ($C = 0$).

Solution

From Eq. (20.26), one obtains

$$i_{IRR} = \frac{(B-C)}{P} = \frac{145,000}{500,000} = 0.29$$

Let us assume first $i = 0.29$; then from Eq. (20.26) with $C_j = 0$, one has

$$NPV_1 \text{ at } 29\% = 145,000 \times \left[\frac{(1+0.29)^{10}-1}{0.29(1+0.29)^{10}}\right] - 500,000$$
$$= 460,868.5 - 500,000 = US\$(-39,131.5)$$

It has negative sign, and hence $i = i_2$ and $NPV = NPV_2$ of Eq. (20.27). Now we should calculate for a positive NPV with an interest rate <29 %. Let assume that the new interest rate 25 %.

$$NPV \text{ at } 25\% = 145,000 \times \left[\frac{(1+0.25)^{10}-1}{0.25(1+0.25)^{10}}\right] - 500,000$$
$$= 145,000 \times 3.57 - 500,000 = US\$17,722$$

Now, the NPV = NPV_1 at $i = i_1 = 25\%$ is positive, so the new approximate i_{IRR} will be evaluated using Eq. (20.28) as

$$i_{IRR} = 0.25 - 17,722\left[\frac{0.29 - 0.25}{-39,131.5 - 17,722}\right] = 0.2624(26.24\%)$$

For better estimate of the true IRR, the NPV should be evaluated at $i = 0.2624\,(26.24\%)$ as

$$= 145,000 \times \left[\frac{(1+0.2624)^{10}-1}{0.2624(1+0.2624)^{10}}\right] - 500,000$$
$$= 498,807.9 - 500,000 = US\$(-1192.16)$$

The new i_{IRR} will be

$$i_{IRR} = 0.25 - 17,722\left[\frac{0.2624 - 0.25}{-1192 - 17,722}\right] = 0.2616(26.16\%)$$

Similarly, a more accurate i_{IRR} will be obtained.

20.9 Effect of Depreciation

The following terms are defined to better understand the effect of depreciation:

Initial cost/investment (P): This is also referred to as the "**First cost/initial value/single amount**." It is the total installed cost (purchase price, delivery, and installation fee) of the solar system.

Salvage value (S): This is the expected market value at the end of the useful life of the solar system. It can be negative if the cost of dismantling/disposing of the system is more than the salvage value; it can also be zero.

Depreciation (C_d): This is an expenditure that is responsible for decreasing the value of the system over time. Mathematically, it is defined as

$$C_d = P - S \tag{20.29}$$

Depreciation rate (D_t): This is defined as the fraction of the first cost (P) removed through depreciation. Straight-line (SL) depreciation is the simplest and most often used method. Mathematically, it can be expressed as follows:

$$\text{Annual depreciation,} \quad D_n = \frac{(P - S)}{n} \tag{20.30}$$

where n is the life of the solar thermal/photovoltaic system.

The present value of annual depreciation (D_n) without tax is given by

$$P_D = \frac{(P - S)}{n} \left[\frac{1}{(1+i)} + \frac{1}{(1+i)^2} + \frac{1}{(1+i)^3} \cdots + \frac{1}{(1+i)^n} \right] \tag{20.31}$$

$$\text{or} \quad P_D = \frac{(P - S)}{n} \frac{(1+i)^n - 1}{i(1+i)^n} = \frac{(P - S)}{n} F_{RP,i,n} = (P - S)F_{SLP,i,n}$$

where the straight-line depreciation conversion factor $F_{SLP,i,n}$ is given by

$$F_{SLP,i,n} = \frac{1}{n} \frac{(1+i)^n - 1}{i(1+i)^n} \tag{20.32}$$

If i is the interest rate before tax and t is tax benefit on i, then the interest rate after tax benefit is given by $r = i(1 - t)$.

The cash flow of the unacost with tax is shown below
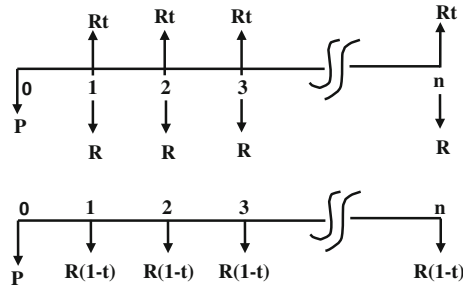
The present value of the unacost with tax is given by

$$P_T = \frac{R(1-t)}{(1+r)} + \frac{R(1-t)}{(1+r)^2} \cdots + \frac{R(1-t)}{(1+r)^n} = R(1-t)F_{RP,i,n} \qquad (20.33)$$

The cash flow of the unacost with depreciation and tax is shown below:
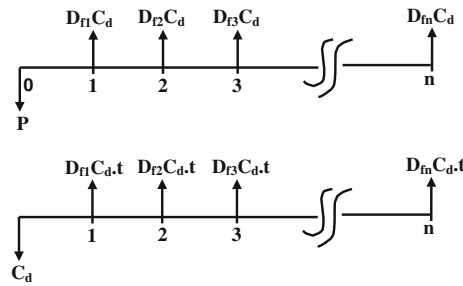
The present cost with depreciation and tax is shown below:

$$P = C_d - D_n t \left[\frac{1}{(1+r)} + \frac{1}{(1+r)^2} + \frac{1}{(1+r)^3} + \cdots + \frac{1}{(1+r)^n} \right]$$
$$= C_d \left[1 - tF_{SLP,i,n} \right] \qquad (20.34)$$

After knowing the present value, P, one can write an expression for the unacost (R) and capitalized cost (K) with depreciation and cost as follows:

$$R = PF_{PR,i,n} = C_d \left[1 - tF_{\text{SLP},i,n}\right] F_{PR,i,n} \qquad (20.35)$$

and

$$K = PF_{PK,i,n} = C_d \left[1 - tF_{\text{SLP},i,n}\right] F_{PK,i,n} \qquad (20.36)$$

Book value (B): Book value is defined as original cost minus the accumulated depreciation. At the beginning of the first year, the book value of depreciation is the initial **cost/investment** at $n = 0$. The book value is usually determined at the end of each year.

Mathematically, the book value (B_n) at the nth year is expressed as

$$(B_n) = \text{Initial cost/investment} \ (P) - \text{accumulated depreciation cost} \left(\sum_1^n D_n\right)$$

$$(20.37)$$

For example, a PV with an initial cost/investment (P) of US\$15,000 has a salvage value (S) of US\$5000 after 5 years.

An annual depreciation of a PV system $= \frac{(15,000-5000)}{5} = \$2000$.

The book value at the end of the current year equals the book value at the beginning of the next year. The PV system is depreciated until the book value equals the salvage/scrap value.

Annual depreciation ($)	Accumulated depreciation cost at year end ($)	Book value at year end ($)
		(P) 15,000
2000	2000	13,000
2000	4000	11,000
2000	6000	9000
2000	10,000	7000
2000	12,000	(S) 5000

Recovery period (n): The recovery period in years (n) is the period during which a user is able to write off a portion of an asset's value each year until the end of it's useful life. It is also referred to as the "**expected life**" in years.

Objective Questions

20.1 The capital-recovery factor (F_{PR}) is always
      (a) >1   (b) >1   (c) =1   (d) none of these
      Answer: (a)

20.2 The compound-interest factor (CIF) (F_{PS}) is always
      (a) <1   (b) >1   (c) =1   (d) none of these
      Answer: (b)

20.3 The present-value factor (F_{SP}) is always
      (a) >1   (b) >1   (c) =1   (d) none of these
      Answer: (a)

20.4 The compound-interest operator is always
      (a) <1   (b) >1   (c) =1   (d) none of these
      Answer: (b)

20.5 The sinking fund factor (SFF), F_{SR} is always
      (a) <1   (b) >1   (c) =1   (d) none of these
      Answer: (a)

20.6 The sinking fund factor (SFF), F_{SR} is
      (a) proportional to F_{SR} (b) inversely proportional to F_{SR}
      (c) equal to F_{SR} (d) none of these
      Answer: (b)

20.7 The payback time period depends on
      (a) cash flow   (b) initial investment
      (c) use of these systems   (d) both (a) and (b)
      Answer: (d)

20.8 The project is economically accepted if B/C is always
      (a) <1   (b) >1   (c) =1   (d) none of these
      Answer: (b)

20.9 The rate of return after tax
      (a) increases   (b) decreases   (c) unaffected   (d) none of these
      Answer: (b)

20.10 The conversion factor from straight-line depreciation to the present value
      with tax is
      (a) lower without tax   (b) higher without tax
      (c) equal without tax   (d) none of these
      Answer: (a)

20.11 Straight-line depreciation is
      (a) directly proportional to n (b) inversely proportional to n
      (c) equal to n (d) none of these
      Answer: (b)

20.12 The expression for total depreciation (C_{d}) is given by
      (a) $C_i - C_{sal}$ (b) $C_i.C_{sal}$
      (c) $C_i + C_{sal}$ (d) none of these
      Answer: (a)

20.13   The expression for future depreciation at end of the mth year (FD_m) is given by
  (a) $C_d\left[1-\frac{m}{n}\right]$ (b) $C_d\frac{m}{n}$
  (c) $C_d\left[1+\frac{m}{n}\right]$ (d) none of these
  Answer: (a)

20.14   The expression for book value (B_m) at the end of the mth year is given by
  (a) $C_{sal}+FD_m$ (b) $C_{sal}-FD_m$ (c) $C_{sal}.FD_m$ (d) None of these
  Here, $FD_m = C_d\left[1-\frac{m}{n}\right]$
  Answer: (a)

20.15   The value of unacost after tax is
  (a) reduced   (b) increased   (c) unaffected   (d) none of these
  Answer: (b)

20.16   The value of $F_{PR,r,n}$ is always
  (a) more than $F_{PR,i,n}$ (b) less than $F_{PR,i,n}$ (c) equal to $F_{PR,i,n}$
  (d) none of these
  Answer: (a)

20.17   The expression for $F_{PR,r,n}$ is
  (a) $\frac{r(1+r)^n}{(1+r)^n-1}$ (b) $\frac{(1+r)^n-1}{r(1+r)^n}$ (c) $\frac{i(1+i)^n}{(1+i)^n-1}$ (d) $\frac{(1+i)^n-1}{i(1+i)^n}$
  Answer: (a)

20.18   The expression for $F_{SR,r,n}$ is
  (a) $\frac{r}{(1+r)^n-1}$ (b) $\frac{(1+r)^n-1}{r}$ (c) $\frac{i}{(1+i)^n-1}$ (d) $\frac{(1+i)^n-1}{i}$
  Answer: (a)

20.19   The expression for payback period (n) without interest rate and uniform cash flow is
  (a) $\frac{P}{CF}$ (b) $\frac{CF}{P}$ (c) $P.CF$ (d) none of these
  Answer: (a)

20.20   The tax rate is always
  (a) <1   (b) >1   (c) =1   (d) none of these
  Answer: (a)

Additional References

1. M.A. Hossain, J.L. Woods, B.K. Bala, Renew. Energy **30**, 729 (2005)
2. J. Mumba, Energy Convers. Manag. **37**(5), 615 (1996)
3. A. Kumar, T.C. Kandpal, Sol. Energy **78**(2), 321 (2005)
4. M.S. Sodha, R. Chandra, K. Pathak, N.P. Singh, N.K. Bansal, Energy Convers. Manag. **31**(6), 509 (1991)
5. P. Barnwal, A. Tiwari, Int. J. Agric. Res. **3**(2), 110 (2008)
6. K.K. Humphreys, *Jelen's Cost and Optimization Engineering*, 3rd edn. (McGraw-Hill Inc, New York, 1991)
7. T.B. Leland, T.J. Anthony, *Engineering Economy*, 3rd edn. (McGraw-Hill Inc, New York, 1989)

For More Examples and Problems in this Chapter, Please See the Following References

8. G.N. Tiwari, *Solar Energy: Fundamental, Design, Modelling and Applications* (Narosa Publishing House, New Delhi, CRC Press, New York, 2004)
9. G.N. Tiwari, S. Dubey, *Fundamentals of Photovoltaic Modules and Their Applications* (RSC Publishing, UK, 2010)
10. B. Agrawal, G.N. Tiwari, *Building Integrated Photovoltaic Thermal Systems* (RSC Publishing, UK, 2010)
11. G.N. Tiwari, R.K. Mishra, *Advanced Renewable Energy Sources* (RSC Publishing, UK, 2011)

Appendix I

Conversion of units

(i) Length, m
1 yd (yard) = 3 ft = 36 in (inches) = 0.9144 m
1 m = 39.3701 in = 3.280839 ft = 1.093613 yd = 1650763.73 wavelength
1 ft = 12 in = 0.3048 m
1 in = 2.54 cm = 25.4 mm
1 mile = 2.54 × 10^{-3} cm
1 μm = 10^{-6} m
1 nm = 10^{-9} m = 10^{-3} μm
(ii) Area, m^2
1 ft^2 = 0.0929 m^2
1 in^2 = 6.452 cm^2 = 0.00064516 m^2
1 cm^2 = 10^{-4} m^2 = 10.764 × 10^{-4} ft^2 = 0.1550 in^2
1 ha = 10,000 m^2
(iii) Volume, m^3
1 ft^3 = 0.02832 m^3 = 28.3168 l (litre)
1 in^3 = 16.39 cm^3 = 1.639 × 10^2 l
1 yd^3 = 0.764555 m^3 = 7.646 × 10^2 l
1 UK gallon = 4.54609 l
1 US gallon = 3.785 l = 0.1337 ft^3
1 m^3 = 1.000 × 10^6 cm^3 = 2.642 × 10$^{1\ 2}$ US gallons = 109 l
1 l = 10^{-3} m^3
1 fluid ounce = 28.41 cm^3
(iv) Mass, kg
1 kg = 2.20462 lb = 0.068522 slug
1 ton (short) = 2000 lb (pounds) = 907.184 kg
1 ton (long) = 1016.05 kg
1 lb = 16 oz (ounces) = 0.4536 kg
1 oz = 28.3495 g
1 quintal = 100 kg

(continued)

1 kg = 1000 g = 10,000 mg
1 μg = 10^{-6} g
1 ng = 10^{-9} g
(v) **Density and specific volumes, kg/m^3, m^3/kg**
1 lb/ft^3 = 16.0185 kg/m^3 = 5.787 × 10^{-4} lb/in^3
1 g/cm^3 = 10^3 kg/m^3 = 62.43 lb/ft^3
1 lb/ft^3 = 0.016 g/cm^3 = 16 kg/m^3
1 ft^3 (air) = 0.08009 lb = 36.5 g at N.T.P.
1 gallon/lb = 0.010 cm^3/kg
1 μg/m^3 = 10^{-6} g/m^3
(vi) **Pressure, Pa (Pascal)**
1 lb/ft^2 = 4.88 kg/m^2 = 47.88 Pa
1 lb/in^2 = 702.7 kg/m^2 = 51.71 mm Hg = 6.894757 × 10^3 Pa = 6.894757 × 10^3 N/m^2
1 atm = 1.013 × 10^5 N/m^2 = 760 mm Hg = 101.325 kPa
1 in H$_2$O = 2.491 × 10^2 N/m^2 = 248.8 Pa = 0.036 lb/in^2
1 bar = 0.987 atm = 1.000 × 10^6 dynes/cm^2 = 1.020 kgf/cm^2 = 14.50 lbf/in^2 = 10^5 N/m^2 = 100 kPa
1 torr (mm Hg 0 °C) = 133 Pa
1 Pa (Pascal) = 1 N/m^2 = 1.89476 kg
1 inch of Hg = 3.377 kPa = 0.489 lb/in^2
(vii) **Velocity, m/s**
1 ft/s = 0.3041 m/s
1 mile/h = 0.447 m/s = 1.4667 ft/s = 0.8690 knots
1 km/h = 0.2778 m/s
1 ft/min = 0.00508 m/s
(viii) **Force, N**
1 N (Newton) = 10^5 dynes = 0.22481 lb wt = 0.224 lbf
1 pdl (poundal) = 0.138255 N (Newton) = 13.83 dynes = 14.10 gf
1 lbf (i.e. wt of 1 lb mass) = 4.448222 N = 444.8222 dynes
1 ton = 9.964 × 10^3 N
1 bar = 10^5 Pa (Pascal)
1 ft of H$_2$O = 2.950 × 10^{-2} atm = 9.807 × 10^3 N/m^2
1 in H$_2$O = 249.089 Pa
1 mm H$_2$O = 9.80665 Pa
1 dyne = 1.020 × 10^{-6} kgf = 2.2481 × 10^{-6} lbf = 7.2330 × 10^{-5} pdl = 10^{-5} N
1 mm of Hg = 133.3 Pa
1 atm = 1 kgf/cm^2 = 98.0665 k Pa
1 Pa (Pascal) = 1 N/m^2
(ix) **Mass flow rate and discharge, kg/s, m^3/s**

(continued)

1 lb/s = 0.4536 kg/s
1 ft^3/min = 0.4720 1/s = 4.179 × 10^{-4} m^3/s
1 m^3/s = 3.6 × 10^6 l/h
1 g/cm^3 = 10^3 kg/m^3
1 lb/h ft^2 = 0.001356 kg/s m^2
1 lb/ft^3 = 16.2 kg/m^2
1 l/s = 10^{-3} m^3/s
(x) **Energy, J**
1 cal = 4.187 J (Joules)
1 kcal = 3.97 Btu = 12 × 10^{-4} kWh = 4.187 × l0^3 J
1 W = 1.0 J/s
1 Btu = 0.252 kcal = 2.93 × 10^{-4} kWh = 1.022 × 10^3 J
1 hp = 632.34 kcal = 0.736 kWh
1 kWh = 3.6 × 10^6 J = 1 unit
1 J = 2.390 × 10^{-4} kcal = 2.778 × 10^{-4} Wh
1 kWh = 860 kcal = 3413 Btu
1 erg = 1.0 × 10^{-7} J = 1.0 × 10^{-7} Nm = 1.0 dyne cm
1 J = 1 Ws = 1 Nm
1 eV = 1.602 × 10^{-19} J
1 GJ = 10^9 J
1 MJ = 10^6 J
1 TJ (Terajoules) = 10^{12} J
1EJ (Exajoules) = 10^{18} J
(xi) **Power, watt (J/s)**
1 Btu/h = 0.293071 W = 0.252 kcal/h
1 Btu/h = 1.163 W = 3.97 Btu/h
1 W = 1.0 J/s = 1.341 × 10^{-3} hp = 0.0569 Btu/min = 0.01433 kcal/min
1 hp (F.P.S.) = 550 ft lb f/s = 746 W = 596 kcal/h = 1.015 hp (M.K.S.)
1 hp (M.K.S.) = 75 mm kgf/s = 0.17569 kcal/s = 735.3 W
1 W/ft^2 = 10.76 W/m^2
1 ton (Refrigeration) = 3.5 kW
1 kW = 1000 W
1 GW = 10^9 W
1 W/m^2 = 100 lx
(xii) **Specific heat, J/kg °C**
1 Btu/lb °F = 1.0 kcal/kg °C = 4.187 × 10^3 J/kg °C
1 Btu/lb = 2.326 kJ/kg
(xiii) **Temperature, °C and K used in SI**
$T_{(Celcius, °C)} = (5/9) [T_{(Fahrenheit, °F)} + 40] - 40$

(continued)

$T_{(\text{°F})} = (9/5)\,[T_{(\text{°C})} + 40] - 40$
$T_{(\text{Rankine,°R})} = 460 + T_{(\text{°F})}$
$T_{(\text{Kelvin,K})} = (5/9)\,T_{(\text{°R})}$
$T_{(\text{Kelvin,K})} = 273.15 + T_{(\text{°C})}$
$T_{(\text{°C})} = T_{(\text{°F})}/1.8 = (5/9)\,T_{(\text{°F})}$

(xiv) Rate of heat flow per unit area or heat flux, W/m^2

1 Btu/ft^2 h = 2.713 kcal/m^2 h = 3.1552 W/m^2

1 kcal/m^2 h = 0.3690 Btu/ft^2 h = 1.163 W/m^2 = 27.78 × 10^{-6} cal/s cm^2

1 cal/cm^2 min = 221.4 Btu/ft^2 h

1 W/ft^2 = 10.76 W/m^2

1 W/m^2 = 0.86 kcal/h m^2 = 0.23901 × 10^{-4} cal/s cm^2 = 0.137 Btu/h ft^2

1 Btu/h ft = 0.96128 W/m

(xv) Heat-transfer coefficient, W/m^2 °C

1 Btu/ft^2 h °F = 4.882 kcal/m^2 h °C = 1.3571 × 10^{-4} cal/cm^2 s °C

1 Btu/ft^2 h °F = 5.678 W/m^2 °C

1 kcal/m^2 h °C = 0.2048 Btu/ft^2 h °F = 1.163 W/m^2 °C

1 W/m^2 K = 2.3901 × 10^{-5} cal/cm^2 s K = 1.7611 × 10^{-1} Btu/ft^2 °F = 0.86 kcal/m^2 h °C

(xvi) Thermal conductivity, W/m °C

1 Btu/ft h °F = 1.488 kcal/m h °C = 1.73073 W/m °C

1 kcal/m h °C = 0.6720 Btu/ft h °F = 1.1631 W/m °C

1 Btu in/ft^2 h °F = 0.124 kcal/m h °C = 0.144228 W/m °C

1 Btu/in h °F = 17.88 kcal/m h °C

1 cal/cm s °F = 4.187 × 10^2 W/m °C = 242 Btu/h ft °F

1 W/cm °C = 57.79 Btu/h ft °F

(xvii) Angle, rad

2π rad (radian) = 360° (degree)

1° (degree) = 0.0174533 rad = 60′ (minutes)

1′ = 0.290888 × 10^{-3} rad = 60″ (seconds)

1″ = 4.84814 × 10^{-6} rad

1° (hour angle) = 4 min (time)

(xviii) Illumination

1 lx (lux) = 1.0 lm (lumen)/m^2

1 lm/ft^2 = 1.0 foot candle

1 foot candle = 10.7639 lx

100 lx = 1 W/m^2

(xix) Time, h

1 week = 7 days = 168 h = 10,080 min = 604,800 s

1 mean solar day = 1440 min = 86,400 s

1 calender year = 365 days = 8760 h = 5.256 × 10^5 min

(continued)

1 tropical mean solar year = 365.2422 days
1 sidereal year = 365.2564 days (mean solar)
1 s (second) = 9.192631770×10^9 Hertz (Hz)
1 day = 24 h = $360°$ (hour angle)
(xx) **Concentration, kg/m^3 and g/m^3**
1 g/l = 1 kg/m^3
1 lb/ft^3 = 6.236 kg/m^3
(xxi) **Diffusivity, m^2/s**
1 ft^2/h = 25.81×10^{-6} m^2/s

Appendix II

The value of $f_{0-\lambda T}$ for different λT, μm K, for even increment of λT

λT, μm K	$f_{0-\lambda T}$	λT, μm K	$f_{0-\lambda T}$	λT, μm K	$f_{0-\lambda T}$
1000	0.0003			8000	0.8562
1200	0.0021	4600	0.5793	8200	0.8639
1400	0.0077	4800	0.6075	8400	0.8711
1600	0.0197	5000	0.6337	8600	0.8778
1800	0.0393	5200	0.6579	8800	0.8841
2000	0.0667	5400	0.6803	9000	0.8899
2200	0.1009	5600	0.7010	9200	0.8954
2400	0.1402	5800	0.7201	9400	0.9005
2600	0.1831	6000	0.7378	9600	0.9054
2800	0.2279	6200	0.7451	9800	0.9099
3000	0.2730	6400	0.7692	10000	0.9141
3200	0.3181	6600	0.7831	12000	0.9450
3400	0.3617	6800	0.7961	14000	0.9628
3600	0.4036	7000	0.8080	16000	0.9737
3800	0.4434	7200	0.8191	18000	0.9807
4000	0.4829	7400	0.8295	20000	0.9855
4200	0.5160	7600	0.8390	50000	0.9988
4400	0.5488	7800	0.8479	$\propto$	1

Appendix III

Appendix IIIA

Parameters on a horizontal surface for sunshine hours = 10 for all four weather type of days for different Indian climates (from Chap. 1, ref. [2])

Type of day	Parameters	January	February	March	April	May	June	July	August	September	October	November	December
(a) New Delhi													
a	T_R	2.25	2.79	2.85	2.72	3.54	2.47	2.73	2.58	2.53	1.38	0.62	0.72
	α	0.07	0.10	0.17	0.23	0.16	0.28	0.37	0.41	0.29	0.47	0.59	0.54
	K_1	0.47	0.39	0.33	0.28	0.20	0.27	0.41	0.40	0.23	0.21	0.21	0.28
	K_2	−13.17	−6.25	5.61	38.32	65.04	31.86	−40.57	−55.08	39.92	32.77	30.62	9.73
b	T_R	2.28	2.78	2.89	3.15	5.44	4.72	5.58	5.43	3.23	4.56	0.19	1.83
	α	0.15	0.13	0.14	0.17	0.16	0.20	0.24	0.18	0.31	0.22	1.14	0.42
	K_1	0.51	0.54	0.49	0.46	0.45	0.45	0.53	0.39	0.37	0.42	0.35	0.40
	K_2	−21.77	−28.26	−9.22	−11.55	1.54	23.99	−51.61	9.46	14.07	−9.50	17.47	−0.07
c	T_R	5.88	6.36	6.11	7.77	9.20	10.54	7.13	7.97	5.51	5.01	4.93	3.23
	α	0.27	0.37	0.37	0.31	0.07	0.06	0.41	0.51	0.49	1.26	1.06	0.64
	K_1	0.39	0.36	0.33	0.35	0.56	0.48	0.47	0.35	0.39	0.36	0.31	0.43
	K_2	−14.73	−7.97	10.87	20.45	−56.00	−0.37	−52.27	47.70	35.64	−0.68	13.06	−7.04
d	T_R	7.47	8.97	10.77	11.18	13.69	12.47	8.21	8.58	9.40	7.24	4.30	4.02
	α	0.96	1.04	0.24	0.07	0.07	0.61	1.26	1.10	0.84	1.29	1.43	1.70
	K_1	0.35	0.30	0.43	0.49	0.48	0.46	0.43	0.43	0.41	0.36	0.31	0.38
	K_2	−25.89	−6.48	−36.46	−44.07	−42.58	−62.66	−56.75	−61.08	−27.09	3.90	20.10	−11.78
(b) Bangalore													
a	T_R	3.36	3.27	3.63	5.05	4.24	4.32	5.18	4.75	4.10	2.28	1.66	1.65
	α	0.07	0.13	0.06	−0.06	0.10	0.19	0.10	0.18	0.13	0.33	0.35	0.36
	K_1	0.33	0.35	0.33	0.29	0.21	0.25	0.32	0.23	0.20	0.05	0.03	0.12
	K_2	−18.05	−22.11	−5.44	14.54	47.81	22.40	−26.04	10.14	38.54	107.04	103.64	47.70

(continued)

(continued)

Type of day		Month											
		January	February	March	April	May	June	July	August	September	October	November	December
	Parameters												
b	T_R	3.24	5.25	6.21	5.72	5.90	7.35	4.12	5.27	4.83	2.43	1.89	3.68
	α	0.31	0.24	0.21	0.19	0.25	0.17	0.51	0.44	0.62	0.56	0.78	0.39
	K_1	0.50	0.45	0.48	0.50	0.41	0.50	0.46	0.50	0.33	0.26	0.37	0.41
	K_2	−60.12	−60.50	−80.04	−75.59	−28.55	−103.35	−90.54	−115.27	13.80	69.14	9.08	−33.76
c	T_R	3.70	4.51	7.74	5.83	4.95	4.39	5.68	2.67	6.64	4.71	5.68	2.02
	α	0.96	0.94	0.63	0.98	0.96	1.12	1.07	1.35	0.78	1.03	0.93	1.44
	K_1	0.46	0.57	0.36	0.50	0.53	0.58	0.50	0.55	0.48	0.43	0.36	0.43
	K_2	−63.02	−129.68	−20.76	−61.13	−103.14	−156.14	−108.34	−161.61	−52.93	−26.53	−15.95	−47.21
d	T_R	6.13	7.49	7.35	6.86	6.33	4.84	4.45	6.68	3.94	3.91	3.84	2.80
	α	1.61	1.31	1.41	1.48	1.59	2.00	2.32	1.69	2.16	2.00	2.04	2.58
	K_1	0.29	0.30	0.40	0.45	0.53	0.61	0.41	0.50	0.38	0.42	0.55	0.27
	K_2	36.80	83.73	−39.85	−72.22	−99.52	−213.29	−79.79	−146.94	−88.62	−125.35	−177.28	−12.29
(c) Jodhpur													
a	T_R	1.26	1.33	1.59	2.82	3.72	3.87	3.25	3.39	3.20	2.26	1.56	1.54
	α	0.37	0.38	0.37	0.27	0.21	0.21	0.27	0.28	0.27	0.33	0.39	0.31
	K_1	0.22	0.14	0.18	0.21	0.20	0.13	0.10	0.17	0.26	0.24	0.23	0.26
	K_2	30.67	63.90	56.40	47.66	50.84	87.88	105.23	59.41	14.42	27.40	22.71	9.48
b	T_R	2.34	2.03	3.00	4.07	5.21	5.50	5.07	4.73	3.81	2.90	2.28	3.43
	α	0.46	0.55	0.42	0.31	0.23	0.28	0.37	0.40	0.35	0.38	0.46	0.24
	K_1	0.33	0.29	0.31	0.34	0.33	0.33	0.34	0.33	0.34	0.30	0.33	0.40
	K_2	12.89	43.13	42.22	23.50	31.22	33.40	35.81	29.57	8.71	24.12	12.35	−11.64

(continued)

(continued)

Type of day	Parameters	January	February	March	April	May	June	July	August	September	October	November	December
c	T_R	3.81	4.78	4.04	4.97	6.87	5.58	4.90	5.10	3.40	3.71	3.28	4.23
	α	0.93	1.32	0.98	0.64	0.61	0.67	1.02	0.88	0.97	2.05	1.31	1.06
	K_1	0.43	0.40	0.42	0.47	0.47	0.46	0.41	0.50	0.48	0.53	0.44	0.44
	K_2	−33.72	12.44	−19.11	−26.93	−44.76	−35.15	2.06	−60.42	−26.96	−62.06	−35.85	−32.84
d	T_R	2.25	5.20	7.09	9.33	8.01	3.52	9.62	3.17	1.63	7.67	1.71	1.94
	α	1.89	1.64	2.03	1.59	1.66	2.37	2.37	2.77	3.24	0.86	2.89	2.03
	K_1	0.44	0.46	0.42	0.44	0.43	0.28	0.52	0.44	0.44	0.52	0.36	0.39
	K_2	−19.31	−45.44	−89.92	−149.27	−117.01	60.69	−221.29	−87.34	−77.55	−26.47	−15.46	−14.88
(d) Mumbai													
a	T_R	1.95	1.80	2.88	3.95	5.40	3.20	3.31	4.25	4.22	3.16	2.97	3.27
	α	0.34	0.37	0.23	0.14	−0.02	0.16	0.61	0.33	0.15	0.30	0.23	0.18
	K_1	0.26	0.19	0.28	0.34	0.28	0.25	0.09	0.12	0.24	0.24	0.26	0.30
	K_2	19.77	53.96	27.13	−0.75	30.06	4.55	27.28	47.27	30.02	15.87	9.11	−4.81
b	T_R	2.96	2.68	3.57	4.98	6.25	6.08	7.74	6.70	4.78	3.93	3.40	4.21
	α	0.43	0.49	0.37	0.25	0.15	0.19	0.20	0.37	0.47	0.47	0.45	0.24
	K_1	0.35	0.31	0.35	0.40	0.42	0.44	0.31	0.39	0.41	0.36	0.34	0.37
	K_2	−0.14	24.17	11.73	−13.57	−13.69	−19.52	61.35	22.16	−14.71	5.99	0.60	−14.17
c	T_R	3.06	2.26	3.24	4.39	5.91	5.97	8.17	4.24	5.36	3.16	2.97	3.75
	α	1.14	1.18	1.10	1.00	0.79	0.86	0.62	1.26	0.98	1.13	1.10	0.91
	K_1	0.59	0.58	0.52	0.54	0.60	0.52	0.54	0.43	0.44	0.47	0.57	0.54
	K_2	−59.86	−47.12	−58.09	−78.37	−111.97	−81.79	−95.21	−34.40	−39.31	−28.02	−48.41	−52.45

(continued)

(continued)

Type of day	Parameters	January	February	March	April	May	June	July	August	September	October	November	December
d	T_R	3.38	7.42	4.45	2.30	4.71	4.71	6.41	7.40	7.46	3.22	5.13	3.05
	α	1.71	1.73	2.29	2.08	2.95	2.66	2.68	1.81	2.14	2.15	1.53	1.51
	K_1	0.52	0.56	0.50	0.35	0.41	0.38	0.32	0.47	0.34	0.42	0.57	0.53
	K_2	−59.78	−26.16	−82.34	63.52	−101.81	−87.19	−61.50	−108.37	−38.68	−25.89	−78.03	−40.51
(e) Srinagar													
a	T_R	1.45	5.37	3.31	4.25	5.41	3.63	5.77	6.45	4.06	2.61	4.03	0.72
	α	0.33	−0.36	−0.03	−0.03	−0.12	0.08	−0.09	−0.23	0.03	0.20	−0.37	0.53
	K_1	0.37	0.63	0.69	0.37	0.51	0.33	0.17	0.37	0.46	0.43	0.66	0.33
	K_2	−6.14	−82.86	−94.01	−10.95	−79.57	−13.73	68.06	−42.79	−60.27	−47.83	−37.00	−6.60
b	T_R	3.09	6.98	4.65	6.92	5.86	6.82	7.40	7.58	6.41	4.04	0.04	0.35
	α	0.38	−0.48	0.23	0.06	0.29	0.11	0.00	−0.13	−0.04	0.19	1.16	1.00
	K_1	0.39	0.83	0.59	0.42	0.32	0.63	0.48	0.38	0.48	0.52	0.37	0.41
	K_2	−23.08	−110.23	−107.74	−49.61	0.26	−167.86	−80.06	−13.91	−66.64	−62.52	−14.63	−12.20
c	T_R	2.35	6.59	6.31	7.57	8.69	8.00	9.72	8.23	7.36	5.02	1.86	0.76
	α	1.64	0.86	1.35	0.57	0.61	0.81	0.69	0.90	0.99	1.49	1.47	1.98
	K_1	0.41	0.42	0.48	0.54	0.50	0.39	0.56	0.49	0.44	0.52	0.41	0.31
	K_2	−37.87	−85.68	−180.45	−120.38	−146.97	−87.44	−228.91	−147.96	−62.10	−93.64	−40.07	−12.15
d	T_R	1.69	1.36	7.52	9.09	9.48	10.79	10.93	8.54	8.16	7.75	3.78	2.44
	α	2.63	2.97	1.87	1.35	1.13	1.56	3.08	1.71	3.15	1.70	1.74	2.04
	K_1	0.43	0.36	0.35	0.62	0.92	0.80	0.45	0.75	0.67	0.55	0.48	0.63
	K_2	−41.27	−44.68	−65.17	−254.24	−467.30	−421.63	−129.49	−356.92	−261.85	−119.53	−49.16	−64.02

Appendix IIIB

For cloudy conditions, the value of T_R will be more than 10.0.

The turbidity factor (T_R) for different months (from Chap. 1, ref. [2])

Region	Month											
	1	2	3	4	5	6	7	8	9	10	11	12
Mountain	1.8	1.9	2.1	2.2	2.4	2.7	2.7	2.7	2.5	2.1	1.9	1.8
Flat land	2.2	2.2	2.5	2.9	3.2	3.4	3.5	3.3	2.9	2.6	2.3	2.2
City	3.1	3.2	3.5	3.9	4.1	4.2	4.3	4.2	3.9	3.6	3.3	3.1

Appendix IIIC

Model type	Model name	Model correlations	Remarks
Solar radiation model for calculation of hourly radiation	Hotel model [1][14]	$I_N = I_{ON}[a_0 + a_1 \exp(-k/\cos\theta_z)]$ $a_0 = 0.4237 - 0.00821(6-A)^2$ $a_1 = 0.5055 - 0.00595(6.5-A)^2$ $k = 0.2711 - 0.01858(2.5-A)^2$	The constants a_0, a_1 and k are functions of the altitude of the location, and A is the altitude in kilometres
	Kasten and Young model [2][15]	$I_N = I_{ON}\exp(-m.\varepsilon.T_R)$ $m = \left[\cos\theta_z + 0.15 \times (93.885 - \theta_z)^{-1.253}\right]^{-1}$ $\varepsilon = 4.529 \times 10^{-4}\,m^2 - 9.66865 \times 10^{-3}\,m + 0.108014$	m is air mass, ε is optical thickness of atmosphere, and T_R is the Linke turbidity factor
	Perez et al. model [3][16]	$I_N = I_{ON}\exp[-T_R/(0.9 + 9.4\cos\theta_z)]$	I_{ON} is solar radiation in the extraterrestrial region, and T_R is the Linke turbidity factor
	ASHRAE model [4][17]	$I = I_N\cos\theta_z + I_d$ $I_N = A\exp(-B/\cos\theta_z)$ $I_d = CI_N$	A, B and C are constants depending on locations. These constants were also found by Nijgorodov[18], Machler[19], Iqbal and Parishwad et al.[20]
	Singh and Tiwari model [5][21]	$I_N = I_{ON}\exp\{-(m.\varepsilon.T_R + \alpha)\}$ $I_{HD} = K_1(I_{ON} - I_N)\cos\theta_z + K_2$	α is atmospheric transmittance for beam radiation, I_{HD} is diffuse radiation on horizontal surface, and K_1 and K_2 are atmospheric transmittances for diffuse radiation. Applicable to different weather conditions
	Jamil and Tiwari model [6][22]	$I_N = I_{ON}\exp\left\{-\left((m.\varepsilon)^2 T_{RO} + (m.\varepsilon).T_R + \alpha\right)\right\}$ $I_{HD} = K_0\{(I_{ON} - I_N)\cos\theta_z\}^2 + K_1(I_{ON} - I_N)\cos\theta_z + K_2$	Applicable to different weather conditions. Validated for composite climatic condition of New Delhi, India
Radiation on horizontal surface (decomposition model)	Liu and Jordan model [7][23]	$k_D = 0.384 - 0.416k_t$ $k_t = \frac{I}{I_0}, k_d = \frac{I_d}{I}, k_D = \frac{I_d}{I_0}, k_b = \frac{I_b}{I_0}$	k_t is clearness index, k_d is diffuse fraction, k_D is diffuse coefficient, and k_b is direct transmittance. I, I_b, I_d and I_0 are the global, direct, diffuse, and extraterrestrial irradiances respectively, on a horizontal surface (all in MJm^{-2})

(continued)

(continued)

Model type	Model name	Model correlations	Remarks
	Orgill and Hollands model [8][24]	$k_d = 1.557 - 1.846k_t$ for $0.35 \leq k_t \leq 0.75$ $k_d = 1.0 - 0.249k_t$ for $k_t < 0.35$ $k_d = 0.177$ for $k_t > 0.75$	The model was based on the global and diffuse irradiance values registered in Toronto (Canada 42.81°N) during the years 1967–1971
	Erbs et al. model [9][25]	$k_d = 0.951 - 0.1604k_t + 4.388k_t^2 - 16.638k_t^3 + 12.336k_t^4$ for $0.22 \leq k_t < 0.80$ $k_d = 1.0 - 0.09k_t$ for $k_t \leq 0.22$ $k_d = 0.165$ for $k_t > 0.80$	Correlations developed using data from five stations in the USA with latitudes between 31° and 42°
	Spencer model [10][26]	$k_d = a_3 - b_3 k_t$ for $0.35 \leq k_t \leq 0.75$ $a_3 = 0.94 + 0.0118\|\phi\|$ $b_3 = 1.185 + 0.0135\|\phi\|$	Correlations developed from five stations in Australia (20–45°S latitude) ϕ (degrees) is the latitude
	Muneer et al. model [11][27]	$k_d = 0.9698 + 0.4353k_t - 3.4499k_t^2 + 2.1888k_t^3$ for $0.175 \leq k_t \leq 0.775$ $k_d = 0.95$ for $k_t < 0.175$ $k_d = 0.26$ for $k_t > 0.775$	Correlation developed using data from New Delhi, India
	Hawlader model [12][28]	$k_d = 1.135 - 0.9422k_t - 0.3878k_t^2$ for $0.225 < k_t < 0.775$ $k_d = 0.915$ for $k_t \leq 0.225$ $k_d = 0.215$ for $k_t \geq 0.775$	Correlation developed using data from a tropical site in Singapore
	Reindl et al. model [13][29]	First correlation: $k_d = 1.02 - 0.248k_t$ for $k_t \leq 0.30$ $k_d = 1.45 - 1.67k_t$ for $0.3 < k_t < 0.78$ $k_d = 0.147$ for $k_t \geq 0.78$ Second correlation: $k_d = 1.02 - 0.254k_t + 0.0123\sin\alpha$ for $k_t \leq 0.30$ $k_d = 1.4 - 1.749k_t + 0.177\sin\alpha$ for $0.3 < k_t < 0.78$ $k_d = 0.486k_t - 0.182\sin\alpha$ for $k_t \geq 0.78$	Correlations developed from five locations in the USA and Europe (28–60°N latitude)

(continued)

(continued)

Model type	Model name	Model correlations	Remarks
	Chandrasekaran and Kumar model [14][30]	$k_d = 0.9686 + 0.1325k_t + 1.4183k_t^2 - 10.1862k_t^3 + 8.3733k_t^4$ for $0.24 < k_t \le 0.80$ $k_d = 1.0086 - 0.178k_t$ for $k_t \le 0.24$ $k_d = 0.197$ for $k_t > 0.80$	Correlation developed using data from a tropical environment in Chennai, India
	Lam and Li model [15][31]	$k_d = 0.977$ for $k_t \le 0.15$ $k_d = 1.237 - 1.361k_t$ for $0.15 < k_t \le 0.7$ $k_d = 0.273$ for $k_t > 0.7$	Correlations developed for Hong Kong (22.31 N latitude) with the measured data in 1991–1994
	Boland et al. model [16][32]	$k_d = \frac{1}{1+e^{7.997(k_t-0.586)}}$ for all values of k_t	Correlation developed using data from one location in Victoria, Australia
	Miguel et al. model [17][33]	$k_d = 0.724 + 2.738k_t - 8.32k_t^2 + 4.967k_t^3 + 12.336k_t^4$ for $0.21 < k_t \le 0.76$ $k_d = 0.995 - 0.081k_t$ for $k_t \le 0.21$ $k_d = 0.18$ for $k_t \ge 0.76$	Correlation developed using data from several countries in the North Mediterranean Belt area
	Oliveira et al. model [18][34]	$k_d = 0.97 + 0.8k_t - 3.0k_t^2 - 3.1k_t^3 + 5.2k_t^4$ for $0.17 < k_t < 0.75$ $k_d = 1.0$ for $k_t \le 0.17$ $k_d = 0.17$ for $k_t > 0.75$	Correlation developed using data from Sao Paolo site, Brazil
	Karatasou et al. model [19][35]	$k_d = 0.9995 - 0.05k_t - 2.4156k_t^2 + 1.4926k_t^3$ for $0 < k_t \le 0.78$ $k_d = 0.20$ for $k_t > 0.78$	Correlation developed using data from Athens, Greece
	Soares et al. model [20][36]	$k_d = 0.90 + 1.1k_t - 4.5k_t^2 + 0.01k_t^3 + 3.14k_t^4$ for $0.17 < k_t < 0.75$ $k_d = 1.0$ for $k_t \le 0.17$ $k_d = 0.17$ for $k_t > 0.75$	Correlation developed with neural network technique using data from Sao Paolo site, Brazil

(continued)

(continued)

Model type	Model name	Model correlations	Remarks
Models for predicting the mean hourly global radiation from daily summations	Whillier/Liu and Jordan model [21][37]	$r_0 = (\cos\omega - \cos\omega_0)/kA(\omega_0)$ $A(\omega_0) = \sin\omega_0 - \omega_0\cos\omega_0$ r_0 is the extraterrestrial hourly/daily ratio ω_0 is the sunrise hour angle (in radians) ω is the hour angle	It is assumed that global radiation follows the same hourly distribution as if there were no atmosphere
	Collares-Pereira and Rabl model [22][38]	$r_{CPR} = (a + b\cos\omega)r_0$ $a = 0.4090 + 0.5016\sin(\omega_0 - 1.047)$ $b = 0.6609 + 0.4767\sin(\omega_0 - 1.047)$	r_{CPR} is the extraterrestrial hourly/daily ratio
	Newell model [23][39]	$r_N = (1.5/S_0)\left[1 - 4(t-12)^2/S_0^2\right]$ $S_0 = k\omega_0,\ k = 24/\pi$ ω_0 is the sunrise hour angle (in radians) $\cos\omega_0 = -\tan\phi\tan\delta$	ϕ is the site's latitude, δ is solar declination, and r_N is the extraterrestrial hourly/daily ratio
	Jain model [24][40]	$r_J = \dfrac{1}{\sigma_J\sqrt{2\pi}}\exp\left[-\dfrac{(t-12)^2}{2\sigma_J^2}\right]$ $\sigma_J = 0.461 + 0.192S_0,\ S_0 = k\omega_0,\ k = 24/\pi$ ω_0 is the sunrise hour angle (in radians) $\cos\omega_0 = -\tan\phi\tan\delta$	ϕ is the site's latitude, δ is solar declination, and r_J is the extraterrestrial hourly/daily ratio
	Gueymard model [25][41]	$r_{CPRG} = (a + b\cos\omega)r_0/f$ $f = a + 0.5b(\omega_0 - \sin\omega_0\cos\omega_0)/A(\omega_0)$ $a = 0.4090 + 0.5016\sin(\omega_0 - 1.047)$ $b = 0.6609 + 0.4767\sin(\omega_0 - 1.047)$	Modified Collares-Pereira and Rabl model. r_{CPRG} is the extraterrestrial hourly/daily ratio
	Garg and Garg model [26][42]	$r_G = r_0 - 0.008\sin 3(\omega - 0.65)$	Corrected Whillier/Liu and Jordan model for Indian climatic condition. r_G is the extraterrestrial hourly/daily ratio

(continued)

(continued)

Model type	Model name	Model correlations	Remarks
	Baig et al. model [27][43]	$$r_B = \frac{1}{2\sigma_B\sqrt{2\pi}}\exp\left[-\frac{(t-12)^2}{2\sigma_B^2}\right]$$ $\sigma_B = 0.26 + 0.21S_0,\ S_0 = k\omega_0,\ k = 24/\pi$ ω_0 is the sunrise hour angle (in radians) $\cos\omega_0 = -\tan\phi\tan\delta$	ϕ is the site's latitude, δ is solar declination. It is the corrected Jain model for better accuracy for values of solar radiation during sunrise and sunset. r_B is the extraterrestrial hourly/daily ratio

Appendix IV

Specifications of solar cell material (at solar intensity 1000 W/m^2 and cell temperature 25 °C) and cost (from Chap. 1, ref. [2])

Cell technology	Efficiency (%)	Fill factor (FF)	Aperture area ($10^{-4} \times$ m^2)	Life time[a] (years)	Manufacturing cost (\$/kWp in 2007)	Selling price (\$/ kWp in 2007)
Monocrytalline silicon	24.7 ± 0.5	0.828	4.0	30	2.5	3.7
Multicrytalline silicon	19.8 ± 0.5	0.795	1.09	30	2.4	3.5
Copper indium diselenide (CIS/CIGS)	18.4 ± 0.5	0.77	1.04	5	1.5	2.5
Thin silicon cell	16.6 ± 0.4	0.782	4.02	25	2.0	3.3
Cadmium telluride (CdTe)	16.5 ± 0.5	0.755	1.03	15	1.5	2.5
Amorphous silicon (a-si)	10.1 ± 0.2	0.766	1.2	20	1.5	2.5

[a]Based on experience

Source B. Agarwal, G.N. Tiwari, Development in environmental durability for photovoltaics, Pira International Ltd., UK, 2008
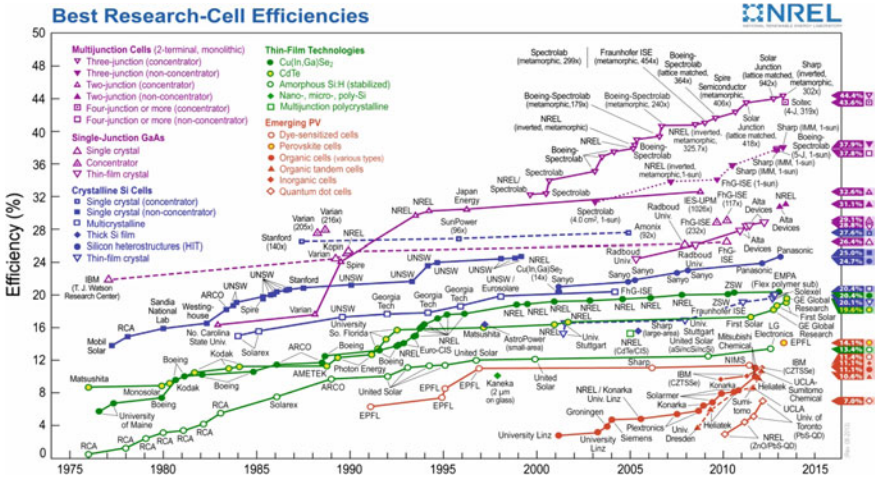
Courtesy of NREL, USA

Appendix V

Table V(a) Properties of air at atmospheric pressure

T (K)	P (kg/ m³)	C_p (kJ/ kg K)	μ (kg/m-s) $\times 10^{-5}$	v (m²/ s) $\times 10^{-6}$	K (W/ m² K) $\times 10^{-3}$	α (m²/ s) $\times 10^{-5}$	Pr
100	3.6010	1.0259	0.6924	1.923	9.239	0.2501	0.770
150	2.3675	1.0092	1.0283	4.343	13.726	0.5745	0.753
200	1.7684	1.0054	1.3289	7.490	18.074	1.017	0.739
250	1.4128	1.0046	1.488	9.49	22.26	1.3161	0.722
300	1.1774	1.0050	1.983	15.68	26.22	2.216	0.708
350	0.9980	1.0083	2.075	20.76	30.00	2.983	0.697
400	0.8826	1.0134	2.286	25.90	33.62	3.760	0.689

The values of μ, K, C_p and Pr are not strongly pressure-dependent and may be used over a fairly wide range of pressures

Table V(b) Properties of water (saturated liquid)

Temperature		C_p (kJ/kg K)	ρ (kg/ m³)	μ_k (kg/m s)	K (W/m K)	Pr	$\frac{g\beta P^2 C_p}{\mu_k}$ (I/m³ K)
°F	°C						
32	0.00	4.225	999.8	1.79×10^3	0.566	13.25	1.91×10^9
40	4.44	4.208	999.8	1.55	0.575	11.35	6.34×10^9
50	10.00	4.195	999.2	1.31	0.585	9.40	1.08×10^{10}
60	15.56	4.186	998.6	1.12	0.595	7.88	1.46×10^{10}
70	21.11	4.179	997.4	9.8×10^4	0.604	6.78	1.46×10^{10}
80	26.67	4.179	995.8	8.6	0.614	5.85	1.91×10^{10}
90	32.22	4.174	994.9	7.65	0.623	5.12	2.48×10^{10}
100	37.78	4.174	993.0	6.82	0.630	4.53	3.3×10^{10}
110	43.33	4.174	990.6	6.16	0.637	4.04	4.19×10^{10}
120	48.89	4.174	988.8	5.62	0.644	3.64	4.89×10^{10}
130	54.44	4.179	985.7	5.13	0.649	3.30	5.66×10^{10}
140	60.00	4.179	983.3	4.71	0.654	3.01	6.48×10^{10}

(continued)

Table V(b) (continued)

Temperature		C_p (kJ/kg K)	ρ (kg/m³)	μ_k (kg/m s)	K (W/m K)	Pr	$\frac{g\beta P^2 C_p}{\mu_k}$ (I/m³ K)
°F	°C						
150	65.55	4.183	980.3	4.3	0.659	2.73	7.62×10^{10}
160	71.11	4.186	977.3	4.01	0.665	2.53	8.84×10^{10}
170	76.67	4.191	973.7	3.72	0.668	2.33	9.85×10^{10}
180	82.22	4.195	970.2	3.47	0.673	2.16	1.09×10^{10}
190	87.78	4.199	966.7	3.27	0.675	2.03	
200	93.33	4.204	963.2	3.06	0.678	1.90	
210	104.40	4.216	955.1	2.67	0.684	1.66	

Table V(c) Properties of metals

Metal		Properties at 20 °C			
		P (kg/m³)	C_p (kJ/kg K)	K (W/m K)	α (m²/s × 10⁻⁵)
Aluminum	Pure	2707	0.896	204	8.418
	Al–Si (silumin, copper bearing) 86 % Al, 1 % Cu	2659	0.867	137	5.933
Lead	Pure	11400	0.1298	34.87	7.311
Iron	Pure	7897	0.452	73	2.034
	Steel (carbon steel)	7753	0.486	63	0.970
Copper	Pure	8954	0.3831	386	11.234
	Aluminum bronze (95 % Cu, 5 % Al)	8666	0.410	383	2.330
Bronze	75 % Cu, 25 % Sn	8666	0.343	326	0.859
Red Brass	85 % Cu, 9 % Sn 6 % Zn	8714	0.385	61	1.804
Brass	70 % Cu, 30 % Zn	8600	0.877	85	3.412
German Silver	62 % Cu, 15 % Ni, 22 % Zn	8618	0.394	24.9	0.733
Constantan	60 % Cu, 40 % Ni	8922	0.410	22.7	0.612
Magnesium	Pure	1746	1.013	171	9.708
Nickel	Pure	8906	0.4459	90	2.266
Silver	Purest	10524	0.2340	419	17.004
	Pure (99.9 %)	10524	0.2340	407	16.563
Tin	Pure	7304	0.2265	64	3.884
Tungsten	Pure	19350	0.1344	163	6.271
Zinc	Pure	7144	0.3843	112.2	4.106

Table V(d) Properties of nonmetals

Material	Temperature (°C)	K (W/m K)	ρ (kg/m^3)	C (kJ/kg K)	α (m^2/s) × 10^{-7}
Asbestos	50	0.08	470	–	–
Building brick	20	0.69	1600	0.84	5.2
Common face	–	1.32	2000	–	–
Concrete, cinder	23	0.76	–	–	–
Stone 1–2–4 mix	20	1.37	1900–2300	0.88	8.2–6.8
Glass, window	20	0.78 (avg)	2700	0.84	3.4
Borosilicate	30–75	1.09	2200	–	–
Plaster, gypsum	20	0.48	1440	0.84	4.0
Granite	–	1.73–3.98	2640	0.82	8–18
Limestone	100–300	1.26–1.33	2500	0.90	5.6–5.9
Marble	–	2.07–2.94	2500–2700	0.80	10–13.6
Sandstone	40	1.83	2160–2300	0.71	11.2–11.9
Fir	23	0.11	420	2.72	0.96
Maple or oak	30	0.166	540	2.4	1.28
Yellow pine	23	0.147	640	2.8	0.82
Cord board	30	0.043	160	1.88	2–5.3
Cork, regranulated	32	0.045	45–120	1.88	2–5.3
Ground	32	0.043	150	–	–
Sawdust	23	0.059	–	–	–
Wood shaving	23	0.059	–	–	–

Table V(e) Physical properties of some other materials

S. No.	Material	Density (kg/m^3)	Thermal conductivity (W/m K)	Specific heat (J/kg K)
1	Air	1.117	40.026	1006
2	Alumina	3800	29.0	800
3	Aluminum	41–45	211	0.946
4	Asphalt	1700	0.50	1000
5	Brick	1700	0.84	800
6	Carbon dioxide	1.979	0.145	871
7	Cement	1700	0.80	670
8	Clay	1458	11.28	879
9	Concrete	2400	1.279	1130
10	Copper	8795	385	–
11	Cork	240	0.04	2050
12	Cotton wool	1522	–	1335
13	Fibre board	300	0.057	1000
14	Glass-crown	2600	1.0	670
15	Glass-window	2350	0.816	712
16	Glass-wool	50	0.042	670
17	Ice	920	2.21	1930
18	Iron	7870	80	106
19	Lime stone	2180	1.5	–
20	Mudphuska	–	–	–
21	Oxygen	1.301	0.027	920
22	Plaster-board	950	0.16	840
23	Polyesterene-expanded	25	0.033	1380
24	P.V.C.—rigid foam	25–80	0.035–0.041	–
25	P.V.C.—rigid sheet	1350	0.16	–
26	Saw dust	188	0.57	–
27	Thermocol	22	0.03	–
28	Timber	600	0.14	1210
29	Turpentine	870	0.136	1760
30	Water (H_2O)	998	0.591	4190
31	Sea water	1025	–	3900
32	Water vapour	0.586	0.025	2060
33	Wood wool	500	0.10	1000

Table V(f) Absorptivity of various surfaces of the Sun's rays

Surface	Absorptivity	Surface	Absorptivity
White paint	0.12–0.26	**Walls**	
Whitewash/glossy white	0.21	White/yellow brick tiles	0.30
Bright aluminium	0.30	White stone	0.40
Flat white	0.25	Cream brick tile	0.50
Yellow	0.48	Burl brick tile	0.60
Bronze	0.50	Concrete/red brick tile	0.70
Silver	0.52	Red sand line brick	0.72
Dark aluminium	0.63	White sand stone	0.76
Bright red	0.65	Stone rubble	0.80
Brown	0.70	Blue brick tile	0.88
Light green	0.73	**Surroundings**	
Medium red	0.74	Sea/lake water	0.29
Medium green	0.85	Snow	0.30
Dark green	0.95	Grass	0.80
Blue/black	0.97	Light-coloured grass	0.55
Roof		Sand gray	0.82
Asphalt	0.89	Rock	0.84
White asbestos cement	0.59	Green leaf	0.85
Cooper sheeting	0.64	Earth (black ploughed field)	0.92
Uncoloured roofing tile	0.67	White leaves	0.20
Red roofing tiles	0.72	Yellow leaves	0.58
Galvanised iron, clean	0.77	Aluminium foil	0.39
Brown roofing tile	0.87	Unpainted wood	0.60
Galvanised iron, dirty	0.89		
Black roofing tile	0.92		
Metals			
Polished aluminium/copper	0.26		
New galvanised iron	0.66		
Old galvanized iron	0.89		
Polished iron	0.45		
Oxidized rusty iron	0.38		

Table V(g) Theoretical model for the thermal conductivity of nano-fluids found in the literature

Models	Thermal conductivity (k) (W/m-K)	Physical models
Maxwell-Eucken [28][10]	$k_{\text{nf}} = k_{\text{bf}} \times \dfrac{[k_{\text{p}} + 2k_{\text{bf}} + 2\phi_{\text{p}}(k_{\text{p}} - k_{\text{bf}})]}{[k_{\text{p}} + 2k_{\text{bf}} - \phi_{\text{p}}(k_{\text{p}} - k_{\text{bf}})]}$ **Remarks:** Spherical particles	Based on the conduction solution through a stationary random suspension of spheres
Bruggeman [29][11]	$k_{\text{nf}} = \dfrac{[(3\phi - 1)k_{\text{p}} + (2 - 3\phi)k_{\text{bf}} + k_{\text{bf}}\sqrt{\Delta}]}{4}$ $\Delta = \left[(3\phi_{\text{p}} - 1)\dfrac{k_{\text{p}}}{k_{\text{bf}}} + (2 - 3\phi)\right]^2 + 8\dfrac{k_{\text{p}}}{k_{\text{bf}}}$ **Remarks:** – Applicable to high-volume fraction of spherical particles – Suspension with spherical inclusions	Based on the differential effective medium (DEM) theory to estimate the effective thermal conductivity of composites at high particle concentrations
Hamilton-Crosser [30][12]	$k_{\text{nf}} = k_{\text{bf}} \dfrac{[k_{\text{p}} + (n-1)k_{\text{bf}} + \phi(n-1)(k_{\text{p}} - k_{\text{bf}})]}{[k_{\text{p}} + (n-1)k_{\text{bf}} - \phi(k_{\text{p}} - k_{\text{bf}})]}$ **Remarks:** Spherical and nonspherical particles, $n = 3$ (spheres), $n = 6$ (cylinders)	Based on the effective thermal conductivity of a two-component mixture when the ratio of thermal conductivity is more than 100
Wasp [31][13]	**Remarks:** Special case of Hamilton and Crosser's model with $n = 3$	Based on effective thermal conductivity of a two-component mixture

Table V(h) Correlation developed for thermal conductivity of nano-fluids

Khanafer and Vafai [32][14]	$k_{nf} = k_{bf} \times \left(1 + 1.0112\phi_p + 2.4375\phi_p \times \left(\frac{47}{d_p nm}\right) - 0.0248\phi_p \left(\frac{k_p}{0.613}\right)\right)$	Al_2O_3–H_2O CuO–H_2O
	Remarks: At ambient temprature	
	$k_{nf} = k_{bf} \times \left[0.9843 + 0.398\phi_p^{0.7383} \left(\frac{1}{d_p(nm)}\right)^{0.2246} \left(\frac{\mu_{nf}(T)}{\mu_{bf}(T)}\right)^{0.0235} -(3.9517) \times \left(\frac{\phi_p}{T}\right) + (34.034) \times \left(\frac{\phi_p^2}{T^3}\right) + (32.509) \times \left(\frac{\phi_p}{T^2}\right)\right]$	
	$\mu_{bf} = 2.414 \times 10^{-5} \times 10^{247.8/(T-140)}$	
	$0 \leq \phi_p \leq 10\%,\ 11 \leq d_p \leq 150\ nm,\ 20 \leq T \leq 70\,°C$	
	$\mu_{nf} = -0.4491 + \frac{28.837}{T} + 0.574\phi_p - 0.1634\phi_p^2 + 23.053 \times \left(\frac{\phi_p^2}{T^2}\right) + 0.0132\phi_p^3 - 2354.735 \times \left(\frac{\phi_p}{T^3}\right) + 23.498 \times \left(\frac{\phi_p^2}{d_p^2}\right) - 3.0185 \times \left(\frac{\phi_p^3}{d_p^2}\right)$	
	$1 \leq \phi_p \leq 9\%,\ 13 \leq d_p \leq 131\ nm,\ 20 \leq T \leq 70\,°C$	

Table V(i) Models of viscosity of nano-fluids

Models	Dynamic viscosity (μ) (kg/m-s)	Physical model
Einstein [33][15]	$\mu_{nf} = \mu_{bf}(1 + 2.5\phi_p)$ **Remarks:** – Infinitely dilute suspension of spheres (no interaction between the spheres) – Valid for relatively low particle–volume fraction $\phi_p < 5\%$	– Based on phenomenological hydrodynamic equations – Considered a suspension containing n-solute particles in a total volume V
Brinkman [34][16]	$\mu_{nf} = \frac{\mu_{bf}}{(1-\phi_p)^{2.5}}$ **Remarks:** – Spherical particles, – Valid for high to moderate particle concentrations – Used Einstein's factor: (1 + 2.5 ϕ_p)	– Based on Einstein model – Derived by considering the effect of the addition of one solute-molecule to an existing solution
Batchelor [35][17]	$\mu_{nf} = \mu_{bf}(1 + 2.5\phi_p + 6.2\phi_p^2)$ $= \mu_{bf}(1 + \eta\phi_p + k_H\phi_p^2)$ Here, Huggins coefficient, $k_H = 6.2$ (5.2 from hydrodynamic effect and 1.0 from Brownian motion) **Remarks:** – Brownian motion – Isotropic structure	– Based on reciprocal theorem in Stokes flow problem to obtain an expression for the bulk stress due to the thermodynamic forces – Incorporated both effects: hydrodynamic effects and Brownian motion
Lundgren [36][18]	$\mu_{nf} = \frac{\mu_{bf}}{(1-2.5\phi_p)}$ **Remarks:** – Dilute concentration of spheres – Random bed of spheres	Based on a Taylor series expansion in terms of ϕ_p

Table V(j) Viscosity models at room temperature based on experimental data (TiO_2–H_2O, CuO–H_2O and Al_2O_3–H_2O)

Reference	Viscosity (μ)	Remarks
Maiga et al. [37][19]	$\mu_{nf} = \mu_{bf}(1 + 7.3\phi_p + 123\phi_p^2)$	Least-square curve fitting of Wang et al. (1999)[20] data, Al_2O_3–H_2O, $d_p = 28$ nm
Khanafer and Vafai [32][14]	$\mu_{nf} = \mu_{bf}(1 + 0.164\phi_p + 302.34\phi_p^2)$	Least-square curve fitting of experimental data (1993, 1999), Al_2O_3-ethylene glycol, $d_p = 28$ nm
Buongiorno [38][21]	$\mu_{nf} = \mu_{bf}(1 + 5.45\phi_p + 108.2\phi_p^2)$	Curve-fitting of Pak and Cho [60][22] data, TiO_2–H_2O, $d_p = 27$ nm
Khanafer and Vafai [32][14]	$\mu_{nf} = \mu_{bf}(1 + 23.09\phi_p + 1525.3\phi_p^2)$	Curve-fitting of Pak and Cho [60][22] data, Al_2O_3–H_2O, $d_p = 13$ nm, $0 \leq \phi_p \leq 0.04\,\%$
Nguyen et al. [39][23]	$\mu_{nf} = \mu_{bf}\left[0.904 \times \exp(0.148\phi_p)\right], \mathbf{d_p = 47\ nm}$ $\mu_{nf} = \mu_{bf}(1 + 0.0025\phi_p + 0.00156\phi_p^2),$ $\mathbf{d_p = 37\ nm}$	Curve-fitting of experimental data, Al_2O_3–H_2O
Nguyen et al. [39][23]	$\mu_{nf} = \mu_{bf}(1.475 - 0.319\phi_p + 0.051\phi_p^2 + 0.009\phi_p^3)$	Curve-fitting of experimental data, CuO–water, $d_p = 29$ nm
Tseng and Lin [40][24]	$\mu_{nf} = \mu_{bf}\left[13.47 \times \exp(35.98\phi_p)\right]$	TiO_2–H_2O, $0.05 \leq \phi_p \leq 0.12\,\%$

Table V(k) Effect of temperature and volume fraction on dynamic viscosity of Al_2O_3–H_2O nano-fluid

Reference	Viscosity (μ)	Remarks
Khanafer and Vafai [32][14]	$\mu_{nf} = 0.44 - 0.254\phi_p^2 + 0.0368\phi_p^2 + 26.33\frac{\phi_p}{T} - 59.311\frac{\phi_p^2}{T^2}$	Curve-fitting of Pak and Cho [60][22] data, and $d_p = 13$ nm, $20 < T(°C) < 70$, $\phi_p = 1.34$ and 2.78 %; units: **mPa-s**
Nguyen et al. [39][23]	$\mu_{nf} = \mu_{bf}(1.125 - 0.0007 \times T(°C))$, $\phi_p = 1\%$ $\mu_{nf} = \mu_{bf}(2.1275 - 0.0215 \times T(°C) + 0.0002 \times T^2(°C))$, $\phi_p = 4\%$	Units: **mPa-s**
Namburu et al. (41, 42)[25−26]	$\mu_{nf} = \exp[A \exp(-BT)]$ Here $A = -0.2995\phi_p^3 + 6.7388\phi_p^2 - 55.44\phi_p + 236.11$ $B = (-6.4745\phi_p^3 + 140.03\phi_p^2 - 1478.5\phi_p + 20341) \times 10^{-6}$	Experimental Al_2O_3–ethylene glycol and water mixture; $1\% < \phi_p < 10\%$, $d_p = 53$ nm, and $238 < T(K) < 323$, units: **mmPa-s**

Table V(I) Effect of temperature and volume fraction on the dynamic viscosity of TiO$_2$–H$_2$O and CuO–H$_2$O nano-fluids

Reference	Viscosity (μ)	Remarks
Duangthongsuk and Wongwises [43][27]	$\mu_{\text{nf}} = \mu_{\text{bf}}(1.0226 + 0.0477\phi_{\text{p}} - 0.0112\phi_{\text{p}}^2)$; $T = 15\,°C$ $\mu_{\text{nf}} = \mu_{\text{bf}}(1.013 + 0.092\phi_{\text{p}} - 0.015\phi_{\text{p}}^2)$; $T = 25\,°C$ $\mu_{\text{nf}} = \mu_{\text{bf}}(1.018 + 0.112\phi_{\text{p}} - 0.0177\phi_{\text{p}}^2)$; $T = 35\,°C$	– Experimental data, TiO$_2$–H$_2$O – $d_{\text{p}} = 21$ nm, $0.2\% \leq \phi_{\text{p}} \leq 2\%$ – Units: **mPa-s**
Khanafer and Vafai [32][14]	$\mu_{\text{nf}} = 0.6002 - 0.569\phi_{\text{p}} + 0.0823\phi_{\text{p}}^2 + 28.8763\frac{\phi_{\text{p}}}{T} - 204.2202\frac{\phi_{\text{p}}^2}{T^2} + 561.3175\frac{\phi_{\text{p}}^3}{T^3}$	Curve-fitting of Pak and Cho [60][22] data, TiO$_2$–H$_2$O, $d_{\text{p}} = 27$ nm, $20 < T(°C) < 70$, $\phi_p = 0.99\%, 2.04\%, 3.16\%$ – Units: **mPa-s**
Namburu et al. [41, 42][25–26]	$\mu_{\text{nf}} = \exp[A\exp(-BT)]$ Here $A = 1.8375\phi_{\text{p}}^2 + 29.643\phi_{\text{p}} + 165.56$, $B = (4 \times 10^{-6}\phi_{\text{p}}^2 - 0.001\phi_{\text{p}} + 0.0186)$	CuO–ethylene glycol and water mixture $1 \leq \phi_{\text{p}} \leq 6\%$, $d_{\text{p}} = 29$ nm, $238 < T(\text{K}) < 323$ – Units: **mmPa-s**
Kulkarni et al. [44, 45][28–29]	$\mu_{\text{nf}} = \exp(\frac{A}{T} - B)$ Here $A = 20587\phi_{\text{p}}^2 + 15857\phi_{\text{p}} + 1078.3$, $B = -107.12\phi_{\text{p}}^2 + 53.54\phi_{\text{p}} + 2.8715$	CuO–H$_2$O, $0.5\% \leq \phi_{\text{p}} \leq 0.15\%$ $d_{\text{p}} = 29$ nm $238 < T(\text{K}) < 323$ – Units: **mmPa-s**

Table V(m) Theoretical models and correlations for thermo-physical properties

Properties	References	Theoretical formulae	Correlations
Density (kg/m³)	Pak and Cho [60][22]	$\rho_{nf} = \rho_p \phi_p + \rho_{bf}(1-\phi_p)$	$\rho_{nf} = 1001.064 + 2738.6191\phi_p - 0.2095T$, $0 \leq \phi_p \leq 0.4\%$, $5 < T(°C) < 40$ Curve-fitting of Ho et al. [46][30] measured the density of Al₂O₃–water nanofluid at different temperatures and nanoparticle volume fraction
Specific heat (J/kg·K)	Pak and Cho [60][22] Xuan and Roetzel [47][31]	$C_{nf} = \frac{\phi_p \rho_p C_{pp} + (1-\phi_p)\rho_{bf} C_{pbf}}{\rho_{bf}}$ $(\rho C_p)_{nf} = (1-\phi_p)(\rho C_p)_{bf} + \phi_p(\rho C_p)_p$	Vajjha and Das [48][32] for Al₂O₃ and SiO₂, ZnO nanofluids $C_{pnf} = C_{pbf}\left[\dfrac{A\left(\frac{T}{T_0}\right) + B\left(\frac{C_{pp}}{C_{pbf}}\right)}{(C+\phi)}\right]$ Nanofluids / A / B / C / Max error (%) / Avg. absolute error (%): Al₂O₃ 0.00089 0.5179 0.4250 5 2.28; SiO₂ 0.00176 1.1937 0.8021 3.1 1.5; ZnO 0.00046 0.9855 0.299 4.4 2.7 $0 \leq \phi_p \leq 0.1\%$ for Al₂O₃ and SiO₂–ethylene glycol and water mixture (60:40 by weight) $0 \leq \phi_p \leq 0.07\%$ for ZnO–ethylene glycol and water mixture (60:40 by weight) $315 < T(K) < 363$
Thermal expansion coefficient (K⁻¹)	Khanafer et al. [49][33] Wang et al. [50][34], Ho et al. [51][35]	$\beta_{nf} = \frac{(1-\phi_p)(\rho\beta)_{bf} + \phi_p(\rho\beta)_p}{\rho_{nf}}$ $\beta_{nf} = (1-\phi_p)\beta_{bf} + \phi_p\beta_p$	A correlation for the thermal-expansion coefficient of Al₂O₃–water nanofluid as a function of temperature and volume fraction of nanoparticles based on data presented in Ho et al. [46][30] $\beta_{nf} = \left(-0.479\phi_p + 9.3149 \times 10^{-3}T - \frac{4.7211}{T^2}\right) \times 10^{-3}$, $0 \leq \phi_p \leq 0.04\%$, $10 < T(°C) < 40$
Thermal diffusivity (mm²/s)		$\alpha_{nf} = \frac{k_{nf}}{\rho_{nf} C_{pnf}}$	

The table inside the Correlations column for Specific heat:

Nanofluids	A	B	C	Max error (%)	Avg. absolute error (%)
Al₂O₃	0.00089	0.5179	0.4250	5	2.28
SiO₂	0.00176	1.1937	0.8021	3.1	1.5
ZnO	0.00046	0.9855	0.299	4.4	2.7

$\phi_p = V_p/V_{bf} + V_p$ volume fraction of nanoparticles, V_p volume fraction of nanoparticles, k_{nf} = thermal conductivity of nanofluids, k_{bf} = thermal conductivity of nanofluids, k_p thermal conductivity of nanoparticles, k_H 6.2, Huggins coefficient, n empirical shape factor, r_p particle radius, h interparticle spacing, t thickness of the nano-layer, k_{layer} thermal conductivity of the nano-layer nanoparticles, k_{layer} thermal conductivity of the nano-layer
Sub-script f fluid, bf base fluid, p nanoparticle, nf nanofluid

Table V(n) Heat transfer coefficient of nano-fluids

Reerences	Nusselt number and heat-transfer coefficient	Remarks
Seider–Tate [52] equation[36]	$(Nu_{nf})_{th} = 1.86 \times \left(Re_{nf} Pr_{nf} \dfrac{D}{L} \right)^{\frac{1}{3}} \left(\dfrac{\mu_{nf}}{\mu_{bf}} \right)^{0.14}$ $Re_{nf} = \dfrac{u_m D}{\mu_{nf}} Pr_{nf} = \dfrac{(C_p)_{nf} \mu_{nf}}{K_{nf}}, Nu_{nf} = \dfrac{h_{nf} D}{K_{nf}}$	– Circular tube
Pak and Cho [53][37]	$Nu = 0.021 Re^{0.8} Pr^{0.5}$	– Circular tube – Limited to dilute concentration up to 3 % – Ultrafine metallic oxide particles suspended in water (γ-Al$_2$O$_3$, TiO$_2$) – Mean diameter 13 nm (γ-Al$_2$O$_3$) and 17 nm (TiO$_2$)
Xuan and Li [54][38]	$Nu_{nf} = c_1 \left(1 + c_2 \phi^{m_1} Pe_d^{m_2} \right) Re_{nf}^{m_3} Pr_{nf}^{m_4}$ $Pe_p = \dfrac{u_m d_p}{\alpha_{nf}} Re_{nf} = \dfrac{u_m D}{\mu_{nf}}$ $Pr_{nf} = \dfrac{\mu_{nf}}{\alpha_{nf}} \alpha_{nf} = \dfrac{k_{nf}}{(\rho C_p)_{nf}}$	<table><tr><td></td><td>C_1</td><td>C_2</td><td>m_1</td><td>m_2</td><td>m_3</td><td>m_4</td></tr><tr><td>Laminar flow</td><td>0.4328</td><td>11.285</td><td>0.754</td><td>0.218</td><td>0.333</td><td>0.4</td></tr><tr><td>Turbulent flow</td><td>0.0059</td><td>7.6286</td><td>0.6886</td><td>0.001</td><td>0.9238</td><td>0.4</td></tr></table> The case $C_2 = 0$ refers to zero thermal dispersion, which corresponds only to the case of the pure base fluid – Limited to dilute up to 2 %
Maiga et al. [55][39]	Laminar flow $Nu = 0.086 Re^{0.55} Pr^{0.5}$ (for constant wall flux) $Nu_{nf} = 0.28 Re^{0.35} Pr^{0.36}$ (for constant wall temperature) Turbulent flow $(Nu_{nf})_{fd} = 0.085 \times Re^{0.71} Pr^{0.35}$	– Circular tube – Al$_2$O$_3$ nanoparticle suspension in water
Fotukian and Esfahany [56][40]	Turbulent flow $h_{nf} = \dfrac{C_{pnf} \rho_{nf} uA (T_{b2} - T_{b1})}{\pi DL (T_w - T_b)_{LM}}$	– Circular tube – CuO–H$_2$O – Turbulent convective heat-transfer performance and pressure drop of very dilute (less than 0.24 % volume)

(continued)

Table V(n) (continued)

Reerences	Nusselt number and heat-transfer coefficient	Remarks				
		Nano-sized particle	Mean diameter (nm)	Density (kg/m³)	Thermal conductivity (J/kg-K)	Specific heat (W/m-K)
		CuO	30–50	6350	69	535.6
Qiang and Yimin [57][41]	**Mouromtseff numbers** Laminar flow $Mo = \left[1 + \left(11.285\phi_p^{0.754}\left(\frac{d_p}{\alpha_{nf}}\right)^{0.218}\right)\right]\frac{\rho_{nf}^{0.33}C_{pnf}^{0.4}K_{nf}^{0.6}}{\mu_{nf}^{-0.07}}$ Turbulent flow $Mo = \left[1 + \left(7.6286\phi_p^{0.6886}\left(\frac{d_p}{\alpha_{nf}}\right)^{0.001}\right)\right]\frac{\rho_{nf}^{0.9238}C_{pnf}^{-0.4}K_{nf}^{0.6}}{\mu_{nf}^{0.5232}}$	– Friction factor: $f_{nf} = \frac{2P_{nf}D_g}{Lu_m^2}$ – Derived from equation of Xuan and Li [54][37] for fully developed internal laminar and turbulent flow at a specific velocity of 1 m/s.				
Gnielinski [58][42]	For single-phase flow $f = (1.58 \times \ln Re - 3.82)^{-2}$ $Nu_{nf} = \frac{(0.125f)(Re - 1000)Pr}{1 + 12.7(0.125f)^{0.5}(Pr^{2/3} - 1)}$	Heat exchanger Al_2O_3–H_2O TiO_2–H_2O				
Duangthongsuk and Wongwises [59][43]	For each flow rate $f = 0.961 \times (Re^{-0.375}\phi_p^{0.052})$ $Nu_{nf} = 0.074 \times Re_{nf}^{0.707} Pr_{nf}^{0.385} \phi_p^{0.074}$ $Re = \frac{VD}{\mu}$ $Pe = \frac{VD}{\alpha_{nf}}$ $Pr = \frac{\mu_{nf}}{\alpha_{nf}}$ $\alpha_{nf} = \frac{k_{nf}}{\rho_{nf}(C_p)_{nf}}$	Heat exchanger Al_2O_3–H_2O TiO_2–H_2O				

$(Pe)_p$ Particle Perclet number of the nanoparticle, Re_{nf} Reynolds number of nanofluids, Pr_{nf} Prandlt number of nanofluids, K_{nf} thermal conductivity of nanofluids, α_{nf} thermal diffusivity of nanofluids, D tube diameter, d_p particle diameter, u fluid velocity, A cross-section area of the tube, D diameter of the tube, L tube length, T_{b1} inlet bulk temperature (K), T_{b2} exit bulk temperature (K), T_w wall temperature of the tube (K), $(T_w - T_b)_{LM}$ logarithmic mean temperature difference, in which T_w is the wall temperature that is the average of 10 measured temperatures on the tube wall at different positions, P_{nf} pressure drop of the pressure drop test section, L length of the pressure drop test section, g acceleration gravity, f friction factor, volume concentration is $\phi_v = [1/(100/\phi_m)((\rho_p/\rho_w) + 1)] \times 100\%$

Appendix VI

List of embodied energy coefficients

Material	MJ/kg	MJ/m^3
Aggregate, general	0.10	150
Virgin rock	0.04	63
River	0.02	36
Aluminium, virgin	191	515,700
Extruded	201	542,700
Extruded, anodised	227	612,900
Extruded, factory painted	218	588,600
Foil	204	550,800
Sheet	199	537,300
Aluminium, recycled	8.1	21,870
Extruded	17.3	46,710
Extruded, anodised	42.9	115,830
Extruded, factory painted	34.3	92,610
Foil	20.1	54,270
Sheet	14.8	39,960
Asphalt (paving)	3.4	7140
Bitumen	44.1	45,420
Brass	62.0	519,560
Carpet	72.4	–
Felt underlay	18.6	–
Nylon	148	–
Polyester	53.7	–
Polyethylterepthalate (PET)	107	–
Polypropylene	95.4	–
Wool	106	–
Cement	7.8	15,210
Cement mortar	2.0	3200
Fibre cement board	9.5	13,550

(continued)

(continued)

Material	MJ/kg	MJ/m³
Soil-cement	0.42	819
Ceramic	–	–
Brick	2.5	5170
Brick, glazed	7.2	14,760
Pipe	6.3	–
Tile	2.5	5250
Concrete	–	–
Block	0.94	–
Brick	0.97	–
GRC	7.6	14,820
Paver	1.2	–
Pre-cast	2.0	–
Ready mix, 17.5 MPa	1.0	2350
30 MPa	1.3	3180
40 MPa	1.6	3890
Roofing tile	0.81	–
Copper	70.6	631,160
Earth, raw	–	–
Adobe block, straw stabilised	0.47	750
Adobe, bitumen stabilised	0.29	–
Adobe, cement stabilised	0.42	–
Rammed soil cement	0.80	–
Pressed block	0.42	–
Fabric	–	–
Cotton	143	–
Polyester	53.7	–
Glass	66.2	–
Float	15.9	40,060
Toughened	26.2	66,020
Laminated	16.3	41,080
Tinted	14.9	375,450
Insulation	–	–
Cellulose	3.3	112
Fibreglass	30.3	970
Polyester	53.7	430
Polystyrene	117	2340
Wool (recycled)	14.6	139
Lead	35.1	398,030
Linoleum	116	150,930
Paint	90.4	118/l

(continued)

Material	MJ/kg	MJ/m³
Solvent based	98.1	128/l
Water based	88.5	115/l
Paper	36.4	33,670
Building	25.5	–
Kraft	12.6	–
Recycled	23.4	–
Wall	36.4	–
Plaster, gypsum	4.5	6460
Plaster board	6.1	5890
Plastics	–	–
ABS	111	–
High density polyethelene (HDPE)	103	97,340
Low density polyethelene (LDPE)	103	91,800
Polyester	53.7	7710
Polypropylene	64.0	57,600
Polystyrene, expanded	117	2340
Polyurethane	74.0	44,400
PVC	70.0	93,620
Rubber	–	–
Natural latex	67.5	62,100
Synthetic	110	–
Sand	0.10	232
Sealants and adhesives	–	–
Phenol formaldehyde	87.0	–
Urea formaldehyde	78.2	–
Steel, recycled	10.1	37,210
Reinforcing, sections	8.9	–
Wire rod	12.5	–
Steel, virgin, general	32.0	251,200
Galvanised	34.8	273,180
Imported, structural	35.0	274,570
Stone, dimension	–	–
Local	0.79	1890
Imported	6.8	1890
Straw, baled	0.24	30.5
Timber, softwood	–	–
Air dried, roughsawn	0.3	165
Kiln dried, roughsawn	1.6	880
Air dried, dressed	1.16	638
Kiln dried, dressed	2.5	1380

(continued)

Material	MJ/kg	MJ/m^3
Mouldings, etc.	3.1	1710
Hardboard	24.2	13,310
MDF	11.9	8330
Glulam	4.6	2530
Particle bd	8.0	–
Plywood	10.4	–
Shingles	9.0	–
Timber, hardwood	–	–
Air dried, roughsawn	0.50	388
Kiln dried, roughsawn	2.0	1550
Vinyl flooring	79.1	105,990
Zinc	51.0	364,140
Galvanising, per kg steel	2.8	–

Appendix VII

Heating values of various combustibles and their conversion efficiencies

Fuel	Heating value (kJ/kg)	Efficiency of device
Coal coke	29000	70
Wood	15000	60
Straw	14000–16000	60
Gasoline	43000	80
Kerosene	42000	80
Methane (natural gas)	50000	80
Biogas (60 % methane)	20000	80
Electricity	–	95

Appendix VIII

Steam table for saturation vapor pressure

Temp. (K)	P (N/m^2)	Temp. (K)	P (N/m^2)	Temp. (K)	P (N/m^2)
273	610.8	304	4491.0	334	20860.0
274	656.6	305	4743.0	335	21840.0
275	705.5	306	5029.0	336	22860.0
276	757.6	307	5318.0	337	23710.0
277	812.0	308	5622.0	338	25010.0
278	871.8	309	5940.0	339	26150.0
279	934.5	310	6274.0	340	27330.0
280	1001.2	311	6624.0	341	28560.0
281	1072.0	312	6991.0	342	29840.0
282	1147.2	313	7375.0	343	31160.0
283	1227.0	314	7777.0	344	32530.0
284	1311.6	315	8198.0	345	33960.0
285	1401.4	316	8639.0	346	35430.0
286	1496.5	317	9100.0	347	36960.0
287	1597.3	318	9583.0	348	38550.0
288	1703.9	319	10086.0	349	40190.0
289	1816.8	320	10612.0	350	41890.0
290	1936.2	321	11162.0	351	43650.0
291	2062.0	322	11736.0	352	45470.0
292	2190.0	323	12335.0	353	47360.0
293	2337.0	324	12961.0	354	49310.0
294	2485.0	325	13613.0	355	51350.0
295	2642.0	326	14340.0	356	53420.0
296	2808.0	327	15002.0	357	55570.0
297	2982.0	328	15641.0	358	57800.0
298	3166.0	329	16511.0	359	60110.0
299	3360.0	330	17313.0	360	62490.0
300	3564.0	331	18147.0	361	64950.0
301	3778.0	332	19016.0	362	67490.0
302	4004.0	333	19920.0	363	70110.0
303	4241.0				

Appendix IX

Physical properties of some liquids

Liquid	Density kg/m^3	Viscosity $\times 10^3$ (Ns/m^2)	Melting point (K)	Boiling point (K)	Thermal conductivity (W/m K)	Specific heat (J/kg K)	Latent heat $\times 10^4$ (J/kg)	Heat of vaporization $\times 10^4$ (J/kg)
Acetic acid	1049	1.219	290	391	0.180	1960	18.1	39
Acetone	780	0.329	178	330	0.161	2210	8.2	52
Ammonia	665	–	–	–	0.558	4606	–	–
Crude oil	800	1.379	–	–	0.155	–	–	–
Ethyl alcohol	789	1.197	156	352	0.177	2500	10.4	85
Glycerine	1262	1495	293	563	0.270	2400	19.9	83
Mercury	13546	1.552	234	630	7.6	140	1.17	29
Olive oil	920	85	–	570	0.17	1970	–	–
Paraffin oil	800	1000	–	–	0.15	2130	–	–
Turpentine	870	1.49	263	429	0.136	1760	–	29
Sea water	1020	1.02	264	377	–	3900	33.0	–
Water	998	1.00	273	373	0.591	4190	33.4	226

Glossary

Absorber Plate A component of the solar flat-plate collector that absorbs solar radiation and converts it into heat

Absorptance The ratio between radiation absorbed by a surface (absorber) and the total amount of solar radiation striking the surface

Acceptance Angle Half of the angular aperture of an optical system

Active Solar Heating Heating by solar energy using an additional energy source (usually electricity) for pumping water or blowing air

Active Solar Still In this case, water in a basin is heated through the glass cover as well as through an external source such as a flat-plate collector

Air-Heating System Air heating by solar energy

Air Ingredient The two main components of air are nitrogen (79 %) and oxygen (approximately 20 %). Air also consists of an optimum level of oxygen (20.94×10^4 ppm) and carbon dioxide (320 ppm)

Air Mass Atmospheric attenuation defined as the ratio of the optical thickness of the atmosphere through which direct radiation passes to the optical thickness if the Sun is at its zenith

Air Collector Device used to convert the Sun's energy to heat air

Air Pressure Same as **Atmospheric Pressure**

Air Temperature A measure of how hot or cold the air is

Albedo The ratio of amount of light reflected by a surface to the light falling onto it

Alternating Current (AC) An electric current that alternates direction between positive and negative cycles, usually 50 or 60 times/s. Alternating current is the current typically available from power outlets in a household

Altitude The height of the Sun in a vertical plane at the altitude angle

Altitude Angle The Sun's rays make an angle above the horizontal plane as measured in a vertical plane

Amorphous Silicon A disordered thin-film PV material, unlike crystalline silicon, manufactured by depositing layers of doped silicon on a substrate at low temperature

Ampere A unit of electrical current; a measure of electrons flowing through a conductor

Ampere-hour (Amp-hr) Measure of electrons flowing for a period of time

Anaerobic Digestion The process by which organic matter is decomposed by bacteria in the absence of oxygen to produce methane and other byproducts

Anemometer An instrument used for measuring wind speed

Angle of Incidence The angle formed by a ray incident on a surface and perpendicular to the surface at the point of incidence

Annual Mean Daily Insolation Average solar energy per square meter available per day over the whole year

Annual Solar Saving Annual energy savings due to the use of solar-energy devices

Antifreeze A substance added to water to lower its freezing point; solar water heaters usually use a mixture of water and propylene glycol, instead of only water, to prevent freezing

Antireflection Coating A thin coating of a material applied to a photovoltaic cell surface to reduce light reflection and increases light transmission

Aperture In optics, a hole or an opening through which solar radiation travels

Apparent Solar Time (True Solar Time) Daily apparent motion of the true, or observed, Sun; it is based on the **apparent solar day**, which is the interval between two successive returns of the Sun to the local meridian; solar time can be crudely measured by a sundial

Array Any number of photovoltaic modules connected together electrically to provide a single electrical output; an array is a mechanically integrated assembly of modules or panels together with support structure (including foundation and other components as required) to form a free-standing field installed unit that produces DC power

Atmosphere of the Earth A layer of gases surrounding Earth and retained by Earth's gravity; the atmosphere protects living organisms by (i) absorbing ultraviolet solar radiation (UV radiation), (ii) warming the surface through heat retention (greenhouse effect), and (iii) reducing the temperature extremes between day and night (diurnal temperature variation)

Atmosphere Optical Path The quantity of light removed from a beam of radiation by scattering or absorption during its path through the atmosphere (medium)

Atmospheric Pressure Force per unit area exerted against a surface by the weight of air above that surface in the Earth's atmosphere

Audit An energy audit seeks energy inefficiencies and prescribes improvement

Automatic Tracking A device that permits a solar collector to track or to follow the Sun during the day without manual adjustment (usually for concentrating collectors)

Azimuth Angle Same as **solar azimuth angle**

Balance of System (BOS) Term used in photovoltaics that represents all components and costs other than that of PV modules

Band GAP The difference in energy between the state of the highest valance band and the conduction band

Battery A collection of cells that store electrical energy; each cell converts chemical energy into electricity, or vice versa, and is interconnected with other cells to form a unit for storing useful quantities of electricity

Battery Capacity The maximum total electrical charge, expressed in ampere-hours (AH) that a battery can deliver to a load under a specific set of conditions

Battery Cell The simplest operating unit in a storage battery; it consists of one or more positive electrodes or plates, an electrolyte that permits ionic conduction, one or more negative electrodes or plates, separators between plates of opposite polarity, and a container for all of the above

Battery Available Capacity The total maximum charge, expressed in ampere-hours, that can be withdrawn from a cell or battery under a specific set of operating conditions including discharge rate, temperature, initial state of charge, age, and cutoff voltage

Battery Energy Capacity The total energy available, expressed in watt-hours (kilowatt-hours), that can be withdrawn from a fully charged cell or battery. The energy capacity of a given cell varies with temperature, rate, age, and cutoff voltage

Battery Cycle Life The number of cycles, to a specified depth of discharge, that a cell or battery can undergo before failing to meet its specified capacity or efficiency performance criteria

Beam Radiation This is radiation propagating along the line joining the receiving surface and Sun; also known as "direct radiation"

Biofuel A product from biomass

Biogas A mixture of methane (CH_4), carbon dioxide (CO_2), and some trace gases

Biomass Organic material of nonfossil organic (i.e., living or recently dead plant and animal tissue) matter including aquatic, herbaceous and woody plants, animal waste, and a portion of municipal waste

Biot Number (Bi) A dimensionless number that gives a simple index of the ratio of heat-transfer resistances inside of (L/K) and at the surface (1/h) of a body; it can also be defined as the ratio of surface heat-transfer coefficient to unit conductance of a solid over the characteristic dimension

Black body A perfect absorber and emitter of radiation; a cavity is a perfect black body; lampblack is close to a black body, whereas aluminum (polished) is a poor absorber and emitter of radiation

Blackbody Radiation Energy converted electrodynamically from the black body's pool of internal thermal energy at any temperature greater than absolute zero

Blackened Surface See **Absorber Plate**

Book Value The value at which an asset is carried on a balance sheet; it is the difference between the initial cost and the accumulated cost

Bouguer's Law (Beer's Law, Bouguer–Lambert Law; Lambert's Law) The attenuation of a beam of light by an optically homogeneous (transparent) medium

Brightness The subjective human perception of luminance

BTU British thermal unit; the amount of heat required to increase the temperature of one pound of water by 1°F; 3411 BTU equals 1 kWh

Cadmium Telluride (CdTe) A crystalline compound formed from cadmium and tellurium and used as an infrared optical window as well as a solar cell material; it is usually sandwiched with cadmium sulfide to form a p-n junction photovoltaic solar cell; typically CdTe cells use an n-i-p structure

Calorie The amount of heat required to raise the temperature of 1 g of water by 1 °C

Calorific Value The energy content per unit mass (or volume) of a fuel that will be released in combustion (kWh/kg, MJ/kg, kWh/m^3, MJ/m^3)

Candela (cd) An SI unit of luminous intensity; an ordinary candle has a luminous intensity of 1 cd

Capital-Recovery Factor (CRF) The ratio of constant annuity to the present value of receiving that annuity for a given length of time

Carbon Dioxide (CO_2) A colorless, odorless gas that is formed during normal human breathing; it is also emitted by combustion activities used to produce electricity; CO_2 is a major cause of the greenhouse effect, which traps radiant energy near the Earth's surface

Carbonization A process whereby wood is heated with restricted air flow from a high-carbon product by removing volatile materials from it

Cash Flow Diagram A tool used by accountants and engineers to represent the transactions that will take place over the course of a given project including initial investments, maintenance costs, projected earnings, or savings resulting from the project as well as the salvage and resale value of equipment at the end of the project

Cell A device that generates electricity traditionally consisting of two plates or conducting surfaces placed in an electrolytic fluid

Celsius The international temperature scale, named after Anders Celsius, in which water freezes at 0 °C and boils at 100 °C

Central Power Tower A configuration of independently tracking solar collectors focusing the reflected solar radiation onto a receiver placed on the top of tower

Charge Rate Current applied to a cell or battery to restore its available capacity; this rate is commonly normalized by a charge control device with respect to the rated capacity of the cell or battery

Charge Controller A component of a photovoltaic system that controls the flow of current to and from the battery to protect the batteries from over-charge and over-discharge; the charge controller may also indicate the system's operational status

Chromosphere (Literally, "color sphere") A thin layer of the Sun's atmosphere just above the photosphere approximately 2000-km deep

Circuit A system of conductors (i.e., wires and appliances) capable of providing a closed path for an electric current

Clear Sky A sky condition with few or no clouds (usually taken as 0–2 tenths covered with clouds); clear skies have high luminance and high radiation and thus create strong shadows relative to more cloudy conditions; the sky is brightest nearest the Sun, whereas away from the Sun it is approximately three times brighter at the horizon then at the zenith

Closed Cycle In this case a working fluid is returned to the initial stage at end of cycle and is recirculated

Clerestory Window A wall with windows between two different (roof) levels; the windows are used to provide natural light into a building

Coefficient of Performance (COP) The ratio of the change in heat at the "output" (the heat reservoir of interest) to the supplied work of any thermal system

Cogeneration Joint production of heat and work, most often electricity and heat

Collector A device that converts incoming solar radiation to heat

Collector Efficiency The ratio of useful (heat) energy converted by a solar collector to the radiation incident on the device

Collector-Efficiency Factor (F′) The ratio of actual rate of heat transfer to the rate of heat transfer if the absorber plate were at fluid temperature

Collector Plate A component of a solar flat-plate collector that absorbs solar radiation and converts it into heat

Collector Tilt Angle An angle between the horizontal plane and the surface of the solar collector

Compact Fluorescent Light (CFL) A modern light bulb with integral ballast using a fraction of the electricity used by a regular incandescent light bulb

Concentrating Collector A solar collector that reflects solar radiation (direct radiation) to an absorber plate for the production of high temperatures

Concentration Ratio The ratio of aperture area to receiver area

Condensation The process of vapor changing into a liquid state during which heat is released

Conductance (C) A measure of the ease with which heat flows though a specified thickness of a material by conduction; its unit is W/m^2 $°C$

Conduction The process by which heat energy is transferred through materials (solids, liquids, or gases) by the molecular excitation of adjacent molecules

Conduction Band The energy band in which electrons move freely

Conductivity The quantity of heat that will flow through 1 m^2 of material of 1-m thickness in 1 s when there is a temperature difference of 1 $°C$ between its surfaces

Conductor A substance or body capable of transmitting electricity, heat, and sound

Convection The transfer of heat between a moving fluid medium (liquid or gas) and a surface or the transfer of heat within a fluid by movement within the fluid

Convective Zone The range of radii of a star in which the Sun's energy is transported primarily by convection

Conservation of Energy Total amount of energy in any closed system; it remains constant

Core The central region of Earth having a radius of 3470 km; the radius of Earth measures 6370 km outside of which lie the mantle and crust

Crystalline Silicon A type of PV cell made from a single crystal or from poly-crystalline slices of silicon

Cost-Benefit Analysis (B/C) A process by which business decisions are analyzed.

Current The flow of electrons through a conductor

Dark Current The constant response (current) exhibited by a receptor of radiation (solar cell) during periods when it is not actively exposed to light

Daylight Factor Illumination inside a building

Daylight Hours The duration of time between sunrise and sunset

Day Lighting The practice of placing windows or other openings and reflective surfaces in a building so that natural light provides effective internal lighting during the day

Declination The angle of the Sun's rays made with respect to north or south of the equatorial plane

Deep Discharge Battery A type of battery that is not damaged when a large portion of its energy capacity is repeatedly removed (i.e., motive batteries)

Density Weight (mass [kg]) per unit volume

Depreciation Decline in the value of assets over the given period of time.

Depth of Discharge (DOD) Ampere-hours removed from a fully charged cell or battery expressed as a percentage of rated capacity; e.g., the removal of 25 A-h from a fully charged cell rated for 100 A-h results in a 25 % depth of discharge

Design Heat Load Total heat loss from a building during the most severe winter conditions that the building is likely to experience

Design Month The month has the lowest mean daily insolation value around which many stand-alone systems are planned

Diffuse Radiation Solar radiation reaching the surface due to reflection and scattering effect from the atmosphere

Diffusion Length Mean distance through which a free electron or hole moves before recombining with another hole or electron

Digester A huge vessel where chemical or biological reactions are performed

Direct Combustion Burning of biomass in the presence of oxygen

Direct Current (DC) The complement of AC, or alternating current, presents one unvarying voltage to a load; this is standard in automobiles

Direct Gain Same as **Direct Solar Gain**

Direct Radiation Radiation coming in a beam from the Sun, which can be focused due to its direction

Direct Solar Gain Thermal energy gain in building through a glazed window

Discharge The removal of electric energy from a battery

Discount Rate (d) Annual interest divided by capital including interest $[i/(1 + i)]$; this rate is lower than the interest rate and it considers the initial value as the nominal value minus a discount ($i - d = id$)

Diurnal Recurring every day or having a daily cycle

Dopants A chemical impurity added, usually in minute amounts, to a pure semiconductor to alter its electrical properties

Doping The addition of dopants (material with an excess of electron/holes) to a semiconductor

Double-Exposure Solar Air Heater In this case, both sides of an absorber are exposed to solar radiation to heat air for space heating/drying

Double Glazing Two panes of glass with a space between the panes

Dry-Bulb Temperature The temperature of a gas of mixture or gases indicated by an accurate thermometer after correction for radiation

Duct A pipe, tube, or channel that conveys a substance (usually warm or cold air)

Dye-Sensitized Solar Cell Solar cell composed of a porous layer of titanium dioxide nanoparticles immersed under an electrolyte solution and covered with a molecular dye (platinum-based catalyst) that absorbs sunlight; this is a low-cost solar cell belonging to the group called "thin-film solar cells"

Earth The Earth is the third planet from the Sun and is the densest and fifth largest of the eight planets in the solar system

EAHE Earth–air heat exchanger; used to transfer ground heat for heating/cooling of a space

Efficacy The efficiency by which a lamp converts electricity to visible radiation, i.e., the capacity to produce an effect (effectiveness); expressed in lumens per watt (lux)

Efficiency The ratio of output power (or energy) to input power (or energy) expressed as a percentage

Electromagnetic Spectrum The entire range of wavelengths or frequencies of electromagnetic radiation extending from gamma rays to the longest radio waves including visible light

Electronic Ballasts An improvement over core/coil ballasts used to drive fluorescent lamps

Elevation The height of a geographic location above a fixed reference point, e.g., the Earth's sea level, as an equipotential gravitational surface

Embodied Energy Amount of energy required to produce an object in its present form; an inflated balloon's embodied energy includes the energy required to manufacture and inflate it

Emissive Power Energy radiated (only by emission) from a body per unit area per unit time from zero to ant wavelength

Emissivity The ratio of radiant energy emitted by a body to that emitted by a perfect black body

Emittance A measure of the ability of a material to give off heat as radiant energy

Energy The ability to do work

Energy Band Gap An **energy** range in a solid where no electron states can exist

Energy Density Energy per unit area

Energy Intensity The ratio of energy used in a sector to activity in that sector, e.g., the ratio of energy use to constant dollar production in manufacturing

Energy Storage This is accomplished by a device or a physical medium that stores some form of energy to perform some useful operation at a later time

Equation of Time The difference between apparent solar time and mean solar time

Equinox The times of the year when the Sun passes over the celestial equator and when the day of length and night are almost equal; it happens twice a year

ERC External-reflection components defined as illumination inside a building due to the external reflection of solar radiation

Evacuated Tubular Collector (ETC) A solar collector that uses a vacuum between the absorber and the glass to reduce the top-loss coefficient (insulate the absorber plate) by reducing convective losses

EVA Ethylene–vinyl–acetate foil; it is used for module production to cover the cells

Exergy Available energy to be used for work; it refers to the second law of thermodynamics

Extrinsic Semiconductor A semiconductor that has been doped by a doping agent, which gives it different electrical properties than an intrinsic (pure) semiconductor

Extraterrestrial Region An enclosure (space) between the top of the atmosphere and the Sun

Fermentation The conversion of carbohydrates to alcohols in the absence of oxygen under anaerobic conditions for food processing

Fermi Level Term used to describe the top of the collection of electron energy levels at absolute zero temperature in a forbidden gap of a semiconductor

Fill Factor (FF) For an I–V curve, the ratio of maximum power to the product of the open-circuit voltage and the short-circuit current; a measure of the "squareness" of the I–V curve

Fin A surface that extends from an object to increase the rate of heat transfer to or from the environment by increasing convection/conduction

Fin Efficiency The ratio of actual heat transfer to heat transfer if the entire fin area were at base temperature

Forward Bias In this case, the *p*-type is connected with the positive terminal, and the *n*-type is connected with the negative terminal

First-Generation Solar Cell Crystalline solar cells made from silicon (sand) are first-generation solar cells; these are the most expensive with the highest efficiency

Flat-Plate Collector A solar-collection device for gathering the Sun's heat consisting of a shallow metal container covered with one or more layers of transparent glass or plastic; either air or a liquid is circulated through the cavity of the container whose interior is painted "black" and the exterior well insulated

Focusing Collector See **Concentrating Collector**

Forbidden Gap Gap that exists between the conduction and the valance band, in which electrons cannot normally exist

Forced Circulation Same as **Forced Mode**

Forced Convection A type of heat transport in which fluid motion is generated by an external source (e.g., a pump, fan, suction device, etc.)

Forced Mode In this case, the hot water from a flat-plate collector is moved to an insulated storage tank by a water pump

Fourier Number (Fo) (Fourier Modulus) Ratio of the heat-conduction rate to the rate of thermal-energy storage

Frequency $f = c/\lambda$ or $f = E/h$

Free Convection (Natural Convection) A type of heat transport that works only by density differences in the fluid occurring due to temperature gradients

Fresnel Collector A type of concentrating solar collector consisting of a concentric series of rings with a reflecting surface

Fuel Cell A device combining a fuel with oxygen in an electrochemical reaction to generate electricity directly without combustion

Gallium Arsenide (GaAs) A crystalline, high-efficiency semiconductor/photovoltaic material

Gamma rays Frequencies of gamma rays varies from 2.4×10^{23} Hz (1 GeV) to the local plasma frequency of the ionized interstellar medium (approximately 1 kHz)

Generator A device that produces electricity

Geothermal Energy Energy contained in the Earth's interior

Glare Visual perception caused by a very bright light or a high contrast of light, thus making it uncomfortable or difficult to see

Glasshouse Same as **Greenhouse**

Glazing Material Transparent or translucent materials, usually glass or plastic, used to cover an opening without impeding (relative to opaque materials) the admission of solar radiation and light

Global Radiation The sum of direct, diffuse, and reflected radiation

Greenhouse (Glasshouse) A building (house) made of transparent materials where plants are grown; these structures range in size from small sheds to very large buildings

Greenhouse Effect Global warming resulting from the absorption of infrared solar radiation by carbon dioxide and other traces of gases present in the atmosphere; the term is a misnomer in that in actual greenhouses warming occurs primarily to the restriction of air flow

Greenhouse Gases (GHG) Gases that contribute to the greenhouse effect by absorbing and emitting thermal infrared radiation in the atmosphere, carbon dioxide, nitrous oxide, methane, water vapor, ozone, and variety of chlorofluorocarbons (CFCs)

Grid A utility term for the network of wires that distribute electricity from a variety of sources across a large area

Heat Capacity or Thermal Capacity A measurable physical quantity that characterizes the amount of heat required to change a substance's temperature by a given amount

Heat Exchanger Device that passes heat from one substance to another; in a solar hot-water heater, for example, the heat exchanger takes heat harvested by a fluid circulating through the solar panel and transfers it to domestic hot water

Heat Pipe (Heat Pin) A heat-transfer device that combines the principles of both thermal conductivity and phase transition to efficiently manage the transfer of heat between two solid interfaces

Heat-Removal Factor (F_R) Ratio of actual rate of heat transfer to the rate of heat transfer if the absorber plate were at fluid inlet temperature

Heat Transfer The exchange of thermal energy from one physical system to another

Heat-Transfer Coefficient The proportionality-constant coefficient between heat flux (heat flow per unit area [q/A]) and temperature difference ΔT (the thermodynamic driving force for the flow of heat); the inverse of thermal resistance

Heat-Transfer Effectiveness The ratio between actual heat-transfer rate and maximum possible heat-transfer rate

Heat Loss Thermal-energy loss to the atmosphere due to a temperature difference

Honeycomb A mass of hexagonal cells built either by an infrared transparent material or an infrared specularly reflecting material; also known as "transparent insulating material" (TIM)

Hour Angle The angular displacement of the Sun east or west of the local meridian due to the rotation of Earth on its axis at 15°/h with morning being negative and afternoon being positive

Hydropower Energy in falling water converted into mechanical energy and then into electrical energy

I–V Curve Plot of current versus voltage characteristics of a solar cell, module, or array; I–V curves used to compare various solar cell modules and determine their performance at various levels of insolation and temperatures

Iluminance The amount of lumens per unit area

Incandescent Bulb A light source that produces light by heating a filament until it emits photons

Incident Radiation The quantity of radiant energy striking a surface per unit of time and area

Indirect Gain Thermal mass (such as rock or contained liquid) positioned between the Sun and a building space (room) to be heated

Infiltration A term used in heating, ventilation, and air conditioning for air leakage into buildings

Inflation rate The rate of increase of a price index (consumer price index) or the percentage rate of change in price level over time; the rate of decrease in the purchasing power of money is approximately equal

Infrared Radiation (IR) The part of electromagnetic radiation (waves) whose wavelength lies between 0.75 and 1000 μm

Insolation (or Incident Solar Radiation) The amount of sunlight falling on a place

Isolated Gain Thermal energy of solar energy is stored in separate unit before use for thermal heating

Instantaneous Efficiency Ratio of the rate of useful energy to the rate of input energy

Insulation A material that keeps energy from crossing from one place to another; on an electrical wire, it is the plastic or rubber that covers the conductor; in a

building, insulation makes the walls, floor, and roof more resistant to the outside (ambient) temperature

Insulator A material that is a poor conductor of electricity or heat

Intercept Factor The ratio of the fraction of power reaching the collector of a concentrator to the total power arriving at its entry aperture in a given direction

Intrinsic Semiconductor (Undoped Semiconductor/i-type Semiconductor) A pure semiconductor without any significant presence of dopant species

Inverter Electrical device that changes direct current (DC) into alternating current (AC)

IRC (internal-reflection component) Illumination inside a building due to the internal reflection of solar radiation

Irradiance The presence of electromagnetic radiation incident on the surface; it has an SI unit of W/m^2; the total amount of radiation present at all frequencies

Irradiation Same as **Irradiance**

Irreversible Process A process that is not reversible; it refers to the second law of thermodynamics

Isolated Gain When solar radiation collection and storage are thermally isolated from the living spaces of the building for the purpose of either heating or cooling

Joule A unit of energy or work; 1 J = 1 W second

Kilowatt (kW) 1000 W; energy consumption at a rate of 1000 J/s

Kilowatt-Hour (kWh) One kilowatt of power used for 1 h; a typical house uses 750 kW/h/month

Kinetic Energy The energy of motion

Kirchhoff's Law (Thermal Radiation) A general statement equating emission and absorption in heated objects

Laminar Flow (Streamline Flow) When a fluid flows in parallel layers with no disruption between the layers

Latent Heat Storage Phase-change material (PCM) used as a storage medium

Latitude The angular position of a location north or south of the equator

Life-Cycle Costing A method for estimating the comparative costs of alternative energy or other systems; life-cycle costing takes into consideration such long-term costs as energy consumption, maintenance, and repair

Life-Cycle Costs The entire cost of an energy device including the capital cost in present dollars and the cost as well as the benefits discounted to the present

Light-Emitting Diode An efficient source of electrical lighting typically lasting 50,000–100,000 h

Load A set of equipment or appliances that uses electrical power from the generating source, battery, or PV module

Local Time (Mean Solar Time) Our clocks use mean solar time (local time), which is uniform, i.e., averaged over 1 year (365.243… days)

Longitude A geographic coordinate that specifies the east–west position of a point (location) on the Earth's surface

Low-E Window Window that reflects infrared (IR) heat back into a room instead of absorbing and transmitting it to the outside

Manifold The folding together of multiple inputs and outputs

Maximum power point (MPP) The voltage at which a PV array produces maximum power

Maximum-power point tracker (MPPT) A power-conditioning unit that increases the power of a PV system by ensuring operation of the PV generator at its maximum power point (MPP); the ability to do so can depend on climate and the battery's state of charge

Mean Radiant Temperature (MRT) The area mean temperature of all objects surrounding the body

Mean Solar Time (Local Time) Our clocks use mean solar time, which is uniform, i.e., averaged over 1 year (365.243… days)

Medium-Temperature Solar Collector A solar thermal collector designed to operate in the temperature range of 80–100 °C

Megawatt 1,000,000 W

Module The smallest self-contained, environmentally protected structure housing interconnected photovoltaic cells and providing a single direct-current (DC) electrical output

Monthly Mean Daily Insolation The average solar energy per square meter available per day of a given month

Natural Convection same as **Free Convection**

Night-Sky radiation Reversal of the daytime-insolation principle; just as the Sun radiates energy during the day through the void of space, so also can heat energy travel unhindered at night from the Earth's surface back into space; on a clear night, any warm object can cool itself by radiating long-wave heat energy to the cooler sky; on a cloudy night, the cloud cover acts as an insulator and prevents heat from travelling to the cooler sky

NOCT Nominal operating cell temperature; the estimated temperature of a PV module when operating under 800 W/m^2 irradiance, 20 °C ambient temperature, and wind speed of 1 m/s; NOCT is used to estimate the nominal operating temperature of a module in its working environment

Nonconvective Zone (NCZ) The zone where salt concentration and temperatures are nearly constant. This separates the upper **convective** zone (UCZ) and the lower **convective** zone (LCZ) in a solar pond

Nonporous Air Heater A solar air heater with a metallic absorber

Nonrenewable Energy Sources Energy derived from finite and static stocks of energy

N-Type Semiconductor A semiconductor produced by doping an intrinsic semi-conductor with an electron-donor impurity (e.g., phosphorous in silicon)

NTU Number of transfer units; it is used to evaluate the rate of heat transfer through a heat exchanger

Nuclear Fusion The process by which two or more atomic nuclei of hydrogen join together, or "fuse," to form a single heavier nucleus of helium; this process occurs at the centre core of the Sun and usually is accompanied by the release of large quantities of energy

Number of Transfer Units (NTU) A method used to calculate the rate of heat in counter-current heat exchangers

Nusselt Number The ratio of convective to conductive heat transfer across (normal to) the boundary

Off the Grid Not connected to power grid

One-Axis Tracking A solar system capable of rotating about one axis and tracking the Sun from east to west

Open-Circuit Voltage (V$_{oc}$) The maximum possible voltage across a solar module or array; it occurs in sunlight when no current is flowing with infinite resistance between two noses

Open Cycle When the working fluid is renewed at the end of each cycle

Open-Sun Drying Direct drying of crops using solar energy

Optical Efficiency (Zero-Loss Coefficient) The ratio of solar energy passing through the panel glazing to the overall solar energy striking the panel

Organic Solar Cell It uses organic electronics (a branch of electronics that deals with conductive organic polymers or small organic molecules for light absorption [photons] and charge transport across electrodes

Orientation The arrangement of a solar device along a given axis to face in a direction best suited to absorb solar radiation

OTEC (Ocean Thermal-Energy Conversion) A process that exploits the natural temperature difference (gradient) between shallow and deep ocean water as the driving potential for a simple thermodynamic cycle that can extract work out of the temperature gradient

Overall Heat-Transfer Coefficient The inverse of total thermal resistance across all boundary layers

Overall Thermal Efficiency Ratio of useful energy to input energy for a given period, which can be hourly, daily, monthly, and yearly

Overcharging Leaving batteries on charge after they have reached their full state of charge (100 % charge)

Parabola A geometrically curved shape to focus sunlight on a single point

Parabolic Concentrating Cooker A solar cooker that uses a parabolic disk to focus sunlight

Parabolic Mirror A device with a large, shiny, and curved surface that focuses solar radiation on a specific point

Parallel Flat Plat A plate in which the absorber and glazing material are parallel

Passive Solar Design A building design that makes use of structural materials using no moving part to heat or cool the space inside

Passive Solar Heater A solar water or space heating system that moves heated water or air without using a fan, motor, or pump

Passive Solar House Same as **Solar House**

Passive Solar Still When the water in the basin is only heated through the glass cover of a solar still

Passive Solar Water Heater Solar water-heating system with natural/thermosyphon circulation

Payback Period (Payback Time/Payment Time) The length of time required to recover the cost of an investment

Payback Time Same as **Payback Period /Payment Time**

Payout Time Same as **Payback Period/Payback Time/Payment Time**

PCM Phase-change material

Peak Sunshine Hours The number of hours per day during which solar radiation averages 1000 W/m^2

Peak watt (W_p) Power output of a PV module under standard test conditions, i.e., 1000 W/m^2 and 25 °C

Pelletization A process in which wood is compressed and extracted in the form of rods and cubes

Periodic Motion Any motion that repeats in equal time intervals

Phase-Change Materials (PCM) A substance with a high heat of fusion during melting and solidifying at a certain temperature; it is capable of storing and releasing large amounts of energy as per requirement

Photon The elementary particle of electromagnetic energy; light (Greek photos, light)

Photosphere The deepest region of a luminous object, usually a star or the Sun, that is transparent to photons of certain wavelengths

Photovoltaic Array A number of PV modules that are electrically connected in series or parallel to provide the required rated power

Photovoltaic-Conversion Efficiency The ratio of electric power produced by a photovoltaic device to the power of the sunlight incident on the device

Photovoltaic Device A device that converts light directly into DC electricity; same as solar cell; this is also referred as to as the "photovoltaic effect"

Photovoltaic Effect Same as **photovoltaic device**

Photovoltaic Module N assembled set of interconnected solar cells connected in series

Photovoltaics (PV) A technology for using semiconductors to directly convert light into electricity

Photovoltaic Thermal A system to produce electrical as well as thermal energy

Planck's constant (h) Its value is 6.626×10^{-34} Js $= 4.135 \times 10^{-15}$ eVs

Planck's Law This describes the electromagnetic radiation emitted from a black body at absolute temperature T

P–N Junction This is formed at the boundary between a P-type and N-type semiconductor created in a single crystal of semiconductor by doping

Polycrystalline Silicon A material used to make PV cells that consists of many crystals in contrast to a single crystal silicon

Porous Air Heater A solar air heater with porous absorber

Potential Energy The energy that an object possesses as a result of its elevation in a gravitational field

Power The rate at which energy is consumed or produced; the unit is the watt

Power Density Power per unit area (W/m^2)

Power Factor The cosine of the phase angle between the current and voltage of a circuit

ppb Parts per billion

ppm Parts per million

Present Value Factor (PVF) ratio of present value to future value for a given lifetime of a system

PV See photovoltaic

PVT A photovoltaic thermal system to produce electrical as well as thermal energy

Pyranometer A type of actinometer used to measure broadband (total) solar irradiance on a planar surface; a sensor designed to measure solar radiation flux density (in watts per square meter) from a field of view of 180°

Pyrheliometer An instrument for the direct measurement of normal solar irradiance

Pyrolysis Canonization at a high-process temperature

R-value Thermal resistance of material, which is the inverse of the heat-transfer coefficient

Radiant Emittance Same as **Radiant Energy**

Radiant Energy (Radiant Exitance or Radiant Emittance) Energy in the form of electromagnetic waves emerging from the surface; it has an SI unit of W/m^2; the total amount of radiation present at all frequencies

Radiant Exitance Also known as **Radiant Self-Exitance,** Same as **Radiant Energy**

Radiant Exposure Same as **Irradiation**

Radiant Self-exitance Same as **Radiant Energy**

Radiation Electromagnetic waves that directly transport energy through space; sunlight is a form of radiation

Radiative Cooling Cooling of a roof exposed to the night sky

Radiosity Same as **Radiant Exitance**

Rate of Return (ROR)/Return on Investment (ROI)/Rate of Profit (ROP) The ratio of money gained or lost (whether realized or unrealized) on an investment relative to the amount of money invested

Reflectivity The ratio of radiant energy reflected by a body to that falling on it

Reflector A device that can be used to reflect solar radiation

Refrigeration A process in which work is done from one location to another by transferring heat

Relative Humidity A term used to describe the amount of water vapor in a mixture of air and water vapor

Renewable Energy Sources An energy source that renews itself without effort; fossil fuels, once consumed, are gone forever, whereas solar energy is renewable in that the sunlight we harvest today has no effect on the sunlight we can harvest tomorrow

Resistor Any electronic component that restricts the flow of electrical current in circuits

Reverse Bias In this case, the p-type is connected with the negative terminal, and the n-type is connected with the positive terminal

Reversible Process A process that can be reversed after it has taken place without change in either the system or its surroundings; it also refers to first law of thermodynamics

Respiration The process by which energy in organic molecules is released by oxidation

Rock-Bed Storage A type of thermal storage medium used in passive solar heating or cooling consisting of an underground accumulation of rocks serving as a heat exchanger

Salvage Value An estimated value that an asset will realize on its sale at the end of its useful life

Second-Generation Cell A thin-film solar cell that is significantly cheaper to produce than a first-generation cells but has a lower efficiency

Selective Surface A special surface that has high absorption and low emissivity; a means of increasing operation temperature and/or efficiency

Selectivity The ratio of radiation absorption (*alpha*) to radiation emission (*epsilon*)

Semiconductor A material, such as silicon, that has a crystalline structure that will allow current to flow under certain conditions; semiconductors are usually less conductive than metals but do not insulate like rubber

Sensible Heat Storage A heat storage system that uses a heat-storage medium and where the additional or removal of heat results in a change in temperature

Short-Circuit Current (I_{sc}) Current across the terminals when a solar cell or module in strong sunlight is not connected to a load (measured with an ammeter)

Short-Wavelength Radiation It varies from 0.26 to 2.6 μm

Silicon (Si) The most common metalloid and a chemical element that has atomic number 14; silicon is the eighth most common element (27.7 % of the crust) in

the universe by mass and is more widely distributed in the form of dusts and sands

Silicon Wafer Same as **Wafer**

Single-Crystal Structure A material having a crystalline structure such that a repeatable or periodic molecular pattern exists in all three dimensions

Sinking-Fund Factor (SFF) The ratio of the annuity payment (unacost) to a specified sum at some given future time period (future value)

Sinking-Fund Depreciation The actual loss in value of a machine for each year

Solar-Absorption Process A low temperature–driven solar cooling system

Solar Air Collector Same as **Solar Air Heating**

Solar Air Heating A solar thermal technology in which energy from the Sun is captured by an absorbing medium and used to heat air

Solar Air Conditioning Any air-conditioning (cooling) system that uses solar power

Solar Cooling Cooling of an enclosure by solar energy

Solar-Desiccant Cooling An open-cycle system using water as a refrigerant in direct contact with air unlike the solar-absorption process

Solar Distillation A process by which brackish/saline water is purified using solar energy

Solar Distiller A device used for the purification of brackish/saline water using solar energy

Solar Dryer A device that uses solar energy to dry substances, especially food/crop

Solar Flat-plate Air Collector Same as **Solar Air Collector**

Solar House House exposed to solar energy

Solarium A plastic/glass house attached to a room of a building for thermal heating

Solair Temperature The effective ambient air temperature, which includes the effect of solar intensity and long-wavelength radiation exchange between the ambient air and the sky

Solar Altitude Angle Same as **altitude angle**

Solar-Azimuth Angle The horizontal angle between the projection of Sun's rays (beam radiation) and due south in the northern hemisphere or between the Sun's rays (beam radiation) and due north in the southern hemisphere in a horizontal plane

Solar Cabinet Dryer A device that uses solar radiation for crop drying

Solar Cell A device that converts light energy or solar radiation (photons) directly into DC electricity

Solar-Cell Module Groups of encapsulated solar cells framed in glass or plastic units; usually the smallest unit of solar electric equipment available to the consumer

Solar Concentrator A device that uses reflective surfaces in a planar, parabolic trough, or parabolic bowl configuration to concentrate solar radiation onto a smaller surface

Solar Constant A measure of solar flux density; the amount of incoming solar electromagnetic radiation per unit area that would be incident on a plane perpendicular to the rays in an extraterrestrial region at the mean distance from the Sun to the Earth (one astronomical unit [AU]); the accepted value is approximately 1367 W/m^2

Solar Cooker A device that uses solar radiation for food cooking

Solar Declination The angle of the Sun north or south of the equatorial plane

Solar Distillation A process to produce drinking water or to produce pure water for lead acid batteries, laboratories, and hospitals and in producing commercial products, such as rose water, using solar energy

Solar Electricity Electricity that is obtained using solar energy

Solar Energy Radiant light and heat from the Sun, which has been harnessed by humans since ancient times using a range of ever-evolving technologies

Solar Fraction Same as **Solar-Savings Fraction**

Solar House A house where windows, walls, and floors are made to collect, store, and distribute solar energy in the form of heat in the winter and reject solar heat in the summer without the use of mechanical and electrical devices

Solarium A room built largely of glass to afford; exposure to the Sun; also referred to as a "sunroom"

Solar-Incident Angle The angle at which an incoming solar beam strikes a surface

Solar Oven Same as **Solar Cooker**

Solar Pond A pool of saltwater that acts as a large-scale solar thermal energy collector with integral heat storage for supplying thermal energy such as process heating, desalination, refrigeration, drying, and solar-power generation; it has three layers: (i) the UCZ (upper **convective** zone); (ii) the NCZ (**nonconvective** zone; and (iii) the LCZ (lower **convective zone);** and (iii) the LCZ (lower **convective zone)**

Solar Radiation The radiant energy received from the Sun from both direct and diffuse or reflected sunlight

Solar Spectrum The total distribution of electromagnetic radiation emitted from the Sun

Solar Still A device consisting of one or several stages in which brackish water is converted to portable water by successive evaporation and condensation with the aid of solar heat

Solar-Savings Fraction (Solar Fraction) The amount of energy provided by solar technology divided by the total energy required

Solar Spectrum Radiation emitted from Sun having wavelength between 0 and infinity

Solar Time The passage of time based on the Sun's position in the sky; the fundamental unit of solar time is the day; there are two types of solar time, apparent solar time (sundial time) and mean solar time (clock time)

Solar Wall Azimuth Angle The angle between normal to the wall and the projection of Sun's rays on a horizontal plane

Solar Water Heater A water heater that depends on solar radiation as its source of power

Specific Heat The quantity of heat required to raise one kilogram of a substance by one degree centigrade (J/kg/°C)

Specific Humidity The ratio of water vapor to dry air in a particular mass

Spectral Irradiance The total radiation for each frequency in the spectrum separately. It is measured in SI units W/m^3 or, commonly, $W\,m^{-2}\,nm^{-1}$ or $W\,m^{-2}\,\mu m^{-1}$

Speed of light (c) Its value is 299,792,458 (3×10^7) m/s in a vacuum

SSP Water Heater Heating and storage capacity of thermal energy in one unit

Standard Meridians This occurs every 15° of longitudinal displacement from the prime meridian (e.g., 15° W, 30° W, 45° W, etc.)

Standard Test Condition A condition having 1000 W/m^2 solar radiation and 25 °C ambient air temperature with air mass of 1.5

Standard Time The result of synchronizing clocks in different geographical locations within a time zone to the same time rather than using the local meridian, i.e., as in local mean time or solar time

Stratification The building up of layers of water/air temperature in a storage tank/room

Stefan's Law Also known as **Stefan–Boltzmann law**

Stefan–Boltzmann Law The total energy radiated per unit surface area of a black body per unit of time (known variously as black-body "**irradiance**," "**energy flux density**," "**radiant flux**," or "**emissive power**") is directly proportional to the fourth power of the black body's thermodynamic temperature T (also called **absolute temperature**); also known as "**Stefan's law**"

Streamline Flow Same as **Laminar Flow**

Sun An almost perfectly spherical star at the center of the solar system consisting of hot plasma interwoven with magnetic fields

Sun–Earth Angles All angles defined at the Earth with respect to the Sun

Sunshine Recorder A device that records the amount of sunshine at a given location

Sun's Rays Rays of sunlight that appear to radiate from a single point in the sky

Surface Azimuth Angle An angle between the line due south and the projection of normal to an inclined plane in a horizontal plane

Sustainable Material or energy sources that, if managed carefully, will provide at the current level indefinitely

Temperature A physical property of matter that quantitatively expresses the common notions of hot and cold; objects of low temperature are cold, whereas various degrees of higher temperatures are referred to as "warm" or "hot"

Terrestrial Region An enclosure (space) between Earth and the bottom of the atmosphere

Thermal Air Conductance Equivalent to heat-transfer coefficient for an air gap

Thermal Capacity Same as **Heat Capacity**

Thermal Comfort The state of mind in humans that expresses satisfaction with the surrounding environment by heating, ventilation, and air-conditioning design, etc.

Thermal Comfort Cooling Cooling performed by solar air conditioning

Thermal Conductivity The property of a material's ability to conduct heat

Thermal Diffusivity A physical property of material that refers how fast heat diffuses through the material

Thermal-Load Levelling This determines the room air fluctuation; for more fluctuation, there is more thermal load levelling

Thermal Mass A material used to store heat (thermal energy), thereby slowing the temperature variation within a space

Thermal Storage A solid or liquid medium that stores sensible heat

Thermal-Storage Wall A south-facing glazed wall that stores solar thermal energy; generally known as a "Trombe wall"

Thermodynamic System A physical system that contains a large number of atoms/molecules

Thermoelectric Effect The direct conversion of temperature differences to electric voltage and vice versa

Thermosyphon A closed-loop system in which water automatically circulates between a solar collector and a water storage tank above it due to the natural difference in density between the warmer and cooler portions of a liquid

Thermal Resistance The temperature difference across a structure when a unit of heat energy flows through it in unit time; the inverse of heat-transfer coefficient

Thermal Storage Any of several techniques to store heat energy using either the heat capacity of a material, the latent heat of phase change, or the heat of chemical dissociation

Thermosyphon A closed-loop system in which water automatically circulates between the flat-plate collector and storage tank placed above flat-plate collector due to pressure difference

Thin-film Photovoltaic Cell (TFPV) Same as **Thin-film Solar Cell** (TFSC)

Thin-film Solar Cell (TFSC)/Thin-film Photovoltaic Cell (TFPV) A solar cell made by depositing one or more thin layers (thin film) of photovoltaic material on a substrate; the thickness range of such a layer is wide and varies from a few nanometers to tens of micrometers

Third-Generation Solar Cell It (polymer, nanocrystalline cells, and dye-sensitized solar cells) does not need the p–n junction necessary in a traditional semiconductor with silicon-based cells (First-Generation Solar Cells)

Threshold Condition of Solar Radiation The level of solar radiation after which the solar system starts performing; it depends on the climatic and design parameters of each solar system

Thin-Film Silicon Most often this is amorphous (noncrystalline) material used to make photovoltaic (PV) cells

Tilt Angle The angle at which solar collector is tilted upward from the horizontal surface to receive maximum solar radiation

Time Constant The rise time characterizing the response to a time-varying input of a first-order, linear time-invariant

Total Radiation Sum of beam and diffuse radiation

Tracking The adjustment made to a solar-concentrating collector to track or follow the Sun's path across the sky

Transfer Medium A substance (air, water, or antifreeze solution) that carries heat from a solar collector to a storage area or from a storage area to a collector

Transmission Transporting bulk power over long distance

Transmittance The ratio of solar radiation transmitted through glazing to the total radiant energy falling on its surface

Transwall A thermal storage wall that is semitransparent in nature

Trombe Wall A glazed thermal-storage wall facing solar radiation

Trough A type of concentrating collector with one-axis tracking

Turbidity The cloudiness or haziness of a fluid caused by individual particles (suspended solids) that are generally invisible to the naked eye, similar to smoke in air

Turbine Generator A device that uses steam, heated gas, water flow, or wind to cause a spinning motion that activates electromagnetic forces to generate electricity

Turbulent Flow (Turbulence) A flow regime characterized by chaotic and stochastic property changes generally due to high forced flow

Two-Pass Air Heater In this case, fluidflows on both sides of the absorber

Uniform End of Year Annual Amount (Uniform Annual CostUnacost) An annualized sum of all relevant costs just like the amount of an installment-loan payment

Unacost (Uniform Annual Cost) The same **as Uniform end of year annual amount**

U-Value The amount of heat that flows in or out of a system at steady state, in 1 h, when there is a 1° difference in temperature between the fluid inside and outside

UV Radiation Same as **Ultraviolet (UV) Radiation**

Ultraviolet (UV) Radiation A portion of the electromagnetic radiation in the wavelength range of 4–400 nm

Valence Band The highest energy band in a semiconductor (holes are in majority) that can be filled with electrons

Ventilation The exchange of room air between rooms to the outside ambient air as per requirement; generally it measured in terms of the number of air changes per hour

Visible Light (Radiation) Electromagnetic radiation, with a wavelength between 0.38 (380 nm) and 0.78 μm (760 nm), that can be detected by the human eye

Volt The measure of potential difference between two electrodes

Wafer A thin slice of semiconductor material, such as a silicon crystal, used in the fabrication of integrated circuits and other micro-devices

Wall Solar Azimuth Angle Same as **Solar Wall Azimuth Angle**

Water Heating The process of generating domestic hot water by employing a flat-plate collector and using solar radiation

Watt Measure of power (or work) equivalent to 1/746 of horse power

Watt Hour (Wh) A common energy measure derived by multiplying the power times the hours of use; grid power is ordinarily sold and measured in kilowatt hours

Wavelength The distance between two similar points of a given wave

Wein's Displacement Law ($\lambda T = 2877.58$ μm K) The wavelength distribution of thermal radiation from a black body at any temperature has essentially the same shape as the distribution at any other temperature, except that each wavelength is displaced on the graph

Wet-Bulb Temperature A type of temperature measurement that reflects the physical properties of a system with a mixture of a gas and a vapor, usually air and water vapor

Wind Tower A traditional architectural element, mainly a part of residential houses, to catch cooler breezes at a higher level above the building and to direct it into the interior room of the building

Wind Turbine A device to convert kinetic energy associated with wind into mechanical energy

Zenith The top of the sky dome, i.e., perpendicular to a horizontal plane); a point directly overhead 90° in altitude angle above the horizon

Zenith Angle The angle between the Sun's ray and the zenith (perpendicular to a horizontal plane)

References

1. H.C. Hottel, A. Whiller, in *Transactions of the Conference on Use of Solar Energy*. The Scientific Basis, vol. II(I), Section A (University of Arizona Press, Tucson, 1958), 74
2. F. Kasten, A.T. Young, Appl. Opt. **28**, 4735 (1989)
3. R. Perez, P. Ineichen, E. Maxwell, R. Seals, A. Zelenka, ASHRAE Trans. **98**, 354 (1990)
4. American Society of Heating, *Refrigeration and Air-conditioning Engineers. ASHRAE Applications Handbook (SI)* (ASHRAE, Atlanta, 1999)
5. H.N. Singh, G.N. Tiwari, Energy **30**, 1589 (2005)
6. M.J. Ahmad, G.N. Tiwari, CIGR E-J **10**, 1 (2008)
7. B.Y.H. Liu, R.C. Jordan, Sol. Energy **4**, 1–19 (1960)
8. J.F. Orgill, K.G.T. Hollands, Sol. Energy **19**, 357 (1977)
9. D.G. Erbs, S.A. Klein, J.A. Duffie, Sol. Energy **28**, 293 (1982)
10. J.W. Spencer, Sol. Energy **29**(1), 19 (1982)
11. T. Muneer, M.M. Hawas, K. Sahili, Energy Convers. Manag. **24**(4), 265 (1984)
12. M.N.A. Hawlader, Int. J. Ambient Energy **5**, 31 (1984)
13. D.T. Reindl, W.A. Beckman, J.A. Duffie, Sol. Energy **45**, 1 (1990)
14. J. Chandrasekaran, S. Kumar, Sol. Energy **53**, 505 (1994)
15. J.C. Lam, D.H.W. Li, Build. Environ. **31**(6), 527 (1996)
16. J. Boland, L. Scott, M. Luther, Environmetrics **12**, 103 (2001)
17. A. Miguel, J. Bilbao, R. Aguiar, H. Kambezidis, E. Negro, Sol. Energy **70**, 143 (2001)
18. A.P. Oliveira, J.F. Escobedo, A.J. Machado, J. Soares, Appl. Energy **71**, 59 (2002)
19. S. Karatasou, M. Santamouris, V. Geros, Int. J. Sustain. Energ. **23**, 1 (2003)
20. J. Soares, A.P. Oliveira, M.Z. Boznar, P. Mlakar, J.F. Escobedo, A. Machado, J. Applied Energy **79**, 201 (2004)
21. A. Whillier, Arch. Meteorol. Geophys. Bioclimatol. **B8**, 197 (1956)
22. M. Collares-Pereira, A. Rabl, Sol. Energy **22**, 155 (1979)
23. T.A. Newell, Sol. Energy **31**, 339 (1983)
24. P.C. Jain, Solar Wind Technol. **1**, 123 (1984)
25. C. Gueymard, J. Sol. Energy Eng. Trans. ASME **108**, 320 (1986)
26. H.P. Garg, S.N. Garg, Sol. Wind Technol. **4**, 113 (1987)
27. A. Baig, P. Akhter, A. Mufti, Renew. Energy **1**, 119 (1991)
28. J.C.A. Maxwell, *Treatise on Electricity and Magnetism*, II edn. (Clarendon Press, Oxford, UK, 1881)
29. D.A.G. Bruggeman, Ann. Phys. Leipzig **24**, 636 (1935)
30. R.L. Hamilton, O.K. Crosser, I&EC Fundam **1**, 182 (1962)
31. F.J. Wasp, Solid–liquid slurry pipeline transportation. Trans. Tech. 1977 (Berlin)
32. K. Khanafer, K. Vafai, Int. J. Heat Mass Transf. **54**, 4410 (2011)
33. A. Einstein, Ann. Phys. Leipzig **19**, 289 (1906)
34. H.C. Brinkman, J. Chem. Phys. **20**, 571 (1952)
35. G. Batchelor, J. Fluid Mech. **83**, 97 (1977)

36. T. Lundgren, J. Fluid Mech. **51**, 273 (1972)
37. S. Maiga, S.J. Palm, C.T. Nguyen, G. Roy, N. Galanis, Int. J. Heat Fluid Flow **26**, 530 (2005)
38. J. Buongiorno, ASME J. Heat Transfer **128**, 240 (2006)
39. C.T. Nguyen, F. Desgranges, G. Roy, N. Galanis, T. Maré, S. Boucher, H.A. Mintsa, Int. J. Heat Fluid Flow **28**, 1492 (2007)
40. W.J. Tseng, K.C. Lin, Mater. Sci. Eng. A **355**, 186 (2003)
41. P.K. Namburu, D.P. Kulkarni, D. Misra, D.K. Das, Exp. Therm. Fluid Sci. **32**, 397 (2007)
42. P.K. Namburu, D.K. Das, K.M. Tanguturi, R.S. Vajjha, Int. J. Therm. Sci. **48**, 290 (2009)
43. W. Duangthongsuk, S. Wongwises, Int. J. Heat Mass Transf. **52**, 2059 (2009)
44. D.P. Kulkarni, D.K. Das, G. Chukwa, J. Nanosci. Nanotechnol. **6**, 1150 (2006)
45. D.P. Kulkarni, D.K. Das, S.L. Patil, J. Nanosci. Nanotechnol. **7**, 2318 (2007)
46. C.J. Ho, W.K. Liu, Y.S. Chang, C.C. Lin, Int. J. Therm. Sci. **49**, 1345 (2010)
47. Y. Xuan, W. Roetzel, Int. J. Heat Mass Transf. **43**, 3701 (2000)
48. R.S. Vajjha, D.K. Das, ASME **131** (2009)
49. K. Khanafer, K. Vafai, M. Lightstone, Int. J. Heat Mass Transfer **46**, 3639 (2003)
50. K.S. Wang, J.H. Lee, S.P. Jang, Int. J. Heat Mass Transfer **50**, 4003 (2007)
51. C.J. Ho, M.W. Chen, Z.W. Li, Int. J. Heat Mass Transfer **51**, 4506 (2008)
52. E.N. Seider, G.E. Tate, Ind. Eng. Chem. **28**(12), 1429 (1936)
53. B.C. Pak, Y.I. Cho, Exp. Heat Transfer **11**(2), 151 (1998)
54. Y. Xuan, Q. Li, Trans. ASME **125** (2003)
55. S.E.B. Maiga, C.T. Nguyen, N. Galanis, G. Roy, T. Mare, M. Coqueux, Int. J. Numer. Meth. Heat Fluid Flow **16**(3), 275 (2006)
56. S.M. Fotukian, M.N. Esfahany, Int. Comm. Heat Mass Transfer **37**, 214 (2010)
57. L. Qiang, X. Yimin, Sci. China (Series E) **45**(5), 408 (2002)
58. V. Gnielinski, Int. Chem. Eng. **16**, 359 (1976)
59. W. Duangthongsuk, S. Wongwises, Exp. Therm. Fluid Sci. **33**, 706 (2009)
60. B.C. Pak, Y.I. Cho, Exp. Heat Transfer **11**, 151 (1999)